

NUREG/CP-0027, V. 3
C.1

NUREG/CP-0027
Vol. 3



**NUCLEAR WASTE
MANAGEMENT
LIBRARY**

Proceedings of the International Meeting on Thermal Nuclear Reactor Safety

SANDIA NATIONAL LABORATORIES
823 LIBRARY, MS-0731
P. O. BOX 5800
ALBUQUERQUE, NM 87185-0731

Held at Chicago, IL
August 29-September 2, 1982

Sponsored by
American Nuclear Society
Nuclear Reactor Safety Division
Chicago Section

Cosponsored by
European Nuclear Society
Canadian Nuclear Society
Japan Atomic Energy Society

In Cooperation with
U.S. Nuclear Regulatory Commission
International Atomic Energy Agency

The views expressed in these proceedings are not necessarily those of the U. S. Nuclear Regulatory Commission.

The submitted manuscript has been authored by a contractor of the U.S. Government under contract. Accordingly the U.S. Government retains a nonexclusive, royalty-free license to publish or reproduce the published form of this contribution, or allow others to do so, for U.S. Government purposes.

Available from

GPO Sales Program
Division of Technical Information and Document Control
U.S. Nuclear Regulatory Commission
Washington, DC 20555

Printed copy price: \$13.00

and

National Technical Information Service
Springfield, VA 22161

Proceedings of the International Meeting on Thermal Nuclear Reactor Safety

Held at Chicago, IL
August 29-September 2, 1982

Date Published: February 1983

Sponsored by
American Nuclear Society
Nuclear Reactor Safety Division
Chicago Section

Cosponsored by
European Nuclear Society
Canadian Nuclear Society
Japan Atomic Energy Society

In Cooperation with
U.S. Nuclear Regulatory Commission
International Atomic Energy Agency

FOREWORD

The International Meeting on Thermal Nuclear Reactor Safety, held August 29-September 2, 1982, in Chicago, Illinois, is part of an ongoing series of meetings on the subject of nuclear reactor safety, jointly sponsored by the *American Nuclear Society* (through its *Nuclear Reactor Safety Division*) and the *European Nuclear Society*. The cosponsorship by the *Canadian Nuclear Society* and the *Japan Atomic Energy Society*, as well as the cooperation received from the *U.S. Nuclear Regulatory Commission* and the *International Atomic Energy Agency*, further attests to the importance and international character of the meeting.

The *Chicago Section* of the American Nuclear Society served as host of the meeting, having carried, through the Organizing Committee, the responsibility for the local arrangements and the financial aspects.

The safety of nuclear power reactors is a subject that, of necessity, has to be dealt with in an international framework. It is for this reason that the meeting organizers have also made a major effort to encourage participation from countries other than those represented by the cosponsoring professional societies. In this respect should be mentioned the valuable contributions, both in the organizational and the technical aspects of the meeting, made by representatives from countries with major nuclear power programs such as Argentina, Brazil, Mexico, the Republic of China (Taiwan), and the Republic of (South) Korea.

High distinction was bestowed on the meeting by three Honorary Chairmen, namely: James R. Thompson, Governor of Illinois; André Giraud, Professor at the University of Paris-Dauphine and Minister of Industry and Technology in the immediate-past government of France; and Joseph M. Hendrie, Senior Scientist at Brookhaven National Laboratory and past Chairman of the U.S. Nuclear Regulatory Commission, to whom the meeting organizers wish to express great appreciation for their support and valuable contributions.

It is not possible to individually acknowledge all persons who contributed to the meeting. As regards the *technical content* of the meeting, major contributions were made by those who accepted responsibility for organizing and coordinating the Special Sessions and Panel Discussions, namely: R. A. Bari (BNL), R. D. Cheverton (ORNL), R. S. Denning (BCL), J. W. Hickman (SNL), W. Y. Kato (BNL), D. A. Meneley (OHC), M. Rosen/E. Iansiti (IAEA), and E. Yaremy (AECL). An important contribution was also made by Annick Carnino (EdF), who accepted primary responsibility for coordinating the papers from France. We are greatly indebted to Long-Sun Tong, the Representative of the U.S. Nuclear Regulatory Commission on the Technical Program Committee, for his numerous and valuable contributions. Many thanks are also due to the members of the International Advisory Committee, the Technical Program Committee and the Paper Review Committee; in particular we wish to express our thanks to those members of the Paper Review Committee, who came from far to make an essential contribution, namely: Karel Brinkmann (ECN), Eric Hellstrand (Studsvik), Morris Rosen (IAEA), Wolfgang Schikarski (KFK), Jean Stolz (EdF), Roberto Treviño (CNSNS), and Hermann Unger (UST).

With respect to the *non-technical part* of the meeting organization, we wish to express our great appreciation to Miriam Holden (ANL) for her valuable advice and assistance concerning numerous aspects, including hotel arrangements and registration. Great appreciation is also due to Joyce Kopta (ANL) for her valuable advice and assistance in the preparation of the Meeting Program and Proceedings. Our special gratitude goes to Joan Cooley (ANL), Barbara Heineman (ANL), Beverly Korelc (ANL), Dena Rottner (NWU), Alice Townsend (ANL), Jill Wadas (ANL), Julia Wertelka (ANL), and Carol Whalen (ANL) for their numerous and valuable contributions made before, during, and after the meeting.

In the final analysis, the success or failure of a meeting depends on its attendees — authors, session chairmen, panelists, and others — they make the meeting. Therefore, last, but not least, we wish to thank all attendees for their participation in, and contributions to, this meeting which, it is hoped, has served a useful purpose by providing a forum for fruitful exchange of information, by promoting the safety of nuclear power reactors, and by contributing to international cooperation in the field of nuclear safety.

STEERING COMMITTEE

Donald T. Eggen (NWU)	General Chairman
Adolf Birkhofer (GRS)	General Co-Chairman
Norman C. Rasmussen (MIT)	Chairman, Technical Program Committee
Jan B. van Erp (ANL)	Co-Chairman, Technical Program Committee
Elmer E. Lewis (NWU)	Chairman, Publications Committee
André Gauvenet (EdF)	Chairman, International Advisory Committee
Dietrich Buenemann (GKSS)	Chairman, ENS Representatives on the Technical Program Committee
Wladimir Paskievici (EPM)	Chairman, CNS Representatives on the Technical Program Committee
Yasumasa Togo (UT)	Co-Chairman, JAES Representatives on the Technical Program Committee

REPRESENTATIVES OF COOPERATING ORGANIZATIONS

U. S. Nuclear Regulatory Commission: L. S. Tong

International Atomic Energy Agency: M. Rosen

HONORARY CHAIRMEN

The Honorable James R. Thompson,
Governor of Illinois

André Giraud, Professor at the University of Paris-Dauphine,
Minister of Industry and Technology of France

Joseph M. Hendrie, Senior Scientist Brookhaven National Laboratory,
Past Chairman US Nuclear Regulatory Commission

ORGANIZING COMMITTEE

Donald T. Eggen (NWU)	Chairman	Elmer E. Lewis (NWU)	Publications
Raymond M. Crawford (SAI)	Treasurer	Donald R. MacFarlane (ETA)	Publicity
Joseph Edelstein (Fluor)	Activities	John T. Madell (FAI)	Deputy Chmn.
Donald R. Ferguson (ANL)	Deputy Chmn.	Martin Plys (FAI)	Students
Mary Goodkind (ESCOR)	Guests	William J. Sturm (ANL)	Publications
James W. Henning	Audio/Visual	Bruce W. Spencer (ANL)	Poster Sessions
C. Daniel Henry (ETA)	Tours	Tom R. Tramm (CECo)	Registrar
Miriam L. Holden (ANL)	Arrangements	Jan B. van Erp (ANL)	Technical Program
Dennis J. Kilsdonk (ANL)	Audio/Visual	Norman Weber (S&L)	Publications
Joyce A. Kopta (ANL)	Publications		

AMERICAN NUCLEAR SOCIETY

Nuclear Reactor Safety Division

Chicago Section

Executive Committee:

Joseph C. Turnage (SNR)	Chairman
Walter Y. Kato (BNL)	Vice Chairman
Dirk A. Dahlgren (SNL)	Secy.-Treas.
William Kerr (UM)	Past Chairman
Robert Avery (ANL)	Past Chairman

Brian R. T. Frost (ANL)	Chairman
Mary Goodkind (ESCOR)	Chairman-Elect
Dennis O'Boyle (CECo)	Secretary
F. O. (Whitey) Hurd (WEC)	Treasurer
Tom R. Tramm (CECo)	Past Chairman
Joseph Edelstein (Fluor)	Past Chairman
Donald R. MacFarlane (ETA)	Past Chairman

Program Committee:

Joseph A. Murphy (NRC)	Chairman
George F. Flanagan (ORNL)	Past Chmn.
Alan Waltar (HEDL)	Past Chmn.

REPRESENTATIVES OF CO-SPONSORING SOCIETIES

Canadian Nuclear Society

W. Paskievici (EPM), Chairman
W. T. Hancox (AECL)
D. A. Meneley (OHC)
E. Yaremy (AECL)

European Nuclear Society

D. Buenemann (GKSS), Chairman	W. Jeschki (Wuerenlingen)
L. Bindler (BN)	P. Mostert (KEMA)
K. Brinkmann (ECN)	A. Rastas (TVO)
A. Carnino (EdF)	H. Teague (UK-AEA)
A. Hassid (NIRA)	H. Unger (USt)
M. Israel (EdF)	G. Volta (JRC)

Japan Atomic Energy Society

R. Kiyose (UT), Chairman
Y. Togo (UT), Co-Chairman

TECHNICAL PROGRAM COMMITTEE

N. C. Rasmussen (MIT), Chairman	J. W. Hickman (SNL)
R. A. Bari (BNL)	J. F. Jackson (LANL)
W. R. Corcoran (CE)	R. J. Johnson (TVA)
W. B. Cottrell (ORNL)	J. A. Murphy (NRC)
D. Dahlgren (SNL)	E. O'Donnel (EC)
L. W. Deitrich (ANL)	V. E. Schrock (UCB)
R. S. Denning (BCL)	R. Seale (UA)
R. Duffey (EPRI)	G. Sherwood (GE)
D. T. Eggen (NWU)	R. R. Stiger (EG&G)
H. K. Fauske (FAI)	J. C. Turnage (SNR)
G. Flanagan (ORNL)	J. B. van Erp (ANL), Co-chairman
E. Fuller (SLI)	L. J. Ybarrondo (EG&G)

INTERNATIONAL ADVISORY COMMITTEE

A. Gauvenet (France, EdF), Chairman	S. Levine (USA, NUS)
A. Alonso (Spain, JEN)	W. Loewenstein (USA, EPRI)
R. Avery (USA, ANL)	M. Nozawa (Japan, JAERI)
R. Bello (Mexico, CNSNS)	D. Okrent (USA, UCLA)
D. Beninson (Argentina, CNEA)	M. Rosen (IAEA, Vienna)
A. Birkhofer (FRG, GRS)	D. Smidt (FRG, KFK)
B. R. T. Frost (USA, ANL)	K. Stadie (OECD)
A. Gonzalez (Argentina, CNEA)	J. Stolz (France, EdF)
J. H. Jennekens (Canada, AECB)	W. Stratton (USA, LANL)
W. Y. Kato (USA, BNL)	L-S. Tong (USA, NRC)
G. Kinchin (UKAEA)	R. Treviño (Mexico, CNSNS)
L. Lederman (Brazil, CNEN)	W. Vinck (CEC, Brussels)
S-H. Lee (Korea, KAERI)	

PAPER REVIEW COMMITTEE

N. C. Rasmussen (MIT), Chairman	J. F. Jackson (LANL)
S. Asselin (TEC)	W. Y. Kato (BNL)
L. Baker, Jr. (ANL)	R. Lindsay (ANL)
R. Bari (BNL)	D. A. Meneley (OHC)
C. Bowers (ANL)	C. J. Mueller (ANL)
K. Brinkmann (ECN)	L. Potash (INPO)
J. Buchanan (ORNL)	W. Quapp (EG&G)
R. Christie (TVA)	M. Rosen (IAEA)
D. Dahlgren (SNL)	W. Schikarski (KFK)
R. S. Denning (BCL)	B. W. Spencer (ANL)
Z. Domaratzki (AECB)	J. Stolz (EdF)
D. T. Eggen (NWU)	L-S. Tong (NRC)
H. K. Fauske (FAI)	R. Treviño (CNSNS)
G. Flanagan (ORNL)	H. Unger (UST)
B. R. T. Frost (ANL)	J. B. van Erp (ANL), Co-chairman
W. T. Hancox (AECL)	R. Vogel (EPRI)
E. Hellstrand (Studsvik)	E. Yaremy (AECL)
J. W. Hickman (SNL)	J. Young (CE)
J. Ireland (LANL)	

COORDINATORS OF SPECIAL SESSIONS AND PANEL DISCUSSIONS

R. A. Bari (BNL)	Session 28
R. D. Cheverton (ORNL)	Sessions 7 and 11
R. S. Denning (BCL)	Sessions 17 and 21
J. W. Hickman (SNL)	Session 18
W. Y. Kato (BNL)	Session 6
D. A. Meneley (OHC)	Session 22
N. C. Rasmussen (MIT)	Sessions 1 and 32
M. Rosen (IAEA)	Session 2
E. Yaremy (AECL)	Session 10

ACRONYMS OF ORGANIZATIONS

AECB	Atomic Energy Control Board (Canada)
AEC-Greece	Atomic Energy Commission of Greece
AECL	Atomic Energy of Canada Limited
ANL	Argonne National Laboratory
ARL	Alden Research Laboratory (Worcester, MA)
AS	Anstalt fuer Stroemungsmaschinen GmbH (Austria)
ASA	Applied Science Associates, Inc.
ASEA	ASEA-Atom (Sweden)
BCL	Battelle Columbus Laboratories
BEC	Boston Edison Co.
BN	Belgonucléaire
BNL	Brookhaven National Laboratory
B&W	Babcock & Wilcox Co.
CE	Combustion Engineering Co.
CEA	Commissariat à l'Energie Atomique (France)
CEC	Commission of the European Communities
CECo	Commonwealth Edison Co.
CEGB	Central Electricity Generating Board (UK)
CMET	Center for Mineral and Energy Technology (Canada)
CNEA	Comision Nacional de Energia Atomica (Argentina)
CNEN	Comissão Nacional de Energia Nuclear (Brazil)
CNSNS	Comision Nacional de Seguridad Nuclear y Salvaguardias (Mexico)
COGEMA	Compagnie Generale des Matieres Nucleaires (France)
CPC	Consumers Power Co.
CSDL	Charles Stark Draper Laboratory
CU	Carleton University (Canada)
DE	Davis Engineering Ltd. (Canada)
DOE	Department of Energy
DPC	Duke Power Co.
EA	Empresarios Agrupados (Spain)
EC	Envirosphere Company/Ebasco Services, Inc.
ECN	Energy Research Center (The Netherlands)
EdF	Electricite de France
EERM	Ettablissement d'Etudes de Recherches Météorologiques (France)
EES	Electrowatt Engineering Services (London or Zurich)
EG&G	EG&G Idaho, Inc.
EI	Energy Incorporated
ENACE	Empresa Nuclear Argentina de Centrales Electricas SA (Argentina)
EPM	Ecole Polytechnique de Montréal (Canada)
EPDC	Electric Power Development Co., Ltd. (Japan)
EPRI	Electric Power Research Institute
ESA	Engineering Science & Analysis
Escor	Escor, Inc.
ESI	Ebasco Services, Inc.
ETA	ETA Engineering, Inc.
FAI	Fauske & Associates, Inc.
FEPC	Federation of Electric Power Companies (Japan)
Fluor	Fluor Power Services, Inc.
Framatome	Framatome, SA (France)

ACRONYMS FOR ORGANIZATIONS (Contd.)

GA	General Atomic Co.
GE	General Electric Co.
GKSS	Gesellschaft fuer Kernenergieverwertung in Schiffbau und Schiffahrt mbH, Geesthacht (FRG)
GPC	General Physics Corporation
GRS	Gesellschaft fuer Reaktorsicherheit (FRG)
Halden	Halden Project (Norway)
HEI	Heat Engineering Institute (USSR)
Hitachi	Hitachi, Ltd. (Japan)
HTRB	Hochtemperatur-Reaktorbau GmbH (FRG)
IAEA	International Atomic Energy Agency
INEL	Idaho Nuclear Engineering Laboratory
INPO	Institute for Nuclear Power Operation
INS	Institute of Nuclear Safety (Japan)
IT	Intermountain Technologies, Inc.
IVO	Imatran Voima Oy (Finland)
JAERI	Japan Atomic Energy Research Institutes
JBF	JBF Associates, Inc.
JEN	Junta de Energia Nuclear (Spain)
JRC	Joint Research Centre - Ispra (Italy)
KAERI	Korea Advanced Energy Research Institute
KEMA	N. V. Keuring van Electriche Materialen (The Netherlands)
KFK	Kernforschungszentrum Karlsruhe
KLA	Kernkraftwerk Leibstadt AG (Switzerland)
Ktech	Ktech Corp.
KWU	Kraftwerk Union AG (FRG)
LANL	Los Alamos National Laboratory
LLNL	Lawrence Livermore National Laboratory
LPL	Louisiana Power and Light
LU	Lehigh University
MESA	Studio MESA (Italy)
MIT	Massachusetts Institute of Technology
MU	McMaster University (Canada)
NAIG	Nippon Atomic Industry Group Co., Ltd. (Japan)
NEC	NucleDyne Engineering Corporation
NII	Nuclear Installations Inspectorate (UK)
NIRA	Nucleare Italiana Reattori Avanzati S.P.A. (Italy)
NRC	Nuclear Regulatory Commission (U.S.)
NSAC	Nuclear Safety Analysis Center
NU	Northeast Utilities
NUS	NUS Corporation
NWU	Northwestern University
OECD	Organization for Economic Cooperation and Development
OHC	Ontario Hydro Company (Canada)
ORNL	Oak Ridge National Laboratory
PLG	Pickard, Lowe and Garrick, Inc.
PNL	Pacific Northwest Laboratory

ACRONYMS FOR ORGANIZATIONS (Contd.)

RI	Rockwell International
Risø	Risø National Laboratory (Denmark)
S&A	Stevenson and Associates
SAI	Science Applications, Inc.
SEC	Sukegawa Electric Co., Ltd. (Japan)
S&L	Sargent & Lundy
SLI	S. Levy, Inc.
SNL	Sandia National Laboratories
SNR	Summit Nuclear Resources
SPB	State Power Board (Sweden)
Studsvik	Studsvik Energiteknik AB (Sweden)
SUNY	State University of New York
S&W	Stone & Webster Engineering Corp.
Sydskraft	Sydskraft (Sweden)
TAI	Tech. Aid Inc.
TC	Toshiba Corp. (Japan)
TEC	Technology for Energy Corporation
TEPC	Tokyo Electric Power Company (Japan)
TPC	Taiwan Power Company (Taiwan)
TRC	Technical Research Centre (Finland)
TUM	Technische Universitaet Muenchen (FRG)
TVA	Tennessee Valley Authority
TVO	Teollisuudon Voima Oy (Finland)
UA	University of Arizona
UCB	University of California at Berkeley
UCLA	University of California, Los Angeles
UdP	Universita di Pisa (Italy)
UFRJ	Universidade Federal Rio de Janeiro (Brazil)
UKAEA	UK Atomic Energy Authority
USt	University of Stuttgart (FRG)
UT	University of Tokyo (Japan)
UWa	University of Waterloo (Canada)
UW	University of Wisconsin
VEPCO	Virginia Electric and Power Co.
WEC	Westinghouse Electric Corp.
WLA	Wood-Leaver and Associates, Inc.
Wuerenlingen	Federal Nuclear Research Center (Switzerland)
YAEC	Yankee Atomic Electric Co.

VOLUME 1

Page

Special Address: What About the Future of Nuclear Energy?	
A. Giraud (<i>COGEMA</i>)	1
Luncheon Address: Man-Machine Relations in Nuclear Energy—And Elsewhere	
A. Gauvenet (<i>EdF</i>)	17

SESSION 1

CURRENT ISSUES IN NPP SAFETY

Chair: N. C. Rasmussen (*MIT*)

The Use of Probabilistic Risk Assessment for Safety Evaluation	
A. Birkhofer (<i>GRS</i>)	25
Issues and Trends in Canadian Reactor Safety Practice	
G. L. Brooks (<i>AECL</i>)	35
Operating Experience of Light Water Reactors in Japan	
S. Hamaguchi (<i>FEPC</i>)	42
Recent Nuclear Power Safety Initiatives at the International Atomic Energy Agency	
M. Rosen (<i>IAEA</i>)	48

SESSION 2

NATIONAL PROGRAMS IN NPP SAFETY

Chair: M. Rosen (*IAEA*)
K. Stadie (*OECD*)

Regulatory Actions during the Transition Period from Construction to Operation	
R. Bello (<i>CNSNS</i>)	59
A Review of the Brazilian Experience in the Licensing of Nuclear Power Plants	
L. Lederman and J. J. Laborne (<i>CNEN</i>)	66
Nuclear Power Plant Safety-Related Experience in Finland	
A. J. Rastas (<i>TVO</i>) and B. A. O. Regnell (<i>IVO</i>)	71
Scientific/Engineering Judgement in Swedish Reactor Safety Assessment	
S. O. W. Bergström (<i>Studsvik</i>)	81
The Regulatory Use of Probabilistic Safety Analysis in Argentina	
A. J. Gonzalez (<i>CNEA</i>)	87

SESSION 3

RADIOLOGICAL SOURCE TERMS - 1

Chair: C. Devillers (*CEA*)
J. Griffith (*DOE*)

Effect of Core Chemistry on Fission Product Release	
S. W. Tam, P. E. Blackburn, and C. E. Johnson (<i>ANL</i>)	101
Volatile Fission-Product Source Term Evaluation Using the FASTGRASS Computer Code	
J. Rest (<i>ANL</i>)	111
A Generalized Model for Predicting Radionuclide Source Terms for LWR Degraded Core Accidents	
S. L. Nicolosi and P. Baybutt (<i>BCL</i>)	122

	<u>Page</u>
Plate-Out Modelling in Assessing Fission Product Retention in Advanced Gas-Cooled Reactor Primary Circuits	
E. M. Hood, A. R. Taig, and P. N. Clough (<i>UKAEA</i>)	131
Uncertainties in LWR Meltdown Accident Consequences	
R. E. Kurth and P. Baybutt (<i>BCL</i>)	140
Transient Fission Product Release during Dryout in Operating UO₂ Fuel	
I. J. Hastings, C. E. L. Hunt, J. J. Lipsett, and R. G. Gray (<i>AECL</i>)	150
Fission Product Source Terms Measured during Fuel Damage Tests in the Power Burst Facility	
D. J. Osetek, J. J. King, and R. M. Kumar (<i>EG&G</i>)	162

SESSION 4

PRA-1; METHODS AND TECHNIQUES

Chair: W. Vinck (*CEC*)
W. Paskievici (*EPM*)

Assembling and Decomposing PRA Results: A Matrix Formalism	
D. C. Bley, S. Kaplan, and B. J. Garrick (<i>PLG</i>)	173
A Methodology for Seismic Risk Analysis of Nuclear Power Plants	
S. Kaplan, H. F. Perla, and D. C. Bley (<i>PLG</i>)	183
Accident Sequence Binning: A Method to Integrate the Individual Analyses of a Probabilistic Risk Assessment	
B. F. Putney, Jr., and W. J. Parkinson (<i>SAI</i>)	193
A Mathematical Framework for Quantitative Evaluation of Software Reliability in Nuclear Safety Codes	
C. J. Mueller, E. E. Morris, C. C. Meek (<i>ANL</i>), and W. E. Vesely (<i>NRC</i>)	202
Comparison of Deterministic and Stochastic Techniques for Estimation of Design Basis Floods for Nuclear Power Plants	
S. I. Solomon, K. D. Harvey (<i>UWa</i>), and G. J. K. Asmis (<i>AECEB</i>)	210
Analytic Methods for Uncertainty Analysis in Probabilistic Risk Assessment	
D. C. Cox and P. Baybutt (<i>BCL</i>)	223
A Methodology for Assessing Uncertainties in the Plant-Specific Frequencies for Initiating Events in the Presence of Population Variability	
I. A. Papazoglou (<i>BNL</i>)	231
Methodology and Code for Specifying Probabilistic Risk Coefficients	
D. E. Fields (<i>ORNL</i>)	239
A Fast Analytical Method for the Addition of Random Variables	
V. Senna, R. L. Milidiu, P. V. Fleming, M. R. Salles, and L. F. S. Oliveira (<i>UFPRJ</i>)	245

SESSION 5

NON-LOCA AND SMALL-BREAK-LOCA TRANSIENTS

Chair: W. Hancox (*AECL*)
E. Hellstrand (*Studsvik*)

Assessment of Calculational Methods and Results for Large PWR Feedwater Line Break and Steam Line Break Accidents	
K. S. Chung, M. F. Kennedy, and P. B. Abramson (<i>ANL</i>)	255
Steam-Generator-Tube-Rupture Transients for Pressurized Water Reactors	
D. Dobranich, R. J. Henninger, and N. S. DeMuth (<i>LANL</i>)	264
Predictions on Angra 1 Behaviour during Startup Tests Using the ALMOD Code	
C. T. M. Camargo (<i>CNEN</i>)	276

RETRAN Operational Transient Analysis of the Big Rock Point Plant Boiling Water Reactor	
G. R. Sawtelle, J. D. Atchison, R. F. Farman (<i>EI</i>), D. J. VandeWalle, and H. G. Bazydlo (<i>CPC</i>)	285
TRAC-BD1/MOD1, An Improved Analysis Code for Boiling Water Reactor Transients	
W. L. Weaver, M. M. Giles, J. D. Milton, and C. C. Tsai (<i>INEL</i>)	294
A Systematic Evaluation of Transients in Swedish BWR Power Plants	
K. J. Laakso (<i>ASEA</i>)	303
Safety-Related Dynamic Response Measurements on CEGB Reactors at Power	
M. J. Bridge (<i>CEGB</i>)	313
RETRAN-02-MOD001 Modeling of Kuosheng Unit 1 Transient Analyses	
E. Lin, P. C. Chen, J. K. Hsiue, and R. Y. Yuann (<i>TPC</i>)	325
Design and Instrumentation of LOBI U-Tube Steam Generators for Small Break and Special Transients Tests	
W. L. Riebold, T. R. Fortescue, and K. H. Gunther (<i>JRC</i>)	335
Calculation of a BWR "Partial ATWS" Using RAMONA-3B	
D. I. Garber, D. J. Diamond, and H. S. Cheng (<i>BNL</i>)	342

SESSION 6

SAFETY GOALS

Chair: W. Y. Kato (*BNL*)
Y. Togo (*UT*)

Development of Risk-Based Safety-Related Criteria for Licensing CANDU Nuclear Power Reactors	
W. Paskievici (<i>EPM</i>), A. Pearson (<i>Consultant</i>), and J. T. Rogers (<i>CU</i>)	353
Safety Policy in the Production of Electricity	
E. Siddall (<i>AECL</i>)	363
Dealing with Uncertainties in Examining Safety Goals for Nuclear Power Plants	
W. R. Rish and J. J. Mauro (<i>ESI</i>)	377
Proposed Safety Goals for Nuclear Power Plants	
F. J. Remick, D. K. Rathbun, and J. N. Wilson (<i>NRC</i>)	387
Safety Goals for Nuclear Power Plants: The Position in the United Kingdom	
R. D. Anthony (<i>NII</i>)	393
Considerations on a Proposed Rationale for Quantification of Safety Goals	
A. Birkhofer and A. Jahns (<i>GRS</i>)	403
Safety Goals as Applied in Canada	
Z. Domaratzki (<i>AECB</i>)	409
A French View on the Proposed NRC Policy on Safety Goals	
P. Y. Tanguy (<i>CEA</i>)	414

SESSION 7

PRESSURIZED THERMAL SHOCK - 1

Chair: R. Noel (*EdF*)
M. Vagins (*NRC*)

The Integrity of PWR Pressure Vessels during Overcooling Accidents	
R. D. Cheverton, S. K. Iskander, and G. D. Whitman (<i>ORNL</i>)	421
Thermal-Hydraulic Considerations for Pressurized Thermal Shock in PWR's	
R. A. Hedrick and R. D. Dabbs (<i>SAI</i>)	431
Nonlinear Fracture Mechanics Analysis and Experiment on Thermal Shock Behavior of RPV Plates	
G. Yagawa, K. Ishihara, and Y. Ando (<i>UT</i>)	438

An Experimental and Theoretical Study for the Evaluation of the Residual Life of the Primary Circuit of LWR's

A. C. Lucia (*JRC*) 448

SESSION 8

PRA-2; SYSTEMS APPLICATIONS OF RELIABILITY AND RISK METHODS

Chair: L. Lederman (*CNEN*)

I. Wall (*EPRI*)

Auxiliary Feedwater System Reliability

T. J. Raney (*ESI*) 457

Reliability Analysis of a BWR Decay Heat Removal System

R. N. Dumolo (*EES*) and A. Tiberini (*KLA*) 464

Estimating Failure-to-Close Probabilities for Pressurizer Valves

W. W. Weaver (*B&W*) 473

Reliability of the Emergency AC Power System at Nuclear Power Plants

R. E. Battle (*ORNL*), D. J. Campbell (*JBF*), and P. W. Baranowsky (*NRC*) 479

The Risks due to Fires at Big Rock Point

W. A. Brinsfield (*WLA*) and D. P. Blanchard (*CPC*) 489

The Program to Study the Reliability of Safety Systems in the PALUEL 1300 MWe

PWR Power Plant: Organization, Methodology, First Conclusions

M. Llory, A. Villemeur, and P. Brunet (*EdF*) 497

Analysis of Station Blackout Accidents for LWRs

A. M. Kolaczowski, A. C. Payne, Jr. (*SNL*), and P. W. Baranowsky (*NRC*) 511

Use of Risk Concept in Safety Evaluation, Licensing and Decision Making:

Practice and Trends in the European Community

W. Vinck and G. van Reijen (*CEC*) 521

SESSION 9

MAN/MACHINE INTERFACE - 1; HUMAN FACTORS

Chair: Z. Sabri (*LPL*)

A. Vuorinen (*IAEA*)

Human Reliability and the Man/Machine Interface: What Do We Do After the Control Room Review?

J. D. Folley, Jr., and D. L. Schurman (*ASA*) 533

Review and Evaluation of Human Error Reliability Data Banks

D. A. Topmiller, J. S. Eckel, and E. J. Kozinsky (*GPC*) 541

Additional Emergency Procedure Based on NSSS Physical States Approach

P. Cadiet, G. Depond, and H. Sureau (*EdF*) 550

Design of Test and Emergency Procedures to Improve Operator Behaviour in French Nuclear Power Plants

M. Griffon-Fouco (*EdF*) and M. Gomolinski (*CEA*) 555

Survey of How PRAs Model Human Error

E. M. Dougherty, Jr. (*TEC*) 565

Dynamic Human Operator Modelling by the ESCS Analysis Technique

A. Amendola (*JRC*) and G. Reina (*MESA*) 575

SESSION 10**MAN/MACHINE INTERFACE - 2; MACHINE SIDE**

Chair: J. H. Hopps (CSDL)
E. Yaremy (AECL)

Integrated Operator/Plant Interface Design in CANDU Nuclear Power Plants	
T. O. McNeill and N. Yanofsky (AECL)	587
Conception of a PWR Simulator as a Tool for Safety Analysis	
J. M. Lanore, P. Bernard, J. Romeyer Dherbey, C. Bonnet, and P. Quilichini (CEA)	593
Multivariate Alarm Handling and Display	
P. J. Visuri (Halden)	598
THE STAR-CONCEPT: A Method for the Definition and Generation of Computer-Based Systems to Support the Operator during Normal and Disturbed Plant Situations	
L. Felkel and H. Roggenbauer (GRS)	608
A Monitoring and Diagnostic System of Fission Product Transport and Release in Nuclear Power Plants	
H. Kodaira, S. Kondo, and Y. Togo (UT)	618

SESSION 11**PRESSURIZED THERMAL SHOCK - 2**

Chair: R. Bello (CNSNS)
G. Whitman (ORNL)

The Consequence of the Coincidence of Irradiation Embrittlement; Surface Cracking and Pressurized Thermal Shock (PTS) in RPVs of LWRs	
K. Kussmaul, J. Jansky, and J. Föhl (UST)	631
The EPRI Program Concerning Reactor Vessel Pressurized Thermal Shock	
V. K. Chexal, T. U. Marston, and B. K. H. Sun (EPRI)	644

SESSION 12**PRA-3: DATA BASES AND SPECIAL APPLICATIONS**

Chair: G. Flanagan (ORNL)
M. Hayns (UKAEA)

Synthesis of the Data Base for the Ringhals 2 PRA Using the Swedish ATV Data System	
G. Johanson (SPB) and J. R. Fragola (SAI)	661
The In-Plant Reliability Data System (IPRDS) History, Status, and Future Effort	
J. P. Drago (ORNL) and J. R. Fragola (SAI)	671
Limited Scope Probabilistic Risk Assessments (Mini-PRAs) for Environmental Reports	
R. L. O'Mara and W. T. Hotchkiss (S&W)	678
A PRA-Based Approach to Establishing Priorities for Equipment Qualification Needs	
D. E. Leaver, W. A. Brinsfield, J. F. Quilliam (WLA), and R. N. Kubik (EPRI).	683
The Use of Operator Action Event Trees to Address Regulatory Issues	
W. A. Brinsfield, R. G. Brown (WLA), and P. Donnelly (CPC)	690
Risk Assessment of Filtered-Vented Containment Options for a BWR Mark III Containment	
F. T. Harper and A. S. Benjamin (SNL)	697
Risk Reduction Analysis of Severe Accident Prevention and Mitigation Systems	
S. W. Hatch, P. R. Bennett, D. D. Drayer, and A. S. Benjamin (SNL)	706

Some Perspectives on Risk Presentation from the German Risk Study	
J. Ehrhardt and A. Bayer (KFK)	716

VOLUME 2

SESSION 13

FUEL PERFORMANCE EVALUATION

Chair: M. Israel (EdF)
W. Quapp (EG&G)

LWR Fuel Performance during Anticipated Transients with Scram	
P. E. MacDonald, Z. R. Martinson (EG&G), T. C. Rowland (GE), and M. Tokar (NRC)	729
FRAP-T6 Calculations of Fuel Rod Behavior during Overpower Transients	
R. Chambers and S. C. Resch (EG&G)	736
Influence of Mechanical Anisotropy on the LOCA Deformation Behavior of Zircaloy Cladding Tubes	
E. Ortlieb, G. Cheliotis, and H. G. Weidinger (KWU)	744
Development and Application of an Asymmetric Deformation Model to Describe the Fuel Rod Behaviour during LOCA	
A. K. Chakraborty and J. D. Schubert (GRS)	754
Comparison of BALON2 with Cladding Ballooning Strain Tables in NUREG-0630	
S. C. Resch and E. T. Laats (EG&G)	762
A Method of Predicting the Temperature Response of Ballooning Fuel Cladding for PWR LOCA Conditions	
K. H. Ardron and S. A. Fairbairn (CEGB)	768
A Statistical Margin to DNB Safety Analysis Approach for LOFT	
S. A. Atkinson (EG&G)	781
Uncertainty of Measured and Calculated Steady State Fuel Rod Behavior	
E. T. Laats (EG&G)	791

SESSION 14

RADIOLOGICAL SOURCE TERMS - 2

Chair: B. W. Spencer (ANL)

Atmospheric Transport Model for Radiological Emergency Preparedness for Complex Terrain	
D. Robeau (CEA), C. Blondin (EERM), M. Dumas and N. Parmentier (CEA)	803
The Use of Principal Components Analysis and Three-Dimensional Atmospheric Transport Models for Reactor Accident Consequence Evaluation	
P. H. Gudiksen, J. J. Walton (LLNL), D. J. Alpert, and J. D. Johnson (SNL) ...	813
Retention of Fission Products by BWR Suppression Pools during Severe Accidents	
W. J. Marble, T. L. Wong, F. J. Moody, and D. A. Hankins (GE)	821

SESSION 15

SMALL-BREAK LOCA ANALYSIS

Chair: B. W. Spencer (ANL)

RELAP5 Analysis of LOFT and Zion Nuclear Power Plant Small Break LOCAs	
S. M. Modro, T. C. deBoer, and T. H. Chen (EG&G)	839

	<u>Page</u>
Comparisons of TRAC-PF1 Calculations with Semiscale MOD-3 Small-Break Tests S-07-10D, S-SB-P1, and S-SB-P7	
M. S. Sahota (LANL)	851
Effect of Pump Operation following a Small Break in a Pressurized Water Reactor	
J. L. Elliott, J. F. Lime, and G. J. E. Willcutt, Jr. (LANL)	861
Experiences About a Two-Phase Model SMABRE in a Full Scale PWR Simulator	
J. Miettinen, M. Hänninen (TRC), and M. Tiitinen (IVO)	872
Large and Small Loss of Coolant Accident Occurring during Residual Heat Removal Cooling Mode	
H. Boileau, J. L. Gandrille, and J. C. Megnin (Framatome)	882
Post-Test Analysis of the LOFT Experiment L3-6 with the Code RELAP4 MOD6	
Y. Macheteau, D. Menessier, J. Peltier, and J. B. Thomas (CEA)	891
ROSA-III Small Break Test Analysis in RELAP5/MOD1	
M. Kato, N. Abe, K. Itoya (NAIG), F. Masuda (TC), and K. Tasaka (JAERI)	900
The LOCA/ECC System Effects Tests at ROSA-III Changing the Break Area as Test Parameter	
K. Tasaka, M. Suzuki, Y. Koizumi, Y. Anoda, H. Kumamaru, and M. Shiba (JAERI)	910

SESSION 16

DEGRADED CORE ANALYSIS - 1

Chair: B. W. Spencer (ANL)

Phenomenological Investigations of Cavity Interactions Following Postulated Vessel Meltthrough	
B. W. Spencer, D. Kilsdonk, J. J. Sienicki (ANL), and G. R. Thomas (EPRI)	923
Thermochemical Aspects of Fuel-Rod Material Interactions at $\sim 1900^{\circ}\text{C}$	
H. M. Chung (ANL) and S. M. Gehl (EPRI)	938
Combustion of Hydrogen-Steam-Air Mixtures Near Lower Flammability Limits	
R. K. Kumar, H. Tamm, W. C. Harrison, J. Swiddle, and G. Skeet (AECL)	951
Experimental Investigations of Spontaneous and Triggered Vapour Explosions in the Molten Salt/Water System	
H. Hohmann, H. Kottowski, H. Schins (JRC), and R. E. Henry (FAI)	962
Ignition Effectiveness of Thermal Heating Devices in Hydrogen-Air-Steam Mixtures	
H. Tamm, R. MacFarlane (AECL), and D. D. S. Liu (CMET)	972
Steam Explosions of a Metallic Melt as Its Degree of Oxidation Increases: Fe, $\text{FeO}_{1.0}$, and $\text{FeO}_{1.2}$	
L. S. Nelson (SNL) and P. M. Duda (Ktech)	981
Debris Bed Quenching Studies	
D. H. Cho, D. R. Armstrong, L. Bova (ANL), S. H. Chan (UW), and G. R. Thomas (EPRI)	987
Transient Core Debris Bed Heat Removal Experiments and Analysis	
T. Ginsberg, J. Klein, C. E. Schwarz, J. Klages (BNL), and J. C. Chen (LU) ...	996
The Effect of Water to Fuel Mass Ratio and Geometry on the Behavior of Molten Core-Coolant Interaction at Intermediate Scale	
D. E. Mitchell and N. A. Evans (SNL)	1011
Heat Transfer Between Immiscible Liquids Enhanced by Gas Bubbling	
G. A. Greene, C. E. Schwarz, J. Klages, and J. Klein (BNL)	1026
The TMI-2 Core Examination Plan	
D. E. Owen, P. E. MacDonald, R. R. Hobbins, and S. A. Ploger (EG&G)	1038
A Debris Bed Model to Predict the Effect of Gas Influx from Below on the Dryout Heat Flux	
E. Gorham-Bergeron (SNL)	1049

SESSION 17**RADIOLOGICAL SOURCE TERMS - 3**

Chair: P. Mostert (KEMA)
R. Vogel (EPRI)

Release Rates and Chemical States of Volatile Fission Products	
R. L. Ritzman (SAI) and D. Cubicciotti (EPRI)	1059
Fission Product Chemistry Under Reactor Accident Conditions	
D. F. Torgerson, D. J. Wren, J. Paquette, and F. Garisto (AECL)	1069
Influence of Variable Physical Process Assumptions on Core-Melt Aerosol Release	
G. W. Parker, G. E. Creek, and A. L. Sutton, Jr. (ORNL)	1078
The Vaporization of Structural Materials in Severe Accidents	
R. A. Lorenz (ORNL)	1090
Aerosol Transport Analysis of LWR High-Consequence Accidents Using the HAA-4A Code	
John M. Otter (RI)	1100

SESSION 18**PRA-4; PLANT APPLICATIONS**

Chair: A. Carnino (EdF)
J. W. Hickman (SNL)

Insights from the Interim Reliability Evaluation Program Pertinent to Reactor Safety Issues	
D. D. Carlson (SNL)	1109
The Interim Reliability Evaluation Program (IREP) Analysis of Millstone Unit 1	
P. J. Amico, A. A. Garcia (SAI), J. J. Curry (NRC), D. W. Gallagher, M. Modarres (SAI), and J. A. Radder (NU)	1116
Arkansas Nuclear One Unit One Risk Analysis Results	
G. J. Kolb (SNL) and D. M. Kunsman (SAI)	1125
HTGR Optimization of Safety Using Probabilistic Risk Assessment	
C. J. Everline, F. A. Silady, W. J. Houghton, and B. I. Shamasundar (GA)	1134

SESSION 19**DEGRADED CORE ANALYSIS - 2**

Chair: R. A. Bari (BNL)
P. Hosemann (KFK)

SCDAP: A Light Water Reactor Computer Code for Severe Core Damage Analysis	
G. P. Marino (NRC), C. M. Allison (EG&G), and D. Majumdar (DOE)	1145
Development of MARCH 2	
P. Cybulskis, R. O. Wooton, and R. S. Denning (BCL)	1158
MARCH1B: BNL Modifications to the MARCH Computer Code	
W. T. Pratt, J. W. Yang, R. D. Gasser, W. S. Yu, R. Jaung, J. Zahra, and R. A. Bari (BNL)	1167
Analysis of Postulated Severe LWR Accidents	
R. E. Henry, H. K. Fauske, J. R. Gabor, M. A. Kenton, G. M. Hauser, R. W. MacDonald (FAI), T. F. Ewing, D. R. MacFarlane (ETA), and E. L. Fuller (TEC)	1177
Fuel Performance during Severe Accidents	
B. J. Buescher, G. E. Gruen, and P. E. MacDonald (EG&G)	1185

Impact of Meltdown Accident Modeling Developments on PWR Analyses	
F. E. Haskin (SNL) and C. J. Shaffer (ET)	1191
Assessment of Heat Transfer Models in Molten-Core-Concrete Interaction Codes	
I. K. Paik, S. I. Abdel-Khalik, and M. L. Corradini (UW)	1199
Status of Major Modeling Phenomena in the ANL/NSAC Core Heatup And Redistribution (ANCHAR) Code	
C. H. Bowers, R. P. Hosteny (ANL), and G. R. Thomas (EPRI)	1209

SESSION 20

NPP OPERATIONAL ASSESSMENT

Chair: P. E. Ahlström (SPB)
J. Buchanan (ORNL)

Precursors to Potential Severe Core Damage Accidents: 1969-1979	
J. W. Minarick and C. A. Kukiela (SAI)	1225
PWR - Safety Related Operating Experience Feedback Organization of Electricite de France	
R. Capel (EdF)	1234
Development of an In-House Safety Analysis Capability for Plant Operational Support	
R. W. Cross and N. A. Smith (VEPCO)	1244
Operating Experience Review for Nuclear Power Plants in the Systematic Evaluation Program - Oyster Creek	
G. T. Mays (ORNL) and K. H. Harrington (JBF)	1247
Operational Analysis - An Approach to Safety and Planning	
D. J. Harvey, R. E. Grazio, N. H. Williams (BEC), and D. D. Buckley (TAI)	1257
Analysis of the Main Causes of Failure in the Atucha I PWR Moderator Circuit Branch Piping	
J. Porto (CNEA) and G. Sánchez Sarmiento (ENACE)	1263

SESSION 21

RADIOLOGICAL SOURCE TERMS - 4

Chair: R. S. Denning (BCL)
W. Schikarski (KFK)

Best Estimate Calculations of Fission Product Release to the Environment for Some PWR Core Melt Accident Sequences	
W. Schoeck and H. Bunz (KFK)	1281
Iodine Behavior in PWR Accidents Leading to Severe Core Damage	
M. Lucas, C. Devillers, J. Fermandjian, and D. Manesse (CEA)	1290
High Temperature Fission Product Chemistry and Transport in Steam	
R. M. Elrick and R. A. Sallach (SNL)	1299
Source Term Assumptions for Realistic Accident Analyses	
S. J. Niemczyk and L. M. McDowell-Boyer (ORNL)	1307

SESSION 22**NPP SAFETY-RELATED OPERATIONAL EXPERIENCE**

Chair: D. A. Meneley (OHC)
J. Stolz (EdF)

Safety Evaluation of Operational Occurrences as Applied to Oconee Nuclear Station

S. T. Rose and P. M. Abraham (DPC)	1321
The Impact of Procedures on Operator Performance	
E. J. Kozinsky (GPC)	1326
Reactor Operation Feed-Back in France	
C. Feltin, B. Fourest, and J. Libmann (CEA)	1334
Commonwealth Edison Operating Experience: The People Factor	
L. Soth (CECO)	1340
Nuclear Power Plant Safety and Reliability Improvements Derived from Operational Experience Analysis	
E. L. Zebroski and S. L. Rosen (INPO)	1345

SESSION 23**DEGRADED CORE ANALYSIS - 3**

Chair: Y. Togo (UT)
A. Torri (PLG)

The Role of Steam Vapor Explosions during Core Meltdown of LWR's	
H. Unger, R. Bisanz, M. Bürger, and W. Schwalbe (USt)	1357
Steam Pressure Spike in FWR Plant Under Severe Accident Conditions	
J. W. Yang and W. T. Pratt (BNL)	1366
Application of Hydrodynamic and Thermal Fragmentation Models and a Steady State Thermal Detonation Model to Molten Salt-Water Vapor Explosions	
M. Bürger, W. Schwalbe, and H. Unger (USt)	1378
Steam Explosions - Their Relationship to LWR Safety Assessments	
S. G. Bankoff (NWU), D. H. Cho (ANL), A. W. Cronenberg (ESA), H. K. Fauske, R. E. Henry, M. N. Hutcherson, T. J. Marciniak (FAI), R. C. Reid (MIT), and G. R. Thomas (NSAC)	1388
Proposed Model for Fuel-Coolant Mixing during a Core-Melt Accident	
M. L. Corradini (UW)	1399
An Assessment of LWR Fuel Foaming Potential during Core Meltdown Accidents	
A. W. Cronenberg (ESA), D. W. Croucher, and P. E. MacDonald (EG&G)	1409
Cooling of Debris Beds - Methods of Analysis for LWR Safety Assessments	
R. E. Henry, M. Epstein, and H. K. Fauske (FAI)	1421
Hydrogen Evolution during LWR Core Damage Accidents	
L. Baker, Jr. (ANL), M. Epstein, H. K. Fauske, R. E. Henry, and J. C. Leung (FAI)	1433
Fuel Rod Temperature Transients during LWR Degraded Core Accidents	
F. Briscoe (UKAEA), J. B. Rivard, and M. F. Young (SNL)	1443

VOLUME 3**SESSION 24****LICENSING CRITERIA: DEVELOPMENT AND COMPARISON**

Chair: Z. Domaratzki (AECB)
R. Treviño (CNSNS)

A General Siting Regulation and Population Distribution Criteria for Greece	
J. Kollas and G. Yadigaroglu (AEC-Greece)	1455
Development of French Technical Safety Regulations: Safety Fundamental Rules	
Ph. Lebouleux (CEA)	1465
A Comparison of LOCA Safety Analysis in the USA, FRG, and Japan	
L. P. Leach, L. J. Ybarrondo (EG&G), E. F. Hicken (GRS), and K. Tasaka (JAERI)	1475
A Methodology for Performing the Design Review of Plant Shielding and Environmental Qualification Required After TMI-2	
J. A. Carretero (EA)	1485
Estimated Releases and Offsite Doses After a Loss of Coolant Accident.	
A Comparison between USA and German Regulations	
J. P. Carmena (EA)	1492
Harmonization of Safety Practices and Criteria Relating to the Safety of Light Water Reactor Nuclear Power Plants within the European Community	
W. Essler and W. Vinck (CEC)	1501
US Licensing Requirement Tracking and Integration from Abroad	
J. Tapia and X. Jardi (EA)	1511

SESSION 25**LOCA ANALYSIS**

Chair: B. W. Spencer (ANL)

Moderator Boiling on the External Surface of a Calandria Tube in a CANDU Reactor during a Loss-of-Coolant Accident	
G. E. Gillespie, R. G. Moyer, and P. D. Thompson (AECL)	1523
Thermal Behaviour of a CANDU-PHW Reactor Fuel Channel Containing Nearly Stagnant Steam	
G. E. Gillespie, W. C. Harrison, J. G. Hildebrandt, and G. A. Ledoux (AECL) ..	1534
Refilling and Rewetting of Horizontal Fuel Channels	
W. T. Hancox, V. S. V. Rajan, F. W. Barclay, B. N. Hanna, and B. H. McDonald (AECL)	1545
Analysis of Transient Dry Patch Behavior on CANDU Reactor Calandria Tubes in a LOCA with Late Stagnation and Impaired ECI	
J. T. Rogers (CU) and T. C. Currie (DE)	1556
A Simplified Method for Predicting Afterheat Power from Uranium-Fueled PWR Fuel Assemblies	
J. C. Ryman, O. W. Hermann, C. C. Webster, and C. V. Parks (ORNL)	1567
Prediction of Critical Flows of Hot Water from Orifices and Tubes	
Y. S. Chen (NRC)	1574
COMPARE Containment Subcompartment Analysis Code Evaluation	
R. G. Gido and A. Koestel (LANL)	1583

SESSION 26**MAN/MACHINE INTERFACE - 3**

Chair: B. W. Spencer (ANL)

A Method for Improving Accident Sequence Recognition in Nuclear Power Plant Control Rooms

C. D. Heising (MIT) and S. C. Dinsmore (YAEC)	1599
The Feasibility of On-line Fuel Condition Monitoring	
D. A. Petti, D. J. Osetek, D. W. Croucher, and J. K. Hartwell (EG&G)	1608
An Integrated Accident Monitoring System, A Computerized Informational Aid to Improve the Overall Response to Abnormal Situations	
C. H. Neuschaefer (CE)	1617
Regional Overpower Protection in CANDU Power Reactors	
C. M. Bailey, R. D. Fournier, and F. A. R. Laratta (AECL)	1627
Simulators of Function	
J. Rabouhams and J. Stolz (EdF)	1637
Improved Method for Reactor Diagnosis Using Noise Analysis Based on Multivariable Time Series Modeling	
R. Oguma, K. Matsubara, and K. Hayashi (JAERI)	1641
Multilevel Flow Modelling of Process Plant for Diagnosis and Control	
M. Lind (Risø)	1653
Development of an In-Vessel Water Level Gauge for Light Water Power Reactors	
K. Ara, N. Wakayama (JAERI), and K. Kobayashi (SEC)	1667
Computer Assisted Training	
R. Felgines and J. Stolz (EdF)	1681

SESSION 27**LOCA-RELATED EXPERIMENTS AND ANALYSIS**

Chair: B. W. Spencer (ANL)

Blowdown and Cold Water Injection Experiments: Comparisons with the FIREBIRD-III and RELAP-5 Codes

A. C. D. Wright (AECL), G. Proto, A. Alemberti, G. Bimbo (NIRA) and M. Z. Caplan (AECL)	1691
Two-Phase Flow Behaviour of Axial Pumps	
W. G. Kennedy (CE), W. Kastner (KWU), G. J. Kanupka, J. D. Fishburn (CE), A. Lang (AS), K. Riedle, and G. Seeberger (KWU)	1706
The Experiment Prediction for LOFT Nuclear Experiments L5-1 and L8-2	
T-H. Chen and S. M. Modro (EG&G)	1720
Influence of Break Size on Blowdown for Large Breaks	
L. Piplies, C. Addabbo, and W. L. Riebold (JRC)	1730
Effect of Noncondensable Gas on Natural Circulation in the Semiscale MOD-2A Facility	
K. Soda (INS) and G. G. Loomis (EG&G)	1743
Influence of Downcomer Volume and Gap Width on Blowdown	
H. Städtke, D. Carey, and W. L. Riebold (JRC)	1751
Reflooding of a PWR Bundle-Effect of Inlet Flow Rate Oscillations and Spacer Grids	
P. Clément, R. Deruaz, and J. M. Veteau (CEA)	1763
Containment Emergency Sump Studies to Investigate Unresolved Safety Issue A-43	
G. G. Weigand, M. S. Krein, M. J. Wester (SNL), and M. Padmanabhan (ARL)	1771
PHEBUS Program - First Results on PWR Fuel Behavior in LOCA Conditions	
R. Del Negro, M. Reocreux, J. Pelce, B. Legrand, and Ph. Berna (CEA)	1781

Reflood Experiments with Simultaneous Upper and Lower Plenum Injection in the REWET-II Rod Bundle Facility	
T. Kervinen (TRC)	1791
Mist Core Cooling during the Reflood Phase of PWR-LOCA	
P. Ihle, K. Rust (KFK), and S. L. Lee (SUNY)	1801
Experiments on Heat Transfer Crisis in Triangular Lattice Configuration	
V. I. Kisina, A. S. Konjgov, D. L. Prozerov, N. V. Tarasova (HEI), K. L. Eerikainen, O. M. Tiihonen, and T. A. Vanttola (TRC)	1810
BWR Loss of Coolant Integral Tests: Parallel Channel Effect	
M. Murase, M. Naitoh (Hitachi), and T. Gomyoo (TEPC)	1819

SESSION 28

DEGRADED CORE ANALYSIS - 4

Chair: M. Fontana (TEC)
H. Unger (USt)

SASYST - A New Approach in Total Plant Simulation during Severe Core Damage Accidents	
R. Rühle, R. Bisanz, W. Scheuermann, F. Schmidt, and H. Unger (USt)	1829
Analysis of the TMI Incident Using EXMEL and MELSIM3	
R. Bisanz and F. Schmidt (USt)	1838
The USNRC Severe Fuel Damage Research Program	
M. Silberberg, R. W. Wright, G. P. Marino (NRC), P. E. MacDonald, T. M. Howe, B. J. Beuscher, R. W. Miller (EG&G), P. S. Pickard, R. L. Coats, and J. B. Rivard (SNL)	1844
Severe Accident Trends in Light Water Reactors	
R. A. Bari, W. T. Pratt (BNL), and J. F. Meyer (NRC)	1854
Sensitivity of Degraded Core Cooling Accident Predictions to the Assumed Levels of Operability of Engineered Safety Systems	
P. Cybulskis (BCL)	1864

SESSION 29

LARGE-BREAK LOCA ANALYSIS

Chair: F. D'Auria (UdP)
L. Ybarrondo (EG&G)

Posttest Analysis of Semiscale Large-Break Test S-06-3 Using TRAC-PF1	
B. E. Boyack (LANL)	1871
COBRA/TRAC Analysis of the PKL Reflood Test K9	
C. A. Wilkins and M. J. Thurgood (PNL)	1880
The Emergency Core Cooling Function of the Moderator System in CANDU Reactors	
C. Gordon and C. Blahnik (OHC)	1889
Experience in Small Break LOCA Calculations by RELAP 4 Computer Codes	
N. Cerullo, G. Galassi, M. Mazzini, and F. Oriolo (UdP)	1899
On the Existence of Early Core Rewet during Large-Break LOCA Transients in a Commercial PWR	
P. N. Demmie (EG&G)	1914
TRAC Analysis of the System Pressure Effects Tests in the Slab Core Test Facility	
S. T. Smith (LANL)	1923
Loss of Coolant Accidents in HTGR's	
U. Weicht and W. Wachholz (HTRB)	1931

SESSION 30**SAFETY-RELATED DESIGN CONSIDERATIONS**

Chair: A. Gauvenet (*EdF*)
W. Loewenstein (*EPRI*)

A Functional Design Approach to PWR Safety

M. K. De, J. A. Rumancik, A. J. Impink, and J. R. Easter (<i>WEC</i>)	1943
Determination of Environmental Conditions for Equipment Qualification in Buildings Outside Containment	
R. F. Miller and F. A. Elia, Jr. (<i>S&W</i>)	1958
Value-Impact Analysis of Severe Accident Prevention and Mitigation Systems	
A. S. Benjamin, S. W. Hatch, D. R. Strip, P. R. Bennett, D. D. Drayer, and V. L. Behr (<i>SNL</i>)	1969
Depressurizer System for Small Pipe Breaks in Passive Containment System (PCS)	
O. B. Falls, Jr., and F. W. Kleimola (<i>NEC</i>)	1981
Utilization of the Safety Functional Analysis Techniques to Optimize the Separation Requirements in Case of Fire	
L. Martin Alvarez (<i>EA</i>)	1991
Design Considerations for Implementing a Vent-Filter System at the Barseback Nuclear Power Plant	
K. Johansson (<i>Studsvik</i>), L. Nilsson (<i>ASEA</i>), and Å. Persson (<i>Sydskraft</i>)	2001

SESSION 31**DYNAMIC LOADS/STRUCTURAL ANALYSIS**

Chair: T. Kuroda (*EPDC*)
L. Pease (*AECL*)

Seismic Qualification of Equipment Located in CANDU Nuclear Power Plants

A. C. Heidebrecht and W. K. Tso (<i>MU</i>)	2013
Experimental and Analytical Studies on the Seismic Behaviour of CANDU-PHW Cores	
T. Kuroda (<i>EPDC</i>) and C. G. Duff (<i>AECL</i>)	2023
Use of the Delphi Approach in Seismic Qualification of Existing Electrical and Mechanical Equipment and Distribution Systems	
J. D. Stevenson (<i>S&A</i>)	2037
Large-Scale, Two-Phase Jet Impingement Experiments at Marviken	
D. C. Slaughterbeck, D. C. Mecham (<i>IT</i>), J. E. Collén, and O. Sandervåg (<i>Studsvik</i>)	2045
Calculation of Steam-Water Jet Impingement Forces	
B. A. Kashiwa and T. D. Butler (<i>LANL</i>)	2052
Break Flow and Two-Phase Jet Load Model	
G. G. Weigand and S. L. Thompson (<i>SNL</i>)	2063
German Standard Problem No. 4 and 4a Loadings and Response of a Feedwater Line due to Pipe Break and Ensuing Check Valve Closure	
T. Grillenberger (<i>TUM</i>) and W. Ch. Müller (<i>GRS</i>)	2073
Static and Dynamic Tests on Reinforced Concrete Shear Walls at High Loads	
E. G. Endebrock and R. C. Dove (<i>LANL</i>)	2083
Qualification of Unreinforced Manholes in Thin-Walled Piping of Auxiliary/Emergency Cooling Water Systems	
Zs. Revesz (<i>EES-Zurich</i>)	2092

SESSION 32

PANEL DISCUSSION: WHERE DO WE GO FROM HERE?

Chair: N. C. Rasmussen (MIT)
P. Tanguy (CEA)

Review of Man-Machine Interface and Safety-Related Design Considerations	
D. Buenemann (GKSS)	2105
Review of Fuel Performance Evaluation, Dynamic Loads/Structural Analysis, and Operating Experience	
D. A. Meneley (OHC)	2107
Review of Degraded Core Analysis	
P. Tanguy (CEA)	2111
Review of LOCAs, Transients, and Pressurized Thermal Shock	
L. S. Tong (NRC)	2114

* * * * *

List of Attendees	2117
--------------------------------	------

SESSION 24

LICENSING CRITERIA: DEVELOPMENT AND COMPARISON

Chair: Z. Domaratzki (*AECB*)
R. Treviño (*CNSNS*)

A GENERAL SITING REGULATION AND POPULATION DISTRIBUTION CRITERIA FOR GREECE

J. Kollas and G. Yadigaroglu

Nuclear Regulatory Service
Greek Atomic Energy Commission
Aghia Paraskevi, Attiki, Greece

ABSTRACT

A new national regulation for nuclear power plant siting is described. The main body of the regulation is similar in contents to the IAEA Code of Practice in siting, but exceeds its scope in certain areas and covers all aspects of the impact of the plant on the population and the environment of the region, including non-radiological effects. The regulation is accompanied by appendices which refer to site suitability criteria with respect to the radiological consequences from the operational states of the plant and with respect to accidents, including core-melt accidents; these reflect the particular geographic and demographic situation of Greece.

INTRODUCTION

The Nuclear Regulatory Service (NRS) of the Greek Atomic Energy Commission (GAEC) has developed a national siting regulation for nuclear power plants¹ entitled "Criteria and Methods for Proving the Suitability of a Proposed Site for the Installation of a Nuclear Power Plant" (Regulation KT-1). Regulation KT-1 is intended for the regulatory process related to site approval, which is a separate step preceding the construction permit in Greece.

The starting point of Regulation KT-1 is the IAEA Code of Practice on siting² and practically all the IAEA code requirements are contained in the Greek regulation. Regulation KT-1, however, exceeds the scope of the IAEA code in several areas³.

This paper presents the main features of the Greek siting regulation with emphasis on the population distribution criteria contained in two appendices of Regulation KT-1.

THE LICENSING SYSTEM⁴

In Greece, large nuclear installations are governed by a licensing system established by Decree-Law No. 854 of March 15, 1971, pending the adoption of more detailed regulatory provisions. Under this Decree, nuclear installations, i.e. installations generating nuclear power or which use, fabricate, process, or store nuclear fuels in large quantities, or radioactive products or, finally, installations for the storage and management of radioactive wastes, are governed by a prior licensing system.

The GAEC, a public body, is placed now under the authority of the Minister of Research and Technology⁵, and is responsible for proposing measures for the protection of individuals and property against radiation, and for seeing that these measures are applied. The GAEC is consulted concerning applications to import and use radioactive materials and to operate nuclear installations. The NRS is the regulatory branch of

the GAEC, responsible for all matters related to the licensing, siting, and safety of nuclear installations.

The licensing procedure for nuclear installations is conducted according to Decree-Law No. 854 in the four following stages:

- site license
- construction or modification license
- license for preoperational testing
- license for normal operation or transfer of ownership.

Each successive license is delivered by the Minister of Energy and Natural Resources⁵ after obtaining the opinion of the GAEC. The flow chart for the licensing procedure in Greece is presented in Fig. 1.

Site License

The Presidential Decree No. 610 published in 1978, in implementation of Decree-Law No. 854 provisions, established the licensing requirements for siting of the nuclear power plants for electricity generation operated by the Public Power Corporation (PPC), the national public utility.

In essence, the license is granted on the basis of a site-suitability and environmental report prepared by the applicant and evaluated by the GAEC. The application for a license, to be submitted to the Minister of Energy and Natural Resources, must be accompanied by a report proving the suitability of the proposed site and providing the necessary information for site suitability evaluation from the viewpoints of plant safety and protection of the population and the environment, with emphasis on radiological aspects.

The application is first checked by a competent department of the Ministry of Energy and Natural Resources, and is then forwarded to the GAEC for advice. Following the advice of the GAEC, and if the application is favorably received, the Minister of Energy and Natural Resources publishes his decision in the Official Gazette, granting the license for a given site and specifying its boundaries. If the application is rejected, he notifies the PPC accordingly, giving the reasons for his refusal.

Granting of the site license means that the proposed site is considered suitable for a nuclear power plant and enables preparatory site work to be started.

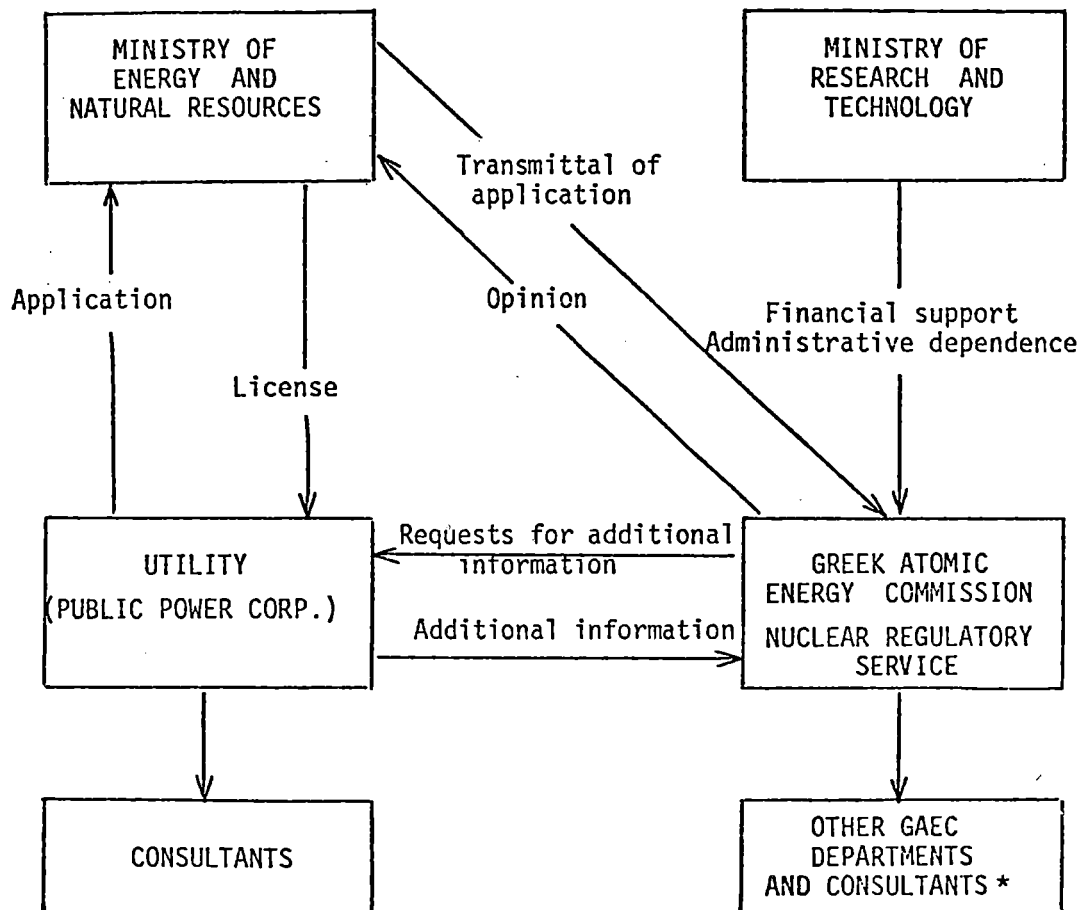
THE SITING REGULATION AND POPULATION DISTRIBUTION CRITERIA

The starting point of Regulation KT-1 is the IAEA Code of Practice on siting², as was mentioned above. Differences in scope and content from the IAEA code and the reasons for developing a national siting regulation are outlined in Ref. 3.

Essentially all the IAEA code requirements are contained in the first three chapters of the main body of the Greek regulation. Table I reproduces the table of contents of Regulation KT-1, which is divided into five chapters and five appendices.

In the first chapter, the scope and the purpose of Regulation KT-1 are defined, the relationship between non-compulsory safety guides and KT-1 is established, and general criteria and principles expressing the general philosophy of the regulation are listed. The general approach regarding population distribution in the plant region is also introduced in this chapter, while specific acceptance criteria regarding population distribution are dealt with in Appendices B and C.

In the second chapter, methods for determining design bases for external events are established. These concern external natural events as well as external man-induced events and refer in detail to floods; waves; tornados; windstorms and hurricanes; earthquakes; surface faulting; slope instability; surface collapse, subsidence



* National and foreign governmental organizations, international organizations, private consultants, etc.

Fig. 1. The Licensing Procedure in Greece.

TABLE I

Table of Contents of Proposed Regulation KT-1

-
1. GENERAL
 - 1.1 Scope and purpose
 - 1.2 Definitions
 - 1.3 Regulatory Guides
 - 1.4 General criteria and principles
 - 1.5 Criteria on population distribution in the plant region
 2. METHODS FOR DETERMINING DESIGN BASES FOR EXTERNAL EVENTS
 - 2.1 Criteria for determining design bases for external natural events
 - 2.2 Criteria for determining design bases for external man-induced events
 - 2.3 Floods
 - 2.4 Waves
 - 2.5 Tornados, windstorms, and hurricanes
 - 2.6 Earthquakes
 - 2.7 Surface faulting
 - 2.8 Slope stability
 - 2.9 Surface collapse, subsidence or uplift
 - 2.10 Soil liquefaction
 - 2.11 Aircraft crashes
 - 2.12 Other man-induced events
 - 2.13 Water availability for residual heat removal
 3. METHODS FOR EVALUATING THE CHARACTERISTICS OF THE REGION
 - 3.1 Location and population characteristics
 - 3.2 Dispersion through air
 - 3.3 Dispersion through water
 - 3.4 Food chain
 - 3.5 Ecology
 - 3.6 Land use
 - 3.7 Ambient radioactivity
 4. PLANT FEATURES
 - 4.1 Basic technical features of the plant
 - 4.2 Heat removal system
 - 4.3 Sources and radioactive waste handling system
 - 4.4 Non-radioactive wastes
 5. METHODS FOR THE DETERMINATION OF THE IMPACT OF THE PLANT ON THE POPULATION AND THE ENVIRONMENT OF THE REGION
 - 5.1 Extent of study for the determination of the consequences
 - 5.2 Radiological impact
 - 5.3 Waste heat disposal impact
 - 5.4 Chemical and biological pollution
 - 5.5 Changes in land use
 - APPENDIX A. DEFINITIONS
 - APPENDIX B. RADIOLOGICAL CONSEQUENCES FROM THE OPERATIONAL STATES OF THE NUCLEAR POWER PLANT
 - APPENDIX C. SITE SUITABILITY CRITERIA WITH RESPECT TO ACCIDENTS
 - APPENDIX D. GEOLOGICAL AND SEISMOLOGICAL SITE SUITABILITY CRITERIA^a
 - APPENDIX E. CRITERIA FOR THE NON-RADIOLOGICAL ENVIRONMENTAL IMPACT OF THE NUCLEAR POWER PLANT^a
-

^aIn preparation.

or uplift; soil liquefaction; aircraft crashes; and to other man-induced events having the potential for generation of fires, toxic and corrosive releases, severe explosions, or the production of gas clouds with subsequent deflagration or detonation; missile generation, etc.

In the main body of Regulation KT-1, quantitative acceptance criteria are given only for man-induced external events; the following probabilistic criterion is adopted in such cases: If the level of risk from the man-induced activities is considered as negligible, i.e. specifically if the probability of adverse consequences is lower than 10^{-7} per year, no further analysis and definition of design bases are required.

The second chapter includes also certain criteria concerning cooling water availability for residual heat removal: if the probability of the consequences of natural or man-induced events on the long-term availability of cooling water for residual heat removal cannot be reduced to acceptable levels, then such events shall be considered in the design bases for the residual heat removal system of the plant.

The third chapter refers to criteria and methods for the collection, study, and presentation of the physical, natural, and man-made characteristics of the region which could either be affected by the construction and operation of the plant, or could influence the impact of the plant on the population and the environment.

The remaining two chapters of the main body of Regulation KT-1, as well as all appendices, except the appendix containing the definitions, cover areas beyond the scope of the IAEA code on siting. This stems from the particular requirements of the Greek regulatory process. Indeed, in Greece, site approval is decoupled from the subsequent safety analysis review leading to the construction permit for the proposed plant, as shown in Fig. 2. Problems arising from this situation were resolved by requiring that assumptions be made regarding plant-specific information that is not available during the site-approval phase. Therefore, in the fourth chapter, the technical characteristics of plant design and operation, and the assumptions which determine the radiological consequences from the various operational states and accident situations, or influence the impact of the plant on the environment are identified. This is done in a conservative manner, taking into account the fact that at the site-license stage, the determination of certain information is by necessity approximate.

The Greek regulation must also address all aspects of the environmental impact of the nuclear power plant, including non-radiological effects. This is done in the fifth chapter, where the criteria and the general methods for determining the impact of the construction and operation of the plant on the population and the environment of the region are spelled out. The environmental impacts from new auxiliary constructions directly related to the plant are also considered. The determination of the impact of the plant shall be based on the assumptions with regard to the estimated magnitudes of releases, taking into account plant design and the design of items important to safety of the plant.

Four appendices are envisaged at this time, beyond the appendix containing the definitions, to complete Regulation KT-1. The first three appendices have already been drafted. The last two, containing geological and seismological site suitability criteria and criteria for the non-radiological environmental impact of the nuclear power plant, respectively, are in early stages of preparation.

Appendix A contains all the necessary definitions of terms and is similar to the corresponding part of the IAEA Code of Practice².

Radiological Consequences from the Operational States of the Nuclear Power Plant

Appendix B of Regulation KT-1 contains the permissible radiological exposure limits for the population due to the operational states of the plant. These are defined to include normal operation as well as anticipated operational occurrences⁶. In this appendix a limit of 5 mrem (0.05 mSv) per unit for an effective annual whole-body dose due to releases of gaseous and liquid radioactive substances is specified. This dose is limited to 15 mrem (0.015 mSv) for multiunit nuclear power stations. For

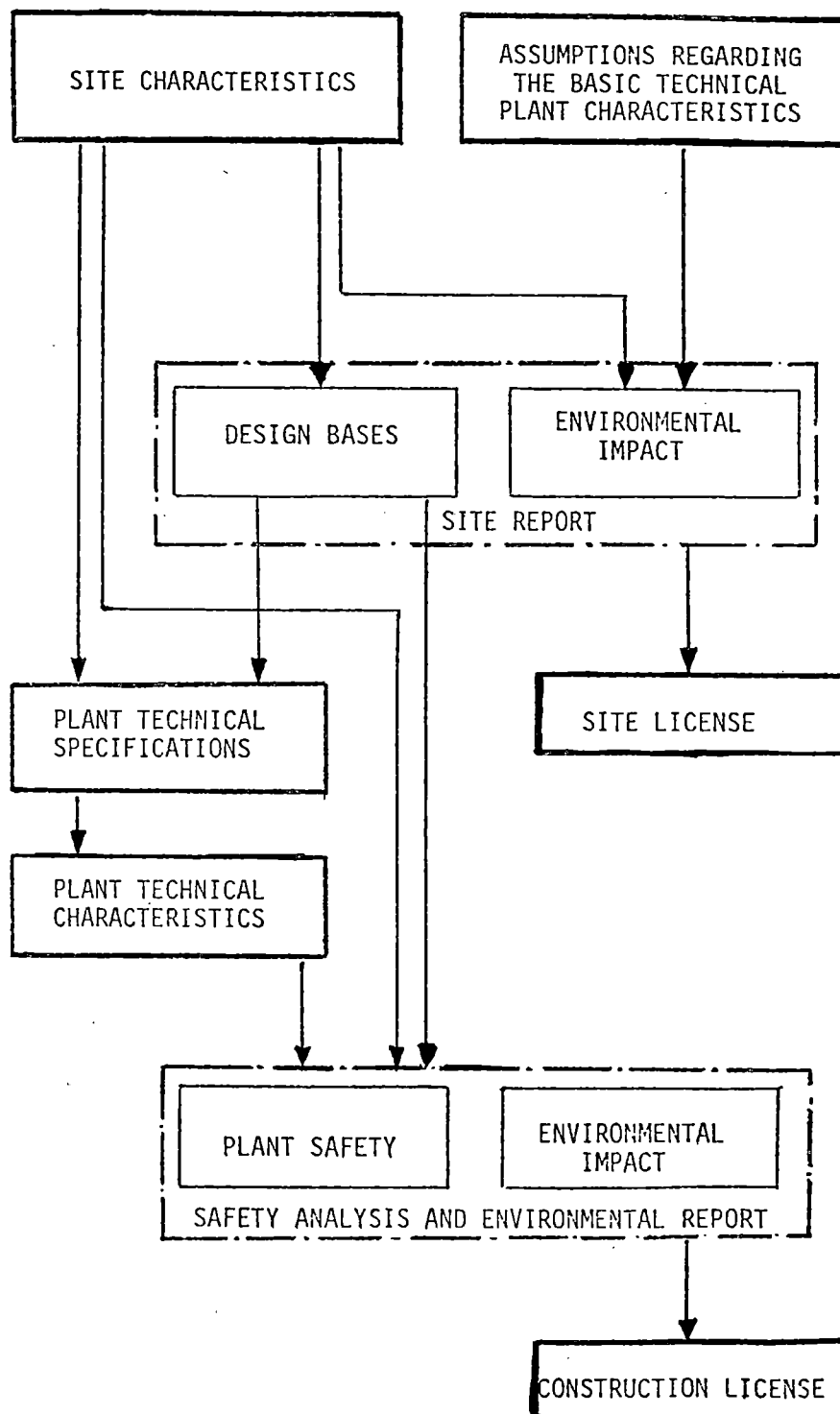


Fig. 2. The Flow of Information for the Site and Construction Licenses.

the calculation of the effective whole-body doses the recommendations of the IRP⁷ are taken into account, and the sum of the weighted doses for the various organs is calculated using the weighting factors of Ref. 7. The annual dose is meant to be the 50-year dose-equivalent commitment resulting from operation of the plant during one year. All possible direct or indirect pathways by which the radioactive substances may reach the individual, including the food chain, are to be taken into consideration. This dose refers to an individual, member of a critical group postulated to reside at the most unfavorable point, from the radiological point of view, outside the controlled zone (CZ) of the unit. The CZ is defined as the zone within which the applicant has absolute control of all activities. As a minimum, the CZ is a circle of 650 m radius. The most unfavorable point outside the CZ is defined as the point where the maximum exposure is expected, not taking into account whether this point is inhabited or not, and assuming that the food for the individual residing at this point originates from the region of the maximum radioactive-food-chain related contamination. When the CZ exceeds the area of a circle of 1000 m radius from the unit, then the above-mentioned doses refer to the most unfavorable point at or beyond 1000 m. This provision was included to avoid the possibility of allowing large releases by choosing a very large CZ area.

Appendix B also introduces societal-risk criteria by first limiting the annual collective whole-body dose of the population residing within a radius of 80 km from the station to less than one percent of the corresponding natural background radiation dose. This is done in order to limit total releases from plants to very low levels, in accordance with the latest available technology, and mitigate possible long-term adverse consequences to the general public. This first limit being independent of population density, a second limit of 500 person-rem (5 person-Sv) per unit or station is also imposed in order to give preference to low-population-density areas.

Site Suitability Criteria with Respect to Accidents

Appendix C defines criteria regarding the suitability of sites for the installation of nuclear power plants with respect to nuclear accidents. The first part of this appendix considers all accidents except those that lead to core melt and specifies requirements in terms of two criteria. The first criterion considers the radiological impact of plant operation and is a probabilistic one: the average annual expected dose from the spectrum of accidents considered (a probabilistic measure of risk) should not exceed the allowable corresponding doses from the operational states specified in Appendix B, i.e.

$$\sum_{i=1}^N P_i D_i \leq D^*$$

where P_i is the annual probability of occurrence of accident A_i ,

D_i is the dose resulting from accident A_i , and

D^* is the corresponding limiting dose defined in Appendix B.

The choice of a discrete spectrum of accidents A_i must be conservatively representative of the real continuous spectrum. Generic results from previous studies, such as the Reactor Safety Study⁸, can be used if realistic models for the calculation of the doses D_i and the corresponding accident probabilities P_i are not available for the specific site and plant considered.

The second criterion is a deterministic one and establishes a maximum acceptable effective whole-body dose of 5 rem (0.05 Sv) for any single accident, with the exception of core melt accidents. The procedures of Appendix B are also used here for the calculation of the doses.

The second part of Appendix C deals with site suitability criteria with respect to core melt accidents. To test site suitability under these extreme conditions, an arbitrarily defined reference accident, such as the one described in Table II, is

used. The conditions of Table II refer to an atmospheric release corresponding to core melt followed by containment failure by overpressurization, and results in the highest release for almost all radioisotopes⁸.

TABLE II

Core-Melt Reference Accident (BWR/PWR Conditions)

Time of release	20 / 2.5 hr
Duration of release	3 / 0.5 hr
Height of release	Ground Release
<u>Source Term</u> (fraction of core inventory)	
Xe, Kr	1 / 0.9
Organic I	0.007
I	0.9 / 0.7
Cs, Rb	0.5
Te, Sb	0.3
Ba, Sr	0.1 / 0.06
Ru, Mo, Rh, Tc, Co	0.03 / 0.02
La, Nd, Y, Ce, Pr, Nb, Am, Cm, Pu, Np, Zn	0.004

A series of parametric calculations of individual doses⁹, as well as results from international studies^{8, 10, 11} of very serious but improbable accidents brought the following two basic conclusions:

1. The probability for prompt (direct) effects (i.e. deaths and radiologically induced illnesses up to 60 days after the accident) at distances greater than 20 km from the reactor is negligible.
2. Effective emergency measures in the vicinity of the reactor (0-20 km distance) are necessary and result in a drastic reduction of the direct consequences from the very serious accident.

The following two criteria of Appendix C evolved from these conclusions:

- a) a minimum distance of 20 km from the outer boundaries of the plant to the nearest population center of 20,000 people or more, and
- b) site suitability for effective implementation of emergency measures.

Another factor dealt with in Appendix C is the demographic idiomorphy of the country. Indeed, Greece has two large population centers of limited area, namely the metropolitan areas of Athens and Thessaloniki. These have average population densities near 10,000 km⁻², while the rest of the country exhibits a small average population density of about 40 km⁻². This large heterogeneity in population distribution allows the reduction of the total collective dose in case of a core melt accident, provided that the collective dose to the very large population centers is kept at low levels. Our studies⁹ led to the conclusion that for distances between plant and population center of the order of 100 km, and for sites with favorable air flow patterns, the average 7-day collective whole-body dose to the population center from the reference accident of Table II is comparable to the annual dose from background radiation.

For this reason, and in order to reduce the total collective dose from a core melt accident, the mean 7-day whole-body population dose from the reference accident, to population centers of 500,000 people or more is limited to the corresponding annual population dose due to natural radioactivity. In addition to the above criterion, it is required that such large population centers be situated at least 50 km from the proposed site of the nuclear power plant.

CONCLUSIONS

The Greek siting regulation provides an excellent example of improvement and implementation to the regional idiomorphy of a country of the IAEA Code of Practice on siting. The regulation covers areas extending beyond the minimum safety objectives spelled out in the IAEA document due on one hand to the special conditions met in Greece, and on the other hand to an effort to specify quantitative criteria for site selection.

ACKNOWLEDGEMENT

The regulation described in this paper resulted from the collective work of the Nuclear Regulatory Service Staff. Constructive comments of IAEA experts and Public Power Corporation Staff are acknowledged.

REFERENCES

1. This regulation has been approved by the Governing Board of the GAEC. Ministerial approval and official publication are pending.
2. "Safety in Nuclear Power Plant Siting. A Code of Practice," IAEA Safety Series No. 50-C-S, International Atomic Energy Agency, Vienna (1978).
3. G. YADIGAROGLU, "Development of National Siting Regulations Based on the IAEA NUSS Code of Practice," paper presented at the Joint IAEA/ISO Seminar on Selection and Implementation of Safety Standards for Nuclear Power Plants, Vienna, 15-18 December 1980 (IAEA paper SR-54/28).
4. "Description of Licensing Systems and Inspection of Nuclear Installations," Nuclear Energy Agency, OECD (1980).
5. Prior to a recent reorganization of the Greek Government, the GAEC was under the authority of the Ministry of Coordination, while licenses were granted by the Ministry of Industry and Energy.
6. Normal Operation: Operation of a nuclear power plant within specified operational limits and conditions, including shutdown, startup, power operation, shutting down, maintenance, testing, and refueling.
Anticipated Operational Occurrences: All operational processes and situations deviating from normal operation which are expected to occur once or several times during the operating lifetime of the plant and which do not cause any significant damage to items important to safety nor lead to accident conditions.
7. "Recommendations of the International Commission of Radiological Protection," ICRP Publication 26, Annals of the ICRP 1, No. 3 (1977).
8. "Reactor Safety Study - An Assessment of Accident Risks in U.S. Commercial Nuclear Power Plants," Report WASH-1400, Nuclear Regulatory Commission (1975).

9. L. CAMARINOPOULOS AND G. YADIGAROGLU, "Large-Population-Center and Core-Melt-Accident Considerations in Siting," to be published in Nuclear Technology.
10. Federal Ministry for Research and Technology, "German Risk Study - Main Report. A Study of the Risk Due to Accidents in Nuclear Power Plants," EPRI Report NP-1804-SR, Electric Power Research Institute (1981).
11. P. HEDEMANN et al., "Calculation of the Individual and Population Doses on Danish Territory Resulting from Hypothetical Core-Melt Accidents at the Barseback Reactor," Report RISØ No. 356, Risø National Laboratory (1977).

DEVELOPMENT OF FRENCH TECHNICAL SAFETY REGULATIONS :
SAFETY FUNDAMENTAL RULES

(Règles Fondamentales de Sûreté)

par : Ph. LEBOULEUX

C.E.A. - I.P.S.N

(FRANCE)

ABSTRACT

The technical regulation related to nuclear safety in France is made of a set of regulation texts, of a different nature, that define the requirements for the construction, commissioning and operation of nuclear facilities.

Simultaneously, the safety authorities (Service Central de Sûreté des Installations Nucléaires : SCSIN) issue recommendations or guides which are not strictly speaking regulations in the juridical sense; they are called "Règles Fondamentales de Sûreté" (RFS).

The RFS set up and detail the conditions, the respect of which is deemed to be complying with the French regulation practice, for the subject to which they relate. Their purpose is to make known rules judged acceptable by safety authorities, thus making the safety review easier.

The RFS program is described.

A RFS - or a letter - can also give the result of the examination of the constructor and operator codes (RCC) by safety authorities.

INTRODUCTION

Within a general regulation defining a licensing procedure particularly rigorous, the safety evaluation of the first nuclear facilities built in France required special investigation of all technical difficulties. A number of references were, however, available : regulatory documents and publications outlining good engineering practice for comparable industrial activities, as well as foreign regulations and codes.

The increase in the number of nuclear installations controlled and particularly the implementation of the French nuclear power program demonstrated the multiple needs for safety requirements which exhibit the two main features of any regulations : definition of basic rules unrelated to any specific projects; uniformity of measures adopted for comparable projects. The raw material for this approach was provided by the lessons learned from early experience and the findings of initial investigations.

Concomitant to the development of the technical regulation of nuclear safety, the availability of texts having a reduced regulatory range but stating precise technical rules on specific points was considered as a need.

After recalling the main elements of the general regulation and of nuclear safety technical regulation, this paper points out the features of basic safety rules ("Règles Fondamentales de Sûreté - RFS"), and describes their publication program. Finally it indicates the possibility to complete the examination of the constructor and operator codes by means of a RFS (or a letter).

I - FRENCH NUCLEAR SAFETY REGULATION

1.1 - Procedures and organization

Insofar as this presentation is concerned, the regulations make the following provisions:

- authorization of Basic Nuclear Installations, i.e. reactors and other major nuclear facilities, is granted in a Decree issued by the Prime Minister subsequent to a report by the Minister of Research and Industry, following an advice by the Inter-ministerial Commission on Basic Nuclear Installations (CIINB) established by the same Decree, and concurrence of the Minister of Health;

- the Authorization Decree establishes the characteristics of the installation and specific requirements to be fulfilled by the Operator, in addition to implementation of the relevant general regulations;

- the General Technical Regulations (GTR) pertaining to the safety of Basic Nuclear Installations are issued in Orders signed by the Minister of Research and Industry.

The agency at the Ministry of Research and Industry in charge of activities related to the safety of nuclear installations, particularly the preparation of General Technical Regulations, is the Service Central de Sûreté des Installations Nucléaires (SCSIN) or Central Office for Safety of Nuclear Installations.

The SCSIN subjects each installation to a technical evaluation on the basis of the Preliminary Safety Analysis Report submitted by the Operator. These technical evaluations are conducted by the Nuclear Safety Department at the CEA (Institut de Protection et de Sûreté Nucléaire or Protection and Nuclear Safety Institute). This Department reports its findings to a group of experts (Groupe Permanent) appointed by the Minister of Research and Industry. After review, the Groupe Permanent issues an opinion in conjunction with proposed technical requirements. The Authorization Decree is then prepared in view of the Groupe Permanent's observations and proposals.

1.2 - Technical regulation

The technical regulation related to nuclear safety in France is made of a set of regulation texts, of a different nature, that define the requirements for the construction, commissioning and operation of nuclear facilities.

It includes:

- regulations with a general scope; such as "Basic Safety Principles" (issued as a draft), Protection against ionizing radiation or pressure vessel regulations;

- requirements applying to a given type or a given serie of plants (as an example, the Minister of Industry has issued requirements concerning 1300 MWe PWRs (letter CAB-900 MZ dated September 3, 1979);

- technical specifications which are issued with the licence given for each particular plant.

In each above category, texts are also classified according to their generality into three levels : basic principles, general criteria, specific technical requirements

II - THE SAFETY FUNDAMENTAL RULES

Simultaneously with the regulatory effort recalled above, the safety authorities (Service Central de Sûreté des Installations Nucléaires "SCSIN") issue recommendations or guides which are not strictly speaking regulations in the juridical sense; they are called "Règles Fondamentales de Sûreté" (RFS).

The RFS set up and detail the conditions, the respect of which is deemed to be complying with the French regulation practice, for the subject to which they relate. Their purpose is to make known rules judged acceptable by safety authorities, thus making the safety review easier. They aim to benefit from the advantages offered by standardization while being open to technical advances.

A basic safety rule applies in principle to any nuclear facility for which the decree authorizing the construction is issued more than one year after the rule publication. Owing to the interest of standardization, this period is extended to three years, except if otherwise mentioned, if the considered unit is identical to one unit whose construction has already been permitted.

As the safety fundamental rules are also established with an aperture to technical advance, the publication of a rule does not result in an obligation of modification or of additional justification for the facilities, either operating, or being built, except when otherwise stated.

Moreover, the Service Central de Sûreté des Installations Nucléaires keeps the right to modify at any time, if deemed necessary, any basic safety rule, and to detail the conditions of application if the case may be.

Besides, taking into account the RFS does not decrease the utility's responsibility, in particular as regards the regulatory requirements in effect. Under these circumstances, an utility may be able not to apply one RFS if it demonstrates that the safety objectives of the rule are achieved by other means that it proposes within the frame of regulatory procedures.

For PWRs, a RFS program is under way according to a plan given in appendix I with the main following scopes :

- general plant design and installation general principles;
- general design of the elementary systems;
- interface rules;
- rules applying to operation study;
- general rules relative to various systems, structures or equipments.

The present work does not intend to fill exhaustively this plan, but is focused on the subjects where the prompt obtention of regulatory tools seems to have the most efficient effect.

As for now, thirteen RFS have been published by SCSIN or are being reviewed by the Groupe Permanent; they relate in particular to the single failure criterion, to the

taking into account of some external hazards or events (ismic motions, aircraft crashes, industrial environment) and to the quality assurance (see appendix II).

Other rules are being written according to the working schedule given in appendix III which includes in particular rules concerning safety classes and design of materials.

III - EXAMINATION OF THE COMPATIBILITY OF CODES BY SAFETY AUTHORITIES

At the suggestion of governmental authorities, the French nuclear installation constructors and operators have undertaken to compile a collection of the rules used for design and construction of pressurized water reactor nuclear power plants. This document headed "Recueil des règles de conception et de construction" - RCC - (Collection of design and construction rules) is limited to the Nuclear Island and includes several parts :

- RCC - P for the processes (design rules)
- RCC - M for the mechanical equipments
- RCC - G for the civil engineering
- RCC - E for the electric equipments
- RCC - I for the provisions against fire
- RCC - C for the nuclear fuel

Safety authorities do not participate directly to the writing of those texts, the general scope of which goes beyond the strict frame of safety concerns.

After appropriate revision and examination of their compatibility with the licensing regulatory practices by safety authorities, the codes can supplement the technical regulation.

The RFS or a letter is a mean to give the result of the examination and to define the conditions for which the use of these codes is accepted.

Presently, the RCC-M and RCC-G have been the subjects of a RFS and RCC-P (900 MWe) of a letter; the examination of the safety aspects of RCC-E and RCC-I is being completed; for the RCC-C the examination is only beginning (see appendix IV).

IV - CONCLUSION

A few years ago, the scope of regulatory actions to be accomplished was considerable. Today, some progress has been made after it was considered preferable to avoid performing this work in a systematic manner. The capabilities unmobilized for such priority tasks as licensing and safety research and development were thus focussed on those areas which could most benefit from rapid preparation of regulatory tools.

REFERENCES

1. Ph. LEBouleux - C. Gilguy., La réglementation technique et la normalisation en matière de sûreté nucléaire en FRANCE,
Seminar on Selection and implementation of Safety Standards for NPPS - ISO - AIEA - VIENNE 1980.
2. M. LAVERIE - C. Houze - Ph. LEBouleux., La réglementation technique générale et la normalisation - Annales des Mines - Juin 1980.

APPENDIX I

TABLE OF CONTENTS OF SAFETY FUNDAMENTAL RULES

(Nuclear Power plant units equipped with a pressurized water reactor)

I - GENERAL DESIGN AND INSTALLATION PRINCIPLES OF THE PLANT

- I.1 General plant layout description
- I.2 Protection against externally generated hazards
- I.3 General design and installation principles

II - BASIC STRUCTURES AND SYSTEMS DESIGN

- II.1 Successive barriers against the release of radioactive products
 - II.1.1 Fuel cladding
 - II.1.2 Reactor coolant system
 - II.1.3 Containment barrier
 - II.1.4 Other barriers
- II.2 Engineered safety features
 - II.2.1 Emergency core cooling system
 - II.2.2 Containment spray system
 - II.2.3 Containment atmosphere control system
 - II.2.4 Steam generator auxiliary feedwater system
- II.3 Auxiliary systems
 - II.3.1 Fuel handling and storage system
 - II.3.2 Refueling and storage pools cooling and water treatment system
 - II.3.3 Ventilation systems
 - II.3.4 Residual heat removal system
 - II.3.5 Chemical and volume control system and reactor boron and water make-up system
 - II.3.6 Component cooling water system and essential cooling water system
 - II.3.7 Radioactive waste treatment systems
- II.4 Electrical systems
 - II.4.1 Instrumentation and control systems
 - II.4.2 Electrical power

III - INTERFACE CRITERIA

III.1 Installation criteria

III.2 Nuclear steam supply system and structures interface

III.3 Nuclear steam supply system and other balance of plant systems interface

IV - OPERATING CONDITION AND ANALYSIS CRITERIA

IV.1 Equipment classification

IV.2 Equipment operating conditions

IV.3 Reactor coolant system (main primary circuit) operating conditions

IV.4 Accident analysis

V - GENERAL RULES APPLICABLE TO CERTAIN SYSTEMS, STRUCTURES AND COMPONENTS

V.1 Radiation protection

V.2 Other general rules

APPENDIX II

"REGLES FONDAMENTALES DE SÛRETE" published or
being published on July 1st 1982 (PWRs)

Number	Title	date of application
I.2.a	Hazards related to aircraft crashes	Aug 5, 1980
I.2.b	Risks of emission of missiles following bursting of turbine - generator set.	Aug 5, 1980
I.2.c	Determination of seismic displacements to be taken into account for safety	Oct 1, 1981 (provisional)
I.2.d	Hazards related to industrial environment and communication ways	May 7, 1982
I.2.e	Flood hazards	being presented to "Permanent Group"
I.3.a	Application of the single failure criterion in safety analysis	Aug 5, 1980
I.3.b	Seismic instrumentation	being presented to "Permanent Group"
II.2.2.a	Design of the containment spray system	Aug 5, 1980
V.1.a	Determination of the activity released out of the fuel	Janv 18, 1982
V.1.b	Meteorological measurements	Jun 10, 1982
V.2.a	General provisions on quality assurance	Nov 1 st , 1981 (provisional)
V.2.b	General rules applicable to civil engineering works	Jul 30, 1981
V.2.c	General rules applicable to the construction of mechanical materials	Apr 8, 1981

APPENDIX III

"REGLES FONDAMENTALES DE SÛRETE" being written (PWRs)

Chapter I.2

- Rules relative to earthquakes
 - . building behaviour
 - . equipment behaviour

Chapter IV

- Rules relative to safety classes of mechanical and electrical materials.
- Rules relative to seismic classes of materials.
- Rules relative to design of mechanical materials, of civil engineering works, of supports, of electrical materials.
- Rules relative to in service monitoring and inspection.

Chapter V

- Rules relative to the radioactivity inventory to be taken into account in accident studies :
 - . instrumentation range
 - . access to materials
 - . material qualification
 - . releases

APPENDIX IV

EXAMINATION OF COMPATIBILITY OF CODES

Code	Reference text	Date
RCC-P (900 MWe)	letter SIN n° Z 3229-80	Aug 01, 1980
RCC-M	RFS V.2.c	Apr 08, 1981
RCC-G	RFS V.2.b	Jul 30, 1981
RCC-E	} RFS under way of publication	
RCC-I		

A COMPARISON OF LOCA SAFETY ANALYSIS IN THE
USA, FRG, AND JAPAN

L. P. Leach and L. J. Ybarrondo
EG&G Idaho, Inc.
Idaho Falls, Idaho 83415, USA

E. F. Hicken
Gesellschaft für Reaktorsicherheit
Garching, FRG

K. Tasaka
Japan Atomic Energy Research Institute
Tokai, Japan

ABSTRACT

The bases for loss-of-coolant accident (LOCA) safety analyses required by reactor licensing regulations in the United States of America (USA), Federal Republic of Germany (FRG), and Japan are investigated and related to new data obtained since the regulations were established. The licensing approaches used in the three countries are similar in that a conservative calculation is called for, the necessary conservatism is unspecified, and new research data have had only limited effect on changing the regulations.

INTRODUCTION

Reactor safety research in connection with the LOCA began in the 1960s, and since that time, an extensive data base has been accumulated. In this paper^a the LOCA safety analysis methods and regulations applied toward licensing nuclear reactors in the USA, FRG, and Japan are described and evaluated. The conservatism of valid reactor licensing criteria for the three countries is addressed.

REACTOR LICENSING REGULATIONS

The bases for the reactor licensing regulations for the USA, FRG, and Japan are presented, and similarities and differences among the regulations are highlighted.

Regulations in the USA

The basic requirements for performing LOCA safety analyses for licensing reactors in the USA are defined in the United States Code of Federal Regulations, 10 CFR 50.46, "Acceptance Criteria for Emergency Core Cooling Systems for Light Water Nuclear Power Reactors."¹ This is supplemented by additional detail in 10 CFR 50 Appendix K, "ECCS Evaluation Models,"² and a number of regulatory guides. The USA regulations

a. Work supported by the U.S. Nuclear Regulatory Commission, Office of Nuclear Regulatory Research under DOE Contract No. DE-AC07-76ID01570, by the Japanese Atomic Energy Research Institute, and by the Federal Republic of Germany--Gesellschaft fuer Reaktorsicherheit.

grew out of an extensive series of ECCS (emergency core cooling system) hearings in 1972 and 1973. They were originally designated as "Interim Acceptance Criteria"³ in anticipation of the large increase in LOCA/ECCS data that have been obtained over the last decade. There were numerous short comings in the technical data base at the time the regulations were established. Therefore, an overall approach to produce calculated results that were conservative relative to the specified criteria was adopted. This approach requires the use of limiting data on important variables such as decay heat production and heat transfer coefficients, and nonphysical behavior such as discarding of emergency core coolant (ECC) water. This conservatism is in addition to other conservatisms in design (for example, single-failure criterion and seismic requirements) and accident consequence analysis (for example, equipment malfunctions, source term, and weather conditions).

Regulations in the FRG

LOCA safety analysis in the FRG is governed by the Atomic Energy Act, Safety Criteria,⁴ and government guidelines.⁵ The overall procedure is based on not exceeding defined radiation exposure guidelines. In addition to the criteria used in the USA, the FRG has the requirement that a reactor core must be coolable. This requirement is not specified in detail, but is demonstrated in a "core damage report," which permits the use of a probabilistic approach in assessing the effectiveness of ECCSs. The FRG regulations require the use of 106% normal power and a local peaking factor of 2.5 which lead to calculated peak clad temperatures of 300 to 400 K higher than those in best estimate calculations (see Table I).

The FRG guidelines for using conservative assumptions are relatively flexible. Usually, new analytical and experimental results are taken into account. Data from small break LOCA analyses have been available for several years.

Regulations in Japan

The Japanese guide for LOCA safety analysis is "Acceptance Criteria for Performance of ECCS for Light Water Cooled Nuclear Power Reactors."⁶ A new version was

TABLE I
Difference Between FRG Conservative and Best Estimate
Peak Clad Temperature Calculations

Phenomena	Range of Difference Between Calculated Conservative and Best Estimate (K)
Fq-factor ^a	100-150
ECCS availability	100
Decay heat	50-80
Gap heat conductance	50-100
Heat transfer coefficient (cladding-fluid)	50-100

a. Power distribution factor (including overpower assumption).

issued by the Special Committee on Safety Standards of Reactors on July 20, 1981. Although this guide is in many respects similar to the USA regulations, it is much more flexible than the USA regulations or the old Japanese regulations.

In most cases, the new Japanese criteria allows for the introduction of new data. For example, the decay heat curve from American Nuclear Society (ANS) Standard 5.1 (1979) and the homogeneous equilibrium critical flow model are specifically allowed. In addition, characteristics and core cooling capability of the ECCS call for the use of experimental data to justify the models used rather than specifying the criteria or approaches.

CONSERVATISM IN THE REGULATIONS

Since the promulgation of the reactor licensing regulations in the USA, FRG, and Japan, an extensive data base has been accumulated. Key experimental facilities contributing to this data base include the Two Loop Test Apparatus (TLTA),^{7,8,9,10} Semiscale,¹¹ and Loss-of-Fluid Test (LOFT)¹² facilities in the USA; the Rig of Safety Assessment (ROSA),¹³ Cylindrical Core Test Facility (CCTF), and Slab Core Test Facility (SCTF) facilities in Japan; the Primar Kreis Lauf (PKL)¹⁴ facility in West Germany; and the Loop Blowdown Investigation (LOBI)¹⁵ facility at Ispra, Italy, sponsored by the FRG for the first test series. Analytical capabilities to describe LOCA/ECCS behavior have been extensively improved, using the data from these facilities and from a wide range of smaller more basic experiments.

Conservatism in the licensing regulations were evaluated using the following methods:

1. Direct evaluation of experimental data
2. Comparison of licensing calculations to experimental data
3. Comparison of validated best estimate calculations with licensing calculations.

The first method is illustrated in Fig. 1, which shows measured cladding temperature from a wide range of LOCA experiments in the Japanese ROSA-III test facility. The measured temperatures are well below the safety criteria specified in the licensing regulations. The second and third methods are illustrated in Fig. 2, which compares a Nuclear Regulatory Commission (NRC) licensing calculation, a best estimate calculation, and experimental data from LOCA Experiment L2-3 performed in the LOFT reactor in the USA. The best estimate calculation is substantially below the licensing calculation and the measured data are even lower yet! Table I illustrates the conservatism in peak clad temperature resulting from the use of FRG licensing assumptions rather than a best estimate calculation. Figs. 1 and 2 and Table I vividly illustrate that despite different reactor systems, initial conditions, and analysis methods, the intended objective to imposing conservative criteria in the three countries has been uniformly successful. Comparison of the overall requirements in the USA, FRG, and Japan is given in Table II. The acceptable technical features are compared in Table III.

In most cases, there is now sufficient data to support use of best estimate modeling techniques with specified uncertainties. The new licensing rule adopted in Japan allows for the introduction of some of these new data, including new data relative to the decay heat term. Calculations have not been performed as yet with this new criteria.

As mentioned earlier, although the licensing criteria recognized the need for analysis of small break as well as large break LOCAs, there is very little guidance explicitly addressing the small break analysis techniques in the USA. For example, the methods of calculating natural circulation flow rate and heat removal are not

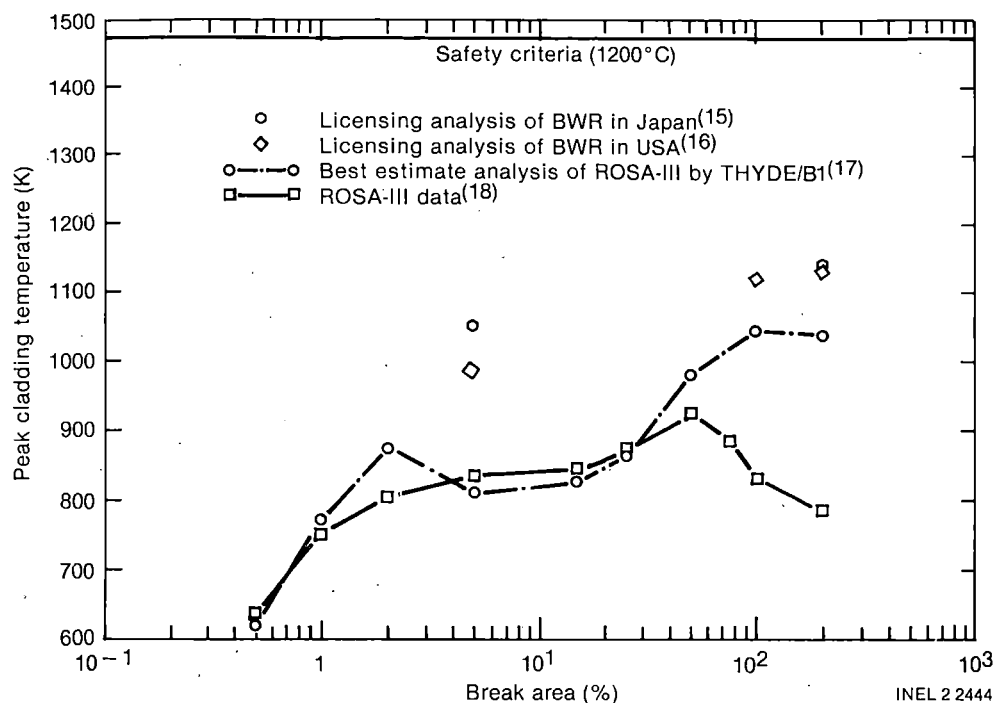


Fig. 1. Measured cladding temperature compared with specified safety criteria.

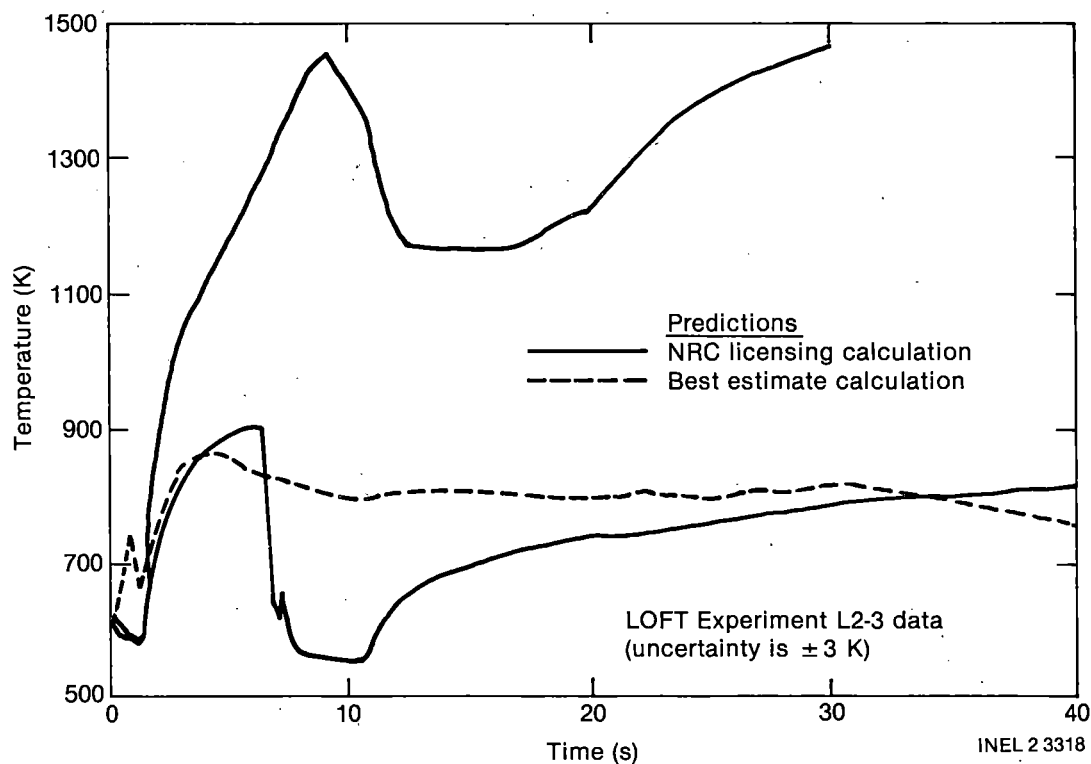


Fig. 2. Comparison of calculated and measured cladding temperature.

TABLE II
Comparison of Overall Requirements

Item	USA	Japan	FRG
Regulation	10 CFR 50.46, "Acceptance Criteria for Emergency Core Cooling Systems for Light Water Nuclear Power Reactors," March 1975	"Acceptance Criteria for Performance for ECCS for Light Water Cooled Nuclear Power Reactors," July 20, 1981	"Risk-Guidelines for Pressurized Water Reactors, October 1981
Peak clad temperature limit	$\leq 1204^{\circ}\text{C}$	$\leq 1200^{\circ}\text{C}$	$\leq 1200^{\circ}\text{C}$
Maximum clad oxidation	$\leq 17\%$	$\leq 15\%$	$\leq 17\%$
Maximum H ₂ generation	$\leq 1\%$	Low enough to maintain integrity of containment	$\leq 1\%$
Coolable geometry	Coolable geometry	Coolable geometry	Coolable geometry
Long-term cooling	Core temperature low/remove decay heat	Remove decay heat	Remove decay heat; no long-term steam flow into the containment

TABLE III
Comparison of Acceptable Technical Features

Item	USA	Japan	FRG
Sources of Heat			
Initial power	1.02 x licensed worst peaking	1.02 x licensed worst peaking	1.06 x licensed worst peaking (e.g., $F_{q,\max} = 2.5$)
Fission heat	Minimum plausible reactivities	Conservative	
Decay of actinides	To yield highest temperature	To be included	Not included
Fission product decay	1.2 x ANS Standard, October 1971	(1+2 σ) x ANS Standard 5.1, 1979	1.2 x ANS Standard 5.1, 1979

TABLE III (continued)

Comparison of Acceptable Technical Features

Item	USA	Japan	FRG
Sources of Heat (continued)			
Metal water reaction	Baker Just Not steam limited. Inside also on ruptured rods	Evaluated by experiment infinite vapor source. Inside also on ruptured rods	$\leq 1\%$ of zirconium in core
Internal heat transfer	Taken into account	Taken into account	Taken into account
Pressurized water reactor (PWR) primary to secondary heat transfer	Taken into account	Taken into account	Taken into account
Swelling and Rupture of Cladding and Fuel	Taken into account	Taken into account	$\leq 10\%$ rod failure
Blowdown Phenomena			
Break characteristics and flow	a. Break spectrum to double-ended breaks b. Discharge model or Moody, 1965 c. Noding near the break	a. Break spectrum from small-break with break flow corresponding to the capacity of auxiliary water supply system to double-ended break b. Discharge model $2\% < x < 100\%$ Moody, 1965 $x < 0\%$ Henry-Fauske or Zaloudek $0\% < x < 100\%$ HEM $100\% < x$ Murdock-Bauman c. Noding near the break	a. Break spectrum to double-ended breaks, 20 cm^2 pressure vessel bottom leak b. Experimentally verified discharge model or Moody, 1965 c. Noding near the break
Frictional pressure drops	Realistic	Realistic	Realistic
Momentum equation	Justify omission of terms	Justify omission of terms	Not specified

TABLE III (continued)

Comparison of Acceptable Technical Features

Item	USA	Japan	FRG
Critical heat flux (CHF)	Must assure in range Not permitted until reflood Equal < mean value of data	Should be justified by experimental data	a-d. Experimentally verified correlations, conservative assumptions
a-d. Correlations			
e. Rewet			e. Not permitted until reflood
Post-CHF heat transfer correlations			Experimentally verified correlation or modified Dougall-Rohsenow correlation
Pump modeling	Justified by data	Justified by data	Justified by data or conservative assumptions
Core flow distribution during blowdown	Realistic	Realistic	20% flow reduction
ECC bypass	Subtract ECC injected until end of blowdown	Subtract bypassed ECC or injected ECC until end of blowdown	Subtract ECC injected until end of blowdown
Postblowdown phenomena, heat removal by ECCs			
Single-failure criterion	Most damaging single failure	Most damaging single failure	Most damaging single failure plus repair
Containment pressure	Conservative	Conservative	80% of calculated value
PWR reflood rate	Locked pump impellers	Justified by data	Justified by data
Steam interactions with ECC water in PWRs	Zero flow in unbroken pipes unless justified by data	Justified by data	Justified by data
Refill and reflood heat transfer for PWRs	Applicable experimental data	Conservative correlations based upon applicable experimental data	Adiabatic heatup during refill or applicable experimental data for reflood or modified Dougall-Rohsenow correlation

TABLE III (continued)

Comparison of Acceptable Technical Features

Item	USA	Japan	FRG
Postblowdown phenomena, heat removal by ECCs (continued)			
Convection heat transfer coef- ficients for boiling water reactor (BWR) fuel rods under spray cooling	Based on appropri- ate experimental data	BWR-FLECHT	Applicable experi- mental data
BWR channel box under spray cooling	Based on appropri- ate experimental data	Yamanouchi correlation	Applicable experi- mental data

addressed explicitly. A second area not explicitly addressed in the licensing criteria is the method of dealing with multiple failure events. The accident at the USA Three Mile Island plant has made the need for addressing such events apparent, although no methodology for so doing has been established (other than a recognition that probabilistic risk assessment includes evaluation of multiple failure events).

CONCLUSIONS

In general, the licensing approaches used in the USA, FRG, and Japan are similar in that a conservative calculation is called for, the necessary conservatism is unspecified; and new research data have had only limited effect on changing the regulations. Although FRG regulations and the new Japanese regulations are flexible enough that more use will be made of the new data, it is doubtful that their practical use will allow changes in plant power or operation beyond that which would be allowed by the USA regulations. Based on these data, it is our judgment that the application of the regulations is needlessly over conservative. In addition, there are a number of areas not addressed by the regulations that should and can be revised with the techniques and data base accumulated since their promulgation.

In conclusion, we recommend a reevaluation of the overall LOCA analysis licensing approach, using the best features of the regulations adopted in the USA, FRG, and Japan. We recommend that this new approach be objective rather than prescriptive in nature so as to better allow for the continual and rapid use of new research data as they are obtained. We believe that such an approach can benefit the public of all countries involved by providing safer and more productive nuclear reactor systems.

NOTICE

This paper was prepared as an account of work sponsored by an agency of the United States Government, the Federal Republic of Germany, and Japan. Neither the United States Government, Japan, or the Federal Republic of Germany nor any agency thereof, or any of their employees, makes any warranty, expressed or implied, or assumes any legal liability or responsibility for any third party's use, or the

results of such use, of any information, apparatus, product or process disclosed in this paper, or represents that its use by such third party would not infringe privately owned rights. The views expressed in this paper are not necessarily those of the U.S. Nuclear Regulatory Commission, JAERI, or FRG, GRS.

REFERENCES

1. United States Code of Federal Regulations, Title 10, Section 50.46 (10 CFR 50.46) "Acceptance Criteria for Emergency Core Cooling Systems for Light Water Nuclear Power Reactors," (March 1975).
2. United States Code of Federal Regulations, Title 10, Section 50 (10 CFR 50) Appendix K, "ECCS Evaluation Models," (October 27, 1979).
3. Final Environmental Statement Concerning Proposed Rule Making Action: "Acceptance Criteria for Emergency Core Cooling Systems for Light-Water-Cooled Nuclear Power Reactors," Volumes 1 and 2, Docket No. RM-50-1, United States Atomic Energy Commission (May 9, 1973).
4. Der Bundesminister des Innern: "Sicherheitskriterien fuer Kernkraftwerke." Verabshiedet vom Laenderausschuss fuer Atomkernenergie am 12. Oktober 1977, Bekanntmachung vom 21. Oktober 1977 im Bundesanzeiger Nr. 206 vom 3 November 1977; Druck and Versand: GRS, Koeln.

[Federal Minister of the Interior: "Safety Criteria for Nuclear Power Plants." Passed by the Atomic Energy Committee of the State on October 12, 1977. Published October 21, 1977, in Bundesanzeiger (like Federal Register) No. 206, on November 3, 1977; Druck and Versand: GRS, Koeln.]

5. Reaktor-Sicherheitskommission: RSK-Leitlinien fuer Druckwasserreaktoren, 3 Ausgabe, 14 Oktober 1981. Druck and Versand: GRS, Koeln.

[Commission for Reactor Safety (RSK): RSK-Guidelines for Pressurized Water Reactors, 3rd Edition (October 1981). Druck and Versand: GRS, Koeln.]

6. Special Committee on Safety Standards of Reactors, Nuclear Safety Commission, Japan, "Acceptance Criteria for Performance of ECCS for Light Water Cooled Nuclear Power Reactors," (July 20, 1981).
7. W. S. HWANG et al., "BWR Blowdown/Emergency Core Cooling Program 64-Rod Blowdown Heat Transfer (8x8 BDHT) Final Report," GEAP-NUREG-2397 (September 1978).
8. L. S. LEE et al., "BWR Large Break Simulation Tests BWR Blowdown/Emergency Core Cooling Program," Volumes 1 and 2, NUREG/CR-2229 (March 1981).
9. D. S. SEELY et al., "BWR Low Flow Bundle Uncovery and Test Analysis," NUREG/CR-2231 (August 1981).
10. W. S. HWANG, "BWR Small Break Simulation Tests with and without Degraded ECC Systems," Topical, BWR Blowdown/Emergency Core Cooling Program, NUREG/CR-2230 (January 1982).
11. M. L. PATTON, "Semiscale Mod-3 Test Program and System Description," NUREG/CR-0239, TREE-NUREG-1212 (July 1978).
12. L. P. LEACH and G. D. MCPHERSON, "Results of the First Nuclear-Powered Loss-of-Coolant Experiments in the LOFT Facility," Nuclear Safety, 21, 4 (July-August, 1980).

13. Y. ANODA et al., "ROSA-III System Description," JAERI-M 9243 (December 1980).
14. B. BRAND, R. KIRMSE, W. WINKLER, Specification, OECD-CSNI LOCA Standard Problem No. 10: "Refill and Reflood Experiment in a Simulated PWR Primary System (PKL)," KWU, Erlangen R513 (December 1979).
15. W. L. RIEBOLD, "LOBI Experimental Programme A--Testmatrix Part A1 and A2," Commission of the European Communities, J.R.C.-Ispra Technical Note Nr. I.06.01.111.79.

A METHODOLOGY FOR PERFORMING THE DESIGN REVIEW OF PLANT
SHIELDING AND ENVIRONMENTAL QUALIFICATION
REQUIRED AFTER TMI-2

José A. Carretero

Empresarios Agrupados, S.A.
Magallanes, 3, Madrid - 15, Spain

ABSTRACT

After TMI-2, the NRC issued several documents requiring a design review of plant shielding and environmental qualification for spaces/-systems which may be used in post-accident operations.

The objective of this requirement was to confirm the shielding provided around systems that may contain highly radioactive materials as a result of an accident, which may unduly limit personnel occupancy or degrade safety equipment by radiation.

The objective of this paper is to describe a methodology developed to obtain the inputs needed for shielding and dose calculations.

It has to be pointed out that criteria for determination of vital areas, system flow paths and fluid data were not well defined by the NRC and the events considered were beyond design basis.

The paper describes (1) the approach adopted, exposing the conservative hypothesis applied to meet the intention of requirements, (2) more significant differences in this job between PWR and BWR, and (3) some complementary applications of the work developed.

INTRODUCTION

Based on the experience of TMI-2, the NRC issued requirements by letters to all operating licensees and operating license applicants to perform radiation and shielding design review which would confirm adequate access to vital areas and protection to safety equipment during accident conditions.

The required shielding review should be performed according to criteria beyond design basis accidents. Previous work is then required to determine inputs for shielding calculations that are not as well defined as for usual shielding design.

The objective of this paper is to describe the methodology employed to define inputs, but is not intended to describe detailed characteristics of the computer programmes used in shielding calculations.

The most significant differences between PWR and BWR are also analyzed.

The prime objective of the shielding design review is to comply with license requirements of the NRC, but the method developed permits complementary applications which can be as useful in the design as in plant operation.

REASON FOR THE SHIELDING DESIGN REVIEW

The purpose of the NRC requirements on this subject was to confirm that (1) personnel occupancy and access to vital areas are not unduly limited, and (2) safety equipment is not unduly degraded by radiation levels during accident conditions. It should be considered that shielding design is calculated using most restrictive sources from normal plant operation, except in the control room. Otherwise, wall thickness would be penalized in excess by accident condition inputs.

REFERENCE DOCUMENTATION

NRC technical positions for the shielding design review have had clarifications. NRC requirements and technical positions for operating licensees and operating license applicants are incorporated in NUREG 578¹, NUREG 660², NUREG 694³ and mainly in NUREG 737⁴.

Requirements for construction permit applicants are included in NUREG 718⁵ and cited reference documents.

REVIEW METHODOLOGY

NRC requirements and technical positions for shielding design review are employed together with information included in the accident analysis of SAR Chapter 15, to define a "worst case" from the shielding point of view. It has to be pointed out that issued requirements do not lead to a single accident with the most restrictive conditions, but these have to be determined from different types of accidents giving an envelope named "worst case".

The indicated information and the design documentation is used to determine:

- a. Systems outside containment, which may potentially contain highly radioactive fluids, and flow paths
- b. Characteristic data from fluids in the "worst case" (pressure, temperatures, sources and dilution factors)
- c. Vital areas which may require continuous occupancy or infrequent access for the control and mitigation of consequences of the accident.

The accident sequences and assumptions considered in developing the system actuation model are the most restrictive to the shielding, i.e., those which lead to maximum extension of contamination to the systems and/or maximum concentration of radioactive sources in systems. Although, on some occasions, this actuation model may be incongruent with other assumptions or criteria employed, it has to be considered to develop a "worst case", e.g., in a BWR 6. The ECCS contamination at zero time can be postulated for the criterion of maximum extension of the contamination, but the prompt actuation of ECCS could probably prevent significant damage to the core, the cause of radioactive materials released.

The next step is to consider the plant general arrangement and to proceed with geometrical patterns and computer calculations.

For dose calculation, the combined PANDORA and EVITA (property of Empresarios Agrupados) computer programmes, prepared on the basis on the Point Kernal dose calculation method and which calculate the point dose on the basis of Equation (1) (or the integrated dose by means of a similar equation) have been used.

$$D(d,s,t) = \int_g R(d,g,s) \times I(s,g,t) \quad (1)$$

where:

$D(d,s,t)$ = dose rate (mrem/hour) in the detector "d" and time "t" due to "s" system equipment

$R(d,g,s)$ = dose rate (mrem/hour)/(MeV/s.cm³) in the detector "d" produced by a 1MeV/s.cm³ source in the power group "g" in all "s" system equipment

$I(s,g,t)$ = specific intensity (MeV/s.cm³) in the "s" system, power group "g" and time "t".

Finally, the following are obtained:

- a. Evolution of dose rate for personnel in each vital area considered with the time after the beginning of the accident.
- b. Integrated doses for equipment required during the accident.

This information is used to check habitability and/or accessibility of personnel to vital areas, as well as the radiation qualification of equipment required to be operable during accident conditions.

Corrective actions, which have to be taken when the checking does not give satisfactory results, may be as follows:

- a. Post-accident procedural controls
- b. Increased permanent or temporary shielding
- c. Design changes

The adopted corrective action should be taken considering specific circumstances on a case-by-case basis to obtain the best alternative.

DISCUSSION OF CRITERIA APPLIED

The speed with which NUREG 578 was published gave rise to many doubts in the industry regarding the interpretation of the criteria and their application to shielding design review. As a consequence of this, in NUREG 737, the NRC published a clarification of the requirements, which in some cases it completed and in others significantly changed the basic review hypotheses. However, significant differences may be seen in the published results of already performed studies, which can only be attributed to the NRC's lack of precise technical positions in certain areas, as well as to the generally very conservative practice normally used in shielding design.

A Mark III BWR-6 may be used as an example. The RHR is a system which in analysis may be assumed to contain high radioactivity levels; but this system has various actuation modes, some of which are only expected to be used in normal operation and not during an accident and even less during an accident with a significant release of fission products. Since no strict criterion on the accident sequence to be considered has been established, it may occur that the analyst assumes, conservatively, that such modes are used under hypotheses of high core degradation, which would significantly affect the resulting doses. However, in view of the system logic characteristics and the post-accident coolant sampling capacity, it may be assumed that it should not be considered that an RHR mode such as steam condensation will be used under such conditions. In a different way, the RHR normal shutdown mode - which one might assume may be used by the operator instead of the alternative shutdown - through the suppression pool - should be considered, in spite of the fact that he has to reset the isolation logic and have available information on core damage by means of the sample. What is not so clear in the NUREG 737 clarifications is whether in this case the fluid may be considered as depressurized - reactor pressure should decrease to below 135 psig - and therefore as having 50% iodines and 1% fission products or whether, on the contrary, it should be assumed that it also contains 100% of noble gases.

Another aspect in which the basic hypotheses may give rise to very diverse results is that of accessibility to vital areas. In NUREG 737 some zones to which

access would only be required if repairs were to be done within 30 days of the accident are identified as vital areas, although only as a guide, but these zones are not vital for safe shutdown since there are redundant controls in the control room. The consideration of more or less vital areas and greater or less staying time gives noticeably different results.

A case in point is the accident sampling panel. The requirements have established the maximum allowable sampling time, but have not clearly defined at which moment after the accident the sample should be taken or how many samples should be taken throughout the duration of the accident.

In view of the shielding design reviews already performed by the plants, an additional clarification by the NRC of its position in the indicated areas and the degree of confidence in the logic and mechanical devices involved in limiting the extension of contamination between systems (e.g., applicability of the single failure criterion) might be very useful in the optimization of modifications which may result from this type of study.

DIFFERENCES BETWEEN PWR AND BWR

The most significant difference between the "worst case" in modern PWR and BWR is that PWR has to consider 100% of the core equilibrium noble gas inventory contained in the recirculation coolant outside containment, while it is very difficult to imagine the same situation⁶ in BWR because the boiling characteristic would release these gases from the coolant as soon as it is depressurized.

However, the "worst case" is more restrictive in other cases for BWR; e.g., ECCS is considered to be pumping water containing radioactive sources since the beginning of the accident in BWR, while in a PWR it does not happen until injection systems take water from containment sumps, which occurs about 20 minutes after the beginning of the accident.

REVIEW APPLICATIONS

There are several applications of this shielding design review. Some are implicit in NRC requirements, but others are complementary applications that may be obtained explicitly according to the particular necessities of each plant. These applications are as follows:

- a. Plant specific knowledge of the accessibility to the buildings during accident conditions. This information is used in general arrangement of equipment, instrumentation and control design, emergency guidelines and emergency procedural controls.
- b. Plant specific integrated doses to equipment and components required to be operable during accident conditions for checking the radiation qualification.

- c. Plant specific values of dose rates in areas as well as in process fluids for better specifications of required ranges of radiation monitoring instrumentation.
- d. Identification of all potential flow paths for extension of contamination to clean systems. This information is useful in emergency guidelines.
- e. Identification of emergency operation sequences which lead to minimum volume of contaminated fluids. This information is useful in the review of radwaste treatment capability for plant recovery.
- f. Computer programme availability for determination of the actual source intensity in equipment and doses in vital areas, from actual sources which are determined through isotopic analyses of coolant and containment atmosphere samples taken with the post-accident sample systems.

CONCLUSIONS

The modifications resulting from this review do not usually affect the plant construction schedule because there is a series of alternatives available to the designer: (1) procedural controls, (2) increased shielding and (3) design changes.

The implementation of modifications is easier if the review is done in an intermediate design stage, since design can incorporate modifications without further problems, while in an advanced design stage increased shielding may be necessary.

It is thus concluded that it is desirable to perform the review in an intermediate stage of the project and to verify the conclusions when the project is more advanced.

ACKNOWLEDGEMENT

This work was performed under the auspices of Hidroeléctrica Española, S.A. and C.N. Valdecaballeros.

REFERENCES

- 1. NUREG-578, "TMI-2 Lessons Learned, Task Force Status and Short-term Recommendations", Item 2.1.6.B.
- 2. NUREG-660, "NRC Action Plan Developed as a Result of the TMI-2 Accident", Item II.B.2.
- 3. NUREG-694, "TMI-2 Related Requirements for New Operating Licensees", Item II.B.2.

4. NUREG-737, "Clarification TMI Action Plan Requirements", Item II.B.2.
5. NUREG-718, "Proposed Licensing Requirements for Pending Applications for Construction Permits and Manufacturing License", Item II.B.2.
6. Document NSAC/17 - "Designing for Post-Accident Radiological Conditions", Section B.3.

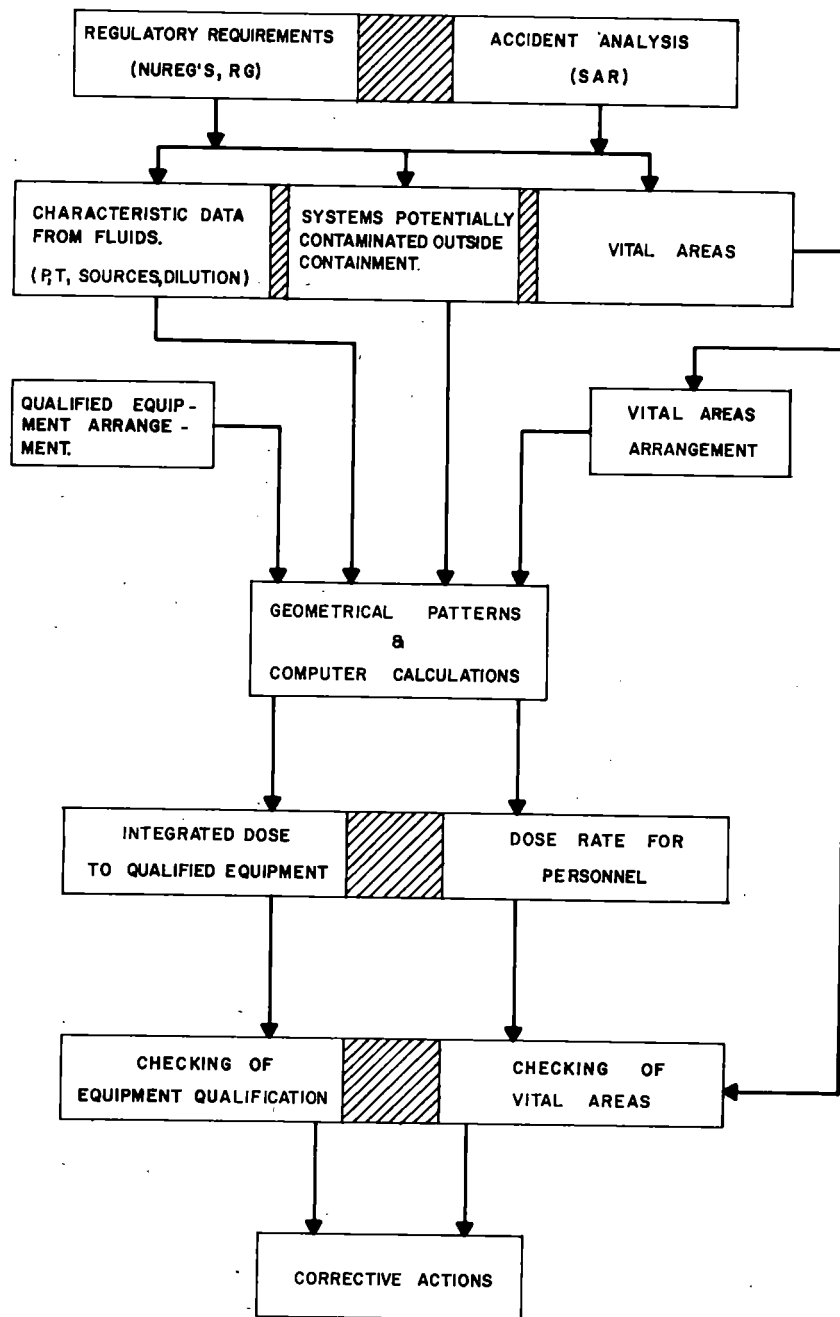


FIGURE 1 REVIEW METHODOLOGY BLOCK DIAGRAM

ESTIMATED RELEASES AND OFFSITE DOSES AFTER A
LOSS OF COOLANT ACCIDENT. A COMPARISON BETWEEN
USA AND GERMAN REGULATIONS

J.P. Carmena

Empresarios Agrupados
Magallanes, 3, Madrid - 15, Spain

ABSTRACT

One of the ways of evaluating the adequacy of structures, systems and components with respect to public health and safety is to analyze the radiological consequence of accidents, particularly the loss of coolant accident (LOCA). This paper compares the different assumptions, related to the release of radioactive material, recommended by the USA and German regulations. In a conservative analysis of this type of accident in PWR's, we conclude that the differences found cannot only be justified by design particularities of the safety features incorporated in each type of reactor and, accordingly, a uniformity in the assumptions made should be internationally sought.

INTRODUCTION

The loss of coolant accident is, to date, one of the most restrictive used to evaluate the structures, systems and components of a nuclear power plant in such a way that the radiological impact on its surroundings is permissible, even in the event of this foreseeable accident.

However, the hypotheses to be used in the calculation of this impact on PWR type reactors are not concretely established by nuclear standards. Taking two important countries in the nuclear field which have developed their own designs for this type of plant, Germany and the USA, it may be seen that the different standards issued for the licensability of nuclear power plants indicate very different hypotheses for the performance of analyses for this type of accident.

This paper aims to compare the different hypotheses with regard to the release of radioactivity in the event of a LOCA indicated in German Standard RSK 2.2 (1981)⁵ and USA Regulatory Guide 1.4 (1974)¹, presently in force, and finally recommends some guidelines to follow in search of an international regulation, especially useful for third countries importing this technology and who face this disparity of hypotheses which leads them to very different results, depending on the criteria applied.

BRIEF DESCRIPTION OF SOME ASPECTS OF THE TWO TYPES
OF PWR NUCLEAR POWER PLANTS

For a complete understanding of the hypotheses compared hereinafter, a brief description of the two types of plants to which they apply is advisable, paying special attention to the design details and the radioactive release paths in each type of plant, which might justify the discrepancies.

The KWU KONVOI Model has been used to represent the German type of reactor and Figure 1 indicates the layout of the Reactor Building, safeguards and radioactive release paths¹². It may be observed that the approximately semispherical Reactor Building houses a spherical steel containment within which is contained the nuclear steam supply system: reactor, pumps and generators, as well as the passive safeguard system: accumulators. This sphere must withstand the pressure generated by a LOCA, thus avoiding uncontrolled release of radioactive products. The primary coolant pipe rupture takes place inside this steel containment which is automatically isolated at the outbreak of the accident. The radioactivity contained in the primary coolant, and part of that contained in the fuel, escapes through the break to the containment atmosphere, from where it is partly eliminated through absorption by walls and structures. Owing to the existing high pressure caused by the accident, this radioactivity leaks to the annulus. This is kept depressurized by the annulus emergency ventilation system, thus avoiding uncontrolled leaks to the outside. Radioactive products are released by this system through the plant stack, after passing through the system filters. This latter design concept especially influences the last phases of the dosis calculations on the plant surroundings, reducing them appreciably.

The Westinghouse PWR model has been taken to represent the US type of reactor, outlined in Figure 2¹¹. It may be seen from this model that the Reactor Building coincides with the containment. This containment houses the nuclear steam supply system: reactor, pumps and generators, as well as the passive safeguard systems. In the event of a LOCA, it is this which must withstand the pressure, avoid uncontrolled release of radioactive products and shield the outside from possible direct radiation. The primary coolant pipe rupture occurs inside containment which is also isolated automatically during the first few seconds. The radioactivity contained in the primary coolant, and part of that contained in the fuel, escapes through the rupture to the containment atmosphere from where it is partly eliminated through absorption by walls and structures and by the effects of the containment spray system. This safeguard also reduces the pressure within the area. Due to the difference in pressure between the material and external atmospheric pressure, radioactive leaks, distributed throughout the area, are produced directly to the environment, which implies release at ground level, influencing this concept in the last phases of the doses calculation. To reduce the radioactivity inside containment, recirculation systems with filters for containment atmosphere are envisaged. The safeguard internals are housed in a separate building, as indicated. This implies the need for special care in the design of the ventilation systems in the event of leaks in the safeguards during the accident mitigation phase.

So as to make a quantitative evaluation of the effects of these release phenomena, the different standards indicate some models and hypotheses which are compared as follows.

COMPARISON OF THE TWO PROPOSED MODELS

In order to evaluate the release of radioactivity to the atmosphere, the two standards analyzed herein, German⁵ and US¹, recommend the following hypotheses, summarized in Table I.

1. Radioactive Material Released from the Fuel as a Result of the Accident

Regulatory Guide 1.4 (1974)¹ considers that the release of radioactive material from the fuel to the containment atmosphere, referring to the equilibrium inventory developed for maximum full-power operation, is the following:

25% of the iodines	91% of this 25% is to be assumed to be in the form of elemental iodine, 5% in the form of particulate iodine, and 4% in the form of organic iodides
100% of the noble gases	

RSK 2.2 (1981)⁵ considers that the release of radioactive materials from the fuel to the containment atmosphere, referring to the inventory developed for an effective dwell time of 2.5 years of full-power operation, is the following:

10% of noble gases
3% of iodines
2% of the volatile solids (e.g. Cs, Te, Ru)
0.1% of the other solids

As may be observed, there is a noticeable difference between the proposed values. This difference cannot be justified by different designs of fuel rods, core geometry or safeguards in each type of plant, but rather by considering the problem from a different angle.

In our opinion, the values which the US standards indicate do not exactly represent a LOCA, but rather, as indicated in NUREG 0771⁹, aim to present a Design Basis Accident (DBA) which does not respond to any actual sequence, since it neither follows the sequence of the accident nor takes into account the safeguard systems. What cannot be estimated is whether this exaggeration of effects, primarily envisaged in the design of safeguard systems and components, is also justified for radiological calculations for licensing purposes, where perhaps it would be more advisable to use more realistic values.

The German data correspond to a realistic analysis of a momentary loss of coolant in the core. According to ref. 13, two phenomena, one short-term and one medium- and long-term, are brought about. In the short-term, during the first phase of the accident (a question of a few seconds), the overheating of the element causes the rupture of some of the fuel claddings, releasing into the containment atmosphere fission products contained in the fuel rod gaps. In the medium- and long-term, in the phase of core reflooding, the diffusion of fission products is caused through fuel rods, thence to the gap and, from there, through the flood water to the outside.

Therefore, with regard to leaks to the containment atmosphere, it is the first phase (short-term) which has the greatest influence. During this phase, only the fraction obtained by multiplying the fraction of broken claddings by the fraction of fission products contained in the fuel rod gaps is released.

TABLE I

Summary of US and German Assumptions and Limits for Dose Calculation During LOCA

	Radioactive Mat. Released from Core to Cont.	Radioactive Mat. Removal Inside Containment	Radioactive Mat. Leaked from Containment	Meteorological Post-Accident Considerations	Dose Limits (Sv) (1 Sv = 100 rem) Body Thyroid	
<u>US Regulation</u>						
Noble Gases	100%	Evaluated on in- dividual case basis	Technical Spec. leak rate to en- vironment 100% - 0-1 day 50% - 1-30 days	Pasquill dif- fusion theory applied to ground level emission in: - Exclusion area boun- dary (0-2h) - Low popula- tion zone boundary (0-30d)	0.25	3
Iodides	25%					
<u>German Regulation</u>						
Noble Gases	10%	0%	Technical Spec. leak rate to an- nulus for first 24 hours	Pasquill dif- fusion theory corrected by Fortak, Klung and Vagt models applied to elevated emission	0.05	0.15
Iodides	3%	75%	Annulus emer- gency exhaust system flow rate to environment through filters Effectiveness: 0% noble gases 99% org iodines 99.99% el. iodines 99.9% others			
Volatile Solids	2%	97.5%				
Other Solids	0.1%	97.5%				

2. Radioactive Material Removal Inside Containment

Once the radioactive isotopes leak to the containment atmosphere through the rupture, certain removal phenomena may be observed inside containment, ensuring that not all the radioactivity released may leak to the exterior.

The US standard, Regulatory Guide 1.4¹ takes into account the effects of radiological decay as well as other removal features, such as sprays, natural deposition, recirculating filters or any other safety system. The values of the removal probabilities are to be calculated individually in each design of containment and safety system. In reference 10, formulae are given for the determination of these values based on data which are difficult to evaluate in the licensing process, such as the difference in temperature between the wall and containment air, bubble viscosity, diameter of drops and particles, etc.; thus the evaluator is faced with a series of parameters which are either supplied as standard, in which case he would arrive at standard removal probability values, or are to be evaluated, with the consequent difficulty, greatly aggravated by the lack of definition of design during the first stages of the licensing process.

The criterion of the German standards is that a decrease in the radioactivity released is brought about due to deposition and condensation (spraying is not included in the design of these plants). The recommended radioactive fraction values which, it is estimated, remain in the containment atmosphere are the following:

- 1 for noble gases
- 0.25 for iodines, the resultant halogens being composed of 85% elemental halogens, 10% organic halogens and 5% aerosols
- 0.025 for solid substances

The adoption of either of the criteria does not bring about differing results. We thus have removal probability values, applicable in the event of preliminary evaluations when there are too few data and a model of the removal phenomena based on the actual plant design. It is clearly more appropriate to apply the second criterion, whenever possible.

3. Radioactive Material Leaked from Containment

Once the concentrations of radionuclides in the containment atmosphere have been determined, two things may be calculated:

- Dose rates and integrated doses, based on considerations of time, on materials, equipment and operating personnel who are in the containment building, or who have to go there.
- Rates of radioactive leakage to the exterior, based on the leaks from the containment and their treatment. At this point, the differences in containment design makes direct comparison between the hypotheses impossible.

The design of US PWR containments causes leaks to be made directly to the atmosphere, assuming that this leak rate is either incorporated or to be incorporated as a technical specification requirement at peak accident pressure for the first 24 hours, and at 50% of this leak rate for the remaining duration of the accident¹.

In the case of double containments (BWR) whose design is comparable to the German plants, the US standards assume that the leak rate from the primary containment to the annulus is that incorporated in the technical specifications for the duration of the accident. The leakage should be assumed to pass directly to the emergency exhaust system without mixing in the surrounding reactor building atmosphere², and to be released directly to the exterior.

German standards specify that the calculations shall be based on the specified maximum integral leak rate until the practical equalization of pressures inside and outside the containment vessel. Following such equalization, no further leakage needs to be postulated, a duration of 24 hours being estimated. The radioactive material which thus leaks to the annulus mixes with the air therein, passing through the emergency exhaust system and, after filtering, to the exterior. In this process, and before filtering, part of the elementary iodine is converted into organically bound iodine. Thus the total iodine in the filter supply air shall be assumed to contain 50% organic iodine. The separation efficiencies postulated with regard to the effectiveness of the filters intended for the control of the accident are as follows:

- 0% for noble gases
- 99% for organically bound halogens
- 99.99% for elemental halogens
- 99.9% for all other substances

Comparing both hypotheses in the cases of double containment, the US one is more conservative since it does not consider the dilution of radioactive products in the annulus atmosphere (except in certain cases), and neither does it envisage or consider the installation of filters. Although, in order to form an opinion on this point, the design and layout of the emergency exhaust systems must be known, in principle these systems may be designed to favour this dilution, especially bearing in mind that they are not subject to extreme LOCA conditions.

4. Meteorological Post-Accident Considerations

Once the discharge rate of radioactivity to the outside as a function of time is known, radiation concentrations in the atmosphere surrounding the plant may be determined.

Here again, there is a design difference between the two types of plant, since in the US plants, the radiation is released at ground level, and in the German plants through the stack, thus leading to two different diffusion models.

US regulations recommend the use of site specific meteorological factors calculated as indicated in ref. 14, but if these are not available, it defines an atmospheric diffusion model¹ based on Pasquill's theory for groundlevel emission considering building wake correction factors for the first interval. The post accident period is divided into several intervals: 0-8 hours, 8-24 hours, 1-4 days and 4-30 days, associating to each one a specific weather category (A to F), and wind speed and direction. In this way, a diffusion factor is calculated for each time interval, function of the distance from the emitting structure. Thus, doses to the public finally depend on the distance from the containment and, in the event of ground-level emission, they decrease as the distance increases. This makes it necessary to establish some points in the plant's surroundings at which doses may be measured, since the maximum dose is very close to the building. To this end, the US regulation⁶ introduces the concepts of exclusion area and low population zone in the plant surroundings, implying that, within these areas, the doses may exceed the limits considered.

The German regulation⁵ considers an atmospheric diffusion model for elevated (stack-height) emission, taking ground elevation, roughness, etc., into account. Pasquill's diffusion theory, considering also Fortak, Klung and Vagt models according to location, is used to determine the atmospheric diffusion coefficients. The post-accident period is divided into four intervals: 0-8 hours, 8-24 hours, 1-4 days, and 4-100 days, associating with each one a weather category, wind speed or direction, much the same as in the US regulation. As a result, we get a diffusion factor for each time interval, function of distance and stack height. For a determined stack height, the highest of these values will be taken at a distance from the plant and the doses at this point determined and compared with the established limits.

It is observed that, apart from the different values obtained by applying each model, which is justifiable due to the difference in the type of release and the correction factor applied, the US regulation introduces the concepts of restricted areas throughout plant operation (exclusion and low population areas) for accident prevention and establishes limits for the boundary of such areas, allowing higher values within such areas. The German regulation, however, defines the dose limit for the most unfavourable point, so that no area has values exceeding these established dose limits.

5. Dose Calculations and Limits

With both models described previously, we have reached the dose calculation points in the surroundings of the nuclear power plant with the radioactive material released (concentration of radioisotopes in air of plume).

The US regulation⁶ requires the calculations of whole body dose due to gamma and beta ray emission from the plume and the radiation exposure due to inhalation of radionuclides in the air breathed (as defined in ref. 1). These must not be exceeded for an individual located at any point on the exclusion area boundary for two hours immediately after the radioactive release, or for an individual located at any point on the low population zone for the entire period of the passage of the radioactive cloud through the values of 0.24 Sv (25 rem) to the whole body or 3. Sv (300 rem) to the thyroid from iodine exposure.

The German regulation³ requires the determination of the same doses - to whole body and thyroid gland - as well as to bones (as defined in ref. 7), to the most exposed individual outside the power plant site. The values of these doses must not exceed 0.05 Sv (5 rem) or 0.15 Sv (15 rem) for the entire duration of the accident⁸.

CONCLUSIONS

From the analyses of the assumptions and expected results of both models, we deduce that the differences found cannot be justified only by design particularities of each type of plant.

It is not the purpose of this paper to define the best approach to adopt, but to indicate the different interpretations of the phenomena produced by the accident, as well as the varying points of view with regard to the establishment of dose limits.

Although, in the opinion of the author, both systems are conservative, it seems fitting that a more detailed analysis of each assumption carried out by world experts in each material would be desirable, so as to verify the criteria and to be able to evaluate properly, from the radiological point of view, the design of the different safety features incorporated into each type of power plant, in order to obtain homogeneous grades of conservatism which are suitable from both practical and credible points of view.

REFERENCES

1. Regulatory Guide 1.4, "Assumptions used for Evaluating the Potential Radiological Consequences of a Loss of Coolant Accident for Pressurized Water Reactors", Rev. 2 (1974).
2. Regulatory Guide 1.3, "Assumptions used for Evaluating the Potential Radiological Consequences of a Loss of Coolant Accident for Boiling Water Reactors", Rev. 2 (1974).
3. Safety Criterion 2.3, "Radiation Exposure of the Environment. Loss of Coolant Accident within the Containment of PWR's", GRS (1976).
4. "RSK Guidelines for Pressurized Water Reactors", 2nd Edition, January 24, 1979.
5. "RSK Guidelines for Pressurized Water Reactors", 3rd Edition, October 14, 1981.
6. 10CFR 0.735-1: Code of Federal Regulations.
7. Per Bundesminister für Bildung und Wissenschaft: Emissionsquellstärke vor Kernkraftwerken: Schriftenreihe Kernforschung, 6.1972.
8. Verordnung über den Schutz vor Schäden durch Ionisierende Strahlen (Strahlenschutz Verordnung - StrlSchV), Entwurf vom 11.3.1976.
9. NUREG 0771, "Regulatory Impact of Nuclear Reactor Accident Source Term Assumptions" (1981).
10. NUREG/CR 0009, "Technological Bases for Models of Spray Washout of Airborne Contaminants in Containment Vessels".
11. "Systems Summary of a Westinghouse Pressurized Water Reactor Nuclear Power Plant", G.C. Masche - Westinghouse.
12. "Pressurized Water Reactor", Kraftwerk Union.
13. "Fortschritte in der Sicherheitsbeurteilung von Kernkraftwerken", 5. GRS Fachgespräch München 22-23 October, GRS-41 (February 1982).
14. Regulatory Guide 1.145, "Atmospheric Dispersion Models for Potential Accident Consequence Assessments of Nuclear Power Plants".

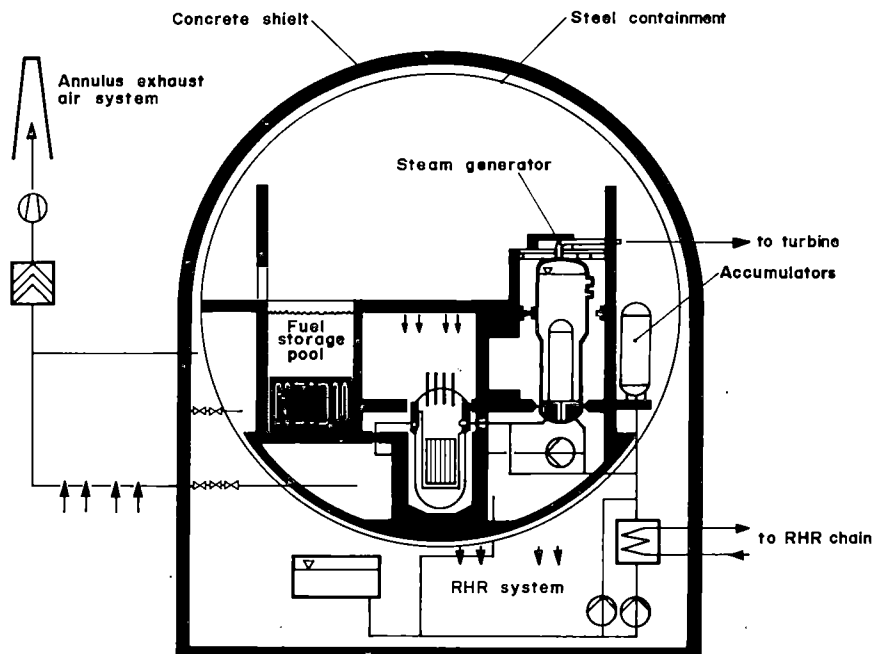


Figure 1. Schematic Representation of the Different Type of Reactor Building Designs - German (KWU).

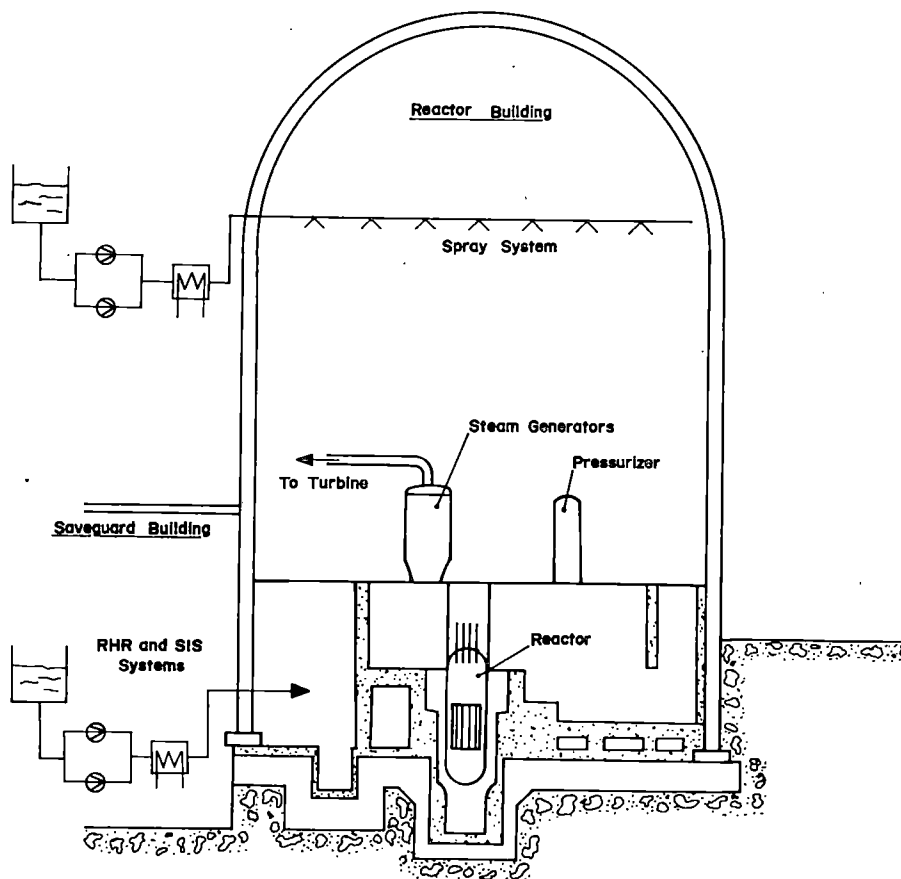


Figure 2. Schematic Representation of the Different Type of Reactor Building Designs - USA (Westinghouse).

HARMONIZATION OF SAFETY PRACTICES AND CRITERIA
RELATING TO THE SAFETY OF LIGHT WATER REACTOR
NUCLEAR POWER PLANTS WITHIN THE EUROPEAN COMMUNITY

W. Essler, W. Vinck

Commission of the European Communities
200 rue de la Loi, 1049 Brussels

ABSTRACT

This paper describes efforts undertaken by the Commission of the European Communities (CEC) to harmonize technological safety practices, rules and requirements for light water reactors (LWRs). Activities carried out and scheduled for treatment by Working Group No 1 (WG1) on safety of LWRs are outlined and comments on some of the individual tasks performed are presented.

INTRODUCTION

The Council Resolution of 22 July 1975 on the technological problems of nuclear safety [1] reinforced the ongoing Community action in respect of the progressive harmonization of safety requirements and criteria and foresees proceeding in three stages. The first stage is the exchange of information and the inventory of the methodologies, criteria and standards applied in the different member states. The second stage consists of identifying the similarities and dissimilarities and analyzing reasons for their existence. The aim of the third stage is the establishment of Recommendations pursuant to Article 124 second indent of the Euratom Treaty. This Commission action is mainly performed within the framework of a working group (Working Group No 1 on safety of light water reactors) with the active collaboration of the representatives from regulatory bodies, licensing authorities and/or associated safety and control organizations, utilities and equipment vendors.

The paper outlines activities carried out and scheduled for treatment by this working group and contains comments on some of the individual tasks carried out. The discussion primarily concentrates on:

- a document formally approved by the Commission, which compiles the safety principles for light water reactor nuclear power plants (LWR NPPs)
- an overview of WG1 activities
- safety issues which have received priority after the TMI accident such as: safety objectives, qualifications and training of reactor operators, siting practices and related considerations and emergency planning and preparedness.

The views expressed in the present paper do not necessarily reflect those of the Commission.

SAFETY PRINCIPLES FOR LWR NPPS

During the work relating to the first and second stages mentioned above, it was realized that a harmonization of safety requirements, although possible at certain levels, is not necessarily practicable at all levels because criteria and standards often refer to a specific aspect of a protective function which may be achieved in different ways. It appeared, therefore, that any specific and in-depth harmonization can only be based on a previous harmonization effort on the basic principles of safety, on which requirements and criteria depend.

A set of basic safety principles and a scheme for subsequent requirements and criteria for light water reactor nuclear power plants was established [2]. The document underlines the importance of accident prevention and confirms the current safety philosophy - called defense-in-depth - which focuses on high quality design, the consideration of failures, the assurance of physical barriers and others to limit the release of radioactivity to the public.

The policy upon which the safety principles for LWR NPPs are based takes - among other things - the form of a requirement that in normal operation the Recommendations of the International Commission on Radiological Protection and the requirements of the Euratom directive on radiation protection standards [3] are followed with regard to exposure to radiation of persons on-site and members of the public.

The document consists of three parts:

- . Fundamental safety principles
- . General safety principles
- . Subjects for safety requirements

The fundamental and general safety principles summarize those criteria and concepts which are considered in national rules and regulations. In more general terms, the fundamental safety principles state the basic objectives relating to design, construction, commissioning, operation and decommissioning which are to provide reasonable assurance that there is no undue risk to the workers, the public and the environment.

The policy adopted by the CEC to achieve these objectives is expressed by the following fundamental principles:

- . to confine the radioactive products
- . to reduce to a minimum the release of radioactive materials
- . that as a result of normal operation of a power station no person shall receive doses of radiation in excess of the appropriate limits
- . that the exposure of individuals to radiation shall be kept as low as reasonably achievable
- . that the collective dose equivalent to site personnel and the public as a result of the operation of a nuclear installation shall be kept as low as achievable
- . to take all reasonably practicable steps to prevent accidents
- . to minimize the radiological consequences of any accident, and
- . the more serious the potential consequences of an accident, the smaller should be the probability of its occurrence.

The general safety principles constitute those necessary to achieve the objectives laid down in the fundamental safety principles, i.e. to avoid accidents and limit the radiological consequences of the operation of the NPP during all operational states and accident conditions. These principles are related to the design and layout of the plant, the provision of safeguards, operating procedures, the provisions made for detecting abnormal conditions and mitigating the consequences of nuclear

accidents, the performance of a safety evaluation, the establishment and implementation of a quality assurance programme (for design, construction, commission and operation phases), the provision of safe operation by an efficient and adequate organization, the continuous surveillance (testing and maintenance) and sufficiently qualified and trained personnel who can perform the required task, etc.

The third part of the document lists the main key words (subjects) for safety requirements to fulfil the general safety principles and pertaining to the phases siting, design, construction, commissioning, operation and decommissioning and to the areas safety evaluation, QA, radiological protection including waste treatment ergonomics and emergency planning.

With respect to this part of the document, during 1981 a scheme of work was set up and priorities assigned concerning the activities to be treated.

OVERVIEW ON WG1 ACTIVITIES

Obviously, all EC countries operating NPPs have considered the impact of the TMI accident on regulatory review, safety research, design, operation, quality assurance, etc, and have carefully considered the applicability of the results of the USA investigations into the TMI accident. As a consequence, priorities in many areas have been shifted and, during 1980, a review of the orientations and objectives of WG1 activities was undertaken for the coming years. The review discussed in detail the strategy and priority of activities. Consultations between members of the working group had produced the following criteria relating to the selection of subjects and tasks:

- to handle items of importance for safety and usefulness at European level;
- to avoid duplication of activities undertaken by other international organizations such as the IAEA;
- to consider subjects already treated by IAEA but for which supplements are possible and desirable at EC level;
- subjects for which rules have already been established in member states;
- reference was made to the continuing utility of WG1 activities as a forum of exchange of information between countries with nuclear programmes and those with little or no programmes to keep them involved in the developments;
- in particular, the delegates from authorities and associated safety and control organizations have stressed the fact that regulations and guidelines, etc, should be focused on major safety issues and should be based on a comprehensive approach to the plant as a whole or ultimately the risk to the public at large. Such philosophy requires the establishment of overall safety objectives on criteria for "how safe is safe enough?", the aim of which should be a safety concept with realistic residual risk and appropriate safety measures.

The following is a listing of WG1 activities, underway or envisaged, which have obtained high priority assignment:

- Permanent Activities
 - . Information update and consultation and comments on drafts or revisions of national and international criteria, rules, standards, safety guides, etc.

- . Compilation of national and international regulations, rules, standards, safety guides, etc: catalogue and classification of technical safety standards, rules and regulations for NPPs and nuclear fuel cycle facilities.
 - . Survey of national and international programmes for development of criteria, standards, regulations, etc.
 - . Exchange of technical information on specific incidents having a significant effect on safety.
- Activities to result in status reports, synthesis reports or ultimately in recommendations in the sense of Article 124 of the EUR Treaty:
- . Safety goals/objectives.
 - . Practices with regard to fault and accident conditions that determine the design of an NPP (list and definition of initiating events and methods to be dealt with).
 - . Emergency planning and preparedness.
 - . QA in operating NPPs.
 - . QA-basic requirements.
 - . Hydrogen formation, control and consequences relating to severe core accidents.
 - . Personnel qualifications and training.
 - . Overpressure protection of primary circuit.
 - . Electric power supply.
 - . Reactor protection system (comparison of national specifications, regulations and guidelines)
 - . Containment leak testing methods.
 - . Fire protection for NPPs.
 - . Safety aspects of siting of NPPs.
 - . General requirements relating to safety evaluation (information to be given by safety reports and supporting documents).
 - . Reporting requirements in case of abnormal occurrences (reporting systems of abnormal occurrences implemented in EC countries).
 - . Environmental qualification of safety equipment.
 - . Seismic catalogue and maps for regions (potential sites) in EC countries.
- Independent safety evaluation of PWR NPPs in a member country.

In connection with WG1 activities, the Commission contributes to coordinating the action of experts from different specialized institutions in member states relating to the safety evaluation on specific aspects for NPPs at the request of a member country. In establishing a common view on the safety of certain systems, these experts who are used to different regulations, rules and methods perform a practical and pragmatic exercise of harmonization of methodologies and safety rules and thus contribute to the systematic efforts of harmonization which the Commission undertakes.

- In support of the activities carried out by Working Group No 1, the "Catalogue and classification of technical safety standards, rules and regulations for nuclear power reactors and nuclear fuel cycle facilities" was established by DIN under CEC study contract [4]. Steps were initiated so that in the future the catalogue will also present a survey of the programmes for development of criteria, codes and standards in as many countries as possible and from international organizations. It is in order here to ask those responsible for setting up such programmes to provide regular input to the Commission and DIN efforts in order to arrive at a complete overview of standards, rules and regulations under development or planned.

OVERALL SAFETY OBJECTIVES

It may be said that there is much evidence of an increasing use of probabilistic analysis in EC countries. Typically, fault and event trees for safety systems have been developed and are intensified and expanded to other systems. As the use of such methods increases with time it is obvious that finally an overall safety goal must be defined. In EC countries with major programmes increased efforts are underway.

During 1981, a special Task Force was created comprising members from licensing authorities, associated safety and control organizations and utilities which started discussions on this important issue, since it was realized that:

- safety objectives related to the protection of the public can contribute to harmonizing the regulations applicable for NPPs within member states and between member states.
- such goals can familiarize the public with the safety rules applied by the authorities and safety and control organizations, designers, etc, and thus enhance the confidence of public opinion in operating NPPs.
- the quantification of safety goals together with the use of probabilistic risk assessment (PRA) techniques are necessary to provide consistency in evaluating changes which are proposed as improvements to safety and are likely to affect future NPP design and to come to comparable safety levels.
- the quantification of safety objectives would enable the licensee to achieve the desired result in a way which is safe and practical in an NPP. The licensee's actions to meet the safety goals would be subject to review by the licensing authority and would reduce the number of prescriptive requirements. This would ultimately result in an accelerated licensing procedure.

The overall safety goal is to reduce the risk and to make the residual risk as small as reasonably achievable. So the fundamental approach to ensure an acceptably safe nuclear plant is to impose an adequate safety standard of engineering against design basis accidents so that the chances of large accidents are sufficiently reduced.

There is also a need for the examination of accident sequences beyond the design basis to avoid unacceptable contribution to the overall risk. Primary emphasis is placed on prevention of accidents since it is realized that design improvements reduce risks more than large scale mitigation devices.

The concept applied by EC countries is based on the idea of risk presented by tables which establish the consequences of different size and respective probabilities of event sequences. As a general rule, consequences are expressed in terms of individual dose equivalents at the site boundary. According to Table I₆ the range of probabilities of event sequences (classes) falls between 1/year and 10^{-6} /year and this range is divided into 4 classes. To each event class corresponds a consequence which defines the limit values of dose (protection goals) which may not be exceeded. For the dose limit values given in Table I, criteria are under development which, when observed, will avoid the consequence limits being exceeded. Such criteria may refer to fuel temperature limits and heat loads, pressure limits, etc. It should also be noted that the establishment of the list of event sequences and assignment of the event sequences into probability classes is still underway and consequently the data given in Table I are of a preliminary nature.

The line beyond which an event sequence may not be considered in design is generally placed at $<10^{-6}$ /year and then are pertaining to the residual risk. However, there may be event sequences with lower probability than 10^{-6} /year which

must be considered in design and in the licensing procedure.

The safety goal for certain man-made events like airplane crashes, explosions and fires at industrial facilities is frequently expressed by the condition that the probability of the event, P_i , should be negligible; the event is not considered in the design basis of the NPP when, for example, $P_i < 10^{-7}$ /year.

Events in class 4 may be divided into conceivable accidents and hardly conceivable accidents. They are not considered in the design basis of the NPP and are taken into account by site selection and emergency planning and preparedness.

More details on this subject are presented in another paper to this conference [5].

T A B L E I

Relationship between frequency of class of event sequences and the consequences (dose)

Event designation (a) (class of event sequences)	Frequency (Events/year)	Dose (b) (rem/year)
1. Moderate frequency events any of which may occur in every NPP several times during plant life.	$\geq 10^{-2}$	$\leq 5 \times 10^{-2}$
2. Events or fault sequences which are not expected during the life of a plant, but which cannot be excluded during the life of several plants at a site.	$< 10^{-2}$ to $\geq 10^{-4}$	$\leq 5 \times 10^{-1}$
3. Event sequences which are not expected to occur during the lifetime of a particular plant, but whose occurrence is considered in the design.	$< 10^{-4}$ to $\geq 10^{-6}$	5 to 15
4. Hypothetical events or fault sequences with a very remote probability, whose occurrence is not considered in the design. The plant should have certain characteristics to mitigate the consequences of such hypothetical events.	$< 10^{-6}$	$> (5 \text{ to } 15)$

(a) These classes of events correspond to those presented in [2].

(b) Maximum dose received by a person staying two hours at the border of the site.

OPERATOR QUALIFICATION AND TRAINING

The investigations into the training of operators after the TMI-2 accident showed that training as well as operating procedures could be improved, especially for emergency situations.

Many areas are presently under study. Some of the major items addressed refer to the establishment of the position of a shift technical advisor, review of accidents and related procedures, control room access, training requirements for mitigating core damage, increased use of simulators, improvement of qualifications of NPP personnel, minimum shift staffing and proper number of individuals in the control room, delineation of the responsibility and task of the shift, etc.

Some items of interest are briefly commented in the following:

- Operator training has been intensified and expanded to include degraded core training and contingency procedures. Typically accident emphasis has shifted from large break to small break accidents.

- It is generally accepted that persons selected for reactor operator training (i.e. operators and supervisors) should prove several years of experience - for example in the operation of fossil fired plants, ships or petrochemical plant - and should be subject to ability tests. The training should then be carried out at existing NPPs in combination with training schools. Each trainee should also have regular access to a control room simulator.

- A basic question is to define which of the control room operators should have a technical degree as it is now generally recognized that, in addition to more intensive training, operators should have more basic education in the engineering science of the plant design and how it functions. It is also felt that symptom-oriented procedures rather than scenario-oriented training requires a higher educational level of operators. Opinions on this are still divergent. There is a tendency to associate a degreed engineer with shift operations in assigning a shift technical advisor position or safety engineer to each plant to advise, among other things, operators in case of severe accidents. In other countries the assignment of a safety engineer appears unnecessary, since operators have the level of a shift technical advisor.

- Utilities, vendors and authorities regard simulators as a key to effective training of shift personnel. Increased simulator training time has been specified and simulators are being adjusted to the actual needs. Besides increasing the number of simulators, new simulators are under development with improved performance. These simulators will enable the training of low probability accidents such as design basis accidents and current incidents or off-normal condition which have been experienced in operating NPPs.

- It is essential to have a replica simulator for each power station design (e.g. convoi projects), but not for each power station. Such a simulator should be installed in a single centre (e.g. training institution) as this allows the maximum use of extremely expensive equipment.

- The question of approval and reapproval of the operating staff by the national safety authorities is under discussion and divergent. A minimum requirement could be that the safety authority verifies that simulator training and medical check-ups (including physical and psychological fitness) take place at regular intervals, e.g. one every two years and possibly approve operator training curricula.

- When initial qualification and requalification examinations are required, they could be attended by authority delegates. The use of simulators in examinations will be stressed in the future.

- It is also felt that both curriculum and instructor qualifications should be subject to periodic review by the national safety authority in the future.

- Some thinking should be done as to what staff other than shift staff should be trained on simulators.

SITING PRACTICES AND RELATED CONSIDERATIONS

Siting criteria as well as other safety standards of nuclear reactors depend on the policy of each country which has its own sovereignty. But the very basic and fundamental philosophy of safety related matters including siting should have something in common among nations which use the same or similar types of reactors and/or which have common national borders. As the number of NPPs sited near borders in EC countries increases, the Commission of the European Communities tries to encourage member states to apply a consistent approach in siting matters.

In order to reach this objective:

. The requirements of the national environmental policy should be met and in the future possibly those of border countries in cases where NPPs are located within a certain radius from borderlines or under certain circumstances.

. Siting policy should be open and accessible.

. Every reasonable effort must be made to inform and educate the public and to facilitate discussion.

Contrary to states which have at least partially low density populated and industrialized regions, remote siting or more distance as a substantial barrier cannot be a solution in most of the cases in EC countries. Instead EC countries have to look for safety measures which reduce the probability of the occurrence of accidents and guarantee a limitation of the consequences should an accident occur, and to apply high standards of operation in NPPs.

The basic practices or siting criteria used to decide a site's suitability are similar in all EC countries. These criteria are in many aspects similar to those applied in the USA, but the weighting of parameters considered is variable between countries and allows flexibility to authorities and utilities. Radiation protection factors are among the more important ones and include provisions for the routine release of radioactive wastes, the ease of applying counter-measures after an accident and the minimizing of the consequences of an accident.

As to the interrelationship between the scale of a possible accident and the choice of a site, it appears that the choice is mainly influenced by the moderate scale of accidents which affects only the population near the plant and for which counter-measures must be possible in providing emergency plans. Due to the small likelihood of severe accidents, their importance in site selection is not great. It was clearly established that at considerable distances from a site the difference between European sites is small, i.e. the consequences from severe accidents would be roughly the same [6].

EMERGENCY PLANNING AND PREPAREDNESS

Emergency plans in EC countries were revised and are still subject to or in the process of change. Emergency planning is now considered an important element in safety requirements and in most EC countries emergency plans must now even be implemented for NPPs located near the national borders. There are bilateral agreements established or in preparation which are designed a) to exchange information in case of reactor accidents which may result in radiological consequences in another country or

b) to provide mutual assistance in case of accidents. Such agreements would essentially ease legal problems such as crossing the frontier by rescue teams and equipment.

Distinct features of emergency plans are being compared in order to get some insight into the basic criteria, procedures, facilities, equipment, etc and a good estimate of the investment necessary for effective mutual assistance.

Some of the problem areas are commented upon in the following:

. It is clear that a nuclear emergency plan must form an integral part of the arrangements made to deal with non-nuclear emergencies and therefore depends on the national situations in the member states. Major accidents are too rare to justify a standing emergency team large enough to cope with all eventualities. Therefore arrangements exist for calling in support from other nuclear installations and other organizations (and countries). It is recognized, however, that a basic minimum stock must be provided to cover all the action, including counter-measures for the first days of the scale needed by the largest size of accident for which plans are being made.

. There is a critical evaluation of the necessary emergency centres and facilities underway. Practical experience of serious accidents has emphasized the need for more than one control centre and for the clear demarcation of control centre functions. No single structure of control centres has yet emerged as being generally preferred but in general one can find:

a) remote from the site:

- . emergency operation support centre
- . emergency press briefing centre

b) on-site:

- . technical support centre (emergency site operation)
- . radiation protection centre

There is agreement on a secondary emergency control centre located on or off-site.

. The greatest difficulty in making decisions about counter-measures is posed by the need to forecast the course of an accident and to estimate doses and dose reductions from situations that have not yet arisen. For this reason the initiation of the first phase of counter-measures should be based on NPP conditions as well as on measured releases of activity or environmental measurements.

. Factors in planning policy for counter-measures are the level of dose and the amount of dose that can be avoided. Counter-measures may include evacuation, the use of stable iodine and the control of foodstuffs, especially milk. EC countries have specified quantitative values on the initiation and scale of counter-measures (emergency reference levels). Counter-measures would be considered if the effective absorbed doses are likely to be in excess of a few rads. Typically, evacuation would be advisable only if the whole body dose due to exposure in open air over a period of several hours would attain values beyond 25 rem. Confinement indoors is considered an effective counter-measure. It is anticipated that any evacuation of the public around a site would only be required to a maximum distance of about 5 km. Monitoring for control of agricultural produce would be conducted to approximately 30 to 40 km. But these distances may be modified depending on the severity of the accident.

. Distribution of iodine blockers to the general public is not viewed in some countries as a viable counter-measure to be taken. Such measures may, however, be efficient and effective for selected groups like personnel of monitoring teams and police, on-site personnel and off-site emergency response support personnel.

. The seemingly low numbers relating to the evacuation zone are based on recent developments related to accidents involving extensive core damage which demonstrate that the source term is smaller than believed so far. Recent research developments suggest that iodine volatility has been grossly overestimated under water or steam-water mixtures and, furthermore, pressure and containment vessels appear to sustain loadings originating from possible steam explosion. Presently, design changes are being considered by EC countries which would minimize the release of radioactive gases during accident conditions (e.g. by providing filters).

REFERENCES

1. Council Resolution of 22 July 1975 relative to technological problems of nuclear safety. Official Journal of the European Communities No C 185/1, of 14 August 1975.
2. Commission of the European Communities. Safety principles for light water reactor nuclear power plants. COM(81) 519 final.
3. Council Directive of 15 July 1980 amending the Directives laying down the basic safety standards for the health protection of the general public and workers against the dangers of ionizing radiation. Official Journal of the European Communities L 246, Volume 23, 17 September 1980.
4. Commission of the European Communities, DIN Deutsches Institut für Normung e.v. Nuclear Standards. Catalogue and classification. Beuth 1981.
5. W. VINCK, G. VAN REIJEN. Possibilities and limitations of the development and the quantification of safety objectives. Commission of the European Communities. Brussels, Belgium.
International meeting on thermal nuclear reactor safety. August 29-September 2, 1982, Chicago,.
6. Commission of the European Communities. Nuclear safety in the context of the European Communities. The report of the Expert Group on Nuclear Safety. COM(80) 808 Final. Brussels, 10 December 1980.

US LICENSING REQUIREMENT TRACKING AND
INTEGRATION FROM ABROAD

Jesús Tapia and Xavier Jardí

Empresarios Agrupados
Magallanes, 3, Madrid - 15, Spain

ABSTRACT

An enormous amount of new licensing requirements and experiences are being developed in the US every day due to the process of licensing which issues a requirement for each operational event. Integration of these in the design, construction and operation of nuclear plants is an unachievable task if the traditional methods of filing and diffusion of papers are used.

The present paper discusses a methodology useful to make the requirements known by the persons concerned in an A/E firm outside the US. Four steps are made to achieve this goal:

1. Finding the new information from abroad: A comparison of methods and a criticism of the results is included
2. Assimilation of the new item and integration of the same. The qualification, functions and purpose of the technical team which develops this stage are described
3. Mechanization of the information into a data bank. The structuring and retrievability of data are explained
4. Synthesis and diffusion to persons concerned. The systematic process of selection and distribution of documentation through the use of the data bank are explained.

INTRODUCTION

The traditional licensing requirements in the USA are based on the definition of general safety objectives such as in-depth defence, general design criteria and on the development of these for more concrete cases through such specific standards as regulatory guides and BTP. This method is based on general postulations, the application and interpretation of which gives rise to specific standards.

As a result of the recent abnormal operating events, the licensability system is changing over from the deduction method to an endless casuistry caused even by various offices or Task Forces. This gives rise to an enormous amount of requirements which have to be met for plant licenses to be obtained. Both licensability personnel and plant design, construction and operating engineers are overwhelmed by this amount of requirements.

In the USA, the nuclear industry's reply to this casuistry has been through coalitions between plant owners who discuss the new requirements with the NRC and establish their own common organizations (NSAC, INPO), which analyze the new requirements and operating experience so that they might result in greater safety.

The situation is slightly different in countries far from the USA. It should be understood that in countries where there are not so many plants, the resources devoted to regulation and nuclear research are far less. Therefore, such countries do not have their own regulatory requirements to cover all nuclear power plant safety aspects; where there are no specific national standards, the Authorities apply the requirements of the country of origin of the reactor. All the NRC requirements become known to the Authorities of the country, through the existence of agreements and treaties for the exchange of information and evaluation. There is a logical delay in their transference and in their assimilation by foreign regulatory bodies but, in the majority of cases, they also become licensing requirements in these countries, with the only difference that they are requirements taken from other countries and, therefore, applied even more rigorously than in the country of origin. Moreover, the fact that there are fewer plant owners in these countries prevents the creation of powerful common bodies to respond to and analyze the requirements.

In view of this situation, the countries using American nuclear technology in practice are obliged to accept the NRC requirements and the responses and analyses of the owners' organizations.

Therefore, taking part in the actual process of gestation, development, discussion and evolution of requirements and licensing information is worthwhile so as to avoid delays in the acquisition of data important to the projects or misinterpretations caused by taking the criteria out of the original context. This participation can be achieved through agreements and treaties between the NRC and the Regulatory Agency of the country. The integration of the utilities' technical staff into U.S. owners' groups is also of interest, as is the regular attendance of technical meetings chaired by the ANS, AIF, IEEE, ASME and other, similar, organizations.

In order to collaborate and give proper support in resolving the danger of technical isolation, it has been thought wise to give special emphasis to establishing a well-designed method for following up the licensing requirements with a view to: (1) having prompt and accurate knowledge of the requirements, (2) selecting the most important, (3) assimilating them in an integrated manner, (4) distributing them to the interested parties so that plant design, construction and operation take them into account, and (5) speeding up the Licensing process based on the knowledge, fulfilment or justification of exceptions.

The method is shown graphically in Figure 1 and is described in the following paragraphs.

METHODOLOGY FOR KNOWLEDGE OF REQUIREMENTS

Conventional Methodology

The traditional sources of knowledge of requirements are basically the following:

- a. Standards and regulations (10 CFR, ASME, Regulatory Guides, Branch Technical Position, etc.)
- b. Periodic publications (Inside NRC, Nuclear News, Nuclear Standard News, etc.)
- c. Subscriptions to series of documents supplied by NTIS or other informative organizations (Nuclear Power Experiences, etc.)
- d. General information transmitted by the main suppliers of the nuclear system.

The traditional method poses certain problems which are illustrated below:

- a. Delay between the occurrence of an event or issuing a requirement and the reading of the document. This delay is caused by factors inherent to the process of preparation and distribution of publications, and is further increased for foreign countries because the publications take so much longer to arrive
- b. Lack of knowledge of the history and preparation of the requirements, since there are few documents in draft form, Minutes of Meeting and transcripts received by the traditional method
- c. This method does not guarantee the receipt of all requirements of interest, giving rise to the possibility of important gaps in knowledge
- d. Lack of a system and persons responsible for tracking requirements. The receipt of documents in the way a library receives them is not conducive to systematic assimilation of same, but rather to chance knowledge and then not necessarily by those who most require it. Unanalyzed documentation is stored on tables and files without being assimilated or used.

Present Methodology

There are two types of requirement, each needing a different methodology. On the one hand, there are data whose acquisition is required immediately, although in summarized form. These are data required, for example, for initiating certain studies or decisions which constitute a critical path at a certain stage of the project, for example the NRC requirements or exceptions to performing diesel reliability tests. If the matter is raised by the national licensing authority during the testing stage, NRC requirements on the matter have to be known immediately. On the basis of this information, a discussion with the Administration may be started or it may be decided to begin a study to justify the similarities to other diesels previously tested. In such cases, speed in acquiring the datum is more important than accuracy. The immediate acquisition of information requires the use of modern telecommunication methods. Although the use of what are now conventional

means, such as the telephone or telex, may be sufficient in certain cases, telephone/computer or computer/computer communication techniques offer more advantages, since the transmission of information does not require the presence or collaboration of the person receiving the information, provided that the information may be located in the computer. Since the NRC is equipped with a modern documentation control system, in the future it may be useful to establish computerized contact with the NRC system.

On the other hand, there is another type of information which has to be received continually since it reflects the daily evolution of requirements and the plants' response to the same. Table I shows the documents usually used as sources of information on licensing requirements. The table has been divided into five paragraphs, basically in descending order of binding nature. This information is acquired by more conventional means, by post or by subscription. A "standing request" including the basic information has been defined. This is automatically received without prior request. The number of documents in the standing request is limited and deals with those aspects consulted systematically and which need to be studied before the normal date of receipt of microfilmed subscriptions, which constitute the third source of significant information on licensing requirements.

INFORMATION PROCESSING

The average monthly number of documents received by the methods described above exceeds five hundred. Their length varies from one-page letters to documents of several hundred pages. Handling this amount of information requires a computerized data bank system. Two aspects should be considered in the information computerizing process: structuring information to put it in the bank and the definition of methods of access to input information.

Structuring of Information in the Data Bank

A double classification system is used; one depending on the type of document, and the other depending on content.

Classification by type of document is performed by administrative personnel, once guidelines have been defined by technical personnel. Depending on the type of report, the following process, which deals with the selection and classification of each document, is followed.

- a. Information on administrative procedures applicable to the USA but not the country in question is discarded (hearings, intervenors, antitrust, number of copies, etc.).
- b. Technical information not applicable to the types of reactor in design or operation in the country is filed but not put into the bank.
- c. Operating events or reports which are not significant (LER, Operation reports, etc.) are not considered. Significant operating experiences are summarized in other reports and the detailed compilation of each operating event is not required.

TABLE I

Systematic Information of Special Interest

A. REGULATIONS

- Advanced and Proposed Notices
- Petitions for Rulemaking
- Final Rules

B. ACCEPTED CRITERIA

- Regulatory Guides
- Standard Review Plan (including Branch Technical Position)
- Generic Letters
- TMI Action Plan Letters
- Code Committee Documents (ASME, IEEE, etc.)

C. INSPECTION AND ENFORCEMENT ACTIVITIES

- Bulletin, circular and info. notices
- Inspection reports

D. REPORTS

- NUREG
- Standard Tech. Spec.
- National Laboratories Report (ORNL, BNL, LASL, ANL, SANDIA, UCRL)
- Other Organization Reports (NSAC, EPRI, EGG, ERDA, EPA, TID, BEIR, ICRP, WASH)

E. U.S. LICENSING PROCESS

- SAR (Safety Analysis Reports)
- ES (Environmental Statement)
- Technical Specifications
- Test Procedures
- NRC & ACRS Meeting and Letters
- SER (Safety Evaluation Report)
- NRC Requests for Information
- USI (Unresolved Safety Issues) and GTI (Generic Technical Issues)
- Vendor Reports (NEDO, WCAP, etc.)

- d. Repetitive documentation is avoided (for example, only one specific IE Bulletin is filed and classified, even though it is sent to several plants).
- e. Each remaining document is given a generic and a sub-generic name. If the information is docketed, the generic name corresponds to the docket number. The sub-generic names of such documents represent the type of document (PSAR, Tech. Spec., Environmental Report, etc.).

If the information is non-docketed, it is assigned a generic name which corresponds to the issuing agency (EPRI, NRC, UCRL, etc.) or to the initials of a series of documents (NUREG, etc.). The sub-generic names of documents in this group indicate the collections within a publication series (e.g., within EGG, subgeneric names CAAP, EA, etc., are included) or the types of documents of the organization (e.g., within the generic name NRC, there are subgeneric names such as IE, GL, SECY, etc.).

Classification by content requires the dedication of technical personnel. The method of assigning keywords to each document is used. A limited number of these has been chosen, based on the frequency of use throughout the life of the information service. Component names and properties, characteristics and parameters are used. The use of very extensive and detailed lists complicates the assignation and information tracking processes.

Access to Information

Access to information is conceived with the same criteria as its input.

Lists may be requested on the basis of the type of document or date of issue or receipt or on the basis of content or keywords.

INTERACTION BETWEEN USERS AND THE INFORMATION CENTRE

Information needs of design, construction or operating personnel are determined by two basic factors: the general need for information to keep them up to date in such a rapidly changing field and the specific solution to particular problems related to design acceptability by the Administration.

In general, in keeping oneself up to date one comes up against the problem of there being so much documentation that someone working in a specific field would find it impossible to read it all. This is one of the problems which the information service tries to solve by using the procedures described in the preceding paragraphs. A matrix is established, which makes a correspondence between subject matter and users, which is used as a basis for issuing specific lists by areas so that distribution of subject matter of no interest to the user is avoided as far as possible. This table is handled directly by the computer. The subjects are defined by the most significant keywords.

However, the information centre's help in solving specific problems is more important. These problems are related to the interpretation of requirements or standards, the resolution of licensability or testing questions, the selection of

proposals with a view to their acceptability by the licensing Authorities, the development of studies with accepted hypotheses and methods and, in general, with the adaptation of the design to the ever-changing licensing requirements. In these cases, the use of the data bank is two-fold. On the one hand, the Licensability personnel require access to the bank as a back-up in the preparation of Summary Reports on Main Topics or Specific Studies about User's Concerns. On the other hand, a favourable situation is arising in which each design engineer uses the bank directly through interactive screens for specific and specialized problems in which the direct work of the specialist achieves greater efficiency than through the indirect channel of licensing personnel.

The interpretation and application of the requirements are the main subjects of interest and consultation. Table II gives a summary of some of the representative cases which have arisen in the last few years. Since standards deal with general cases with a very wide application, the interpretation and consideration of specific problems is required. The interpretation of a particular paragraph of a standard requires and is based on, firstly, an overall knowledge of all standards and reports issued on that subject. Secondly, the principles of Common Law are applied, i.e. the various previous NRC (Nuclear Regulatory Commission) actions in similar situations are observed and the position of the plants which was not questioned or was approved in the Safety Evaluation Reports is considered as acceptable. Thirdly, a case-by-case consultation with the Regulatory Agency's experts would be necessary.

There is much less use of the service as a back-up in the selection of proposals, although there have been some cases, for example, the selection of condenser tube materials or the acceptability of some systems such as the solidification method for the Radwaste System. One of the factors to be weighed when making the selection is component licensability. For this reason, statistics on approved components or licensing problems with such components are interesting. Nevertheless, this philosophy basically applies to new or very special systems in which problems are suspected.

Another important aspect of interaction between information and design is the establishment of criteria, hypotheses and methodology for developing new studies or design parameters. One of the first stages in the development of new specialized groups, such as the analysis of probabilistic risks or reliability studies, is the compilation and analysis of criteria, procedures and studies accepted for other plants. The same philosophy applies to present matters whose requirements are under discussion. The environmental qualification of electrical components or the design and installation of post-accident monitoring instrumentation requires daily contact with documentation on the subject.

As a final point on the interfaces between design and information, there are two specific fields with an abundance of documentation and great repercussion on design: post-TMI requirements and Inspection and Enforcements requirements. These subjects have been dealt with by a detailed procedure and an accurate follow-up. Specific dossiers have been prepared on each subject which deals with the definition of requirements, the response to some of American plants and owners groups and the detailed analysis of applicability and impact on Spanish plants which have been analyzed. The client, assessed by the Engineers, has taken specific actions and made specific modifications.

TABLE II

Examples of Subjects on Interpretation of Requirements

A. REGULATORY GUIDES

- A.1 R.G. 1.52
 - Acceptability of a single filter in redundant trains, for old plants
- A.2 R.G. 1.63
 - Interpretation of generic requirements on electrical penetrations on the basis of compliance proposed by the plants
- A.3 R.G. 1.68.3 (old 1.80)
 - Acceptability criteria for air loss test in safety pneumatic valves with accumulators
- A.4 R.G. 1.92
 - Specific details on modal and spatial response combination for seismic response analysis

B. BRANCH TECHNICAL POSITIONS

- B.1 ASB 3.1
 - Simultaneous rupture of high energy lines outside containment and SSE. Conflict between ANS 52.1 and BTP
- B.2 ASB 9.5.1
 - Consideration of high or normal site seismicity to determine seismic classification of hose stations
 - Simultaneity of fire and other accidents, when the former is caused by the latter in non-qualified electrical circuits
 - Acceptance criteria for structural barriers as qualified to withstand fire for 3 hours
- B.3 EICSB-15
 - Present non-applicability of this position (regarding classification of Reactor Coolant Pump Breakers) although it has not been withdrawn
- B.4 RSB 5.1
 - Plant response and exceptions to cold shutdown requirements with safety equipment

C. OTHERS

- C.1 NUREG CR-446
 - Clarification of its non-mandatory nature
- C.2 IEEE-308
 - IE Classification of Space Heaters for Class IE Motors. Dependence on the damage which they could cause during an earthquake

As a specific aspect in Spain, the follow-up of the so-called reference plant is of interest, since it is also subject to interactions between the information service and design. This is a concept which is not delineated with complete precision and, naturally, does not imply total similarity. There are cases of reference plants with different capacities, types of containment or site characteristics, even though they are on the lines of the Spanish plant. This concept is used by the Licensing Authorities and has become a sort of pattern or model which is used to measure the safety of the facility itself. Nowadays, there is a greater tendency towards "reference design" than to the reference plant. The reference design may be a type of envelope of the characteristics of American plants of the same type of those of the particular country. In any case, it is worthwhile making a comparison with the reference plant as a measure prior to evaluation by the Regulatory Agency. This requires an analysis of the NRC conditions in the SER, and also the responses from the utilities and an evaluation of the impact which these requirements have on our plant.

CONCLUSIONS

Several interesting conclusions may be drawn from the above explanation.

Nowadays, the Licensing man cannot base his work only on a file or his own memory. This would cause him professional anxiety since he would consider it impossible to be familiar with all the numerous licensing requirements. The present excess of paper should be reduced by the selection, structuring and precision of an information service.

Modern information processing means to acquire, distribute and apply the present requirements were described and found adequate.

The application of these methods is an effective tool for a dynamic, organized technical group.

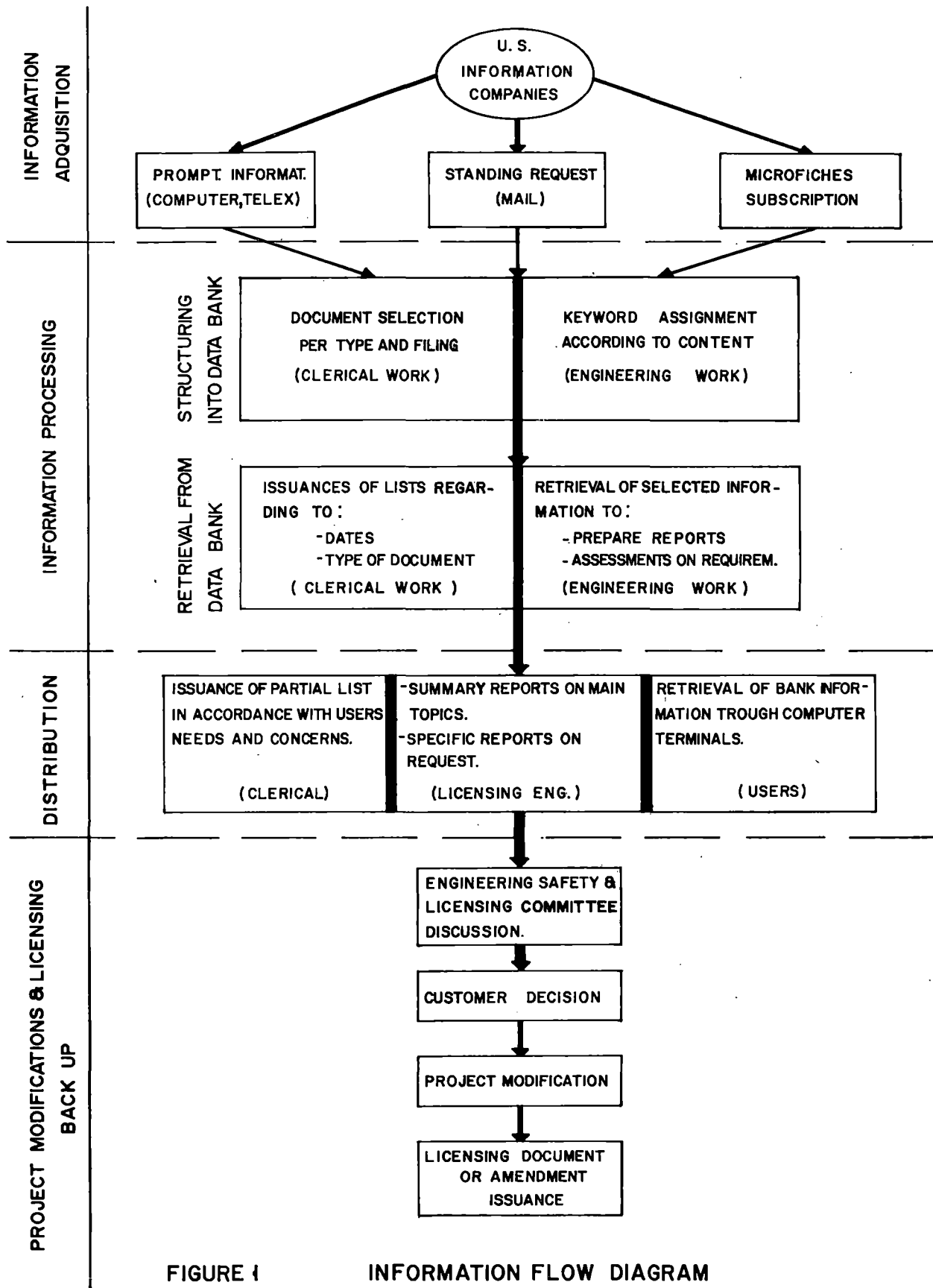


FIGURE 1

INFORMATION FLOW DIAGRAM

SESSION 25

LOCA ANALYSIS

Chair: B. W. Spencer (ANL)

MODERATOR BOILING ON THE EXTERNAL SURFACE
OF A CALANDRIA TUBE IN A CANDU REACTOR
DURING A LOSS-OF-COOLANT ACCIDENT

G.E. Gillespie and R.G. Moyer

Whiteshell Nuclear Research Establishment
Pinawa, Manitoba, ROE 1LO, Canada

P.D. Thompson

Atomic Energy of Canada Engineering Company
Mississauga, Ontario, Canada

ABSTRACT

Each fuel channel in a CANDU-PHW* reactor consists of a pressure tube inside a calandria tube, with a gap containing insulating gas between them. The calandria tubes are surrounded by cool heavy-water moderator. This water would act as a supplementary heat sink during postulated loss-of-coolant accidents if the primary cooling and emergency coolant injection systems failed to remove the decay heat from the fuel. In such cases, the heat would be transferred radially to the heavy-water moderator and removed by its cooling system.

If a pressure tube were to overheat and deform into contact with its calandria tube, the heat transfer to the moderator would increase. The heat stored in the pressure tube would cause a spike in the heat flux, which might result in film boiling on the outside of the calandria tube. Should film boiling occur, the effectiveness of the moderator as a heat sink might then be reduced.

This paper describes a simple one-dimensional model developed to analyze the thermal-mechanical behaviour of a fuel channel when a pressure tube creeps circumferentially into contact with its calandria tube. Also described is a series of experiments in which a pressure-tube segment is pressurized and heated so that it contacts a surrounding calandria-tube segment. Predictions made using the model are compared with the experimental results.

INTRODUCTION

The CANDU-PHW reactor has a high-pressure primary cooling system and a low-pressure, independently cooled moderator system. The fuel and coolant are separated from the moderator by a fuel channel, which consists of a pressure tube and a calandria tube separated by a gas-filled gap. The zirconium pressure tube is designed to contain the high-pressure heavy-water coolant, and the gas-filled gap is designed to insulate the cool moderator from the hot coolant during normal operation. Figure 1

* Canadian natural-uranium fuelled, heavy-water moderated and cooled reactor (CANada Deuterium Uranium-Pressurized Heavy Water)

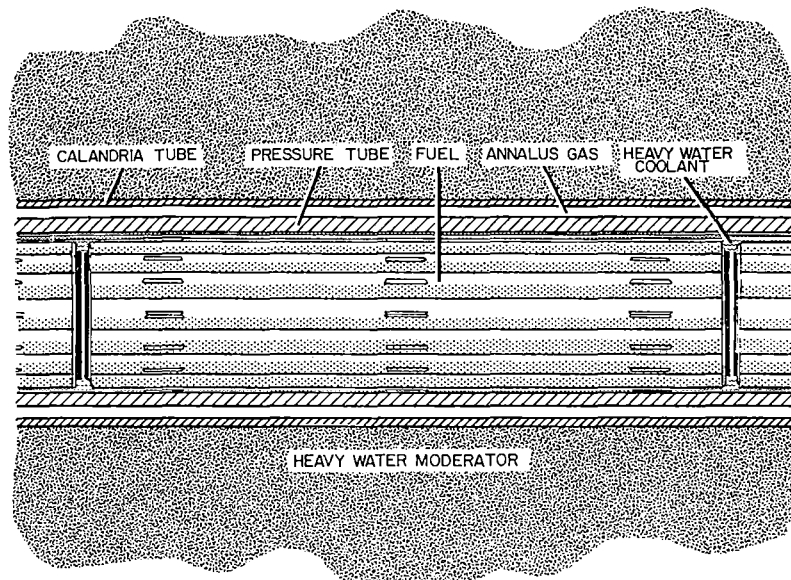


FIGURE 1. FUEL CHANNEL ARRANGMENT

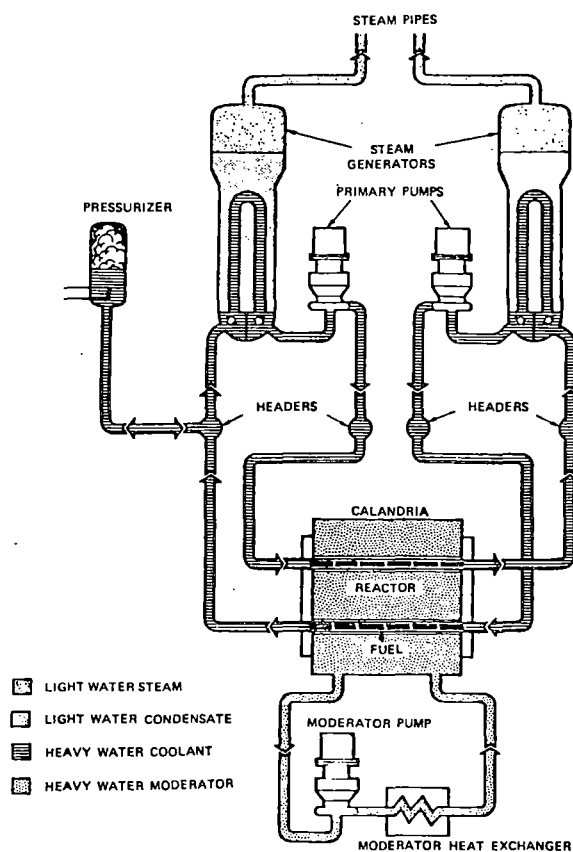


FIGURE 2: Simplified diagram of a CANDU heat transport system

is a schematic of a CANDU fuel channel, and Figure 2 shows a typical arrangement of fuel channels in the reactor core. In this reactor design, each fuel channel is surrounded by cool heavy-water moderator that can act as a sink for heat generated in the fuel if other means of heat removal fail.

For example, if there were a loss-of-coolant accident (LOCA), and coincident impairment of the emergency coolant injection system, the heat generated in the fuel would be transferred mainly by thermal radiation to the pressure and calandria tubes, and then by boiling heat transfer to the moderator. Because radiation is the principal mode of heat transfer in this case, high temperatures in the fuel and pressure tube would result. At elevated temperatures, the pressure tube may deform into contact with the surrounding calandria tube. If its internal pressure were high, the principal deflection of the pressure tube would be radially outwards, and contact would occur completely around the circumference. If the internal pressure were low, the principal deflection would be downwards, and contact would occur in a strip along the bottom.

The initial contact between the hot pressure tube and the cold calandria tube would result in a "spike" in the heat flux to the moderator. The magnitude of the spike would depend on the pressure-tube temperature at contact and the contact conductance between the pressure and calandria tubes. The magnitude of the spike would determine the boiling regime on the calandria tube surface (either film boiling or nucleate boiling) and, thus, the rate of heat removal.

This paper describes a one-dimensional model developed to analyze the thermal-mechanical behaviour of a fuel channel when a pressure tube creeps radially into contact with its calandria tube. Also described are results of experiments [1] in which a pressure-tube segment is pressurized and heated at a constant rate until it contacts a surrounding calandria-tube segment. Predictions of the one-dimensional model are compared with the experimental results.

ANALYSIS

A coupled, one-dimensional thermal-mechanical computer model, CONTACT, was developed to analyze the fuel channel during and after pressure tube/calandria tube contact. The model predicts the deformation of the pressure tube prior to contact, the transfer of heat to the moderator after contact, and the mechanical deformation of the pressure tube and calandria tube following contact.

The deformation of the pressure tube prior to contact is calculated assuming that deformation is time-dependent (creep). The transverse creep rate in an internally pressurized tube is given by

$$\dot{\epsilon}_t = A \exp \left(\frac{-Q}{RT} \right) \sigma_t^n$$

where $\dot{\epsilon}_t$ is the transverse creep rate
 A is the creep constant
 Q is the creep activation energy
 R is the ideal gas constant
 T is temperature
 σ_t is transverse stress
 n is the stress exponent.

Substituting

$$\dot{\epsilon}_t = \frac{1}{r} \frac{dr}{dt} \quad \text{and} \quad \sigma_t = \frac{Pr}{w}$$

where r is the radius

t is time
P is the internal pressure
w is the wall thickness

and using the fact that the volume is constant, yields the following expression, which can be integrated numerically to obtain the inner radius of the pressure tube at any time t:

$$r = r_o + \int_{t_o}^t A \exp\left(\frac{-Q}{RT}\right) r \left(\frac{Pr^2}{r_o w_o}\right)^n dt$$

where r_o is the original inner radius
 w_o is the original wall thickness.

After contact, the pressure and calandria tubes creep at the same rate. Thus

$$A_c \exp\left(\frac{-Q_c}{RT_c}\right) \left(\frac{P_c r}{w_c}\right)^n = A_p \exp\left(\frac{-Q_p}{RT_p}\right) \left(\frac{(P-P_c)r}{w_p}\right)^n$$

where subscript c refers to the calandria tube, subscript p refers to the pressure tube, and r is the inner radius of the combined pressure/calandria tube.

Using the value of P_c determined from the above equation, the pressure-tube radius can be determined by numerically integrating

$$r = r_o + \int_{t_o}^t A_p \exp\left(\frac{-Q_p}{RT_p}\right) r \left(\frac{(P-P_c)r^2}{r_o w_o}\right)^n dt$$

Figure 3 is a schematic of the heat-transfer model used to determine the post-contact thermal behaviour. This model predicts the transient heat transfer along a radius through the pressure and calandria tubes. The heat-conduction equation is solved using a one-dimensional finite-element subroutine. The difficulties in

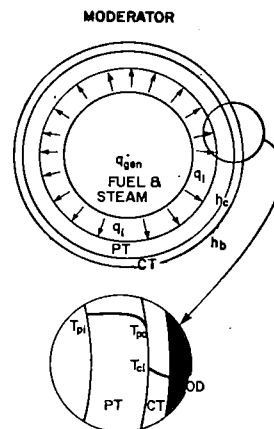


FIGURE 3 SCHEMATIC OF PRESSURE-TUBE / CALANDRIA-TUBE CONTACT HEAT-TRANSFER PROBLEM

analyzing the problem lie in specifying the boundary conditions. The boundary condition on the inside surface of the pressure tube is an incident heat flux, which is determined by the heat generated in the fuel due to the decay heat and the reaction between zirconium and steam.

The heat flux at the outside surface of the calandria tube is described by

$$q_o = h_b(T_{co} - T_B)$$

where q_o is the heat flux to the moderator
 h_b is a pool-boiling heat-transfer coefficient
 T_B is the outside temperature of the calandria tube
 T_{co} is the bulk moderator temperature.

The heat-transfer coefficient, h_b , depends on the type of boiling that occurs with the given subcooling, the saturation temperature, the outside surface temperature of the calandria tube, and the heat flux. In the model, h_b is defined for four regimes [1,2]: subcooled, nucleate boiling, transition boiling, and film boiling. The equations were based on experiments by Thibault [3], Rohsenow [4], Bradfield [5], and Dhiri and Purohit [6], using large diameter horizontal cylinders.

At the interface between the pressure and calandria tubes, the contact conductance determines the rate at which the heat stored in the pressure tube is transferred to the moderator immediately after contact; thus, it also affects the pool-boiling regime. The contact conductance, h_c , is described by the following relationship:

$$q_c = h_c (T_{po} - T_{ci})$$

where q_c is the heat flux between the tubes
 h_c is the contact conductance
 T_{po} is the temperature of the outer surface of the pressure tube
 T_{ci} is the temperature of the inner surface of the calandria tube.

Correlations have been developed that use the surface parameters (hardness, size and shape of surface asperities), the contact pressure and the type of gas between the tubes to predict the contact conductance [7,8]. However, when these predicted values are used in the model CONTACT, incorrect heat flows are predicted for experiments in which pressure-tube segments are deformed circumferentially into contact with surrounding calandria-tube segments. In this paper, the results of such experiments are compared with predictions from the model, based on assumed values of contact conductance. From these comparisons, an improved value for the contact conductance is obtained.

EXPERIMENTS

The experimental apparatus, shown in Figure 4, consisted of a pressure-tube segment, 1.5 m long, surrounded by a calandria-tube segment, 1.8 m long. Inside the pressure tube was a tubular electric heater, 1.0 m long. The apparatus was mounted inside a water tank with viewing ports in the sides, with the water being heated by submerged steam lines.

The experiments were performed by heating the water to the desired temperature, internally pressurizing the pressure tube, and then heating the pressure tube by applying power to the heater.

In each experiment, cine films (at 80 frames per second) were taken of the outer surface of the calandria tube. The type of boiling was noted visually, and the surface temperature of the calandria tube was monitored by 18 thermocouples spot-welded to the surface. Film boiling left a very distinct oxidized area on the surface.

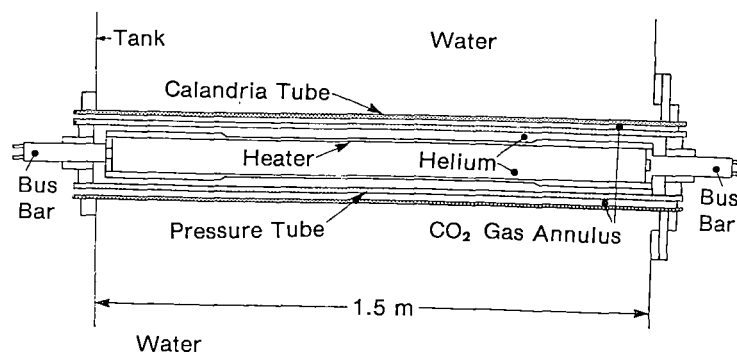


FIGURE 4 EXPERIMENTAL ARRANGEMENT

The experimental conditions and the resulting contact temperatures are listed in Table 1. The pressure-tube temperature at contact is a function of the internal pressure of the tube and its heating rate (controlled by the heater power).

TABLE I

Experimental Conditions

Test	Power (kW)	Pressure (MPa)	Water Temperature (°C)	Contact Temperature (°C)
1	66	4	67	760
2	57	4	85	760
3	66	1	74	860
4	66	1	67	860
5	57	2.5	77	760
6	62	4	81	750
7	66	2.5	77	820
8	66	2.5	77	800
9	62	1	80	900
10	62	4	85	750
11	62	2.8	85	820
12	84	1	85	1000
13	28	0.5	71	1070
14	- *	1.1	71	825
15	- *	0.8	71	900
16	54	2.0	99	800

* Power varied to obtain the desired contact temperature.

Figure 5 summarizes the results of the experiments. Each experiment is plotted as a point, with the pressure-tube temperature at contact as the abscissa and the temperature of the pool of water surrounding the calandria tube as the ordinate. The

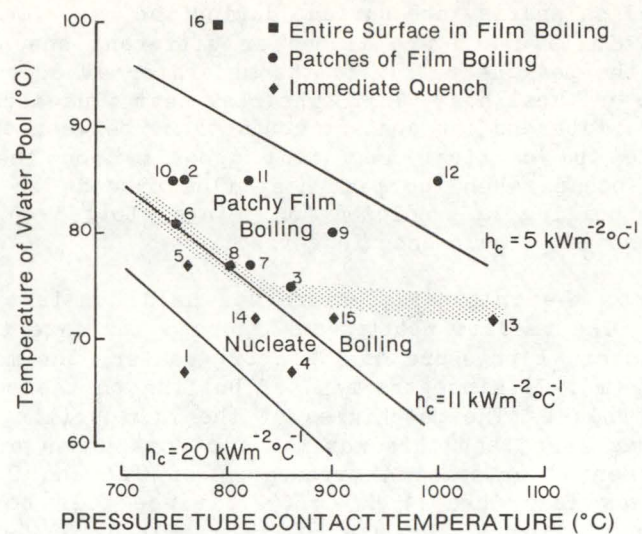


FIGURE 5 SUMMARY OF EXPERIMENTAL RESULTS

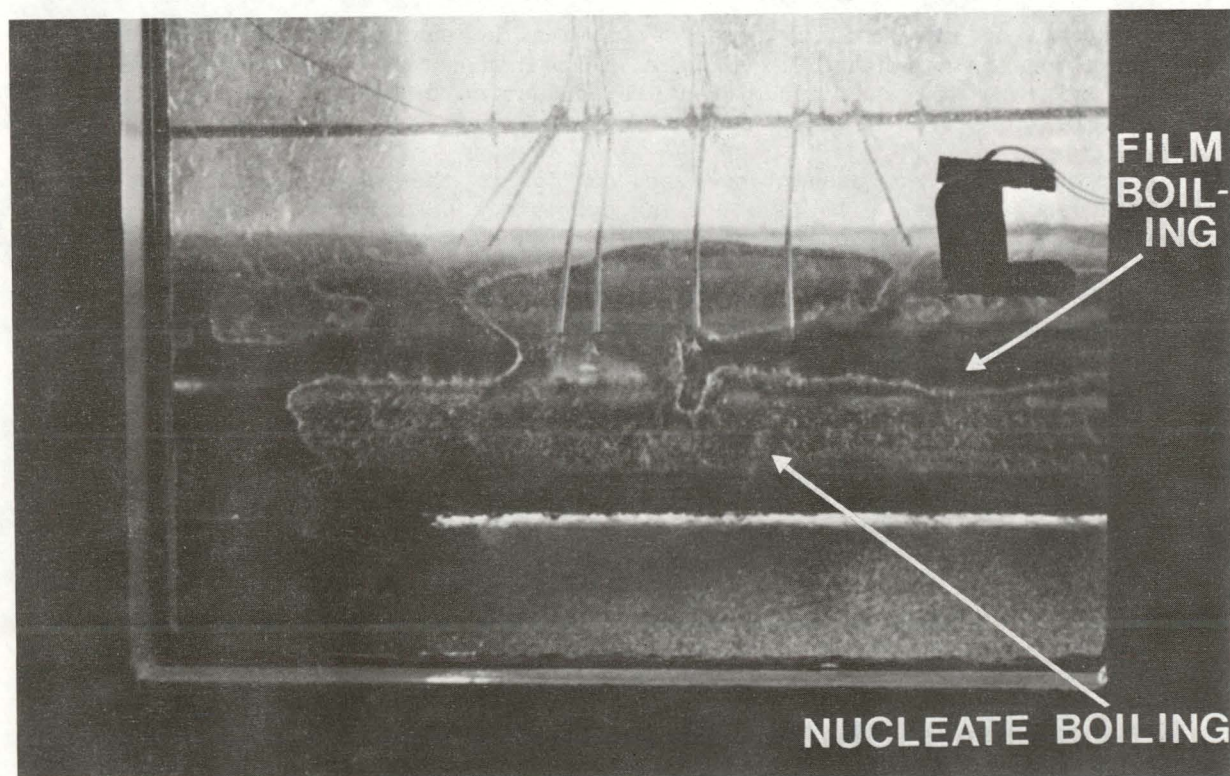


FIGURE 6 BOILING ON CALANDRIA TUBE SURFACE (EXPERIMENT 11)

type of boiling on the calandria-tube surface during the experiment is denoted by the symbols. Also shown in Figure 5 are lines for different assumed contact conductances, showing where the peak heat flux to the moderator at contact, as predicted by the model, equals the critical heat flux. The peak heat flux depends upon the stored energy of the pressure tube and the contact conductance between the pressure tube and calandria tube, while the critical heat flux depends upon the subcooling of the water. Film boiling occurs when the peak heat flux exceeds or equals the critical heat flux; thus, film boiling is predicted for points plotted on the graph above the line if the assumed contact conductance is correct.

In each experiment, the internal pressure was held constant at a value ranging from 0.5 to 4.0 MPa. The results plotted in Figure 5 indicate that, for all of the experiments with an internal pressure of 1 MPa or greater, the maximum local contact conductance was $11 \text{ kW}/(\text{m}^2 \cdot ^\circ\text{C})$ since the type of boiling on the surface was correctly predicted using this value. The patchiness of the film boiling indicates that the contact conductance was less than this maximum for most areas around the circumference. In the experiments performed at pressures of 0.7 and 0.5 MPa, the maximum contact conductance was less than $11 \text{ kW}/(\text{m}^2 \cdot ^\circ\text{C})$, since film boiling would be predicted, and it did not occur. The use of this method to determine the contact conductance assumes that the incident heat flux, determined from the known heater power, and the heat-transfer coefficient at the surface of the calandria tube used in the model, are correct.

In nine of the experiments, film boiling occurred in patches that did not completely cover the area of contact. Figure 6 shows the patches of nucleate and film boiling that occurred in a typical experiment. This behaviour is related to the variation of contact time, temperature, and pressure at a given axial location. The variation of these parameters causes the contact conductance to vary around the circumference.

The patches of film boiling rewet, even when the average incident heat flux is higher than the minimum heat flux required to maintain film boiling. The rewetting is caused by the axial and circumferential conduction of heat through the pressure and calandria tubes from areas of film boiling to areas of nucleate boiling.

To further check the assumptions used to derive the one-dimensional model, an experiment was performed with film boiling completely around the calandria-tube surface. Table 1 lists the conditions used in the experiment (number 16). To obtain this uniform film boiling and the resultant uniform temperatures, the experiment was performed in nearly saturated water. The critical heat flux [9] was a factor of two lower than that of the previous experiments, enabling film boiling to be established over the complete area of contact. The value of subcooling for this experiment was much lower than that expected in the moderator of a CANDU reactor.

Figure 7 shows the temperature of the pressure tube during the experiment in which film boiling occurred completely around the circumference. Figure 8 shows the temperatures obtained from the ring of thermocouples at the axial center of the calandria tube. In the experiment, the power was held constant at 54 kW/m for 250 seconds; then it was increased to 56 kW/m. At 300 seconds, the power was increased to 62 kW/m. At 340 seconds, the internal heater failed and the experiment was terminated. The temperature traces shown in Figures 7 and 8 show that the whole circumference of the calandria tube was surrounded by a steam film and that the behaviour could be reasonably approximated by a one-dimensional model.

Figure 9 compares the average pressure-tube and calandria-tube temperatures obtained during this experiment with the values predicted using the one-dimensional model with a contact conductance of $11 \text{ kW}/(\text{m}^2 \cdot ^\circ\text{C})$ and assuming that the incident heat flux was uniform. The pressure tube heated up very rapidly prior to contact. Contact occurred at 78 seconds, when the pressure-tube temperature was 800°C . The model predicted the heatup very well and the correct contact time and temperature.

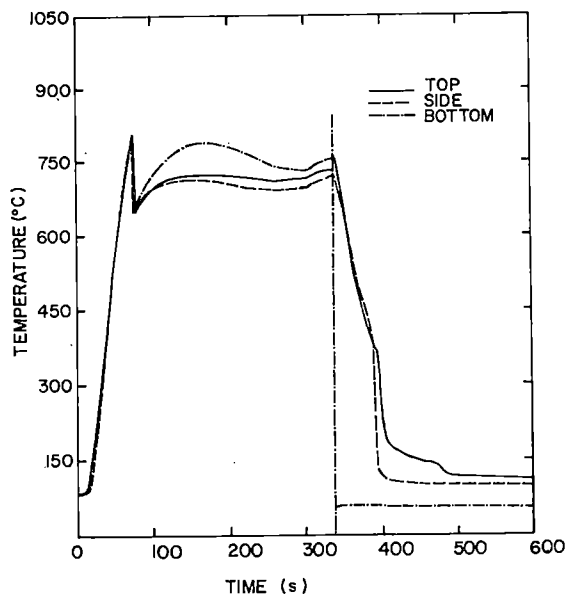


FIGURE 7 TIME VARIATION OF PRESSURE-TUBE TEMPERATURE

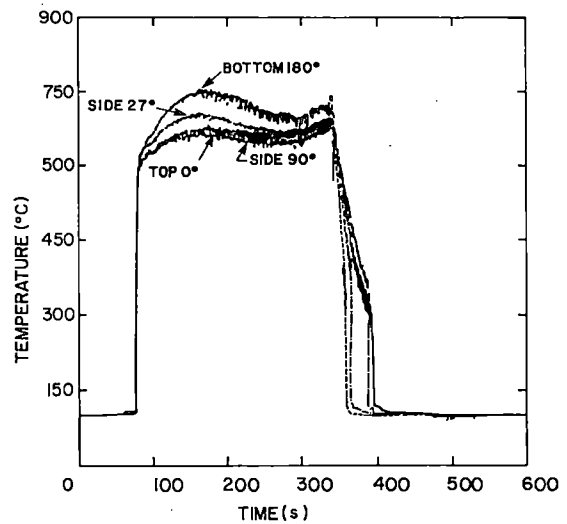


FIGURE 8 TIME VARIATION OF CALANDRIA-TUBE TEMPERATURE

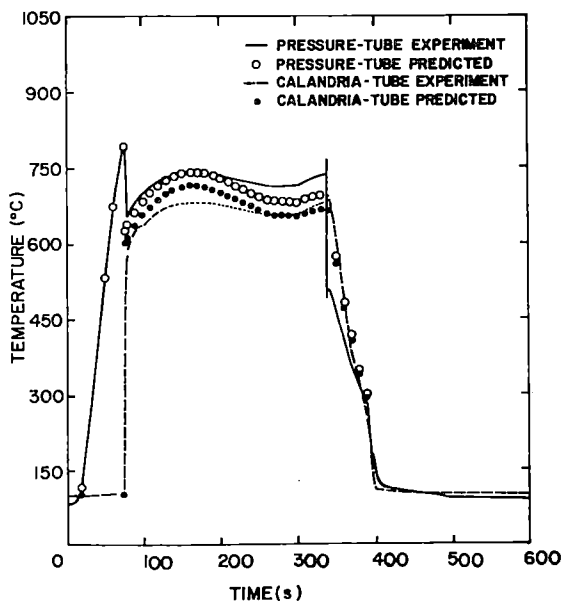


FIGURE 9 COMPARISON OF EXPERIMENTAL RESULTS WITH PREDICTIONS

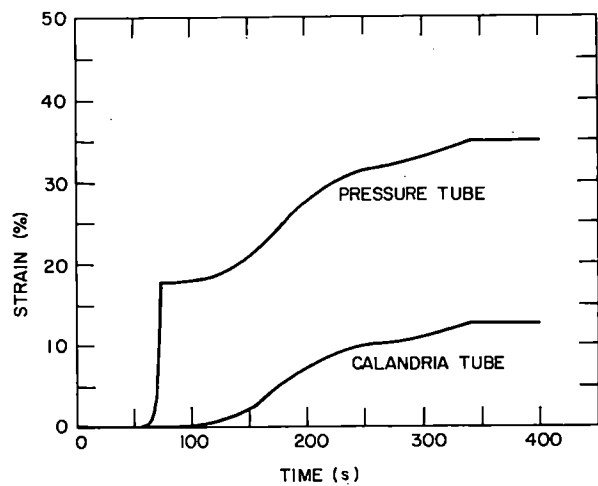


FIGURE 10 PREDICTED STRAIN

Immediately after contact, the pressure-tube temperature fell rapidly and the calandria-tube temperature increased rapidly. Film boiling was established on the surface of the calandria tube. The model predicted this behaviour, but the predicted pressure-tube temperature was lower than that measured and the predicted calandria-tube temperature was greater than that measured, indicating that the assumed value of contact conductance ($11 \text{ kW}/(\text{m}^2 \cdot ^\circ\text{C})$) was higher than the actual value. The temperature of the tubes then slowly increased to a maximum at 165 seconds. This maximum occurred when the heat transmitted through the steam film equalled the heat generated inside the pressure tube. While the calandria tube deformed radially, its surface area increased, whereas the heat flux from its surface depended only on the surface temperature. Therefore, the total heat transferred to the surrounding water increased and the calandria-tube temperature decreased. At 250 seconds, the power was increased to $56 \text{ kW}/\text{m}$, and the rate at which the temperature was falling decreased. At 300 seconds, the power was increased to $62 \text{ kW}/\text{m}$ and the temperatures increased. The model correctly predicted the effects of these power changes. The test was terminated when the heater failed at 340 seconds. Figure 10 shows the strain predicted by the model. The good agreement between the measured and calculated temperatures implies that the strain calculations are reasonably accurate because of the sensitivity of the heat transfer to the surface area. The final deformation of the calandria tube was 15%, close to the calculated value of 13%.

CONCLUSIONS

- (1) The computer model CONTACT gave correct qualitative predictions of the occurrence of film boiling for experiments with an internal pressure $\geq 1 \text{ MPa}$, when a value of $11 \text{ kW}/(\text{m}^2 \cdot ^\circ\text{C})$ was used as the contact conductance.
- (2) The model successfully predicted the behaviour of experiments in which multidimensional effects were not significant. In those in which multidimensional effects were significant, pressure- and calandria-tube temperatures were over-predicted.
- (3) In all of the experiments with subcooling of 14°C or greater, film boiling occurred in patches. These patches eventually rewet because of conduction through the tubes from regions of film boiling to regions of nucleate boiling.
- (4) The purpose of these experiments was not to simulate reactor conditions, but to obtain an understanding of the thermal-mechanical behaviour of a calandria tube as a result of boiling on the external surface. At the expected degree of subcooling in a CANDU reactor, the experiments show that film boiling is unlikely to occur, that heat transfer to the moderator is sufficient to remove the heat generated in the fuel channels and that calandria tubes will not deform.

ACKNOWLEDGEMENT

The financial support of this work by Ontario Hydro is gratefully acknowledged.

REFERENCES

1. G.E. GILLESPIE, "An Experimental Investigation of Heat Transfer from a Reactor Fuel Channel to Surrounding Water", Proceedings of the Canadian Nuclear Society Annual Conference, June 10, 1981.
2. G.E. GILLESPIE, R.G. MOYER, R.S.W. SHEWFELT, "Experiments to Investigate Moderator Boiling when a Pressure Tube Contacts its Calandria Tube", unpublished Report WNRE-401, Whiteshell Nuclear Research Establishment (1980).

3. J. THIBAUT, "Boiling Heat Transfer Around a Horizontal Cylinder and in Tube Bundles", Ph.D. Thesis, McMaster University, Hamilton Ontario, 1978.
4. W.M. ROHSENOW, ed., Developments in Heat Transfer, The MIT Press, Cambridge, Massachusetts, (1964) p. 216.
5. W.S. BRADFIELD, "On the Effect of Subcooling on Wall Superheat in Pool Boiling", Journal of Heat Transfer 89, 269 (1967).
6. V.K. DHIR and G.P. PUROHIT, "Subcooled Film-Boiling Heat Transfer from Spheres", Nuclear Engineering and Design 47, 49 (1978).
7. M.M. YOVANOVICH, "New Contact and Gap Conductance Correlations for Conforming Rough Surfaces", AIAA 16th Thermophysics Conference, AIAA-81-1164, June 1981.
8. M.H. SCHANKULA and D.W. PATTERSON, "A Review of Thermal Contact Conductance Correlations for Pressure Tube-Calandria Tube Contact", Unpublished Report WNRE-155, Whiteshell Nuclear Research Establishment (1982).
9. L.A. BROMLEY, "Heat Transfer in Stable Film Boiling", Chemical Engineering Progress 46, 221 (1950).

THERMAL BEHAVIOUR OF A CANDU-PHW REACTOR FUEL CHANNEL CONTAINING NEARLY STAGNANT STEAM

G. E. Gillespie, W. C. Harrison,
J. G. Hildebrandt, and G. A. Ledoux
Whiteshell Nuclear Research Establishment
Atomic Energy of Canada Limited
Pinawa, Manitoba, R0E 1L0, Canada

ABSTRACT

A unique feature of the CANDU-PHW* reactor design is that the fuel channels are submerged in a low-temperature pool of heavy-water moderator. As with other reactor designs, an Emergency Coolant Injection (ECI) system would act to prevent fuel damage in postulated loss-of-coolant accidents. However, should the ECI system fail or be inadequate, heat transfer to the heavy-water moderator surrounding each fuel channel would limit the maximum temperatures. A computer model, CHAN II, has been developed to analyse the thermal response of the CANDU fuel channel for this situation. The model includes heat transfer radially from the fuel elements to the moderator, and accounts for axial convective heat and mass transfer and the heat and hydrogen produced by the chemical reaction between zirconium and steam.

This paper includes a brief description of the model, predictions of temperatures and hydrogen production obtained using the model for a sample case, and a comparison of the model predictions with the results of experiments in which dry steam flowed through an annulus between two zirconium tubes with the inner tube heated.

INTRODUCTION

In the CANDU-PHW reactor, the hot, high-pressure heavy-water coolant is separated from the cool, low-pressure heavy-water moderator by fuel channels. The fuel channels consist of pressure and calandria tubes separated by gas-filled gaps. Figure 1 is a schematic of a CANDU fuel channel and Figure 2 illustrates the arrangement of fuel channels in the reactor core. A unique feature of the design is that the cool heavy-water moderator surrounding the fuel channels can serve as a supplementary heat sink during a loss-of-coolant accident if emergency coolant injection is insufficient to cool the channel.

The fuel and primary coolant conditions are similar to the conditions assumed for degraded core cooling studies for LWR** power plants, the difference being the moderator heat sink distributed within the core. The heat source is the decaying fuel, augmented by any heat generated by the chemical reaction between zirconium and steam. Since thermal radiation is the main heat-transfer process, high temperatures result. This means that most of the heat initially produced will be stored in the fuel and the pressure tubes.

* CANada Deuterium Uranium - Pressurized Heavy Water

** Light Water Reactor

A computer code, CHAN II, has been developed to predict the fuel channel thermal behaviour and hydrogen production when primary and emergency coolant injection are inadequate. CHAN II uses lumped-parameter models for heat transfer. An experimental program is currently underway to verify the various submodels in the program.

CHAN II is described briefly in this paper, and the results of a sample case are presented. To check the model, a small-scale experiment has been done using a single-element heater with a zirconium sheath to determine the convective and radiative heat transfer and hydrogen production. Results from this experiment are compared with the predictions of the CHAN II model.

DESCRIPTION OF THE COMPUTER MODEL CHAN II

CHAN II [1] is a computer model consisting of a set of time-dependent differential equations derived from a lumped-parameter analysis of the heat generated in the fuel channel, the convective axial heat transfer, via flowing steam and hydrogen, and the radial heat transfer to the moderator, via conduction and radiation. The differential equations are solved using FORSIM [2], a FORTRAN-oriented simulation package.

Each CANDU fuel channel contains 12 or 13 half-metre long fuel bundles (depending on the particular reactor). In the model, the fuel channel is divided into 12 or 13 axial segments which coincide with the fuel bundles. Heat is convected axially from segment to segment by a specified steam flow. Each axial segment is approximated by a system of annular rings, as shown in Figure 3. In the 37-element bundle, the fuel elements are arranged in three rings around a central element. The use of closed rings to model this geometry is conservative for estimating fuel temperatures since radiative heat transfer only occurs between adjacent rings.

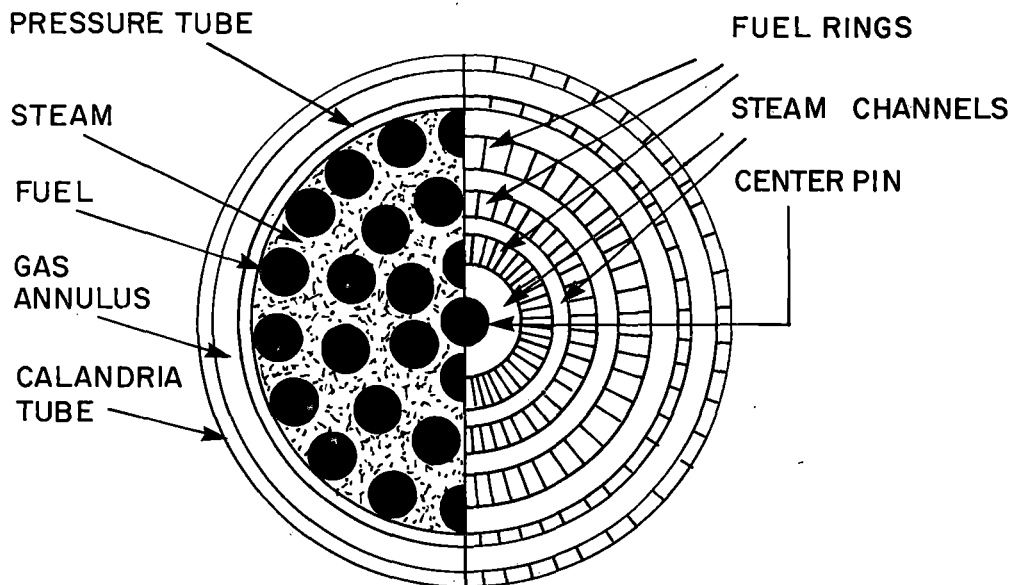


Figure 3: CHAN II Ring Model

Radiation is the principal mode of heat transfer between the fuel rings and between the outer fuel ring and the pressure tube. However, heat will also be transferred by convection if there is steam flow in the channel, or by conduction through the gas mixture if there is no steam flow. The channel initial conditions are taken from models that calculate the thermalhydraulics of the reactor circuit. Since the thermalhydraulic models cannot accurately predict flows when the channel flow is near stagnation, CHAN II is used to determine the thermal behaviour, using assumed steam flows. The temperature distribution in the central fuel pin is assumed to be uniform. Each fuel ring is approximated by two equal-area annular segments, to account for the radial temperature gradient. The heat balance for the inner half is

$$\begin{aligned} \frac{m}{2} C_p \frac{dT_i}{dt} = & \text{heat produced by radioactive decay in half the } \text{UO}_2 \\ & + \text{heat produced by the zirconium-water reaction on the} \\ & \text{inner half of the sheath} \\ & + \text{heat radiated from adjacent inner fuel ring} \\ & - \text{heat convected to the gas mixture} \\ & - \text{heat transferred across the fuel ring.} \end{aligned}$$

For the outer half the heat balance is:

$$\begin{aligned} \frac{m}{2} C_p \frac{dT_o}{dt} = & \text{heat transferred across the fuel ring} \\ & + \text{heat produced by radioactive decay in half the } \text{UO}_2 \\ & + \text{heat produced in the outer half of the fuel} \\ & \text{sheath by the zirconium-water reaction} \\ & - \text{heat radiated to the adjacent outer fuel ring} \\ & \text{(or pressure tube)} \\ & - \text{heat convected away by the gas mixture.} \end{aligned}$$

where m is the mass of the fuel in the ring

C_p is the specific heat of the fuel in the ring

T_i is the temperature of the inner half of the ring

T_o is the temperature of the outer half of the ring

t is time.

The decay heat is specified using the decay power fraction given by Whittier et al. [3]. The heat produced and the hydrogen liberated by the zirconium-water reaction are calculated assuming that the reaction rate is parabolic, using constants measured by Urbanic and Heidrick [4].

The heat transferred radially from the fuel to the moderator passes through the pressure and calandria tubes. These tubes are modelled as zirconium rings separated by a gas annulus. The heat capacity of the zirconium in the pressure tube is accounted for in the program, but since the calandria-tube temperature is held relatively constant by the surrounding moderator, and since it is thin relative to the pressure tube, its heat capacity is neglected. Initially, the gas gap between the two tubes will insulate the pressure tube, and its temperature will increase until it deforms into contact with the calandria tube. The type of contact depends upon the internal pressure. If the pressure is high, the tube creeps circumferentially until it "balloons" into contact. If the pressure is low, creep bending of the pressure tube occurs until it "sags" into contact with the bottom of the surrounding calandria

tube (CANDU-PHW channels are horizontal). During deformation of the pressure tube before contact, the change in radiation form factor and gas conduction length between the pressure tube and calandria tube has very little effect on the heat transfer. A separate thermal-mechanical analysis is used to predict pressure tube deformation and, thus, the time of contact. In the contact region, the heat transfer between the pressure and calandria tubes is modelled using an empirical equation for the contact conductance [5], while in the non-contact region, heat continues to be transferred by radiation and conduction through the gas gap. The contact and non-contact regions used in CHAN II are thermally coupled by circumferential conduction in the pressure and calandria tubes.

A pool-boiling boundary condition [6] is specified on the outside of the calandria tube. Before contact, either subcooled convection or nucleate boiling is used (determined by the calandria-tube surface temperature). After contact, either nucleate boiling or film boiling is specified over the contact region. A "spike" in the heat flux to the moderator occurs when the pressure tube contacts the calandria tube. This spike is caused by the change in the heat-transfer mode between the tubes, which allows the heat stored in the pressure tube to be rapidly released. If this spike exceeds the critical heat flux, film boiling is assumed, but if it is less than the critical heat flux, nucleate boiling continues.

EXPERIMENTAL VERIFICATION

A series of small-scale experiments is underway to verify the submodels used to calculate the heat transfer by radiation and convection. The results are being used to check the ability of the lumped-parameter analysis to follow the transient temperature behaviour of the tubes and to predict the amount of hydrogen produced by the reaction between steam and zirconium. Typical results from one such experiment are discussed here.

Figure 4 is a schematic of the apparatus, which consists of a boiler, a superheater, a test section, a condenser and a hydrogen trap. The experimental test section consists of a tantalum heater element, 500 mm long, electrically insulated by alumina cylinders from the surrounding 9.53-mm (outside diameter) zirconium sheath. Five type-K thermocouples are spotwelded directly to the outside of the heated sheath at 120-mm intervals. Surrounding the sheath is a 19.6 mm (inside diameter) by 0.95 mm thick zirconium flow tube that, in turn, is insulated by a layer of alumina beads, 66 mm thick. Five type-K thermocouples are spot-welded on the outside of the flow tube at the same axial locations as those on the heater sheath. The experiment was performed using the following procedure:

- Helium was passed through the superheater and test section to heat the test section and prevent steam from condensing on the surface during the period of initial steam injection.
- Steam was injected into the flow system at a rate of 2 g/s. The steam temperature at the inlet to the test section was 650°C.
- After the apparatus reached thermal equilibrium, a constant voltage was applied across the heating element.
- The temperatures were recorded at one-second intervals, and the hydrogen production was monitored visually throughout the experiment.

Figure 5 shows the heater power during the experiment. The heater power decreased from its initial value since the temperature of the heating element increased, causing the resistance to increase. The measured power and the power curve used in CHAN II to model the electrical power are both shown in Figure 5. Also

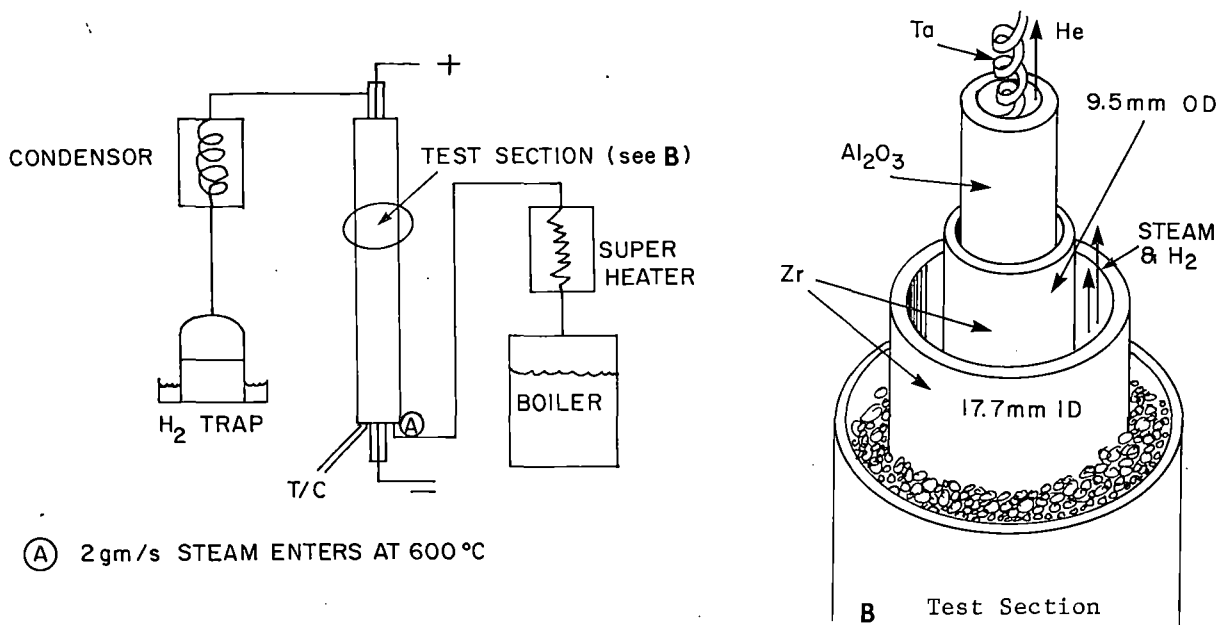


Figure 4: Experimental Apparatus

shown is the total power calculated by CHAN II by adding the heat of the zirconium-steam reaction to the prescribed heater power.

To represent the test section, some modifications were made to CHAN II. The weighted averages of the thermal properties of tantalum and alumina were substituted for those of UO₂ in the heating element.

A pressure tube in a CANDU reactor is surrounded by CO₂ and a calandria tube. The model for heat transfer through the CO₂ assumes that the heat capacity of CO₂ is negligible. In the experiment, the flow tube was insulated by alumina beads, which have a large heat capacity. To accommodate the high heat capacity of the insulation, the shroud tube was modelled by a fuel ring having the thermal properties of zirconium and zero heat generation. The cylinder of alumina was modelled as a pressure tube with the properties of alumina. No flow and zirconium-steam reaction were assumed in the annulus between the zirconium "fuel ring" and alumina "pressure tube". The gap between these rings was set at 0.3 mm, and the heat transfer between them was assumed to be by radiation only.

Normally, the model calculates heat transfer, assuming radiation and conduction through the gas gap to the calandria tube. To model the present experiment, the thermal conductivity of the alumina beads was substituted for that of CO₂ and heat transfer by radiation was deleted.

During the experiment, the temperature of the tube corresponding to the calandria tube varied from 59°C to 69°C. To model the heat transfer from this tube, a moderator temperature of 65°C was assumed. Since the shroud tube was insulated by the 66-mm-thick cylinder of insulation, less than 2% of the total heat generated was transferred radially through it; therefore, the predicted temperatures are insensitive to the assumed moderator temperature.

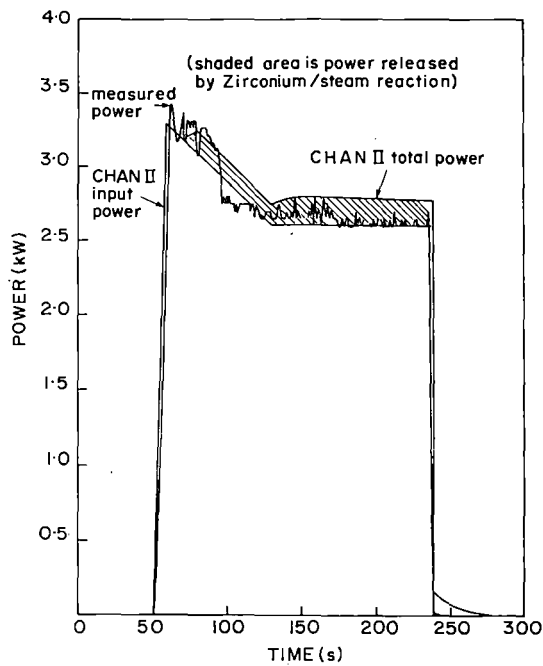


Figure 5: Time Variation of Test Section Power

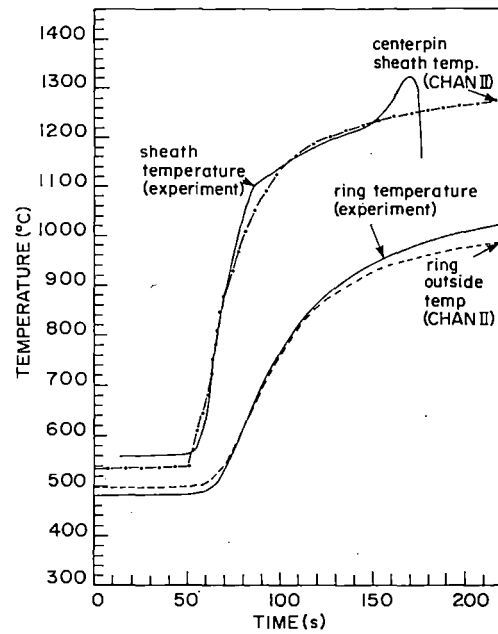


Figure 6: Time Variation of Sheath and Flow-Tube Temperatures

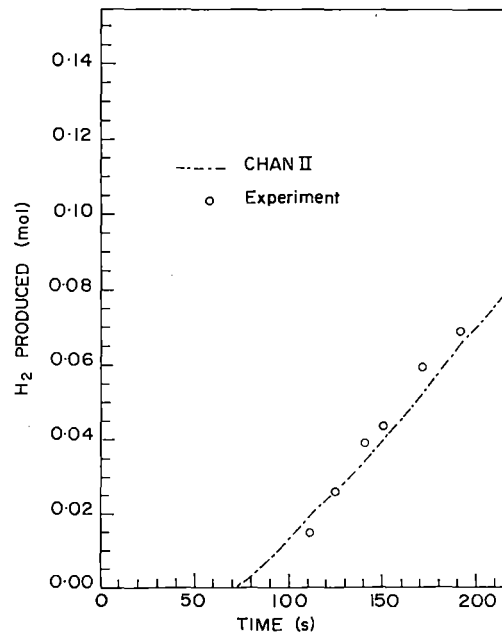


Figure 7: Time Variation of Hydrogen Production

In Figure 6, the temperature variation of the heater sheath and the flow tube 30 mm from the beginning of the heated length are compared with predictions made using CHAN II. The comparisons show that the model predicts the temperature variation with time well. The thermocouple on the heater sheath failed 100 s after the power was turned on, but the flow-tube temperature shows that the good temperature agreement continued throughout the experiment.

In Figure 7, the hydrogen production during the experiment is compared with the predictions made using CHAN II. The amount of hydrogen produced agrees very well with the amount predicted. This is a function of the good agreement between the predicted temperatures of the zirconium surfaces and the accuracy of the correlations derived by Urbanic and Heidrick [4] that are used to model the oxidation of zirconium and the subsequent hydrogen production.

SAMPLE REACTOR CASE

The initial thermal conditions are taken from thermalhydraulic models. In the sample presented, the initial conditions used were taken 80 s from the start of the accident. This time coincided with the end of blowdown for this case, and it was assumed that emergency cooling injection was unavailable. In the example, a steam flow of 30 g/s was assumed, since this value is in the range of flows that produce the highest fuel temperatures. The internal pressure is low, and the pressure tube will sag into contact with its calandria tube. The parameters defining the case are listed in Table 1.

TABLE I

CHANNEL CONDITIONS

Sample Reactor Case

Fuel initial temperature	600°C
Pressure-tube initial temperature	300°C
Moderator temperature	70°C
Steam flow rate	30 g/s
Steam inlet temperature	100°C
Time at beginning of heat-up	80 s
Channel power	6 MW
Channel length	6 m
Fuel bundle length	0.5 m
Fuel bundle elements	37
Fuel bundle rings	3

Figure 8 shows the temperatures predicted by CHAN II for the center fuel pins along the fuel channel at various times. Up to about 500 s, the temperature profile reflects the assumed cosine power distribution plus a skew to the right caused by the axial transfer of heat by the steam flow. After this time, the temperature of the fuel sheath in the center segment is high enough that the zirconium-steam reaction produces a significant quantity of heat. This addition of heat causes the temperature distribution to become sharply peaked near the center of the channel.

Figures 9 and 10 show the predicted radial temperature profiles for the non-contact region and contact region, respectively, at the middle of the channel. The temperatures at a given axial location begin decreasing when the zirconium in the

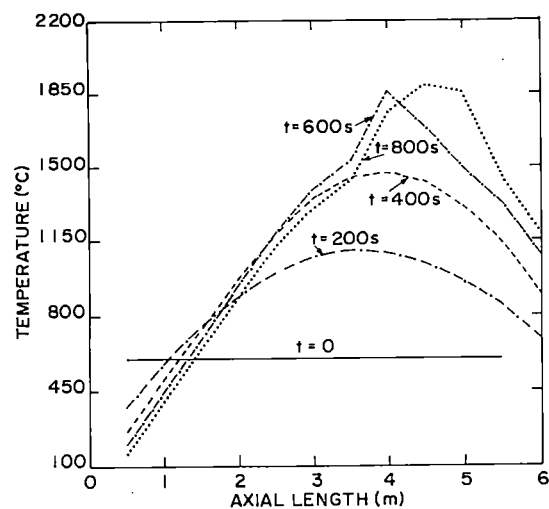


Figure 8: Sample Reactor Case, Axial Center Pin Temperatures

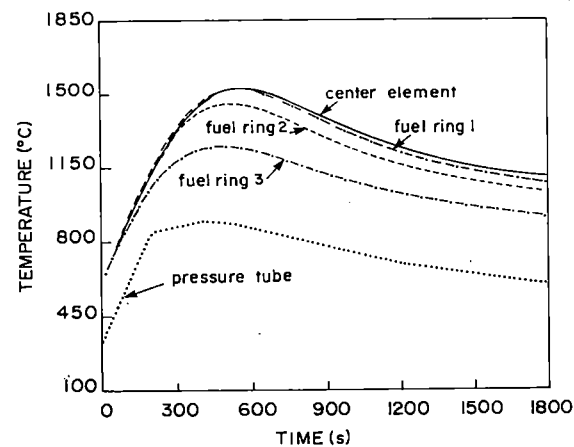


Figure 9: Radial Temperatures of Non-Contact Region (centre of channel)

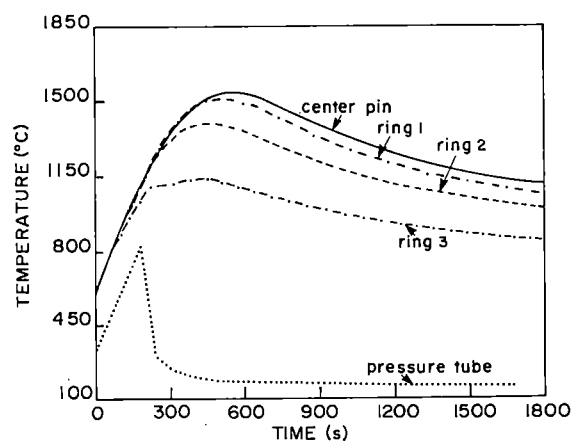


Figure 10: Radial Temperatures of Contact Region (center of channel)

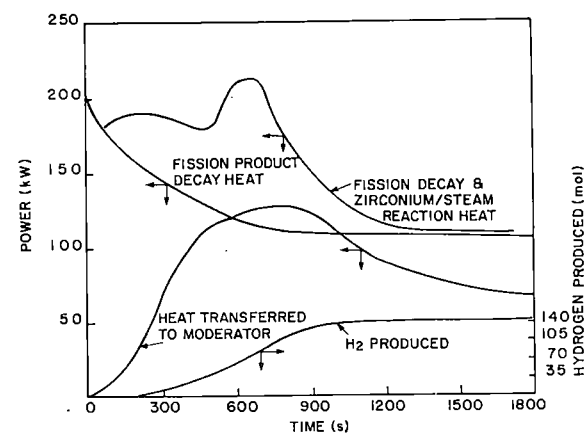


Figure 11: Channel Power, Power transferred to Moderator and Hydrogen Production

fuel sheath is completely consumed and continue to decrease as the decay heat decreases. The temperature rise in the pressure tube follows that of the fuel until it reaches 800°C, at which point a separate mechanical analysis predicts that the pressure tube sags into contact with the calandria tube. The increased heat transfer to the moderator caused by this contact cools the bottom of the pressure tube. This also decreases the rate of temperature rise on the top of the pressure tube (the non-contact area) since heat is transferred circumferentially to the colder portion on the bottom.

Figure 11 shows the fuel decay power, the power added by the zirconium-steam reaction, the power transferred to the moderator and the hydrogen production in the channel. With the initial conditions and steam flow used in this case, the power added by the chemical reaction approaches the decay power for a period of time.

The rate of the zirconium-steam reaction depends principally on the temperature of the zirconium surfaces, but the actual effect of this additional heat on the channel temperatures depends on the steam flow. Figure 12 shows how the predicted peak temperature of the center pin varies as a function of the assumed steam flow for different cases with the same initial conditions. When the steam flow is less than 10 g/s, axial convection heat transfer is weak, all of the steam is consumed by the chemical reaction before leaving the channel and, thus, the peak temperatures increase with increasing flow as more oxygen is available. Balancing this increased heat addition is the increase in convective cooling accompanying the larger flows. For steam flows greater than 20 g/s, the peak temperatures decrease with increasing flow, since the steam removes most of the heat generated.

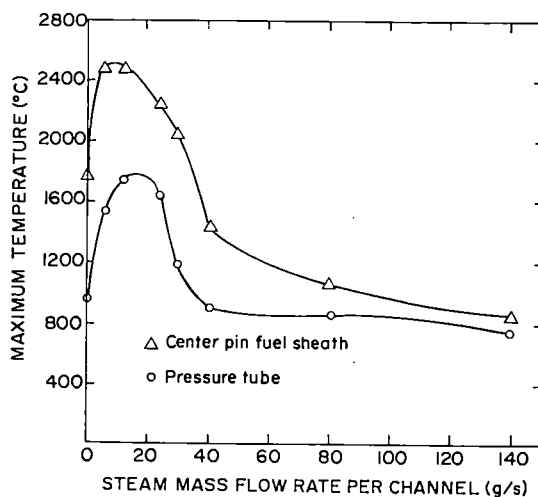


Figure 12: Effect of Steam Flow on Fuel and Pressure Tube Maximum Temperatures

SUMMARY

A computer model has been developed to estimate the thermal behaviour of a CANDU fuel channel during postulated accidents in which the primary cooling and emergency cooling are inadequate. The model accounts for the heat generated (decay power plus zirconium-steam reaction), the heat stored in the fuel, the heat transferred axially by convection, and the heat rejected radially to the moderator.

The good agreement between the computer predictions and the initial results of experiments designed to verify the submodels used in the code is encouraging and indicates that axial convection, radial heat transfer, and hydrogen production are well modelled for these conditions. Further experiments covering a wider range of conditions are continuing.

ACKNOWLEDGEMENTS

The financial support of the program verification portion of this work by Ontario Hydro is gratefully acknowledged.

REFERENCES

1. V.Q. TANG and D.G. VANDENBERGHE, "CHAN II: A Computer Program Predicting Fuel Channel Thermal Behaviour in a Typical CANDU-PHW Reactor Core Following a Loss-of-Coolant Accident", unpublished Report WNRE-494 (1981), Whiteshell Nuclear Research Establishment.
2. M.B. CARVER, D.G. STEWART, J.M. BLAIR and W.N. SELANDER, "The FORSIM VI Simulation Package for the Automated Solution of Arbitrarily Defined Partial and/or Ordinary Differential Equation Systems", AECL 5821 (1979), Atomic Energy of Canada Limited.
3. A.C. WHITTIER, D.W. BLACK and C.R. BOSS, "CANDU Channel Decay Power", AECL-5704 (1977), Atomic Energy of Canada Limited.
4. V.F. URBANIC and T.R. HEIDRICK, "High Temperature Oxidation of Zircaloy-2 and Zircaloy-4 in Steam", Journal of Nuclear Materials, 75, 251 (1978).
5. J. DRYDEN and A.M. STADNYK, "Heat Transfer Between Planar Surfaces of Zr-2 and Zr-2.5wt.%Nb", unpublished Report WNRE-284 (1981), Whiteshell Nuclear Research Establishment.
6. G.E. GILLESPIE, "An Experimental Investigation of Heat Transfer from a Reactor Fuel Channel to Surrounding Water", Proceedings of the Canadian Nuclear Society Annual Conference, June 10, 1981.

REFILLING AND REWETTING OF HORIZONTAL FUEL CHANNELS

W.T. Hancox, V.S.V. Rajan, F.W. Barclay,
B.N. Hanna and B.H. McDonald

Thermalhydraulics Research Branch
Atomic Energy of Canada Limited
Whiteshell Nuclear Research Establishment
Pinawa, Manitoba

ABSTRACT

The core of CANDU-PHW* reactors consists in part of an array of horizontal fuel channels that are individually connected by feeder pipes to headers located above the core. In a loss-of-coolant (LOCA) accident, various flow and heat-removal conditions are possible. To investigate the processes associated with the refilling phase of a LOCA, experiments have been done on full-size channels containing electrically heated rod bundles. The physical phenomena observed in the experiments are described, with emphasis on the modelling requirements. At high refilling rates, homogeneous equilibrium models are shown to be in good agreement with the experiments. At low refilling rates, the flow in the channel is initially stratified, consisting of steam and water streams with different velocities and temperatures. An unequal velocity, unequal temperature (UVUT) model of separated steamwater flow is described, that incorporates the essential physical phenomena. Comparisons between prediction and experiment are presented.

* Canada's natural-uranium-fuelled, heavy-water-cooled and moderated reactor (CANada Deuterium Uranium - Pressurized Heavy Water)

INTRODUCTION

The core of a CANDU-PHW reactor is made up in large part of an array of horizontal fuel channels, each consisting of a pressure tube that contains the fuel bundles and high-pressure heavy-water coolant. The fuel channels are individually connected by small-diameter feeder pipes to headers located above the core at each end. The arrangement of the primary heat-transport circuit is such that some large-break loss-of-coolant accidents (LOCAs) are predicted to produce an initial period of flow stagnation in a group of fuel channels, causing rapid vaporization and ejection of their coolant. The rate at which these channels refill and rewet depends on the persistence of the stagnation condition. In this paper, we discuss the associated fluid-dynamic and heat-transfer processes.

To illustrate the characteristics of the physical processes during refilling, we describe experiments done on a full-size fuel channel containing an electrically heated rod bundle. The experiments were selected to show the full range of refilling and rewetting conditions, from flows dominated by inertial forces at one extreme to flows dominated by gravitational forces at the other. Based on the observed characteristics, a mathematical model is proposed to describe the essential fluid-dynamic and heat-transfer processes. In its most general form, the model considers the steam and water to flow in separate, but interacting, streams. The interaction between the streams is specified by empirical interphase mass, momentum and heat-transfer equations. The ability of the model to describe the important physical processes is demonstrated by comparison with experimental data and two simpler models.

REFILLING EXPERIMENTS

Experimental Facility

Figure 1 shows a schematic of the experimental facility. The horizontal channel consists of a 6-m long, 100-mm diameter Zircaloy flow tube containing a 6-m long bundle of 37 electrically heated 13-mm diameter rods. The channel is connected to inlet and outlet headers, located 10 metres above, by 50-mm diameter pipes. A water injection system, consisting of a pump (or an accumulator), controlled to give a constant discharge pressure up to 900 kPa (or 4 MPa), is connected to the inlet header, or to both the inlet and outlet headers, through a check valve.

The initial conditions for an experiment are established by circulating superheated steam to raise the temperature of the pipes to 300°C and then isolating the loop with an internal pressure (usually 5.5 MPa) greater than the injection pressure. Next, electrical power is supplied to the rods, and when their surfaces reach the desired temperature (usually $\sim 400^\circ\text{C}$), blowdown of the loop is initiated by opening a gas-actuated valve in the discharge line from the outlet header. The discharge rate is determined in part by the size of the orifice plate located downstream of the blowdown valve. The desired channel flow conditions are achieved by an appropriate combination of injection pressure, injection mode, and orifice (or break) size.

During an experiment the following transient measurements are made:

- rod surface temperature, using thermocouples imbedded in the stainless steel sheaths. Typically 30 thermocouples, distributed throughout the rod bundles, are monitored to provide a detailed picture of the motion of the rewetting front.
- coolant density and flow regime, using three-beam gamma-ray densitometers located on horizontal pipes close to the inlet and outlet of the channel.
- injection flow rate, using calibrated orifice plates.
- coolant pressure and temperature at various points in the facility.

Experimental Results

The initial conditions for the experiments to be discussed here are given in Table I, as well as a summary of the results. Figures 2 and 3 show selected transients measured during experiments 774 and 768. These experiments differ only in the mode of injection used: in experiment 774 injection was to the inlet header, while in experiment 768 it was to both the inlet and outlet headers. Three stages are evident:

- blowdown of the loop to the injection pressure,
- refilling of the inlet header and feeder, and
- rewetting and refilling of the channel.

The most striking difference between the two experiments occurs in the channel-refilling stage. In experiment 774, the channel refills slowly (~ 0.9 kg/s), with marked flow stratification evident in the rod temperature histories, while in experiment 768 refilling is rapid (~ 1.9 kg/s), with essentially no flow stratification.

In experiment 774, the inflow of water is determined by the rate of discharge of steam through the break. As evident in Figure 3, the rod temperature histories show that the injected water flows in a layer along the bottom of the channel, rewetting the lower rods. Steam generated during rewetting flows out through the upper part of the channel, removing heat from the upper rods and gaining substantial superheat. As the injection proceeds, the water level rises, progressively rewetting more rods, until the channel is refilled.

In experiment 768, the outlet header is filled with water and water is discharged through the break. Steam generated in the channel is condensed in the outlet header. The combined effect of the condensation and increased discharge rate reduces the pressure in the outlet header (relative to experiment 774) and increases the header-to-header pressure drop. As a result, the average flow rate through the channel is 1.9 kg/s, twice that in experiment 774. At this flow rate (see Figure 3,) a piston-like rewetting front propagates through the channel, rapidly refilling it. Upper and lower rods rewet almost at the same time.

The above experiments are typical of those listed in Table I. Figure 4 gives an overall summary of the results. We have chosen to represent the duration of flow stratification by the time difference between the rewetting of the bottom and top rods at the channel outlet. As evident, the experimental data show clearly that prolonged stratification can be expected when the average refilling rate is less than 1 kg/s (the corresponding mass velocity is $340 \text{ kg/(m}^2\text{s)}$).

MATHEMATICAL MODEL

To predict the full range of the refilling processes described above mathematical models are required that permit the steam and water to flow in separate, but interacting, streams with unequal velocities and temperatures. Suitable models can be derived from the local instantaneous differential conservation laws and interface jump conditions, using space and time averaging to remove the need to treat the interfaces explicitly. A system of one-dimensional conservation equations for each phase results. One such system of equations for phase k ($k=1$ for gas; $k=2$ for liquid) has the following form [1]:

(i) mass conservation

$$\frac{\partial}{\partial t} \alpha_k \rho_k + \frac{1}{A} \frac{\partial}{\partial x} A \alpha_k \rho_k u_k = m_{ki} \quad (1)$$

(ii) momentum conservation

$$\begin{aligned} \frac{\partial}{\partial t} \alpha_k \rho_k u_k + \frac{1}{A} \frac{\partial}{\partial x} A \alpha_k \rho_k u_k^2 + \alpha_k \frac{\partial p_k}{\partial x} + (p_k - p_i) \frac{\partial \alpha_k}{\partial x} \\ + (-1)^{k-1} M_a \sum_{j=1}^2 \left(\frac{\partial u_j}{\partial t} + u_j^* \frac{\partial u_j}{\partial x} \right) = \tau_{kw} + \tau_{ki} - m_{ki} u_{ki} + \alpha_k \rho_k b_x \end{aligned} \quad (2)$$

(iii) energy conservation

$$\begin{aligned} \frac{\partial}{\partial t} \alpha_k \rho_k H_k + \frac{1}{A} \frac{\partial}{\partial x} A \alpha_k \rho_k u_k H_k - \alpha_k \frac{\partial p_k}{\partial t} - (p_k - p_i) \frac{\partial \alpha_k}{\partial t} \\ + (-1)^k M_a u_k \sum_{j=1}^2 \left(\frac{\partial u_j}{\partial t} + u_j^* \frac{\partial u_j}{\partial x} \right) = q_{kw} - q_{ki} - \tau_{ki} u_{ki} + m_{ki} h_{ki} + \alpha_k \rho_k u_k b_x \end{aligned} \quad (3)$$

$$\text{where } H_k = h_k + u_k^2/2$$

In the above equations α_k , ρ_k , u_k , p_k and h_k denote, respectively, area fraction, density, x -component of velocity, pressure and enthalpy of phase k ; A is the flow cross-sectional area; p_i is an averaged interface pressure; b_x is the x -component of the body force; M_a is the apparent (or virtual) mass and u^* is a convective velocity; m_{ki} is the phase- k mass transfer per unit volume from the interface; u_{ki} is the k -phase interface velocity associated with momentum and mass transfer; h_{ki} is the enthalpy of k -phase at the interface; τ_{ki} and q_{ki} denote, respectively, the momentum and heat transfer per unit volume from phase k to the interface; and τ_{kw} and q_{kw} denote, respectively, the momentum and heat transfer per unit volume from phase k to the wall.

The interphase transfer terms in the above equations must satisfy the following jump conditions:

$$\sum_{k=1}^2 m_{ki} = 0 \quad (4)$$

$$\sum_{k=1}^2 (\tau_{ki} - m_{ki} u_{ki}) = 0 \quad (5)$$

$$\sum_{k=1}^2 \left\{ m_{ki} (h_{ki} + u_{ki}^2/2) + q_{ki} - \tau_{ki} u_{ki} \right\} = 0 \quad (6)$$

The conservation equations (1) to (3) and the interphase jump conditions (4) to (6) contain 28 unknowns. Additional equations are provided by noting that $\sum \alpha_k = 1$, and by the thermodynamic state equations $\rho_k = \rho_k(h_k, p_k)$. To close the system, empirical equations are provided for the remaining terms as functions of the primary flow variables α_k , u_k , h_k and p_k . Included are equations for:

- (i) interface parameters u_{ki} and h_{ki} .
- (ii) phase-to-interface transfers τ_{1i} , q_{1i} and q_{2i} . The remaining transfer terms τ_{2i} , m_{1i} and m_{2i} are then determined using the interphase jump conditions (4) to (6).
- (iii) phase-to-wall transfers τ_{kw} and q_{kw} .
- (iv) phase-to-interface pressure differences $(p_k - p_i)$.
- (v) virtual mass M_a and convection velocity u_k^* .

The particular functional forms of the closure equations used depend on the flow structure (or regime); that is, whether the steam and water are mixed (bubble or droplet flow) or separated (horizontal-stratified or vertical-annular flow). We currently use a simplified version of the flow-regime map developed by Mandhane et al [2] to select the appropriate closure equations. Details of the procedure and the closure equations are given in reference [3]. Of particular importance are the phase-to-interface pressure difference $(p_k - p_i)$ and the virtual mass terms (the final term on the left-hand side of equations (2) and (3)). The former is the dominant factor influencing the stability of the interface between the phases when they are separated. For stratified flow in the channel, we use an equation of the form

$$p_k - p_i = \rho_k g \left\{ y_i - \frac{(-1)^k}{A \alpha_k} \int_{y_k}^{y_i} y \, dA \right\} \quad (7)$$

where y_i denotes the position of the interface and y_k the boundary of phase k in a flow cross section. The integral in equation (7) incorporates the geometry of the rod bundle, which tends to stabilize the interface.

The virtual mass terms are important only when the steam and water are mixed. Mixed flows are characterized by strong coupling between the phases and by small differences between the phase velocities and temperatures. The virtual mass terms reinforce the coupling provided by interface transfer terms and ensure that the velocities at which interfacial waves propagate remain real [1]. We have adopted the functional form proposed by Drew and Lahey [4].

The conservation equations (1) to (3), using the closure equations described above, are hyperbolic for the complete range of flow regimes. The equations are incorporated in the computer code RAMA [5] and are solved using a characteristic finite-difference procedure [6,7].

COMPARISON BETWEEN MODEL AND EXPERIMENT

In general, even the simplest flow-boiling model (homogeneous equilibrium, or equal-velocity, equal-temperature model, (EVET)) accurately predicts experiments with high refilling rates (>1 kg/s). This is expected because the observed flows are approximately homogeneous. Below we focus attention on experiment 774, which showed marked stratification.

Figures 5 and 6 compare calculated and measured transients. Predictions made with the model described above are denoted by UVUT (unequal velocity, unequal temperature). Also shown are predictions made using RAMA with EVET and EVUT (equal-velocity, unequal-temperature) models [6]. As evident, neither the EVET model nor the EVUT model are in good agreement with the experiment. This is particularly so for the rod temperature histories. The EVET model assumes that the steam and water are uniformly distributed over the flow cross-section and that they are in thermal equilibrium. This means that the sink temperature for heat transfer is the local saturation temperature. In this case, the lower rods are predicted to have the same temperature as the upper rods.

The EVUT model assumes that the steam and water streams have different temperatures, but equal velocities. Also, the stratification of the steam and water streams is allowed for. Hence, it removes two weaknesses of the EVET model - the assumption of thermal equilibrium and homogeneity - and should yield more accurate predictions. As evident, although there is some improvement in agreement between prediction and experiment, the EVUT model does not predict the same degree of stratification as observed in the experiment (see Figure 6b). It predicts that the flow is initially stratified, but as cooling proceeds, the injected water quickly steepens into a vertical front. This is believed to be an artifact of the assumption of equal steam and water velocities. As might be expected, the predicted upper rod temperatures are greater than those observed in the experiment.

The UVUT model, described above, allows the steam and water to flow in separate streams with different velocities and temperatures. Hence, it removes the assumptions of both mechanical and thermal equilibrium. As evident, the agreement between the model and experiment is much improved. The major shortcoming is the predicted transition from stratified flow to mixed flow at about 120 seconds (see Figure 6b) and the resultant gradual steepening of the rewetting front. To improve the prediction, refinements are required in the empirical flow-regime map. We intend to study flow-regime transitions in channels containing rod bundles to provide a data base for developing improved transition criteria.

CONCLUSIONS

The main conclusions are:

- (i) Refilling of horizontal fuel channels typical of CANDU-PHW reactors is characterized by marked flow stratification when the average mass velocity is less than $340 \text{ kg}/(\text{m}^2 \cdot \text{s})$, and the bottom fuel rods can be expected to rewet before the upper rods. At higher mass velocities, the rewetting front is piston-like and the channel refills rapidly.
- (ii) Mathematical models based on homogeneous equilibrium flow underpredict peak rod temperatures and refilling times when the mass velocity is less than $340 \text{ kg}/(\text{m}^2 \cdot \text{s})$. The prediction error increases with decreasing mass velocity.
- (iii) Mathematical models that consider the steam and water to flow in separate streams with different velocities and temperatures offer the promise of greatly improved prediction accuracy. To realize this promise, further research is needed to refine flow-regime transition criteria, particularly for flow in channels containing rod bundles.

REFERENCES

1. Hancox, W.T., Ferch, R.L., Liu, W.S. and Nieman, R.E., "One-Dimensional Models for Transient Gas-Liquid Flows in Ducts", Int. J. Multiphase Flow, 6, 25-40, 1980.
2. Mandhane, J.M., Gregory, G.A. and Aziz, K., "A Flow Pattern Map for Gas-Liquid Flow in Horizontal Pipes", Int. J. Multiphase Flow, 1, 537-553, 1974.
3. Hanna, B.N., McDonald, B.H., Scarth, D.A. and Krishnan, V.S., "Development and Application of a Two-Fluid Model for RAMA", Proceedings of the Simulation Symposium on Reactor Dynamics and Plant Control, Canadian Nuclear Society, April 1982.
4. Drew, D.A. and Lahey, R.T., "Application of General Constitutive Principles to the Derivation of MultiDimensional Two-Phase Flow Equations", Int. J. Multiphase Flow, 5, 243-264, 1979.
5. Barclay, F.W., Nieman, R.E. and Hasinoff, M.P., "Transient Heat Transfer and Fluid Mechanics of a Recirculating Pressurized Water Loop during Blowdown and Cold Water Injection", Canadian Journal of Chemical Engineering, 59, 201-212, 1981.
6. Banerjee, S. and Hancox, W.T., "On the Development of Methods for Analysing Transient Flow-Boiling", Int. J. Multiphase Flow, 4, 437-460, 1978.
7. Hancox, W.T. and McDonald, B.H., "Finite Difference Algorithms to Solve the One-Dimensional Flow-Boiling Equations", ANS/ASME/NRC Topical Meeting on Nuclear Reactor Thermalhydraulics, NUREG/CP-0014, Saratoga Springs, October 1980.

TABLE I
SUMMARY OF EXPERIMENTAL CONDITIONS AND RESULTS

Test Number	INITIAL CONDITIONS				RESULTS		
	Injection Pressure (MPa)	Channel Power (kW)	Rod Surface Temp. (°C)	Break Size	Average Refilling (kg/s)	Duration of Flow Strati- fication (s)	Max. Rod Temp. (°C)
<u>Injection to inlet header</u>							
517	0.8	100	400	6.3	0.3	370	588
521	0.4	50	400	42.3	0.6	65	447
522	0.8	100	400	6.3	0.3	315	553
524	0.8	50	400	6.3	0.3	236	451
525	0.4	50	400	42.3	0.5	244	434
567	4.0	300	317	6.3	1.7	9	393
568	3.0	300	313	6.3	0.9	42	423
580	3.0	300	400	6.3	0.95	57	479
595	2.0	300	400	42.3	2.5	3	445
774	2.0	300	400	6.3	0.9	141	684
839	2.0	300	400	6.3	0.8	132	653
840	2.0	300	400	12.9	0.95	31	517
842	2.0	300	400	36.9	1.9	4	487
843	2.0	300	400	42.3	2.0	3	489
844	2.0	300	400	70	2.0	3	468
845	2.0	300	400	100	2.1	3	468
848	2.0	200	400	2.5	0.3	347	780
851	2.0	300	400	13	0.7	35	503
852	2.0	300	400	20	1.1	14	484
853	2.0	300	400	37	1.7	4	473
855	2.0	200	400	2.5	0.25	>315	>780
856	2.0	300	400	6.3	0.6	134	661
<u>Injection to both headers</u>							
646	0.8	100	400	42.3	0.7	59	535
644	0.8	100	400	6.3	0.4	118	476
647	0.5	100	400	42.3	0.5	165	477
648	0.5	100	400	6.3	0.3	322	535
581	2.0	300	400	6.3	1.1	20	545
582	2.0	300	400	42.3	1.7	8	486
583	3.0	300	400	42.3	2.3	2	486
597	4.0	300	400	6.3	2.6	6	482
749	1.5	300	400	6.3	0.8	65	571
768	2.0	300	400	6.3	1.9	23	560
771	2.0	300	600	6.3	0.85	40	712

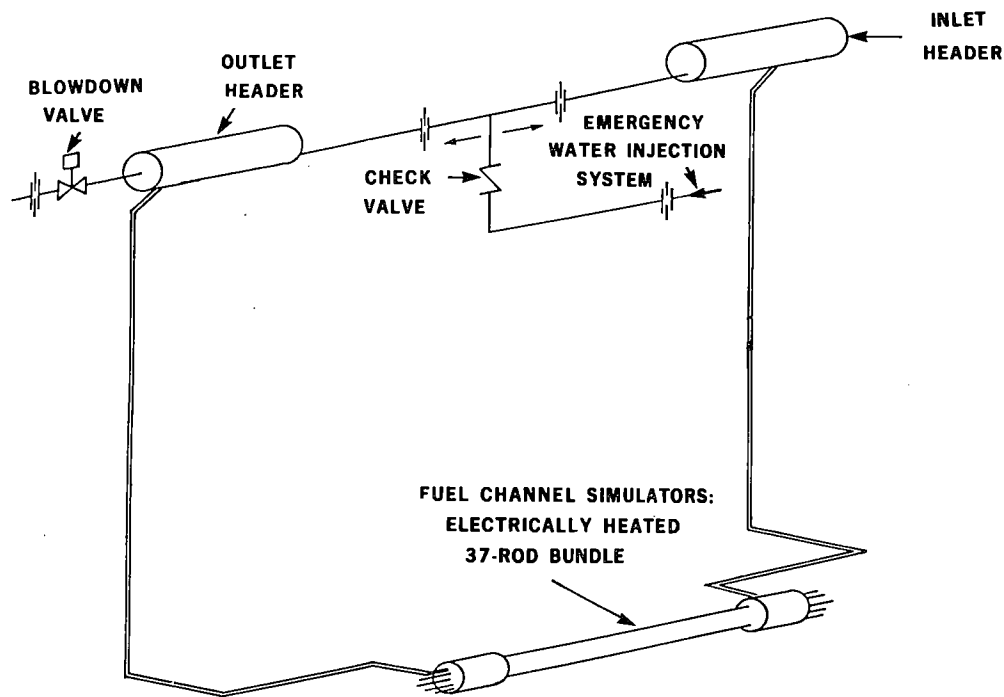


Figure 1: Schematic of the Experimental Facility

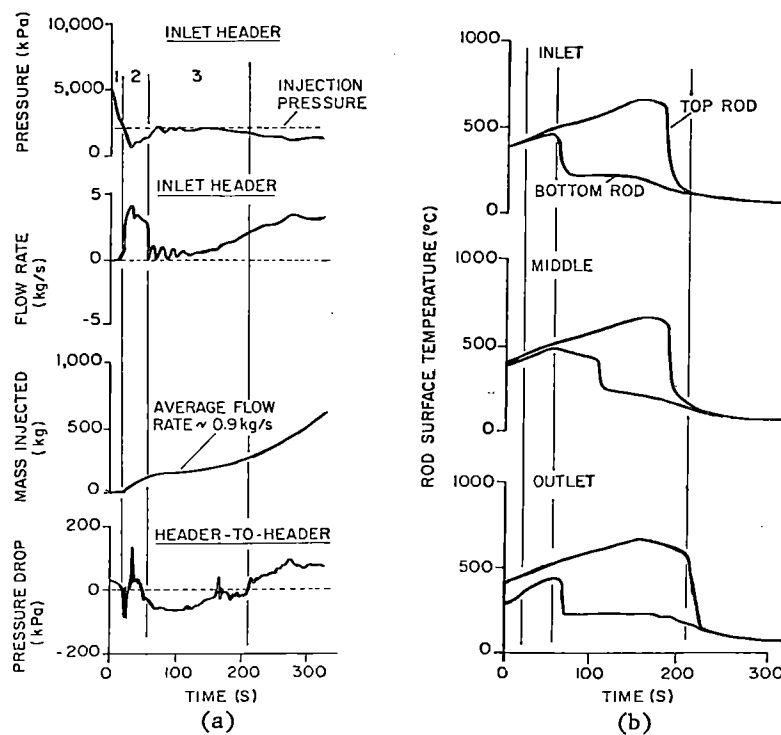


Figure 2: Transients Measured During Experiment 774.
 (a) Flow and Pressure Transients
 (b) Rod Temperature Transients

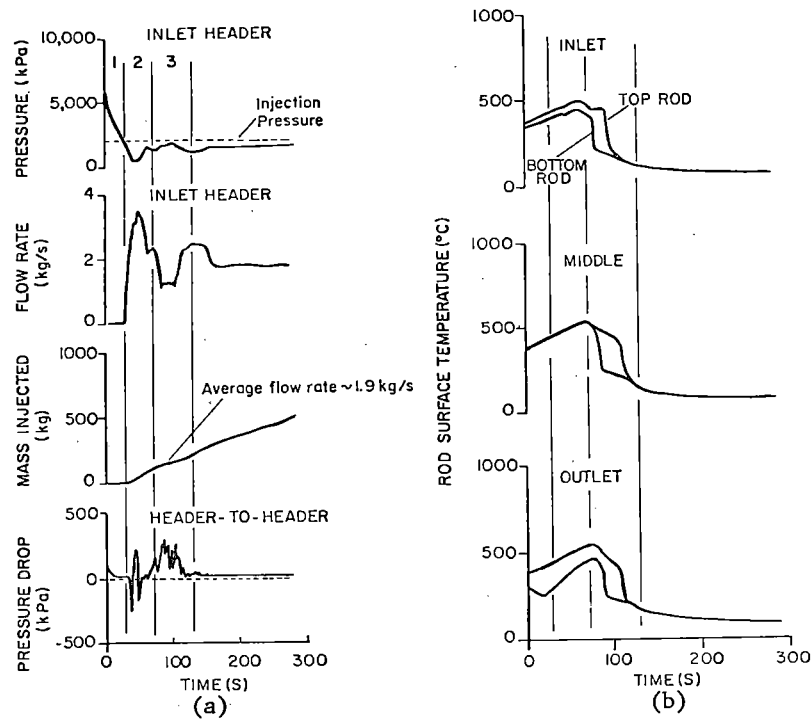


Figure 3: Transients Measured During Experiment 768.
 (a) Flow and Pressure Transients
 (b) Rod Temperature Transients

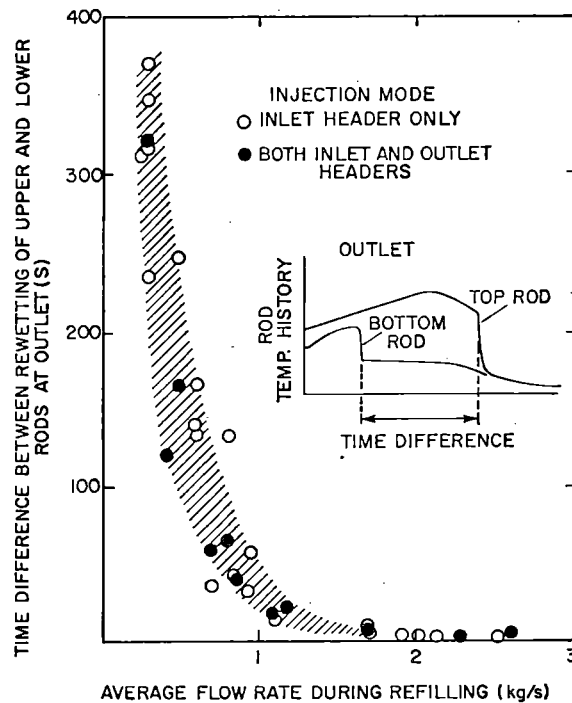


Figure 4: Duration of Flow Stratification as a Function of the Refilling Flow Rate

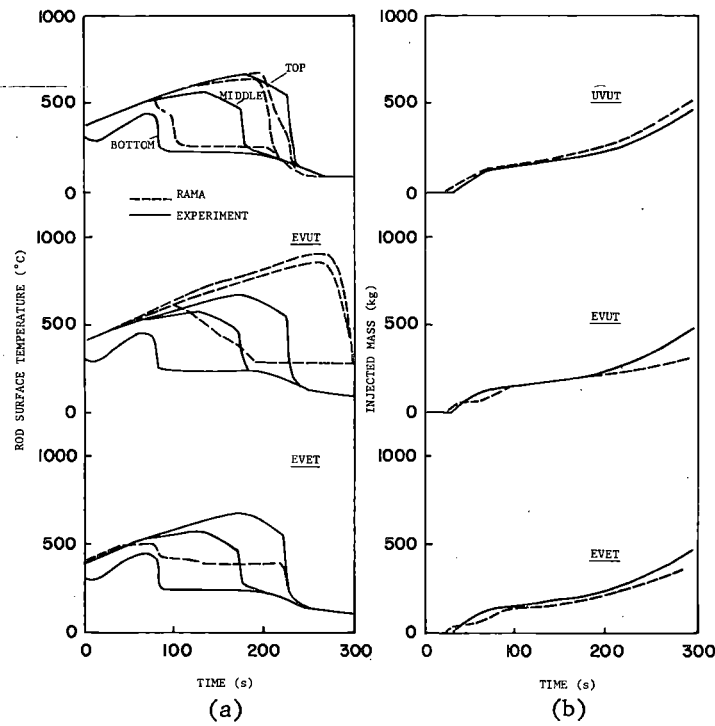


Figure 5: Calculated and Measured Transients for Experiment 774.
 (a) Rod Temperature Transients at the Channel Outlet
 (b) Cumulative Mass Injected

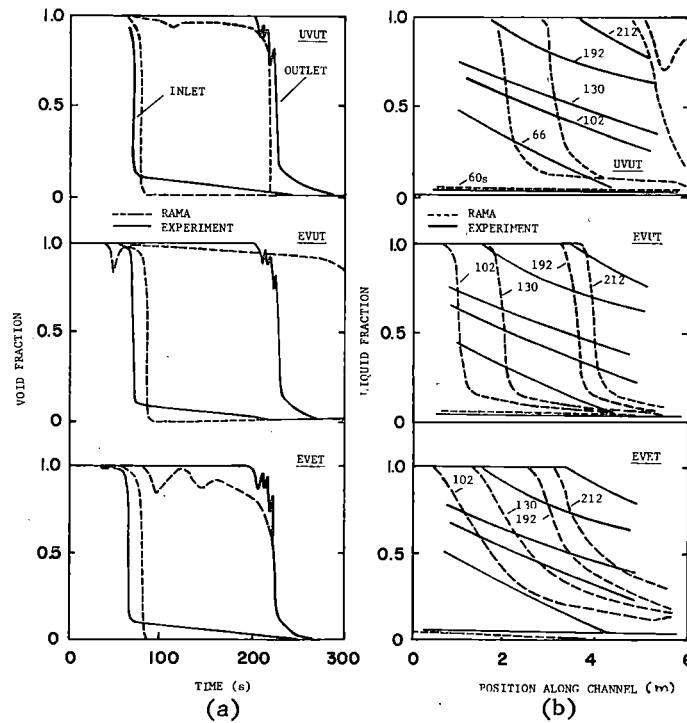


Figure 6: Calculated and Measured Transients for Experiment 774.
 (a) Void Fraction at the Inlet and Outlet of the Channel
 (b) Liquid Fraction Profiles in the Channel

ANALYSIS OF TRANSIENT DRY PATCH BEHAVIOR ON CANDU REACTOR CALANDRIA
TUBES IN A LOCA WITH LATE STAGNATION AND IMPAIRED ECI

J.T. Rogers

Carleton University
Ottawa, Ontario, Canada

T.C. Currie

Davis Engineering Ltd.
Ottawa, Ontario, Canada

ABSTRACT

An analytical method to describe the behavior of transient dry patches on CANDU reactor calandria tubes has been developed. Dry patches may form following the sagging of a pressure tube onto a calandria tube in certain low-probability scenarios in which a loss-of-coolant accident occurs with subsequent failure or impairment of the emergency cooling injection function.

Results of the analysis show that the dry patches will not grow beyond a few degrees on each side of the bottom of the calandria tube and will rewet within a few tens of seconds, with the values depending on the specific CANDU reactor design and the mechanism of dry patch formation and rewetting. Maximum local calandria tube temperatures reached during the transient will be about 550°C to 700°C. There will be no significant effects (<15°C) on fuel, sheath and maximum pressure tube temperatures.

The analytical results provide confidence that pressure tube and calandria tube integrity will not be threatened by dry-patch formation in the LOCA scenarios studied.

INTRODUCTION

In a CANDU reactor, the heavy-water coolant flowing through the horizontal fuel channels is contained within Zircaloy pressure tubes which also support the fuel bundles. Surrounding each pressure tube is a stagnant gas annulus with its outer boundary formed by a concentric calandria tube. Outside the calandria tube is the cool heavy-water moderator contained in the calandria itself. See Figure 1. The purpose of the gas annulus is to keep heat losses from the coolant to the moderator at acceptable levels during normal operation. The moderator is kept at a low temperature (<80°C) by a separate cooling circuit. The cool moderator surrounding the calandria tubes provides a potential heat sink following a loss-of-coolant accident (LOCA) should the emergency coolant injection (ECI) flow fail or be impaired.

In certain LOCA scenarios, stagnation of the coolant occurs late in the blowdown period when the coolant pressure is low. Under such conditions, should the ECI be ineffective, pressure tubes will sag onto calandria tubes when the temperatures of the pressure tubes in the affected fuel channels reach a sufficiently high value, about 900 - 1000°C [e.g., 1].

Sudden high localized heat fluxes will occur on the calandria tube because of the rapid discharge of stored heat from the pressure tube immediately following pressure tube contact with the calandria tube. It has been concluded [e.g., 1-5] that the peak transient heat fluxes on the calandria tube will not result in the occurrence of critical heat flux for those CANDU reactors, such as the Bruce units, in which the calandria tube remains submerged in the moderator during the accident sequence. In those CANDU reactors, such as Douglas Point, in which moderator dump is used as one of the safety shutdown methods, calandria tube cooling following a LOCA is provided by falling films produced by spray headers in the top of the calandria. Analysis has indicated that these falling films will probably be disrupted by the high local heat fluxes following pressure tube sagging which will cause film blow-off by bubble nucleation or film break-up into rivulets by Marangoni instability [6,7].

To assess the consequences of falling film disruption in reactors like Douglas Point and the consequences of dry-patch formation in the highly-improbable event of CHF occurring on calandria tubes in reactors like Bruce, a modified version of the computer program IMPECC [2-5] has been developed that allows for dry-patch formation, growth and eventual shrinkage and disappearance as quenching and rewetting occur on the calandria tube.

This paper describes briefly the analytical models and mathematical methods used in IMPECC and in the modification allowing for transient dry patch behavior, gives results for the Bruce and Douglas Point reactors and discusses the implications of these results.

ANALYTICAL MODELS AND MODIFIED IMPECC COMPUTER PROGRAM

Basic IMPECC Model and Program

The analytical models and the mathematical methods used in the basic IMPECC computer program as well as results obtained by its application to various CANDU reactors are given in references 2 to 5 and 8. Modifications to the basic IMPECC models and methods to account for transient dry patch behavior have been described in reference 9. A brief description only of the basic IMPECC model will be given here.

The model permits a detailed analysis of the transient thermal behavior of the fuel elements and pressure and calandria tubes following a LOCA with no ECI flow. The model allows for decay heat generation in the fuel elements and accounts for heat transfer and heat storage effects. An option allows for heat generation from the Zircaloy-water reaction in a simplified manner. The model also allows for the non-axisymmetric conditions which result from the pressure tube sagging onto the calandria tube and the bundle slumping to the bottom of the pressure tube.

The model considers three periods following the end-of-blowdown (EOB) after a LOCA with no ECI flow. These periods are:

- a) the period between EOB and the moment at which the pressure tube sags onto the calandria tube. During this period, the fuel bundle, pressure tube and calandria tube are assumed to have a normal configuration (Figure 1);
- b) the period between the sagging of the pressure tube onto the calandria tube and the slumping of the fuel bundle to the bottom of the pressure tube. During this period, the fuel bundle itself is assumed to retain its normal configuration, and the pressure tube is assumed to contact the calandria tube as shown in Figure 2;
- c) the period following the slumping of the fuel bundle into the bottom of the pressure tube. Since there is little experimental information available on bundle slumping, the approach taken was to assume two configurations as

limiting cases: the normal, open, bundle shown in Figure 2 and the maximum-packing configuration shown in Figure 3. It is expected that the actual thermal behavior of a slumped bundle will be bracketted by the results for these two cases. Results of analyses with these two configurations have shown that predicted peak fuel temperatures are not very sensitive to the assumed configuration [3,4].

Modifications to IMPECC to allow for bundle slumping before pressure tube sagging have been made [5]. Results show that peak fuel and pressure tube temperatures and calandria tube heat fluxes are quite insensitive to the order of pressure tube sagging and bundle slumping [5].

For the thermal analysis of the contacting pressure and calandria tubes, an implicit finite-difference technique is used in a sub-routine, CONCYL, with variable circumferential and radial node spacings established by the time-temperature variation itself. Analysis of heat transfer between the tubes accounts for contact conductance over a locally-deformed strip and for circumferentially-varying heat transfer rates across the eccentric gas gap between the tubes. Heat transfer across the eccentric gas gap is by gas conduction and radiation. The analysis allows for non-continuum effects in the narrowest portion of the gas gap. The program incorporates a model of contact conductance between non-conforming surfaces, allowing for gas conduction in the gap region, which is supported by experimental results described in reference 8. Boundary conditions on the outer surface of the calandria tube consist of either natural convection or nucleate boiling heat transfer coefficients, the choice of which is dictated in the program by the instantaneous local conditions.

For its normal configuration, the model represents the fuel bundle by concentric rings containing the same total masses of UO_2 and Zircaloy as in the actual fuel elements in the corresponding rings of the bundle, thus simulating their heat capacities. For the standard CANDU 37-element bundle, such as used in a Bruce reactor unit, four rings are used, consisting of four fuel nodes and seven sheath nodes. For a 19-element bundle, such as used in the Douglas Point reactor, three rings are used consisting of three fuel nodes and five sheath nodes. The model allows for conduction within the UO_2 fuel, contact conductance between the fuel and the sheath, conduction through the sheath and radiation and conduction through stagnant steam between the fuel-element rings. The interface boundary condition between the models of the fuel bundle and the pressure and calandria tubes is represented by a circumferentially-varying, time-dependent thermal resistance resulting from radiation and conduction heat transfer.

For the slumped configuration, the actual thermal contacts between the fuel elements were determined by using CONCYL to establish appropriate shape factors. Use of CONCYL in this way required the elimination of the fuel sheath nodes, although the thermal resistances of the sheath and the interface between the sheath and the pellet are accounted for. The interface boundary condition between the bundle and the pressure tube is handled as before except that the actual thermal contacts between the elements and the pressure tube are allowed for, using CONCYL. In the program, the bundle is assumed to slump at a specified time or at a specified temperature of specific fuel elements or fuel sheaths.

IMPECC does not account for the heat generated by the Zircaloy-steam reaction using the temperature-dependent reaction kinetics which govern the expected solid-state diffusion-controlled reaction, but, as mentioned earlier, an option is available in which this heat source is accounted for in a simplified manner [5,9], as follows. The heat generation rate as a function of time resulting from the Zircaloy-steam reaction for a maximum-power channel in a Bruce-A reactor unit following a critical LOCA with no ECI for late-stagnation conditions has been established at Whiteshell Nuclear Research Establishment using the computer program CHAN [1]. This heat generation rate as a function of time, for a steam flow rate in the channel, 12 gm/s, which results in the maximum temperature rises of the fuel sheaths because of the

Zircaloy-steam reaction, is applied as an additional heat source term in this option.

Initial conditions used for the IMPECC program are those for the appropriate end-of-blowdown (EOB) state as predicted using blowdown codes such as RODFLOW [10].

Modifications to IMPECC to Account for Transient Dry Patches on a Calandria Tube

The modified version of IMPECC to allow for transient dry patch behavior is described in detail in reference 9, and a summary is given here.

Heat transfer degradation is assumed to occur at a node on the calandria tube when its temperature reaches a value corresponding to CHF on the boiling curve. The degraded heat transfer region advances node-by-node as the temperature beyond the edge of the region reaches the critical value. The specified critical heat flux is an input variable to the program, and may be the true critical heat flux for a submerged tube or the film disruption heat flux for a film-cooled tube. Quenching and rewetting of a node at the edge of the degraded region is assumed to occur when its temperature drops below a specified quenching temperature.

To predict the calandria tube outer-surface temperatures and heat fluxes for this case requires appropriate heat transfer coefficient correlations to be used for the various heat transfer regimes involved. The heat transfer regimes and the transition points between regimes are shown in Figure 4, as described below. In the natural convection and nucleate boiling regimes, the correlations used are those in the standard version of IMPECC. In the film boiling regime, Gillespie's modification [11] of the Dhir and Purohit correlation [12] for sub-cooled film boiling is used, and radiation heat transfer is accounted for. In the transition boiling regime, an approximate boiling curve was established by linear interpolation between the specified critical heat flux and the minimum film-boiling heat flux.

To permit the code to follow accurately the rapid changes as a dry patch forms or rewets at a node, IMPECC was modified by increasing the number of nodes in the anticipated region of the dry patch and by sub-dividing further the already small time steps used after pressure tube contact with the calandria tube. The sub-divided time steps are termed minor time steps while the normal time steps are termed major time steps. Choleski matrix decomposition [13] is used to permit small minor time steps (e.g., 3.6 milliseconds) to be used without requiring excessive computer time. The radiation components of the coefficients in the matrix are held constant during a major time step, that is, they do not change from one minor time step to the next. By treating the problem as linear between major time steps, the factorization of the finite-difference coefficient matrix, which is very time consuming, does not have to be performed at the minor time steps. This simplification helps to ensure an overall rapid calculation procedure.

RESULTS

Submerged Calandria Tubes - Bruce Reactor

In the two cases run for a Bruce reactor unit, input conditions were those for a maximum power channel with the pressure tube assumed to sag onto the calandria tube at 1000°C and the bundle assumed to slump when the temperature of the fuel in the outer fuel ring reached 1300°C. Other input conditions were the same as those for the Bruce standard case for a LOCA caused by a large inlet header break [e.g., 3,4,5].

The value of critical heat flux used in the Bruce cases, 240 W/cm², is the predicted "steady state" critical heat flux for a submerged tube under uniform heat flux conditions with a nominal sub-cooling of 30°C [2]. However, critical heat flux will not actually occur should local heat fluxes near the contact line exceed this value when a pressure tube sags onto a calandria tube. First of all, as stated above,

the predicted value applies for a uniform heat flux distribution around the circumference, while the actual distribution at and following pressure tube contact is highly non-uniform, with the highest heat flux at the bottom and a very low heat flux near the top (typically less than 20 W/cm^2). For horizontal cylinders under both pool boiling and upward cross-flow boiling, CHF always occurs at the top of the tube [14]. Furthermore, even if the critical position were at the bottom of the tube, critical heat flux would not be expected to occur because of the very small area and exceedingly short time over which the calculated local heat flux exceeds the nominal CHF value, which results in insufficient energy transfer during the heat flux peaking period for CHF actually to occur [2,3,4,5,8]. Nevertheless, for the present cases it is assumed that CHF will occur locally when the predicted heat flux reaches 240 W/cm^2 .

Many variables govern the effective rewetting temperature or apparent quenching temperature [e.g., 15,16]. For the present conditions, the most realistic estimates of the quenching temperature can be obtained from the correlations for the minimum film boiling temperature of Bradfield [17] and of Dhir and Purohit [12]. For the nominal moderator sub-cooling of 30°C , these correlations predict minimum film boiling temperatures of 483°C and 442°C respectively. For zero sub-cooling, minimum film boiling temperatures of 296°C and 202°C , respectively, are predicted. Because of uncertainties in the application of the correlations to the present conditions resulting from geometric and material differences and because of uncertainties in the actual value of the local sub-cooling, the values of rewetting temperatures used in the Bruce runs were taken as 250°C and 350°C . Even the higher of these two values should be conservative notwithstanding the uncertainties mentioned above, while the lower value is very conservative.

Results for the quenching temperature (T_Q) of 350°C , probably the more representative value, are given in Figures 5 and 6. Figure 5 gives the outer surface temperature and heat flux at the bottom of the calandria tube ($\theta = 0^\circ$) as a function of time just before and immediately following sagging of the pressure tube onto the calandria tube. For the assumed critical heat flux of 240 W/cm^2 , the dry patch forms almost instantaneously, following which the local surface heat flux drops rapidly to a minimum value of about 20 W/cm^2 . A maximum temperature of about 530°C is reached on the outer surface of the calandria tube about 2.0 seconds after the pressure tube sags. After the peak temperature is reached, the calandria tube temperature drops relatively slowly until the quenching temperature of 350°C is reached about 5.0 seconds after the pressure tube sags, following which the temperature plummets to about 135°C . Upon rewetting, the local heat flux rises rapidly to a value just below the assumed CHF value and then decreases moderately quickly.

Further information for this case is given in Figure 6 in which the temperatures and heat fluxes on the calandria tube are shown as functions of angular position at about one second after the pressure tube sags onto the calandria tube. Also shown are the surface temperatures and heat fluxes on the calandria tube for essentially the same conditions for the expected case in which CHF does not occur, taken from earlier runs using the standard version of IMPECC.* The results for the two cases agree quite well beyond the edge of the dry patch, giving confidence to the predictions for the transient dry patch analysis. Similar agreement was obtained at all other times after contact.

The effect of quenching temperature on the calandria tube temperature transient is shown in Figure 7. As expected, the peak temperature reached is higher, about

* There is a slight difference between the conditions for the two sets of runs in that the earlier results were obtained assuming a constant and uniform temperature at the outer surface of the calandria tube. The use of this boundary condition instead of the more realistic one of a variable heat transfer coefficient on the calandria tube has been shown earlier to result in no significant differences in local values of heat fluxes and pressure tube, fuel and sheath temperatures at any time [4].

593°C compared to about 530°C, for the lower quenching temperature and it occurs somewhat later. Calandria tube cool-down proceeds more slowly for the lower quenching temperature, with quenching occurring at about 14 seconds for $T_Q = 250^\circ\text{C}$ compared to somewhat less than 6 seconds for $T_Q = 350^\circ\text{C}$.

The growth and shrinkage of the dry patches for the two quenching temperatures are shown in Figure 8. Although the maximum extent of the dry patch at $T_Q = 250^\circ\text{C}$ is about twice that at $T_Q = 350^\circ\text{C}$, the actual size is still quite small, covering only about 6 degrees.

The study also showed that a transient dry patch would have only a slight effect on the maximum temperature of the pressure tube, less than 10°C at the most, since the maximum temperature of this component occurs at a position well away from the dry patch.

The results also showed that a transient dry patch would have negligible effects on the fuel temperatures during the transient, with predicted temperatures differing by less than 1°C at the most, irrespective of the quenching temperature. This finding reflects the relatively high thermal resistance between the fuel bundle and the outer surface of the calandria tube as well as the small area affected by the dry patch and the small period of time involved.

Cases were also examined in which the film boiling heat transfer coefficient was reduced by ignoring the effect of sub-cooling. This change had the effect of reducing the film boiling heat transfer coefficient by factors between 3 and 6 depending on the temperature level. While this change resulted in larger dry patches requiring longer to rewet completely, and hence higher calandria tube peak temperatures, these peak temperatures were not very sensitive to the lower film boiling heat transfer rates. The peak temperatures reached with the lower film boiling heat transfer rates were about 580°C and 650°C for $T_Q = 350^\circ\text{C}$ and 250°C respectively, compared to about 530°C and 593°C when the effect of sub-cooling on the film-boiling heat transfer coefficient is allowed for. The reduced film-boiling coefficients had essentially no effect on the pressure tube maximum temperatures nor on fuel temperatures.

The foregoing results show that, in the highly improbable event of CHF occurring on the calandria tube following pressure tube sagging, the maximum calandria tube temperatures reached would be quite moderate and the very small dry-patch formed by CHF would soon rewet. There would be no threat to the integrity of the calandria tube. There would be essentially no effects on the fuel, sheath, and local maximum pressure tube temperatures.

Falling-Film Cooled Calandria Tubes - Douglas Point Reactor

The Douglas Point reactor uses moderator dump as one of its safety shut-down mechanisms. Subsequent cooling of the calandria tubes is by sprays from headers at the top of the calandria which form falling films on the calandria tubes. Under LOCA conditions with impaired emergency coolant injection, these films must provide a heat sink for the decay heat of the fuel, for heat generated by the Zircaloy-water reaction and for fuel channel stored heat, a function performed in other CANDU reactors which do not use moderator dump for shut-down purposes by the bulk moderator itself [3]. Potential mechanisms of film disruption are flow starvation, non-uniform surface tension effects (Marangoni instability) and film blow-off by bubble nucleation effects. Studies of these disruption mechanisms under conditions relevant to the Douglas Point reactor are described in references 4, 6 and 7.

These studies indicated that two mechanisms of falling film disruption might exist for the conditions of concern here: Marangoni instability and film blow-off by bubble nucleation.

The analyses in reference 6 indicate that film disruption by Marangoni instability

may occur at quite low heat fluxes, of the order of 10 W/cm^2 , for conditions of concern here. However, Marangoni instability does not result in the film departing from the surface but in the film breaking up into rivulets which remain on the surface. Thus, adequate cooling is provided on the portions of the surface covered by the rivulets. Whether cooling of the rest of the surface is adequate will depend on the spacing and width of the rivulets [4].

The analyses of reference 6 also indicate that film blow-off by bubble nucleation, for relevant Douglas Point reactor conditions, will probably occur at local heat fluxes of about 100 to 135 W/cm^2 .

To assess transient dry-patch behavior on the Douglas Point reactor calandria tubes, the modified version of IMPECC was run for Douglas Point conditions assuming that film critical conditions, i.e. complete film disruption, occurred at a local heat flux of 125 W/cm^2 .

The quenching temperature for the present case will be governed by parameters similar to those governing conventional rewetting by top-flooding [e.g., 15]. The correlation of Yu has been recommended for use in such cases in the critical evaluation of the literature by Butterworth and Owen [15], and was used here. The estimated quenching temperature for the present conditions, ignoring the beneficial effect of film sub-cooling, is about 330°C . Another approach, based on the observed relation between the quenching temperature and the homogeneous nucleation temperature [15], leads to a quenching temperature of about 210°C . Considering these estimates, and that a lower value is more conservative in this case, a quenching temperature of 250°C was assumed for this study.

The heat transfer coefficient correlation used for the film blow-off region is again that of film boiling, but no benefit of sub-cooling was assumed. The resulting heat transfer coefficients for the present conditions are quite low, of the order of $0.015 \text{ W/cm}^2\text{K}$.

Results for the Douglas Point reactor are given in Figure 9, where the growth and shrinkage of the dry patch are shown. Although the general behavior is quite similar to that for the dry patches on a Bruce reactor calandria tube, as shown earlier, the maximum extent of the dry-patch is somewhat greater for the same quenching temperature (12° compared to 6°) and the time to rewet is much longer, about 90 seconds compared to about 14 seconds. The maximum calandria tube temperature reached under the dry patch is about 700°C , a few seconds after contact.

The results show that, should a LOCA occur in the Douglas Point reactor with impaired emergency coolant injection, with the falling film blown off a calandria tube when the pressure tube sags onto it, the dry area would not be very extensive and would rewet in a reasonably short time. The maximum temperatures reached by the calandria tube are moderate, and higher-than-normal temperatures do not cover a large area nor persist for a long time. Therefore, we conclude that the integrity of the calandria tube will not be jeopardized during the transient film blow-off.

A comparison of predicted fuel, sheath and maximum pressure tube temperatures for the present case of a transient dry patch, at the moment that the patch rewets, to the temperatures at the same time after pressure tube/calandria tube contact for a previous case in which no film disruption was assumed shows that there is very little effect on fuel, sheath and maximum pressure tube temperatures, less than 15°C at the most.

These results have been obtained for a maximum fuel element power rating of 28 W/cm , corresponding to 70% of full power for the Douglas Point reactor. However, the transient dry patch behavior, being essentially a result of stored-heat effects rather than power-level effects, will not be affected significantly by a change in power level. Therefore, the results will apply also for 100% full power. Although

some numerical inaccuracy may have occurred in this case because the dry patch extended into nodes with a relatively coarse mesh and some time steps were relatively long, this inaccuracy probably did not have very significant effects on the results.

CONCLUSIONS

In this paper, we have described the development of the modified IMPECC program which permits the analysis of the behavior of transient dry patches on a calandria tube in certain LOCA scenarios.

Major conclusions reached can be summarized as follows:

1) In the highly improbable event that CHF occurs when a pressure tube sags onto a calandria tube following a LOCA with impaired emergency coolant injection in a Bruce reactor, a dry patch would form and grow to a maximum extent of about 3 to 6 degrees on each side of the bottom of the calandria tube. The dry patch would rewet within about 6 to 14 seconds. The maximum local calandria tube temperature reached would be less than 600°C. Calandria tube integrity would almost certainly be maintained. There would be negligible effects on fuel, sheath and maximum pressure tube temperatures. Pressure tube integrity would not be threatened. These results are not very sensitive to the magnitude of the film boiling heat transfer coefficient.

2) In the Douglas Point reactor the analysis shows that, for film disruption by bubble nucleation, the dry patch formed following pressure tube/calandria tube contact will reach a maximum extent of about 12° on each side of the bottom of the calandria tube and will completely rewet within about 90 seconds. The maximum local calandria tube temperature will be about 700°C. Calandria tube integrity will almost certainly be maintained. There will be small increases (less than 15°C at the most) in fuel, sheath and maximum pressure tube temperatures above those that would otherwise occur. Pressure tube integrity will not be jeopardized. These results are not affected significantly by reactor power level.

3) The analyses have been done ignoring heat generated by the Zircaloy-steam reaction. However, the conclusions are valid for cases in which Zircaloy-water reactions would eventually occur. The reason for this conclusion is that the dry-patch behavior and its effect on calandria tube temperature, and thus integrity, is essentially governed by the effects of stored heat in the pressure tube at the time that the pressure tube sags onto the calandria tube. With the Zircaloy-water exothermic reaction allowed for, the pressure tube would simply sag onto the calandria tube somewhat earlier in time. Also, because of the poor thermal coupling between the calandria tube and the other components as well as the small areas affected and limited periods involved, we would expect the occurrence of a transient dry patch to have very minor effects on fuel, sheath and maximum pressure tube temperatures should a Zircaloy-water reaction occur at these surfaces.

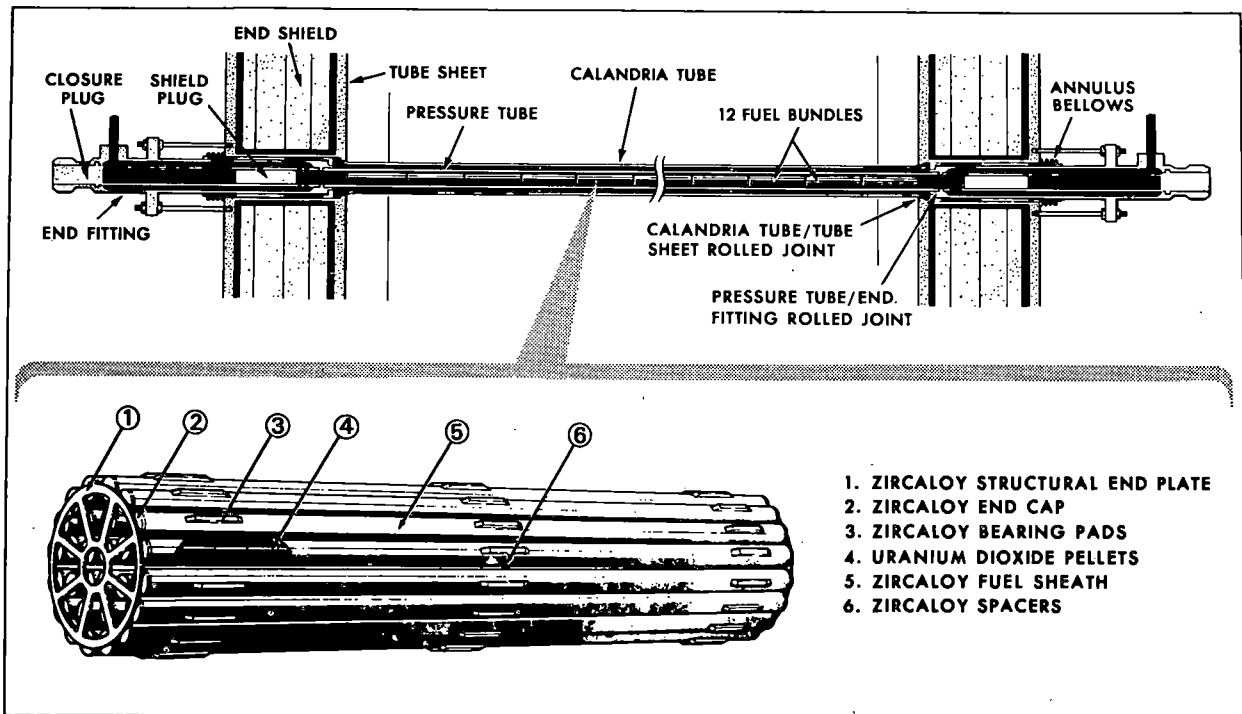
ACKNOWLEDGEMENTS

The work described in this paper was undertaken for the Atomic Energy Control Board under contract OSU 80-00237. Permission of the AECB to publish this paper is appreciated.

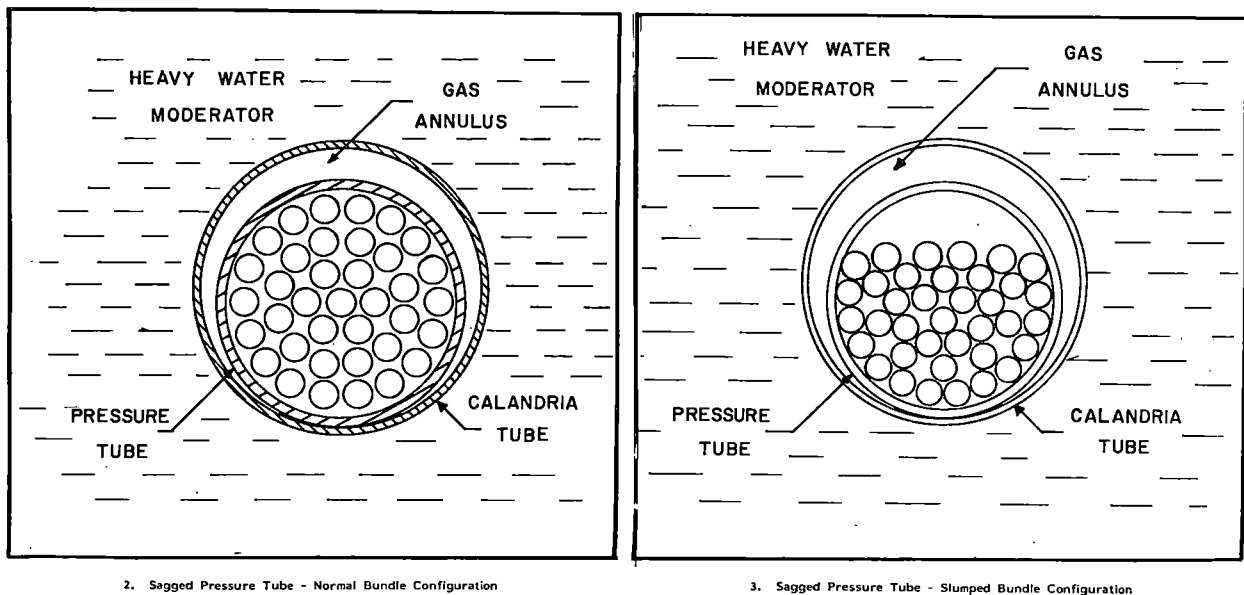
The authors thank Allison Rogers for preparing the figures and Mrs. R. Thomas for typing the report.

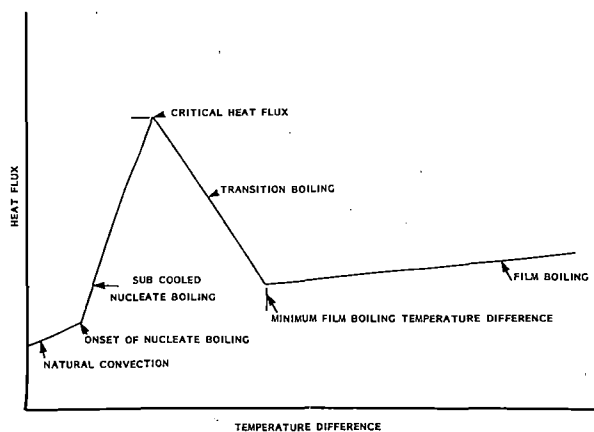
REFERENCES

1. W.T. HANCOX, CANDU Safety Research: A Status Report, Proc. 2nd Annual Conf., CNS, p.140, June 10, 1981.
2. J.T. ROGERS and T.C. CURRIE, A Model for Thermal Analysis of a CANDU Fuel Channel Following a LOCA with Delayed ECC Flow. Paper presented at CNA 18th International Conference, Ottawa, Ont., June 14, 1978, Dept. of Mech. and Aero. Eng., Carleton University, May, 1978.
3. J.T. ROGERS, CANDU Moderator Provides Ultimate Heat Sink in a LOCA, Nuclear Eng. Int., 24, 280, p.38, Jan., 1979.
4. J.T. ROGERS, Studies of Loss-of-Coolant and Loss-of-Regulation Accidents, 1977-1979, Dept. of Mech. and Aero. Eng., Carleton University, Atomic Energy Control Board Report, Oct., 1979.
5. J.T. ROGERS, Loss-of-Coolant Accidents with Impaired Emergency Coolant Injection with and without Additional Heat Sinks. Dept. of Mech. and Aero. Eng., Carleton University, Atomic Energy Control Board Report, Feb., 1981.
6. J.T. ROGERS, Falling Film Flow, Heat Transfer and Breakdown on Horizontal Tubes, Dept. of Mech. and Aero. Eng., Carleton University, Atomic Energy Control Board Report, Nov., 1980.
7. J.T. ROGERS, Laminar Falling Film Flow and Heat Transfer Characteristics on Horizontal Tubes, Can. J. Chemical Engineering, 59, 213, April, 1981.
8. T.C. CURRIE and J.T. ROGERS, Heat Transfer Between Contacting Non-conforming Surfaces with Application to CANDU Reactor Safety Analysis, in Heat Transfer in Nuclear Reactor Safety, Hemisphere Publishing Corp., 1982.
9. J.T. ROGERS, Thermal and Hydraulic Behavior of CANDU Cores Under Severe Accident Conditions, Dept. of Mech. and Aero. Eng., Carleton University, Atomic Energy Control Board Report, Feb., 1982.
10. J.N. ELLIOTT, RODFLOW. A Program for Studying Transients in a Power Reactor Cooling Circuit, AECL Report TDAI-11, June, 1968.
11. G.E. GILLESPIE, An Experimental Investigation of Heat Transfer from a Reactor Fuel Channel to Surrounding Water, Proc. 2nd Annual Conf., CNS, p.157, June 10, 1981.
12. V.K. DHIR and G.P. PUROHIT, Sub-cooled Film Boiling Heat Transfer from Spheres, Nuclear Eng. and Design, 47, 49-66, 1978.
13. G. DAHLQUIST, A. BJORCK and N. ANDERSON, Numerical Methods, Prentice-Hall Inc., 1974.
14. J.T. ROGERS, Critical Heat Flux on CANDU Reactor Calandria Tubes, A Study for AECL, Carleton University, Nov., 1972.
15. D. BUTTERWORTH and R.G. OWEN, The Quenching of Hot Surfaces by Top and Bottom Flooding, AERE-R7992, Mar., 1975.
16. Y. LEE and M. SALCUDEAN, A Study of the Process of Rewetting of Hot Surfaces by Flooding, Final Report to the Atomic Energy Control Board, Univ. of Ottawa, 1979.
17. W.S. BRADFIELD, On the Effect of Sub-cooling on Wall Superheat in Pool Boiling, J. of Heat Transfer, 89, 3, 269-270, Aug., 1967.

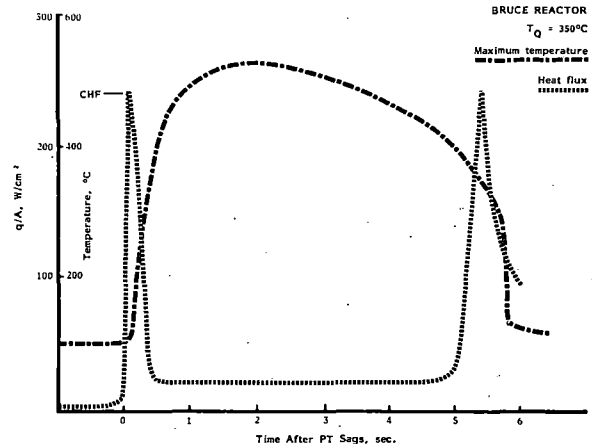


1. Cross-section of CANDU Reactor Fuel Channel

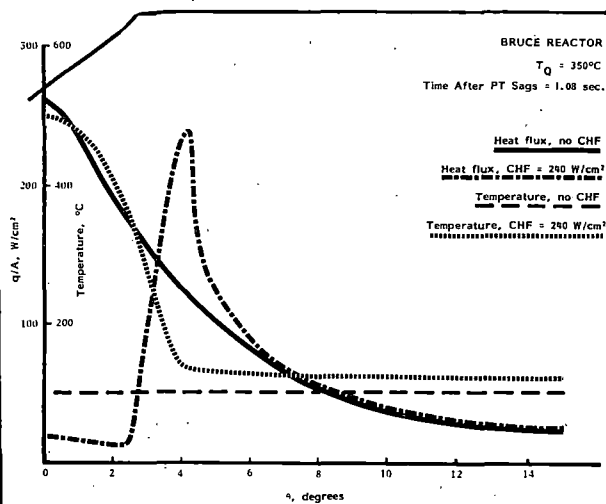




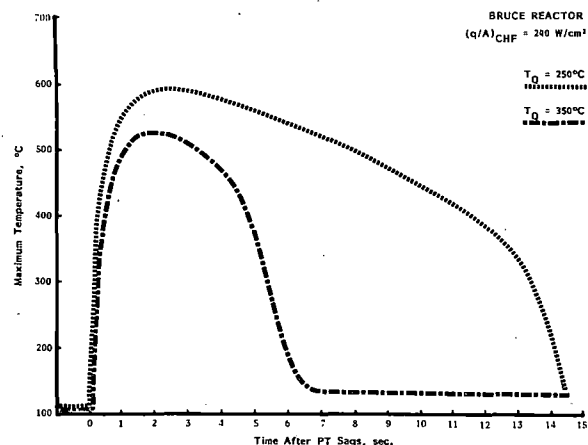
4. Heat Transfer Regimes on Calandria Tubes



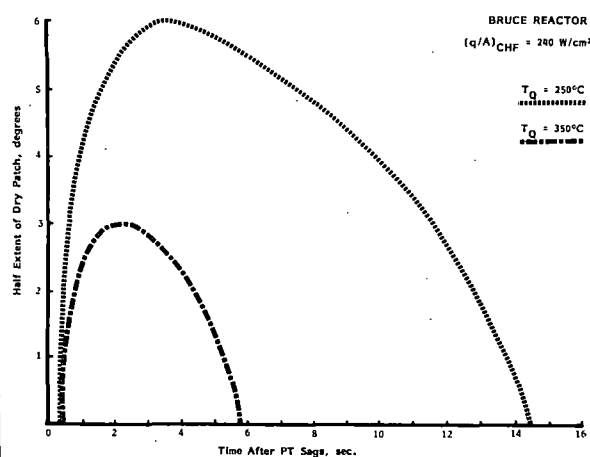
5. Effect of CHF on Temperature and Heat Flux at Bottom of Calandria Tube



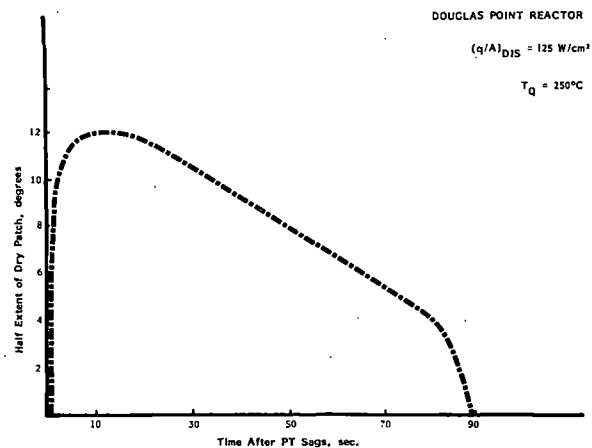
6. Effect of CHF on Calandria Tube



7. Effect of Quenching Temperature on Calandria Tube Temperature Transient



8. Growth and Shrinkage of Dry Patch, Bruce Reactor



9. Growth and Shrinkage of Dry Patch, Douglas Point Reactor

A SIMPLIFIED METHOD FOR PREDICTING AFTERHEAT POWER FROM URANIUM-FUELED PWR FUEL ASSEMBLIES

J. C. Ryman, O. W. Hermann, C. C. Webster, and C. V. Parks

Computer Sciences at Oak Ridge National Laboratory
Oak Ridge, Tennessee 37830, U.S.A.

ABSTRACT

The SAS2 and ORIGEN-S computer codes of the SCALE system have been used with ORIGEN-S data libraries and a 27-group ENDF/B-V cross-section library to generate a tabulation of afterheat power data for uranium-fueled PWR assemblies. The tabulations were made for eight combinations of enrichment and burnup, for cooling times extending to 110 years, and for both "typical" and "conservative" irradiation histories. Based on comparisons of SAS2/ORIGEN-S calculations with measured values and ANSI method calculations, and on a simple uncertainty analysis, a prescription has been developed for using the tabulation, with appropriate safety factors, to predict conservative values of afterheat power.

INTRODUCTION

The design of independent spent fuel storage installations requires knowledge of the heat generation rate in the fuel to be stored. To meet this need for uranium-fueled PWR assemblies, a tabulation of afterheat power data has been generated by using the SAS2 and ORIGEN-S computer codes of the SCALE code system¹ with the ORIGEN-S data libraries and a 27-group ENDF/B-V cross-section library collapsed from the 227-group CSRL-V library.² The SAS2 code¹ is a shielding analysis module which, as a part of its burnup calculations, generates burnup-dependent ORIGEN-S data libraries with updated (cell-averaged) cross sections for major actinide and fission product nuclides (e.g., U, Pu, Am, and Cm isotopes, ¹³³Cs, ¹³⁵Xe, etc.). The ORIGEN-S code¹ is an updated version of the well-known ORIGEN code³ used here to perform fuel depletion and afterheat power calculations with burnup-dependent cross-section libraries.

QUALIFICATION OF CODES AND DATA LIBRARIES

To assess the qualification of the SAS2 and ORIGEN-S codes and their data libraries to predict afterheat power, a study⁴ was performed in which calculated

nuclide inventories were compared to measured values for assemblies from the Yankee-Rowe,⁵ H. B. Robinson Unit 2,⁶ and Turkey Point Unit 3⁷ reactors. In addition, calculated values of afterheat power were compared to measured values⁸ for three assemblies from Turkey Point Unit 3. Details of the comparisons can be found in Ref. 4. It was found that, while calculated quantities of uranium nuclides compared well with measured values, the calculations predicted greater quantities of most plutonium, americium, and curium isotopes than the measurements indicated. It was estimated that, for a fuel burnup near 30 GWD/MTU, this overprediction of actinide inventories corresponds to an overestimate of from 0.6 to 1.4% in the total afterheat power (10 to 20% in actinide power) at a cooling time of 2.5 years. Only a few uncorrected measurements of fission product activities were available for comparison;⁶ but when estimates of known measurement errors were considered, the calculated fission product activities were probably no more than 4 to 8% conservative. An overprediction of about 4% corresponds well to the observed differences in calculated and measured afterheat power, shown in Table I.

TABLE I
Afterheat Power of Turkey Point Unit 3 Assemblies

Burnup (MWD/MTU)	Cooling Time (d)	Afterheat Power (W/assembly)					Percent Difference
		Measured Total	Calculated			Total	
			Light Element	Actinide	Fission Product		
27863	864	1550	36.7	98.8	1500	1635.5	5.52
28430	962	1423	35.8	97.7	1350	1483.5	4.25
26485	963	1284	33.3	82.4	1240	1355.7	5.58

Considering the expected uncertainty of $\pm 5\%$ in the measured values,⁸ the calculated values are in excellent agreement, and are conservative by amounts consistent with the observed differences in the calculated and measured nuclide inventories.

AFTERHEAT POWER CALCULATIONS

Following the qualification of SAS2 and ORIGEN-S for the prediction of PWR afterheat power, fuel inventory and afterheat power calculations were performed for 14x14, 15x15, and 17x17 PWR fuel lattice geometries. It was found that for a 3.3 wt % ²³⁵U enrichment and a burnup of 33 GWD/MTU, the 17x17 geometry gave the most "conservative" predictions of nuclide inventories and afterheat power. Differences in nuclide inventories were generally no greater than 3%, and differences in afterheat power never exceeded 0.6% for cooling times up to 10 years.

Using a 17x17 fuel lattice geometry, afterheat power calculations were performed for the eight combinations of enrichment and burnup shown in Table II. Calculations were made for two different kinds of irradiation history: (1) a "typical" history of three cycles each with 80% full-power irradiation and 20% down time, and (2) a "conservative" history in which the third cycle had 100% full-power operation. The specific power during irradiation was 37.5 MW/MTU, and the irradiation time was varied to achieve the desired burnup. Twenty-one cooling times from discharge to 110 years were used.

TABLE II

Burnup and Initial U Composition for Afterheat Power Cases

Case	Burnup (GWD/MTU)	U Composition (Wt %)		
		^{234}U	^{235}U	^{238}U
1	18	0.022	2.5	97.478
2	27	0.022	2.5	97.478
3	33	0.029	3.3	96.671
4	55	0.029	3.3	96.671
5	40	0.035	4.0	95.965
6	46	0.035	4.0	95.965
7	50	0.040	4.5	95.460
8	55	0.040	4.5	95.460

The total (light element + actinide + fission product) afterheat power for the conservative irradiation history of cases 1, 3, 6, and 8 is shown in Fig. 1. Tabulations and plots for all cases can be found in Ref. 4.

As a further check on the SAS2/ORIGEN-S method, the fission product afterheat power was calculated by the method described in Sections 3.2, 3.4, and 3.5 of American National Standard ANSI-ANS-5.1-1979⁹ for the eight cases with typical irradiation histories. This method is based on data for a 23-term exponential fit to $F_i(t, T)$, the afterheat power (MeV s^{-1} per fission s^{-1}) at t seconds after an operating period of T seconds at a constant fission rate of nuclide i in the absence of neutron capture in fission products. Thermal fission of ^{235}U and ^{239}Pu , and fast fission of ^{238}U were considered. The effect of neutron capture in fission products was accounted for by a simple multiplicative factor $G(t)$, defined in the standard. Total afterheat power for the ANSI method was found by adding the light element and actinide afterheat power from ORIGEN-S to the ANSI method fission product afterheat power, as permitted by the standard.

The total afterheat power from the SAS2/ORIGEN-S and ANSI methods for case 3 with a typical irradiation history is shown in Fig. 2. In general, the ANSI method fission product afterheat power was greater than that from ORIGEN-S for cooling times less than 10 years. The maximum differences occurred near a cooling time of two years and ranged from 40% in case 1 to 9% in case 8. Comparison of ANSI and ORIGEN-S results for test cases with no neutron capture showed that these differences were caused by conservative values of the neutron capture correction factor in the ANSI method. This was confirmed by the small differences in fission product afterheat power of less than 1 or 2% for cooling times greater than 10 years, when the capture effect is small.

SIMPLIFIED METHOD FOR PREDICTING AFTERHEAT POWER

A simple prescription was developed for predicting conservative values of afterheat power for uranium-fueled PWR assemblies. This prescription uses the tabulations of total afterheat power in Ref. 4 for cases 1 to 3 and 5 to 8 (Case 4 was used in conjunction with case 3 only for assessing the effect of enrichment on afterheat power).

The prescription for predicting conservative values of afterheat power follows. In this prescription, the term "2 σ uncertainty" is not used in a strictly statistical

sense, but is taken to mean twice the value of the uncertainty due to random errors plus an estimate of any nonconservative bias.

For the purpose of following the prescription, the operating history of the assembly will be divided into three operating cycles of equal burnup. Note that the lengths of the three cycles are not necessarily equal.

(1) If the third cycle of the operating history has at least 10% downtime in the last 30% of the cycle time and at least 20% downtime in the last 70% of the cycle time, use the tabulated values of afterheat power for a "typical" operating history. Here, 10 and 20% downtime mean 10 and 20% of the time for the entire last cycle. Otherwise, use the tabulated values for a "conservative" operating history. Both sets of tabulations can be found in Appendix C of Ref. 4.

(2) Calculate the burnup of the assembly plus a 2σ uncertainty ($B_{\max} = B + 2\sigma_B + \Delta B_{\text{bias}}$) and then compute the afterheat power at the tabulated cooling times by linear interpolation in burnup (using B_{\max}) between the tabulated values.

(3) Compute, by linear interpolation between the enrichments for the tabulated cases, the enrichment E_I corresponding to the burnup B_{\max} . If the interpolated enrichment E_I is greater than the actual enrichment E , increase the values of afterheat power from step 2 by 0.5% for each difference of 0.1 in the wt % ^{235}U enrichment.

(4) Calculate the average specific power of the assembly plus a 2σ uncertainty (in MW/MTU) for the following time intervals: (a) the last 10 days of operation, (b) the last 30 days of operation, (c) the last 60 days of operation, (d) the time equivalent to the last one-half (in burnup) of the last operating cycle, (e) the last operating cycle, and (f) the entire operating history. When computing the average specific power for each interval, do not include any downtime in the calculation. For example, if the last 30 days includes 5 days of downtime, the average power is the burnup for the last 30 days divided by 25 days. In addition, compute a specific power equal to 88% of the maximum specific power (including a 2σ uncertainty) during the last operating cycle. Then, find the maximum of these seven values. This value will be called $P_{\max, \text{avg}}$, the maximum average specific power.

(5) If $P_{\max, \text{avg}}$ is >37.5 MW/MTU, multiply the values of afterheat power from step 3 by the ratio ($P_{\max, \text{avg}}/37.5$). If the assembly specific power (plus a 2σ uncertainty) immediately before discharge (P_{dis}) is >37.5 MW/MTU, the afterheat power at discharge should be multiplied by the ratio ($P_{\text{dis}}/37.5$) instead of the ratio ($P_{\max, \text{avg}}/37.5$).

(6) After the corrections of step 5, afterheat power for cooling times not in the table should be computed by interpolation which is logarithmic in afterheat power and linear in time.

(7) Multiply the values of afterheat power from step 6 by a safety factor of (a) 1.15 at discharge, or (b) 1.08 for cooling times greater than one day. For cooling times between discharge and one day, determine the safety factor by linear interpolation between 1.15 and 1.08.

(8) If the fuel assembly can be shown to have an initial effective ^{59}Co content (see Appendix E of Ref. 4) of no more than 142.96 g/MTU, including uncertainty, the calculation is finished. Otherwise, an additional safety factor of 0.5% of the afterheat power from step 7 should be added for every 10% excess of ^{59}Co over 142.96 g/MTU. The calculation is now complete.

A similar procedure, outlined below, was developed for using tabulated values of light element and actinide afterheat power in combination with values of fission product afterheat power from the ANSI method.

(1) Select the tabulated values of light element and actinide afterheat power in Appendix D of Ref. 4 for either the "typical" or "conservative" operating history as prescribed in step 1 of the last section.

(2) Calculate the burnup of the assembly plus a 2σ uncertainty ($B_{\max} = B + 2\sigma_B + \Delta B_{\text{bias}}$), and then compute the light element plus actinide afterheat power at the tabulated cooling times by linear interpolation in burnup between the tabulated values.

(3) Compute, by linear interpolation between the enrichments for the tabulated cases, the enrichment E_I corresponding to the burnup B_{\max} . If the interpolated enrichment E_I is greater than the actual enrichment E , increase the values of afterheat power from step 2 by 2% for each difference of 0.1 in the wt % ^{235}U enrichment.

(4) Compute the maximum average specific power $P_{\max, \text{avg}}$ as in step 4 of the preceding section.

(5) If $P_{\max, \text{avg}}$ is >37.5 MW/MTU, multiply the values of afterheat power from step 3 by the ratio $(P_{\max, \text{avg}}/37.5)$. Otherwise, no correction is made.

(6) After any corrections in step 5, afterheat power for cooling times not in the table should be computed by interpolation which is logarithmic in afterheat power and linear in time.

(7) Compute the total afterheat power by adding the values of light element and actinide afterheat power from step 6 to the fission product afterheat power (plus appropriate uncertainty, e.g., 2σ) from the ANSI method.

(8) Multiply the values of total afterheat power from step 7 by a safety factor of 1.06.

(9) If the initial effective ^{59}Co content of the fuel assembly (see Appendix E of Ref. 4) including uncertainty, exceeds 142.96 g/MTU, add an additional 0.5% to the values of afterheat power in step 8 for every 10% excess of ^{59}Co over 142.96 g/MTU. The calculation is now complete.

The corrections for an irradiation history in which the specific power exceeds 37.5 MW/MTU were based on comparisons of afterheat power calculated with ORIGEN-S for cases having the same burnup but different irradiation histories. The safety factors were determined from comparison of the calculations and measurements discussed earlier, comparison with ANSI method results and from an analysis of the uncertainties in the SAS2/ORIGEN-S method. Details are given in Ref. 4.

Because of its simplicity and ease of use, the prescriptions outlined above and the tabulations of afterheat power⁴ are being used by the Nuclear Regulatory Commission to develop a regulatory guide¹⁰ for spent fuel heat generation in an independent spent fuel storage installation.

ACKNOWLEDGMENT

This work was sponsored by and performed for the Office of Nuclear Regulatory Research, U. S. Nuclear Regulatory Commission under Interagency Agreement DOE 40-543-75 with the U. S. Department of Energy under contract W-7405-eng-26 with the Union Carbide Corporation.

REFERENCES

1. SCALE: A Modular Code System for Performing Standardized Computer Analyses for Licensing Evaluation, NUREG/CR-0200 (ORNL/NUREG/CSD-2), Vols. 1-3 (October 1981)
2. W. E. Ford, III et al., CSRL-V: Processed ENDF/B-V 227-Neutron-Group and Point-wise Cross-Section Libraries for Criticality Safety, Reactor and Shielding Studies, NUREG/CR-2306 (ORNL/CSD/TM-160) (June 1982).
3. M. J. Bell, ORIGEN -- The ORNL Isotope Generation and Depletion Code, ORNL-4628 (May 1973).
4. J. C. Ryman, O. W. Hermann, C. C. Webster, and C. V. Parks, Fuel Inventory and Afterheat Power Studies of Uranium-Fueled Pressurized Water Reactor Fuel Assemblies Using The SAS2 and ORIGEN-S Modules of SCALE with an ENDF/B-V-Updated Cross-Section Library, NUREG/CR-2397 (ORNL/CSD-90) (June 1982).
5. J. B. Melehan, Yankee Core Evaluation Program Final Report, WCAP-3017-6094 (January 1971).
6. D. O. Campbell, "Hot-Cell Studies," in LWR Fuel Reprocessing and Recycle Program Quarterly Report for Period July 1 to September 30, 1976, ORNL/TM-5660 (November 1976).
7. S. D. Atkin, Destructive Examination of 3-Cycle LWR Fuel Rods from Turkey Point Unit 3 for the CLIMAX-Spent Fuel Test, HEDL-TME 80-89 (June 1981).
8. F. Schmittroth, G. J. Neely, and J. C. Krogness, A Comparison of Measured and Calculated Decay Heat for Spent Fuel Near 2.5 Years Cooling Time, TC-1759 (August 1980).
9. American National Standard for Decay Heat Power in Light Water Reactors, ANSI/ANS-5.1-1979, American Nuclear Society, LaGrange Park, IL, 1979.
10. Spent Fuel Heat Generation in an Independent Spent Fuel Storage Installation, Draft Regulatory Guide, U. S. Nuclear Regulatory Commission, Washington, DC (to be published).

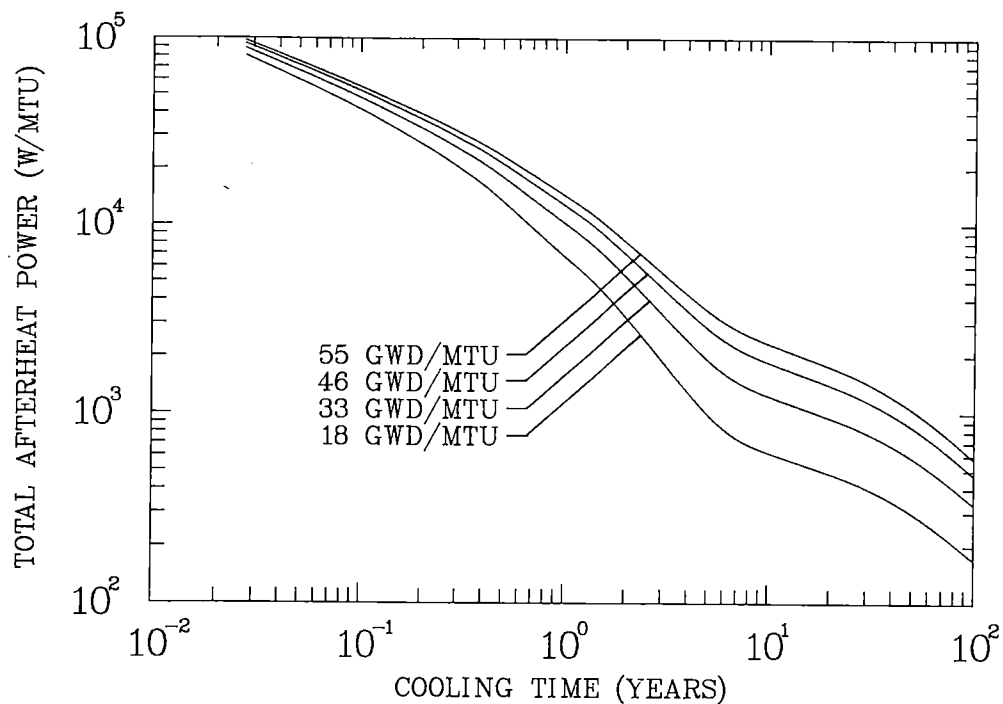


Fig. 1. Total afterheat power for cases 1, 3, 6, and 8, based on a conservative irradiation history for a 17x17 PWR fuel assembly.

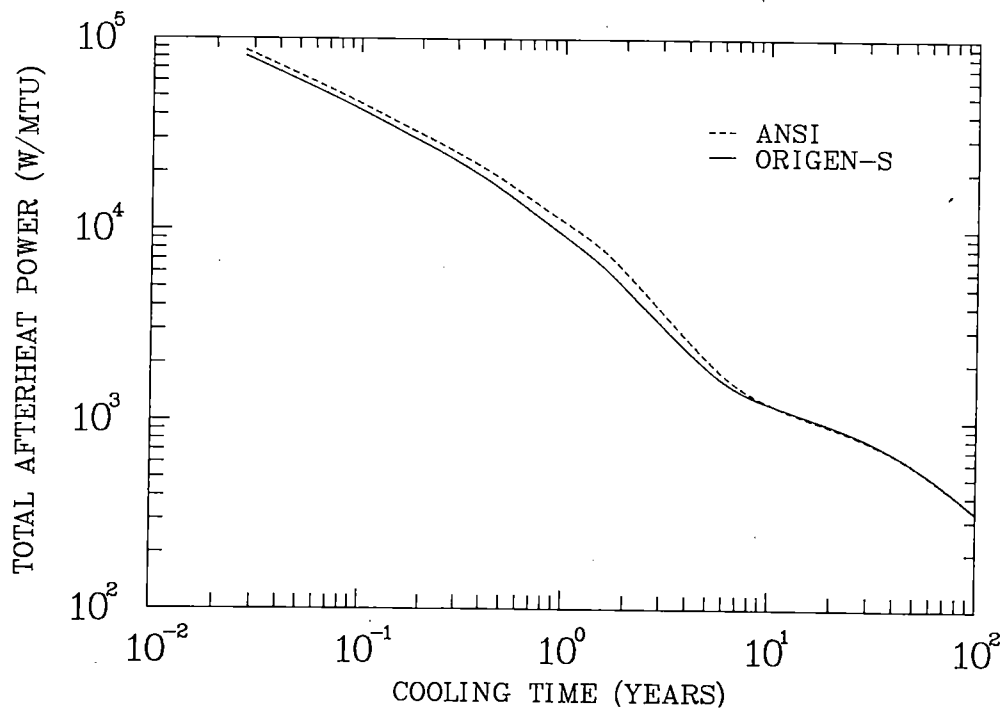


Fig. 2. Afterheat power from the ANSI and SAS2/ORIGEN-S methods for case 3 (3.3 wt % ^{235}U , 33 GWD/MTU) with a typical irradiation history.

PREDICTION OF CRITICAL FLOWS OF HOT WATER FROM ORIFICES AND TUBES

Y. S. Chen

U.S. Nuclear Regulatory Commission
Washington, D.C. 20555, U.S.A.

ABSTRACT

An analytical method using a critical flow correlation has been developed for small break loss-of-coolant accident (LOCA) analyses. To assess the proposed method, variety of experimental data obtained from both sharp-edged orifices and tubes were used. The maximum discrepancy in most cases was found to be within 7%. It is recognized, however, that if the proposed analytical approach is to become fully applicable to a typical pressurized water reactor plant under LOCA conditions, more test data are definitely needed especially at high system pressure (>9 MPa) and under subcooled flow conditions.

INTRODUCTION

Critical flow rate through a pipe break is a key parameter in the analysis of a postulated loss-of-coolant accident (LOCA) in nuclear reactor systems. For breaks resulting from a small hole in a primary coolant pipe or in a small pipe, a sharp-edged orifice or a sharp-edged tube can be the approximation. For breaks resulting from the shearing-off of a small pipe, a short length of tube with a sharp inlet edge can be the approximation. One purpose of the present study is to develop a critical-flow analytical method for the analysis of a postulated small break LOCA; the method will be based on a critical flow correlation formulated by Tikhonenko and his co-workers [1]. Another purpose is to identify the area where further experimental research on critical flow might be required.

It should be recognized that, for subcooled or very low quality two-phase flows, proper critical flow correlations or models are not yet available for accurate calculations of flow rates particularly in orifices or short tubes. The much publicized homogeneous-equilibrium model was found to underpredict the critical flow rate in an orifice geometry by as much as 150% [2,3,4]. In fact, the current critical flow calculation approach, which can be easily found in many LOCA computer codes, of using Moody or any other models in conjunction with the discharge multiplier (or coefficient) is considered inadequate because the approach becomes invalid when these codes are to be used as predictive tools for LOCA analyses.

The effects of the tube diameter (D) and tube length (L) on critical flow rate have been studied by some previous researchers. Nevertheless, it is not yet certain whether the tube length, or the length-to-diameter ratio, or both should be the governing parameter regarding the non-equilibrium effects. In the analysis of their experimental data, Tikhonenko and his co-workers found that the influence of L and

L/D on critical flow rates can be taken into account by the dimensionless length index L^* , which was defined as

$$L^* = \frac{L}{R} \left(\frac{L}{D} \right)^{1/4} \quad (1)$$

where

$$R = \left(\frac{\sigma}{\gamma_l - \gamma_g} \right)^{1/2}$$

Characterizing the average size of vapor bubbles

σ = surface tension

γ_l = liquid specific weight

γ_g = vapor specific weight

The relationship between critical mass flux (G_c) and hydraulic mass flux (G_h) for each region as shown in Fig. 1 is described with good accuracy by

$$\frac{G_c}{G_h} = a_i (L^* K_p)^{-b_i} \quad (2)$$

For saturated water, values of a_i and b_i for each region are constant, but for subcooled liquid, they depend on the inlet subcooling. The subscript, i , describes to which region in Fig. 1 that the coefficients a_i and b_i should belong. Through processing all 222 critical flow data points, Tikhonenko¹ et al. found that the value of a_i and b_i can be determined based on some empirical formulas [1]. The parameter $K = (P_o/P_c)^{1/8}$ takes into account the influence of initial pressure found in long tubes. In the original paper [1], the parameter K was defined as $(P_{so}/P_c)^{1/8}$; hence the effect of the initial saturation pressure corresponding to the inlet fluid temperature instead of the initial inlet pressure is considered. We believe that this is a typographical error in the original paper. It is worth mentioning that, for both subcooled and saturated water, statistical processing of the test data in Ref. 1 has shown that relations (1) to (2) are accurate to within $\pm 7.4\%$ with confidence coefficient of 0.95. These relations, however, were recommended only for use with initial pressures ranging from 1 to 9 MPa, relative inlet fluid subcooling (Δp_{so}) equal to or less than 0.5, and tube diameter (D) greater than or equal to 10 mm. Nevertheless, the present study will show that some of these applicable ranges can be extended.

CRITICAL FLOW FROM ORIFICES

We should point out that calculations of the critical mass flux by using Eqs. (1) and (2) require determination of the mass flux, G_h , in the "hydraulic discharge mode." Fig. 2 shows the empirical relationship between the inlet pressure and the mass flux G_h for the case of subcooled and saturated water discharging

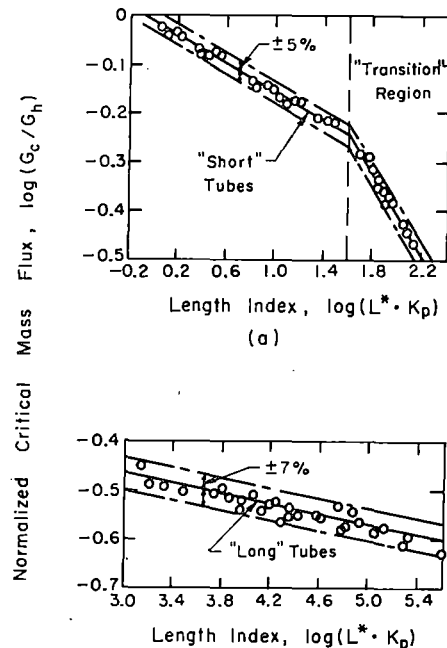


Figure 1. Experimental Data on Critical Mass Fluxes of Saturated Water in Dimensionless Coordinates: (a) "Short" Tubes and "Transition" Region, and (b) "Long" Tubes.

through a sharp-edged orifice. The relationship was derived based on an orifice-discharge formula, Eq. (3), and the test data of Ref. 5. When the inlet stagnation pressure (P_o) is less than 10 MPa and the upstream fluid is at saturation, the value of G_h can be calculated by using the following equation:

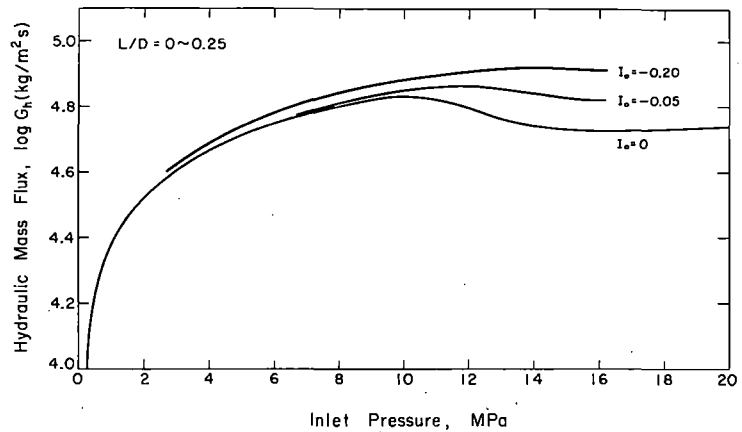


Figure 2. Relationship Between the Calculated Hydraulic Mass Flux and the Inlet Pressure in a Sharp-Edged Orifice Geometry.

$$G_h = \mu_h \sqrt{2 \rho_o (P_o - P_r)} \quad (3)$$

where

P_r = receiver pressure

P_o = upstream inlet pressure

ρ_o = fluid density at inlet

$\mu_h = 0.59$ (discharge coefficient)

For incompressible fluids (e.g., subcooled liquid and saturated water), the orifice discharge coefficient μ_h can be approximately evaluated by Idelchik's empirical formula [6]. But, for subcooled liquid or saturated water at the inlet pressure greater than 10 MPa, no hydraulic formula could be found to calculate G_h , and under these circumstances the empirical curves as shown in Fig. 2 were established by using Eqs. (1) and (2) together with the measured critical flow rates.

It should be reminded though that even with G_h given, the proposed critical flow correlation still cannot be directly applied to a sharp-edged orifice in which the length-to-diameter ratio (L/D) in most cases is less than 0.25. However, we have found that for the case of $L/D < 0.25$, the critical mass flux can be predicted with good accuracy if the length index L^* defined in Eq. (1) is redefined as

$$L^* = \frac{0.008132}{R} \quad (4)$$

and if the calculated value of the maximum critical mass flux, G_c , is limited not to exceed the G_h value. For the case of $L/D > 0.25$, relations (1) to (2) together with certain empirical curves related to G_h have to be employed. This will be discussed in the next section.

A comparison of the critical mass flux of saturated water discharging through a sharp-edged orifice under choked conditions is shown in Tables I to III. Tables I to III also show that the maximum discrepancy between the calculated critical mass flux and measured values is less than 6%. Test data used in the comparison were obtained from three different data sources [1,5,7]. Based on data comparison results, we can conclude that, for saturated critical flows discharging through sharp-edged orifices with $L/D < 0.25$, the present critical flow analytical method is applicable at least for system pressures ranging from 0.392 to 10 MPa.

We note that in the flow discharge processes liquid superheats close to the spinodal line probably occur at the inlet stagnation pressure (P_o) greater than 10 MPa; i.e., when the inlet pressure is greater than 10 MPa, homogeneous nucleation begins to occur and the vapor phase will appear suddenly [5,8]. As a result, the mass flux discharging through an orifice will start to decrease as shown in Fig. 2. Fig. 2 also reveals that increasing the inlet liquid subcooling increases the spinodal line limit. This result is not unexpected since the effect of liquid subcooling is to enhance liquid metastability and decrease homogeneous nucleation. The parameter shown in Fig. 2 is the subcooling index, I_o , which was defined as

$$I_o = \frac{h(P_o) - h_{sat}(P_o)}{h_{fg}(P_o)} \quad (5)$$

where

$h(P_o)$ = liquid enthalpy corresponding to the inlet pressure

$h_{sat}(P_o)$ = saturated liquid enthalpy corresponding to the inlet pressure

$h_{fg}(P_o)$ = latent heat enthalpy corresponding to the inlet pressure

CRITICAL FLOW FROM TUBES

As discussed earlier, the present method can be used to predict critical flow for subcooled and saturated water in tubes with a sharp inlet edge. To do this, the hydraulic mass flux G_h has to be first determined. But no formula or suggestion as to how to determine the value of G_h was given by Tikhonenko and his co-workers. The only clue given in Ref. 1 about G_h is that it is a function of the inlet pressure, back pressure (receiver pressure) and hydraulic discharge coefficient μ_h . In Ref. 1, the parameter μ_h was defined as

$$\mu_h = (1 + k_{in} + f_r \frac{L}{D})^{-0.5} \quad (6)$$

where

k_{in} = form loss coefficient at tube inlet

f_r = resistance coefficient of a tube

TABLE I.

Critical mass fluxes of saturated water discharged from a sharp-edged orifice ($L = 0.35 \sim 0.45$ mm, $D = 3.5 \sim 4.5$ mm, and $L/D \approx 0.1$) [5].

P_o (MPa)	Test data G_c (K_g/m^2s)	Prediction G_c (K_g/m^2s)	Error (%)
2.5	33333	35283	5.8
4	41550	43451	4.6
5	46430	47731	2.8
6	50641	51315	1.3
7.5	55333	55879	1.0
9	57051	58884	3.2
10	58182	61573	5.8

TABLE II.

Critical mass fluxes of saturated water discharged from a sharp-edged orifice ($L = 0.1 \sim 0.2$ mm, $D = 10 \sim 25$ mm, and $L/D \approx 0.0096$) [1].

P_o (MPa)	Testing data G_c (K_g/m^2s)	Prediction G_c (K_g/m^2s)	Error (%)
1	22909	22909	0.0
4	42658	43451	1.9
9	60256	58884	-2.3

Thus, the coefficient μ_h is a function of tube inlet geometry, tube size, tube roughness and Reynolds number. For a sharp-edged inlet from a reservoir, the value of the form loss coefficient k_{in} in a tube is equal to 0.5, and the coefficient f_r is a function of Reynolds number and tube surface roughness. The information about μ_h has been useful in this study. For instance, based on Eq. (6), we were able to convert the test data obtained in glass and copper tubes by Uchida and Nariyai [7] into the data for commercial steel pipes.

Based on the measured value of G_c together with Eqs. (1) and (2), we have obtained Figs. 3 to 5. Both Figs. 3 and 4 illustrate the empirical relationship between the variable G_h and tube length L while the inlet stagnation pressure is expressed as a parameter. For the calculation of critical flow in short tubes, i.e., $L < 0.1$ meter, Fig. 3 is to be used. Notice that this figure clearly illustrates the fact that the value of G_h decreases as L decreases when tube length is less than 0.06 meter. This is probably due to the contracting effect of the metastable water jet. For tube length L greater than 0.1 meter, Fig. 4 is to be used. This figure shows that the value of G_h decreases as L increases, and that the effect of tube length on G_h becomes less pronounced as the inlet pressure increases. Both Figs. 3 and 4 are applicable only for saturated water and very low quality two-phase mixtures at system pressures less than 9 MPa. For inlet pressures greater than 9 MPa, no experimental data are yet available.

For subcooled liquid flows, the empirical relationship between G_h and tube length L is shown in Fig. 5 while the subcooling index I_o is expressed as a parameter. Although Fig. 5 was established at the system pressure of 9 MPa, it can be extended to system pressures less than 9 MPa. The test data used to establish Figs. 3 to 5 were those from Refs. 1, 9 and 10. The test data used to verify the predictive capability of the proposed critical flow correlation together with the empirical curves as shown in Figs. 3 to 5 are those of Sozzi and Sutherland [2], Uchida and Nariyai [7], and Zaloudek [11].

Sozzi and Sutherland [2] collected some data of critical flow rates measured in a variety of nozzles. The data obtained from tubes with a sharp inlet edge were also included. The tube diameter used is 12.7 mm. The inlet stagnation pressure was varied from 4.138 to 6.897 MPa (or 41.4 to 69 bar) and the stagnation temperature ranged from 506 to 561 K (or 232 to 288°C). The L/D ratio ranged from 0.374 to 50. The test fluid was low quality two-phase mixtures. Table IV shows that the predicted values of the critical mass flux by using the proposed correlation

TABLE III.

Critical mass fluxes of saturated water discharged from a sharp-edged orifice ($L \approx 0.0$, $D = 4$ mm, and $L/D \approx 0.0$) [7].

Po (MPa)	Test data G_c (K_g/m^2s)	Prediction G_c (K_g/m^2s)	Error (%)
0.785	20833	20091	-3.6
0.687	19583	18787	-4.0
0.589	17917	17549	-2.1
0.491	15694	15868	1.1
0.392	13889	13980	0.7
0.294	11250	10862	-3.5

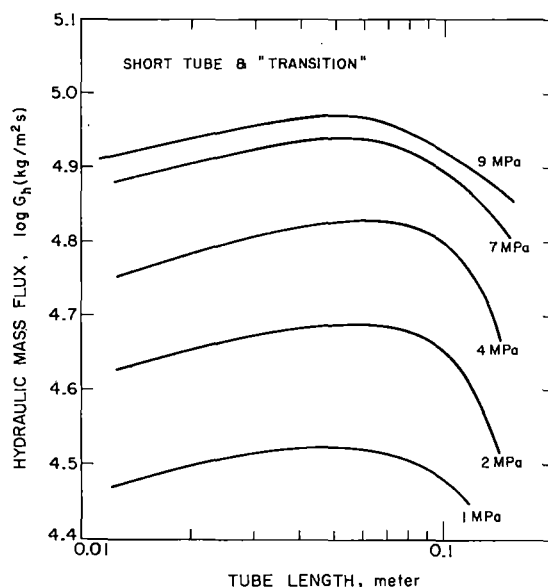


Figure 3. Relationship Between the Calculated Hydraulic Mass Flux and Tube Length for Short Tubes and Tube in "Transitional" Region.

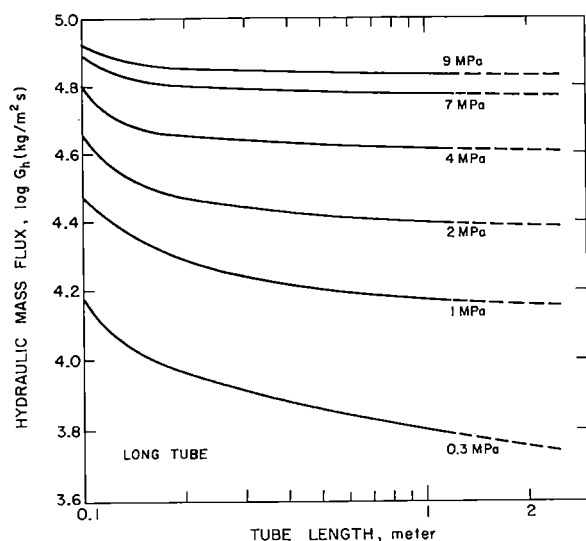


Figure 4. Relationship Between the Calculated Hydraulic Mass Flux and Tube Length for Long Tubes.

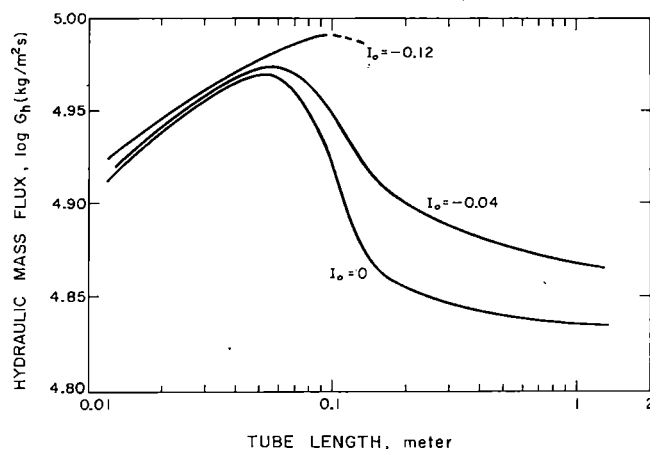


Figure 5. Effect of Subcooling on the Hydraulic Mass Flux and Tube Length at the Inlet Pressure of 9 MPa.

TABLE IV

A Comparison of the Critical Mass Flux of Saturated Water from Long Tubes (Diameter = 12.7 mm)

L/D	Stagnation Pressure, P_o (MPa)	Stagnation Temperature, T_o (K)	Quality (%)	Test Data G_c (Kg/m ² s)	Predicted G_c (Kg/m ² s)	Error (%)
15	6.869	557.7	0.15	26119	26211	0.4
	6.545	554.4	0.28	24654	25089	1.8
	6.255	551.4	0.30	23434	24268	3.5
	6.848	557.4	0.40	24898	25308	1.7
	6.579	554.8	0.40	24410	25039	2.8
	6.338	552.3	0.45	23434	24132	3.0
	5.952	548.2	0.09	23092	24351	5.5
25	6.890	557.9	0.1	24044	24019	0
	6.455	553.5	0.3	22701	22887	0.8
	6.552	554.5	0.2	22945	23399	2.0
	6.283	551.7	0.25	22945	23043	0.4
	6.883	557.8	0.30	22823	23302	2.1
	6.614	555.1	0.30	22823	23326	2.2
	6.386	552.8	0.35	22823	22770	-0.2
40	6.897	557.9	0.2	22750	23077	1.4
	6.483	553.8	0.3	22067	22208	0.6
	6.986	558.8	0.25	22360	22980	2.8
	6.828	557.3	0.35	22360	22516	0.7
	6.828	557.3	0.15	23043	23082	0.2
	6.255	551.4	0.30	21774	21979	0.9
50	6.690	555.9	0.30	21774	22086	1.4
	6.890	557.9	0.10	21115	22887	8.4
	6.379	552.7	0.20	21115	22072	4.5
	6.386	552.8	0.20	21481	22130	3.0

compared very well with the test data. All but one data point are within 5.5% error.

Uchida and Nariyai [7] performed critical flow tests at low pressures (0.196 to 0.785 MPa) in copper, brass and glass tubes. These tubes have 4 mm inside diameter and have length varying from 0 to 2.5 meter (i.e., $0 < L/D < 625$). The tubes also have a sharp-edged entrance and through which initially subcooled or saturated water discharged to the atmosphere. The predicted results of the critical mass flux compared well with Uchida's test data. Figures 9 to 12 show comparisons of Uchida's experimental results with Moody, Levy and Fauske's predictions [7], and the present calculations.

For subcooled liquid under choked conditions, the present analytical method has also been verified with Zaloudek's subcooled data [11]. Zaloudek investigated the critical flow phenomenon of initially subcooled liquid discharging through short tubes. The tube length ranged from 0.8 to 127 mm. The tube has a sharp entrance edge and its diameters are 6.35, 12.7 and 15.9 mm, respectively. The upstream pressure ranged from 0.69 to 2.414 MPa (6.9 to 24.1 bar). Two types of choking phenomena were identified by Zaloudek. The first type occurred near the vena contracta at the tube inlet when localized flashing occurred as the pressure dropped below the corresponding saturation pressure. The second type of choking occurred at the tube exit when the receiver pressure fell below saturation pressure. From the practical point of view, especially for LOCA applications, the second type of choking is much more important, hence only the data obtained from this kind of choking have been used for this study.

The predicted results using the present method compared very well with Zaloudek's data. All data points are within 7.0% error. The maximum subcooling index (I_o) in the test data used for data comparison is -0.2425, which corresponds to a 47 K subcooling at the inlet pressure of 2.413 MPa. The value of the subcooling index (I_o) for a typical pressurized water reactor plant operating at a system pressure of 15.17 MPa is about -0.38. Hence, with respect to operating conditions of a typical PWR plant, the data used for this study cover up to a two-thirds range of liquid subcooling.

CONCLUSIONS AND RECOMMENDATIONS

We have developed an analytical method using a critical flow correlation for small break LOCA analyses. The correlation, which was formulated by Tikhonenko and his co-workers, takes into account the effect of tube geometry, tube form loss, skin friction, thermal nonequilibrium, and initial thermal and hydraulic conditions. For sharp-edged orifice, the proposed method for the calculation of critical flow is applicable to the system pressure up to 10 MPa. For subcooled or saturated water at the system pressure greater than 10 MPa, the applicability of the proposed method is yet to be further verified with more test data. For tubes with a sharp inlet edge, the proposed method is applicable to the system pressure up to 9 MPa, and to a two-thirds of liquid subcooling of PWR operating conditions. Therefore, we suggest that any future critical flow test conducted in tubes or orifices with a sharp-edged geometry should be made under subcooled flow conditions with the system pressure greater than 9 MPa.

REFERENCES

1. L. K. Tikhonenko, L. R. Kevorkov and S. Z. Lutovinov, "Critical Discharges of Hot Water from Tubes", Thermal Engineering, 26(5),
2. G. L. Sozzi and W. A. Sutherland, "Critical Flow of Saturated and Subcooled

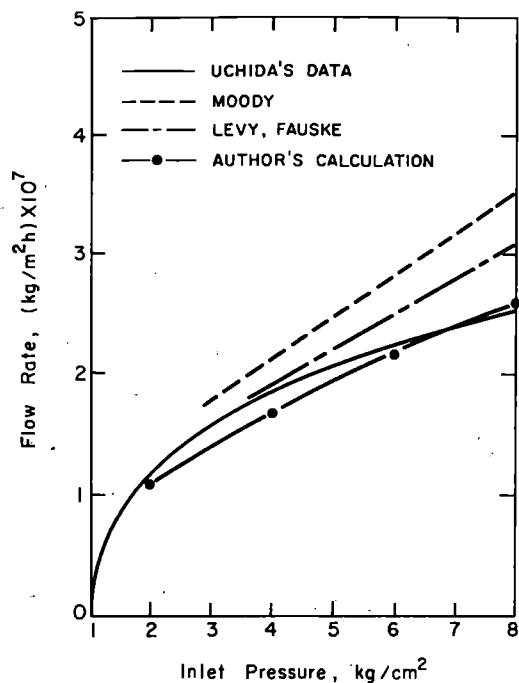


Figure 6. Comparison of UCHIDA'S Experimental Result with Author, Moody, Levy, and Fauske's Prediction for 535 mm Long Pipe.

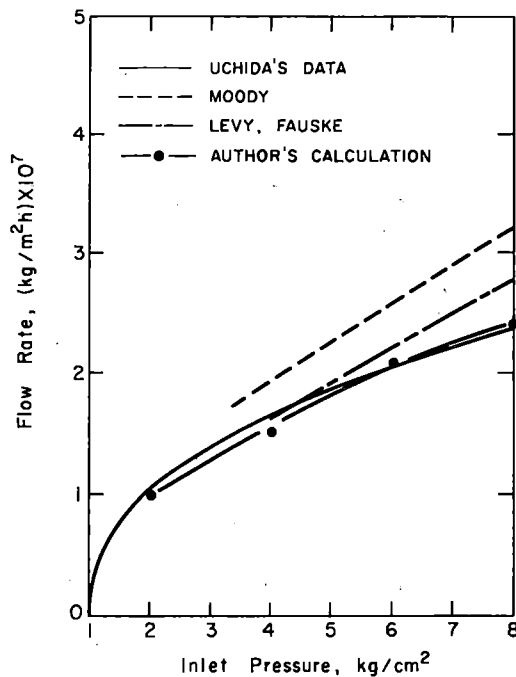


Figure 7. Comparison of UCHIDA'S Experimental Result with Author, Moody, Levy, and Fauske's Prediction for 990 mm Long Pipe.

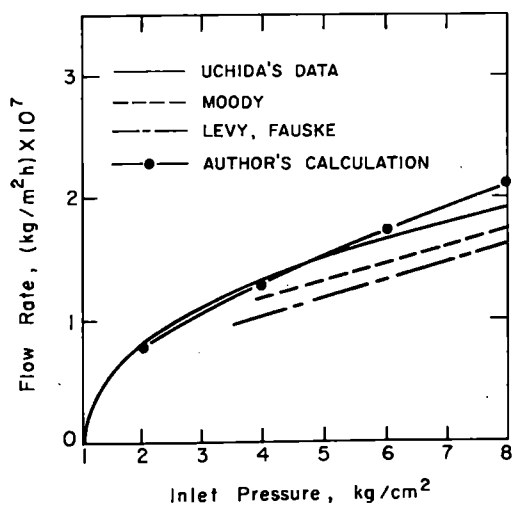


Figure 8. Comparison of UCHIDA'S Experimental Result with Author, Moody, Levy, and Fauske's Prediction for 2155 mm Long Pipe.

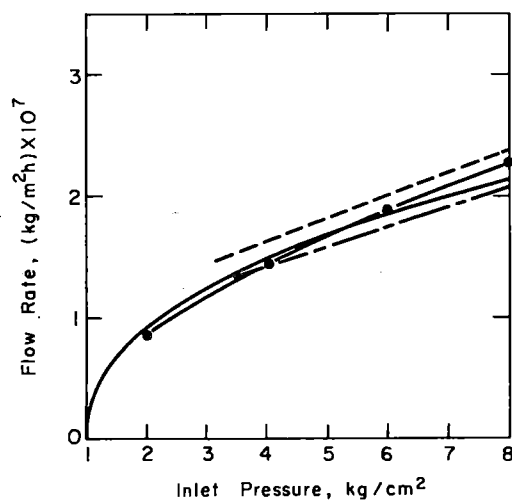


Figure 9. Comparison of UCHIDA'S Experimental Result with Author, Moody, Levy, and Fauske's Prediction for 1450 mm Long Pipe.

Water at High Pressure", General Electric Report NEDO-13418 (July 1975).

3. R. L. Collins, "Choked Expansion of Subcooled Water and the I. H. E. Flow Model", ASME Journal of Heat Transfer, Vol. 100 (May 1978).
4. U. Simon, "Blowdown Flow Rates of Initially Subcooled Water", ANS Topical Meeting on Water Reactor Safety, CONF-730304 (March 1973).
5. D. H. Khlestkin and V. P. Kanishchev, "Investigation of the Processes of Discharge of Very Wet Steam/Water Mixture", Thermal Engineering, 26(5) (1979).
6. I. E. Idelchik, "Handbook of Hydraulic Resistance, Coefficients of Local Resistance and of Friction", AEC-TR-6630, U. S. Department of Commerce, National Technical Information Service (1960).
7. H. Uchida and H. Nariai, "Discharge of Saturated Water through Pipes and Orifices", Proceedings of the Third International Heat Transfer Conference, Vol. V (1966).
8. J. H. Lienhard and Amir Karimi, "Homogeneous Nucleation and the Spinodal Line", ASME Journal of Heat Transfer, Vol. 103 (1981).
9. L. R. Kevorkov, S. Z. Lutovinov and L. K. Tikhonenko, "Influence of the Scale Factors on the Critical Discharge of Saturated Water from Straight Tubes with a Sharp Inlet Edge", Thermal Engineering, 24(7) (1977).
10. A. A. Avdeev, V. N. Mainanik, and V. K. Shanin, "Procedure for Calculating Flashing Adiabatic Flows", Thermal Engineering, 24(8) (1977).
11. F. R. Zaloudek, "Steam-Water Critical Flow from High Pressure Systems", Hanford Atomic Products Operation Interim Report, HW-80535 (1964).

COMPARE CONTAINMENT SUBCOMPARTMENT ANALYSIS CODE EVALUATION

R. G. Gido and A. Koestel

Los Alamos National Laboratory, Energy Division
Los Alamos, NM 87545, U. S. A.

ABSTRACT

Nuclear power plant subcompartment analyses are required to determine the containment pressure distribution that might result from a loss-of-coolant accident. The pressure distribution is used to calculate structural and mechanical design loads. The COMPARE code is used widely to perform subcompartment analysis. However, several simplifying assumptions are utilized to facilitate solution of the complex transient, two-phase, multidimensional flow problem. In particular, it is assumed that the flow is homogeneous, in thermodynamic equilibrium, and one-dimensional. In this study, these assumptions are evaluated by performing simplified transport and relaxation analyses. This results in definition of (a) geometric features and early-time periods that produce significant deviations from reality and (b) specific areas that require further study.

I. INTRODUCTION

A nuclear power plant loss-of-coolant accident (LOCA) could release rapidly a large quantity of high-energy water into the containment. The water would vaporize and flow to containment subcompartments such as the reactor cavity, steam generator, and pressurizer compartments. This would result in pressure differentials and component loads (forces and moments) on walls, piping, and the reactor pressure vessel. Excessive component loadings must be avoided so that the negative consequences of the LOCA are not increased[1]. Containment subcompartment analysis deals with the determination of the pressure differentials in the compartments so that component loads can be determined for mechanical and structural design.

Subcompartment analysis is done conveniently by computer codes such as COMPARE[2-4], which is used by the US Nuclear Regulatory Commission and analysts in the United States and Europe. However, COMPARE utilizes several simplifying assumptions to perform the transient, two-phase, multidimensional flow analysis required. It therefore is important that the deviations from physical reality imposed by the simplifying assumptions are understood. This has been done to some extent by comparing COMPARE-calculated results with Battelle-Frankfurt test results[5,6], and with calculated results from the more sophisticated BEACON code[7]. However, such comparisons often do not provide fundamental understanding of the differences in the comparisons. This presentation is an analytical evaluation of the COMPARE assumptions to provide greater

understanding of the deviations from physical reality. A more complete description of the procedures and results of this evaluation is presented in Ref. 8.

To put the COMPARE code simplifications into perspective, consider what a comprehensive code would include. Because two phases are involved, each can have different thermodynamic and transport properties and different velocities. In the most complex representation, each phase requires satisfaction of the conservation equations of mass, momentum, and energy. Six first-order differential equations result. These equations must be solved with (1) constitutive relations that describe the interactions between the phases and (2) the effects of the compartment walls and vents.* Involved are the transfers of mass, momentum, and energy between the fluid phases and the walls. The thermodynamic equations of state are also included in the array of equations. A two-dimensional grid of cells must be considered because two-dimensional flow effects are important.

A comprehensive formulation such as has been described will account for the various physical phenomena known to occur during transient two-phase flow through a system of subcompartments connected by vents. Included are, (1) compressibility, (2) slip and other related phase interactions caused by nonequilibria, (3) two-dimensional effects such as those causing a vena contracta or jet spreading due to turbulent diffusion, (4) momentum flux as caused by nonstagnation conditions and by nonsteady flow, (5) wall interactions such as liquid-phase deposition and re-entrainment, friction and heat transfer, (6) inertia as related to nonsteady flow, and (7) mass and energy charging transients. Clearly, a computer simulation becomes complex if all the known physical characteristics and interactions of the flow are included. However, simplifying assumptions can drastically reduce the code complexity.

The major COMPARE assumptions are that the two-phase flow is homogeneous, in equilibrium, and one-dimensional. The homogeneous equilibrium assumption implies that the entire liquid phase is finely dispersed in the gaseous (vapor and air) phase and that the net interphasic mass and heat transfer and velocity slip are zero. Average mixture properties and the equations for a single-phase flow can be used. The resulting equations are simple and easy to solve on a computer, but the validity of the assumptions must be assessed.

Homogeneity implies a well-dispersed liquid phase. However, it should be recognized that homogeneity and equilibrium can be dependent on each other. For example, the rate of liquid-drop deposition on a wall and the rate of liquid-phase entrainment from the wall film eventually results in a dynamic equilibrium where the two rates become equal. To support the combined homogeneous equilibrium assumption, (1) the equilibrium amount of the liquid phase retained as a film should be small compared to the dispersed liquid and (2) the entire liquid phase should be dispersed without slip. Also, rapid flow acceleration and pressure change, such as occur through a vent, can make the equilibrium theory inaccurate unless relaxation calculations show that nearly equal phase velocities can be assumed. This depends on the length and diameter of the restriction and the size of the liquid drops. If there is much slip, the vent mass flow computed from the homogeneous equilibrium theory will be in error.

*Vent as used in this report means a reduced flow area between an upstream and a downstream reservoir.

Two-dimensional flow can result in the formation of a vena contracta in the vent thereby introducing a deviation from the one-dimensional assumption. The one-dimensional flow assumption of COMPARE eliminates the need for a multi-dimensional grid of cells and the complexity of including the turbulent diffusion of heat, mass, and momentum.

The following evaluation defines the limitations of the major simplifying assumptions used in COMPARE. The assumptions and the phenomena neglected by the assumptions are given in Table I.

II. DISCUSSION

A. Break Node Boundary Condition

COMPARE utilizes the simplification that the LOCA break flow goes into a break node where a homogeneous mixture in equilibrium is created for use as a boundary condition for the remainder of the analysis. The mixture consists of the break flow added over the time step plus the node contents at the beginning of the time step. This simplification avoids the possibility that the break flow is introduced as a liquid-water and steam mixture with defined flow direction, with slip, and not in equilibrium. The simplification is justified on the basis of (1) the drop sizes being small (10 to 100 μm) due to aerodynamic and thermal fragmentation[9] and (2) a high level of turbulence caused by the

TABLE I

COMPARE Assumptions and Phenomena Neglected by
the Assumptions

<u>Assumption</u>	<u>Phenomenon Neglected</u>
Homogeneity	Liquid-phase deposition to and entrainment from surface
Equilibrium Thermal, mechanical (slip), and chemical (diffusion) between phases	High pressure gradient (vent expansion)
One-Dimensional Flow	Vena contracta and jet expansion by turbulent mixing
Polytropic Vent Expansion	Expansion may be more nearly isentropic
Momentum Based on Local Compressibility only	Convective compressibility effect on momentum through the momentum flux terms, which are not present in the simplified form of the momentum equation used in COMPARE

large amount of kinetic energy in a confined region. Of course, there may be situations where the assumption of a break node flow that is homogeneous and in equilibrium is invalid.

The region surrounding the break node provides the boundary condition for the remainder of the COMPARE analysis. At this point, the flow structure is assumed to be a homogeneous dispersion of fine drops in a gas-vapor cloud. Because this is immediately downstream of the break, there is no need for introducing other complications, such as, (1) metastability and nucleation in the liquid phase and (2) the property discontinuities encountered at the saturated-liquid line during an isentropic expansion.

The size of the drops formed just downstream of the break is crucial to the validity of the homogeneous equilibrium assumption because relaxation, as related to the interphasic rate processes, is strongly dependent on the drop diameter. It will be shown that a dispersion of small drops in a large channel is conducive to homogeneous equilibrium flow as assumed in the COMPARE code.

B. Homogeneity

The previous discussion establishes the basis for the break node in COMPARE representing a boundary condition consisting of a homogeneous two-phase mixture with the liquid totally entrained. As this mixture flows from the break node to the other nodes or compartments, the state of homogeneity could be changed because of liquid mass transfer. This could include deposition to form a liquid film on surfaces and entrainment from the liquid film (film entrainment).

Deposition caused by mass removal associated with condensation has been traditionally ignored (except for ice-condenser containments) in subcompartment analysis because it was estimated that the energy removal was small because of the short time (approx. 0.1 s, see Ref. 10) for peak forces and moments to be reached. In addition, it was felt that neglecting the energy removal would result in higher pressure differences across components and, therefore, conservatively high component forces and moments.

The effect of subcompartment mass-transfer deposition and film entrainment from the resulting film is addressed directly in Ref. 11, which considered deposition to peripheral surfaces only and ignored deposition on obstacles. This analysis shows that the decrease in the amount of entrained liquid caused by deposition is negligible, which results in a corresponding negligible amount of film entrainment.

In summary, then, we believe that net entrainment does not change from the 100% level assumed to be established in the break node. As a result, the state of homogeneity will be maintained. The analysis will now consider how the equilibrium state of the two-phase flow might be altered as it encounters changes in flow geometry under transient conditions.

C. Equilibrium Considerations

The term "equilibrium" implies thermodynamic equilibrium. This means that the two phases are in (1) chemical equilibrium with no potential for interphasic mass transfer, (2) thermal equilibrium with the liquid and vapor temperatures equal, and (3) mechanical (inertial) equilibrium with the liquid (u_l) and vapor (u_g) velocities equal, which means that the slip ($S = u_g/u_l$) is one.

The pressure gradient associated with vent flow changes the kinetic-energy distribution between the phases (slip) by accelerating each phase to a different velocity. The thermal balance is also disturbed. The potential for establishing mechanical equilibrium involves the drag force between the dispersed liquid and the gas (or vapor), which tends to reduce the slip ratio. Problems of this type can be resolved by applying the momentum equation followed by use of the Reynolds analogy to determine the energy and mass transfer. Inertial and thermal equilibrium are related by the Reynolds analogy for momentum, energy and mass transfer.

1. Mechanical. Mechanical non-equilibrium (slip) can have a large effect on the vent flow rate. This can be demonstrated by comparing the mass fluxes, G , based on (1) an isentropic expansion (thermodynamic equilibrium), and (2) an idealized limiting case where there is slip only with thermal and chemical equilibrium maintained.

Figure 1 shows the mass flux for the isentropic expansion of two-phase water, see Ref. 8 for details. Note that the maximum G (critical flow rate) of $\sim 1.71 \text{ Mg}/(\text{s}\cdot\text{m}^2)$ [$350 \text{ lb}_m/(\text{s}\cdot\text{ft}^2)$] occurs at a value of 0.6 for the ratio of the throat (p_t) to upstream stagnation pressure (p_o). Figure 2 shows how the mass flux is affected by slip for three values of p_t/p_o (0.45, 0.60, and 0.90), see Ref. 8. Note that mass flux varies considerably with slip with a maximum at slip values of approximately seven.

COMPARE uses the assumption that the slip is one at the vena contracta. The validity of this assumption depends on how close to thermodynamic equilibrium the two-phase flow is in the region of a high pressure gradient. To make this determination, it is necessary to apply the interphasic transfer relations, which are affected by the vent size and drop diameter.

The drag force on a drop acts to accelerate the drop velocity towards the vapor velocity. This occurs between the vent opening and the vent contracta and results in a slip ratio near one at the termination of the expansion. Similarly, if the gaseous phase is not saturated, there is a trend toward thermal and chemical equilibrium.

The analysis for slip is presented in Ref. 8 and the results are plotted in Fig. 3. This figure shows the slip S at the vena contracta plotted versus the parameter Φ . Note that Φ is a dimensionless number that includes the necessary quantities for estimating the slip in vent flow, that is, density ratio, vent size, drop diameter, and Reynolds number. This analysis is based on the exchange of momentum between the gaseous phase and the drop as they flow through the vent.

2. Thermal. Reference 8 presents a thermal-equilibrium analysis with results in terms of a ratio of the inertial relaxation time (τ) to the thermal relaxation time τ_T . The thermal relaxation time is based on the exchange of energy between the gaseous phase and the drop as they move through the vent. This analysis results in ratios of 0.90 to 0.71 over the range of pressures between 0.10 to 0.69 MPa (14.7 to 100 psia). The significance of this analysis is that thermal equilibrium would be maintained approximately if mechanical equilibrium is maintained, which is approximately true for subcompartments as discussed in Sec. II.C.1.

3. Chemical. If the flow through a vent is saturated, the trend toward chemical equilibrium will coincide with the trend toward thermal equilibrium. However, when the gaseous mixture is not saturated and in thermal equilibrium, vapor diffusion from the liquid phase will continue the approach toward a saturated state until both thermal and chemical equilibrium are attained. The COMPARE assumption that the two phases are in chemical equilibrium is not evaluated in this report because (1) the analysis is complex and (2) a chemical-equilibrium evaluation is currently being performed at Los Alamos by application of the BEACON[7] computer code, which has nonequilibrium capability.

4. Application. The previous analyses show that thermodynamic equilibrium can be assumed if the slip and the relaxation ratio are both near unity at the termination of a vent expansion flow and chemical equilibrium is maintained. The resulting expansion would have a minimum dissipation caused by drag and a minimum amount of irreversibility caused by interfacial heat and mass transfer, which becomes an isentropic expansion in the limit.

For subcompartment problems such as those analyzed by COMPARE, Φ values between 1 and 20 are obtained for a flow equivalent diameter of 1 m (3.23 ft) and drop sizes of 10 to 100 μm . Figure 3 shows that the resulting slip at the critical flow minimum area (vena contracta) will be close to one. This means that the mechanical equilibrium of the two-phase flow will not be significantly disrupted and indicates that the COMPARE assumption of mechanical equilibrium is a good approximation for subcompartment problems. Note that Φ values are estimated to be about 10^{-3} to 10^{-2} for small-scale experiments, for which considerable slip (~ 10) is indicated in Fig. 3.

The COMPARE assumption of thermal equilibrium for subcompartment analysis also appears to be a good approximation because (1) the assumption of mechanical equilibrium is a good approximation, and (2) as shown previously, the ratio of inertial to thermal relaxation times is between 1.0 and 0.7 in the pressure range 0.1 to 0.7 MPa (14.7 to 100 psia), which encompasses approximately the pressure levels encountered in subcompartment analysis.

The foregoing criteria for equilibrium are approximate. A rigorous analysis would require the integration of the local irreversibilities along the entire pressure gradient to determine the net generation of entropy. This would then determine the value of polytropicity for use in the compressible flow equation, see Sec. E.

D. Momentum Considerations

1. One-Dimensional Flow Equation. Channels of uniform cross section with large length-to-diameter ratios may have large total-head (total-pressure) loss during a transient because of wall friction and momentum flux. For this particular situation, COMPARE assumes that the flow is incompressible during a computer time step, which only accounts for local compressibility ($\partial\rho/\partial x$, where ρ is density and x is length). As a result, the COMPARE momentum equation may predict an erroneous total-head response across a nodal volume during rapid flow changes. This error can be quantified by comparing the relaxation time (τ) for progressing from a state of convective compressibility to one of convective incompressibility ($\partial(\rho u)/\partial x \rightarrow 0$) with a representative transient.

Reference 8 develops the conservative form of the one-dimensional momentum equation for the change in total pressure (Δp),

$$\Delta p = p_{T,j} - p_{T,j+1} = \frac{f}{4} \Delta x \frac{(\rho u^2)_i}{2} + \Delta x \frac{d(\rho u)_i}{dt} + \left[\frac{(\rho u^2)_{j+1}}{2} - \frac{(\rho u^2)_j}{2} \right], \quad (1)$$

for comparison with the COMPARE equation for the change in total pressure,

$$\Delta p_C = p_{T,j} - p_{T,j+1} = \frac{f}{4} \Delta x \frac{(\rho u^2)_i}{2} + \Delta x \frac{d(\rho u)_i}{dt}, \quad (2)$$

where p_T is total pressure. These equations are for the constant-area-channel nodal volume i that is Δx long, and located between axial locations j and $j+1$. Friction factor is represented by f and time by t .

The difference between Eqs. (1) and (2) is the bracketed term, which contains the difference between the outlet and inlet momentum fluxes. For incompressible flow during a time step, continuity requires that the bracketed

term be equal to zero. However, a transient with a sudden large change in pressure or flow compressibility can make the difference in momentum flux in Eq. 1 significant. An idealized-flow problem is used in Ref. 8 to estimate the effect of momentum flux (convective compressibility) on the total-head (total pressure) response. The problem assumes (1) a sudden input of choked flow from an infinite reservoir into a channel, (2) time is measured after the shock wave passes the downstream nodal boundary ($j+1$), and (3) accounting for only mass and momentum is sufficient.

The result of the Ref. 8 analysis is Fig. 4, which plots the ratio of the total-head pressure differences $\delta p_C / \delta p$ vs time (t) normalized by the relaxation time (τ). The figure shows that the maximum difference in the total-head response between the two equations [Eqs. (1) and (2)] occurs at time zero at which, $\Delta p_C / \Delta p = 2$ and $\Delta p - \Delta p_C = (\rho u^2)_j / 2$, since $u_{j+1} = 0$ at $t/\tau = 0$.

As an example in the application of these results, Ref. 8 uses the example of a sudden critical flow of air ($u_j = 326.2$ m/s) introduced at the inlet to a duct 1-m-diam with the total-pressure response ratio to be determined 1 m from the inlet (that is, $\Delta x = 1$ m). The relaxation time for the nodal volume is 1.53×10^{-3} s. Thus, for ratios of $t/\tau > 10$ (Fig. 4), the COMPARE momentum equation (Eq. 2) will give a valid total-head response for values of $t > 1.53 \times 10^{-2}$ s. This suggests that the nodal volumes be designed such that the transient time of interest is much greater than the relaxation time for convective compressibility if the COMPARE momentum equation is used.

2. Transient Jet Diffusion. The variation of total head throughout the system of subcompartments and vents is required to compute the transient flow. If the flow were isentropic, the total head would remain constant. However, wall friction, jet diffusion, and dissipation resulting from nonequilibrium effects between the phases cause a decrease in total head along the flow path. The total head also depends on time when the flow is nonsteady. Jet diffusion caused by flow from a vent to a downstream subcompartment is a major contributor to the total-head loss. Factors affecting the loss include the diffusional area ratio, compressibility, momentum flux, and time during transient flow. Note that an experimental loss coefficient is not necessary if conservative equations are used.

A simplified analysis is presented in Ref. 8 to show how the diffusional total-head loss coefficient (K) varies with time during nonsteady flow. The transient total-head loss coefficient is related to that for steady incompressible flow namely, $K_1 = (1 - A_o/A_d)^2$, where A_o is the jet area and A_d is the downstream area to which the jet can diffuse. The transient time is related to a relaxation time. COMPARE assumes that $K = K_1 = 1$ when $A_o/A_d \ll 1$ and also assumes $K = K_1$ to be valid during non-steady flow. The purpose of the analysis is to define the valid limitation of the COMPARE assumptions. The analytical results are summarized by Fig. 5. The curves indicate that for values of the area ratio $A_d/A_o > 6$ or for the time ratio $t/\tau > 3$ the resulting error is small ($\sim 10\%$) when using the steady-state incompressible K_1 as the total-head loss coefficient during non-steady flow. To use a value of unity for K_1 , the area ratio (A_d/A_o) should exceed a value of 20.

An example of the utility of the analysis is presented in Ref. 8. The example determines the relaxation time (τ) required to approach the transient flow state beyond which the steady-state incompressible total-head loss coefficient (K_1) is valid. The example is based on (1) an area ratio (A_d/A_o) of 4, (2) a minimum jet radius of 1 m (r_o), and (3) a critical flow of air ($u_o = 326.2$ m/s). A relaxation time of 0.034 s (τ) results. Because the limit at which K is approximately equal to K_1 is $t/\tau = 3$, $t = 3 \times 0.034 = 0.102$ s. Thus, COMPARE will predict a valid total-head response when the transient time is greater than 0.102 s for the conditions assumed in the example.

If there is insufficient compartment space to fully diffuse a jet to the compartment wall, the total-head loss as computed for full diffusion will have to be reduced. The amount of reduction can be estimated by means of the multiplier developed in Ref. 8. When two opposing vents are exceptionally close together as in compartment R-4 of Ref. 12, direct jet impingement will control the total head at the downstream vent.

The multiplier developed in Ref. 8 is supported by the measurements obtained in compartment R-4. This particular vent-flow condition of incomplete diffusion is a deviation from the COMPARE one-dimensional flow assumption, which should be taken into account in the computations.

E. Polytropic vs Isentropic Flow Equations

An isentropic process can be assumed during expansion from a reservoir to a vena contracta if the two phases are in thermodynamic equilibrium (chemical, thermal, and mechanical). For such an expansion, the total head remains constant. However, if the phases are not in equilibrium, dissipation and irreversible heat transfer will result in a net gain in entropy and a total-head loss coefficient greater than zero. COMPARE combines irreversible effects into a total-head loss coefficient of 0.5. Because it is estimated in Sec. C that near-isentropic conditions could prevail because subcompartment vents are large and liquid drops are small, it is desirable to evaluate the difference between the mass flux for isentropic expansion G_I and for COMPARE's polytropic expansion G_C . The analysis is presented in Ref. 8 for choked flow and results in values for the ratio G_C/G_I of 0.781 for air and 0.788 for steam at 1 bar. These ratios represent limiting values because two-phase expansion is not isentropic.

Mass flow rate (\dot{m}) is a product of the flow area A_F and the mass velocity G . In COMPARE, the minimum geometric area, A_G , is used for A_F . The isentropic approach would account for the vena contracta area being $A_G \times C_c$, where C_c is the contraction coefficient. The ratio of mass flow rates becomes $\dot{m}_C/\dot{m}_I = G_C/G_I \times 1/C_c \approx 1$ because of the mass flux ratios and the fact that $0.6 < C_c < 0.8$ [13].

F. Two-Dimensional Flow Effects

1. Vena Contracta. It is well known that flow through restrictions exhibit multidimensional effects that are accounted for by a multiplier referred to as the contraction coefficient C_c . The formation of a vena contracta is the manifestation of multidimensional flow. The assumption of one-dimensional flow through a vent implies no contraction, that is, $C_c = 1$.

The amount of contraction of the flow through a restriction depends on the geometry of both the upstream reservoir and the restriction and the flow compressibility, but is independent of the Reynolds number beyond a certain limiting value. Experiments have shown that the mass flow rate continues to respond to changes in discharge pressure for all pressure ratios. Although the mass flux may indicate limiting or choking values, the amount of contraction changes the mass flow rate beyond the critical pressure ratio.

Reference 8 presents values of the contraction coefficients C_c for air ($\gamma = 1.4$) to indicate the quantitative effect of geometry and compressibility. In particular, C_c is determined as a function of (1) the ratio of the minimum geometric area A_0 to the upstream area A , which represents the geometric effect, and (2) the ratio of the throat pressure (p_t) and the upstream pressure, p , which represents the compressibility effect. C_c is shown to vary from a value of 0.60 for $A_0/A = 0.059$ and $p_t/p = 1.00$ (incompressible flow) to a value of 0.80 for $A_0/A = 0.25$ and $p_t/p = 0.53$ (compressible flow).

Analytical procedures are available for computing the contraction coefficient and can be introduced into a computer program, see Ref. 13. The previous analysis shows that considerable variation in the computed mass flow can result, especially if the mass velocity is multiplied by the vent area

(contraction coefficient of unity). For example, a deviation of as much as 40% in the mass flow rate can be expected for sharp-edged vents if one-dimensional flow is assumed without the use of a contraction multiplier.

2. Turbulent Spreading of Jets. COMPARE tacitly implies by its one-dimensional assumption that the vent flow immediately diffuses to stagnation in downstream nodes. However, in reality, a considerable flow path length is required for diffusion, as is quantitatively evaluated in Ref. 8. To account for this multidimensional flow process, a multidimensional-mesh computer program, such as BEACON [7], is required. The process of diffusion is controlled by turbulent mixing, the modeling of which would require considerable sophistication.

III. CONCLUSIONS AND RECOMMENDATIONS (Regarding the COMPARE Code)

A. Conclusions

1. A key assumption is that the break can be modeled by a boundary condition describing a homogeneous mixture in thermodynamic equilibrium.

2. The assumption that the initial homogeneity will continue downstream of the break is reasonable because there is very little net liquid-drop deposition to surfaces.

3. The assumptions of mechanical and thermal equilibria were found to be reasonable because vent flow dimensions are large relative to drop sizes. However, the assumption of complete thermodynamic equilibrium requires the additional assumption of chemical (flashing) equilibrium, which is true only if the gaseous mixture surrounding the liquid drops is saturated.

4. The one-dimensional flow equation (with inertia) is reasonable when the flow is approximately incompressible. However, compressibility and momentum flux are important for a short period of time following a rapid change in flow. During this time interval, the COMPARE equation predicts a greater loss in total pressure, see Fig. 4.

5. The assumption of stagnation conditions downstream of a minimum flow area during transient conditions is reasonable when the downstream flow area is large relative to the minimum flow area. However, when the minimum flow area approaches that of the downstream flow area, the downstream transient total pressure becomes dependent on inertia and momentum flux. This also applies to a vena contracta in a duct.

6. Flow from a reservoir to a flow restriction is quasistatic and approximately isentropic because the phases have been determined to be in near-thermodynamic equilibrium. The polytropic flow equation can be used to approximate flows that deviate slightly from thermodynamic equilibrium by introducing small total-head loss coefficients.

7. The one-dimensional flow assumption does not account for two-dimensional effects, such as a vena contracta and jet diffusion. For jet diffusion, the axial and transverse dimensions are important because the total head loss is dependent on the extent of diffusion.

B. Recommendations

1. The assumption that the break results in a homogeneous mixture in thermodynamic equilibrium should be evaluated.

2. The assumption of chemical equilibrium should be evaluated.

3. The BEACON code should be used to support the conclusions reached by this study and to perform the evaluations recommended. In particular, the extent to which equilibrium exists and the effect of multiple dimensions.

ACKNOWLEDGEMENT

Work performed under the auspices of the Office of Nuclear Reactor Regulation, U.S. Nuclear Regulatory Commission.

REFERENCES

1. "Standard Review Plan for the Review of Safety Analysis Reports for Nuclear Power Plants," Section 6.2.1.2, Office of Nuclear Reactor Regulation, U.S. Nuclear Regulatory Commission report NUREG-75/087 (May 1980).
2. R. G. Gido, G. J. E. Willcutt, Jr., J. L. Lundsford, and J. S. Gilbert, "COMPARE-Mod 1 Code Addendum," Los Alamos National Laboratory report NUREG/CR-1185, LA-7199-MS, Addendum 1 (November 1979).
3. R. G. Gido, J. S. Gilbert, R. G. Lawton, and W. L. Jensen, "COMPARE-Mod 1: A Code for the Transient Analysis of Volumes with Heat Sinks, Flowing Vents, and Doors," Los Alamos National Laboratory report LA-7199-MS (March 1978).
4. R. G. Gido, C. I. Grimes, R. G. Lawton, and J. A. Kudrick, "COMPARE: A Computer Program for the Transient Calculation of a System of Volumes Connected by Flowing Vents," Los Alamos National Laboratory report LA-NUREG-6488-MS (August 1976).
5. J. W. S. Gregory, J. R. Campbell, R. G. Gido, and A. J. Webb, "Comparison of COMPARE/RELAP3 Subcompartment Calculations with Battelle-Frankfurt C-Series Test Results," Los Alamos National Laboratory report NUREG/CR-2177, LA-8866-MS (May 1981).
6. J. W. Bolstad, R. G. Gido, W. S. Gregory, P. E. Littleton, and G. J. E. Willcutt, Jr., "Comparison of COMPARE Mod-1 Subcompartment Calculations with Battelle-Frankfurt D-Series Test Results," Los Alamos National Laboratory report NUREG/CR-1817, LA-8615-MS (November 1980).
7. E. S. Idar, J. F. Lime, and R. G. Gido, "Comparison of COMPARE and BEACON Subcompartment Analyses of Battelle-Frankfurt Containment Tests," Los Alamos National Laboratory report NUREG/CR-2849, LA-9461-MS (August 1982).
8. A. Koestel and R. G. Gido, "COMPARE Containment Subcompartment Analysis Code Evaluation," Los Alamos National Laboratory Internal Memorandum Q-7-82-349 (August 1982).
9. A. Koestel, R. G. Gido and D. E. Lamkin, "Drop-Size Estimates for a Loss-of-Coolant Accident," Los Alamos National Laboratory Report NUREG/CR-1607, LA-8449-MS (August 1980).
10. R. G. Gido, J. S. Gilbert et al., "Subcompartment Analysis Procedures," Los Alamos National Laboratory Report NUREG/CR-1199, LA-8169-MS (December 1979).
11. A. Koestel, R. G. Gido and J. S. Gilbert "Film Entrainment and Drop Deposition for Two-Phase Flow," Los Alamos National Laboratory Report LA-8475-MS (1980).

12. G. Mansfeld, "Nonstationary Pressure Build Up in Full-Pressure Containments After a Loss-of-Coolant Accident: Comparison Between Theoretical and Experimental Results", Proc. of Topical Meeting on Thermal Reactor Safety, Sun Valley, ID, Am. Nuc. Soc. report CONF-770708 (July 31 - August 4, 1977).
13. A. Koestel and R. G. Gido, "Compressibility Effects on Containment Subcompartment Loss Coefficients," Los Alamos National Laboratory report (to be published).

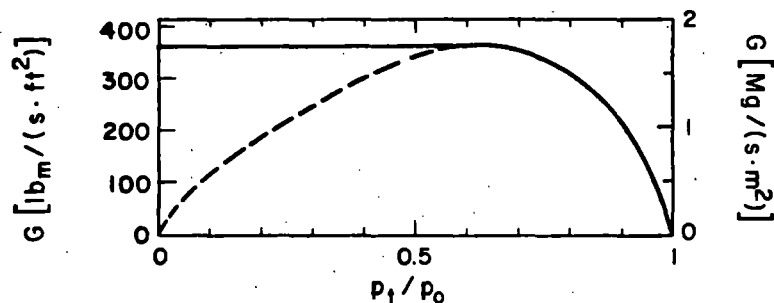


Fig. 1.

Mass flux (G) vs ratio of throat pressure (p_t) to upstream stagnation pressure (p_0) for two-phase water at an upstream pressure of 0.689 MPa (100 psia), upstream quality of 0.3 and slip of one.

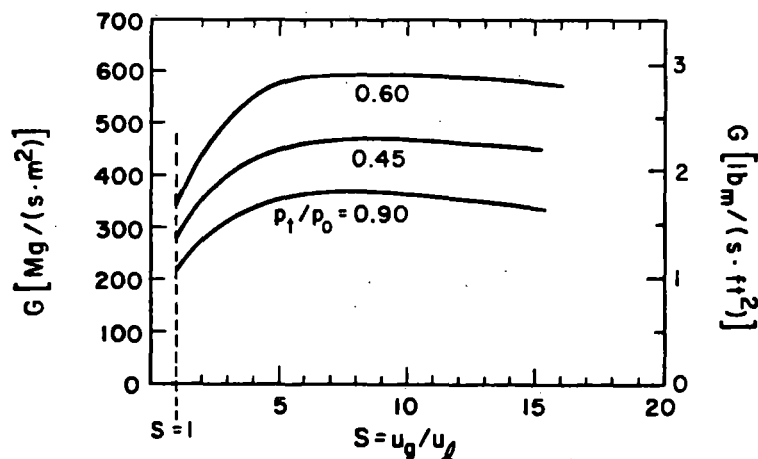


Fig. 2.

Effect of slip (S) on two-phase water mass flux (G) for several ratios of throat-to-upstream stagnation pressures (p_t/p_0) from an upstream stagnant condition of 0.689 MPa and quality of 0.3.

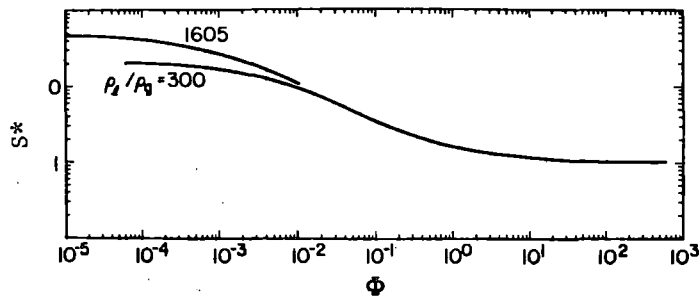


Fig. 3.

Slip at the critical-flow vena contracta (S^*) vs parameter grouping Φ for density ratios of the liquid (ρ_l) to gas (vapor) (ρ_g) phases of 300 and 1605, which correspond to saturated water at 0.59 MPa (85 psia) 0.10 MPa (14.7 psia). Typical values for Φ are 1 to 20 for subcompartment problems and 0.001 to 0.01 for small scale experiments. Φ is a dimensionless number proportional to the ratio of the gas to liquid density and the ratio of the vent diameter to drop diameter squared.

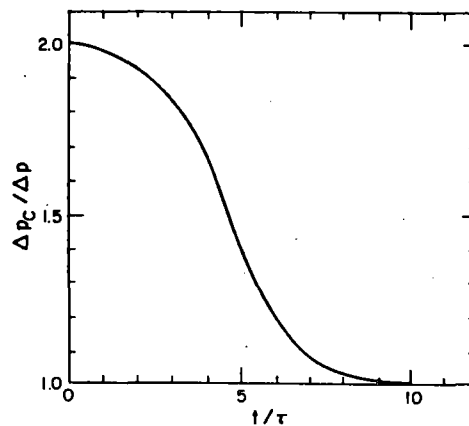


Fig. 4.

Shown is the effect of momentum flux on rapid-transient total-pressure difference as a function of time (t) normalized by a relaxation time (τ). The COMPARE difference (Δp_C) does not account for the momentum flux, which is accounted for in (Δp).

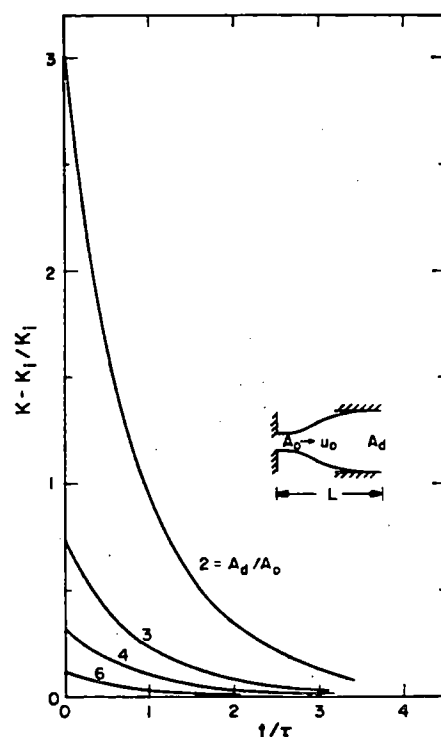


Fig. 5.

Error in using the steady-state loss coefficient (K_1) for diffusion in COMPARE as a function of normalized time (t/τ) and the ratio of downstream area (A_d) to the jet area (A_0). K is the correct transient, compressible total-head loss coefficient for diffusion.

SESSION 26

MAN/MACHINE INTERFACE - 3

Chair: B. W. Spencer (ANL)

A METHOD FOR IMPROVING ACCIDENT SEQUENCE RECOGNITION
IN NUCLEAR POWER PLANT CONTROL ROOMS

C.D. Heising and S.C. Dinsmore*

Nuclear Engineering Department
Massachusetts Institute of Technology
Room 24-207
Cambridge, MA 02139

*As of March 1, 1982
Yankee Atomic Electric Company
Framingham, Massachusetts

ABSTRACT

This work adapts fault trees from plant-specific probabilistic risk analyses (PRAs) to construct and quantitatively evaluate an alarm analysis system for the engineered safety features (ESFs). The purpose is to help improve reactor operator recognition and identification of potential accident sequences. The PRA system fault trees provide system failure mode information which can be used to construct alarm trees. These alarm trees provide a framework for assessing the plant indicators so that the plant conditions are made more readily apparent to plant personnel. In the alarm tree, possible states of each instrumented alarm are identified as "true" or "false". In addition, a "warning" status is defined and integrated into an alarm analysis routine. The impact of this additional status conditioned on the Boolean laws used to evaluate the alarm trees is examined. An application is described for a BWR high pressure coolant injection system (HPCI) that would be utilized during many severe reactor accidents.

1.0 INTRODUCTION

Traditional power plant control rooms have between 400 and 2,000 annunciations, usually arranged in panels which run along the top of the control boards [1]. The control boards themselves include many controller lights and analogue indicators. The audible alarm and individual flashing light triggered by the arrival of any annunciated alarm is a principal method of rapidly alerting the operations staff that an abnormal condition has developed. Both the alarms received and the order of their detection depend on the initiating event (or cause) and the disturbance which develops from it.

Modern control room designs replace the bulky annunciator pannels with CRTs [2]. The versatility of a CRT allows the display of both traditional alarm messages and complex processed information (past trends, system mimics, etc.). Unfortunately, CRT alarm display is not effective when myriad alarms are received [3].

This paper proposes a technique to base an alarm analysis system on the plant models developed in Probabilistic Risk Assessment studies. The resulting alarm analysis system would only display one message for any system whose alarms indicated a problem. This would reduce the demand on the operator to rapidly interpret a large number of alarms. Additional information specific to a failed system could be referenced and displayed on the screen on demand.

Both the construction process and the quantification of the "reliability" of the resulting alarm analysis system for a HPCI system is described [4]. An expansion of the alarm analysis system to enable the prediction of possible future consequences of the apparent accident sequence is discussed.

2.0 ALARM ANALYSIS

The use of computers to assist the operations staff in identifying the cause of abnormal plant conditions began in the mid 1960's [5,6]. Typically, the computer analysis is started by inserting any alarms received into a previously constructed alarm pattern - a data base. Each alarm is represented in the pattern by one or more uniquely labeled logic flags. When an alarm is received, its logic flag(s) is changed from FALSE (0) to TRUE (1). The alarm analysis routine performs various Boolean operations with these logic flags. The results (TRUE or FALSE) of selected operations represent the output of the alarm analysis routine - the display on the CRT is the output of the alarm analysis system.

The structure of the pattern reflects the expected logical grouping of alarms for various failure paths. A graphical representation of an alarm pattern resembles a fault tree (Figure 1). Information is presented to the operations staff by displaying messages triggered by the results of the analysis routine. This information usually consists of 1) the apparent prime cause alarm [5,6,7], 2) the apparent last alarm received attributable to the prime cause [5,6,7], and 3) other diagnoses or suggestions [6,7,8]; depending on the complexity of the alarm analysis system.

It was initially thought that filtering the alarms to display only the most relevant information would enable the operators to correct most problems before a reactor trip [9]. However, many alarms are only activated after a critical situation has developed, and a very rapid response is required to avoid a shutdown.

One computer alarm analysis system in operation for six years has not been useful. Two problems were cited: 1) the rapid nature of the fault progression associated with the prevalent paths, and 2) the difficulty of defining fault progression paths between various areas in the plant [9].

2.1 PROPOSED ALARM ANALYSIS ROUTINE

In view of the difficulties discussed above, an alternative type of alarm monitoring is proposed. Instead of attempting to model failure paths throughout the entire plant, only selected, well defined systems would be analyzed. The Engineered Safety Systems are ideal candidates; having been subject to extensive analysis utilizing fault tree methods. Additionally, the operability of these systems is crucial during severe disturbances, precisely when a large number of alarms are generated.

While the primary purpose of the proposed analysis routine is to determine the operability of specific systems, identification of the cause of the problem is still attempted. However, provisions are provided to allow the detection and verification of a system failure even if no specific failure path is found. Specifically, an intermediate ("Warning") status was introduced and several Boolean operators ("and", "or", and "conditional not") were modified to include a response to this input.

2.2 PROPOSED ALARM ANALYSIS SYSTEM

The display generated by the alarm analysis system is separated into two levels. The first level would only display the system name and observed status. The second level would display detailed information about a specific system on demand. The display format of the second level could be alphanumeric messages or a "picture" of the alarm pattern with observed alarms highlighted [10].

If the alarm analysis routine successfully detects the failure of a Safety System, this information could be used in an event tree structured data base. An

analysis routine, similar to the alarm analysis routine, could logically combine the operability of various systems to predict the likely range of consequences for the present state of the plant. This information could also be displayed on demand. The appropriate event tree for an initiating event could be selected by the operator or by an auxiliary alarm analysis routine.

Although not as standardized as fault trees, event trees are under continuous development and refinement. Their logical structure and intimacy with fault trees make them ideal for use in this system. Figure 2 depicts the information flow from the system instruments through the consequence selection for a fully implemented alarm-consequence system.

2.3 DEFINITION OF INSTRUMENT PERFORMANCE STATES

The first step in the analysis is to define the concurrent status of both the ESF and its corresponding instrumentation. To do this, we define the mutually exclusive conditions "True" (T) to refer to either an ESF system failure or the ESF instrumentation indicating that the system is failed, "False" (F) to refer to either an operational ESF system or the ESF instrumentation indicating that the ESF system is operational, and "Warning" (W) to refer to either a noncritical component or sub-system failure or the ESF instrumentation indicating a partially failed ESF system.

As a function of these definitions, we can specify the system status determined by the alarm analysis conditioned on system failure Ts, as follows: {Ti/Ts}, {Fi/Ts}, {Wi/Ts}, and {Ti/Fs}; where {Ti/Ts} means that the alarm analysis, Ti, indicates a system failure when, indeed, the system has failed; {Fi/Ts}, that the alarm analysis indicates no system failure when the system has failed; {Wi/Ti}, the case where the alarm analysis indicates a partial failure when the system has actually failed; and {Ti/Fi} the "false alarm" case where the alarm analysis falsely reports a total system failure.

2.4 PROBABILITY CALCULATIONS FOR THE ALARM ANALYSIS PERFORMANCE

We are interested in calculating the probabilities of observing the states described above. This calculation is performed utilizing quantitative information from the fault tree. The probability of each system state defined by any set of component failures can be quantified - as is each failed state in fault tree analysis. One relation which holds true for every failed system state is:

$$P\{Ti/Ts\} + P\{Wi/Ts\} + P\{Fi/Ts\} = 1 \quad (\text{Eq. 1})$$

which states that the alarm analysis must output either a "True", "False", or "Warning" status.

The probability of each system state, the probability of the component failures, is used as a weighing factor to assess the overall ability of the alarm analysis routine to perform as desired. Additionally, if the alarm pattern is relatively simple, the instrument failure probabilities conditioned on their standby indication can be included in the analysis.

The quantification proceeds by simulating the operation of an alarm analysis routine which has been modified to include the calculation of the parameters discussed above. The results of the calculations reflect the system's structure and failure modes, the instrumentation's properties (position and reliability), the structure of the alarm pattern, and the operation of the analysis routine. Any of these factors can be changed, with varying degrees of difficulty, and the effects quantitatively compared.

3.0 APPLICATION OF THE ALARM ANALYSIS METHOD

To illustrate the alarm analysis method, the high pressure coolant injection (HPCI) of a BWR was analyzed [4]. Plant-specific information on the HPCI instrumentation was provided by the Boston Edison Co. for its Pilgrim-I station. The instrument types, symbols, standby status, and estimated unavailabilities (conditioned on the standby status) are given in Table I.

Since the HPCI system for the Pilgrim-I plant is very similar to that of the Peachbottom Plant analyzed in WASH-1400, the WASH-1400 system diagram and fault trees were utilized [11]. The HPCI instrumentation for Pilgrim-I was added to the system diagram (Figure 3).

3.1 CONVERSION OF FAULT TREE DATA TO ALARM PATTERN DATA

One of the major problems in constructing an alarm pattern is which failure paths to include. Past data bases tended to expand until the available memory space was filled. A suggestion has been made that only the most likely accident sequences be included in the data base [8]. Fault tree analysis, with its systematic and quantitative approach, provides an excellent source of the most likely system failure modes.

To construct the alarm tree (or alarm pattern), each of the system's failure states, represented by the minimum cut sets, is evaluated to determine the expected reflection of that state in the system's instrumentation. Additionally, those component failures which may not fail the system, but which may occur more often than any cut set, need to be similarly evaluated. Such components are often included in multi-component minimum cut sets; however, in some cases, additional work may be required to include all the applicable components in the system.

In general, there are not enough alarms to provide much distinction between the component failures, however there are other indicators in the control room. Of the 22 "alarms" included in the sample alarm pattern (Table I), 9 were valve position indicators. With these 22 alarms, the 84 component failures identified in the fault tree were grouped into 19 alarm lists. Sixteen of these contained one alarm unique to that list, with an average of 5 alarms per list. Most of the grouped component failures were functionally related (the relays in a valve closing circuit), however, several groups of unrelated components were unavoidable. These groups of unrelated components represent the maximum "resolution" of any fault identification by the analysis system.

If pre-processing of signals is included, analogue information such as increasing pressure or decreasing level can be used. In this case, the "alarm" is generated when a monitored parameter exceeds some pre-selected limits [8].

3.2 CONSTRUCTION OF THE ALARM PATTERN

The conversion process described above yields a set of "alarm lists", each list represents a possible observable system state. The three possible categories of states introduced earlier are 1) fully operational (False), 2) failed (True), or 3) partially operational (Warning). The operability of each state is assigned to one of the three categories based on the success criteria of the system. The assigned operability of the system is also the desired "top event" status, given the occurrence of the alarms in its list.

The emphasis on evaluating system failure indicates that this set of lists should be coalesced into a single logical structure whose "top event" represents system failure. One structure can be obtained by linking each alarm in a list by an AND gate. Each of the lists, in turn, could be linked with an OR gate. However, the resulting pattern relies heavily on the accuracy of the alarm lists and the reliability of the instrumentation. Linking the individual alarms offers greater flexibility in the interpretation of the alarms observed during a system failure. The alarm pattern used in the analysis presented in this paper is shown in Figure 1.

3.3 RESULTS OF THE ANALYSIS OF THE BWR HPCIS ALARM SYSTEM

Results of the analysis are given in Table II. They are indicated as a function of three alarm tree logic propagation schemes, according to how the "warning" status is treated. The results shown are the conditional probabilities of observing a given alarm routine output, or top event, status (i.e., "True", "Warning", or "False") given a particular status of the high pressure injection system, either failed (Ts) or operational (Fs). The fourth row entry in Table II, $P_{Ti/Fs}$, is the probability of getting a "false alarm". These results reflect the ability of the alarm analysis routine to produce the correct, or desired, system status for all the failure modes considered; weighed by the probability of observing each failure mode.

It can be seen that utilizing only the normal Boolean states (True-False) the alarm analysis routine fails to detect a system failure, ($P_{Fi/Ts}$), 4% of the time. Only .1% is attributable to instrument failures, the rest arises due to simplifications introduced when the alarms were linked into a pattern. These simplifications were made because, when the individual alarms were linked, it was found difficult to retain each of the individual sequences without an excessively complex pattern.

If the Boolean laws are modified according to the scheme designated T-W-F, the previously missed system failures are now displayed as "Warning" states. If the Boolean laws are modified according to the scheme designated T-Wm-F (which allows a "Warning" to be upgraded to a "TRUE"), the probability of not detecting a system failure with a "True" top event status is less than originally attributable to instrument failure (.04% vs. .1%). This implies that, not only is the pattern more flexible in detecting system failed state, it is also capable of bypassing instrument failures.

The price for this resistance to instrument failures is a small increase in the false alarm probability, ($P_{Ti/Fs}$). The increase is small since two or more instruments must fail, or an instrument failure must occur concurrently with a partial system failure, to generate a spurious "True" top event status.

The identification of a failure mode was defined as a continuous and unambiguous (only one "true" input to any "or" gate) "True" path from the top event to one or more end events (alarms). Under these conditions it is stipulated that the observed path arose from the existence of an included, and observed, failure mode. The analysis of the pattern indicated that 88% of the time a failure existed, the failure was identified in this manner. Due to the requirement that a "True" path exist, the inclusion of the "Warning" status does not affect this parameter.

4.0 CONCLUSIONS

The probabilities discussed above represent upper bounds for all parameters except the false alarm, which represents a lower bound. The effects of component failures not included in the fault tree were not included in the probabilistic analysis. However, an analysis which includes such components would be performed with the same techniques. Additionally, the final values are not meant to represent absolute quantities; only to provide a systematic, quantitative method to compare various system - alarm analysis proposals.

As discussed in section 2.4, several parameters of the alarm analysis system can be varied. The alarm pattern and analysis routine ultimately chosen can be used to monitor the operability of specific systems, and identify the failure mode when possible. Simple alarm patterns are easy to construct, store, access, and modify. If some type of "Warning" status is included in the analysis routine, even the simple pattern promises to reliably detect system failure. The loss of specific failure mode identification is not considered as important, since it may be unlikely that any failure mode assumed will ever actually occur.

REFERENCES

1. Human Factors Methods for Nuclear Control Room Design, EPRI NP-118-5Y, Summary Report (June 1979).
2. G.M. Lilly and M.F. Binney, "Impact of the Westinghouse Control Room on the Reliability Maintenance and Operational Aspects of a Nuclear Power Station," IAEA-SM-226/73.
3. The Human: The Key Factor in Nuclear Safety, Conference Record for 1979 Standards Workshop on Human Failure and Nuclear Safety, Myrtle Beach, South Carolina (1979).
4. S. Dinsmore, "A Method to Improve Accident Sequence Recognition in Nuclear Power Plant Control Rooms," S.M. Thesis, Nuclear Engineering Department, M.I.T. (March 1982).
5. P.C.M. Key and P.W. Heywood, "Alarm Analysis and Indication at Oldbury Nuclear Power Station," in Automatic Control in Electricity Supply, I.E.E. Conf. Publ. 16, Pt. 1 (1966), p. 295-317.
6. D. Welbourne, "Alarm Analysis and Display at Wylfa Nuclear Power Station", Proc. IEE, Vol. 115, No. 11 (November 1968).
7. E. Hollo, "Some Points of Advanced Alarm System Design," RIS0-M-1908 (1977).
8. B. Frogner and C.H. Meyer, "A Method for On-Line Power Plant Disturbance Analysis," Third Power Plant Dynamics, Control, and Testing Symposium, Knoxville, Tennessee (September 7-9, 1977).
9. J.C. Green and G.H. Taylor, "A Review of the Performance of the Station Computer since the Commencement of Power Operation," IAEA-SM-226/11.
10. L. Burger and E. Zobor, "On-Line Analysis in the Hierarchical Control System of the WWR-SM Research Reactor," IAEA-SM-226/17 (1979).
11. Reactor Safety Study, WASH-1400, Appendix I and II, U.S. Nuclear Regulatory Commission (1975).

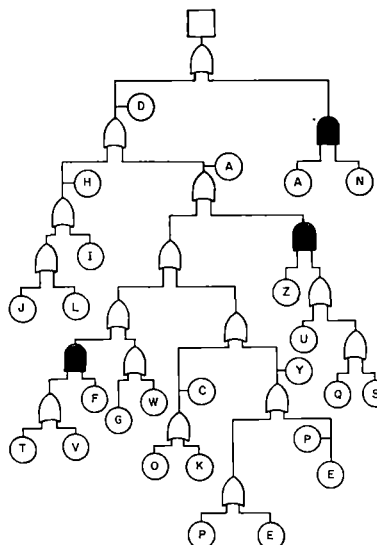


Fig. 1. HPCIS Alarm Pattern.

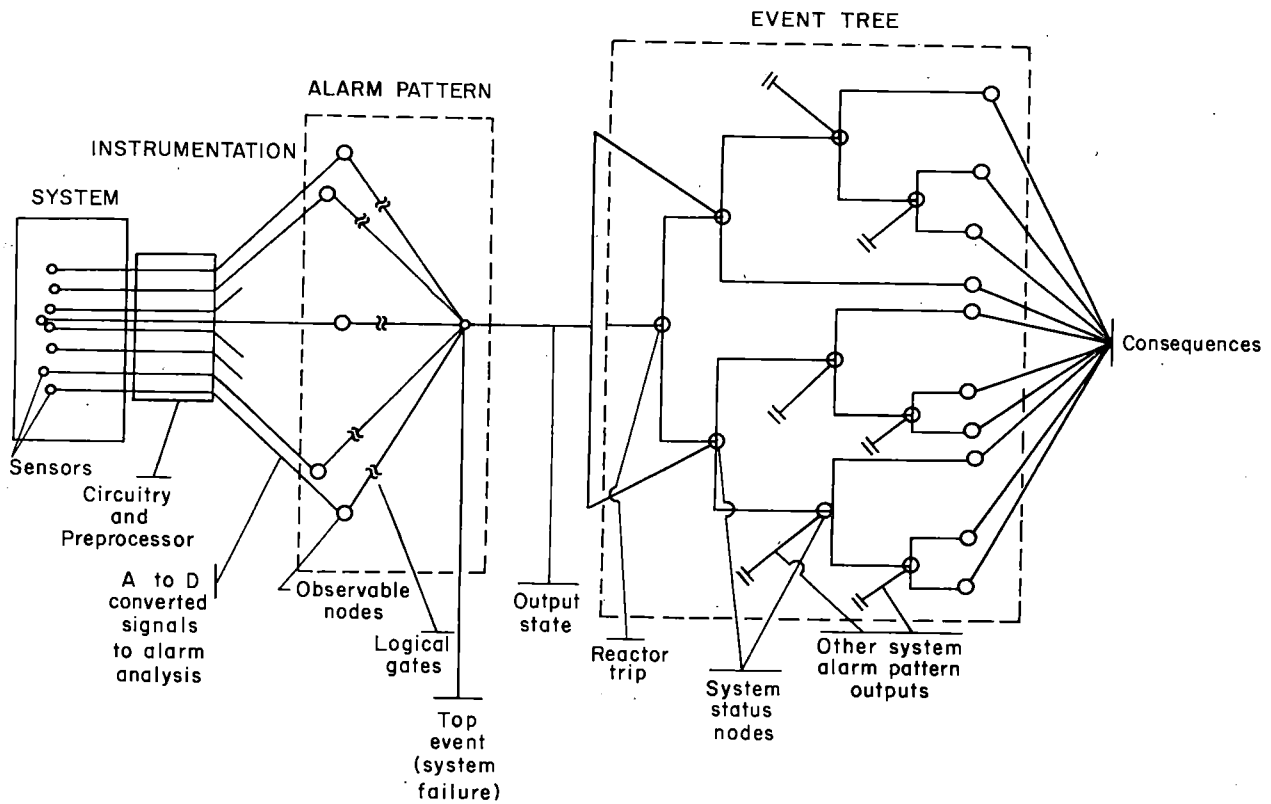


Fig. 2. Fully Implemented Alarm - Consequence System.

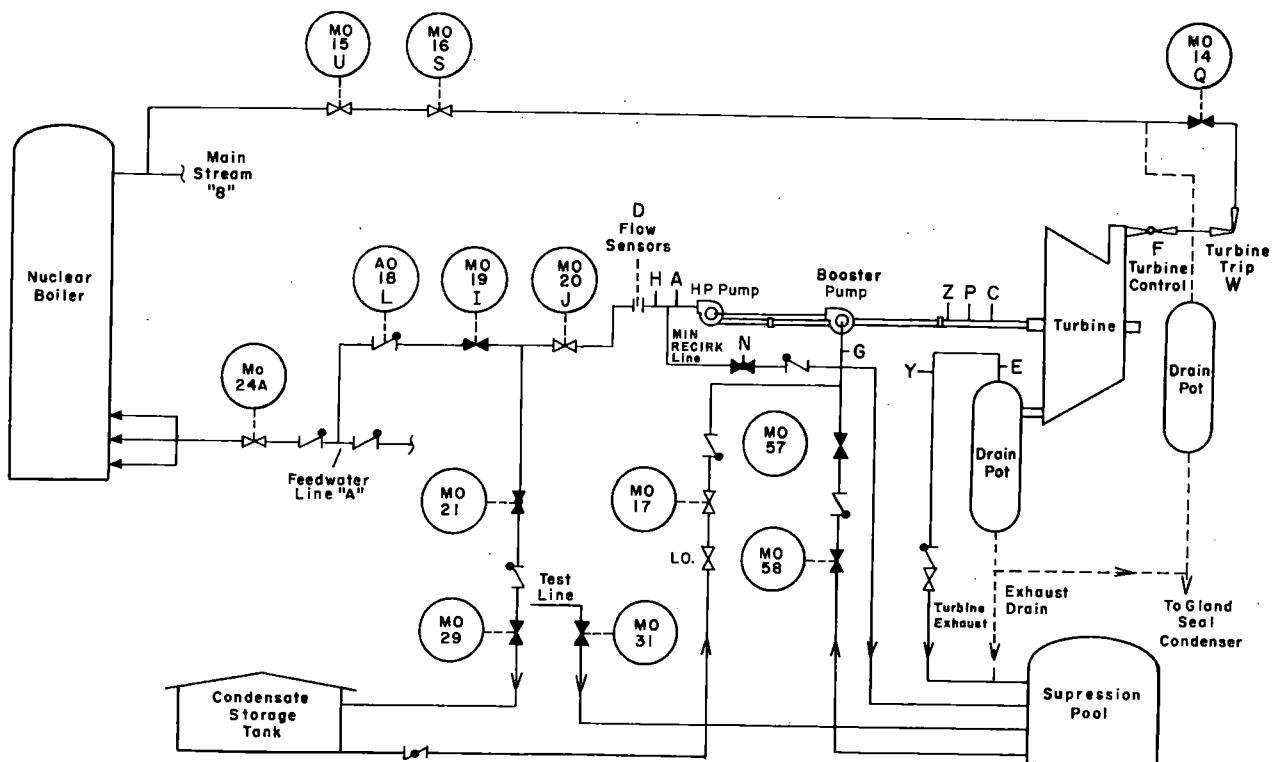


Fig. 3. HPCI System with Instrumentation.

TABLE I

Instrumentation Unavailabilities

<u>Instrument Symbol - Name</u>	¹ <u>Normal Indication</u>	<u>Unavailability of TRUE Status</u>	<u>Unavailability of FALSE Status</u>
A - Low Pressure Pump Outlet	TRUE	4.5×10^{-4}	4.5×10^{-6}
C - ² High Speed Turbine	FALSE	0	0
D - Low Flow Pump Discharge	TRUE	4.5×10^{-4}	4.5×10^{-6}
E - ³ High Pressure Turbine Exhaust	FALSE	4.5×10^{-6}	4.5×10^{-4}
F - Hydraulic Control Valve Light	⁴ TRUE	7×10^{-4}	7×10^{-5}
G - ² Low Pressure Pump Inlet	TRUE	0	0
H - High Pressure Pump Outlet	FALSE	4.5×10^{-6}	4.5×10^{-4}
I - MOV-19 Light	⁴ TRUE	7×10^{-4}	7×10^{-5}
J - MOV-20 Light	⁵ FALSE	7×10^{-5}	7×10^{-4}
L - AO-18 Light	⁵ FALSE	7×10^{-5}	7×10^{-4}
M - High Level Sump	FALSE	4.5×10^{-6}	4.5×10^{-4}
N - MOV-25 Light	⁶ TRUE	7×10^{-4}	7×10^{-5}
O - Pump Room Leak	FALSE	4.5×10^{-6}	4.5×10^{-4}
P - Turbine Vibration	FALSE	4.5×10^{-6}	4.5×10^{-4}
Q - MOV-14 Light	⁴ TRUE	7×10^{-4}	7×10^{-5}
S - MOV-16 Light	⁵ FALSE	7×10^{-5}	7×10^{-4}
T - Steam Line Leak	⁵ FALSE	4.5×10^{-6}	4.5×10^{-4}
U - MOV-15 Light	⁵ FALSE	7×10^{-5}	7×10^{-4}
V - Low Pressure Hydraulic Oil	FALSE	4.5×10^{-6}	4.5×10^{-4}
W - Pneumatic Control Valve Light	⁴ TRUE	7×10^{-4}	7×10^{-5}
Y - ³ High Pressure Turbine Exhaust	FALSE	0	0
Z - Low Speed Turbine	TRUE	4.5×10^{-4}	4.5×10^{-6}

¹The High Pressure Core Injection System is normally in a standby condition.

Some alarms may be disabled in this condition.

If an alarm is disabled, the unavailability of both the TRUE and FALSE states should be equal to the higher value.

²These are control alarms which trip the turbine by closing the Hydraulic Control Valve.

They are assigned a zero unavailability.

³There are two High Pressure Turbine Exhaust Alarms, one initiates a turbine trip. Instrument Y is arbitrarily assigned the trip.

⁴This valve is closed in the standby alignment. When the system is operating, closure of the valve represents a failure event.

⁵This valve is open in the standby alignment. When the system is operating, closure of the valve represents a failure event.

⁶MOV-25 is the minimum flow bypass valve which is open in the standby alignment. When the system is operating, the opening of this valve represents a failure event.

TABLE II

Results of Alarm Tree Analysis of BWR-HPCIS Alarm System

Probability (per demand) of of Instrument Status Conditioned on HPCIS Status*	LOGIC GATE PROPAGATION SCHEME		
	T-F	T-W-F	T-W _{MOD} -F
$P\{T_I/T_{HPCIS}\}$	0.96	0.96	$1-\epsilon^{**}$
$P\{F_I/T_{HPCIS}\}$	4.2×10^{-2}	1.2×10^{-7}	1.2×10^{-7}
$P\{W_I/T_{HPCIS}\}$	NA	4.2×10^{-2}	3.9×10^{-4}
$P\{T_I/F_{HPCIS}\}$	2.8×10^{-7}	2.8×10^{-7}	2.9×10^{-7}

*Definition of Events: T_I = instruments indicate HPCIS has failed T_{HPCIS} = HPCIS is in a failed state F_I = instruments indicate HPCIS has not failed F_{HPCIS} = HPCIS is in an operational state W_I = instruments indicate a "warning" that the HPCIS may have failed $** \quad \epsilon \ll 1$ NOTE: For T-F case, $P\{T_I/T_{HPCIS}\} + P\{F_I/T_{HPCIS}\} = 1$ For other cases, $P\{T_I/T_{HPCIS}\} + P\{W_I/T_{HPCIS}\} + P\{F_I/T_{HPCIS}\} = 1$

THE FEASIBILITY OF ON-LINE FUEL CONDITION MONITORING^a

D. A. Petti, D. J. Osetek, D. W. Croucher, and J. K. Hartwell

EG&G Idaho, Inc.
Idaho Falls, Idaho 83415

ABSTRACT

The relationship between fuel rod damage and fission product release is investigated to assess the feasibility of using on-line gamma spectroscopy of reactor coolant to estimate not only numbers of detected fuel rods, but also the type of core damage which may occur during an accident or off-normal transient. Fission product release signatures for various fuel conditions and accident scenarios are compared, and unique indicators of fuel damage, ranging from cladding pinholes to severely damaged fuel rods, are suggested. The configuration of monitoring hardware and data analysis software are described, and the benefits, development needs, and usefulness of the envisaged power plant system are discussed.

INTRODUCTION

The level of pinhole defects in the core is usually monitored at power plants by analyzing the radioactivity of coolant grab samples. The basic principle involved in assessing defect level deterioration is to compare the relative behavior of different isotopes of certain fission product elements, specifically iodine and xenon. This same basic approach is enhanced with on-line monitoring by increasing both the number of samples analyzed and the number of isotopes included in the analysis. On-line monitoring has proven to be a successful means of determining defect levels in LMFBR and CANDU fuel.^{1,2} Advanced data acquisition and reduction equipment and appropriate gamma spectrometers have provided core defect levels in a near real-time manner, eliminating the time delay and personnel exposure associated with the collection of grab samples. Knowledge of the magnitude and rate of change of the defect level has been used to assess plant refueling strategy and the effects of plant operation on defect deterioration.

Extending on-line monitoring to assess more severe fuel damage situations, although it is only in the experimental stage, could provide important information needed to assess operator actions and emergency procedures. Since the magnitude and timing of fission product release from damaged nuclear fuel rods are strongly dependent on fuel behavior parameters such as fuel temperature and fragmentation, they

a. Work supported by the U.S. Nuclear Regulatory Commission, Office of Nuclear Regulatory Research, under DOE Contract No. DE-AC07-76ID01570.

are thought to be unique to a given damaged fuel condition. Greater or lesser fuel damage will produce distinguishably different fission release signatures. The validity of this hypothesis is accepted,³⁻⁵ although the practicality of accurately assessing various fuel conditions using on-line monitoring and fission product signatures is uncertain. The objective of this paper is to investigate the feasibility, limitations, and requirements of a fission product monitoring system capable of rapidly assessing a wide range of core conditions at a nuclear power plant.

TECHNICAL BASES

Fission products can be separated into several different volatility groups. The more volatile species, such as noble gases and iodine, are released more rapidly from fuel than the less volatile species, such as lanthanum and cerium. The rate of release of all species increases with fuel temperature, and the amount of each species released is generally proportional to the amount of fuel damaged. The fission product release signature resulting from a specific damaged fuel condition can be predicted using present best-estimate release rate constants⁶ and the fuel temperature history. Conversely, the probable condition of a fuel rod(s) can be estimated from the measured fission product release signature and knowledge of fission product behavior.

A flowchart of a release signature calculation is shown in Fig. 1. Element release rate constants, based on NUREG-0772 data, are calculated using a fuel rod temperature history. The release rate constants and the fuel rod power history are then input to the ORIGEN-2 computer code⁷ to calculate both the total inventory and the amount released as a function of time. The quantity released is divided by the total inventory to obtain release fraction signatures. The following describes a possible method of obtaining fuel condition estimates using fission product signatures.

An accurate estimate of fuel rod condition should consider the severity, extent, and rate of change of damage in the core. Methods for determining the extent and severity of damage in the core during normal operation are already in use. The ratios of short-lived to long-lived isotopes of certain elements, such as $^{133}\text{I}/^{131}\text{I}$, have been used to determine the number of defective rods in the core.⁸ Based on extensive data, French researchers⁹⁻¹¹ have developed a computer code, PROFIP, that is capable of estimating the number of defective rods, the average size of the defect, the range of UO_2 temperatures, and the burnup of the defective rod.

Characterizing the extent of damage more severe than cladding defects, in terms of the number of failed rods, becomes more difficult and uncertain. In severe accident situations, the severity of fuel damage will vary throughout the core. Fuel bundles in the center of the core may be severely damaged due to oxidation, fuel melting, or liquefaction, whereas bundles at the core periphery may only contain cladding ruptures. Distinguishing among these varied conditions with an on-line monitor may not be possible. However, interpretation of the response of a monitor will yield an averaged damage estimate that is weighted toward the fuel condition that produces the largest fission product release.

To determine the severity of damage, the release fractions of a nonvolatile and a volatile fission product can be compared. Since nonvolatile isotopes would be released in very small quantities for conditions of mild damage, the ratio of nonvolatile to volatile species would be very small. This ratio would approach one for conditions of severe damage. As a specific example, release signatures for ^{142}Ba and ^{131}I were calculated using the procedure diagrammed in Fig. 1 for four fuel conditions characterized by fuel temperatures of 1570, 1875, 2500, and 3200 K, indicative of increasing amounts of fuel rod damage. The four corresponding ratios of ^{142}Ba

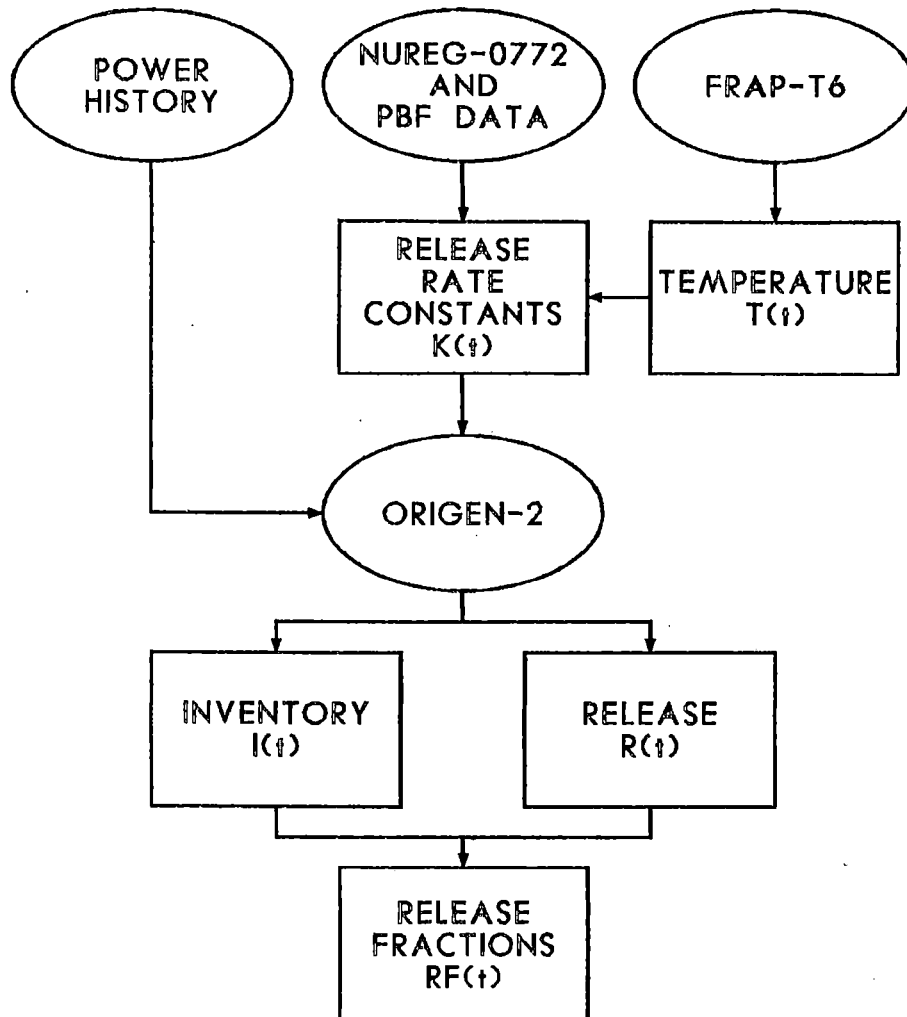


Figure 1. Release signature calculation.

and ^{131}I shown in Fig. 2 range from 10^{-4} , representative of a pinhole defect, to 0.5, for severely damaged fuel. The dynamic range offered by the ratio makes it a useful parameter for estimating fuel damage severity.

Detailed analysis of data from fuel failure tests in the Power Burst Facility may provide additional indicators of fuel condition. Figure 3 compares the ratio of noble gas to iodine release fractions for eight power-cooling-mismatch (PCM) and reactivity initiated accident (RIA) tests.³ Note that the ratio is substantially higher for those tests that produced fuel melting than for instances where only fuel fracturing occurred. It has also been observed that the type and duration of the transient event affects the release of nonvolatile fission product species. During an RIA in which the fission products are rapidly released from the rod, the release of Ba and La is due to the release and subsequent decay of their volatile, short-lived I and Xe precursors. However, in a longer duration PCM event, the precursors decay to more non-volatile species prior to significant release from the rod, such that lesser amounts of Ba and La are released to the primary coolant system.

With minor modifications, the fuel condition monitor could also determine the presence of fuel particles in the sample stream and, thus, provide an additional estimate of the severity of the fuel damage. A gamma spectrometer that monitors radiation from a particle filter placed upstream of the filtered coolant spectrometer could

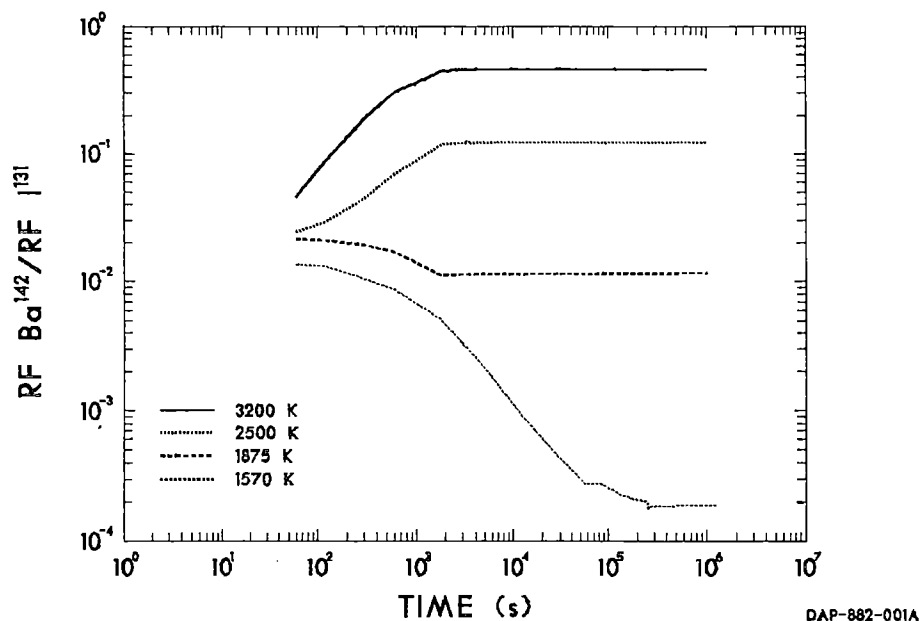


Figure 2. Ratio of isotopic release fractions for different fuel conditions.

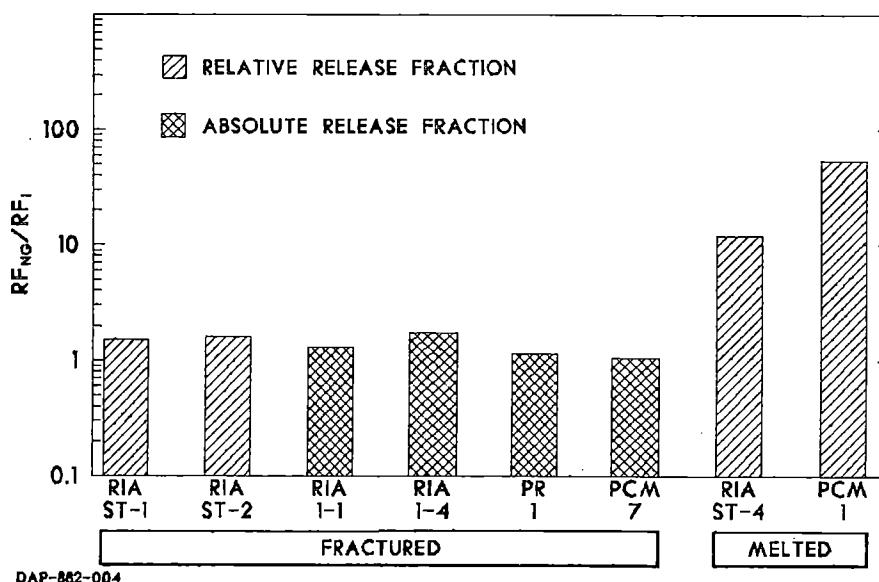


Figure 3. Noble-gas-to-iodine ratio of various PBF tests.

detect any fuel particles released during an accident. The presence of nonvolatile isotopes, such as Ru, Ce, and Zr on the filter, would indicate the presence of fuel particles in the coolant loop.

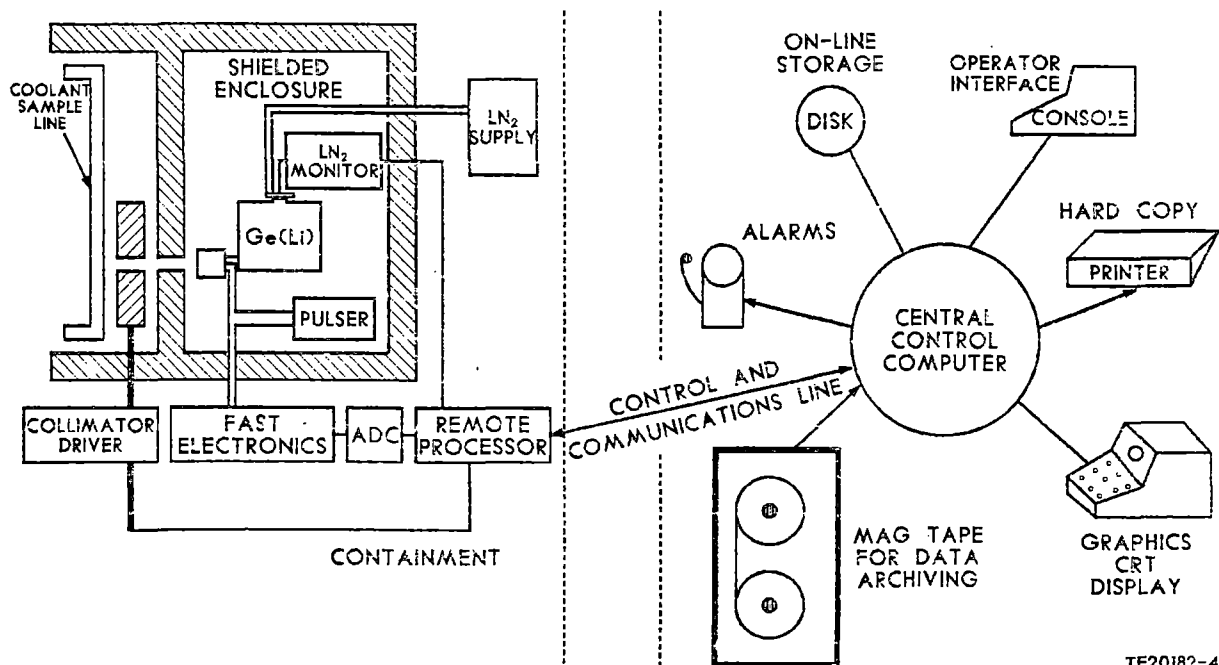
The extent of damage in the core during off-normal conditions can be determined, in part, by the magnitude of the release fractions. Although larger release fractions imply that more of the core is damaged, they alone cannot determine the extent of core damage uniquely. Since the release fractions are based on total core inventory, severe failure (~100% release of volatile isotopes) of one fuel bundle would appear similar to moderate fuel damage (~20% release of volatile isotopes) of five bundles. To classify the extent of core damage uniquely, an estimate of the severity of the fuel damage is needed first. For example, if the release fraction of a volatile

species is low (~ 0.05) and the fuel is severely damaged, as determined by the nonvolatile-to-volatile release fraction ratio, then the damage is localized. If the release fraction of a volatile species is low and the severity of the fuel damage is moderate, then a significant percentage of the core ($\sim 25\%$) is damaged. For conditions of mild damage, a low volatile release fraction implies that the damage is extensive. Thus, once the severity of the fuel damage is known, the extent of core damage can be determined.

The rate of change of fuel rod condition is proportional to the fractional release rate (rate of change of release fraction). If the release fraction has reached an equilibrium value, then the fractional release rate is zero and the damage has stabilized. Damage is increasing if the release fraction is increasing, with the rate of damage progression being proportional to the release rate. Thus, the use of fission product release signatures, the ratio of signatures, and the rate of change of signatures characterize the extent, severity, and rate of progression or stabilization of fuel damage.

SYSTEM DESIGN

On-line gamma spectrometer systems have been developed for use in both special research reactors¹² and commercial power plants.⁵ These on-line monitoring systems incorporate automatic data processing equipment and are usually implemented in a distributed architecture, an example of which is shown in Fig. 4. A small, remote computer provides support for the gamma spectroscopic equipment, while a larger processor at the operator location provides system control and sequencing, spectral analyses, data reduction, and report generation. Since it is essential that the on-line spectrometer be protected against environmental effects, the system must be filled with liquid nitrogen, remotely and automatically, and equipped to operate reliably and unattended over a wide range of coolant concentrations. To accommodate



TF20182-4

Figure 4. System diagram for the Fuel Condition Monitor.

varying coolant radioactivity levels, systems with special "fast" analog electronics to achieve high count rates and variable collimators to control the radioactivity reaching the detector have been developed. These spectrometers also utilize an ultra-stable, dual amplitude pulser which injects electrical pulses across the germanium detector. The injected pulses are processed through the analog electronics chain and provide specific energy calibration for each spectrum and system operation validation. The germanium detector must be enclosed in a lead-polyethelyne shield for protection from background radiation. The shield is sealed and vented through a relief valve to allow the boiloff of liquid nitrogen to back pressure the shield, preventing detector contamination in the event of airborne contamination in the containment building.

SYSTEM OPERATION

Figure 5 is a flow diagram indicating the logic required to estimate fuel condition. As indicated in the figure, all parts of this logic are not available as operating computer programs, but the feasibility of each has been investigated separately.

Each spectrum acquired by the gamma ray spectrometer is analyzed using a suitable spectrum analysis program such as GAUSS.¹³ The measured count rate for each identified photopeak is then converted to an isotopic concentration in the coolant using the calibration data stored in memory. Certain plant operating data such as average core power and primary coolant system flow rate, temperature, and pressure are used to adjust the calibration data set. The calculated fission product concentrations are then output to the user, or the results are integrated over the appropriate sample volume to provide released quantities of measured isotopes.

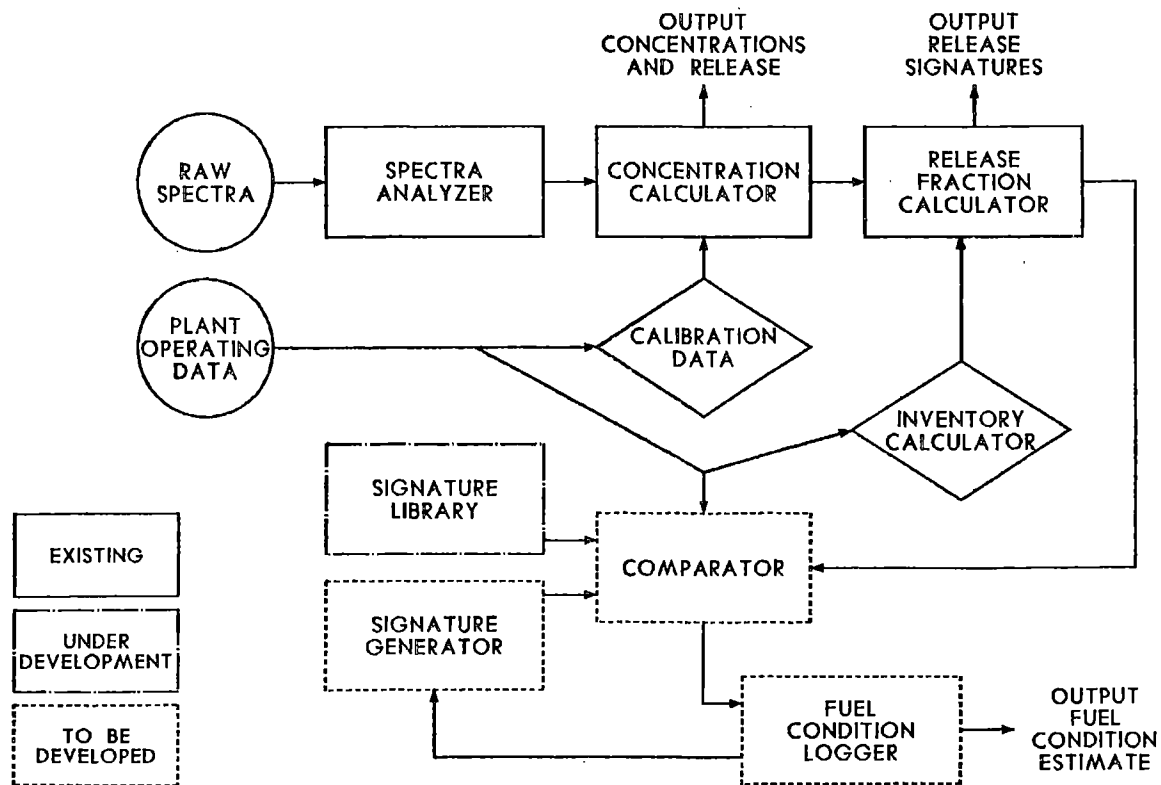


Figure 5. Software flow diagram for the Fuel Condition Monitor.

Release fraction histories or release-to-birth ratios are available from the Release Fraction Calculator, which divides the isotopic concentrations in the coolant by the corresponding core inventory. The time-dependent isotopic inventories are determined by the Inventory Calculator, which uses the core power history, fuel rod data, and a program such as ORIGEN. These time-dependent signatures are also provided to the Comparator, which examines the features in each signature for similarities to other signatures stored in the Signature Library, a set of fission product signatures for a variety of specific fuel conditions. Plant hydraulic data are used to correct for mixing and delay times to avoid misinterpretation of the measured signature. Special algorithms are then employed to calculate certain isotopic signature ratios (e.g., $^{142}\text{Ba}/^{131}\text{I}$) to determine the severity of fuel damage. The estimated fuel condition is provided to the Fuel Condition Logger, which tracks the changes in estimated fuel condition and outputs the current estimate and the history of estimates to the user. The signature generator then uses the current estimate to generate a complete "predicted signature" for analysis in the comparator. Any outstanding features of the predicted signature that are not found in the measured signature are used to improve the next fuel condition estimate. Noted discrepancies can also be provided to the user for evaluation.

The sophisticated data processing software required by the Fuel Condition Monitor to perform the functions shown in Fig. 5 is under development, but still in the initial stages. A reasonably modern computer is expected to handle such processing in a near-real-time manner, making the yet undeveloped portion of the fuel condition monitor appear feasible.

DEVELOPMENT NEEDS

The accuracy of monitors of this kind is expected to be higher during less severe fuel damage situations than during very severe accidents. Nevertheless, additional development in specific areas could potentially expand the versatility of the fuel condition monitor to include severe fuel damage conditions. Accurate release rate constants over a wide variety of fuel conditions would enhance the accuracy of the monitor. Although the temperature dependence of release rate constants has been investigated,⁶ the dependence of the constants on fuel fracturing, oxidation, melting, liquefaction, and burnup needs to be defined. To predict fuel conditions during severe accidents more precisely, the effect of fission product transport, chemistry, and rapidly changing thermal-hydraulic conditions on isotopic release signatures needs to be addressed. Fission product retention or deposition in the primary system must be considered to avoid misinterpretation of the measured signatures. At present, little data exist on fission product release and transport during severe fuel damage accidents. However, fuel and fission product behavior data from experiments being conducted at the Idaho National Engineering Laboratory to simulate severe fuel damage accidents¹⁴ could be applied to address these development needs.

CONCLUSION

On-line gamma spectroscopy is a feasible means of determining fuel condition during both normal and off-normal conditions. Once the development needs are addressed, the fuel condition monitor could potentially provide early information about the extent, severity, and rate of progression or stabilization of fuel damage over a wide range of fuel conditions. The availability of regular coolant radiochemistry data offered by on-line monitors would greatly enhance fuel defect monitoring, primary coolant radiation level monitoring, and other routine plant performance monitoring. The additional value, however, of a fuel condition monitor lies in its potential to

greatly reduce the number and severity of fuel damage incidents by offering the plant operator near-real-time information for interpreting the effectiveness of mitigating actions.

ACKNOWLEDGMENTS

The authors wish to thank R. M. Kumar and G. S. Reilly for their work in preparation of data in support of this paper and P. D. Randolph and J. W. Mandler for their technical review and comments.

NOTICE

This paper was prepared as an account of work sponsored by an agency of the United States Government. Neither the United States Government nor any agency thereof, or any of their employees, makes any warranty, expressed or implied, or assumes any legal liability or responsibility for any third party's use, or the results of such use, of any information, apparatus, product or process disclosed in this paper, or represents that its use by such third party would not infringe privately owned rights. The views expressed in this paper are not necessarily those of the U.S. Nuclear Regulatory Commission.

REFERENCES

1. D. B. LAMBERT et al., "Recent Improvements in Identifying Fission Product Sources in the Experimental Breeder Reactor II," Nucl. Tech., 39, (1978), pp. 275-282.
2. J. M. CUTTLER and P. GIROUARD, "On-Line Detection of Failed Fuel in CANDU Power Stations," Specialists' Meeting on the Behavior of Defected Zirconium Alloy Clad Ceramic Fuel in Water Cooled Reactors, IAEA Proceedings, IWGFPT/6 (May 1980), pp. 49-53.
3. D. J. OSETEK, J. J. KING and D. W. CROUCHER, "Fission Product Release Signatures for LWR Fuel Rods Failed During PCM and RIA Transients," in Proc. ANS/ENS Topical Meeting on Reactor Safety Aspects of Fuel Behavior, Sun Valley, Idaho, August 2-6, 1981.
4. R. BERAHA et al., "Fuel Survey in Light Water Reactors Based on the Activity of the Fission Products," Nucl. Tech., 49 (1980), pp. 426-434.
5. J. W. MANDLER, "On-Line Reactor Coolant Monitoring," Trans. Am. Nucl. Soc., 39, (1981).
6. Nuclear Regulatory Commission, Technical Bases for Estimating Fission Product Behavior During LWR Accidents, NUREG-0772, (1981).
7. M. J. BELL, ORIGEN--The ORNL Isotope Generation and Depletion Code, ORNL-4628 (1973).

8. D. H. LOCKE "Mechanisms of Deterioration of Defected LWR Fuel," Specialists Meeting on the Behavior of Defected Zirconium Alloy Clad Ceramic Fuel in Water Cooled Reactors, IAEA Proceedings, IWGFPT/6, (May 1980).
9. R. BERAHA, et al., "Fuel Survey in the Light Water Reactor Based on the Activity of the Fission Products," Nucl. Tech., 49 (1980) pp. 426-434.
10. P. BESLU et al., "PROFIP Code: A Model to Evaluate the Release of Fission Products from a Defective Fuel in PWR," Specialists' Meeting on the Behavior of Defected Zirconium Alloy Clad Ceramic Fuel in Water Cooled Reactors, IAEA Proceedings, IWGFPT/6, (May 1980).
11. P. BESLU et al., "Description of a Method to Determine the Characteristics of Defective Fuel from Water Activity Measurements," Specialists' Meeting on the Behavior of Defected Zirconium Alloy Clad Ceramic Fuel in Water Cooled Reactors, IAEA Proceedings, IWGFPT/6 (May 1980).
12. D. J. OSETEK et al., "The Power Burst Facility Fission Product Detection System," Review Group Conference on Advanced Instrumentation for Reactor Safety Research, NUREG/CP-0007 (October 1979).
13. J. C. CLINE, M. H. PUTNAM, and R. G. HELMER, "GAUSS VI: Computer Program for Automatic Batch Analysis of Gamma-Ray Spectra from Ge(Li) Spectrometers," NCR-1113 (1973).
14. B. J. BUESCHER, D. J. OSETEK, and S. A. PLOGER, "Power Burst Facility Severe Fuel Damage Test Series," Proc. ANS Reactor Conference on Fast, Thermal, and Fusion Reactor Experiments, Salt Lake City, April 12-15, 1982.

AN INTEGRATED ACCIDENT MONITORING SYSTEM, A COMPUTERIZED
INFORMATIONAL AID TO IMPROVE THE OVERALL RESPONSE TO
ABNORMAL SITUATIONS

C. H. Neuschaefer, NUPLEX 80 Product Manager
Instrumentation and Controls Engineering
Nuclear Power Systems
Combustion Engineering, Inc.
Windsor, Connecticut

ABSTRACT

There is a need to improve the man machine interaction in nuclear power plants that operators can respond better to potentially adverse situations. This can be done with an Accident Monitoring System, which is a plant monitoring, information processing, and graphic display system. The system functions during normal plant operation and is also designed to aid the staff in fulfilling its role, particularly during "ill-defined" events and situations of stress. This system is based on a man-machine design philosophy and computer technology and provides an incremental improvement over most existing operator-control room interfaces.

The Accident Monitoring System consists of the Critical Functions Monitoring and Qualified Safety Parameter Display Systems. It provides plant information in the control room, as well as other locations, such as a technical support center and an emergency operations facility. The information includes: 1) simple and direct CRT safety parameter displays, 2) hierarchically organized CRT plant information displays for verification, diagnosis and feedback on the overall plant state, 3) a qualified IE signal processor and plasma display and 4) inadequate core cooling instrumentation processing and displays.

INTRODUCTION

For significant periods of time during the TMI event, the operations staff and off-site authorities were unaware of the safety status of the plant. Failure to recognize the actual state of the plant resulted in (1) inappropriate actions that contributed to the core damage and (2) a series of misrepresentations to the public. This event pointed up the need for improved operational safety and emergency response. In its definition of operational safety, the Nuclear Regulatory Commission includes "human factors engineering...integration of the human element in the design and regulation of system safety..." (1) Emergency response is the timely and effective reaction to abnormal events to minimize the event's effects on the plant and the environs. To be prepared for effective emergency response, nuclear plants need to have facilities and personnel onsite and offsite equipped and prepared for an emergency.

The accident Monitoring System (AMS) integrates the operations staff role, the Critical Safety Functions philosophy, and computer technology to produce a plant monitoring, information processing, and information display system capable of aiding the operational staff during abnormal events, particularly ill-defined events, and situations of stress. The system provides plant data to onsite and offsite personnel and

and facilities in a manner that enables them to determine the plant status and to respond effectively in the event of an accident. The system meets the spectrum of licensing requirements for processing and display in an integrated cost effective system.

INTEGRATED MAN-MACHINE DESIGN PHILOSOPHY

Even before the proliferation of requirements, C-E's post-TMI evaluations identified the desirability of improved information presentation to the operations staff. In fact, the development of the AMS has been a systematic outgrowth of the development of the Nuplex 80 TM Advanced Control Center. (2-5)

The guiding safety philosophy used to establish the design basis for the AMS is the Critical Safety Functions approach, which has recently been developed. (6) From this safety philosophy, a design basis was established, which, in turn, led to the Accident Monitoring System design, implementation, design verification, man-machine validation, and subsequent integration into plant operation and operator training programs. (7)

The overall plant design and administrative controls that govern its operation must ensure safe and economic generation of electricity. In particular, the plant design, technical specifications, procedures and operations staff must be such that the consequences of plant events are acceptable. Power plants are designed with multiple barriers and redundant and diverse automatic safety systems to effect reliable control in abnormal situations. Pre-TMI emphasis was on increased reliability of automatic safety systems and plant designs. Post-TMI has brought to the foreground a basic item in the safe operations of nuclear power plants: the importance of the operator in plant control and safety. This is not a new philosophy, but an increased emphasis on an existing philosophy.

The operator is an integral part of a control system whose function is to maintain an initially acceptable plant state and to take appropriate corrective actions during transients to control the plant and maintain safety. An initially acceptable plant state is one in which the plant is operated within the design basis initial conditions established by the safety analysis. The operator maintaining an acceptable plant state is analogous to an automobile driver with a well maintained braking system maintaining a minimum braking distance. This ensures that the safety systems, the brakes (which have finite reaction times), can be effective. Appropriate corrective actions are those that assist in controlling the plant and keeping it safe. The operator, as an active element of the control system, must assess the data, decide, and act. In a conventional nuclear power plant control room, the operator's task consists of collecting and interpreting information from the control boards and acting to control the power plant. The human limitations in information processing must be recognized. These include rates of transfer of information in and out of memory, recognition of patterns of information by memory matching, short-term memorization of data, and decision making in the face of many variables, all of which can be further limited by stress.

Traditionally, operators' safety-related control actions have been based on emergency or abnormal operating procedures, which, in turn, were based on design basis event analyses. Certain symptoms would be recognized, appropriate event-oriented procedures would be executed and, implicitly, the safety functions would be maintained. This is primarily rule-and skill based behavior and is appropriate when an event can be defined. However, not all events are well defined, i.e. symptom sets from control room instruments cannot always be correlated to an event and its associated procedure. In such cases, the operator may be deluged with so much information that he may not be able to discern the event, particularly when under stress. Therefore, under these circumstances, symptom-event oriented approaches are not always efficient, since there may be no clear, unambiguous symptom-event set. In these situations, where normal

rule or skill-based behavior (8) do not help, the operator himself must decide how to control the plant. He must link the symptoms to a new procedural approach and actions. To do this, he must rely on his innovative, adaptive, intellectual capacity. This kind of behavior is often called knowledge-based behavior. (8)

A safety function approach to plant operation coupled with a computerized plant information processing system provides a systematic means to: assess plant safety, unload the human, and effect proper operator control actions independent of event-symptom diagnosis. This operational philosophy and computer aid can assist the operator in maintaining a safe plant, particularly during ill-defined events.

Critical safety functions themselves, then, are a group of actions that maintain the safety of the plant by preventing core melt or minimize radiation release to the general public.* The concept is that a nuclear power plant can be maintained in a safe and stable condition if a small number of critical functions are properly performed. The critical functions are:

- 1) Core Reactivity Control
- 2) RCS Inventory Control
- 3) RCS Pressure Control
- 4) Core Heat Removal Control
- 5) RCS Heat Removal Control
- 6) Containment Isolation Control
- 7) Containment Pressure and Temperature Control
- 8) Radiological Emission Control

Using safety functions, the operator observes the plant's state, through logic determines if safety functions are jeopardized, and, if so, determines appropriate "success paths" and takes control actions along these success paths to ensure the safety functions are accomplished. By monitoring these key functions, for example, core reactivity, and taking action to control the reactivity within prescribed limits, the operator can maintain the safety of the plant even if he is unfamiliar with the particular event at hand. The more knowledgeable an operator, the better; but with the critical safety functions, the operator has a systematic means to respond to emergencies without figuring out the event and at a time when his ability to reason, might be impaired because of stress. The operator still has to reason, but with the safety functions the choices he has to make are mapped out.

The Critical Safety Functions are analogous to an emergency medical team's response to an accident, the cause of which is uncertain. They would check the critical functions of the victim, for example, pulse, for they know that no matter what caused the accident, the heart must be beating for the victim to survive.

Conceivably, an operator can use the safety functions approach with any kind of a control room. The information he needs is available. The success that the operator will have using the Critical Safety Functions, however, is related to the availability of well presented, useful information. The operator's "window on the process" must be designed to effectively present the proper amount of information in an efficient manner and to prevent information overload.

* C-E introduced the safety function concept and the importance of the operator's role(6) and, subsequently, industry(9) and NRC(10) recognized its potential for improving the safety of nuclear power plants.

ACCIDENT MONITORING SYSTEM

Here's where the Accident Monitoring System comes in. It is a computerized information processing, monitoring, and display system that uses the critical safety functions to help the operator monitor the plant state and assess safety status. It performs much of the logic to help the operator determine if safety functions are jeopardized. The operator can then call up additional detailed information from a hierarchy of displays, if necessary, to help him diagnose and determine appropriate "success paths" so he can take control actions to ensure that safety functions are accomplished. The AMS does not overload the operator with information. The AMS also provides plant status information to offsite facilities to aid personnel there in their role of plant safety assessment for emergency planning.

The AMS (Fig. 1) consists of two major subsystems:

1. The Critical Functions Monitoring System (CFMS)
2. The Qualified Safety Parameter Display System (QSPDS)

CRITICAL FUNCTIONS MONITORING SYSTEM

The Critical Functions Monitoring System (CFMS) is the center of the integrated AMS. The CFMS consists of a single 32-bit Perkin-Elmer process minicomputer, designed for high availability, I/O equipment, and a fully graphic system including 2 display generators and 6 color CRT's. Two CRT's are located in each of the control room, Technical Support Center (TSC) and Emergency Operations Facility (EOF). The number can be varied. The CFMS (Fig. 2) provides several plant information processing functions, including input processing, integrated plant information and display processing, critical function algorithms/safety parameter display, trending, and historical data storage and retrieval functions. It provides the information in the control room, Technical Support Center (TSC) and Emergency Operations Facility (EOF) as well as to other locations, as necessary.

As discussed, the operators role is central to the design of the AMS, and plant safety, in particular, the key role items of "initial plant setup" and maintaining assurance that plant "safety functions" are maintained. The Critical Function Monitoring System portion of the AMS is the primary safety parameter display system. It provides direct and simple identification of plant safety status via critical function monitoring and alarms. It further provides additional information via its hierarchical displays. Information displayed in a manner to assist the operator: to verify, analyze and diagnose conditions, in determining appropriate actions and in monitoring the plant's response by providing feedback. The CFMS display structure is top down hierarchically oriented. Its structure is based on a functional approach (specifically, Critical Safety Functions). The idea is to structure the operator interface to assist the operator in coping with complexity during abnormal operations. Reference 11 discusses the use of multilevel descriptions of plant data related to the different levels of human abstraction and aggregation to assist in coping with complex situations in process control. This top down function oriented approach helps guide the operator around complexities.

Safety Parameter Display/Critical Functions

The AMS critical function algorithms are designed to assess key plant parameters, filter the plant information, deduce the status of plant safety functions, and provide this information to the operator. References 12 and 13 discuss the needs for and improvements with logical filtering and alarm inhibition to reduce or eliminate irrelevant alarms, particularly during stressful situations. The algorithms are functional, i.e. system/operational oriented and not event symptom oriented. The safety status of the plant is provided by a "go" or "no go" display of the status of each of the critical safety functions. The CFM display hierarchy provides for the safety status display as the top level (Level 1) display page. If a safety function is in jeopardy,

the associated box outline color becomes magenta. This level 1 display is the primary safety parameter display.

Hierarchical Information Presentation

The CFM's sectorable three level hierarchically structured plant information system further provides integrated plant information and displays. This allows the operator to rapidly assess the overall plant status, diagnose the causes, determine appropriate success paths, and monitor the effect of his actions on the overall plant process. In order to provide a presentation of information that is meaningful, it is vital that the physiological and psychological capabilities and limitations of the operator be considered. The CFMS hierarchy and display system take these into consideration. Some of these considerations are listed below.

1. Abnormal events and even more so "ill-defined" events are often accompanied by a high stress level in the operators.⁽¹⁴⁾ Hence the upper level overview information display should be designed to accommodate this. The upper level CFMS page is designed to include only discrete YES/NO presentations to provide important information with as little required operator processing as possible.
2. It is important that an information display system allow the user to A) know where he is, B) know where the information he wants is, and C) know how to get between the two. The CFMS uses a three level tree structured hierarchy to organize the display pages in the system. The upper level of the hierarchy contains information related to the broad overview of the critical functions required to maintain the plant in a safe and stable condition (hence plant safety status). The second level contains information organized according to the major systems in the plant and the third level provides detailed subsystem information.

The hierarchy is designed to be "self guiding" with the primary advantage that the information is organized in a structured, spatial and system oriented fashion. This allows the user to move through the hierarchy with a minimum of key strokes, no dialogs and no required memorization or guide books. All levels are connected to allow the operator to easily move vertically as well as horizontally through the display hierarchy. This hierarchical structure allows the information presentation and representation to be tailored to the specific requirements of the operator. The operator controls the breadth and detail of the information he wishes to view and the computer assures through the hierarchy that the operator is always informed of another page that may have other important information. The self directing hierarchy coupled with the straightforward and simple page control keyboard allows a large amount of information to be presented in an effective manner.

3. Designing and fabricating the NUPLEX 80 Advanced Control Center has provided C-E with much experience in the design of graphic display systems. The CFMS displays use this experience including.
 - a. A set of predesigned graphic symbols that have been developed from operator interviews, identification and confusion tests, and timing studies.
 - b. A systematic color and shape code grammar that ensures that the dynamic behavior of symbols is effective and understandable to the operator.
 - c. A methodology for the design and development of graphic displays.

The requirements of the operator and the need to design an effective process-man interface is an important portion of the overall systems approach toward the design of an integrated AMS

Reference 16 provides the hierarchy and typical displays.

QUALIFIED SAFETY PARAMETER DISPLAY SYSTEM (QSPDS)

The Qualified Safety Parameter Display System (QSPDS) consists of two safety grade Class 1E channels (Fig. 3). Each channel contains qualified Class 1E microprocessor based signal processing, a plasma display and page control module and fiber optic data link to the CFMS. The QSPDS will accept and process Class 1E plant signals and provide human factors engineered displays and will transmit isolated information to the CFMS for overall plant information integration, logging, primary operator displays, and transmittal to offsite facilities (e.g. TSC, EOF).

The QSPDS design basis includes the following:

1. A qualified signal processor system and display to address the NUREG 0737, II.F.2, inadequate core cooling requirements including:
 - a) Saturation margin monitoring
 - b) Reactor vessel level and temperature monitoring
 - c) Core exit temperature monitoring
2. A Class 1E signal processor and control room display including ICC and other plant parameters and the capability to expand it e.g., adding safety grade Reg. Guide 1.97 parameters into an integrated display. In addition to the obvious human factors benefits of this it can save valuable control room/board space, and
3. A qualified isolated data link to the Critical Functions Monitoring Systems providing isolated 1E information to be integrated into overall plant information and human factors engineered displays. This reduces the need for 1E I/O cabinets and isolation (including Reg. Guide 1.75) to the primary system.

In addition as necessary the existing design can without modification serve to provide qualified seismic backup Safety Parameter Display System that satisfies criteria set forth in NUREG-0696 regarding uninterrupted performance during and subsequent to events that could occur during the life of the plant (including earthquakes).

The essential signal processing performed in the base QSPDS consists of 1E qualified signal processing and SPDS and ICC functions. A functional description of this processing follows.

Qualified Safety Parameter Processing and Display

NUREG 0696 requires a Safety Parameter Display System (SPDS) that must display a minimum set of plant parameters that defines the safety status of the plant. Furthermore, this system must function during all events that could happen, including earthquakes. C-E has concluded that a system that monitors the plant's critical safety functions and provides the control status of each of these is such a system. Specifically, the CFMS, as discussed previously, provides the ability to assess whether the safety functions are controlled or not (and hence plant safety status) and the associated status of plant systems and presents this to the operator as a simple and direct safety status identification. The QSPDS provides a two-channel Class 1E/seismic front end processor and backup SPDS displays. A two-channel processor is cost effective, since it provides a single failure proof processing of 1E inputs, and allows a number of other functions to be performed in a reliable manner. Once such a safety grade processing exists, it is a simple matter to define displays based on a safety parameter approach and to allow this system to also function as a backup SPDS.

The QSPDS processes a number of measured plant variables that relate to detecting the status of each of the plant's critical functions (refer to CFMS discussion for identification of functions). Since the QSPDS is a backup SPDS, the number of inputs, processing and displays are reduced from the primary system. However, the backup SPDS contains the key measured plant variables for providing an assessment of the plant safety status. The variables are chosen from those associated with the Primary

SPDS and critical safety functions and those used to indicate integrity of barriers to radioactive release and are sufficient for the operators to assess plant safety status. Further diagnosis and actions will be based on control board instrumentation once the overall safety status assessment is made. The QSPDS provides for an integrated presentation of information. The QSPDS provides a hardware integration in the common processor and plasma display in lieu of separate IE signal processing units and control board meters. Furthermore, the QSPDS provides functional integration of information and operator presentation through the safety function concept and operator displays. For example, the inadequate core cooling variables (refer to next section) are processed and displayed according to the Core Heat Removal Safety function since they are a subset of that function.

The QSPDS processing includes input checking, signal conditioning, conversion to engineering units, parameter calculations as necessary (e.g. ICC parameters), alarm setpoints and displays hierarchy. The QSPDS displays are arranged in a self guiding hierarchy of information readily accessible to the operator by a Page Control Module (PCM). It consists of top level displays of the key variables listed by safety function and more detailed Inadequate Core cooling information. The display directory hierarchy and typical display sets are shown in Reference 16.

Inadequate Core Cooling Monitoring

C-E has concluded that the NUREG-0737, II.F.2 requirements can be satisfied by monitoring the following three parameters, which are sufficient to detect the approach to, existence of, and recovery from inadequate core cooling over the full range of ICC from normal operation to complete core uncovering:

- a) Saturation margin
- b) Reactor vessel level (inventory)
- c) Core exit temperature

By monitoring the status and trend of these parameters, the possible coolant states associated with an ICC incident are encompassed and plant control of the Core Heat Removal safety function is monitored. The ICC parameters are calculated in the QSPDS and information provided via data link to the CFMS for primary display, trending, data storage, and data retrieval. In addition, the information is available at the IE plasma displays. The plasma displays and overall QSPDS display hierarchy was discussed in previous section.

The following is a description of the ICC processing performed. Saturation Margin. The Saturation Margin function uses the following plant inputs to the QSPDS: reactor coolant system (RCS) hot and cold leg RTD temperatures, reactor vessel upper head HJTC unheated junction temperatures, core exit thermocouples temperatures and pressurizer pressure. These inputs are used to calculate the individual saturation margins (subcooled or superheated) at the RCS locations, alarm on a predetermined amount of subcooled margin existing in the RCS, and calculation of core exit superheat conditions, if the core should ever be uncovered. The saturation margin information is on the SPDS plasma display and also on more detailed displays.

Reactor Vessel Level and Temperature. The QSPDS provides the reactor vessel level/temperature processing, and heater control for a Heated Junction Thermocouple (HJTC) system. The inputs are from the HJTC probe assembly. A HJTC probe assembly consists of a separator tube with eight HJTC sensors spaced inside the tube covering the range from the fuel alignment plate to the top of the reactor vessel head. One of the unique features of this device, aside from the fact that it was designed specifically as a device for measuring level (inventory) inside a PWR reactor vessel, is that it also provides fluid temperature information as well. Reference 15 provides a detailed description of the HJTC/RVLS principle of operation, system description and design verification test program and results. The QSPDS integrates the reactor vessel level and temperature functions with the other ICC information.

In particular, the QSPDS processes the three HJTC inputs, which are HJTC differential temperature (ΔT), HJTC heated junction temperature, and HJTC unheated junction temperature. The processing includes:

1. Determination of collapsed liquid level above the core from the ΔT signal compared to a threshold setpoint. Essentially a low ΔT below threshold is a covered indication and a high ΔT is an uncovered indication, and
2. Provisions of an alarm output when a reactor vessel level other than full is indicated, and
3. Conversion of unheated junction thermocouple readings to provide fluid temperature indication, and
4. Provision of control logic to develop a setpoint to control the heated junction heater controller power supplies for proper HJTC operation. The heater controller power supplies are also provided as part of the QSPDS.

The level and temperature information is primarily displayed as part of the ICC/Core Heat Removal safety function and also in more detailed informational displays.

Core Exit Temperature. The core exit temperature function uses an array of core exit thermocouple inputs that typically map the entire core exit radial and axial plane. The processing includes: conversion of raw TC inputs to temperature units, calculation of a representative core exit temperature from the array (this representative temperature is used in the saturation margin calculation to determine superheat condition, which would result should the core uncover) and providing an alarm output when core exit temperature reaches a predetermined high value. The core exit temperature information is displayed on the ICC/Core Heat Removal safety function display and more detailed individual display pages.

REFERENCES

1. U.S. Nuclear Regulatory Commission, "TMI-2 Lessons Learned Task Force Final Report," USNRC Report NUREG-0585, October 1979.
2. J. E. Myers, Jr. and T. G. Schultz, "The Design of a Computer Based Power Plant Control Center," Institute of Electrical and Electronics Engineers 1974 Nuclear Power Systems Symposium, Washington, D. C., December 1974.
3. J. E. Myers, Jr. and J. W. Veirs, Jr., "An Advanced Control Center Design for Nuclear Power Plants," Proceedings of American Power Conference, Chicago, Illinois, April 1975, C-E Publication TIS-4514.
4. T. G. Schultz and E. M. Brown, "Power Plant Computer System Reliability and Availability," International Atomic Energy Agency Specialist's Meeting on Nuclear Power Plant Control Room Design, IEEE Power Engineering Society, San Francisco, California, July 1975.
5. M. M. Danchak, "The Man-Process Interface Using Computer Generated CRT Displays," Instrument Society of America, Power Symposium, New Orleans, Louisiana, May 1977, C-E Publication TIS-5187.
6. W. R. Corcoran, et al, "The Critical Safety Functions and Plant Operation," Nuclear Technology, Volume 55, 3, 690-712, December 1981; Combustion Engineering Publication TIS-7158.
7. "Combustion Engineering Emergency Procedure Guidelines Development," Nuclear Power Systems Division Report CEN-156, June 1981.

8. L. P. Goodstein and Jens Rasumussen, "The Use of Man-Machine System Design Criteria in Computerized Control Rooms," Riso National Laboratory, Denmark, 1980.
9. D. Cain and E. Zebroski, "The Conceptual Design of a Power Plant Safety Panel," Nuclear Engineering International, August, 1980.
10. U. S. Nuclear Regulatory Commission, "Functional Criteria for Emergency Response Facilities," USNRC Report NUREG-0696, February 1980.
11. J. Rasmussen and M. Lind, "Coping with Complexity," RIS0 National Laboratory, Denmark, June 1981.
12. B. B. Thomassen and J. Augustin, "Alarm Generation, a Concept Based on Automatic Logical Filtering," OECD Halden Reactor Project, HPR260, Halden, Norway, May 1980.
13. Bjorn Wahlstrom, "Inhibition of Alarms During Nuclear Power Plant Operation," Technical Research Center of Finland, presented at Enlarged Halden Programme, Lillehammer, Norway, June 1980.
14. T. O. Sargent, "Towards Accurate Emergency Response Behavior," The Sargent Group Inc. publication, April 1981.
15. Carl H. Neuschaefer, "A Reactor Vessel Level Monitoring System, An Aid to the Operators in Assessing an Approach to Inadequate Core Cooling," Institute of Electrical and Electronics Engineers Nuclear and Plasma Sciences Society, 1981 Nuclear Science Symposium, San Francisco, California, October 1981, C-E publication TIS-6759.
16. Carl H. Neuschaefer, "An Integrated Accident Monitoring System", International Meeting on Thermal Nuclear Reactor Safety, Chicago, Illinois, August 29 - September 2, 1982, C-E publication TIS-7123.

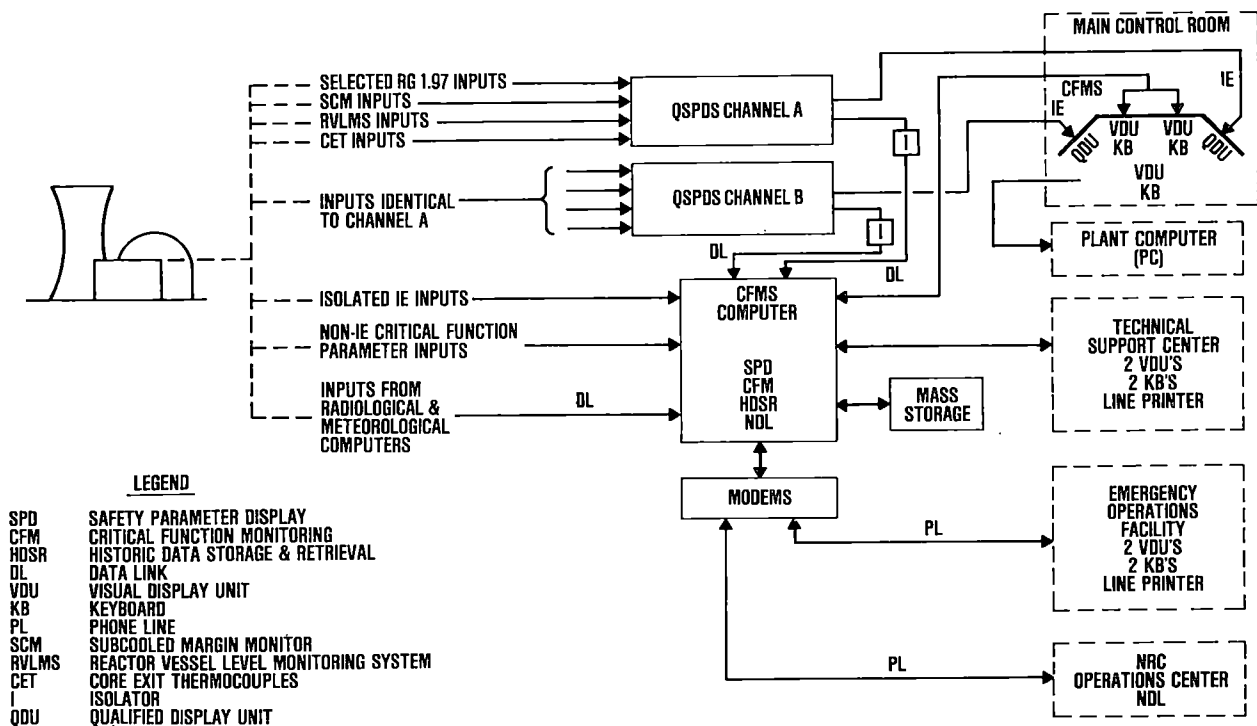


Fig. 1. Typical Accident Monitoring System (AMS).

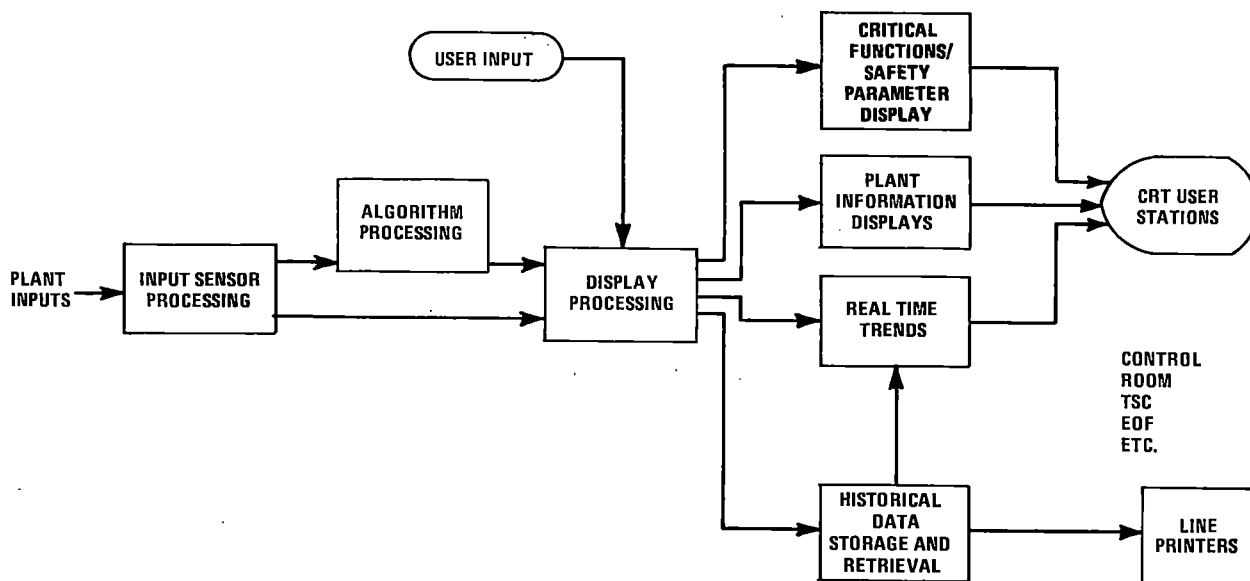


Fig. 2. Critical Functions Monitoring System (CFMS).

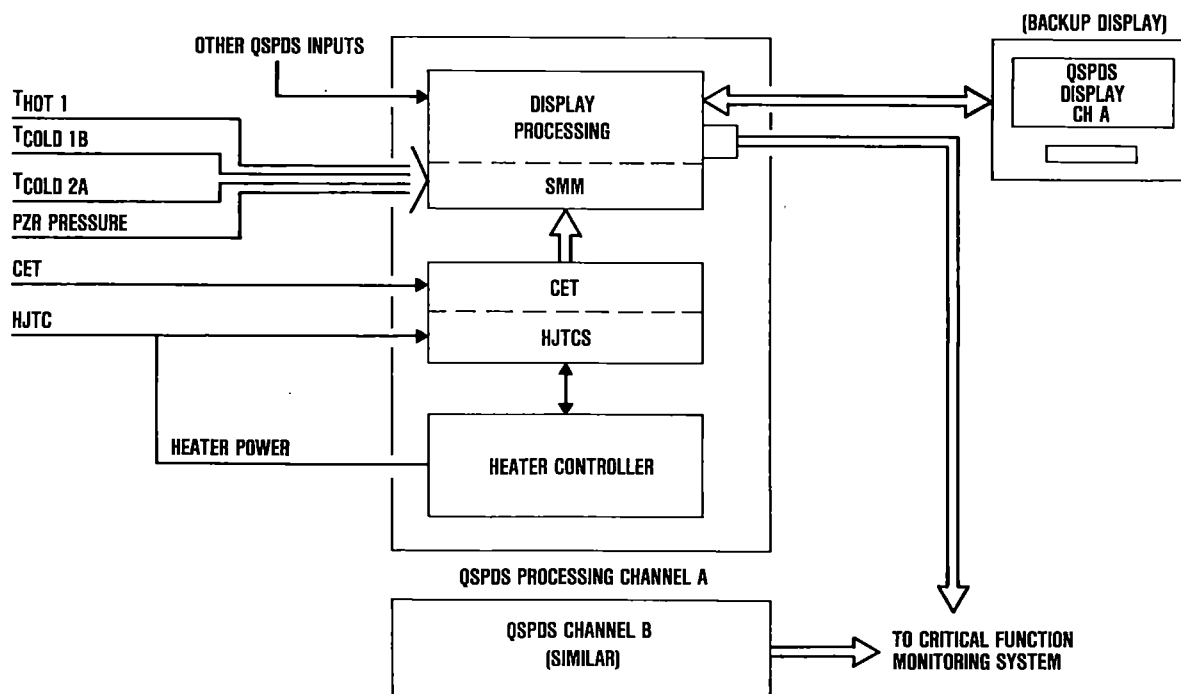


Fig. 3. Qualified Safety Parameter Display System.

REGIONAL OVERPOWER PROTECTION IN CANDU POWER REACTORS

C.M. Bailey, R.D. Fournier and F.A.R. Laratta
Atomic Energy of Canada Limited - Engineering Company
Sheridan Park, Mississauga, Ontario, Canada
L5K 1B2

A B S T R A C T

The Regional Overpower Protection (ROP) trip in a CANDU power reactor protects the core against fuel overpowers, whether the result of local peaking within the core or due to an uncontrolled power transient. This paper outlines the design-basis safety requirements, the equipment used to provide the trip, the analytical approach and procedures for design optimization.

To design the ROP trip means to select the optimum locations, trip setpoints and channelization of a set of self-powered in-core flux detectors for the trip. On-power fuelling, a relatively large reactor core, and the number and variety of in-core reactivity control devices in the CANDU reactor result in a large number of possible flux and power distributions which must be protected against overpowers. The design optimization problem is defined by the safety requirements and economic constraints, and is solved by Boolean reduction techniques. A final step is optimization of the reference channel power distribution.

INTRODUCTION

CANDU [1] power reactors are characterized by on-power fuelling and a relatively large reactor core. These factors result in a continuously changing burnup distribution and a potential for slow flux and power oscillations due to xenon. Reactor control thus involves a number of types of spatially-distributed reactivity control devices and spatial control in three dimensions using dual on-line computers. Combined, these factors result in a need for protection against localized fuel bundle and channel [2] overpowers throughout the core for a wide variety of potential flux shapes.

To provide this protection, CANDU power reactors are equipped with Regional Overpower Protection (ROP) trip systems. There are two such ROP systems in CANDU, one for each shutdown system. If either ROP system senses an overpower condition in the reactor, it immediately "trips" or actuates its associated shutdown system, which then rapidly shuts down the reactor.

An overpower is defined as a fuel bundle or channel power in excess of specified safety-related limits. These overpower limits are separate from and above the normal operating limits on channel and bundle powers.

The ROP trip has evolved from relatively simple neutron overpower trips on earlier CANDU reactors to comprehensive designs on current reactors. The latest designs are the product of well-evolved optimization techniques applied to the problem of providing protection for a wide variety of possible flux shapes, while minimizing restrictions on reactor operating margins. A subsequent probabilistic analysis is used to assess the overall performance of the ROP designs and the adequacy of the safety margins.

SAFETY REQUIREMENTS

Defense-in-Depth Approach

CANDU safety philosophy is based on a defense-in-depth approach to limit the occurrence and consequences of potentially unsafe conditions. Thus, there are three separate reactor systems which independently act to prevent overpowers in the reactor fuel: the Reactor Regulating System (RRS), which controls both the distribution and overall level of neutron flux and power within the core (i.e., spatial control and bulk reactivity control); and two fully independent shutdown systems - Shutdown System No. 1 (SDS1), and Shutdown System No. 2 (SDS2).

Each shutdown system is actuated by a number of process and neutronic trips, one of which is the Regional Overpower trip. If due to an RRS failure, a potential overpower arises in the core, each shutdown system must be equally capable of detecting the condition and initiating a shutdown.

To assure their independence, the two shutdown systems are required to be diverse in design and principle of operation, spatially separate and functionally equivalent. For example, they use different shutdown mechanisms - vertically oriented mechanical shutoff rods, dropped under gravity, for SDS1, and liquid poison injection via horizontal tubes for SDS2. (See Figures 1 and 2).

ROP Functional Requirements

The function of the ROP systems is to protect the reactor against overpowers in the reactor fuel, whether due to a localized peak while the reactor as a whole remains at normal power, or the result of an uncontrolled power excursion due to a Loss-of-Reactivity-Control (LORC).

An LORC is a very unlikely occurrence in a CANDU reactor. The reactor regulating system is designed to have a high degree of reliability and availability. Two independent and identical computers are used to control the reactor power level and spatial distribution (as well as for other reactor and plant control functions). All functions essential to reactor operation are incorporated in both computers, one being in control while the other is in backup mode. Most potential failures of the regulating programs result in a "fail-safe" condition, the reactor automatically being shut down.

Despite this inherently fail-safe design, CANDU reactors are provided with a variety of appropriate trip parameters which will cause a reactor trip if Loss-of-Reactivity-Control does occur. This include trip on high log rate of increase of neutron power (fast LORCs), high primary heat transport pressure (intermediate rate LORCs), as well as the high neutron power or ROP trip.

ROP is the primary trip for slow LORCs, but also acts as a backup trip for the more rapid transients. Because of the flux detector response characteristics and the lack of transport delays in transferring thermal power to the coolant, the most

restrictive LORC is a slow, gradual increase in reactor power. Thus, the "slow" LORC serves as a basis for design of the ROP systems.

In many types of Loss of Coolant accidents, voiding of the in-core coolant produces a reactivity increase and a rapid rise in bulk power. For such LOCAs, ROP also yields an early and effective trip. Thus, ROP provides not only the basic protective trip during 'slow' LORCs but also an effective backup trip signal in both shutdown systems for other types of transients, such as fast and intermediate rate LORCs and some Loss of Coolant accidents.

In the operating reactor, variations from the nominal flux and power distribution are normal and to be expected, and must be taken into account in the ROP design. Aside from changes due to burnup and refuelling, perturbed power shapes will occur during various operating modes such as a startup after a short shutdown (xenon override), withdrawal of adjuster rods, or insertion of mechanical control absorbers. Other perturbed power shapes would occur if a reactivity device were to malfunction for some reason.

An LORC transient, if it were to occur, could happen while the reactor is in one of these perturbed shapes. Or, with a strongly peaked perturbation, overpower limits could be exceeded locally while the reactor as a whole remains at normal power. (This would require temporary loss of spatial control and the flux-mapping stepback function by the regulating system). In either case, the ROP systems must trip the reactor before an overpower occurs.

Design-Basis Overpower Criterion

For the ROP trips, the basic safety requirement is that the integrity of the primary heat transport (PHT) system be maintained if an overpower were to occur. The ROP system must trip the reactor before excessive fuel overheating could result in a failure of the pressure tubes. Then, in the event of fuel failure, any released radioactivity is retained within the PHT system, preventing any possibility of a release to the public.

Although AECL experiments have demonstrated that CANDU fuel can be operated in dryout and melting conditions without damage to pressure tubes, prevention of fuel centreline melting is nevertheless set as a convenient but conservative safety design criterion for CANDU ROP systems.

For the 37-element fuel used in most current CANDU reactors, centreline melting is calculated to first occur under post-dryout conditions, either as an immediate consequence of the dryout or (more commonly) at a somewhat higher power. The limiting channel powers derived on the basis of the centreline melting criterion are known as "critical channel powers" or CCPs. These limiting CCPs are calculated on the basis of CHF (critical heat flux) correlations derived from full-scale laboratory experiments and fuel temperature calculations based on accumulated experimental data on CANDU fuel.

DESCRIPTION OF CANDU ROP SYSTEMS

General Description

Each ROP system consists of 20 to 50 self-powered in-core flux detectors, contained within the core in vertical or horizontal tubes known as assemblies, together with associated amplifiers, trip comparators, display and test circuits, and other trip logic circuitry. (Figures 1 and 2). (In the latest CANDU designs, all trip

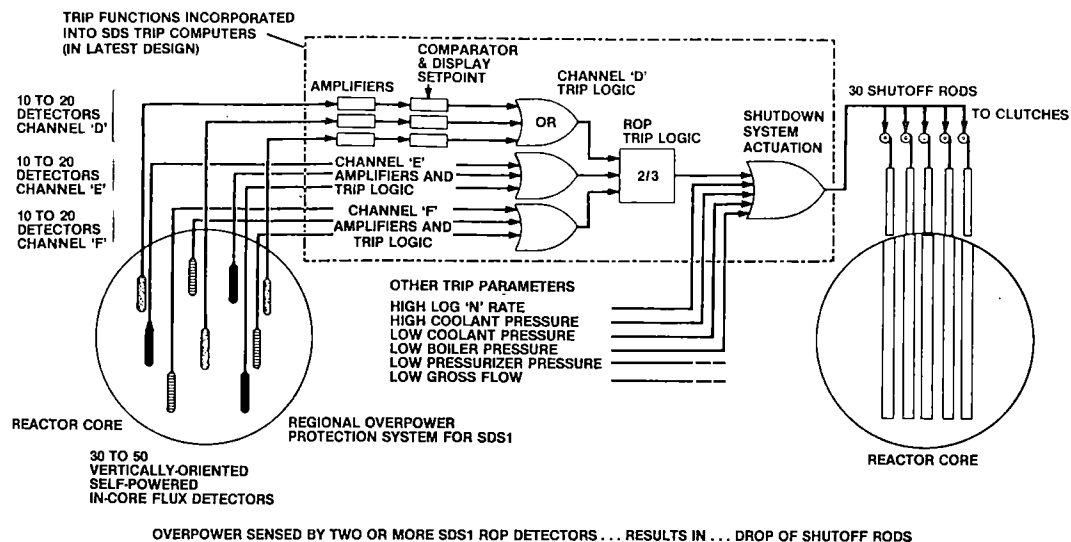


FIGURE 1 ROP TRIP FOR SHUTDOWN SYSTEM No.1

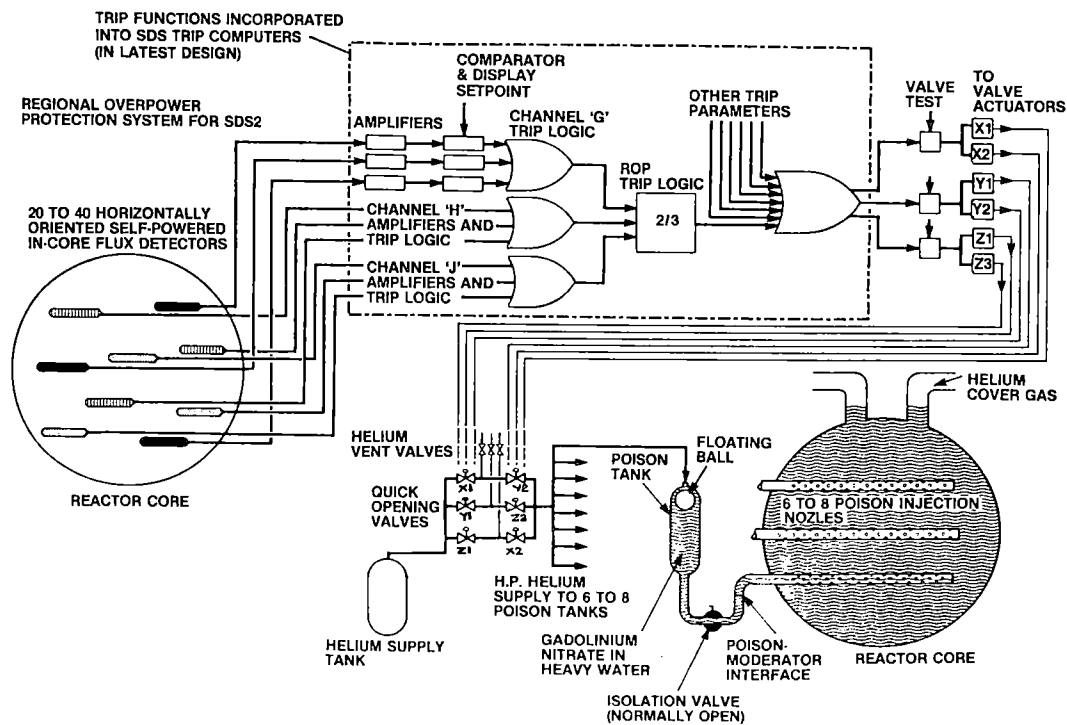


FIGURE 2 ROP SYSTEM FOR SHUTDOWN SYSTEM No.2

logic, display and test functions are incorporated into the Shutdown System trip computers.)

The flux detector assemblies are located within the relatively cool low-pressure moderator, between and perpendicular to the fuel channels. To ensure physical separation, the SDS1 ROP detectors and shutdown mechanisms are vertically oriented, while the SDS2 detectors and poison injection tubes are horizontal. As is indicated on the figures, the detectors in each ROP system are divided into 3 subsets, each associated with one of the shutdown system "trip channels".

Each ROP detector has a preset trip setpoint. If the signal from any detector in a trip channel exceeds the detector's setpoint, then that trip channel is tripped. Trip by any 2 of the 3 channels initiates a reactor shutdown.

Thus, although the two ROP systems together have from 50 to 100 detectors, reactor shutdown will occur if as few as two detectors, in different trip channels (but the same ROP system) were to "see" a high local flux in excess of their preset setpoints.

The detector and assembly locations for each ROP system are carefully optimized to ensure coverage of any flux shape that could arise in the operating reactor, while minimizing any potential for spurious trips and possible restrictions on reactor operating powers due to inadequate margins to trip. (See final sections).

Two Out of Three Coincidence

Trip on 2 out of 3 coincidence is extensively used in reactor safety systems (including ROP in CANDU) to ensure a high level of system reliability and availability. In a 2 out of 3 coincidence system, trip sensors and associated relays are triplicated, and a trip is initiated when any two trip channels indicate a 'trip' condition.

Thus, if a sensor or trip channel were to fail 'unsafe' (i.e. not provide a trip signal when required), the remaining two channels would continue to provide protection. On the other hand, if a sensor or trip channel were to fail 'safe' (i.e. provide a spurious trip signal), this would not, in itself, produce a spurious trip of the reactor. This redundancy against both types of failure provides a high level of reliability and availability, and allows the system to be easily tested while the reactor operates.

Although a trip is initiated on a 2 out of 3 coincidence basis, for design purposes the concept of 2/3 coincidence implicitly requires that at least one detector in each of the three trip channels must 'see' each overpower condition.

Detector Characteristics

Figure 3 shows one type of the prompt-responding self-powered in-core flux detectors used in the ROP systems to measure local flux and power.

These detectors are basically co-axial cables, with a metallic outer sheath (often of Inconel), a mineral oxide insulation layer, and a metallic central wire called an emitter. Placed in a radiation flux, the detector produces a current proportional to the magnitude of the flux without any external voltage being applied. (For additional information, see references [3], [4], [5].)

In the ROP detectors, the larger-diameter sensitive section extends over 2 to 3 lattice pitches (57 to 85 cm) - short enough to see any localized perturbation while being long enough to reduce sensitivity to refuelling of an adjacent fuel channel. The drawn reduced-diameter section forms a lead-cable extending to a connector jack

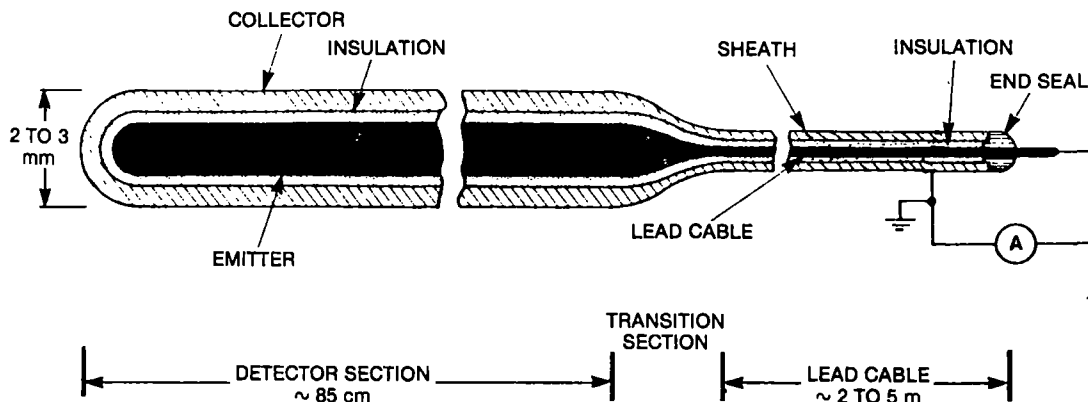


FIGURE 3 SELF-POWERED IN-CORE FLUX DETECTOR FOR CANDU ROP SYSTEMS

at the end of the assembly tube, where connecting cables feed the signal to amplifiers and the trip logic.

In current reactors, two types of detectors prompt-responding have been employed for ROP: Inconel-Inconel detectors, and those with Platinum-clad emitters. Dynamic compensation in the signal amplifier is used to obtain a signal matching the dynamic variation of the power to the fuel.

ROP FLUX SHAPES

The flux and power distributions in the core when the overpower occurs affect not only the peak bundle and channel powers, but also how well the ROP flux detectors "see" the overpower condition. Hence, the possible flux shapes that could arise in the reactor are a basic element of the ROP design process.

The basic design requirement is that the ROP trips must provide overpower protection for any flux, power and burnup distribution, and any device configuration, normal or abnormal, that could arise in the operating reactor, together with any possible changes in local zone controller or xenon levels.

Refuelling Ripple and Recalibration

Because of on-power fuelling, the core in an operating CANDU reactor will typically have channels and bundles with a mixture of widely varying irradiations (burnups) and varying powers. As fuel in a channel reaches its maximum burnup it is discharged and replaced with fresh fuel. The resulting variation in individual channel powers about their time-average values is known as refuelling ripple.

A basic simplification in the ROP design process is to separate the effect of refuelling ripple from the other flux-shape variations - i.e., those due to reactivity devices or xenon changes. The perturbation cases used to design the ROP systems are thus based on an idealized ripple-free nominal power distribution with time-average or equilibrium-burnup fuel properties.

The effect of refuelling ripple is accounted for subsequently, while the reactor operates, through a recalibration procedure essentially as follows:

- a) the maximum ratio of the current (rippled) channel power to the reference power for that channel is calculated; this parameter is called the Channel Power Peaking Factor or CPPF;
- b) the ROP detectors are recalibrated to the product of the CPPF and the current reactor power (i.e. so that their readings will equal the CPPF when the reactor is at 100% power);
- c) the recalibration is done at frequent intervals, while the reactor is operating in a reasonably steady condition; errors that might creep in between recalibrations are provided for in a portion of the overall error allowance.

To illustrate, if the CPPF is 1.08 and the reactor is at 100%, the ROP detectors will be reset during recalibration to read 108%. Not only are the detectors now calibrated to the current flux shape but the margin between each detector and its setpoint is reduced by 8%, just as some channel powers are 8% closer to their CCPs than they were in the original ROP analysis with an unrippled reference core. The CPPF recalibration procedure is conservative since it applies to all parts of the core a maximum ripple factor that is appropriate and needed in only certain parts of the core.

In practice, adjustments are made to the recalibration procedure outlined above, both for operational convenience and to take into account the conservatism.

Reactivity Control Mechanisms

The number and variety of reactivity control mechanisms have a significant impact on the design of the ROP systems. In a CANDU reactor, five means are used for short or long-term adjustment and control of reactivity and power levels:

- a) Liquid zone controllers: 14 or 20 individual compartments filled with variable amounts of light (ordinary) water (a mild absorber in a D₂O reactor); used for continual fine flux control-bulk and spatial;
- b) Adjuster rods: 21 to 27 solid absorber rods, grouped into banks; the adjusters normally reside in the core and have two purposes: core power shaping (axial and radial flattening), and to provide positive reactivity upon their removal (i.e. for startups, reactivity "shim", etc).
- c) Mechanical control absorbers (MCAs): 4 in number, similar in design to shutoff rods and normally held out of core; the MCAs may be driven into core to compensate for excess overall reactivity, or dropped into core to initiate a rapid power reduction or "stepback".
- d) Moderator poison: a boron salt dissolved in the moderator for long-term reactivity adjustments, and a gadolinium salt (burnable poison) for short-term adjustments.
- e) Refuelling: typically at a rate of about 2 to 5 channels per day, with either 4 or 8 fuel bundles of 12 in a channel replaced per visit.

On-line control of spatial power distribution in a CANDU reactor using these mechanisms is described in reference [6].

Design-Basis Case-Set

The ROP systems are designed on the basis of a comprehensive set of perturba-

tion simulations, known as the design-basis case-set, representative of all normal operating conditions and device configurations and any abnormal device configurations that could arise in the operating reactor.

Experience has shown that if:

- a) the ROP design has a reasonably-sized and well-distributed set of detectors;
- b) the design-basis includes cases representative of all normal operating configurations, all single-device abnormal configurations, and certain types of double-device abnormal conditions;
- c) where appropriate, the case-set includes variations representing the range of possible zone controller actions (or includes an error term for zone controller actions); and
- d) for xenon, major transients only (such as startups) need be included,

then the ROP design will also generally cover any related unanalyzed configurations, with different core burnup patterns, zone controller levels, xenon levels, device burnups or device insertions, as well as covering combined device perturbations where the individual device cases had been included.

The ROP design-basis set would typically include the following types of cases:

- (1) Normal Operating Cases
 - normal core with zone controllers at various average levels (20 to 80%)
 - MCAs fully or partially inserted, in banks of two
 - startup (xenon override after short shutdown, all adjusters out)
 - reactor power stepbacks (to 90, 75 or 50% F.P.)
 - adjuster withdrawals for reactivity "shim"

These cases would be simulated with and without normal spatial control.

- (2) Abnormal Configurations
 - one or more zone controller compartments drained
 - general zone controller malfunctions
 - loss of spatial control (harmonic xenon transients)
 - adjusters removed (single, and various combinations)
 - out of sequence adjuster withdrawals
 - MCAs inserted: single rod, 3 rods
 - MCAs inserted with adjusters being withdrawn
 - operations with shutoff rod inserted into core
 - and other cases as appropriate.

Typically, there would be 150 to 500 cases in the design-basis set, plus several hundred additional cases to "test" the validity of the coverage.

DESIGN OPTIMIZATION

The ROP design process also has a significant economic aspect - the potential derating or reduction in margin to trip during normal reactor operations due to non-optimal ROP design. Achievable reactor operating powers can be significantly affected by the choice of detector locations and channelization for the ROP design.

(Trip margins and deratings are closely linked. If the ROP trip margin is inadequate for a certain operating condition, there will be an increased risk of a spurious trip occurring due to refuelling, zone controller movements, etc. To avoid

this, the operator may choose to operate at a reduced power - derate - in order to maintain an adequate margin. Typically, a minimum margin to trip will be determined by the operating utility, based on operating experience, judgment and analysis of the indifference point between the incremental cost of the energy lost due to the derating against the incremental cost of additional spurious trips.)

This results in an optimization problem - to select a set of ROP detector locations, setpoints and channelization that will provide ROP protection, on a 3 channel basis, for all cases in the design-basis set, while minimizing the resultant restrictions on the flux shapes representative of normal operating conditions. These cases, a subset of the design-basis set, are called the "economic case set".

The incentive for optimization is considerable. The present worth to the reactor operator of each additional percent of reduced derating or increased operating trip margin may be of the order of \$10 to \$20 million per reactor unit. Using the optimization procedures outlined below, current CANDU designs attain performance, in terms of the normal operating powers allowed by the ROP systems, equal to theoretical limits for the more common operating configurations and within 1% for the less common conditions.

The CANDU ROP design optimization procedure is embodied in a proprietary code called ROVER and includes the following steps:

- a) A set of potential detector locations is assembled (e.g., at 0.5 lattice pitch intervals along 20 to 50 potential assembly locations), and the flux detector readings and required trip setpoints are calculated for each detector and case.
- b) For each design-basis case, the 3 or 4 detector locations that "least derate" the economic (operating) cases are found. (This may be the least weighted-average derating or on an incremental basis).
- c) For some cases, even the best detector locations may produce some derating of some of the economic cases. These "irreducible" deratings will allow additional detectors to be included in the coverage-set for other cases (i.e. beyond the initial 3 or 4) without incurring any additional derating of the economic case-set.

This results in a matrix of detector locations (at least 3 but generally more per case) against cases, known as the "coverage matrix". This is a set of "best" detector locations which have the minimum possible effect on deratings or trip margins for the economic case-set.

- d) The next step is a Boolean reduction of the initial coverage matrix to eliminate cases with similar coverage requirements. This results in a "reduced coverage matrix", which is the irreducible kernel of cases, with unique coverage requirements, imbedding in it the maximum attainable performance over the economic cases.
- e) The 'reduced coverage matrix' is then channelized, or grouped into 3 unique subsets, and the trip setpoints required to provide coverage of the design-basis set are determined. Additional detectors may be added to improve redundancy or to assist with channelization.

A final step in the design optimization is to optimize the reference channel power distribution (used as a basis for the calculated CPPFs and thus as a target for fuelling operations), in order to improve operational trip margins and/or the degree of redundancy in a given detector layout.

This process is called "reforming" the reference power shape. Basically, it is achieved by reducing the reference channel power for the most limiting channels,

while increasing powers for other less limiting channels. A larger increase in power can thus be tolerated for the limiting channels, which can be used to increase operating trip margins or to improve redundancy in coverage for the limiting case.

The gain in margins will only be realized to the extent to which the new reference power shape can be fuelled to as easily as the previous one. If the new reference shape is harder to fuel to, this may result in higher CPPFs and reduced operating margins, thus offsetting at least part of the original gain in margins.

A subsequent probabilistic analysis is used to assess the overall performance of the ROP designs and the adequacy of the safety margins.

REFERENCES

1. "CANDU" stands for Canada Deuterium Uranium
2. The fuel bundles and hot D_2O coolant in a CANDU reactor are contained in separate pressure tubes referred to as "fuel channels", which pass through the relatively cool, low-pressure D_2O moderator.
3. C.J. Allan and G.F. Lynch, "Signals Produced by Inconel Mineral Insulated Coaxial Cables in Neutron and Gamma-Ray Fields", Report AECL-6876, Chalk River Nuclear Laboratories (July 1980).
4. C.J. Allan, "A New Self-Powered Flux Detector", Report AECL-6681, Chalk River Nuclear Laboratories (1979 November).
5. C.J. Allan, "Response Characteristics of Self-Powered Flux Detectors in CANDU Reactors", paper for IAEA International Symposium on Nuclear Power Plant Control and Instrumentation, 1978 April 24-28, Cannes, France. Also issued as report AECL-6171, Chalk River Nuclear Laboratories (1978 May).
6. E.M. Hinchley and G. Kugler, "On-Line Control of the CANDU-PHW Power Distribution", Report AECL-5045, Atomic Energy of Canada Limited (1975 March).

SIMULATORS OF FUNCTION

Jacques RABOUHAMS - ELECTRICITE DE FRANCE - Direction de la Production
et du Transport

Jean STOLZ - ELECTRICITE DE FRANCE - Conseiller du Directeur de la
Production et du Transport

ABSTRACT

In order to compensate the lack of field experience of the control room operators before going on full scope simulator, E.D.F. is developing the simulators of function. These simulators dispose of all the commands and indicators which are in the control room for the particular function.

Two simulators (Turbine and generator, Volumetric control system) are operating at BUGEY training center. Nine simulators of each type will be available at the end of 1983. Three other simulators are on studies : reactor control system, steam generator and primary pump.

All the simulators will be also used for retraining control room operators every year.

INTRODUCTION

During pre-starting operation of nuclear units, the operational staff was able to have a good experience, indispensable before attending full scope simulator courses. All elementary functions are starting up and testing one by one. Operators can obtain a good knowledge of systems including size, functioning, incidents. Now 20 units are in operation and this experience can hardly be obtained by new operators because of good plant factor. In consequence, function simulators have two principal goals :

- compensation of the lack of experience before going on full scope simulator
- retraining.

Their use must increase the effectiveness of full scope simulator training and enhance the operational reliability by the possibility of permanent retraining.

FRENCH FUNCTION SIMULATOR PROGRAMME

In order to satisfy the two principal goals :

- initial training (before full scope simulator) in a training center,
- retraining on site,

the simulators of function have been design to be easily transportable. So they are compact and a 220/380 ac source is sufficient to ensure their functioning.

At present time, five elementary functions have been defined :

- Turbine Generator
- Volumetric control system
- Reactor control system
- Steam generator
- Primary pump.

Turbine generator and volumetric control system prototypes are operating at BUGEY training center. Nine simulators of each type will be available at the end of 1983. Turbine generator will have two different configurations :

- 900 MW C.P.1 (24 units up to BLAYAIS included)
- 900 MW C.P.2 (10 following PWR units).

Reactor control system prototype is under commissioning and will be available at the end of 1983. At that time, a serie of simulators will be ordered. Steam generator and primary pump simulators are on study. By the way, prototypes of 1300 MW unit are also on study.

GENERAL DESCRIPTION OF SIMULATORS OF FUNCTION

All simulator will have a similar design to Turbine-Generator and Volumetric control system ones. A simulator of function has the look of a compact furniture divided into three parts :

- operator's desk,
- instructor's desk,
- location for computer, peripheral utilities, interface.

All commands and regulation relays are positioned on an horizontal pannel with pedagogical organization which represents an active synoptic. Indicators recorders, video screen are on vertical pannel. Individual alarms are on a top oblique pannel. Each operator's desk has a specific design dependant of the function. All commands and indicators have the same functioning as a real control room.

The instructor's desk is on lateral side of the compact furniture. It is made of several commands and alarms used by the instructor, and a video screen for initialisation, incident or local command facilities. For the two prototypes, the instructor has disposition of five initialisation instances, 30 incidents possibilities, 10 local commands to cover the roundman's operation. The instructor has also the possibility to stop the phenomenon into the last configuration.

The video screen can be used for the representation of main circuits of the simulated function, several datas can be shown. They may have variable values.

The operator has the possibility of selectioning through a list a particular data he wants to see on the recorder.

The interface is the main communication system between the computer and desk operator and instructor equipment. It realizes the different conversions of analogical, binary, numerical signals. The computer is a Mitra 115 (32K possibilities

with 32K extension possibilities) from S.E.M.S.

At this time, for the prototype, there are :

384 binary inputs

64 analogical inputs

320 binary outputs

320 analogical outputs.

The two prototype simulators of function have been made by Thomson CSF Simulator department. The dimensions of simulators are 2,2 m x 1,8 m x 1,6 m and the weight is 800 kg.

UTILISATION OF SIMULATORS OF FUNCTION

These simulators are used during three kinds of training session :

- initial operators training,
- operators retraining,
- staff outside the control room concerned by functioning.

The initial operator training is for all new shift advisor, shift supervisor, assistant shift supervisor, control room operator. The duration of the training is one week and the number of trainees is four for each session. This training is located into the training centers (8 centers) where are also the instructors. Two trainees are working on simulator under the control of the instructor, two others are preparing with the help of procedures and technical documentation under the control of the instructor.

The duration of on site retraining is about 3 days for each simulator and for four trainees. The simulator of function is in that case transported on the site under the control of the training center where it usually is located. The retraining programme is made by instructor according to the plant Management, the retraining is made by instructor with the participation of shift supervisors.

Special sessions are organized in training centers for the staff concerned by the functioning (instrumentation technician, physicist, ...).

The maintenance of the simulators is made by the different training centers for the first degree of failure, by BUGEY training center for the second degree of failure. BUGEY conserves also the soft maintenance, no modification can be obtain without the authorization of BUGEY training center. Of course, retraining is always completed yearly by a week period on the full scope simulator in BUGEY training center.

By the way, simulator of function can be used for demonstration into theoretical courses.

CONCLUSION

These simulators will take place between basic theoretical simulator located at GRENOBLE Atomic Study Center and full scope simulator. The Mitra 115 computer will probably be changed to a Mitra 225 whose performances are better. These simulators must give a very good preparation before the full scope simulator, by the knowledge of physical and nuclear phenomenon. They permit on site retraining as necessary, on normal and abnormal operational condition for the main plant systems.

IMPROVED METHOD FOR REACTOR DIAGNOSIS USING NOISE ANALYSIS
BASED ON MULTIVARIABLE TIME SERIES MODELING

R. Oguma, *K. Matsubara and K. Hayashi

Japan Atomic Energy Research Institute, Tokai Research Establishment
Tokai-mura, Ibaraki-ken, JAPAN

*Japan Atomic Energy Research Institute, Oarai Research Establishment
Oarai-machi, Ibaraki-ken, JAPAN

ABSTRACT

This paper presents an improved method dedicated to reactor diagnosis studies using multivariable noise analysis of process signals from an operating reactor plant. The method includes various computational algorithms, based upon multivariable time series modeling, for system dynamics analysis in both time and frequency domains and for newly developed signal transmission path analysis.

As the practical applications of the method, the paper deals with some results from noise analysis of process signals with PRBS(pseudo-random-binary-sequence) perturbations measured at JPDR-II(Japan Power Demonstration Reactor-II), and also from noise application to a fuel performance study aiming at evaluation of heat transfer characteristics of in-reactor irradiation test fuel rods. In addition, the paper includes on-line computer-based leak monitoring system developed for an irradiation test facility in JMTR(Japan Materials Testing Reactor).

INTRODUCTION

Process signals from a nuclear reactor plant fluctuate randomly around their mean values due to various disturbances occurring in the reactor core as well as other plant systems. The noise components of these signals are rich in information on the operational status of the reactor plant. Therefore, if we can extract properly this information, it will be quite useful for surveillance of the reactor plant and for detecting disturbances and anomalies before they develop into serious malfunctions.

Recent advancement of new methods of multivariable noise analysis based on time series modeling and their application to safety related studies on nuclear reactors have made it possible to extract valuable information on the plant status[1-12] which may not be available by conventional noise analysis based on e. g. FFT(Fast Fourier Transform). Development of further sophisticated method for extracting the most possible information efficiently from fluctuating signals may lead to more powerful means for surveillance and diagnosis of the reactor plant.

In the present paper, we first summarize various computational algorithms in terms of multivariable autoregressive(MAR) modeling that are used for the noise analysis and diagnostic studies presented in this paper. Then we present a new method called STP(Signal Transmission Path) analysis as a tool to investigate noise sources and their propagation mechanisms in multivariable random processes. The analysis is carried out through evaluation of three functions in frequency domain, i. e. noise power

contribution(NPC) ratio, partial coherence(PCH) and partial noise power contribution(PNPC) ratio derived from the MAR modeling.

The STP analysis is performed for process signals measured at PRBS perturbation experiment in JPDR-II in order to demonstrate its feasibility. It will be indicated that this new approach has a potential usefulness for reactor diagnosis by providing information, in more reliable and appropriate manner than conventional methods, with respect to noise sources and their propagation paths as well as to cause-consequence relation among variables under evaluation.

As the practical application of the noise analysis method based on MAR modeling, we present two applicational results; the one from fuel performance study carried out at JMTR using instrumented fuel rods in an attempt to evaluate heat transfer characteristic of the fuel rods under irradiation, and the other from the development of on-line computer-based leak monitoring system for the OWL-1(Oarai Water Loop-1), one of the irradiation facilities in JMTR.

These results suggest that the noise analysis method presented here has a wide applicability to various safety related studies of nuclear reactors.

METHOD FOR INFORMATION EXTRACTION BASED ON MAR MODELING

In this chapter, an outline of the noise analysis method based on the MAR modeling will be given.

Let us consider a multivariable linear, discrete time, stochastic system with r -dimensional measurement variables $X(k)=[x_1(k), x_2(k), \dots, x_r(k)]$ described by

$$x_i(k) = \sum_{j=1}^r \sum_{m=1}^L g_{ij}(m)x_j(k-m) + n_i(k), \quad (i=1, 2, \dots, r, i \neq j) \quad (1)$$

where L denotes the model order; $\{g_{ij}(m)\}$ is the impulse response of x_i to x_j and n_i the noise term which induces random variations in the system via x_i , and hence is called the noise source of x_i . It is assumed that n_i is subject to independent stationary random process with zero mean and the power spectral density(PSD) of $Q_{ii}(f)$. Here it should be noted that Eq.(1) indicates a case in which there exists a closed-loop between a pair of variables, e. g. x_i and x_j via $\{g_{ij}(m)\}$ and $\{g_{ji}(m)\}$. Therefore, the feedback effect is taken into account automatically in the system representation.

Given a set of time series data from the system of the form Eq.(1), we can extract information on the various properties that the system contain, via the MAR modeling. The MAR model for the measurement variables mentioned above is described by

$$x_i(k) = \sum_{j=1}^r \sum_{m=1}^M a_{ij}(m)x_j(k-m) + e_i(k), \quad (2)$$

where $a_{ij}(m)$ denotes the AR coefficient and M the order of the AR model. The additive term e_i is the driving source of random variation for x_i and follows white Gaussian random process with zero mean and the variance σ_{ii} . Then, the following relations hold between the two equations:

$$n_i(k) = \sum_{m=1}^M a_{ii}(m)n_i(k-m) + e_i(k), \quad (3)$$

$$g_{ij}(1) = a_{ij}(1), \quad (4)$$

$$g_{ij}(m) = a_{ij}(m) + \sum_{s=1}^{m-1} a_{ii}(s)g_{ij}(m-s).$$

where $a_{ij}(m)=a_{ii}(m)=0$ for $m>M$. In the frequency domain, we also have the following relations:

$$G_{ij}(f) = a_{ij}(f)/a_{ii}(f), \quad (5)$$

$$Q_{ii}(f) = \sigma_{ii}/|1 - a_{ii}(f)|^2, \quad (6)$$

$$a_{ij}(f) = \delta_{ij} - \sum_{m=1}^M a_{ij}(m)\exp(-i2\pi fm), \quad (7)$$

where $\delta_{ij}=1$ for $i=j$, otherwise $\delta_{ij}=0$ and $G_{ij}(f)$ represents the frequency response of x_i to

x_i . Therefore, once the MAR modeling is accomplished, we can apply it to investigate system dynamics as well as the property of the noise sources.

As for the MAR modeling technique, since it has already been applied elsewhere[1],[7] in the nuclear engineering field, its description will be omitted here.

Describing the system model Eq.(1) in a vector form, it becomes

$$X(k) = \sum_{m=1}^M G(m)X(k-m) + N(k), \quad (8)$$

where $\{G(m)\}$ represents the impulse response matrix with $\{g_{ij}(m)\}$ in the (i,j) element and zero in the (i,i) element, and N the noise source vector with n_i in the i -th element. With a minor calculation using Eq.(8), we obtain the PSD matrix $P(f)$ for X as

$$P(f) = H(f)Q(f)H^*(f)^T, \quad (9)$$

where

$$H(f) = [I - G(f)]^{-1}, \quad (10)$$

which represents the closed-loop frequency response matrix. Superscript $*$ and T denote the complex conjugate and the transpose, respectively. Matrix $Q(f)$ is the PSD matrix of the noise source N of which (i,i) element is $Q_{ii}(f)$ and (i,j) element ($i \neq j$) is zero due to mutual independence of each noise source. From Eq.(9) the PSD of x_i , $P_{ii}(f)$, results in

$$P_{ii}(f) = \sum_{j=1}^r |H_{ij}(f)|^2 Q_{jj}(f), \quad (11)$$

where $H_{ij}(f)$ is the (i,j) element of $H(f)$ and $|\cdot|$ the determinant. Hereafter the argument f will be omitted unless specifically necessary.

NPC Ratio, PCH and PNPC Ratio.

In Eq.(11), the portion in the PSD of x_i which is brought about by the noise source n_j is given by

$$c_{ij}(f) = |H_{ij}(f)|^2 Q_{jj}(f). \quad (12)$$

Hence denoting the ratio of Eq.(12) to Eq.(11) as $\Gamma_{ij}(f)$, then it becomes

$$\Gamma_{ij}(f) = c_{ij}(f)/P_{ii}(f) = |H_{ij}(f)|^2 Q_{jj}(f) / \sum_{k=1}^r |H_{ik}(f)|^2 Q_{kk}(f). \quad (13)$$

The NPC ratio, as clear from Eq.(13), evaluate the degree of influence of each noise source on the specified variable using the closed-loop frequency response Eq.(10), in which all the effective $G_{ij}(f)$ s are included implicitly. In this respect, the NPC ratio provides information about the global effect of the individual noise sources on the variable concerned but not on the local effect that the noise source of one variable affects the other variable via direct STP. The local effect of the noise source can be evaluated by means of PCH and PNPC ratio and through their mutual comparison.

Consider a direct dynamic relationship between a pair of variables among those in Eq.(1), after removing all the linear effect of other variables. For simplicity here, take the variable pair (x_1, x_2) . Let $x_1|3...r$ and $x_2|3...r$ denote conditioned variables for x_1 and x_2 , respectively, with the linear effect of $[x_3, x_4, \dots, x_r]$ on x_1 and x_2 removed. Then they satisfy

$$\begin{bmatrix} x_1|3...r(k) \\ x_2|3...r(k) \end{bmatrix} = \sum_{m=1}^M \begin{bmatrix} 0 & g_{12}(m) \\ g_{21}(m) & 0 \end{bmatrix} \begin{bmatrix} x_1|3...r(k-m) \\ x_2|3...r(k-m) \end{bmatrix} + \begin{bmatrix} n_1(k) \\ n_2(k) \end{bmatrix}, \quad (14)$$

which represents a subsystem made up of dynamic interrelation between x_1 and x_2 , and of the noise sources n_1 and n_2 alone. Following the same procedure as obtaining Eq.(11), PSDs of $x_1|3...r$ and $x_2|3...r$ result in

$$\begin{aligned} P_{11|3\dots r}(f) &= \{|G_{12}|^2 Q_{22} + Q_{11}\} / \Delta, & P_{22|3\dots r}(f) &= \{|G_{21}|^2 Q_{11} + Q_{22}\} / \Delta, \\ P_{12|3\dots r}(f) &= \{G_{21}^* Q_{11} + G_{12} Q_{22}\} / \Delta, \end{aligned} \quad (15)$$

where $\Delta = |1 - G_{12} G_{21}|^2$; $P_{11|3\dots r}(f)$, $P_{22|3\dots r}(f)$ and $P_{12|3\dots r}(f)$ are PSDs of $x_1|3\dots r$ and $x_2|3\dots r$ and cross-power spectral density (CPSD) between them, respectively. Hence, they are called conditioned PSDs with respect to x_1 and x_2 , when eliminating the effect of $[x_3, x_4, \dots, x_n]$ on these variables. It can be also interpreted that these conditioned PSDs represent the PSDs derived when omitting all the possible STPs transmitting the signals to x_1 or x_2 from the remaining variables.

Let the coherence function between $x_1|3\dots r$ and $x_2|3\dots r$ denote $\gamma_{12|3\dots r}^2(f)$, then it can be written as

$$\gamma_{12|3\dots r}^2(f) = \frac{|P_{12|3\dots r}|^2}{P_{11|3\dots r} P_{22|3\dots r}} = \frac{|G_{21}^* Q_{11} + G_{12} Q_{22}|^2}{\{|G_{12}|^2 Q_{22} + Q_{11}\} \{|G_{21}|^2 Q_{11} + Q_{22}\}}, \quad (16)$$

which represents the PCH between x_1 and x_2 when conditioned by $[x_3, x_4, \dots, x_n]$.

Let us denote the ratio of the portion in the PSD of $x_1|3\dots r$ which is brought about by n_2 , to the net PSD of $x_1|3\dots r$ as $\Gamma_{12|3\dots r}(f)$, and that of $x_2|3\dots r$ which is brought about by n_1 , to the net PSD of $x_2|3\dots r$ as $\Gamma_{21|3\dots r}(f)$. Then we have

$$\Gamma_{12|3\dots r}(f) = \frac{|G_{12}|^2 Q_{22}}{|G_{12}|^2 Q_{22} + Q_{11}}, \quad \Gamma_{21|3\dots r}(f) = \frac{|G_{21}|^2 Q_{11}}{|G_{21}|^2 Q_{11} + Q_{22}} \quad (17)$$

The NPC ratio thus derived is here termed partial noise power contribution (PNPC) ratio of x_1 to x_2 (or x_2 to x_1) when eliminating all the STPs from other variables.

STP Analysis

In earlier, the NPC function has been applied to noise analysis of power reactors with emphasis on investigating noise sources in BWRs[2]-[5] and a PWR[6], carrying out diagnostic studies for power reactors[7]-[11], etc. However, for a multivariable system with feedback, the NPC analysis, in some cases, does not necessarily provide sufficient information for the proper understanding of the noise sources. The difficulty occurs especially when one intends to evaluate cause-consequence relationship or direct correlation between two variables. Bearing this in mind, here we propose a new method of noise analysis termed "STP(signal transmission path) analysis". This approach intends to identify noise sources and their propagation mechanisms by characterizing signal power which generated from the noise source of a variable and propagates through STP network in the system to a specified variable. The analysis is performed using the three functions, i. e. the NPC ratio, PCH and PNPC ratio defined previously.

Relationship amongst NPC ratio, PCH and PNPC ratio: We consider here the mutual relationship amongst the three functions.

The NPC analysis, as clear from Eq.(13), evaluates the contribution ratio of the noise source power which is transmitted via all possible STPs to the PSD of the variable concerned. Therefore, it yields information about the global effect of the noise source. On the other hand, the local effect that the noise source power is transmitted directly between a particular pair of variables does not appear explicitly on the NPC function. The local effect of the noise source power can be evaluated through mutual comparison of the PCH and PNPC ratio, i. e. PCH-PNPC comparison. Using Eqs.(16) and (17), it can be theoretically shown that between x_1 and x_2 the two functions have intimate relations relative to the local effect of the noise source power as follows:

- i) If there is no direct STP between x_1 and x_2 , then

$$\gamma_{12|3\dots r}^2(f) = \Gamma_{12|3\dots r}(f) = \Gamma_{21|3\dots r}(f) = 0,$$

for all frequencies of interest.

- ii) If there is an STP from x_1 to x_2 ; subsystem between x_1 and x_2 is composed of an open-loop structure with signal flow from x_1 to x_2 , then

$$\gamma_{12|3\dots r}^2(f) = \Gamma_{21|3\dots r}(f), \quad \Gamma_{12|3\dots r}(f) = 0,$$

for all the frequencies of interest. Similar argument holds for the case with an STP from x_2 to x_1 .

- iii) If there is feedback between x_1 and x_2 , then the PCH function takes a different pattern from the PNPC function for either direction of the signal flow.

Hence, the relations i)-iii) between the PCH and PNPC functions can be used to advantage to identify the STP structure between x_1 and x_2 and thus the local effect of the noise source power transmitted directly between the two variables. It is easily noted that the PCH-PNPC comparison also enables to evaluate cause-consequence relationship, to detect feedback, and to evaluate direct correlation between the two variables.

It is obvious that the PCH and PNPC functions defined for the variables (x_1, x_2) can apply to a pair of variables arbitrarily chosen from those in Eq.(1). Concerning the relation between the NPC and PNPC functions, they turn out to be identical when dealing with two variable systems. In this case, the PCH is also coincident with ordinary coherence.

As developed in the previous section, the three functions used in the STP analysis can be calculated using the identified MAR model, of which the procedure is as follows:

- i) Identify the MAR model for a set of measured variables and check the noise source independency.
- ii) Evaluate the NPC ratio to each variable, which allows examination, from the global point of view, of the possible noise sources.
- iii) Perform the PCH-PNPC comparison for a selected pair of variables, which yields information on the local effect of the noise propagation.

More detailed description on the STP analysis is given in Ref.[12].

STP ANALYSIS FOR PRBS-EXPERIMENT DATA FROM JPDR-II

The STP analysis was performed, in an attempt to demonstrate its feasibility, for process signals from the JPDR-II plant which have been collected in the reactor dynamics experiment using the PRBS perturbations at power level of 45 MWt. In the experiment, mutually independent PRBS signals were applied at two terminals, i. e. one at the bypass pressure regulator (BPR) valve and the other at the master controller (MC) set point of forced circulation pumps. In Fig. 1, a schematic diagram of the JPDR-II plant is shown to indicate the locations of signals' measurement points. The analysis was conducted for four variables, i. e. neutron density (N), vessel pressure (P), BPR valve position (BPR) and MC set point (MC). The latter two variables are disturbance sources artificially introduced to the system. The data set used for the present analysis consists of time series data with a sampling interval of 0.5 sec and sample size of 2000.

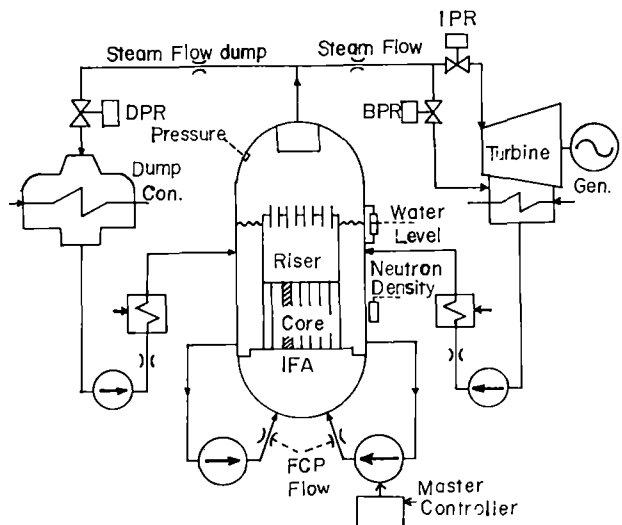


Fig. 1 Schematic diagram of the JPDR-II plant.

Figure 2 shows in a cumulative form the NPC ratios to N and P from individual noise sources. Considerable influence of BPR and MC is seen upon both N and P but the NPC ratio from N to P and that from P to N are quite small, indicating that BPR and MC are predominant disturbance sources to N and P.

The direct STP existing between two variables are evaluated via the PCH-PNPC comparison, from which three examples are shown in Fig. 3. It is seen that there is a feedback effect between N and P(Fig. 3-(a)), and that the system exhibits an open loop structure between N and MC with causal direction from MC to N(Fig. 3-(b)) and between P and BPR with causal direction from BPR to P(Fig. 3-(c)).

These results indicate that the PCH-PNPC comparison is effective for identifying the causality as well as for detecting the feedback existing between the selected pair of variables. Through PCH-PNPC comparison, it turns out that in the present system, BPR and MC are exogenous variables giving rise to disturbances to N and P and that the feedback effect is active between N and P. These achievements are quite reasonable in the light of the physical consideration of the JPDR-II dynamics together with the experimental conditions.

Information on the causality and feedback is in some cases essential for the correct understanding of noise sources and their propagation paths. The results of the analysis of process signals from JPDR-II clearly demonstrate that the present approach is effective for extracting this kind of information.

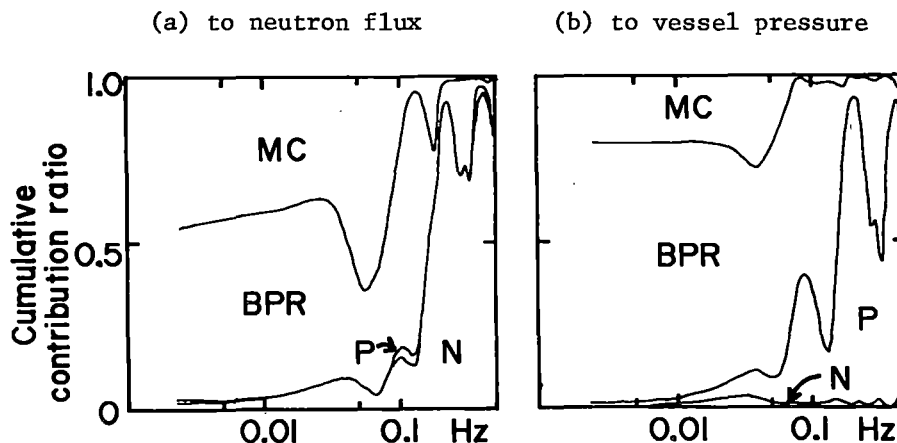


Fig. 2 Cumulative representation of noise power contribution ratios to neutron flux(a) and to vessel pressure(b).

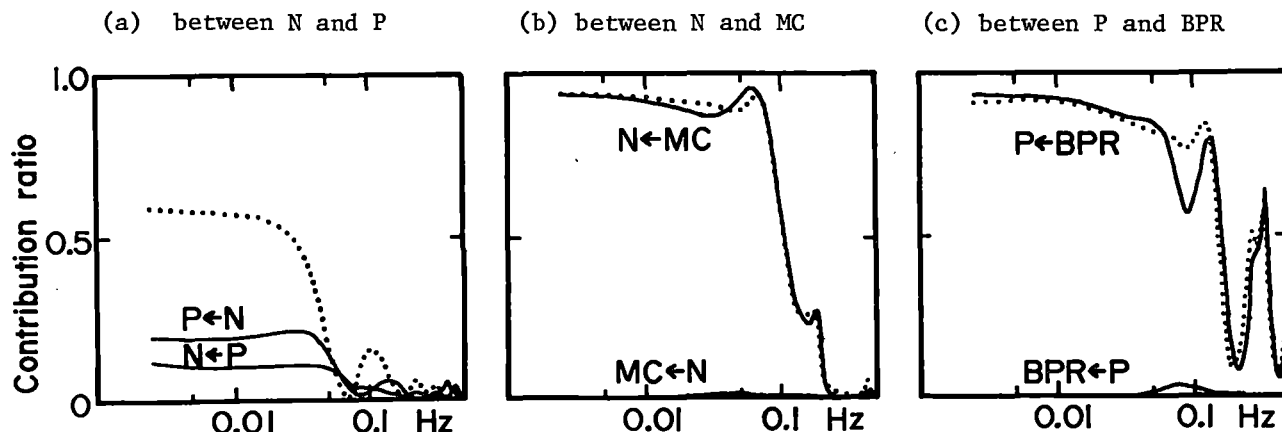


Fig. 3 Comparison of partial coherence and partial noise power contribution ratio for each pair of variables.

APPLICATION TO FUEL PERFORMANCE STUDY

Accurate evaluation of the heat transfer characteristics of the fuel rods under irradiation is thought to be important from the viewpoint of reactor safety, since it may bring about information on the safety related parameters of the fuel rod, e. g. gap conductance between the fuel and clad. The AR modeling was applied to a pair of signals of a fuel center thermocouple installed in each fuel rod and a neutron detector in order to identify the dynamics model of the fuel center temperature in response to the rod power change. The dynamics model thus empirically determined was used to estimate time constant of the temperature response and thereby to evaluate the fuel heat transfer characteristics.

Method to Evaluate Heat Transfer Characteristics of Fuel Rod

For an infinitely long cylindrical fuel rod with uniform time-dependent power production $q(t)$ per unit volume, with constant thermal parameters, and surrounded by a coolant whose temperature T_c is assumed to be constant, the differential equation for non-stationary heat conduction can be described as

$$k_f \left\{ \frac{1}{r} \frac{\partial}{\partial r} T_f(r, t) + \frac{\partial^2}{\partial r^2} T_f(r, t) \right\} + q(t) = \rho c_f \frac{\partial}{\partial t} T_f(r, t), \quad (18)$$

where $T_f(r, t)$ denotes the fuel temperature in radial position r and at time t . Parameters k_f , ρ and c_f are thermal conductivity, density and specific heat capacity, respectively, of the fuel. The boundary conditions for this equation are

$$-k_f \frac{\partial}{\partial r} T_f(r, t) \Big|_{r=R} = h \{ T_f(R, t) - T_c \}, \quad \frac{\partial}{\partial r} T_f(r, t) \Big|_{r=0} = 0 \quad \text{and} \quad T_f(0, t) \neq \infty \quad (19)$$

where R is the fuel radius and h the heat transfer coefficient from the fuel surface to the coolant. Taking the Laplace transform for Eq.(18), the transfer function $G(r, s)$ from neutron flux to the fuel temperature is analytically obtained as

$$G(r, s) = \frac{T_f(r, s)}{q(s)} = \sum_{i=1}^{\infty} \frac{E_i F_i(r)}{\tau_i s + 1}, \quad (20)$$

with boundary condition,

$$-E_i J_1(\xi_i R) + \frac{h}{k_f} J_0(\xi_i R) = 0, \quad (21)$$

where $J_0(\cdot)$ and $J_1(\cdot)$ express 0-th and 1-st order Bessel functions. E_i , $F_i(r)$ and τ_i in Eq.(21) are given as follows:

$$E_i = \left\{ \frac{1}{\xi_i^2 k_f} \right\}^2 / \left[\left\{ \frac{h}{\xi_i^2 k_f} \right\}^2 + 1 \right], \quad F_i(r) = \frac{J_0(\xi_i r)}{J_0(\xi_i R)} \quad \text{and} \quad \tau_i = \frac{\rho c_f}{\xi_i^2 k_f}. \quad (22)$$

τ_i is generally called i -th mode time constant with the following order in magnitude:

$$\tau_1 > \tau_2 > \dots > \tau_i > \dots$$

Therefore, if the 1-st mode time constant τ_1 which is the largest of τ_i 's can be determined experimentally, we can evaluate the heat transfer coefficient h by substituting k_f , ρ , c_f and the estimated time constant into Eqs.(21) and (22).

For the estimation of τ_1 , we can apply the noise analysis technique based on the MAR modeling. As the procedure of the noise analysis to estimate the time constant of the fuel temperature response, first we identify the AR model for a pair of measurement noise data of the fuel center temperature and the neutron flux. Once the model is achieved in the form of Eq.(2), the frequency response of the fuel center temperature to the neutron flux can be estimated using Eq.(5). Then secondly the time constant is determined through the least-squares fitting of the transfer function in terms of rational function to the frequency response.[13]

Noise Experiment and the Results

The noise experiment was conducted, as a preliminary study, at JMTR for four instrumented fuel rods during its steady power operation. The individual rods are equipped with fuel center thermocouple and have different initial gap size as a function of the design parameter. The main parameters of the fuel rods are shown in Table I.

Table I Design Parameters of Fuel Rods

	Rod 1	Rod 2	Rod 3	Rod 4
Fuel Diameter	10.68 (mm)	10.58	10.48	10.38
Diam. Clearance	0.11 (mm)	0.21	0.31	0.41
Clad Thickness	0.86 (mm)			
Pellet Length	11 (mm)			
Fuel Stack Leng.	616 (mm)			
Fuel Density	95.0 \pm 1.5 %TD			
Enrichment	1.5 \pm 0.05 w/o U-235			

Table II Mean Value of Each Signal Measured at the Noise Experiment

	Rod 1	Rod 2	Rod 3	Rod 4
Rod Power	307 (W/cm)	315	253	250
Fuel Cent. Temp.	1093 ($^{\circ}$ C)	1319	1223	1206
Assemb. Inlet T.	248 ($^{\circ}$ C)			
Assemb. Outlet T.	263 ($^{\circ}$ C)			
Pressure	72 (ata)			

Table III Result of the AR model identification and estimation of the 1-st mode time constant of temperature response for each fuel rod.

	Rod 1	Rod 2	Rod 3	Rod 4
Model Order	M=13	14	13	10
Time Constant	7.9-8.8 (sec)	7.9-9.3	8.1-10.6	15.9-17.9

During the noise experiment, the reactor power has been kept constant at 50 MWt, and signals from the fuel center thermocouple for each fuel rod and from the neutron detector are recorded onto analog data recorder after the bias suppression and the amplification for each signal. Steady state values of signals determining the experimental condition are shown in Table II. The measured signals were afterward reproduced and fed into digital computer to perform the analysis according to the procedure described previously. The result of the model identification and the time constant estimation for each fuel rod are given in Table III.

The heat transfer coefficient evaluated for each fuel rod in terms of the time constant of the temperature response and the related thermal parameters is shown in Fig. 4 together with the estimate from a fuel thermal code[14]. Error bar in the figure indicates the uncertainty which occurred in

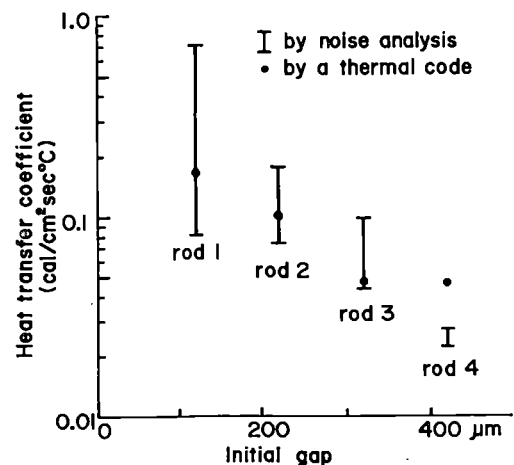


Fig. 4 Comparison of the heat transfer coefficient estimates derived from noise analysis and a thermal code.

the least-squares fitting of the time constant. The results from the two different approaches show qualitatively good agreement. It should be noteworthy that the noise analysis approach as presented here has an advantage in the sense that it does not require the knowledge of each rod power which is indispensable to the conventional experimental approach using mean values of the measurement signals.

A NEW METHOD FOR LEAK DETECTION USING DEWMETER IN OWL-1 LOOP

The problem of early detection of abnormal water leakage from nuclear reactor plants is particularly important to reducing a release of fission products and the resultant contamination. The MAR modeling was applied to develop a sensitive leak detection method for the OWL-1 loop.

Most equipments of the OWL-1 loop system are contained in the loop cubicle of a volume about 115 m³. The cubicle is segregated by a thick concrete wall and is ventilated. A considerable amount of experience on leak monitoring has been accumulated at JMTR up to now through the tests carried out on different methods, in which the use of dewmeters is thought to be promising.[15] Figure 5 illustrates the air flow path to and out of the cubicle together with the location of the dewmeters. The dewmeters used here for measuring humidity of the supply and the exhaust air in the ventilation system is a Dewcel meter with assured measurement range of -10 ~ 50 °C. The signal's outputs of the dewmeters are sampled every 10 sec and are recorded on a chart recorder.

In order to obtain a sensitive indication of leaks, here, time series analysis based on MAR modeling was applied to information processing of the signals from the dewmeters. The method is based on the ability of the identified MAR model to estimate the current state on the ambient humidity; the change in the humidity caused by the water leakage would lead to deviation of the measured humidity from the estimation by the MAR model, thus detecting the leakage.

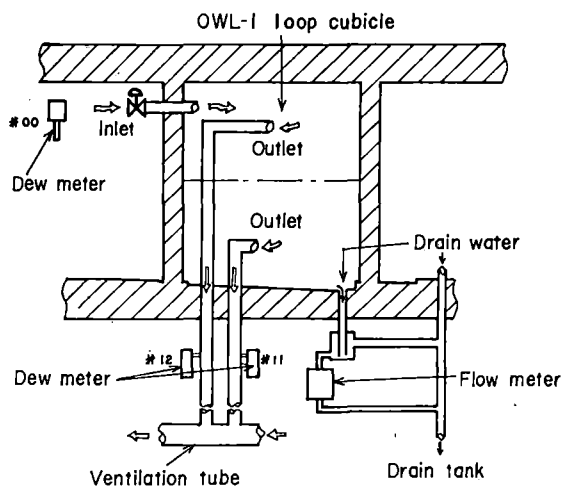


Fig. 5 Diagram showing air flow paths for the cubicle ventilation and location of dewmeters.

Method for Leak Detection and Results of Data Analysis

Given a set of sample record on the supply and exhaust dewpoint signals, the MAR modeling technique developed in the previous chapter can be conveniently applied to identify the dynamics model relating the two signals. The dynamic relationship between the exhaust dewpoint, $To(k)$ and the supply dewpoint, $Ti(k)$ can be represented by an AR model with exogenous variable (ARX model) as follows:

$$To(k) = \sum_{m=1}^M a(m)To(k-m) + \sum_{m=1}^M b(m)Ti(k-m) + v(k), \quad (23)$$

where $a(m)$ and $b(m)$ are coefficients of the system model and $v(k)$ denotes the noise term. This ARX model can be easily derived by applying the MAR modeling; by taking the corresponding elements in the identified MAR model for To and Ti . Once the ARX model was obtained, the exhaust dewpoint can be estimated by inputting the supply dewpoint signal to the identified model, i. e.

$$\hat{To}(k) = \sum_{m=1}^M a(m)\hat{To}(k-m) + \sum_{m=1}^M b(m)Ti(k-m), \quad (24)$$

where $\hat{T}_o(k)$ denotes the estimate of $T_o(k)$. If a leak has occurred, the estimates of the exhaust dewpoint would deviate from the measurement value. Hence, monitoring the time behavior of the difference $[T_o(k) - \hat{T}_o(k)]$ would lead to efficient leak detection.

Figure 6 shows an example of the exhaust dewpoint estimation based on Eq.(24) for the normal data without leaks from the OWL-1 loop. The estimated values follow quite well the original measurement data in a sense of mean value, indicating the validity of the identified model.

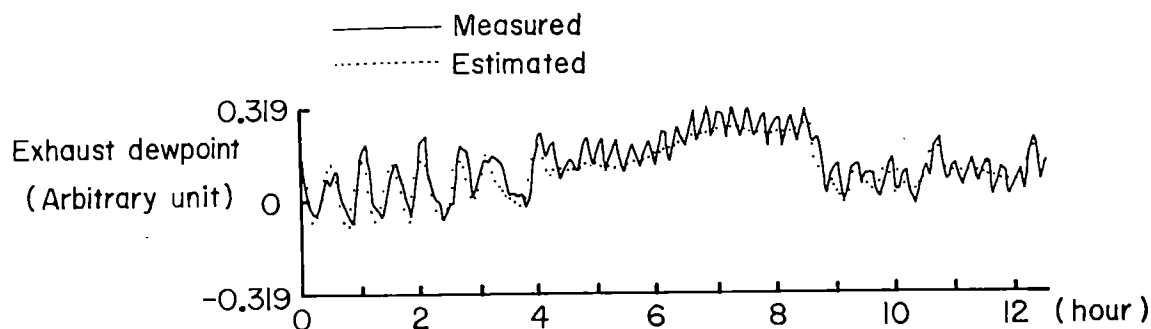


Fig. 6 An example of the exhaust dewpoint estimation based on identified dewpoint dynamics.

A computer algorithm for an on-line leak monitor was developed on the basis of the model identification. This leak monitor consists of two steps of data processing; the first step for evaluating the difference signal $[T_o(k) - \hat{T}_o(k)]$ which includes the identified model, and the second for smoothing the difference signals.

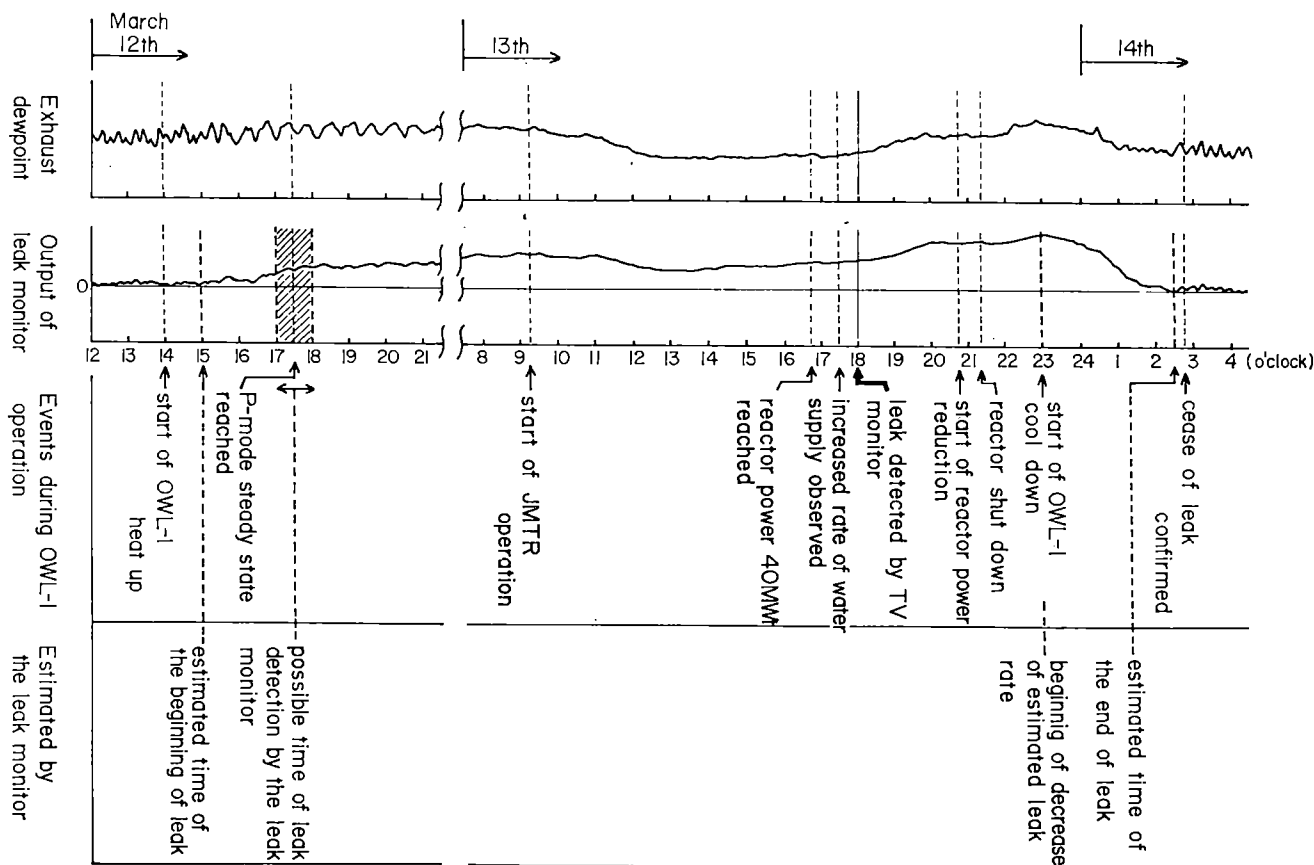


Fig. 7 Evaluation of time history of water leakage occurred during OWL-1 loop operation by leak monitor designed.

The latter is composed of Butterworth lowpass filter of the third order, with which one can cut off the signal's high frequency components not needed for leak monitor.

This leak monitor was applied to analyze the data collected when abnormal water leakage occurred at the OWL-1 loop. In Fig. 7, the results of the leak monitoring are summarized together with the events observed during the loop operation. From the figure, the followings can be pointed out:

- i) It is inferred that the leak from the loop became evident about one hour after starting the OWL-1 loop heating up (14 o'clock on March 12th).
- ii) Reaching steady condition of the loop operation, the leak rate estimated also became steady.
- iii) Almost at the same time when the operator started to decrease the temperature and pressure of the loop, the estimated leak rate also began to decrease.
- iv) There is not much discrepancy between the confirmed and estimated time of the end of leak.

Especially iii) and iv) among these features indicate the present analysis to be fairly reliable. Considering the time history of the leak estimated by the leak monitor applied here, it is conjectured that the leak could have been detected by the present method, at least, when the loop operation attained P-mode(coolant condition of pressurized water reactor) stationary condition.

The results obtained in the present analysis indicate the potential usefulness of the method for early detection of water leakage.

CONCLUDING REMARKS

Various methods for information extraction from multivariable random processes were developed on the basis of the MAR modeling. Those methods were successfully applied to safety related studies of nuclear reactor, i. e. evaluation of thermal behavior of fuel rods under irradiation and leak detection problem for OWL-1 loop. Especially, the basic idea of the leak monitoring system developed here is thought to be applicable also to commercial power plants.

A new method of multivariable noise analysis called "STP analysis" was firstly introduced as a tool to investigate noise sources and their propagation mechanisms. Application to signals measured in PRBS-perturbation experiment at JPDR-II indicated that the method has a potential of identifying the causality as well as detecting the feedback existing between a selected pair of variables. Correct evaluation of the causality and feedback is very important especially for analyzing power reactor noise with complicated reactivity feedback. Even in such a case, the STP analysis is effective and is thus expected to be more powerful tool than conventional methods.

Results of the applicational studies presented in the paper suggest that we can apply the noise analysis method based on the MAR modeling to various problems of information processing with a view to establishing more advanced techniques for diagnosis and surveillance of nuclear reactor plants.

ACKNOWLEDGEMENT

Authors are deeply indebted to Mr. K. Itami, Chief of Irradiation Sec. II in JMTR, for providing them with the dewpoint data measured at OWL-1, and to Mr. M. Sato, Chief of Project Engineering Sec. in JMTR, for permission of noise measurement using instrumented fuel rods, 77LF-33J.

Thanks are also due to Mr. H. Ando in Project Engineering Sec. for his assistance in executing fuel thermal code "FREG-4", and to Mr. Y. Shinohara, Chief of Reactor Control Lab., for his encouragement and valuable advice.

REFERENCES

1. B. R. UPADHYAYA et al, "Multivariate Signal Analysis Algorithms for Process Monitoring and Parameter Estimation in Nuclear Reactors", Ann. of Nucl. Energy 7, 1 (1980).
2. K. FUKUNISHI, "Noise Source Estimation of Boiling Water Reactor Fluctuation by Autoregression", Nucl. Sci. Eng. 67, 295 (1978).
3. K. MATSUBARA, "Identification of Channel Void Generation Noise in BWR", J. Nucl. Sci. Technol. 17[10], 737 (1980).
4. M. KITAMURA and B. R. UPADHYAYA, "Cause-and-Effect Analysis of Neutronic and Process Signals in a Boiling Water Reactor", Prog. Nucl. Energy 9, 195 (1982).
5. B. G. BERGDAHL and R. ESPEFALT, "Multivariate Signal Analysis for Process Source Identification", Prog. Nucl. Energy 9, 149 (1982).
6. M. KITAMURA et al, "Multivariate Autoregressive Analysis of PWR Plant Operating Reactors", Trans. Am. Nucl. Soc. 32, 625 (1979).
7. K. FUKUNISHI, "Diagnostic Analysis of Nuclear Power Plant Using Multivariate Autoregressive Processes", Nucl. Sci. Eng. 62, 215 (1977).
8. Y. ANDO et al, "BWR Simulation Diagnosis by Noise Analysis", Prog. Nucl. Energy 1, 163 (1977).
9. R. OGUMA, "Investigation of Resonant Power Oscillation in Halden Boiling Water Reactor Based on Noise Analysis", J. Nucl. Sci. Technol. 17[9], 677 (1980).
10. B. R. UPADHYAYA and M. KITAMURA, "Stability Monitoring of Boiling Water Reactors by Time Series Analysis of Neutron Noise", Nucl. Sci. Eng. 77, 480 (1981).
11. S. KANEMOTO et al, "Identification of Pressure Control System Dynamics in BWR Plant by Multivariate Autoregressive Modeling Technique", J. Nucl. Sci. Technol. 19[1], 58 (1982).
12. R. OGUMA, "Signal Transmission Path Analysis in Multivariable Random Processes and its Application to At-Power Reactor Noise", Nucl. Sci. Eng. (submitted for publication).
13. K. YAMASHITA et al, "A Method to Find Transfer Function from Frequency Response Data", (in Japanese) Control Engineering 14[11], 667 (1970).
14. H. ANDO et al, "Fuel Centerline Temperature Measurement Experiment in JMTR (II); Experiment Analysis of the First Test Assembly", (in Japanese), Report JAERI-M 9202, Japan Atomic Energy Research Institute (1980).
15. "Operational Report on JMTR Irradiation Facilities in 43rd Cycle", (in Japanese) Irradiation Sec. II (1979).

MULTILEVEL FLOW MODELLING OF PROCESS PLANT FOR DIAGNOSIS AND CONTROL

Morten Lind

Risø National Laboratory
DK 4000 Roskilde, Denmark

ABSTRACT

The paper describes the multilevel flow modelling methodology which can be used to construct functional models of energy and material processing systems. The models describe mass and energy flow topology on different levels of abstraction and represent the hierarchical functional structure of complex systems. A model of a nuclear power plant (PWR) is presented in the paper for illustration. Due to the consistency of the method, multilevel flow models provide specifications of plant goals and functions and may be used as a basis for design of computer-based support systems for the plant operator. Plant control requirements can be derived from the models and due to independence of the actual controller implementation the method may be used as a basis for design of control strategies and for the allocation of control tasks to the computer and the plant operator.

INTRODUCTION

The operation of large industrial installations such as nuclear power plants or chemical processing units involves operator decisions which depend critically on proper information about the required plant functions and the associated necessary control constraints. This information is usually only available to the operator in the form of written documents or is given to him as part of the training. Although information about the state of plant functions is essential for the understanding of plant behaviour, existing man-machine interface designs do not support the operator in thinking in functional terms. The introduction of computers in the control rooms of modern processing systems has aggravated this situation because the level of automation has been increased without attempts to make the functional structure of the total plant complex transparent to the operator. The operator is still left with information which essentially is on the level of the individual sensors. These deficiencies of the man-machine interface may not be important during normal operation, but can be serious in accident situations. This has recently been stressed at the TMI accident where the operators did not know - and could not be expected to know - what was going on in the plant. Rasmussen and Lind (1981) have proposed a solution to these problems based on the idea of using a computer-based man-machine interface. The task of the computer should be to integrate measured data into plant state information related to different levels in an abstraction hierarchy (Fig. 1). The levels in the hierarchy, which can be identified by analysing verbal protocols recorded in power plant control rooms, correspond to different representations of plant function and support different problem solving strategies.

In the present paper we will discuss a methodology called multilevel flow modelling (MFM) which can be used to construct functional models of energy and material processing systems and which belong to the level of abstract function. A multilevel flow model is essentially qualitative as it represents functional structure

LEVELS OF ABSTRACTION

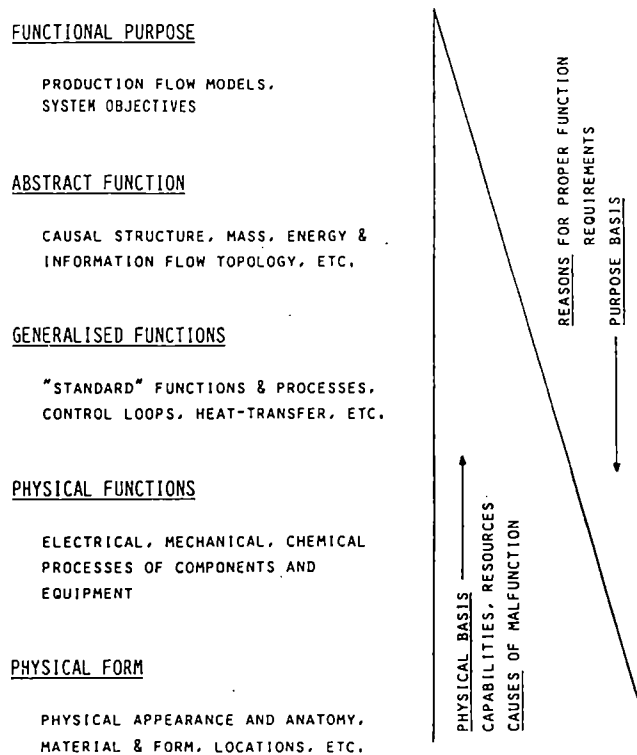


Figure 1. The abstraction hierarchy used for representation of functional properties of a technical system.

of the process plant considered. The modelling method is based on the identification of mass and energy flow structures on different levels of physical aggregation in the plant. It may be used as a basis for man-machine interface design as it provides a systematic way of identifying plant goals and functions and the plant state information required in control and decision making. Due to the consistency of the MFM method, the models produced can be considered as providing functional specifications of the plant. This property makes MFM models attractive as a basis for design of advanced operator aids such as systems for automated diagnosis (Lind, 1981) or for synthesis of operating instructions (Lind, 1979). Within the broader context of the abstraction hierarchy, MFMs may also provide a basis for design of integrated "cognitive" systems where the computer and the operator cooperate in plant supervision and control (Lind, 1982, and Hollnagel and Woods, 1982). Before describing the multilevel flow modelling method we will discuss how functional specifications appear as a result of the process design and how these relate to the levels of abstraction in Fig. 1. Later it will become clear how MFMs provide a systematic framework for organizing this information into a set of interrelated goal and function hierarchies.

SPECIFICATION OF PLANT GOALS AND FUNCTIONS

The specification of goals and functions of plant subsystems is an integral part of the process design, i.e. the activity where the physical structure of the plant is synthesized. However, the identification of subsystem goals and function depends on the actual design strategy adopted. The description given below relates to a formalized "systems approach" to the process design. Gregory (1979) characterizes the

systems approach as "a managerial procedure --- relying upon the identification of the objectives to be attained, the specification of the functions needed to achieve those objectives, the quantification of performance in terms of output quality and value, the specification of parts of the system needed, their interrelationships, and the optimal configuration to achieve the objectives, given the environment, constraints, and resources". This top-down approach is suitable for the development of radically new designs. Another design strategy is used when new designs are obtained by adaptations or modification of existing designs. From the point of view of such an evolutionary design process, the top-down formalized approach may rather be used as basis for a review of the consistency of design decisions.

The systems approach to process design can be described in terms of the abstraction hierarchy (Fig. 1). During design of the plant, the functions of the system and its physical implementation are developed by iteratively considering the plant at various levels of abstraction and in increasing degree of detail (Fig. 2). During this design process, the physical system is identified. But, as the degree of physical detail increases during the design process, so does the number of degrees of freedom in functional states, and control paths relating desired target states or goals with necessary control actions must be introduced to constrain the possible operational states. Another result of the plant design process is the identification of operating modes, i.e. system configurations and functional states corresponding to different overall safety or production goals. In this way the desired states of functions, equipment and components will be identified during design at different levels of abstraction, and the necessary information or control constraints will be identified in terms related to these levels. Due to the coupling between levels of aggregation and abstraction during design, this leads to a conceptual fragmentation of the functional specifications and the associated control requirements. On the high levels of abstraction we deal with the whole system and specify states of the overall plant production function. As we go down in the hierarchy we become more oriented towards components, i.e. we specify states of pumps and valves.

In order to formalize the functional specifications it is necessary to be able to use the same language on all levels of aggregation. As shown below multilevel flow models can be used as a consistent framework for dealing with functional specifications in a uniform language and can be considered as a formalized abstraction

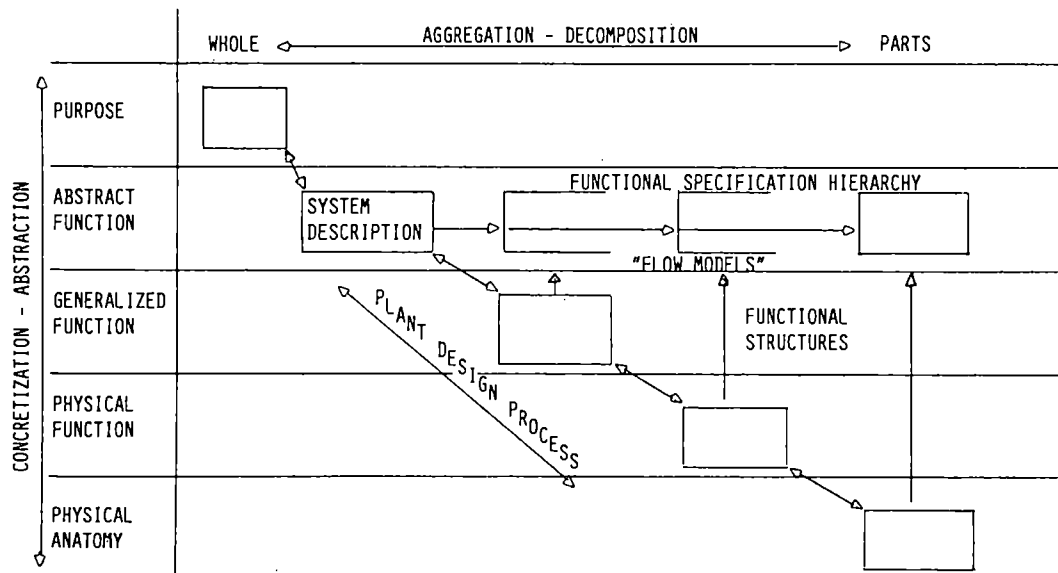


Figure 2. Derivation of goals and functional specifications during the design process.

hierarchy. Fig. 2 shows how specifications developed during the design can be translated into information related to an MFM. The flow model can be considered as obtained by a decomposition of the overall plant mass and energy flow structure, where the decomposition is guided by the design information on system purposes and functions.

THE FUNCTIONAL STRUCTURE OF PROCESS PLANTS

In this section I will briefly describe characteristics of the functional structure of process plants. This may give a general indication of the nature of the complexity to be handled when specifying plant functional requirements. The degree of complexity of the plant functional structure is furthermore an indicator of the difficulty of the control tasks involved in operating the plant. Some important characteristics of functional structure in process plants are:

- A component, an equipment or a plant subsystem may have several purposes or goals.
- Plant and subsystem goals may be multiple and partially conflicting.
- A plant function may have several alternative physical implementations.
- The functional structure changes depending on operating mode.

The one to many and many to one mappings describing the relations between plant physical structure and plant functions are consequences of process plants being systems and having subsystems with multiple operating goals and the results of the design for reliable operation. The features of plant functions as described above can be represented in an MFM together with a map of the physical structure as described below.

MULTILEVEL FLOW MODELS FOR FUNCTIONAL SPECIFICATION

The main goal of multilevel flow modelling is to describe the functional structure of process plants in terms of a set of interrelated mass and energy flow structures on different levels of physical aggregation. The basic concepts used are closely related to thermodynamics which is the basis for every consistent approach to modelling physical phenomena in process plants. Flow modelling can be used for providing both descriptive and normative models. A descriptive model represents the actual behaviour of the system, whereas a normative model represents the system in terms of how it is intended to behave (Simon, 1969). This distinction is important for understanding how flow models are used for functional specification and for avoiding pitfalls in applying the methodology for this purpose. The modelling approaches in the two cases are basically different as the normative model requires a top-down function-oriented holistic approach whereas the descriptive modelling is a bottom-up atomistic approach starting with minute details and ending with a level of detail determined by simplifying assumptions.

Flow modelling may be applied for descriptive purposes as the first conceptual step in the development of a conventional simulation model. In this way a flow model describes the qualitative structural aspects of the problem to be analysed. This type of model is useful as an analytical tool for the study of actual plant behaviour and limiting functional properties. Such a model will necessarily only describe one single functional level. When the flow modelling approach is used to provide normative models specifying intended function we obtain multilevel structures representing the plant as a functionally organized system adapted to its environment - as an artificial system (Simon, op.cit.).

BASIC MODELLING CONCEPTS

The flow modelling method is a diagrammatic method aimed at describing qualitative aspects of the function of material and energy processing plants. The result of the modelling is a graph, called a flow structure, or a set of graphs describing the topology of mass and energy flow paths in the plant. Each node in a flow structure represents the function of a plant subsystem, i.e. related basically to a set of interconnected physical components. It is an assumption that subsystem functions belong to a very restricted set of basic so-called flow functions. A flow structure is accordingly a functional network representing the plant on a level of physical detail given by the decomposition into subsystems. It is an important aspect of the methodology that this physical decomposition is motivated by functional considerations. Two distinct functional elements (nodes) in a flow structure may, as a result, correspond to two overlapping plant subsystems, i.e. they may share components.

The basic flow functions used for modelling are storage, transport, distribution, barrier, source/sink and support functions. Furthermore, we will also need the concept of a condition. The individual functions will be explained below and their symbols in flow structured are shown in Fig. 3. The performance parameter mentioned is a plant variable which can be used to evaluate the success of the system to perform its intended function.

- The storage function represents the property of a system to act as a buffer or accumulator of mass or energy. We distinguish between mass storage and pure energy storage but note that a mass storage in some cases may imply energy storage too. The storage function is characterized by a performance parameter indicating the level of mass or energy accumulated by the system. In the case of multicomponent processes, a storage function may include the interchange of mass between the different chemical species (chemical reactions). The performance
















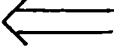
	MASS	ENERGY	INFORMATION
STORAGE			
TRANSPORT			
DISTRIBUTION			
BARRIER			
SOURCE/SINK			
SUPPORT			
FLOW PATH			
CONDITION			
DECOMPOSITION			

Figure 3. Symbols used in flow modelling.

parameter will in this case be a vector indicating the levels of mass accumulated for the individual species.

- A transport function represents the property of a system to provide transfer of materials or energy between two other systems. As for the storage function, we distinguish between mass and pure energy transport. A transport function is characterized by a performance parameter indicating the rate of flow of the mass or energy transferred.
- A distributor function represents the property of a system to provide a balance between the total rates of incoming and outgoing flows. Again we distinguish between material and pure energy distribution. The performance parameter is a vector characterizing the ratios between rates of the individual ingoing/outgoing flows and the total ingoing/outgoing flows.
- A barrier function represents the property of a system to prevent the transfer of materials or energy between two other systems. We distinguish between material and pure energy barriers.
- A source/sink function represents the property of a system to behave as an infinite reservoir of mass or energy. No physically realizable system has in principle unlimited capability of delivering or receiving mass or energy. However, this representation may in many cases be perfectly adequate.
- A support function represents the property of a system to provide the conditions necessary to allow another system to perform its function. The performance parameter associated with a support function is the variable defined by the condition to be provided. The variable has no fixed type as it depends on the actual case. Any plant variable may be chosen such as e.g. temperature, pressure or flow variables.

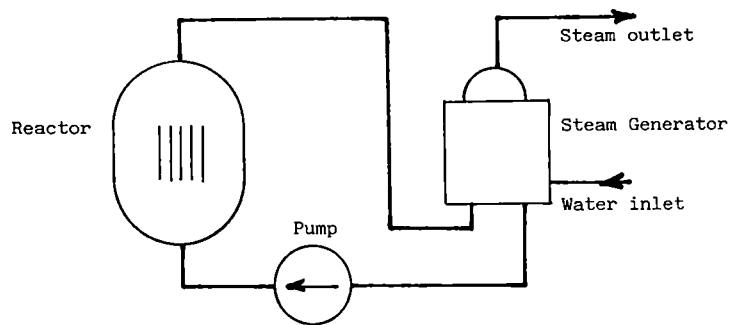
The basic flow functions can be interrelated to create a functional network - a flow structure. The relations are created by links called flow paths as defined in Fig. 3.

A condition can be associated with any of the flow functions described above, except the support, to describe that the system function modelled can only be achieved under certain specified operating circumstances. These may be "natural" physical constraints which should not be violated (cladding integrity) or "artificial" constraints which are determined by the designer's control decisions. A condition is related to a support function which provides the means for reaching these necessary conditions. This relation is indicated by a link in the flow structure called an information flow path. This path has an attribute a predicate defining the truth function to be satisfied by the performance parameter of the support function. The predicate quantifies the requirements to be met for the conditioned flow function. Several conditions may be related to a given flow function in which case all the associated predicates should be true.

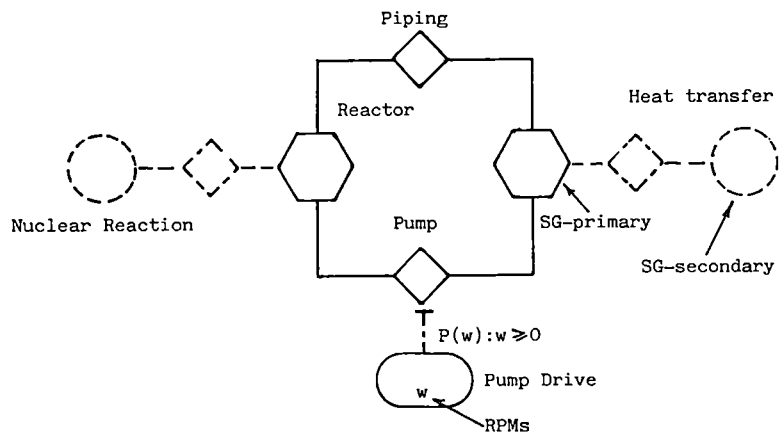
A SIMPLE EXAMPLE

As an illustration of the modelling approach we will describe some models of a simple system as depicted in Fig. 4.

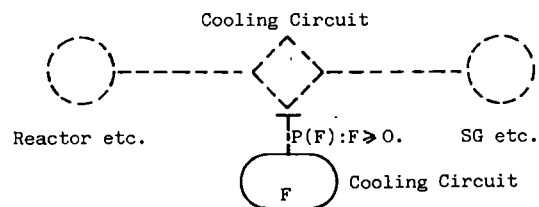
The example chosen is a very simple reactor coolant system comprising a reactor as an energy source, a pump for providing flow and a steam generator. Flow model A describes system function with a high level of detail and specifies the functional degrees of freedom in terms of performance parameters (not indicated in the diagram) for the individual flow functions. Note that the transport node modelling the pumping function is conditioned by the pump drive. The condition for existence of the



Physical Structure



Flow Structure A



Flow Structure B

Figure 4. A simple example illustrating the use of the flow modelling methodology for describing a system on different levels of abstraction.

transport function is given as a predicate $P(w)$ where w is the shaft angular velocity. Flow model B describes the same system at a high level of abstraction as the function of the cooling circuit is specified as an energy transport node. This model describes the intent of the plant designer as it specifies the purpose of the cooling circuit. The energy transport is conditioned by a support function representing the circulation of fluid in the primary. The plant parameter critical to the existence of the energy transport is the rate of flow F in the primary and the condition to be satisfied is given by a predicate $P(F)$ which should be true.

MULTILEVEL FLOW MODELS AND DECOMPOSITION OF FLOW FUNCTIONS

The flow modelling framework described above can be used to describe plant function on any level of aggregation but it is not sufficient for representing the relations between plant functions on different levels. Thus, in the example in Fig. 4 we described two functional aspects of the same system, but we did not model explicitly the relation between the energy transportation aspect of the reactor coolant system and the circulation of fluid in the system. This relation can be represented by introducing a flow modelling concept (see Fig. 3 for the associated symbol) to indicate a functional decomposition of a flow function. The usefulness of this concept becomes clear when it is realized that the decomposed function always can be described in terms of the basic flow functions, i.e. as a flow structure. This recursion is possible because the basic flow function applies on any level of physical detail and makes it possible to construct multilevel flow models describing how the system is organized into several functional levels. Such a model may cover the whole range of functional aspects related to the process plant as a whole down to aspects dealing with minute details concerning the function of e.g. the auxiliary systems to a lubrication pump. An example of a nuclear power plant model will be discussed later.

As an illustration of the use of functional decomposition in flow modelling consider the example in Fig. 5. This example shows a model of a feedwater system consisting of a feed and a condensate pump and a feedwater tank. Two models are provided, on level 1 the feedwater system is described as a mass transport system, which indeed is the function intended of such a system. On level 2 the transport node on level 1 is decomposed into subfunctions (note that the decomposition is in the direction opposite to the arrow), which in this case can be associated with the components of the system.

This example shows a general aspect of a decomposition that it increases the functional degrees of freedom. From considering only the flow F_1 on level 1 we consider two flows F_2 and F_3 and a mass level M on level 2. This implies that F_2 and F_3 should be coordinated in order to ensure that the model on level 1 is an adequate description of the overall function of the feedwater system. We can accordingly consider the transport node on level 1 as specifying the goal of the function described on level 2 and the double arrow implies that a control mechanism (automated

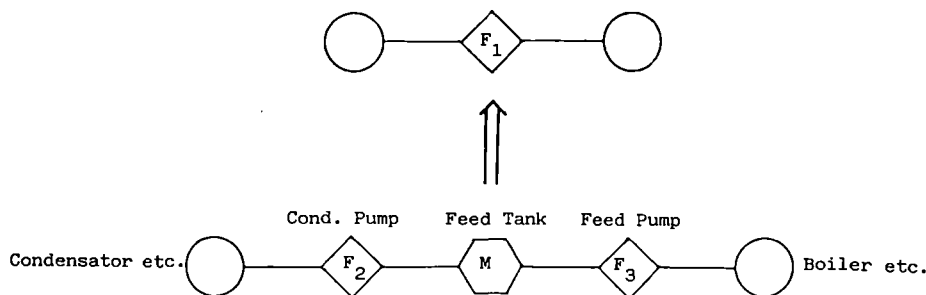


Figure 5. Example illustrating the use of functional decomposition in flow modelling.

or the operator) is required to constrain the variability on level 2. A possible constraint could be $F_1 = F_2 = F_3$. This corresponds to the choice of a specific control strategy and F_1 will be the reference for the resulting control loop. The aspects of functional decomposition discussed here in terms of an example are general, i.e. flow functions can be considered as goals when decomposed and the decomposition implies a control constraint. However, when a support function is decomposed, the associated condition is considered as the goal and not the support function itself.

OPERATING MODES AND THE MODELLING OF FUNCTIONAL ALTERNATIVES

In complex processing plants it is often the case that critical functions may be accomplished in several alternative ways. As examples may be mentioned the main and the auxiliary feedwater system as being alternative systems for the provision of feed flow to the steam generators. Similarly, a condition may be provided by several alternative support systems. These alternatives can also be represented in a multilevel flow model. On the plant level functional alternatives are treated by developing an MFM for each operating mode, i.e. the models are separate. This could also be done on the subsystem level but may lead to the generation of a complex hierarchy of separate models. In order to avoid this, alternatives are only allowed to lead to separate models if they are exclusive. Otherwise they will be considered as belonging to the same operating mode. It is possible to identify three different situations where alternatives should be taken into account.

- A flow function may have several decompositions. However, these alternatives cannot be relevant at the same time otherwise it would reflect an ambiguous design goal and could not be realized. Accordingly, we should only consider the case where the alternatives are exclusive. In this case the alternatives should be represented in separate flow models defining alternative sub-operating modes.
- A flow function may have several conditions. If these conditions should all be satisfied at the same time, there are no problems. But if they are mutually exclusive we are dealing with a situation involving different physical implementations of the same support function. This means that we are dealing with different operating modes which should be modelled separately.

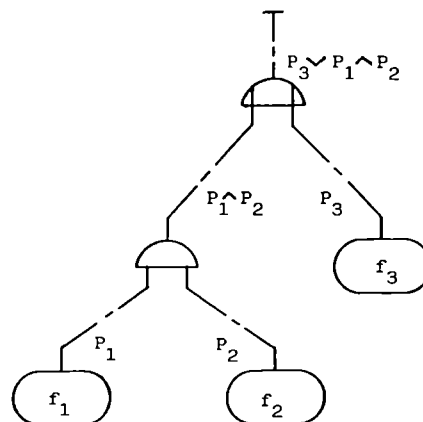


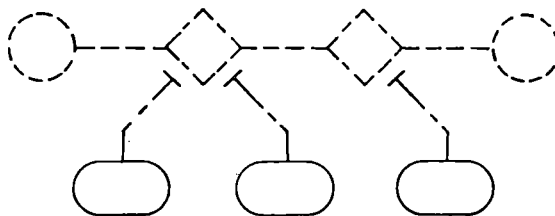
Figure 6. Logical network illustrating how several support functions (f_1 , f_2 and f_3) may contribute to the same condition. Condition predicates P_1 , P_2 and P_3 are combined using AND and OR operations.

- A condition may be satisfied by several support functions. This case can be treated by combining conditions into a logic network as exemplified in Fig. 6. It is clear that arbitrarily complex logical networks can be constructed by using AND and OR operations on condition predicates.

DERIVATION OF CONTROL REQUIREMENTS FROM FUNCTIONAL SPECIFICATIONS

Plant control requirements are clearly closely related to functional specifications, but where the latter describes what should be achieved the specification of control requirements deals with how goals are reached and plant functions established. In the following I will show that MFMs introduced above as a formalism for functional specification can also be used for specification of plant control requirements. The two uses depend on two different interpretations of the information contained on each functional level in the model.

When coming from above functional specifications describe means for reaching goals (defined on next higher level).



When coming from below functional specifications define goals (for the level below).

Figure 7. A flow model specifies plant goals and functions but also provides specification of control requirements when taken together with information about actual state of flow functions.

Considering now as an example the flow model shown in Fig. 7. Such a model defines the causal flow of mass and energy in a plant on the particular level selected, and the functional degrees of freedom in changing levels and flows can be readily identified. Each node in the flow model represents from this point of view a subfunction. But as discussed earlier nodes could also be considered as goals of subsystems on the next lower functional level. Conditions correspond similarly also to goals for subsystems the function of which is defined on the next lower level. A flow model on one level induces accordingly a set of control requirements on the next lower level, i.e. a set of target states to be reached by proper manipulation of the controllable mass and energy variables (degrees of freedom) on the next lower level. This applies by recursion to all the levels in an MFM and we can conclude that we have two different interpretations of the information provided in the model, one for the specification of plant system goals and functions and the other for specification of control requirements. This situation is illustrated in Fig. 7 and it should be noted that the two interpretations correspond to the two ways an operator could use the information in an MFM during diagnosis or control (Rasmussen and Lind, 1981). The possibility of applying two interpretations is the property which makes MFMs useful for transfer of information from plant design into control design (Rasmussen and Lind, 1982), and from the whole design phase into operator training and plant operation.

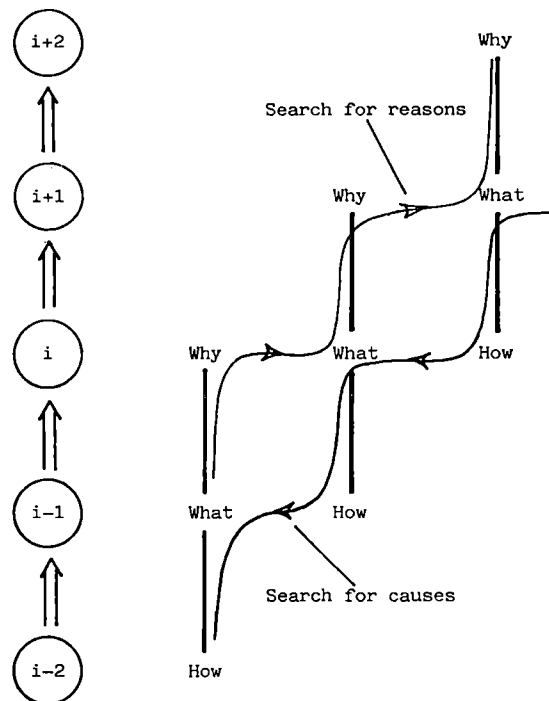


Figure 8. Illustration of the use of why, what and how questions for searching through an MFM. Each circle corresponds to a flow structure. The search routes depicted correspond to a search for reasons and causes. More complex search patterns are possible depending on the use of model information.

This point can be further elaborated by considering three consecutive levels $i-1$, i and $i+1$ in a sequence of levels in an MFM as illustrated in Fig. 8. Assuming that level i describes the function of a particular plant subsystem under investigation in a given model application, then level $i+1$ will describe why this function is required. Similarly, level $i-1$ will describe how the plant function on level i is established and level i will relate to what is going on in the plant subsystems considered. The triple of why, what and hows can be shifted upwards or downwards (see Fig. 8) as the subsystem considered changes and provides a systematic functionally motivated strategy for searching through model information. This may be important for the use of MFMs in training as it provides a way of organizing plant knowledge into a coherent structure. The why, what and hows may also be important for an operator in diagnosis if supported by an information display designed on the basis of an MFM plant model (Goodstein, 1982, Rasmussen and Lind, 1981). In constructing an MFM model it is also necessary to consider the triple as it guides the modeller in the choice of plant aspect to address at a given instant in the modelling (enforces the systems approach).

A MULTILEVEL FLOW MODEL OF A PWR

In order to illustrate the modelling method I will now show an example of a nuclear power plant (PWR) model. The model (Fig. 9) is not complete in any sense but illustrates the characteristics of a multilevel flow model. The presentation of a reasonably complete model would be outside the scope of this paper.

The plant is modelled from two points of view, one dealing with the overall safety goal of preventing release of radioactive materials to the environment and the other dealing with the goal of plant energy production. These two goals are described

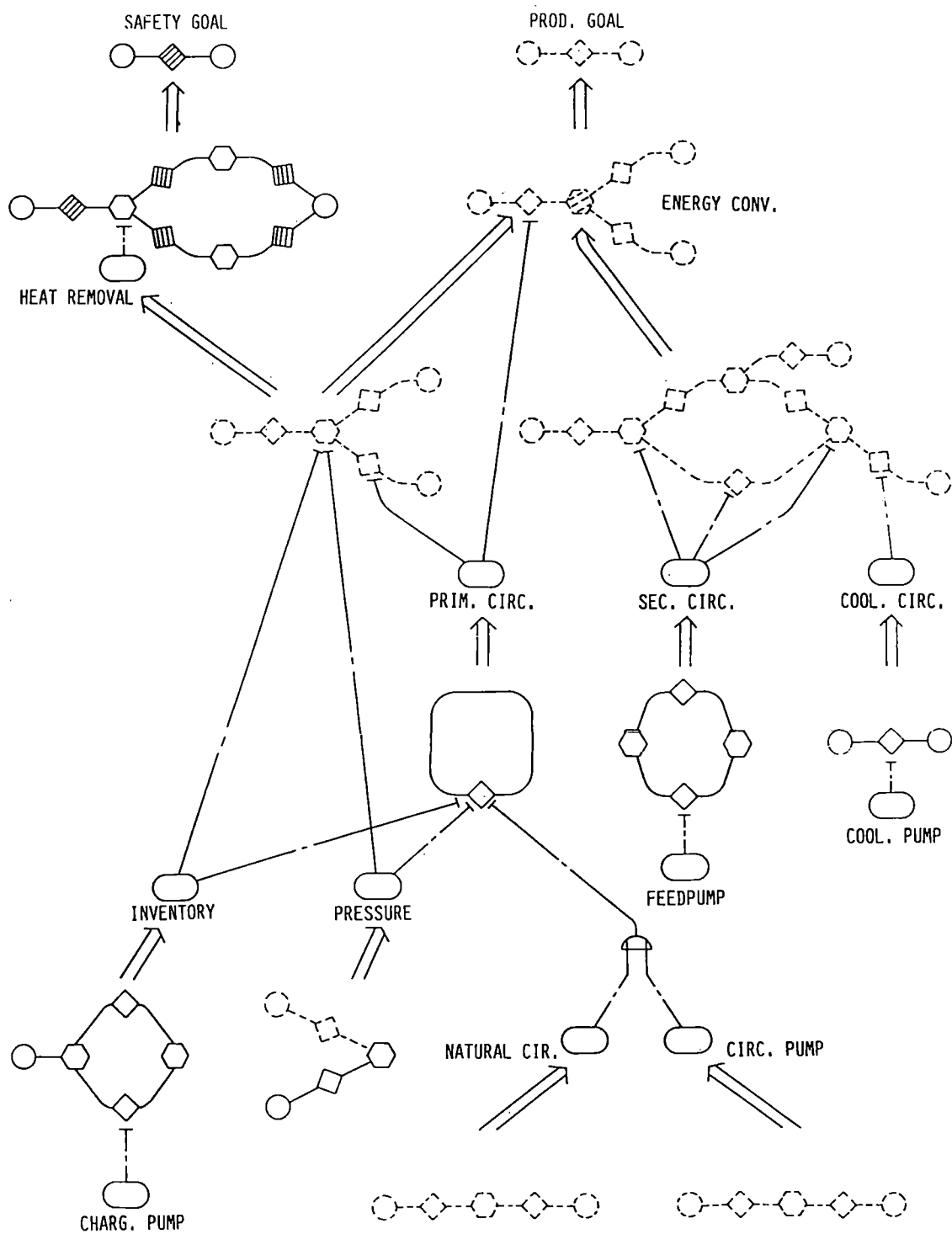


Figure 9. Multilevel flow model of a nuclear power plant (PWR).

in the flow modelling terms and the two goals are decomposed into subgoals with associated plant subfunctions. The safety aspect is described by modelling the flow of radioactive materials through the system. This model includes the safety barriers: cladding, RCS boundary and containment. The availability aspect is described by modelling the RCS and steam generator as an energy transport system. If taken separately, the two plant goals would lead to two goal and function hierarchies, one dealing with the safety issue and the other with the energy production issue. This would disguise the fact that safety and production functions have a common physical basis by being functional aspects of the same system. These relationships appear directly in the PWR model (Fig. 9) as the two functional hierarchies merge together on the lower levels which represent the function of physical components.

APPLICATIONS OF MULTILEVEL FLOW MODELS

Several applications of multilevel flow models have been considered (Lind, 1979, 1981, 1982a and 1982b). They may be used as a system analytical tool in plant design to provide a basis for planning of overall control strategies (Rasmussen and Lind, 1982) and as a consistent basis for identification of critical events in risk analysis (Rasmussen and Pedersen, 1982). Furthermore, they may be used as a basis for design of man-machine interfaces by providing a structure to the plant information which should be displayed to the operator. This structure reflects the plant designer's intentions. In more advanced computer-based operator support systems a set of flow models may provide the knowledge base necessary assisting the operator in diagnosis of plant malfunctions. Flow models may also be considered as a basis for operator training.

ACKNOWLEDGEMENTS

This work is part of the joint Scandinavian NKA/LIT project on Human Reliability supported by the Nordic Council of Ministers.

The support of Westinghouse Electric Corporation, Pittsburgh, USA in providing me with technical information for the PWR modelling is greatly appreciated.

REFERENCES

- L. P. GOODSTEIN, "Computer Based Operating Aids". To be presented at Design 1982 in Birmingham, September, 1982.
- S. A. GREGORY, "Design Strategies and Tactics". Paper presented at ICE Symposium: Current Design Thinking, September 12-14, 1979, Aston University, England.
- E. HOLLNAGEL and D. D. WOODS, "Cognitive Systems Engineering". Risø-M-2330, 1982.
- M. LIND, "The Use of Flow Models for Design of Plant Operating Procedures". Risø-M-2341. Paper presented at: IWG/NPPCI Specialists Meeting of Procedures and Systems for Assisting an Operator during Normal and Anomalous Nuclear Power Plant Operation Situations, December 5-7, 1979, Garching, F. R. Germany.
- M. LIND, "The Use of Flow Models for Automated Plant Diagnosis". In: Rasmussen, J. and Rouse, W. B. (Eds.), "Human Detection and Diagnosis of System Failures". Plenum Press, New York, 1981.
- M. LIND, "Artificial Intelligence Techniques in Process Plant State Identification". Paper presented at: SAIS-82 Workshop on Artificial Intelligence, April 23-25, 1982a, UPMail Uppsala University, Sweden.

M. LIND, "Generic Control Tasks in Process Plant Operation". Paper presented at the 2nd European Annual Manual, Bonn, F. R. Germany, 1982b.

J. RASMUSSEN and M. LIND, "Coping with Complexity". Risø-M-2293, 1982. Paper presented at the European Annual Conference on Human Decision and Manual Control, Delft, 1981.

J. RASMUSSEN and M. LIND, "A Model of Human Decision Making in Complex Systems and Its Use for Design of System Control Strategies". Paper presented at the American Control Conference in Arlington, Virginia, June 14-16, 1982.

J. RASMUSSEN and O. M. PEDERSEN, "Formalized Search Strategies for Human Risk Contributions: A Framework for Further Development". Risø-M-2351, 1982.

H. A. SIMON, "The Sciences of the Artificial". The MIT Press, 1969.

DEVELOPMENT OF AN IN-VESSEL WATER LEVEL GAUGE FOR LIGHT WATER POWER REACTORS

K. Ara and N. Wakayama

Japan Atomic Energy Research Institute
Tokai-mura, Naka-gun, Ibaraki-ken, 319-11 JAPAN

and

K. Kobayashi

Sukegawa Electric Co., Ltd.
Namekawa-honchoh, Hitachi-shi, Ibaraki-ken, 317 JAPAN

ABSTRACT

The in-vessel water level gauge, in principle, is based on the measurement of the temperature distribution on the surface of a long sheathed heater-pin which is partially immersed in water. Instead of adopting the measurement with many thermocouples, a binary-coded thermocouple array consisting of differential thermocouple trains (DTCTs) is settled on or in the sheath of a heater-pin to give a binary output related to the water level. Thus, this new-type of water level gauge was named BICOTH (Binary-Coded Thermocouple-array with Hheater).

After feasibility tests of the method with a prototype BICOTH, two types of in-vessel BICOTH were fabricated. One was a heater-pin type in which five DTCTs were settled in the heater-pin sheath to identify twenty-three different water-levels in the range of 2.6 meters. The other was a flexible-wires type, consisting of five metal-sheathed DTCTs with a diameter of 1.6 mm and with heater wires installed inside with each DTCT. The performance of each type was examined under the conditions of cold water and high-temperature, high-pressure water, and encouraging results were obtained. In this paper, the principle and the tests results are presented.

INTRODUCTION

The accident at Three Mile Island 2 (TMI-2) lives in one's memory as the most serious event at a commercial nuclear power plant. Many lessons were learned through intensive investigations of the accident. Several recommendations and requirements were proclaimed from the governmental authorities being responsible for nuclear safety. These included improvements in instrumentation; namely, more direct and unambiguous measurement of parameters such as the water level in the reactor vessel and the relief valve position, extended-range of the measurement of important parameters such as the in-core thermocouples and radiation monitors, and others. This motivated the development of an in-vessel water level gauge.

Some possible ways of in-vessel water level measurement were reviewed by USNRC¹, and the heated thermocouple (HTC) was evaluated as the most promising method². Oak Ridge National Laboratory (ORNL) developed an in-vessel liquid level probe based on the differential HTC³; and Combustion Engineering, Inc., a liquid level monitoring system based on the same concept⁴. Idaho National Engineering Laboratory developed the system based on the HTC with an unique heater-current feedback method⁵. All these

were tested with excellent results.

The concept of water level measurement based on the HTC was introduced about 20 years ago⁶. The HTC has a very simple structure, and consequently is very reliable and durable. Therefore, it is a matter of course that the HTC is noticed again here. However, the HTC is basically a sort of liquid level switch, so that an array of many HTCs is needed for wide-range and continuous liquid-level monitoring. In actual in-vessel application, this creates many problems with cabling especially with sealing at the cable penetration at the pressure boundary. Therefore, in practice, the maximum number of HTCs to be arrayed may be limited to five or so; but this bears a poor measuring resolution and accuracy as compared with the differential pressure method.

The in-vessel water level gauge presented here is of a more unique method; it minimizes the trouble of cabling and realizes a better measuring resolution without losing the merits of high reliability and durability through the combined usage of thermocouples and electric heaters.

PRINCIPLE OF IN-VESEL WATER LEVEL GAUGE, BICOTH

The in-vessel water level gauge, in principle, is based on the concept of measuring the temperature distribution on the surface of a metal-sheathed heater-pin which is partially immersed in water. When the energized heater-pin is partially in water, the surface temperature of the heater-pin sheath along its axis changes steeply in the vicinity where the surface is in contact with the water, as shown in Fig. 1. Conversely, it is possible to detect the water level if one can identify the position where the surface temperature of heater-pin changes steeply. This concept can be realized easily by fitting up the heater-pin surface with an array of thermocouples, as shown in Fig. 2. The temperature distribution on heater-pin surface can be measured with the usual series array of thermocouples, and the profile of temperature distribution can be obtained directly from the outputs of thermocouples. Also, if one deals with the thermocouple outputs as differences between the outputs of neighbouring thermocouples, a large signal is obtained from the thermocouples which are fitted on

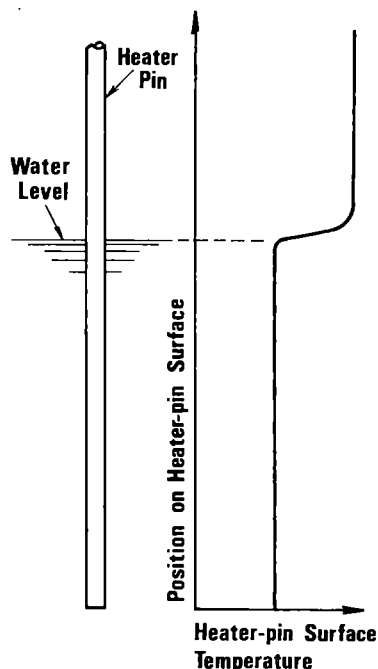


Fig. 1 Heater-pin and its surface temperature distribution.

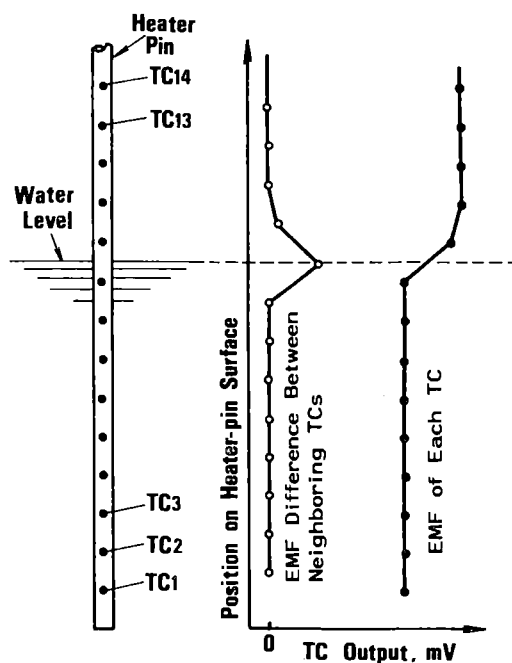


Fig. 2 Measurement of temperature distribution on the surface of heater-pin with many thermocouples.

just above and below the position where the water surface exists. However, if one intends to detect the water level with a good resolution by this method, many thermocouples are needed; for instance, 31 thermocouples for a measuring range of 3 meters with a resolution of 10 cm, resulting in 62 lead wires for the thermocouples in total. This number becomes very troublesome in practice, particularly in cabling especially at the penetration at the pressure boundary of a reactor vessel. Thus, a new method has been explored to decrease the actual number of thermocouple lead wires.

Here, we introduce a differential thermocouple train (DTCT). The DTCT consists of several pairs of differentially connected thermocouples; and all the pairs are connected in series, as shown in Fig. 3. If the differential hot-junctions of each pair are under an isothermal condition (e.g., Case A of the figure), the output of DTCT approaches zero, i.e. "0"; and when this condition is broken between two hot-junctions of one of the pairs (Case B), a certain output voltage, i.e. "1", appears due to the differential electromotive force between these two hot-junctions. This generates a binary output in discrete steps with movement of the water level position as shown in the right-hand side of the figure. Therefore, if we make a metal-sheathed DTCT as shown in Fig. 4 and settle it on the heater-pin surface instead of the usual series array of thermocouples, we can obtain a binary output with change of the water level. Based on these concepts, the BICOTH (Binary-Coded Thermocouple-array with Heater) has been proposed for in-vessel water level measurement⁷.

The fundamental configuration of the BICOTH is shown in Fig. 5. The measuring range is divided to 10 "quantized" sections, and a different number based on a binary gray code is assigned to each section. Then, the binary-coded thermocouple-array composed of four DTCTs is installed inside the heater-pin sheath. Here, each DTCT's pairs of differential hot-junctions are arranged in order to generate one digit of a four-digit binary number assigned to each section. Accordingly, the output signals of the DTCTs correspond to the binary numbers assigned to each section where the water surface exists, as shown in Fig. 5(d). In comparison with the usual series array of n thermocouples which can distinguish $(n - 1)$ quantized sections in the measuring range, n DTCTs can distinguish $(2^n - 1)$ sections; and, as a result, the BICOTH can decrease greatly the total numbers of necessary lead wires.

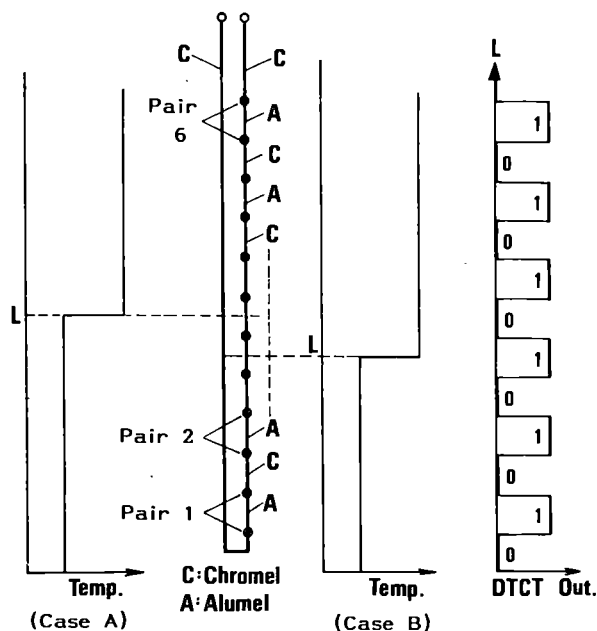


Fig. 3 Differential thermocouple train (DTCT) and its operating characteristics.

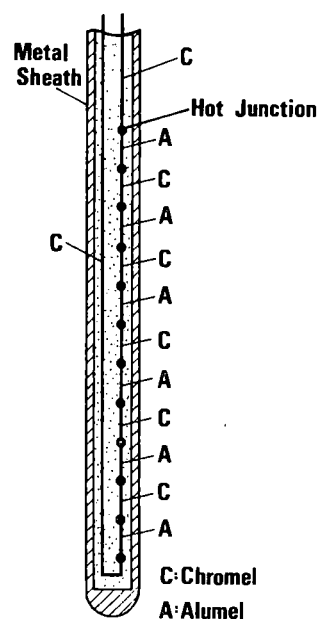


Fig. 4 Metal-sheathed DTCT.

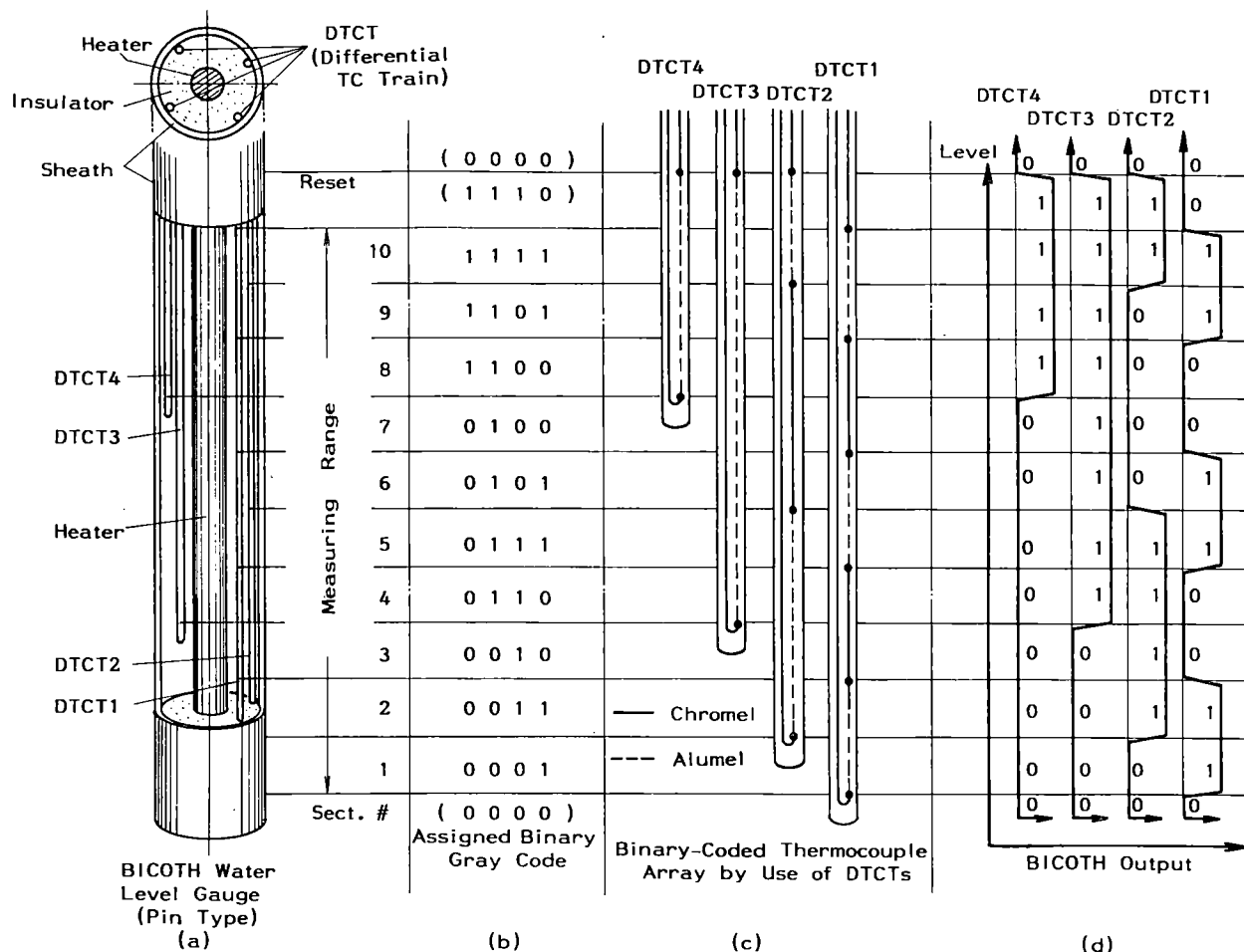


Fig. 5 Fundamental configuration and operating characteristic of BICOTH water level gauge.

FEASIBILITY TEST OF THE METHOD

For feasibility tests, a prototype of the BICOTH water level gauge (BICOTH-WLG) shown in Fig. 6 was fabricated. The measuring range of about 1160 mm was divided to 10 quantized sections with numbers of the binary gray-code. Before assembling the prototype BICOTH-WLG, trial production of metal-sheathed MgO-insulated DTCTs with a diameter of 1.6 mm was carried out by using an ordinary production line for sheathed thermocouples. After production, positions of hot-junctions in each DTCT were found out by heating and searching along the sheath with an alcohol lamp. The intended positions of hot-junctions were realized within an error of about 10% even in the first trial. While assembling, the section lengths were adjusted properly according to the real positions of hot-junctions in the produced DTCTs.

The feasibility tests were carried out to examine the static characteristics at room temperature. The assembled prototype BICOTH-WLG was installed in a water tank. Instead of changing the water level, the prototype BICOTH-WLG was moved down by a step of about 20 mm. The temperature of water was about 20 °C, and that of heater-pin surface above the water level was about 200 °C. The result is shown in Fig. 7. One can see that the correct signals were obtained at every section. The ranges of rise from "0" to "1" and fall from "1" to "0" are about 50 mm.

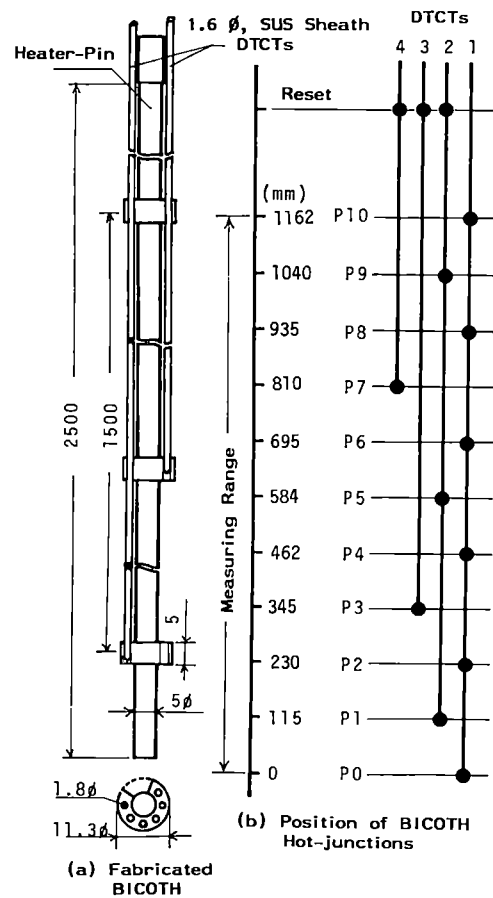


Fig. 6 Prototype BICOTH-WLG for feasibility tests.

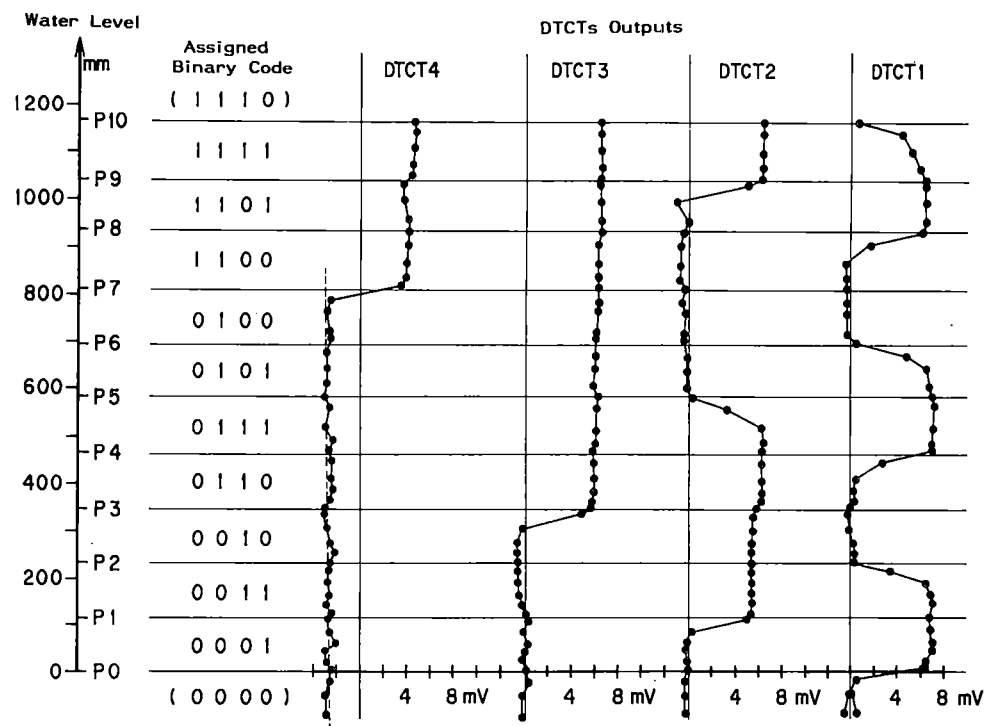


Fig. 7 Calibration results of feasibility tests for prototype BICOTH-WLG.

DEVELOPMENT OF IN-VESSEL BICOTH WATER LEVEL GAUGES

Heater-pin Type BICOTH-WLG and Tests

Since the excellent characteristics of the BICOTH-WLG were confirmed, as was expected, through the feasibility tests, development of the BICOTH-WLG was started for use in reactor vessels. On the initiative step of designing the in-vessel BICOTH-WLG, the following two items were taken into account: (1) long-term stable performances under PWR in-core environments of normal reactor operation, and (2) adequate responses to transient water level changes for assisting operators in accurate understanding of core-cooling conditions during accidents. This induced a concept of the in-vessel BICOTH-WLG having a durable structure and a proper transient response as well as excellent static characteristics.

The most durable structure seems to be where the DTCTs are installed inside the heater-pin sheath, preventing them from direct contact with high-temperature and high-pressure water. The proper transient response, on the other hand, seems to be obtained by adjusting the position of DTCTs between the heater-wire and the surface of heater-pin sheath. Generally, the time response becomes faster for increasing water level and slower for decreasing level when the DTCTs is positioned closer to the heater-pin surface. With these considerations, the heater-pin type BICOTH-WLG shown in Fig. 8 was designed and fabricated. The inconel-sheathed MgO-insulated DTCTs, I1 - I5, were settled in grooves on the surface of stainless steel heater-pin sheath of 20 mm in diameter. Then, they were covered with a stainless steel tube for protection against high-temperature and high-pressure water environments. Here, four MgO-insulated heater-wires were employed in the heater-pin to make uniform the circumferential temperature distribution on the heater-pin surface. In addition, the DTCTs, O1 - O5, were fitted on the cover tube only as a reference to evaluate transient performances of the group of DTCTs, I1 - I5. After assembly, a slight swaging-and-annealing was carried out. The measuring range of about 2600 mm was divided into 23 sections with 20 100-mm-long quantized sections from the bottom to the position of 2000 mm, and 3 200-mm-long quantized sections above 2000 mm. Each section was assigned with a different number of a 5-digits binary gray-code, and the DTCTs were arrayed according to the arrangement of these numbers.

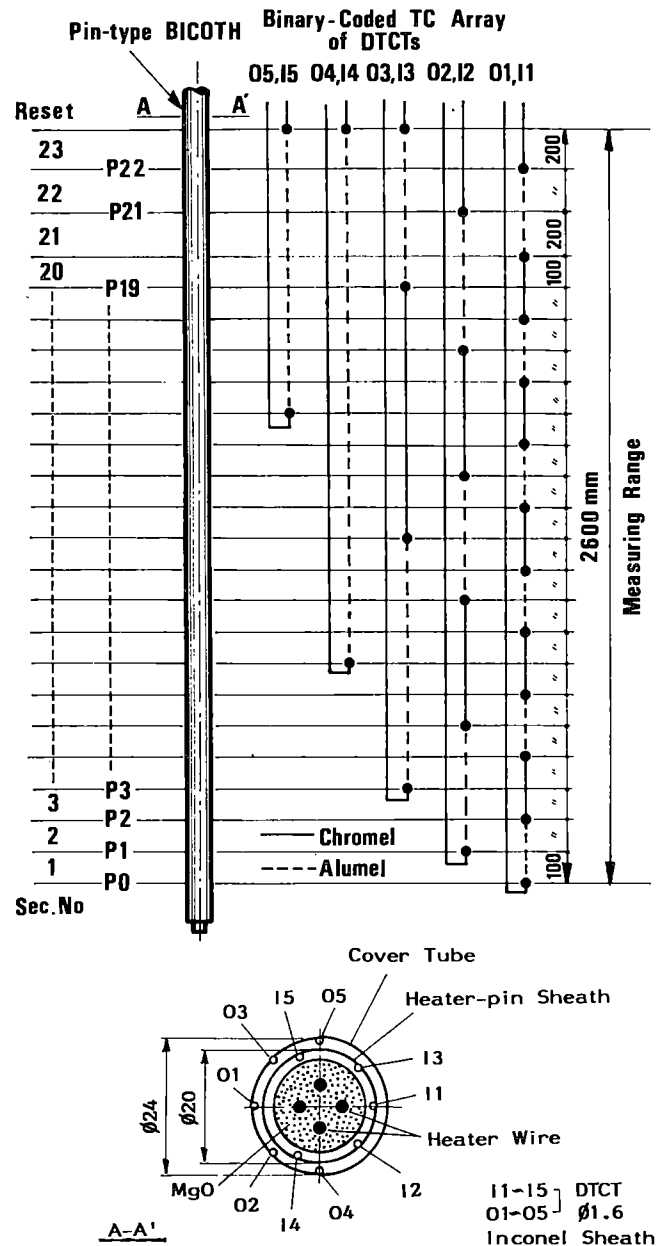


Fig. 8 Heater-pin type BICOTH-WLG.

The fabricated BICOTH-WLG was tested under an atmospheric cold water condition and a PWR-simulated high-temperature/high-pressure water condition. The atmospheric cold water calibration tests were carried out in the same way as the formerly discussed feasibility tests. During the tests, the input power of heater was regulated so that the step amplitude of DTCT output was about 8 mV, corresponding to the temperature difference of about 200 °C. The result is shown in Fig. 9. Although the gradients of "rise range" and "fall range" are not so steep as compared with those of the prototype for feasibility tests, very stable and well-shaped curves have been obtained. In the figure, a discrimination level between "0" and "1" is set up at half of the step amplitude of DTCT output for finding out the borders of the quantized sections. The positions of these borders are actually shifted down about 50 mm from the positions of DTCT's hot-junctions which were checked in an inspection after fabrication, but each of their relative positions agrees fairly well. This position shift is caused from unsharpness of steps in DTCT outputs.

Subsequently, the high-temperature/high-pressure water calibration tests were made under a simulated PWR condition. The result is shown also in Fig. 9, compared with the atmospheric test result. Here, the input power of heater was regulated again for better comparison so that the step amplitude of DTCT output was about 8 mV. One can see that the BICOTH-WLG has excellent static characteristics even under PWR condition and say that the result of the atmospheric calibration agrees well with that of high-temperature/high-pressure calibration.

After the static calibration tests, the dynamic responses for transient changes of water level were examined under atmospheric cold water condition. The results are shown in Figs. 10 - 11. Here the responses of DTCT I5 are presented for a step change of water level; i.e., a water level change passed through the position of a hot-junction of DTCT I5 at a very fast speed. One sees that the "50% response time" for the step change is about 12 sec in case of increasing water level, and 13 min in decreasing water level. Consequently, an overly fast continuous change of water level distorts the shape of DTCT output or decreases its amplitude. The typical examples are shown in the figures. Figure 10(B) shows a ramp response of DTCT I1 for continuous increase of water level with a speed of 20 cm/min, and figure 11(B) for continuous decrease with a speed of 1.1 cm/min. Therefore, for a clear discrimination of "0" and "1" in transient conditions, some adaptive means would be necessary: an automatic change of discrimination level in accordance with the change of amplitude, multi-level discrimination with unique signal processing, and so on. Also, the utilization of time differentiation of DTCTs output signals might be useful for this purpose. As a conclusion, it may be said that the transient response of the pin-type BICOTH-WLG is adequate from a practical point of view.

Flexible-wires Type BICOTH-WLG and Tests

On employing the BICOTH-WLG to power reactors or facilities for safety research, some limitation may exist in the space for installation. In such cases, it will be required to make the BICOTH-WLG as small as possible; and in some cases, to be flexible for installation through a curved guide tube. A flexible-wires type BICOTH-WLG was, therefore, designed. In contrast with the structure of heater-pin type BICOTH in which DTCTs are settled on the heater-pin sheath, the flexible-wires type has heater-wires inside with the sheathed DTCTs. Figure 12 shows the produced flexible-wires type BICOTH-WLG. Heater-wires and DTCTs wires are encased with MgO insulator in a stainless-steel sheath with a diameter of 1.6 mm. Five DTCTs having heater wires are arranged around a stainless-steel support rod and make a binary-coded thermocouple array. Here, the unflexible support rod is adopted because the purpose of the trial production was to investigate fundamental characteristics of the flexible-wires type, so that the flexibility of whole assembly was lost. The assembly will become flexible if a bundle of all DTCTs is installed inside a flexible support such as a spring-shaped sleeve. Also, this structure will protect the DTCTs from rubbing with an outer guide tube.

The produced BICOTH-WLG was tested in the same partial, comparative way as the heater-pin type. The result is shown in Figs. 13 - 15. Figures 14(A) and 15(A) show

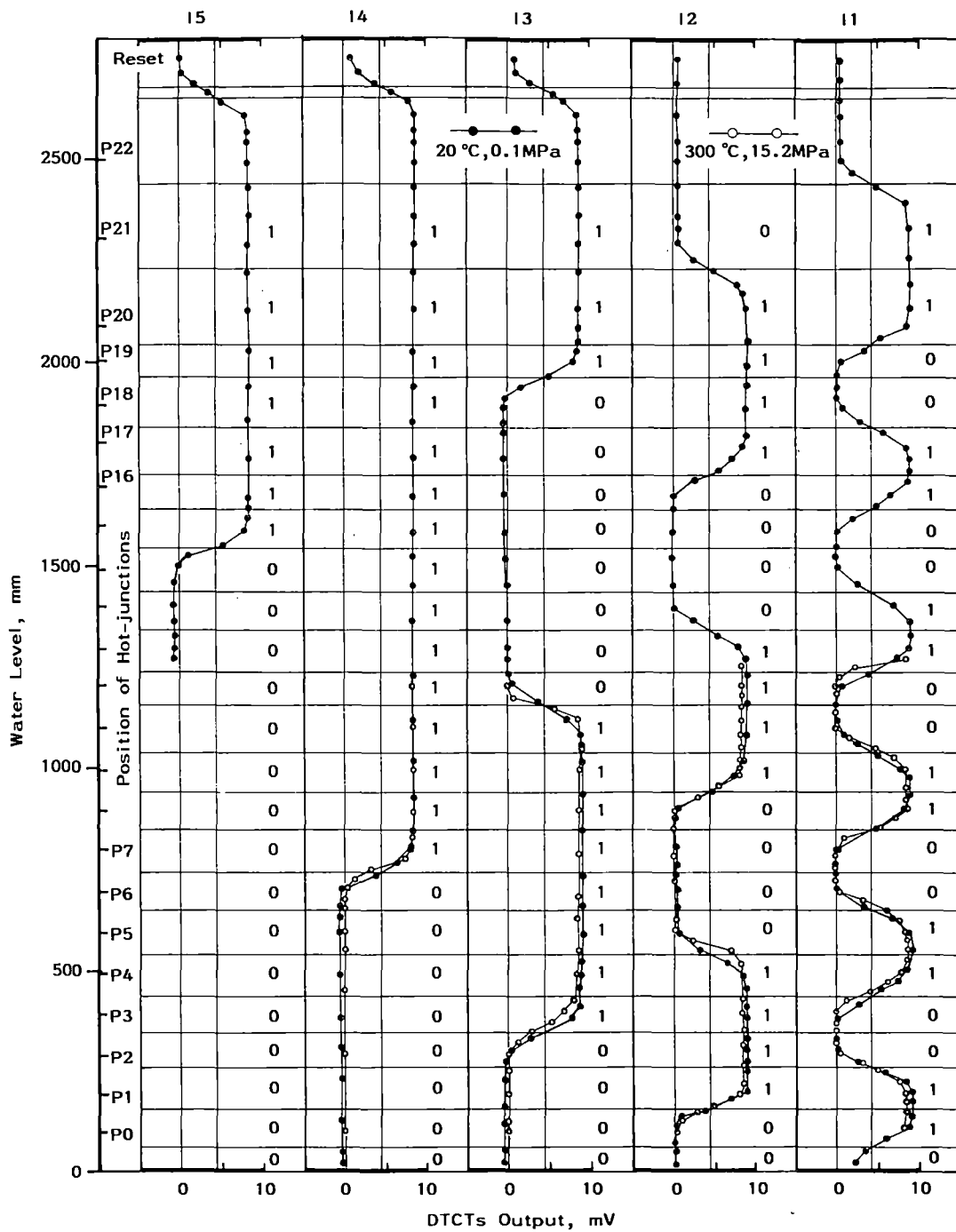


Fig. 9 Calibration results for heater-pin type BICOTH-WLG.

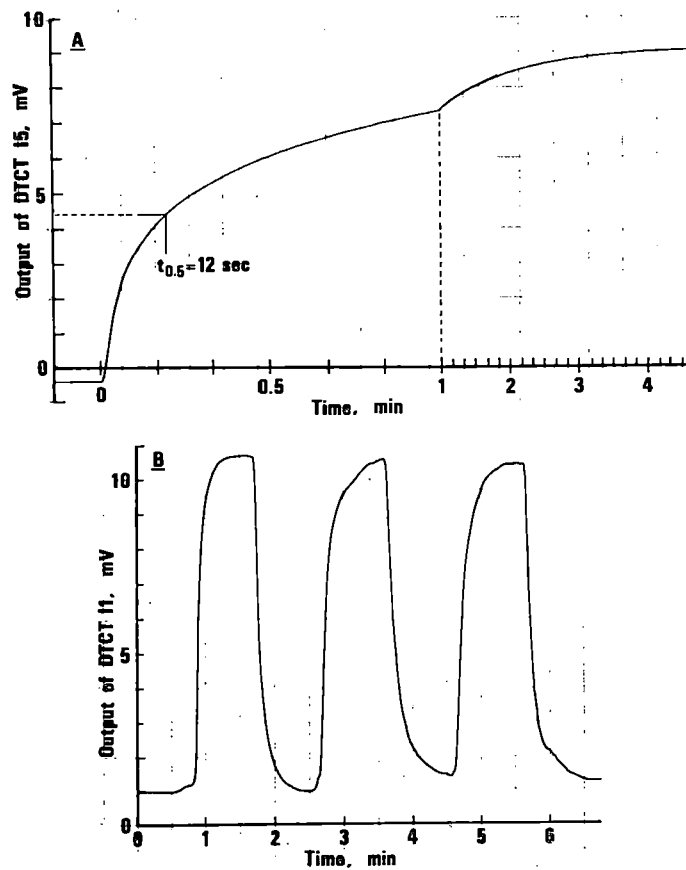


Fig. 10 Transient responses of heater-pin type BICOTH-WLG for increasing water level.

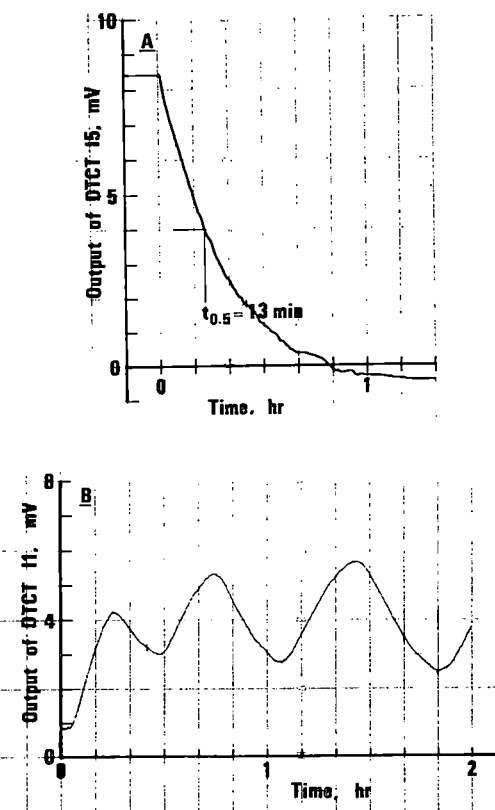


Fig. 11 Transient responses of heater-pin type BICOTH-WLG for decreasing water level.

responses of DTCT TH5 for step increasing and decreasing water level, respectively. Figure 14(B) shows a ramp response of DTCT TH1 for continuous increase of water level with a speed of 47.2 cm/min, and 15(B) for continuous decrease with a speed of 19 cm/min. As compared with the heater-pin type, steps of static characteristic curves are sharp, and dynamic responses are faster. This results from small heat capacity of the flexible-wires type. Conversely, however, this means that the flexible-wires type tends to be affected significantly by surrounding environments. Unevenness of the step shown in Fig. 13 is an indication of this environmental effect; i.e., the wind blowing during tests. Therefore, it may need some means to prevent such disturbances like a shroud tube. Also, automatic regulation of heater input-power will be effective to make constant the amplitude of the step. Even though the flexible-wires type has several superior properties as compared with the heater-pin type, its durability and reliability seem to be inferior. This will be a key point to be solved in actual application.

DISCUSSION AND CONCLUSION

Excellent performance characteristics of the BICOTH-WLG were confirmed through the trial fabrications and the tests. Along with the fact that the wide-range water level measurement can be achieved by the BICOTH-WLG with a comparatively precise resolution, the number of necessary lead-wires is small. Therefore, the cabling especially at the pressure boundary penetration does not induce a large number of problems, even if a redundant system such as 2-out-of-4 system is constructed. In other words, a very reliable system can be constructed without cabling troubles by employing redundant BICOTH-WLG system. Further, the structure of BICOTH-WLG is quite durable; its main elements are the heater-pin (or heater-wires) and the sheathed DTCTs. All of these are based on the same technology as for simulated fuel rods and

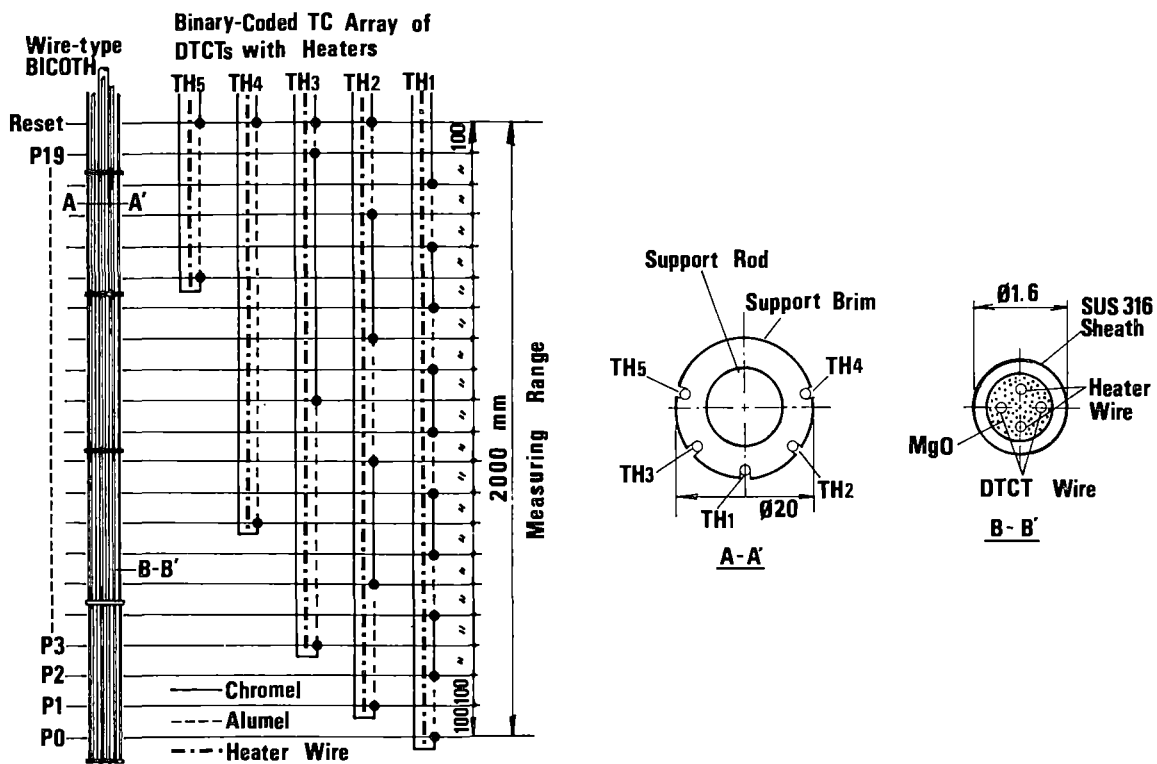


Fig. 12 Flexible-wires type BICOTH-WLG.

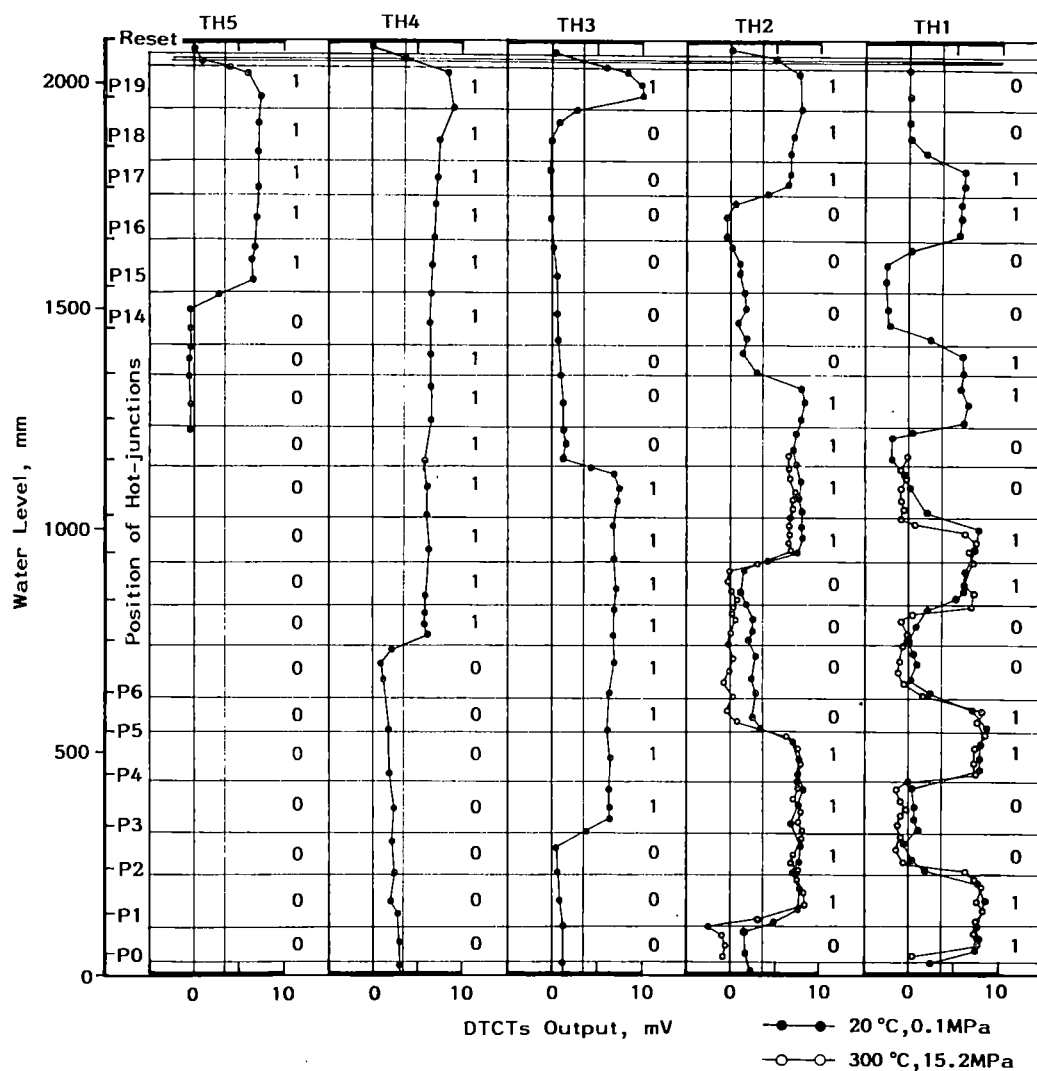


Fig. 13 Calibration results for flexible-wires type BICOTH-WLG.

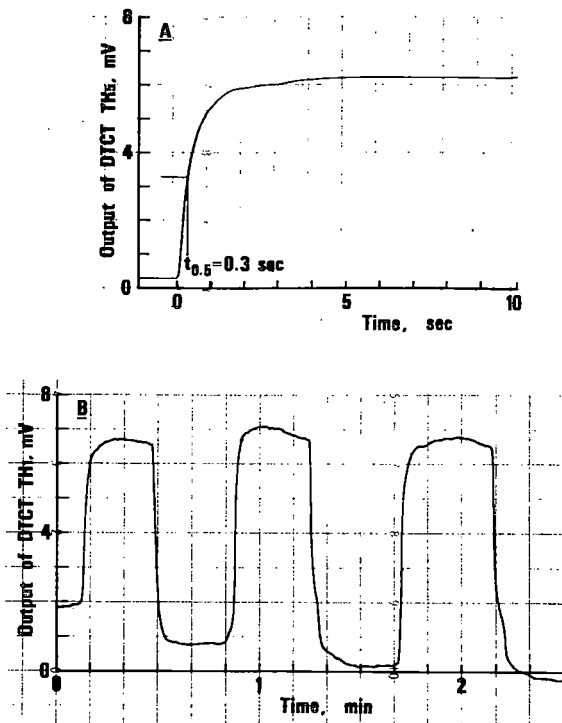


Fig. 14 Transient responses of flexible-wires type BICOTH-WLG for increasing water level.

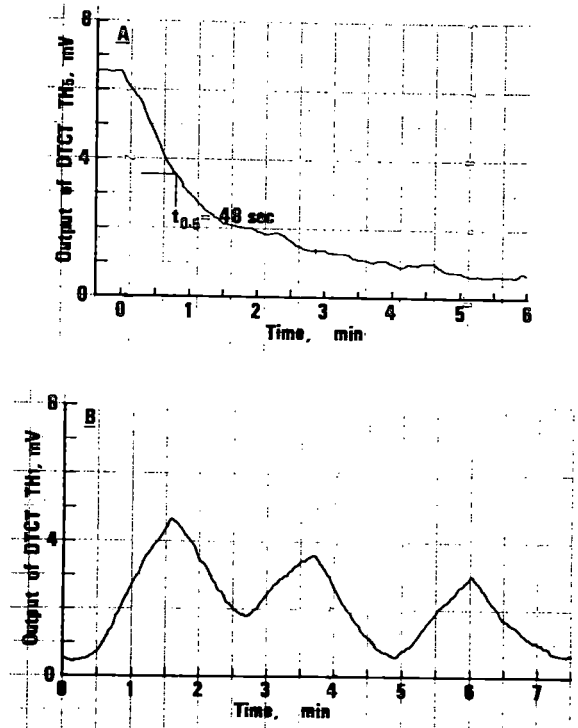


Fig. 15 Transient responses of flexible-wires type BICOTH-WLG for decreasing water level.

sheathed thermocouples, which have experienced wide success in safety research programs and in real power reactors, respectively. Therefore, the BICOTH-WLG can not only respond directly to the in-vessel water level, but also can be expected to survive and to function properly even under accident conditions. This is very essential to meet the new requirement which was proclaimed after investigation of the TMI-2 accident.

Dynamic characteristics of the BICOTH-WLG as well as static ones depend on its structure and materials. This suggests possibility of further improvements: a more proper structure and selection of materials will form a better heat-conducting circuit to produce better characteristics. Also, modification of structure will produce some possibility of new application such as sodium level detection in FBR, detection of boiling initiation in PWR and FBR, and detection of abnormal boiling condition in BWR.

Furthermore, the BICOTH-WLG is a digital sensor so that its connection with a computer is very easy. This allows complicated signal processing without difficulty and also produces a possibility of earlier detection of abnormal core-cooling initiation. When the in-vessel BICOTH-WLG system is employed with the present system in PWRs and BWRs, this possibility will be enhanced by comparing indications of both systems.

As mentioned above, the BICOTH-WLG has a great potential as an in-vessel water level gauge. However, there are many subjects to be solved until actual in-vessel application will have been practiced; that is, development of a unique signal processing and water-level detection algorithm, improvement of static and dynamic characteristics if necessary, more detail examinations and evaluations for adaptability under accident conditions, system design and evaluation of its reliability, and others. For these studies, participation of many researchers and engineers will be very beneficial and be welcome.

ACKNOWLEDGEMENT

The authors are deeply indebted to Mr. S. Morimoto for his great contribution to this work, and wish to thank Messrs. D. H. Miyasaki and H. Adachi for their valuable advices in preparation of the paper.

REFERENCES

1. Proc. of the U.S. Nuclear Regulatory Commission, Meeting on Reactor Vessel Liquid Level Measurement, Report NUREG/CP-0016, U.S. Nuclear Regulatory Commission (1980).
2. R. L. Anderson, "State of the Art for Liquid Level Measurements Applied to In-vessel Coolant Level for Nuclear Reactors", in Proc. of the U.S. Nuclear Regulatory Commission, *ibid.*, p. A-1.
3. K. G. Turnage, "In-vessel Liquid Level Probes for PWRs, Part I: Thermal Devices", in Proc. of the U.S. Nuclear Regulatory Commission, Review Group Conference on Advanced Instrumentation Research for Reactor Safety, Report NUREG/CP-0015, U.S. Nuclear Regulatory Commission (1980), p. I.2-1.
4. C. H. Neuschaefer, "A Reactor Vessel Level Monitoring System, an Aid to the Operators in Assessing an Approach to Inadequate Core Cooling, IEEE Trans. N.S., NS-29, 669 (1982).
5. J. V. Anderson, "Heated Thermocouple Liquid Level System", in Proc. of the U.S. Nuclear Regulatory Commission, Review Group Conference on Advanced Instrumentation Research for Reactor Safety, Report NUREG/CP-0015, U.S. Nuclear Regulatory Commission (1980), p. V.4-1.

6. G. F. Popper, "Lecture Notes on In-core Instrumentation for the Measurement of Hydrodynamic Parameters", Report ANL-6452, Argonne National Laboratory (1961).

7. K. Ara, et al., "Development of In-vessel Water Level Gauge" (in Japanese), in Proc. of the Fall Meeting of the Atomic Energy Society of Japan, E1 and E2 (1981).

COMPUTER ASSISTED TRAINING

Roland FELGINES - ELECTRICITE DE FRANCE - Direction de la Production Transport
Service de la Production Thermique

Jean STOLZ - ELECTRICITE DE FRANCE - Conseiller du Directeur de la Production
et du Transport

3 Rue de Messine
75384 Paris Cedex 08, France

ABSTRACT

Before fulfilling his task, operating personnel of nuclear power plants of Electricité de France follow a training programme prior to their licensing. After that, during operation, it is absolutely necessary, for a safe operation of nuclear power plants, to maintain and increase their knowledge and know-how by re-training.

Computer assisted training is a part of that continuing action. It has been tried for one year in four nuclear plants including 2 or 4 units of 900 MW power each. A 400 hours programme is now in operation. It includes re-training on systems circuitry, on operation specifications and procedures.

The EDF system is based on a central computer and use of specialized terminals in each plant.

If conclusive, this system will be extended to about 30 nuclear power units in the beginning of 1983 and also to other requirements than just operation people re-training needs.

INTRODUCTION

The Thermal Production Department of E.D.F. faced with several problems of training and keeping our personnel updated on the knowledge which they need, taking into consideration the nuclear program (21 units of 900 MW and 13 units of 1300 MW), has been conducting beginning 1981 a CAT experiment in 4 PWR plants.

This test which involved about 700 employees operation staff of nuclear power plants has been carried out on the reactor coolant system. This test ended in June 1982 and has led to a generalization of this system to all the French nuclear power plants.

INTEREST IN CAT

CAT, may improve the training because :

- it is a structured training based on analysis and logic,

- it is a system with an active pedagogy :
 - . use in groups,
 - . course presented as exercises,
 - . dialogue with the system inside the group,
- it allows a measure of the training work,
- it is used on the work site (control room),
- it is available all day long,
- always programs may be added with new modules.

APPLICATION OF CAT IN THE TRAINING OF STAFF

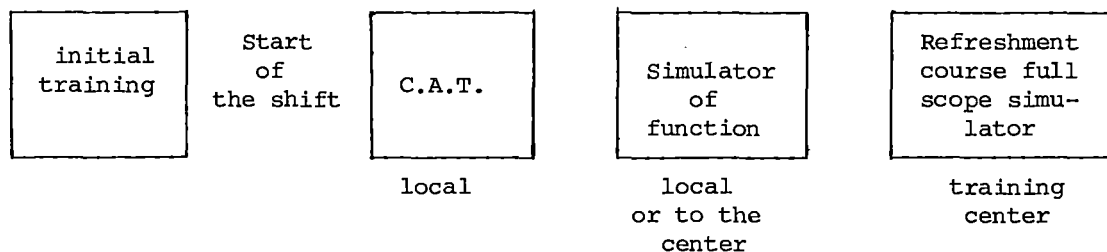
Computer based training seems to be very efficient to improve the operations personnel of nuclear power stations to improve the knowledge particularly when such training is conducted on their working premises during working hours.

That knowledge is directly related to their professional activity; it is initially acquired as part of centralized training activities set up by the Thermal Production Department in order to properly prepare employees to their speciality and function; computer based training specifically addresses here the follow-up need to maintain and up-date that knowledge while performing their job.

These activities are conducted either locally, or in specialized centers :

- local activities are organized in each plant under management responsibility, in particular shift managers. The subject matter includes keeping up basic knowledge plus safety and health physics. CAT seems to provide substantial support for such local activities aiming at refreshing speciality related knowledge.
- activities in specialized centers are generally reorientation courses supported by simulators and simulators of function.

The following diagram may be given for the 24 hours staff



- maintenance of knowledge -

CONTENTS OF THE COURSES

The program includes about 400 training hours as exercises for :

- reactor coolant system of a 900 MW unit,
- general accident malfunction instructions,

- actual accidents,
- health physics.

1) The circuits

We covered each circuit at 4 levels :

- A) circuit description
- B) normal circuit operation
- C) circuit operating instructions
- D) circuit malfunction instructions.

A) Circuit description :

This level is intended for the patrol and operations technicians. It covers the circuit technology and the main characteristics which this personnel should know.

- . circuit components,
- . component location,
- . values, parameters (pressure, temperature, flow-rates...),
- . patrols to be performed on the circuit.

B) Normal circuit operation :

This level is intended for the control room supervisors. It presents :

- . the circuit configuration under normal operation,
- . the various parameters or values displayed in the control room,
- . instrumentation and control

C) Circuit operating instructions : (Appendix 2)

These are intended for the whole operations team and describe the circuit in various configurations.

These modules are presented in the form of manipulations :

- . opened or closed valves,
- . set up,
- . starting or stopping a circuit, etc...

D) Circuit malfunction instructions :

As the preceding modules, this course is intended for the operations team and it presents the main malfunctions which may occur on the circuit and how to deal with them.

2) General accident-malfunction instructions.

We present the instructions in 2 forms :

- . the logical flow of the operating instruction, that is, the various manipulations or operations to be performed in chronological sequence,
- . the whys and wherefores of the various operations and manipulations and the analysis of the consequences.

3) Accident library.

We have two types of modules :

- the presentation of an incident animated from time to time by precise questions in relation with the French operating staff experience (which instruction is to be applied, what to do now ? which reasoning may justify such an action...) with a possibility to ask for information screens (such as the module of GINNA).
- a concise information (some screens and may be some exercises) on incidents and first conclusions, especially on the behaviour of an unit further to an incorrect action.

4) Health Physics.

We have two modules RP1 and RP2 which correspond to two levels of training :

RP1 for the whole staff,
RP2 for foremen.

These two modules are part of the yearly refreshment course of the staff after initial training. The session is of 2 days including the actual operations under the supervision of training staff.

PREPARING THE COURSES

It is very important that the course objective be very clear for those preparing the course : initial acquisition or routine maintenance or updating of knowledge. This influence course presentation as well as choice of questions. It is also necessary to know the users well, initial training, the work they are performing, the language they use, etc...

We must permanently pay attention to the formulation of questions : if we are not careful, they may lose their significance for the students, either because of ambiguity or lack of precision.

Three main concerns have influenced the working methodology :

- the desire to associate personnel from participating plants into the best process,
- to best suit the needs of operations personnel,
- to make sure that the information, values, figures and all parameters used in the course are correct.

To take the first point into account, we performed the following steps :

- . definition of the systems to be studied as well as priorities and major items (technology, diagrams), in cooperation with operations supervision and management.
- . as the courses were being prepared, keeping the corresponding engineers informed of work progress. These engineers were our contacts for all questions requiring good operating knowledge.
- . presenting the course document to future users (operation team) for criticism and modification before machine input.

The second point was taken into account by ensuring the participation of shift supervisors who had started-up and operated the 900 MW plant units and had trained field people.

For the third point, we were registered as a satellite of the TRICASTIN power station for documentation purposes, and this guaranteed automatic updating of the documents which we were using. Furthermore, the courses were validated in the plant by the users themselves before final use for personnel training. These checks covered vocabulary, comprehension of questions, pertinence of chosen answers.

The courses were prepared by engineers knowledgeable about the capabilities and contents of the software used.

Machine input is performed by typist, from documents written by the engineers. This personnel knows how to use the commands for controlling the screen, and takes initiatives in the area of presentation, laying out the pages on the screen, as well as choosing colors, unless specific instructions are given.

USE IN POWER PLANT AND USER RECEPTION

A) Use in power plants.

There are 2 computers by two units. One computer is installed in the room between the two control rooms, the other one is in the training room of the spare shift. A computer is also installed in the Health Physics department.

The courses are available permanently and the use is subject to the agreement of the shift supervisor and under his instructions. It concerns the maintenance of knowledge of the shift.

Employees naturally gathered themselves into "level groups" (patrol man/control room supervisor, control room supervisor/shift supervisor).

Discussion arose spontaneously within these groups either to explain the questions in more detail or to build the answer or to provide additional comments.

The whole shift uses CAT but in different ways. Most users are field operators and the percentage of users decreases according to the ranking.

The incident courses pertaining to actual accidents are used with the participation of the Health Physics engineers. These sessions and programs are organized for each shift.

B) User reception.

The first contacts were perceived as a discovery. Curiosity was aroused, the diagrams were attractive, and their quality was appreciated. Certain users tried to "trick" the machine but this aspect disappeared very quickly.

There didn't seem to be any apprehension at the keyboard. Those with the habit were not surprised; for the others, the "hunt and peck" was a bit long, and also, they tried to shorten the answers.

The users quickly realized that "the machine" was not there to give them a hard time, and when the student did not find the answer and the latter appeared on the screen, a certain relief appeared.

The self evaluation displayed at the end of each module was well accepted. It should be noted that an effort was made to explain that this evaluation is anonymous and not stored in computer memory.

- It is necessary that a good information of users be carried out before the implementation of CAT in power plants.

- It is important that the management be concerned and interested in CAT, especially the shift supervisors.
- The users in most cases use the non directive strategy which enables them to have access to the whole course.

In appendix 3 we give the usage statistics over about 6 months.

To conclude, operations people were definitely interested in computer-assisted education.

This interest arises :

- from the novelty of the product,
- from the quality of the presented displays. People were really quite sensitive to the way this tool relates to their specialty. The color diagrams of circuits, taps, valves with a layout and coding which are familiar to them was favorably received. Conversely, the machine's rejection of an answer which they felt to be correct was severely disapproved and raised lively discussions among the participants. These rejections led them to better analyse questions and to look for key words in the answer.
- from the advantage of this tool :
 - . permanent availability (day, night, weekend).
 - . very easy and immediate access without preparation, thus encouraging use even for short periods of time.
 - . location of the screens in the vicinity of the control room.
 - . group work at the speed chosen by the group.
- possibility of dialogue with the machine in the group which make the training more interesting.

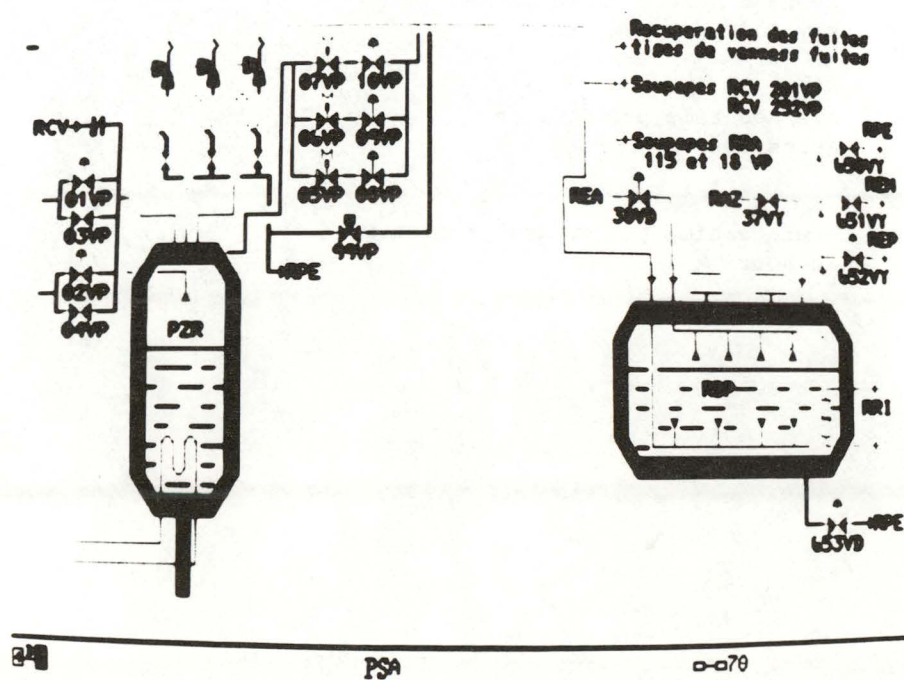
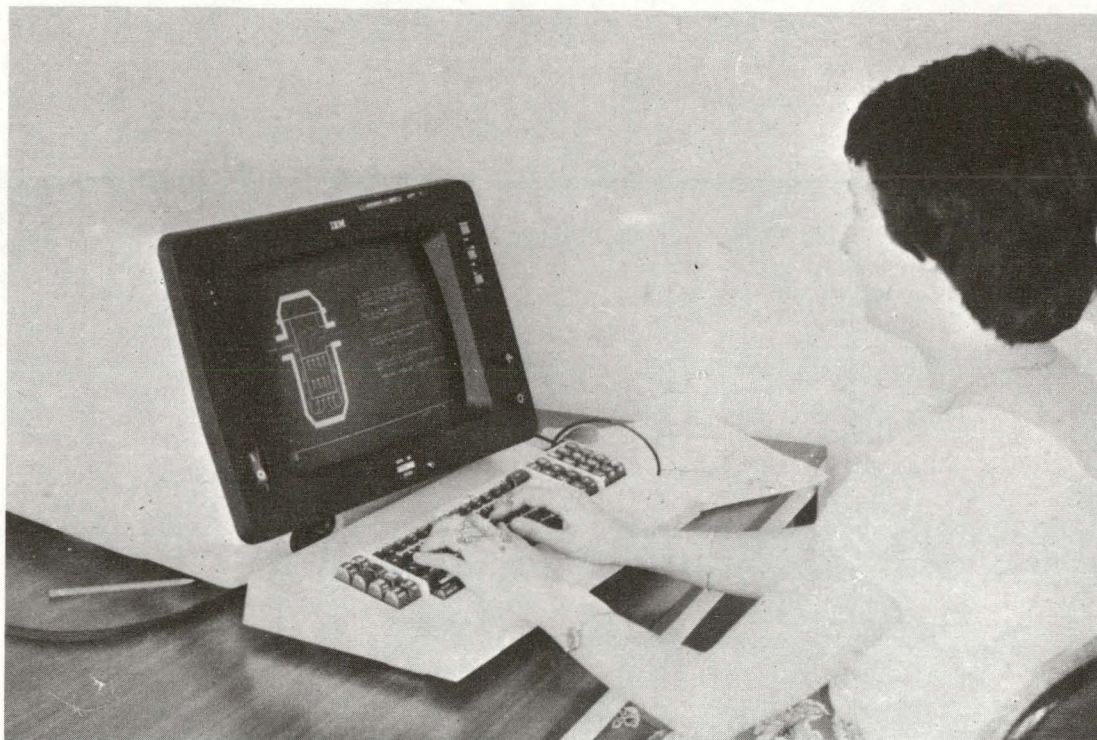
PROSPECTS

A) For the operations staff.

- . develop a program for the 1300 MW level,
- . check the advantages for the fast reactor systems,
- . create a course on the secondary system based on generally applicable principles.

B) In other fields.

- . create courses for clerical and accounting personnel,
- . study the possibility of presenting model method sheets for maintenance personnel.



APPENDIX 3

1.	Duration in months	:	6
2.	Use days	:	180
3.	Number of terminals	:	13
4.	Number of student register	:	600
5.	Number of student accesssees	:	12 225
6.	Use time in hours	:	7 960
7.	Average use time per day and per terminal in hours	:	3,4
8.	Average number of accesssees per day and per terminal	:	5
9.	Average time per student accesssees in hours	:	0,65
10.	Average time per student register in hours	:	13,3

SESSION 27

LOCA-RELATED EXPERIMENTS AND ANALYSIS

Chair: B. W. Spencer (ANL)

BLOWDOWN AND COLD WATER INJECTION EXPERIMENTS:
COMPARISONS WITH THE FIREBIRD-III AND RELAP-5 CODES

A.C.D. Wright (b), G. Proto (a), A. Alemberti (a),
G. Bimbo (a), and M.Z. Caplan (b)

(a) Nucleare Italiana Reattori Avanzati S.P.A.,
Genoa, Italy

(b) Atomic Energy of Canada Limited - Engineering Company,
Mississauga, Ontario, Canada

ABSTRACT

The thermohydraulics computer codes FIREBIRD-III and RELAP-5 have been used to simulate a cold water injection experiment done at Westinghouse Canada Incorporated and a blowdown plus injection experiment done in the RD-12 loop at Whiteshell Nuclear Research Establishment. The cold water injection experimental facility contains two parallel horizontal channels, each containing a 6-m long, 37-element electrically heated bundle. RD-12 is an integrated facility containing pumps, boilers and two electrically heated test sections.

Parametric trends have been studied by simulating several additional cold water injection experiments using FIREBIRD-III.

The predictions of the two codes are compared to measurements. Overall, the predictions are reasonable, although some discrepancies occur. In particular, FIREBIRD-III underpredicts channel refill time at low injection pressure. RELAP-5 predicts channel refill time well. Oscillations observed during refilling are qualitatively predicted by RELAP-5, although the amplitude and frequency are overpredicted.

INTRODUCTION

This paper describes the simulation of thermohydraulics experiments involving heated, horizontal channels, using the codes FIREBIRD-III¹ and RELAP-5².

The experiments were done to provide data₃ for code verification. The horizontal channel geometry is relevant to CANDU reactors³.

The codes FIREBIRD-III and RELAP-5 are described in some detail in the following Section. FIREBIRD-III is a major tool for safety analysis of CANDU plants. RELAP-5 is used worldwide for safety analysis of light water reactors.

The FIREBIRD-III simulations were conducted by AECL-EC personnel, while the RELAP-5 simulations were performed at NIRA.

FIREBIRD-III predictions are compared with data from several experiments, to summarize the parametric trends. Of these experiments, two (tests 508 and B7907) have been simulated using RELAP-5. The predictions of both codes are compared in detail with measurements from the latter two experiments. In general, the predictions are reasonably good.

THE CODES

FIREBIRD-III

FIREBIRD-III¹ is a thermohydraulics network code which solves the one-dimensional thermal equilibrium fluid conservation equations for single- and two-phase flow in a pipe. The conservation equations, together with the equation of state and constitutive equations, are reduced to a system of ordinary differential equations by volume nodalization. This system is then solved implicitly. Slip and drift correlations are available as a user option to treat unequal phase velocities. Rewetting is assumed to occur whenever a node becomes saturated.

FIREBIRD-III is equipped with a "hot pin" sheath temperature calculation which is uncoupled from the bulk thermohydraulics. If the two-phase mass flux is calculated to be less than $245 \text{ kg/m}^2\text{-s}$, the flow is assumed to be stratified. Upper rods are assumed to be steam cooled in this situation.

Homogeneous equilibrium fluid property derivatives are discontinuous at phase transitions. In FIREBIRD-III, the derivatives are adjusted to be continuous through the phase transitions. The enthalpy range over which the derivatives are smoothed is fixed in the code, as determined by matching one point in the pressure transient for cold water injection test 569.

RELAP-5

RELAP-5² is a digital computer program which solves the one-dimensional conservation equations for each phase, assuming equal pressures for the phases. The equations are coupled by expressions for the interphase heat and mass transfer.

RELAP-5 MOD 1 Release 14 required modification to allow the temperature of the Time Dependent Volumes to vary with time.

Since RELAP-5 was designed for LWR analysis, it does not model heat transfer in a stratified horizontal channel. Further, no specific rewetting model is included in the code. Hydraulically, stratification is assumed whenever the mass flux is less than $150 \text{ kg/m}^2\text{-s}$.

The numerical solution uses a Taylor series expansion of the fluid property derivatives, truncated at the second term. No smoothing is introduced at the transition from two-phase to single-phase. This leads to a mass error at the transition, which can be reduced by reducing the time step. However, in general this is not sufficient to ensure numerical stability.

COLD WATER INJECTION TEST FACILITY AND PROCEDURE

The cold water injection tests were carried out by Whiteshell Nuclear Research Establishment personnel at Westinghouse Canada Incorporated. The test program was 50% funded by Ontario Hydro.

Figure 1 is a schematic of the test facility, showing instrumentation. The test sections are located 5 m and 10 m below the headers. Each test section consists of a 103-mm ID Zr-2 flow tube containing a 6-m array of 37 indirectly electrically heated rods. Injection to both headers is supplied by a pump whose discharge pressure is controlled. The outlet header is fitted with a fast-acting valve in a pipe leading to a catch tank. Opening the valve creates a break whose size is governed by a sharp-edged orifice. Thermocouples are provided for fluid, pipe and heater surface temperature measurements at various locations throughout the loop. Fluid pressures and injection flows are also measured.

The tests were carried out in the following manner: Initially the system was filled with superheated steam. Bundle power was initiated. The break was triggered when any of the rod surface thermocouples exceeded a prescribed temperature. When the system pressure fell below the injection pressure cold water began to flow into the headers. The test was terminated when the heater surfaces were completely rewet, and a steady subcooled flow had been established.

In some of the tests only the bottom channel was used, and/or injection water was supplied to the unbroken header only. The test channel powers ranged from 50 to 300 kW, and injection pressures ranged from 400 to 3000 kPa.

FIREBIRD-III COMPARISONS WITH COLD WATER INJECTION TESTS

To outline the parametric trends and provide an overview of FIREBIRD-III capability, predictions for 6 cold water injection tests are summarized in this Section. Table I gives the test conditions.

TABLE I

Cold Water Injection Tests Used for Code Verification

Test No.	Injection*	Number of Channels	Break Area (cm ²)	Injection Pressure (kPa)	Channel Power (kW)
508	BH	2	2.67	890	100/100
569	IH	1	8.07	3000	300
583	BH	1	8.07	3100	300
517	IH	1	1.20	840	100
521	IH	1	8.07	380	50
771	BH	1	1.20	2000	300

*
IH - Injection to inlet header only
BH - Injection to both headers

Two of the most important parameters in the tests are the channel refill time and the sheath temperature turnaround time. Figure 2 illustrates the definition of these times in terms of a typical top rod sheath temperature transient at the outlet of a channel.

Figures 3 and 4 compare the FIREBIRD-III predictions with the measurements for refill time and turnaround time, respectively. The predictions are good at high injection pressure when channel refilling flows are strong. The code underpredicts channel refill and turnaround times at low injection pressure when refilling is slow. This is at least partly due to an underprediction of pressure during the mixing of cold water with steam in the headers. The pressure transient is better predicted for high pressure tests. Code comparisons with low pressure test 508 are discussed in more detail in the following Section.

CODE COMPARISONS WITH TEST 508

For both code simulations, initial (break initiation) test conditions, including fluid, pipe and heater temperatures, and fluid pressures were taken as inputs. The measured injection pump discharge pressure and the downstream-of-the-break pressure were input as time-dependent boundary conditions.

FIREBIRD-III Results

Figure 5 compares the predicted inlet header pressure with the measurement. The code underpredicts the minimum pressure reached during the filling of the inlet header. This is related to the lack of thermal non-equilibrium in the code. Without property derivatives smoothing the depressurization rate would be even greater. The underprediction of header pressure causes an overprediction of injection flow (Figure 6).

Figure 7 shows the predicted and measured sheath temperatures for the top rod at the outlet of the top channel. The prediction is for the "hot pin". The over-predicted injection flow leads to an underpredicted turnaround and refill time.

The code predicts channel flow oscillations during the refilling of the inlet feeders. These are manifested as oscillations in the predicted inlet header pressure (Figure 5) in qualitative agreement with the measurements. FIREBIRD-III does not capture the higher frequency oscillations associated with refilling of the heated channels.

Overall the FIREBIRD-III predictions for test 508 reproduce the basic phenomenology of the experiment.

RELAP-5 Results

Due to strong pressure and enthalpy gradients, the potential exists for numerical oscillations in the transition from single-phase to two-phase. To minimize this effect neighbouring volumes must be as similar as possible.

The two-temperature, two-velocity models were selected for this simulation and the multiplier discharge coefficient was taken equal to 1.0.

RELAP-5 underpredicts the inlet header pressure (Figure 8) immediately following injection. This indicates that the RELAP-5 non-equilibrium model is insufficient. The assumption that one of the phases is at the saturation temperature leads to too much condensation during the mixing of cold water with steam.

The pressure underprediction leads to an overprediction of injection flow (Figure 9). The predicted pressure begins to rise after the headers are full, and the feeders and channels become saturated. However, because of the overpredicted flow, the channel inlet is predicted to begin rewetting about 30 seconds early (Figure 10).

The predicted quenching temperature agrees well with the data. The overall circuit refill time is overpredicted by only 20 seconds (Figure 8). This good agreement indicates that the discharge flow is well-predicted.

Pressure and mass flow oscillations can be noticed in the prediction and in the experiment both at low and high frequency: the former, observed during feeder refilling, are about the same as experimentally seen, the latter, which are due to the channel rewetting, show a frequency and amplitude two or three times greater than the measured values. This discrepancy is due to the lack of feedback between the flow regime prediction and the heat transfer mode. As a consequence, all the heated rods of a given volume are predicted to be involved simultaneously in the stored energy release. In the experimental transient, stratification causes rewetting and energy release to proceed from the lowest rods to the highest rods. Consequently, the vapour generation rate is more controlled and the oscillation amplitude and frequency are lower than predicted.

The experimental mechanism leads to a faster rewetting, as shown in the sheath temperature comparison (Figure 10). Nevertheless, the average trend is well predicted as are the most significant phenomena which take place in the refilling transient.

Figure 11 compares measured and predicted flows in the inlet feeder of the bottom channel. Qualitatively, the agreement is good, apart from a general early prediction of the oscillations. The measurement is not as accurate as the injection flow measurements (Figures 6 and 9) but can be used as a qualitative indication of oscillation characteristics.

EXPERIMENT B7907, FACILITY AND PROCEDURE

Experiment B7907 was carried out on the RD-12 loop at Whiteshell Nuclear Research Establishment. RD-12 is a light water pressurized loop which has the same configuration and components (heated horizontal channels, boilers, headers, feeders and pumps) as the primary heat transport system of a CANDU reactor³ (Figure 12). Components are not geometrically scaled to reactors.

The test simulated was a 0.361 cm^2 inlet header break with injection. The loop was brought to its initial steady state by running the pumps at 2100 rpm and setting each directly heated test section at 920 kW. The break was initiated by opening a fast acting valve. At this time (time 0) the boiler feedwater was turned off. The test section power was decreased to 7% at 2 s. The Emergency Coolant Injection (ECI) isolation valves were manually opened when the primary heat transport pressure dropped to the injection pressure (5.1 MPa(a)). The experiment was complete when the loop was full and cold.

CODE COMPARISONS WITH EXPERIMENT B7907

This experiment exhibits a late stagnation. That is, the depressurization of the broken header is balanced by the degraded pump head at Pump 1, resulting in a near zero header-to-header pressure drop across the broken test section. This low pressure drop results in low test section flow ($< 1 \text{ l/s}$) as well as a long circuit refill time ($\sim 600 \text{ s}$) providing a severe test of the codes.

After the break, the primary heat transport system starts to blow down. During the blowdown phase (0 - 20 s), the circuit pressure is controlled by the break and the boiler secondary side. The secondary side remains an effective heat sink due to the power reduction to 7% at 2 s. When the pressure reaches 5.1 MPa(a) the ECI valves open (20 s). This is the start of the refill period.

During the refill period, the boilers become a heat source. The circuit depressurization is now predominantly controlled by the outflow through the break and the inflow of cold (20°C) injection water. The pressure in the injection tank is input to the codes as a boundary condition. Therefore the ECI flow is a function of circuit pressure.

The pressure transient and the total refill time (570 s) are thus the most representative parameters of the overall circuit response.

As no information is available on RD-12 two-phase pump behaviour, the Semiscale pump characteristics were assumed. However, the FIREBIRD-III pump model uses coolant properties at the pump suction while RELAP-5 uses coolant properties averaged between the pump suction and discharge. This will result in different predictions of pump behaviour for each code.

FIREBIRD-III Results

Figure 13 shows the FIREBIRD-III prediction of the pressure in the broken header. The agreement is very good. This results in a good prediction of the onset of injection (20 s) and the refill time (520 s).

FIREBIRD-III predicts the late stagnation period as seen in the experiment. Figure 14 shows the predicted header-to-header pressure drop across Test Section 1 to be in good agreement with experiment.

The top and bottom pin sheath temperatures in the first test section node are shown in Figure 15. The first sheath temperature excursion is consistent with that of the test. The temperature is overpredicted later on due to an underprediction of header-to-header pressure drop as a result of an underprediction of pump head (Figure 16) during this time. The consistent agreement of predicted sheath temperature and pressure drop indicates that the stratification threshold of 245 kg/m²-s assumed in FIREBIRD-III is reasonable for RD-12.

FIREBIRD-III captures the circuit phenomenology and shows reasonable agreement with experiment. For this case, the FIREBIRD-III pump treatment gives a good prediction of pump performance.

RELAP-5 Results

The reference case was run using the abrupt area change option at the break and the inertial effect of the volume upstream of the break was arbitrarily increased. A sensitivity study on break discharge was performed by changing both the multiplier discharge coefficient and the inertia of the break junction.

The reference prediction for the broken header pressure (Figure 17) is reasonable except for an overprediction during the middle of the transient and an underprediction in steady state. The total refill time is also overpredicted by 100 seconds. The pressure overprediction is related to the early prediction of upstream pump head recovery (Figure 18). This leads to an underprediction of energy discharge but an overprediction of mass discharge.

The effect of break area was studied by reducing the break area to 80% of its actual value (Case A). This produces a good prediction of refill time, but the overprediction of pressure remains (Figure 19). The pump head was predicted to recover early for Case A also.

Finally, a run was done using the correct volume upstream of the break, and eliminating the abrupt area change option (Case B). The pressure transient is reasonably well-predicted (Figure 20) but the refill time is strongly overpredicted.

This is believed to be caused by an overprediction of mass discharge between 100 and 200 seconds. The overprediction begins after the temporary recovery of the pump early in the transient and is sustained by the cold water injection to the broken header.

RELAP-5 provides a reasonable prediction of the RD-12 circuit phenomena. For this case, the RELAP-5 pump treatment does not adequately predict the pump behaviour. The discrepancy in predicted pump behaviour may be related to the differences between the Semiscale pump and the RD-12 pump. The boundary condition corresponding to the secondary side is another source of uncertainty.

SUMMARY

FIREBIRD-III predictions have been compared with data from cold water injection experiments and an RD-12 blowdown plus injection experiment. The predictions are generally in reasonable agreement with the measurements, although channel refill time and sheath temperature turnaround time are underpredicted at low pressure. This is at least partly due to an early underprediction of the system pressure during the mixing of cold water and steam in the headers.

The simulation of RD-12 test B7907 shows that FIREBIRD-III can reproduce the basic features of a blowdown plus injection in a figure-of-eight circuit. Circuit pressure and refill times are well-predicted, as is the stagnation in the broken pass.

RELAP-5 has been successfully used to simulate tests 508 and B7907. The results show that the code can handle the complicated phenomenology of the refilling of parallel horizontal channels (test 508). This also holds true for a circuit prediction in which break and pump flows and voids fluctuate (test B7907).

The RELAP-5 results obtained for test 508 appear to be better than for test B7907, although from a numerical point of view test 508 was the more difficult. Discrepancies in test B7907 can be attributed to uncertainties in the two-phase behaviour of the RD-12 pumps and uncertainties in the secondary side boundary conditions.

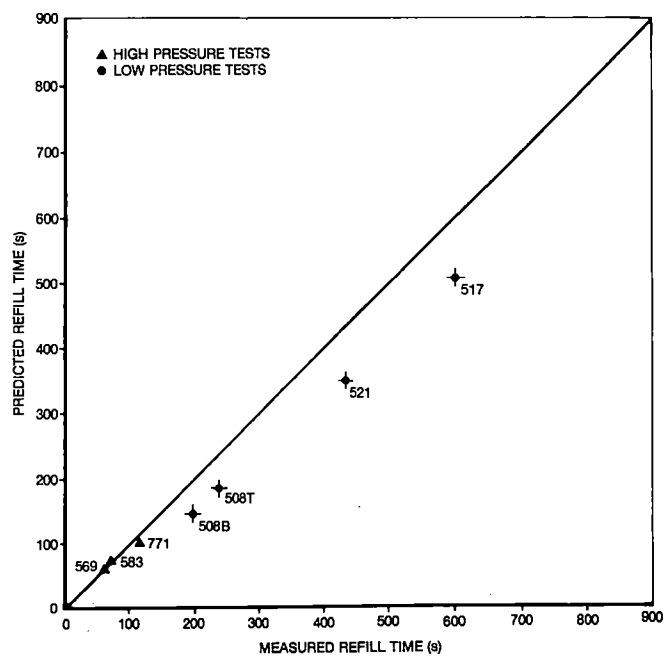
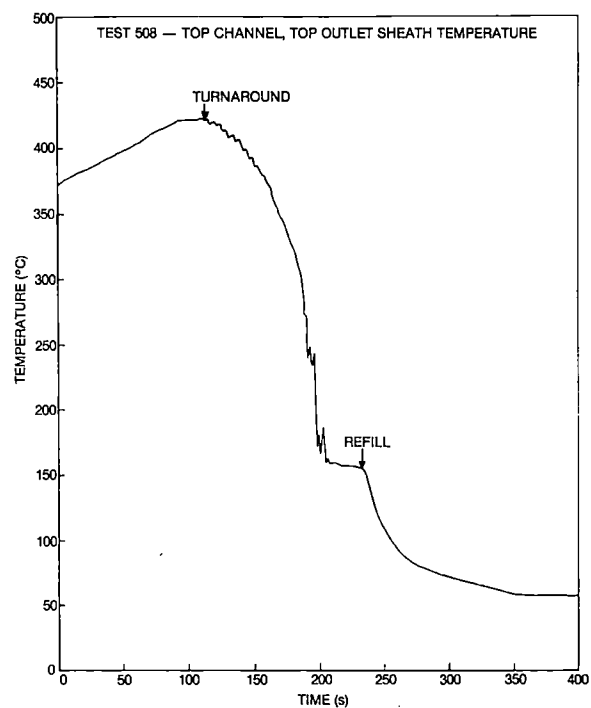
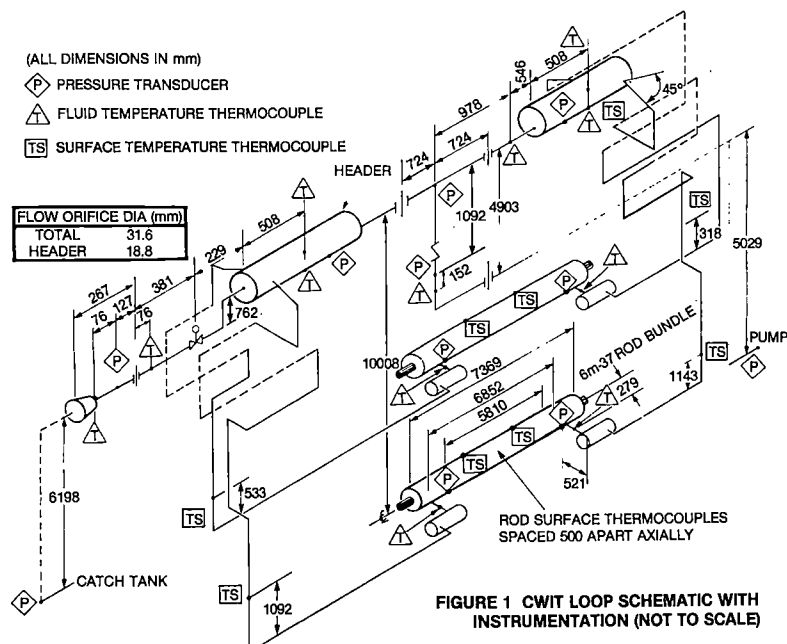
In test 508, RELAP-5 overpredicts the steam condensation rate during cold water injection. This occurs to a lesser degree in the FIREBIRD-III prediction, in spite of the homogeneous equilibrium assumption. The FIREBIRD-III pressure minimum prediction is better because of the property derivatives smoothing treatment.

The lack of RELAP-5 heat transfer modelling in a stratified channel affects the prediction of stored energy release from the heaters. However, the pressure and flow oscillations are qualitatively well predicted. In FIREBIRD-III, the oscillations are damped, but this does not significantly affect the predicted refill time.

Differences between the FIREBIRD-III and RELAP-5 predictions for test B7907 are related to the different treatment of the pumps, and different treatment of secondary side boundary conditions.

REFERENCES

1. M.R. Lin et al, "FIREBIRD-III Program Description", AECL-7533, 1982.
2. V.H. Ransom et al, "RELAP-5/MOD1 Code Manual", Volume 1, EG&G Report No. NUREG/CR-1826, March 1981.
3. "CANDU Nuclear Power System, AECL Report no. TDSI-105, January 1981.



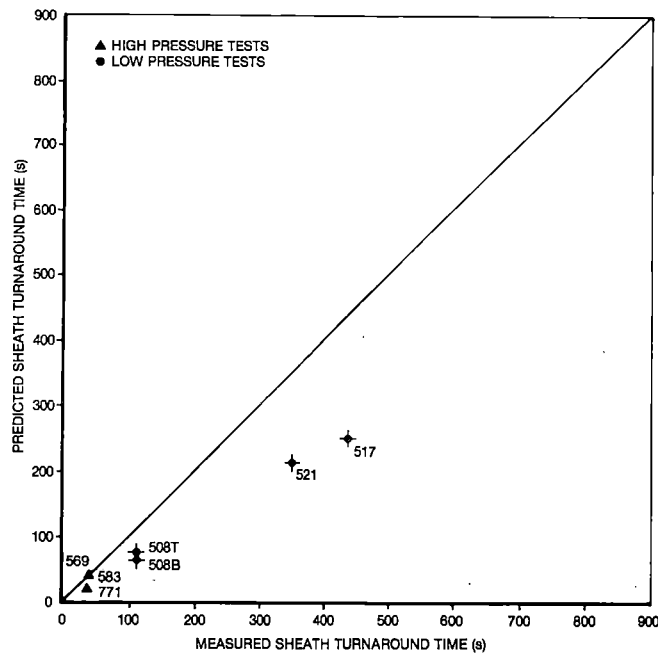


FIGURE 4 COMPARISON OF SHEATH TURNAROUND TIMES

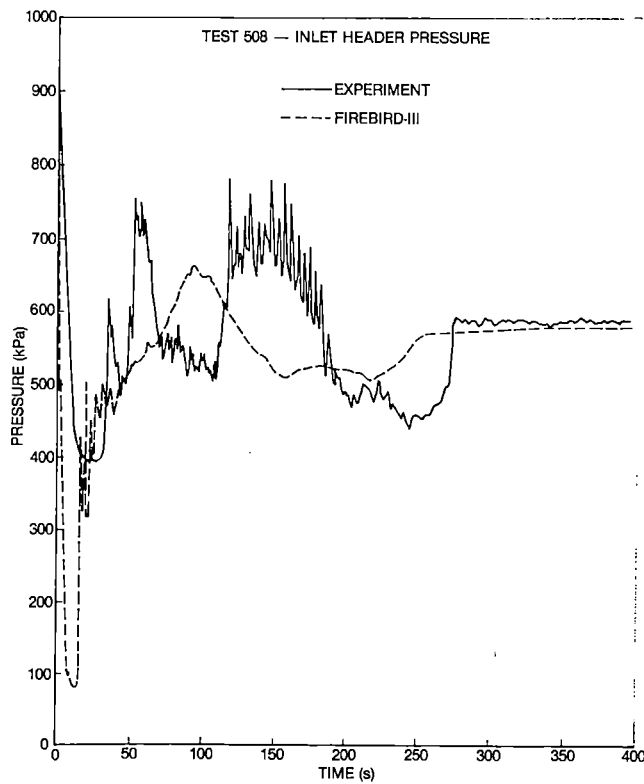


FIGURE 5 COMPARISON OF FIREBIRD-III PREDICTION WITH TEST 508 (INLET HEADER PRESSURE)

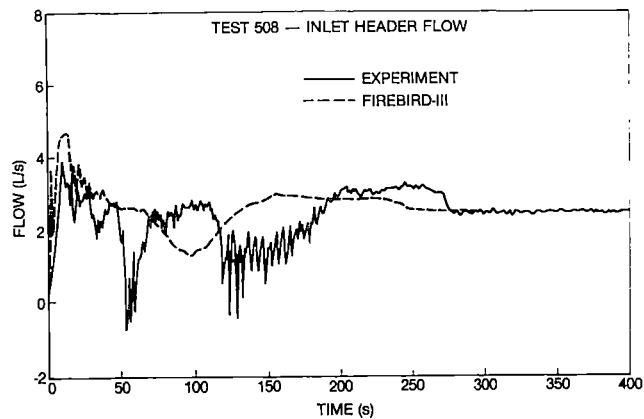


FIGURE 6 COMPARISON OF FIREBIRD-III WITH TEST 508 (INLET HEADER FLOW)

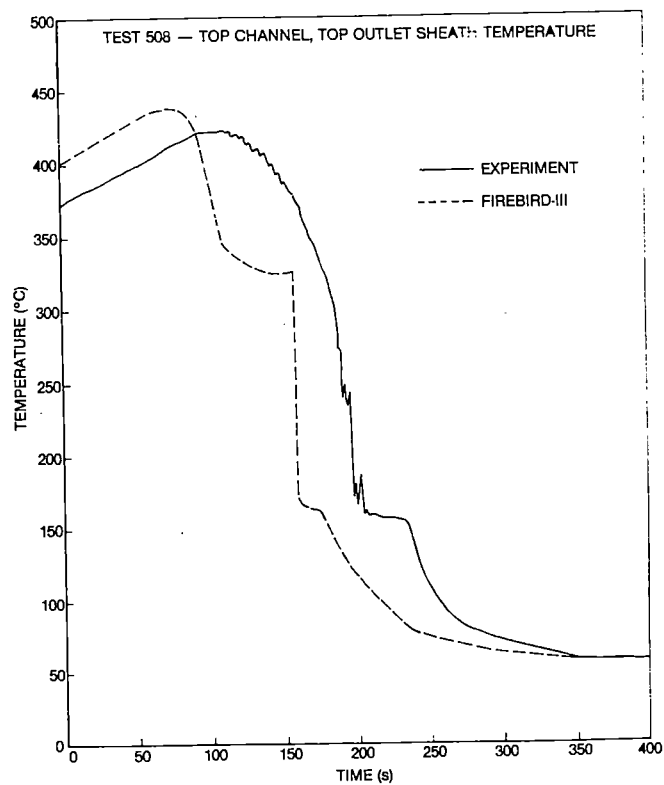


FIGURE 7 COMPARISON OF FIREBIRD-III PREDICTION WITH TEST 508 (TOP CHANNEL, TOP OUTLET SHEATH TEMPERATURE)

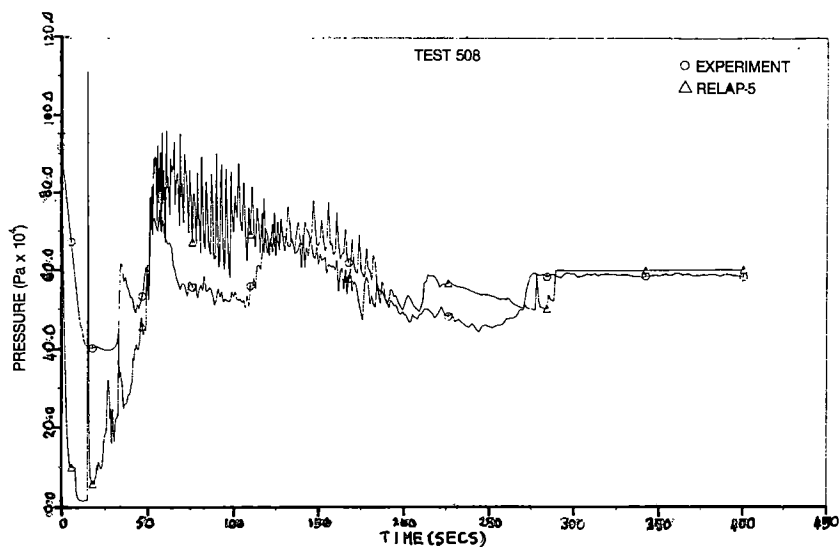


FIGURE 8 INLET HEADER PRESSURE (EXP. AND CALCULATED)

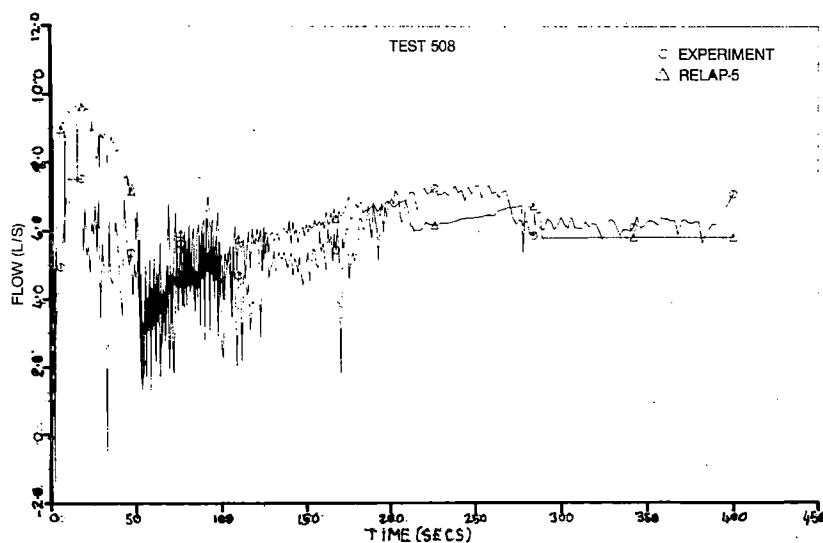


FIGURE 9 TOTAL INJECTION MASS FLOW (EXP. AND CALCULATED)

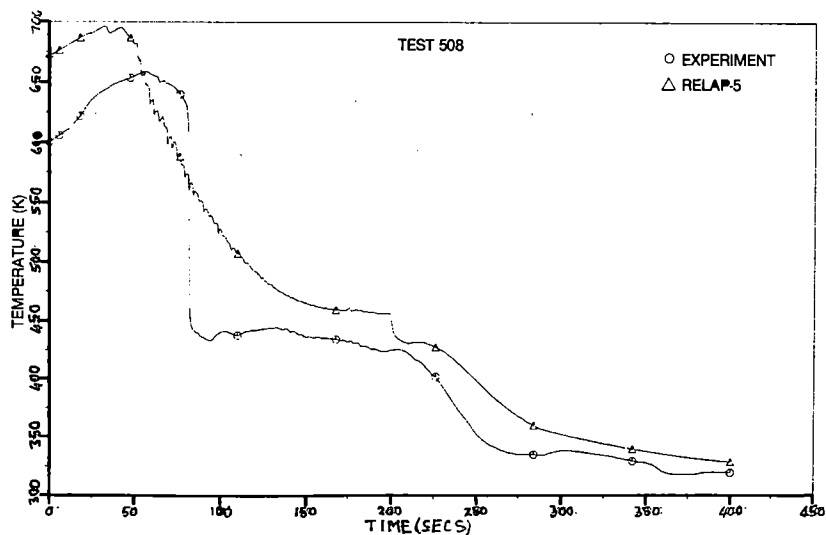


FIGURE 10 TOP CHANNEL, INLET SHEATH TEMPERATURE (EXP. AND CALCULATED)

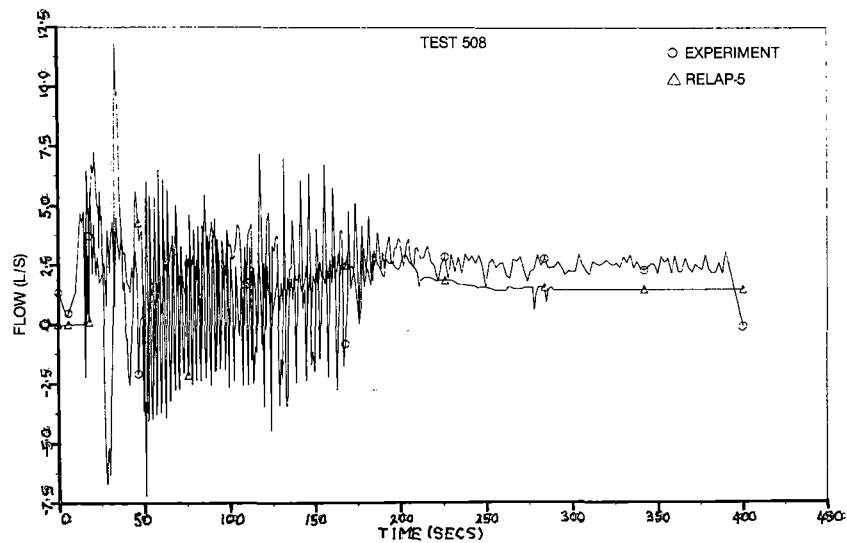


FIGURE 11 BOTTOM CHANNEL INLET FEEDER FLOW

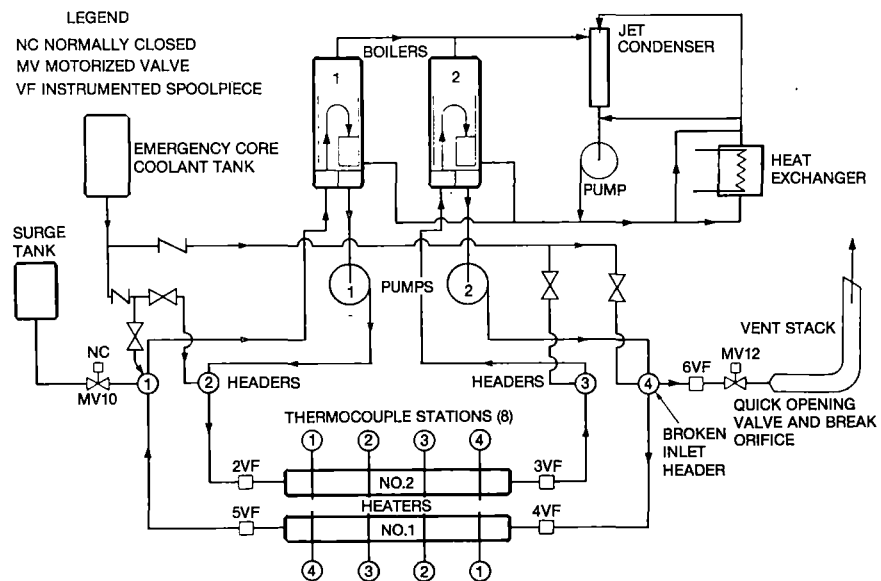


FIGURE 12 RD-12 LOOP SCHEMATIC DIAGRAM

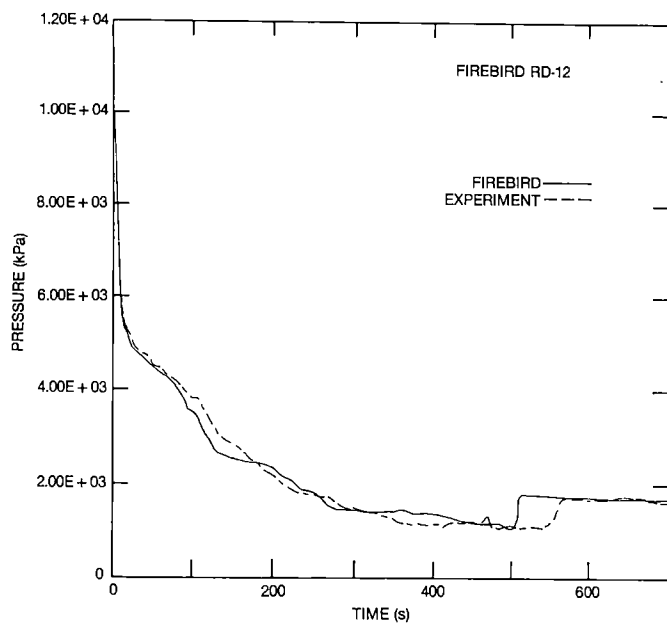


FIGURE 13 COOLANT PRESSURE IN BROKEN HEADER

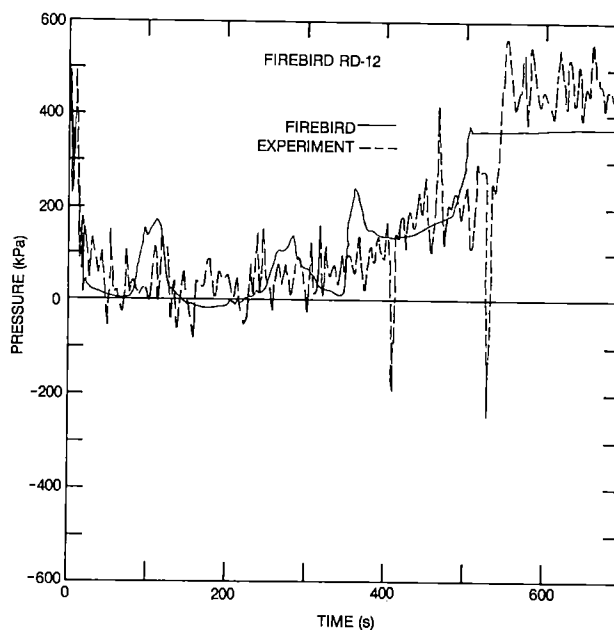


FIGURE 14 HEADER TO HEADER PRESSURE DROP ACROSS TS1

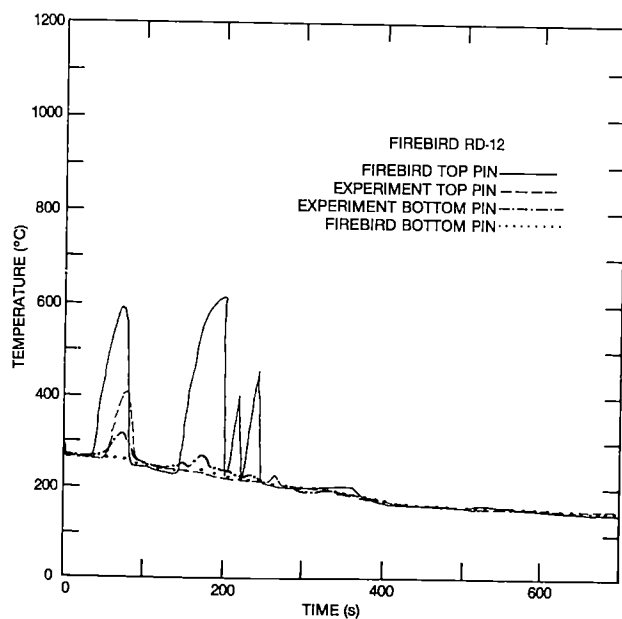


FIGURE 15 SHEATH TEMPERATURE IN TS1 FIRST TS NODE

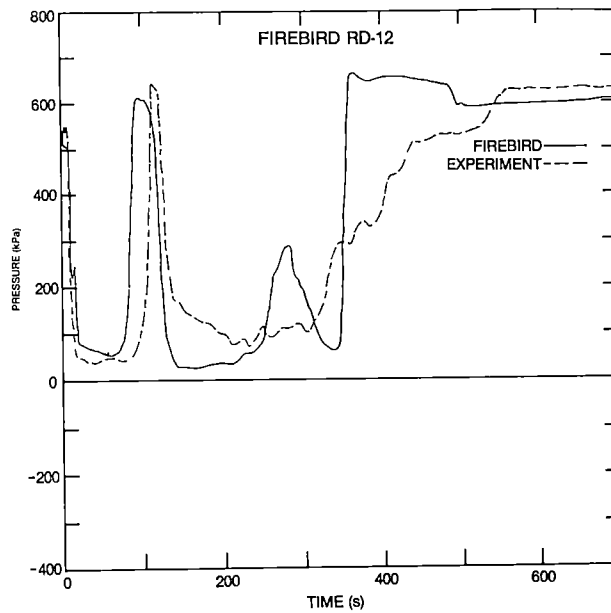


FIGURE 16 PUMP TWO HEAD

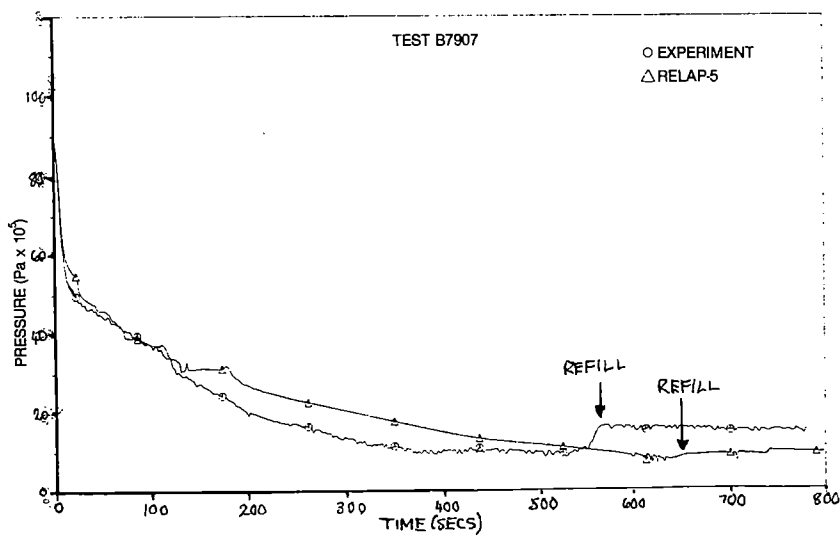


FIGURE 17 COOLANT PRESSURE IN HEADER 4 (BROKEN HEADER)

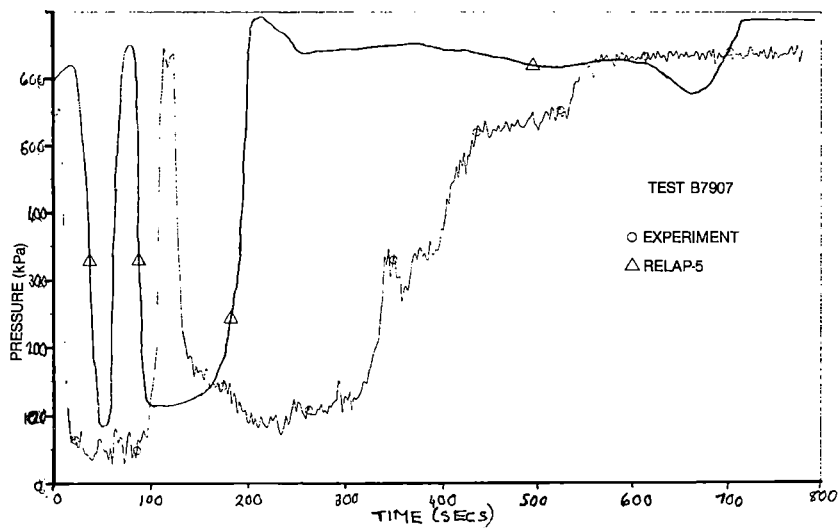


FIGURE 18 PUMP 2 HEAD

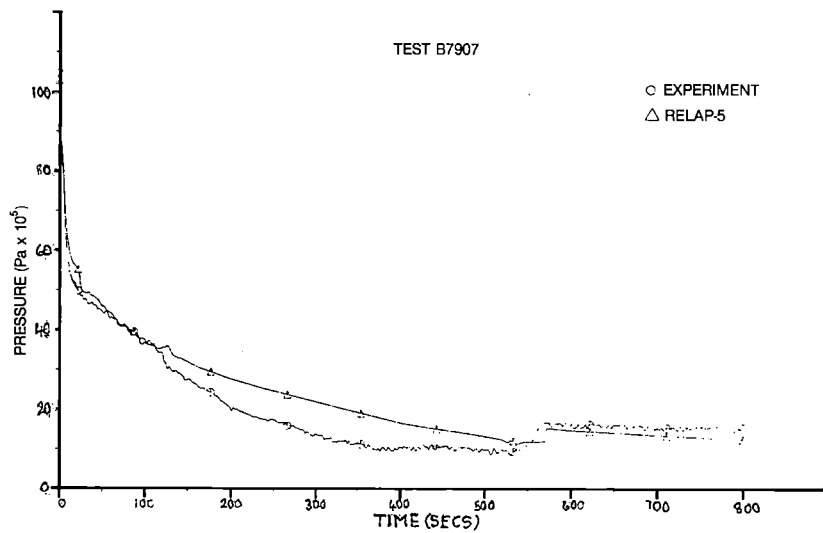


FIGURE 19 CASE A COOLANT PRESSURE IN HEADER 4

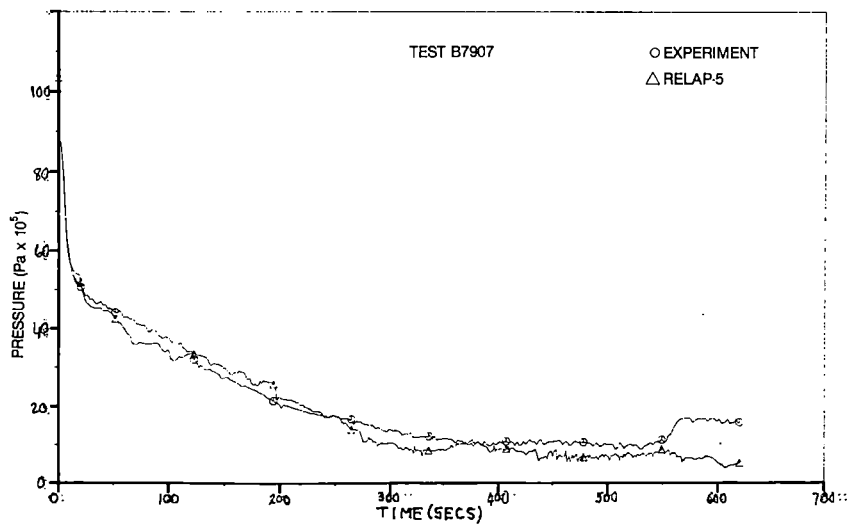


FIGURE 20 CASE B COOLANT PRESSURE IN HEADER 4

TWO-PHASE FLOW BEHAVIOUR OF AXIAL PUMPS

W. G. Kennedy - Combustion Engineering Inc., Windsor, Conn. USA
W. Kastner - Kraftwerk Union AG, Erlangen, FRG
G. J. Kanupka - Combustion Engineering Inc., Windsor, Conn. USA
J. D. Fishburn - Combustion Engineering Inc., Windsor, Conn. USA
A. Lang - Anstalt für Strömungsmaschinen GmbH, Graz, Austria
K. Riedle - Kraftwerk Union AG, Erlangen, FRG
G. Seeberger - Kraftwerk Union AG, Erlangen, FRG

ABSTRACT

The LOCA analysis for a PWR requires a model of the primary coolant pump under single and two-phase flow conditions. To verify and improve this model an experimental program was carried out. A one-quarter and a one-fifth scale model of an axial flow type pump used in many KWU-PWR's were tested under steady-state and transient conditions over ranges typical for a PWR LOCA. The steady-state data can be plotted as hydraulic similarity curves $H/H_R = f(Q/Q_R, N/N_R)$ but with the void fraction and absolute pressure as additional parameters. The transient data from blowdown tests for various break sizes follow the corresponding steady-state values closely as long as critical flow conditions in the pump are not reached.

SCOPE OF WORK

The LOCA analysis for a PWR requires a mathematical model of the reactor coolant pump (RCP) behaviour under single and two-phase flow conditions, which takes into account the complex interaction between the fluid in motion and the rotating impeller in the two-phase mixture during a postulated accident. Some models used until now are based on scarce experimental data gained on test pumps which do not cover the geometrical and hydraulic conditions of RCP's. To verify and improve these models for KWU's axial flow type RCP a research project sponsored by the German Federal Ministry of Research and Technology was carried out. A one-quarter and a one-fifth scale model of an axial flow type pump were tested under steady-state conditions with single-phase water, steam and with two-phase mixtures, that is for void and pressure ranges typical for a PWR LOCA. The ranges of flow rate and speed of the tested one-fifth scale model pump in comparison with the operating range of RCP's in event of hypothetical LOCA's are shown in Fig. 1. To insure the applicability of the steady-state experimental data to the LOCA transients, blowdown tests for various break sizes were run with the one-fifth scale pump.

SCALING LAWS

The application of model pump tests to full scale pumps relies on laws of similarity. At conditions above a certain Reynolds and below a certain Mach number, which have generally been adhered to in the test program, the basic square-root relationship between velocities in and pressure differences across the pump exists. This allows the pump characteristics to be drawn as hydraulic similarity curves for single-phase flow. In exploring any two-phase effects on the scaling laws, two sizes of the same pump model were tested, and tests at hydraulically similar points involving various pump speeds were carried out, i. e. different absolute velocities at constant impeller entrance flow angles. Since both size and speed variations have not shown any remarkable differences, it seems to be demonstrated that the regular scaling laws also apply to a significant range of two-phase flow conditions.

MODEL PUMPS

Two model pumps of the type shown in Fig. 2 were designed with impeller diameters of 150 and 200 mm for the experiments. Besides the geometric similarity to a typical RCP they are also similar in regard to the seal system, bearing oil supply, bearing and cooling systems. The rated pump data of the full size RCP and the two model pumps are listed in Fig. 3.

TEST FACILITY

The pump test facility located at Combustion Engineering Inc., Windsor, Conn. was designed to provide single and two-phase steam/water conditions and transient blowdown capability at pressures up to 83 bar. Maximum steady-state flow capability was 0.28 m³/s with the 150 mm test pump ($1.4 \cdot Q_R$) and 0.38 m³/s with the 200 mm test pump ($1.09 \cdot Q_R$). Index R means rated.

The basic elements of the test facility are shown in Fig. 4. Water from the high pressure drum and boiler steam were mixed. Before entering the test pump the two-phase mixture flowed through a measuring section and a down-scaled elbow typical for the reactor system geometry. On exiting from the test pump the mixture entered another measuring section and returned to the high pressure drum. Transient loop blowdowns were run by means of a branch connecting pipe containing a stop valve and a rupture disc assembly. The steam-water mixtures could be supplied to either the test pump suction or discharge through a reversible piping arrangement. This allowed testing of the pump in both flow directions.

INSTRUMENTATION

The instrumentation besides monitoring the loop and the test pump provided data for mass flow rate, head, pump speed and hydraulic torque. Due to a matrix of test points which specified forward and reverse flow and likewise forward and reverse rotation of the model pump, the information on quality, void and density was required at both the pump inlet (before the elbow) and outlet. Fig. 5 shows a schematic of the test pump instrumentation.

STEADY-STATE-TESTS

Testing procedure

The test loop was initially set up for the required flow direction, i.e. forward or reverse. Based on the particular type of test points to be run, the loop was then set up for one of three basic operating modes:

- single-phase water flow
- single-phase steam flow
- two-phase flow

For single-phase water tests water was circulated by the booster and/or test pumps around the test loop. Steam was fed into the high pressure drum to obtain the specific temperature of loop water called for by the test point parameters.

Single-phase steam points were obtained by admitting steam to the mixing tee while the loop was empty. The steam flowed through the test pump to the high pressure drum. The booster pumps were not used.

Two-phase test points were achieved by admitting steam to the mixing tee while saturated water was circulated in the loop by the booster and/or test pumps.

Test matrix

Some 600 steady-state tests were chosen to cover the range relevant to a PWR LOCA, to meet the hydraulic aspects essential for an assessment of the head characteristics (e.g. design point of the model pumps) and to permit a comparison with other two-phase pump tests. The scheme of the steady-state test matrix can be seen from Fig. 6.

Test results

The test results can be presented in many different forms which facilitate scaling from model tests to full size pumps and extrapolating to hydraulic conditions outside the tested range. Here we chose dimensionless groups such as

$$\frac{H/H_R}{(N/N_R)^2 + (Q/Q_R)^2} = f \left(\frac{N/N_R}{Q/Q_R} \right)$$

and

$$\frac{T/T_R}{(N/N_R)^2 + (Q/Q_R)^2} = f \left(\frac{N/N_R}{Q/Q_R} \right)$$

relations first used by Suter /1/ and Gluckman /2/, but present these functions in a modified form. Fig. 7 and 8 show results for the 150 mm pump for the whole range of pump operation with the void fraction as a parameter. In this case, a significant dependency of pump head and torque on void can be seen primarily in the regimes of normal pumping (forward flow, forward rotation) and dissipation (with reverse flow and forward rotation).

The degradation of the head with increasing void fraction at the pump inlet for rated volumetric flow and pump speed and different pressures is shown in more detail in Fig. 9. Taking the curve for 66 to 72 bar the head started to degrade continuously from zero void up to 0.30. The head declined more steeply near 0.40 void fraction, reached a minimum of 13 percent near a void fraction of 0.75, and then rose in an increasingly steep recovery to higher all-steam values. The reason for the head degradation is assumed to be the occurrence of a more and more severe phase separation adversely affecting the boundary layer and causing the flow to deviate from the rotating and guide blade contours, and also changing the velocity triangles. The result was a strong influence on the efficiency of the pump.

The higher pressures tended to suppress the two-phase effects, while lower pressures generally magnified the two-phase effects, even leading to negative head values at pressures below 55 bar. The more severe two-phase effects at low pressures were expected due to the increased size of bubbles and greater differences between steam and water densities, which promote the friction between the phases and the pump resistance.

The curves of head degradation are appropriate for comparing test results from various flow-category pumps, Fig. 10. The single-phase (water) performance of pumps varies considerably with design and does not correlate simply with any single index such as specific speed. Two-phase flow effects also vary with pump design. The data of the radial flow type pump /3/ shows rapid and strong head degradation starting at low void fractions. The head curve for the axial flow pump is less precipitous and is quite similar to that for the mixed flow pump tested within a C-E/EPRI program /4/. For maximum degradation, in both cases, the head drops down to about 15 % of the water value. The similarity of the 200 and 150 mm test pump data was considered good (not shown in this diagram).

TRANSIENT TESTS

Testing procedure

All blowdown tests were preceded by a period of steady-state operation with loop circulation, if any, generated by the test pump because the booster pump rotors were locked during the blowdown runs. A few seconds before blowdown started, loop circulation was interrupted by closing the valve in the return line to the high pressure drum and, if desired, the test pump motor power was turned off. Then rupture of the diaphragms at the end of the blowdown line initiated depressurization of the loop, and the fluid flashed to progressively higher void fractions until flow through the pump was all steam.

Test matrix

To achieve a large variety of transient operating conditions blowdown tests were run for different sets of specifications. These comprised both forward and reverse flow, four modes of pump operation and six break sizes, as can be seen from Fig. 11. One test with the pump removed, and a piping elbow substituted, served to check out the transient test procedures, instrument response, and data handling. It also provided data on the blowdown behaviour of the test loop with-

out any effect of the pump. The network of the further tests was, in part, tailored to provide data to assess the onset and extent of flow choking in the pump, which became apparent during the testing.

Test results

Fig. 12 shows hand-smoothed average curves which were drawn for a typical blowdown transient. The test system depressurized rapidly during the initial fraction of a second after rupture, indicating a subcooled blowdown period. Then the pump suction pressure decayed at a nearly constant rate during most of the saturated blowdown period, while the pump discharge pressure fell rapidly to a fraction of the upstream pressure. This pressure ratio is further discussed below relative to possible flow choking in the pump. A mixture of saturated water and steam was expelled through the break for a period of the order of 60 seconds after rupture. At that time, near 125 seconds in the plot, a distinct change in the slope of the pressure-time curves took place due to depletion of the liquid, so that the fluid became mostly steam expanding as a compressible gas. Soon afterwards, the suction side as well as the discharge side of the test pump was essentially voided of liquid, and the void fraction reached a value of approximately 1.0.

The volumetric flow rate behaviour shows an initial rapid increase from the pre-rupture stagnation value, quickly reaching a "plateau" of nearly steady or slowly rising values which lasted for about 40 seconds. As the piping became voided of liquid, the volumetric flow rate again increased rapidly, reaching a peak value before slowly falling off.

From sets of blowdown curves such as those in Fig. 12, "snapshots" of operating conditions and pump performance parameters were extracted at various void fractions (see dots) for comparison with steady-state performance curves at the same void fractions. Such a comparison is shown in Fig. 13 for head values at 0.40 void fraction from forward flow blowdowns. Agreement with steady-state performance was much closer for smaller breaks without critical (choked) flow in the test pump. Agreement was also found to be good even for a large break (100 % break size, 0.75 rated speed) at low void fractions just after rupture, when the transient changes were strong but critical flow had not been reached.

To see when choking occurred in individual blowdowns, the pressures and mass flow rates were compared against theoretical critical flow values as a function of time for two test runs, which had 57 and 100 % break sizes respectively, Fig. 14. These curves indicate that choking in the test with constant speed of 0.75 rated and 100 % break size started near 0.35 void fraction. By using a single selected value for the throat area, good agreement between measured mass flow rates and the Homogeneous Equilibrium Model was reached for the whole blowdown transient as soon as the critical pressure ratio was exceeded. For the test with 0.75 rated speed but 57 % break size it appeared from looking at the pressure ratio and using the same value of throat area that choking never occurred.

From this the conclusion can be drawn, that the pressure ratio

$$\left[\frac{p_{\text{upstream}}}{p_{\text{downstream}}} \right]_{\text{EXP}} \quad \bigg/ \quad \left[\frac{p_{\text{upstream}}}{p_{\text{throat}}} \right]_{\text{HEM}}$$

gives evidence whether choking occurred or not. A stronger pressure drop than theoretically necessary for choking gives a pressure ratio greater than unity.

Fig. 15 shows the comparison of the pressure ratios based on blow-down measurements and homogeneous equilibrium theory for 0.40 upstream void fraction in forward flow blowdowns with locked rotor, constant speed and free-wheeling pump modes. This check indicates that for 0.40 upstream void there was strong likelihood of choking in the test pump for a break size of at least 40 % for the locked rotor blowdowns, and at least 50 to 70 % for the 0.40 and 0.75 constant speed and the free-wheeling blowdowns.

At about the same break sizes as where the pressure ratios rose past unity the curves of the mass flux ratio G_{EXP}/G_{HEM} for both constant 75 % of rated speed and free-wheeling leveled off. A further increase of mass flow rates was not possible due to choking in the pump. The curves for 40 % speed and for locked rotor were only partially defined by experimental data, but they were compatible with the trends of the complete curves and showed a shift toward smaller break sizes for the pressure ratio crossover past unity. This shift was expected because the lower pump speeds caused more turning of the flow in the pump impeller, with more pressure loss and an effectively smaller flow area.

When choking occurred the curves of the mass flux ratio must reach unity, Fig. 15. From this statement the effective minimum flow areas in the test pump for various pump modes can be calculated, as the throughput is known from measurements with drag discs, turbine meters and gamma densitometers and the theoretical critical mass flow rate is given by the Homogeneous Equilibrium Model. As a function of the normalized speed, resulting critical cross-sections in the 150 mm test pump are shown in Fig. 16. The minimum flow areas increase only slightly with the speed, which was zero for locked rotor, and 40 and 75 % for constant speed. With the calculated critical cross-section for the free-wheeling blowdown the speed at which choking is indicated is about 50 %.

CONCLUSIONS

- From the tests performed it seems to be demonstrated that the scaling laws which apply to single-phase flow also are valid for a significant range of two-phase flow conditions.
- The degradation of head and torque with changing void fraction is also a function of the pressure, especially at low pressure levels.
- The test results can be presented as cyclic curves for head and torque under both single- and two-phase flow conditions, taking into account the two-phase flow effects by void and pressure, e.g.

$$\left[\frac{H/H_R}{(N/N_R)^2 + (Q/Q_R)^2} \right]_{TP} = \left[\frac{H/H_R}{(N/N_R)^2 + (Q/Q_R)^2} \right]_{SP} \cdot f_1(p) \cdot g_1(\alpha_F)$$

and

$$\left[\frac{T/T_R}{(N/N_R)^2 + (Q/Q_R)^2} \right]_{TP} = \left[\frac{T/T_R}{(N/N_R)^2 + (Q/Q_R)^2} \right]_{SP} \cdot f_2(p) \cdot g_2(\alpha_F)$$

with correction functions of p and α_F for each pump regime.

- Behaviour of axial and mixed flow type pumps agreed very well but was quite different from radial pump performance.
- No discernible influence of test model scale could be ascertained.
- The transient test results agree with steady-state data quite closely if no choking in the pump occurred.
- A criterion for critical flow conditions occurring in the pump was found to be dependent on the ratio between the pressures at pump inlet and outlet, break size and speed.
- The above criterion is supported by the mass flux behaviour during blowdowns, i.e. leveling off at values corresponding to critical mass flow rates. From this behaviour the effective minimum flow areas in the pump, as a function of the speed, could be calculated.

NOMENCLATURE

Letters

f, g	Function
G	Mass flux (flow/area)
H	Pump head
N	Pump speed
p	Pressure
Δp	Pressure difference
Q	Volumetric flow rate
T	Hydraulic torque normalized for density
t	Time
V	Velocity
α_F	Void fraction
ρ	Density
θ	Temperature (Index R: Resistance Thermometer, Index T: Thermocouple)

Indices

EXP	Experiment
HEM	Homogeneous Equilibrium Model
R	Rated
SP	Single-Phase
TP	Two-Phase

REFERENCES

- /1/ P. SUTER
Representation of Pump Characteristics for
Computation of Water Hammer
Sulzer Technical Review, 1966, pp. 45 - 48

- /2/ R. GLUCKMAN and M. W. E. CONEY
An Investigation of the Four-Quadrant Performance
of a Centrifugal Pump with Single and Two-Phase
Flow of Refrigerant 12
European Two-Phase Flow Group Meeting, Ispra, Italy,
Paper A4, 1979

- /3/ D. J. OLSON
Experimental Data Report for Single- and Two-Phase
Steady-State Tests of the 1 1/2 - Loop Mod-1 Semiscale
System Pump
Report ANCR-1150, Aerojet Nuclear Company, 1974 A

and

Single- and Two-Phase Performance Characteristics of
the Mod-1 Semiscale Pump under Steady-State and Tran-
sient Fluid Conditions
Report ANCR-1165, Aerojet Nuclear Company, 1974 B

- /4/ W. G. KENNEDY, M. C. JACOB, J. C. WHITEHOUSE,
J. D. FISHBURN, G. J. KANUPKA
Pump Two-Phase Performance Program
Project 301
Report EPRI-NP-1556, Vol. 1 - 8, Sept. 1980

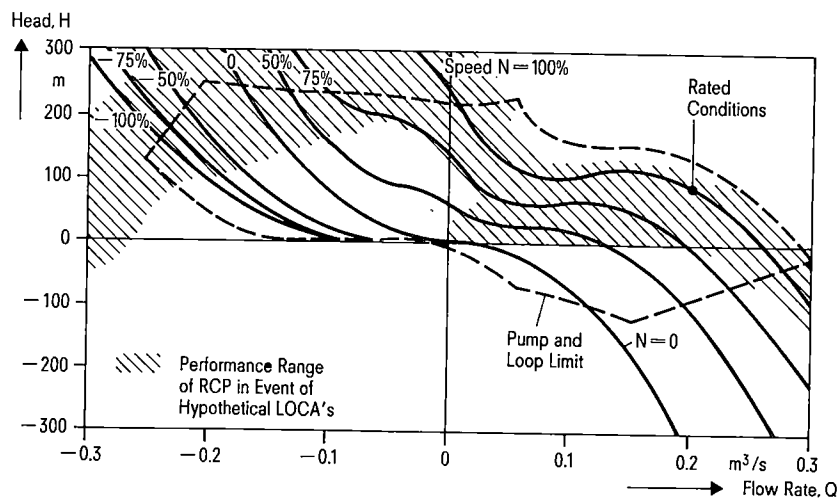


Fig. 1 Characteristic Properties of the 150 mm Test Pump with Single - Phase Flow

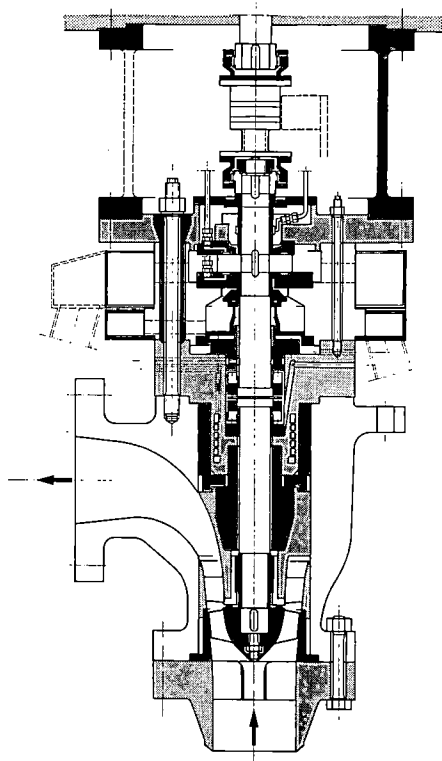


Fig. 2 Model Pump

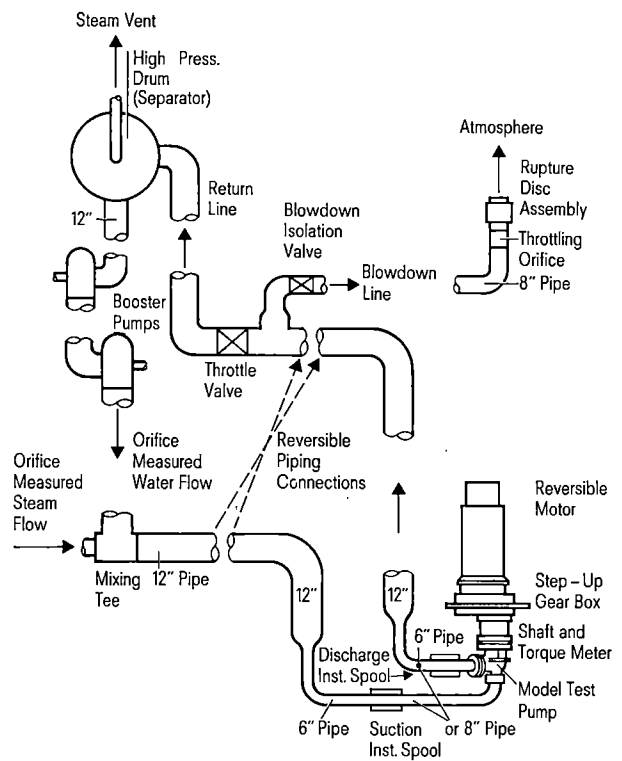


Fig. 4 Basic Elements of Test System

Title	Reactor Coolant Pump Type	Scale - Model Pumps		Units
		1 : 4	1 : 5	
Dia. of Impeller	853	200	150	mm
Volume Flow	6.46	0.35	0.20	m ³ /s
Head	92.0	93.3	89.5	m
Hydraulic Torque	—	616.0	257.3	Nm
Speed	1490	6360	8480	min ⁻¹

All Ratings for Cold Water Density, 998 kg/m³

Fig. 3 Rated Pump Parameters

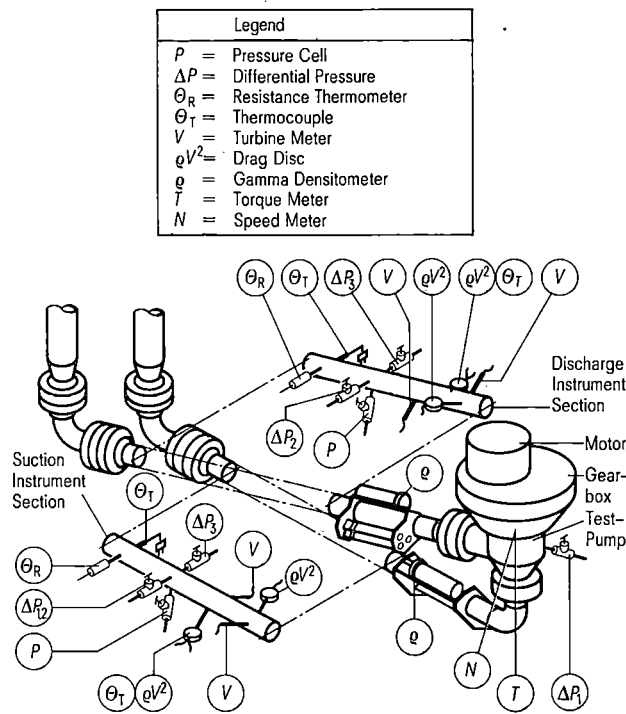


Fig. 5 Test Pump Instrumentation

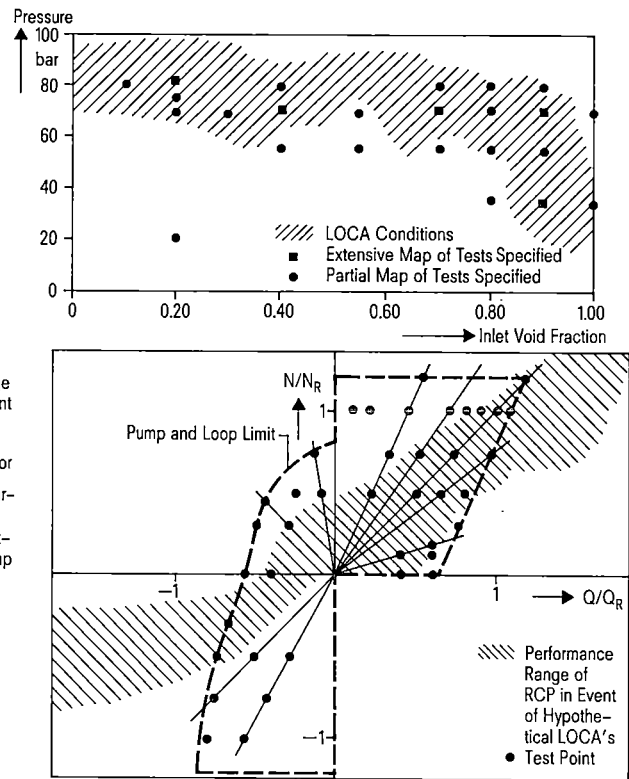


Fig. 6 Steady - State Test Matrix

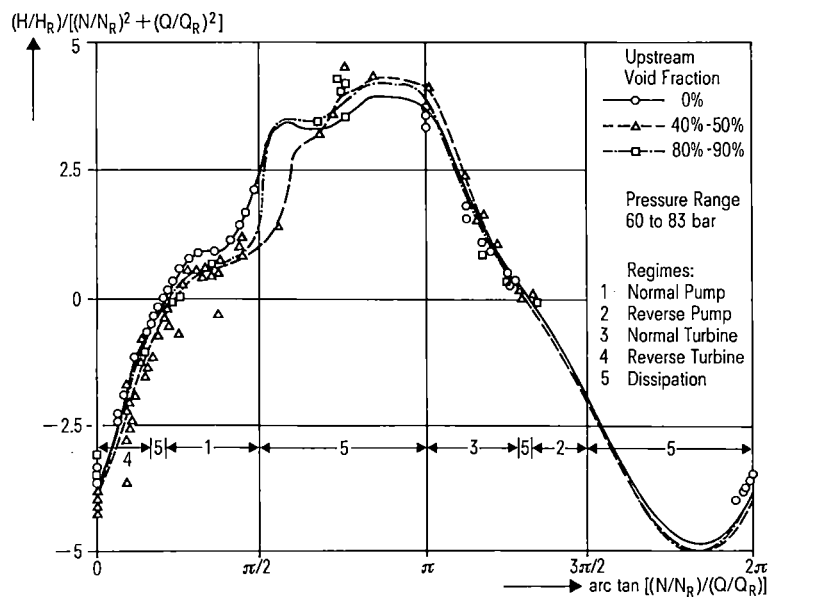


Fig. 7 Cyclic Head Curves for Single- and Two-Phase Flow with the 150 mm Test Pump

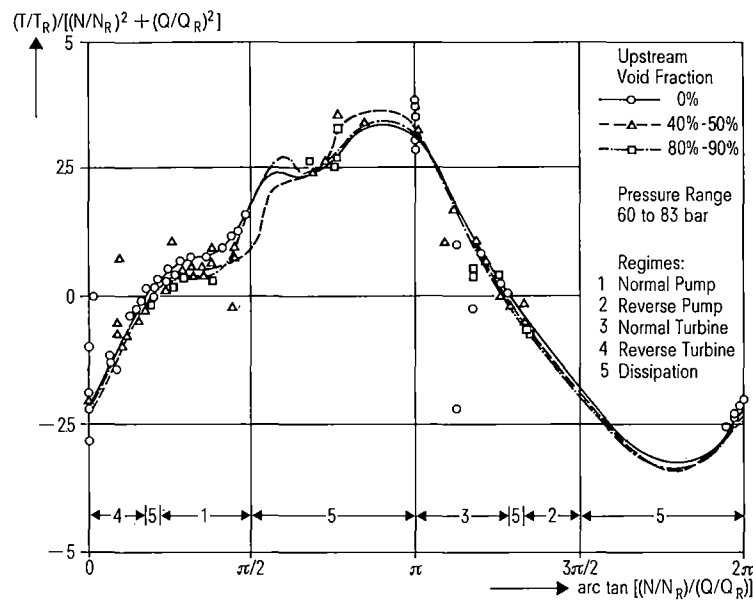


Fig. 8 Cyclic Torque Curves for Single- and Two-Phase Flow with the 150 mm Test Pump

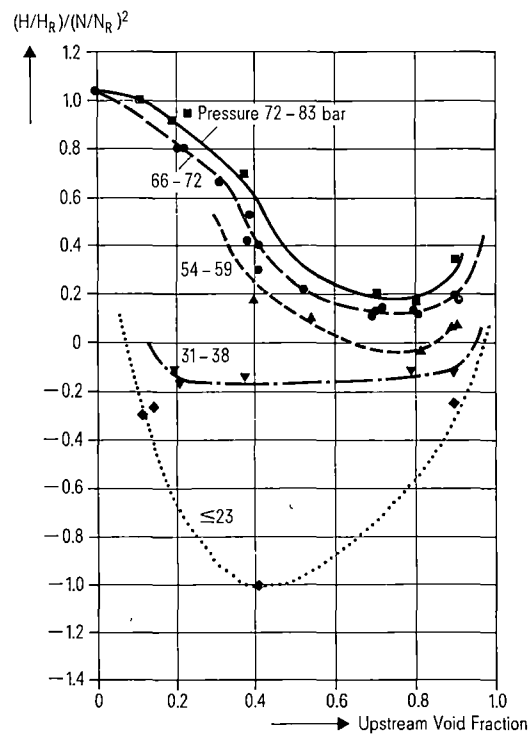


Fig. 9 Head Degradation as Function of Void and Pressure for Forward Flow, Volumetric Flow and Pump Speed Near Rated with the 150 mm Test Pump

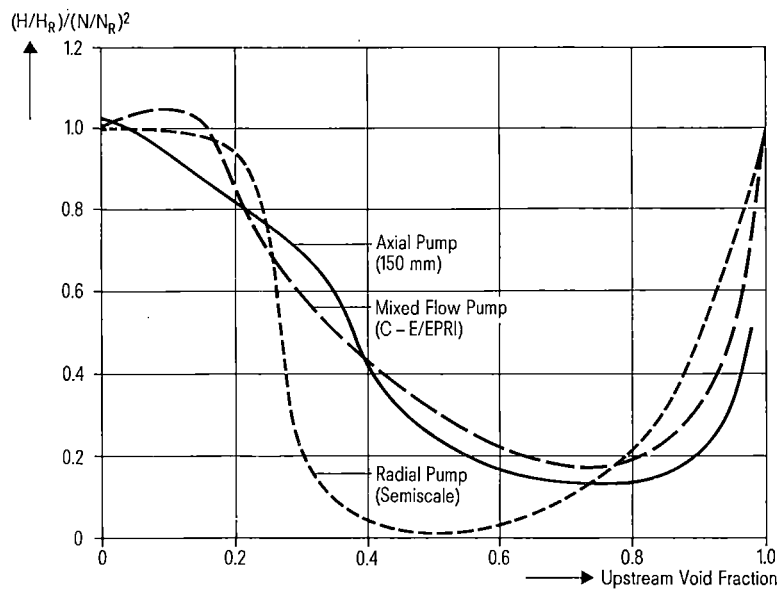


Fig. 10 Comparison of the Two-Phase Flow Behaviour of Different Test Pumps at about 69 bar for Speed and Volumetric Flow Near Rated, Forward Flow

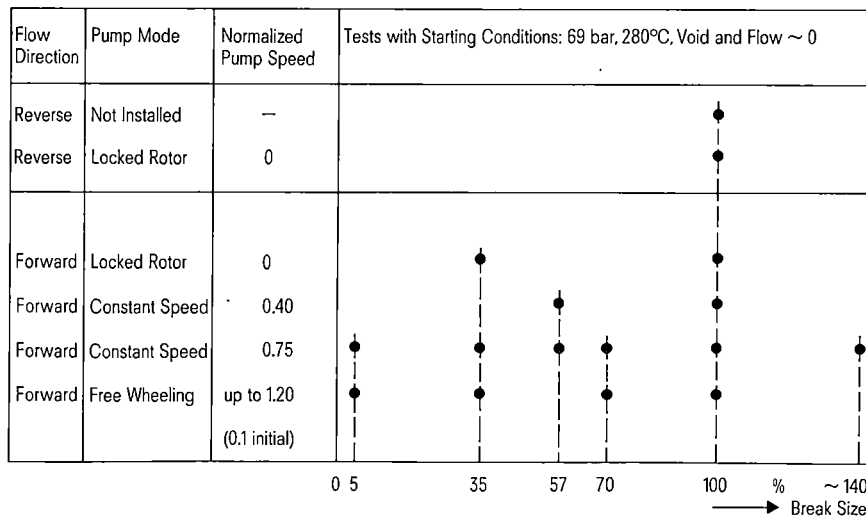


Fig. 11 Transient Test Matrix

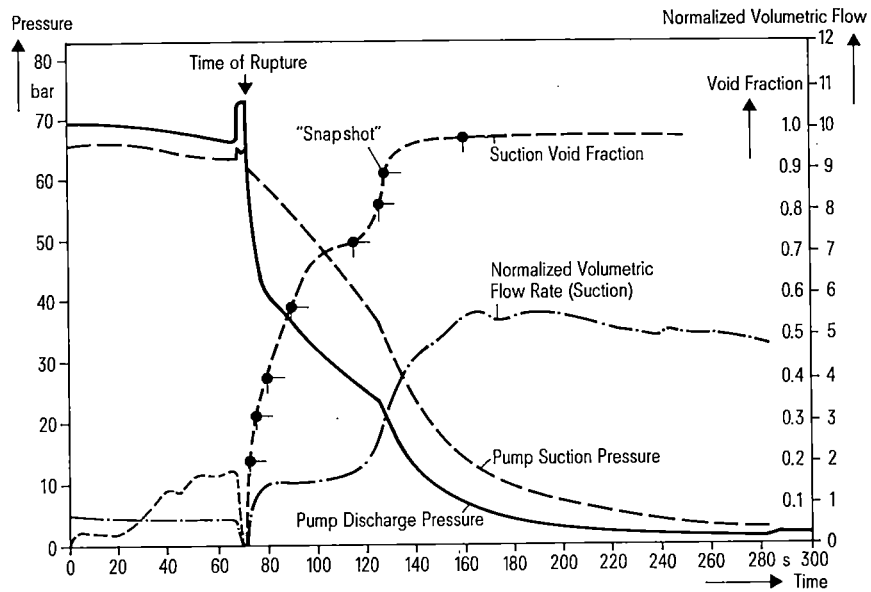


Fig. 12 Transient Test No. 4473 with 100% Break Size at 0.75 Rated Speed

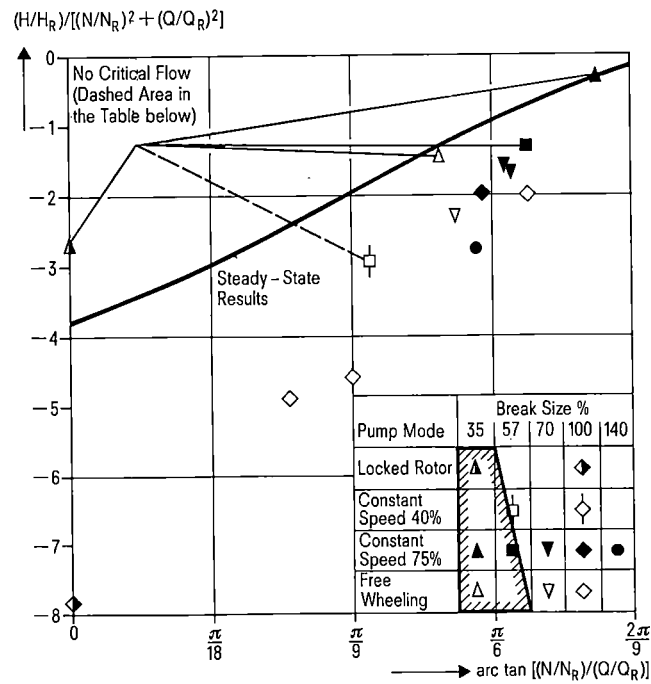


Fig. 13 Comparison of Steady-State versus Transient Data from Forward Flow Blowdowns at 69 bar and 40% Void with the 150 mm Test Pump

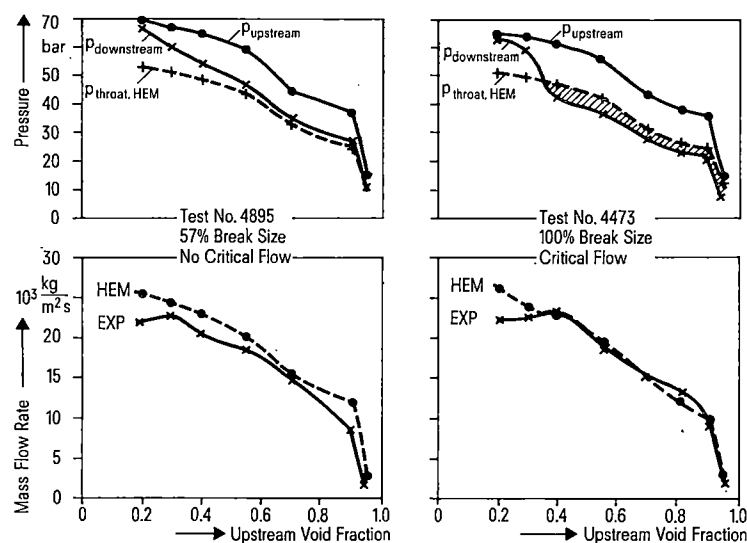


Fig. 14 Check for Choked Flow Conditions in the 150 mm Test Pump in Forward Flow Blowdowns with Constant Speed 75% Rated

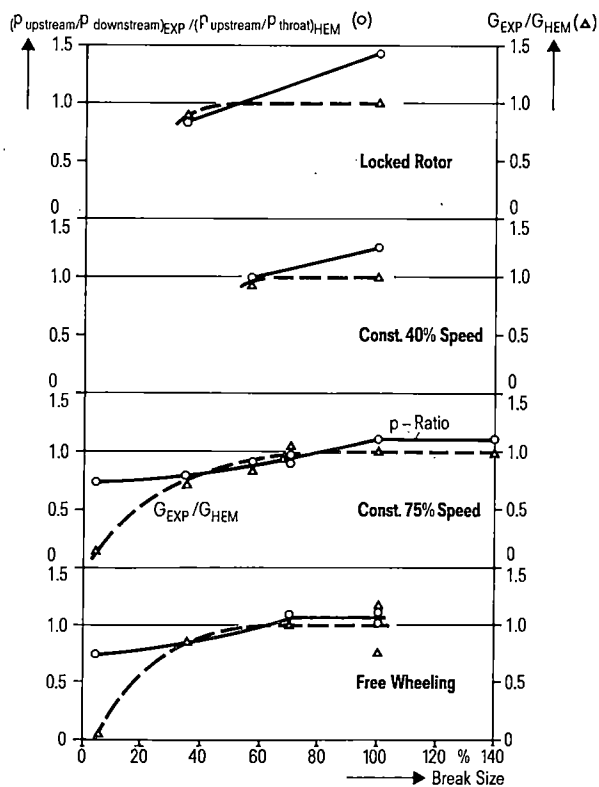


Fig. 15 Check for Choked Flow Conditions in the Model Pump (150 mm) at 0.40 Void Fraction in Forward Flow Blowdowns

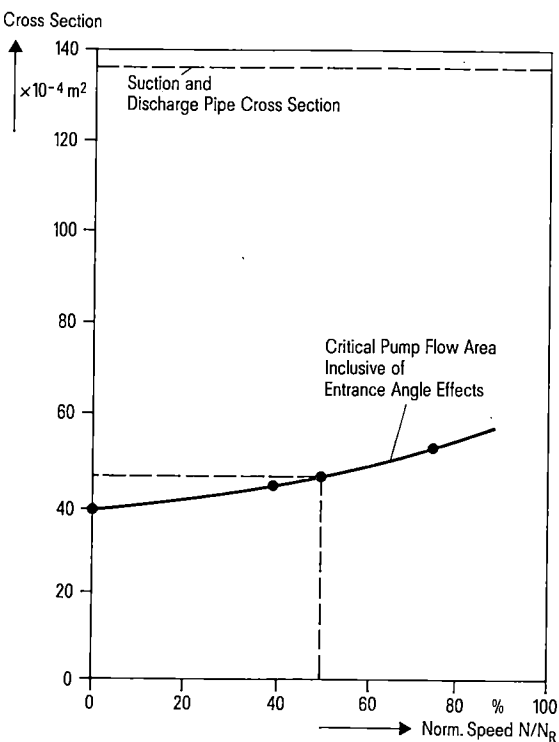


Fig. 16 Calculated Critical Cross-section in the 150 mm Test Pump (Inclusive of Entrance Angle Effects) as Function of Impeller Speed at Forward Flow, 40% Void Fraction

THE EXPERIMENT PREDICTION FOR LOFT NUCLEAR
EXPERIMENTS L5-1 AND L8-2

Tien-Hu Chen and Slawomir M. Modro

EG&G Idaho, Inc.
P.O. Box 1625
Idaho Falls, Idaho 83415

ABSTRACT

The LOFT Experiments L5-1 and L8-2 simulated intermediate break loss-of-coolant accidents with core uncovering. This paper compares the predictions with the measured data for these experiments. The RELAP5 code was used to perform best estimate "double-blind" and "single-blind" predictions. The double-blind calculations are performed prior to the experiment and use specified nominal initial and boundary conditions. The single-blind calculations are performed after the experiment and use measured initial and boundary conditions while maintaining all other parameters constant, including the code version. Comparisons of calculated results with experimental results are discussed; the possible causes of discrepancies are explored and explained. RELAP5 calculated system pressure, mass inventory, and fuel cladding temperature agree reasonably well with the experiment results, and only slight changes are noted between the double-blind and single-blind predictions.

INTRODUCTION

The Loss of Fluid Test (LOFT) facility [1] at the Idaho National Engineering Laboratory is a 55-MW(t), volumetrically scaled pressurized water reactor (PWR) used to simulate the thermal-hydraulic responses expected in a commercial reactor during postulated accidents. The experiments of interest simulate loss of coolant accident (LOCA) scenarios evolving from various accident initiators.

Prior to each experiment, the reactor system responses are modeled using the thermal-hydraulic computer code with specified experiment conditions. These calculations are used both to predict the experiment outcome and to evaluate the modeling techniques.

The RELAP5/MOD1 code [2] was used to perform best estimate "double-blind" and "single-blind" predictions. The double-blind calculations (a) are performed prior to the experiment, (b) use specified nominal initial and boundary conditions, and (c) provide a basis for evaluating the best estimate analytical modeling techniques.

The single-blind calculations (a) are performed after the experiment, (b) use measured initial and boundary conditions [3] while maintaining all other parameters constant (including the code version), and (c) were performed to evaluate the effects of the differences between specified and actual initial and boundary conditions.

This paper compares predictions with measured data for LOFT Experiments L5-1 and L8-2, which simulated intermediate break LOCA with core uncovering.

DESCRIPTION OF EXPERIMENTS

Experiments L5-1 and L8-2 were conducted on September 24 and October 12, 1981, respectively, by EG&G Idaho, Inc., for the U.S. Nuclear Regulatory Commission.

The LOFT facility is instrumented so that the system conditions can be measured and recorded during the experiments. The LOFT plant configuration used for conducting the experiments is illustrated in Fig. 1. The break location for these experiments is at the broken loop cold leg. Both experiments simulated a shear break in one of four emergency core cooling (ECC) system injection pipes [28.5-cm (11.2-in.) inside diameter] in a commercial four-loop PWR.

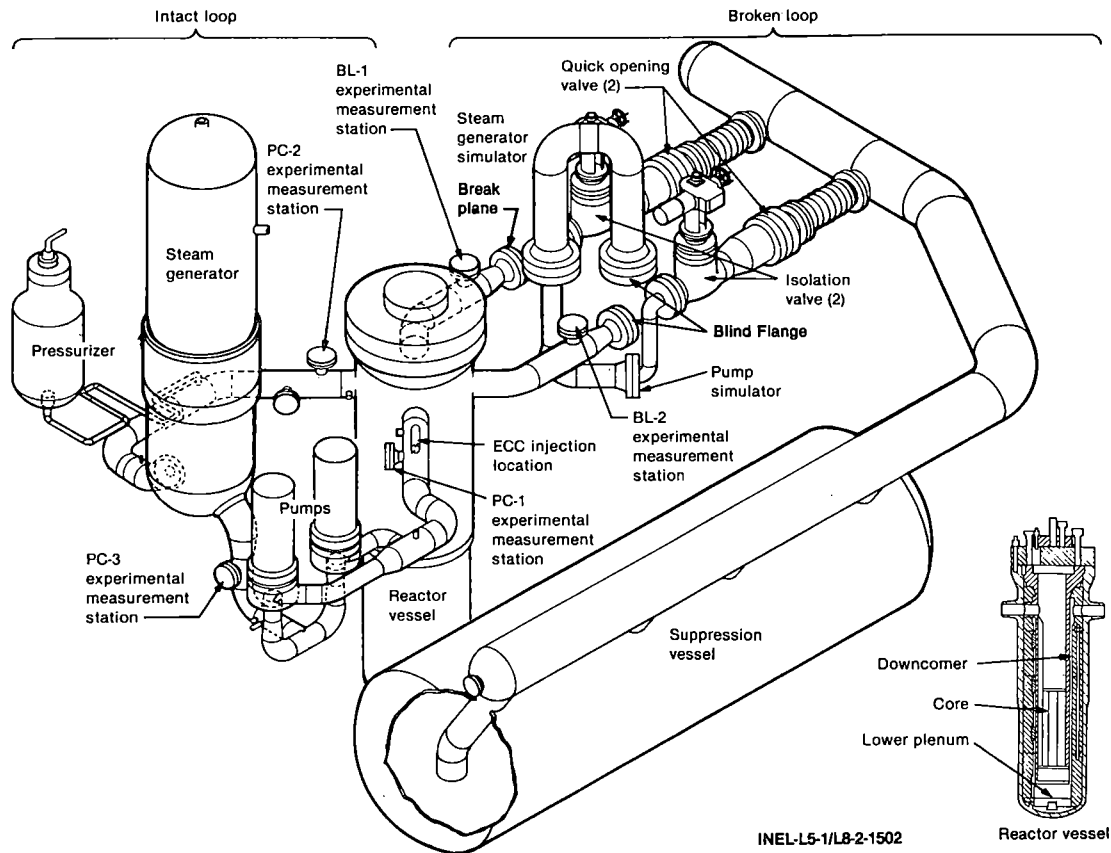


Fig. 1. LOFT system configuration.

Experiment L5-1 was designed to provide data to evaluate the effectiveness of degraded ECC system performance (only three of four accumulators available) during an intermediate size break LOCA. The accumulator pressure was changed from a nominal setpoint of 4.22 MPa (600 psig) to 1.66 MPa (228 psig). This pressure setting is used in some Combustion Engineering PWR designs, which is the limiting condition for worst case ECC system operation. The liquid volume of a single LOFT facility accumulator was scaled to represent three of four accumulators available for a large commercial PWR.

Experiment L8-2 duplicated the initial portion of the L5-1 experiment up to the time of accumulator injection. Both experiments provided data on repeatability of LOFT experiments. The single LOFT facility accumulator and low-pressure injection system (LPIS) were deliberately inhibited to produce a sustained core uncover in order to study a potential plant recovery procedure involving restarting the reactor coolant pumps (RCPs).

When a fuel cladding temperature of 811 K (1000°F) was reached, the RCPs were restarted and brought to full speed for determining whether the forced steam flow in a nearly empty reactor coolant system (RCS) could significantly affect the fuel cladding temperature rise.

Initial conditions (which were essentially the same for both experiments) are given in Table I together with the corresponding RELAP5/MOD1 input values used for performing the double-blind (D-B) and single-blind (S-B) calculations.

Prior to conducting the L5-1 and L8-2 experiments, the RELAP5/MOD1 code was used to perform the experiment predictions (double-blind calculations) using the specified nominal initial and boundary conditions [4,5]. The method for performing the experiment prediction is to begin with a best estimate nominal calculation (base case) and then perform sensitivity calculations on phenomena that are known to have larger uncertainty. The phenomena of larger uncertainty examined in the experiment predictions included critical flow through the break, the pump frictional torque, and the correlations used to calculate critical heat flux. Of these, the calculated system behavior was most influenced by changing the critical flow discharge coefficients. The sensitivity calculations used a subcooled break discharge coefficient of 0.84 and a two-phase discharge coefficient of 0.84 [6,7] instead of the nominal calculation with both coefficients of 1.0.

TABLE I
Initial Conditions for Experiments L5-1 and L8-2
and the RELAP5 Input Values

Parameter	Measured Value		RELAP5 Input Value	
	L5-1	L8-2	D-B	S-B
Core power (MW)	45.9 ± 1.2	46.0 ± 1.2	50.0	45.9
Hot leg pressure (MPa)	14.93 ± 0.08	14.86 ± 0.06	15.00	14.99
(psia)	2165.3 ± 11.6	2155.2 ± 8.7	2175.5	2174.6
Cold leg temperature (K)	552.3 ± 0.9	552.4 ± 0.9	555.01	551.38
(°F)	534.4 ± 1.6	534.7 ± 1.6	539.33	532.80
Core temperature (K)	27.0 ± 1.2	26.9 ± 1.2	29.0	26.92
difference (°F)	48.6 ± 2.2	48.4 ± 2.2	52.2	48.5
Mass flow rate (kg/s)	308.2 ± 4.0	311.0 ± 4.0	317.6	321.4
(Mlbm/hr)	2.45 ± 0.03	2.47 ± 0.03	2.52	2.55

CODE AND MODEL DESCRIPTIONS

The RELAP5/MOD1 computer code, Cycle 13 [8], was used to perform the experiment predictions described in this paper. RELAP5/MOD1 is an advanced one-dimensional, fast-running computer code designed for thermal-hydraulic analysis of experimental nuclear reactors and related systems. RELAP5 is based on a two-fluid, nonequilibrium hydrodynamic model. The basic governing equations of the hydrodynamic model consist of two phasic continuity equations, two phasic momentum equations, and a mixture energy equation. Nonequilibrium phasic temperatures are computed by using the mixture energy equation supplemented by the assumption that one of the phases is at saturation. RELAP5 has models to represent feedback control systems, stratified horizontal flow, and reactor neutronics.

The nodalization diagram for the LOFT facility used for the experiment predictions is shown in Fig. 2. This model contains 104 volumes, 109 junctions, and 79 heat

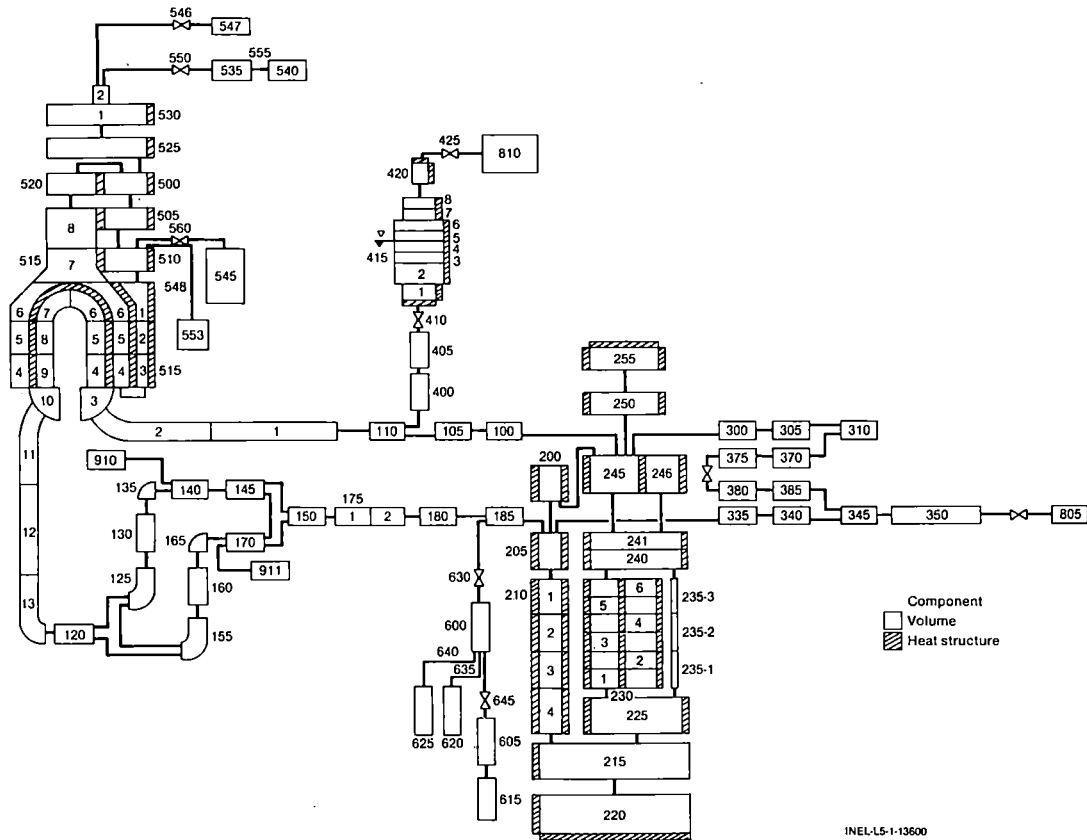


Fig. 2. LOFT RELAP5 nodalization diagram.

structures. This model is based on the standard nodalization model described in detail in Ref. 9. The standard model was changed to represent the LOFT system configuration and to incorporate either the specified or the measured initial and boundary conditions, as appropriate, for Experiments L5-1 and L8-2. In addition, changes to the standard model were made as experience was gained in use of the code. The changes included the following:

1. Heat transfer to the outside of the steam generator steam dome and downcomer was added to allow calculation of ambient heat losses
2. The reactor vessel wall heat slabs were modified to allow heat transfer to the environment
3. Heat slabs representing the 10 hottest pins were added to the core volumes to allow calculation of the peak cladding temperatures
4. Heat slabs were added to account for heat transfer from the pressurizer walls to the fluid
5. The number of core volumes was increased from three to six to provide more detailed information in the core
6. The number of volumes in the pressurizer was increased to nine to provide a better calculation of pressurizer level
7. Reactor coolant pump injection flow was added to properly account for the system mass inventory

8. The steam generator and pump simulator volumes in the broken loop hot leg were removed because they were to be flanged off during the test
9. The accumulator and the injection line were remodeled using the recently available accumulator component model
10. Reactor coolant pump two-phase head and torque multipliers were changed to agree with data obtained from the LOFT L3-6 pumps-on small break experiment [10].

COMPARISON OF EXPERIMENTAL DATA WITH EXPERIMENT PREDICTIONS

Comparisons of double-blind nominal and sensitivity calculations to the measured data for Experiment L5-1 (Fig. 3) indicate that the system behavior was better predicted with break discharge coefficients (C_d) of 0.84. The calculation with coefficient of 1.0 overpredicted the depressurization rate, which in turn affected the predicted times of occurrence of significant events. However, both calculations (with $C_d = 0.84$ and 1.0) correctly predicted the phenomena that occurred during Experiments L5-1 and L8-2 in the proper sequences. Therefore, in the following discussion, the measured data of Experiments L5-1 and L8-2 are compared with the double-blind and single-blind predictions performed using a break coefficient of 0.84.

Experiment L5-1

Figure 4 compares the calculated and measured reactor vessel upper plenum pressure for Experiment L5-1. The double-blind and single-blind predictions are in very good agreement with the experimental data. The slightly underpredicted pressure in the calculations that resulted after 200 s was due to the calculated accumulator flow being slightly less than what actually occurred.

Figure 5 shows the comparison of measured and calculated mass flow rates at the break. Both calculated mass flow rates agree very well with the experimental data.

Figure 6 presents the comparison of measured and calculated reactor coolant system (RCS) mass inventory. Both predictions of calculated coolant mass in the RCS are in excellent agreement with the experimental data. The double-blind and single-blind calculations each slightly overpredicted the RCS coolant mass before 90 s and underpredicted it after 90 s. The slightly larger deviation in both experiment predictions after 190 s was due to the calculated low accumulator injection flow.

Figures 7 and 8 compare the calculated and measured intact and broken loop cold leg densities. The calculated and the measured densities are generally in reasonably good agreement, although slight deviations from the measured data can be seen between 20 and 60 s. The overpredicted density in the broken loop cold leg during that period

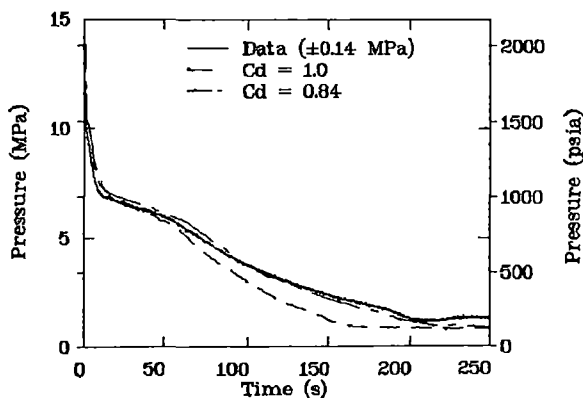


Fig. 3. Pressure comparison with break discharge coefficients (C_d) of 1.0 and 0.84 for L5-1 experiment.

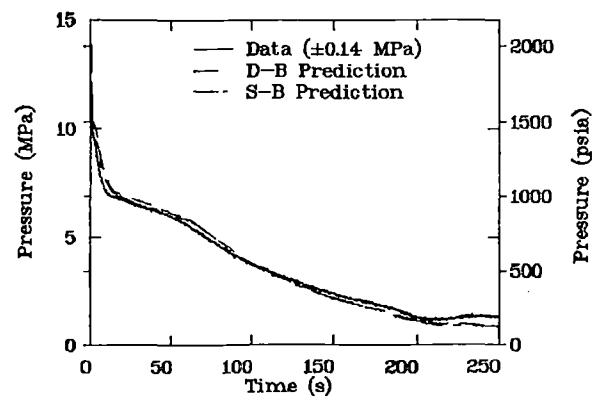


Fig. 4. Pressure comparison for D-B and S-B prediction for L5-1 experiment.

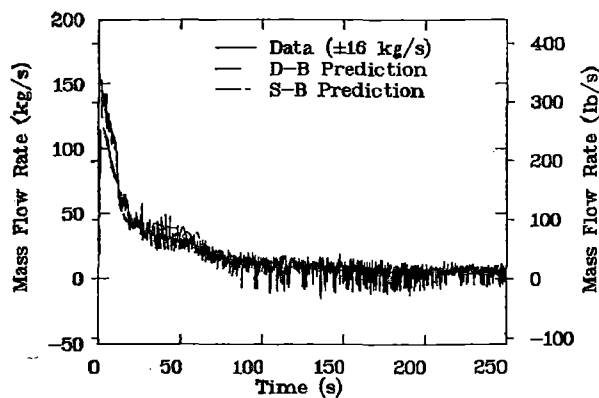


Fig. 5. Break mass flow rate comparison for L5-1 experiment.

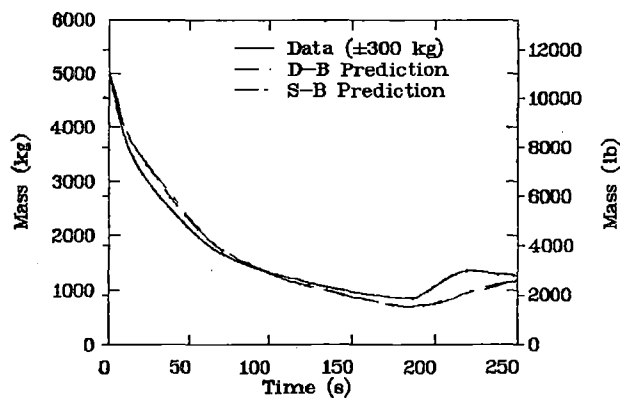


Fig. 6. Mass inventory comparison for L5-1 experiment.

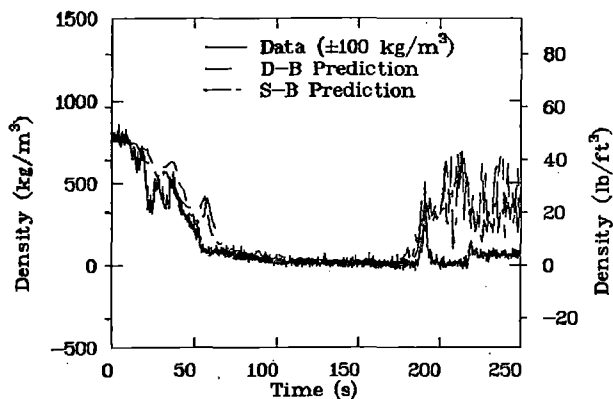


Fig. 7. Intact loop cold leg density comparison for L5-1 experiment.

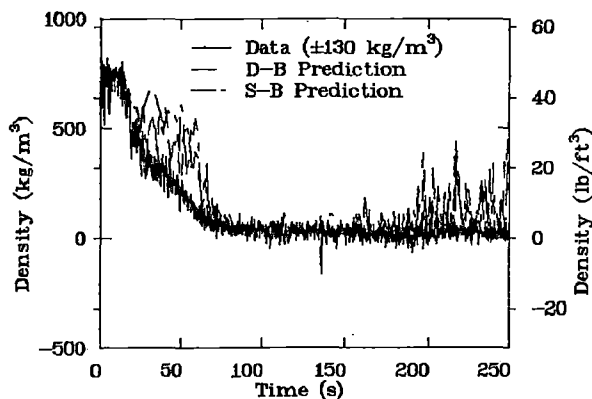


Fig. 8. Broken loop cold leg density comparison for L5-1 experiment.

corresponded to fuel cladding temperature oscillations. High void fractions were calculated to occur in the core due to excessive vapor generation moving liquid from the core to the lower plenum and downcomer, and causing high density flow in the broken loop cold leg. In the intact loop cold leg, a measured density increase at about 190 s was caused by the accumulator injection, followed by a decrease when the liquid drained into the downcomer. Both calculations showed a density increase, but not the decrease. This difference may be attributed to a small calculated draining of liquid from the intact loop cold leg into the downcomer.

Figure 9 shows the comparison of calculated and measured fluid temperatures in the upper plenum. The calculated and measured coolant temperatures are in good agreement as long as the fluid is saturated. The measured temperature showed a large fluid superheating after 140 s in the upper plenum. Both calculations failed to predict the superheated fluid temperatures that actually occurred in the upper plenum during the later part of the experiment. This difference between calculated and measured coolant temperatures were caused by the incorrect RELAP5 modeling of the non-equilibrium conditions. RELAP5 will not maintain enough superheated steam, because the superheated steam will be immediately condensed into liquid by the interfacial mass transfer model when any liquid is present. Therefore, a superheated fluid condition cannot be calculated without a continuous supply of superheated steam.

Figure 10 compares the measured fuel cladding temperatures with the calculated temperatures near the core hot spot from 0.84 to 1.12 m (33 to 44 in.) from the bottom of the active core. The core thermal response during the heatup was also reasonably

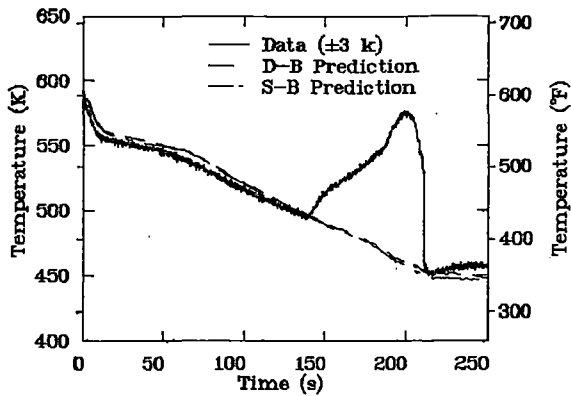


Fig. 9. Coolant temperature comparison for L5-1 experiment.

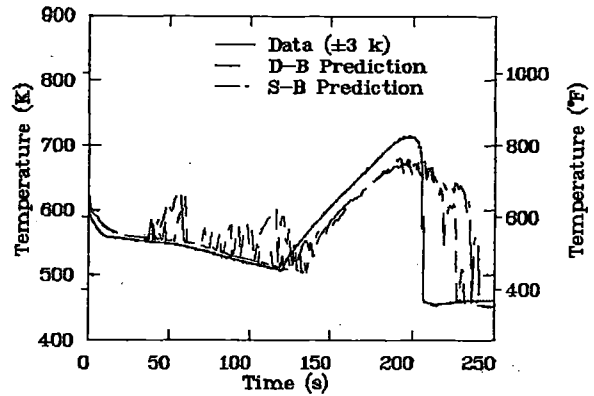


Fig. 10. Fuel cladding temperature comparison for L5-1 experiment.

well predicted. However, several low-amplitude, short-duration temperature oscillations prior to the principal dryout were calculated. The predicted quench of the fuel cladding temperature was also calculated to occur late compared with the data. The minor temperature oscillations are caused by the fuel cladding heat flux reaching the critical value due to periodic and almost complete voiding calculated to occur in the core. It appears that improper interfacial drag was calculated during these periods. The late fuel cladding temperature quench was due to the effect of the calculated lower rate of accumulator injection. The calculated maximum fuel cladding temperature was lower than the measured peak value, which can probably be attributed to (a) the calculated accumulator flow injecting slightly earlier than in the experiment, (b) the lack of fluid superheating in the calculation, and (c) the minor temperature oscillations that were calculated to occur during the heatup.

Experiment L8-2

The double-blind and single-blind predictions for Experiment L8-2 were performed with initial conditions identical to those of Experiment L5-1. Also, results for the first 175 s of Experiment L8-2 transient are identical to those of Experiment L5-1. Therefore, only comparisons of the double-blind and single-blind predictions with the measured data for the relevant system hydraulic and thermal parameters during the later portion of the Experiment L8-2 transient are discussed.

Figure 11 shows the comparison of the calculated and measured reactor vessel upper plenum pressures. Both predicted pressures are in very good agreement with the experimental data. The slight increase in the measured pressure at approximately 305 s was due to the accumulator flow injection into the system, which terminated the experiment but was not modeled in the calculation [11].

Figure 12 shows the comparison of the break mass flow rate. Both calculated mass flow rates compare very well with measured data. The large difference after 310 s was due to accumulator flow which, again, was not modeled.

Figures 13 and 14 present the comparisons of the calculated and measured intact and broken loop cold leg densities. The calculated densities are generally in good agreement with the measured values during the subcooled and two-phase saturated blow-down transients. Slightly larger deviations, similar to Experiment L5-1 calculations, are shown during the transition period.

Figure 15 indicates the RCP speed comparison. The RCP response as a free turning turbine is very well predicted up to its restart time (237.5 s). A constant pump speed was specified in the double-blind calculation, and a pump speed versus time table was specified as code input in accordance with measured data in the single-blind calculation. There are differences in the predicted RCP restart time because the pump restart was initiated at a cladding temperature of 866 K (1100°F) in the double-blind

experiment prediction instead of the 811 K (1000°F) that occurred during the experiment. The difference in the single-blind calculation is due to the lower calculated cladding temperature compared to the measured data.

Figure 16 shows the comparisons of calculated and measured coolant temperature in the reactor vessel upper plenum. The measurements indicate that fluid superheating

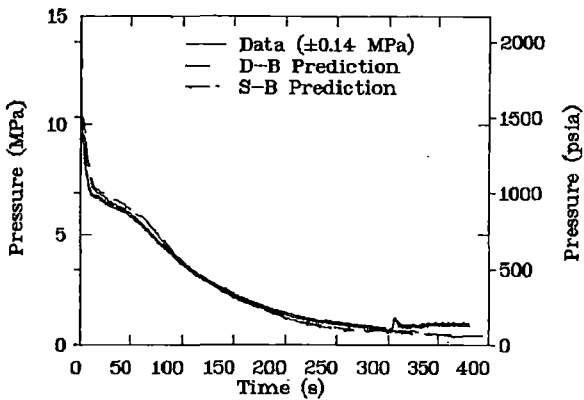


Fig. 11. Pressure comparison for L8-2 experiment.

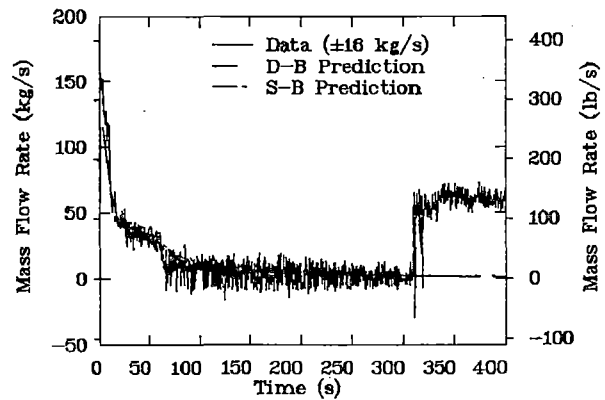


Fig. 12. Break mass flow rate comparison for L8-2 experiment.

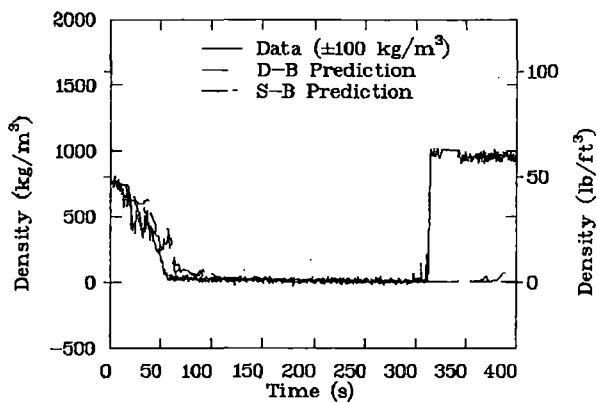


Fig. 13. Intact loop cold leg density comparison for L8-2 experiment.

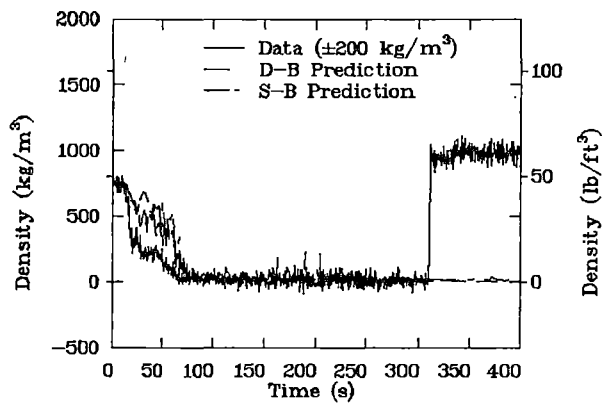


Fig. 14. Broken loop cold leg density comparison for L8-2 experiment.

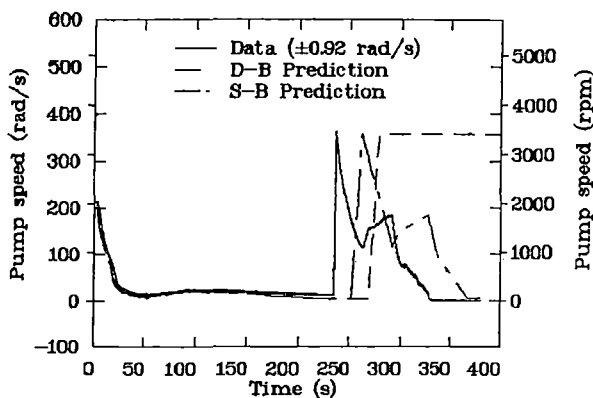


Fig. 15. Pump speed comparison for L8-2 experiment.

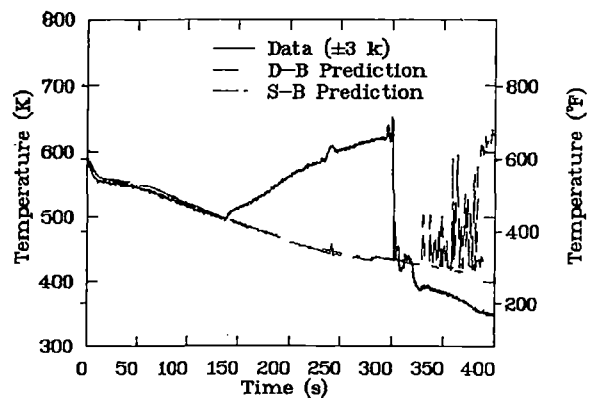


Fig. 16. Coolant temperature comparison for L8-2 experiment.

occurred in the RCS; however, RELAP5 predicted that the fluid temperature would remain saturated. The reasons for this disparity are the same as discussed for Experiment L5-1.

Figure 17 presents the comparison of fuel cladding temperatures at the location between 0.84 to 1.12 m (33 to 44 in.) from the bottom of the active core. The calculated and measured fuel cladding temperatures are in reasonably good agreement until the RCPs restart time (the RCPs were restarted in the experiment when the cladding temperature reached 811 K). Although RELAP5 incorrectly predicted that the heatup rate would decrease when the RCPs were restarted, the code correctly predicted that the fuel cladding temperatures would increase continuously and eventually reach the experiment termination criteria, although 90 s late. The calculated heatup rate decrease was due to a heat transfer regime change when the RCPs were restarted. The fluid in the core was already superheated when the RCPs restarted. The proper heat transfer mechanism should have been forced convection to superheated steam with the RCPs operating. Because the code was unable to predict the fluid superheating, a two-phase natural convection heat transfer correlation was chosen to compute the heat transfer coefficients, which were larger than those that would have been obtained from a forced convection to superheat steam correlation. This resulted in a slightly lower fuel cladding heatup rate being calculated.

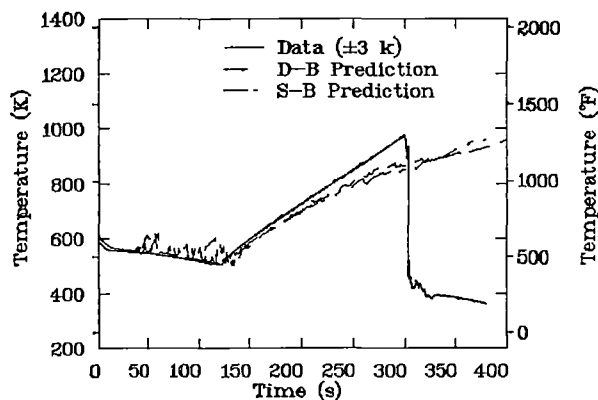


Fig. 17. Fuel cladding temperature comparison for L8-2 experiment.

CONCLUSIONS

The comparisons of the calculated and measured data for Experiments L5-1 and L8-2 indicate that most of the important system thermal-hydraulic parameters were predicted reasonably well in the RELAP5 double-blind and single-blind calculations. In general, the calculated results agree with the experimental data within the uncertainty ranges of the instruments, although some minor differences are observed for certain short periods in the transients. Furthermore, only slight changes are noted between the double-blind and single-blind calculations.

The RELAP5 code adequately calculated important safety-related phenomena such as system depressurization, RCS coolant mass inventory, and core heatup and quench (although slightly delayed). However, fluid superheating in the core and upper plenum was not calculated. Also, the code-calculated cladding temperature oscillations were not observed in the experiment.

The significance of the double-blind and single-blind calculations is that the L5-1 and L8-2 experiments are the only intermediate break and severe core transient experiments scheduled to be performed at the LOFT facility and analyzed with the RELAP5 code. The results obtained and presented in this paper reveal deficiencies in some RELAP5 analytical models (such as the accumulator, heat transfer, and interfacial drag models) that were not found in previous analyses of small and large break LOCA.

NOTICE

This paper was prepared as an account of work sponsored by an agency of the United States Government. Neither the United States Government nor any agency thereof, or any of their employees, makes any warranty, expressed or implied, or assumes any legal liability or responsibility for any third party's use, or the results of such use, of any information, apparatus, product, or process disclosed in this paper, or represents that its use by such third party would not infringe privately owned rights. The views expressed in this paper are not necessarily those of the U.S. Nuclear Regulatory Commission.

REFERENCES

1. D. L. Reeder, "LOFT System and Test Description (5.5-Ft Nuclear Core 1 LOCEs)," Report NUREG/CR-0247, TREE-1208, EG&G Idaho, Inc. (1978).
2. V. H. Ransom et al., "RELAP5/MOD1 Code Manual, Volume 1: System Models and Numerical Method," Report EGG-2070, EG&G Idaho, Inc. (1980).
3. D. L. Jarrel and Janice M. Divine, "Experiment Data Report for LOFT Intermediate Break Experiment L5-1 and Severe Core Transient Experiment L8-2," Report NUREG/CR-2398, EGG-2136, EG&G Idaho, Inc. (1981).
4. R. P. Jordan, "LOFT Experiment Operating Specification Intermediate Break Test Series L5, Test L5-1," Report EGG-LOFT-5436, EG&G Idaho, Inc. (1981).
5. D. B. Wood, "LOFT Experiment Operating Specification Core Uncovery/Degraded Core Cooling Test L8-2," Report EGG-LOFT-5544, EG&G Idaho, Inc. (1981).
6. L. K. Tikhonenko et al., "Critical Discharges of Hot Water from Tubes," Thermal Engineering, 26 5 (1979).
7. H. K. Fauske, "The Discharge of Saturated Water Through Tubes," Chemical Engineering Progress, Symposium Series, 61 59 (1961).
8. This analysis was performed using RELAP5/MOD1, Cycle 13, a production version of the RELAP5/MOD1 code which is filed under Idaho National Engineering Laboratory Computer Code Configuration Management (CCCM) Archival Number F00341.
9. E. J. Kee, P. J. Schally, and L. Winters, "Base Input for LOFT RELAP5 Calculations," Report EGG-LOFT-5199, EG&G Idaho, Inc. (1980).
10. T. H. Chen, "Primary Coolant Pump Performance During LOFT L3-6 Experiment," Report EGG-LOFT-5414, EG&G Idaho, Inc. (1981).
11. Experiment L8-2 was defined as terminated when the hottest cladding temperature was greater than 950 K (1250°F).

INFLUENCE OF BREAK SIZE ON BLOWDOWN FOR LARGE BREAKS

L. Piplies, C. Addabbo, W. L. Riebold

Commission of the European Communities
EURATOM, Joint Research Centre - Ispra Establishment
LOBI Project, Heat Transfer Division
I-21020 ISPRA/Varese (I)

ABSTRACT

The transient thermal-hydraulic behaviour of a simulated pressurized water reactor (PWR) primary cooling system during the blowdown period of a loss-of-coolant accident (LOCA) is being investigated in the LOBI¹ test facility. The overall objective of the LOBI experimental programme is to provide and/or extend the data base required for assessing the capabilities of computer codes to predict integral blowdown-refill experiments for a range of system components operational conditions and for pipe ruptures of different sizes and at various locations within the primary cooling system.

This paper summarizes the essential results of four loss-of-coolant experiments covering the large-to-intermediate break spectrum. These tests were cold leg breaks with intact loop cold leg emergency core coolant (ECC) injection. Break sizes ranged from single-ended 1 x 0.25A, through 1 x 0.5A and 1 x 1A up to the double-ended 2 x 1A break size. A comparative analysis of the essential test results shows that the influence of break size on blowdown in the LOBI facility is mainly confined to core thermal-hydraulic response.

INTRODUCTION

The LOBI project is being executed in the Ispra Establishment of the Euratom Communities in the framework of a R&D contract between the Bundesminister für Forschung und Technologie, Bonn, Federal Republic of Germany, and the Commission of the European Communities.

The general objectives of the LOBI experimental programme consist essentially in the investigation of the transient thermal-hydraulic behaviour of a simulated PWR primary cooling system during the blowdown period of a loss-of-coolant accident, and in the application of the experimental results to check and improve blowdown computer codes and associated analytical models.

¹ Loop Blowdown Investigations

During the first phase of the programme (December 79 - June 82) 25 large-to-intermediate break blowdown tests have been performed. In addition, three small break scoping tests have also been carried out. The influence of the following parameters on the thermal-hydraulic behaviour of the scaled facility during blowdown has been investigated:

- Break size
- Break location
- Downcomer gap width
- Pump operation mode
- Heating power
- Accumulator injection mode and rate.

With respect to the influence of break size on blowdown for cold leg breaks and with intact loop cold leg injection, the break spectrum has been covered by tests ranging from single-ended 1 x 0.25A, through 1 x 0.5A and 1 x 1A up to the double-ended 2 x 1A break size. In this paper the influence of break size on blowdown in the LOBI facility is assessed through a comparative analysis of the essential test results.

FACILITY DESCRIPTION

A view of the LOBI facility is given in Figure 1. It is a 1 : 700 scale model of a four-loop 1300 MWe PWR and has two primary loops, the intact loop representing three loops and the broken loop representing one loop of a PWR. Both primary loops are active loops each containing a circulation pump and a steam generator.

The main coolant circulation pumps are radial type pumps and are equal in size. The different steady-state mass flows in each loop are thus established by different pump speeds. The intact and broken loop steam generators are different in volume and tube number but equal in height. The reactor pressure vessel model contains an electrically heated rod bundle with 64 rods (8 x 8 array) and a heated length of 3.9 m. The nominal heating power is 5.3 MW. The downcomer is of annular shape and for the tests described in this paper it had a gap width of 50 mm (a downcomer gap width of 12 mm was later installed). An upper head simulator is connected to the upper plenum and upper downcomer region. A schematic drawing of the pressure vessel with the heated section is shown in Figure 2. The height, and relative heights of components are scaled 1 : 1, thus preserving gravitational heads.

In the present test facility configuration only the accumulator ECC injection system is represented. ECC water can be supplied from two accumulators, one for each loop; cold or hot leg as well as combined injection can be simulated. Heat is removed from the steam generators by an active secondary system containing two condensers, a cooler and a feedwater circulation pump. The effluent from the simulated break is discharged into a concrete bunker which is vented to atmosphere, thus the containment back pressure is not simulated.

A comprehensive measurement system suited to resolve fast transients and a high speed data acquisition system are used to monitor and record the main thermo-hydraulic parameters prior and during the transient in PCM format on an analog tape.

SYSTEM CONFIGURATION AND INITIAL CONDITIONS

System configuration for the four tests referred to herein was essentially the same. Cold leg break between primary circulation pump and pressure vessel inlet nozzle was simulated. ECC water injection from the accumulator system was made only into the intact loop cold leg. The high pressure as well as the low pressure injection system are not represented. The pressurizer was connected to the intact loop.

Convergent-divergent nozzles of different throat diameter were used to simulate the required break sizes. It is noted that the downcomer gap width of 50 mm is out-of-scale with respect to both power to volume and pressure drop scaling criteria¹. Thus break sizes of 2 x 1A, 1 x 1A, 1 x 0.5A and 1 x 0.25A represent break sizes of 2 x 0.75A, 1 x 0.75A, 1 x 0.38A and 1 x 0.19A respectively, when reference is made to the ratio of break size to actual primary system volume of the LOBI facility with the 50 mm downcomer gap width installed.

The specified and actual primary system initial conditions are summarized in Table I. The power supplied to the rod bundle was programmed to follow the calculated energy release from an appropriate nuclear fuel model during the simulated transient / 1 /. The feed water mass flow to the steam generator secondary side was reduced to zero after blowdown was started. Further information on secondary side operational conditions and boundary conditions is contained in /2, 3, 4, 5 /.

TEST RESULTS

The effect of break size on depressurization rate of the primary cooling system during blowdown can be seen in Figure 3 which compares the pressure responses in the intact loop cold leg (a short time plot is shown in the insert) which are almost identical to the lower plenum pressure responses. Clearly, depressurization rate decreases with break size which limits the rate of discharge and hence depletion of primary system fluid inventory during both the subcooled and subsequent saturated phases of the blowdown transient. Also, in the early transient depressurization rate changes with the occurrence of flashing at various locations in the primary cooling system.

Immediately following the start of blowdown system pressure drops quickly to the saturation pressure corresponding to hot legs and upper plenum fluid temperatures. For the larger, double-ended, 2 x 1A blowdown test saturation pressure in the upper pressure vessel internals is reached within 100 ms after initiation of blowdown, whereas for the single-ended 1 x 1A, 1 x 0.5A and 1 x 0.25A blowdown tests it is reached within 200 ms, 400 ms and 1 s, respectively. Thereafter a flashing front propagated through the whole primary cooling system. The transition from subcooled to saturated conditions in the cold legs occurred at about 3.4 s, 5.4 s,

¹ A volume scaled downcomer would yield a 7 mm gap width whereas a 25 mm gap width would preserve the same pressure drop due to wall friction as in the reference plant.

TABLE I. Specified and Actual Initial Test Conditions

Primary System ^{a)}	Specified	Actual			
Test		A1- ϕ 4R	A2-59	A2-55	B-RIM
Break Size		2x1A	1x1A	1x0.5A	1x0.25A
Mass Flows in KG/s					
Intact Loop in KG/s	21.07	21.1	20.7	21.0	21.0
Broken Loop	7.03	7.0	7.3	7.3	7.0
Pressure in MPa					
Upper Plenum	15.5	15.3	15.4	15.4	15.3
Fluid Temperatures in °C					
Intact Loop : vessel outlet	323	327	319	320	320
vessel inlet	290	298	288	288	289
Broken Loop : vessel outlet	323	333	324	326	326
vessel inlet	290	298	288	289	289
Pressurizer	345	346	348	349	348
Core Power in MW	5.28	5.12	5.13	5.26	5.19
Accumulator					
Fluid Temperature °C	30	32	31	31	32
Liquid Volume Litres	224	224	224	224	224
Gas Volume Litres	56	56	56	56	56
Actuation Pressure MPa	2.7	2.7	2.7	2.7	c. 2.6

a) The Scaling Factor for Mass Flows, Core Power and All Primary System Components Except the Downcomer is 1:7 $\phi\phi$

7.5 s and 8.5 s going from the larger 2 x 1A down to the smaller 1 x 0.25A break size blowdown tests.

As the primary system fluid inventory depleted due to fluid discharge through the break, heater rod bundle heat transfer degraded considerably causing departure from nucleate boiling (DNB) over the whole heated length for the 2 x 1A and 1 x 1A break tests. DNB was localized in the upper bundle region for the 1 x 0.5A test whilst no boiling crisis occurred in the 1 x 0.25A test. The onset of DNB for the spectrum of breaks considered is shown in Figure 4 where the average times with one standard deviation are presented (TC's time response is not accounted for).

After the occurrence of DNB a first rewet of the bundle was observed for each test where boiling crisis was experienced, see Figures 5 and 6 which illustrate the envelopes of heater rod temperatures (central and intermediate zones of the 8 x 8 square lattice) at the upper (level 9) and middle (level 6) bundle elevations, respectively. This very first rewet was mainly caused by a reestablished core flow in the 2 x 1A and 1 x 1A tests. For the 1 x 0.5A blowdown test where relatively low quality fluid persisted in the bundle during the early transient, rewet was caused by the initial decay of the heating power.

The reestablished positive core flow which typifies the very initial blowdown phase in the LOBI facility with the large 50 mm downcomer gap width (and although to a less extent also with the 12 mm downcomer gap width) installed is the result of the transition from subcooled to saturated critical flow at the break nozzle. Figure 7 depicts fluid densities in the core entry for each of the four break sizes. The core entry density in the 2 x 1A blowdown test drops quickly soon after initiation of blowdown due to large core flow reversal and then recovers as positive core flow is momentarily reestablished. Thereafter the density drops continuously and starts to recover again only when ECC injection starts. The same trend characterizes the 1 x 1A blowdown transient. Here, however, the initial drop of density is very mild. The 1 x 0.5A and 1 x 0.25A blowdown transients are characterized by relatively high core entry fluid density.

In the larger 2 x 1A and 1 x 1A break size tests the initial rewet was followed by the onset of dryout at about 10 s and 22 s, respectively. No dryout occurred in the 1 x 0.5A and 1 x 0.25A tests. The temperature rise after dryout in the 2 x 1A test was generally higher than in the 1 x 1A test. As primary cooling system depressurization continued accumulator actuation pressure (2.7 MPa) was reached and ECC water injection started. Figure 8 illustrates heater rod bundle temperature distribution for each of the four tests at the time of the respective ECC injection time (see insert). It can be seen that heater rod temperatures were at about primary system fluid saturation temperature in the 1 x 0.25A and 1 x 0.5A break tests. Large temperature gradients were present above level 6 for the 1 x 1A and above level 5 for the 2 x 1A break tests.

Figure 9 illustrates the thermal status of the heater rod bundle at primary system pressure of 1 MPa which is regarded as the set pressure for the low pressure injection ECC system in the reference plant (1300 MWe KWU-PWR). As mentioned earlier, in the present system configuration only the accumulator injection system is represented. Referring to Figure 9 for the 1 x 0.25A and 1 x 0.5A break size tests rod temperatures were at system saturation temperature over the whole heated

length. For the 1 x 1A break size test they were slightly above saturation temperature up to level 7 and above this level a well defined region of high temperature existed. For the 2 x 1A break size test heater rod temperatures departed from saturation temperature from level 6 upward. The higher heater rod temperatures below level 6 in the 1 x 1A break size test as compared to the 2 x 1A break size test is presumably due to the generally higher initial heater rod temperatures and system pressure which occurred in the 1 x 1A test.

Figure 10 through Figure 13 illustrate a three-dimensional development of heater rod temperatures for each of the four tests. Here average heater rod temperature is produced at each instrumented level. It should be noted that such an averaging procedure resulted in some cases in distortions of the dryout and rewetting processes.

As to the primary system major active components such as steam generators and circulation pumps, their effect on overall primary system thermohydraulic behaviour was not relevant. Rather, the coupling between fluid flow and heat transfer in the bundle which was mainly governed by the break flow, characterized the system response for the range of breaks investigated in this series of tests.

CONCLUDING REMARKS

With regard to the influence of break size on blowdown in the LOBI facility the experimental investigation has shown that the coupling between fluid flow and heat transfer in the bundle which is directly related to the break size through the break flow resulted in an early DNB over the whole heated length of the bundle for the 2 x 1A and 1 x 1A break size tests. DNB was localized in the upper bundle elevation in the 1 x 0.5A break size test whilst no boiling crisis occurred in the 1 x 0.25A break size test. Following an initial rewet caused by a reestablished positive core flow, dryout was measured only for the large 2 x 1A and 1 x 1A break size blowdown tests.

REFERENCES

1. H. STÄDTKE, L. PIPLIES, "Performance of Directly Heated Rods as Nuclear Fuel Rod Simulators in the LOBI Facility", Proceedings of the International Symposium on Fuel Rod Simulators, Gatlinburg, Tennessee, October 1980.
2. L. PIPLIES, "Quick Look Report on LOBI Test A1-04R", LQC 80-03, Communication No. 3802, Euratom-J.R.C. (1980).
3. L. PIPLIES et al., "Quick Look Report on LOBI Tests A2-59 and A2-59R", LQC 82-16, Communication No. 3960, Euratom-J.R.C. (in preparation).
4. C. ADDABBO, G. DE SANTI, "Quick Look Report on LOBI Test A2-55", LQC 82-12, Communication No. 3945, Euratom-J.R.C. (1982).
5. C. ADDABBO, G. DE SANTI, "Quick Look Report on LOBI Test B-R1M", LQC 82-08, Communication No. 3815, Euratom-J.R.C. (1982).

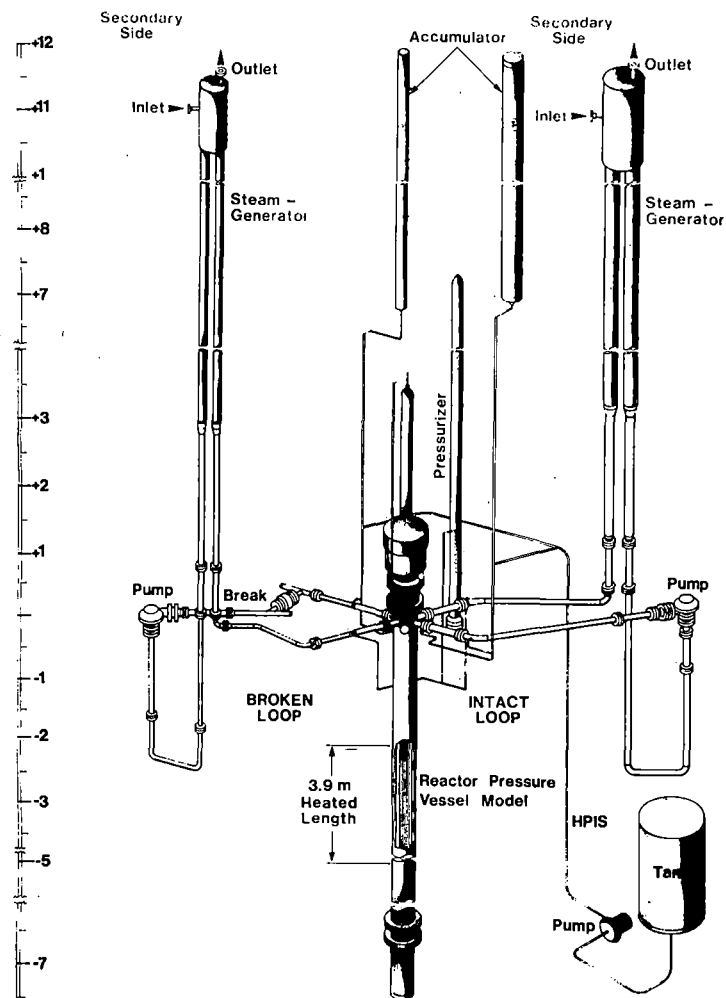


Figure 1 LOBI Test Facility

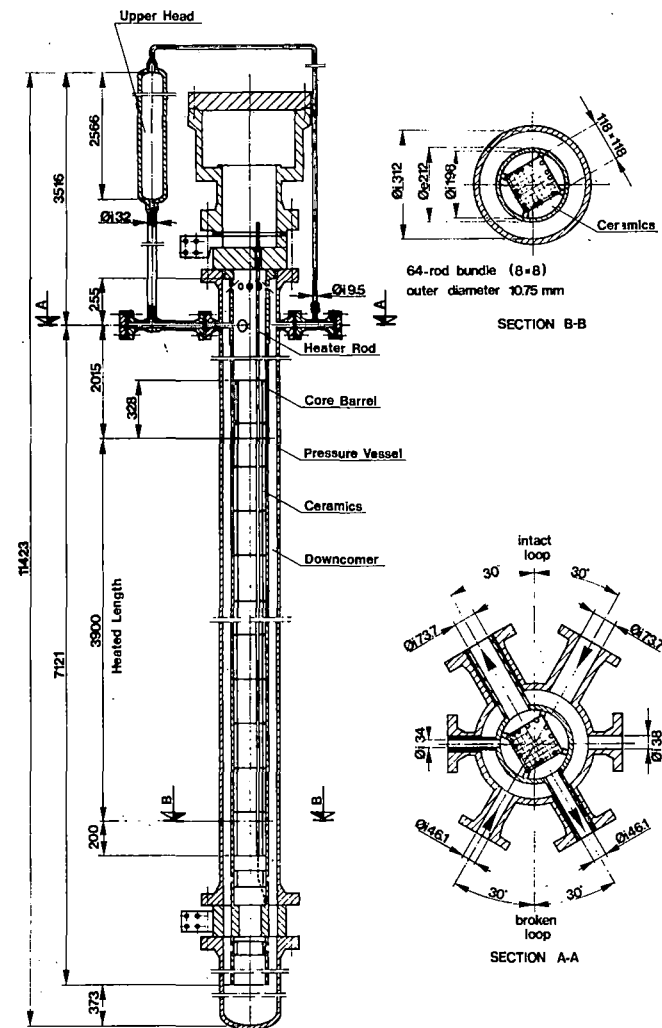


Figure 2 Schematic Drawing of the Reactor Pressure Vessel Model with Heated Section

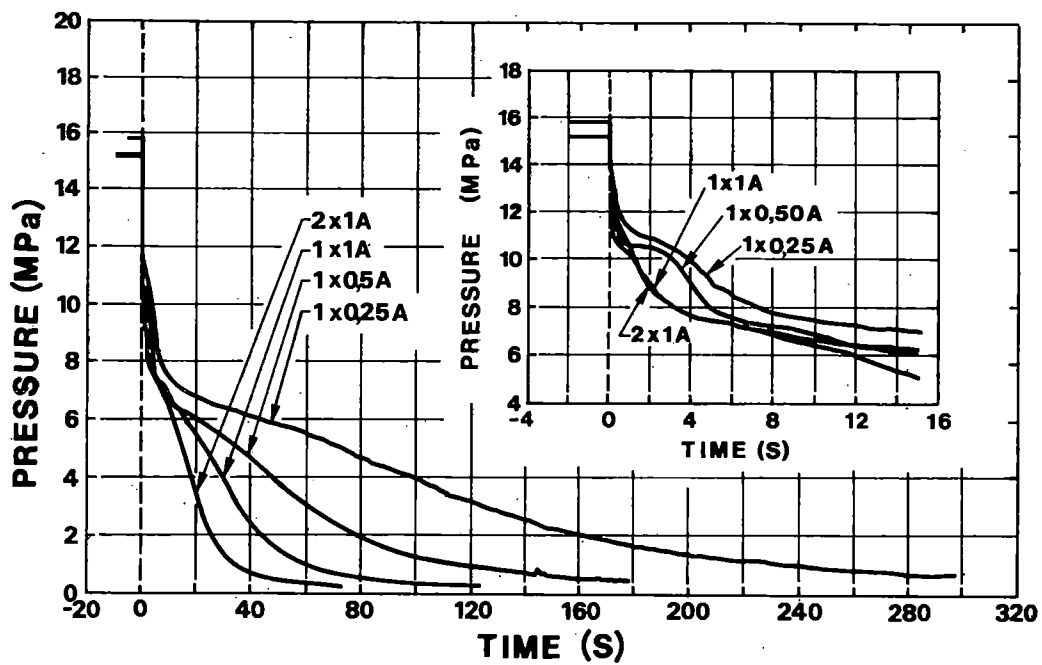


Figure 3 Pressure in the Intact Loop Cold Leg for 2 x 1A, 1 x 1A, 1 x 0.5A and 1 x 0.25A Break Size Blowdown Tests

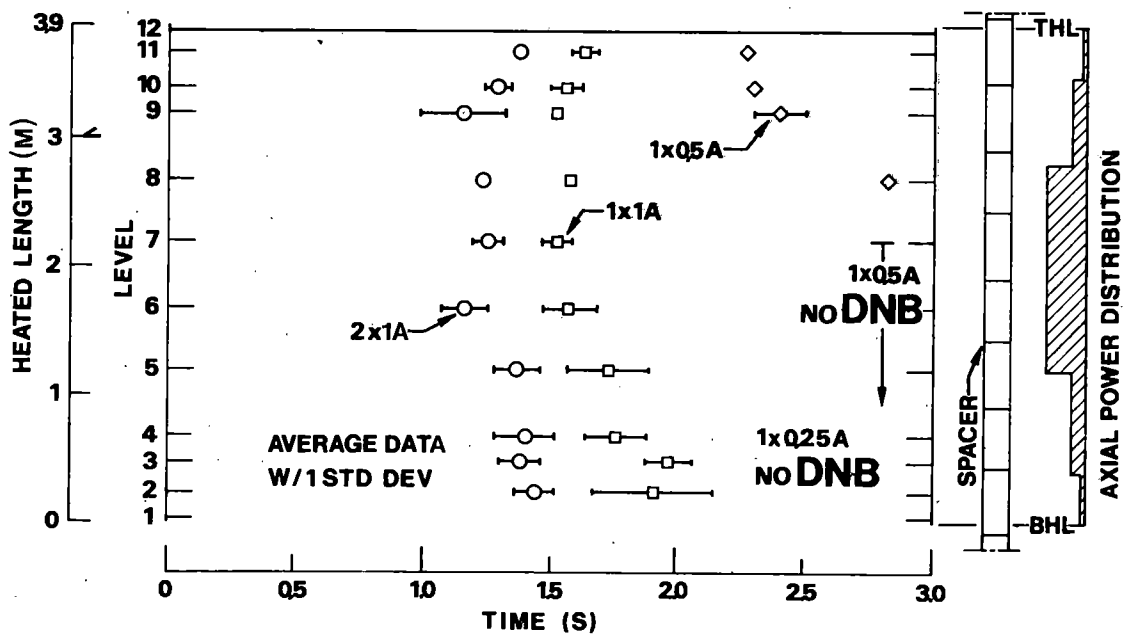


Figure 4 Time to DNB

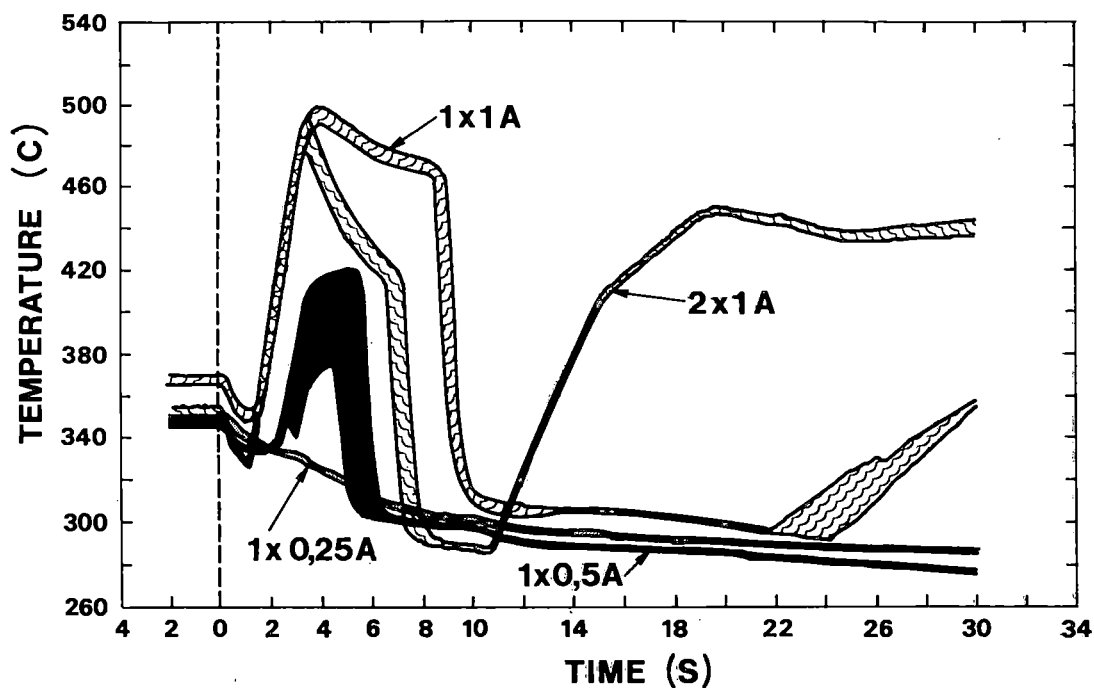


Figure 5 Envelopes of Heater Rod Temperature (Central and Intermediate Zones) at Level 9

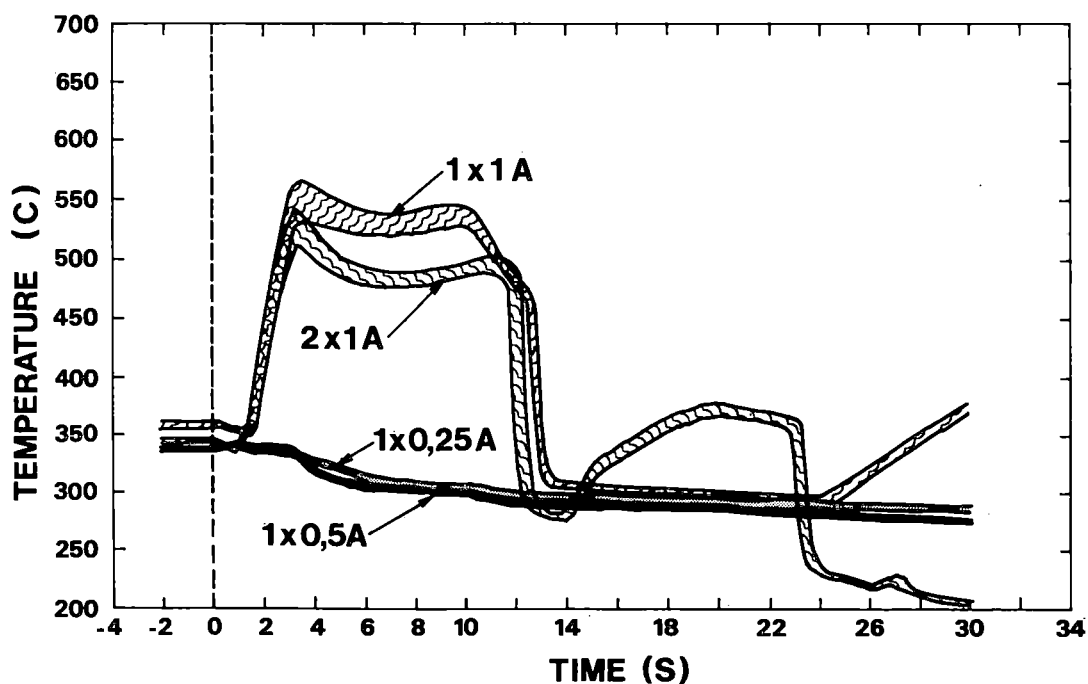


Figure 6 Envelopes of Heater Rod Temperatures (Central and Intermediate Zones) at Level 6

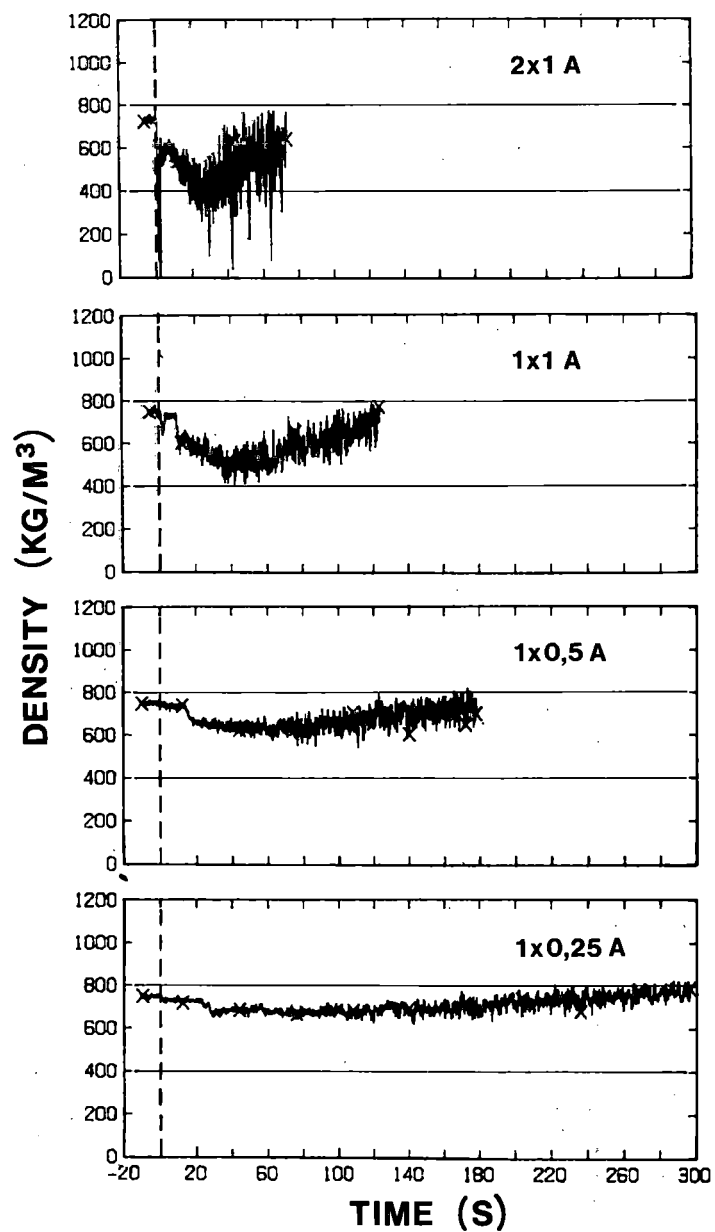


Figure 7 Density in the Core Entry

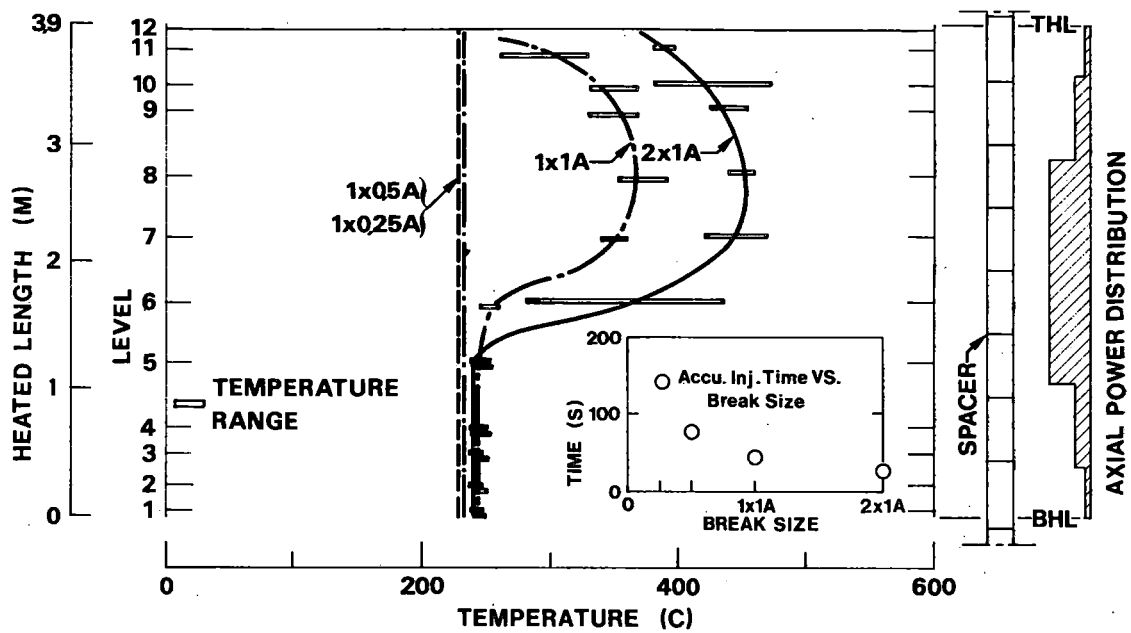


Figure 8 Heater Rod Bundle Axial Temperature Profile at Accumulator Injection Time (insert)

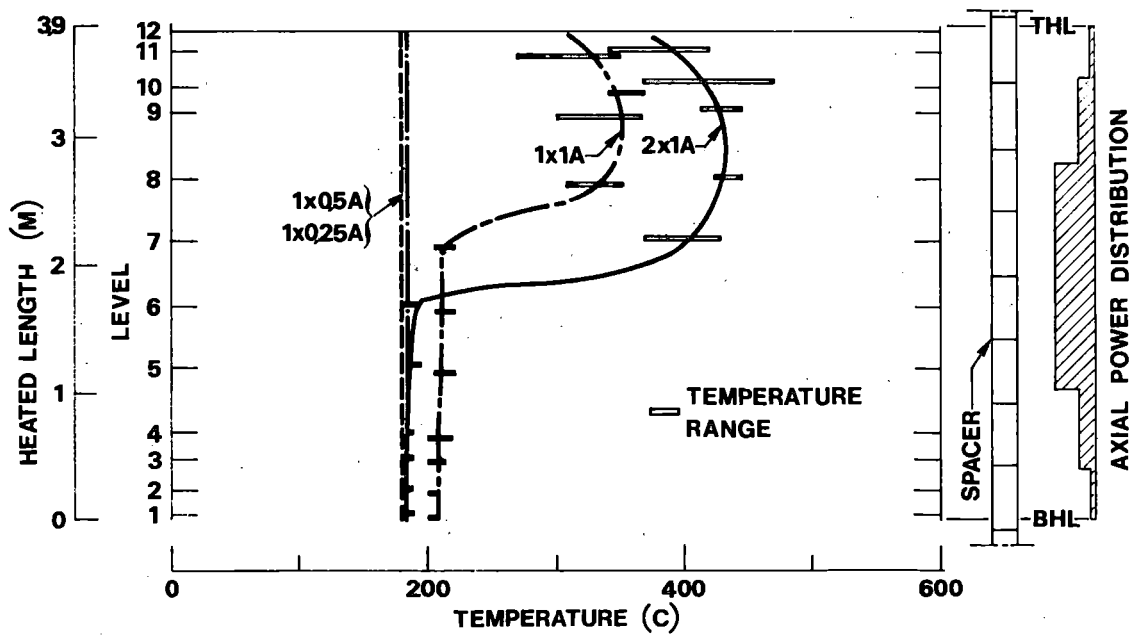


Figure 9 Heater Rod Bundle Axial Temperature Profile at Primary System Pressure of c. 1 MPa

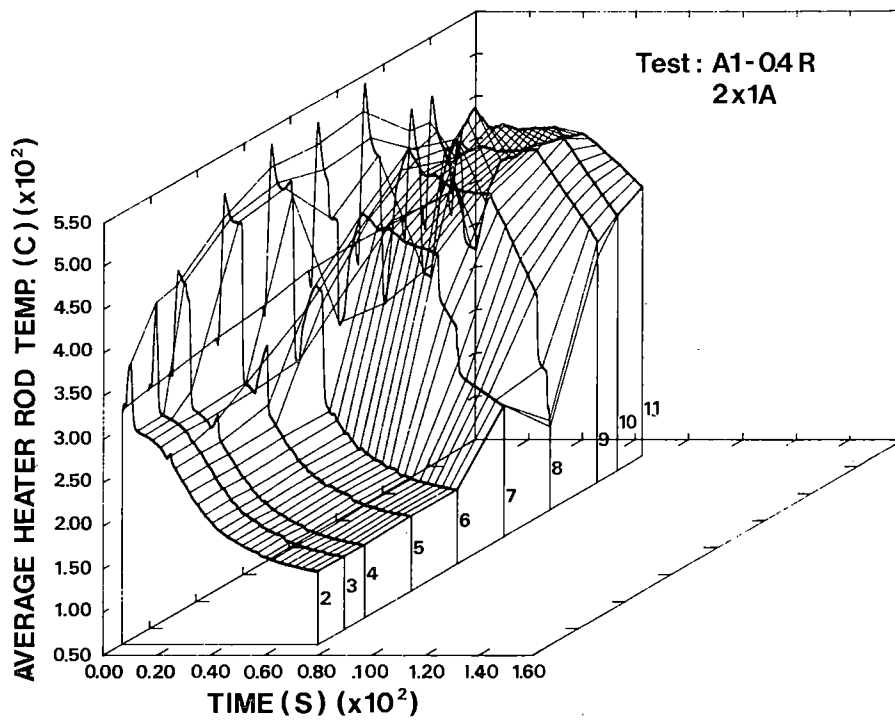


Figure 10 Development of Axial Profile of Heater Rod Temperature for
Test A1-04R (2 x 1A)

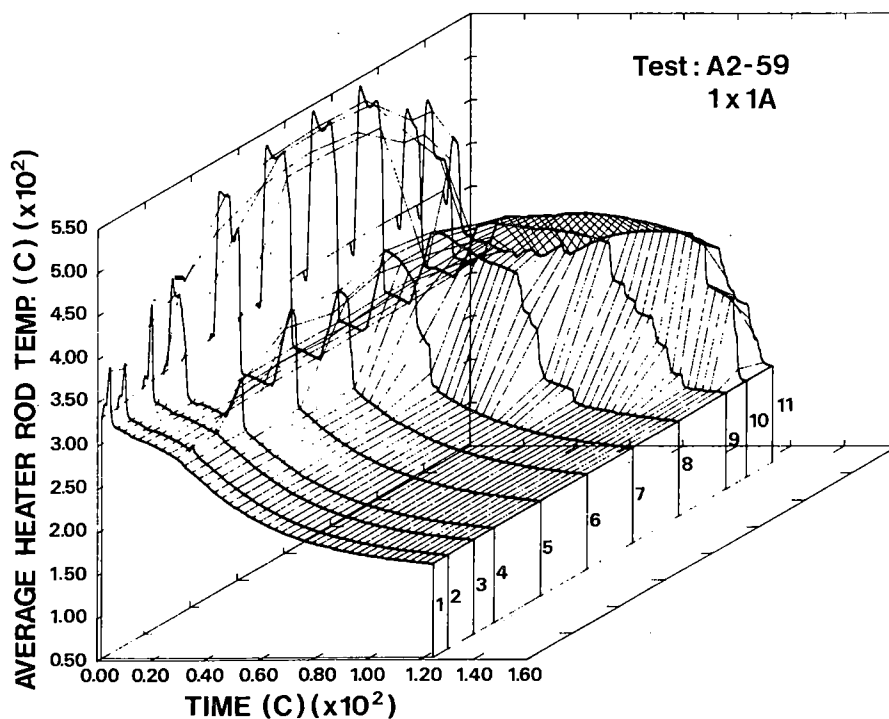


Figure 11 Development of Axial Profile of Heater Rod Temperature for
Test A2-59 (1 x 1A)

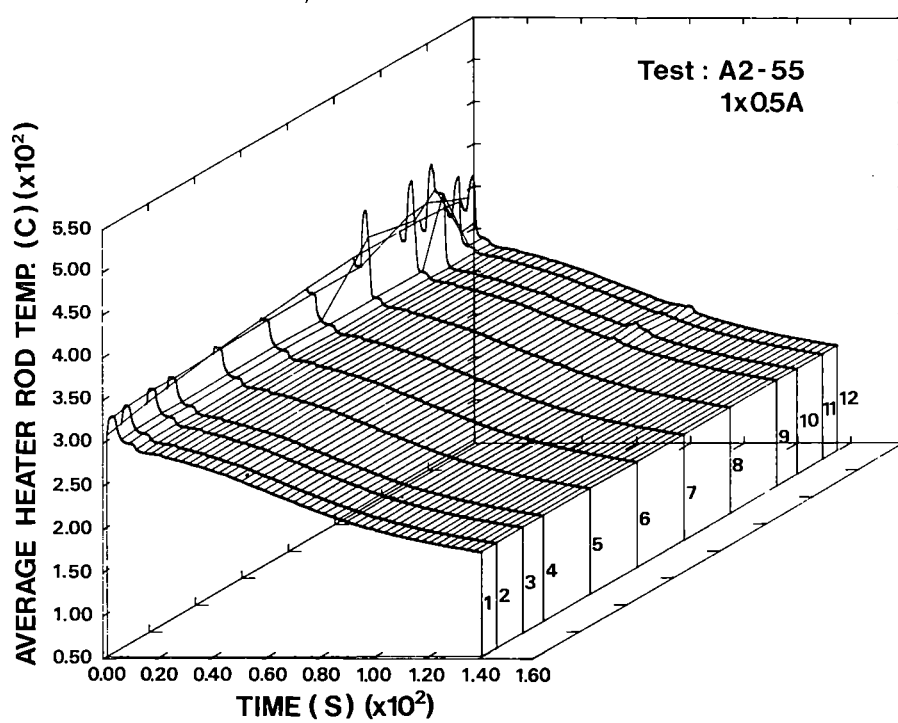


Figure 12 Development of Axial Profile of Heater Rod Temperature for Test A2-55 (1 x 0.5A)

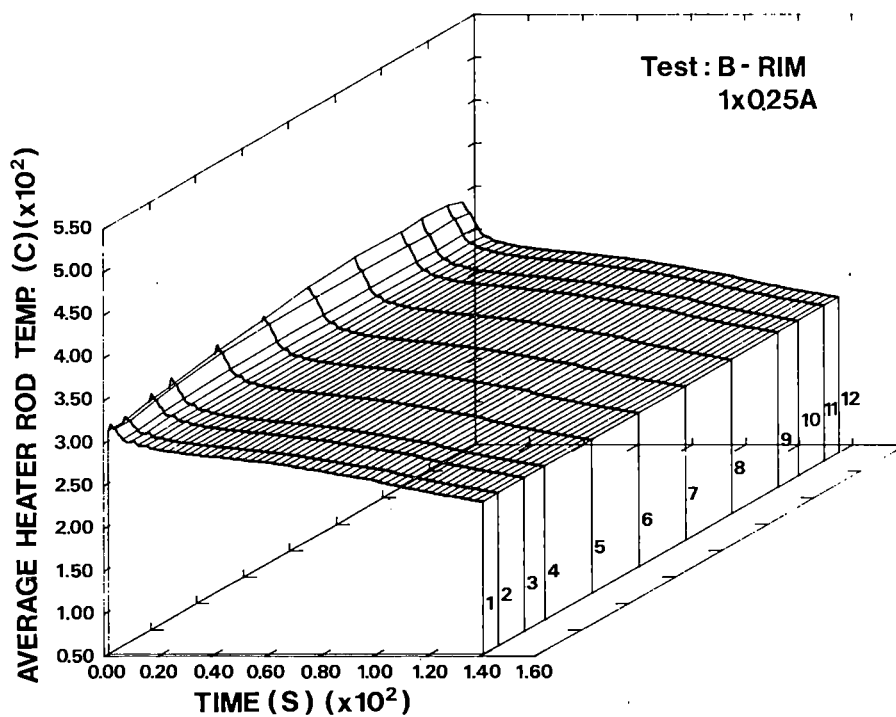


Figure 13 Development of Axial Profile of Heater Rod Temperature for Test B-R1M (1 x 0.25A)

EFFECT OF NONCONDENSIBLE GAS ON NATURAL CIRCULATION IN THE SEMISCALE MOD-2A FACILITY

K. Soda

Institute of Nuclear Safety, Japan
2-14-28 Mita, Minatoku, Tokyo, Japan

G. G. Loomis

Idaho National Engineering Laboratory, EG & G Idaho, Inc.,
P.O.Box 1625, Idaho Falls, Idaho 83415

ABSTRACT

Results are presented from an experimental investigation of the effect on noncondensable gas on natural circulation in a scaled model of a pressurized water reactor primary coolant system (Semiscale Mod-2A). Specifically, the effect of various nitrogen gas concentrations (in the coolant) on steady, two-phase and reflux natural circulation cooling modes has been identified and quantified. The Semiscale experiments were performed at high temperature and pressure (6.1 to 11.1 MPa) and included visual observations at key piping locations which aided in the interpretation of the the data.

INTRODUCTION

This paper presents results from an experimental investigation of natural circulation cooling with presence of noncondensable gas as it pertains to the safety aspects of pressurized water reactors (PWR's). Natural circulation flow is important as a core heat rejection mechanism during PWR accidents or transients involving loss of pumped flow. The presence of noncondensable gas during natural circulation has become an important safety issue since the Three Mile Island accident. The experimental investigation was performed in the Semiscale Mod-2A system which is a small, non-nuclear, high-pressure, experimental facility modeled from a PWR.

Specifically this paper examines the effects of noncondensable gas on natural circulation flow rate and heat transfer to the steam generator. Additionally, the migration of the noncondensable gas throughout the system is examined. The effect of noncondensable gas on system behavior was examined for two-phase liquid continuous natural circulation and the reflux cooling mode. Two-phase natural circulation is driven by fluid density differences created by core heat generation and steam generator heat removal. The reflux mode is characterized by steam from the core being condensed in the steam generator and the condensed liquid running back into the core through the hot leg.

SYSTEM DESCRIPTION AND TEST PROCEDURE

Semiscale Mod-2A is a scaled model representation of the primary system of a PWR plant, with a fluid volume of about 1/1705 of a PWR. The scaling philosophy followed in the design of the Mod-2A system (modified volume scaling) preserves most of the important first-order effects thought important for small break loss-of-coolant transients. Most notably the 1:1 elevation scaling of the Semiscale system is an important criterion for preserving the factors influencing natural circulation behavior. The Mod-2A system consists of a pressure vessel with external downcomer and simulated reactor internals; an intact loop with a tube and shell inverted U-tube active steam generator, pressurizer, and pump. For the natural circulation experiments an additional broken loop was disconnected and only the vessel and a single loop were used as shown on Figure 1. The intact loop pump was removed and replaced with an instrumented spool piece that has a scaled hydraulic resistance representative of a locked rotor pump condition. Within the Semiscale Mod-2A steam generator, volume scaling dictates six primary tubes (two long, two medium, and two short tubes). The vessel was modified for these tests by removing the vessel upper head. The simulated core consists of a 5 x 5 array of internally heated electric rods, 23 of which were equally powered. The rods are geometrically similar to nuclear rods with a heated length of 3.66 m and an outside diameter of 1.072 cm. External heaters are installed in a relatively uniform manner on the vessel and loop piping to offset environmental heat loss. The heaters are controlled by four independent, variable power supplies.

The nitrogen gas injection system consisted of valves, a pressure regulator and metering tank connected to the steam generator inlet piping such that injections of discrete volumes of nitrogen were possible. The amount of nitrogen gas injected into the system was calculated from pressure changes in the metering tank.

Measurements in the system include an extensive network of metal and fluid thermocouples and differential pressure measurements. In the steam generator, a long and short tube are extensively instrumented with both primary and secondary side fluid thermocouples and several primary side differential pressure measurements. Average fluid density is measured in the loops and vessel with X-ray and gamma densitometers. Volumetric flow is measured with turbine meters and momentum flux is measured with drag screens. Optical probes in the pressure boundary, and associated video equipment, were used to visually observe fluid flow behavior. These probes were installed in the steam generator inlet and outlet plena and in the vertical loop piping at the steam generator inlet and outlet. Visual observations were found to be a powerful tool for determining the existence of, and transition between, the natural circulation modes. A special reflux meter was attached to the steam generator inlet piping to catch condensed fluid as it left the steam generator. The reflux meter consisted of a tee in the primary piping connected to a standpipe, with a differential pressure measurement to measure the level of condensate. The reflux meter could be reset with a drain valve without adversely reducing system pressure.

Prior to initiation of an experiment, the system was filled with demineralized water and vented to ensure a liquid-full system. The system was heated using core power as a heat source and the steam generator secondary as a heat sink. Single-phase natural circulation flow (driven by density gradients in the loop) was used to thermally condition the system to obtain specified single-phase, steady-state conditions. Both the two-phase natural circulation and the reflux cooling mode were established by draining discrete amounts of fluid from the primary system. To establish the desired two-phase natural circulation condition, fluid was drained from the vessel until the system mass inventory was about 88.5% of the initial. For reflux, conditions were established at 57.3% inventory. After establishing steady initial conditions, nitrogen gas was introduced into the steam generator inlet plenum in increments of 1 to 2% of system volume. After an injection of nitrogen, sufficient time was allowed for conditions to stabilize. For all cases discussed in this paper,

the core power was 30 kW (representing 1.5% of full power) and the steam generator tubes were covered (collapsed secondary liquid level). The secondary fluid remained saturated at 6.0 MPa by using continuous feed and bleed. Primary pressure was dependent variable (values of 6.2 to 12.2 MPa were observed). The pressurizer was used only to establish initial conditions and then valved out of the system at the onset of system drain. Therefore, all system mass inventories are referenced to the full system without the pressurizer fluid. The leak rate was negligible and therefore no makeup was required. Four different banks of external heaters for the hot leg, cold leg, pump suction, and vessel-plus-downcomer were used to maintain a nearly zero temperature gradient from component-to-component thus simulating a net adiabatic boundary. However, for the reflux test, the pump suction and cold leg external heaters were turned off to eliminate boiling of stagnant water in the pump suction piping.

RESULTS AND DISCUSSIONS

The presence of noncondensable gas generally degrades heat transfer between a fluid and a solid surface. However, previous work (References [1]-[7]) concerns only the local effect of noncondensable gas on heat transfer and no work has been reported to date on the effects on noncondensable gas on natural circulation in an integral test facility at representative PWR pressures. The Semiscale Mod-2A experiments are unique in that hydraulic conditions were typical of those expected in a large PWR and extensive measurements including visual observations were made.

Effect of Noncondensable Gas on Two-Phase Natural Circulation

Discrete amounts of nitrogen gas were injected into the steam generator inlet piping during two-phase natural circulation. A total of 13 data points were obtained and the test conditions and important system parameters are summarized in Table I. A total amount of nitrogen gas equal to about 50% of the scaled volume of noncondensable gas present in accumulators and fuel rod plena of a PWR was injected.

The overall loop natural circulation mass flow rate was found to decrease as nitrogen gas was injected. Figure 2 presents the loop mass flow rate and the system pressure as a function of nitrogen gas volume injected into the system. The amount of nitrogen gas is in terms of the volume fraction of nitrogen relative to the system volume at measured system pressure and temperature.

The system pressure increased as more nitrogen gas was injected because nitrogen as a noncondensable gas occupied space in the system and pressurized the entire system. The initial introduction of nitrogen into the system had a large effect on loop mass flow rate as shown in Figure 2. The mass flow rate dropped to a magnitude typical of single-phase natural circulation after the first injection of nitrogen (the amount of nitrogen equaled about 1.4% of the system volume at system pressure and temperature).

The drop in mass flow rate from a peak two-phase natural circulation value to a nearly single-phase value is attributed to system pressurization caused by an interruption in two-phase natural circulation flow following the nitrogen injection. When the nitrogen was first introduced, a nitrogen bubble formed in the steam generator tubes which effectively blocked the continuous natural circulation flow. As a result of the cessation of natural circulation flow, the system pressure increased which caused the nitrogen bubble to compress. Eventually, the nitrogen bubble was compressed enough to allow a bridging of flow from the upflow side to the downflow side of the steam generator tubes which effectively restarted natural circulation flow. Once the flow restarted the system pressure dropped and a steady natural circulation condition was reached. The system pressure dropped to a value equal to

TABLE I.

Test Conditions for Test S-NC-5^{a,b}

Number	Mass Inventory (% of total)	Primary Pressure (MPa)	Cold Leg Fluid Temperature (K)	Hot Leg Fluid Temperature (K)	Injected N ₂ Volume ^c (%)	Loop Mass Flow Rate (kg/s)
1	100	11.1	549	570	0.0	0.28
2	88.5	6.5	549	553	0.0	0.61
3	88.5	7.5	551	563	1.4	0.29
4	88.5	7.8	551	566	2.5	0.27
5	88.5	8.0	548	567	3.4	0.24
6	88.5	8.3	547	569	4.3	0.23
7	88.5	8.6	547	571	5.2	0.22
8	88.5	8.3	546	569	7.4	0.23
9	88.5	8.8	548	573	8.8	0.21
10	88.5	8.4	547	574	11.4	0.21
11	88.5	9.7	549	576	11.5	0.20
12	88.5	9.9	549	577	12.6	0.19
13	88.5	10.3	550	579	13.2	0.19

a. Secondary pressure was 5.94 MPa throughout the test.

b. Core power was 32.2 kW.

c. Based on total system volume at pressure and temperature.

TABLE II.

Test Conditions for Test S-NC-6^{a,b}

Number	Mass Inventory (% of total)	Primary Pressure (MPa)	Fluid Temperature (K)	Fluid Temperature (K)	N ₂ (% of System Volume)	Reflux Rate (kg/s)
1	57.25	6.1	549	550	0.0	0.0113
2	57.25	6.1	550	550	0.86	0.0182
3	57.25	6.5	554	555	2.98	0.0178
4	57.25	7.1	558	560	5.00	0.0167
5	57.25	7.7	566	566	6.34	0.0175

a. Core power was 31.9 kW.

b. Secondary pressure was 5.95 MPa.

about 1 MPa higher than the pre-nitrogen injection pressure which was sufficient pressure to maintain a natural circulation condition of single-phase liquid and nitrogen bubbles.

Therefore, the injection of nitrogen gas was equivalent to reducing the void fraction of the fluid in the hot leg, core, and steam generator upside tubes. This in turn reduced the overall density gradient between the hot side and cold side of the steam generator which is the driving mechanism for natural circulation flow. Further introduction of nitrogen increased the system pressure, but only slightly decreased the mass flow rate. The slight decrease in mass flow rate was partly attributed to an increase in hydraulic resistance caused by the presence of nitrogen. Also, the reduction in mass flow rate could be accounted for due to an increase in the flow resistance in the steam generator, where some of the tubes were blocked by the nitrogen.

Injected nitrogen migrated into the vessel upper plenum and several of the steam generator tubes. Nitrogen gas in the upper plenum did not influence the natural circulation flow rate; however, the nitrogen that migrated into the steam generator tubes did stall the flow in several tubes. Nitrogen in the tubes became stagnant and remained in the top of the U-tubes. The amount of stagnant nitrogen increased as further injection was continued. However, in the rest of the system, including the rest of the U-tubes, a smooth and continuous two-phase natural circulation was observed throughout the test. Visual observations and fluid temperature measurements indicated that the two-phase flow consisted of liquid water and nitrogen bubbles. Figure 3 shows an estimated fluid inventory in the system (based on tube differential pressure transducers). It was observed that among the three instrumented steam generator tubes (out of total of six), the short tube and middle tube indicated stalled flow, and the long tube indicated normal two-phase natural circulation. Stall occurred when the flow was blocked by nitrogen gas in the U-bends.

Even though some of the tubes were stalled because of the presence of a noncondensable gas, the overall primary-to-secondary heat transfer rate in the steam generator was not degraded at acceptable primary pressures.

Effect of Noncondensible Gas on Reflux Cooling Mode

Discrete amounts of nitrogen gas were injected into the steam generator inlet piping during the reflux cooling mode. The test conditions and important system parameters for a total of five data points are presented in Table II. A total amount of nitrogen gas equal to 24% of the scaled volume of noncondensable gas present in accumulators and fuel rod plena of a PWR was injected. The reflux rate (the amount of condensed steam in the steam generator upflow side tubes running back to the vessel) was changed drastically when the nitrogen was first injected into the steam generator inlet plenum as shown on Figure 4. Prior to nitrogen injection the reflux rate (measured by the reflux meter) showed that nearly one-half of the steam generated in the core was condensed in the upside of the steam generator and the remainder was condensed in the downside. When the noncondensable gas was injected, the condensation occurred in the upside only and the measured hot leg refluxing rate was nearly 100% as shown on Figure 4. This remained true for all amounts of nitrogen gas that were injected. Visual observations through optical probes clearly showed the cessation of steam condensation in the downflow side of the steam generator tubes after the first nitrogen injection.

Figure 5 shows that estimated fluid distribution in the system after injecting a nitrogen volume equal to 5.0% of the system volume. Nitrogen gas collected in the steam generator tubes such that steam condensation occurred in only the upflow side of the steam generator tubes. Even though nitrogen gas prevented condensation in the downflow side, the overall heat removal rate between the primary and the secondary remained the same and the steam generator acted as an effective heat sink at acceptable primary pressures.

CONCLUSION

- 1) Nitrogen injection into the steam generator inlet piping during both two-phase and reflux natural circulation did not preclude effective rejection of core heat to the steam generator at acceptable pressures.
- 2) The effect of injecting nitrogen into the steam generator inlet piping during two-phase natural circulation was an increase in system pressure and a decrease in mass flow rate. The loop mass flow rate was reduced to value similar to those observed for single-phase conditions after the first injection of an amount of nitrogen equal to 1.4% of the total system volume. Further introduction of nitrogen increased the system pressure, but only slightly decreased the mass flow (this was true for volumes of nitrogen up to 13% of the total volume). As more nitrogen was injected into the system, the system pressure increased because the nitrogen occupied more volume. The mass flow rate appears to have decreased due to an effective increase in hydraulic resistance.
- 3) The effect of injecting nitrogen during the reflux cooling mode was to completely eliminate condensation in the steam generator tube downflow sides (as supported by visual observations). However, all of the steam created in the core was adequately condensed in the upflow side of the steam generator. This occurred for all amounts of nitrogen injected into the system (up to 6.3% of the system volume). Therefore, even though the normal 1:1 split of steam condensation in the upflow and downflow sides of the steam generator was interrupted when nitrogen was injected, system fluid conditions stabilized at acceptable pressures.

ACKNOWLEDGEMENT

This work was supported by the U.S. Nuclear Regulatory Commission, Office of Nuclear Regulatory Research under DOE Contract No. DE-AC07-76ID01570.

REFERENCES

1. Sparrow, E.M. and Lin, S.H., "Condensation Heat Transfer in the Presence of a Noncondensable Gas", J. Heat Transfer, 86, 430(1964)
2. Sparrow, E.M. and Minkowycz, Y., "Condensation Heat Transfer in the Presence of Noncondensibles, Interfacial Resistance, Superheating, Variable Properties, and Diffusion", Int. J. Heat Mass Transfer, 9, 1125(1966)
3. Mori, Y. and Hijikata, K., "Free Convective Condensation Heat Transfer with Noncondensable Gas on a Vertical Surface", Int. J. Heat Mass Transfer, 16, 2229(1973)
4. Sage, F.E. and Estrin, J., "Film Condensation from a Ternary Mixture of Vapors upon a Vertical Surface", Int. J. Heat Mass Transfer, 19, 323(1976)
5. Borinshansky, V.M. and et al., "Effect on Uncondensable Gas Content on Heat Transfer in Steam Condensation in a Vertical Tube", Heat Transfer-Soviet Research, 9, 35(1977)
6. Weiss, H. and Gutfinger, C., "Film Condensation Inside Tubes in the Presence of a Noncondensable Gas", Israel Journal of Technology, 15, 255 (1977)
7. Kotake, S., "Film Condensation of Binary Mixture Flow in a Vertical Channel", Int. J. Heat Mass Transfer, 21, 875 (1978)

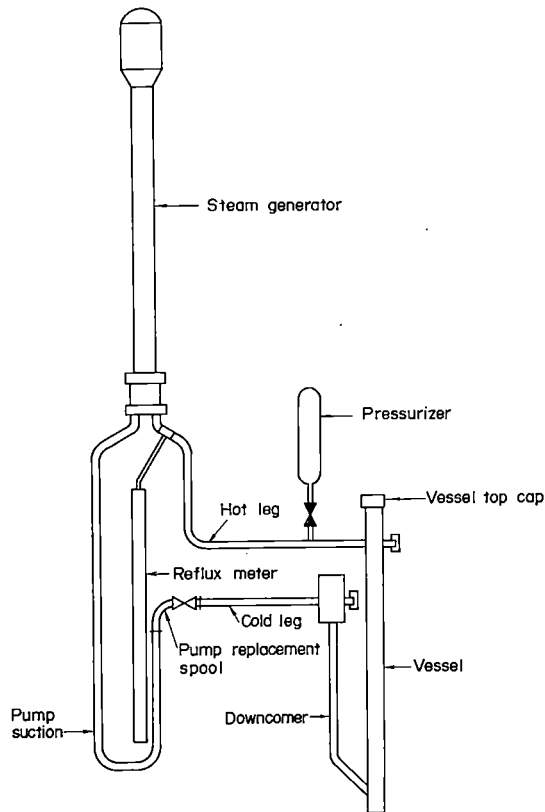


Figure 1. System configuration for Tests S-NC-5 and S-NC-6

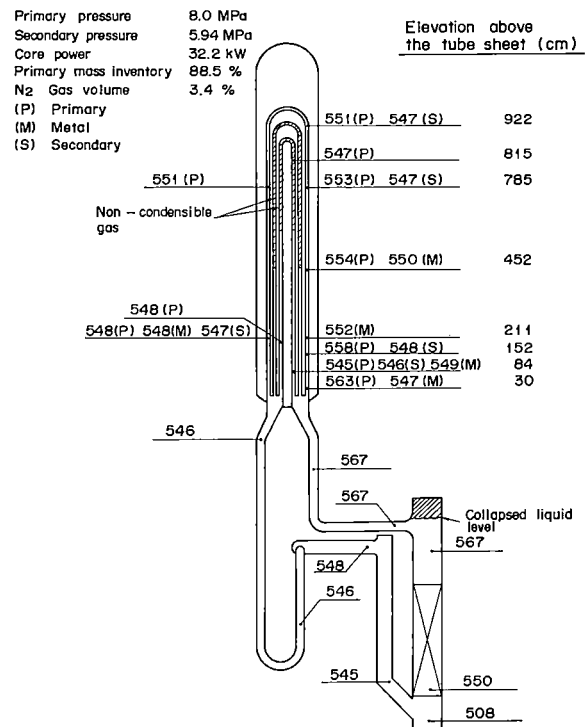


Figure 3. Fluid temperature and mass distribution after injecting a nitrogen volume equivalent to 3.4% of the system volume during two-phase natural circulation

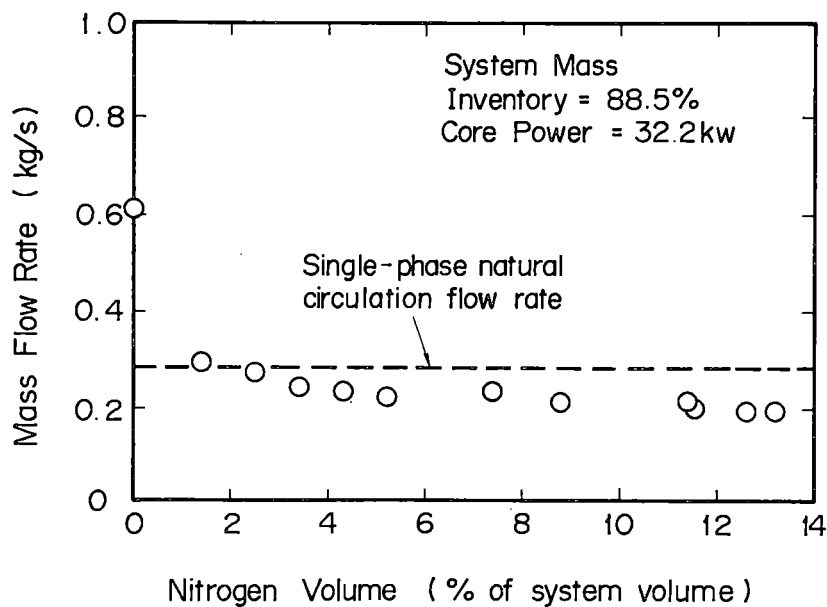


Figure 2. Loop mass flow rate as a function of the volume of injected nitrogen (percent of system volume at system temperature and pressure).

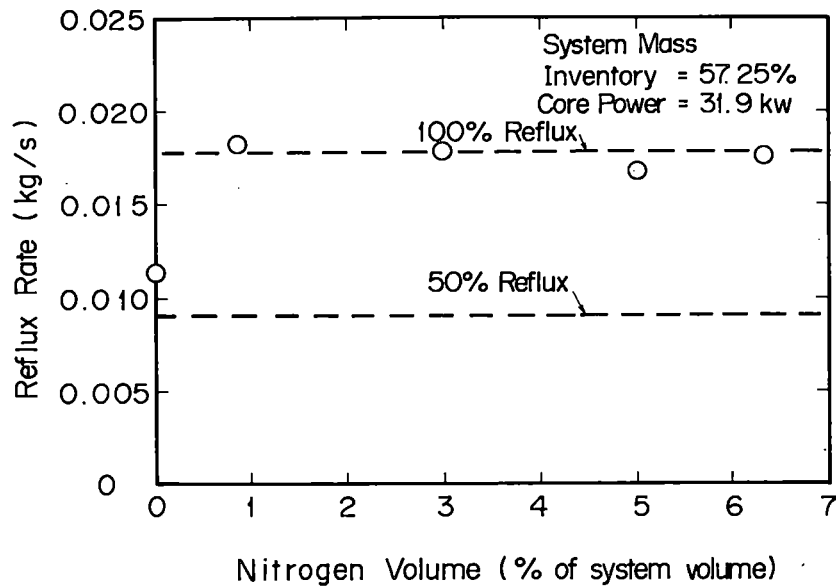


Figure 4. Hot leg reflux rate as a function of nitrogen injection

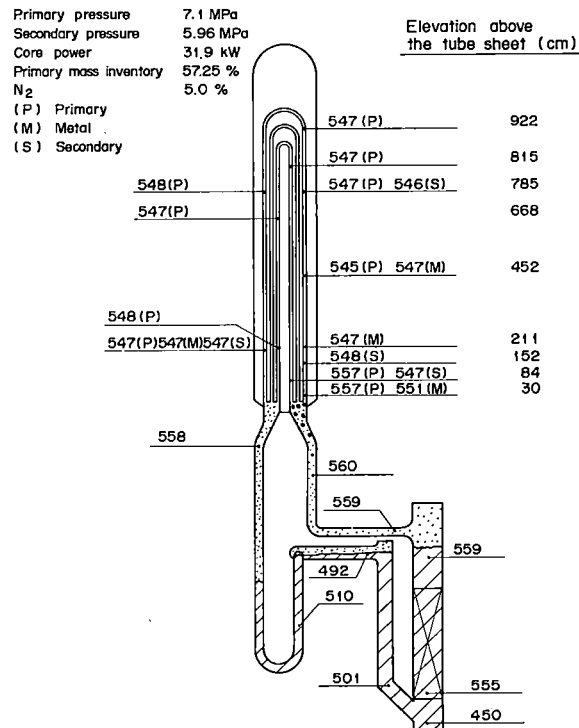


Figure 5. Fluid temperature and mass distribution during reflux cooling after injecting a nitrogen volume equivalent to 5.0% of the system volume during reflux natural circulation cooling mode.

INFLUENCE OF DOWNCOMER VOLUME AND GAP WIDTH ON BLOWDOWN

H. Städtke, D. Carey, W. L. Riebold

Commission of the European Communities
EURATOM Joint Research Centre - Ispra Establishment
LOBI Project, Heat Transfer Division
I-21020 ISPRA/Varese (I)

ABSTRACT

Experimental results from two LOBI large break blowdown/refill tests, with different downcomer volumes and gap widths, have been analysed. Both tests, which simulated a 2A offset shear break in the cold leg pipe of a PWR, were performed with nearly the same initial and boundary conditions. The experimental data show a strong influence of the downcomer volume and gap width on the thermo-hydraulic behaviour of the system during the blowdown and refill period of the transient. The analysis of the reasons for this different behaviour is supported by results from RELAP4/Mod 6 test predictions which, in general, agree well with the measured data.

INTRODUCTION

The LOBI¹-test facility / 1 / was built and is operated by the Joint European Research Centre (J.R.C.) in Ispra, Italy. The LOBI facility was designed to simulate the thermal-hydraulic behaviour of the primary coolant system of a pressurised water reactor during the blowdown and the beginning of the refill period of a Loss of Coolant Accident. In the first part of the LOBI test programme / 2 /, large break blowdown tests with different break sizes and different break locations were performed within the framework of a contract between the Commission of the European Communities and the "Bundesminister für Forschung und Technologie" in Germany. Following the commissioning of the test facility in 1979, 25 large break blowdown tests have been successfully performed up to the end of June 1982.

LOBI TEST FACILITY

The LOBI test facility has, similar to Semiscale and LOFT, a two-loop configuration where the "intact loop" represents three unbroken loops of a four loop PWR.

¹ Loop Blowdown Investigations

Within the "broken loop" pipe ruptures of different sizes can be simulated at three different break positions (hot leg, cold leg, pump suction leg). Both loops contain steam generators and circulation pumps. A view of the LOBI test facility is shown in Fig. 1.

The nuclear core is simulated by an electrically heated 64 rod bundle with a full length "heated section" of 3.9 m. The heater rods, which have the same outer diameter as the nuclear fuel rods of the reference plant, are directly heated hollow tubes. A stepped axial cosine profile is achieved by five sections with different tube wall thicknesses. The fission power and the release of the decay-heat and the stored energy of the nuclear fuel rods are simulated by an appropriate electrical power-time curve which has to be determined prior to each test based on pre-test predictions / 3 /.

All the components in the primary system of the test facility have their full heights and are arranged at their original elevations. The volumes of the components, the mass flows in the system and the nominal power input have been scaled down from a 1300 MWe reference reactor plant by a factor of 1/712. This results in a nominal power for the LOBI facility of 5.3 MW.

An exception to this scaling concept is the annular shaped downcomer of the facility. A volume scaled downcomer would result in a gap width of 7 mm which is not acceptable for two reasons: (1) the large surface area-to-volume ratio and the corresponding high heat transfer from the downcomer walls to the fluid¹ could prevent the penetration of ECC water into the downcomer and lower plenum, (2) the small hydraulic diameter of the downcomer could possibly suppress the occurrence of two-phase counter-current flow, which is expected to be an important effect in the refilling of the reactor downcomer and lower plenum after the ECC injection has started.

Although the downcomer problematic is well known from the Semiscale test programme / 4 /, no general scaling concept for the downcomer gap size is available at present. The rational scaling criteria may also be different for the different periods of the LOCA (blowdown, refill period), depending on the governing physical phenomena.

For this reason it has been decided to perform blowdown tests with two different downcomer gap widths. In the first test series a gap width of 50 mm was used which resulted in 6.3 times too large a downcomer volume and therefore in a strong distortion of the mass distribution in the scaled system. In a second test series the downcomer gap width was reduced to 12 mm by installing a downcomer filler. The 12 mm gap width was chosen as a compromise between the volume scaled downcomer (7 mm gap width) and a downcomer which would yield the same pressure drop due to wall friction as in the reference reactor (25 mm gap width for the scaled facility). For the downcomer filler a honeycomb structure was used in order to reduce the amount of stored heat in the downcomer walls. Although the 12 mm gap width still gives too large a downcomer volume (1.7 times larger than the volume scaled downcomer), the volume and mass distribution is more representative of the reactor

¹The downcomer walls are not thermally insulated

cooling system. The cross sections of the LOBI pressure vessel with the two different downcomer gap sizes are shown in Figure 2.

LOBI TESTS A1-04R (50 MM DOWNCOMER GAP WIDTH)
AND A1-66 (12 MM DOWNCOMER GAP WIDTH)

The tests A1-04R and A1-66 have been selected for the investigation of the influence of the downcomer volume and gap size during the blowdown and early refill period. Apart from the different gap width of the annular shaped downcomer, 50 mm for test A1-04R and 12 mm for test A1-66, the tests also differ in the flow resistance of the accumulator injection line. Test A1-04R was performed without any flow restriction in the injection line. This resulted in an atypically large ECC injection rate. The installation of orifice plates in the later LOBI test Programme (including test A1-66) gave, due to the increased flow resistance, a more reactor-typical ECC injection characteristic.

Tests A1-04R and A1-66 were performed with nearly the same initial and boundary conditions. These include:

- (1) nominal initial conditions for pressure, temperature and mass flows in the primary and secondary system
- (2) same break configuration and break location: double-ended (non-communicative) break in the cold leg pipe between pump and pressure vessel
- (3) same break area of $2 \times 7.069 \cdot 10^{-4} \text{ m}^2$ which corresponds to a relative break size¹ of $2 \times 0.75A$ in the case of test A1-04R and $2 \times 1.0A$ in the case of test A1-66
- (4) same mode of ECC injection: accumulator injection only into the cold leg pipe of the intact loop with an actuation pressure of 2.7 MPa.

There was no low pressure ECC injection for tests A1-04R and A1-66. In both tests, the LOBI model containment was connected with the atmosphere and, therefore, nearly atmospheric pressure existed downstream of the break during the whole transient. These limitations may result in reactor-atypical behaviour during the low pressure period of the transient ($p < 1.0 \text{ MPa}$).

The circulation pumps in the intact and broken loops were controlled using prescribed pump speed versus time curves as shown in Fig. 3. These pump speed-time curves, which are nearly identical for tests A1-04R and A1-66, were determined in order to give a similar pump head (pressure difference over the pump) behaviour as expected for the reactor pump for the same transient.

The transient electrical power curves shown in Fig. 4 simulate the heat release from nuclear fuel rods due to fission power, decay heat of the fission products and the stored heat in the nuclear fuel. The curves are calculated from the results of a pre-test prediction assuming a nuclear fuel rod bundle instead of the

¹ The relative break size is defined as the break area-to-primary system volume ratio of the test facility related to the same ratio for the reactor system.

electrically heated bundle in the LOBI test facility. Large differences in the heat transfer conditions in the core region resulted in different electrical power curves for tests A1-04R and A1-66 during the blowdown transient.

TEST PREDICTIONS

Pre-test and post-test predictions for the tests A1-04R and A1-66 were performed with the RELAP4/Mod 6 code. As can be seen from the figures, the predicted values describe fairly well the measured system behaviour. This is considered to justify the use of the predicted data for the test analysis in those cases where no, or no reliable, measurements were available e.g. fluid temperatures and vapor qualities in the core region and mass flows in the downcomer and core.

SYSTEM BEHAVIOUR FOR TEST A1-04R AND TEST A1-66 DURING BLOWDOWN AND EARLY REFILL PERIOD

After initiation of the blowdown the system pressure decreased very rapidly (within 100 ms) from its initial value to the saturation pressure corresponding to the fluid temperature in the upper plenum and hot leg pipes (Fig. 5). This pressure drop was accompanied by a sudden reversal of flow in the core region (Fig. 6). A slower depressurization followed as evaporation started in the upper plenum and hot leg pipes and the evaporation front propagated into the core and steam generator U-tubes.

Due to the rapid increase in vapour content in the core (Fig. 7) and the resulting expansion of the two-phase fluid the (absolute) core mass flow decreased such that nearly stagnation conditions occurred in the core region between 1 s and 2 s into the blowdown transient (Fig. 6). Both the increased vapour content and the reduced (absolute) core flow led to a DNB over the whole heated length of the bundle at about 1 s after blowdown initiation as can be concluded from the sudden increase in the heater rod temperatures at that time (Fig. 9 and 10). The heater rod temperatures subsequently reached a first maximum at 2.5 s (test A1-66) and at 3.2 s (test A1-04R), when the electrical power input to the bundle was reduced to 32 % of its initial value (Fig. 4).

During the first 2.6 s of the blowdown, before the system pressure has fallen below the saturation pressure corresponding to the initial fluid temperature in the cold leg pipe and downcomer region, the system behaviour as described above is nearly identical for tests A1-04R and A1-66. From this agreement it can be concluded that, as long as single phase (subcooled) liquid conditions remain in the downcomer, the amount of liquid in the downcomer region and the downcomer gap size have only a minor effect on the overall system behaviour. However, this may be true only because the flow resistance of the downcomer is small compared with other parts of the pressure vessel, e.g. upper and lower plenum with internals, core region.

Between 2 s and 3 s of the transient evaporation also started in the intact loop cold leg pipe and in the downcomer region. Beginning at this time the course of the transient became extremely influenced by the downcomer volume and gap size.

The evaporation of the liquid and the accompanying strong expansion of the two-phase fluid in the downcomer region led to a further decrease in the system depressurisation rate (Fig. 5). The expansion of the two-phase fluid in the downcomer also caused a change in the pressure distribution and, as a consequence, the re-establishment of a positive core mass flow (Fig. 6). These effects were much more pronounced in test A1-04R where the initial amount of liquid in the downcomer was 4.2 times larger than in test A1-66. During the subsequent time period, the system pressure in test A1-04R was higher up to 2.0 MPa than that for test A1-66. In test A1-66, the positive core flow was only temporary. After most of the liquid in the downcomer had evaporated the core mass flow reduced again and after 8 s into the transient nearly stagnation conditions existed in the core. In test A1-04R, however, the positive core flow remained until the end of the blowdown transient.

The initial amount of 'cold' liquid in the downcomer region also influenced the residual water mass in the lower plenum (Fig. 11). In test A1-04R a high fluid density existed throughout the whole blowdown transient, whereas in test A1-66 the amount of residual water in the lower plenum reduced continuously from 7 s until the initiation of the ECC injection.

The behaviour of the heater rod temperatures, as shown in Fig. 9 and 10, is directly related to the core mass flow and the fluid density at the core inlet. After the power reduction at 3.2 s for test A1-04R, the relatively large positive core mass flow and the high fluid density in the lower plenum led to a fall in the vapour quality in the core (Fig. 7) together with a partial rewetting of the heater rods and a rapid drop in their surface temperature (Fig. 9 and 10).

The increased core mass flow between 3 s and 7 s in test A1-66 also resulted in a fall of the heater rod temperatures. However, after nearly stagnation conditions were reached in the core at about 8 s, the core completely voided and from 10 s onwards superheated vapour conditions existed in the core (Fig. 8). Consequently heater rod temperatures rose again until the core power was reduced to 8 % of its initial value when the vapour cooling became sufficient to maintain the temperatures relatively constant but at a level significantly higher than the first maximum (Fig. 9 and 10).

The injection of subcooled water from the accumulator started, at 24 s in test A1-04R and at 18 s in test A1-66, when the primary system pressure had fallen below the activation pressure of 2.7 MPa. Due to the differences in the injection line flow resistance different injection rates were measured and predicted for tests A1-04R and A1-66 as shown in Fig. 12.

As explained above, completely different conditions existed in the pressure vessel in tests A1-04R and A1-66 at the time of initiation of ECC injection from the accumulator. These differences, which were a result of the different downcomer volumes in the two tests, probably had a strong influence on the subsequent refill behaviour of the pressure vessel.

For test A1-04R (50 mm downcomer gap width), the refilling of the downcomer was predicted to start 4.5 s after the initiation of ECC injection as indicated by the positive liquid mass flow rate at the inlet to the downcomer in Fig. 13. The

fraction of the injected water which penetrated the downcomer increased continuously and about 10 s after ECC injection had started more than 50 % of the ECC water flow was entering the upper part of the downcomer. During the refill period counter current flow conditions were predicted to occur in the downcomer region. A fraction of the water which enters the downcomer is evaporated, if it comes into contact with the hot walls of the downcomer channel, causing an upward flow of vapour. The superficial velocity of this vapour flow was sufficiently below the Wallis flooding criteria and, therefore, it is expected that counter-current flow limitations did not prevent the refill of the pressure vessel in the case of test A1-04R. Only a small fraction of the ECC water which entered the lower plenum remained there (Fig. 11). Due to the core flow still being positive (Fig. 6), most of this water flowed into the core causing a decrease of the vapour quality (Fig. 7) and an improvement in the cooling of the heater rod bundle.

For test A1-66 (12 mm downcomer gap width) the penetration of the ECC water into the top of the downcomer was predicted to occur 5 s after the initiation of ECC injection. Only about 30 % of the ECC water was predicted to penetrate the downcomer compared to 50 % in test A1-04R. The lower penetration rate appears to be a result of the reduction in downcomer gap width from 50 mm to 12 mm. This reduction in gap size, by increasing the surface-to-flow area ratio by a factor of 4, increased the potential for heat transfer from the downcomer walls to the fluid. Consequently, higher evaporation rates and upward vapour velocities resulted which restricted the penetration of liquid into the downcomer.

Most of the liquid which penetrated as far as the bottom of the downcomer was collected in the lower plenum as shown by the density increase between 18 s and 30 s (Fig. 11). However, beginning at 30 s in the experiment and 35 s in the prediction, short periods of complete voiding of the downcomer and lower plenum occurred indicating interruptions in the refill of the pressure vessel. It is assumed that liquid periodically entered the lower part of the core which contained superheated vapour with temperatures up to 550 °C (Fig. 8). This caused a rapid evaporation which forced the liquid from the downcomer and lower plenum into the broken loop cold leg and towards the break. This process was repeated, at intervals of 5 s to 8 s, several times.

The refill behaviour, as described above, is probably strongly influenced by the containment pressure. Primary pressures 60 s after blowdown initiation were still 0.3 to 0.5 MPa. This led to relatively large critical break mass flow rates due to the low containment pressure of 0.1 MPa. The vessel side break was fed mostly by ECC water which bypassed the pressure vessel. An increased, and more correctly simulated, containment pressure would reduce the break mass flow during the late refill period and thus, probably, decrease the amount of ECC bypass.

CONCLUSIONS

- (1) Downcomer gap width and volume had little effect upon the system behaviour during blowdown whilst fluid conditions remained subcooled in the downcomer.
- (2) The larger downcomer, due to the increased amount of coolant, caused a slower depressurization rate following the propagation of the evaporation fronts into

the 'cooler' parts of the circuit.

- (3) The larger downcomer volume resulted in more fluid remaining in the pressure vessel, particularly the lower plenum, and in positive core mass flows during the late blowdown and refill period. This provided good cooling of the heater rod bundle during the whole transient.
- (4) The smaller downcomer gave a more reactor typical system behaviour during the blowdown period due to the more accurate representation of the fluid mass distribution in the primary system.
- (5) The smaller downcomer gap width inhibited ECC penetration and refill of the pressure vessel as a result of increased heat transfer from the downcomer walls to the fluid, increased evaporation rate and higher vapour velocities in the upward direction.

REFERENCES

1. W. L. RIEBOLD, H. STÄDTKE, "LOBI - Influence of PWR Loops on Blowdown. First Results", Trans. Am. Nucl. Soc. 38, 734 (1981).
2. W. L. RIEBOLD, "LOBI Experimental Programme A - Testmatrix A1 and A2", Technical Note I.06.01.111.79, J.R.C. Ispra, 1979.
3. H. STÄDTKE, L. PIPLIES, "Performance of Directly Heated Rods as Nuclear Fuel Rod Simulators in the LOBI Facility", Proceedings of the International Symposium on Fuel Rod Simulators, Gatlinburg, Tennessee, October 1980.
4. T. K. LARSON, E. A. HARVEGO, "Semiscale Program Summary: A Review of Mod 3 Results", Nuclear Safety, Vol. 22, No. 2, May-June 1981.

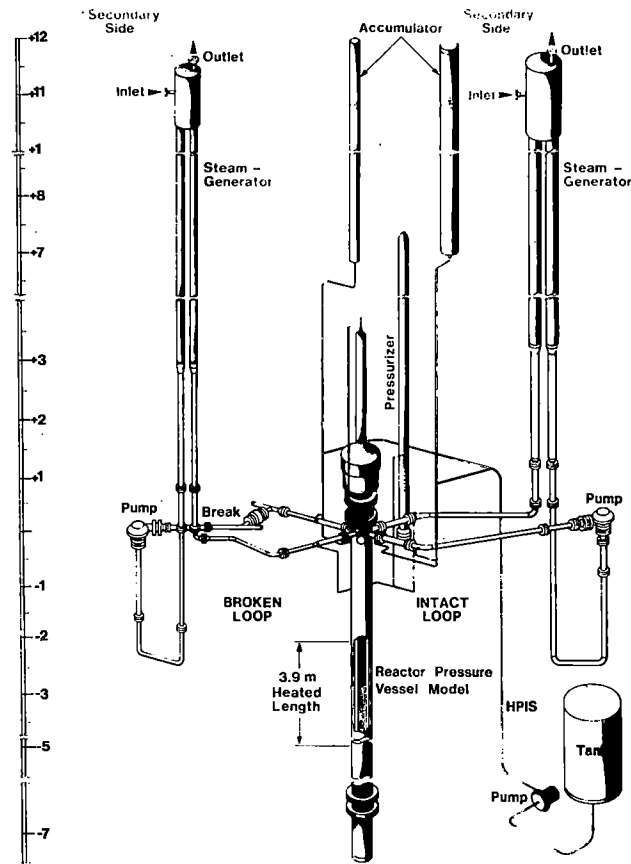


Fig. 1: LOBI Test Facility

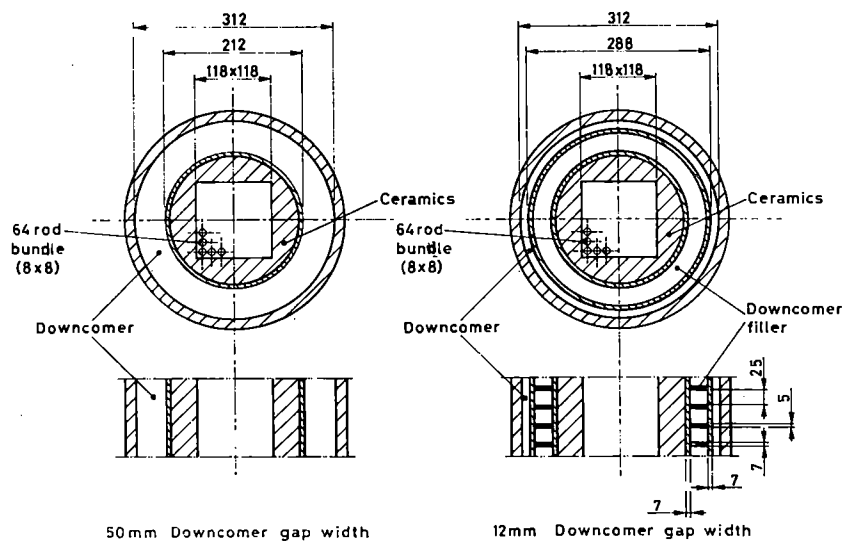


Fig. 2: Cross Section of LOBI Pressure Vessel

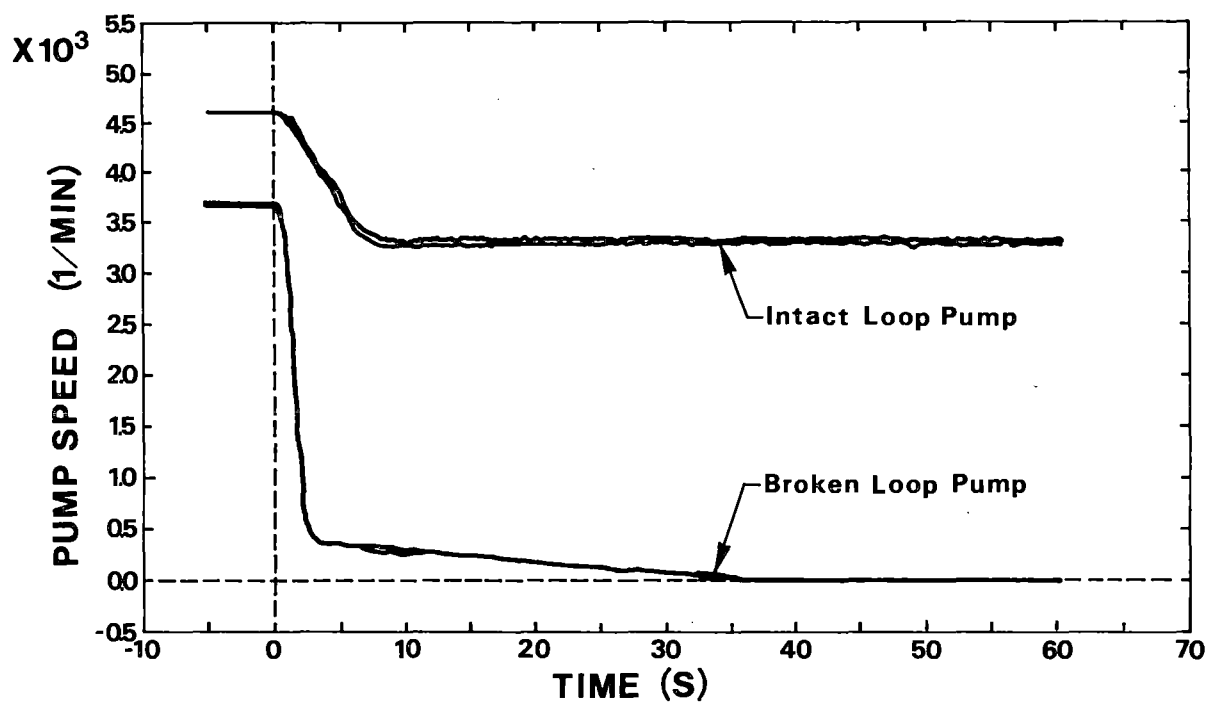


Fig. 3: Pump Speeds for Intact and Broken Loop Pump, Test A1-04R and A1-66

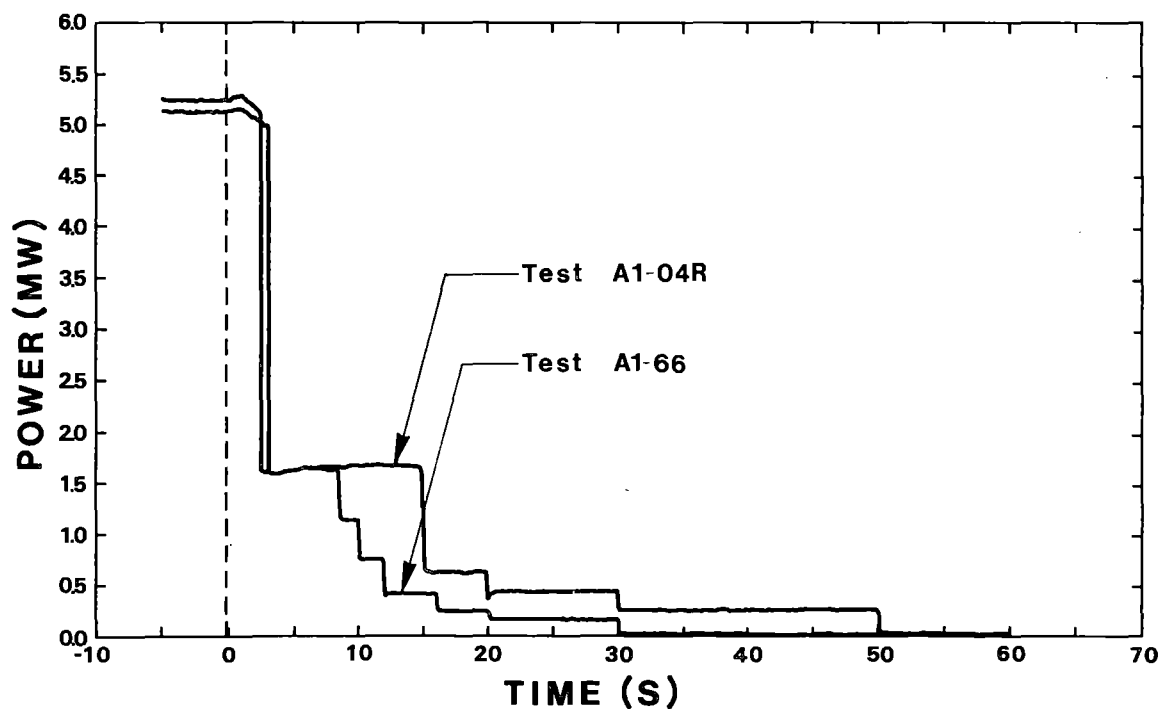


Fig. 4: Electrical Power Input

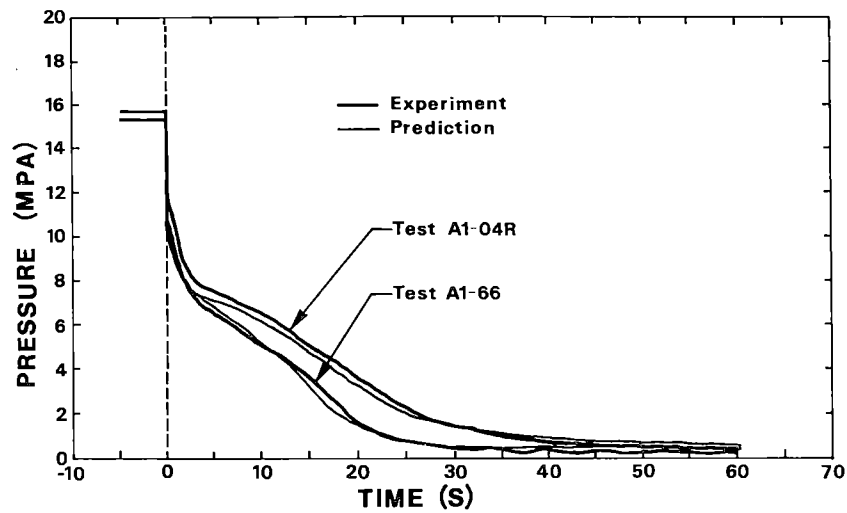


Fig. 5: Pressure in Lower Plenum

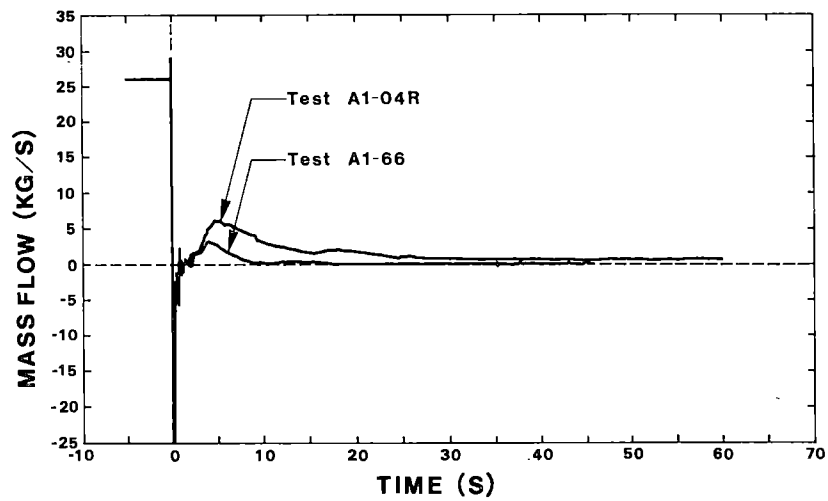


Fig. 6: Calculated Mass Flow in Core Middle Section

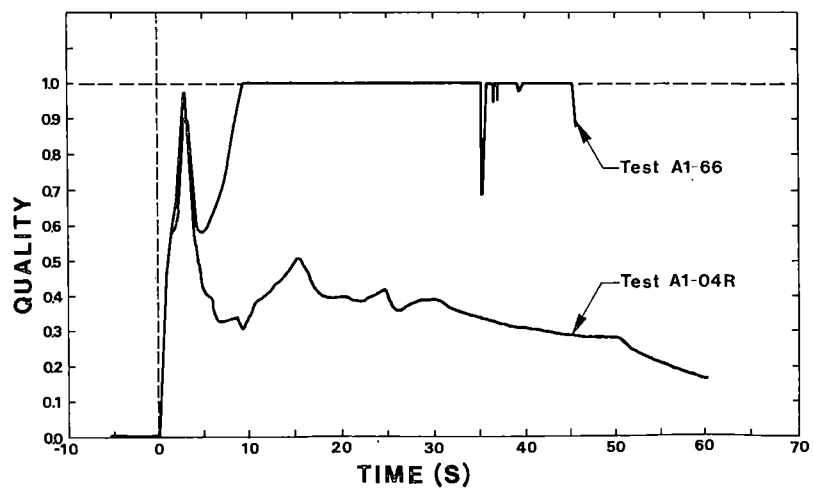


Fig. 7: Calculated Vapor Quality in Upper Part of Core Middle Section

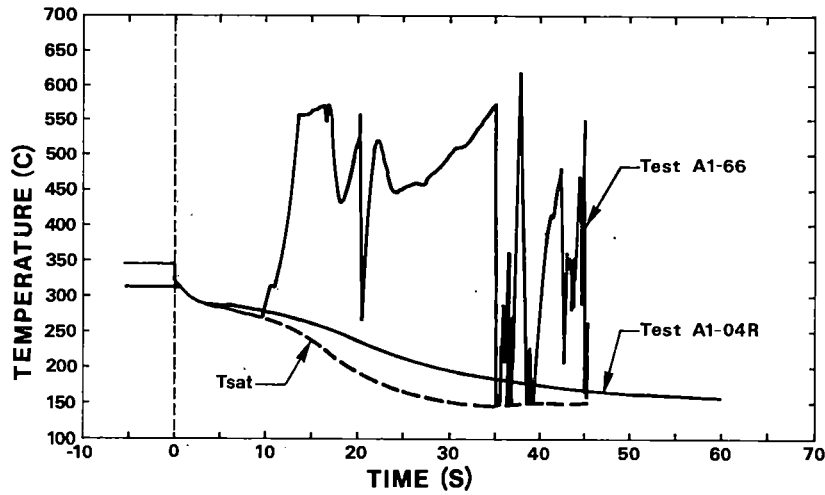


Fig. 8: Calculated Fluid Temperatures in Upper Part of Core Middle Section

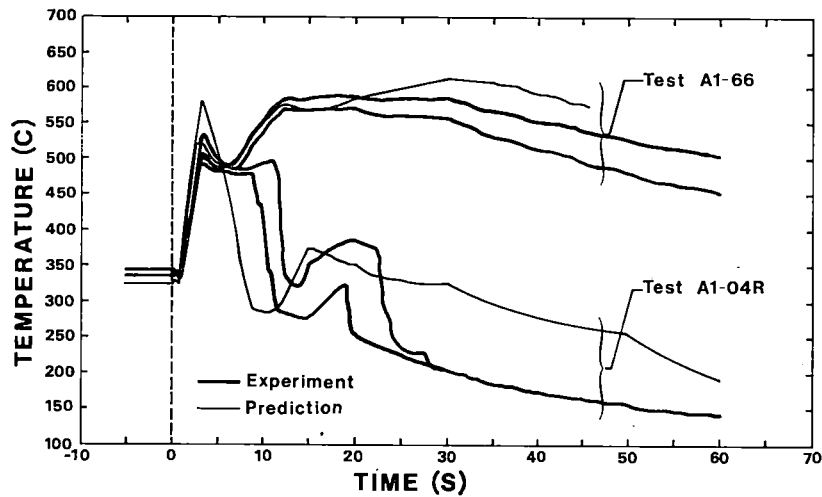


Fig. 9: Heater Rod Surface Temperatures, Lower Part of Middle Section

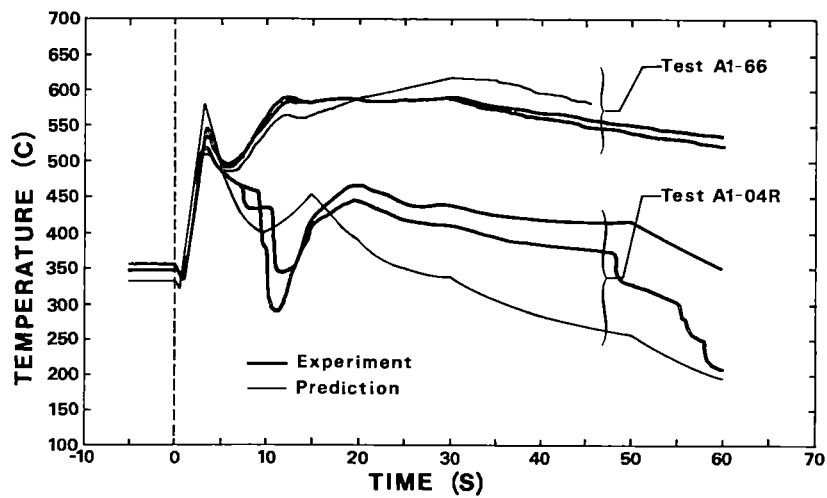


Fig. 10: Heater Rod Surface Temperatures, Upper Part of Middle Section

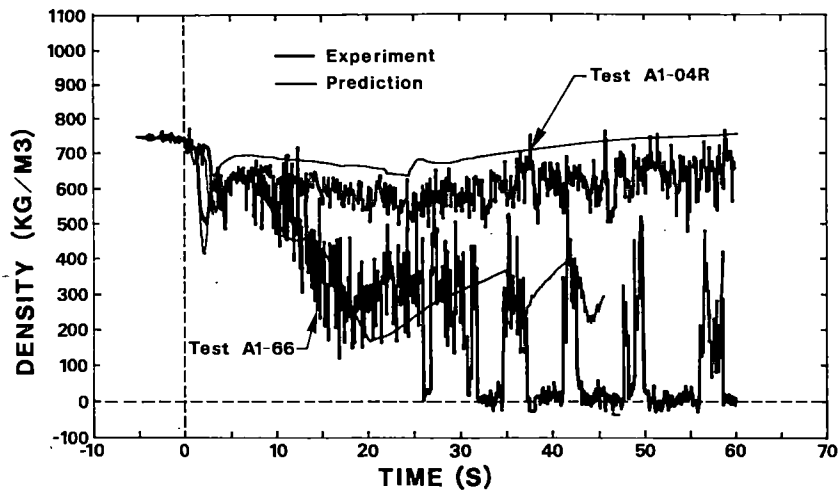


Fig. 11: Fluid Density in Lower Plenum

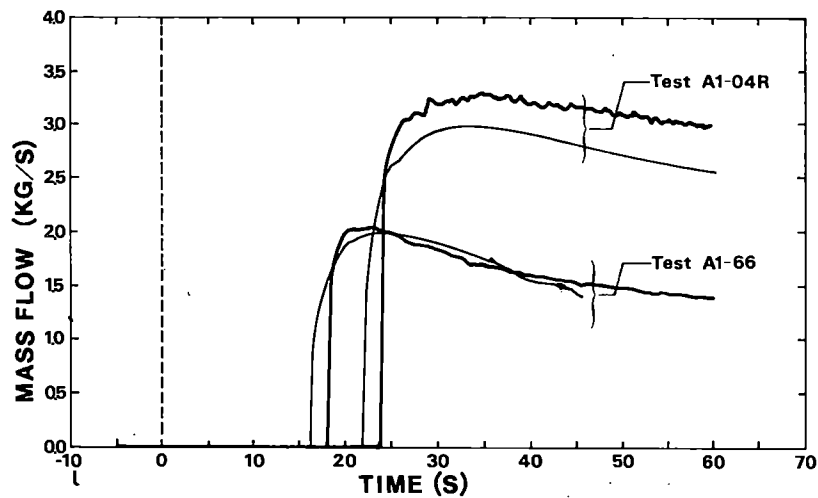


Fig. 12: ECC Mass Flow from Accumulator

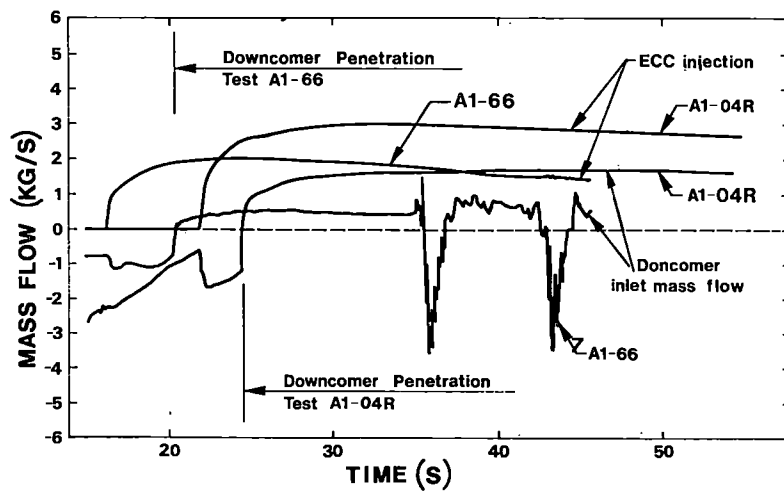


Fig. 13: ECC Injection Mass Flow and Liquid Mass Flow at Downcomer Inlet, Results of Test Predictions

REFLOODING OF A PWR BUNDLE-EFFECT OF INLET FLOW RATE OSCILLATIONS AND SPACER GRIDS

P. Clément, R. Deruaz, J.M. Veteau

CEA-CENG - 85X - 38041 GRENOBLE CEDEX-FRANCE

ABSTRACT

Flooding rate oscillations are expected to occur in a PWR during the reflooding phase after a LOCA. A special device was introduced in ERSEC loop, which enables to check the effect of well controlled oscillations including reverse flow, in a full length 6 x 6 rod bundle. Results are compared with those obtained in the case of constant inlet flow rates. Special attention is devoted to the applicability of these results to the case of actual fuel rods.

Spacers located all along the cladding of fuel rods are shown to significantly influence both heat transfer in the dry region and quench front propagation. Results clearly show that the effects are strongly dependent upon the design of spacer grids and provide a useful data base to take into account these effects in reflood models.

INTRODUCTION

The thermal behaviour of fuel elements during the reflooding phase of a PWR core after a LOCA depends on complex and interacting phenomena occurring in the core and the primary circuit.

Physical modeling of the core thermal hydraulics is generally based upon separate effect tests performed with :

- single test sections like tubes (internal flow)
- electrically heated rod bundles

Inlet flow rate oscillations, which are expected to occur in the core during the reflooding phase, and are encountered in some large integral tests, may affect phenomena like quench front propagation and entrainment of water, and as a consequence, influence the heat transfer in the dry region.

To investigate this problem, reflooding experiments were performed on ERSEC loop with a full length 6 x 6 rod bundle and a special device making use of a two head piston pump.

Likewise, spacers located all along the cladding of fuel rods in a reactor core influence the cooling efficiency in comparison with results obtained on smooth heated walls like tubes. In order to clarify these grids effects, reflooding experiments were performed on the ERSEC loop, with the 6 x 6 rod bundle previously used for flow rate oscillation tests and different kinds of spacers, with or without turbulence promoters.

EXPERIMENTAL SETUP

The ERSEC loop has been used for re-flood studies at a maximum pressure of 6 bar on full length (3.66 m) electrically heated rod bundles (max. power supply 480 KW).

Water at constant fixed temperature is supplied at the bottom of the test section either by a centrifugal pump (constant inlet flow rate) or by the device involving a two head piston pump (oscillating inlet flow rate).

The geometry of the bundle is the same as for 17 x 17 PWR assembly (outer rod diameter 9.5 mm, square pitch 12.6 mm) maintained by 7 spacer grids axially distributed about each 60 cm along the test section.

The rods are heated by a coil (fig.1) giving a stepped approximation of a chopped cosine axial power profile (axial peak factor 1.65), compacted magnesia being the insulation material. Four kinds of rods, instrumented with 4 thermocouples, were used in the test section, providing 16 levels of wall temperature measurements.

These temperatures, as well as the entrained liquid mass velocity at the outlet of the test section and the overall pressure drop were measured and recorded all along a run.

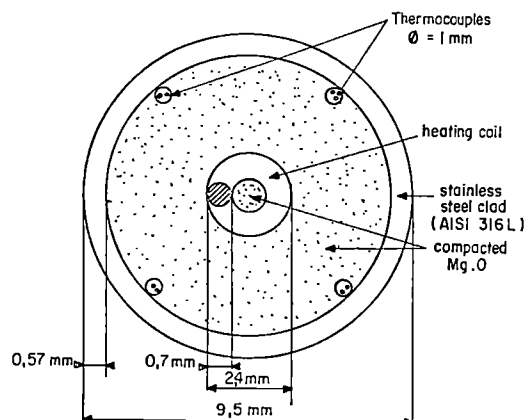


Fig. 1 : Rod structure

INLET FLOW RATE OSCILLATION EFFECTS

In previous experiments on the 6 x 6 rod bundle, oscillating flow rate showed no effect on the reflooding behaviour. However, reverse flow were absent, and new experiments have been performed involving positive and negative alternations of flow rate to study the hydrodynamic effects and the influence of a possible temperature rise in the region of the clad left uncovered during the negative phase of oscillation.

In order to impose at the inlet of the test section an oscillating flow rate (OFR) in well defined conditions :

- constant inlet water temperature
 - positive and negative amplitudes and frequency of oscillations separately adjusted and controlled,
- a two head piston pump was used (fig.2), which feeds alternately the test section and the storage tank.

The time averaged mass velocity entering the test section is

$$\bar{G} = \frac{1}{2} (G^+ - G^-)$$

where G^+ and G^- are the mass velocities delivered by each head.

Two kinds of experiments were performed :

- one with a constant flow rate G (CFR)
- three with different G^+ and G^- corresponding to the same $\bar{G} = G$ (OFR)

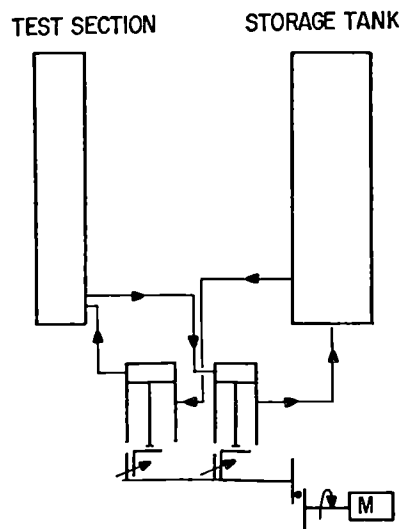


Fig. 2 : The two head pump device

Runs with no reverse flow ($G^- = 0$) were done again in order to compare the results with those obtained previously with a 3-way valve and then detect a possible influence of the injection device. The effect of the oscillation period Θ was also investigated. The range of parameters was :

pressure : 1 bar
inlet water subcooling : 20 and 80°C
initial wall temperature : 600°C
inlet mass velocity (averaged) : 2.5, 6, 10 g/cm²s
oscillation amplitude : - 15 to + 28 g/cm²s
period : 2 and 4 s, imposed heat flux : 3 or 4.5 W/cm²

Fig. 3 and 4 show the comparison between (respectively) quench times t_q and maximum wall temperature rises ΔT_{Wmax} obtained for CFR and OFR tests.

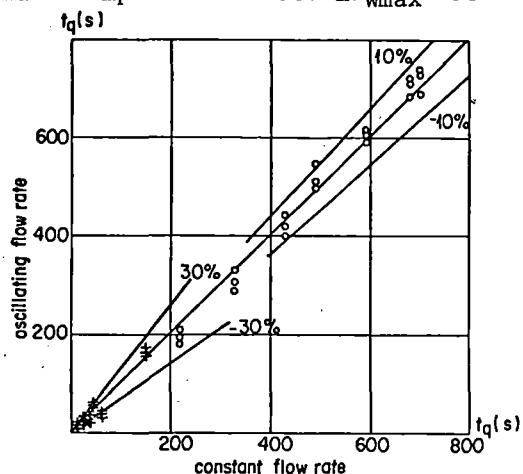


Fig. 3 : Quench times,

Influence of the oscillation amplitude (range - 15 to + 28 g/cm²s ; o: $\bar{G} = 2.5$ g/cm²s ; +: $\bar{G} = 10$ g/cm²s ; $\Theta = 2$ s).

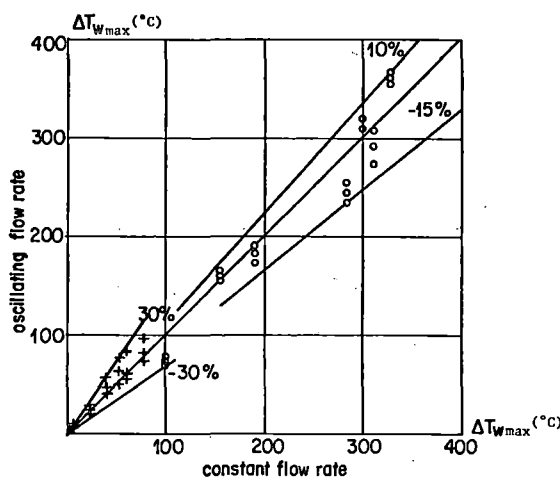


Fig. 4 : Maximum wall temperature rises,

Influence of the oscillation amplitude (range - 15 to + 28 g/cm²s ; o: $\bar{G} = 2.5$ g/cm²s ; +: $\bar{G} = 10$ g/cm²s ; $\Theta = 2$ s).

For these two important quantities, it is seen that :

- rather large discrepancies ($\pm 30\%$) occur at low values, but involving variations smaller than 40°C for the ΔT_{Wmax}
- while the agreement is close to $\pm 10\%$ for $t_q > 200$ s and + 10, - 15% for $\Delta T_{Wmax} > 150^\circ\text{C}$.

The 4 second period tests show the same kind of results.

Now, it is necessary to know if these results obtained on electrically heated rods are valid for actual fuel rods or not.

Indeed, during a negative alternation of the inlet flow rate, the rods may be partly dried or not : when dewetting occur, the clad temperature rises prior to rewetting coming with the next positive alternation, and if this temperature rise ΔT_W is sufficiently large, the quench front progression may be slowed down.

Such a result seems not to happen during our tests :

- recorded ΔT_W are smaller than 10°C
- the quench front velocity has been shown to be practically unchanged in case of OFR.

However, this result does not necessarily hold for fuel rods, for the clad temperature rise results both from the flattening of initial radial temperature profil $T(r)$ due to the decrease of the heat transfer coefficient h at the outer surface of the clad, and from the local residual power W_R . So, for given h , W_R and oscillation period, ΔT_W depends on $T(r)$ and on the internal constitution of the rod, which is quite different for heater elements and fuel rods.

To investigate this problem, transient conduction calculations were performed for the two kinds of rods.

Among the initial and hydrodynamics sets of conditions investigated, these leading to the highest ΔT_W were :

- very steep initial radial temperature profile $T(r)$, at the location of the quench front just prior to reverse flow
- hydrodynamics conditions at the quench front leading to large rewetting velocities U_q (which values are different for fuel rod and heater element mainly due to the different material of the clad)
- small heat transfer coefficient h (10^{-2} W/cm²°C) at the outer wall of the clad.

Fig. 5 shows an example of temperature profile evolution versus time for the two kinds of rods : large differences between the wall temperature rises ΔT_W are observed.

The existence and quasi instantaneous time response of the gap ($\approx 10^{-4}$ s) lead to far greater ΔT_W in the early instants for fuel rods (in the range 50 - 350°C depending on U_q and h) than for heater rods (range 20 - 200°C).

So, if reverse flow induces the dry out of the wall upstream the initial quench front elevation, calculations show that a simple application of the results obtained with heater rods to fuel rods is not obvious : the temperature rise of the clad in the dewetted region can reach values which may affect the quench front progression during the next positive alternation of the inlet flow rate.

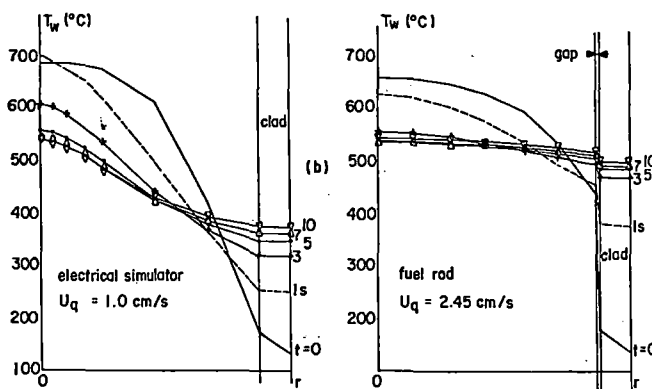


Fig. 5 : Time evolution of $T(r)$; conditions at the quench front : imposed heat flux : 5.25 W/cm². Value of h : 10^{-2} W/cm²°C. pressure : 1 bar. Thickness of the gap : 80 μ m.

On the other hand, this application is undoubtedly possible if the wall remains rewetted by a liquid film during negative alternations. This last situation is probably more realistic, and is supported by the following remarks :

- no important ΔT_W was observed after quench during the tests
- quench front propagation was not significantly different in cases of CFR and OFR tests
- the existence of a liquid film ahead of the two phase level in boil-off experiments was already suggested as the main explanation of the differences of apparent two phase level observed between boil-off and level swell experiments previously performed on the ERSEC loop.

It remains however that a proof of that would only be possible with the help of liquid film detectors located along the clad of the rods, a not yet solved problem as far as we know.

SPACER GRIDS EFFECTS

Spacers located along the cladding of fuel rods influence the cooling efficiency in comparison with results obtained on smooth surfaces like tubes :

- heat transfer in the dry region is increased at the level and just ahead of spacer grids due to turbulence, acceleration of the flow, possible breakup of the entrained droplets, and cooling fin effect of the grid itself

- quench front propagation is expected to be accelerated, at least at the level of grids, which have a low thermal inertia and no internal heat source.

In order to obtain experimental results about these effects, we have performed reflood experiments on the 6 x 6 rod bundle with 3 kinds of spacer grids :

- slight grids (S G) which are "minimum technically achievable spacer grids" especially designed and manufactured in order to reduce two phase flow disturbances and however able to hold the rods in the right position during the transient (a bundle without grids could not be chosen as reference case, due to superimposed deformation effects)
- grids used in French PWR, without its turbulence promoters (G)
- same as above, with turbulence promoters (MG) (standard French PWR mixing grid).

The following range of parameters was investigated :

constant inlet mass velocity : 2.5, 6, 10 g/cm²s
 imposed heat flux : 3 or 4.5 W/cm²
 initial wall temperature : 600°C
 pressure : 1,6 bar
 inlet subcooling : 20, 80°C

The thermal behaviour of the rods is strongly influenced by the geometry of the spacers, not only near each grid, but also for :

- the overall quench time t_q
- the overall turn around time t_t
- the maximum wall temperature ΔT_{wmax}

Fig. 6 shows differences as great as 100% between the SG and MG results.

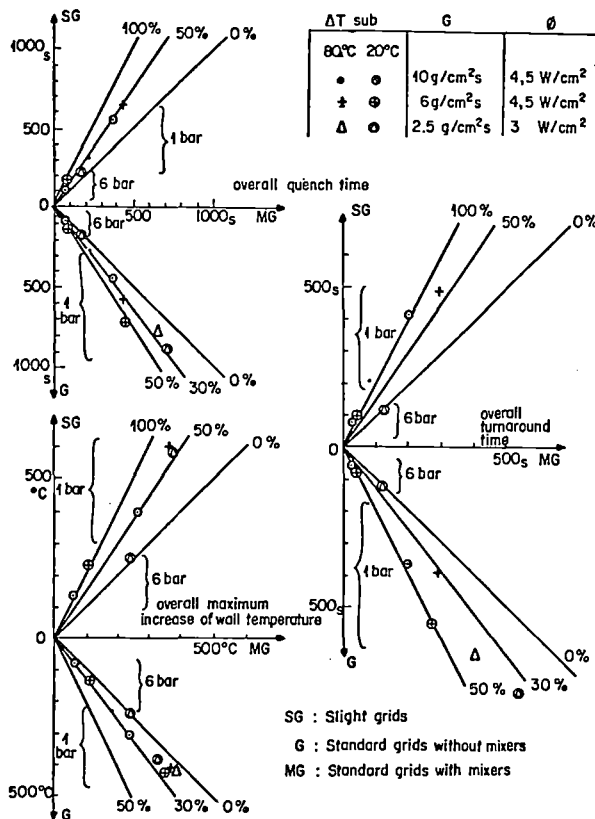


Fig. 6 : Comparison of overall results for 3 kinds of grids

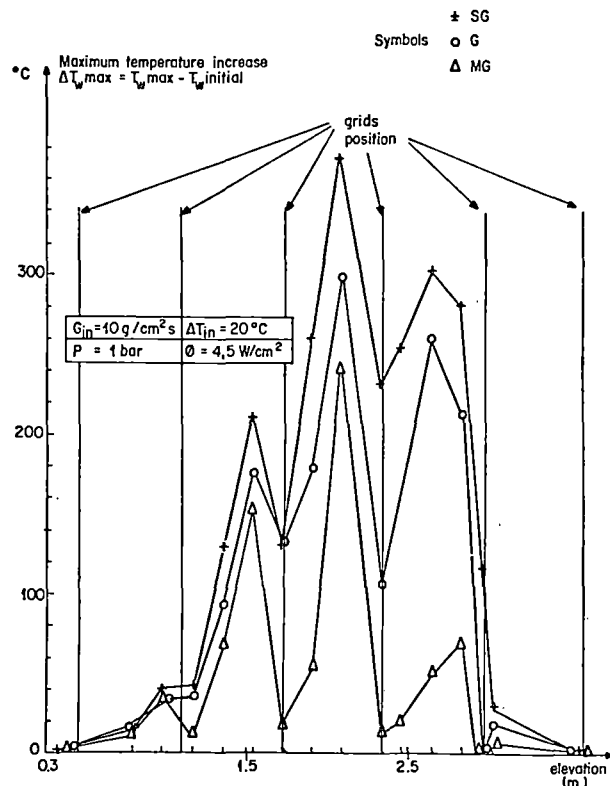


Fig. 7 : Comparison of ΔT_{wmax} for the three kinds of spacer grids at high inlet mass velocity.

However, these overall results are the consequences of several effects which mechanisms cannot be explained without looking more precisely to the local phenomena. Fig. 7, where ΔT_{Wmax} has been plotted versus elevation for the 4 rods surrounding the central subchannel and for the three kinds of grids in the case of a high inlet mass velocity experiment, shows a strong variation between SG, G and MG, increasing with elevation, and leading to several hundred degree celsius differences in ΔT_{Wmax} at the upper grid locations.

There is also an effect of the spacer geometry on the quench time as shown on figure 8 :

For G and MG experiments, prequenching sometime arises at the 4 upper grid locations, probably due to collecting of the entrained droplets in the dry region by the grids, and is followed in the MG experiments by the development of a secondary quench front from the fourth grid level.

This behaviour is not observed for the SG which offers less impact area for droplets and resistance to the steam water flow, and vanishes for the 3 kinds of grids at low inlet mass velocity, because the entrained mass flow rate becomes too small.

The low inlet mass velocity involves and additional phenomenon in the lower part of the test section :

The wall temperature rise (fig. 9) is higher for MG than for G between grids, which seems inconsistent with previous results obtained at high inlet mass velocity.

The proposed mechanism is the increased collection of water on the lower MG, and possible fall back of large drops from these grids, these drops being not entrained by steam which velocity is rather small in this region (below 5 m/s).

This explanation is supported by the fact that at the same time the quench front moves faster for MG and the entrainment of liquid (measured at the outlet of test section), which start is delayed, is smaller for MG than for G.

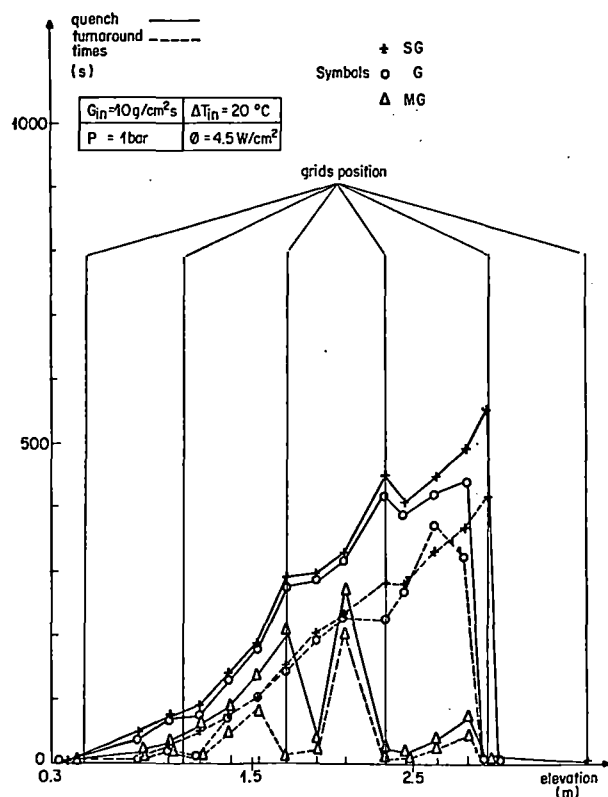


Fig. 8 : Comparison of reflooding significant quantities for the three kinds of spacer grids at high inlet mass velocity.

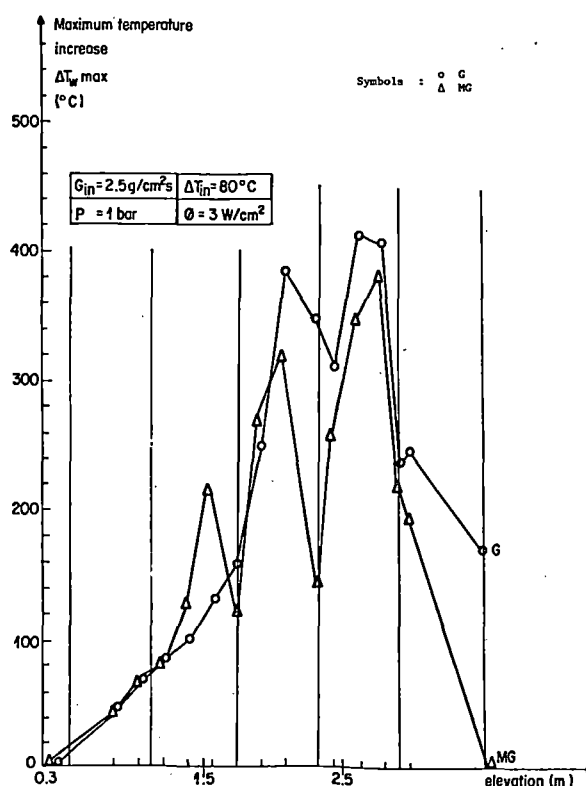


Fig. 9 : Comparison of ΔT_{Wmax} for two kinds of spacer grids at low inlet mass velocity.

Finally, runs performed at 6 bar show differences between the 3 kinds of grids smaller than those at one bar, especially the effect on ΔT_{wmax} (fig. 6 and 10).

This seems to denote the importance of the role played by the liquid flow rate in the dry region (water entrainment is smaller at 6 bar than at 1 bar), which is a leading parameter for the grids effect.

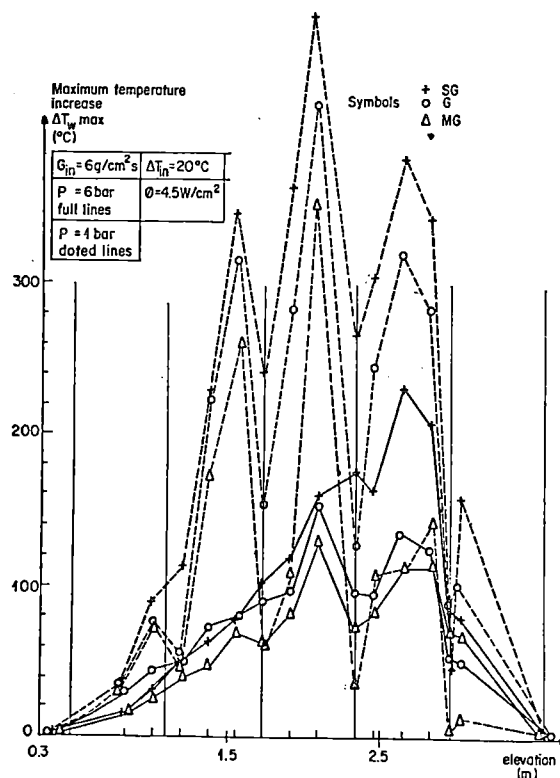


Fig. 10 : Comparison of ΔT_{wmax} for the three kinds of spacer grids at 1 and 6 bar.

GENERAL CONCLUSIONS

A series of reflood tests was performed on a 6 x 6 full length rod bundle, which contributes to give some insight about the influence of inlet flow rate oscillations and spacer grids geometry upon the thermal hydraulic behaviour of a PWR core during the reflooding phase of a LOCA.

For the inlet flow rate oscillation effect study, runs with constant and oscillating flow rate, including reverse flow, were achieved : for the range of parameters investigated, and for the electric simulators used, no significant differences were observed between oscillating and constant inlet flow rate between entrained mass flow rates, quench front velocities, heat transfer in the dry region, and the clad did not undergo a significant temperature rise in the region which, in principle, can be dewetted during the negative alternations.

These results lead to the conclusion that a liquid film is likely to remain on the wall during reverse flow, in which case the transposition of experimental results to fuel rods raises no particular problem.

For the spacer grids effect study, runs with 3 kinds of spacers, and constant inlet flow rate were achieved, the effect of parameters like pressure, inlet flow rate and subcooling was investigated, and it was shown that :

- the overall enhancement of heat transfer in the dry region is strongly related to entrained liquid flow rate through this region
- quench front propagation is accelerated due both to early quenching at grid elevation and improvement of precursory cooling.
- the effect of spacers is drastically increased by turbulence promoters.

So, it is clear that there is no chance to succeed in describing heat transfer in rod bundles with models only adjusted from experiments on tubes.

If the chosen way is to use overall correlations, this work shows that they must be established from experiments in bundles with actual grids.

A physical treatment of grids effects requires addition of modification of two phase flow at the level and ahead of grids, and accounting for the resulting enhancement of heat transfer, including heat transfer between phases.

For this purpose, more detailed information, involving more sophisticated instrumentation and flow visualization would be of interest.

CONTAINMENT EMERGENCY SUMP STUDIES TO
INVESTIGATE UNRESOLVED SAFETY ISSUE A-43

G. G. Weigand, M. S. Krein* and M. J. Wester**
Sandia National Laboratories
Albuquerque, New Mexico

M. Padmanabhan
Alden Research Laboratory of WPI
Holden, Massachusetts 01520

ABSTRACT

A systematically structured test program designed to characterize the hydraulic behavior of full-scale emergency core cooling system (ECCS) sumps under a broad range of geometric configurations and flow conditions has been conducted. The effects of potential accident induced perturbations on sump performance were also evaluated. These perturbations included screen blockage, nonuniform approach flows, break flow and ice condenser drain flow impingement, and obstructions. In addition, the effects of elevated water temperature and the performance of vortex suppression devices have been established. The results show that the vortices are unstable and that vortex size and type is not a reliable indicator to adjudge air ingestion or swirl behavior. Measured air withdrawal rates were generally less than 1-2 percent and the measured swirl in the outlet pipes was small. An envelope curve analysis of the data was developed, and it gives the "bounded" performance response of the sump as a function of the flow variables.

These results are being used to develop comprehensive design and review guidelines for ECCS sumps. Additionally, the test results will be used in developing the resolution of Unresolved Safety Issue A-43, "Containment Emergency Sump Performance".

INTRODUCTION

This paper presents the results of a parametric study^{1,2} of geometric and hydraulic parameters, and provides detailed design and evaluation guidance for rectangular type Emergency Core Cooling System (ECCS) sumps with two horizontal or vertical suction pipes; the study was conducted to aid in the resolution of Unresolved Safety Issue A-43 (USI-A43), Containment Emergency Sump Performance, which addresses the issue of a long-term cooling capability for ECCS sumps in nuclear power stations. In particular, we are addressing the issue of the sump, during the recirculation mode, providing the necessary flow of coolant to safety systems following a LOCA. A disruption of long-term cooling to the reactor core could lead to core damage.

A few years ago, the hydraulic performance of the ECCS sumps started to receive renewed attention as an important component of the residual heat removal system in nuclear power stations. Excessive pressure losses, ingestion of air from free surface vortices or break jets impinging near the sump, and swirling flow in the pump

*M. S. Krein Co.

**The Dikewood Corp.

suction lines can result in degraded recirculation system performance. Various types of hydraulic model studies of particular sumps showed that such undesirable flow conditions can exist, and that remedial measures were needed to ensure satisfactory long-term pump operation.^{3,4,5} As a result, the hydraulic performance of ECCS sumps, as an ingredient of pump suction hydraulics, was designated by the NRC as an unresolved safety issues, USI-A43.

Since the available sump design guidelines were not supported by an adequate data base, it was not possible to assess the adequacy of ECCS sumps, both in service and proposed, without requiring model or in-situ tests. The basic objective of this research was to develop general engineering and numerical guidelines, consistent with the NRC Regulatory Guide procedures, which would allow an evaluation of ECCS sumps to determine the adequacy of their hydraulic performance. This information can also serve as a sound basis for the design of ECCS sumps in future plants. Plants found to have deficient sumps may require redesign or installation of remedial devices, such as vortex suppressors. A secondary objective of the program, therefore, concerned the testing of vortex suppressors.

The approach to meeting the basic objective was to systematically generate a data base covering the range of geometric and flow variables typical of ECCS sumps, including strong flow perturbations caused by potential screen blockage, approach flow distribution, transients, break flows, etc. The effects of elevated water temperature and vortex suppressors were also evaluated. This data base is used to establish interrelationships between variables and bounding criteria. Since some of the hydraulic phenomena of concern, particularly air ingestion, could involve scale effects if tested at a reduced scale, a full-scale experimental facility was constructed.

TESTING AND ANALYSIS PROCEDURES

Alden Research Laboratory of Worcester Polytechnic Institute, under contract to Sandia National Laboratories, is performing the sump experiments. The test plan considers 14 different flow and geometric variables, and it considers most flow issues concerning unusual flow conditions in containment sumps. The test plan is divided into five parts: (1) factorial testing, (2) secondary geometric variable sensitivity tests, (3) severe flow perturbation tests, (4) vortex suppression tests and (5) design or operational tests of special concern in ECCS sumps. In (1), primary sump flow and geometric variables are studied using a fractional factorial matrix of tests. A fractional factorial matrix developed by Sandia was used since it is an efficient way to test a large number of variables, it provides a wide range of parameter variations, and the interdependency of different variables can also be determined. In (2), the effect on sump performance of secondary geometric variables is tested by holding all sump variables, but one, constant and testing several values of this one variable. In (1) and (2), the approach flow to the sump was reasonably uniform and unperturbed (low ambient circulation). Parts (3) and (4) are tests where the approach flow was severely perturbed. In (3), screen blockage (up to 75% blockage), nonuniform approach flow patterns including streaming, impinging break and drain flows, flow obstructions, and flow transients were considered. In (4), the effectiveness of several vortex suppressors was evaluated. In (5), several operational items such as temperature or cover plate effects were evaluated.

Sump performance has been characterized in this investigation by four dependent parameters: void fraction (percent air ingestion), surface vortex type, inlet swirl angle, and sump loss coefficient. Surface vortex type provides a qualitative assessment of surface activity. Vortex activity was classified by a scale of vortex severity that ranged from an incoherent surface swirl (type 1) to a fully developed air core vortex (type 6) (see Figure 1).

The inlet swirl angle provides a qualitative assessment of the tangential velocities in the pipe. Void fraction measurements provide a quantitative assessment of the levels of air withdrawal; and the sump loss coefficient provides a measure of the sump energy losses.

In this analysis, the most widely used variable was the Froude number (defined as U/\sqrt{gs} where s is the depth of water over the pipe inlet, U is the pipe velocity, and g is the acceleration of gravity).

The sump performance data were analyzed primarily using a bounding envelope analysis. In this analysis, boundary curves indicate the maximum response of the data for each of the hydraulic performance parameters (void fraction, vortex type, swirl, and loss coefficient) as a function of the sump flow variables, in particular the Froude number. For most of the test configurations, the values of the dependent variables (particularly void fraction and swirl angle) were so small that any functional correlation, with independent variables (Froude number, submergence, etc.), was obscured by measurement accuracy and the complex time-varying nature of the three-dimensional flows in the sump.

Since the experimental data cover a wide range of ECCS sump geometries, flow parameters, and flow perturbations, they provide a means of defining an envelope of maximum values for the dependent performance parameters. This envelope (or boundary) is valid for any sump and flow conditions provided there is a similarity of characteristics between the sump being considered and the data base. Using the envelope analysis, we can confidently predict under what conditions the void fraction, vortex type, or swirl will not exceed some prescribed value. Thus, this type of analysis can form the basis for establishing design guidelines.

A full-scale test facility⁶ shown in Figure 1, was used to conduct the sump tests. The test facility consists of a main tank with sump, suction pipes with variable diameters and positions, a pump pit tank, and associated piping for the simulation of break and drain flows. The maximum capacity of the main tank is 250,000 gallons of water with the ability to position false walls within the tank to achieve a wide range of sump configurations. A continuous filtration system provides water quality down to 10 microns and a heating system is capable of increasing the temperature of the water to 165°F.

RESULTS AND CONCLUSIONS

In this section, it is only possible to provide a brief and summary account of the most significant results. Further detail and the complete description of the test results and their analysis can be found in References 1 and 2.

Envelope Analysis

The most significant result was the development of bounding (or envelope) curves for key sump design parameters. The sump performance test program generated a data base covering a broad range of ECCS geometric variables, flow conditions (including potential accident conditions), and design options (horizontal or vertical inlets, single or dual pipes, etc.). An envelope analysis was applied to this broad range of data and resulted in boundary curves that describe the maximum expected air withdrawal, surface vortex activity, swirl, and sump head loss as a function of key sump flow variables (Froude number, velocity, etc.).

Figures 2, 3, and 4 show typical envelope analysis curves for air withdrawal, surface vortex activity, and swirl in sumps with dual, horizontal outlets. Figures 5, 6, and 7 show typical envelope analysis curves for air withdrawal, surface vortex activity, and swirl in sumps with dual, vertical outlets.

General Sump Performance (All Tests)

Free Surface Vortices -- Vortex size and type resulting from a given geometric flow condition are difficult to predict and are not reliable indicators of sump performance. Performance parameters -- void fraction, pressure loss coefficient, and swirl angle -- are not well correlated with observed vortex formations.

Air Ingestion -- Measured levels of air ingestion, even with freestanding air core vortices, were generally less than 1-2 percent. Maximum values of air ingestion with deliberately induced swirl and blockage conditions were less than 7 percent for horizontal inlets and 10-12 percent for vertical inlets; these high levels always occurred for high flow and low submergence. For submergences of 8 feet or higher, none of the configurations tested indicated air-drawing vortices that ingested more than 1 percent air over the entire flow range even with severe flow perturbations.

Swirl (measured 14 diameters from suction inlet) -- Flow swirl within the intake pipes, with or without flow perturbations, was very low. In almost all cases, the swirl angle was less than 4° . The maximum value for severely perturbed flows was about 8° and occurred during the screen blockage test series.

Sump Head Losses -- Suction pipe intake pressure loss coefficient for most of the tests, with and without flow perturbations, was in the range of 0.8 ± 0.2 and agreed with recommended hydraulic handbook values.

Sump Performance During Accident Conditions (Perturbed Flow)

Screen Blockage -- Screen blockage up to 75 percent of the sump screen resulted in air ingestion levels similar to those noted under "Air Ingestion" above.

Nonuniform Approach Flow Distributions -- Nonuniform approach flows, particularly streaming flow, generally increased surface vortexing and the associated void fraction.

Drain and Break Flow -- Drain and breakflow effects were generally found not to cause any additional air-ingestion. They reduced vortexing severities by surface wave action.

Obstructions -- Obstructions with hydraulic radii less than 2 ft had no influence on vortexing, air withdrawals, swirl, or inlet losses.

Transients -- Under transient, start-up conditions, momentary vortices were strong, but no air-core vortices giving withdrawals exceeding 5 percent void fraction (1 minute average) were observed.

Geometric and Design Effects (Unperturbed Flow Tests)

In general, no consistent trends applicable for the entire range of tests were observed in the data between the hydraulic response of the sump (air withdrawal, swirl, etc.) and secondary geometric parameters. However, for some ranges of flow and submergences, the following observations are applicable:

Greater depth from containment floor to the pipe centerline reduces surface vortexing and swirl.

Lower approach flow depths with higher approach velocities may cause increased turbulence levels serving to dissipate surface vortexing.

There is no advantage in extending the suction pipe beyond 1 pipe diameter from the wall.

Suction pipe inlets located with less distance to the sump wall and greater pipe spacing reduces vortexing and swirl.

Placing pipe outlet some distance above the floor helps avoid withdrawal of any debris collected on the sump floor.

Design or Operational Items of Special Concern in ECCS Sumps

Vertical Outlets -- Comparison of vertical outlet data to corresponding horizontal outlet data showed some, but no major differences, in the hydraulic performance of vertical outlet sumps and horizontal outlet sumps of the same geometry and flow conditions: average vortex types agreed within ± 1 ; air withdrawals were somewhat higher for vertical outlet sumps, usually within 1 percent void fraction (30 minute averages) and 4 percent void fraction (1 and 5 minutes averages); swirl angles differed only within ± 1 degree. As in the case with horizontal outlets where sump performance was best with pipe projections close to the wall, vertical pipe outlets with perturbations performed best when placed close to the wall rather than at the center of the sump.

Cover Plate -- A solid top cover plate over the sump was effective in suppressing vortices as long as the cover plate was submerged and proper venting of air from underneath was provided. No air-drawing vortices were observed for the submerged cover plate tests, and no significant changes in swirl or loss coefficients occurred.

Elevated Water Temperature -- Changing water temperature over the range from 40°F to 165°F had no significant effect on horizontal outlet sump performance parameters.

Vortex Suppressors

Cage shaped vortex suppressors made of floor grating to form cubes 3 and 4 ft on a side, and single layer horizontal floor grating over the entire sump area, were both found to be effective in suppressing vortices and reducing air-ingestion to zero. These suppressors were tested using 12-inch outlet pipes, and with the water levels ranging from 0.5 to 6.5 ft above the top of the suppressors. Adverse screen blockages were used in conjunction with sump configurations which produced considerable air-ingestion and strong vortexing without the suppressors; thus, suppressors' effectiveness were tested when hydraulic conditions were least desirable. The suppressors also reduced pipe swirl and did not cause any significant increase in inlet losses. Both the cage shaped grating suppressors as well as the horizontal floor grates were made of standard 1.5 inch floor grates.

Tests on a cage shaped suppressor less than 3 ft on a side indicated the existence of air-core vortices for certain ranges of flows and submergences, even though air-withdrawals were found reduced to insignificant levels.

Either properly sized cage shaped suppressors made of floor grating, or floor grating over the entire sump area, may therefore be used to reduce air-ingestion to zero in cases where the sump design and/or approach flow creates otherwise undesirable vortexing and air-ingestion.

ACKNOWLEDGMENTS

The authors would like to gratefully acknowledge the support of the Department of Energy and the U. S. Nuclear Regulatory Commission.

REFERENCES

1. G. G. Weigand, M. S. Krein, M. J. Wester, M. Padmanabhan, A Parametric Study of Containment Emergency Sump Performance, NUREG/CR-2758, SAND82-0624, ARL-46-82, Sandia National Laboratories, Albuquerque, NM, July 1982.
2. M. S. Krein, M. J. Wester, Results of Vertical Outlet Sump Tests, NUREG/CR-2759, SAND82-1286, Sandia National Laboratories, Albuquerque, NM, to be published.

3. M. Padmanabhan, Assessment of Flow Characteristics Within a Reactor Containment Recirculation Sump Using a Scale Model -- McGuire Nuclear Power Station, Alden Research Laboratory WPI, May 1978.
4. T. G. Fain, Model Study of the Sequoyah RHR Sump, Report No. WM28-1-45-102, Tennessee Valley Authority, Division of Water Management, October 1978.
5. USNRC Docket No. 50-308, "Trip Report - Western Canada Hydraulics Laboratories, LTD, ANO-2 Model Tests", 1978.
6. W. W. Durgin, M. Padmanabhan, C. R. Janik, The Experimental Facility for Containment Sump Reliability Studies (Generic Task A-43), Alden Research Laboratory WPI, December 1980.

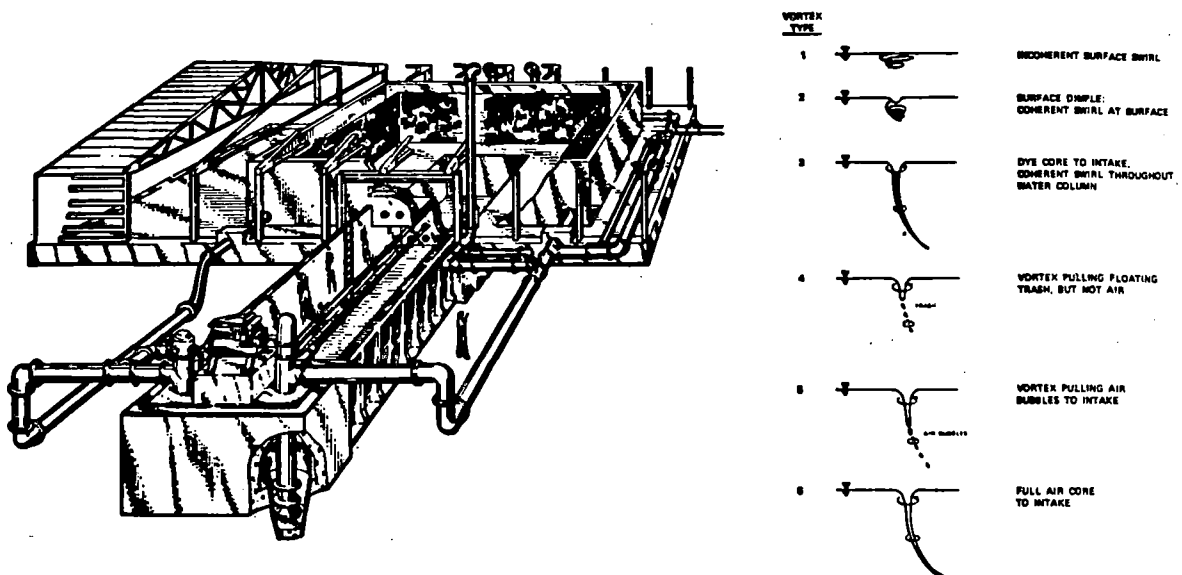


Figure 1. Perspective view of full-scale ECCS test facility and numerical scale for surface vortex classification

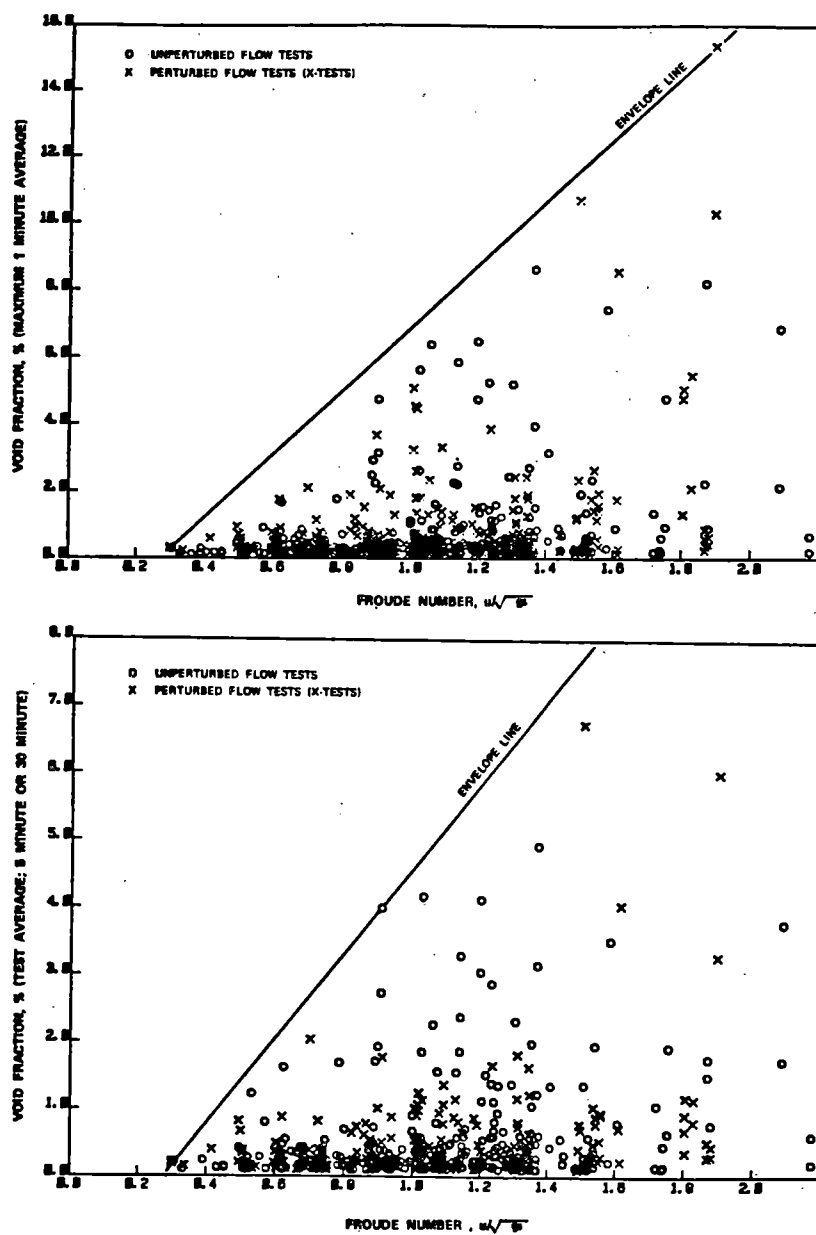


Figure 2a,b. Void fraction (% by volume) as a function of Froude number; horizontal outlet configuration

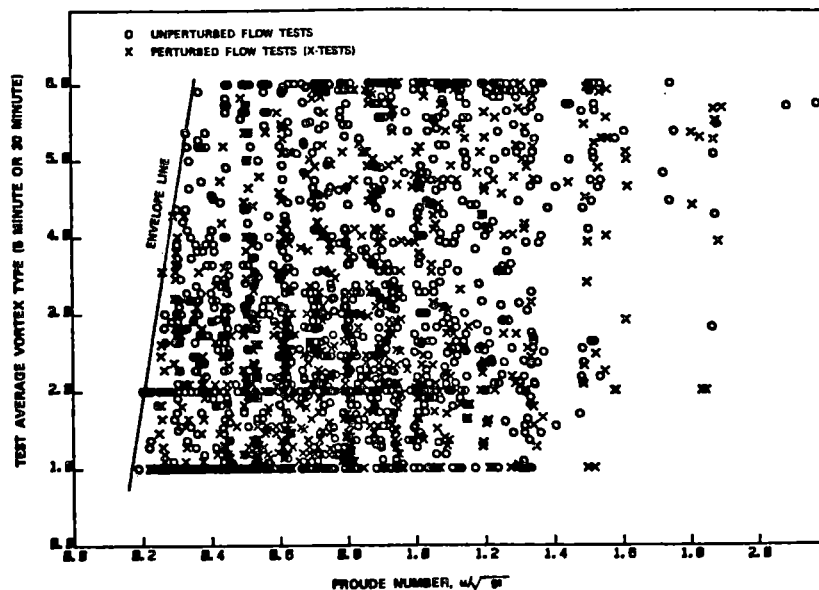


Figure 3. Surface vortex type as a function of Froude number; horizontal outlet configuration

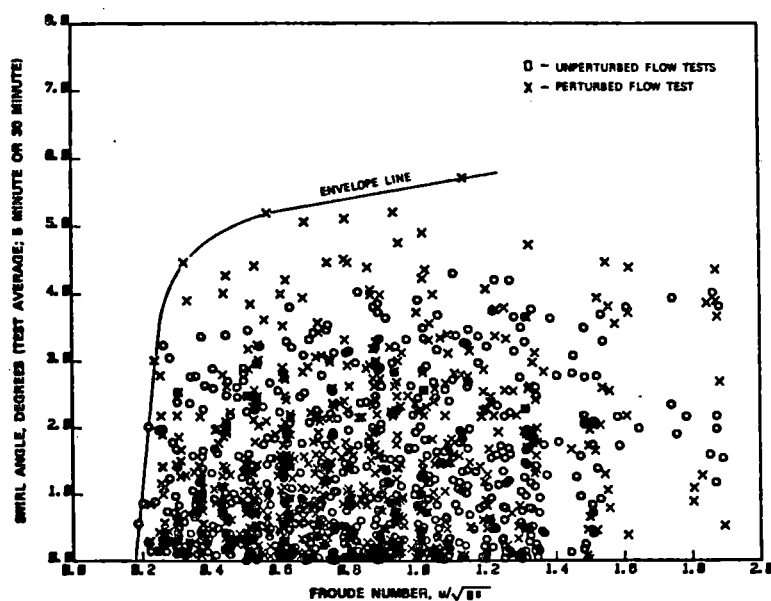


Figure 4. Swirl as a function Froude number horizontal outlet configuration

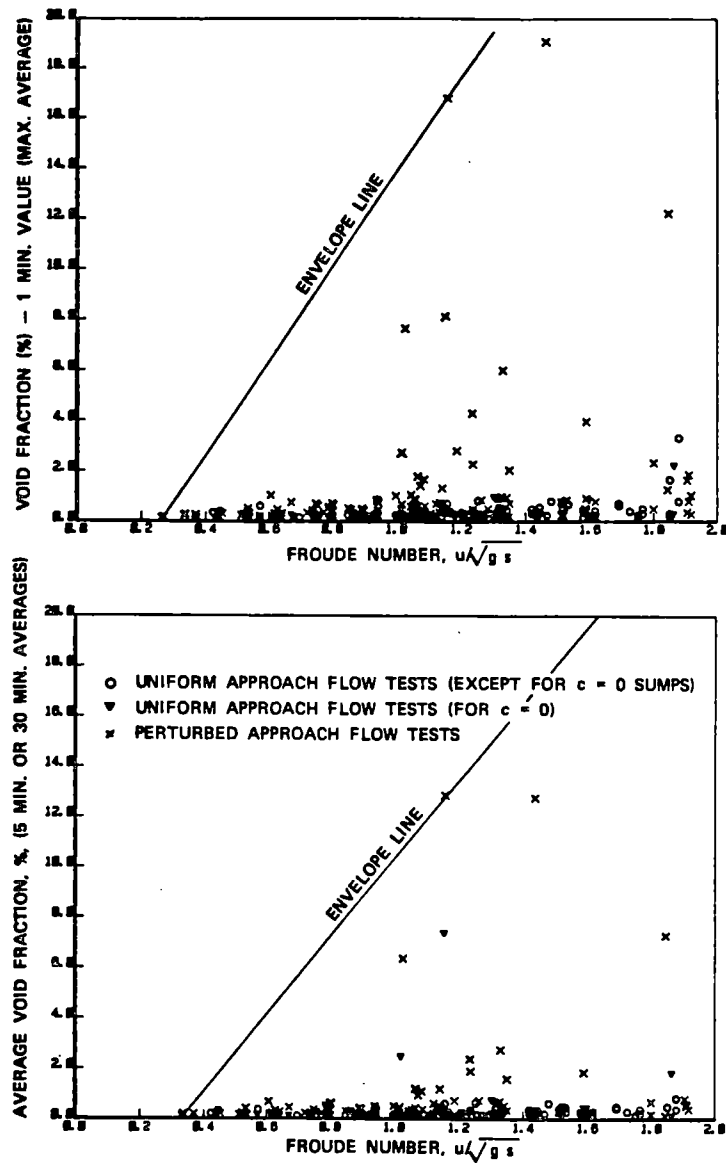


Figure 5a,b. Void fraction data for various Froude numbers; vertical outlet configuration

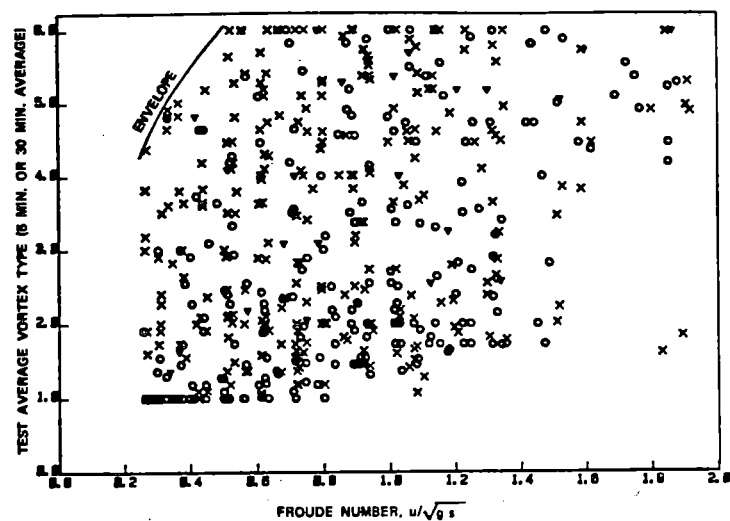


Figure 6. Surface vortex type as a function of Froude numbers; vertical outlet configuration

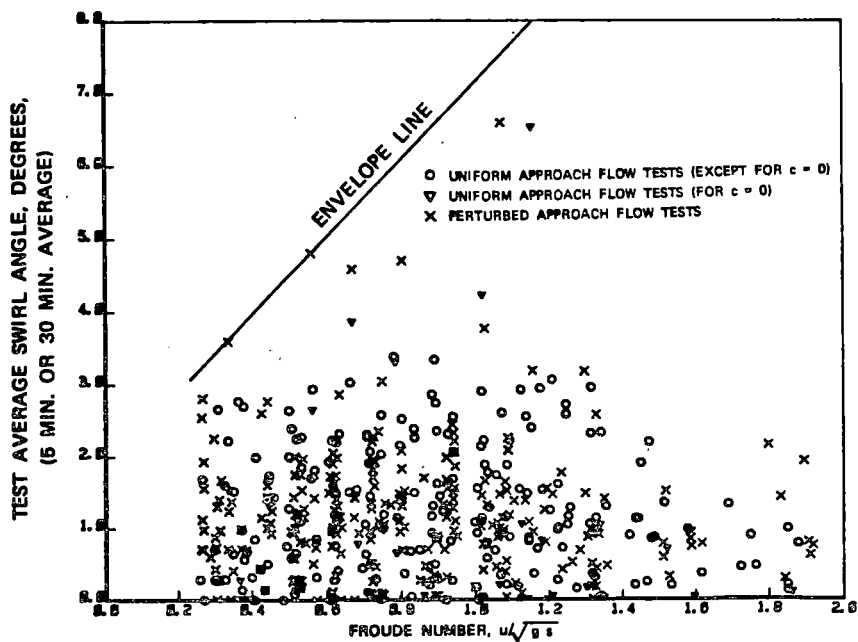


Figure 7. Swirl as a function of Froude number; vertical outlet configuration

PHEBUS PROGRAM - FIRST RESULTS ON PWR FUEL BEHAVIOUR IN LOCA CONDITIONS

R. DEL NEGRO^{**}, M. REOCREUX^{**}, J. PELCE^{*}, B. LEGRAND^{**}
Ph. BERNA^{**}.

* DSN CEN/FAR, B.P. n° 6
92260 Fontenay-aux-Roses

** DSN/SRS CEN/CADARACHE
B.P. n° 1, 13115 St Paul-lez-Durance

ABSTRACT

In the first PHEBUS test with pressurized rods some rods burst and clad temperature reached 1100°C in the 25 rods bundle. There is now a lot of valuable experimental results and their analysis is in progress. The Phase II on fuel behaviour in case of a large LOCA will start at the beginning of 83. The onset of the SFD program is foreseen to take place on the first months of 85.

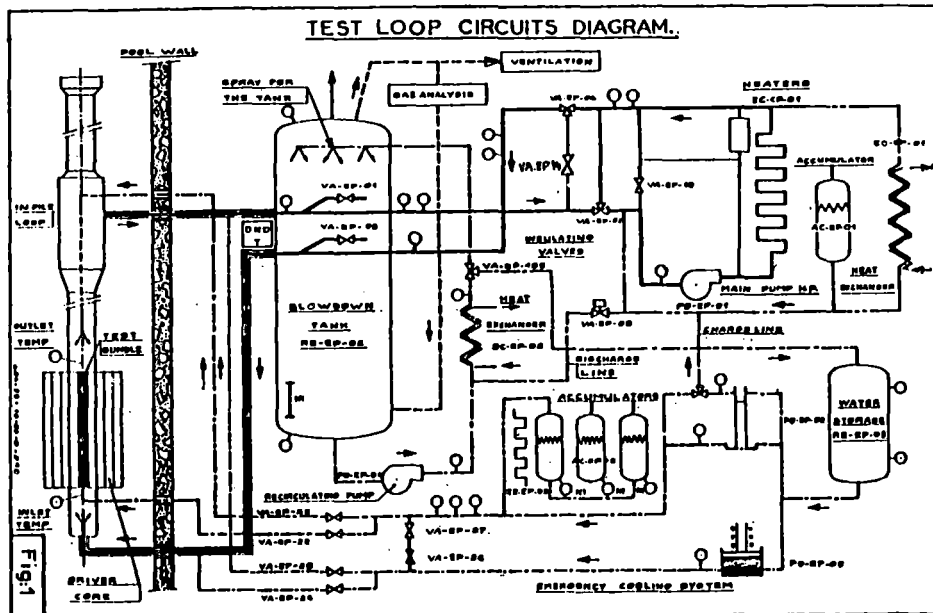
I - INTRODUCTION AND THE OBJECTIVES OF THE PHEBUS PROGRAM

The French government has decided in 1969 to equip France with a large number of power pressurized water reactors. Following this decision, the French atomic energy commission(CEA) has launched a vast program of research including safety aspects for this type of reactor.

For the needs of the safety analysis, special emphasis has been put on the fuel behaviour in accidental conditions and at first in LOCA conditions. The nuclear PHEBUS facility has been designed for that. The PHEBUS loop is specially devoted to provide experimental results about the integral thermomechanical behaviour of the PWR fuel rods under prescribed accidental thermohydraulic conditions. These experimental results are to be used to validate the French fuel code such as CUPIDON[1], and to check the ability of FRAP T4 [2] to predict PHEBUS experimental results, the qualification of which is in progress on analytical test results.

After a short description of the PHEBUS facility and the general strategy of the program, this paper indicates at which point we are got and gives a survey on the experimental results already obtained and their first analysis.

II - DESIGN OF THE IN-PILE PHEBUS



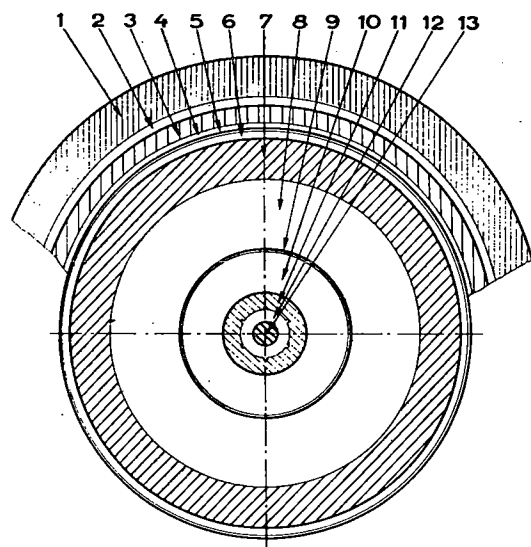
The test train, which consists essentially of a PWR type assembly with 25 fuel rods (fissile length : 0,8 m), is placed in an in-pile part of the loop (see fig.1) where the same working and accidental conditions as a PWR are reproduced. In the steady state the fluid conditions are : pressure 15.5 MPa , fluid temperature 320°C , fluid velocity in the test section 5 ms^{-1} ; the driver nuclear core allows a linear power up to 57 KW m^{-1} to be obtained (hot point of the test assembly) during about 10 minutes before the experimental transient.

The main characteristics of the transient are :

- PWR fuel rods residual power simulation,
- "blowdown" by opening of one or two fast operating valves (hot or/and cold leg break),
- "refilling and reflooding" by emergency injection circuits consisting of an accumulator, a high pressure pump and a low pressure pump,
- accidental temperature history can be represented by delaying the injection which can be actuated manually or automatically, 4 injection points available (2 above the fuel. 2 below the fuel).

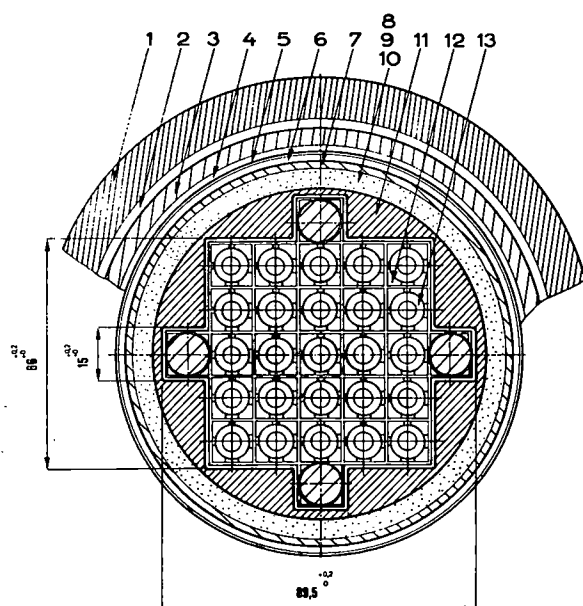
About 150 sensors equip the facility, they determine the evolution of the experimental parameters during the test : pressures, temperatures (fluid, structures, cladding, fuel), power level, injection mass flow rate ... Two two-phase flow spool pieces (turbine; venturi, γ densitometer) are installed one on the cold leg and the other one on the hot leg to determine the mass flow rate and the quality. After the test, the test train is unloaded and the state of the test assembly is given by post-irradiation examination.

One can see on the figures 2 and 3 the view of the cross-sections respectively for the 1 rod channel and the 25 rods bundle.



DESIGNATION	MATERIAL
cell { 1 Safety tube	Zircaloy 4
2 Vacuum	Vacuum
3 Pressure tube	Inconel 625
4 Water	Water
5 Shroud	Zircaloy
6 Water	Water
7 Stringer	Zircaloy 4
8 Vacuum	Vacuum
9 Radiation shield	Zircaloy 2
10 Vacuum	Vacuum
11 Columbium tube	Niobium
12 Water	Water
13 Fuel rod	

Fig.2: ONE ROD CHANNEL SECTION (MID CORE PLANE)



DESIGNATION	MATERIAL
cell { 1 Safety tube	Zircaloy 4
2 Vacuum	Vacuum
3 Pressure tube	Inconel 625
4 Water	Water
5 Shroud	Zircaloy
6 Water	Water
7 Stringer	Zircaloy 2
8 Zirconium	Zirconium
9 lagging	ZrO ₂
10 Tungstène strip	Tungstène
11 Zircaloy case	Zircaloy 2
12 Water	Water
13 25 fuels rods	

Fig.3: 25 RODS BUNDLE SECTION (MID CORE PLANE)

III - GENERAL STRATEGY OF THE PHEBUS PROGRAMME

The programme of the PHEBUS tests has been divided into four Phases.

The phase I is performed so as to see :

- if in Phebus we can reproduce around the fuel rods typical thermohydraulic conditions of a power reactor LOCA.
- How to describe the Phebus loop in the calculation data so that the Relap IV mod 6 code could simulate its transient behaviour and the thermomechanical response of the fuel rods. The Phase I is already well advanced.

The Phase II which is specially devoted to the study of the thermomechanical behaviour of the PWR rods will start at the beginning of 83. The prescribed thermohydraulic boundary conditions around the fuel rods will be adjusted by sensitivity calculations of Relap IV mod 6 to specify the scenario of the main loop valves during the test.

The first five tests of the Phase II, will investigate which damages and up to which extent pressurized fuel rods will suffer when submitted to the pessimistic licensing thermohydraulic transient, such as defined by the clad temperature transient of figure 4. Some of these tests will be conducted until safety criteria are fully reached.

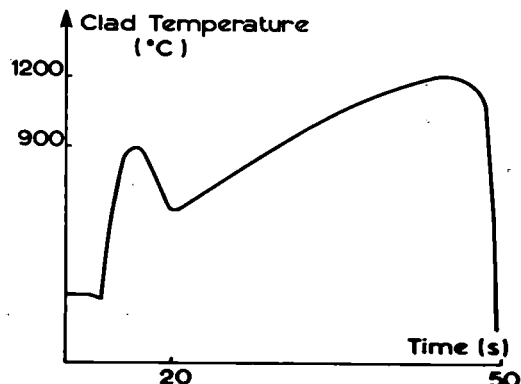


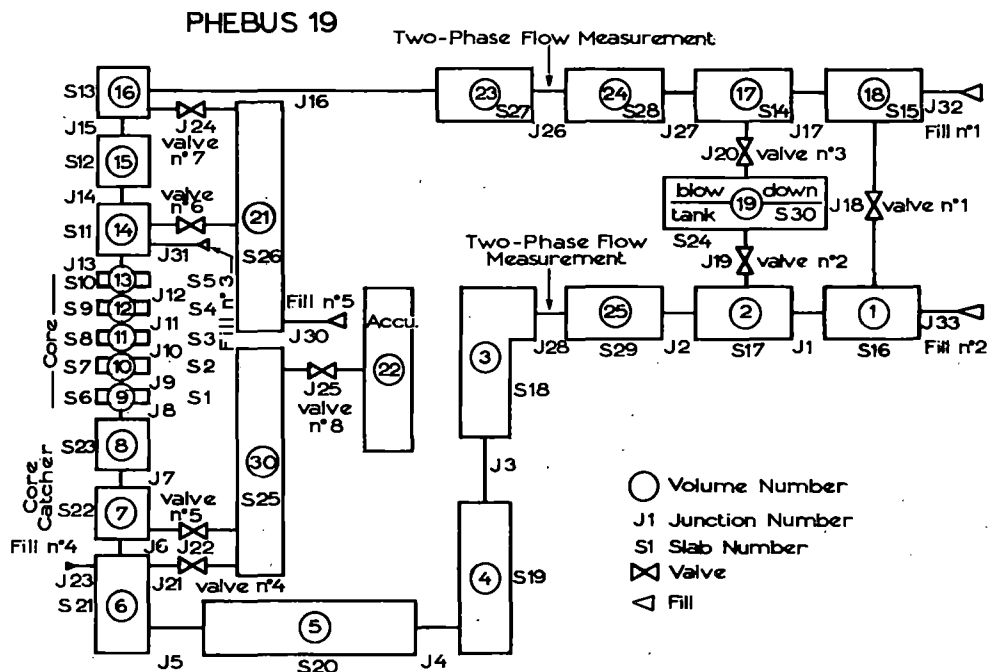
Fig.4: PROTOTYPICALLY CLAD TEMPERATURE TRANSIENT

The tests will be carried out on 25 rods bundles. Damages will be considered under the aspects of deformation (ballooning), rupture, external and internal oxidations. The ballooning will be considered as a possible cause of preventing the coolability by blockage. The effects of a rupture at the first clad temperature peak will be also investigated. A sixth and last test is due to see what difference it makes with a 25 preirradiated rods bundle.

From the Phase III to the Phase IV, the process of degradation of the PWR fuel rod assemblies will be progressively investigated under SFD conditions, but with a different design of test train. The Phase III is to start at the very beginning of 1985.

Guidance and Exploitation of the tests. At present Relap IV mod 6 is the base code for helping in the guidance of the tests as it has been said a little before. The description of the Phebus loop is indicated in figure 5. Some data of the code such as those which concern the rupture have been drawn from French analytical experiments.

The exploitation of Phase I's results is chiefly used to optimize the modeling of the Phebus loop so that this code would be able to describe as well as possible the thermohydraulic within the bundle during Phase II.



As Relap IV mod 6 has proved to be not suitable to describe reflooding along short heating lengths, a simple but realistic module PHEDRE adjusted to the ERSEC tests in Grenoble is under development at Cadarache for this purpose.

However for the Phase II, we shall preferentially use the fuel codes FRAP T4 and CUPIDON for taking benefit of the results of the tests. These codes will be thermohydraulically fed either by Relap IV mod 6 or by experimental results.

For the moment pretest and posttest computations are performed with the three codes.

IV - ADVANCEMENT POINT OF THE PHEBUS PROGRAM

IV.1 Phase I (see Table I)

IV.1.1 One rod test

Table I. Phase I's one rod tests

Test	Linear power hot point (kW m ⁻¹)	Injection delay	Date
101	0	Not delayed	03.12.80
102	57	Delayed up to 800°C (cladding temp.)	14.04.81
103	57	Delayed up to 1000°C (cladding temp.)	29.10.81
104	57	Delayed up to 1200°C (cladding temp.)	1982

Three of the four double-break tests on one non-pressurized rod channel are done (101, 102, 103) and the clad temperature has reached 940°C for the test 103. Some interesting procedures have been implemented to take benefit of the results of this kind of nuclear test.

At first the problem was to compute the rod power time function starting from the known driver core power time function. It was found for the test 102 using iteratively FRAP T4, that the ratio between these two functions (i.e. the coupling factor) was a constant with the time, as neutronics let it expected. For that, Ross and Stoute gap conductance with relocation model was employed ; clad TC measurement was taken as fluid temperature ; and a very large value was attributed to the clad-fluid thermal exchange coefficient. On the figure 6, one can see that there is a very small difference between the calculated fuel temperature at iteration convergence and the measured one. Consistently the so-calculated value for the coupling factor was 381 which is not far from the neutronics evaluation : 340 and the thermal hydraulic evaluation by inventory : 385.

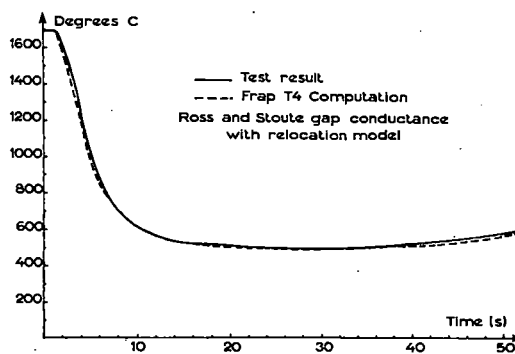


Fig.6 : TEST 102-CENTER LINE TEMPERATURE

Secondly so as to predict reflooding duration for the test 104, the thermal exchange coefficient between fluid and clad has been evaluated via FRAP T4 again, during the quenching period of the test 103. It was assumed that the coupling factor calculated for the test 102 by the above-mentioned method was still valid, because the test 103 was set to be a prolonged test 102.

In a first FRAP T4 computation, measured clad temperature was taken as fluid temperature and a very large value was attributed to the clad-fluid thermal exchange coefficient. That gave us a good evaluation for the heat transfer flux from clad to fluid. Dividing this result by the difference of measured T_{clad} to T_{sat} , we got a first value for the thermal exchange coefficient. This value was then checked by a second FRAP T4 computation (with T_{fluid} taken equal to T_{sat}). Downstream the quenching front, the so-calculated thermal exchange coefficient was used to calculate the quenching velocity via Ellion's correlation [3].

As expected from the results of the ERSEC-PHEBUS-CORE out-of-pile facility tests in GRENOBLE for such a so shorter heating length than that of PHEBUS, this quenching velocity happened to depend only weakly on the time, therefore on the axial position of quenching.

Another confirmation of the validity of the approach was given by the good comparison between the quenching velocity average value issued from this approach : 0.078 m/s and a direct evaluation from the delay between the slope shiftings in the clad temperature measurement curves :

$$0.077 \text{ m/s.}$$

IV.1.2. - 25 rods test (see Table II)

Table II. Phase I's 25 rods tests

Test	Break location	Linear power kW m ⁻¹ (hot point)	Injection delay	Fuel rods internal pressure Mpa	Date
206	hot leg	0	no	0.1	24.04.80
207	"	27	no	0.1	03.06.80
208	cold leg	0	no	0.1	22.05.80
209	"	27	no	0.1	10.06.80
210	double break	0	no	0.1	4.06.81
211	"	27	no	0.1	9.09.81
212	"	40	no	0.1	26.11.81
213A	"	40	yes	0.1	24.06.82
215P	"	40	yes	0.1 3.5	8.07.82
213 B,C	"	40	gradual injection	0.1	from sept to Dec 82
215R	"	40	yes	3,5	Beginning of 83

All the four single break tests with 25 non-pressurized rods bundles of the Phase I are performed (206, 207, 208, 209) and the Relap IV mod 6 results are in fairly good agreement with the experimental results for these tests (see figure 7).

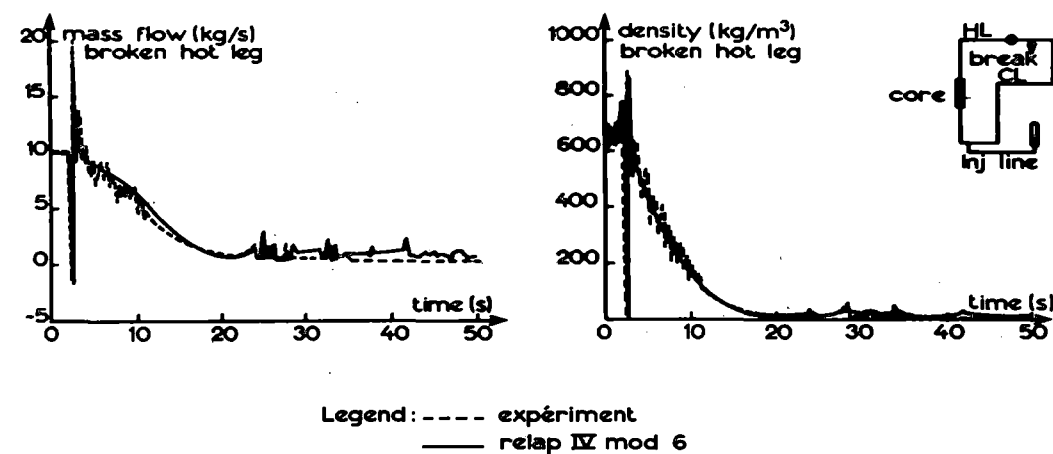


Fig.7: TEST 207 COMPARISON BETWEEN EXPERIMENT
AND POST COMPUTATION RESULTS

As concerns the double-break tests with 25 rods bundles, four tests have been performed (210, 211, 212, 213 A) with non-pressurized rods and for the last of them the clad temperature has reached 1100°C (see fig. 10). A first 25 pressurized rods bundle test (215P) has also been carried out (July 8th 82). The examination of the first available experimental results shows that this test has led to rod rupture and to a clad temperature rise up to 1100°C too (see fig. 8).

This last test can be considered as a successful demonstration of the PHEBUS experimental ability to submit fuel rods to severe temperature and pressure transients as in a LOCA. However the present shape of transient is not quite suitable because of the occurrence as in LOFT tests L2-2 and L2-3 of an early rewetting before the end of the blowdown phase (see figures 8, 9 and 10). On the other hand although thermohydraulic continues to be fairly well predicted by Relap IV mod 6 (see figure 11) in the loop far from the bundle (as for single break tests, see fig. 7), the thermohydraulic behaviour is only represented for orders of magnitude and physical tendencies within the bundle (see also fig. 8, 9 and 10).

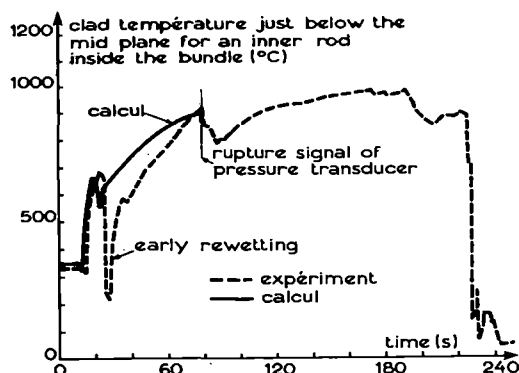


Fig. 8: TEST 215 P (WITH PRESSURIZED RODS)
COMPARISON BETWEEN EXPERIMENT
AND PRECOMPUTATION RESULTS

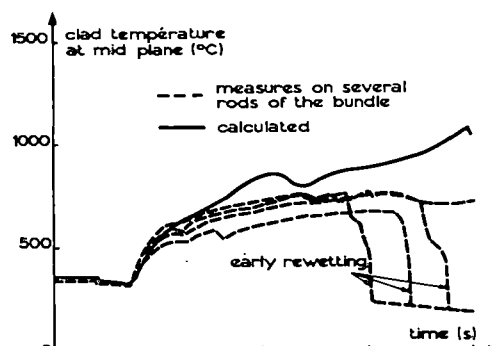


Fig. 9: TEST 212 COMPARISON BETWEEN EXPERIMENT
AND POSTCOMPUTATION RESULTS

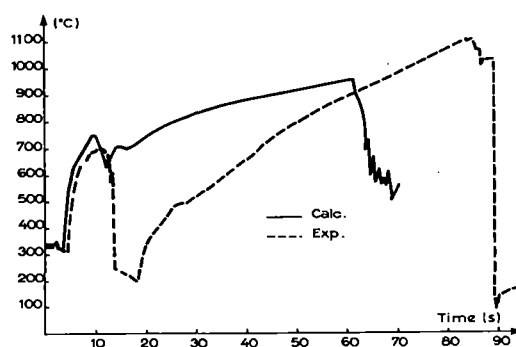


Fig. 10: TEST 213 - COMPARISON BETWEEN EXPERIMENT
AND PRECOMPUTATION RESULTS

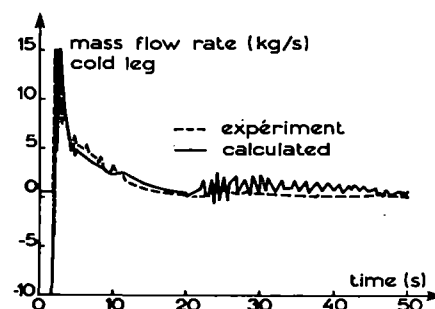


Fig. 11: TEST 212 COMPARISON BETWEEN
EXPERIMENT AND POSTCOMPUTATION
RESULTS

That results from attempting to locate stagnation point in the bundle leads to cope with difference effects. The Relap IV mod 6 data set for describing Phebus loop needs to evolve on. For that purpose, taking into account the results of the two last tests will be useful because both of them give a long adiabatic rise of the clad temperature. But it will be not sufficient, in particular for the usual refilling and reflooding phases (up to now, refilling and reflooding were rather abrupt). So the following tests with non-pressurized rods of the Phase I will be devoted to sensitivity studies with respect to the main loop parameters (the most important of them being probably the break ratio) so as to identify what affects the early rewetting and what in the Relap IV mod 6 data set is insufficient. The other test with pressurized rods of Phase I will serve just before the Phase II :

- firstly to check how has improved our ability both to realize a more suitable temperature transient and to describe thermohydraulic conditions within the bundle, since the July 8th test,

- secondly to see how higher clad temperature tahn 1204°C (2200°F) can be safely reached with the present design of the PHEBUS test train.

IV.2 - Phase II

The feasibility of a long plateau for the clad temperature at the safety criteria limit has been estimated by a simple pessimistic code, so it seems to be secured.

IV.3 - Phase III and IV

A new design for the test train has been proposed. The hability of this new type of test train to simulate core SFD situations is at present under study.

V - CONCLUSION

In-pile Phebus loop has proved to be able to submit PWR fuel rod bundles to severe temperature and pressure transients as in a LOCA. In the 215P test, pressurized fuel rods have burst.

The last tests of the Phase I will be now devoted to sensitivity and checking tests so that we should be able for Phase II, reserved for fuel behaviour study, to avoid early rewetting and to get better prediction of the thermohydraulic conditions around the fuel rods with Relap IV mod 6 through data set improvement. Probably the procedures implemented for taking benefit of the results of one rod tests will be helpful for that.

ACKNOWLEDGMENT

The authors would like to mention that Mrs M. BERNE, MM. B. ADROGUER, B. CLEMENT, C. HUEBER and R. SENEMEAUD have largely contributed to the preparation of this paper.

REFERENCES

- 1 M. CHAGROT : Specialist meeting on fuel element performance computer modelling. AIEA Blackpool 13 - 17 Mars 1978. CUPIDON : A code modelling the thermal and mechanical behaviour of a PWR fuel rod during a LOCA.
- 2 L.J. SIEFFREN et al, FRAP T4 : A computer code for the transient analysis of oxide fuel rods CDAP 78 027, (1978).
- 3 M.E. ELLION : A study of the Mechanism of Boiling Heat Transfer, Jet Propulsion Laboratory, Memo 20.88, CIT, (1954).

==A-A-A-A-A-A-A-A-A-A-A-A-A-A-A-A==

REFLOOD EXPERIMENTS WITH SIMULTANEOUS UPPER
AND LOWER PLENUM INJECTION IN THE REWET-II
ROD BUNDLE FACILITY

Timo Kervinen

Nuclear Engineering Laboratory,
Technical Research Centre of Finland
Lönnrotinkatu 37, 00180 Helsinki 18, Finland

ABSTRACT

A series of 27 reflood experiments has been carried out in a full-length electrically heated rod bundle facility. The primary objective of these tests was to study the effects of a simultaneous upper plenum and downcomer coolant injection and to provide data for the verification of computer codes. The experimental results indicate that an upper plenum injection alone cools the test rods slowly, a simultaneous coolant injection to the downcomer improves cooling significantly, and a downcomer injection alone cools the test rod bundle best if the total value of the coolant flow rate is the same in these three different cases. If the coolant injected to the upper plenum increases the total flow rate, the quench time of the test rods decreases at all elevations. Quenching time and clad temperature histories calculated with the computer codes NORCOOL-I and FLOOD4 are in a reasonable quantitative agreement with experiments in the case of pure downcomer injection. Qualitative trends were predicted reasonably well in most other cases.

1. INTRODUCTION

As a result of a postulated Loss-Of-Coolant Accident (LOCA) in a light water-cooled nuclear reactor the water inventory in the reactor core is reduced and the fuel clad temperature begins to increase due to the fission product decay heat and the energy stored in the fuel. The overheated dry core is cooled down by the emergency core cooling water, injected into the core either by top spray or by bottom flooding. This reflood phase of the LOCA is characterized by complicated heat transfer phenomena. The hot fuel rods cannot rewet until the clad temperature is brought down to the Leidenfrost temperature. It is important to understand the temperature behaviour of the fuel clad, which forms the first barrier against the release of fission products from the fuel.

The aim of the REWET research project is to improve the understanding of the basic phenomena of the reflood phase and to provide experimental data for the development and verification of reflooding codes under conditions simulating pressurized water reactors in use in Finland. These reactors have certain unique features, which make them different from most other PWR designs, in particular, the injection of ECC water directly into the upper plenum and the downcomer of the reactor vessel.

The program was started with the REWET-I single fuel rod simulator facility [1], and it is being continued with the REWET-II facility, which has 19 full-length electrically heated fuel rod simulators and scaled reactor volumes and primary loops.

The aim of the first REWET-II test series reported here was to study the effect of a simultaneous upper plenum and downcomer coolant injection in general.

The experiments performed in the REWET-II facility were calculated before and after the tests using two computer codes NORCOOL-I and FLOOD4, which differ in the degree of complexity.

2. TEST FACILITY AND TEST CONDITION

2.1 Test Facility

The REWET-II test facility was designed to investigate the phenomena during the reflood phase of an LWR LOCA. The scaling factor between the reference power reactor, the VVER-440 reactors Loviisa 1 and 2, and the test section of the facility is 1:2333 referring to the number of fuel rod simulators. The main design principles are accurate simulation of the specific features of rod bundle geometry and the primary system elevations. The steam generators and the primary pumps are currently simulated as flow resistances. Fig. 1 shows schematically the REWET-II test facility.

The test section of the REWET-II facility consists of 19 indirectly electrically heated full-length fuel rod simulators in a triangular grid (Figs. 2 and 3), an upper plenum, a lower plenum and a downcomer. An intact primary loop and a broken loop in the test facility simulate the five intact loops and the broken loop of the simulated PWR, respectively. The heating coil of the fuel rod simulators is inside a stainless steel tube packed in magnesium oxide. The axial power distribution of the fuel rod simulators is shown in Fig. 4. The test section is thermally isolated.

The primary measurements in the experiments are rod surface temperatures from thermocouples distributed radially and axially throughout the bundle (Figs. 3 and 4), pressure difference along the test section, coolant flow rates and heating power.

The data acquisition system consists of a measurement and control processor, a digital voltmeter and a desktop computer with 217 kilobytes tape cartridge drive and 115 kilobytes user memory. During a test 96 data channels are scanned once a second. A maximum of 30000 readouts can be collected during 8 minutes and 40 seconds.

The main characteristics of the test facility are listed in Table I.

TABLE I

REWET-II facility characteristics

Fuel rod simulators:		Fuel rod simulator bundle	
Heated length	242 cm	power	0 - 90 kW
Outer diameter	0.91 cm	Average fuel rod simulator	
Power distribution	chopped cosine	power	0 - 4,7 kW
Axial peaking factor	1.5	Flooding rate	0 - 15 cm/s
Number of rods in bundle	19	System pressure	0.1 - 1.0 MPa
Wall thickness of housing	0.2 cm	Maximum cladding	
Bundle arrangement	triangular	temperature	1000 °C
Lattice pitch	1.22 cm	Coolant temperature	15 - 120 °C
ECC injection location	upper plenum and / or downcomer		

2.2 Test Procedure and Test Conditions

Before the start of each test run various accessories and instruments are checked for their operability and the test facility is heated by a flow of saturated steam at 600 kPa to minimize the condensation of the reflood-generated steam on the inner walls of the upper plenum and the primary loops. The coolant feed lines are pre-heated by allowing water from the coolant storage tank to flow through it. After pre-heating the liquid level in the lower plenum was established at a point just below the heated length of the core. The specified electrical power was then applied to the rod simulators and when the test rod clad temperature reached the specified value, the test was initiated by starting the ECC injection to the downcomer or/and to the upper plenum.

The test matrix of the 27 tests carried out so far is shown in Table II.

TABLE II

Test matrix

Experiment		R	2	3	4	5	6	7	8	9	10	11	12	13	14	15	16	17	18	19	20	21	22	23	24	25	26	27
Power	30 kW	X	X	X	X	X				X	X		X					X	X		X	X	X	X	X	X	X	X
	40					X	X	X			X		X	X	X	X		X									X	
Flooding Rates	DC 0.0345 kg/s	X		X					X	X			X	X	X		X	X	X		X		X	X		X		X
	0.0690	X			X	X	X				X		X	X		X		X		X		X	X		X			
	0.1725																										X	
	0.3450							X				X																
LP	0.0345		X						X				X	X	X		X	X	X		X		X	X				
	0.0690			X			X						X															
	0.1725																										X	
	0.3450												X															
Coolant Temp.	DC 10 C												X	X			X											
	50	X	X		X	X	X	X	X	X	X	X	X					X	X		X	X	X	X	X	X	X	X
	100															X	X											
LP	10															X												
	50		X	X		X		X		X		X						X		X		X	X		X	X		
	100												X	X			X											
Pressure	100 kPa	X	X	X	X	X	X	X	X	X	X	X	X	X	X	X	X	X							X	X	X	X
	400																		X	X		X	X	X				

0.0345 kg/s $\hat{=}$ 2 cm/s

0.0690 kg/s $\hat{=}$ 4 cm/s

0.1725 kg/s $\hat{=}$ 10 cm/s

0.345 kg/s $\hat{=}$ 20 cm/s

30 kW $\hat{=}$ 6.5 W/cm

40 kW $\hat{=}$ 8.7 W/cm

2.3 Test Results

In these reflooding experiments, where the lower plenum was full of water at the start of the experiments, the reflooding mechanism was nearly similar in the three compared modes of ECC water injection. After the initiation of water injection to the downcomer or/and to the upper plenum, the quenching front started to progress upwards and oscillations of about 0,3 Hz occurred in the test rod bundle. Entrained droplets or the falling liquid film quenched the upper end of the test rods. The falling liquid film and the bottom flooding level met at an elevation of about 1970 mm, at which location thermocouples at various radial positions indicated either early quenching (about 30 s after start) or late quenching (more than 100 s after start). Thermocouples located at the elevation of 1740 mm indicated primarily the longest quenching time.

In all experiments the highest measured cladding peak temperature occurred at the highest heating power location of the fuel rod simulators (see Fig. 4).

The variation of these temperatures was between 575 °C (experiment 11) and 755 °C (experiment 2). The variation of measured cladding temperature rise (peak temperature minus initial temperature) was between 30 °C and 265 °C, which were measured in the experiments 21 and 3, respectively. Lower values of the maximum cladding temperature and temperature rise were measured in the case of downcomer coolant injection and higher values in the cases of pure upper plenum or simultaneous coolant injection.

The average quenching front progression rate upwards was in the test series between 0,4 (experiment 4) and 0,6 cm/s (experiment 5). Fig. 5 shows a comparison of quenching front progression in different cases of coolant injection. It is seen that the quenching front rises nearly with the same speed for the first 700 mm or so. This implies that up to this moment the water injected into the upper plenum flowed rapidly downwards.

At a fixed total flow rate (designed here 100 %) a pure downcomer injection was the most effective of the three injection modes compared. A pure upper plenum injection cooled the test rods slowly, and a simultaneous coolant injection to the downcomer improved cooling significantly. If the total flow rate is increased by upper plenum injection, the cooling with simultaneous coolant injection to the upper plenum and to the downcomer is slightly more effective than pure downcomer injection. This result was observed at a flow rate of 100 %/100 %. Figs.6 and 7 show comparisons of cladding temperature histories.

2.4 Computer code predictions

The test predictions are calculated using the advanced NORCOOL-I /2/, developed in the nordic NORHAV nuclear safety program, and the simpler FLOOD4 /3/ computer codes.

NORCOOL-I consists of two basic models, a fuel rod model and a model for the two-phase flow. The fuel rod model is a heat conduction mode. The two-phase flow model is based on a solution of the conservation equations for mass, momentum and energy, and the equation of state. The flow regimes covered by NORCOOL-I are single phase liquid, bubbly flow, inverse annular flow, film flow and dispersed flow. Thermodynamic equilibrium is not assumed and the steam is allowed to be superheated and the water subcooled. The coupling between the fuel rod model and the two-phase flow model is taken into account through a number of physical models and correlations for the heat transfer, which include conduction, convection and thermal radiation.

FLOOD4 code was developed in the Semiscale Program at the Idaho National Engineering Laboratory (INEL) as an analytical tool to calculate expected results during reflooding experiments and to relate them to the results expected in a PWR during reflooding. The FLOOD4 model contains several empirical correlations based on the semiscale test. FLOOD4 has about 3000 commands, which is one tenth of the size of NORCOOL-I.

A comparison of calculated and measured clad temperature responses at three different elevations in the case of downcomer injection alone is presented in Fig. 8. The maximum clad temperature is higher in the calculations than in the experiments, but the time of temperature turnover agrees well with the measured data. After the turnover the NORCOOL-I calculations indicate a more rapid decrease of clad temperature and an earlier quenching. The quenching temperature observed in the experiments was between 400 - 500 °C. In the NORCOOL-I code this temperature is a result of calculations of rewetting front velocity based on the Leidenfrost temperature and an effective heat transfer coefficient. The calculated quenching temperature was slightly too high.

The reference prediction by the FLOOD4 code shows good agreement with the experimental data in the middle of the test rod. In the lower part of the test rod the prediction shows a lower maximum clad temperature and an earlier quenching time. In the upper part of the test rod the clad temperature increases until the quenching front reaches this area (Fig. 9).

Predicted clad temperatures and quenching times by both NORCOOL-I and FLOOD4 differ more from the experimental data in the cases of simultaneous and pure upper plenum injection than in pure downcomer injection. In agreement with the experiments, the calculations indicate that the quenching front propagates upwards and the falling liquid film quenches only the uppermost end of the test rod having very low power.

3. CONCLUSIONS

In order to improve the understanding of the specific effects of simultaneous ECC injection to the downcomer and to the upper plenum during the reflood phase of a PWR-LOCA and to evaluate the capabilities of the NORCOOL-I and FLOOD4 computer codes, reflood tests have been carried out in the REWET-II rod bundle facility with corresponding pretest computer code calculations. The following conclusions are drawn from the results available so far:

1. Upper plenum injection alone cools test rods slowly, a simultaneous coolant injection to the downcomer improves cooling significantly, and downcomer injection alone cools the test rod bundle best if the total value of the coolant flow rate is the same in these three different cases. If the coolant injected to the upper plenum increases the total flow rate, the quenching time gets shorter at all elevations.

2. A part of the ECC water injected to the upper plenum flows down through the test rod bundle and increases the velocity of the quenching front rising upwards. Further experiments are needed to investigate this phenomenon.

3. The NORCOOL-I and FLOOD4 computer codes are capable of calculating fairly well the temperature history and the quenching time in the case of pure downcomer injection during the reflood phase. In the case of simultaneous upper plenum and downcomer injections the understanding under what conditions and how rapidly the water injected to the upper plenum may flow down through the core into the lower plenum is decisive for predicting core cooling. Therefore, in later experiments this will be one of the main aspects.

4. ACKNOWLEDGEMENT

The REWET-test program is being carried out by The Technical Research Centre of Finland (VTT) in co-operation with the Lappeenranta University of Technology (LTKK). The work is primarily sponsored by the Finnish Ministry of Trade and Industry. The financial support from the International Atomic Energy Agency and the Academy of Finland is gratefully acknowledged.

The authors express their thanks for the significant contributions to several members of the staff of the Department of Energy Technology of the LTKK and the Nuclear Engineering Laboratory of VTT.

REFERENCES

1. Kervinen, T. et al., "REWET-I Single Pin Reflood Experiments". Technical Research Centre of Finland, Nuclear Engineering Laboratory, Report 49, Helsinki June 1980.
2. Andersson, J.G.M., et al., "NORCOOL-I, A model for Analysis of a BWR under LOCA Conditions", a revised report, NORHAV-C-47, August 1977.
3. Shumway, R.W., "Core reflood dynamics code-FLOOD4", U.S. Development of Energy report EGG-SEMI-505, October 1979.

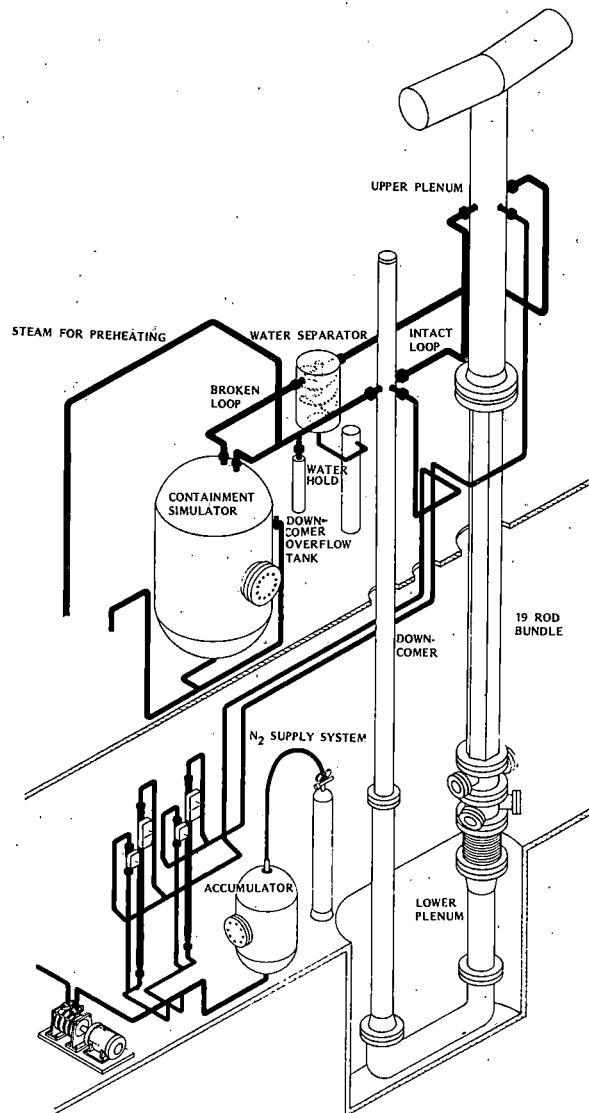


Fig.1. REWET-II test facility.

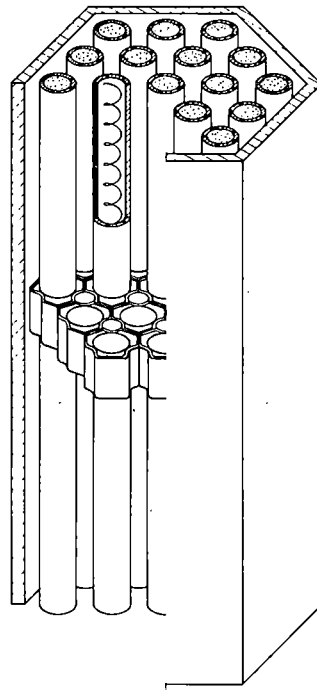


Fig. 2. Test rod arrangement in the REWET-II facility.

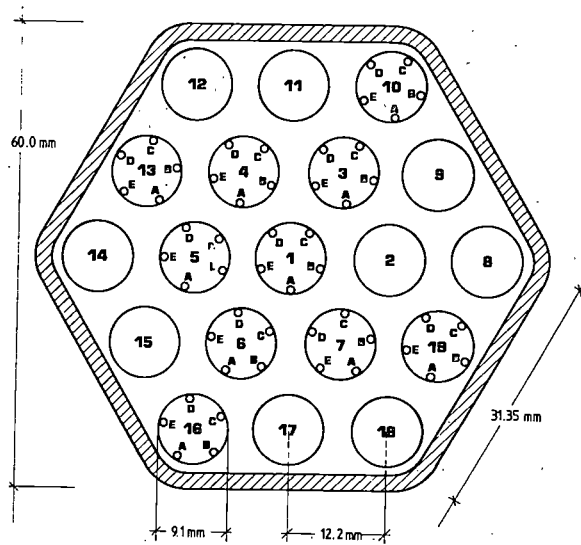


Fig. 3. Plan view of the REWET-II core showing heater rod thermocouple locations.

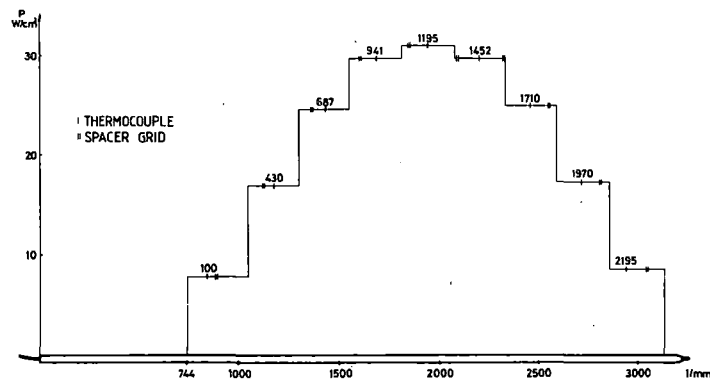


Fig. 4. REWET-II heater rod axial power distribution showing spacer grid and thermocouple locations.

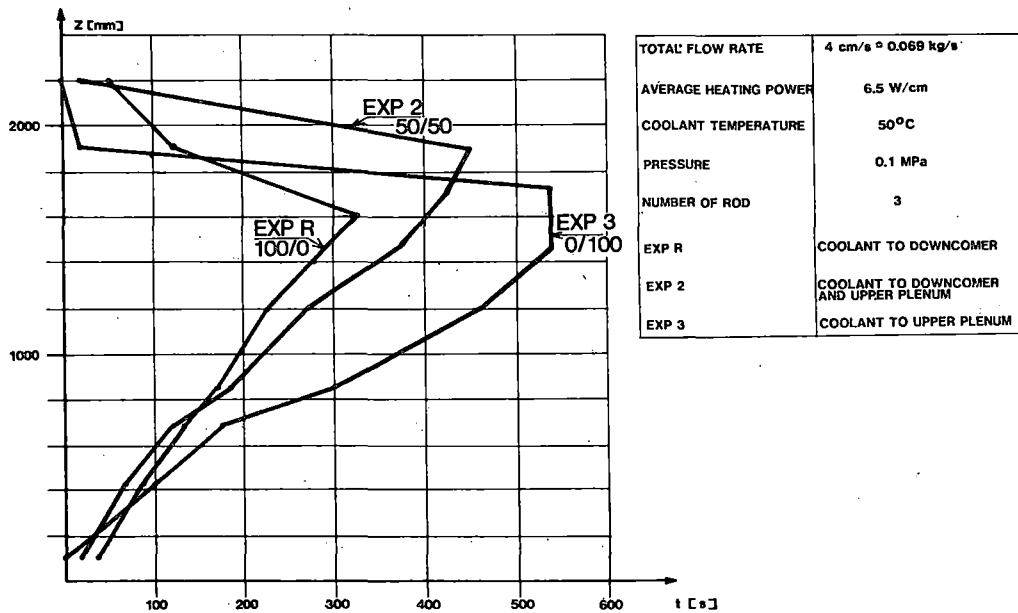


Fig. 5. Comparison of quench front progression with the downcomer (EXP R), the upper plenum (EXP 3) and the simultaneous coolant injection (EXP 2).

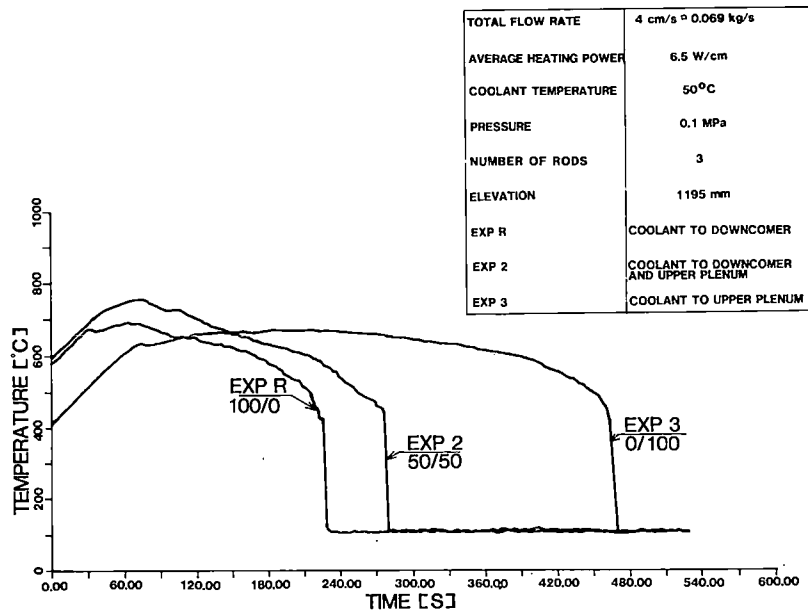


Fig. 6. Clad temperature histories in the cases of the upper plenum (EXP 3), the downcomer (EXP R) and the simultaneous coolant injection (EXP 2).

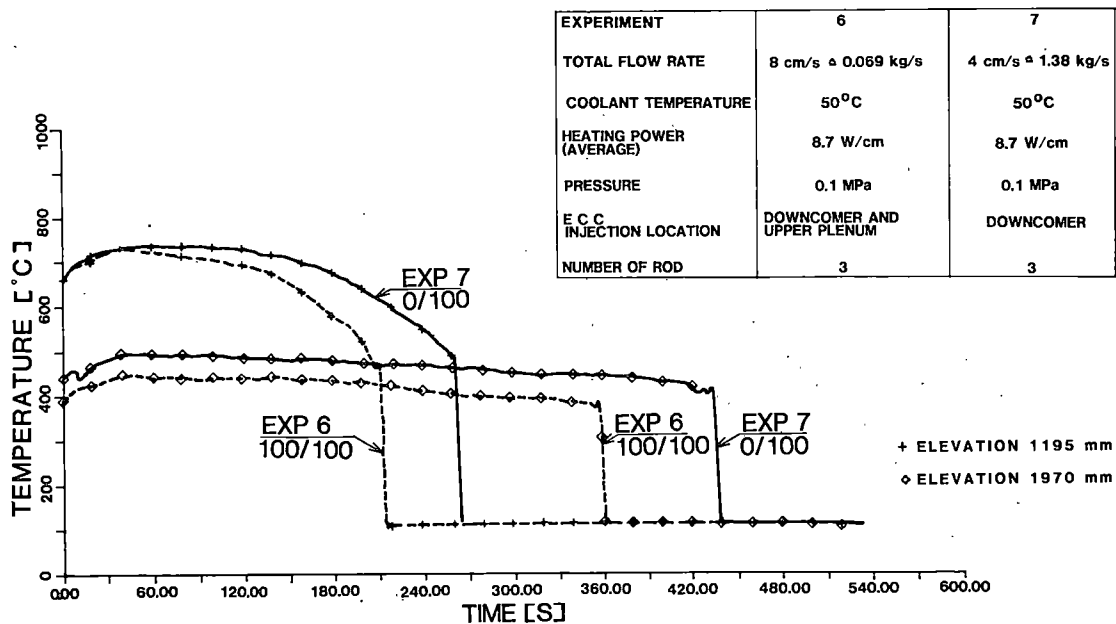


Fig. 7. Effect of total flow rate on clad temperature histories in the cases of the downcomer (EXP 7) and the upper plenum injection (EXP 6).

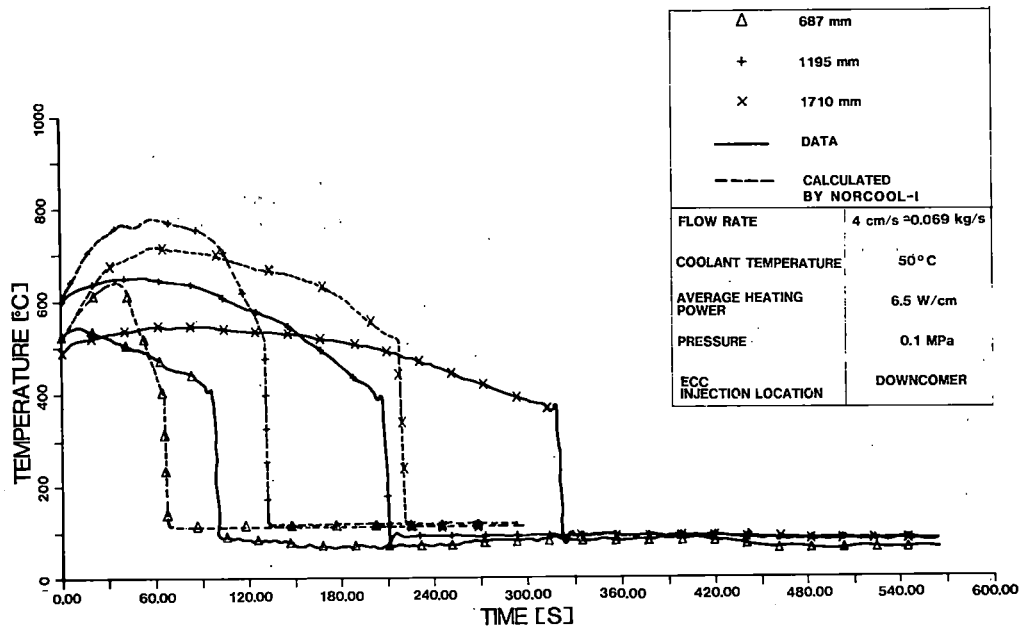


Fig. 8. Comparison of experimental and NORCOOL-I calculated clad temperature histories (Experiment R).

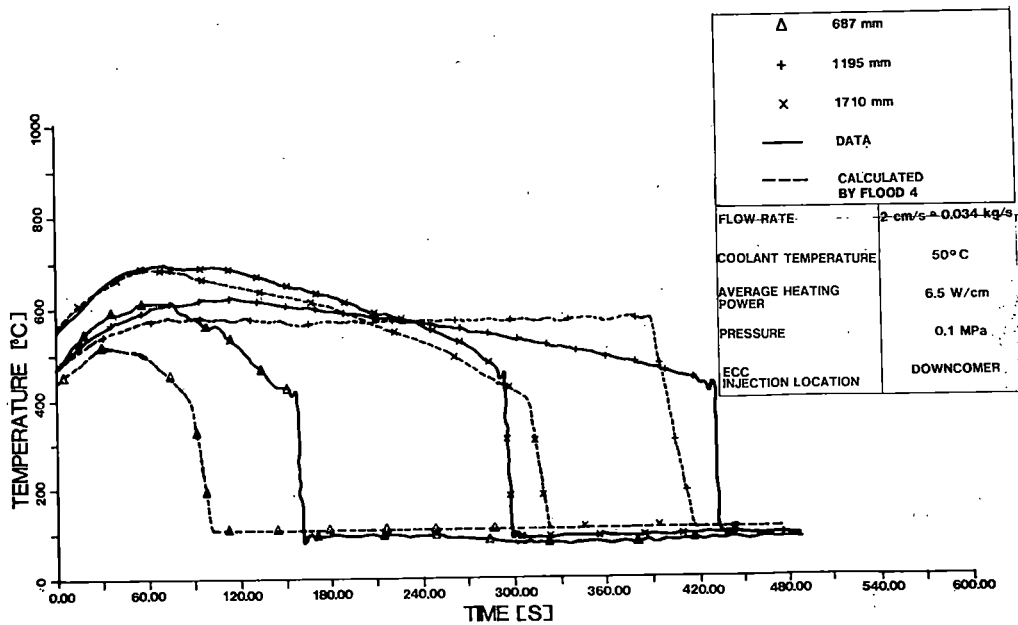


Fig. 9. Comparison of measured and FLOOD4 calculated clad temperature histories (Experiment 4).

MIST CORE COOLING DURING THE REFLOOD PHASE OF PWR-LOCA

P. Ihle and K. Rust

Institut für Reaktorbauelemente
Projekt Nukleare Sicherheit
Kernforschungszentrum Karlsruhe
Postfach 3640, 7500 Karlsruhe 1
Federal Republic of Germany

and

S.L. Lee

Department of Mechanical Engineering
State University of New York at Stony Brook
Stony Brook, N.Y. 11794, U.S.A.

ABSTRACT

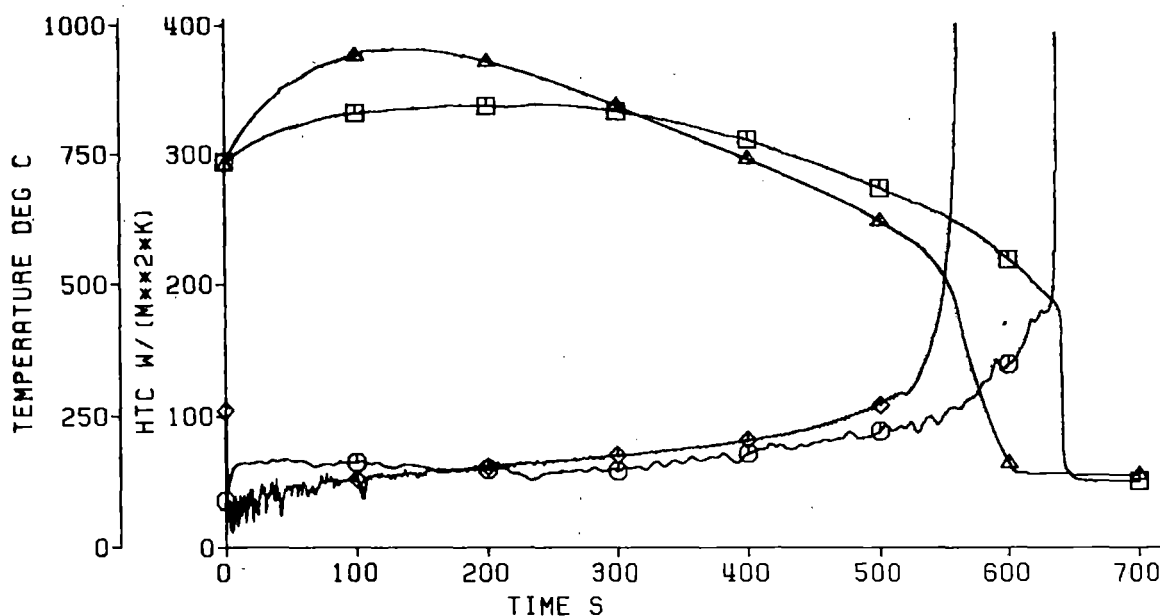
A transient thermal-hydraulic experiment in a simulated rod bundle is reported here in the hope of gaining an insight into the most important heat transfer mechanisms which are responsible for the development of the cladding temperature transient and therefore of great interest to analytical model development. The enhanced mist cooling downstream of the grid spacers has been identified as one of the most significant of such mechanisms and a correlation has been formulated for this mode of droplet heat transfer over realistic ranges of system parameters.

INTRODUCTION

The prediction of the peak cladding temperature during the transient of the re-flood phase of a PWR-LOCA is a matter of great importance in reactor safety. For example, the acceptance criteria for emergency core cooling systems for light-water cooled nuclear power reactors in the United States requires that each evaluation model shall include a provision for predicting cladding swelling and rupture from consideration of the axial temperature distribution of the cladding and from the difference in pressure between the inside and outside of the cladding, both as functions of time [1]. Unfortunately such a prediction has always been found grossly inadequate apparently due to a general lack of understanding of the physics in the mist flow portion of re-flood phase in existing analytical prediction models as shown in the comparison of the predicted and measured cladding temperature of Fig. 1, the details of which will be explained later.

EXPERIMENTAL ARRANGEMENT

The test facility as shown in the sketch of Fig. 2 was designed for simulation of idealized re-flood conditions in a PWR core using forced feed, system pressure and geometry as constant parameters during each test [2]. System effects and interaction between cooling and deformation were excluded. A 5 x 5 array of simulated fuel rods of German PWR dimensions of 3.9 m heated length with chopped cosine axial rod power distribution, 10.75 mm outer diameter and 14.30 mm pitch was used. The rods were heated electrically by embedding heating elements in MgO. In the NiCr-cladding of 1 mm thick-



FEBA-test No. 223
 flooding velocity 3.8 cm/s
 system pressure 2.1 bar
 feedwater temperature 40 deg C

□ FEBA: clad temperature
 △ RELAP: clad temperature
 ○ FEBA: heat transfer
 ◇ RELAP: heat transfer

elevation:
 2840 mm from bottom

heat transfer related to
 saturation temperature

Fig. 1 FEBA-experiment - RELAP-calculation Temperatures and Heat Transfer Coefficients.

ness, thermocouples were completely embedded to reduce coolant channel disturbances. Unshielded Chromel-Alumel thermocouples sheathed by an Inconel tube of 0.25 mm outside diameter were placed in the center of the bundle subchannels for the measurement of the temperatures of the water and steam coolant phases [3]. These thermocouples have a response time which is sufficiently short to detect steam superheat during the early portion of a reflood test and a capacity which is sufficiently high to prevent a too early quenching due to the passage of water droplets present in the flow. Temperatures, pressures, pressure differences, flow rates, water carry-over and rod power were recorded digitally at a scan frequency of 10 cycles/s.

COMPARISON BETWEEN EXPERIMENT AND ANALYSIS

The conventional thinking about bottom flooding is that a hot dry wall is cooled by a parallel stream carrying the water droplets generated from the bottom [4]. The significant mechanisms in this heat transfer mode are usually assumed to be superheated steam convection, droplet cooling and liquid carry-over [5], the last of which becomes less important at levels in the subchannels far above the quench front. Furthermore, during refill and reflood when reflood rates are small, say less than 2.5 cm/s, heat

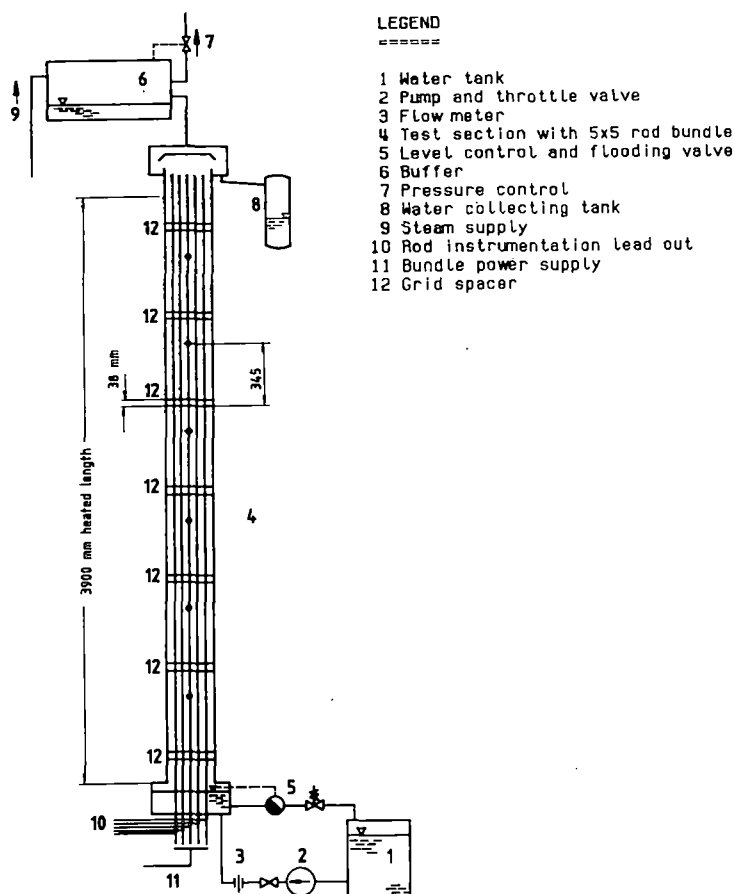


Fig. 2 Sketch of Test Facility.

transfer calculations are normally based on the assumption that cooling is only by steam [1], apparently on account of a believed lack of sufficient population of smaller droplets from the bottom which serve as efficient cooling agents due to their high surface area to mass ratios.

To check on the afore-mentioned assumption, a preliminary test was conducted with a relatively low flooding velocity of 3.8 cm/s and a system pressure of 2.1 bar. Figure 1 shows the measured cladding temperatures at a distance of 2840 mm above the bottom end of heated bundle length compared with corresponding analytical predictions by the RELAP4/MOD6 computer code. From this comparison, it is clear that the assumed mechanisms of heat transfer are not adequate, particularly in the initial period of reflooding, to bring the calculated temperatures down to the measured level.

ENHANCEMENT OF MIST COOLING

An additional, possibly plausible mechanism of heat transfer during reflooding is the cooling effect of smaller droplets generated from the thermally relatively inactive large droplets which are intercepted by the grid spacers located at distributed intervals along the whole length of the bundle [6]. To check on the validity of this suggested physical model, a direct measurement of droplet dynamics across the grid spacer is needed. Such an endeavor would have been considered nearly unrealizable until the recent development by Lee and Srinivasan [7] of a special laser-Doppler anemometry technique for the *in situ* simultaneous measurement of velocity and size of relatively large particles in a dilute two-phase suspension flow. Using this optical scheme, Lee et al. [8] conducted a series of systematic studies of the influence of a simulation grid spacer plate on the droplet size population and velocity distribution in the mist flow downstream for several pre-selected initial mean droplet sizes in the millimeter range in the mist flow upstream. Their results reveal that regardless of the initial mean droplet size in the mist flow upstream of the grid spacer plate, the mean droplet size in the mist flow downstream of the grid spacer plate has been found to assume a stabilized value on the order of 200 microns. The measured order-of-magnitude increase in the population of the smaller droplets in the mist flow downstream of the grid spacer plate is indeed due to the re-entrainment of droplets from the accumulated liquid from the deposition on the plate of some of the droplets, including some of the

larger ones, in the initial flow upstream of the plate.

To ascertain the effect of enhanced mist cooling downstream of the grid spacer, further measurement and correlation of axial temperature distribution behind a grid spacer and an understanding of the transient natural convection in a slow vertical dispersed flow have long been anticipated [4]. Figure 3 shows the measured cladding temperature, fluid temperature, and heat transfer coefficient relative to the saturation temperature corresponding to the system pressure at an elevation of 3385 mm above the bottom end of heated bundle length for a test with a low flooding velocity of 2.2 cm/s and a system pressure of 4.1 bar. In much of the initial period of reflooding, in this case, the temperature of the vapor is higher than that of the cladding and consequently the convective heat transfer is actually from the superheated steam to the cladding instead of the measured overall loss of heat from the cladding to the dispersed flow. The only exception to this is the fact that at the very beginning, the measured heat transfer is indeed from the flow to the cladding as expected. This discrepancy in much of this period excluding the very beginning can be attributed to the effect of evaporative cooling of the smaller droplets in the flow most likely due to the presence of the grid spacers in the subchannel.

Figure 4 presents a comparison among heat fluxes measured at three different axial locations, one at 200 mm upstream, one at 100 mm downstream, and one at 400 mm downstream of the leading edge of a grid spacer. The heat flux for the axial location of 100 mm downstream of the grid spacer leading edge is more than fifty percent higher than those for the other two axial stations, indicating clearly the effect of enhanced droplet cooling in the region immediately downstream of the grid spacer.

MEASUREMENTS AND ANALYSES

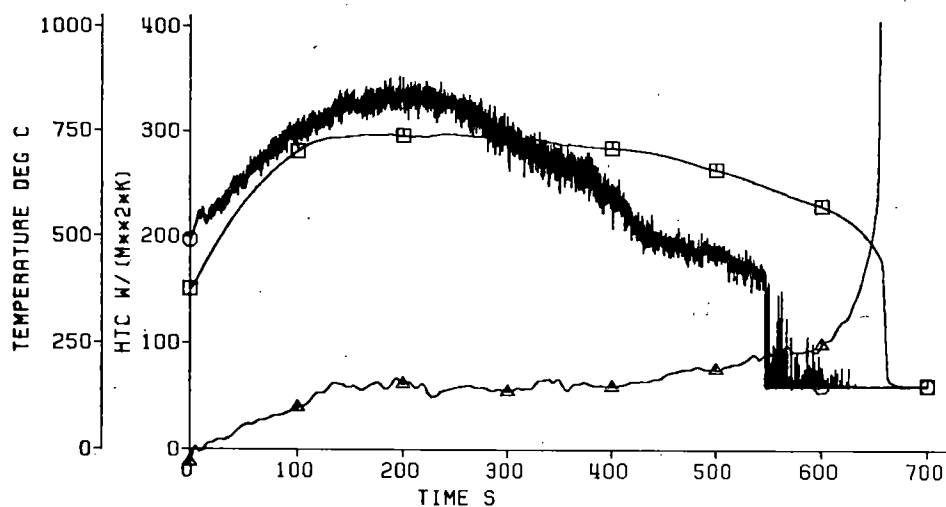
In total, six individual tests were conducted, one for each of the various combinations of three system pressures of approximately 2, 4 and 6 bars and two flooding velocities of 3.8 and 5.8 cm/s. In each test, the usual standard of 120 percent ANS for transient decay heat simulation with an initial bundle power of 200 kW was adopted. The measuring station was selected at a fixed level of 345 mm downstream of a grid spacer in the upper portion of the subchannel as indicated in Fig. 2. Temperature transients for both the cladding and the flow were carefully monitored.

CHARACTERISTIC TIME SCALE FOR MIST FLOW

As expected, the running time for a test varies greatly from test to test. In order to be able to analyze the test results on some rational basis, a suitable characteristic time scale would have to be found with particular attention paid to the mist flow portion of the transient. Since the quenching of the flow probe generally marks the end of the loosely defined mist flow regime, the flow probe quench time seems to be the logical choice for the required characteristic time scale. Within the scatter of the experimental data due to the uncertainty in the determination of time of flow probe quenching, the following correlation was established for the quench time of the flow probe:

$$T_Q^* = (C_{00} + C_{01} Re^{-1}) + (C_{10} + C_{11} Re^{-1}) P^{-1} + (C_{20} + C_{21} Re^{-1}) P^{-2} \quad (1)$$

$$\begin{aligned} C_{00} &= 0.57317 \times 10^1 & C_{01} &= -0.15738 \times 10^5 \\ C_{10} &= -0.93267 \times 10^1 & C_{11} &= 0.71458 \times 10^5 \\ C_{20} &= 0.21643 \times 10^2 & C_{21} &= -0.98885 \times 10^5 \end{aligned}$$



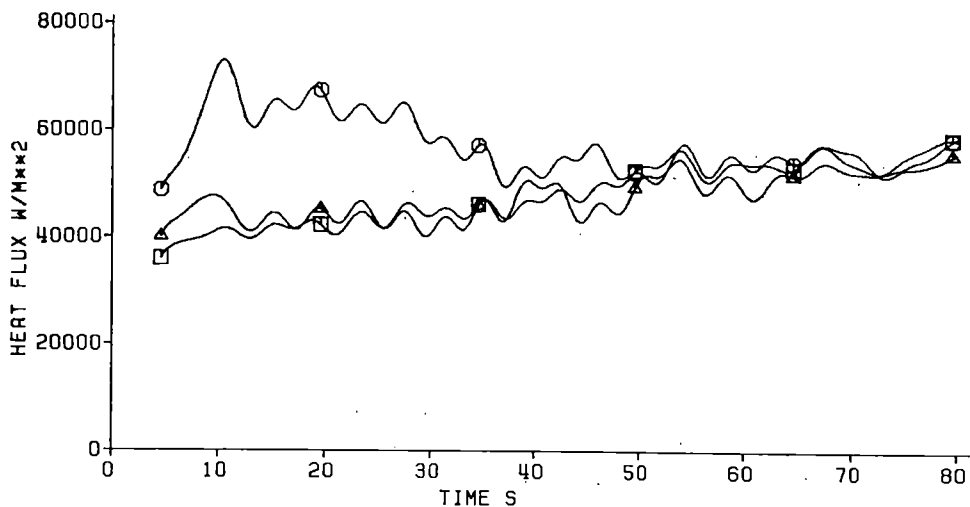
FEBA-test No. 284
 flooding velocity 2.2 cm/s
 system pressure 4.1 bar
 feedwater temperature 40 deg C

□ clad temperature
 ○ fluid temperature
 ▲ heat transfer

elevation:
 3385 mm from bottom

heat transfer related to
 saturation temperature

Fig. 3 FEBA-experiment Temperatures and
 Heat Transfer Coefficient.



FEBA-test No. 282
 flooding velocity 3.8 cm/s
 system pressure 4.1 bar
 feedwater temperature 40 deg C

□ 200 mm upstream of
 grid spacer leading edge
 ○ 100 mm downstream of
 grid spacer leading edge
 ▲ 400 mm downstream of
 grid spacer leading edge

height of grid spacer 38 mm

Fig. 4 Effect of Grid Spacer on Heat Transfer in
 Mist Flow.

where $T_Q^* = T_Q \cdot (V/L)$	Dimensionless probe quench time
T_Q	Probe quench time
V	Flooding velocity at bundle inlet
L	Axial distance from bundle bottom end
$Re = \frac{V \cdot d_H}{\nu}$	Flooding Reynolds number
d_H	Hydraulic diameter of subchannel
ν	Kinematic viscosity of water (at saturation)
P	Normalized system pressure, bar

A plot of the comparison of this correlation, Eq. (1), with experimental data is shown in Fig. 5.

MIST COOLING ENHANCEMENT DOWNSTREAM OF GRID SPACER

A transient heat balance based on the measured cladding and fluid temperatures and the physical properties of the heater rod materials and the fluid under local flow conditions led to the determination of the local heat flux, \dot{q}_{total} . On the other hand, a transient mass balance led to the determination of the local vapor mass flux, \dot{m}_v :

$$\dot{m}_v = \dot{m}_i - \dot{m}_{co} - \dot{m}_b \quad (2)$$

where \dot{m}_v	Mass flux of vapor
\dot{m}_i	Mass flux of injected water
\dot{m}_{co}	Mass flux of carry-over
\dot{m}_b	Mass flux of water stored in bundle deduced from pressure drop measurement

By the use of this local vapor mass flux together with the local flow properties and physical properties of vapor under local flow conditions, we can obtain the local vapor heat transfer coefficient, h_v , with reference to the local vapor temperature from the Dittus-Boelter correlation equation for single-phase convective heat transfer [9]:

$$Nu_v = 0.023 \cdot Re_v^{0.8} \cdot Pr_v^{0.4} \quad (3)$$

where $Nu_v = \frac{h_v \cdot d_H}{k}$	Vapor Nusselt number
h_v	Vapor heat transfer coefficient based on difference between cladding and vapor temperatures
k	Vapor thermal conductivity
$Re_v = \frac{U_v \cdot d_H}{\nu_v}$	Vapor flow Reynolds number
$U_v = \frac{\dot{m}_v}{A \cdot \rho_v}$	Vapor velocity
\dot{m}_v	Vapor mass flux in bundle

A	Cross-section area of bundle
ρ_v	Vapor density
Pr_v	Vapor Prandtl number
ν_v	Vapor kinematic viscosity

The local droplet heat flux, \dot{q}_d , can then be determined as follows:

$$\dot{q}_d = \dot{q}_{total} - h_v(\theta_c - \theta_v) \quad (4)$$

where θ_c and θ_v are the measured cladding and vapor temperatures respectively.

Within the scatter of the data due to the various experimental uncertainties, the following correlation was established for the local droplet heat transfer:

$$\begin{aligned} Nu_d = & [(C_{101} Re_\ell^{-1} + C_{102} Re_\ell^{-2}) + (C_{111} Re_\ell^{-1} + C_{112} Re_\ell^{-2}) Re^{-1}] \cdot T' \\ & + [(C_{201} Re_\ell^{-1} + C_{202} Re_\ell^{-2}) + (C_{211} Re_\ell^{-1} + C_{212} Re_\ell^{-2}) Re^{-1}] \cdot (T')^2 \\ & + [(C_{301} Re_\ell^{-1} + C_{302} Re_\ell^{-2}) + (C_{311} Re_\ell^{-1} + C_{312} Re_\ell^{-2}) Re^{-1}] \cdot (T')^3 \\ & + [(C_{401} Re_\ell^{-1} + C_{402} Re_\ell^{-2}) + (C_{411} Re_\ell^{-1} + C_{412} Re_\ell^{-2}) Re^{-1}] \cdot (T')^4 \end{aligned} \quad (5)$$

$C_{101} = 0.22851 \times 10^9$	$C_{111} = -0.72922 \times 10^{12}$
$C_{201} = -0.18093 \times 10^{10}$	$C_{211} = 0.57371 \times 10^{13}$
$C_{301} = 0.54325 \times 10^{10}$	$C_{311} = -0.17245 \times 10^{14}$
$C_{401} = -0.55725 \times 10^{10}$	$C_{411} = 0.17725 \times 10^{14}$
$C_{102} = -0.30952 \times 10^{14}$	$C_{112} = 0.11003 \times 10^{18}$
$C_{202} = 0.24887 \times 10^{15}$	$C_{212} = -0.87328 \times 10^{18}$
$C_{302} = -0.75366 \times 10^{15}$	$C_{312} = 0.26355 \times 10^{19}$
$C_{402} = 0.77681 \times 10^{15}$	$C_{412} = -0.27141 \times 10^{19}$

$$\text{where } Nu_d = \frac{d_H \cdot \dot{q}_d}{k(\theta_v - \theta_s)}$$

Droplet heat transfer Nusselt number

\dot{q}_d

Droplet heat flux

θ_s

Saturation temperature of water

$$Re_\ell = \frac{U_v \cdot \ell}{\nu_v}$$

Flow Reynolds number based on downstream distance from grid spacer

ℓ

Distance downstream of leading edge of grid spacer

$$T' = T/T_Q$$

Normalized time

T

Time

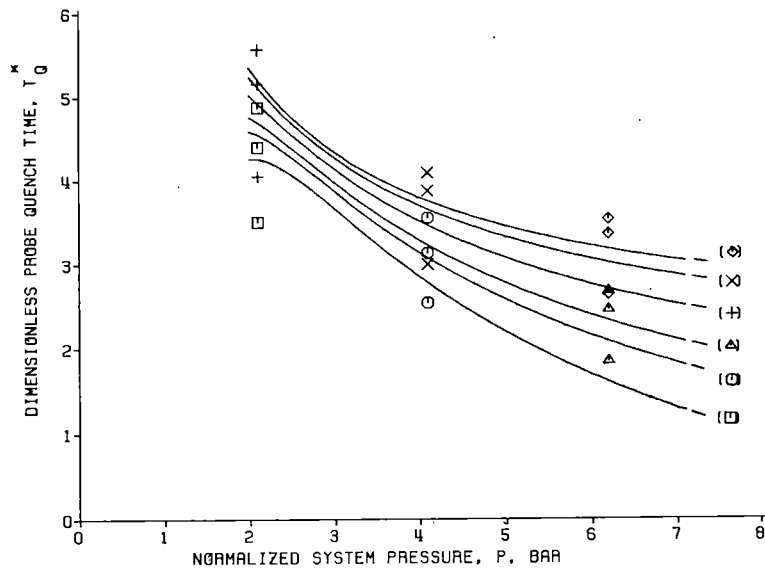


Fig. 5 Probe Quench Time Correlation.

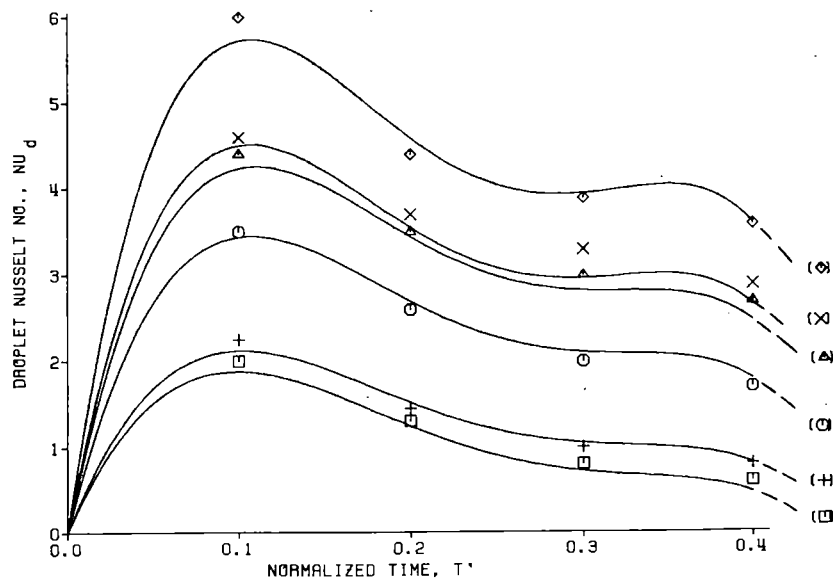


Fig. 6 Droplet Heat Transfer.

A plot of the comparison of this correlation, Eq. (5), with experimental data is shown in Fig. 6.

CONCLUSIONS

The enhanced mist cooling downstream of the grid spacer has been identified as the most important additional heat transfer mechanism which is responsible for the observed significant lowering of the peak cladding temperature during transient of reflood phase of a PWR-LOCA.

The flow probe quench time, which is related to the passage of the mist regime of the flow, has been correlated over realistic ranges of system parameters. The use of this flow probe quench time as a characteristic time scale has made possible the formation of a correlation for the enhanced droplet heat transfer downstream of the grid spacer.

ACKNOWLEDGEMENTS

The authors would like to express their appreciation to the Institut für Reaktorbauelemente, Kernforschungszentrum Karlsruhe, for its support and to the U.S. Nuclear Regulatory Commission for its encouragement. In addition, they would also like to thank Mr. W. Hame of PTF, Bruchsal, for his assistance in the programming.

REFERENCES

1. "ECCS Evaluation Models", Appendix K, Part 50 - Licensing of Production and Utilization Facilities, *Federal Register*, 39, No. 3, p. 1003 (1974).
2. Rust, K. and Ihle, P., "Heat Transfer and Fluid Flow During Reflooding of Blocked Arrays", in *Proc. ANS/ASME/NRC Int. Topical Meeting on Nuclear Reactor Thermal Hydraulics*, Saratoga Springs, New York, (1980), p. 1237.
3. Ihle, P. and Mueller, St., "Experience with Steam Temperature and Water Detection Probes for Transient Mist Flow in Hot Rod Bundles", in *Proc. ANS/ASME/NRC Int. Topical Meeting on Nuclear Reactor Thermal Hydraulics*, Saratoga Springs, New York, (1980), p. 970.
4. Tong, L.S. and Bennet, G.L., "NRC Water-Reactor Safety-Research Program", *Nuclear Safety*, 18, No. 1, p. 1 (1977).
5. Cadek, F.F., Dominicis, D.P., and Leyse, R.H., "PWR FLECHT: Final Report", USAEC Report WCAP-7665, Westinghouse Electric Corp. (1971).
6. Era, A. et al., "Heat Transfer Data in the Liquid Deficient Region for Steam-Water Mixtures at 70 kg/cm² Flowing in Tubular and Annular Conduits", Italian Report CISE-R-184, (1966).
7. Lee, S.L. and Srinivasan, J., "An LDA Technique for In Situ Simultaneous Velocity and Size Measurement of Large Spherical Particles in a Two-Phase Suspension Flow", *Int. J. of Multiphase Flow*, 8, p. 47, (1982).
8. Lee, S.L., Rob, K. and Cho, S., "LDA Measurement of Mist Flow Across Grid Spacer Plate Important in Loss of Coolant Accident Reflood of Pressurized Water Reactor", in *Proc. Int. Symp. on Application of Laser-Doppler Anemometry to Fluid Mech.*, Lisbon (1982), p. 5.3.1.
9. Welty, J. R., *Engineering Heat Transfer*, John Wiley & Sons, New York (1978).

EXPERIMENTS ON HEAT TRANSFER CRISIS
IN TRIANGULAR LATTICE CONFIGURATION

V.I. Kisina, A.S. Konjlov,
D.L. Prozerov and N.V. Tarasova

All-Union Heat Engineering Institute (VTI)
Avtozavodskaja ulitsa 14/23, Moscow 109068, USSR

K.L. Eerikäinen, O.M. Tiihonen and T.A. Vanttola

Technical Research Centre of Finland (VTT)
P.O.B. 169, SF-00181 Helsinki 18, Finland

ABSTRACT

Heat transfer crisis experiments were performed in a test facility (1.5 MW) simulating the Soviet VVER-440 reactor core. Four triangular rod bundles with different heat flux distributions were studied, each of which consisted of 19 directly electrically heated rods. The experiments were conducted in full pressure (12.3 MPa) at small mass flow rates ($< 1100 \text{ kg/m}^2\text{s}$) and large steam qualities. Several different values of critical heat flux could be discovered in the stationary experiments, when critical steam quality and mass flow rate were kept constant. This is equal to the phenomenon that has earlier been reported for tubes, but in the bundles it took place in 15-20 % smaller steam qualities than in the tubes. A delay in the appearance of crisis was observed in flow decay transient tests.

INTRODUCTION

When critical heat flux has been measured as a function of steam quality in tubes, a zone has been found, where heat transfer crisis does not depend on heat flux [1-6]. An experimental programme was carried out on a thermal-hydraulic loop at VTI Moscow. In this test series it was possible to measure, if a similar phenomenon would appear in a nuclear reactor rod bundle. Other heat transfer and hydraulic parameters were also studied.

TEST PROGRAMME

The test section was constructed in a loop that included a pump, two control valves and a heater-cooler system. It simulated a Soviet VVER-440 pressurized water reactor core (Table I). The experimental rod bundle was heated directly by DC-current.

Mass flow rate and hydraulic characteristics of the rod bundle were measured by differential pressure transducers located along the bundle. Water inlet temperature and rod temperatures were obtained by thermocouples. Some of them were welded on the inside walls of the rod simulators, while the others were hanging freely in the rods.

Four rod bundles were studied during the test programme. Two of them had uniform heat flux distribution both axially and radially. The third bundle was axially uniform but radially strongly nonuniform. In this bundle four of the central rods had a heat flux twice as large as the others. The fourth bundle was radially uniform but axially cosinusoidal.

Most of the experiments were performed in stationary conditions. Some transient tests with decay of mass flow rate were also run. All experiments were performed at the operating pressure of the VVER-440 reactor. Parameter variations of the tests can be seen in Table II.

SUPPLEMENTARY CALCULATIONS

Local conditions in the bundle, such as steam quality, could not be measured directly in the experiments. Therefore they were calculated by the subchannel code COBRA-IV-I available at VTT. The bundle was divided into subchannels with boundaries drawn between centres of the adjacent rods. Heat loss from the bundle to the surrounding by-pass channel was also calculated. Local steam quality was obtained by the Miropolskii correlation [7].

Single-phase turbulent mixing between subchannels was evaluated based on beginning of boiling data of the radially nonuniform bundle. It appeared to be more intensive than predicted by some earlier models (e.g. Rowe [8]). This phenomenon is probably due to the spacer grids of the bundle. Two-phase turbulent mixing was calculated by the Beus model [9].

EXPERIMENTAL RESULTS

All the measured stationary critical heat fluxes have been plotted as a function of local steam quality in Fig. 1. The points have been grouped according to mass flow rate during crisis condition.

It can be seen immediately that the results of the radially nonuniform bundle differ remarkably from the other results. This is apparently due to failure of the subchannel model to predict local steam quality, when there are rods with different heat fluxes facing the same subchannel. In this case rod centered subchannel division would obviously be better, but it has not been tried so far.

TABLE I

Characteristics of the test sections

lattice type	triangular
number of rods	19
heated length	2300...2500 mm
rod diameter	9.1 mm
pitch to diameter ratio	1.34
number of spacer grids	11
spacer grid type	honeycomb
maximum power	1.5 MW

TABLE II

Operating conditions in critical heat flux tests

pressure	12.3 MPa
boiling temperature	326.3 °C
inlet subcooling	-0.39...-0.23
mass flow rate	460..1080 kg/m ² s
rate of change of the flow in transients	-20...-130 kg/m ² s ²

In the radially uniform bundles the measured heat fluxes are usually smaller than in the radially nonuniform bundle. The behaviour of crisis is also totally different. Critical heat flux comes down at a certain steam quality in the radially uniform bundles. The lowest heat flux values have been reached by the axially cosinusoidal bundle. The critical steam quality, where the drop takes place, decreases nearly linearly as function of increasing mass flow rate (Fig. 2). In the covered range of heat fluxes (390-1035 kW/m²) no departure or return to heat flux dependence can be found.

The calculated steam qualities of the radially uniform bundles are more reliable than those of the radially nonuniform bundle because of more symmetrical boundaries of the central subchannels.

In the transient experiments mass flow rate was decreased linearly with different rates of change. Transient crisis always appeared later than the corresponding stationary crisis. The delay was usually about one second in time. Deviation from the stationary crisis conditions can be found to enlarge as a function of transient speed (Fig. 3). The large scattering of the points is due to the fact that the experimental loop could not be controlled well enough in the transient tests. Often decreasing of flow rate had to be interrupted before appearance of crisis and therefore many of the points in Fig. 3 are probably somewhere between stationary state and actual transient.

DISCUSSION

Steam quality of the experiments is so large that at least all the crises of the radially uniform bundles are dryouts in the annular flow regime. Here the vertical part of the burnout curve Fig. 1 can be explained qualitatively according to Doroshchuk et al. [1-4] as follows. A thin, smooth micro-film of liquid has been formed on the heated surface just upstream of the dryout point. Steam generation in the film is so intensive that it prevents the droplets in the channel core to deposit on the film. However, heat flux is not large enough to enhance mechanical entrainment of the droplets from the film before the smooth part of annular flow, or to allow formation of steam film on the heated surface.

Nearly all the results concerning the limiting steam quality have been obtained by tube experiments, but KWU rod bundle data has been compared to the tube data with reasonably good agreement [10]. In our experiments the Soviet VVER-440 rod bundle has for the first time been tested in the corresponding circumstances. The behaviour is in principle similar to that of the tubes. However, in the bundles the limiting steam quality with the same pressure and equivalent hydraulic diameter is lower than in the tubes [5] (Fig. 2).

There are two possibilities for the difference between tube and rod bundle results. One is that geometric complexity of the rod bundle (spacers etc.) increases amount of entrained droplets thereby reducing critical steam quality at the point of dryout. The other is that local steam quality at dryout has been underestimated by the subchannel calculations. It is important to note that the calculated steam quality is very sensitive to mixing parameters even in the central subchannels, if the bundle is no larger than 19 rods.

There are a lot of relatively simple critical heat flux correlations that extend to the steam qualities of our tests. Most of them are based on tube experiments. In Fig. 4 there is a comparison of some of these correlations to our experimental points of the radially uniform bundles. Surprisingly, many of them perform fairly well even though they do not account for the drop of heat flux. Bowring correlation [11] gives partially conservative prediction. Bezrukov correlation [12] follows the lower limit of the points. This formula is based on experiments in a rod bundle that simulated VVER-conditions. The simple GE correlation [11] and Biasi correlation [13] are near the upper limit of the points where the drop of critical heat flux starts.

According to all the reference correlations, except Bezrukov, critical heat flux decreases as a function of mass flow rate. This behaviour is in agreement with our experiments.

Some observations can be made of the crisis points of the radially nonuniform bundle, even though absolute values of steam qualities are not correct. These crises do not seem to have any dependence on mass flow rate. An explanation is that the effect of mass flow rate on critical heat flux is changing sign in the tested steam qualities. In subcooled conditions the effect is positive while in large steam qualities it is negative.

Critical heat flux of the radially nonuniform bundle usually decreases nearly linearly as a function of steam quality. In two mass flow rate groups (800-900 and 900-1000 kg/m²s) there is, however, a critical heat flux value (~ 1050 kW/m²) below which crisis does not depend on heat flux.

Delay of dryout in flow decay transients can be explained only qualitatively so far. Annular flow starts at larger steam quality, if mass flow rate is increased. If we follow path of a flow element before it enters crisis, we observe that in flow decay transients there is less time from the beginning of annular flow to the crisis moment compared to that of the stationary case with the same mass flow rate at the crisis point. Therefore there is also less time for the entrained droplet flow to develop and consequently flow is dryer in the channel core in the beginning of the crisis.

CONCLUSIONS

Heat transfer crisis experiments have been conducted on four rod bundles simulating the Soviet VVER-440 reactor. The tests were performed in full pressure in large steam qualities and small mass flow rates compared to the normal operating conditions of the reactor. Inlet flow to the bundles was always subcooled.

A limiting steam quality could be observed, where local dryout conditions do not depend on heat flux. The limiting steam quality decreases nearly linearly, when mass flow rate is increased. The steam quality is about 15-20 % lower in the bundle geometry of the experiments than in an equivalent tube. All the measured critical steam qualities were, however, larger than 0.4.

The dependence of crisis on heat flux appears again when heat flux is larger than about 1050 kW/m² in an axially uniform bundle in our test conditions. Theoretically the limit should be smaller in axially sinusoidal bundles, but it was not observed in our experiments.

The later appearance of crisis in flow decay transients can be explained qualitatively as a delay in forming of annular flow pattern.

Calculation of local steam quality in radially nonuniform small bundles proved to be difficult. More experimental information would be needed in this field.

REFERENCES

1. V.E. DOROSHCHUK, L.L. LEVITAN, F.P. LANTSMAN, "Recommendations for Calculating Burnout in a Round Tube with Uniform Heat Release", Teploenergetika 2, (12) (1975).
2. V.E. DOROSHCHUK, R.I. NIGMATULIN, "An Investigation into Burnout in a Steam Generating Tube with a Cosinusoidal Law of Heat Release", Teploenergetika 25, (3) (1978).

3. V.E. DOROSHCHUK, "Origin of Burnout in Tubes of Subcooled Water and Wet Steam", Thermal Engineering 27, (8) (1980).
4. V.E. DOROSHCHUK, "Some Features of Burnout with Annular Flow of Steam-Water Mixture in a Tube", Thermal Engineering 28, (4) (1981).
5. L.L. LEVITAN, F.P. LANTSMAN, E.I. DEDNEVA, "Investigation of the Influence of Tube Diameter on Burnout of the Second Kind", Thermal Engineering 28, (7) (1981).
6. D.M. FRANCE, T. CHIANG, R.D. CARLSON, "Experimental Evidence Supporting Two-Mechanism Critical Heat Flux", Int. J. Heat. Mass Transfer, 25 (1982).
7. Z.L. MIROPOLSKII, et al, "Steam Content with Forced Flow of Steam-Water Mixture, with Supply of Heat and Adiabatic Conditions", Teploenergetika 18, 5 (1971).
8. D.S. ROWE, "A Thermal-Hydraulic Subchannel Analysis for Rod Bundle Nuclear Fuel Elements", The Fourth International Heat Transfer Conference, Paris-Versailles, (1970).
9. S.G. BEUS, "A Two-Phase Turbulent Mixing Model for Flow in Rod Bundles", WAPD-T-2438, (1972).
10. P. SUCHY, et al, "Application of Tables of Critical Heat Fluxes to Rod Bundles", Trans. Am. Nucl. Soc. Enc ' 79 Conference, (1979).
11. J.C.M. LEUNG, "Transient Critical Heat Flux and Blowdown Heat Transfer Studies", ANL/RAS/LWR 80-2, Ph.D. thesis, Northwestern University (1980).
12. Yu.A. BEZRUKOV et al, "Experimental Investigation and Statistical Analysis of Data on Burnout in Rod Bundles for Water-Moderated Water-Cooled Reactors", Teploenergetika 23, 2 (1976).
13. L. BIASI et al, "Studies on Burnout, Part 3, A New Correlation for Round Ducts and Uniform Heating and Its Comparison with World Data", Energia Nucleare 14 (1967).

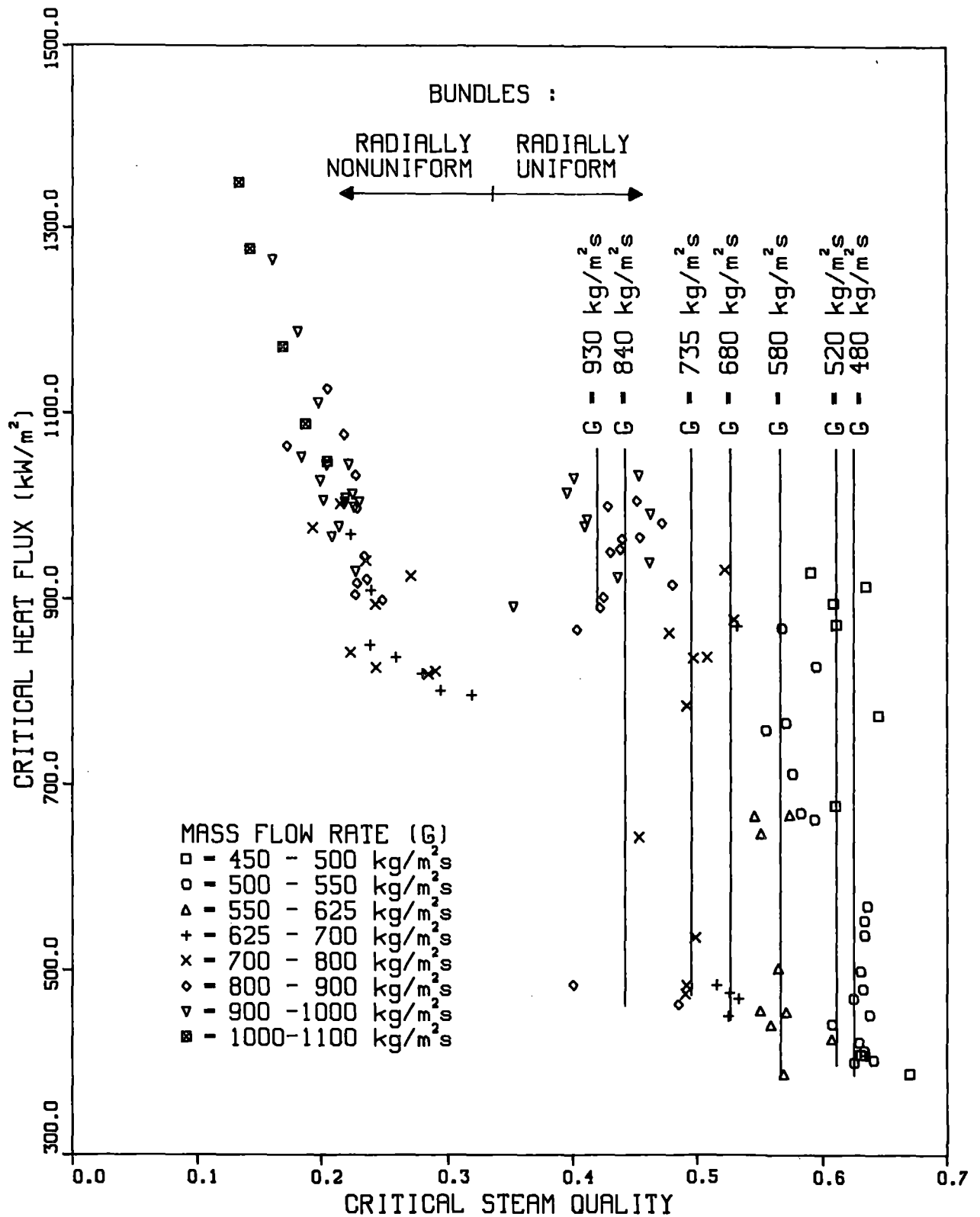


FIG. 1. CRITICAL HEAT FLUX POINTS IN VVER-440 TYPE ROD BUNDLES ($p=12.3 \text{ MPa}$). STEAM QUALITY IN THE RADIALLY NONUNIFORM BUNDLE IS UNDERESTIMATED.

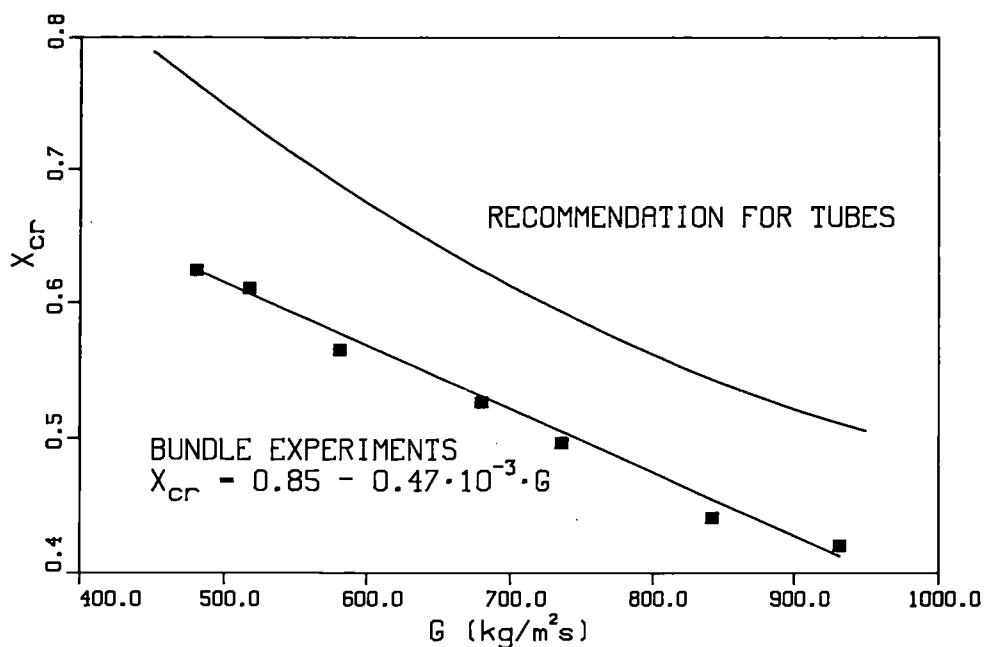


FIG. 2. CRITICAL STEAM QUALITY VERSUS MASS FLOW RATE IN THE RADIALLY UNIFORM BUNDLES WHEN DRYOUT DOES NOT DEPEND ON HEAT FLUX. IN COMPARISON THE CURVE FOR TUBES IN EQUIVALENT CIRCUMSTANCES ($D_e = 8.94 \text{ mm}$, $p = 12.3 \text{ MPa}$).

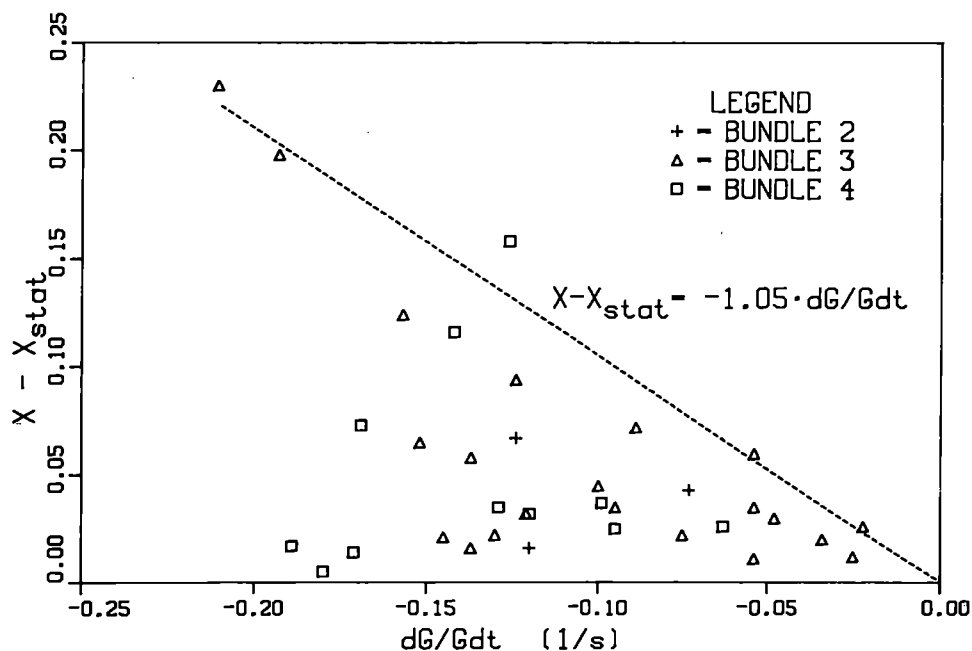


FIG. 3. INCREASE OF LOCAL STEAM QUALITY FROM THE STATIONARY VALUE AT THE MOMENT OF CRISIS VERSUS RELATIVE RATE OF CHANGE OF FLOW ($p = 12.3 \text{ MPa}$). BUNDLE 2 IS UNIFORM. BUNDLE 3 IS RADIALLY NONUNIFORM. BUNDLE 4 IS AXIALLY COSINUSOIDAL.

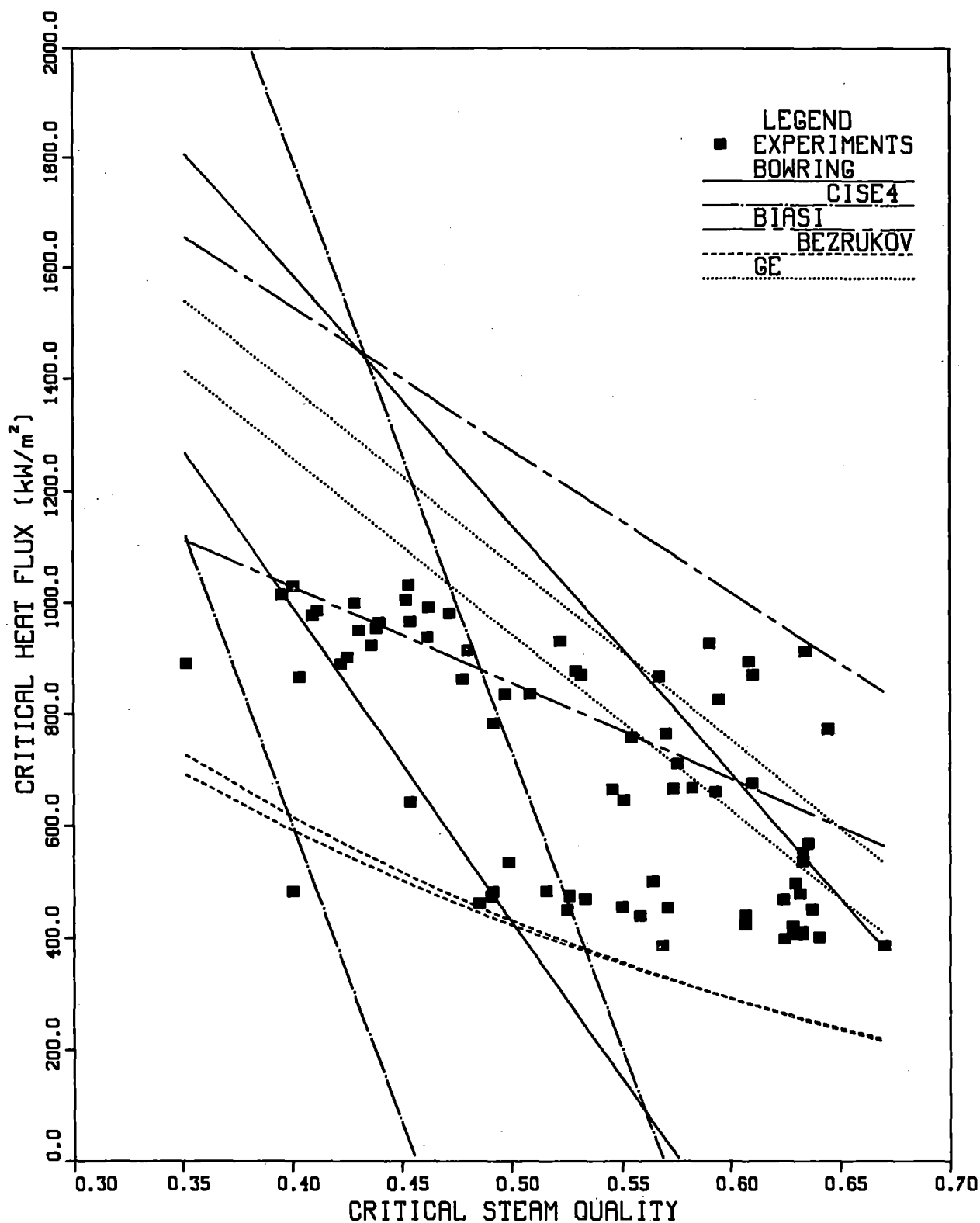


FIG. 4. CRISIS POINTS OF RADIALLY UNIFORM BUNDLES COMPARED TO SOME CORRELATIONS (12.3 MPa). THE UPPER LINE OF EACH CORRELATION IS OBTAINED BY MASS FLOW RATE $480 \text{ kg/m}^2\text{s}$ AND THE LOWER BY $930 \text{ kg/m}^2\text{s}$ (BEZRUKOV VICE VERSA ON THE LEFT).

BWR LOSS OF COOLANT INTEGRAL TESTS :
PARALLEL CHANNEL EFFECT

M. Murase, M. Naitoh
Energy Research Laboratory, Hitachi Ltd.
Hitachi, Ibaraki, Japan

and T. Gomyoo
The Tokyo Electric Power Company
Chiyodaku, Tokyo, Japan

ABSTRACT

Simulation tests of a BWR loss of coolant accident (LOCA) were conducted in the Two Bundle Loop (TBL), and the parallel channel effect was evaluated. The test results indicated that flow paths for falling water from the upper plenum and updraft steam from the lower plenum were separated in the two bundles after the termination of the lower plenum flashing. As a result, the peak cladding temperature (PCT) was lower in the higher power bundle with much updraft steam than for the lower power bundle with much falling water. The flow separation was induced by counter current flow limitation (CCFL) at bundle inlets and outlets. CCFL at the bundle inlet was sometimes broken by subcooled water or the decrease of the depressurization rate due to feed water flashing ; such a break made the PCT difference in the two bundles small. In small breaks, the parallel channel effect was not significant due to a low depressurization rate and, consequently, the thermal-hydraulic responses were similar in the two bundles.

INTRODUCTION

The present blowdown and emergency core cooling (BD/ECC) program was planned to obtain and evaluate BD/ECC data during a hypothetical loss of coolant accident (LOCA) in a BWR plant. The principal objective of this program was to evaluate the parallel channel effect with different bundle powers. For this purpose, the Two Bundle Loop (TBL) with two full-sized, electrically heated bundles was constructed, and simulation tests of the recirculation line breaks were performed. The test results indicated that the flow paths for falling water from the upper plenum and updraft steam from the lower plenum were separated in the two bundles after the termination of the lower plenum flashing, and that the flow separation affected rod surface temperatures (1, 2). Similar flow separation during a LOCA was observed in the Steam Sector Test Facility with full-sized, unheated bundles (3), and the Parallel Channel Effect Freon Loop with three small-scaled, heated bundles (4).

This report discusses the characteristics of the parallel channel effect, its effect on the peak cladding temperatures (PCT), and the influence of break size on the parallel channel effect.

EXPERIMENTAL

Test Apparatus

The TBL shown in Fig.1 is scaled to a BWR5/251 plant with 764 fuel bundles. The TBL consists of a main steam line, a feed water line, two recirculation lines, emergency core cooling systems (ECCSs), a pressure vessel and its internals. Main features include two full-sized, electrically heated bundles with maximum powers of 5 and 6 MW. The total power is limited to 10 MW due to the capacity of the power supply system. The bundle consists of 63 heated rods and one water rod. The heights of the internals are the same as the reference BWR from the bottom of the jet pumps to the upper plenum. The regional volumes, flow areas and flow rates are scaled on a 2 to 764 basis, following the bundle ratio of the TBL to the reference BWR. The blowdown lines are connected to the broken loop and the pipe break is simulated by the operation of quick open valves.

About 400 signals are recorded on a magnetic tape. The data acquisition system has the capacity of memorizing about 300,000 data points and a maximum data sampling rate of 2,500 points per second. The main measurements are flow rates and temperatures of every line, pressure, 256 rod surface temperatures, 18 differential pressures in the bundles, 20 differential pressures in the vessel, and 10 water levels in the lower plenum and annulus.

Test Conditions

The test parameters are break diameters, bundle power combinations and available ECC modes as listed in Table I. The 28 mm break diameter simulates a full-sized guillotine rupture of a recirculation line, that is a design basis accident (DBA). Initial bundle powers are significantly different, except in Run 119. Initial bundle powers of 4, 5 and 6 MW simulate the low power of the peripheral bundles and the average and high powers of the core center bundles, respectively. For the DBA simulation tests, a single failure of ECCSs is assumed. A BWR5 plant contains a high pressure core spray system (HPCS), a low pressure core spray system (LPCS) and three low pressure coolant injection systems (LPCIs); the ECCS pumps are driven by three diesel generators. For the single failure, a diesel generator is assumed unavailable. In small breaks, only the HPCS is operated.

The initial conditions before the break are the same as for the normal operating conditions of the reference BWR, except for water level in the pressure vessel. The tests are started from a scram water level and the bundle powers are controlled following the ANS+20% decay heat curve, which is modified after considering the differences in thermal properties between fuel rods and heater rods.

RESULTS AND DISCUSSION

Characteristics of Parallel Channel Effect

Fig.2 shows differential pressures and rod surface temperatures at the center, and differential pressures at the bottom of the bundles in Run 107. There was little difference in thermal-hydraulic characteristics between the two bundles during the blowdown period for about 30 seconds after the break. However, after the termination of the lower plenum flashing, the differential pressures in the lower power bundle-A were higher at the bottom, but lower in the center region, than for the higher power bundle-B. This was caused by the following. In bundle-A, the steam generation rate was small and coolant inflow based on counter current flow limitation (CCFL) at the upper tie plate was large. Much coolant remained in the bottom of bundle-A due to the updraft steam from the lower plenum (i.e., CCFL at the bundle inlet). On the other

hand, only a small amount of coolant was in the bottom of bundle-B and the amount of updraft steam became significant to equalize the total differential pressures throughout the bundles. The steam flow entrained the coolant in the bottom resulting in a higher heat transfer coefficient, and the rod heatup initiation was delayed in the higher power bundle-B. The CCFL at the bundle inlet was broken down at about 65 seconds due to subcooled water injected by ECCSs.

The difference of thermal-hydraulic responses in the two bundles are clearly shown in Fig.3. The figure plots the heatup initiation times and maximum rod surface temperatures at the center of each rod. In the lower power bundle-A with much falling water, heatup initiation of rods was early, but 30% of the rods never heated up. Only 10% of the rods reached a high temperature, 90% of the rods remained below the initial temperature of about 305°C. These facts indicate that water fell locally into the bundle. On the other hand, heatup initiation times were all within a short time period and rods heated up more uniformly in the higher power bundle-B.

The features of the parallel channel effect were the separation of flow paths for falling water and updraft steam, which could be detected by the difference in differential pressures at the bottom of the two bundles, and the difference in rod heatup initiation times between the two.

Parallel Channel Effect on Peak Cladding Temperatures

Fig.4 shows the pressure in the steam dome, rod surface temperatures at the center and differential pressures at the bottom of the bundles in Runs 108 and 139. The power of bundle-A in Run 108 was nearly identical with the power of bundle-B in Run 139 (Table I). The thermal-hydraulic responses in Runs 108 and 139 without HPCS were similar to the responses in Run 107 with HPCS (Fig.2). After the termination of the lower plenum flashing, at about 30 seconds, the differential pressures in the bottom region were higher in the lower power bundle than in the higher power bundle, and the heatup initiations of rods were earlier in the lower power bundles. In Run 139, the initial feed water temperature was 220°C and liquid in the feed water line began flashing at about 70 seconds. The feed water flashing (FWF) made the depressurization rate low, and CCFL at the bundle inlet was broken due to a lower steam generation rate in the lower plenum. After the initiation of LPCS and LPCI injection, CCFL at bundle inlets occurred again before the lower plenum was refilled with the ECC water at 195 seconds. On the other hand, the initial feed water temperature in Run 108 was low, 190°C, compared with the 215°C of the reference BWR, and CCFL at the bundle inlet was continued until the reflooding period was reached. The increasing rate of the rod surface temperature in the higher power bundle was larger in Run 139 than that in Run 108 due to the CCFL break at the bundle inlet, even though the bundle power was lower in Run 139.

Fig.5 shows peak cladding temperatures (PCTs) in each bundle without HPCS. In Runs 108 and 119, CCFL at the bundle inlets was continued until the reflooding period was reached, due to low feed water temperature, and the difference in PCTs between the two bundles was large. This shows that the flow paths for falling water and updraft steam were separated even with nearly identical powers in Run 119, and indicates that the parallel channel effect was only slightly affected by the bundle power difference. On the other hand, the difference of PCTs between the two bundles was small in Run 139 due to the CCFL break at the bundle inlet and, consequently, a weak parallel channel effect.

In Run 107, the difference in PCTs was also small as noted in Fig. 2 due to the CCFL break. Rod surface temperature responses after the CCFL break were similar between Runs 107 and 139.

Break Size Effects

A feature of the parallel channel effect in the two bundles was the separation of flow paths for falling water and updraft steam, which was well shown in the differences of differential pressure responses (i.e., fluid mass distributions) and

rod heatup initiation times. In the smaller breaks with HPCS, the vapor-liquid mixture level in the bundles was kept at a high level and the rods never heated up in some cases. Therefore, the parallel channel effect was evaluated only by the differential pressure responses for these breaks.

Fig.6 shows the pressure in the steam dome, rod surface temperatures at the center, and differential pressures in the center and bottom regions. In Run 134 with a 15 mm break diameter, the transient responses were slower than for the larger breaks, but the thermal-hydraulic phenomena were similar. After termination of the lower plenum flashing, at about 50 seconds, the differential pressure in the lower power bundle-A was higher in the bottom than for the higher power bundle-B. In bundle-A, the mixture level was below the center (i.e., zero differential pressure in the center) and some rods heated up at about 100 seconds. In bundle-B, the mixture level was higher than the center and rod surface temperatures were kept low. In Run 135 with a 10 mm break diameter, the depressurization rate was low and the mixture level was continuous from the lower plenum throughout the bundles. Therefore the thermal-hydraulic responses were similar in the two bundles.

CONCLUSIONS

Simulation tests of a LOCA were conducted using the Two Bundle Loop. Evaluation of test data led to the following conclusions :

1. A significant parallel channel effect was the separation of flow paths for falling water and updraft steam in the two bundles, which was induced by CCFL at bundle inlets and outlets. As a result, heatup initiation of rods was early and local in the bundle with much falling water and was delayed in the bundle with much updraft steam.
2. The peak cladding temperature (PCT) was higher in the early heatup bundle even with lower power than in the delayed heatup bundle when CCFL at the bundle inlet was continued until the reflooding period. The difference of the PCTs decreased due to the CCFL break at the bundle inlet, which was caused by subcooled water at the bundle inlet or the decrease of depressurization rate due to feed water flashing.
3. In smaller breaks, the parallel channel effect was not significant because of the low depressurization and low steam generation rates, and, consequently, the thermal-hydraulic responses were similar in the two bundles.

ACKNOWLEDGEMENT

This test program was jointly funded by Japanese BWR-user utilities, Hitachi Ltd. and Toshiba Corporation. The authors wish to express appreciation to members of this program for fruitful discussions.

REFERENCES

1. M.Naitoh, M.Murase and R.Tsutsumi, "Large Break Integral Test with TBL-1, Hitachi BWR Integral Facility," Paper presented at 9th Water Reactor Safety Research Information Meeting, Gaithersburg, Maryland (1981).
2. M.Murase, et. al., "Two-Bundle Loop for LWR Large-Break Integral Test," Trans. Am. Nucl. Soc., Vol.41, P.390 (1982).

3. J.A. Findlay, "BWR Refill/Reflood Test Results," Paper presented at 9th Water Reactor Safety Research Information Meeting, Gaithersburg, Maryland (1981).

4. R.T.Lahey, W.Conlon and M.Fakory, "Parallel Channel Effects During the Emergency Core Cooling of a BWR," Paper presented at 9th Water Reactor Safety Research Information Meeting, Gaithersburg, Maryland (1981).

Table I

Test Conditions

Run No.	Break Diameter(mm)	Initial Power (MW)		Available ECC Mode
		Bundle-A	Bundle-B	
107	28 ^a	4.0	5.9	HPCS+LPCS+LPCI
108	28 ^a	4.1	5.9	LPCS+3LPCI
119	28 ^a	4.9	4.9	LPCS+3LPCI
120	20	4.0	5.7	HPCS
134	15	4.0	5.6	HPCS
135	10	4.0	5.8	HPCS
139	28 ^a	5.0	3.9	LPCS+3LPCI

^a 28mm simulates a full-sized guillotine rupture of a recirculation line.

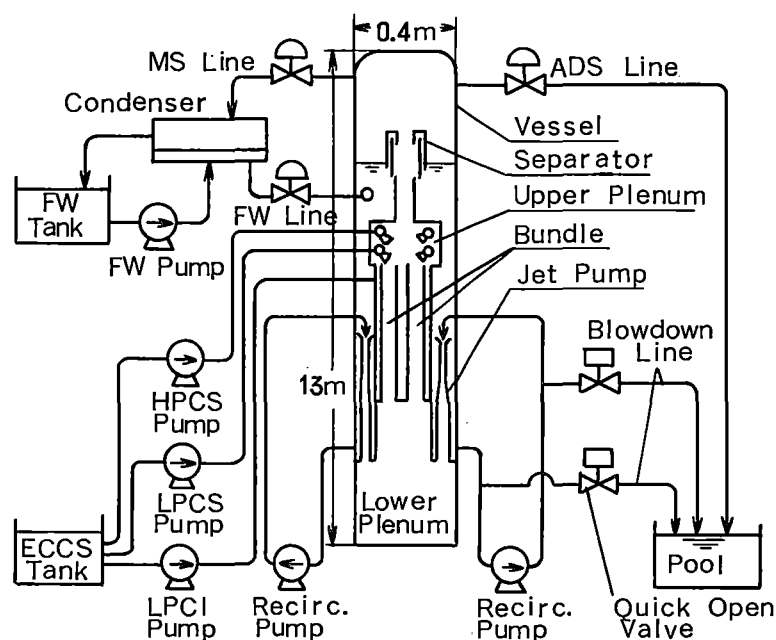


Fig.1 Schematic diagram of the TBL facility

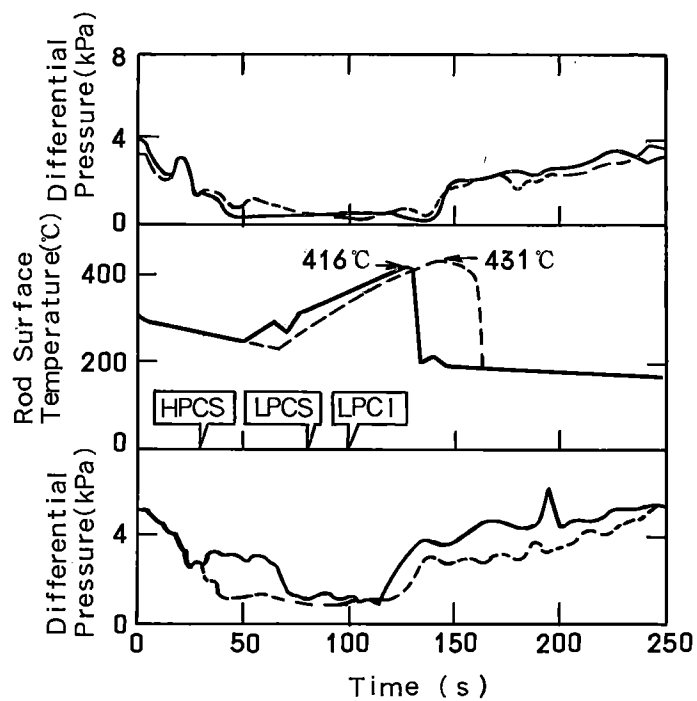


Fig.2 Differential pressures and rod surface temperatures at the center, and differential pressures at the bottom (Run 107 ; Bundle-A, — ; Bundle-B, ----)

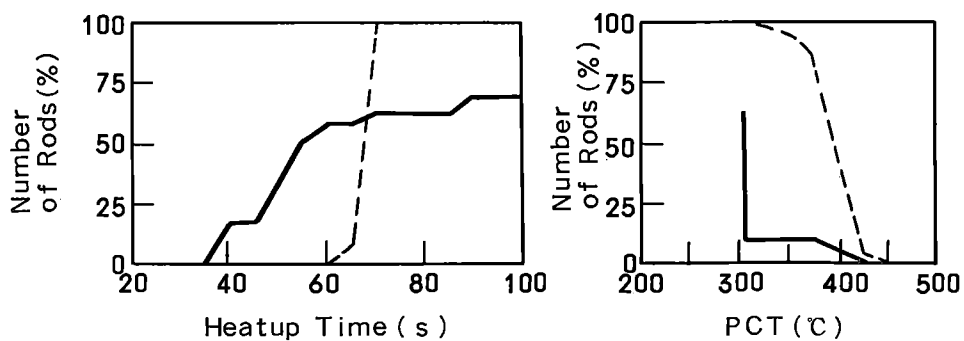


Fig.3 Heatup initiation times and peak cladding temperatures at the center of each rod (Run 107 ; Bundle-A, — ; Bundle-B, ----)

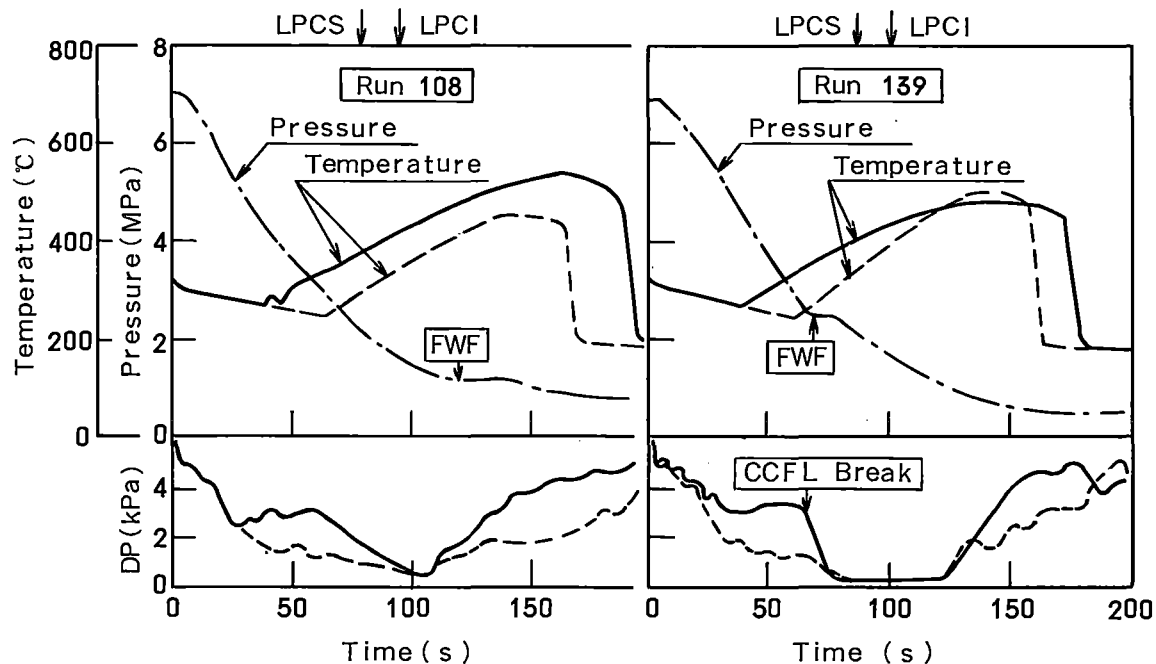


Fig.4 Vessel pressure, rod surface temperatures at the center and differential pressures at the bottom (Runs 108 and 139 ; Bundle-A, —; Bundle-B, ----)

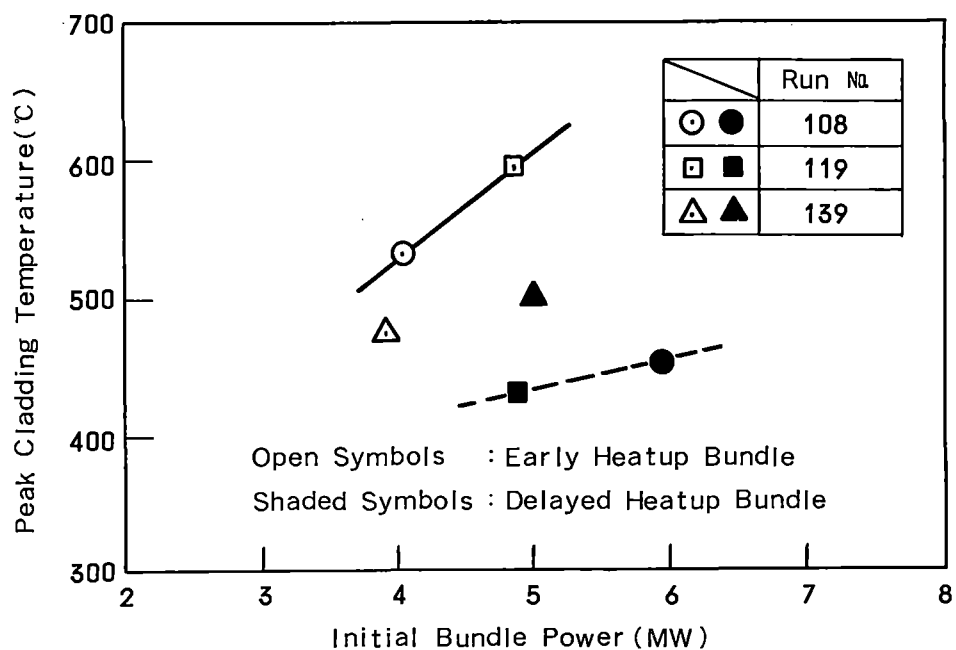


Fig.5 Peak cladding temperatures in each bundle without HPCS operation

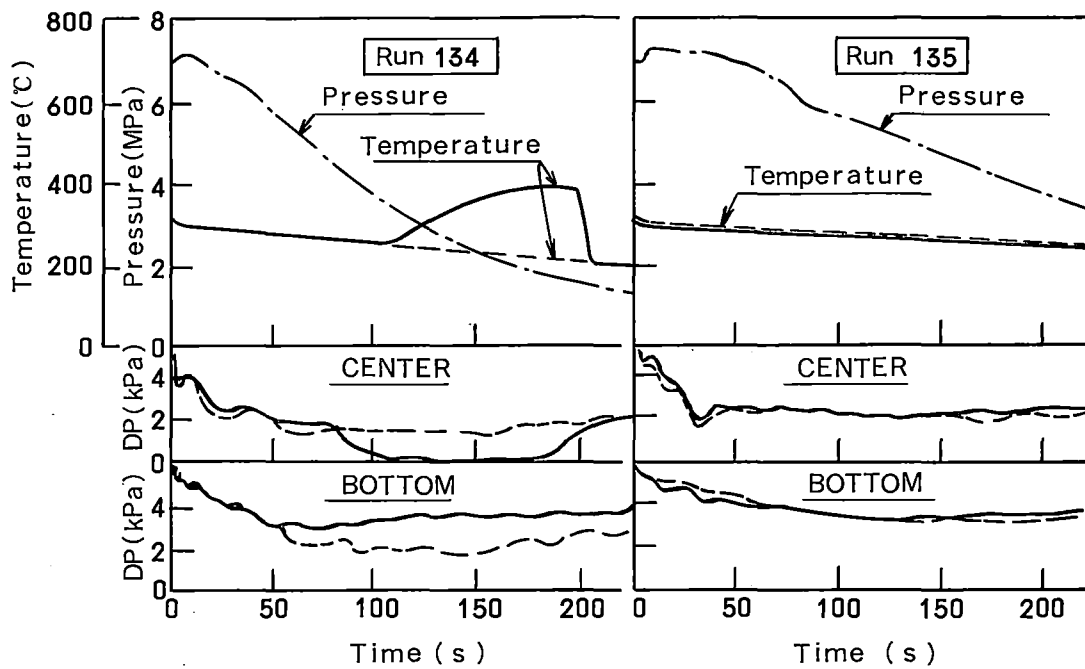


Fig.6 Vessel pressure, rod surface temperatures in the center, and differential pressures in the center and bottom (Runs 134 and 135 ; Bundle-A — ; Bundle-B, - - - -)

SESSION 28

DEGRADED CORE ANALYSIS - 4

Chair: M. Fontana (*TEC*)
H. Unger (*USt*)

Panel Discussion on
DEGRADED CORE ANALYSIS

Chair: M. Fontana (*TEC*)

Panelists

H. K. Fauske (*FAI*)
W. Hancox (*AECL*)
P. Jones (*JRC*)
R. Mattson (*NRC*)
D. Okrent (*UCLA*)
H. Teague (*UKAEA*)
H. Unger (*USt*)

SASYST - A NEW APPROACH IN TOTAL PLANT SIMULATION
DURING SEVERE CORE DAMAGE ACCIDENTS

R. Rühle, R. Bisanz, W. Scheuermann, F. Schmidt and H. Unger

University of Stuttgart
Institut für Kernenergetik und Energiesysteme,
Pfaffenwaldring 31, 7000 Stuttgart 80
Federal Republic of Germany

ABSTRACT

The complex modeling of reactor safety problems requires new and non-conventional computer techniques. The IKE-Safety Analysis-System (SASYST) utilizes such techniques. SASYST is based on the RSYST software system and features well introduced computer codes like SSYST, EXMEL, KESS, MELSIM, RELAP, TRAC, SAP, ADINA to analyze safety problems of various degrees of complexity. Code application, representation of the results and statistical analysis can also be performed easily using the RSYST concept.

A broad variety of reactor safety related problems can be treated in a less conservative way using the advanced techniques of SASYST. Thus the many new features of the system qualify it to become a flexible tool in nuclear safety analysis. To demonstrate some of these capabilities of SASYST, the MELSIM and LUECKE modules were applied to simulate a high pressure core melt accident.

INTRODUCTION

Since the TMI incident it is apparent that one has to be prepared to analyze such types of accidents and one also knows that the past core melt programs were much too pessimistic in predicting core behavior under conditions similar to those which occurred at TMI. However, a thoughtful analysis reveals that there is no single effect which could remove all the conservativities. Instead, we have to take into account a broad variety of improvements which have to be taken from physics, chemistry, thermohydraulics, structural mechanics, or material sciences. Also, the interaction of these effects may be different under different conditions. Therefore, if we want to analyze LWR core melt accidents, complicated systems have to be used which require new and non-conventional computer techniques. This is especially true if our ultimate goal is to give reactor engineers and operators actual support in managing and terminating reactor meltdown accidents.

THE IKE SAFETY ANALYSIS SYSTEM SASYST

Based on these considerations, the Institut für Kernenergetik und Energiesysteme e.V. (IKE e.V.) started the development of a general Safety Analysis System (SASYST). The present status of the system is shown in Fig. 1. The system can be used to analyze single rod and bundle experiments as well as reactor meltdown accidents. Various degrees of accuracy might be achieved by using different modules. Well introduced systems like TRAC, ADINA, SAP, RELAP, SSYST, MELSIM, or KESS are paths of SASYST.

RSYST manages the data transfer and provides capabilities to exchange data between subsystems, to compare different results and to display the behavior of arbitrary parameters. Several special features of the system qualify it to manage local and international data exchange and interpretation and possibly to become a tool which can be used on site to analyze reactor conditions during long term accident sequences with time ranges between ten minutes and several hours. The most important ones are

- a) the system runs on small machines
- b) the system allows user interactions
- c) the system allows interruptions for detailed analysis of special conditions
- d) the system is able to incorporate detailed results from fast and large background computers
- e) the system provides well defined data interfaces and numerous auxiliary routines for data management and interpretation.

SOFTWARE COMPONENTS OF SASYST

The software components of SASYST are the general purpose software tools of RSYST /1/.

In RSYST all calculations are done using a sequence of user called functional modules (Fig. 2). The module data interfaces are managed by the RSYST system. All data are accessed by abstract data type modules /2/. The information hiding principle first introduced by Parnas /3/ is used extensively. By these techniques the engineer can formulate his algorithms free of data management problems. Additionally changes in data structures do not influence the programming of application modules.

Besides the application module programmer level and the software system programmer level at least two more user access levels of RSYST are available (Fig. 3). These are the application system engineer level and the calculation engineer level. The system engineer formulates complex module sequences to describe his complex physical models. For this the RSYST language allows free combination of modules and data in any order. The new module sequences are stored in the data base. The calculation engineer performs parameter studies and evaluates results using modules and predefined module sequences.

Fig. 4 shows the main components of the software system RSYST. The data base stores all data like input data, material libraries, results, texts for module or project descriptions and module sequences. The entire module input and output is handled versus the data base. The user may use the data base to evaluate data, write reports, for interactive graphics, or to do statistical analysis (Fig. 5).

The dialog system controls all dialog or batch input. It also allows to get input from the data base. In dialog mode it establishes a link to the information system. This allows the user to get module information (documentation, help), data base and system status information at any dialog point. Besides this, the information system informs about the possibilities of SASYST and writes documentation reports of the modules.

The monitor allows to execute module sequences formulated in RSYST language. In SASYST time integration is done in a very flexible way using this monitor. Besides the specific nuclear safety modules of SASYST, there are general purpose modules for data base manipulation and transformation of data. Graphic display and statistical analysis are also available.

All those components may be used from one module. On the other hand, for large programs, which originally were not written as RSYST modules (e.g. RELAP) only those components needed to do a specific task may be used independently. Most commonly the access to the data base is used in order to get input data or to store results for further processing.

RSYST software may be used from single stand alone modules. It is also possible to generate automatically module systems which enclose a class of modules to solve a given physical problem. SSYST-EXMEL for fuel rod analysis and KESS for whole core analysis under severe core damage conditions are examples for this kind of modular systems, both use RSYST-I software technology. In contrary to this SASYST is not intended to be a defined system containing a fixed number of modules. Instead SASYST is a growing collection of programmes, modules and systems which should all have a more or less consistent data interface. All these data are managed using the RSYST data base. SASYST serves as a flexible tool, that allows flexible combinations of modules and programs to solve new problems in nuclear safety analysis. If a certain problem is fixed new systems may be build easily - by linking together all modules necessary to cover the problem.

A typical sequence of modules within SASYST which represents a coupling of thermal hydraulics, fuel element or core behavior, and structural mechanics analysis is shown in Fig. 6. Thermal hydraulic codes, like RELAP5, TRAC or other simpler codes are used in order to predict the heat transfer coefficient and the fluid temperatures along the fuel rod in axial direction, within a predefined time intervall. The core or fuel rod behavior codes (at present SSYST, EXMEL or MELSIM) calculate temperature distributions in fuel rods and structures. The following structural mechanics calculations result in displacements and stresses which might be feed back into the codes mentioned above, but also in containment analysis codes. The sequence of modules can be restarted for any number of time intervals.

The basic RSYST software is running on CDC, IBM, VAX and PDP 11/40 computer systems. In 1983 IKE will have access to a CRAY1 with an IBM 3083 and a CYBER-174 station at the computer center of the University of Stuttgart. IKE owns a VAX 11/780 as a front end and graphics device. RSYST will be installed at all these computers (Fig. 7) and handle the data tranfers using its data base. In this configuration each module or programme may run in the computer surrounding which is best suited to it. Therefore SASYST may be distributed around the local Stuttgart network. At present this is realized on our actual computer system. Thus we run RELAP on a CDC. The results are written to the RSYST data base and transfered to our VAX computer. There the data are used as boundary conditions in SSYST or KESS runs. The VAX results may be feed back or combined with the CDC results for graphical interpretation.

PAST, PRESENT, AND FUTURE APPLICATIONS OF SASYST SYSTEM

SASYST is application oriented. The development of SASYST was initiated by an increasing number of safety related problems which had to be solved by similar methods. Thus the development of SASYST was not sponsored by a specific organisation. Instead contributions (experiences or money) to the development of SASYST were made during various projects.

One of the first applications of SASYST was in the frame of the analysis of the TMI incident. This analysis will be described in more detail in the following paper /4/.

The number of problems which we have solved successfully with SASYST techniques is growing continously. At the same time the degree of complexity of the problems solved is increasng considerably. To give an idea of the flexibility of the SASYST concept we list the most important past and present applications.

Past applications of SASYST

- Analysis of blow down experiments of PNS
(development of SSYST)
- Analysis of melting experiments of PNS
(development of EXMEL)
- Investigation of low pressure melt down accidents
(development of MELSIM, LUECKE, and KESS)
- Analysis of the TMI incident
(development of high pressure version of MELSIM)
- Determination of initial condition for steam explosions
(see paper 243 of this conference)
- Test train design for SUPER SARA experiemnts
- Statistical analysis of various thermalhydraulics codes
(DRUFAN, RELAP, COBRA)
(development of data exchange techniques between
IKE and installations which run the codes)

Present applications of SASYST

- Design of severe fuel damage experiments
- Interpretation of severe fuel damage experiments
- Transformation of experimental results into reactor codes
- Core melt and thermalhydraulics calculations for the
German Risk Study Phase B
- Determination of recoolable reactor states during severe
damage accidents
- Investigation of small leak problems
- Improvement of high pressure melting capabilities
- Investigation of the influence of core heat up on structural
analysis problems.

The techniques and the capabilities of SASYST are open ended. Thus SASYST is a tool which is easy adaptable to solve future questions. Some of the future applications of SASYST may be the following.

- Analysis and interpretation of new inpile and out-of-pile
severe fuel damage experiments
- Comparison of results from different severe fuel damage
experiments performed at various installations
- Improvement of experiments of minor value
- Simulation of operator actions during core heat up incidents

- Investigation of the behavior of the reactor pressure vessel under thermal shock conditions
- Analysis of containment structures
- Model development for debris bed formation and coolability investigations
- Sensitivity analysis of core melt and related calculations.

Of course this list has to be concretized in the future.

The SASYST development depends on codes and data from all institutions involved in reactor safety and plant analysis. Therefore we are very much interested in a close cooperation with as many installations as possible. We believe that tools and ideas incorporated in SASYST will help to facilitate this cooperation.

REFERENCES

1. R. RÜHLE, "RSYST I - III - Experience and Further Development", Atomkernenergie (ATKE), Bd. 26 (1975)
2. E. DENERT, "Software-Modularisierung", Informatik Spektrum 2-4, Oktober 1979, s. 204
3. D.L. PARNAS, "On the Criteria to be Used in Decomposing System into Modules", CACM 15, 12 (72), 1053-1058
4. R. BISANZ and F. SCHMIDT, "Analysis of the TMI Incident Using EXMEL and MELSIM-2" Int. Meet. on Thermal Reactor Safety, Paper 246, Chicago 1982

FIGURES

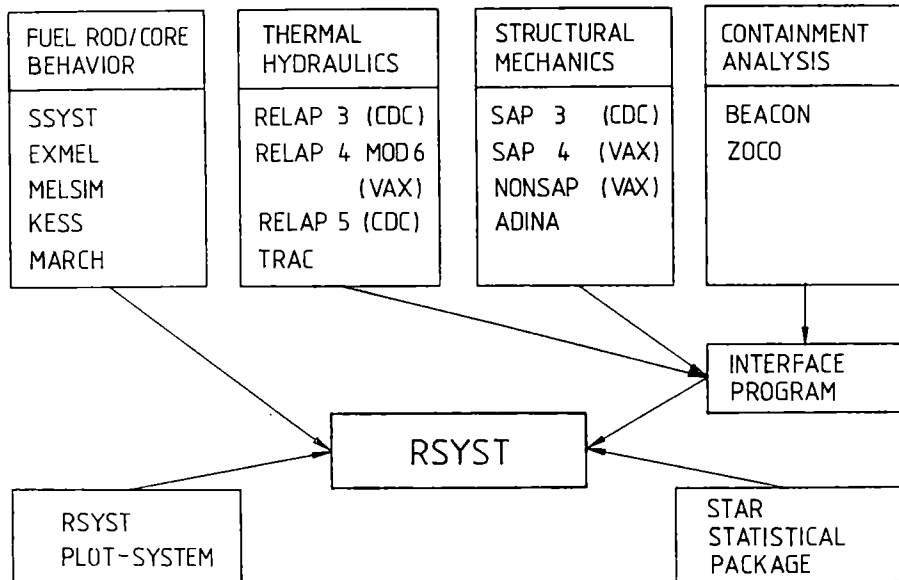


Fig. 1: The IKE-Safety Analysis System (SASYST)

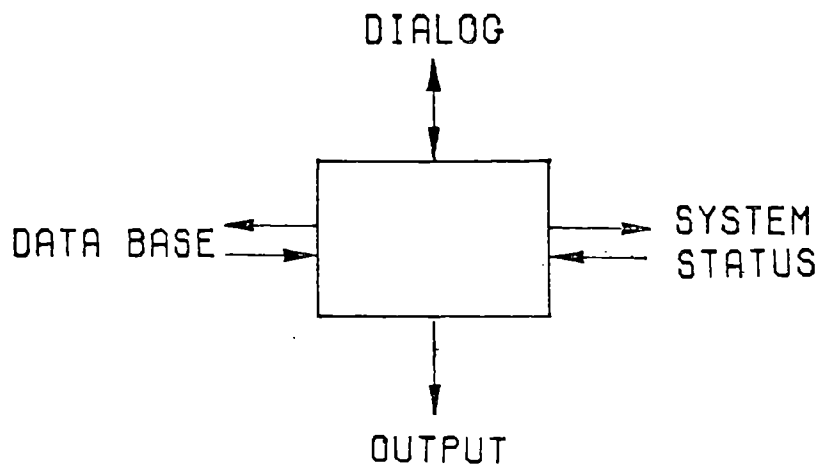


Fig. 2: Module Interfaces in RSYST

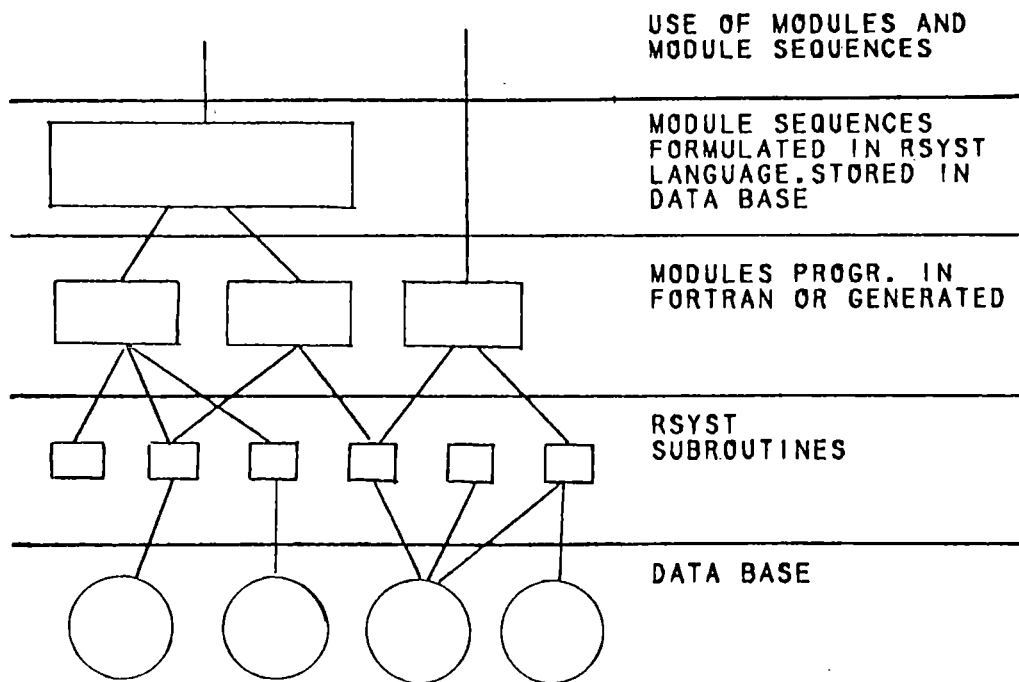


Fig. 3: Levels of Problem Formulation in RSYST

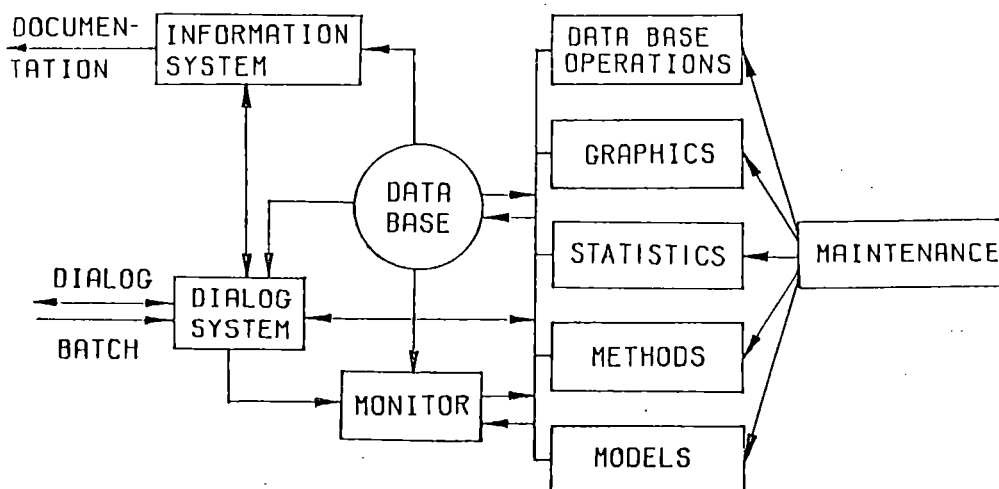


Fig. 4: Components of the RSYST Software System

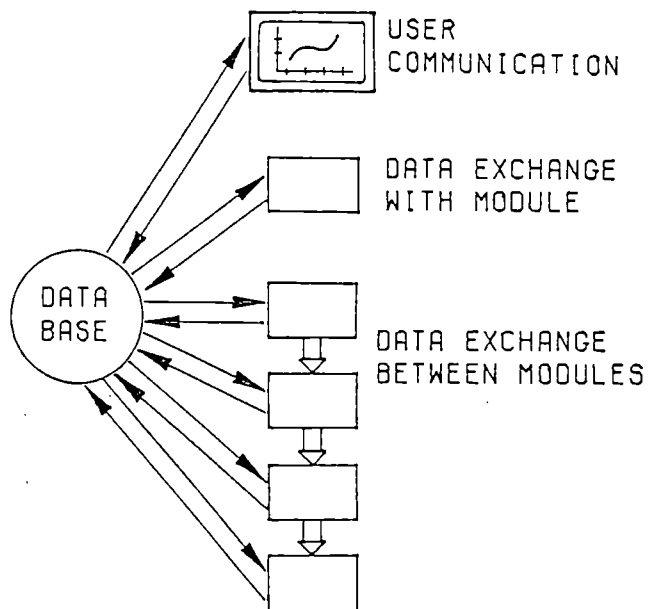


Fig. 5: Use of RSYST Data Base

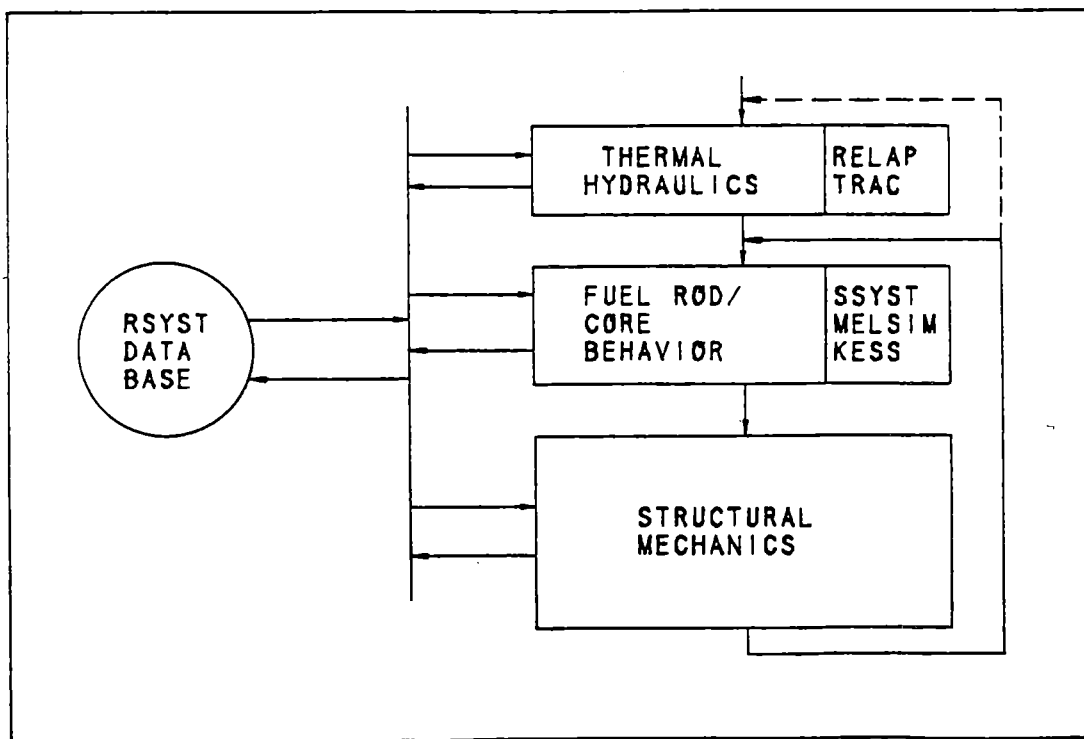


Fig. 6: Example of Problem Oriented Module Sequence in SASYST

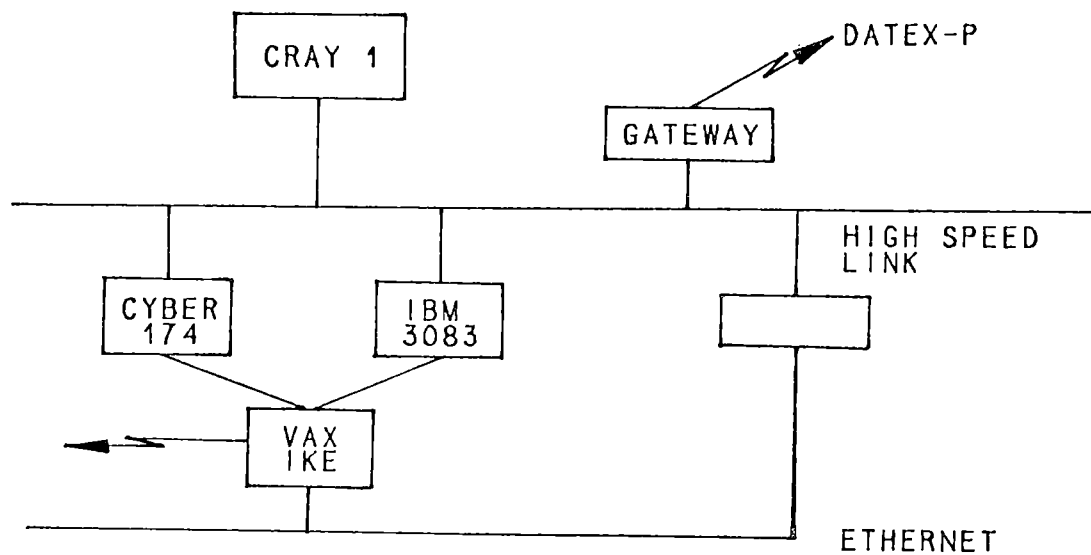


Fig. 7: Local Computer Network of the University of Stuttgart (Status 1983)

ANALYSIS OF THE TMI INCIDENT USING EXMEL AND MELSIM3⁺

R. Bisanz, and F. Schmidt

University of Stuttgart
Institut für Kernenergetik und Energiesysteme,
Pfaffenwaldring 31, 7000 Stuttgart 80,
Federal Republic of Germany

ABSTRACT

Calculations for the dry out phase of the TMI-2 incident (114 min to 174 min) were performed with the program systems SSYST-EXMEL and MELSIM3 which are both included into the safety system SASYST. Both EXMEL and MELSIM3 predict liquified fuel in the reactor center. However the reactor geometry is still coolable at the end of the calculations, which was caused by the reflooding of the core. From the temperature distribution at that time we conclude that during the reflooding approximately 90 % of the fuel rods were destroyed due to embrittlement. The embrittlement took place in the upper axial sections with a lower boundary of approximately 1.5 m beyond the top of the fuel elements. A film was made to investigate the transient development of the computer results. The film also gives support in understanding the calculational results and comparing different code systems.

INTRODUCTION

Estimates of the core damage of the TMI-2 reactor vary quite considerably /1/. Predictions of the core status are connected with large uncertainties. However in comparing different calculated results one might get some insight into the computer codes used to do the calculations and into the physical reasoning of various groups working in the severe core damage area.

It were reasons like these which lead us to try an analysis of the destruction of the TMI core with programs developed in the frame of the German core melt research project. Two systems are especially suited to analyse the core damage.

The first code system is the EXMEL system /2/. EXMEL was primarily developed to analyse the slumping experiments done at Karlsruhe (Hagen's experiments /3/). Due to the modular design it was easy to extend the system to model fuel rods under reactor conditions. Also TMI conditions and selected TMI fuel bundles could be simulated. Thus it was possible to transfer experimental insight to reactor situations.

The second code system is the MELSIM system /4/. MELSIM was primarily developed to analyse large break accidents. An early version of the code is included into the KESS system /5/. There MELSIM is considered to belong to the best estimate part of KESS. However the KESS version of MELSIM only allows the treatment of low pressure melting. Therefore improvements had to be installed to enable MELSIM to treat partially molten cores under high pressure.

⁺Work performed under BMI grant SR 0253

Both code systems seem to give reasonably agreeing results for the analysis. The results fit well within the frame of the uncertainties mentioned before. Both tend to support the optimistic view of the incident.

To judge our findings we shall first give a quick review of the boundary and initial conditions used for the analysis. Our time dependent results are visualized in a film. Therefore only a few graphs are included into this paper. A more detailed description is given in /6/. To support our conclusions we have repeated the MELSIM calculations with the assumption that coolant pump 2B would not be restarted at 174 min. Thus no reflooding occurs, the core melting progresses, and finally (approximately 25 minutes after the beginning of melting) the core breaks down.

THE TMI-2 INCIDENT: BOUNDARY AND INITIAL CONDITIONS FOR THE CALCULATIONS

The core damage simulation was started with conditions which corresponded to the reactor status at 114 minutes after the beginning of the incident. Initial conditions were calculated using SSYST /7/. The following assumptions were made

- the water level had reached the upper core (3.66 m)
- the pressure was 52 bar initially
- the water in the core was saturated
- the cold pressure in the fuel was 33 bar
- the initial oxide layer thickness was 3×10^{-5} m
- the power distribution was taken from NRC literature /8/.

Of special interest are the time dependent boundary conditions. The boundary conditions have a strong influence on the temperature history. However - due to the lack of experimental data - it also is very difficult to determine reliable values. Fortunately we were able to rely on work done at EPRI. Water level, pressure history and after heat were taken from Ref. /9/. These data were fed into the program systems and transferred into data like vapour temperature, mass of vapour available for the $\text{Zr-H}_2\text{O}$ reaction, or heat transfer coefficients.

The calculations were terminated at the 174 minutes mark. At this time coolant pump 2B was restarted, the pressure increased to 151,7 bar, and the core was cooled down quite rapidly.

IMPROVEMENTS OF MELSIM FOR THE HANDLING OF SEVERE CORE DAMAGE ACCIDENTS

The original version of the MELSIM code, which is included into the official version of the KESS system, allows only the treatment of large break loss of coolant accidents. To handle high pressure core melt accidents several changes had to be made. Due to the modular structure of the code systems these changes could be performed quite easily. The main improvements which characterize the version 3 of MELSIM /10/ are the followings

- coupling with thermohydraulic results of different codes
- possibilities to feed in subcooled water
- improvement of the model for heat transfer from fuel rods to coolant
- inclusion of ballooning
- inclusion of heat transfer between fuel and clad
- remodeling of the melting process due to the experiences in EXMEL
- options to calculate single rods or bundles.

This new version of the MELSIM code is part of the SASYST system which was described in the preceding paper.

MAIN RESULTS OF THE ANALYSIS OF THE TMI INCIDENT

The core damage calculations were done with EXMEL and MELSIM. Additionally results of the TMI-BOIL /11/ code were available. A comparison of temperature histories at the hottest points in the rod with the highest power is given in Fig. 1. We note the following

- Both EXMEL and MELSIM predict temperature histories which are in reasonably good agreement.
- The new version of MELSIM is able to treat
 - a) single rods
 - b) bundles
 - c) partial melting
 - c) high pressure melting.
- Fuel liquification is predicted almost at the same time point.
- No temperature rises occur during the liquification phase.
- The liquification process terminates the Zr-H₂O reaction thus reducing the heat sources at the melting parts quite considerably.

The temperature field at the end of the MELSIM calculation is shown in Fig. 2. Here we can see

- Slumping ($T > 2500$ K) did not occur which means that the core remained coolable.
- Eutectic melting ($2000 \text{ K} < T < 2200 \text{ K}$) started in the upper third of the core.
- Strong oxidation ($T > 1500 \text{ K}$) occurred in the upper part of the core only. Oxidation rates up to 100 % were found in the hottest parts.

If we assume that all the material which was strongly oxidized was embrittled during the reflooding process we may conclude

- Approximately 90 % of the fuel rods were destroyed during reflooding
- The embrittlement affected only parts of the fuel rods in axial positions above 2 m
- The embrittled material should not show significant portions of molten UO₂.

RESULTS OF SUPPORTING CALCULATIONS

To see what would have happened if coolant pump 2B would not have been restarted we postulated a second case of thermohydraulic boundary conditions. It might be characterized by the swell level of the water in core which is compared in Fig. 3 with the water level of the simulation calculation. The new curve was calculated by the module KOCH of KESS under the assumption that any water supply was stopped 145 minutes after trip. Typical results for this hypothetical case are shown in Fig. 4 which gives the axial temperature distribution of the innermost MELSIM zone as a function of time. We now note the following

- Eutectic melting starts about at the 160 min mark (which is much the same as in the simulation calculation).
- Melting of UO₂ and overheating starts 7 minutes after the beginning of melting. This was faster than in the TMI simulation.
- Slumping and material movements can be noted 10 minutes after the beginning of melting.

- About 35 minutes after the beginning of the melting we note that molten material has reached the support structure which fails approximately 5 minutes later.

Of course these time intervals depend on the actual form of the thermohydraulic boundary conditions. Thus they can only give us an estimate how much time was available at TMI. However they support our general finding that in any high pressure incident sequence we have investigated up to now the core remains coolable as long as 50 % of the power can be used to vaporize saturated cooling water.

REFERENCES

1. D.W. CROUCHER, "Status of the TMI-2 Core: A Review of Damage Assessments" ANS Topical Meeting, Sun Valley (1981)
2. W. TÜRK, F. SCHMIDT, H. UNGER, "Abschlußbericht zum Forschungsvorhaben BMFT - RS 205" (Sept. 1979)
3. S. HAGEN, H. MALAUSCHEK, "Bundle Experiments on the Meltdown Behavior of PWR Fuel Rods", Trans. Am. Nucl. Soc. 33 505 (1979)
4. R. BISANZ, W. SCHEUERMANN, W. GULDEN and H. UNGER, "Abschlußbericht zum Forschungsvorhaben MBFT - RS 316", Teil 1 (März 1980)
5. K. HASSMANN, R. BISANZ, W. GULDEN, W. SCHEUERMANN, "Das Kernschmelzsystem KESS" Tagungsbericht der Jahrestagung Kerntechnik, Düsseldorf (1981)
6. W. TÜRK, F. SCHMIDT, R. BISANZ, "Theoretische Untersuchungen zum Verhalten der Brennstäbe während des Störfalles im TMI-2 Reaktor und rechnerische Übertragung auf einen deutschen Druckwasserreaktor vom Typ Biblis" Abschlußbericht zum BMFT Vorhaben SR 0253 IKE 4-102 (Mai 1981)
7. W. GULDEN et al., "SSYST1 - Ein Programmsystem zur Berechnung des LWR Brennstabverhaltens bei Kühlmittelverluststörfällen" KFK-2496 and IKE 2-32 (1977)
8. M. L. PICKLESIMER, "Bounding Estimates of Damage to Zircaloy Fuel Cladding in the TMI-2 Core at Three Hours after the Start of the Accident" Memorandum for File (June 1979)
9. K. H. ARDON, "Modeling of the Liquid Level During Uncovering of the TMI-2 Core" ANS/ENS Top. Meet. on Therm. Reactor Safety, Knoxville 1980, and private communications (see also EPRI estimates in /1/)
10. R. BISANZ, "Dissertation in preparation"
11. G. P. MARINO, J. M. MARKS, "Calculation of Fuel Rod Temperatures Reached in the TMI-2 Incident", NRC (Oct. 1979), and private communications.

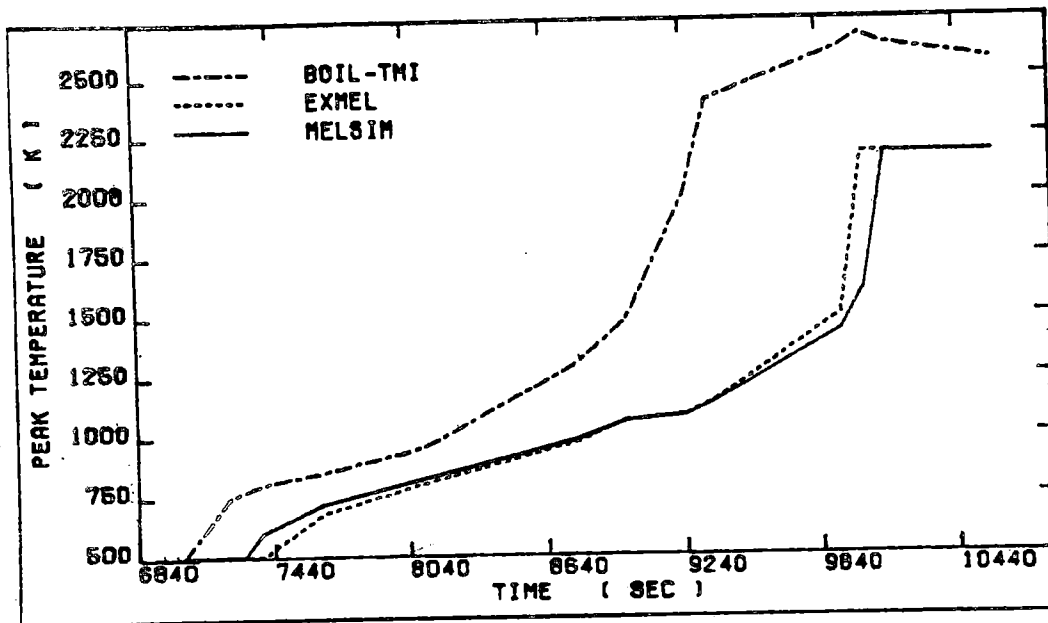


Fig. 1: Comparison of fuel element peak temperatures as calculated by BOIL-TMI, EXMEL and MELSIM (note BOIL-TMI predicts the peak temperature at a slightly higher position of the fuel bundle)

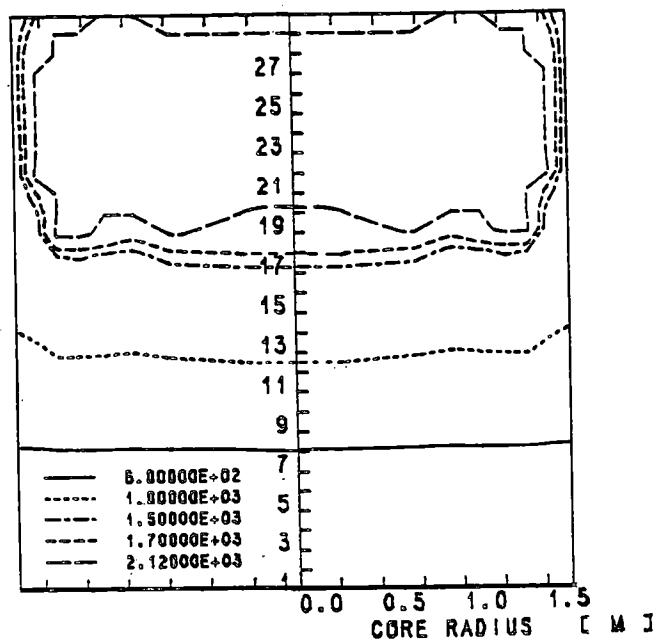


Fig. 2: Temperature distribution in the TMI-2 core at the end (190 min) of reflooding as predicted by MELSIM

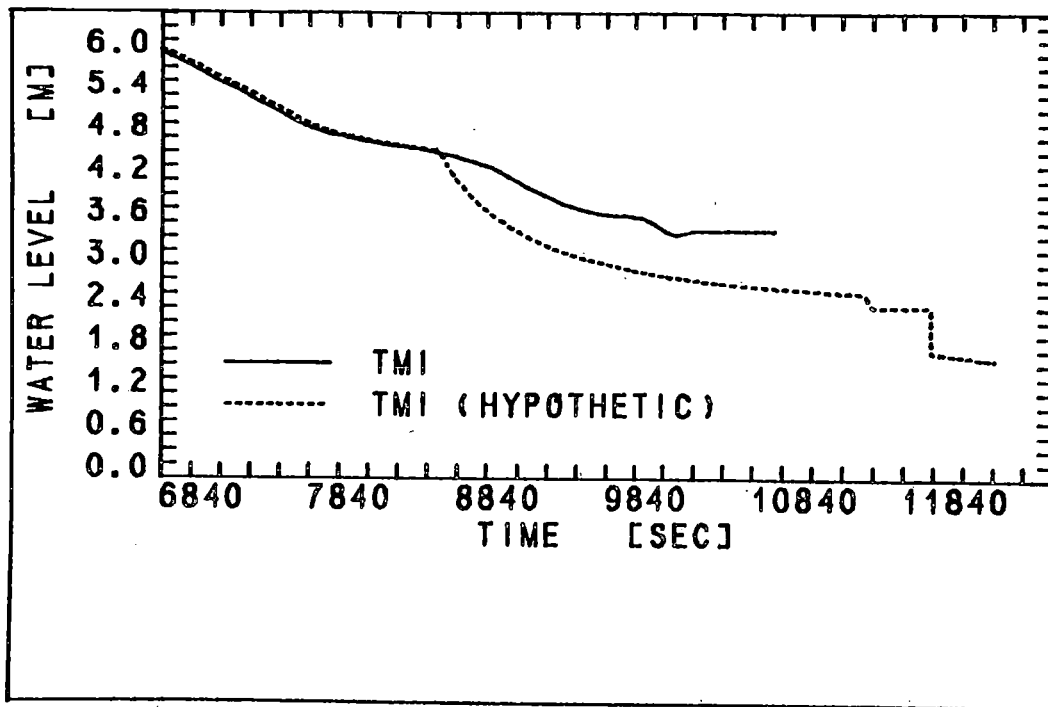


Fig. 3: Comparison of different water level assumptions

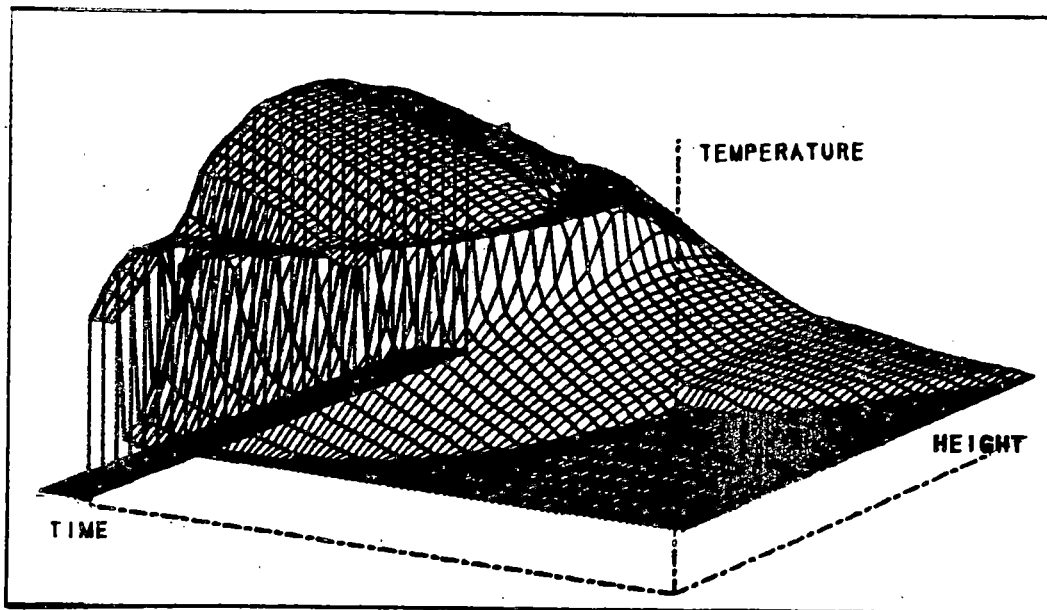


Fig. 4: Temperature distribution in the first radial core zone as calculated by MELSIM under hypothetical conditions

THE USNRC SEVERE FUEL DAMAGE RESEARCH PROGRAM

M. Silberberg, R. W. Wright, and G. P. Marino
Office of Nuclear Regulatory Research
U. S. Nuclear Regulatory Commission

P. E. MacDonald, T. M. Howe, B. J. Beuscher, and R. W. Miller
EG&G Idaho, Inc.

P. S. Pickard, R. L. Coats, and J. B. Rivard
Sandia National Laboratories

ABSTRACT

As part of its response to the TMI-2 accident and to considerations of severe accidents in the regulatory process, the USNRC has initiated a program of research on Severe Fuel Damage (SFD). The purpose of this program is to develop, for a range of accident conditions beyond the design basis, a data base and verified analytical models for assessing the state of a severely damaged core, the hydrogen generation, the fission product release, the coolability of the damaged core by reflooding, and also, when relevant, the progression of core melt to reactor-vessel failure for use in Probabilistic Risk Assessment (PRA). As currently planned, the four-part integrated program consists of: first, integral (multi-effect) in-pile tests in PBF and possibly NRU; second, separate-effects phenomenological experiments in ACRR and in the laboratory; third, analysis, including a Severe-Core Damage Analysis Package (SCDAP) that integrates the models developed from the SFD experiments and an interfacing Melt Progression Model (MELPROG) and fourth, benchmark data from the TMI-2 core examination. The foundation of the SFD program is the PBF Phase-1 series of five tests covering both core-uncovery and reflood conditions for fuel temperatures up to 2400K that will be performed in 1982 and 1983.

DISCUSSION

Program Objectives

As part of its response to the TMI-2 accident, and following the recommendations of the Kemeny Commission and the Rogovin Special Inquiry Group that reviewed the accident, the U.S. Nuclear Regulatory Commission has started a program of research on LWR behavior in the severe fuel damage regime [2, 3]. The accident at TMI-2 demonstrated that severe fuel damage resulting in large hydrogen and fission-product release to the containment does not necessarily result in massive core melt and pressure vessel failure. In the absence of evidence to the contrary, this has been assumed in the past, as, for example, in the reactor safety study, WASH-1400 [1]. Results of this research on the state of severely damaged reactor cores under severe LWR accident conditions are applicable both to accidents in which in-vessel

accident recovery is achieved, and to those which proceed through melt progression to vessel failure with the ex-vessel core-melt threat to the containment.

The objective of the NRC Severe-Fuel-Damage (SFD) research program is to provide a technical basis for decisions and actions by the U.S. Nuclear Regulatory Commission for the range of accident conditions beyond the current design basis that involve severe fuel damage. Applications of the data base and verified analytical models from the Severe Fuel Damage research program will include:

1. Regulatory decisions for accident conditions beyond the design basis.
2. Improved risk assessment methodology and codes.
3. Assessment of possible refinements in systems and procedures.
4. Planning for severe-accident management and emergency response.
5. Information to the public and to other government units during the course of any severe accident.

The TMI-2 accident demonstrated the importance of this last item, and that the Commission has responsibilities in this area.

The technical issues that are addressed by the Severe-Fuel-Damage research program are as follows:

1. Fission-product release from the core, including timing and chemical form.
2. Hydrogen release from the core, including timing.
3. Relevant in-vessel fuel behavior, including the conditions at reactor vessel failure for assessing containment loading.
4. Coolability limits of severely damaged cores, including requirements on coolant supply and timing.

All of these issues require a general knowledge of the state of the reactor core, including temperature distributions, chemical reactions, and material relocation for the range of conditions of the higher probability severe-accident sequences. All these issues involve complicated interactions among these phenomena, so the severe fuel damage program addresses the state of the core over the range of severe-accident sequences. All these issues involve complicated interactions among these phenomena, so the severe fuel damage program addresses the state of the core over the range of severe accident sequences and conditions in order to obtain information on the above technical issues. The program addresses all of these technical issues, and its need evolves from all of the above issues, not from any one alone.

The sequence of the important thermal-hydraulic, chemical, and material-relocation phenomena involved in severe fuel damage under core-uncovery conditions is as follows:

1. Fuel heat-up from the decay-heat, steam cooling imbalance.
2. Oxidation of Zircaloy by steam, oxidation heating, and hydrogen generation.
3. Fuel liquifaction, i.e., fuel dissolution in molten Zircaloy metal cladding [4].

4. Relocation of liquified fuel and possible molten-fuel blockage formation [4, 5].
5. Liquified and molten fuel attack on core structure and the reactor vessel.
6. Nature of debris formed by reflood quenching-steam generation.
7. Coolability of the severely damaged core by reflooding.

The amount, timing, and chemical form of the fission-product release within the core are determined by the above phenomena.

The Research Program

The NRC Severe Fuel Damage research program is a four-part integrated program of in-reactor and laboratory experiments and analysis. Determining the state of the reactor core over the relevant range of severe accident conditions to the accuracy necessary to resolve the desired technical issues is a difficult, but we think not intractable technical problem. However, there is no single set of experiments or single test facility that can provide all the required data. In order to cover the range of parameters between a necessarily few large in-pile integral tests, and to provide the required level of confidence in the results, verified models of the governing phenomena are required. Separate-effects experiments for model development are needed along with the large-scale integral tests. The models can then be applied to the reactor accident sequence, rather than trying to decide "how prototypic is an individual test," and how much reliance can be placed upon the direct application of its results under different conditions. An outline of the scope and purpose of the Severe Fuel Damage research program is given in Table I.

The first part of the integrated program consists of integral (multi-effect) in-pile tests in the PBF test reactor and also possibly the NRU test reactor to provide early scoping data on the governing phenomena and on large-scale multi-pin interactive effects. Later, proof tests of the models and codes developed in the Severe Fuel Damage program may be performed. The second part of the program consists of separate-effects experiments on the governing phenomena, both in the ACRR test reactor and in the laboratory, to furnish a data base for model development and to cover the necessary parameter space on a cost-effective basis. The third part of the program consists of analysis and development of the mechanistic severe-core-damage-analysis codes SCDAP and MELPROG. The Severe Core Damage Analysis Package (SCDAP) treats the development of fuel damage in the original core volume, starting with intact rods [6]. The Melt Progression Model (MELPROG) treats the relocation of liquified (ternary mixture) and molten fuel through the attack on and failure of the reactor vessel [4, 5, 7]. SCDAP and MELPROG will furnish a mechanistic basis for advanced risk assessment codes such as MELCOR, and for evaluating existing codes such as MARCH [8]. The fourth part of the severe-fuel-damage program is benchmark data from the examination of the TMI-2 core. There is continuous active interaction and feedback between the analysis and the experimental programs. At the beginning of the program, an extensive analysis was started in the risk-analysis format to determine the phenomenological uncertainties that have the greatest effect on risk. This analysis is proceeding from the work done in the Zion and Indian Point risk assessments [9, 10, 11]. Results of this analysis will guide the research program as it proceeds.

The usefulness of experiments in the severe core damage regime has been questioned on the basis that there are so many different accident sequences

TABLE I

Integrated Severe Fuel Damage Research Program

Need: Verified severe fuel damage data/models covering a broad range of parameters and accident sequences.

Approach: Integrated Research Program:

- o Integral (Multi-Effect) in-pile tests - PBF, NRU (?)
 - Essential scoping rod-bundle data
 - Too few tests to cover parameter space
 - PIE data on fuel damage
 - Only in-vessel source-term data available
- o Separate effects phenomenological experiments - ACRR, Lab
 - Optical real-time data for model development
 - Very cost-effective coverage of parameter space
 - Early high-temperature data to fuel melting
 - Debris coolability limits under recovery
 - Basic Zircaloy oxidation, fuel liquifaction data (KfK Data)
- o Severe core damage analysis and model development (SCDAP code)
- o Melt progression analysis and experiments
 - In-depth analysis of problem and experiment needs
 - Experiments as required
 - Melt progression analysis (MELPROG code)
- o Benchmark data from TMI-2 examination.

and core-damage state points that only a small fraction of them may be covered by experiment. It has been argued that valuable resources should not be expended upon such a difficult task. If the program output were only the data from large-scale integral tests, this argument might be valid. However, with a coordinated program of integral tests, separate-effects phenomenological experiments, and analytical modeling of the governing phenomena, the accident state-point parameter space is covered by the analytical models, and it is not necessary to perform integral experiments near each accident state point of interest. A few integral experiments in significant regions of the accident-state-point parameter space are needed, as scoping experiments to identify governing phenomena, and as bounding experiments, and later for verification of integral models. Separate-effects phenomenological experiments, both in the laboratory with non-reactor materials and in test reactors with reactor materials and temperatures, will then be used to acquire a data base for the development of phenomenological models. This approach makes tractable, although still very difficult, the research needed to acquire an understanding of reactor behavior during accidents involving severe core damage.

Integral In-Reactor Tests

The integral in-reactor test component of the Severe Fuel Damage program consists primarily of integral tests in PBF. The five tests in Phase I of this program will be performed in 1982 and 1983, and will provide integral scoping data on the progression of fuel damage under core uncover conditions up to 2200 to 2400K. The test fuel in PBF can be operated at full prototypic LWR power for about 1 week before the experiment transient is performed. In this way the fuel is preconditioned, and the short-lived fission product inventory, including iodine, is built up. With preirradiated test fuel, the week of pretest power operation, broken into two parts around a 2-week shutdown, provides measurable quantities of all important fission-product isotopes and the essentially correct cesium-to-iodine ratio. These PBF tests are our only source of significant integral data on fission-product release and chemical form in the in-core thermal-hydraulic and chemical environment of severely damaged cores. These tests will also furnish integral data on hydrogen generation in the severely-damaged core environment. The characteristics of the severely damaged fuel will be obtained from post-test examination. This series of integral PBF tests is the foundation of the NRC Severe Fuel Damage research program, and will form the necessary base for the in-pile and laboratory separate-effects experiments on governing phenomena as well as for the models in the integral damaged-fuel behavior code, SCDAP [6].

In the five Phase I PBF tests, 1-meter long bundles of 32-rods of test fuel will be exposed to core-uncovery accident sequences. The initial test will be performed at a low heating rate (less than 0.5°C/sec) to fully oxidize the Zircaloy cladding before quenching by reflooding, so that formation of the liquified fuel-clad ternary solution will not occur. Two of the tests will use a higher heating rate (about 4°C/sec) to produce considerable liquified fuel, and two will use preirradiated fuel and estimated TMI-2 heating rates. One test with each of the last two heating rates will be cooled slowly from the maximum temperature to preserve as much as possible the fuel configuration at the maximum temperature, and the other two tests will be reflooded to produce quench debris. The last two tests with TMI-2 heating rates will use preirradiated fuel that has been run at power for 1 week to build up the short-lived fission-product inventory, so that fission-product source-term data applicable to an operating PWR may be obtained. The last test will include a rod with low-melting control-rod materials. Post-test examination of the debris in these tests will yield debris size distributions, compositions, and permeability for use in separate-effects experiments in ACRR on core-debris coolability limits. The test matrix for the PBF Phase I tests is given in Table II.

TABLE II

PBF Phase I Test Matrix

Test No.	Heating Rate (K/s)	Irradiated Rods	Control Rods	Cooling	Test Date
SFD-ST	< 0.5	No	No	Quench	Sept 82
SFD-1	> 4.0	No	No	Slow	Dec. 82
SFD-2	> 4.0	No	No	Quench	May 83
SFD-3	TMI-2	Yes	No	Quench	Sept 83
SFD-4	TMI-2	Yes	Yes	Slow	Dec 83

There has been preliminary planning for possible Phase 2 follow-on Severe Fuel Damage tests in PBF. These tests would proceed to higher temperatures above 2700K where massive dissolution of the fuel in molten Zircaloy metal and resulting fuel relocation are expected to occur [5]. Effects of irradiated fuel and control-rod materials would be investigated further, along with fission product release in the higher-temperature environment. These tests would also furnish integral data on melt-progression effects. Decisions about possible Phase 2 Severe Fuel Damage tests in PBF are dependent upon resource considerations and the results of Phase 1, and have not yet been made.

A small number of integral Severe Fuel Damage tests may also be performed in the NRU reactor at Chalk River, which can accommodate 21-rod full-length fuel bundles. In short bundle tests, it is not possible to reduce the steam flow at a given decay-heat power, in order to maintain prototypic ΔT across the bundle, and still have the proper scaling conditions when oxidation heating becomes dominant. Thus, a few full-length check tests on oxidation effects are desirable. Subject to resource availability, two or three tests on these oxidation effects may be performed in 1983 and 1984.

Phenomenological Separate-Effects Experiments

The second major part of the Severe-Fuel-Damage program consists of separate-effects experiments in the ACRR test reactor and in the laboratory on the governing phenomena. Experiments in ACRR on Debris Formation and Relocation (DFR) will provide continuous-in-time visual diagnostics data on the development of severe fuel damage throughout core-uncovery accident sequence. Debris characterization data from reflood quenching at various times in the accident sequences, for use in assessing damaged-core coolability by reflooding, will also be obtained. Data from these separate-effects experiments will be used to develop phenomenological models of the governing processes for use in the mechanistic integral severe core damage code SCDAP and the mechanistic melt-progression code MELPROG. The time-continuous data from these ACRR phenomenological separate-effects experiments under different conditions complement very effectively the necessarily limited severe-fuel damage data from post-test examination of the few integral PBF tests. These ACRR DFR experiments will also provide a very cost-effective way of covering the range of parameter space relevant for LWR severe accident assessment.

Two series of five DFR experiments in ACRR are planned for the period 1983 to 1985. In these experiments a 50 cm long bundle of nine fuel rods, with one rod displaced for axial visualization of the central experiment rod, are exposed to flowing steam in a core-uncovery accident sequence for a 50 cm section of an LWR core. There is time-continuous optical diagnostics of the center-rod surface and temperature, of material motion, and of downstream temperature and hydrogen content. Reflood quench debris for the assessment of damaged core coolability by reflooding will be produced in some of the experiments. After the initial experiments, all accident sequences will be followed to maximum temperatures up to fuel melting (3000K) if that is reached in the sequence. These experiments will

provide the only data available on damaged fuel behavior and relocation in this very-high temperature regime until possible later Phase 2 PBF tests. The experiment matrix for the ten DFR ACRR experiments in Series 1 and 2 is given in Table III. These experiments cover slow-cooled and quenched debris, BWR as well as PWR fuel and quench mode, spacer effects, and the effects of fuel cracking for model development. This half-factorial matrix is a reduction from the original 2D experiment full-factorial matrix planned to cover the desired parameter range, and is considered minimal for this purpose.

A series of phenomenological separate-effects experiments has also been started in ACRR to determine the range of core conditions (if any) for which simple reflood is not sufficient to cool the debris and terminate the accident, and to determine the reflood conditions (pressure and flow velocity) necessary to achieve coolability under these circumstances. Considerable data and rather sophisticated analytical models of the dry-out coolability limits of beds of decay-heated particulate fuel debris under liquid pools have been developed in fast-reactor safety research.

A series of three LWR-specific core-debris coolability experiments will be performed in ACRR in 1982 and 1983 that will be extensions of previous LMFBR safety experiments. The purpose of these experiments is to validate the current fast-reactor debris-coolability models for LWR accident conditions. The LWR-specific conditions that require experimental verification, in addition to the change to water coolant, are high pressure, very deep debris beds, inlet flow, and particularly the characteristics of LWR core debris. It is known that the characteristics of core debris are a major determinant of the dry-out coolability limit under reflood conditions. With the results of these initial three LWR debris-coolability experiments, it will be decided if further ACRR experiments are required for the assessment of the coolability limits of LWR severe accident debris.

The three planned ACRR debris-coolability experiments will have debris beds that are 50 cm deep, use stagnant water, and will cover the pressure range up to 13.5 MPa (2,000 psi). The three beds will have unstratified coarse LWR debris, unstratified fine LWR debris, and stratified debris. Any follow-on experiments would investigate the effects of inlet flow, bed depth changes, non-fuel materials in the bed, and fuel-pin stubs in the bed.

Laboratory separate effects experiments have been started on Zircaloy oxidation in the presence of flowing steam, including hydrogen-blanketing effects. Laboratory experiments may also be performed on the thermodynamics and kinetics of the reactions between UO_2 , Zircaloy, and steam and on the fuel liquification process produced by the ternary (U, Zr, O) interaction [4]. Much information in these areas is produced by the strong program at KfK in the Federal Republic of Germany, and international exchange may be used for this data. KfK will also be getting important laboratory data on the coolability limits of very deep (2 m) inductively heated particle beds.

Analysis and Model Development

The objective of the Severe-Fuel-Damage research program is to develop a data base and verified analytical models of risk-significant fuel behavior for the range of conditions of the higher-probability severe-accident sequences. These models will then be incorporated into the mechanistic severe-accident fuel behavior codes SCDAP and MELPROG [6, 7]. These mechanistic codes become the technical basis for advanced risk-assessment codes such as MELCOR, which must use simplified, fast-running damaged fuel-behavior modules. SCDAP and MELPROG will also furnish an important tool for analysis of the results of Severe-Fuel-Damage experiments in a consistent framework and for future experiment planning. The analytical part of the Severe-Fuel-Damage research

TABLE III

ACRR Debris Formation and Relocation Experiment Matrix

	<u>Test</u>	<u>Inlet SFS</u>	<u>Inlet Conds.</u>	<u>Rel. Pres.</u>	<u>Fuel Pre-Cracking</u>	<u>Spacer Pos.</u>	<u>PWR or BWR</u>	<u>PIE</u>	
<u>SERIES 1</u>									
Scoping (Slow Cool)	DF-1	L	L	+	Y	L	P	PIE--Early Damage	
	DF-2	H	L	-	Y	L	P	PIE--Severe Damage	
<hr/>									
BWR vs. PWR	DF-3	H	H	-	Y	L	B	PIE--If Different	
Spacer LOC	DF-4		DF-2 Conditions		Y	H	P	--	---
Fuel Cracking	DF-5		DF-2 Conditions		N	L	P	--	---
<hr/>									
								Quench Flow	Quench Position
<hr/>									
<u>SERIES 2</u>									
Separate Effects with Quench	DQ-1	L	L	+	Y	L	P	L	L
	DQ-2	H	L	-	Y	L	P	H	L
	DQ-3	L	H	-	Y	L	P	L	H
	DQ-4	H	H	-	Y	L	P	H	H
<hr/>									
Quench Mode	DQ-5		DF-2 Conditions		L	L	P	Top Quench	

L=Low, H=High, Y=Yes, N=No, Relative Rod Pressure, +=Position, -=Negative, P=PWR, B=BWR

SFS=Steam Flow Rate

program includes development of mechanistic models of damaged-fuel behavior on the basis of information developed in the Severe-Fuel-Damage research program and other available information.

At the beginning of the Severe-Fuel-Damage research program, an indepth analysis was started to determine the phenomenological uncertainties in the current analysis of severe accidents that have the greatest impact upon risk and upon the uncertainties in risk assessment. This analysis used the risk-assessment format, and is a cooperative project with the NRC Probabilistic Risk Assessment research program. A preliminary report on this work will be issued in late 1982, and a final report in late 1983. Results of this analysis will guide the future development of the Severe Fuel Damage research program.

The Severe Core Damage Analysis Package, SCDAP, under development at EG&G, is a mechanistic integral accident analysis code on the behavior of severely-damaged-fuel during severe-accident-transients [6]. SCDAP treats the core-wide development of fuel damage with a fuel-pin model and includes thermal hydraulics, oxidation and hydrogen generation, fuel liquifaction by molten Zircaloy and local displacement, fission product release and chemical form, core-rubble formation by reflood-quenching, and damaged-core coolability by reflooding. SCDAP is a modular code, and some of the models in the current MOD 0 of SCDAP have little or no supporting data base. As experimental information is obtained in the Severe-Fuel-Damage research program, individual new or improved models will be developed and used in future versions of SCDAP. SCDAP MOD 0 has already been completed along with reports on its individual modules. The MOD 1 version will be completed in October 1983.

The Melt Progression Model, MELPROG, under development at Sandia, is a mechanistic analysis code that treats core-wide melt progression in uncovered severe accidents from the original core geometry, through the attack on the reactor structure and the reactor vessel, to vessel failure [7]. MELPROG will give the mode of vessel failure and the conditions at vessel failure for use in analysis of the ex-vessel core-melt threat to the containment, and for use in risk assessment. MELPROG MOD 0 will be completed in 1983, and a later version will incorporate results of the Severe Fuel Damage research program.

TMI-2 Core Examination

Examination of the TMI-2 core will provide unique and invaluable benchmark data on the characteristics of severely-damaged fuel. Important information on the governing processes in the development of severe core damage may also be obtained, but the lack of instrumentation and uncertainties about the actual accident transient make the value of this information uncertain before-the-fact. Early recovery and adequate analysis of the TMI-2 core debris will be of great importance to the Severe-Fuel-Damage research program, and information from the TMI-2 core examination will be used in the program as soon as it is available.

REFERENCES

1. Reactor Safety Study, NUREG-75/014, October 1975.
2. J. G. Kemeny, et.al., Report of the President's Commission on the Accident at Three Mile Island, October 1979.
3. M. Rogovin and G. Frampton, Jr., Three Mile Island: A Report to the Commissioners and to the Public, NUREG/CR-1250, Volume I, January 1980.

4. S. Hagen and H. Malaushek, "Bundle Experiments on the Meltdown Behavior of PWR Fuel Rods," Transactions ANS 33:505, November 1979.
5. S. Hagen, Private communication, November 1981.
6. C. M. Allison, et.al., Severe Core Damage Analysis Package (SCDAP) Code Conceptual Design Report, EGG-CDAP-5397, April 1981.
7. SNL-LWR Severe Core Damage Phenomenology Program, NUREG/CR-2725, to be published.
8. R. O. Wooton and H. I. Avci, MARCH (Meltdown Accident Response Characteristics) Code Description and User's Manual, NUREG/CR-1711, October 1980.
9. Zion Probabilistic Safety Study, Commonwealth Edison, 1981.
10. Indian Point Probabilistic Safety Study, Consolidated Edison, 1981.
11. W. B. Murfin, Report of the Zion/Indian Point Study: Volume I, NUREG/CR-1410, August 1980.

SEVERE ACCIDENT TRENDS IN LIGHT WATER REACTORS

R. A. Bari and W. T. Pratt

Brookhaven National Laboratory
Upton, New York 11973

and

J. F. Meyer

U.S. Nuclear Regulatory Commission
Washington, D. C. 20555

ABSTRACT

An analysis is presented of key phenomena and scenarios which imply some general trends for beyond-design-basis accidents in light water reactors. This analysis is based on the insights gained from studies performed over the past three years at Brookhaven National Laboratory (BNL), on pressurized water reactors with large dry or ice condenser containments and of boiling water reactors - with Mark II or Mark III containments. This analysis relies on: 1) extensive use of the MARCH code and improvements to the code made at BNL; and on 2) additional phenomenological evaluations which are not currently addressable within the context of the MARCH code.

INTRODUCTION

The behavior of a light water reactor under severe accident conditions must be determined in order to assess the risk of reactor operation and, if deemed necessary, to develop equipment and/or procedures which would mitigate the consequences of such accidents. The body of knowledge available for this determination includes: limited direct experience, experiments aimed at simulating certain aspects of severe accidents, and analytical studies of postulated accident conditions. It is the purpose of this paper to discuss results obtained via analytical studies and to infer some general trends for beyond-design-basis accidents in light water reactors. This work is based on insights gained from studies of pressurized water reactors (PWR), with large dry or ice condenser containments and of boiling water reactors (BWR) with Mark II or Mark III containments.

Beyond-design-basis, or Class 9, accidents have received increased attention in recent years as a result of the Three Mile Island-2 accident. Emphasis has been given to studies and evaluations which would provide information on both accident prevention and mitigation. Degraded core (but not necessarily full core meltdown) accident analysis has focused particularly on the generation, transport, and combustion of hydrogen. Full core meltdown analysis has focused on, in addition to hydrogen-related problems, a spectrum of potential threats to the containment integrity and on fission product transport. In this paper, all of the above termed accidents will be referred to as severe accidents.

A severe accident will occur when the appropriate plant safety functions fail to adequately respond to an event which affects at least one of the following reactor conditions: heat removal capability, coolant boundary integrity, reactivity control.

Various plant-specific probabilistic risk assessments have been performed which delineate severe accident sequences. Initiating events, both internal and external to the plant, are considered and plant system failures which compromise safety functions are analyzed to obtain the severe accident sequences.

METHODS OF ACCIDENT ANALYSIS

Much of the analysis reported in this paper has been conducted with the aid of the MARCH computer code [1]. The MARCH code models the heat-up of the reactor core following a transient or loss of coolant accident. The code computes the boiloff of water, the zirconium-steam chemical reaction, the melting of the clad and fuel, and the collapse of the core within the reactor vessel. The interaction of core debris with water is computed and the impact of steam and hydrogen on the containment boundary is computed at all stages of the accident. If the core debris breaches the reactor vessel, additional core debris interactions with water are computed and, under specified conditions, the interaction of core debris with concrete in the containment basement is computed. A fuller description of the MARCH code and improvements made to the code at BNL are described in another paper [2] in these Proceedings. In areas where deemed necessary, additional analysis was performed to supplement the MARCH code analysis.

Accident Analysis

For any accident sequence that leads to severe core damage an important question to address is: Will the integrity of the containment building be violated? This is obviously an important question since the containment provides the barrier between the biosphere and the fission products emanating from the damaged reactor core. The failure of the containment boundary may be a result of the severe accident or it may precede core damage. In the latter case, core damage may or may not be correlated with failure of containment integrity. Examples of these situations are: the undetected failure to isolate a containment penetration before and during core damage; the well-known check-valve sequence (Event V) [3].

For those accident sequences for which containment integrity exists at the initiation of core damage, the main concern is whether the accident progression will include loadings on containment which will ultimately lead to its failure. Table 1 provides the loadings which may directly or indirectly threaten containment integrity, their sources, and some options for mitigating these loadings. Of these loadings, steam pressurization is most universally available for various accidents and reactor types. However, the severity of this threat will depend strongly on the availability of the containment heat removal function (e.g., fan coolers and sprays in some PWRs and the suppression pool in BWRs). If a cooling system is to be selected as the beyond-design-basis-accident mitigation scheme, then it must be qualified to withstand the severe accident containment environment and it must operate under the system conditions that caused the accident (e.g., station blackout). Filter/Vent systems have received some attention and consideration as a mitigation option; their design is strongly influenced by the spectrum of accidents that they would potentially mitigate.

Hydrogen combustion requires hydrogen and oxygen in appropriate concentrations, an ignition source and the absence of significant amounts of diluents (e.g., steam) in the containment atmosphere. Combustion is eliminated during normal reactor operation for the Mark I and Mark II BWR containment types because the containment atmosphere is continuously inerted by the presence of a sufficient concentration of

TABLE I

Potential Containment Loadings from Severe Core Damage Accidents

Containment Loading	Source(s)	Mitigation Options
Steam Pressurization	Vessel; Core Debris Interactions with H ₂ O and/or Concrete	- Containment Cooling System - Filter/Vent System
Hydrogen Combustion	Metal-Water Reaction (In-Vessel and Ex-Vessel)	- Controlled Combustion - Combustion Prevention - Pressure Reduction
Carbon Monoxide Combustion	Reaction of CO ₂ (From Concrete) with Metal (in core debris)	as above
Hydrocarbon Combustion	e.g., Lubricants, Insulation in Containment	- Protect - Replace - Remove
Pressurization by Noncondensibles (e.g., CO ₂ , CO, H ₂)	Core Debris/Concrete Interactions	- Containment Cooling System - Filter/Vent System - Core Catcher
Decomposition/Melting of Containment Basemat	Core Debris/Concrete Interaction	- Cool Debris - Core Catcher
Missiles	Reactor Components and Structures	- Missile Shields

nitrogen. A controlled combustion scheme has been developed for the PWR ice condenser containment. This scheme relies on deliberate ignition of hydrogen in the lower containment compartment with dissipation of the resulting heat load in the ice chest.

Combustion of carbon monoxide may occur for those accidents that progress to full core meltdown provided that 1) core-concrete interactions occur and 2) the concrete in a particular reactor basemat is a limestone type with high calcium carbonate content and 3) significant amounts of CO₂ is released from the concrete as a result of the core debris/concrete interaction and 4) the CO₂ is chemically reduced by the metallic component of the core debris to produce carbon monoxide. The combustion properties of CO are generally similar to H₂ and indeed a mixture of CO/H₂ could be present in the containment atmosphere. The mitigation options in this case are the same as for hydrogen combustion.

Combustion of hydrocarbons in the containment may occur directly or synergistically with H₂ combustion. Electrical cable insulations have varying degrees of protection among the reactor plants from such combustion. The question of the combustion hazard related to the insulation in ice condenser chests has been raised in the licensing process for such plants.

The interaction of core debris with concrete provides a source of containment loading by noncondensibles such as CO₂, CO and H₂. This loading can be prevented by replacing the concrete basemat by a core catcher material (e.g., MgO) that does not allow for the production of large quantities of noncondensibles. Alternatively, the partial pressure associated with noncondensibles may be kept sufficiently low by cooling the containment atmosphere.

The above-mentioned loadings refer to thermodynamic loads via the containment atmosphere to the containment structure. Alternatively, the containment boundary may be violated as a result of a breach of the concrete basemat when attacked by molten or re-solidified core debris. There is a lack of large-scale prototypic empirical knowledge in this area and the severity of the problem will depend on the ready availability of a liquid pathway for fission product transport.

Missiles may be accelerated to the containment boundary as a result of the accident progression. The WASH-1400 steam explosion scenario is well-known and its credibility has been called into question by several workers [4-6] in recent years.

An Example: TMLB' and Variations

An accident which illustrates many of the key accident phenomena and accident progression trends is the TMLB' accident of a PWR large, dry containment. In this section this accident and its variations are explored for a typical four-loop 3200 MWt PWR.

The TMLB' transient assumes a loss of the turbine-driven pump train of the auxiliary feedwater system, coupled with a total loss of AC power. Output from the MARCH computer code for a reference TMLB' transient is shown in Figure 1. The TMLB' results in failure of the heat removal capability of the secondary system, which eventually results in overheating of the primary system. The primary system water boils at the pressure set point of the pressurizer relief valves. Without onsite or off-site power, none of the active engineered safety features operate. As a result, the containment building pressure gradually increases as primary system steam is released through the pressure relief valves. The core, which is uncovered at about 240 minutes, melts and slumps at about 300 minutes. When the molten core comes in contact with water in the bottom head, a large quantity of steam is produced, leaves the reactor through the pressure relief valves, and results in a pressure increase in the containment building of 13 psi. With the hot core materials in the bottom head coupled with a high primary system pressure, failure of the head is predicted to occur within approximately 2 minutes. The subsequent depressurization of the primary system results in a 15-psi increase in containment-building pressure.

When the primary system depressurizes as a result of failure of the bottom head, the accumulator tanks inject water into the vessel, starting at 665 psia. The 173,000 lbs of water from the accumulators then falls from the breached reactor vessel onto the core in the reactor cavity. The interaction of hot core materials and accumulator water in the reactor cavity is modeled in the MARCH code using the HOTDROP subroutine. The HOTDROP model assumes that when the molten core materials come in contact with the water, they fragment into a large number of small, spherical particles. The model further assumes that the water can completely flood the resulting debris bed.

In the HOTDROP model, the heat transfer from the core debris particles is limited only by the internal thermal resistance of the individual particles and the

particle/water interface area and heat transfer coefficient. The result is a very rapid energy transfer to the water, with corresponding rapid steam pressurization of the containment building. The core materials are then cooled from 3940°F at the point of head failure to 1160°F after the interaction with the accumulator water. Our analyses indicate that the interaction is water-limited. That is, there is not enough water to quench the core debris if the reactor cavity is assumed to be dry before head failure. This accumulator water and core interaction adds another 26 psi to the containment building pressure load. After all accumulator water has evaporated, the core materials are predicted to reheat to about 2500°F before they attack the concrete, a process which takes about 120 minutes. Because it is assumed in MARCH that the hot core materials do not drive gases from the concrete during this period, the containment building pressure falls. When the core materials begin to attack the concrete, the MARCH code uses INTER to model the core/concrete interaction. The pressure history shown in Figure 1 is strongly dependent on these model assumptions in INTER as discussed elsewhere [4,7].

At no time during the first 15 hours of this accident sequence does the MARCH model predict that the containment building pressure exceeds ~100 psia. This is significantly below the currently assessed containment strengths of several large dry containment buildings. Furthermore, at the time the core is uncovered and significant hydrogen release occurs, the containment building atmosphere is already rendered so inert that hydrogen ignition is prevented. (See Figure 1.)

In order to gain some perspective for this accident the following variations are considered:

- (i) Pump Seal Failure
- (ii) AC Power Restoration
- (iii) Flooded Cavity

(i) Pump Seal Failure (TMLB'S)

During a total-loss-of-AC-power accident, the reactor coolant pump seals cannot be cooled. Under these circumstances, a LOCA induced by failure of the reactor coolant pump seals would likely occur in approximately 1 hour. This accident sequence is identical to the TMLB' reference case up to the point of seal failure. At that point, the accident becomes very similar to a LOCA without AC power in terms of containment building response.

The containment building response is shown in Figure 2. The time to uncover the core was based on an assumed break flow rate of about 200 gal/minute. Under these circumstances depressurization of the primary system allows injection of the accumulator water into the vessel before head failure. Accumulator injection into the vessel contributes greatly to the steam release from the primary system before head failure which increases the steam partial pressure at head failure. This results in significantly higher containment building pressure at head failure for the TMLB'S sequence (80 psia) than for the TMLB' reference case (60 psia). Also, as the accumulators inject into the vessel prior to vessel failure, water is not discharged from this source onto the core debris in the reactor cavity after vessel failure. If we assume that the reactor cavity is dry, then the TMLB'S sequence results in extensive core/concrete interactions immediately after vessel failure. However, comparing Figures 1 and 2 indicates that the TMLB'S sequence does not result in significantly higher containment pressures than predicted for the TMLB' sequence. However, it was noted above that these predictions are strongly dependent on the INTER model in MARCH. An independent analysis carried out at BNL on the containment building response during core/concrete interactions is described in another paper [2] in these proceedings.

(ii) AC Power Restoration

For TMLB' and TMLB'S, at the time hydrogen is released from the primary system, the containment building atmosphere is inert because of the steam. If the reactor cavity is assumed to be relatively dry, then extensive core/concrete interactions will occur. MARCH predicts that over 4000 lb of H₂ could be produced ~15 hours after accident initiation. If containment building heat removal is restored at this stage, then the accompanying reduction in steam partial pressure will render the containment building atmosphere combustible, thereby creating the potential for ignition of a large quantity of hydrogen during one burn. Figure 3 shows the effect of restoring two containment building sprays after 950 minutes for the TMLB' sequence as calculated using the MARCH code. The hydrogen and oxygen mole fractions included in Figure 3 indicate a hydrogen concentration in excess of the lean flammability limit (>4%), which is prevented from ignition by a low oxygen concentration (<6.5%). The effect of the sprays is to reduce the steam mole fraction, which increases the hydrogen and oxygen concentrations. When the oxygen reaches 6.5% by volume, the hydrogen concentration is >14%. A hydrogen concentration of this magnitude may be capable of combustion, but is unlikely to detonate. The pressure rise shown in Figure 3 corresponds to the burning (not detonation) of 3800 lbs of hydrogen over an assumed burn time of 0.1 minutes. However, the above combustion calculation ignores the potential impact of CO. It was noted above that if the reactor basemat consists of limestone concrete then the potential exists for CO generation during core/concrete interactions. At BNL we modified MARCH to consider CO as a combustible rather than as an inert gas as assumed in the original code. For the accident sequence noted above the effect of significant quantities of CO is to increase the mole fraction of combustible gases at the time the oxygen concentration reaches 6.5% by volume. This in turn increases the potential for a detonable mixture.

(iii) Flooded Cavity

In the foregoing analysis it was assumed that the majority of steam condensed in the containment building collects in the sump. The quantity of water in the reactor cavity was assumed to be negligible compared with the amount of water resulting from discharge of the accumulator tanks. In this section we assume that the quantity of water in the reactor cavity is large compared with the amount of water in the accumulator tanks. Substantial quantities of water may be present because of the containment building design, or if the presence of large quantities of water is considered to be an advantage, then building design modifications may be made to insure that this water is available. Water supplied to core debris in the reactor cavity has the potential for preventing the debris from attacking concrete by keeping the core debris cool. Thus, a substantial buildup of combustibles resulting from extensive interactions of the core materials with concrete would be prevented if the core could be rapidly flooded with water and brought into a coolable configuration.

The TMLB' sequence was run under the assumption that the cavity contained an unlimited amount of water to cool the debris to the extent that the core could not reheat and interact with the concrete. The results of this sequence are included in Figure 4. The buildup of hydrogen, after lower plenum failure, is prevented by the presence of water in the cavity. After the core is brought into thermal equilibrium with the water and the rapid steam production and rapid pressure rise have occurred, the decay heat in the core materials continues to boil water at the rate of ~1000 lbs/minute. This rate is sufficient to pressurize the containment building due to steam production. Hence, if a large amount of water is available in the reactor cavity, containment building cooling is essential to prevent the eventual failure of the building by steam overpressurization.

CONCLUSION

The foregoing accident scenario illustrated several general features of severe accidents, particularly in connection with containment loadings. In this regard, severe accidents can be categorized as either those with containment heat removal available or those without containment heat removal capability. In the former category, containment loading by steam pressurization is usually a dominant threat because of the availability of water from the vessel and other repositories. Since core debris coolability usually relies on water providing a direct heat sink, steam generation and, if the core debris has a metallic component, hydrogen generation are potential byproducts of the core cooling process.

Engineered safety features that are designed to accommodate design basis accidents, do not necessarily provide the same mitigation benefits against beyond-design-basis accidents. In certain instances, the operation of the engineered safety features may even aggravate a beyond-design-basis accident. For example, injection of emergency core coolant when the core temperatures reach and exceed $\sim 2000^{\circ}\text{F}$ will lead to additional steam and hydrogen production if the coolant flow is insufficient to rapidly reflood the core. As another example, restoration of containment cooling may transform a steam-inerted hydrogen-oxygen-air atmosphere to a combustible atmosphere as a result of the condensation of steam.

Further studies of severe accidents are warranted. This will provide needed information on the prevention and mitigation of these accidents.

ACKNOWLEDGEMENT

This work was carried out under the auspices of the U. S. Nuclear Regulatory Commission.

REFERENCES

1. R. O. WOOTEN and H. I. AVCI, "MARCH Code Description and User's Manual," NUREG/CR-1711, Battelle Columbus Laboratory, October 1980.
2. W. T. PRATT et al., "MARCH1B: BNL Modifications to the MARCH Computer Code," Proceedings of the International Meeting on Thermal Nuclear Reactor Safety, August 29 - September 2, 1982, Chicago, IL.
3. Reactor Safety Study, U.S. Nuclear Regulatory Commission, WASH-1400 (NUREG-75/014), October 1975.
4. Preliminary Assessment of Core Melt Accidents at the Zion and Indian Point Nuclear Power Plants and Strategies for Mitigating their Effects, U. S. Nuclear Regulatory Commission, NUREG-0850, Vol. 1, November 1981.
5. D. V. SWANSON and M. L. CORRANDINI, "A Probabilistic Analysis of LWR Steam Explosions," Proceedings of the International ANS/ENS Topical Meeting on Probabilistic Risk Assessment, September 20-24, 1981, Port Chester, NY, p. 293.
6. S. G. BANKOFF et al., "Steam Explosions - Their Relationship to LWR Safety Assessments," Proceedings of the International Meeting on Thermal Nuclear Reactor Safety, August 29 - September 2, 1982, Chicago, IL.
7. W. T. PRATT, R. D. GASSER, and R. A. BARI, "Potential Influence of Core-Concrete Interactions on PWR Containment Pressurization," Trans. Am. Nucl. Soc. **39**, 609 (1981).

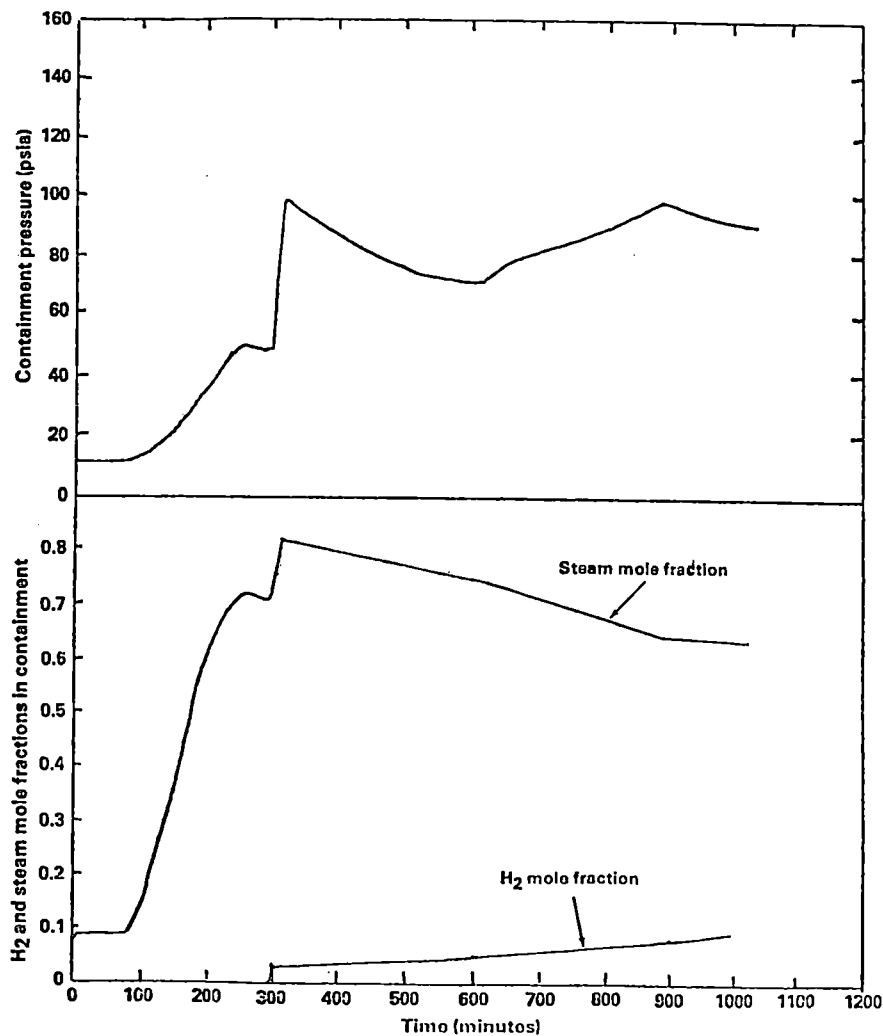


Figure 1
Containment Response for
a 3 TMLB' Dry Cavity
Reference Case

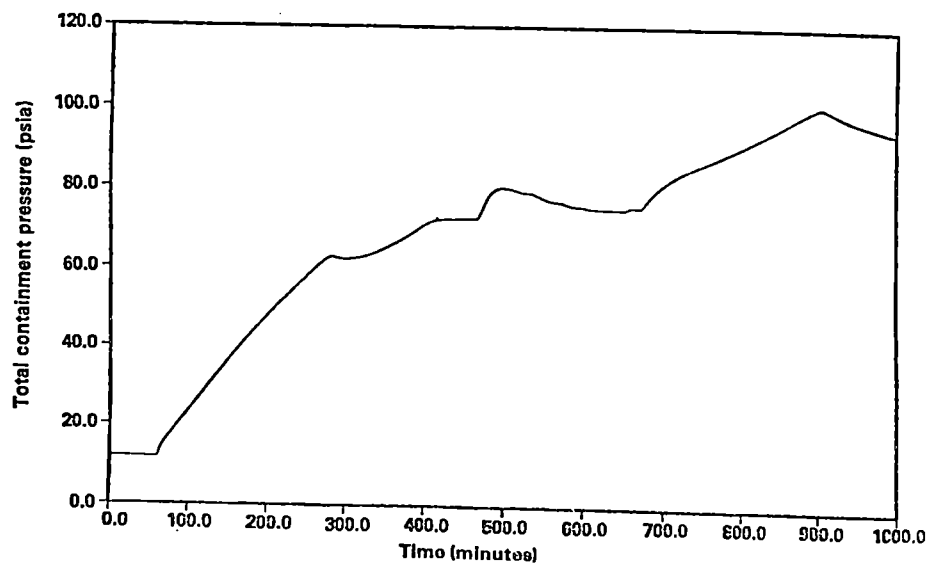


Figure 2
Containment Response
for a TMLB'S Dry
Cavity Case

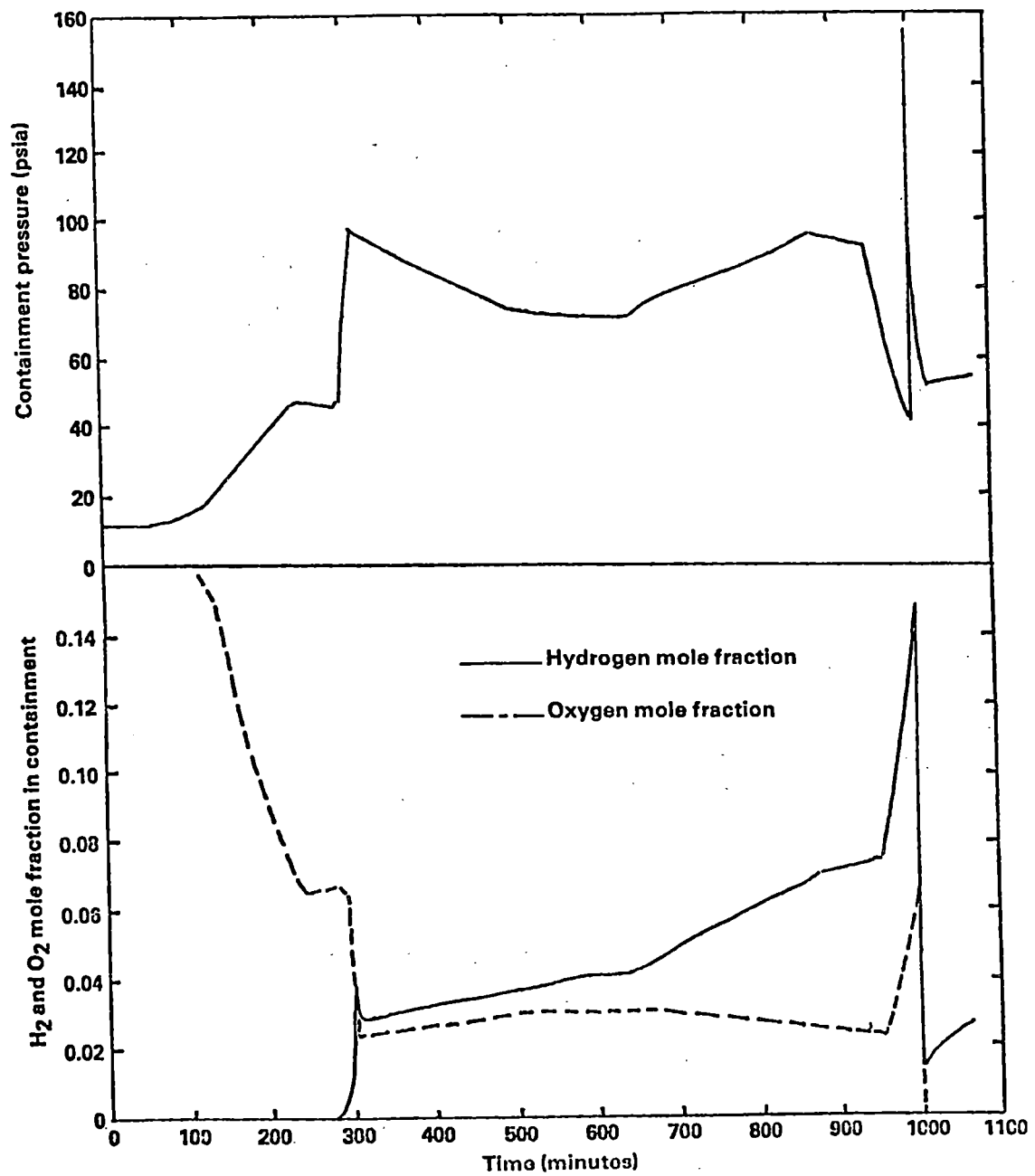


Figure 3 Effect of Starting Spray Operation at 950 Minutes on a TMLB' Dry Cavity Case

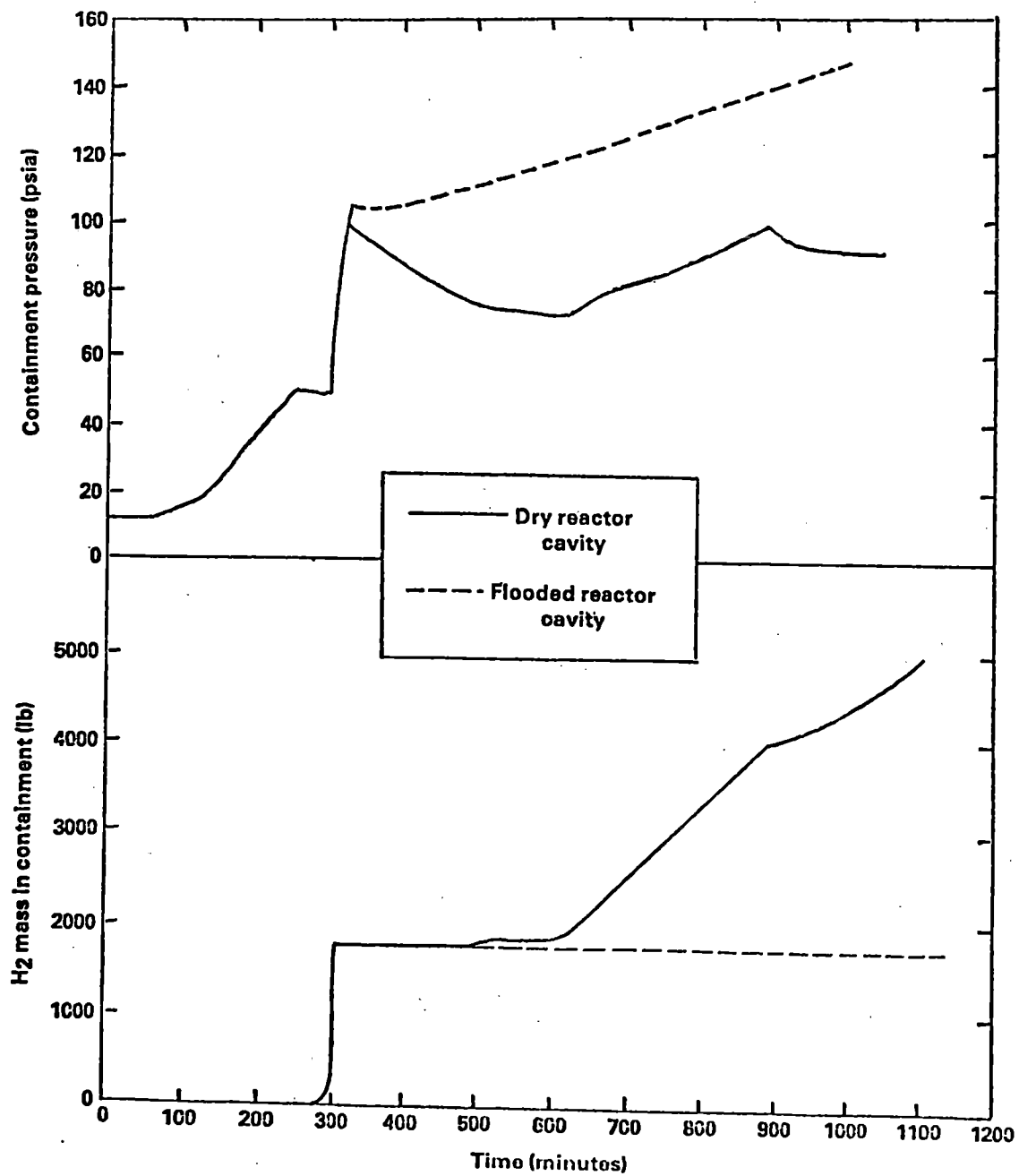


Figure 4 Effect of Flooding Reactor Cavity on a TMLB' Case

SENSITIVITY OF DEGRADED CORE COOLING ACCIDENT PREDICTIONS TO THE
ASSUMED LEVELS OF OPERABILITY OF ENGINEERED SAFETY SYSTEMS

P. Cybulskis

Battelle's Columbus Laboratories
Columbus, Ohio 43201, U.S.A.

ABSTRACT

In the performance of probabilistic risk assessments of reactors, the success criteria for the various engineered safety features must be specified, both for the quantitative evaluation of system failure probabilities as well as for the description of the response of the plant to the various accident events. Often these success criteria are assumed to correspond to the minimum safety features as defined in the safety analysis reports; this was the case in the Reactor Safety Study. Sometimes more realistic minimum safety feature requirements are derived, as has been done in some more recent efforts. Since engineered safety features generally have significant degrees of redundancy and diversity, the assumption of minimum safety feature availability is not necessarily consistent with the most likely levels of operability. Further, the assumptions regarding the levels of operability of certain safety features can have a significant effect on the prediction of the nature and course of the physical processes in any given accident sequence. Specific examples of the potential sensitivity of predicted results to the assumed levels of operability of engineered safety features as inferred from a number of PRA's and related studies are described.

INTRODUCTION

In the performance of probabilistic risk assessments of reactors, the success criteria for the engineered safety features required to cope with various initiating events must be specified. These criteria are required both for the quantitative evaluation of system failure probabilities as well as for the prediction of the response of the plant to the various accident events. The success criteria deal with the minimum number of pumps, heat exchangers, sprays, etc., that must be operable to perform the intended safety function. Since the important engineered safety features may have significant degrees of redundancy and diversity to compensate for possible failures, various levels of success are possible; each of the possible success (or failure) states would in principle have its own probability of occurrence. As a simplification in systems analyses it is convenient to define a single success criterion for each system. In the Reactor Safety Study [1] the success criteria were taken to correspond to the minimum required safety features as defined in the safety analysis for the plants under consideration. Similar approaches have been taken in other risk studies [2-5], though more realistic minimum success criteria for safety system operability have been defined in some cases. The minimum required engineered safety features, however defined, obviously do not represent the most likely levels of operability.

In the evaluation of the physical processes associated with core meltdown accidents, such as the timing of key events, nature of challenges to containment integrity,

etc., success and failure criteria for those engineered safety features that may be operable are once again required. Although it is recognized that a wide variety of partial as well as complete failures are possible, almost always failure is modeled as the complete failure of the affected system. This is an assumption of convenience. Those safety features that are available are typically assumed to be operating at only the minimum required levels. Again, this assumption is not consistent with the most likely levels of operability and can have a significant impact on the prediction of the course of the subsequent events. The accident sequence definition, which should include specification of the levels of operability of appropriate engineered safety features, is a major boundary condition for the analyses of the plant response to any given accident sequence. This paper attempts to point out some areas in which more attention to the specification of these boundary conditions may be required.

ESF FAILURE MODES

In the description of the physical phenomena associated with core meltdown accidents, safety system failures are typically modeled as complete failures, even though it is recognized that a variety of partial as well as complete failures are possible. The assumption of complete failure is one of convenience since it is impossible to analyze the wide spectrum of partial failures that can be postulated. This assumption will influence the nature of the predictions resulting from the analyses. In core meltdown analyses, the rate and extent of reaction between the Zircaloy cladding and steam is frequently found to be steam limited; in some cases, so called dry meltdowns, little or no reaction would be predicted because of this assumption. If a degraded or delayed emergency core cooling system operation is assumed instead of complete failure, more rapid core melting with more extensive zirconium-water reaction can result. Further, the rates of steam and hydrogen input into the containment during the period of principal hydrogen generation have been found to vary with the accident sequence and modeling assumptions considered [6]. With complete emergency core cooling failure, the steam flow to the containment will decrease as that of the hydrogen increases, to the point that mostly hydrogen is released to the containment in the later stages of core heatup. Such a hydrogen flow may be amenable to accommodation by intentional hydrogen burning, for example. For situations involving delayed emergency core cooling initiation on degraded system operation, high steam flows may accompany the hydrogen flows into the containment. Such steam flows may prevent the effective operation of hydrogen ignitors.

Another item of concern similar to the question of complete versus partial failure is the frequent assumption that failure of emergency core cooling injection necessarily implies failure of emergency core cooling recirculation. While there are clearly situations where this is true, there are also others where such an assumption is not necessarily appropriate. For example, there may be cases where the emergency core cooling system recirculation cannot function due to high primary system backpressure; in such cases, one may expect the recirculation to start upon primary system pressure relief upon vessel head failure. Consideration of water injection on the hot core debris would obviously lead to different behavior than if such a possibility is ignored.

ESF LEVELS OF OPERABILITY

Among the most obvious impacts of the assumption of minimum versus design levels of safety system operability is on the prediction of the timing of certain events. For a loss of coolant accident involving rapid primary system depressurization with both emergency core cooling injection and containment spray injection working, the time to empty the refueling water storage tank with minimum system operability was found in the Reactor Safety Study to be about an hour; with full systems operation the corresponding time would be about 20 minutes. For small break loss of coolant accidents, the emergency core cooling system could continue to draw from the refueling water storage tank for a number of hours perhaps, if operating at a minimum level; however, if at the same time the containment spray injection was operating at its

design level, the water in the tank would be exhausted quickly and the time for switching to recirculation would be much shorter. Comparable times and time differences between the two sets of assumptions would apply to many other designs. Table I presents a representative set of times to empty the refueling water storage tank as functions of engineered safety feature levels of operability. The switchover from the injection to the recirculation mode is one of the more frequently encountered emergency core cooling system failure modes encountered in PRA's. The potential variability in time at which this switchover must take place could also influence the probability of failure to do so.

The length of time between the start of the accident and the time of the occurrence of the failure could have an effect on the operator's ability to take the proper action, the likelihood of recovery or repair, and other emergency actions. All other things being equal, the precise timing of the onset of core melting, e.g., due to emergency core cooling recirculation failure, would have little effect on the predicted consequences. There are aspects of accident behavior, however, that would change in time and thus could affect the course and consequences of the accident sequence depending on the timing of specific events. In an ice condenser containment, for example, the ice has a finite lifetime for any particular sequence. Whether core melting takes place with or without the ice present may have a marked influence on the outcome. In the RSSMAP ice condenser analyses in which the failure of the emergency core cooling recirculation was found to be one of the key failure modes, the timing of this failure was based on minimum safety features operation. If design operating conditions were assumed, somewhat different timing of events would be predicted and sequences such as S₂H and S₂HF could be altered significantly.

The interaction of the core debris with water in the reactor cavity has been identified as a key aspect of meltdown accident analysis. Under some assumptions, the rapid vaporization of the water by the core debris can present a significant challenge to containment integrity. Under somewhat different sets of assumptions and boundary conditions, the initial presence and continuing ingress of water into the reactor cavity has been suggested as a possible means of terminating the accident at that point [7]. Aside from many uncertainties related to the phenomena associated with melt-water interactions, the amounts of water that may be present in the cavity and how it gets there can vary with reactor design, accident sequence, as well as ESF assumptions. In some reactor designs, the water on the containment floor can communicate freely with that in the reactor cavity; in such cases, one can expect significant quantities of water in the reactor cavity as long as any of the safety injection systems have or continue to operate. In other designs, the entry of water into the reactor cavity is restricted and the amount of water that may enter the cavity could be sensitive to the specific levels of safety system operation. In the Reactor Safety Study PWR, for example, there is no direct communication between water on the containment floor and that in the reactor cavity; however, a fraction of the containment spray water will find its way into the cavity. Thus, the quantity of water available for interaction with the core debris following vessel head meltthrough will depend not only on the plant design, but also on the level of containment spray operability in any accident sequence.

There is a further point to be made with regard to the earlier example of a small break accident and the dependence of event timing on assumptions regarding containment spray operation. Many PWR designs incorporate containment building coolers as well as spray systems, with the actuation pressure for the latter being higher than that for the former. Thus, in small break and transient induced loss of coolant accident sequences the combination of the containment coolers and heat absorption by structural heat sinks will often maintain the pressure below the spray system actuation setpoint. Thus the spray, although available, may not in fact be actuated for significant portions of an accident sequence. This could have a significant impact on, among other things, fission product removal in such sequences as small break loss of coolant accidents with emergency core cooling failure. Figure 1 illustrates an analysis for an accident sequence to illustrate this point. The results are for a transient with loss of power conversion, auxiliary feedwater, and emergency cooling. During the boiloff of the primary coolant through the relief valve the containment pressure is maintained below the spray setpoint by the containment coolers. The rapid pressure increase

would actuate the sprays, but too late to prevent a serious challenge to containment integrity.

CONCLUSIONS

Consideration of the results of a number of PRA's indicates that specific levels of operability of engineered safety systems that are assumed can influence the prediction of timing as well as the nature of the physical phenomena. The assumption of minimum safety features that is commonly made is not necessarily consistent with the most likely levels of operability. It is suggested that more attention should be given to the definition of the most likely levels of operability and the use of these levels in the analysis of physical phenomena associated with core meltdown accidents. This is particularly true if the binning approach in which only a small number of sequences are treated in detail is utilized.

REFERENCES

1. "Reactor Safety Study, An Assessment of Accident Risks in U.S. Commercial Nuclear Power Plants", WASH-1400 (October, 1975).
2. D. D. CARLSON, et al, "Reactor Safety Study Methodology Applications Program: Sequoyah #1 PWR Power Plant", NUREG/CR-1659/1 of 4 (February, 1981).
3. G. J. KOLB, et al, "Reactor Safety Study Methodology Applications Program: Oconee #3 PWR Power Plant", NUREG/CR-1659/2 of 4 (January, 1981).
4. S. W. HATCH, et al, "Reactor Safety Study Methodology Applications Program: Calvert Cliffs #2 PWR Power Plant", NUREG/CR-1659/3 of 4 (May, 1982).
5. S. W. HATCH, P. CYBULSKIS, and R. O. WOOTON, "Reactor Safety Study Methodology Applications Program: Grand Gulf #1 BWR Power Plant", NUREG/CR-1659/4 of 4 (October, 1981).
6. P. CYBULSKIS, "A Method for the Analysis of Hydrogen and Steam Releases to Containment During Degraded Core Cooling Accidents", NUREG/CR-2540 (February, 1982).
7. COMMONWEALTH EDISON, "Zion Probabilistic Safety Study" (1981).

TABLE I. TIMES TO EMPTY REFUELING WATER
STORAGE TANK

Engineered Safety Features Operability	Time, (min)
MIN ECI & CSI	53
MAX ECI & CSI	22
MAX HP ECI & CSI	49
MAX HP ECI & NO CSI	318
CHARGING ONLY	1167

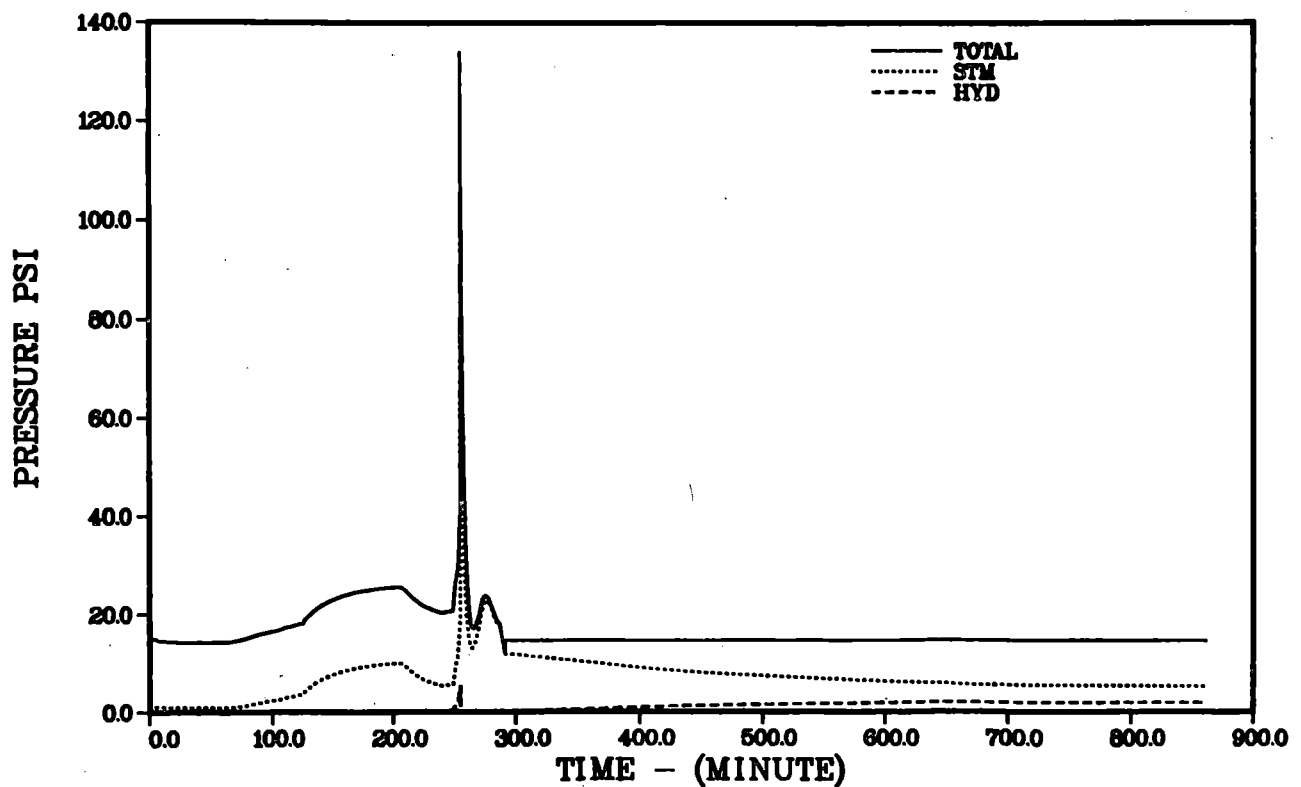


FIGURE 1. PWR TML SEQUENCE CONTAINMENT PRESSURE RESPONSE

SESSION 29

LARGE-BREAK LOCA ANALYSIS

Chair: F. D'Auria (*UDP*)
L. Ybarrondo (*EG&G*)

POSTTEST ANALYSIS OF SEMISCALE LARGE-BREAK TEST S-06-3 USING TRAC-PF1*

B. E. Boyack

Energy Division
Los Alamos National Laboratory
Los Alamos, New Mexico 87545

ABSTRACT

The Transient Reactor Analysis Code (TRAC) is an advanced systems code for light-water-reactor accident analysis. The code was developed originally to analyze large-break loss-of-coolant accidents (LOCAs) and running time was not a primary development criterion. TRAC-PF1 was developed because increased application of the code to long transients such as small-break LOCAs required a faster-running code version. Although developed for long transients, its performance on large-break transients is still important. This paper assesses the ability of TRAC-PF1 to predict large-break-LOCA Test S-06-3 conducted in the Semiscale Mod-1 facility.

INTRODUCTION

The Transient Reactor Analysis Code (TRAC) is an advanced systems code for light-water-reactor accident analysis. The original goal of the TRAC development effort was to provide a unified bench-mark systems code for the analysis of large-break loss-of-coolant accidents (LOCAs). Code adequacy was assessed by comparing predictions with an extensive experimental data base. As a bench-mark code, running time was not a primary concern for the relatively brief large-break-LOCA transients. However, recent emphasis has been placed on prediction of long transients such as small-break LOCAs. For such transients, a fast-running version, TRAC-PF1 [1], has been developed.

An experiment conducted in the Semiscale Mod-1 facility was selected as one element in the TRAC-PF1 developmental assessment program. Test S-06-3 [2] simulated the response of a pressurized water reactor (PWR) to a large-break LOCA. This paper reports the results of TRAC-PF1 predictions of Test S-06-3.

*Work performed under the auspices of the US Nuclear Regulatory Commission.

EXPERIMENTAL FACILITY

The Semiscale Mod-1 system [3] shown in Fig. 1 was a small-scale model of a four-loop PWR. The system included a pressure vessel with core simulator, upper and lower plenums, and downcomer; an intact loop with steam generator, pump, and pressurizer; a broken loop with simulated steam generator and simulated pump; coolant injection accumulators; high- and low-pressure coolant-injection pumps; and a pressure-suppression system with a suppression tank, header, and heated steam supply system. The Mod-1 core contained 40 rods, including 36 active rods that yielded a total core power of 1.004 MW.

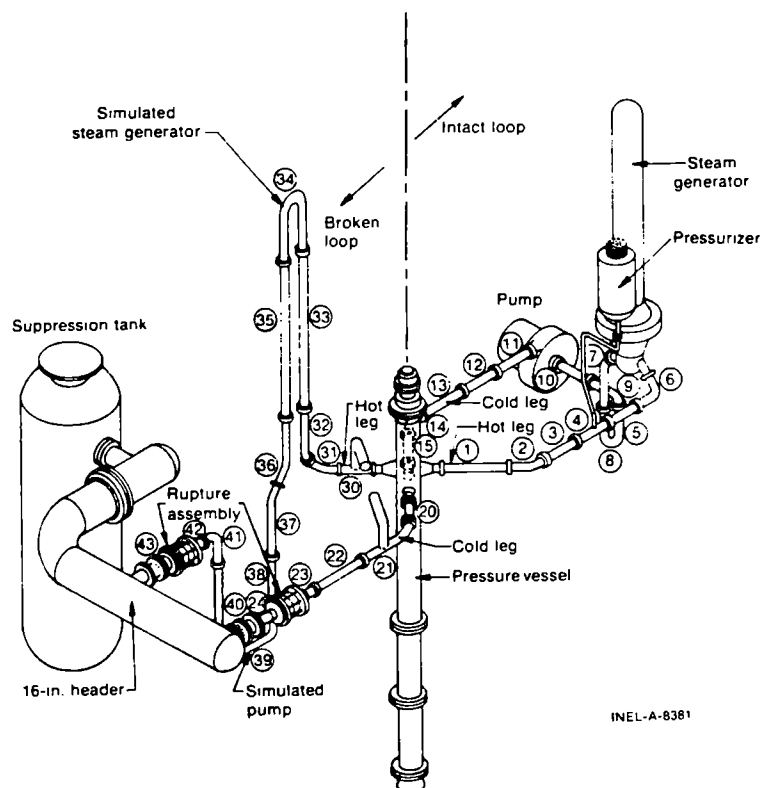


Fig. 1.
Semiscale Mod-1 system for cold-leg-break configuration - isometric.

TRAC MODEL

The TRAC model of the Semiscale Mod-1 facility (Fig. 2) generally corresponds to the hardware configuration. The two primary coolant loops, associated piping, and the test vessel are simulated. Although TRAC-PF1 can model a three-dimensional vessel, all system elements were modeled as one-dimensional components to assess their utility in large-break calculations. The elements used to develop the TRAC-PF1 input model are identified in Table I. The model deviates from the hardware in the following respects:

1. the inlet annulus and downcomer that are inside the pressure vessel are modeled as one-dimensional elements outside the test vessel and
2. the facility containment system is not modeled directly but is represented by a break component with the containment pressure history specified.

The core is divided into eight vertical levels. An average- and a high-power rod are modeled at each core level. The hot- and cold-leg breaks are modeled as finely noded pipe components.

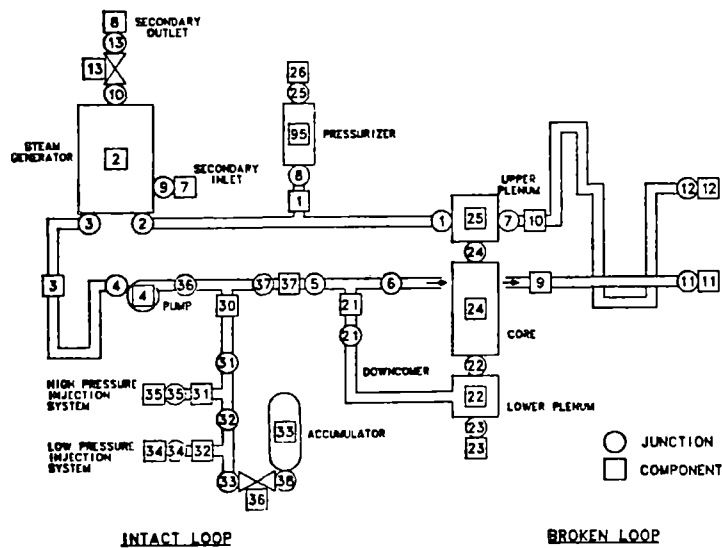


Fig. 2.
TRAC model of Semiscale Mod-1 facility.

TABLE I
System Model Components
Transient Calculation

<u>Component Number</u>	<u>Component Type</u>	<u>Description</u>	<u>Number of Fluid Cells</u>
1	TEE	Intact-loop hot leg	6,5
2	STGEN	Intact-loop steam generator	22,12
3	PIPE	Intact-loop pump suction	6
4	PUMP	Intact loop pump	2
7	FILL	Intact-loop steam-generator feedwater	1
8	BREAK	Intact-loop secondary-pressure set point	1
9	PIPE	Broken-loop cold leg	18
10	PIPE	Broken-loop hot leg	34
11	BREAK	Broken-loop suppression-system set point	1
12	BREAK	Broken-loop suppression-system set point	1
13	VALVE	Intact-loop steam line	2
21	TEE	Downcomer inlet annulus and downcomer	1,7
22	TEE	Downcomer and lower vessel plenum	4,1
23	FILL	Bottom of vessel	1
24	CORE	Vessel core	8
25	TEE	Vessel upper plenum	1,1
26	FILL	Top of pressurizer	
30	TEE	Intact-loop cold leg	1,1
31	TEE	HPIS piping	2,1
32	TEE	LPIS piping	21
33	ACCUM	Intact-loop accumulator	3
34	FILL	LPIS boundary condition	1
35	FILL	HPIS boundary condition	1
36	VALVE	Accumulator valve	2
37	PIPE	Intact-loop cold leg	1
95	PRIZER	Pressurizer	12

ASSESSMENT RESULTS

Steady-state conditions immediately before blowdown initiation were calculated using TRAC-PF1. Table II lists the measured and calculated conditions at blowdown initiation. The largest calculated deviation was the intact-loop cold-leg volumetric flow that exceeded the measured value by ~4.5%. The higher flow rate resulted from matching the hot-leg temperature closely.

Figure 3 compares the calculated and measured system pressures. During the blowdown phase the calculated system pressure decayed more rapidly than the measured system pressure. The influence of a finely noded representation was investigated by modeling the breaks with a critical-flow model using coarse noding. The changes in calculated system pressure decay during blowdown were minor. The emergency core-cooling accumulators, which were tripped on system pressure, were activated at 16.07 s. This was ~2.5 s earlier than measured in the test.

The loop mass flows generally were well calculated by TRAC-PF1. Figure 4 compares the intact-loop mass flows through the pump. The calculated flow decayed ~1 s earlier than measured and became zero at 25 s. A small residual flow was measured throughout the blowdown phase of the test. The comparison between the calculated and measured broken-loop cold-leg entrance mass flows (Fig. 5) is excellent. The calculated and measured core inlet mass flows are compared in Fig. 6.

TABLE II

Test S-06-3 Initial Conditions

	<u>Experiment</u>	<u>Calculation</u>
Core power (MW)	1.004	1.004 ^a
Intact-loop cold-leg fluid temperature (K)	563.	562.1
Hot-leg to cold-leg temperature differential (K)	34.1	34.1
Pressurizer pressure (MPa)	15.769	15.769 ^a
Pressurizer liquid mass (kg)	9.09	9.27
Steam-generator feedwater temperature (K)	497.	497. ^a
Fluid temperature in broken loop on the pump side (K)	562.	562. ^a
Fluid temperature in broken loop on the vessel side (K)	591.	591. ^a
Intact-loop cold-leg flow (l/s)	6.68	6.98

^aSpecified as input parameter to steady-state calculation.

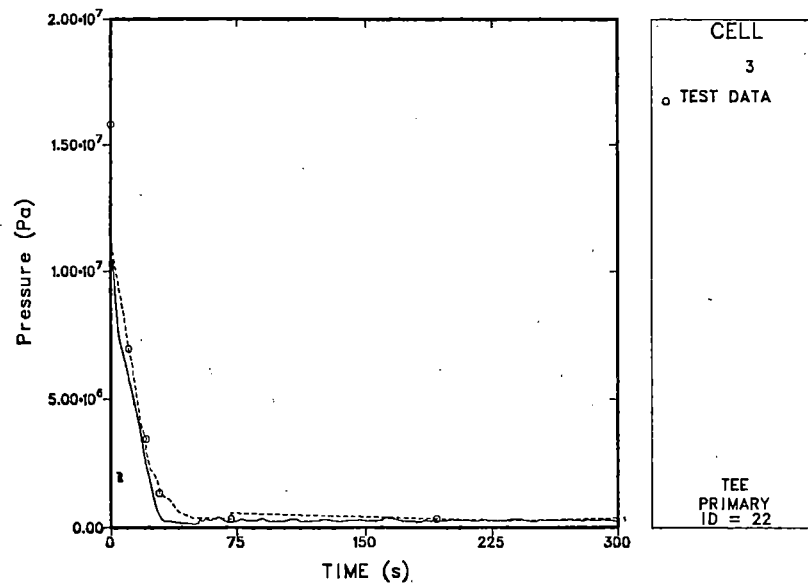


Fig. 3.
Calculated and measured system pressures.

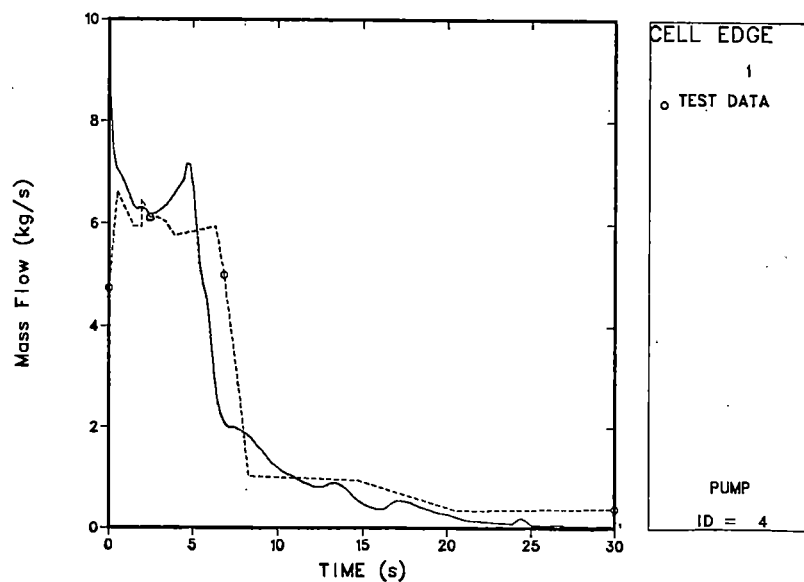


Fig. 4.
Calculated and measured intact-loop pump mass flows.

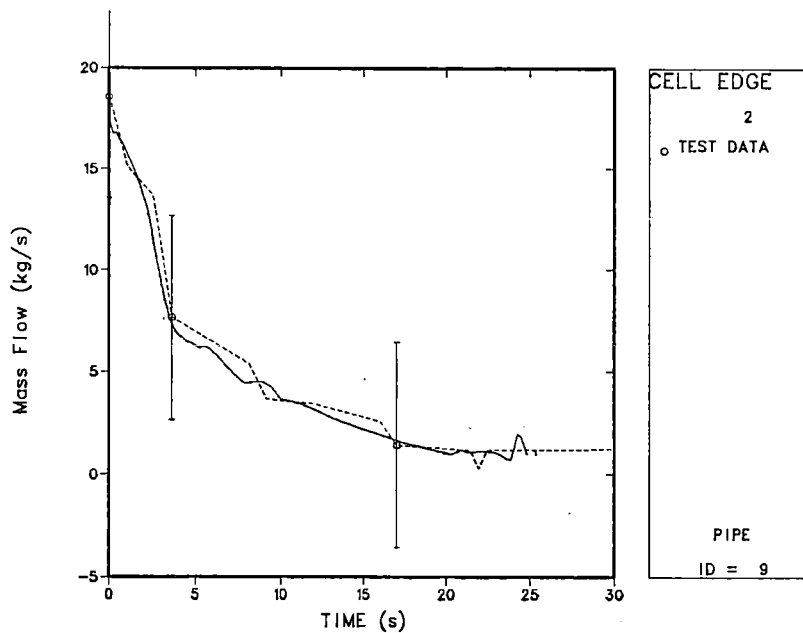


Fig. 5.
Calculated and measured broken-loop cold-leg entrance mass flows.

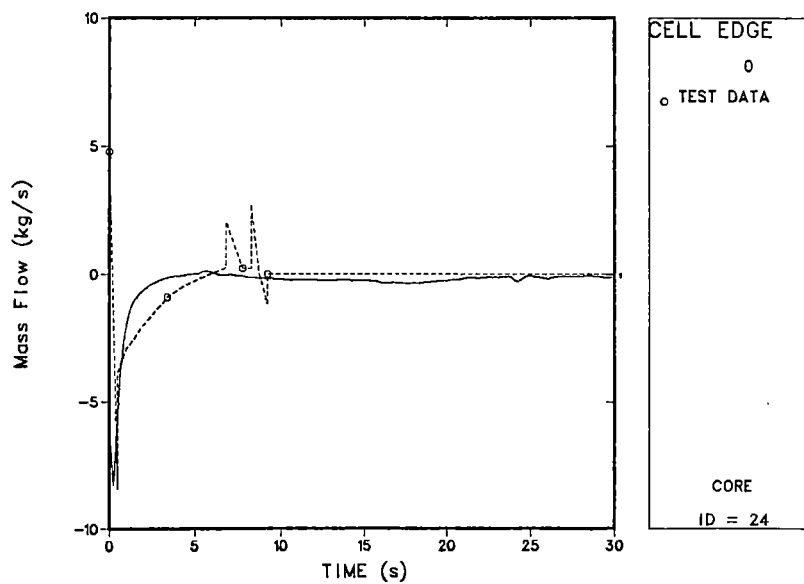


Fig. 6.
Calculated and measured core inlet mass flows.

Within the first second following blowdown initiation, a sharp flow reversal at the core inlet was measured and calculated. The core inlet flow approached zero at ~6 s; the calculated flow decayed more rapidly than the measured. A surge of fluid upward into the core was measured but not calculated between 7 and 10 s.

Figure 7 compares the rod cladding temperature histories at a level near the middle of the heated core. TRAC-PF1 overpredicted the maximum cladding temperature by 125 K. The measured rate of cladding temperature increase during the first 10 s of the blowdown was reduced by the upward flow surge into the core between 7 and 10 s. The excess temperature rise calculated by TRAC-PF1 was a direct consequence of the failure to predict the brief surge flow through the core. A quench was not calculated at 300 s, whereas the measured quench occurred at ~180 s. After reviewing the predicted quenching temperature at all core levels, it was concluded that the wall temperature used in TRAC-PF1 to define the boundary between the transition and film boiling regimes in the boiling curve may be too low. A sensitivity study was conducted by varying the expression that defines the homogeneous nucleation temperature used in calculating the transition wall temperatures. For the study, the homogeneous nucleation temperature was specified at a constant, the saturation temperature at the critical pressure (647.3 K). The predicted time of cladding quenching (Fig. 7) improved markedly, which suggests that further study of the correlation for the homogeneous nucleation temperature is needed.

In an earlier study [4], predictions of Test S-06-3 made with a previous TRAC version, TRAC-PD2, were assessed. In general, the predictions were quite similar. However, TRAC-PD2 calculated the core heatup and cladding quenching phenomena better. A comparison of running times of the code versions revealed an even more significant feature. The CDC-7600 central-processor-unit (CPU) time required to calculate the first 200 s of the Test-S-06-3 transient using TRAC-PF1 was 3211 s; using TRAC-PD2, 19020 s. Thus, TRAC-PF1 is approximately a factor of 6 faster in calculating large-break transient Test S-06-3.

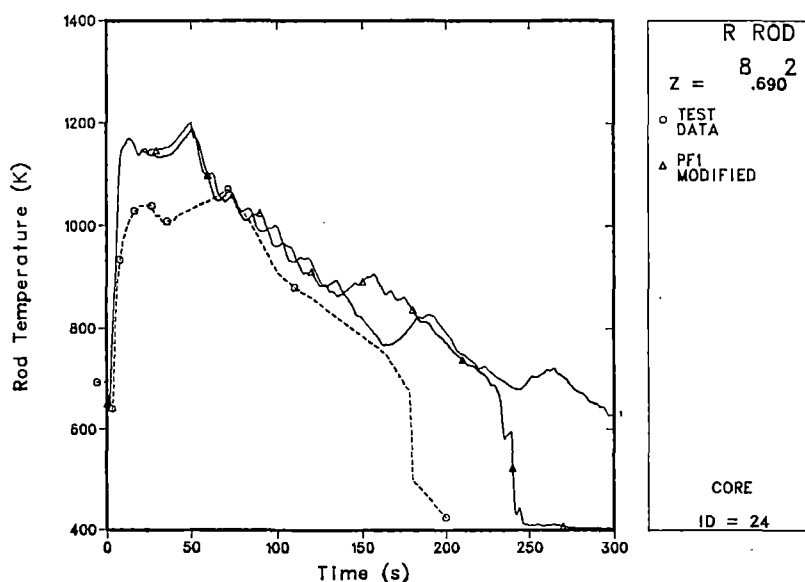


Fig. 7.
Calculated and measured cladding temperatures at mid core.

CONCLUSIONS

A posttest study of Semiscale large-break-LOCA Test S-06-3 has been completed to assess TRAC-PF1 predictions of these transients. In general, TRAC-PF1 predicted the transient well. During the blowdown phase the system pressure was underpredicted. Loop mass flows were predicted well. Quenching of the rod cladding was predicted to occur much later than measured. A parametric study was conducted and the minimum stable film-boiling temperature was increased. A marked improvement in the predicted time of quenching resulted. The results showed that TRAC-PF1 calculated the transient about as well as TRAC-PD2. However, TRAC-PF1 calculated the transient in ~17% of the time. Thus, TRAC-PF1 offers significant improvement in calculation time not only for small-break but also for large-break transients.

REFERENCES

1. J. H. MAHAFFY, D. R. LILES, and T. F. BOTT, "TRAC Methods and Models," Proceedings of the American Nuclear Society Specialists Conference on Small Break Loss-of-Coolant Accident Analyses in LWRs, Monterey, California (August 25-27, 1981), Report WS-81-201, Electric Power Research Institute report (1981).
2. B. L. COLLINS, et al., "Experimental Data Report for Semiscale Mod-1 Test S-06-3 (LOFT Counterpart Test)," Report NUREG/CR-0251, EG&G Idaho, Inc. (July 1978).
3. E. M. FELDMAN and D. J. OLSON, "Semiscale Mod-1 Program and System Description for the Blowdown Heat Transfer Tests (Test Series 2)," Report ANCR-1230, EG&G Idaho, Inc. (August 1975).
4. "TRAC-PD2: An Advanced Best-Estimate Computer Program for Pressurized Water Reactor Loss-of-Coolant Accident Analysis," Report LA-8709-MS, NUREG/CR-2054, Los Alamos National Laboratory, (April 1981).

COBRA/TRAC ANALYSIS OF THE PKL REFLOOD TEST K9

C. A. Wilkins and M. J. Thurgood

Pacific Northwest Laboratory
Richland, Washington

ABSTRACT

Experiments at the Primärkreisläufe (PKL) test facility in Erlangen, Germany, simulated the refill and reflood period following a loss-of-coolant accident (LOCA) in the primary coolant system of a 1300-MW pressurized water reactor (PWR). COBRA/TRAC, a thermal-hydraulics analysis code developed at the Pacific Northwest Laboratory, was used to model experiment K9 of the PKL test series. The COBRA/TRAC code, which utilizes COBRA-TF as the vessel module and TRAC-P1A for the remaining components, was designed to analyze LOCAs in PWRs. PKL-K9 was characterized by a double-ended guillotine break in the cold leg with emergency core cooling water injected into the intact cold legs. COBRA/TRAC was able to successfully predict lower-core temperature profiles and quench times, upper-core temperature profiles until the quench, upper plenum and break pressures, and correct trends in collapsed water levels.

INTRODUCTION

The COBRA-TF computer code [1] has been developed at the Pacific Northwest Laboratory [2] as part of the NRC Water Reactor Safety Research Program. COBRA-TF has been implemented into TRAC-P1A [3] as the vessel module. The resultant code, COBRA/TRAC, is used to analyze loss-of-coolant accidents (LOCAs) in Pressurized Water Reactors (PWRs). This paper reports the application of COBRA/TRAC to a gravity feed, bottom reflood experiment conducted at the Primärkreisläufe (PKL) test facility at Erlangen, Germany. Test K9 was chosen for comparison with COBRA/TRAC predictions. Test K9 is the German standard problem No. 2.

COBRA-TF uses a three-dimensional, three-field representation of two-phase flow. The three fields are the vapor, continuous liquid, and droplet fields. This model allows thermal nonequilibrium between the vapor and liquid phases, and each field is allowed to move with a different velocity. One can, therefore, treat mechanistically a continuous liquid core from which liquid drops are removed and carried away by the vapor phase. This is a cardinal feature of the reflood hydrodynamics during a loss-of-coolant accident. Other strengths of the COBRA/TRAC code include flexible noding, which accommodates complex geometries, and a fine-mesh rezoning fuel rod model. The latter can automatically decrease the rod heat transfer mesh size to resolve the boiling curve in the quench front region or increase the mesh size in low-heat-flux regions.

DESCRIPTION OF EXPERIMENT

The PKL test facility was designed to model the thermal-hydraulic behavior of a 1300-MW PWR. The main components of the facility include a cylindrical vessel [approximately 8.89 m (30 ft) high and 0.489 m (1.6 ft) in diameter], an external pipe downcomer [1.2 m (0.66 ft) in diameter], and three primary coolant loops (one with double capacity). Each coolant loop contained a U-tube steam generator and a cold-leg pump simulator with an orifice plate to model the rotor resistance.

The pressure vessel contained 340 simulated fuel rods, of which 337 were electrically heated. These were arranged in three concentric, separately heated regions to accommodate a radial power profile (Figure 1). The PKL-K9 experiment, however, had uniform radial power and a stepped cosine axial power profile. Upper and lower plenums with their associated internal components were also present.

A separate pipe downcomer was attached to the vessel at the lower plenum. The hot leg of each coolant loop connected the upper plenum to a steam generator. The intact loop piping extended from the steam generator through a pump resistance to the top of the downcomer. In the broken loop, the hot leg proceeded through the rotor resistance and terminated in a pressurized containment tank (4.2 bar initially). The downcomer side of the double-guillotine break was also attached to the pressurized containment tank, which was partially filled with saturated water. Emergency core cooling (ECC) water was injected into the cold legs as well as directly into the top of the downcomer. Before test initiation, the entire system was purged with steam. The secondary sides of the steam generators were filled with water to 7.5 m (24.6 ft). Initial flows in the system were zero. The initial vessel pressure was set to the specified pressure

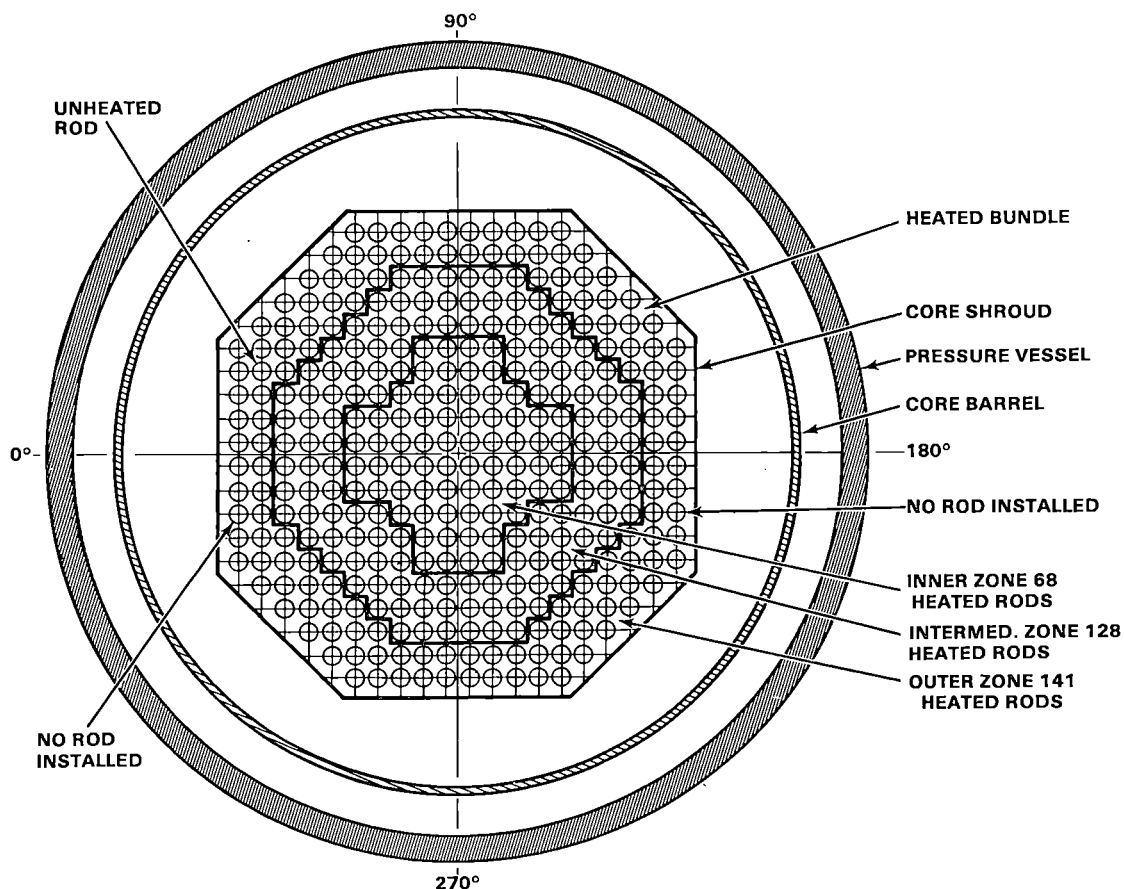


Figure 1. Arrangement of Rods Within the Pressure Vessel

at 4.6 bars. The transient was initiated by venting the containment vessel, resulting in a depressurization of the system, and by injecting ECC water.

COBRA/TRAC MODEL

The COBRA/TRAC model of the experiment used the COBRA-TF vessel module for the vessel and downcomer and TRAC-PLA one-dimensional modules for the remaining components and pipes. A COBRA/TRAC system component schematic for PKL-K9 is illustrated in Figure 2.

Figure 3 illustrates the one-dimensional noding used in the vessel and downcomer. The numbers in Figure 3 correspond to the channel numbers used to model each part of the vessel. A channel is simply a vertical stack of computational mesh cells. Channel 1 represents the volume of the lower plenum, and Channel 2 is the fluid volume of the lower core support plate region of the vessel. The core fluid volume is

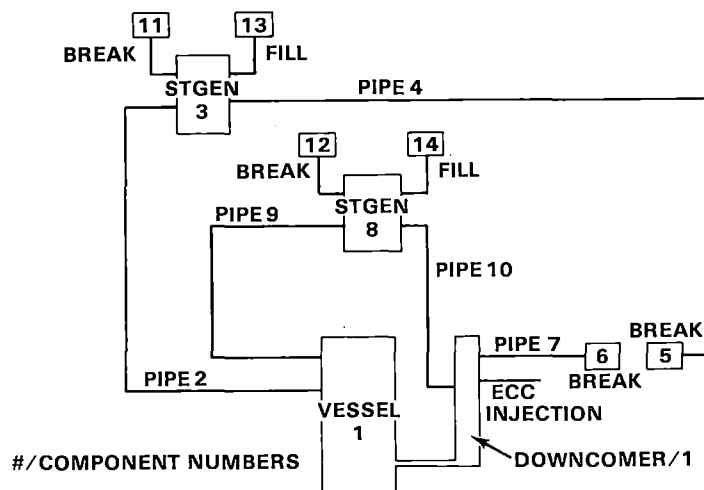


Figure 2. COBRA/TRAC Model of Test PKL-K9

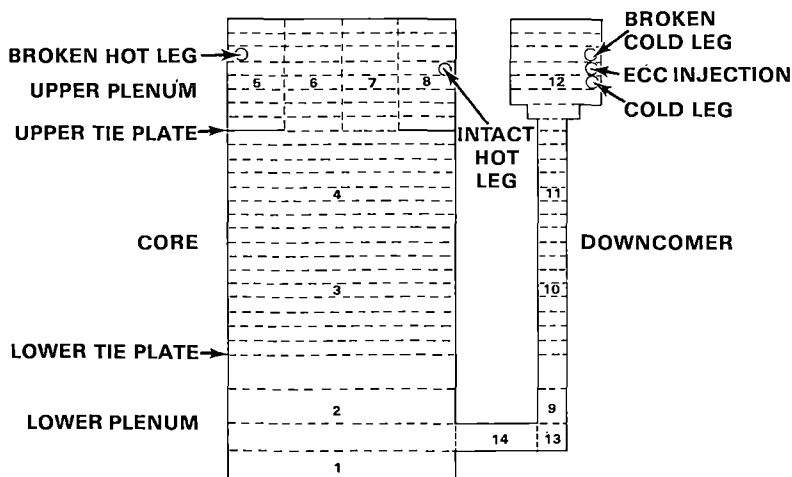


Figure 3. Vessel Mesh for Test PKL-K9

represented by Channels 3 and 4. Channels 5 and 8 in the upper plenum represent the fluid volume directly above the solid portions of the upper core tie plate, and Channels 6 and 7 represent the fluid volume directly above the holes in the upper tie plate. Channels 7 and 8 represent the fluid volume most directly associated with the intact loop hot legs, and Channels 5 and 6 represent the volume associated with the broken loop hot leg. The sum of the areas for Channels 6 and 7 is equal to the total flow area through the upper tie plate, and the hydraulic diameter of these channels is equal to the hydraulic diameter of a single tie plate hole. This mesh arrangement is used to obtain a reasonable estimate of velocity and void profiles between the area above the solid portion of the tie plate and the holes in the tie plate. This is essential to the correct prediction of countercurrent flow limiting (CCFL) at the upper tie plate. CCFL may be important if liquid fallback from the upper plenum to the core should occur. Liquid accumulates in the upper plenum as a result of de-entrainment of liquid drops carried over from the core during the reflood process.

Channels 13 and 14 represent the horizontal length of the downcomer pipe that connects the downcomer to the lower plenum. The downcomer is represented by Channels 9 through 12 with Channel 12 being the expanded portion at the top of the downcomer to which the cold legs are attached. The solid structure of the vessel and downcomer are represented with heat slabs, and the core is represented by a single rod having the average power generation rate and temperature of the core. This rod is connected to Channels 3 and 4 and has a heated length of 3.9 m (12.67 ft).

The three coolant loops of PKL-K9 were modeled in COBRA/TRAC with two loops using equivalent volumetric dimensions. The broken cold leg (pipe 7) and the cold return (pipe 4) from steam generator 3 were connected to break components 6 and 5, respectively. These break components modeled the break pressure history described in the PKL documents [4,5,6]. The intact cold leg (pipe 10), ECC injection, and broken cold leg (pipe 7) were connected to the downcomer at nodes 4, 5, and 6 of Channel 12, as illustrated in Figure 3.

RESULTS

The computer simulation was initiated by setting liquid levels, pressures, and temperatures as specified for the experiment, specifying the containment pressure as a function of time, and injecting ECC water at the specified rate into the top of the downcomer and cold legs.

The injection of cold ECC water into the downcomer immediately overpowered the blowdown by condensing all of the steam available in the vessel. This resulted in a very rapid drop in vessel pressure down to the containment pressure. When the vessel pressure dropped to the containment pressure, condensation was shut off in the calculation since it was assumed that air would flow in from the containment once the vessel pressure dropped below the containment pressure. The measured pressure for the upper plenum (Figure 4) indicates that the vessel pressure did indeed drop below the containment pressure, indicating that perhaps steam rather than air entered the vessel from the containment, allowing further depressurization of the vessel by condensation. This further depressurization was not predicted by the code since condensation was shut off whenever the vessel pressure fell below the containment pressure. This large pressure decrease does not appear in the break pipe pressure (Figure 5), indicating that the break pipe is essentially at the containment pressure.

As liquid from the downcomer filled the lower plenum and lower core support plate regions, bringing water into contact with the bottom of the core, quenching of the bottom of the fuel rods resulted in large vapor generation rates that overpowered the condensation rate in the downcomer and increased the vessel pressure back up above the containment pressure. This occurred at about 24 seconds. From this point on, the

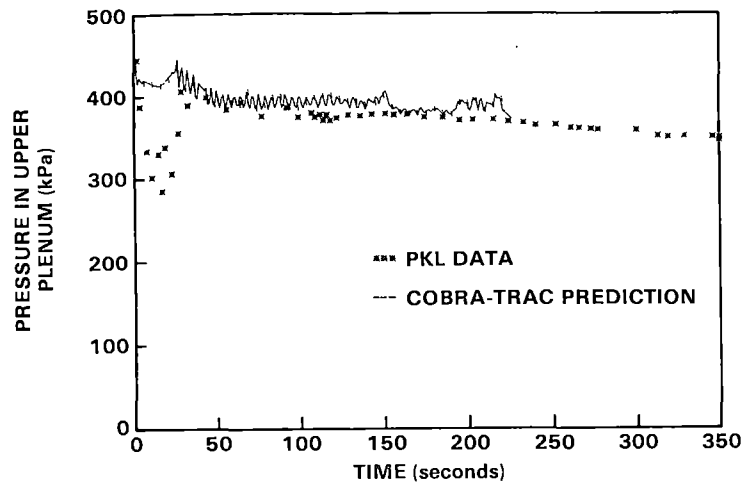


Figure 4. Upper Plenum Pressure Channels 5-8

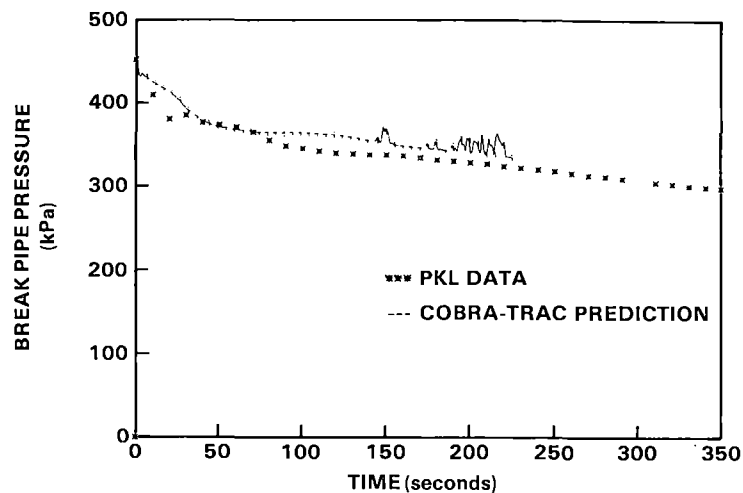


Figure 5. Break Pipe Pressure

predicted pressures are in reasonable agreement with the measured pressures. The pressures are slightly overpredicted, indicating an overprediction of pressure drop through the broken legs. This could be caused by higher predicted vapor flows or by higher loss coefficients than those in the actual experiment.

Flow during the reflood period was as follows. Water flowed from the downcomer into the lower plenum. From here water entered the core where it was carried over, either in the form of steam generated as a result of the heat transfer processes in the core or in the form of liquid drops entrained in the vapor flow. Some of the liquid drops were de-entrained in the upper plenum as a result of interaction with the upper plenum internal components. The steam flowed through the hot legs. Steam flowing through the broken hot leg passed through the steam generator and the pump simulator and entered the containment. Steam flowing through the intact hot leg flowed through the intact loop steam generator and pump simulators into the intact cold leg. Here some of the steam was condensed by the cold ECC water before it entered the top of the downcomer where further condensation took place. Steam not condensed in the cold leg or downcomer flowed out through the broken cold leg, carrying some saturated water with it.

Once reflood began, the back pressure (caused by steam flow through the upper plenum and the intact and broken loops) limited the rate at which water could enter the core. This caused the ECC water to back up into the downcomer pipe and fill the downcomer up to the cold leg level. Any excess water was carried out through the broken cold leg by the steam flow.

Flow oscillation driven by heat transfer processes in the core and the liquid head of the downcomer were computed to occur throughout the test. This oscillatory flow is evident in the core collapsed liquid level as a function of time (Figure 6). Oscillations were also measured; however, the magnitude of the measured oscillations appears to diminish in time while the computed magnitude continues at a nearly constant rate. This indicates that transitions in heat transfer or two-phase flow regimes used in the code may not be exactly correct, leading to an overprediction of core reflood oscillation magnitudes and duration. Collapsed water level predictions showed fairly good agreement with the PKL-reported data, but after 150 seconds the calculated water level appeared to be low.

Cladding temperature profiles at several elevations in the core are shown in Figures 7 through 11. Peak cladding temperatures occur about 25 seconds after the start of the transient. At this time, the lower plenum was full and the bottom of the core was beginning to reflood. Quench front propagation through level 4 (~2.0 m or ~6.4 ft) was fairly well predicted by COBRA/TRAC. Above level 4, the code underpredicted the heat transfer associated with top-down quenching. A plot of the quench front envelope is shown in Figure 12.

The predicted temperature profiles for the lower half of the core showed excellent agreement with the reported data. The quench times showed good agreement also. The quench front in the upper half of the core was not correctly predicted; however, COBRA/TRAC was able to predict the temperatures well until the time at which the quench occurred. The lack of a top quench indicates that the top quench front propagation is not being computed correctly by the code. Improved models for top quenching are currently being developed.

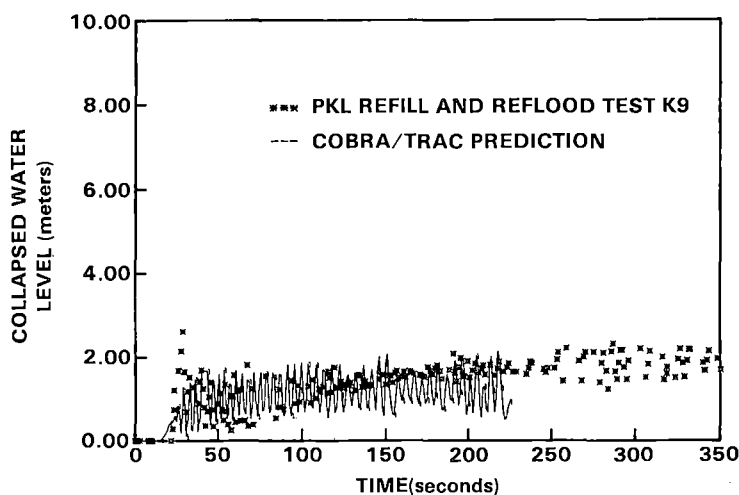


Figure 6. Core Collapsed Water Level

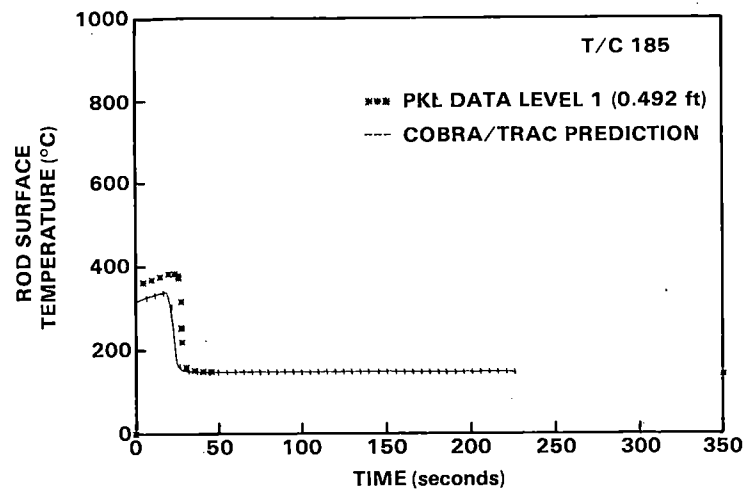


Figure 7. Rod Surface Temperature at Core Level 1 (0.492 ft)

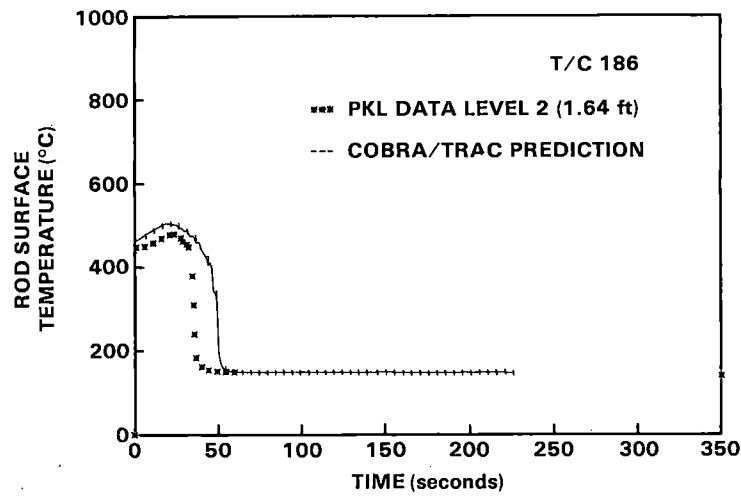


Figure 8. Rod Surface Temperature at Core Level 2 (1.64 ft)

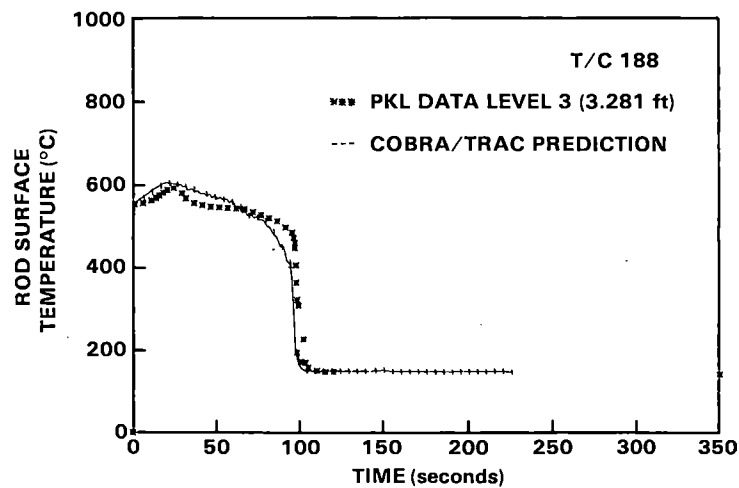


Figure 9. Rod Surface Temperature at Core Level 3 (3.281 ft)

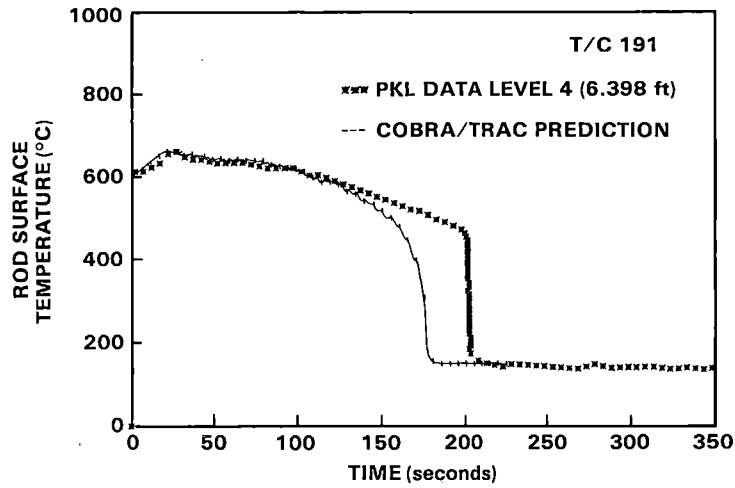


Figure 10. Rod Surface Temperature at Core Level 4 (6.398 ft)

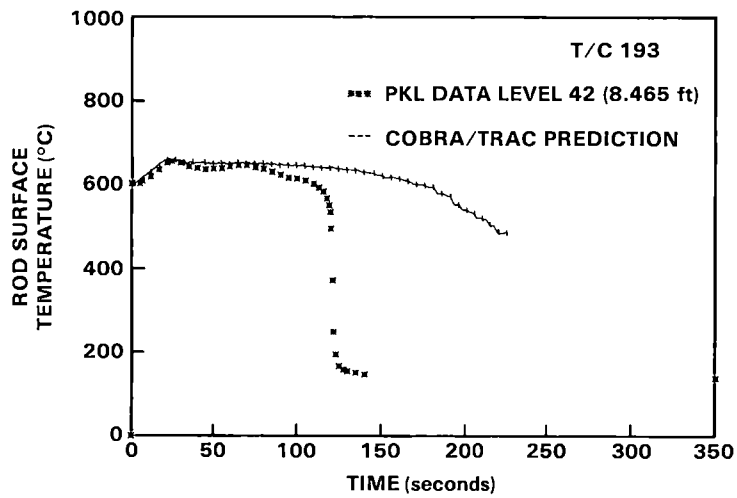


Figure 11. Rod Surface Temperature at Core Level 42 (8.465 ft)

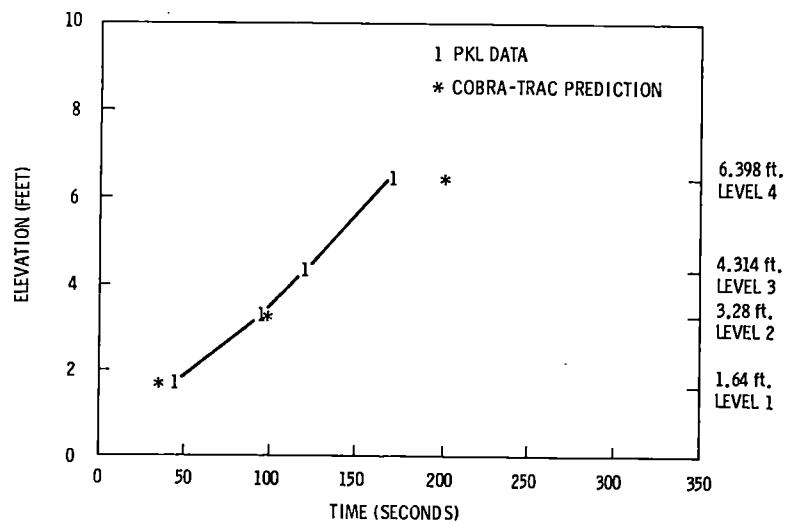


Figure 12. Quench Front Envelope

CONCLUSIONS

COBRA/TRAC predicted the temperature profiles well for PKL Test K9 in the lower half of the core. It had difficulty with quench front propagation in the upper half of the core because the falling-film heat transfer was not correctly modeled. The falling-film heat transfer model has been significantly improved in a more recent version of COBRA/TRAC. Predicted upper plenum pressure, break pressure, and collapsed water level in the core were fairly well in line with the measured data. Reflood oscillations are probably overpredicted in both magnitude and duration and need to be investigated further.

The COBRA/TRAC code used 5.8 CPU hours on a CDC-7600 to calculate the 229.6 seconds of the transient. The code used an average simulation time step of 0.00539 second. A more useful measure of the code calculational efficiency is given by the ratio of the CPU time per time step per mesh cell. For this model, the ratio was 6 msec per time step per mesh cell.

ACKNOWLEDGMENT

This paper is an account of work performed by the Pacific Northwest Laboratory for the U.S. Nuclear Regulatory Commission under a Related Services agreement with the U.S. Department of Energy, Contract DE-AC06-76RLO 1830.

REFERENCES AND ANNOTATIONS

1. M. J. THURGOOD, J. M. KELLY, K. L. BASEHORE and T. L. GEORGE, "COBRA-TF, A Three-Field Two-Fluid Model for Reactor Safety Analysis," in HTD-Vol. 7, Experimental and Analytical Modeling of LWR Safety Experiments, L. E. Hochreiter and G. L. Suzzi, eds., American Society of Mechanical Engineers, New York, New York (1980).
2. The Pacific Northwest Laboratory is operated for the U.S. Department of Energy by Battelle Memorial Institute.
3. D. R. LILES et al., "TRAC-PLA, An Advanced Best-Estimate Computer Program for PWR LOCA Analysis," Report NUREG/CR-0665 (also LA-7777-MS), prepared for the U.S. Nuclear Regulatory Commission by Los Alamos Scientific Laboratory, Los Alamos, New Mexico (1979).
4. B. BRAND, R. MANDL and H. SCHMIDT, "PKL Refill and Reflood Experiment Selected Results from Test K9," Report R51/22/79, Kraftwerk Union (1979).
5. B. BRAND, R. KIRMSE and W. WINKLER, "Refill and Reflood in a Simulated PWR Primary System (PKL)," Specification OECD-CSNI LOCA Standard Problem No. 10, Report R513, Kraftwerk Union (1979).
6. R. E. KIRMSE, "Status of PKL Activities," presented at the 6th Meeting of the CSNI Working Group on Emergency Core Cooling in Water Reactors, Idaho Falls, Idaho, October 1-3 (1979).

THE EMERGENCY CORE COOLING FUNCTION OF
THE MODERATOR SYSTEM IN CANDU REACTORS

C. Gordon and C. Blahnik
Nuclear Studies and Safety Department
Ontario Hydro, Toronto, Canada

ABSTRACT

The moderator in the CANDU design provides an alternate heat sink capable of removing decay heat and maintaining fuel temperatures well below the UO_2 melting temperature, even when the unlikely event of a loss-of-coolant combined with a failure of the emergency coolant injection system is postulated. The role of the moderator and the analysis and experimental basis for the assessment of the emergency core cooling function of the moderator are described. This capability is unique to CANDU-type reactors and contributes to the assurance that the public health risk from operation of CANDU reactors is small.

INTRODUCTION

Heavy-water-moderated pressure-tube reactors are in commercial use for production of nuclear electric power in several countries. Ontario Hydro has an installed capacity of about 5000 MWe and a further 8500 MWe under construction, the majority in the form of CANDU multi-unit generating stations.

The CANDU reactor employs a large number of horizontal fuel channel assemblies surrounded by heavy water moderator within the calandria vessel (Figure 1). The fuel channel assembly provides the pressure boundary between the high-pressure heat transport system and the low-pressure moderator system. They are supported at each end by the calandria/shield tank structure.

The horizontal fuel channel (Figure 2) consists of Zr - 2.5% Nb alloy pressure tubes (about 10 cm inside diameter) rolled into the hub of an alloy steel end-fitting at each end. Each assembly is supported by the end shield structure through a sliding journal/bearing arrangement and partially by the calandria tube/pressure tube annular spacers (garter springs). The end fitting assemblies allow relative axial movement to accommodate thermal expansion, creep and irradiation growth of pressure tubes. The zirconium alloy calandria tube is attached rigidly to the calandria vessel tubesheet, separating the pressure tube from the liquid moderator.

The fuel assembly (fuel bundle) consists of short (0.5 m), closely spaced fuel elements welded to two zirconium alloy end plates and separated from each other by brazed zirconium alloy spacers (Figure 3). The thin-wall (0.4 mm) zirconium alloy cladding is in intimate contact with fuel pellets throughout normal operation (collapsible cladding). The fuel bundle contains approximately 20 kg of natural uranium in the form of high-density sintered UO_2 pellets. The string of bundles in the fuel channel rests on the pressure tube, separated from it by zirconium alloy bearing pads, brazed to outer elements of the fuel bundle.

The fuel channels are arranged into loops, each containing pumps, steam generators, two inlet headers and two outlet headers (Figure 4). The channels are connected in parallel to the headers by feeder pipes to form two "core passes" in each loop. This arrangement provides bi-directional flow through the core such that flow is in opposite directions in adjacent channels. Under normal operating conditions, the heat generated in the fuel is removed by pressurized (~ 10 MPa) heavy water coolant. The coolant flowrate through individual fuel channels is approximately 25 kg/s, driven by a pressure gradient between inlet and outlet headers of about 1 MPa.

The main moderator system has been designed to provide sufficient cooling capacity to remove the maximum heat generated in the moderator during normal operation. It consists of two relatively independent circuits, each with a pump and heat exchanger, feeding a common supply header and draining water from the calandria (Figure 4). The moderator outlet temperature is controlled at the required temperature by controlling the service water flow through the moderator heat exchanger. An auxiliary circuit provides the necessary backup cooling under abnormal operating conditions.

CANDUs are equipped with three primary types of safety systems: shutdown, emergency coolant injection (ECI), and containment. The design of these are unique to the CANDU concept. Briefly, two independent shutdown systems are provided: (1) solid, neutron-absorbing shutoff rods which gravity-drop into the moderator, and (2) a liquid injection system which injects a neutron-absorbing liquid into the moderator through nozzles or injection pipes within the calandria vessel. The ECI system consists of high-pressure injection and low-pressure recovery portions. The containment system in multi-unit CANDU stations consists of a concrete structure forming the majority of the envelope; isolation devices to close off normally open penetrations; pressure relief valves, a large evacuated volume (vacuum building), and a dousing system within the vacuum building to suppress the initial pressure surge following a LOCA; and vault coolers and a filtered-air discharge system to maintain the containment pressure subatmospheric in the long term.

EMERGENCY CORE COOLING REQUIREMENTS

The capability of removing heat from fuel and fuel channels following interruption of normal cooling is referred to as the Emergency Core Cooling (ECC) function. This function is performed by a variety of systems with the objective of providing reliable heat removal to ensure that the regulatory dose limits are met for all postulated LOCA scenarios. In order to predict with confidence any resultant doses to the public, it is first necessary to predict the releases into containment. For practical reasons, to assure a conclusive analysis, a

derived requirement is imposed on the ECC: that fuel channel integrity be maintained. This requirement ensures that a demonstrable coolable geometry is achieved following the accident: In the long-term, this also ensures that water can be supplied into all the fuel channels.

There are two major heat removal systems available for emergency core cooling under LOCA conditions - the ECI system and the moderator. The use of the ECI system is preferred, since it minimizes damage to the reactor (economic consequences). It also minimizes airborne activity releases into containment by minimizing fuel sheath temperature excursions and by providing water along the activity transport path to "scrub" many fission products into solution. The moderator acts as a "standby" heat sink, available to supplement ECI heat removal, or, if necessary, provide heat removal if ECI fails.

Maintaining fuel channel integrity is a derived ECC requirement sufficient (along with containment) to meet the dose criteria imposed by the regulatory agency (AECB) for licensing. Ontario Hydro has also imposed a design target on the ECI system of preventing temperature induced fuel and fuel channel damage following a rupture in the heat transport system up to, and including, the size of the largest feeder. Because of the large amount of small diameter piping in CANDUs, such small LOCAs have a higher, although still low, predicted frequency of occurrence. This requirement is imposed by the utility to limit the economic consequences of these accidents, an approach reinforced by the TMI lesson.

Unimpaired ECI system performance is achieved when all components and supporting process systems function normally. However, the Canadian licensing process has always required analysis of LOCAs assuming both normal and impaired ECI system operation. This paper considers the latter case, which is analogous to a class 9 accident in the context of LWR licensing, during which the moderator can become the dominant heat sink.

THE MODERATOR AS AN ALTERNATIVE HEAT SINK

In a CANDU fuel channel, the fuel bundles and the primary coolant are separated from the pool of moderator by relatively thin pressure and calandria tubes (Figure 1). Under normal operating conditions, the heat transfer to moderator is small, governed by the low conductivity through the gas annulus between pressure and calandria tubes and a relatively low pressure tube temperature. Following some LOCAs, the flow of primary coolant may be disrupted sufficiently to result in a very rapid rise in fuel temperature. Without heat removal by the normal heavy water heat transport medium or the ECI coolant, the heat is transferred from the fuel to the pressure tube which in turn heats up. If the pressure tube temperature excursion is of sufficient magnitude and duration, the pressure tube deforms into contact with the surrounding calandria tube.

The mode of pressure tube deformation depends on the internal pressure. If the pressure is low, the pressure tube sags into contact under the weight of the fuel, at temperatures from about 850°C to about 1000°C. If the pressure is high, it expands radially (balloons) into contact at temperatures ranging from about 700°C to 1000°C.

Upon contact, the stored heat in the pressure tube is suddenly released, causing a peak in the heat flux at the surface of the calandria tube. The mode of heat transfer at the outer surface of the calandria tube is determined by the pressure-tube contact temperature, the contact conductance at the interface between the pressure and calandria tubes and the initial subcooling of the moderator. Figure 5 illustrates the relationship between these parameters, where the dashed lines are the predicted loci of conditions needed to initiate film boiling with different constant values of contact conductance between the pressure and calandria tubes.

Experiments have been performed at Whiteshell Nuclear Research Establishment of AECL^(1,2) jointly funded by AECL and Ontario Hydro, to study the coupled thermal-mechanical processes associated with a hot pressure tube ballooning into contact with a cool calandria tube, which is submerged in a pool of water. A summary of the results is shown in Figure 5. Heating rate, internal pressure and pool temperature were varied to get desired contact and heat-transfer conditions. The solid line denotes the boundary between nucleate-boiling and film-boiling heat transfer.

At lower contact temperatures ($\sim 850^{\circ}\text{C}$), which require high internal pressures to achieve a ballooning contact ($>1\text{ MPa}$), the maximum contact conductance is constant at about 11 kW/m^2 . With decreasing pressure, higher ballooning contact temperatures can be achieved, but these are accompanied by lower contact conductance. The net result is that the rate of heat release from the pressure tube remains constant or actually decreases with increasing contact temperature. A non-ballooning contact, such as sagging of a hot pressure tube under the weight of the fuel, is characterized by a low contact conductance; the release of heat is gradual rather than sudden, and only a minimum water subcooling is required around the calandria tube to avoid film boiling at the tube surface.

It can be seen from Figure 5 that departure from nucleate boiling (dryout) on the outer surface of the calandria tube can be prevented simply by maintaining sufficient moderator subcooling in the fuel channel region of the calandria vessel. The hot pressure tube then rapidly drops in temperature, regains its structural strength, and no further distortion of fuel channel occurs. Furthermore, an efficient heat transport path has been established for cooling of fuel within the fuel channel by heat rejection to the moderator.

Initially, the fuel transfers its heat to the pressure tube by radiation and by conduction through steam or hydrogen (note that convective heat transfer must be severely impaired in the first place to cause the geometry distortion of pressure tube). At some later stage, following the expansion of pressure tube and redistribution of steam flow in the channel, the fuel bundle may collapse, so that heat transfer within the fuel and from the fuel will have a large conduction component. The collapse (or slumping) of fuel bundle increases the rate of heat rejection to moderator; however, the heat fluxes at the surface of calandria tube are well below those associated with the pressure tube ballooning. The heat from fuel is rejected gradually, rather than suddenly, because the thermal properties of fuel are not conducive to rapid heat rejection. Thus, the collapse of fuel causes brief and minor temperature excursions in the contacting area of the ballooned channel; these excursions are insufficient to disrupt the nucleate boiling on the outer surface of calandria tube.

Figure 6 shows the ratio of peak heat flux (PHF) to the moderator and critical heat flux (CHF) at the surface of the calandria tube as a function of moderator subcooling and various assumed fuel collapse conditions. These calculations, which conservatively assumed an infinite contact heat conductance between the fuel surface and the pressure tube (to maximize heat rejection from fuel), show that calandria tube dryout does not occur for any realistic bundle slumping conditions, even at saturated moderator conditions. The bundle is expected to collapse well before the sheath melting temperature ($\sim 1850^{\circ}\text{C}$) is reached in the interior of fuel bundle, at which point the outward facing surfaces of fuel would be well below 1200°C . Thus, the fuel slumping conditions are expected to be in the shaded area of Figure 6. Experiments are in progress to study the collapse behaviour of CANDU fuel over a range of severe temperature excursions. The results to date support our current understanding of fuel temperatures at the time of collapse. Upon completion, these experiments will demonstrate the conservatism of above analyses which are based on fundamental physical principles.

The integrity of fuel channels can be assured even for the most severe LOCAs by maintaining the moderator temperatures at a sufficient level of subcooling to prevent the occurrence of dryout on the outside surface of calandria tube following pressure tube ballooning. It should be remembered that the pressure tube ballooning is the relevant deformation mechanism only in the early stages of certain LOCA scenarios when high temperatures combined with high internal pressures could possibly occur. It should also be noted that the prevention of dryout on the calandria tube is a sufficient, but not essential, condition for the maintenance of fuel channel integrity. Experiments have shown that fuel channels can withstand prolonged periods of widespread dryout (up to 8 minutes prior to rewet) at high internal pressure (up to 4 MPa) without failure.

In order to determine the most stringent subcooling requirement as a function of time following a LOCA, a methodology has been developed to derive the maximum possible pressure tube contact temperature at any time during a depressurization transient. This represents the bounding envelope to the range of possible contact temperatures. Similarly, the bounding envelope of minimum contact temperatures is derived and used to determine the maximum heat load to the moderator from ballooned channels. Figure 7 is an example of the largest subcooling requirement transient for a postulated LOCA scenario in which fuel channels void rapidly right at the start of the accident, and remain cooled only by a minute flow of steam for an indefinite period of time. The subcooling requirements rise as the decreasing system pressure makes possible a higher contact temperature, and then drops sharply when the system pressure drops to a level at which a uniform ballooning contact is no longer achievable.

Also shown in Figure 7 is the corresponding transient of minimum available subcooling (i.e. the subcooling in the hottest region of calandria vessel derived on the basis of largest conceivable moderator heat load). The available subcooling rises from the steady state values as the neutronic heat load decays and the moderator heat exchangers continue to operate.

Similar transients can be derived for a range of postulated LOCA scenarios, with and without postulated impairments of the moderator or ECI systems. On the basis of these analyses, operating conditions for

the moderator system are defined which provide sufficient subcooling in the calandria vessel to cool the fuel channel for the maintenance of fuel channel integrity even for the most severe postulated LOCA.

As shown above, it is possible to determine the minimum required moderator subcooling to avoid onset of calandria tube dryout for any postulated LOCA scenario. The inherent flexibility of the moderator system makes it possible to operate the system in such a way that sufficient subcooling is available even in the hottest region of the moderator pool. To quantify the capability of the moderator to act as a heat sink, detailed calculations of the spatial and temporal distribution of the moderator temperatures and local subcooling have been carried out and verified by experiment.

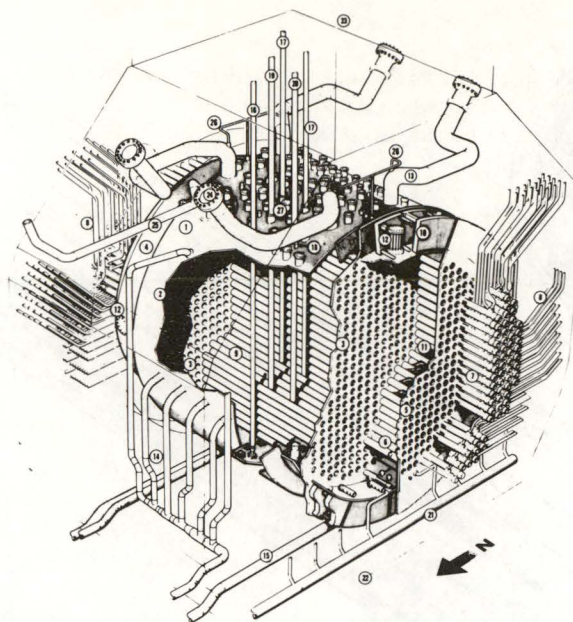
Figure 8 illustrates the average fuel temperatures in a channel with an initial power of 6.7 MW which was assumed to void immediately after a LOCA (with little of the fuel's stored energy removed during channel voiding) and thereafter cooled by a constant flow (25 g/s) of superheated steam (300°C). The reference curve represents the most likely consequence of this postulated scenario in which the pressure tube balloons into contact with its calandria tube at several axial locations, providing an efficient heat rejection path to the moderator. For the derivation of second curve, the heat rejection to moderator was disallowed in the computation. The role of moderator as an important heat sink is clearly evident.

SUMMARY

We have shown that inherent in the CANDU concept is an alternate heat sink capable of maintaining fuel channel integrity and of maintaining fuel temperatures well below UO_2 melting temperatures following a postulated loss-of-coolant accident followed by the failure of the emergency coolant injection system. The design of the moderator system allows changes in operating conditions such that sufficient subcooling in the calandria vessel can be provided to prevent calandria tube dryout. This capability is unique to CANDU-type reactors and contributes to the assurance of safe operation of this reactor type.

REFERENCES

- (1) G.E. Gillespie, "Experimental Investigation of Heat Transfer From A Reactor Fuel Channel to Surrounding Water", Proc CNS Annual Conference, June 10, 1981.
- (2) G.E. Gillespie, R.G. Moyer, P.D. Thompson, "Moderator Boiling On The External Surface Of A Calandria Tube In A CANDU Reactor During A Loss-of-Coolant Accident", (these proceedings).



- | | |
|--------------------------------------|------------------------------|
| 1 CALANDRIA | 15 MODERATOR OUTLETS |
| 2 CALANDRIA MAIN SHELL | 16 SHUT OFF UNIT |
| 3 CALANDRIA SIDE TUBESHEET | 17 ADJUSTER UNIT |
| 4 CALANDRIA SUB SHELL | 18 VERTICAL FLUX DETECTOR |
| 5 FUELLING MACHINE SIDE TUBESHEET | 19 CONTROL ABSORBER |
| 6 LATTICE TUBES | 20 LIQUID ZONE CONTROL UNIT |
| 7 END FITTINGS | 21 END SHIELD COOLING PIPING |
| 8 FEEDERS | 22 SHIELD TANK |
| 9 CALANDRIA TUBES | 23 SHIELD TANK EXTENSION |
| 10 SHIELD TANK SOLID SHIELDING | 24 RUPTURE DISC ASSEMBLY |
| 11 STEEL BALL SHIELDING (END SHIELD) | 25 MODERATOR OVERFLOW |
| 12 MANHOLE | 26 PRESSURE BALANCE LINES |
| 13 EMERGENCY DISCHARGE PIPES | 27 VIEWING PORT |
| 14 MODERATOR INLETS | |

FIGURE 1
REACTOR ASSEMBLY

35-1000-2
REV. 3 1961

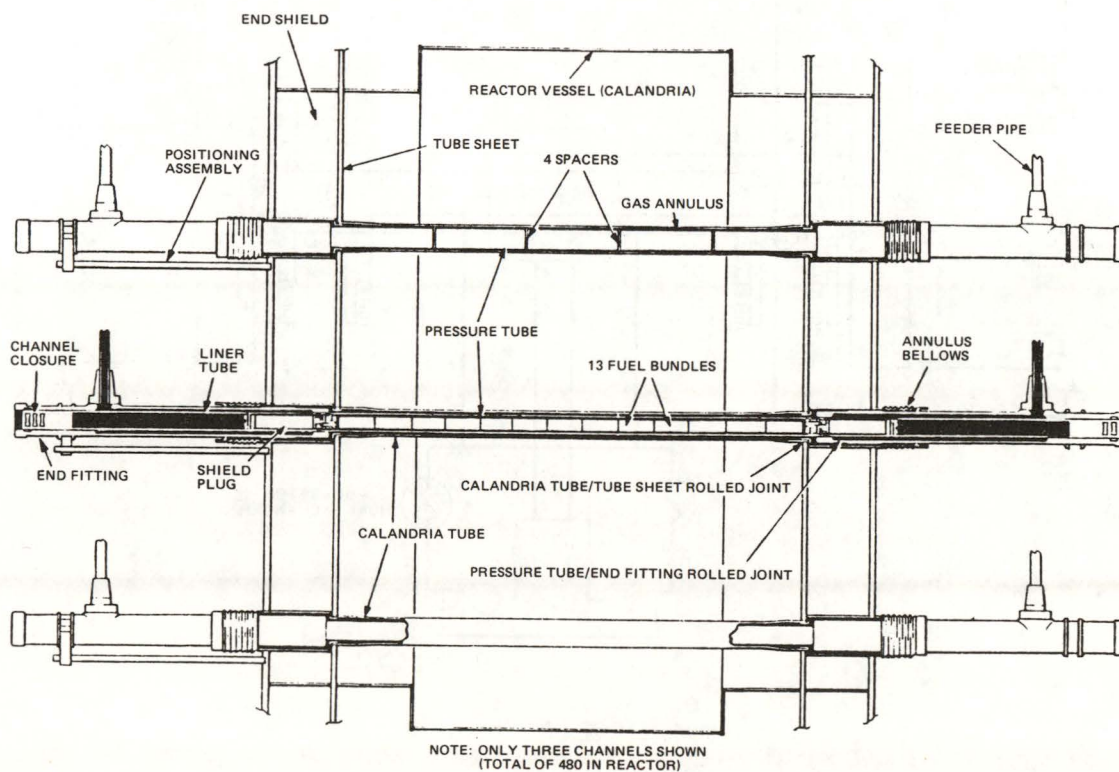


FIGURE 2
SIMPLIFIED DIAGRAM OF FUEL CHANNEL ASSEMBLY

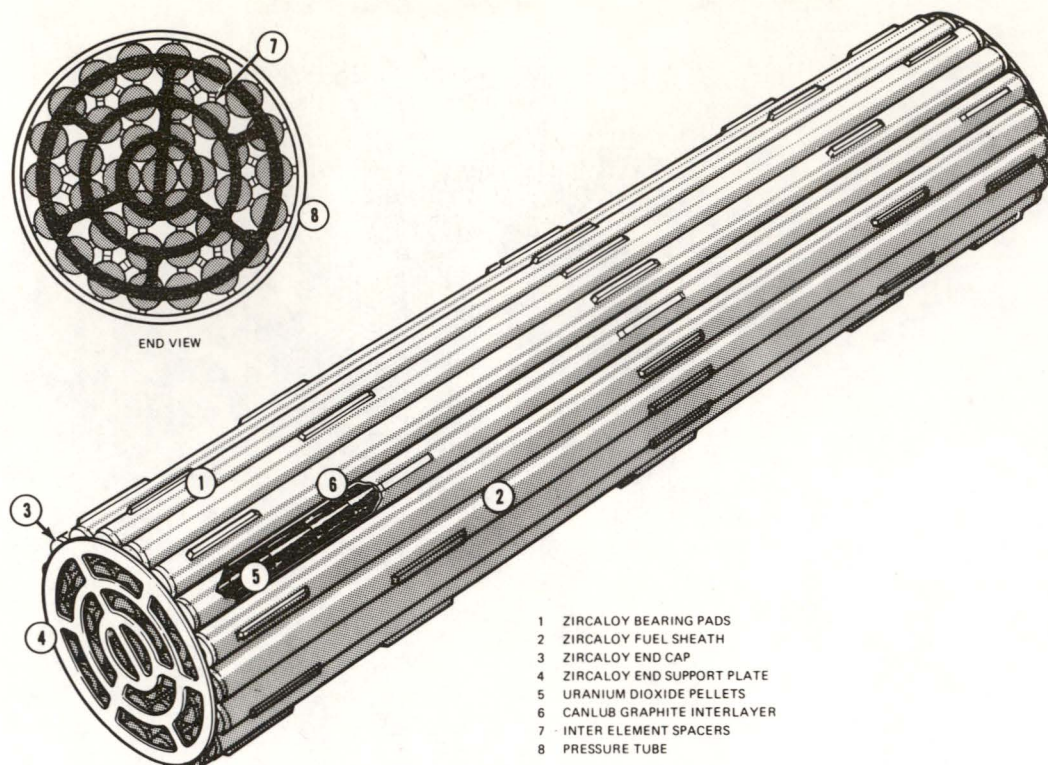


FIGURE 3
FUEL BUNDLE ASSEMBLY

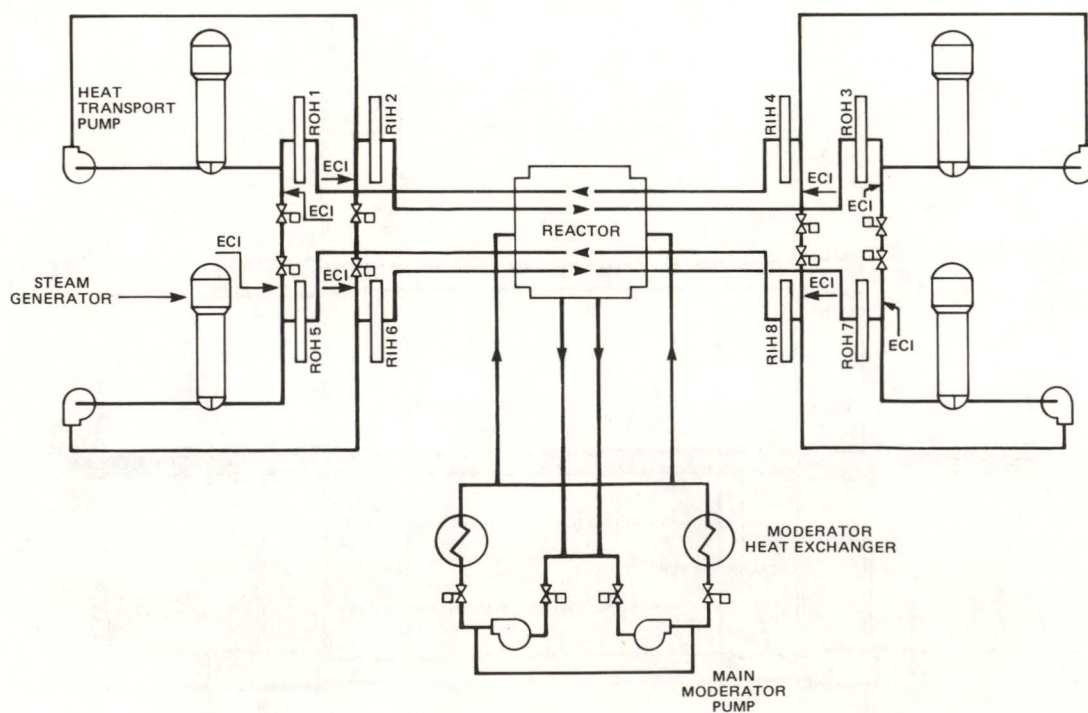


FIGURE 4
HEAT TRANSPORT SYSTEM AND MODERATOR SYSTEM
SIMPLIFIED FLOW SHEET

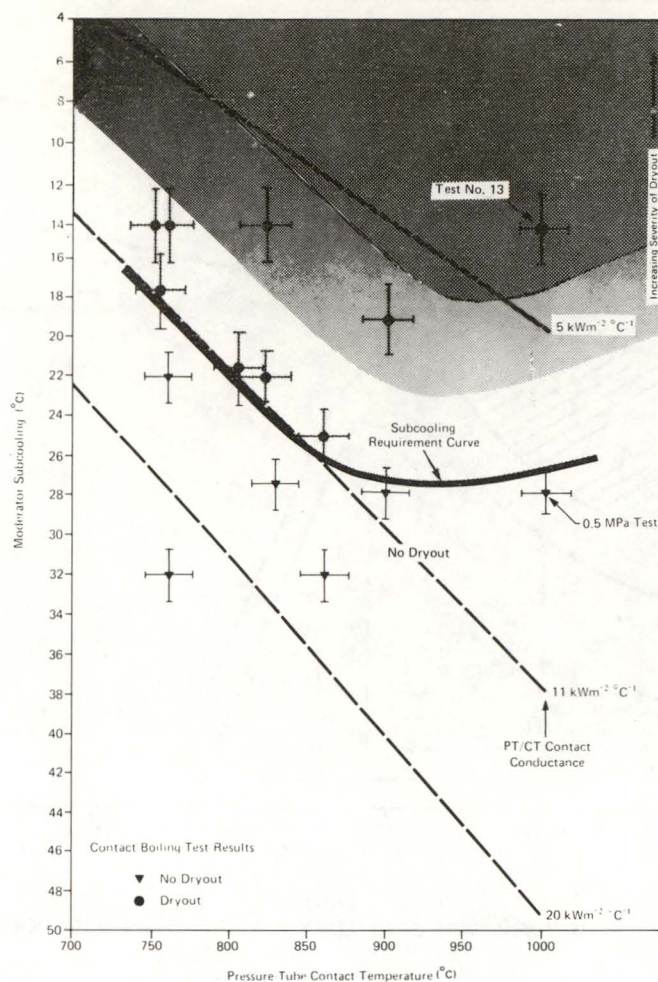


FIGURE 5
CALANDRIA TUBE DRYOUT CURVE

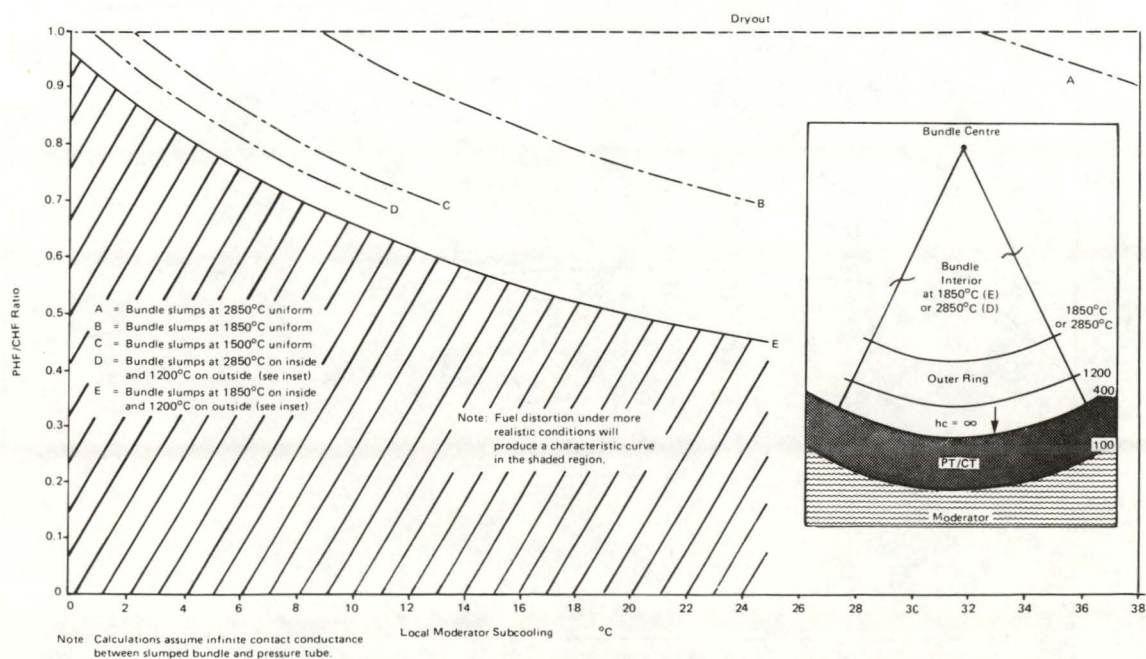


FIGURE 6
PEAK TO CRITICAL FLUX RATIO FOR BUNDLE SLUMPING

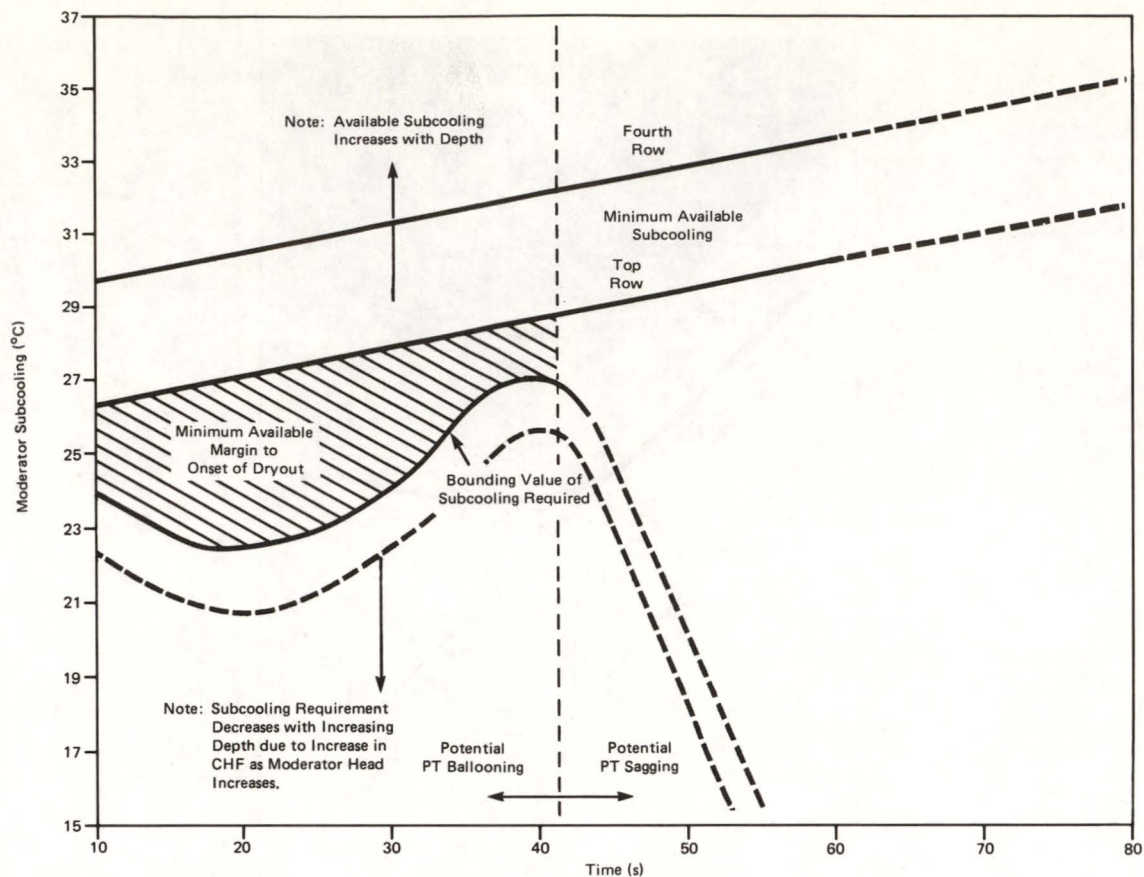


FIGURE 7
MINIMUM MARGIN TO DRYOUT IN LARGE LOCA-LOECI

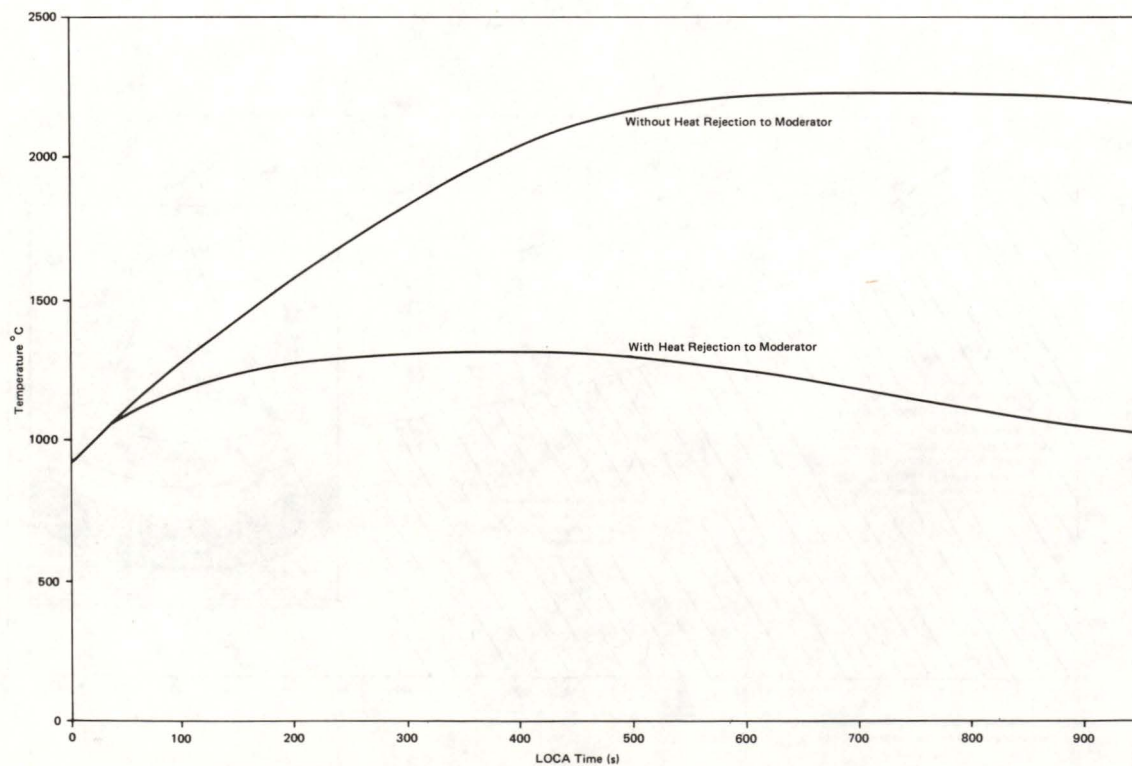


FIGURE 8
EXAMPLE OF EFFECT OF MODERATOR HEAT SINK ON AVERAGE CHANNEL TEMPERATURE

EXPERIENCE IN SMALL BREAK LOCA CALCULATIONS
BY RELAP 4 COMPUTER CODES

N. Cerullo, G. Galassi, M. Mazzini, F. Oriolo

University of Pisa
Dipartimento di Costruzioni Meccaniche e Nucleari
Via Diotisalvi, 2 - I-56100-Pisa - Italy

ABSTRACT

The experience acquired at the "Istituto di Impianti Nucleari" of the University of Pisa on computer code assessment in small LOCA is presented.

From the observation of the smoothed behaviour of thermalhydraulic variables during a small break LOCA, a coarse nodalization was assumed to perform both pre-and post-test analysis in this field.

This approach has been used in calculations related to International Standard Problems (ISP) and LOBI program tests:

- ISP 4 (SEMISCALE TEST S-02-06);
- ISP 9 (LOFT TEST L3-1);
- ISP 11 (LOFT TESTS L3-6/L8-1);
- Shake-down test SD-SL-03 of LOBI program.

The experience gained allows to draw some criteria about the use of RELAP 4 in small break LOCA calculations and to emphasize the need of improvements in this respect.

1. INTRODUCTION

A research program on thermalhydraulic transient in LWR following LOCA's has been carried out for a long time at "Istituto di Impianti Nucleari" (now "Dipartimento di Costruzioni Meccaniche e Nucleari") of the University of Pisa. During the last two years emphasis has been placed on small LOCAs.

In order to state the capability of RELAP 4 Mod. 6 computer code to analyze this kind of problems, the results of some International Standard Problems and of LOBI program tests have been used.

The RELAP 4 code (originally conceived for large LOCA evaluations) was used in a new way, as a "fast run" code, for small LOCA calculations. At the basis there was the observation that the transients subsequent to small breaks - excluding the first phase - is generally smooth, both regarding space and time trends of the main thermalhydraulic quantities, so that contiguous volumes present homogeneous conditions.

Also, without the action of pumps, the phases are separated and a well defined mixture level builds up where possible (vessel, SGs, etc.).

According to the break size, a transient length of perhaps some thousand seconds follows before the intervention of low pressure cooling systems.

This transient behaviour could lead to core uncovering, as in T.M.I. accident, if high pressure injection systems do not restore the water blowing-out of the break. As temporal derivatives of thermalhydraulic variables are slowly varying, it is possible to use a reduced number of control volumes and of balance equations for each node and junction, saving computer time without loss of reliability. However, accurate choices are necessary for a good modelling of the above-mentioned phenomena, in order to evaluate the interaction between liquid and steam phases.

Bearing in mind these considerations, the following tests were analyzed:

- SEMISCALE TEST S-02-06 (ISP 4);
- LOFT TEST L3-1 (ISP 9);
- LOFT TESTS L3-6/L8-1 (ISP 11);
- SHAKE DOWN TEST SD-SL-03 of LOBI Program.

The involved experimental facilities are scaled representations of a four loop PWR.

LOFT^{/1/} and SEMISCALE^{/2/} are operated at the Idaho National Engineering Laboratory by EG&G Idaho Inc. for the USNRC and the Department of Energy, while the LOBI test facility^{/3/} is placed at the Ispra Establishment of the EURATOM Joint Research Centre of the Commission of the European Communities.

2. SEMISCALE TEST S-02-06 (ISP 4)

The test S-02-06 simulates an intermediate (6% Amax) single-ended cold leg break; the hot leg of the blow-down loop is not present in this test.

The maximum electrical power of the core is 1.6 Mw; when the fluid in the pressurizer reaches the pressure set-point of 1800. psia, the power decreases following a trend analogous to nuclear decay heat.

ECCS begin to operate on pressure signal at the pump discharge. Two completely separated systems inject water into the intact loop cold leg and near the break nozzle.

ISP 4 pre-test calculation^{/4/} with RELAP 4-Mod. 2 code and further post-test calculations^{/5/} with RELAP 4-Mod. 5 code were performed by a normal nodalization with poor results; this was due to the lack of adequate correlations for some physical phenomena (critical flow model for Mod. 2, bubble rise models for both Mod. 2 and Mod. 5).

After some years, the ISP 9 analysis^{/6/, /7/} (2,5% break in cold leg) performed by RELAP 4-Mod. 6 code, evidenced the difference on computer time, using normal or reduced nodalization, without loss in the quality and quantity of informations.

On the basis of these results, a new calculation was performed for ISP 4, with a remarkable reduction in control volumes (from 39 to 15) as shown in Fig. 1.

Moreover on the basis of the above said considerations and using the increased code capabilities, new models and correlations have been utilized:

- Henry-Fauske / HEM (without dials) instead of Moody (with $C_D = 0.7$) model, for critical flow;
- Wilson bubble rise model instead of a homogeneous one in vessel and intact loop volumes.

The results are good, with a reduction in running time from a few hours to half an hour.

Fig. 2 shows the comparison among calculated and experimental trends for some significant variables.

Further details on ISP 4 post-test calculations are reported in^{/8/}.

3. LOFT TEST L3-1 (ISP 9)

L3-1 test, chosen by CSNI as ISP 9, simulated a cold leg break, with area 2,5% A_{max}.

LOFT plant was operating at full power (50 Mw), and at nominal values of pressure (2186. psig), mass flow in the primary piping (1055 lb/s) and core inlet temperature (537.5°F).

The reactor scram was actuated simultaneously to the blow-down valve (0. s) and the trip of the main coolant pumps followed immediately (0.04 s) after it.

ECC injections were initiated when pressure reached about 4.4 MPa (634. s) for accumulators and about 1 MPa (4240. s) for LPIS.

A nodalization of only 13 control volumes, 18 junctions and 7 heat slabs, as shown in Fig. 3, has been used to describe this experiment.

The following physical models have been chosen:

- Wilson model for phase separation;
- HF/HEM model, without dials, for critical flow;
- slip and stacked models for correct evaluation of liquid level and therefore of the heat transfer in the vessel.

Details can be found in^{/6/} and^{/7/}.

Some significant results are compared in Figs. 4, 5 and 6 with the experimental ones and with those obtained by EGG using TRAC-PD2 code.

The success is evident from these figures, especially keeping in mind the reduced computing time (ratio 0.9 between CPU time and real time on a computer IBM 370/158).

4. LOFT TESTS L3-6/L8-1 (ISP 11)

Also the LOFT L3-6/L8-1 experiment^{/1/}, ^{/9/}, ^{/10/}, chosen as ISP 11 by CSNI, simulates a small break in the intact loop cold leg, between the primary coolant pumps and reactor vessel, with area 2.5% A_{max}.

In the L3-6 portion of the experiment, the break valve was opened and the LOFT reactor was allowed to blow-down with continuous operation of the reactor coolant pumps during the transient.

The only emergency core cooling system activated during L3-6 was the high pressure injection system (HPIS A).

The low pressure injection system and the accumulator were valved out.

When the primary system pressure declined to 300. psia, the pumps were tripped off. This event initiated the L8-1 portion of the experiment, devised to investigate core uncovering.

Also in this case a coarse nodalization, similar to that in ISP 9 (Fig. 3), and the usual physical models (Wilson, HF/HEM) were used. Volumes 1, 2, 3 and 4 were assumed homogeneous during the pumps operation period; later when the pumps are stopped, the Wilson model was employed.

The details of our calculation on ISP 11^{/11/} show that the agreement with the experimental data is generally good during most of the transient.

An underprediction of primary pressure (Fig. 7) and of cladding temperature can be observed from 800. s on, and is due to the following reasons:

- incomplete modelling of the heat transferred from the piping to the coolant;

- the assumption done by RELAP 4 that each volume is in thermal equilibrium.

The discrepancies evidenced between experimental and calculated pressure trends on steam generator secondary side (Fig. 8) are also due to this latter assumption.

The calculation of ISP 11 reflood phase has been carried out on the basis of the experience acquired through the analysis of the SEMISCALE test S-06-3^{/12/}. From the break isolation time (2460. s), pressure and temperature conditions of the various volumes of LOFT plant are almost uniform and some volumes are empty.

So the previous nodalization has been modified gathering some volumes, but representing the vessel in a more detailed way, as suggested by RELAP 4-Mod. 6 instruction manual. Fig. 9 shows the adopted nodalization.

The heat transfer between primary and secondary loop and between pipes and fluid has been neglected; only vessel structures have been simulated by two slabs, one placed in the downcomer and the other in the lower plenum. The initial conditions have been taken from the previous calculation.

RELAP 4-Mod. 6 reflood heat transfer correlations are used in the analysis.

Pressure and rod cladding temperature results of both blow-down (in the first calculation the blow-down heat transfer correlations have been used during the reflood phase too) and reflood are presented in Fig. 10, together with the experimental data.

These figures clearly show the improvement in the provision of the experimental trends, when the reflood correlations are used: both the rewetting time and the axial temperature distribution are in agreement with the experiment.

5. SHAKE DOWN TEST SD-SL-03 OF LOBI PROGRAM

The test is a single-ended 1x0.4% cold leg break, executed with nominal initial conditions; only cold leg ECC water injection from the accumulators was available^{/13/} on the LOBI plant.

The heating power input was kept at nominal value up to 20. s from the beginning of the transient; thereafter the heating power was decreased down to 3% within 265. s and finally it was set at zero at 1380. s.

The pumps were operated at nominal speed as long as full nominal heating power existed; thereafter they were "coasted down" during the transient according to an exponential pump speed time function, with a half-value time of about 10. s, and finally set at zero after about 90. seconds.

The secondary loop system was operated so that the cooling follows a temperature gradient of about 100°K/h.

The experimental facility has been modelled by a small number of volumes (16) and flow-paths (19), as shown in Fig. 11.

Wilson, HF/HEM, slip and stacked models were used.

In order to avoid the large discrepancy on S.G. secondary pressure (and corresponding deviations on primary system pressure) found in ISP 11, the experimental steam generator secondary side pressure trend has been used as a boundary condition of the problem.

Some parametric analysis were performed in order to evaluate the influence of the choice of stacked volumes and of the introduction of dials.

Sending to^{/13/} for details, some of the most important calculation outputs are presented in Figs. 12 and 13, together with the corresponding experimental results.

From the comparison, conclusions similar to those in the above paragraphs can be drawn.

6. DISCUSSION

The analysis presented in the previous chapters show that the RELAP 4-Mod. 6 code can well simulate transients in which gradients of the thermal-hydraulic variables are smoothed, when a reduced nodalization is used. Moreover particular attention must be given to some physical phenomena such critical two-phase flow, phase separation and mixture level trends, making an appropriate use of the corresponding models implemented in the code (stacked volumes, bubble rise, and slip).

We also emphasize the strong dependence of the depressurization rate in small LOCAs from the correct evaluation of the term of heat addition from core and piping, to the fluid, and of heat loss through the break flow and the primary to secondary circuits heat transfer.

The existing version of RELAP 4-Mod. 6 code is not able to calculate the last term with the necessary accuracy; consequently a very good evaluation of the primary pressure behaviour is not possible.

The use of a reduced nodalization with the consequent reduction in CPU time, allows parametric calculations to be performed without excessive expenses; this can be important in order to analyze the influence on the calculated transient of some particular phenomena (e.g. the above mentioned thermal exchange between primary and secondary circuits), to test the used correlations and to detect their possible weak points.

In particular, the lack in RELAP 4-Mod.6 of a non-equilibrium model is emphasized. The code infact calculates an instantaneous mixing of the subcooled ECCS and/or auxiliary feed water with the fluid present in the volume, with simultaneous steam condensation in order to maintain saturation conditions.

A non-equilibrium model is implemented in the new versions of RELAP code (RELAP 4-Mod. 7 and RELAP 5); it delays the mixing, allowing an improved simulation of the AIS injection and of the S.G. secondary side behaviour.

In conclusion, we can say that further experiences, notwithstanding some new problems, fundamentally confirm our conclusions presented at the ANS "Small Breaks Specialist Meeting" held in Monterey^{/7/}.

The use of a coarse nodalization allows the study of smoothed and slowly variable transients in spite of the inherent inaccuracy of RELAP 4-Mod. 6 code.

As it's sometimes necessary to change the adopted initial nodalization, particularly evidenced in the analysis of LOCA reflood phase, at our Department we think to modify RELAP 4 code in order to allow the automatic change of nodalization and initialization.

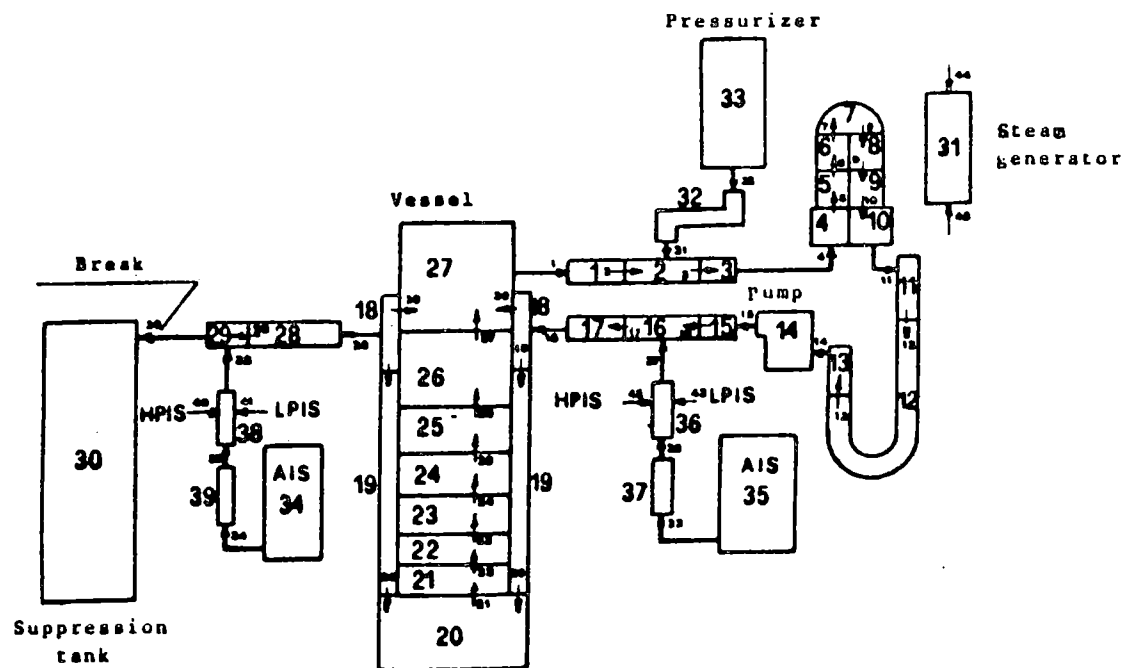
ACKNOWLEDGEMENT

This work has been sponsored by C.N.E.N. (contracts AC-2 and AC-3).

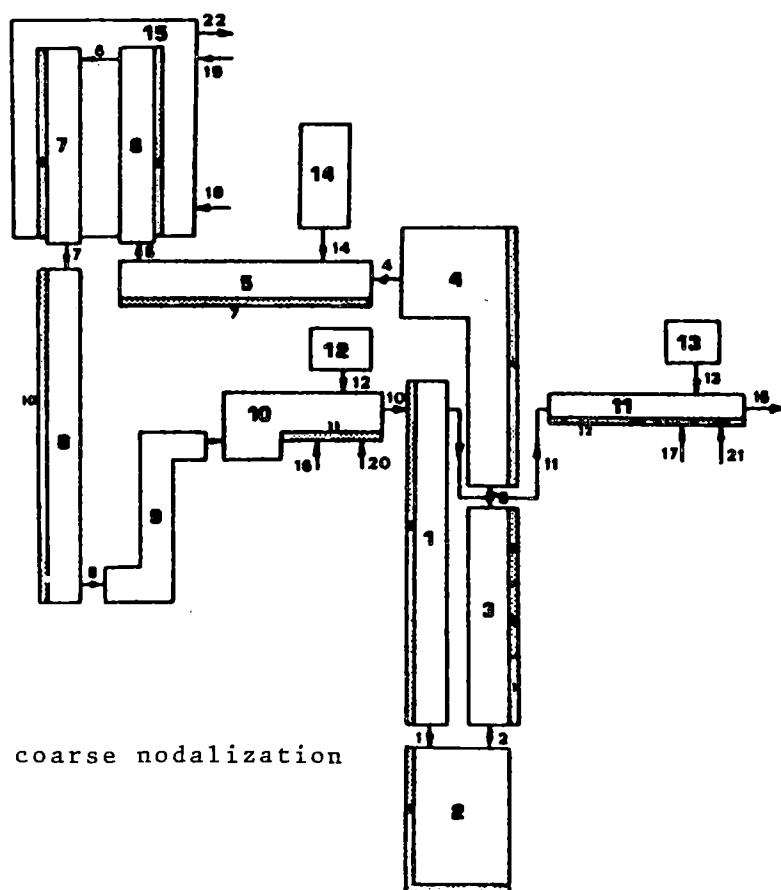
REFERENCES

1. D.L. REEDER, "LOFT System and Test Description (5,5 ft Nuclear Core LOCEs)" - EG&G Idaho Inc. - NUREG/CR - 0247 July 1978.
2. E.M. FELDMAN, D.J. OLSON, "SEMISCALE Mod. 1 Program and System Description for the Blowdown Heat Transfer Tests" - ANCR - 1230, Idaho National Engineering Laboratory, August 1975.

3. W. RIEBOLD et alii, "Specifications LOBI PRE-PREDICTION EXERCISE Influence of PWR Primary Loops on Blow-down (LOBI)" - Commission of the European Communities JOINT RESEARCH CENTRE - ISPRA Establishment TECHNICAL NOTE Nr. 1.06.01.79.25, February 1979.
4. N. CERULLO et alii, "Results of Calculations of NEA-Standard Problem 4 using Relap 4-002 Computer Program" - Presented at the Second NEA-CSNI Workshop on LOCA Standard Problems, Paris Dec. 6-9 1976.
5. N. CERULLO et alii, "Thermohydraulic Problems in LWR's Related to the Assessment of LOCA Computer Relap 4 Code" - XXXV Congresso Nazionale dell'Associazione Termotecnica Italiana - ATI - Saint Vincent, Sept. 15-19 1980.
6. N. CERULLO et alii, "OECD-CSNI Standard Problem n. 9: Calculation of LOFT L3-1 Experiment using Relap 4-Mod. 6 Computer Code" - Atti Istituto di Impianti Nucleari, Università di Pisa, RP433(80). Presented at 8th Meeting of OECD-CSNI Working Group on Emergency Core Cooling and Fuel Behaviour, Ispra, May 4-7 1981.
7. M. MAZZINI et alii, "The Analysis of L3-1 LOFT Test, a Small Break LOCA, by Relap 4-Mod. 6 Computer Code, using Different Nodalizations" - Presented at ANS Specialists Meeting on Small Break LOSS-of-Coolant Accident Analyses in LWR's, Monterey (California), August 25-27 1981.
8. G. GALASSI, "Post Test Calculation of ISP-4 (SEMISCALE Test S-02-06)" - Atti Dipartimento di Costruzioni Meccaniche e Nucleari, Università di Pisa DCMN003 Pisa, 1982.
9. L.T. DAO et alii, "Experiment Data Report for LOFT NUCLEAR Break experiment L3-5/L3-5A" - NUREG/CR-1965, EGG-2060, November 1980.
10. P.D. BAYLESS, J.M. CARPENTER, "Experimental Data Report for LOFT Nuclear Small Break Experiment L3-6 and Severe Core Transient Experiment L8-1" - NUREG/CR-1868, EGG-2075, January 1981.
11. G. GALASSI et alii, "The Analysis of L3-6/L8-1 LOFT Experiments (OECD-CSNI International Standard Problem n. 11) by RELAP MOD. 6 Computer Code" - Atti Istituto di Impianti Nucleari, Università di Pisa RP490(81).
12. F. DONATINI, G. GALASSI, M. MAZZINI, F. ORIOLO, "Analisi del riallagamento del nocciolo, nella prova S-06-3 del Programma SEMISCALE, mediante il codice RELAP 4-Mod. 6" - XXXVII Congresso Nazionale dell'Associazione Termotecnica Italiana - ATI - Padova, 27 settembre - 1 ottobre 1982.
13. P. BROTTINI et alii, "Analisi di post-test dello "shake-down test" SD-SL-03 del programma LOBI" - Atti Istituto di Impianti Nucleari, Università di Pisa, RP491(81).

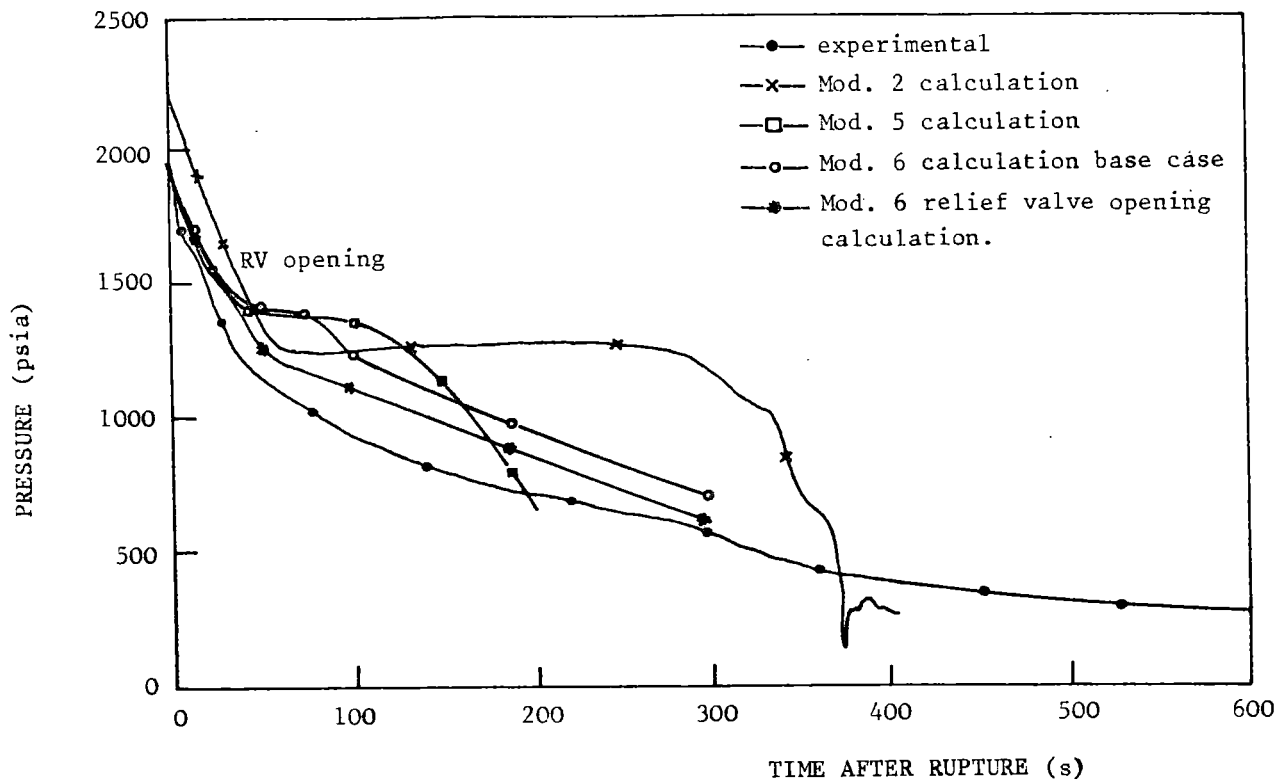


a) standard nodalization

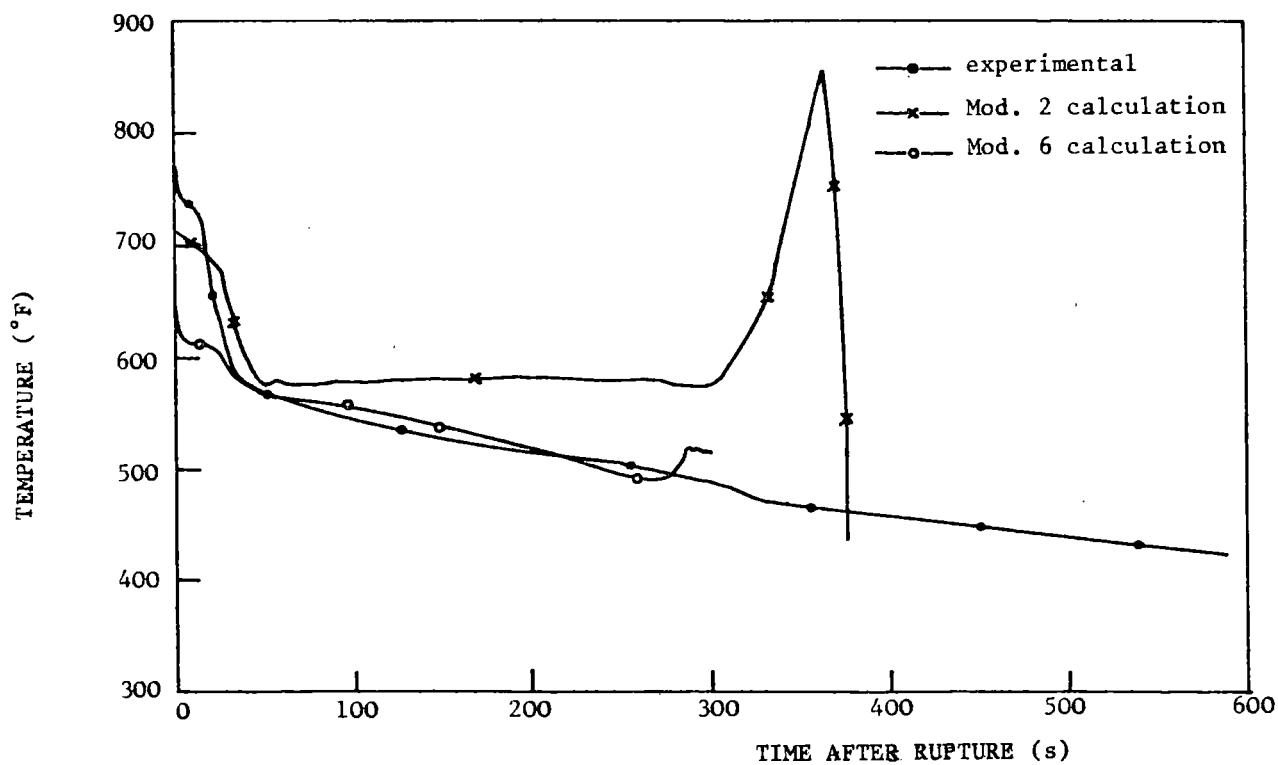


b) coarse nodalization

Fig. 1 - Nodalizations of SEMISCALE apparatus used in I.S.P. 4.



a) upper plenum pressure



b) rod surface temperature (44 inch elevation)

Fig. 2 - Results of I.S.P. 4 calculations

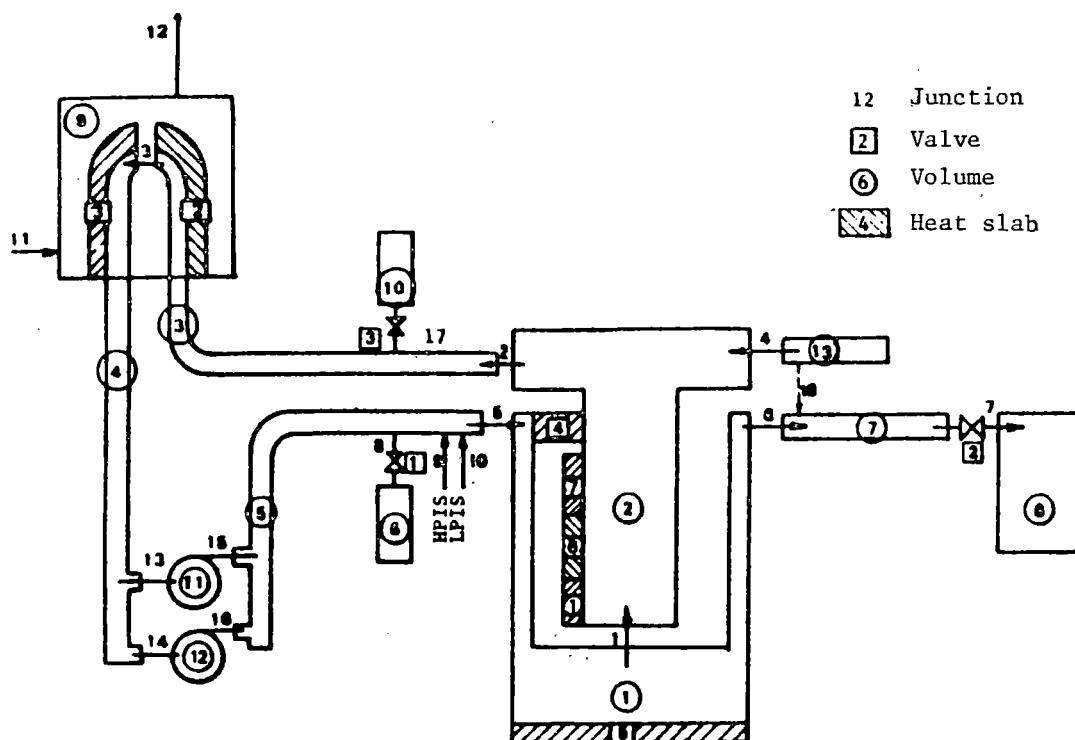


Fig. 3 - Nodalization of LOFT apparatus used in I.S.P. 9 post-test calculations.

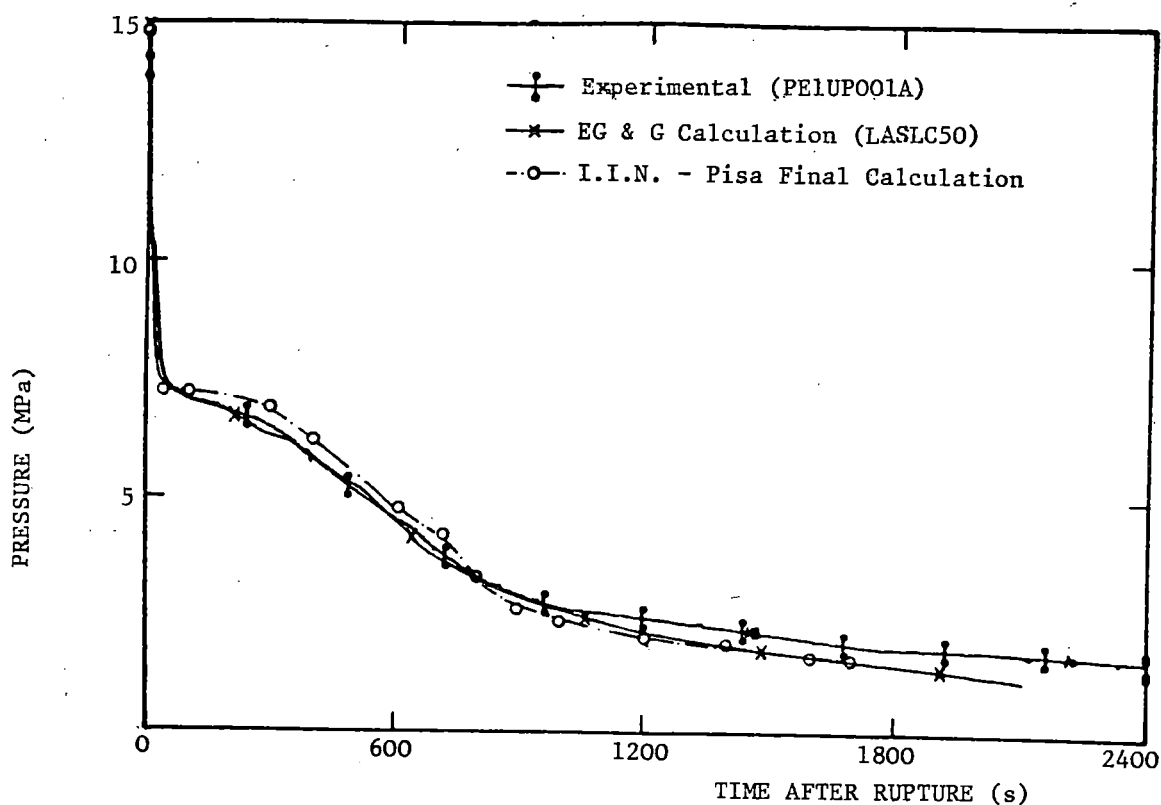


Fig. 4 - I.S.P. 9 upper plenum pressure

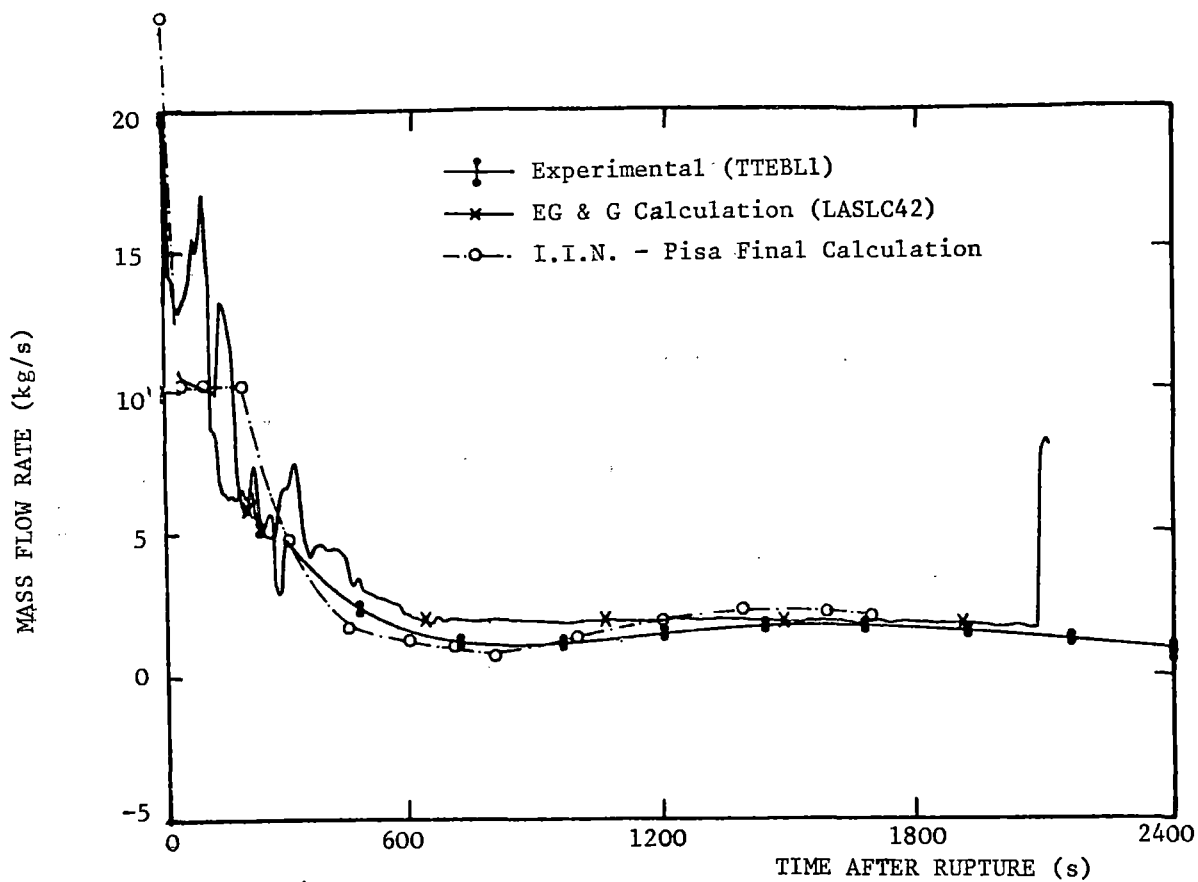


Fig. 5 - I.S.P. 9 break mass flow rate.

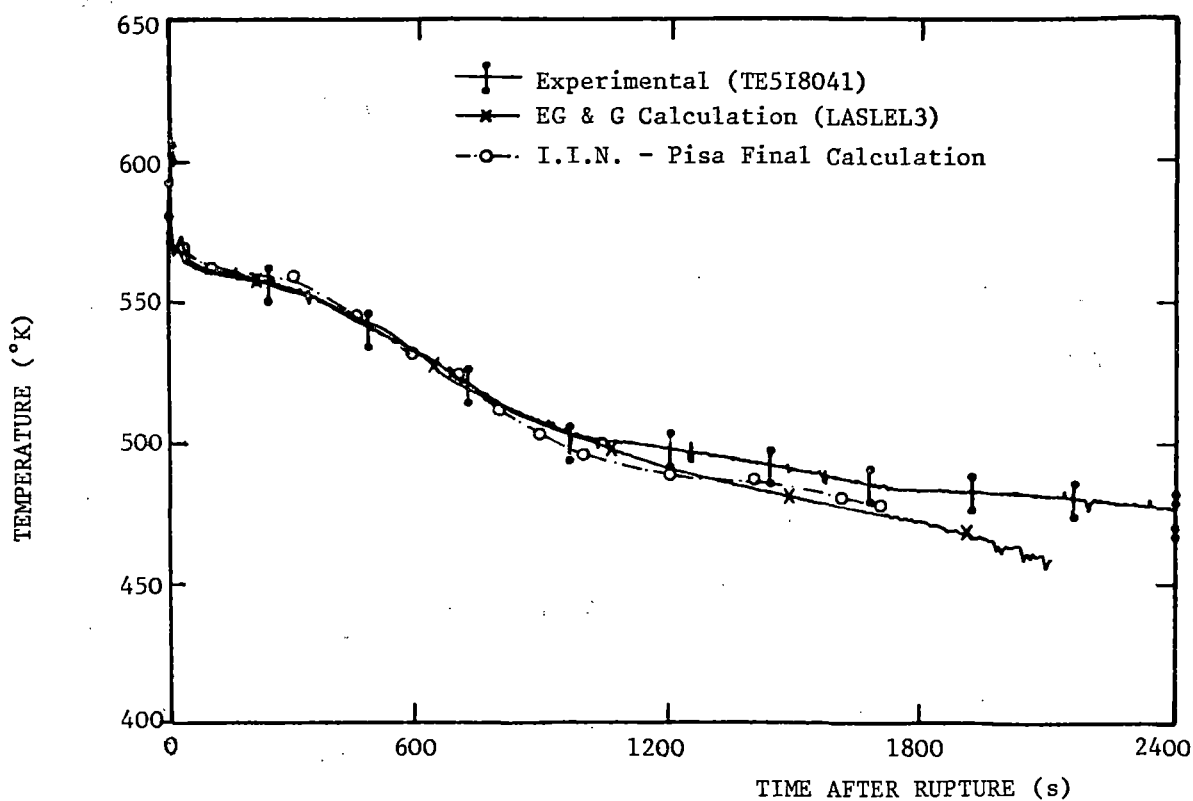
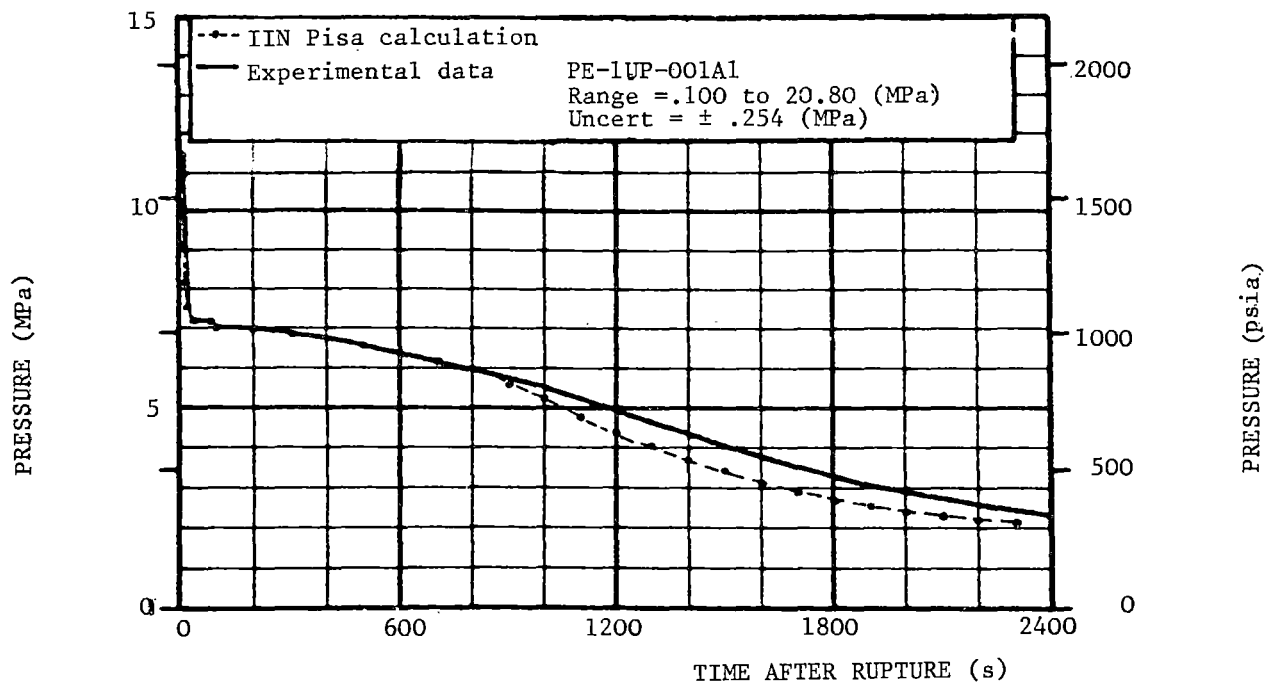
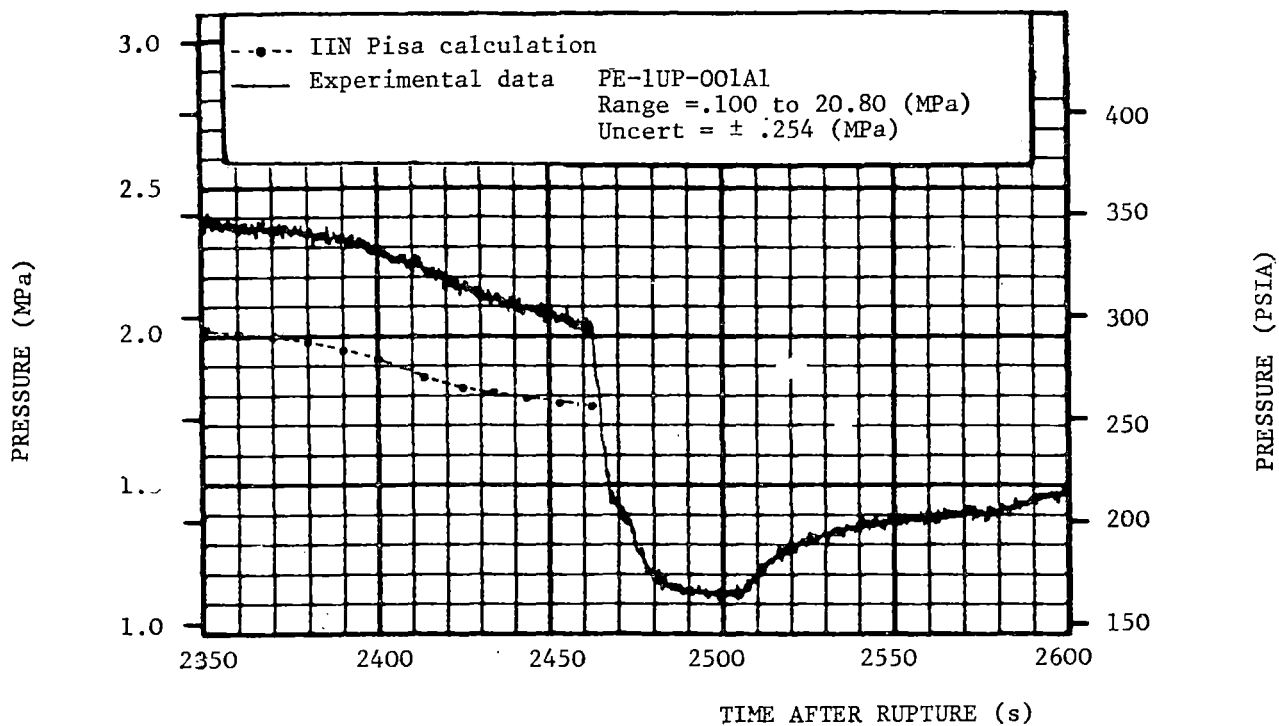


Fig. 6 - I.S.P. 9 rod cladding temperature.



a) L3-6 portion of test



b) L8-1 portion of test

Fig. 7 - I.S.P. 11 upper plenum pressure

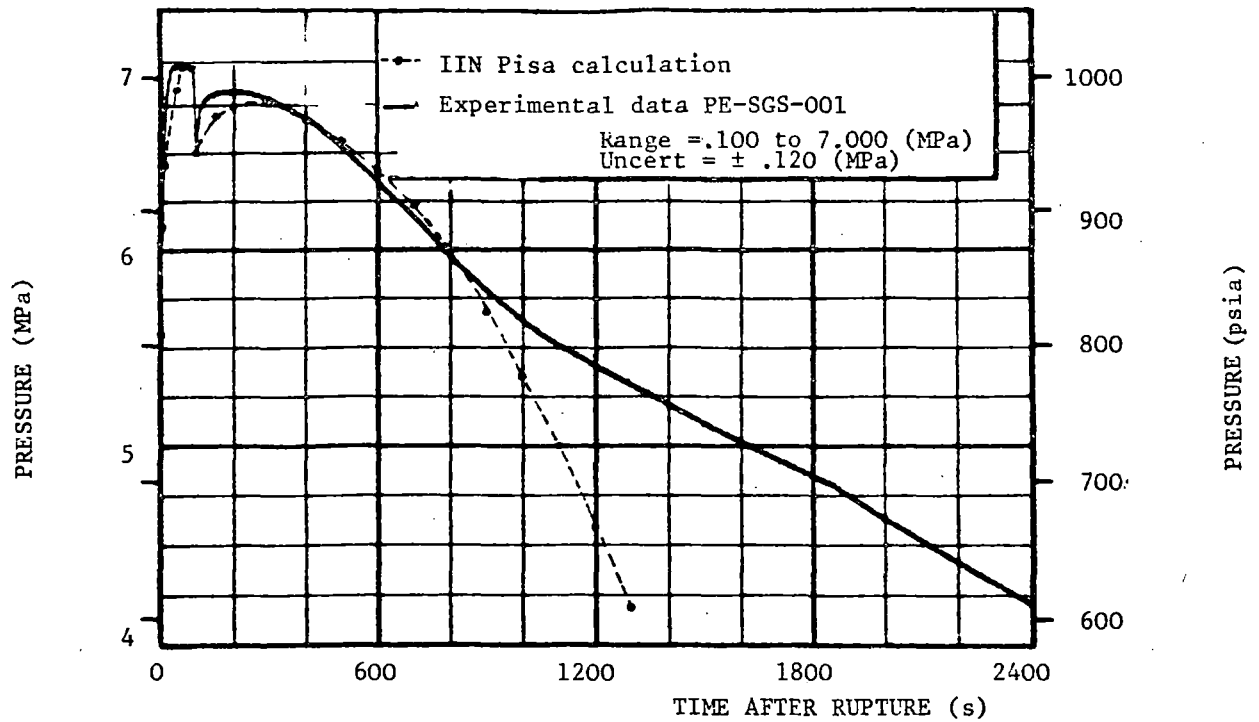


Fig. 8 - I.S.P. 11 pressure in steam generator dome.

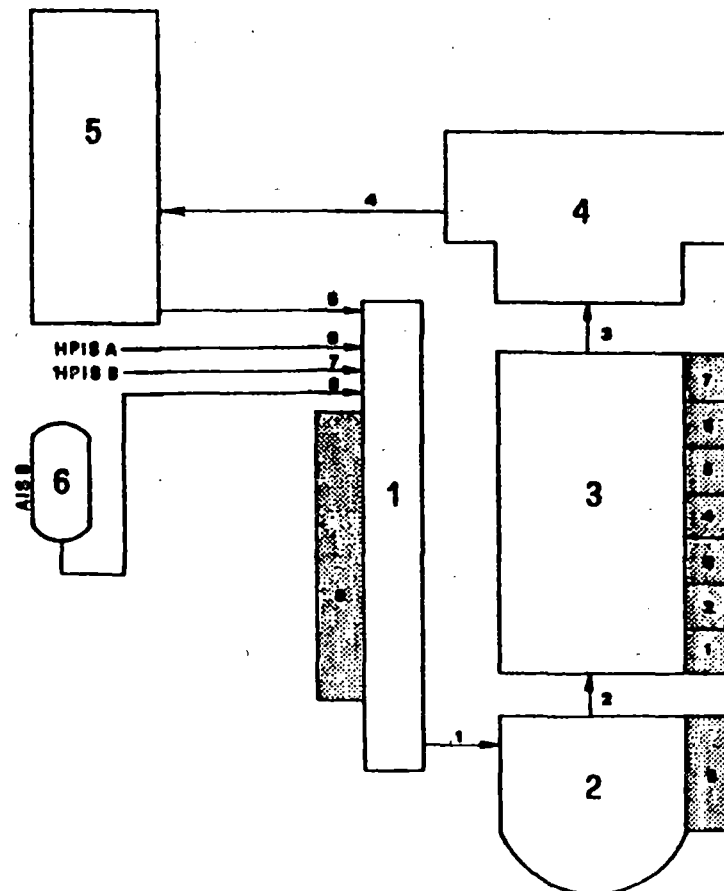


Fig. 9 - I.S.P. 11 reflood nodalization.

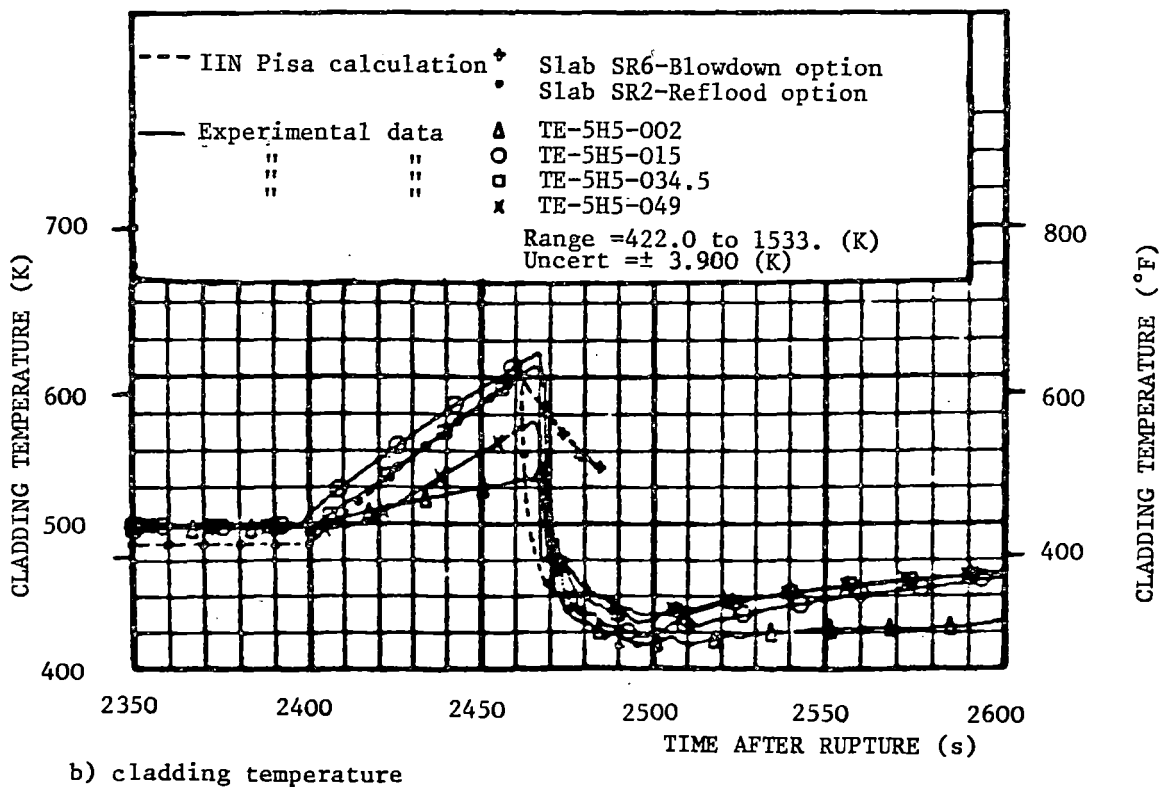
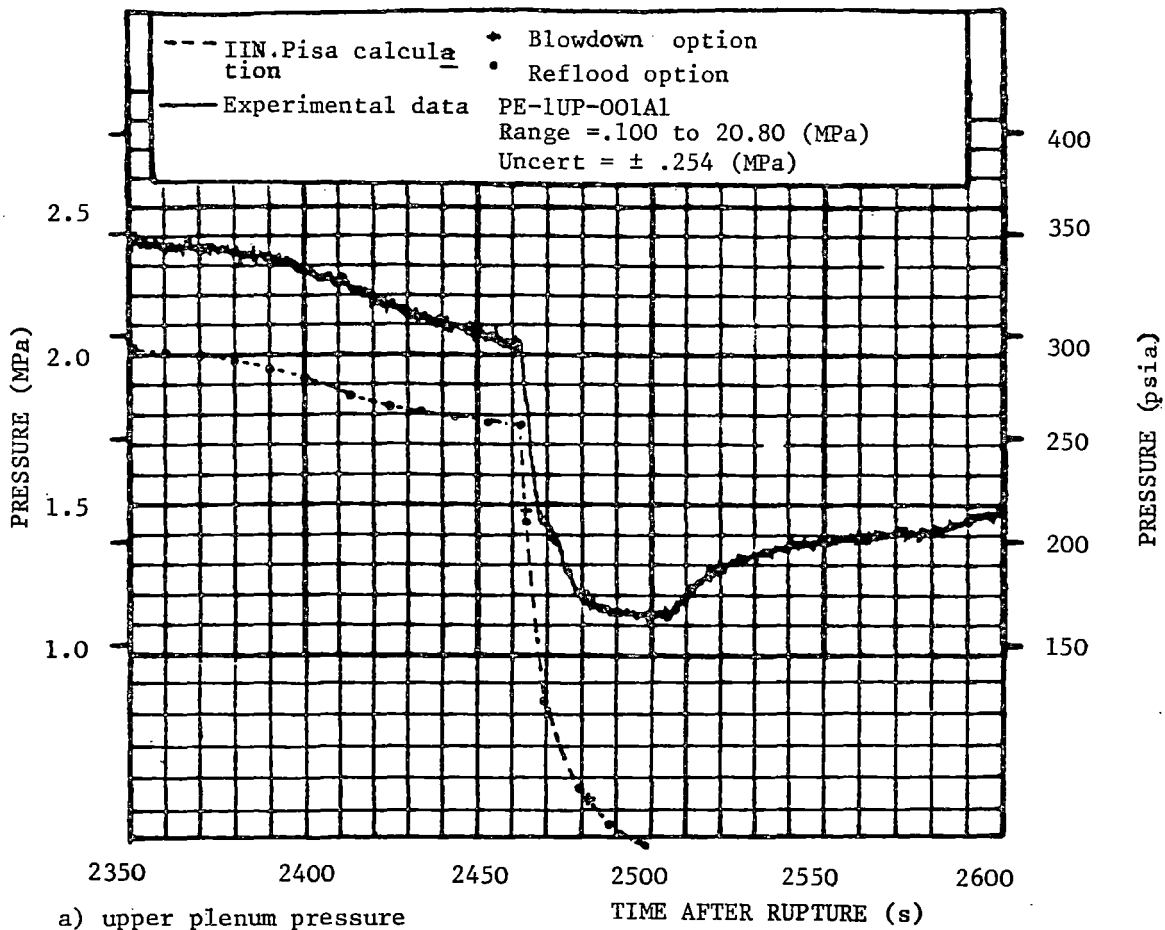


Fig. 10 - I.S.P. 11 reflood phase.

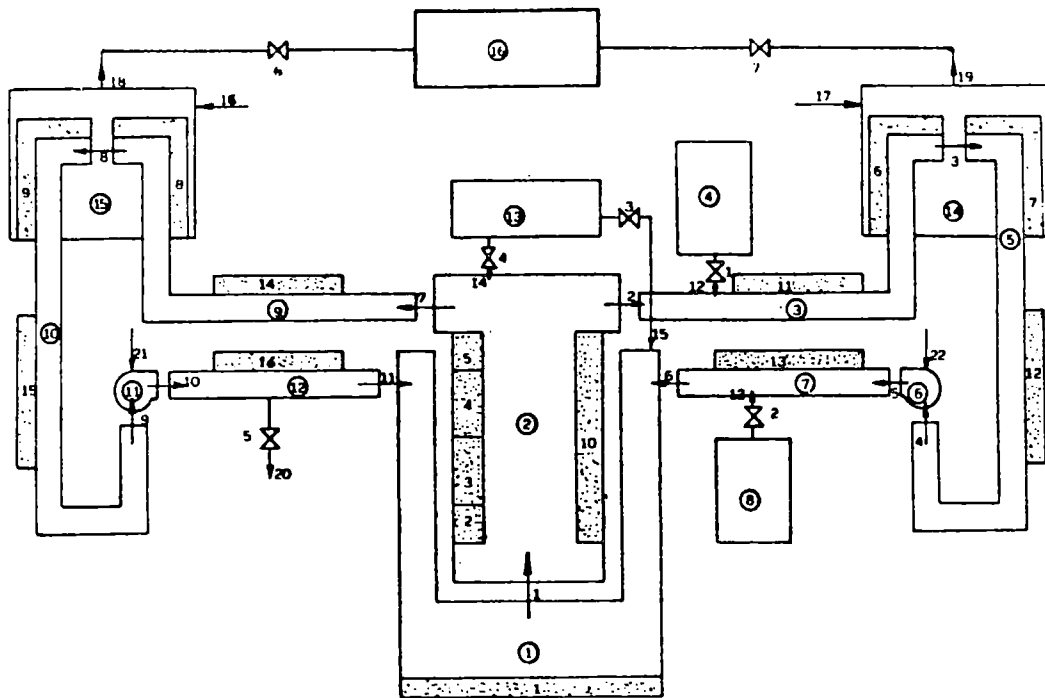


Fig. 11 - Nodalization of LOBI apparatus used in shake-down test SD-SL-03 post-test calculations.

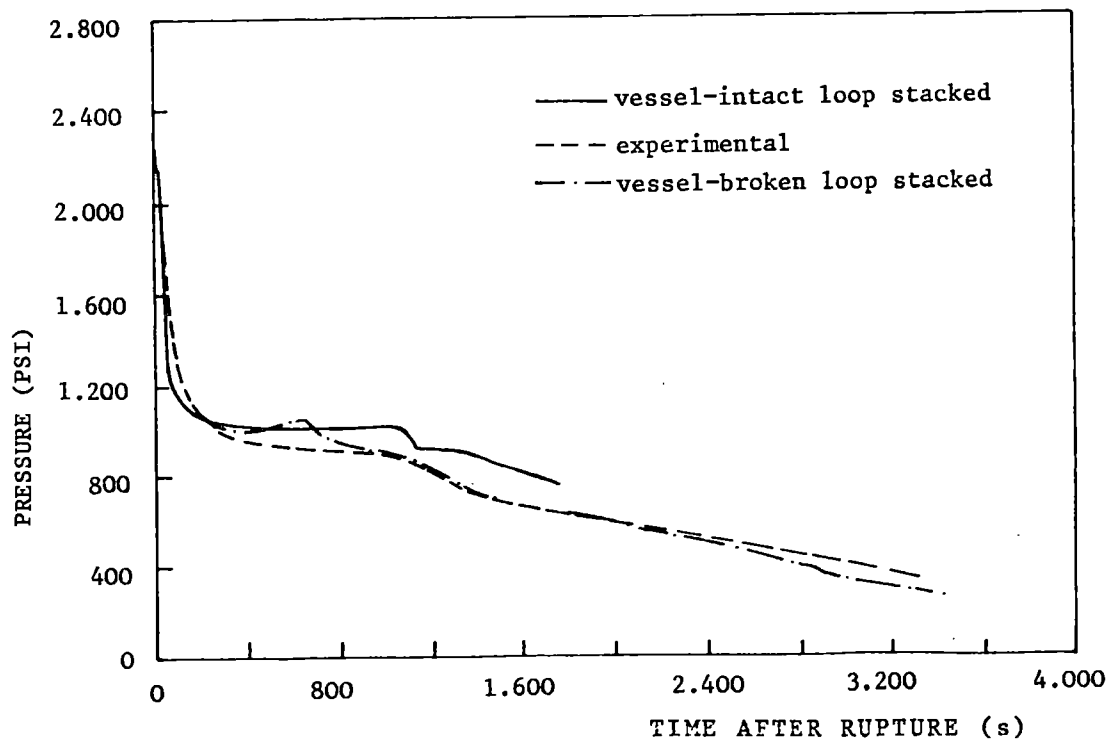
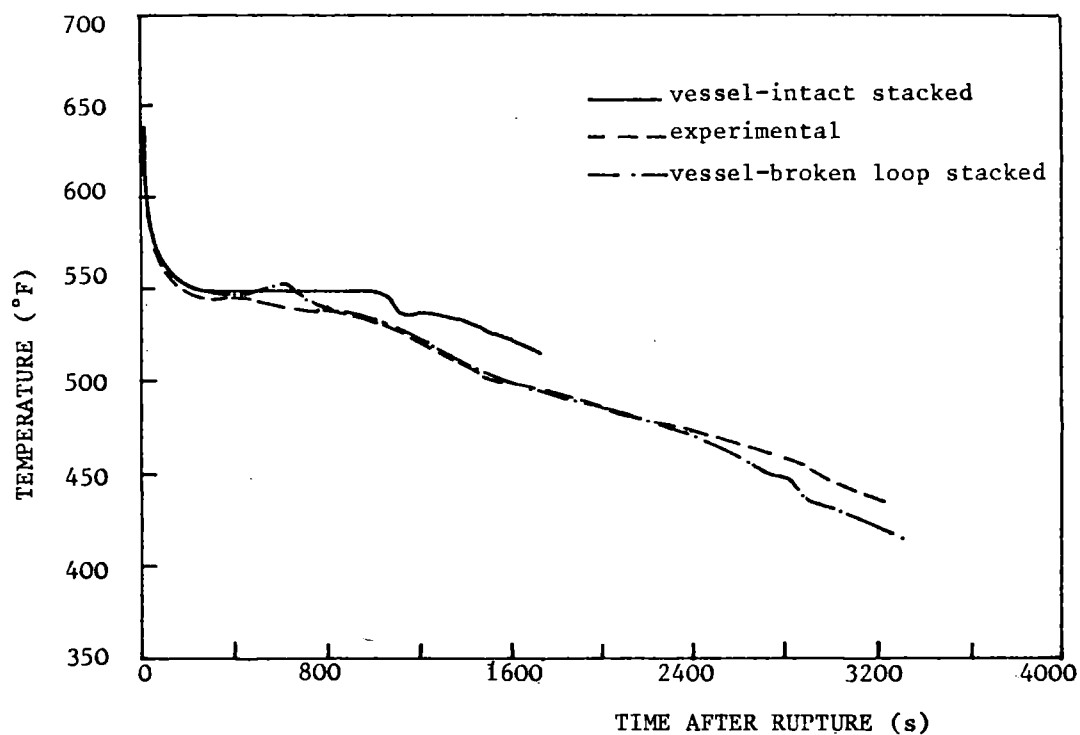
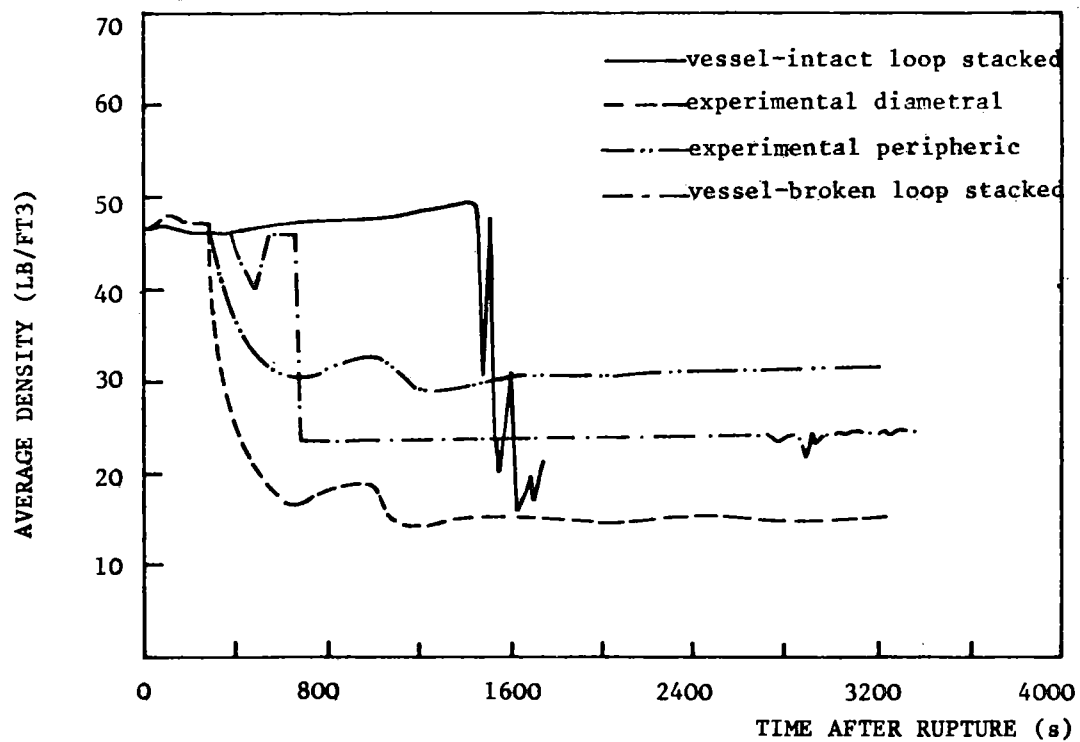


Fig. 12 - LOBI TEST SD-SL-03 upper plenum pressure.



a) Rod surface temperature (slab 4)



b) fluid density in break volume

Fig. 13 - LOBI TEST SD-SL-03

"ON THE EXISTENCE OF EARLY CORE REWET DURING LARGE-BREAK LOCA
TRANSIENTS IN A COMMERCIAL PWR"^a

Paul N. Demmie
EG&G Idaho, Inc.
P.O. Box 1625
Idaho Falls, Idaho 83415

ABSTRACT

Large-break experiments in the Loss-of-Fluid Test (LOFT) Facility showed that the nuclear fuel rods were rewet between 5 and 10 s after break initiation. Computer calculations of large-break loss-of-coolant accident (LOCA) transients in a commercial pressurized water reactor (PWR) predict similar early core rewets if the primary coolant pumps remain powered. A question suggested by these experiments and calculations is, "Can system conditions exist in a commercial PWR which would prevent an early core rewet during a large-break LOCA transient?" A computer study answered this question in the affirmative for 200%, double-ended, cold-leg break LOCA transients in a PWR of the Westinghouse four-loop design. However, the probability of such an accident actually occurring is extremely small. This paper summarizes the results of this study and briefly discusses the implications of these results on nuclear safety issues.

INTRODUCTION

Large-break experiments in the Loss-of-Fluid Test (LOFT) Facility showed that the nuclear fuel rods were rewet (cooled down to fluid saturation temperature) between 5 and 10 s after break initiation.^{1,2} Computer calculations of large-break loss-of-coolant accident (LOCA) transients in a commercial pressurized water reactor (PWR) predict similar early core rewets if the primary coolant pumps (PCPs) remain powered.^{3,4} A question suggested by these experiments and calculations is, "Can system conditions exist in a commercial PWR which would prevent an early core rewet during a large-break LOCA transient?"

To answer this question, a computer study was conducted of the thermal-hydraulic response of a full-scale PWR to a hypothesized LOCA.⁵ This study was intended to determine whether system conditions could exist which would prevent an early fuel rod rewet during a 200%, double-ended, cold-leg (DECL) break LOCA. System conditions were investigated which could lead to early core-flow stagnation, persisting through the blowdown phase of the transient.

a. Work supported by the U.S. Nuclear Regulatory Commission under DOE Contract No. DE-AC07-76ID01570.

An early rewet of all the fuel rods would not occur in LOFT or in a full-scale PWR if the core flow would stagnate for a sufficient period of time early during a large-break LOCA. Stagnant core flow leads to a temperature excursion of the fuel rods. Subsequently, if the temperature of the fuel rod cladding would reach about 1100 K, ballooning and/or failure of some rods could occur, and as the system pressure decreases, fuel rods could rupture. Such an accident scenario is a nuclear safety concern.

As a reference case, a PWR of the Westinghouse four-loop design was considered. Since the design is representative of many PWRs, the results of calculations performed using it as a reference case can be considered typical for many PWRs. Furthermore, the design of the LOFT facility, in which the early fuel rod rewet phenomenon was discovered, is similar.

The early rewet of the fuel rods in LOFT Experiments L2-2 and L2-3 was caused by the powered PCPs reestablishing a positive mass flow through the core early in these experiments. This observation suggested that PCP system conditions should be a major consideration in this study, even though other ways of achieving extended core flow stagnation might exist. These conditions are given and discussed in the following section.

Subsequent sections of the paper (a) present a discussion of the results of the LOCA simulations with these system conditions, and (b) provide the conclusions obtained from this study.

SYSTEM CONDITIONS CONSIDERED

The PCP system conditions considered during a 200%, DECL break LOCA are:

1. All pumps powered
2. All pumps unpowered
3. One intact-loop pump shaft broken and the remaining pumps unpowered
4. Two intact-loop pump shafts broken and the remaining pumps unpowered
5. All pump shafts locked.

The phrase, pumps powered, means that electrical power is being supplied to the pumps; the phrase, pumps unpowered, means that such power is not being supplied. In either mode, the shaft rotation is not inhibited. A broken pump shaft is completely sheared, causing the pump to be incapable of moving fluid. Although the probability of a pump shaft completely shearing simultaneously with a 200% DECL break is extremely small, the simultaneous occurrence of these events was considered possible for the purposes of the study discussed in this paper. A pump shaft locked means that the shaft, and hence the impeller, cannot rotate. In all cases, the pump design prevents reverse rotation.

These pump conditions are representative of the entire spectrum of intact-loop pump performance during a LOCA. At one end of the spectrum, the best performance in delivering fluid to the reactor vessel occurs when all the pumps are powered. At the other end, the worst performance occurs when all the pump shafts are locked. Between these extremes lie, in order of decreasing performance, the remaining pump system conditions listed above.

The first 15 s of the blowdown phase of LOCAs with these conditions were simulated using the RELAP5/MOD1 computer code⁶ with specific modifications (see Reference 5). RELAP5/MOD1 is a one-dimensional, transient system analysis code designed for analyses of light water reactor LOCA and non-LOCA transients. It uses a five-equation, hydrodynamics model consisting of two continuity equations, two momentum equations, and a total energy equation to simulate unequal velocity, unequal temperature, and two-phase flow. All calculations were made with initial conditions corresponding to normal operating conditions for a PWR of the Westinghouse four-loop design.

PRESENTATION AND DISCUSSION OF RESULTS

A summary of the effects of the five sets of pump conditions on fuel rod cladding temperatures during a 200%, DECL break LOCA is given in Table I. The greatest concern about the cladding behavior during these LOCA simulations is whether or not an early fuel rod rewet occurred. Table I shows that such rewets were calculated for all accidents considered, except the LOCA with one intact-loop pump shaft broken. Therefore, there exists in the spectrum of possible intact-loop PCP performance a window which (a) occurs with an extremely small probability and (b) leads to an extended core flow stagnation and the absence of an early fuel rod rewet.

TABLE I. FUEL ROD CLADDING TEMPERATURE BEHAVIOR DURING LOCA SIMULATIONS

System Conditions	Hot Fuel Rod		Average Fuel Rod	
	Rewet	PCT ^a	Rewet	PCT ^a
All pumps powered	Yes	1006 K (1351°F) at 4.6 s	Yes	742 K (878°F) at 3.8 s
All pumps unpowered	Yes	1070 K (1467°F) at 4.6 s	Yes	752 K (894°F) at 4.7 s
One intact-loop pump shaft broken, remaining pumps unpowered	No	1112 K (1543°F) at 14.7 s	No	817 K (1012°F) at 14.4 s
Two intact-loop pump shafts broken, remaining pumps unpowered	Yes	1004 K (1348°F) at 5.0 s	Yes	722 K (841°F) at 4.6 s
All pump shafts locked	Yes	879 K (1123°F) at 2.3 s	Yes	677 K (761°F) at 2.4 s

a. Peak cladding temperature.

In the following five subsections, more detailed analyses are given of the results of the LOCA simulations with the five sets of pump conditions.

A detailed description of the PWR model used for the LOCA simulations is given in Reference 5. This model contains two primary coolant loops: one representing three primary coolant loops of the plant; the other representing a single loop of the plant. To interpret the results presented in this paper, knowledge of the following features of the PWR model is helpful. In this model, the core of the reactor is represented by two, six-volume channels--the hot channel representing the highest powered fuel rod bundle in the core, and the average channel representing the rest of the core. The geometry of the hot channel is that of a single, 15 x 15 fuel rod bundle; the geometry of the average channel is that of the remaining 192 bundles. Crossflow connections exist between volumes at the same elevations in these channels. Each volume in the hot channel contains a heat structure representing an axial portion of the highest powered fuel rod (hot fuel rod) and a heat structure representing an axial portion of the 203 average fuel rods in this channel. Each volume in the average channel contains a heat structure representing an axial portion of the 38,168 fuel rods in the average channel. Each heat structure representing a fuel rod is nodalized axially in six, equal-length segments.

All Pumps Powered

Cladding temperatures for the hot fuel rod are shown in Fig. 1 for the 15-s LOCA simulation with all the pumps powered. The most salient features of the results shown in this figure are the early rewet of the hot fuel rod and the subsequent low cladding temperatures. By about 5.75 s, all parts of the hot fuel rod did rewet. This phenomenon was observed during LOFT Experiments L2-2 and L2-3 and was calculated to occur in the reference plant by the RELAP4/MOD7 computer code.⁷

The explanation of the cladding temperature behavior can be ascertained from an examination of Figs. 2 and 3. Figure 2 is a comparison of intact- and broken-loop, cold leg mass flows. This figure shows that at about 3 s into the transient, the fluid flow into the vessel exceeded the fluid outflow through the cold leg break. The intact-loop pumps, which remained operating, were responsible for providing the larger magnitude of inflow. Positive fluid flow was subsequently reestablished through the core, as is evident in Fig. 3, which shows mass flows near the middle of the hot channel. A sufficient quantity of fluid mass flowing upward through the core caused a bottom-up rewet of all the fuel rods.

All Pumps Unpowered

Cladding temperatures for the hot fuel rod are shown in Fig. 4 for the 15-s LOCA simulation with the pumps unpowered. This figure shows, like the corresponding figure for the LOCA with the pumps powered, that the hot fuel rod did rewet. However, the rewet occurred somewhat later during this LOCA (at about 9 s).

The explanation of the cladding temperature behavior can be ascertained from an examination of Figs. 5 and 6. Figure 5 is a comparison of intact- and broken-loop, cold leg mass flows. This figure shows that slightly after 3.5 s into the transient, the fluid flow into the vessel exceeded the fluid outflow through the cold leg break. Positive fluid flow was subsequently reestablished through the core, as is evident in Fig. 6, which shows mass flows near the middle of the hot channel. As expected, the magnitude of the reestablished positive core flow was somewhat less with the pumps unpowered than with the pumps powered. Nevertheless, fluid mass flowed upward through the core in sufficient quantity to cause a bottom-up rewet of all the fuel rods.

One Intact-Loop Pump Shaft Broken and Remaining Pumps Unpowered

Cladding temperatures for the hot fuel rod are shown in Fig. 7 for the 15-s LOCA simulation with one intact-loop pump shaft broken and the remaining pumps unpowered. This figure shows that the hot fuel rod did not rewet. Furthermore, the results of a continuation of this simulation showed that this fuel rod had not rewet by 30 s into the transient.

The reason for the absence of a fuel rod rewet can be explained by an examination of Figs. 8 and 9. Figure 8 is a comparison of intact- and broken-loop, cold leg mass flows. Although this figure shows that at about 6 s into the transient the fluid flow into the vessel equals the fluid outflow through the cold leg break, there was no time interval from 6 s forward during which the inflow was significantly larger than the outflow. Thus, positive fluid flow through the core was not reestablished, as is evident in Fig. 9, which shows mass flows near the middle of the hot channel. It is evident from this figure that not only did the loss of one intact loop pump cause a failure to reestablish positive core flow, but that this loss also caused nearly stagnant hydraulic conditions in the core. The consequence of this early core-flow stagnation was the absence of a fuel rod rewet.

Two Intact-Loop Pump Shafts Broken and Remaining Pumps Unpowered

Cladding temperatures for the hot fuel rod are shown in Fig. 10 for the 15-s LOCA simulation with two intact-loop pump shafts broken and the remaining pumps unpowered. This figure shows multiple heatup/rewet cycles, culminating in the rewet of the hot fuel rod.

The explanation of the cladding temperature behavior can be ascertained from an examination of Figs. 11 and 12. Figure 11 is a comparison of intact- and broken-loop, cold leg mass flows. This figure shows that the fluid flow into the vessel was less than the fluid outflow through the break from nearly the beginning of the transient until nearly 10 s into the transient. Thus, positive fluid flow through the core was not reestablished, as is evident in Fig. 12, which shows mass flows near the middle of the hot channel. Furthermore, it shows that the loss of two intact-loop pumps caused the fluid to flow downward through the core, which, by 15 s into the transient, led to a top-bottom rewet of the hot fuel rod.

All Pump Shafts Locked

Cladding temperatures for the hot fuel rod are shown in Fig. 13 for the 15-s LOCA simulation with all pump shafts locked. This figure shows that the hot fuel rod did rewet by 4 s into the transient. This accident is by far the least severe transient discussed here.

The explanation of the cladding temperature behavior can be ascertained from an examination of Figs. 14 and 15. Figure 14 presents a comparison of the intact- and broken-loop, cold leg mass flows. This figure shows that the fluid flow into the vessel was always less than the fluid outflow through the cold leg break from near the beginning of the transient. As a consequence, negative fluid flow through the core persisted, as is evident in Fig. 15, which shows mass flows near the middle of the hot channel. Since the pumps were stopped and the break was a 200%, cold leg break, this core flow behavior was expected. Although the mass flow was downward through the core, its magnitude was sufficiently large to cause an early top-bottom rewet of all the fuel rods.

CONCLUSIONS

The system conditions that led to the most severe thermal transient on the fuel rods during a 200%, DECL break LOCA were one intact-loop, primary coolant pump shaft broken and the remaining PCPs unpowered. With these conditions, core flow was calculated to be sufficiently close to stagnation that the fuel rods were not rewet during the first 15 s. All fuel rods were rewet during the first 15 s of the LOCA simulations with the remaining PCP conditions. However, the nature of the rewets was not the same for all these simulations. For the LOCA simulations during which the pumps were powered or unpowered, but without broken shafts, the fuel rods were rewet by a sufficient quantity of liquid flowing upward through the core. These bottom-up rewets occurred because the performance of the intact-loop pumps caused positive core flow to be reestablished. For the simulations during which two intact-loop pump shafts were broken or the pump shafts were locked, the fuel rods were rewet by a sufficient quantity of liquid flowing downward through the core. These top-bottom rewets occurred because the low performance of the intact-loop pumps permitted a significant negative core flow to be maintained during most of the transient.

The nature of these rewets and the intermediate performance of the PCPs in delivering fluid to the reactor vessel under Condition 3 support the conclusion that the system conditions leading to the most severe thermal transient on the fuel rods during a 200%, DECL break LOCA in a four-loop plant are one intact-loop, PCP shaft broken and the remaining PCPs unpowered. Although these special conditions led to a nonrewetting LOCA transient, the probability of their occurring simultaneously with a 200%, DECL break is extremely small. Therefore, the possibility of a nonrewetting, large-break LOCA transient occurring should not be a major concern in the safety of nuclear plants similar to the Westinghouse four-loop design.

NOTICE

This paper was prepared as an account of work sponsored by an agency of the United States Government. Neither the United States Government nor any agency thereof, or any of their employees, makes any warranty, expressed or implied, or assumes any legal liability or responsibility for any third party's use, or the results of such use, of any information, apparatus, product or process disclosed in this report, or represents that its use by such third party would not infringe privately owned rights. The views expressed in this paper are not necessarily those of the U.S. Nuclear Regulatory Commission.

REFERENCES

1. M. McCORMICK-BARGER, "Experiment Data Report for LOFT Power Ascension Test L2-2," TREE-1322, EG&G Idaho, Inc. (1979).
2. P. G. PRASSINOS et al., "Experiment Data Report for LOFT Power Ascension Experiment L2-3," TREE-1326, EG&G Idaho, Inc. (1979).
3. T. L. DeYOUNG, "RELAP4/MOD7 Developmental Checkout: Zion," EGG-CDAP-5308, EG&G Idaho, Inc. (1980).

4. T. C. deBOER, "RELAP4/MOD7 Commercial PWR Large Break Transient Analysis Compared with LOFT Data," EGG-LOFT-5401, EG&G Idaho, Inc. (1981).
5. P. N. DEMMIE, "Primary Coolant Pump Effects on Core Thermal Response During Large Break LOCA Transients in a Commercial Pressurized Water Reactor," EGG-LOFT-5505, EG&G Idaho, Inc. (1981).
6. V. H. RANSOM et al., "RELAP5/MOD1 Code Manual, Volumes 1 and 2," NUREG/CR-1826, EGG-2070, EG&G Idaho, Inc. (1982).
7. S. R. BEHLING et al., "RELAP4/MOD7--A Best Estimate Computer Program to Calculate Thermal and Hydraulic Phenomena in a Nuclear Reactor or Related System," NUREG/CR-1998, EGG-2089, EG&G Idaho, Inc. (1981).

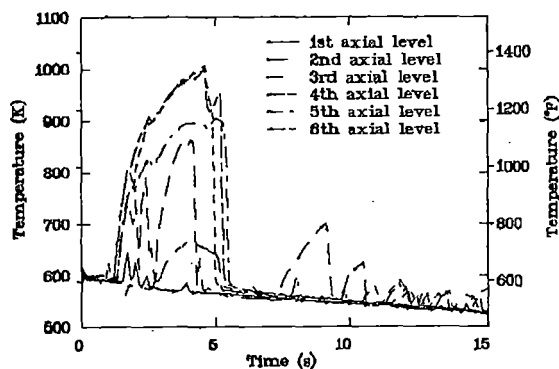


Figure 1. Cladding temperatures for hot fuel rod during a LOCA with pumps powered.

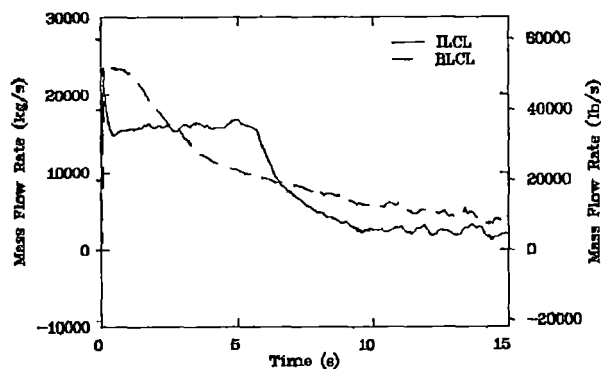


Figure 2. Intact- and broken-loop cold leg mass during a LOCA with pumps powered.

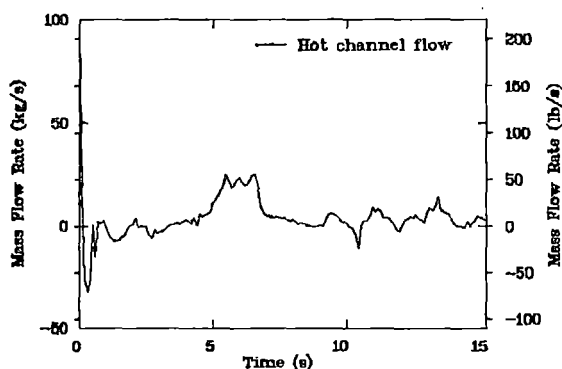


Figure 3. Mass flows at core hot spot during a LOCA with pumps powered.

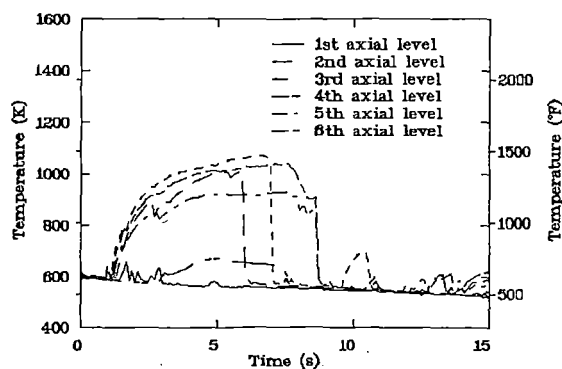


Figure 4. Cladding temperatures for hot fuel rod during a LOCA with pumps powered.

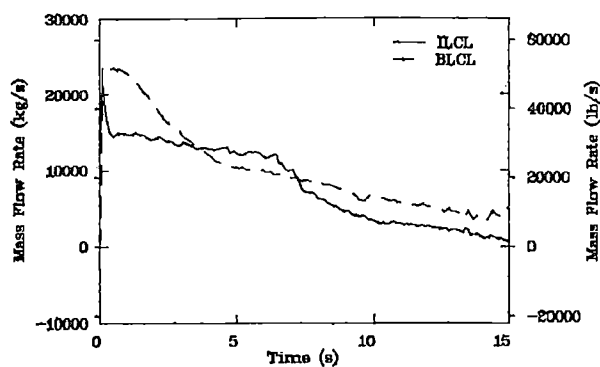


Figure 5. Intact- and broken-loop cold leg mass flows during a LOCA with pumps unpowered.

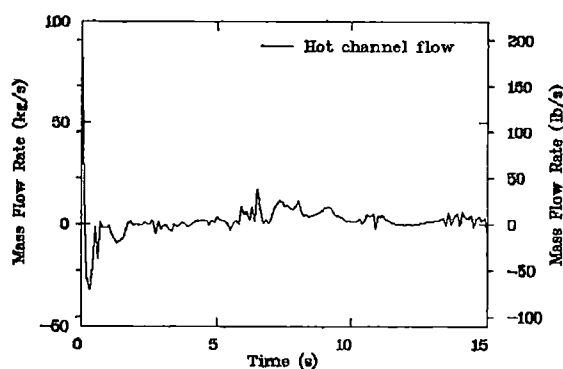


Figure 6. Mass flows at core hot spot during a LOCA with pumps unpowered.

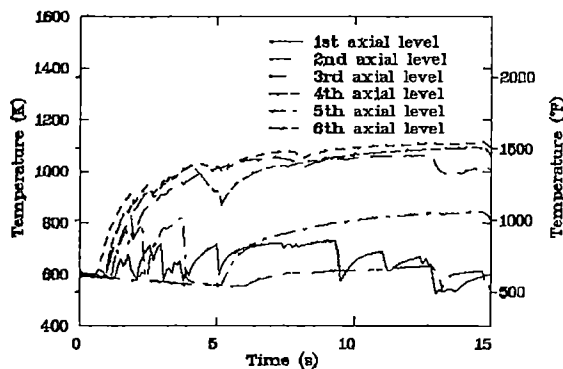


Figure 7. Cladding temperatures for hot fuel rod during a LOCA with one intact-loop pump shaft broken.

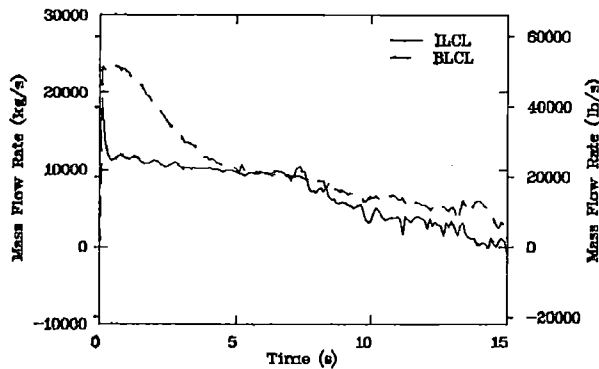


Figure 8. Intact- and broken-loop cold leg mass flows during a LOCA with one intact-loop pump shaft broken.

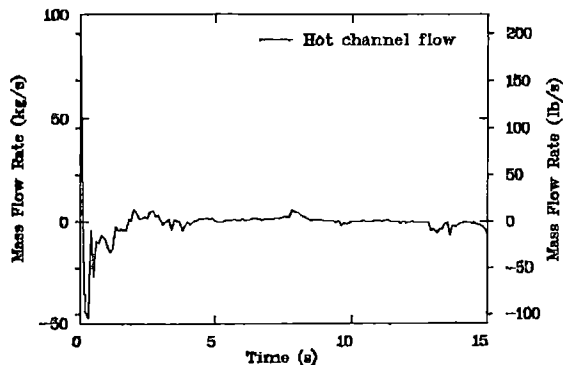


Figure 9. Mass flows at core hot spot during a LOCA with one intact-loop pump shaft broken.

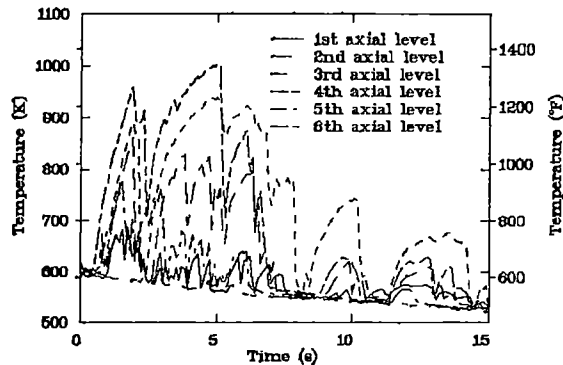


Figure 10. Cladding temperatures for hot fuel rod during a LOCA with two intact-loop pump shafts broken.

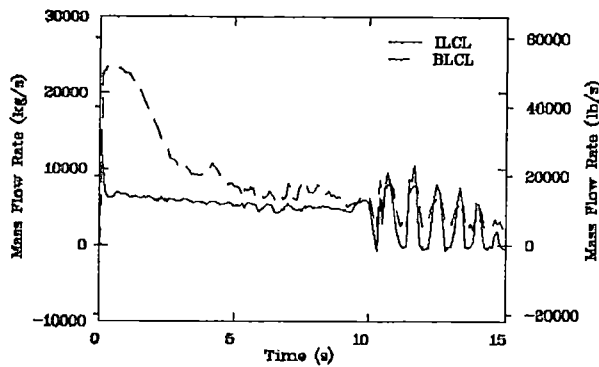


Figure 11. Intact- and broken-loop cold leg mass flows during a LOCA with two intact-loop pump shafts broken.

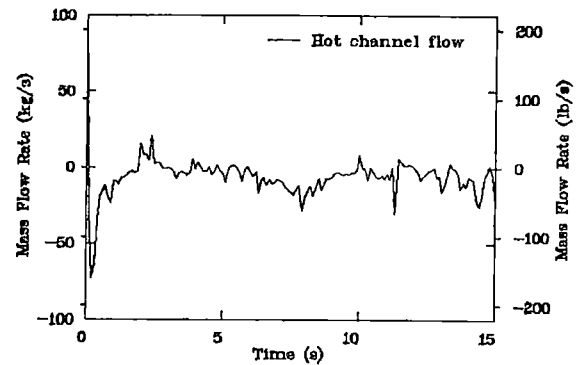


Figure 12. Mass flows at core hot spot during a LOCA with two intact-loop pump shafts broken.

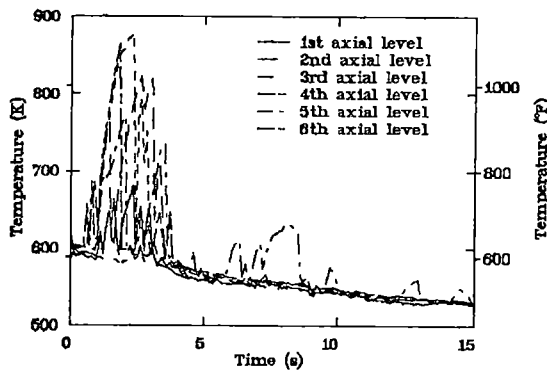


Figure 13. Cladding temperatures for hot fuel rod during a LOCA with pump shafts locked.

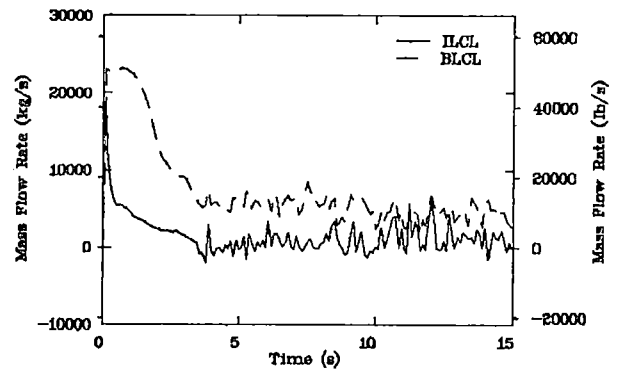


Figure 14. Intact- and broken-loop leg mass flows during a LOCA with pump shafts locked.

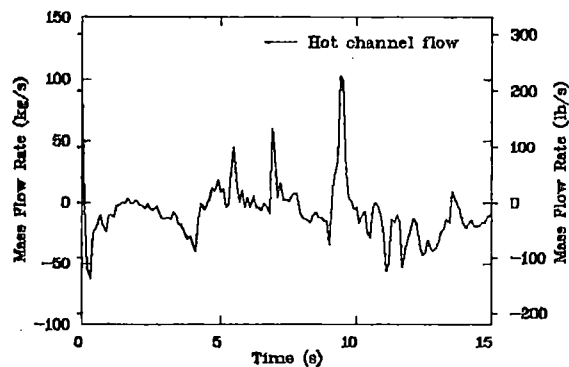


Figure 15. Mass flows at core hot spot during a LOCA with pump shafts locked.

TRAC ANALYSIS OF THE SYSTEM PRESSURE EFFECTS TESTS IN THE SLAB CORE TEST FACILITY

Suzanne T. Smith
Los Alamos National Laboratory
Los Alamos, New Mexico 87545, U.S.A.

ABSTRACT

This paper describes the analysis, using the TRAC computer code, of three system pressure effects reflood tests performed during 1981 at the Slab Core Test Facility at the Japan Atomic Energy Research Institute in Tokai, Japan. Comparisons of the calculated results with the experimental data were very good, particularly for rod temperature histories, core differential pressures, mass inventories, liquid carryover, and fluid velocities in the loops. These comparisons indicate that the TRAC code can predict reasonably well the effects of pressure variations in test conditions. This and similar calculations demonstrate that TRAC is a useful tool for the design of nuclear reactor systems and the analysis of system response during postulated accident sequences.

INTRODUCTION

The TRAC [1] computer code was used to analyze three Slab Core Test Facility (SCTF) system pressure effects tests performed in 1981 at the Japan Atomic Energy Research Institute (JAERI) in Tokai, Japan. These calculations were performed as blind analyses, knowing the actual initial conditions of the tests but with no foreknowledge of the results.

The SCTF is part of a multinational program to obtain data, develop improved correlations, and assess best-estimate computer codes for the analysis of loss-of-coolant accidents (LOCAs) in pressurized water reactors (PWRs) during the end-of-blowdown, refill, and reflood phases by means of experiments in large test facilities in Japan and Germany.

TRAC CODE DESCRIPTION

The analysis tool used for these calculations was the Transient Reactor Analysis Code (TRAC) [1], which has been developed at Los Alamos to provide an advanced best-estimate predictive capability for the analysis of postulated accidents in light water reactors. TRAC provides this analysis capability for light water reactors and

for a wide variety of thermal-hydraulic experimental facilities. It features a three-dimensional treatment of the pressure vessel and associated internals; two-phase nonequilibrium hydrodynamics models; flow-regime-dependent constitutive equation treatment; reflood tracking capability for both bottom flood and falling film quench fronts; and consistent treatment of entire accident sequences, including the generation of consistent initial conditions. It has been assessed against data from a diverse range of experimental facilities.

TRAC-PD2/MOD1 (version 26.2) was the code version used for these calculations.

DESCRIPTION OF THE SCTF

The SCTF is composed of the pressure vessel, primary coolant system, and emergency core cooling (ECC) system. Figure 1 shows an artist's view of the SCTF. The pressure vessel contains the slab core, downcomer, upper and lower plena, core baffle region, and upper head. The facility is full-scale in height and half-scale in width. The slab core consists of eight bundles of electrically-heated rods in a 16 x 16 matrix. These eight bundles are arranged in a row numbered from the innermost bundle (1) representing the core center to the outermost bundle (8) on the downcomer side. There are blockage sleeves near the core midplane in Bundles 3 and 4 to simulate fuel rod ballooning.

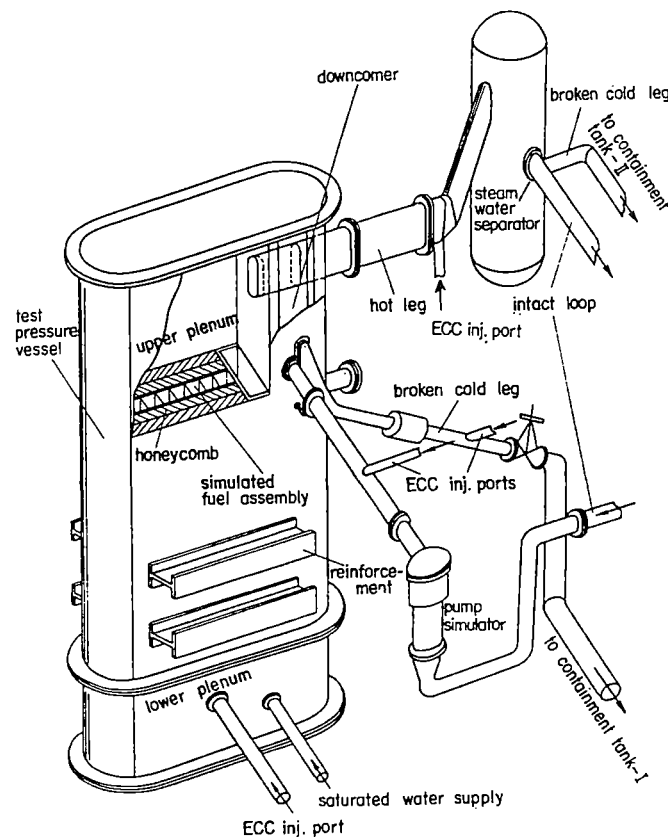


Fig. 1. Artist's view of the Slab Core Test Facility.

The primary coolant system comprises an intact loop, a broken loop with controllable valves simulating the breaks, a steam-water separator, and two containment tanks. ECC water can be injected into the intact cold leg or directly into the plena. The accumulator (ACC) and low-pressure coolant injection (LPCI) system is connected to the pressure vessel at the bottom of the lower plenum on the downcomer side.

TEST OPERATING PROCEDURE

The series of forced-flooding tests discussed herein included Runs 506, 507, and 508 (Run 507, the base case test, was the first of the main test series for this new facility). The initial system pressures were 3.97, 1.98, and 1.5 bars, respectively. For all these tests, the downcomer was blocked at the bottom, allowing flow only in the core and bypass regions. The lower-plenum ACC and LPCI systems were operational, but the cold-leg and upper-plenum ECC systems were not. The initial fluid and structure temperatures were the saturation temperature at the given system pressure. The initial power for all three tests was about 7 MW. The axial power distribution was a chopped cosine, and the radial power distribution was specified as:

Bundles 1 and 2	0.940
Bundles 3 and 4	1.0
Bundles 5 and 6	0.953
Bundles 7 and 8	0.863 .

Initially, the lower plenum was half full of saturated water.

Operation of these tests began by heating the rods electrically until a specified cladding temperature (926 K) was reached ($t = 0$ s). After a 2 s delay, a 20 kg/s ACC flow was initiated and held constant until 17 s, when a 10 kg/s LPCI flow was actuated and held constant until quench. At 6 s, the power began to decrease according to the standard "ANS + actinides" decay curve.

THE COMPUTATIONAL MODEL

The TRAC computational model developed at Los Alamos for the SCTF uses a two-dimensional VESSEL component for the pressure vessel (154 cells) and a three-dimensional VESSEL component for the steam-water separator (8 cells). One-dimensional components comprising 51 computational cells were used for the rest of the primary system. Figure 2 shows schematics of the SCTF pressure vessel and primary system. The hot leg and the lower-plenum ACC/LPCI injection nozzles were modeled as PIPE components, the intact cold leg with the cold-leg ECC injection nozzle as a TEE component, the two segments of the broken cold leg as VALVE components, the two containment tanks as BREAK components attached to each of the broken cold legs, and the cold-leg and lower-plenum ECC injection capability as FILL components. In total, there were 213 computational cells in the TRAC model.

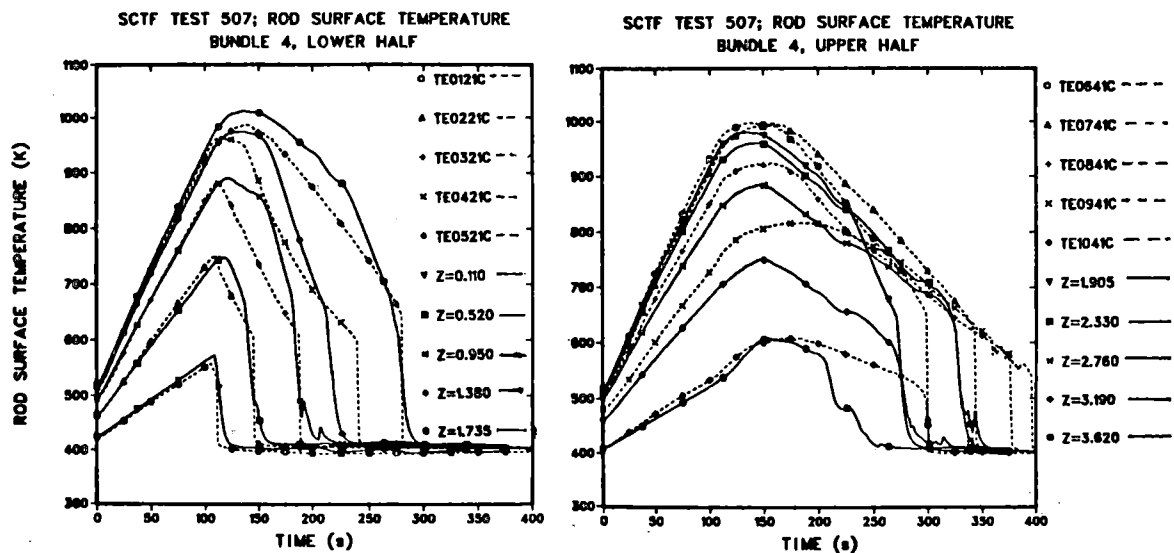


Fig. 3. Comparison of the calculated and experimental cladding temperatures at the ten thermocouple locations for Run 507.

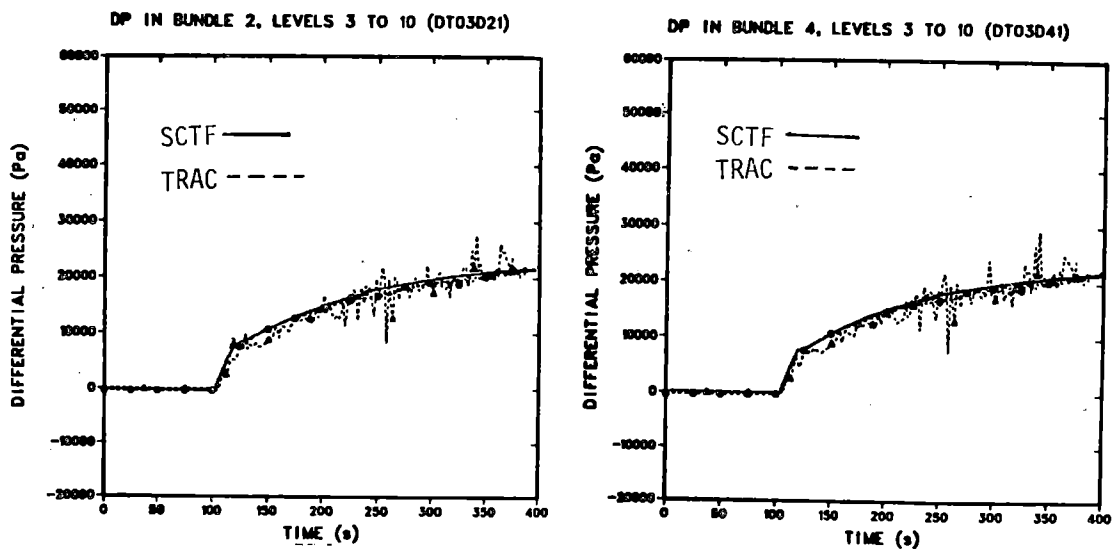


Fig. 4. Comparison of the calculated and experimental core full-height differential pressures for Run 507.

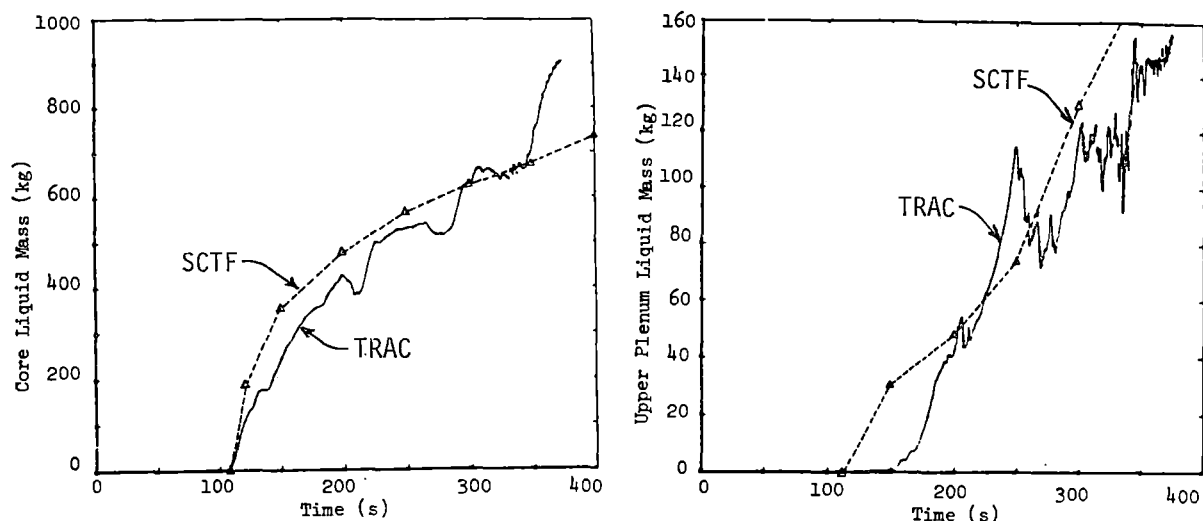


Fig. 5. Comparisons of calculated and experimental liquid mass in the core and upper plenum for Run 507.

accumulation in the separator than the data because of more carryover into the hot leg of the entrained liquid in the calculations.

EFFECTS OF THE SYSTEM PRESSURE VARIATION

The effects of the pressure variation were well-predicted by TRAC, agreeing closely with the trends seen in the tests. The general trend was that the higher the system pressure, the more rapidly the core cooled and quenched.

Maximum cladding temperatures were lower at higher pressure and quench occurred sooner, demonstrated by comparing the quench envelopes for selected bundles for the three runs shown in Fig. 6. The heat-transfer processes were more sedate at lower pressures, with less sputtering steam generation as the quench front progressed through the core. In addition, the lower pressure allowed more liquid fallback into the core from the upper plenum, resulting in more top-down quenching. The higher system pressure produced less liquid carryover into the steam-water separator, as well as less liquid accumulation in the upper plenum, than did the lower pressures. The reason is that, even though higher pressures require lower steam velocities for entrainment, the high-pressure test generated steam more rapidly at the quench front, leaving less liquid for entrainment in the region of the quench front. The calculation of the low-pressure test showed larger steam velocities (because of a lower steam density) with more entrainment than the high-pressure test, so that the core flooding was slower, but still the calculation showed that the core cooled more rapidly than was observed in the experiment. There were some wide-band pressure pulses observed in the calculation that were not seen in the data; the period of the pulses was about the same (50 - 60 s) for all three runs, but the amplitude was considerably less at lower pressure because, for film and transition boiling, the differences in the heat-transfer coefficients are higher at higher pressures [2], indicating more volatile heating processes.

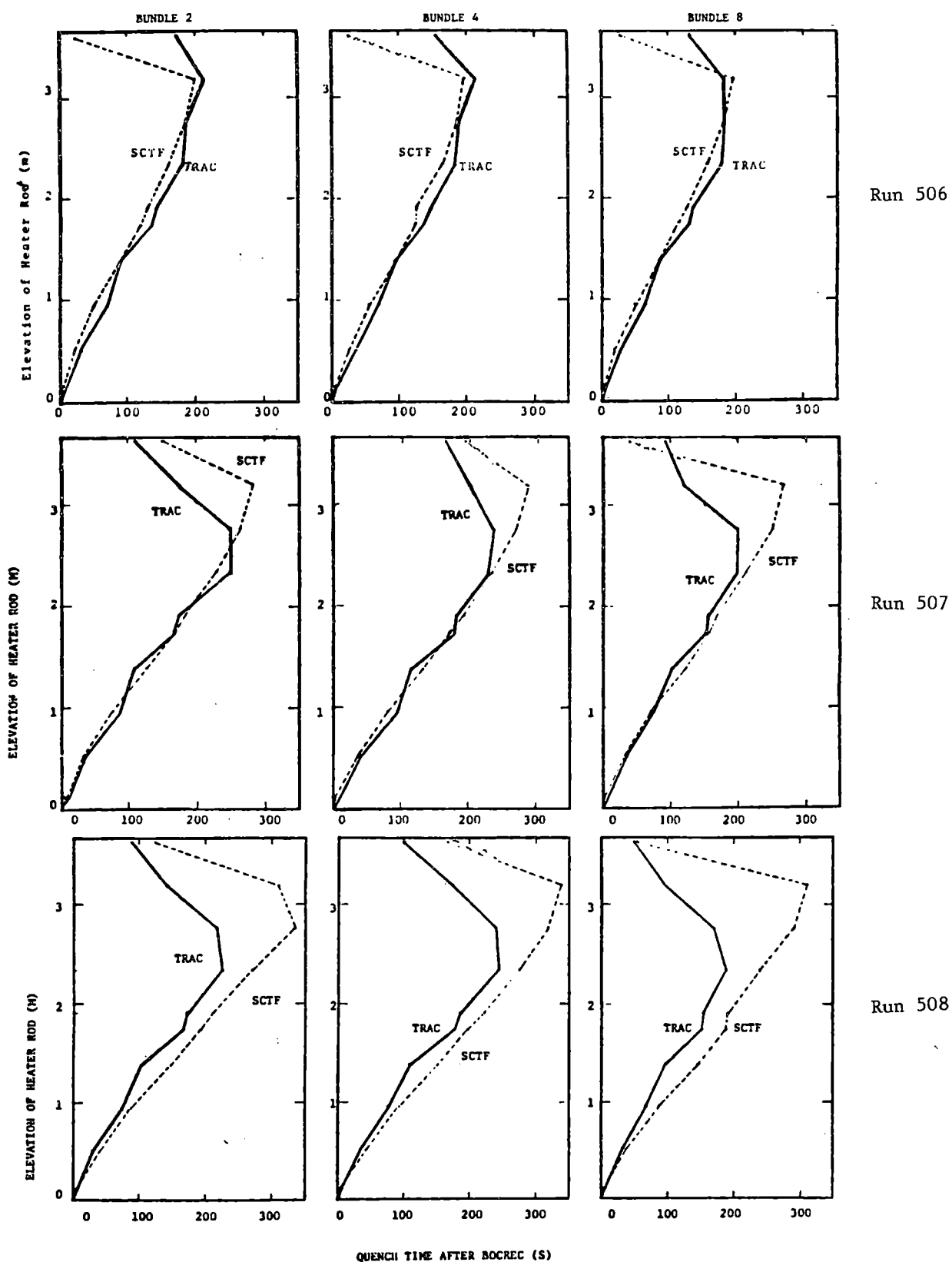


Fig. 6. Comparison of quench times after bottom-of-core-recovery (BOCREC) for Bundles 2, 4, and 8 in Runs 506, 507, and 508.

There was little noticeable effect of the 50% blockages in Bundles 3 and 4 in either the calculations or the data for any of the experiments when the blocked bundles were compared with the unblocked bundles; this was anticipated because of previous experiments [3] at Karlsruhe. However, this may change under gravity-reflood conditions.

CONCLUSIONS

The most important result arising from this study is that both the calculations and the data show that the core quenches sooner at higher pressure. More liquid accumulation in the steam-water separator and more upper plenum liquid pool formation and fallback into the core were seen clearly in both the calculations and the data at lower pressure. In most other areas, the calculations were close to the experimental data, particularly in predicting the trends.

These calculations show that TRAC can predict both the qualitative and quantitative effects of parametric variations in test conditions quite well. This and similar calculations demonstrate that TRAC is a useful tool for the design of nuclear reactor systems and the analysis of system response during postulated accident sequences.

ACKNOWLEDGMENTS

This work was performed under the auspices of the United States Nuclear Regulatory Commission.

Special assistance in plotting the experimental results over our calculated results came from Dr. Yukio Sudo (JAERI) [4], who visited us at Los Alamos during September, 1981, bringing with him the data plots from the first few tests.

REFERENCES

1. Safety Code Development Group, "TRAC-PD2: An Advanced Best-Estimate Computer Program for Pressurized Water Reactor Loss-of-Coolant Accident Analysis," Los Alamos National Laboratory report LA-8709-MS (May 1981).
2. J. G. Collier, Convective Boiling and Condensation, (McGraw-Hill International Book Company, London, 1981), pp. 224-225.
3. P. Ihle, "Flooding Experiments in Blocked Arrays," presented at the Eighth Water Reactor Safety Research Information Meeting, Gaithersburg, Md., October, 1980.
4. Y. Sudo, "Analysis of TRAC and SCTF Results for System Pressure-Effects Tests Under Forced Flooding (Runs 506, 507, and 508)," Los Alamos National Laboratory report LA-9258-MS (March 1982).

LOSS OF COOLANT ACCIDENTS IN HTGR's

U.Weicht/W.Wachholz

Hochtemperatur-Reaktorbau GmbH
Gottlieb-Daimler-Straße 8
6800 Mannheim 1
Federal Republic of Germany

ABSTRACT

Loss of coolant in HTGR's merely means a reduction in coolant density and not a total loss. The auxiliary cooling systems are designed to operate at or near atmospheric pressure. In general, two out of four auxiliary cooling systems are sufficient to remove the decay heat without violating the design limits of the plant.

In the hypothetical case of a depressurisation of the primary circuit and no active cooling at all, part of the coated fuel particles would be damaged within a period of days, leading to a larger increase of activity in the primary circuit and subsequently in the containment. Only if an additional failure of the liner cooling system has to be regarded, non-condensable gases, originating from a desintegration of the concrete pressure vessel, might accumulate within several days in the containment, where they could be drawn off through filtering systems.

INTRODUCTION

The basic concept of the HTGR - with respect to the type of accident under consideration - is characterised by

- its gaseous coolant, i.e. helium
- the all-ceramic reactor core, containing UO_2 or UC_2 fuel kernels coated with pyro-carbon within a graphite matrix
- and the burst-proof concrete pressure vessel furnished with a temperature resistant insulation and a cooling system at its inner surface.

Fig. 1 shows - on a mock-up - the design of the THTR-prototype reactor, just being under construction in Germany. The core consists of nearly 700,000 spherical fuel elements, each of them containing roughly one gramme of fissile and ten grammes of fertile material.

The working pressure of the primary coolant helium is 40 bars,

yielding a total mass of 8500 kg within the primary circuit.

Due to the lower heat transfer and heat transport properties of helium compared to a liquid water or liquid metal coolant, the core power density of HTGR's is lower by a factor of 10 to 50 compared to other reactor systems. On the other hand, the heat capacity of the reactor core and the reflectors is comparatively high and their failure temperature is far beyond the range of operating temperatures. Thus, in HTGR's the rate of temperature change is extremely low in case of a mismatch between power generation and heat removal.

Fig. 2 and 3 illustrate the "good-natured" behaviour of e.g. the THTR: A sudden reduction of the coolant gas flow leads to a slight increase of the mean fuel temperature and hence - due to the negative temperature coefficient of the reactivity - to a reduction of the core power. Within less than five minutes all the thermal parameters of the core have reached a new equilibrium with slightly increased fuel element and gas temperatures and a reduced core power.

Similarly a sudden increase of the reactivity by 10^{-3} is compensated by a moderate increase in the fuel temperatures.

In the following the different types of depressurisation accidents will be discussed (Fig. 4):

Small leakages at different seals and welds up to 10^{-3} per day, i.e. 8 kg per day, are within the bounds of normal operating conditions. This leakage is conducted by the ventilation system - mainly via filters - to the stack and finally to the surrounding environment. The corresponding activity release is less than 2.5 mrem/a. These losses of helium are permanently compensated by the gas purification plant.

Leaks in the primary circuit leading to a depressurisation can occur at one of the numerous penetrations of the concrete pressure vessel, e.g. control rods, instrumentation, gas purification and - in case of a pebble bed reactor - at the charge and discharge tubes. The cross-section for leakages at these penetrations can be restricted by construction to very small values of the order of a few cm^2 , leading to a depressurisation time of several hours. The average probability for such an event is in the order of 10^{-3} /a.

For the follow-up design of the THTR larger leakages can occur at the closures of the larger vessel pods which house the steam generators, blowers or auxiliary cooling systems. Here, the maximum cross section is limited to roughly 200 cm^2 by an appropriate construction and supervision over the life-time. The corresponding depressurisation time is a few minutes; the probability less than 10^{-4} /a.

When discussing loss of coolant accidents in HTGR's it is important to realize, that loss of coolant merely means a reduction in coolant density and not a total loss. The final coolant pressure after depressurisation will be at or near atmospheric pressure, a value, which the decay heat removal systems are designed for.

Fig. 5 shows the plant behaviour of the THTR for the maximum depressurisation rate, if no reactor trip and shut down were initiated: According to the diminishing coolant pressure the core mass

flow and the core power are reduced. The latter being a consequence of the negative temperature coefficient of the reactivity. With proper plant control, the core outlet temperature will be reduced by gradually inserting the control rods in order to avoid an increase of the steam temperature. Without this plant control the core outlet temperature and hence the steam temperature would increase slightly.

In reality, the depressurisation will be recognized by the plant protection system when the primary pressure falls below 35 bars.

In general, HTGR's are equipped with 4 x 50% decay heat removal systems to cope with a depressurisation accident, each of them providing a core flow of approximately 0,5% of the normal gas flow. Thus, the heat removal of two systems balances the decay heat production after 1 - 2 hours and achieves thereafter a steady reduction of the core temperatures. With the availability of two systems out of four, depressurisation accidents within the probability range to be regarded can be tolerated by the plant without exceeding the design limits of components in the primary circuit (Fig. 6 and 7).

Depending on the location and configuration of the leak, air or a mixture of air and helium from the containment atmosphere may enter the primary circuit by a convective mass transfer at the opening. Additionally, any reduction of the temperatures in the primary circuit after the equalization of the inner and outer pressures at the leak, leads to a suction of containment atmosphere into the primary circuit.

In the THTR, which is equipped with a vented containment, atmospheric pressure fluctuation could cause supplementary air ingress.

The total amount of air in the primary circuit, for instance in the THTR, can amount to 300 kg, yielding no undue corrosion problems even under conservative assumptions.

Hypothetical accidents can be postulated by combining a depressurisation with the unavailability of more than two decay removal systems and the liner cooling system.

If only one system were operating with a mass flow in the order of 0,5%, the maximum core temperatures, i.e. the temperatures of the fuel elements in the active zone, would reach nearly 1400°C, which still is far below the failure limit of coated particles. The corresponding core outlet temperature from the bottom reflector attains a maximum of 1100°C which, however, will be considerably reduced by mixing with the cold bypass -flow (back-flow) through the non-operating heat-exchanger and steam generator units.

In the event of no active cooling at all, the total decay heat is stored primarily in the core, the maximum temperatures of which increase within the first 10 h at an average rate of 100°C/h (Fig. 8). Depending on the size, i.e. power output of the reactor, the maximum fuel temperature will stabilize after a few days - for example in a 1200 MW thermal plant - in the range of 2500°C at the location of maximum power density. The majority of the fuel elements, however, attains temperatures less than 2000°C, when particle failures just begin.

Even at the maximum of 2500°C the all-ceramic fuel elements still maintain their stability and strength, but the fuel-particles are damaged. Gaseous fission products as well as metallic ones will diffuse out of the hottest fuel elements, will be absorbed on cooler parts of the core and the primary circuit and will be finally swept partly into the containment.

The reactor internals, i.e. reflectors, the thermal shield and the liner insulation would experience a moderate temperature increase, which - although above design-limits - is even two weeks after the initiating accidental event still far below the temperatures for gross failure of these components.

The behaviour of the concrete pressure vessel is predominantly defined by the liner insulation and cooling system, which - on the longterm - is capable of removing the decay heat from the primary circuit and protects the concrete from desintegration. Unless no further independent failures or malfunctions are postulated for the containment, no undue activity is released to the environment.

Ultimately, if an additional failure of the liner insulation and cooling system is regarded, the concrete of the concrete pressure vessel might desintegrate due to high temperatures, producing non-condensable gases. A pressure relief-system (hand-operated or on a fail-safe basis) limits the containment pressure to uncritical values.

The results of these investigations reveal another important aspect of the HTGR: In case of a loss of coolant accident - the same holds true for other accident scenarios - there is always ample time for emergency measures to bring the plant back into safe conditions or at least to diminish the course of the accident.

Moreover, core heat-up accidents, which are generally accompanied by a loss of coolant, are dominating with respect to the public risk, as was shown in the Accident Initiation and Progression Analysis (AIPA) performed by General Atomic Company.

In summary it can be stated, that loss of coolant accidents in HTGR's can be tolerated within the design limits of the plant; even if additional failures of decay heat removal systems are hypothetically postulated, the environment impact is acceptable.

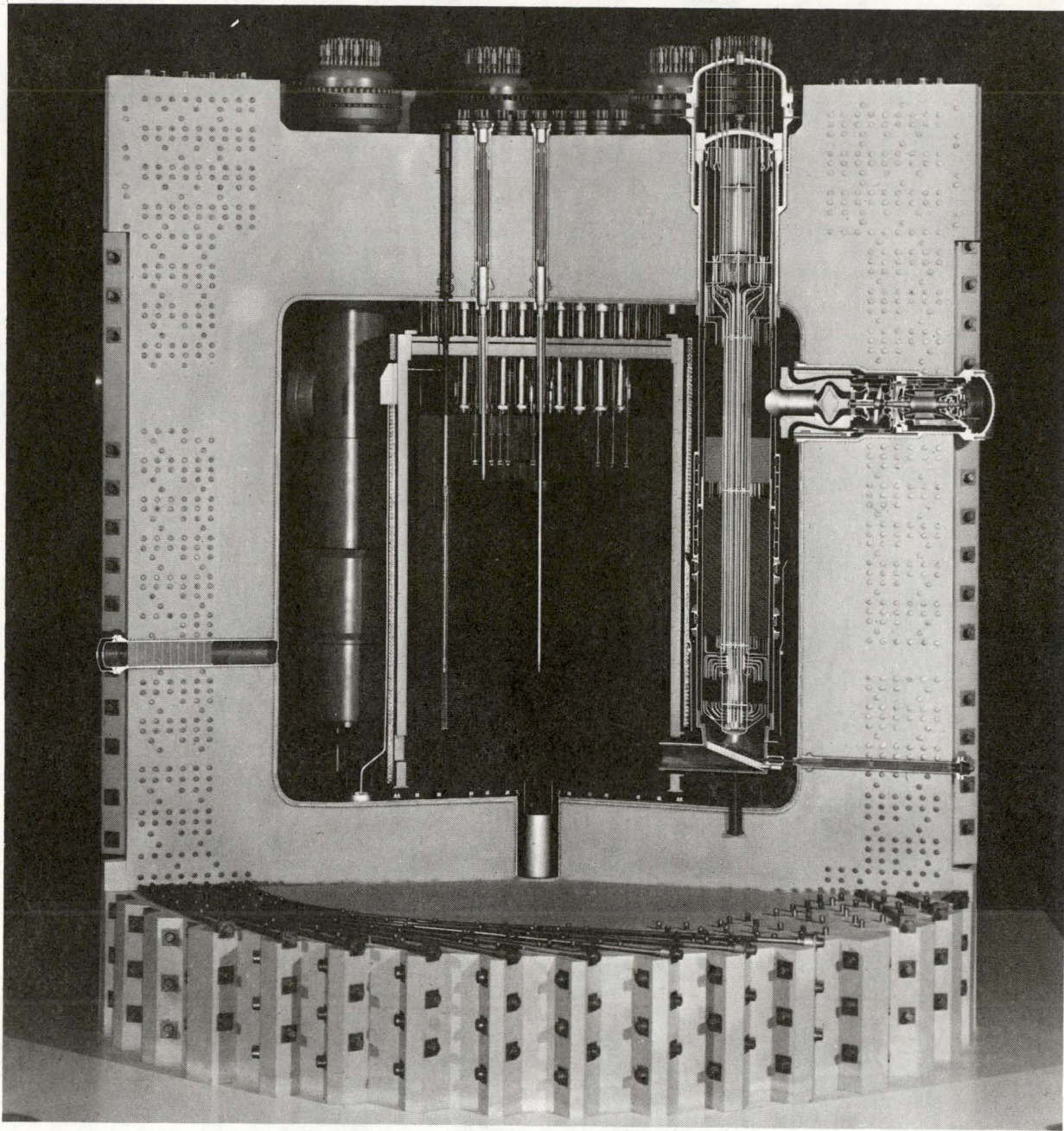


Fig. 1: THTR: CROSS SECTION

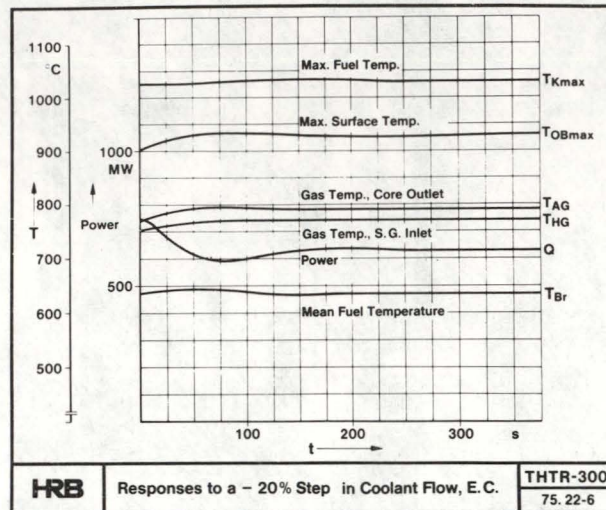


Fig. 2: THTR: SUDDEN REDUCTION OF COOLANT FLOW BY 20%

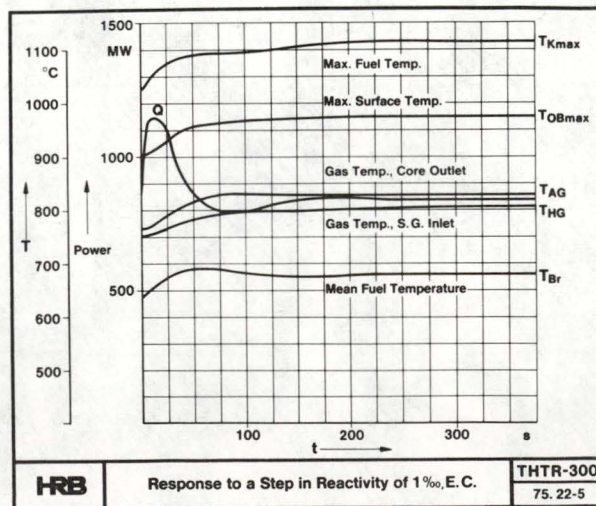


Fig. 3: THTR: SUDDEN INCREASE OF REACTIVITY BY 1‰

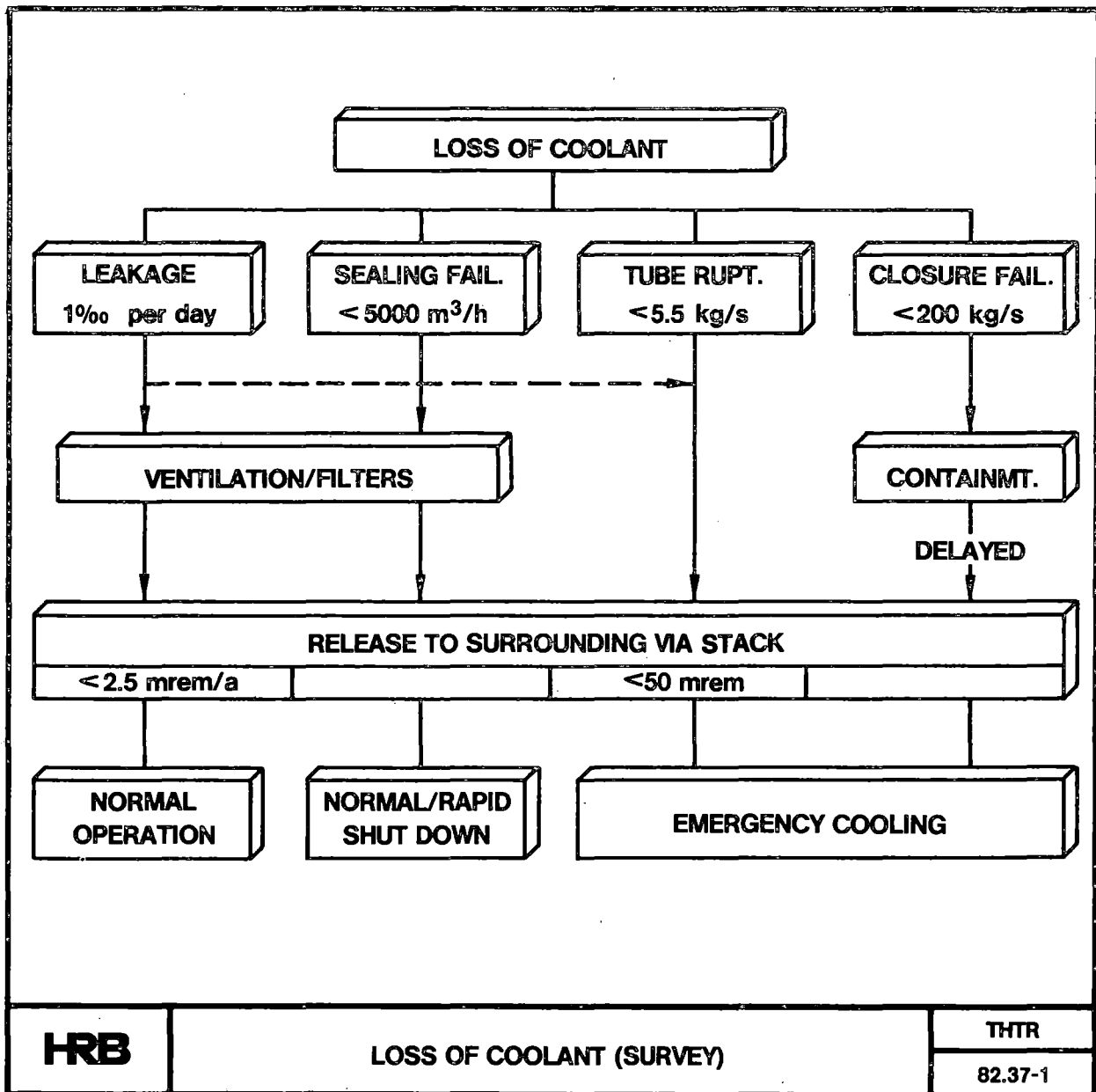


Fig. 4: LOSS OF COOLANT (SURVEY)

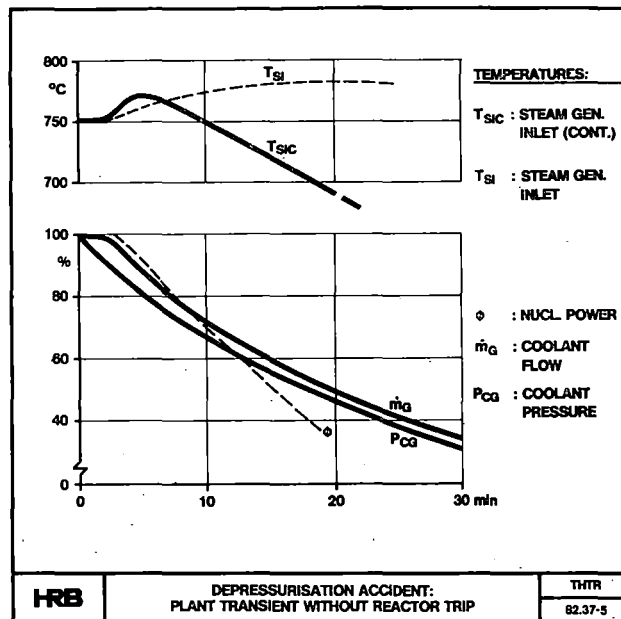


Fig. 5: THTR: DEPRESSURISATION ACCIDENT WITHOUT REACTOR TRIP

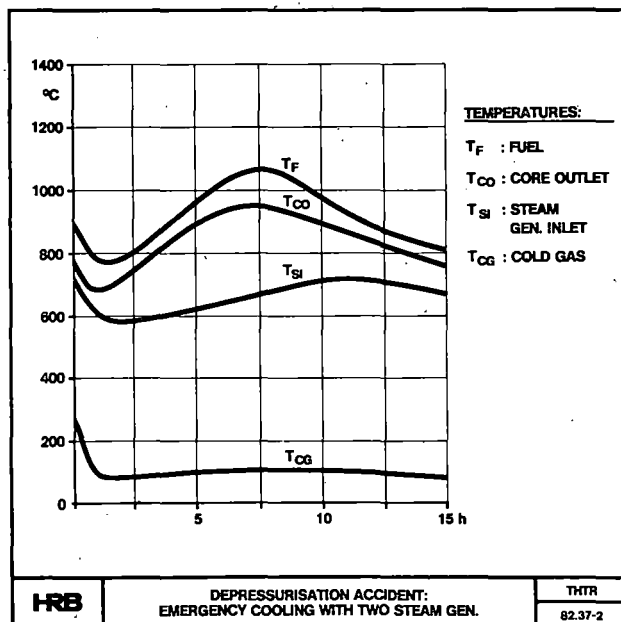


Fig. 6: THTR: DEPRESSURISATION ACCIDENT WITH TWO STEAM GEN.

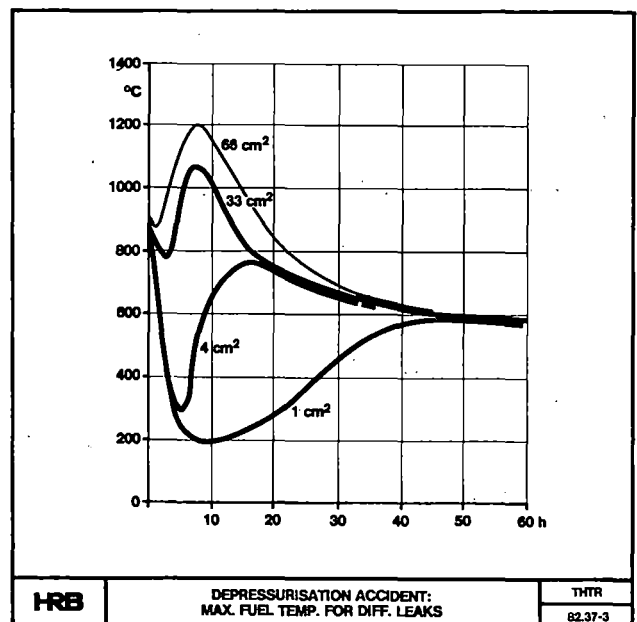


Fig. 7: THTR: DEPRESSURISATION ACCIDENT FOR DIFF. LEAKS

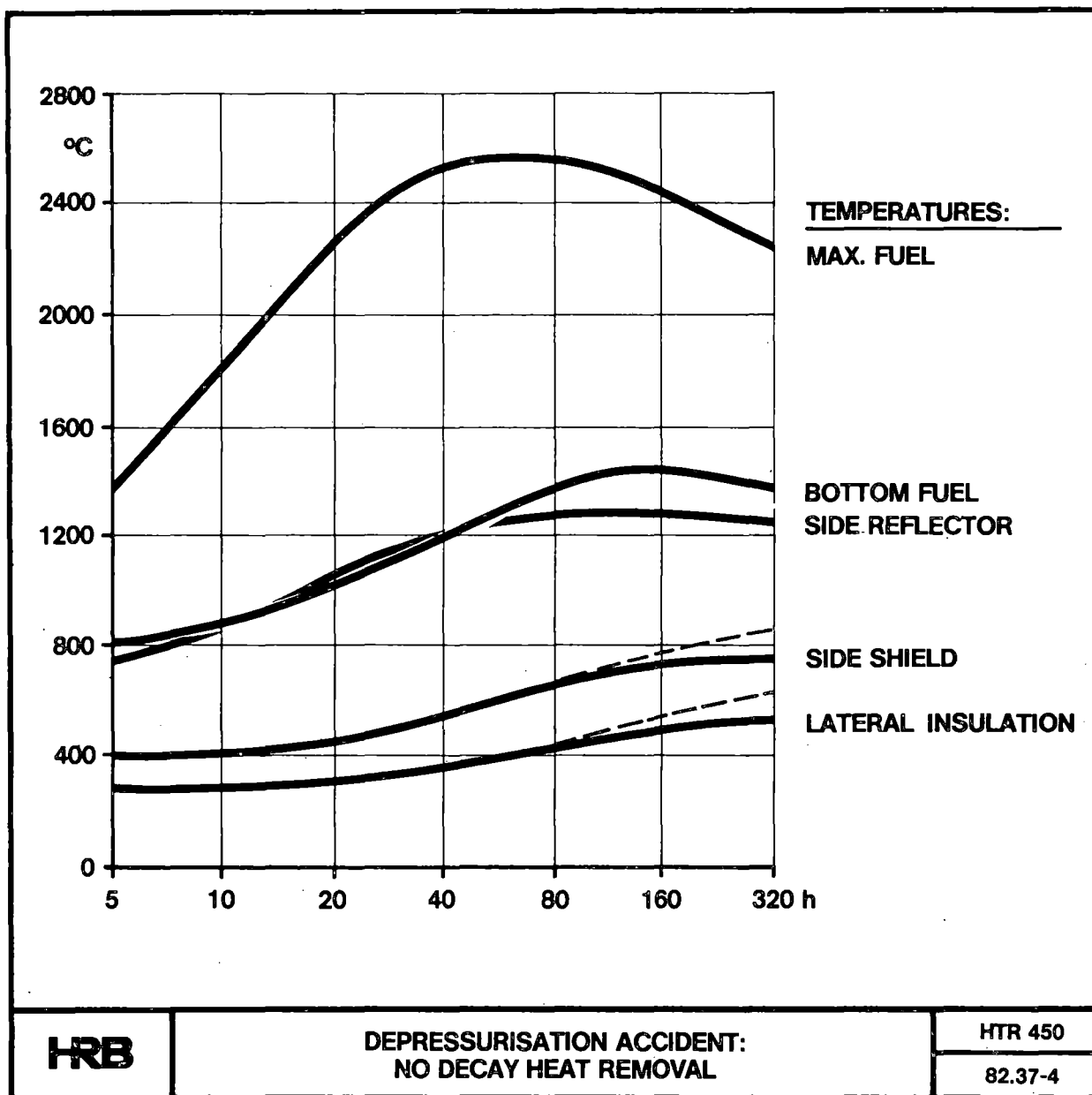


Fig. 8: HTR-450: DEPRESSURISATION ACCIDENT WITHOUT DECAY HEAT REMOVAL

SESSION 30

SAFETY-RELATED DESIGN CONSIDERATIONS

Chair: A. Gauvenet (*EDF*)
W. Loewenstein (*EPRI*)

A FUNCTIONAL DESIGN APPROACH TO PWR SAFETY

M. K. De, J. A. Rumancik, A. J. Impink, and J. R. Easter

Nuclear Technology Division
Westinghouse Electric Corporation
P. O. Box 355, Pittsburgh, PA 15230, U.S.A.

ABSTRACT

The present work in the U.S. nuclear industry directed towards improving response during emergency conditions consists of improvement in emergency procedures, post-accident instrumentation, alarm presentation, and the development of operator aids. This paper contains work in progress for the formulation of a possible basis for such an effort. The basis consists of using a functional relationship chart for PWR safety as a conceptual model for the plant. The functional relationship chart identifies elements important to safety starting from the abstract concepts of fission product barrier maintenance and proceeding to equipment details. The interactions have been structured by using a multilevel flow model of the plant which formulates the purpose, function and supporting systems in terms of mass and energy transport and storage processes, and their functional interrelationship by critical, controllable variables. The methodology for developing a set of critical safety function restoration procedures is also presented to demonstrate application of these concepts.

INTRODUCTION

As a consequence of the accident at TMI, there is presently a considerable effort in the U.S. nuclear industry directed towards improving response during emergency conditions in nuclear power plants. This work consists of improvement in alarm presentation, emergency procedures, post-accident instrumentation, and the development of operator aids. Westinghouse has recognized the importance of establishing the fundamental basis for all such efforts and for coordinating development from such a basis. This paper describes work in progress for the formulation of this basis and the application of these concepts to emergency procedures and alarm prioritization. The results of the present effort will eventually be used in determining the functional specifications for an Advanced Control Room (ACR). (See Abbreviations list)

It has been identified^[1] that there were three main deficiencies in the control room at TMI: (1) There was a lack of adequate post-accident instrumentation and, therefore, the capability to diagnose plant state; (2) the emergency procedures were designed for responses to single events and did not address the occurrence of multiple failures indicated by plant symptoms; and (3) the alarm system did not suitably alert the operators to the changes in plant state, but rather was a source of confusion. This paper describes the present ongoing effort at addressing the above deficiencies and integrating control room functional design aspects. The effort is composed of applications of new design methods which attempt at designing the control room on the functional aspects of the entire plant rather than on single events or on the requirements of each individual system designer. The new methods include the use of plant safety functions and functional flow models of processes to depict systems interactions during accident conditions. There is presently an effort to improve the control room for plant operability and availability also; however, these results are not presented in this paper.

CRITICAL SAFETY FUNCTIONS AND PLANT OPERATIONS DURING EMERGENCY CONDITIONS

This work was initiated in Phase II of the Electric Power Research Institute Disturbance Analysis and Surveillance project,[2,3] during which a functional relationship chart for PWR safety was formulated as a conceptual model of a nuclear power plant. The functional relationship chart identified the primary objective in the design of a nuclear power plant from a public health and safety viewpoint, which is to prevent radioactive releases to the environment. Multiple fission product barriers are designed to achieve this objective, and are kept intact by maintaining critical parameters within limits. Systems and subsystems are provided to perform functions which maintain these critical parameters within limits and are composed of various individual components. Thus, the plant can be envisioned as a multilevel pyramid starting with the objective of preventing radioactive release and broadening continually until the individual component level is reached. Figure 1 is the top section of the aforementioned functional relationship chart and shows the critical parameters (safety functions) in the plant that have to be controlled within limits to maintain the integrity of the barriers which prevent the release of radioactive material to the environment. Also shown are the control requirements and available plant systems.

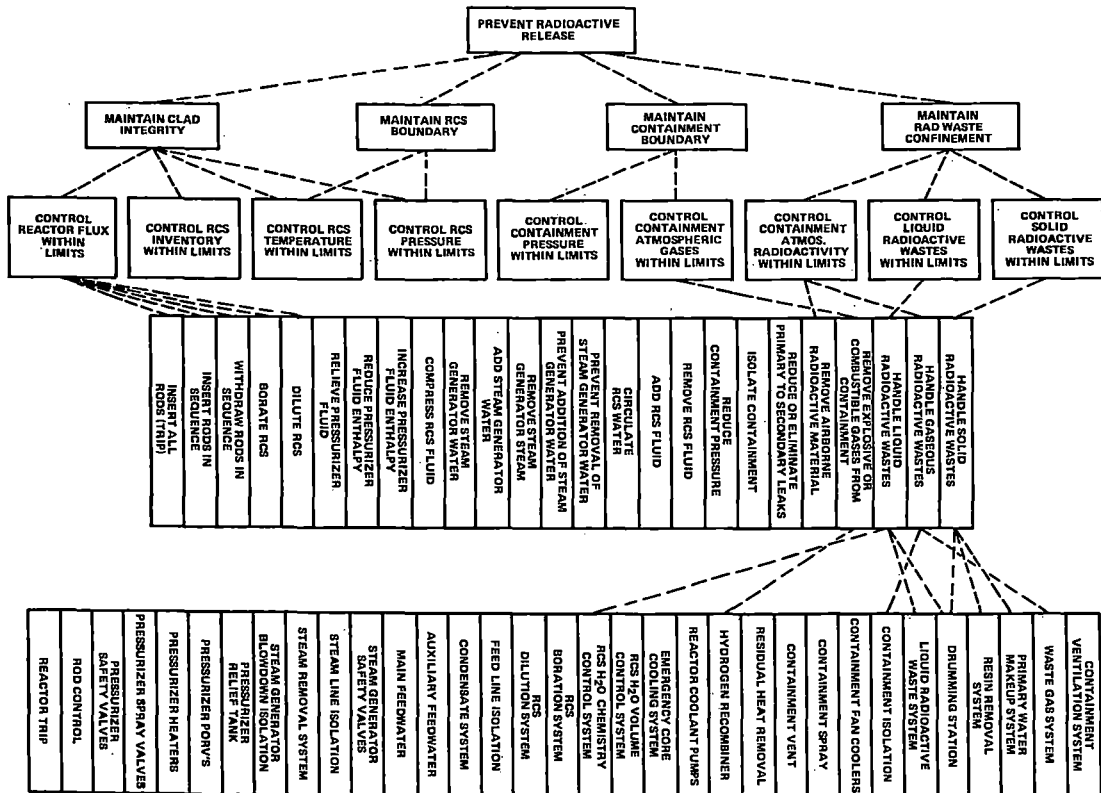
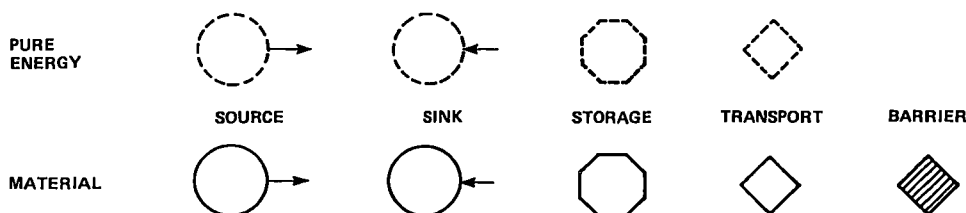


Figure 1. Critical Safety Requirements and Functions Chart

The set of critical safety parameters shown in Figure 1 has been used as the basis for constructing a set of plant safety status trees that would guide an operator to perform appropriate control actions to maintain plant critical parameters within limits. For example, Figure 2 shows the plant safety status tree for the critical parameter, reactor coolant system (RCS) pressure. The endpoints FP-1 and FP-2 in Figure 2 indicate that a response to high or low RCS pressure is required. The curve tagged 1 on the RCS Pressure vs T_{cold} graph is the limit on RCS pressure for overpressurization and vessel integrity concerns. The curve tagged 4 indicates the conditions at which the reactor coolant will change phase. Further, the endpoints are marked according to the priority of response required and are indi-

The diagram illustrates the RPS logic for different temperature conditions. It features two graphs: one for T_{COLD} showing pressure rising above and below limits, and another for T_{HOT} showing pressure falling above and below limits. The logic is represented by a series of interconnected blocks and lines, with numbered callouts (1-4) indicating specific states or transitions. The responses (PH, PR, PL) and functions (FP-1, FP-2) are indicated for each state.



Storage processes include simple accumulation phenomena, i.e., pile-up of material or energy in a volume, and in addition may also include changes of material composition and changes of phase.

Transport processes include the transfer of material and energy between two locations in space by convection, conduction and diffusion phenomena.

A barrier is a permanent physical boundary that only functions to prevent the transport of material or energy across the boundary.

A conditioning subsystem either controls the main process (e.g., Reactor Coolant Pressure Control System), or establishes and maintains proper function of the main system (e.g., component cooling).

A conditioning variable is the physical variable in the main process that is controlled or maintained by a conditioning subsystem.

Processing subsystems function as sources or sinks of material or energy in relation to the main system.

An aggregate is a collection of interrelated transport and storage processes. Aggregates are used for representing plant subsystems for which the internal structure is ignored.

A graphical description of the plant can be made through the use of the symbols shown in Figure 3 and defined above. This graphical description is termed a "flow structure" and describes the plant in terms of its fundamental processes and their relationships as opposed to a description of interconnections of processing components which are shown in piping and instrumentation diagrams (P&ID). The description of a plant in terms of its flow structure allows a decomposition of the plant into its systems and subsystems. This decomposition forms a hierarchy as shown in Figure 4 and depicts the functional relationships between plant processes.

FLOW MODEL DESCRIPTION OF A PWR DURING ACCIDENT CONDITIONS

Figure 5 illustrates the basic plant control problem that has to be addressed for accident situations in a PWR or any fission power producing facility. There are two integral aspects in the problem due to the nature of the fission process and its byproducts: transfer of fission product decay heat, and prevention of the release of fission products to the environment. These then become a complex systems engineering problem for nuclear power plants which have numerous systems and release paths that have to be controlled and monitored. It is necessary to determine why, when, and how various systems are used in the plant, and the consequence of failures of various systems and barriers. Only then can an information system (including alarms) be effectively designed to aid an operator in this complex task.

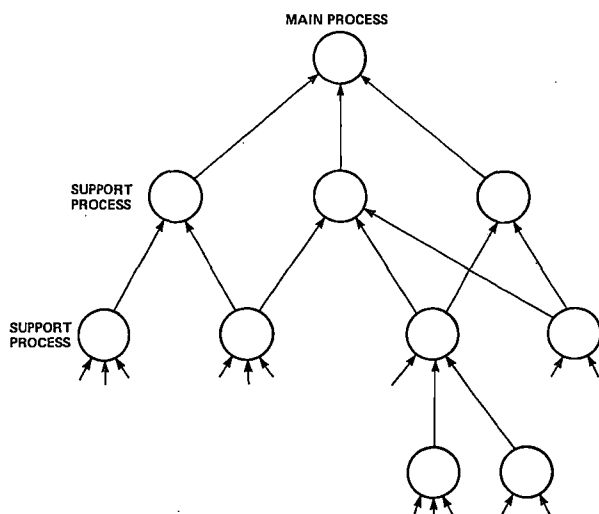


Figure 4. Decomposition of Plant Processes

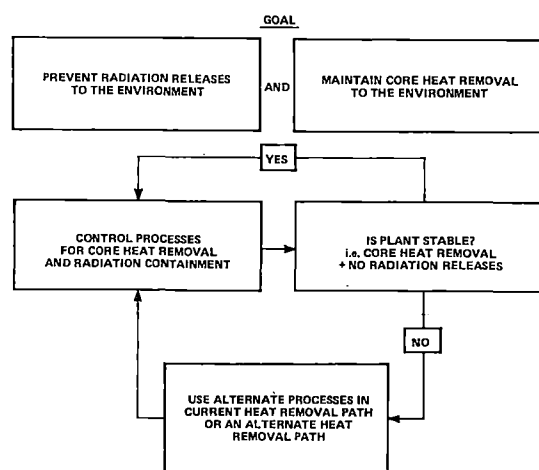


Figure 5. Block Diagram for Plant Control During Accident Conditions

We attempt here to formally model this problem and then deduce the requirements for an information system for a control room. Figure 6 shows, in an aggregate manner using flow model terminology, the goal during emergency plant (Westinghouse SNUPPS) operations, i.e., the prevention of radioactive material release to the environment. Included in this goal is the requirement for continuous decay heat removal to prevent a core melt. Figure 6 shows the barriers in a PWR that defend against radioactive release to the public, i.e., fuel rod material, fuel rod cladding, reactor coolant system boundary, and containment.

The fuel rod material must be prevented from melting to maintain fission products within the crystalline lattice in the solid fuel. As indicated in Figure 6, this first barrier is maintained by controlling the neutron flux in the core to keep the reactor subcritical during accident conditions. The second barrier is the fuel rod cladding. The fuel cladding may fail because of high internal pressure caused by molten fuel or a departure from nucleate boiling in the coolant. As shown in Figure 6, the integrity of the fuel cladding is maintained by controlling neutron flux, and pressure, temperature and inventory of the Reactor Coolant System (RCS). The neutron flux is controlled by the Reactor Trip and Emergency Boration Systems, and the pressure, temperature and inventory of the RCS are controlled by the core and RCS heat removal systems. The third barrier is the RCS boundary. This boundary (reactor vessel, primary piping, etc.) may fail due to overpressure conditions or by exceeding Nil Ductility Transition limits. NDT limits are avoided by controlling RCS pressure and temperature. The final barrier is the containment. The integrity of the containment building is maintained by controlling containment hydrogen concentration, pressure, and temperature. The radioactivity in the containment must also be controlled to avoid high radiation leakage rates and to minimize release if this last barrier is breached. These critical variables are controlled by the Containment Spray and Hydrogen Control Systems.

Also shown in Figure 6 are the barriers (components and piping) of the Secondary Coolant System (SCS), and the auxiliary systems to the RCS and SCS. The transport nodes indicate the existence of paths that result from the use of various plant processes. A correlation between transport nodes in Figure 6 and those in flow models of plant processes used for decay heat removal and other barrier maintenance functions (e.g., Containment Spray System) will identify the detailed release paths and implications of isolating process paths due to the failure of various barriers. The model in Figure 6 only addresses fission products in the core and contaminated coolants as sources of radioactive material. Similar models can be made to address radioactive release from radioactive wastes and spent fuel storage tanks which are independent problems.

Figure 6 shows the conditioning variables (critical safety parameters) that have to be maintained and controlled within limits to meet the overall objective. A distinction can be made here between variables that have to be controlled within limits, e.g., containment pressure and hydrogen concentration, versus variables that have to be continuously controlled to maintain a specific function. For example, the core heat removal function dictates continuous control of RCS pressure, temperature, and inventory. The processes (systems) conditioning the first type of variables are initiated only if the variable exceeds a calculated setpoint, whereas processes supporting heat removal are in continuous operation. It should be noted that the conditioning variables on the various nodes in Figure 6 are identical to the critical safety parameters shown in Figure 1. The material flow model in Figure 6, however, diagrammatically further describes the matter of the problem. The details of the problem may then be described in further detail from this top level model.

Figure 7 shows, as energy flow models, the five distinct core decay heat removal paths (states) available during accident conditions in Westinghouse PWR Standard Nuclear Power Plants (SNUPPS). These five heat removal states (HRS) or paths can be defined as distinctly unique paths, via various coolant systems, through which decay heat may be transported from the core to the environment. They include only the stable plant states. For example, a steam line break into containment requires steam

generator isolation and is not considered a stable plant heat removal state. Also, the cold shutdown heat removal state, to which the plant is transferred after the plant is stabilized following a reactor trip, is not included.

Corcoran^[7] has identified the need for plant state identification and has suggested a tabular verbal format for listing plant states. Analysts, particularly in probabilistic risk assessment, continually consider decay heat energy flow paths as part of their modeling effort. However, there has not been a diagrammatic modeling formalism for describing plant state in terms of the fundamental mass and energy flows until the method proposed by Lind.^[4] Such a formalism is particularly useful for ACR functional design work (procedures, alarms and instrumentation) since it provides a mechanism to formulate and describe the basis for specifying the need for equipment and analytical models. Further, the flow model formalism allows one to model and understand the interrelationship between systems (processes) in various anomalous conditions.

The heat removal states in Figure 7 may be viewed as the goal states the plant should be transferred to for various plant anomalies. Figure 8 shows the correlation between plant anomaly(ies) and heat removal states. This correlation is determined from plant protection systems design bases. The plant should be transferred to HRS-I for all anomalies that dictate a reactor trip and which are not in the main decision flow chart shown in Figure 8. As shown in Figure 7, the decay heat in HRS-I is transferred from the core to the reactor coolant and then to the secondary coolant at the steam generators. The energy is then transferred to the tertiary coolant (circulating water) at the condensers, and then to the environment at the natural draft cooling towers. Also shown in Figure 7 are the variables that must be suitably conditioned by various processes to maintain core heat removal in this state. The question of condenser availability in Figure 8 includes passive (breaks) or active failures that prevent energy transport via the condensers and cooling towers using tertiary coolant. Such failures dictate that the plant operational mode be transferred to HRS-II as shown in Figure 7 where energy is transported from the secondary coolant directly to the environment via the steam generator relief valves. HRS-II is also the desired goal state when the SCS boundary is not intact, e.g., steamline or feedline break, or stuck open condenser steam dump valves. The main steam isolation valves to the condenser are closed for such anomalies.

HRS-III and IV are the result of the RCS boundary not being intact, i.e., a loss of coolant accident resulting from a break, stuck open valve, etc. Steam generator (SG) tubes are not included as part of the RCS boundary here. An SG tube rupture dictates isolation of that particular SG. The heat removal state (path) or the coolant systems supporting energy transport are the same unless all four SGs are unavailable. SG availability is defined as the availability of feedwater to one SG which is intact (SG tubes, feedline, and steamline up to the MSIV and atmospheric steam dump valves). The top legs in HRS-III and IV shown in Figure 7 are determined by similar considerations as for HRS-I and II. The bottom legs for HRS-III and IV are identical; that is, they are a result of reactor coolant spillage into containment. Note that energy in the containment is transported to the environment by the Component Cooling and Essential Service Water systems only during the emergency core cooling recirculation phase. HRS-V in Figure 7 is the ultimate heat removal state which results from the unavailability of all SGs or a large break in the RCS boundary leading to inadequate reactor coolant circulation for heat transport to the secondary coolant.

The flow chart in Figure 8 identifies in a complete manner the basic diagnosis that must be done for plant control during emergency conditions. Plant diagnosis may be accomplished in a number of ways and degrees of reliability. Provided adequate instrumentation is available, the operator may symptomatically diagnose plant state using his own mental pattern recognition capability. However, this method is questionable for multiple failures for which the operator has not had a prior recognition. Alternatively, the operator may be given subflow charts for each question in Figure 8 to guide him in determining plant status. There is presently a considerable

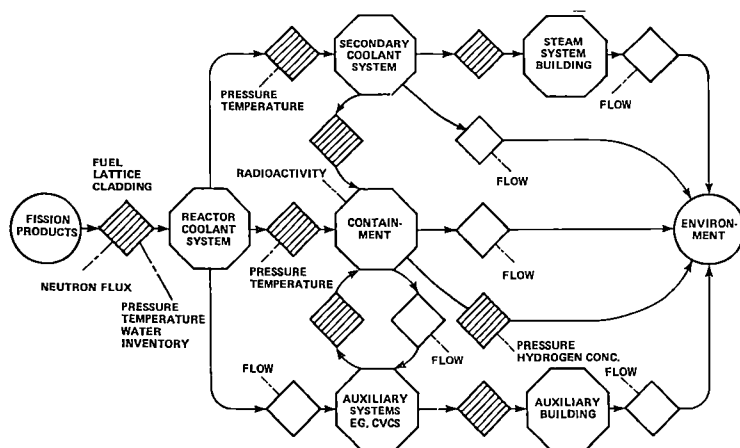


Figure 6. Flow Model of Radioactive Material Transport During Accident Conditions in a PWR

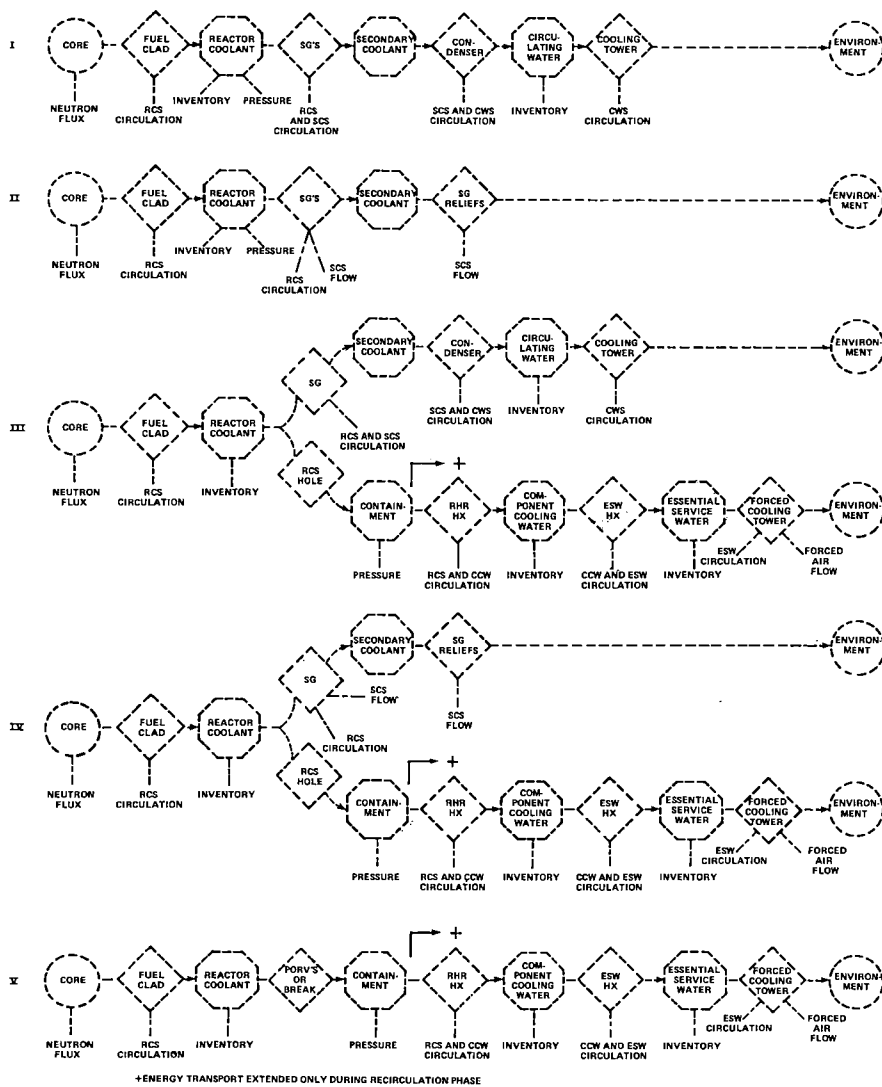


Figure 7. Heat Removal States During Accident Conditions in a PWR

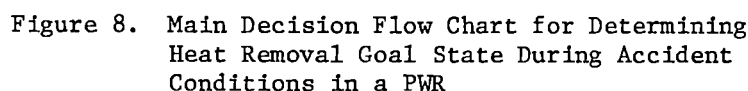


Figure 9 shows process flow models for inventory control in HRS-I and II (Figure 9A), and HRS-III, IV and V (injection phase shown in Figure 9B and recirculation phase in Figure 9C). Figure 9D shows the flow structure for component cooling water (CCW) circulation which supports the pumps used in the processes shown in Figures 9A, B, and C, and also supports energy transport from the containment sump to the essential service water (Figure 7, HRS-III, IV and V). The transport nodes from the containment sump to the RCS in Figure 9c are also identified in the radioactive material transport flow model shown in Figure 6 between the containment and the auxiliary systems since a break in the ECCS in the auxiliary building would release radiation via the vents. These flow models are shown as examples of process flow structure and how supporting processes and/or components are identified. Also illustrated is how the interrelationship between a supporting process (CCW) and the various processes it supports is determined and shown. There are numerous such complex functional interrelationships in a nuclear power plant and these are identified in a full set of flow models. Such a set has been completed for SNUPPS and includes the processes that condition nodes in Figure 6 (e.g., CSS), and all the vital support systems (component cooling, compressed gas and electric power systems) in a nuclear power plant. This complete flow model set forms the basis for a plant diagnostic and alarm system, and may also be a useful systems information format for developing fault and event trees in a risk assessment study.

We have so far discussed a method for describing plant processes and their interrelationships in various plant states. Lind^[4] has also proposed a method, for describing plant state transitions, which is closely related to flow models and conceptually similar to the precedence network theory developed for project management^[13]. In this method, a prior distinction is not made between automatic and

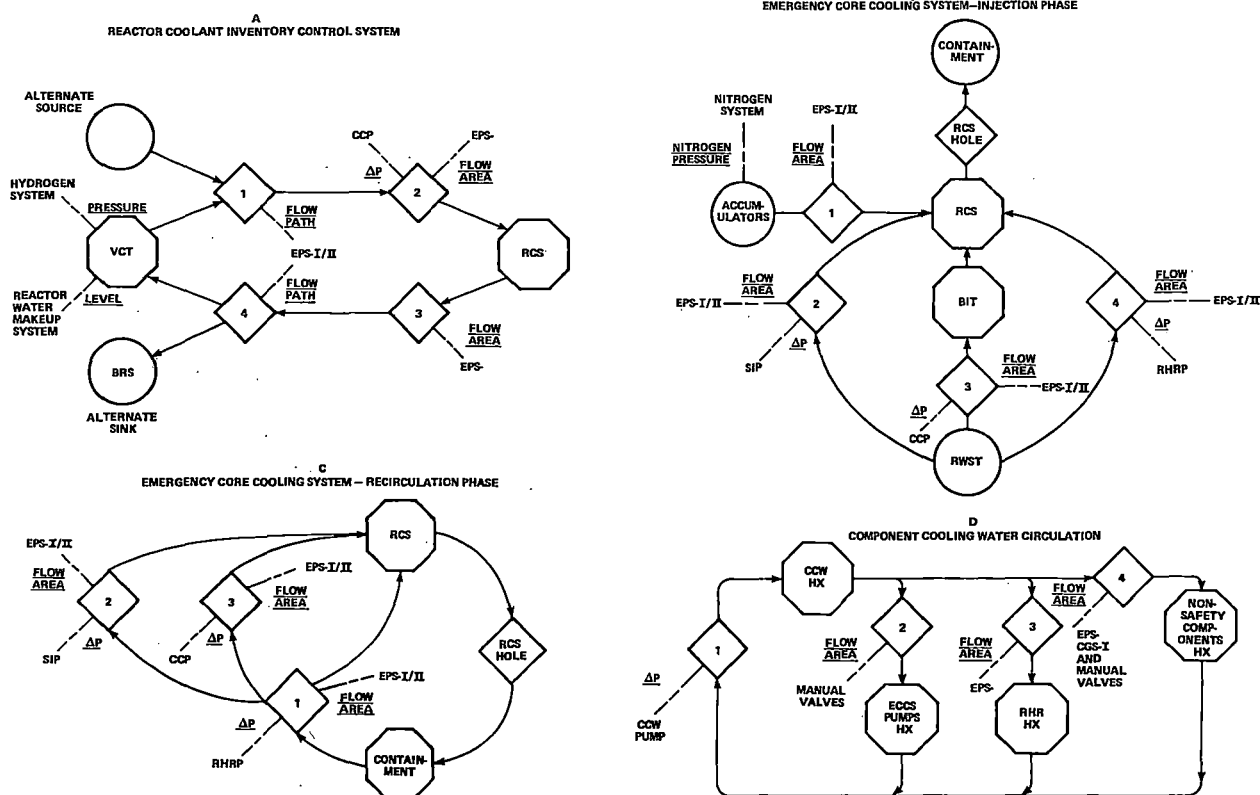


Figure 9. Examples of Flow Models for Processes Supporting Core Heat Removal

manual control actions since there is no formal difference between operating procedures and the specification of control action sequences for automatic systems. In a State Action Network (SAN), one shows the decomposition of control tasks required for a defined plant state transition. The basic postulate is that a task decomposition into sequential and concurrent action sets results from the topology of material and energy flow as described in flow models. The SAN formalism provides a structured method for plant control design, or for describing plant control tasks before any judgements (task analyses) can be made regarding their adequacy.

Figure 10A shows the basic symbol used in a SAN. A process (system or subsystem) or component is taken from an initial state S_1 to S_2 by a set of control actions. State changes can be indicated at various levels of detail, e.g., change in plant HRS, initiation of a process supporting heat removal, or initiation of a component in a supporting process. Therefore, tasks can be decomposed into subtasks and such a decomposition is made similar to the decomposition of flow structure in flow models.

There are basically two categories of control in process plants. One category includes control actions for flow structural changes in the plant. For example, transition from normal operating conditions to HRS-IV requires the activation and deactivation of various processes. Figure 10B shows the format for representing the decomposition into subtasks for the above type of control. The second category of control is the type where further decomposition is not possible due to the task being a functional "whole," e.g., a valve is modulated till a tank reaches a desired set-point. The symbol for such control actions is shown in Figure 10C, and Figure 10D shows how the actions are combined in a control sequence. Figure 10D also shows that two systems (or components) are required to be in a particular state before a control action can be executed on one of them. Figure 10E shows the symbol for a conditional (c) task which is executed depending on the output of some logic other than what

triggered the SAN it is included in. Finally, Figure 10F shows the symbol for representing alternate state actions to accomplish the same control function.

APPLICATION OF STATE ACTION NETWORKS FOR RESPONSE DURING EMERGENCY CONDITIONS IN A PWR

Figure 11 shows the main tasks, as a SAN, for plant transitions to HRS-I through V from normal operations above 15 percent of full power. Essentially, Figure 11 identifies the tasks necessary to suitably condition the heat removal paths identified in Figure 7, namely the control of processes that condition the variables identified in Figure 7. Figure 12 is an example of a decomposition of a task identified in Figure 11 to detailed subtasks. The tasks required to change the flow structure shown in Figure 9B to that in Figure 9C are identified in Figure 12. The subtasks for the components are determined from the identification of the various components needed to condition the variables in Figures 9B and 9C. The relationship between SANs and flow models is due to the nature of control actions required for mass and energy processes. However, not all tasks are related to heat removal. Containment isolation is related to the second aspect of the problem (radiation release) that was discussed earlier with references to Figures 5 and 6. A complete set of conditional control tasks for various combinations of failures of barriers have not been identified in Figure 11 and would affect the use of various processes. Alternatives for control actions for transition to a HRS have also not been shown in Figure 11.

The SAN in Figure 11 for transition into the five heat removal states is an attempt at formulating a response network to respond to passive and active multiple failures. As shown earlier in Figure 5, emergency response can be considered to consist of a transition to a heat removal state, followed by a possible degradation of heat removal state, and responses required to isolate radioactive release paths being formed as a result of the failure of various barriers. The SAN formalism based on heat removal states allows the inclusion of multiple failures into the network in a logically structured manner due to the mass and energy topographic basis.

The logic in Figure 8 triggers the conditional state action for transition to a heat removal state. Figure 8 shows in an aggregate form the categories of possible failures in a PWR and all failures fall into one of the categories. For example, the question "Condenser available?" includes all active and passive failures in the tertiary coolant portion of the plant heat removal path. Isolation of processes due to radiation release concerns may also result in the unavailability of the tertiary coolant system.

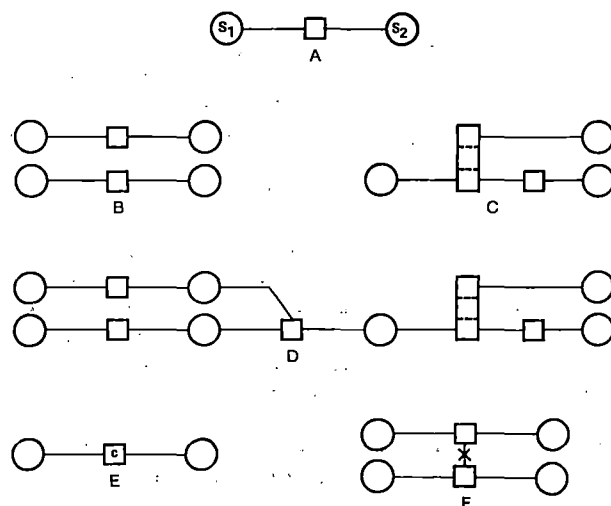


Figure 10. Symbols Used in State Action Networks

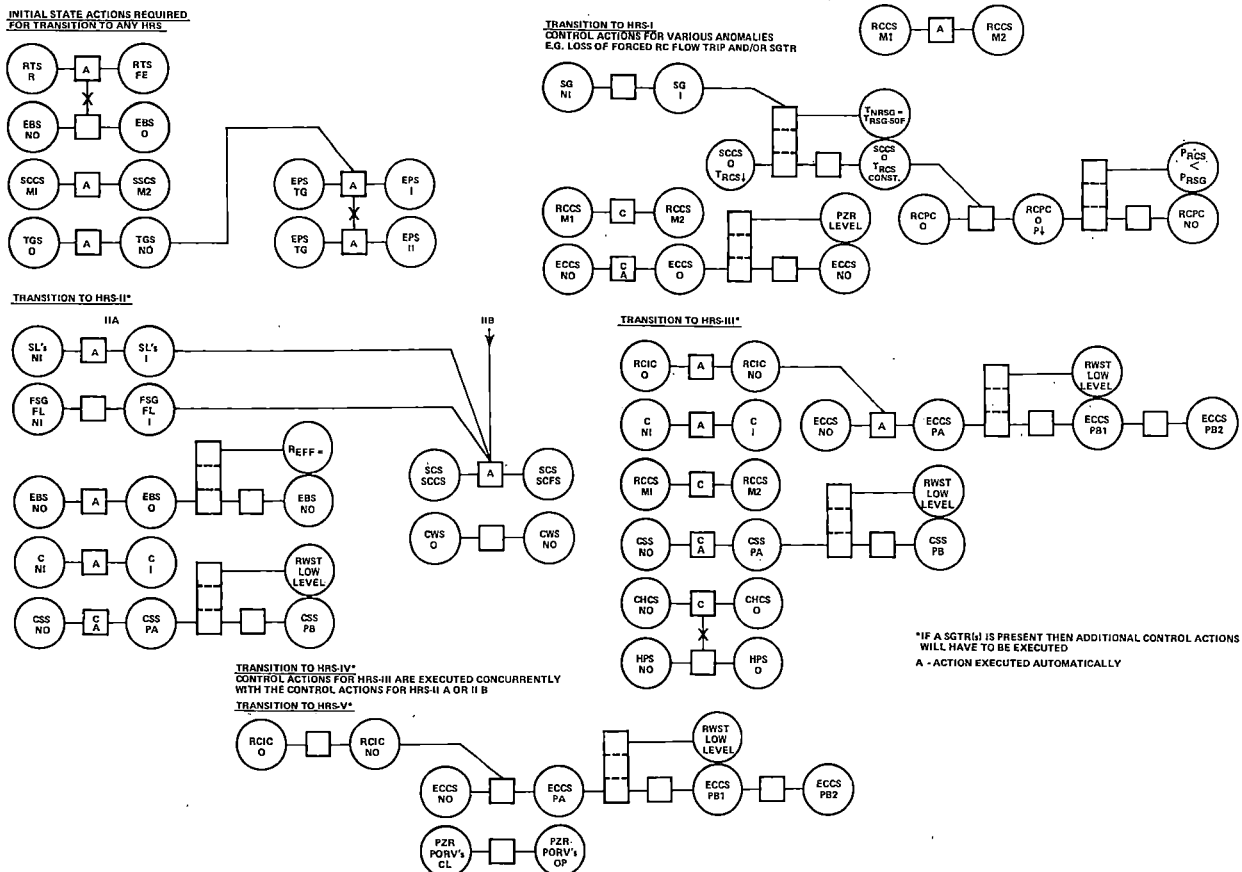


Figure 11. State Action Network for Transition to Heat Removal Goal States During Accident Conditions in a PWR

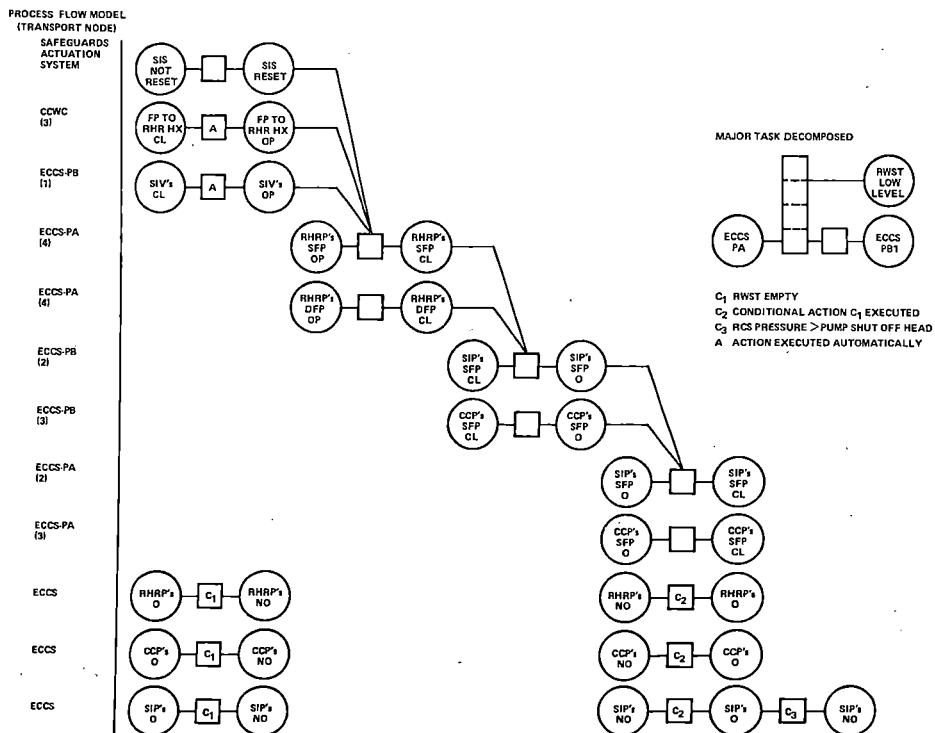


Figure 12. State Action Sequence for ECCS Transition from Injection to Cold Leg Recirculation Phase

Lind^[4] has also proposed that the control heuristics or bases for the specification of state actions should be formulated. The heuristics consist of reasons for the precedence in state actions, preference of alternatives, and prioritization of concurrently required state action sequences. For example, one heuristic would be "reactor coolant must always exist." These heuristics will be the design bases for SANs, and also the knowledge data base for operators executing and monitoring the control actions. The detailed subtasks for the tasks identified in Figure 11 and the control heuristics are presently being developed and formulated.

The development of SANs from flow models for HRSs and radiation release paths is only the first phase of the development of an emergency response network. The second phase of the development will consist of scheduling of the tasks and determining whether the state action sequence can be adequately executed. Time constants from plant dynamic analysis will be necessary for such an evaluation. Control actions can then be designated as being manual or automatic using such schedular information. It should be noted that the above design method for developing an emergency response scheme can also be used for a formal task analysis of existing normal or emergency response networks (procedures). To date, this method is the only formalism that fundamentally describes process plant operations and therefore allows a proper and complete determination of the plant variables that have to be monitored to verify the execution of control actions.

INFORMATION REQUIREMENTS FOR PLANT CONTROL

The information requirements for plant state identification and control during emergency conditions may now be identified from the formulation presented above. The alarm system will be an integral part of the required information and will consist of annunciators that will alert the operating crew to changes in plant state based on the above formulation. The requirements for post-accident instrumentation may then be derived in a formal manner from such informational requirements.

Table I lists the information required for plant control during accident conditions and shows how flow models allow a hierarchical representation of the information. The hierarchy of information for the second and lower levels is based on the decomposition (as shown in Figure 4) of plant flow structure and identification of supporting subprocesses and/or components. See Goodstein^[14] for a complete discussion on an informational hierarchy based on a system's decomposition as illustrated in Figure 4 and discussed in this paper.

TABLE I Hierarchy of Information for Plant Control

Level	Identification
I	Identification of the status of barriers and radiation releases to the environment (see Figure 6) and <u>Identification of the plant heat removal goal state (see Figures 7 and 8).</u>
II	<u>Identification of the capability of the processes conditioning the nodes in the flow models representing the first level. Includes monitoring of the conditioning variables and overall process performance (mainly mass and energy flows).</u>
III	<u>Identification of the status of the nodes and the variables that have to be conditioned to support the above processes. The variables may be conditioned by components or supporting processes.</u> <u>The lowest level identifies the status of individual components.</u>

Table II lists and categorizes the alert conditions that should be addressed by an alarm system for plant control; such a categorization is consistent with the

proposed overall information system philosophy. Category 1 is for power production and has not been dealt with in this paper. Category 2 includes plant anomalies shown in Figure 8 and all other anomalies that dictate a reactor trip and transition to HRS-I. Category 3 includes anomalies in control actions during transition to an HRS, and Category 4 includes recoverable anomalies at steady-state operation at an HRS. Category 5 includes anomalous conditions that dictate a degradation of HRS and are determined by the logic in Figure 8.

TABLE II Categorization of Alarms

- | | |
|----|--|
| 1. | Recoverable anomalies during power production. |
| | a. Anomalies related to a state-action |
| | b. Anomalies not related to a state-action |
| 2. | Anomalies dictating a reactor trip. |
| 3. | Recoverable anomalies related to state actions for transition to a heat removal state (HRS). |
| 4. | Recoverable anomalies during steady HRS operation. |
| 5. | Anomalies dictating a degradation of HRS. |

The various categories require different degrees and types of alert. For example, an alert for Category 3 may be a blinking message on a cathode ray tube (CRT) display which the operator monitors to verify his control actions, whereas anomalies in Category 4 and definitely Category 5 require a much more drastic alert mechanism. The alarm categories include in them anomalies such as loss of barriers and potential release of radioactive material to the environment. An annunciator system based on Figure 6 could be used to alert the operator to execute prescribed conditional control actions for failures of various barriers, or to determine a suitable control action where one has not been prescribed. The urgency of a response would depend on the severity of or potential for release and this can be encoded in the annunciator system as various degrees of alert.

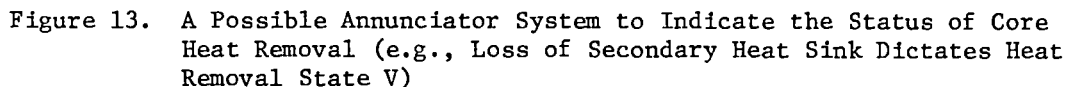
Finally, Figure 13 shows a possible annunciator to indicate the status of core heat removal. Such an annunciator system could be used for two purposes: to alert the operator and indicate the heat removal goal state he must achieve and maintain, and to alert and indicate the "health" of the conditioning variables and therefore processes supporting the current heat removal goal state. The operator can then be directed to displays (based on the informational hierarchy shown in Table I) to investigate the status of the processes conditioning the variables for heat transport. If the operator is unable to restore the "health" of the process(es), he is dictated by the annunciator to a degraded heat removal state to maintain core heat removal and, therefore, plant safety.

CONCLUSIONS

A basis for response during emergency conditions in a PWR has been proposed using two new modeling tools: flow models and state-action networks. The aim of this fundamental approach to such a complex problem is to formulate a common basis for emergency procedures, alarm prioritization, post-accident instrumentation, and advanced diagnostic methods for an advanced control room. The fundamental nature of the formulation allows one to include responses to multiple failures in a logically structured manner, and therefore extend the prescribed capabilities of a control room as much as desired. However, the complexities and utility of the proposed approach will only be realized once a representative application has been made.

ACKNOWLEDGEMENTS

We wish to thank our colleagues from various organizational units in Westinghouse that are involved in the work presented in this paper.



1. Clarification of TMI Action Plan Requirements U.S. Nuclear Regulatory Commission NUREG-0737, November, 1980.
2. Rumancik, J. A., Easter, J. R., and Campbell, L. A., "Establishing Goals and Functions for a Plant-Wide Disturbance Analysis and Surveillance System (DASS)," IEEE Trans. Nucl. Sci., 28, pp. 905-912, (1981).
3. Gallagher, J. M., et al., "A Process for Design of a Plant-Wide Disturbance Analysis and Surveillance System," Report NP-2240, Electric Power Research Institute (1982).
4. Lind, M., "The Use of Flow Models for Design of Plant Operating Procedures," in Proc. IWG/NPPCI Specialists' Meeting on Procedures and Systems for Assisting an Operator During Normal and Anomalous Nuclear Power Plant Operation Situations, December 5-7, 1979, Garching, Federal Republic of Germany, N-38-79, NKA/KRU-PZ (79) 26.
5. Lind, M., "The Use of Flow Models for Automated Plant Diagnosis," in Rasmussen, J. and Rouse, W. B. (Eds) Human Detection and Diagnosis of System Failures, Plenum, New York, 1981.
6. Lind, M., "Multi-Level Flow Modeling of Process Plant for Diagnosis and Control," This conference.
7. Corcoran, W. R. et al, "Nuclear Power Plant Safety Functions," Nuclear Safety, 22, pp. 179-191, 1981.

8. Rasmussen, J., "Models of Mental Strategies in Process Plant Diagnosis," in: Rasmussen, Jr. and Rouse, W. B. (Eds.) Human Detection and Diagnosis of System Failures, Plenum, New York, 1981.
9. Pau, L. F., "Application of Pattern Recognition to Failure Analysis and Diagnosis," Ibid.
10. Hsu, Y. Y. and Hon, A. L. M., "Some Possible Ways to Improve Nuclear Power-Plant Instrumentation", Nuclear Safety, 22, pp. 728-737, 1981.
11. Thie, J. A., "Surveillance of Instrument by Noise Analysis," Nuclear Safety, 22, pp. 728-737, 1981.
12. Byford, R. G. and Geis, C. G., "An Advanced Digital Metal Impact Monitor," IEEE Trans. Nucl. Sci., 29, pp. 993-999 (1982).
13. Burman, P. J., Precedence Networks for Project Planning and Control, McGraw Hill, New York, 1972.
14. Goodstein, L. P., "Computer-Based Operating Aids," in Proc. Design, 82, Birmingham, UK, September 22-23, 1982.

ABBREVIATIONS

ACR	Advanced Control Room	PA	Phase A
BIT	Boron Injection Tank	PB	Phase B
BRS	Boron Recycle System	PORV	Power Operated Relief Valve
C	Containment	PWR	Pressurized Water Reactor
CACS	Containment Air Cooling System	PZR	Pressurizer
CCP	Centrifugal Charging Pump	R	Ready
CCW	Component Cooling Water	RCCS	Reactor Coolant Circulation
CCWC	Component Cooling Water Circulation	(M1/M2)	System (Forced/Natural)
CGS	Compressed Gas System	RCIC	Reactor Coolant Inventory
CHCS	Containment Hydrogen Control System		Control System
CSS	Containment Spray System	RCPC	Reactor Coolant Pressure
(PA/PB)	(Injection/Recirculation)		Control System
CL	Closed	RCS	Reactor Coolant System
CWS	Circulating Water System	RHR	Residual Heat Removal
DFP	Discharge Flow Path	RHRP	Residual Heat Removal Pump
EBS	Emergency Boration System	RSG	Ruptured Steam Generator
ECCS	Emergency Core Cooling System	RTS	Reactor Trip System
(PA/PB)	(Injection/Recirculation,	RWST	Refueling Water Storage Tank
	1 = Cold Leg, 2 = Hot Leg)	Rx	Reactor
EPS	Electric Power System	SAN	State Action Network
(I/II)	(Offsite/Diesel)	SCCS	Secondary Coolant Circulation
ESWS	Essential Service Water System	(M1/M2)	System (Main/Auxiliary)
FE	Function Executed	SCS	Secondary Coolant System
FL	Feedline	SCFS	Secondary Coolant Flow System
FP	Flowpath	SFP	Suction Flow Path
FSG	Faulted Steam Generator	SG	Steam Generator
HPS	Hydrogen Purge System	SCTR	Steam Generator Tube Rupture
HRS	Heat Removal State	SIP	Safety Injection Pump
Hx	Heat Exchanger	SIS	Safety Injection Signal
I	Isolated	SIV	Sump Isolation Valve
M	Mode of Operation	SL	Steamline
MSIV	Main Steam Isolation Valve	SNUPPS	Standard Nuclear Power Plants
NI	Not Isolated	T _{cold}	RCS Cold Leg Temperature
NO	Not Operating	TGS	Turbine Generator System
NRSG	Not Ruptured SG	TMI	Three Mile Island
O	Operating	VCT	Volume Control Tank
OP	Open	ΔP	Differential Pressure

DETERMINATION OF ENVIRONMENTAL CONDITIONS FOR EQUIPMENT QUALIFICATION IN BUILDINGS OUTSIDE CONTAINMENT

R.F. Miller and F.A. Elia, Jr.

Stone & Webster Engineering Corporation
Boston, Massachusetts 02107, U.S.A.

ABSTRACT

A method for determining pressure/temperature/relative humidity envelopes for high-energy line break (HELB) accidents is presented. Established methods used for accidents inside containment are not applicable to the typical multicompartment buildings outside containment. A computer code which models individual compartments and inter-compartment flow, with the additional capability to model the effects of passive heat sinks and active ventilation systems, is described. General results of analyses completed to date are discussed. The important trends of temperature distribution in a building and the sensitivity to various parameters is summarized.

INTRODUCTION

An important aspect of environmental qualification of safety-related equipment is the specification of pressure, temperature, and relative humidity envelopes for high-energy line breaks (HELBs). Although the methods and computer codes used for determination of these conditions inside containment are well established, they are not applicable to the typically compartmentalized buildings outside the containment. These buildings require modeling of individual interconnected compartments, and the flow between them, to determine the pressure and temperature distribution throughout the building.

A computer code, THREED, has been developed by Stone & Webster Engineering Corporation to perform this analysis for both Pressurized Water Reactor (PWR) and Boiling Water Reactor (BWR) plants. Individual pressure and temperature transients are determined for each compartment included in the geometric model of the building. The effects of passive heat sinks and active ventilation systems can be included in the analysis. These effects have been very important in determining the duration of the accident environment.

First, a summary description of the important models and assumptions in the code are presented. This is followed by a discussion of considerations in developing the geometric model of the building being analyzed. This involves dividing the building into individual compartments, and then determining the values of the parameters necessary to calculate the thermodynamic state of each compartment and the flow between compartments. Selected results from an analysis are provided to illustrate the resulting environments for a typical building. The sensitivity of the results to the type and location of the pipe break, and the effects of including

passive heat sinks and an active ventilation system in the calculation are shown. The development of pressure and temperature envelopes from the calculated transients is discussed. Finally, a compilation of general conclusions, based on analyses performed for a variation of building geometries and accident scenerios, is included.

DESCRIPTION OF THE COMPUTER MODELS

The THREED Computer Code was utilized to perform the analyses which are described later in this paper. This code was developed by Stone & Webster Engineering Corporation with the following goals:

1. Provide adequate modeling detail to analyze subcompartments.
2. Optimize computer run time and storage requirements.
3. Simplify the user interface (input/output).
4. Provide a structured programming environment which would easily allow implementation of future changes.

The code is based on the RELAP4 code ^{1,2} and gives similar results. Some simplifying assumptions were made in the code development which do not affect the results for the intended use. These are:

- The complexity of the building model is limited to:
 - Seventy-five control volumes
 - One hundred flow paths
 - One source of mass-energy release
 - Ventilation system(s) with five fans
 - Twenty passive heat sink slabs
 - Five heat sources
- The kinetic energy effects are neglected. This is acceptable since the flowing fluids encountered in subcompartment analysis are generally low density. Sensitivity studies have shown that kinetic energy effects are second order and can be neglected.
- Fans were modeled explicitly, thus, simplifying the input required. Implicit modeling, such as that found in the RELAP4 code for pumps, requires input data which is not generally available for fans.
- The lumped parameter (control volume) approach is utilized.
- The rate at which mass enters the geometric model is independent of the pressure in the "fill" junction.
- Thermodynamic equilibrium is attained in each control volume at the end of each time step.
- Fluid flow is one-dimensional.
- A "staggered-mesh" approach is utilized for solution of the conservation equations.
- Flow is homogeneous unless the Moody Choking option is utilized.
- Flow is incompressible.

Additional modifications were required to satisfy the analysis requirements. These consist of:

- The Homogeneous Equilibrium Model was extended to include two-phase, two-component flow (steam-water-air) which is encountered in sub-compartment analyses.
- Heat sources may be included in any of the control volumes with the limitation stated earlier.
- Passive heat sinks can be included in any of the control volumes. The code utilizes a model based on CONTEMP-LT/026, except that recent condensation assumptions (i.e., condensate mass transfer and revaporization effects) are included. It should be noted that the revaporization effect during condensing heat transfer on heat sinks has a significant effect on the calculated temperature for superheated conditions.

The code numerically integrates the basic field equations which describe the conservation of mass, energy, and momentum. A stream-tube form of the field equations is utilized based on assumptions noted above.

DEVELOPMENT OF THE GEOMETRIC MODEL

In developing a geometric model to evaluate environmental conditions for equipment qualification, two factors are first considered. They are:

- The locations of all equipment of concern must be identified.
- The location of all high and moderate energy piping which might result in elevated temperatures and pressures must be identified.

These locations are then "mapped" onto a drawing showing the general building layout. This drawing will have already been subdivided into "control volumes" based on the presence of cubicle walls, floors, ceilings, etc. Certain discontinuities, such as sudden changes in a room dimension, would also be modeled as a "control volume" boundary if it is expected to be part of a dominant flow path.

In general, vent paths such as doorways and pipe penetrations, must be evaluated in a conservative manner. That is, if a door tends to restrict flow out of an area, assuming that it remains closed is conservative. On the other hand, if a closed door results in a decrease in inflow to the area of concern, it must be assumed to be open unless provisions are made, such as door design or plant administrative control, to assume that the door remains shut during the transient.

Areas which do not contain equipment and do not allow flow through them (dead-ended) may be omitted from the geometric model. This simplifies the model somewhat and will shorten problem execution times.

Areas which will not be affected by any pipe rupture (i.e., remain isolated) are omitted from the model.

The input requirements which must be calculated are:

- The control volume net volumes
- The flow path (junction) flow areas
- The junction loss coefficients
- The geometric inertia terms

Other input is required if certain options are utilized. These consist of:

- Fan curves of flow as a function of head
- Heat source as a function of time
- Heat sink slab thickness and surface area

The model may be sectioned into zones in order to limit the number of different equipment qualification envelopes which result from the analysis. These zones generally will consist of many control volumes and are not part of the geometric model. They do, however, simplify the identification of environmental requirements according to equipment location.

Development of this "Universal Building Model" allows analysis of the various pipe breaks of concern by merely redefining the break location and mass-energy release rates to the model.

This building model approach is invaluable when pipe break analysis is required long after the original analysis is performed. One need merely define the break location and releases and run the new analysis with the building model.

DISCUSSION OF A TYPICAL ANALYSIS

The analysis of a typical Auxiliary Building for a two-unit plant is described. Figure 1 presents a diagram of the geometric model of the lower two levels of the building, identifying the control volumes, or nodes, used for the analysis. The upper levels of the building were included in the model simply as a few large nodes. There is an opening to atmosphere on the upper level. All the levels of the building are analyzed with one model since there is sufficient level-to-level flow area for a pipe break on one level to cause an increase in temperature and pressure on the other levels.

Figure 1 also indicates those areas of the building excluded from the model. These include (1) areas that do not contain equipment of concern and are not located along major flow paths (the corners of the lower level), (2) areas that are sealed from the compartments in which the high-energy lines are located, and thus isolated from the effects of an HELB (both ends of the second level), and (3) compartments that are identical to, and located next to compartments that are included in the model (the central area of the lower level). The motivation for keeping the model to the minimum necessary size is the resultant saving in computer costs. It has been shown that selectively limiting the size of the model does not significantly affect the results of interest.

For each node and for each junction between nodes, the required data were developed as described in the previous section.

A review of piping in the building was performed to identify the locations of high-energy lines. Postulated break locations and sizes were then determined, using the criteria in Standard Review Plans 3.6.1³ and 3.6.2⁴. An evaluation of all the possible break cases narrowed the number requiring analysis to those that could potentially be limiting for the areas of interest. This evaluation was based on the relative magnitude and duration of the mass and energy released from the breaks, and the location of the breaks relative to the areas of interest. Mass and energy release versus time was then determined for each break case requiring analysis.

Table I provides a key for the resulting temperature transients that are shown in Figures 2 through 5.

Figure 2 presents the calculated temperature transients for one particular node, for four different break cases. This particular set of results illustrates that, although the largest break analyzed (break case 1) yields the highest

instantaneous temperature, the smaller breaks become limiting in the long term. Also, the two break cases of a saturated liquid line (break cases 1 and 4) are in the same pipe in the same location, the difference being the break size. Case 1 is a large break which causes automatic isolation of the break flow, while Case 4 is a smaller break which does not. Manual isolation at 30 minutes is assumed for the analysis.

A temperature envelope which is developed to bound all the calculated transients is also shown in Figure 2. Margin is included in the temperature, the time at the higher temperatures, and the time necessary to reduce the temperature to lower values. The final temperature reduction, beyond the calculated transients, is extrapolated based on the rate of decrease at the end of the calculated transient.

Figure 3 shows the variation in temperature through the building during the same break. Temperature swings in the various areas occur unpredictably as flow patterns develop throughout the building. Note that all nodes gradually approach the same long-term transient.

Figure 4 presents a comparison of the same break with and without modeling the ventilation system and passive heat sinks. The heat sinks cause somewhat lower temperatures, as expected, but the effect increases significantly in the long term. A reduction in temperature to 124°F (51°C) was achieved in roughly 30 minutes, where the extrapolation of the other cases would not reach this temperature for many hours.

The apparent insignificance in modeling only the ventilation system, and not the heat sinks, is due to the nature of the break and the distance from the node represented and the system suction and supply points. The break has a short blowdown duration, after which there is no mass and energy release. The ventilation system effects are less noticeable for this type of break than for a smaller, longer duration rupture. The ventilation system supply is at the top level of the building, and the suction points are all located in the center of the building. Figure 4 shows the temperature transient for node 13, which is removed from the expected flow patterns set up by the ventilation system.

Figure 5 shows results for a steam pipe crack on the second level, with operation of the ventilation system, for both with and without heat sinks. The effect of modeling heat sinks is similar to that for the liquid line break case, as previously discussed.

Pressure envelopes are developed similarly. A relative humidity of 100 percent is assumed present for the duration of the accident environment.

GENERAL CONCLUSIONS

The general conclusions, based on analyses performed for various building geometries and accident scenerios, are:

1. The short-term pressure and temperature transients in the area of the pipe rupture are a function of the rate and thermodynamic properties of the blowdown from the pipe, the volume of the compartment in which the rupture occurs, and the flow path characteristics from that compartment.

The short-term temperature transients in other areas of the building are highly dependent on the flow paths that are established in the building. The main flow paths usually lead from the area of the rupture to the building pressure relief, e.g., either vents to atmosphere or an open ventilation system. Temperature transients in compartments located along main flow paths are often higher than in compartments that are located

closer to the rupture, but not in a main flow path. Compartments through which there is little or no flow, i.e., "dead-ended" compartments, experience a relatively small temperature increase.

2. Long-term temperature transients, after break flow has ended, are highly dependent on purging of the building by an active ventilation system, and on heat removal by passive heat sinks. Without consideration of either of these effects, temperatures remain high for a long time.
3. Ruptures in liquid pipes will produce maximum temperatures of roughly 212°F (100°C), depending upon the maximum pressure attained. Ruptures in steam pipes can produce higher temperatures, depending upon the steam conditions, size of the break, and duration of the steam release.
4. The largest postulated break size for a particular pipe does not necessarily result in the most severe temperatures. A large break causes significant changes in a system which may either trip an automatic isolation signal or give the operator indication allowing identification and mitigation of the rupture. A smaller break can go undetected for longer periods of time and produce higher temperatures or longer duration transients. This is especially true for small cracks postulated in steam lines in areas where temperature is not indicated in the control room. The break can go undetected for a long time and produce high local temperatures.

The temperature envelope ultimately developed for use in qualifying equipment is typically a composite of different break cases. The envelope is based on the large breaks in the short term, but smaller breaks are often limiting in the long term.

5. Initial building conditions at the time of the event which maximize the resultant environmental conditions are the maximum pressure, temperature, and relative humidity.
6. Pressurization of a building following a HELB has been found to be fairly uniform, for buildings with vent paths between the different areas and levels of the building.
7. A ventilation system that remains operable following a HELB could cause a more severe temperature transient in a particular area than if it were inoperable. The hot steam environment could be drawn through certain areas by the flow patterns set up by the ventilation system.
8. Temperature transients are so highly dependent on the building geometry that the development of generic envelopes is impractical. The envelopes developed for those compartments in which a major rupture occurs would be unnecessarily severe for many other areas of the building.

REFERENCES

1. AEROJET NUCLEAR COMPANY, "RELAP4/MOD5:A Computer Program for Transient Thermal Hydraulic Analysis of Nuclear Reactors and Related Systems - Users Manual, Vol. I-III," Report No. ANCR-NUREG-1335 (1976).
2. K. V. MOORE and W. H. RETTIG, "RELAP4-A Computer Program for Thermal Hydraulic Analysis," Report No. ANCR-1127, Aerojet Nuclear Co. (1974).
3. U.S. NUCLEAR REGULATORY COMMISSION, Standard Review Plan 3.6.1, "Plant Design for Protection Against Postulated Piping Failures in Fluid Systems Outside Containment," Rev. 1, (NUREG-0800) (1981).
4. U.S. NUCLEAR REGULATORY COMMISSION, Standard Review Plan 3.6.2, "Determination of Rupture Locations and Dynamic Effects Associated with the Postulated Rupture of Piping," Rev. 1, (NUREG-0800) (1981).

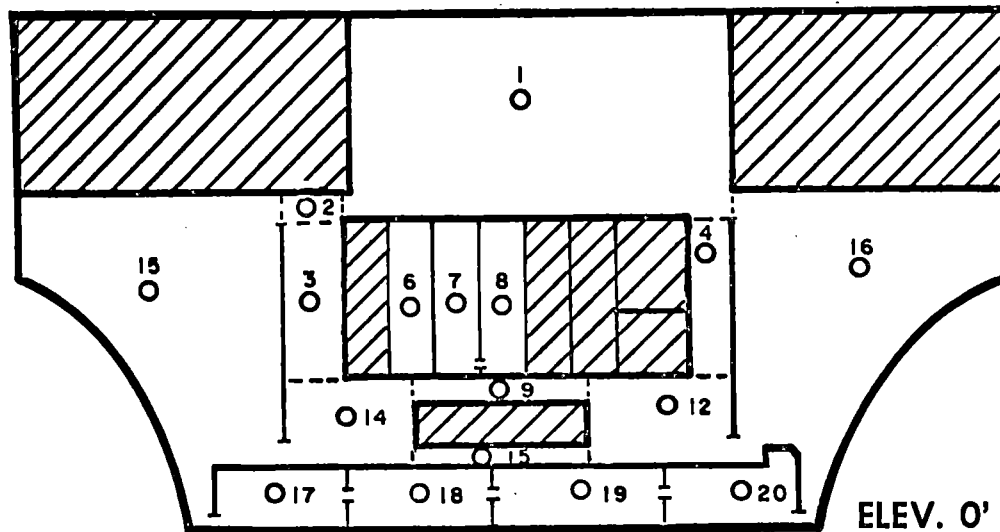
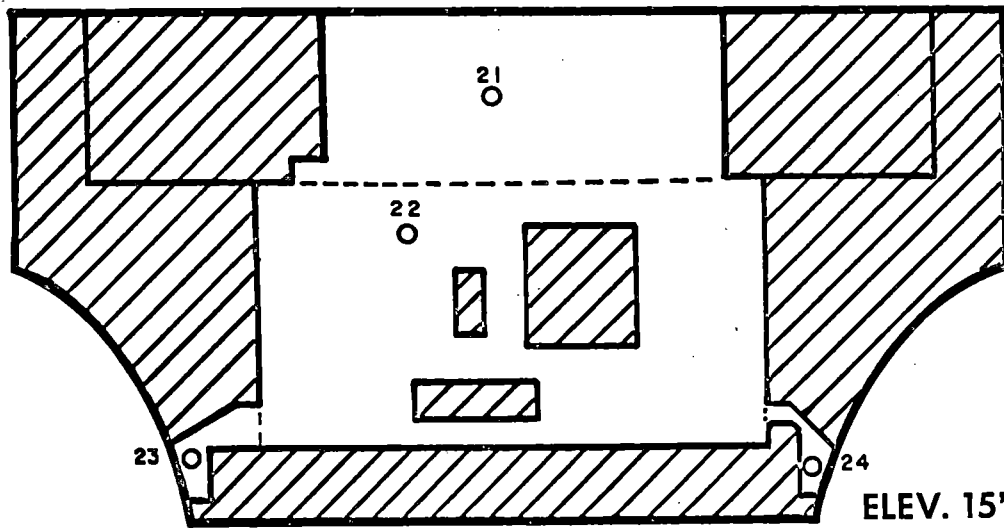
TABLE I

Key to Temperature Curves on Figures 2-5

<u>Figure No(s).</u>	<u>Break Case Number</u>	<u>Curve Symbol</u>	<u>Temperature for Node No.</u>	<u>Type and Location of Break^a</u>	<u>Time and Method of Isolation</u>	<u>Ventilation/ Heat Sinks Modeled</u>
2,3,4	1	○	13	Saturated liquid line break in Node 13	30 sec - Automatic	None
2	2	▲	13	Subcooled liquid line break in Node 13	1800 sec - Manual	None
2	3	◆	13	Subcooled liquid line break in Node 5	1800 sec - Manual	None
2	4	+	13	Saturated liquid line crack in Node 13	1800 sec - Manual	None
3	5	▲	1	Saturated liquid line break in Node 13	30 sec - Automatic	None
3	6	◆	8	Saturated liquid line break in Node 13	30 sec - Automatic	None
3	7	+	22	Saturated liquid line break in Node 13	30 sec - Automatic	None
4	8	▲	13	Saturated liquid line break in Node 13	30 sec - Automatic	Ventilation
4	9	◆	13	Saturated liquid line break in Node 13	30 sec - Automatic	Ventilation and Heat Sinks
5	10	▲	21	Steam line crack in Node 21	900 sec - Manual	Ventilation
5	11	◆	21	Steam line crack in Node 21	900 sec - Manual	Ventilation and Heat Sinks

^a The term "break" refers to a complete circumferential rupture.
The term "crack" refers to a partial rupture, or split.

GEOMETRIC MODEL

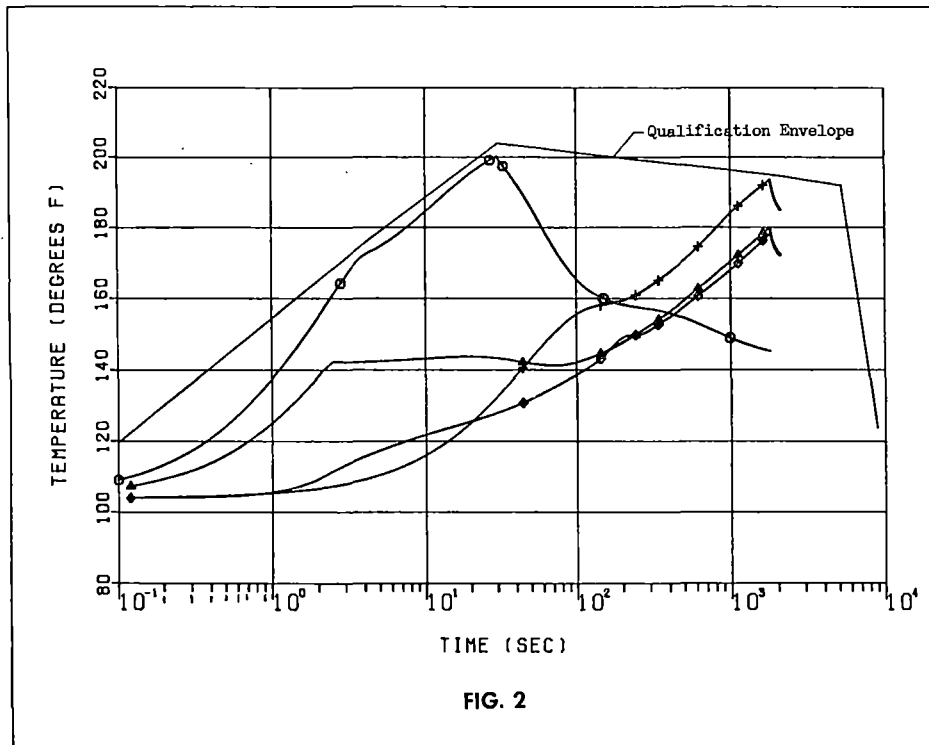


Notes:

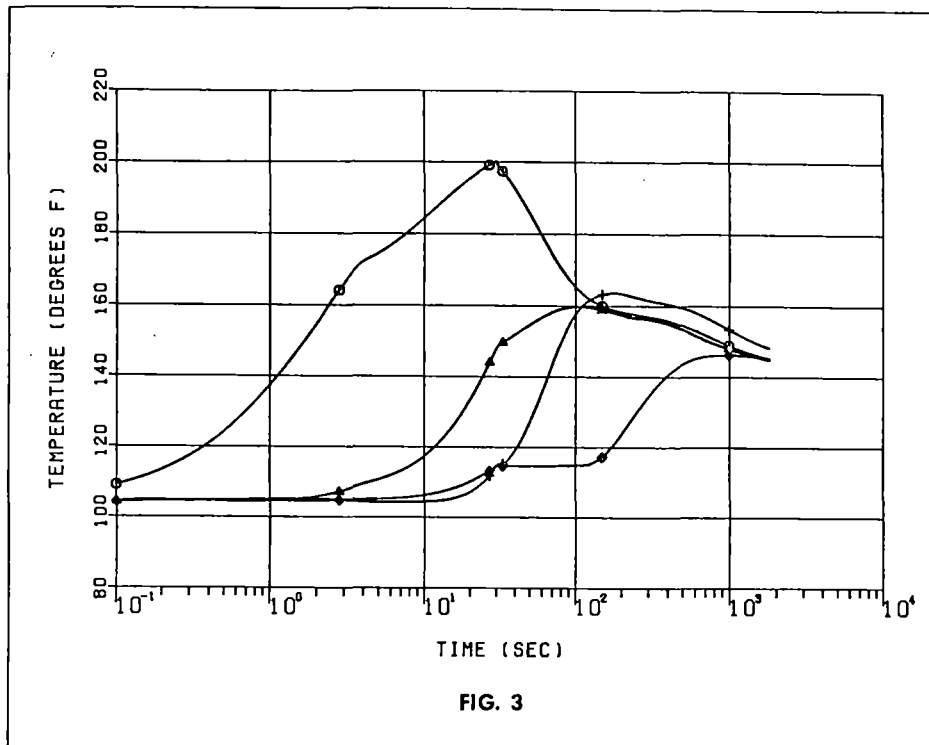
- o Represents node designation.
- Node 5 is a pipe tunnel above Node 9, running between Nodes 13 and 16. Node 10 is a pipe tunnel connecting Nodes 5 and 18. Node 11 is a pipe tunnel connecting Nodes 5 and 19.
- Boundaries between nodes are at doorways, openings, etc., and indicated by a dotted line in some cases.
- Flow paths from the lower level up to the second level are located in Nodes 1, 6, 7, 8, 13, and 16. Flow paths from the second level up to the third level are located in Nodes 21, 22, 23, and 24.
- Intakes to the ventilation system are located in Nodes 6, 7, 8, and 22.

FIG. 1

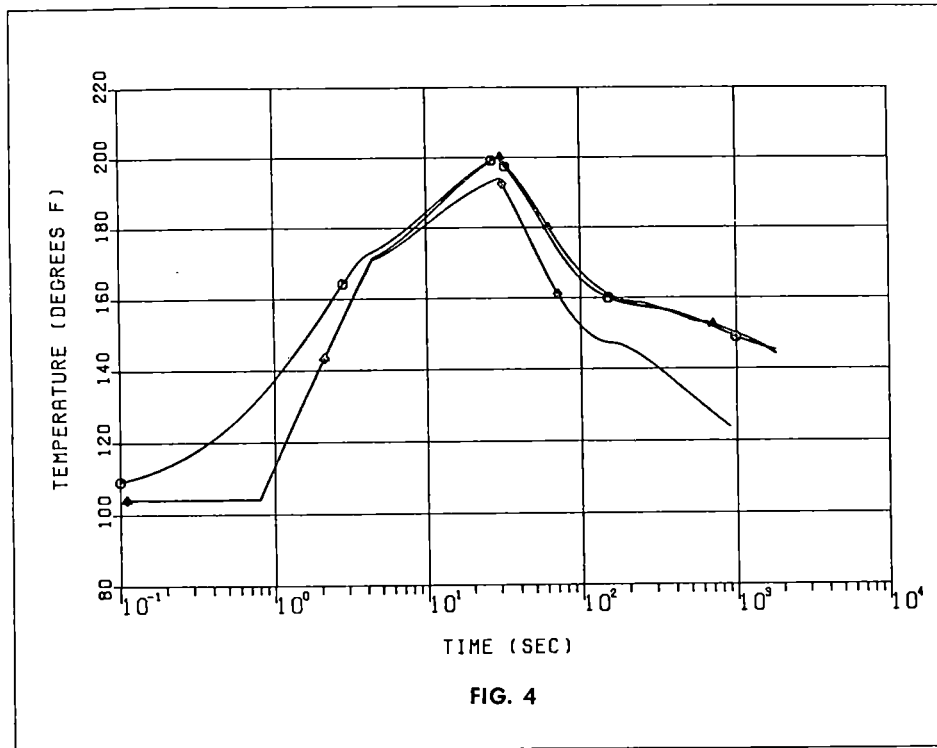
TEMPERATURE TRANSIENT VARIATION FOR DIFFERENT BREAK CASES



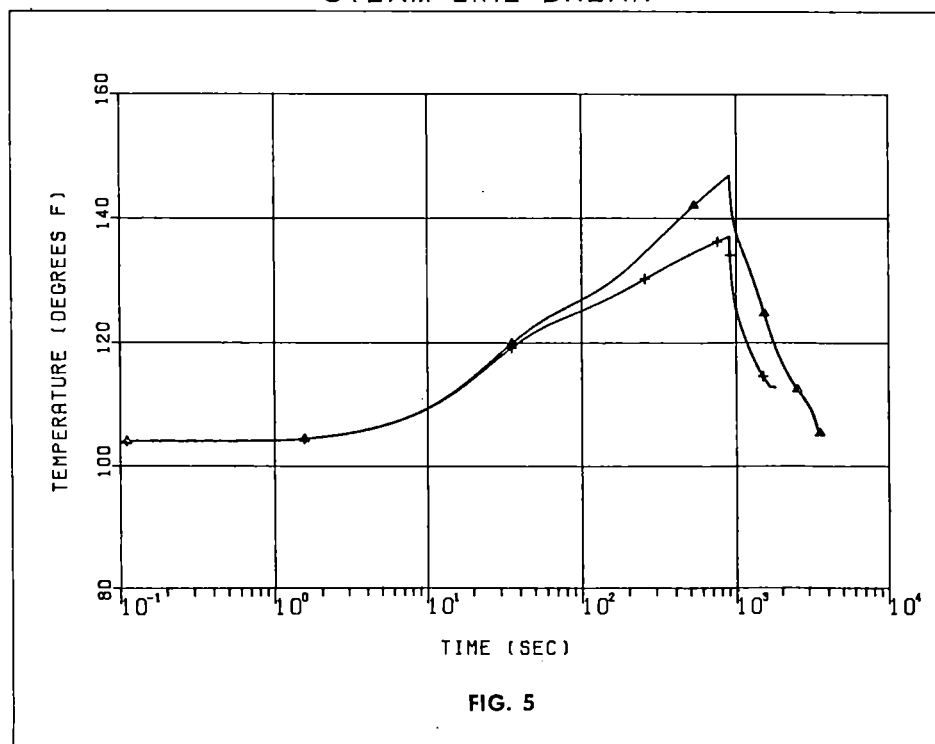
TEMPERATURE TRANSIENT VARIATION FOR DIFFERENT COMPARTMENT LOCATIONS



TEMPERATURE TRANSIENT VARIATION WITH VENTILATION
SYSTEM OPERATION & PASSIVE HEAT SINKS -
LIQUID LINE BREAKS



TEMPERATURE TRANSIENT VARIATION WITH VENTILATION
SYSTEM OPERATION & PASSIVE HEAT SINKS -
STEAM LINE BREAK



VALUE-IMPACT ANALYSIS OF SEVERE ACCIDENT PREVENTION
AND MITIGATION SYSTEMS

A. S. Benjamin, S. W. Hatch, D. R. Strip,
P. R. Bennett, D. D. Drayer, and V. L. Behr

Sandia National Laboratories
Albuquerque, New Mexico 87185, U.S.A.

ABSTRACT

As part of Sandia's Severe Accident Risk Reduction (SARR) Program for the U.S. Nuclear Regulatory Commission, we have been investigating the cost-benefit tradeoffs of filtered-vented containment (FVC) systems, hydrogen control systems, alternate decay heat removal systems, and a variety of other reactor modifications designed to reduce the risk from severe accidents. We have been appraising our results in terms of the Commission's proposed safety goals and in terms of the true costs of reactor accidents.

Some of our preliminary results to date indicate that (1) FVC systems are potentially cost-effective for many BWRs, but apparently not cost-effective for most PWRs; (2) the opposite is true for hydrogen control systems; and (3) the most effective safety approaches include combinations of both preventive and mitigative features. Further analyses are being performed to fully investigate the sensitivity of these results to uncertainties.

INTRODUCTION

Sandia National Laboratories is supporting the NRC severe accident rulemaking activities through a number of technical investigations that broadly address the phenomenological, systems, and human aspects of degraded core accidents. The integration of results from these programs to provide a technical base for regulatory decisions is the responsibility of a program entitled, "Severe Accident Risk Reduction (SARR) Program." Basically, the objectives of the SARR program are to provide an assessment of the values and impacts of a set of degraded core prevention and mitigation features, summarized in Table I, and to assist NRC in formulating rules.

The safety approaches being considered include not only the individual features listed in Table I, but also all plausible combinations of these features, applied both to existing reactors and to new (design-stage) reactors. To quantify these tradeoffs, we have been evaluating the potential reduction in accident risks against the retrofitting and/or implementation costs, and have been appraising our results in terms of the Commission's proposed safety goals and in terms of the true costs of reactor accidents.

The SARR program is being conducted in two phases, the first of which is scheduled for completion around September 1983 and the second two years later. Existing value-impact studies at Sandia on filtered-vented containment systems [1,2], alternate decay heat removal systems [3], and molten core retention devices [4] are being incorporated into the SARR program during the first phase.

Table I. Degraded Core Safety Features Under Consideration

Candidate Improvements	Options
1. Additional Containment Heat Removal	a. Active Versus Passive
2. Containment Atmosphere Particulate Capture	
3. Containment Atmosphere Mass Removal	a. Filtered Versus Unfiltered b. Low Flow Versus High Flow
4. Increased Containment Margins	a. Deliberate Ignition b. Increased Pressure Capability c. Pressure Suppression Features
5. Combustible Gas Control	a. Deliberate Ignition b. Inerting (Prior/Post Accident) c. Heat Sinks (Fogs/Foams)
6. Core Retention Devices	a. Dry Versus Wet b. Active Versus Passive Cooling or No Cooling
7. Missile Shields	a. Gas Detonations or Steam Explosions b. Vessel Thermal Shock
8. BWR Containment Spray System	
9. PWR Primary System Depressurization	a. Automatic Versus Manual b. Additional Relief Capacity c. Pressure Suppression Features d. Radioactivity Removal Systems
10. Add-On Decay Heat Removal Systems	a. High Pressure Versus Low Pressure b. Open Loop Versus Closed Loop c. Primary System Versus Secondary System
11. Specific Prevention Concepts	a. Improved Drain or Valve Design b. Improved Maintenance Procedures c. Improved Control Logic d. Reduction of Common Mode Dependencies

We are conducting Phase I of the value-impact assessment in two parts. In the first part, we obtain a preliminary rating of the candidate safety approaches for each of several existing baseline reactors, which are listed in Table II. The risks from these reactors were originally analyzed in the Reactor Safety Study [5] and the Reactor Safety Study Methodology Applications Program [6]. The rating is based on the following steps:

Step 1: Initial screening of safety approaches. A preliminary analysis is made for each baseline reactor to estimate the risk reduction potential of the candidate safety approaches and to screen out those approaches which provide no possibility of a significant risk reduction benefit.

Step 2: Initial screening of uncertainties. The phenomenological, system, and human response uncertainties are prioritized according to their relative importance in the risk reduction evaluation, and the sensitivity of the results to these uncertainties is assessed.

Table II. Description of Baseline Reactors

Baseline Reactor	Reactor Type	NSS Supplier	Containment Type
Grand Gulf Unit 1	BWR	General Electric	Mark III
Peach Bottom Unit 2	BWR	General Electric	Mark I
Oconee Unit 3	PWR	Babcock and Wilcox	Large, Dry
Calvert Cliffs Unit 2	PWR	Combustion Engineering	Large, Dry
Surry Unit 1	PWR	Westinghouse	Large, Dry Subatmospheric
Sequoyah Unit 1	PWR	Westinghouse	Ice Condenser

Step 3: Development of cost-benefit measures. Procedures are developed to enable us to evaluate the risk reduction results in terms of monetary values.

Step 4: Initial quantification of cost-benefit measures. Based on available estimates of construction cost and reactor downtime, the cost of retrofitting the proposed safety approaches into the baseline reactors is compared to the value of the risk averted.

The analyses and results to be described in this paper pertain to Steps 2 through 4. (A separate paper presents results from Step 1 [7].)

In the second part of Phase I, we shift from plant-specific analyses to more generic analyses, and include a more detailed evaluation of costs and feasibility, both for existing plants and for new plants. The specific steps are as follows:

Step 5: Determination of generic plant categories. Results from NRC's Accident Sequence Evaluation Program (ASEP) [8] are used to group reactors into generic categories.

Step 6: Risk benchmarking. The risk is reevaluated for each generic plant type, based on updated estimates of accident frequency and consequences.

Step 7: Cost and feasibility assessment and evaluation of competing risks. For those safety approaches which appear attractive after Step 4, conceptual designs are developed, the overall feasibility of incorporating these designs into existing or new reactors is assessed, potential system interactions are evaluated, and cost estimates are obtained.

Step 8: Reevaluation of Part 1 results. The risk reduction potentials, sensitivity to uncertainties, and cost-benefit tradeoffs are reevaluated for each generic plant type.

In this paper, we will describe our cost-benefit methodology and will present example results for certain specific cases (namely, cases involving containment venting and hydrogen control). As a preface to the presentation that follows, it is important to mention that the analyses are ongoing and that the results are preliminary. This is particularly the case in our analysis of the influence of uncertainties on the cost-benefit tradeoffs, in our evaluation of the financial aspects of reactor risk, and in our assessment of the effectiveness of certain safety approaches for preventing certain containment failure modes. Further, we have not yet specifically considered accidents initiated by acts of sabotage or by external events such as earthquakes, winds, or airplane crashes. In the Reactor Safety Study, external events were excluded as "not contributing significantly to reactor accident risks." Later studies have shown, however, that external events may be significant contributors for certain plants [9,10]. For all these reasons, the results to be presented should be considered preliminary findings that may be subject to change upon further analysis.

COST-BENEFIT MEASURES

The measures we use to characterize the benefit of various safety approaches are as follows:

- (1) The amount of risk averted (expressed in terms of man-rem averted over the life of the plant).
- (2) The total accident cost averted (including all offsite and onsite costs).
- (3) The cost of offsite effects averted (including offsite health effects and property damage).

The basis for using averted population dose (man-rem) as a measure of benefit stems from the NRC proposed safety goals [11]. Included in the Commission proposal are specific guidelines for acceptable limits of core melting frequency, prompt fatality risks, and latent cancer fatality risks. Also included is a cost-benefit guideline, which is stated as follows: "The benefit of an incremental reduction of risk below the numerical guidelines for societal mortality risks should be compared with the associated costs on the basis of \$1,000 per man-rem averted." Subsequent safety goals proposed by the Atomic Industrial Forum [12] and supported by the American Nuclear Society [13] have agreed to the principle of evaluating the benefit in terms of averted population dose but have argued for a figure of \$100 per man-rem.

The rationale for using actual accident costs in the benefit determination is that it allows cost-benefit analyses to be performed on a dollar-for-dollar basis. On the one hand, it avoids the argument over how the balance between costs and benefits should be fixed, since the break-even point is clearly defined in terms of equal costs. On the other hand, it shifts the argument to the question of how financial risk should be evaluated. Because there is a rather strong sentiment in the nuclear power industry against using total accident costs as a basis for safety regulation, we evaluate the cost-benefit tradeoffs in terms of both the total financial risk (offsite plus onsite) and the offsite financial risk alone.

A method for determining accident costs is described elsewhere [14,15]. In the following paragraphs, we shall summarize some of the key features of the methodology.

Cost of Health Effects

To assign a dollar value to various health effects, we impute a social perception of the worth of a life from the expenditures that society is willing to make in order to prevent a death. This approach leads to widely varying values on human lives, from the low tens of thousands of dollars for some cancer prevention tests and highway maintenance, to hundreds of thousands of dollars per life for some auto

safety features, to millions of dollars per life for some mine safety and radiological standards.

For purposes of the cost-benefit examples to be presented in this paper, we place a value of \$1 million on early fatalities and \$100,000 on early injuries and latent cancer fatalities. The higher figure is larger than most values for traffic safety programs or equipment which are used to prevent prompt deaths, comparable to the early death as defined for our purposes. In addition, it is in the range of the imputed life values based on other considerations such as aircraft safety. The lower figure is in the range (although slightly larger) of imputed life values based on various medical treatments or screening techniques, mostly related to cancers, which are comparable to the delayed deaths caused by radiological accidents.

An analysis of the sensitivity of the total financial risk to the values assigned to health effects has been made [14]. The conclusion is made that for most reactors, the cost of health effects is low compared to the cost of property damage, cleanup, and replacement power.

Property Damage Costs

The economic costs resulting from lost wages, relocation expenses, decontamination of property, lost property, and interdiction of land and farm crops are calculated by the CRAC2 computer code [16]. The costs are evaluated on the basis of statewide averaged land use and land value data, and utilize the actual population distribution surrounding the specific reactor site.

Power Replacement and Cleanup Costs

Estimates of replacement power costs are based on preliminary results from an ongoing research project at Argonne National Laboratory. In this method replacement power costs are estimated on the basis of the cost of replacement fuels and power availability for various regions that span the United States and part of Canada. The dominant factor in determining these costs is the relative proportion of oil-fired backup plants versus economical alternative sources. The cost of replacement power is estimated to be

$$C_o = (0.286 \times R + 0.086) \text{ \$millions per MW year}$$

where R is the fraction of replacement energy by oil-fired or noneconomical power purchases. The values of R vary from .05 to .95, with an average of .41.

Cleanup costs for reactor accidents are difficult to estimate due to a lack of experience and data. For the initial stages of this project we are using a value of 100 million dollars per year for ten years, which represents the cost of early decommissioning or cleanup and repair, depending upon the severity of the accident.

Discounting

It is standard practice in economic analyses to use present value discounting of future income or losses to provide a basis of comparison for economic events that occur at different times, or over a period of time. In this study we have used formulae based on continuous discounting [14,15], at a rate of 4 percent per annum.

Other Costs

There are a number of other costs which have not yet been included in our analyses. Examples are (1) the cost of medical care for injuries and illnesses sustained, (2) the cost of litigation and settlements pursuant to the accident, and (3) various secondary business costs. We will be exploring these other costs in future analyses.

EFFECTS OF UNCERTAINTIES

A key element of the risk reduction evaluation is the treatment of uncertainties. Existing risk assessments are currently thought to be highly dependent upon uncertainties in the following areas:

- (1) Extent of fission product release from fuel and physiochemical form,
- (2) Modeling of fission product retention in primary and containment systems,
- (3) Severity of steam explosions, hydrogen burns, and other pressure spiking phenomena,
- (4) Survivability of safety systems under severe accident conditions,
- (5) Accounting of human interfaces.

To account for these uncertainties, we first define quantitative upper and lower bounds for the parameters involved. In selecting these bounds, we try to reflect the spectrum of expert opinion as defined, on the one hand, by the Reactor Safety Study [5] and subsequent risk assessments [6], and on the other hand, by the evolving industry position [9,10,17,18]. Table III illustrates this bounding of uncertainties for one of the reactors analyzed in this study [19].

Table III. Uncertainty Bounds Used for Peach Bottom Analysis

Source of Uncertainty	Conservative Bound	Nonconservative Bound
1. Containment failure probability from in-vessel steam explosion	0.01	0.
2. Rationale for containment failure from ex-vessel core-water interactions	Large steam explosion in reactor cavity with 50% of debris dispersed to suppression pool	Small steam explosions in reactor cavity with up to 18% of debris dispersed to suppression pool
3. Iodine release form	I ₂ and 0.7% CH ₃ I	CsI and 0.2% CH ₃ I
4. Particulate retention in primary system for accidents of type TW and TC	DF = 1	DF = 10
5. Particulate retention in primary system and containment for other accident types	MARCH/CORRAL Calculation	MARCH/CORRAL calculation plus additional DF = 100-1000
6. Effect of containment failure loads on water delivery systems	All water lines fail	Lines that bypass torus may survive
7. Failure condition for ECCS pumps	NPSH less than design	Water sources depleted
8. Recoverability of containment cooling systems	Common modes and plugged valves nonrecoverable	All faults recoverable (MRT = 19 hours)
9. Recoverability of reactor protection system	RPS nonrecoverable	RPS recoverable (MRT = 2.5 hours)

In the risk reduction evaluation, we calculate two sets of risks, one based on the conservative assumption set and the other based on the nonconservative set, and we take the difference between the two to represent the overall risk uncertainty due to phenomenological and system response unknowns. To date, we have performed an uncertainty analysis for the two boiling water reactors but not for the four pressurized water reactors. Our results will reflect this state of development.

COST-BENEFIT RESULTS

Figure 1 and Table IV illustrate some sample results of our cost-benefit calculations for safety approaches involving filtered-vented containment (FVC) systems and hydrogen control systems. (FVC systems are intended to prevent containment failure from gradual overpressurization, whereas hydrogen control systems are designed to prevent containment failure resulting from hydrogen burning.)

The vertical axes depict the value of man-rem averted (at \$1000 per man-rem) or the value of accident costs averted (both total costs and offsite costs) for the various FVC options and hydrogen control options considered. The estimated retrofitting costs are overlayed in the form of dashed horizontal lines. In this format, an FVC or hydrogen control option would be considered cost effective if the bar depicting its value lay predominantly above the dashed line depicting its cost, and would be considered not cost effective if the opposite were true.

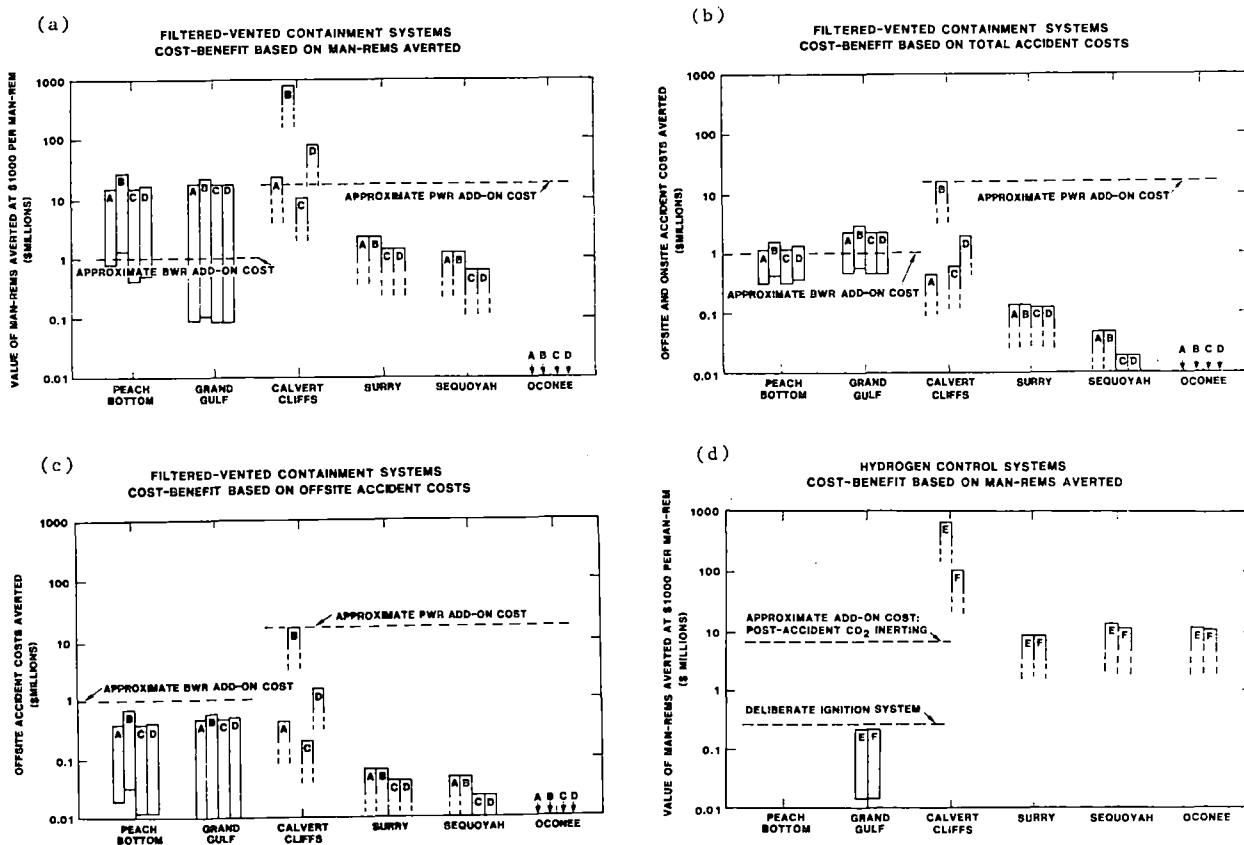


Figure 1. Cost-Benefit Results for Containment Venting and Hydrogen Control Systems

Table IV. Cases Considered for Cost-Benefit Comparison

<u>Case</u>	<u>Containment Configuration Prior to Modification</u>	<u>Modification</u>
A	As analyzed in original PRA	Low-Volume Containment Vent (~15,000 ft ³ /min.)
B	As analyzed in original PRA	High-Volume Containment Vent (~300,000 ft ³ /min.)
C	With hydrogen control and specific preventive fixes (see below)	Low-Volume Containment Vent (~15,000 ft ³ /min.)
D	With hydrogen control and specific preventive fixes	High-Volume Containment Vent (~300,000 ft ³ /min.)
E	As analyzed in original PRA	Hydrogen Control System
F	With specific preventive fixes only	Hydrogen Control System

Identification of Preventive "Fixes" for Cases C, D, and F

1. Improved design or maintenance of the low pressure injection system check valves to reduce the probability of direct containment bypass (Surry, Sequoyah, and Oconee)
2. Improved maintenance of upper-to-lower compartment drains to reduce the probability of common mode failures of emergency core cooling and containment spray recirculation systems (Sequoyah)
3. Improved control logic to prevent the actuation of containment spray recirculation in the event of an empty containment sump (Surry)
4. Modified auxiliary feedwater system, based on improvements to be implemented by November 1982 (Calvert Cliffs)
5. Improved reactor protection system, based on General Electric's proposed ATWS "Fix 3A" (Peach Bottom and Grand Gulf)

As mentioned earlier, high and low uncertainty bounds on the benefit measures have been estimated for the BWRs. The top and bottom of the bars in Figure 1 depict the difference between these bounds. On the other hand, only the high bounds have been estimated so far for the PWRs, and so the bars in these cases are left incomplete.

Cases A, B, and E consider the cost-benefit attributes of FVC and hydrogen control systems applied to the baseline reactors as analyzed in the original PRAs [5,6], whereas Cases C, D, and F consider the incremental effects of adding these systems to containments that have already undergone some modification. These modifications consist of certain preventive "fixes" designed to reduce specific vulnerabilities that were identified in the original PRAs (see Table IV). In Cases C and D, a hydrogen control system is also assumed to have been implemented prior to the addition of containment venting.

All add-on systems were assumed to have a failure rate of 0.01 on demand. We assumed that the FVC systems cannot react fast enough to reduce the risk of containment failure from hydrogen burns, but that a high-volume venting strategy (~300,000 ft³/min) can prevent containment overpressurization both from anticipated transients without scram (ATWS) and from ex-vessel "steam spikes" (i.e., pressurization caused by the quenching of core debris in water in the reactor cavity or on the containment floor). The assumption regarding steam spikes appears to be important only for Calvert Cliffs, where the reactor cavity is designed to retain large amounts of water.

Basis for Retrofitting Costs

Schematics of the containment venting designs used for cost estimation are shown in Figure 2. For the BWR Mark I containment (Peach Bottom), we tapped off from two existing personnel access penetrations (one 30 inches in diameter and the other 24 inches in diameter) located above the suppression pool in the wetwell torus. By choosing to vent from above the pool, we were able to use the existing suppression pool as a fission product scrubber, thereby eliminating the need for any add-on filtration capability. The additions, therefore, consisted mainly of the valving necessary to open and close the vent paths and a main vent line routed from the torus to the turbine building roof, where we chose to exhaust the effluent. Provisions were included to inert the vent line prior to normal operation, since the Mark I containment is also preinerted.

The cost of the BWR Mark I containment venting system was estimated by Holmes and Narver, Inc., (an architect-engineering firm subcontracted by Sandia) to be about \$1.2 million for a high-volume system ($\sim 300,000 \text{ ft}^3/\text{min.}$) and about \$0.9 million for a low-volume system ($\sim 15,000 \text{ ft}^3/\text{min.}$). These costs are quoted in 1980 dollars and include a 15 percent contingency and a 6 percent fee. The system was designed to be seismic category 1; i.e., it was afforded the same level of seismic protection as the containment. Reactor downtime required for retrofitting was estimated to be about 15 days. This estimate was based on the architect-engineer's assessment that the reactor would have to be shut down only for construction within the reactor containment building and not for construction in the turbine building. It was judged that the retrofitting could be accomplished during a normal refueling outage.

A containment venting system has not been specifically designed for the BWR Mark III containment (Grand Gulf). We are currently assuming that the characteristics of the system and costs would be similar to Peach Bottom.

For the PWRs, we designed a BWR-style water-filled suppression pool as a component of the venting system outside containment. (We could have used a submerged gravel scrubber in place of a suppression pool; we estimate that the costs and filtration capabilities would have been similar.) Although the pool had its own

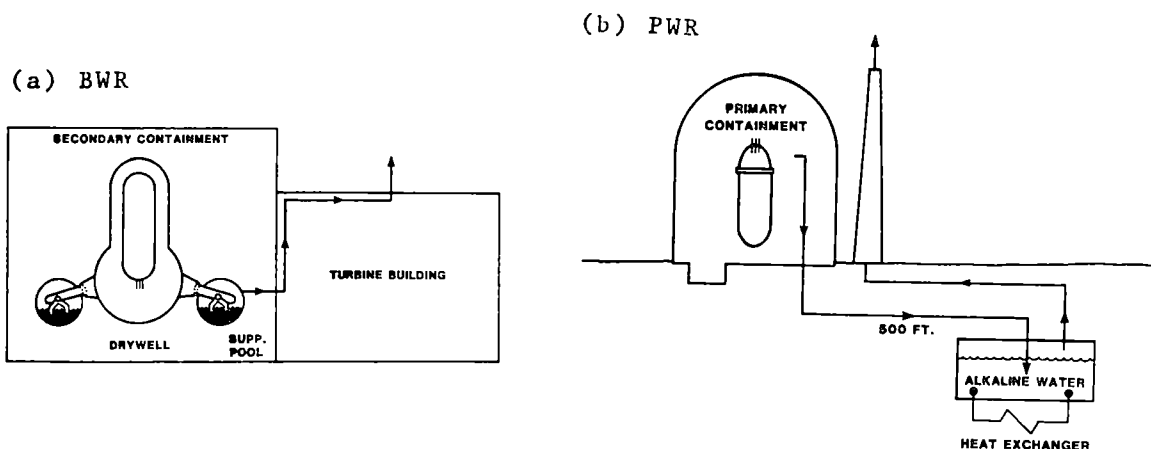


Figure 2. Schematic Showing the Flow Paths for Two Containment Venting Systems: (a) BWR Mark I Containment; (b) PWR Large Dry Containment (Not to Scale.)

heat exchanger, it was designed according to a criterion that in the event of a loss of ac power, the water should remain subcooled for at least 16 hours (so as to remain effective as a fission product scrubber). This criterion set the pool water content at about one million gallons, the size of a BWR suppression pool.

The cost of the PWR containment venting system was estimated by Holmes and Narver to be about \$16 million. The entire system was designed to be seismic category 1. Because the size of the suppression pool was determined by its capacity to retain heat rather than by the venting flow rate, the low-volume and high-volume options were comparable in cost. Since most of the construction occurred far from the reactor containment building, the reactor downtime was assessed to be short and to be easily accommodated during a normal refueling outage.

The cost estimates for hydrogen control systems are based on two concepts developed by General Electric Company, one a deliberate ignition system and the other a CO₂ post-accident containment inerting system [20]. Although these designs were developed for Mark III containment boiling water reactors, we are currently assuming that the costs for pressurized water reactors would be similar. (The Mark I containment BWRs are preinerted and do not require any additional hydrogen control).

The deliberate ignition system includes a separate power source and electrical system. It has recently been suggested that the effectiveness of deliberate ignition systems may be enhanced by modifying the containment spray system in the following two ways: (1) replacing the nozzles with emitters that discharge fog-sized droplets, and (2) eliminating common mode dependencies with the emergency core cooling systems (especially for BWRs). Such modifications have not been included in the cost estimate depicted in Figure 1(d).

DISCUSSION AND CONCLUSIONS

As mentioned in the Introduction, the results shown in Figure 1 are preliminary and the analyses are ongoing. In particular, the following caveats need to be reiterated:

- (1) External events (earthquakes, winds, etc.) have not been included in the risk assessments, nor has the risk of sabotage.
- (2) The effects of uncertainties have been only partially evaluated.
- (3) Assumptions have been made regarding the effectiveness (or lack of effectiveness) of containment venting systems under certain scenarios.
- (4) Several factors have not yet been considered in the evaluation of financial risks from reactor accidents.

Keeping these caveats in mind, the following observation can be made from the results in Figure 1:

First, the estimated value of accident prevention and/or mitigation appears to be much higher when NRC's proposed \$1,000 per man-rem is used as a cost-benefit measure than when either total or offsite accident cost is used. The guideline of \$1,000 per man-rem should, therefore, not be construed as representing a surrogate for actual accident costs.

Second, large differences can be observed among the three large dry PWR containments. In part, this is due to the relatively larger level of risk evaluated in the RSSMAP study for Calvert Cliffs than for Oconee or Surry. Also, the potential benefit of filtered-vented containment systems for these reactors is governed by factors not related to containment type, such as the relative independence of

systems that remove heat from containment (i.e., sprays and fan coolers), the reliability of onsite ac power, and the design of the reactor cavity.

Third, based on man-rem averted or total accident costs, containment venting appears to be potentially cost effective for the BWRs evaluated. The potential cost effectiveness is predicated, however, on a simple, inexpensive containment venting design that uses only the existing suppression pool as a scrubber. A highly efficient add-on filtration system would increase the cost without improving the risk reduction benefit.

Fourth, with the possible exception of Calvert Cliffs, containment venting systems do not appear to be cost effective for the PWRs evaluated, regardless of the cost-benefit measure used. The potential benefit for Calvert Cliffs may be illusory, because it is dependent upon some highly uncertain assumptions regarding the phenomenology of ex-vessel "steam spikes".

Fifth, hydrogen control systems appear to be potentially cost effective for the PWRs, but are apparently not cost effective for the BWR evaluated. Hydrogen control for PWRs would be especially cost effective if it could be shown that a simple deliberate ignition system is capable of preventing containment failure from hydrogen burns with a high degree of reliability. The reliability and effectiveness of deliberate ignition systems is currently under investigation [21].

The cost-benefit examples presented in this paper pertain to safety approaches involving the addition of containment venting, hydrogen control, and specific preventive fixes to existing reactor containments. A wide variety of other safety approaches is also being considered (see Table I), and results from these analyses will be documented at a later time. Future reporting will also include updated iterations of the results presented here.

REFERENCES

1. BENJAMIN, A. S., "Program Plan for the Investigation of Vent-Filtered Containment Conceptual Designs," Sandia National Laboratories, SAND79-1088, NUREG/CR-1029 (1979).
2. BENJAMIN, A. S., "Filtered-Vented Containment System Design Study", Report of the Zion/Indian Point Study, ed. W. B. Murfin, Sandia National Laboratories, SAND80-0617/1, NUREG/CR-1410 (1980), I-1.
3. BERRY, D. L. and BENNETT, P. R., "Study of Alternate Decay Heat Removal Concepts for Light Water Reactors - Current Systems and Proposed Options," SAND80-0929, NUREG/CR-1556 (1981).
4. DARBY, J. L., "A Review of the Applicability of Core Retention Concepts to Light Water Reactor Containments," SAND81-0416, NUREG/CR-2155 (1981).
5. RASMUSSEN, N. C., et al., "Reactor Safety Study," WASH-1400, NUREG-75/014 (1975).
6. "Reactor Safety Study Methodology Applications Program," Volumes 1 through 4, Sandia National Laboratories, SAND80-1897, NUREG/CR-1659 (1981-1982).
7. HATCH, S. W., et al, "Risk Reduction Analysis of Severe Accident Prevention and Mitigation Systems," these proceedings (1982).
8. HARPER, F. T., et al., "Accident Sequence Evaluation Program Phase II Report," Sandia National Laboratories, to be published (1982).

9. "Zion Probabilistic Safety Study," Pickard, Lowe, and Garrick, Inc. (1982).
10. "Indian Point Probabilistic Safety Study," Pickard, Lowe, and Garrick, Inc. (1982).
11. "Safety Goals for Nuclear Power Plants: A Discussion Paper," U.S. Nuclear Regulatory Commission, NUREG-0880 (1982).
12. "A Proposed Approach to the Establishment and Use of Quantitative Safety Goals in the Nuclear Regulatory Process," Atomic Industrial Forum (1981).
13. "Proposed Policy Statement on Safety Goals for Nuclear Power Plants," letter from C. L. Rickard, President American Nuclear Society, to U.S. Nuclear Regulatory Commission, May 18, 1982.
14. STRIP, D. R., "Estimates of the Financial Risks of Nuclear Power Reactor Accidents," Sandia National Laboratories, SAND82-1110, NUREG/CR-2723, to be published (1982).
15. BENJAMIN, A. S., and STRIP, D. R., "Cost-Benefit Considerations for Filtered-Vented Containment Systems," Proc. 17th DOE Nuclear Air Cleaning Conference, to be published (1982).
16. RITCHIE, L., JOHNSON, J., and BLOND, R., "Calculations of Reactor Accident Consequences, Version 2: User's Guide," Sandia National Laboratories, SAND81-1994, NUREG/CR-2326, to be published (1982).
17. LEVENSON, M., and RAHN, F., "Realistic Estimates of the Consequences of Nuclear Accidents," and following articles, Nuclear Technology, Vol. 53 (1981).
18. "Technical Basis for Estimating Fission Product Behavior During LWR Accidents," U.S. Nuclear Regulatory Commission, NUREG-0772 (1981).
19. BENJAMIN, A. S., HARPER, F. T., and CYBULSKIS, P., "Filtered-Vented Containment System Conceptual Design Study and Risk Assessment for a BWR Mark I Containment," Sandia National Laboratories, to be published (1982).
20. "Allens Creek Nuclear Generating Station - Preliminary Safety Analysis Report," Amendment 57 (1981).
21. BERMAN, M. et al, "Analysis of Hydrogen Mitigation for Degraded Core Accidents in the Sequoyah Nuclear Power Plant," Sandia National Laboratories, SAND80-2714, NUREG/CR-1762 (1981).

DEPRESSURIZER SYSTEM FOR SMALL PIPE BREAKS
IN PASSIVE CONTAINMENT SYSTEM (PCS)

O. B. Falls, Jr. and Frank W. Kleimola

NucleDyne Engineering Corporation
Jackson, Michigan, 49201, U.S.A.

ABSTRACT

PCS provides complete protection for the design basis LOCA - double-ended guillotine-type rupture of the largest pipe in the reactor coolant system (RCS) - without the need for onsite or offsite AC power. Incorporated into the PCS the Depressurizer System extends these protective safety features enabling RCS cooldown to safe shutdown for the full spectrum of pipe breaks including the small LOCA. Other than the DC power required for actuation of valves that initiate operation of the Depressurizer System, RCS cooldown is thereafter passive. The System lends itself to flexibility in the design of the depressurizer vessels and the location of the interconnecting piping for variations in the design of a pressurized water reactor (PWR).

INTRODUCTION

The PCS has been under development for over 15 years. These developments have been described in papers presented at meetings. (Ref. 1-6). Although particular emphasis has been directed toward mitigation of the consequences of the complete spectrum of loss-of-coolant accidents (LOCAs) and secondary system pipe breaks, the thrust of the PCS developments have been to provide complete protection to the public against all potential releases of energy and radioactivity resulting from adverse incidents.

In this paper special emphasis is directed toward a Depressurizer System, an added engineered safety feature provided in the PCS to overcome the small break LOCA without need for AC power. In order to describe the function of the Depressurizer System in the small break LOCA, it is necessary to briefly describe the balance of the basic PCS.

For a four-loop PWR the primary reactor containment (PRC) consists of freestanding, interconnected steel cells. These cells individually house the RCS components and safety system components, consisting of water-filled refill, deluge and quench tanks, which are vertically mounted at an elevation above the RCS piping. Separate compartments are provided for the reactor coolant pump motors, the pressurizer, and the control rod drives. The PRC free volume (except for the compartments) and the freeboard in the deluge and quench tanks is maintained in the range of 2 psia during

reactor operation.

In the PCS the main steam isolation valves (MSIV) are immediately outside the PRC. The power-operated relief valves (PORVs) and the safety valves for the steam generator secondaries are inside the PRC and are arranged in such manner as to discharge into the deluge and quench tanks.

The four refill tanks are identical; each tank has about 5800 cu. ft. of internal volume. The eight deluge tanks and eight quench tanks are identical; each tank has about 7000 cu. ft. of internal volume. The total heat sink capacity of the stored water in the refill, deluge and quench tanks is over 1311 million British thermal units (Btu) on being heated from 50F to 212F; the saturation temperature corresponding to the one atmosphere of pressure in the PRC. For comparison, the stored energy in the reactor coolant equals about 303.1 million Btu.

During reactor operation, whenever the RCS is accidentally depressurized from 2250 to the 1000 psia range, the injection of emergency core cooling water initiates passively. As shown in Figure 1 steam flow from the steam generator secondaries is directed through check valves to jet injectors that entrain borated water from the refill tanks for safety injection into the RCS. The refill system is designed to re-flood the core at the rate of 6 inches per second against 100 psia RCS pressure; this rate increases as the RCS back pressure decreases. The refill system has sufficient inventory to refill the reactor vessel over five times; also, there is sufficient heat sink capacity to reduce the steam generator secondary fluid to less than 160F. After RCS blowdown to the back pressure in the PRC, emergency cooling with borated water continues for over four hours with gravity flow from the deluge tanks.

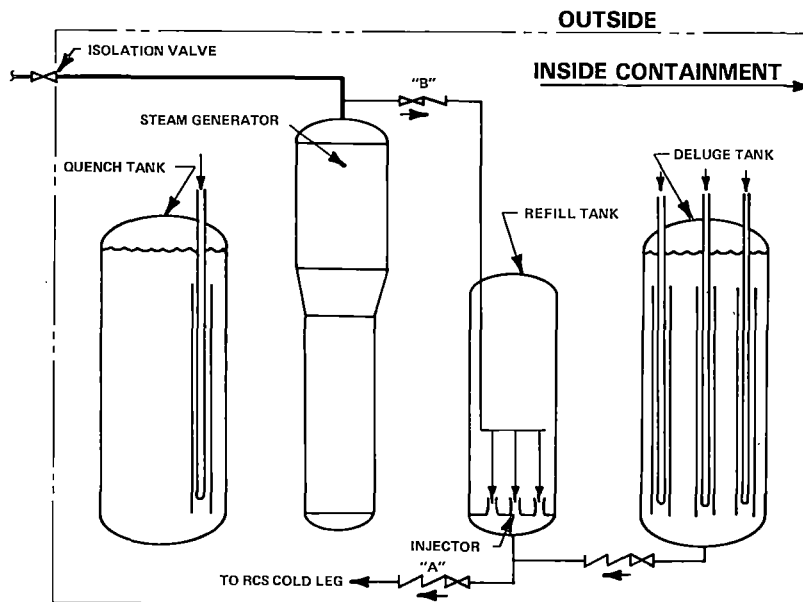


Figure 1

Engineered Safety Systems for LOCA

On the loss of feedwater an emergency flow of makeup water to the steam generator is initiated. In Figure 2, steam from the steam generator secondaries is directed to jet injectors that entrain water from the quench tanks for injection back into the steam generator secondaries. This water from the quench tanks increases in temperature as the water is recycled into the steam generators.

In a LOCA the water in the deluge and quench tanks serve as a heat sink for the RCS blowdown. These tanks have vertically positioned vent pipes (12 in. in diameter) that are perforated with small orifices positioned below the water level. The vent pipes are encircled with solid wall pipes to prevent thermal stratification and adverse hydrodynamic loads. The total vent area from the PRC into the deluge and quench tanks is over 1200 sq. ft.

The steam discharge from the over-pressure valves (PORVs and safeties) at the pressurizer and steam generator secondaries are vented into the deluge and quench tanks. These vents are similar in construction for the quenching of steam as those provided for venting steam from the PRC.

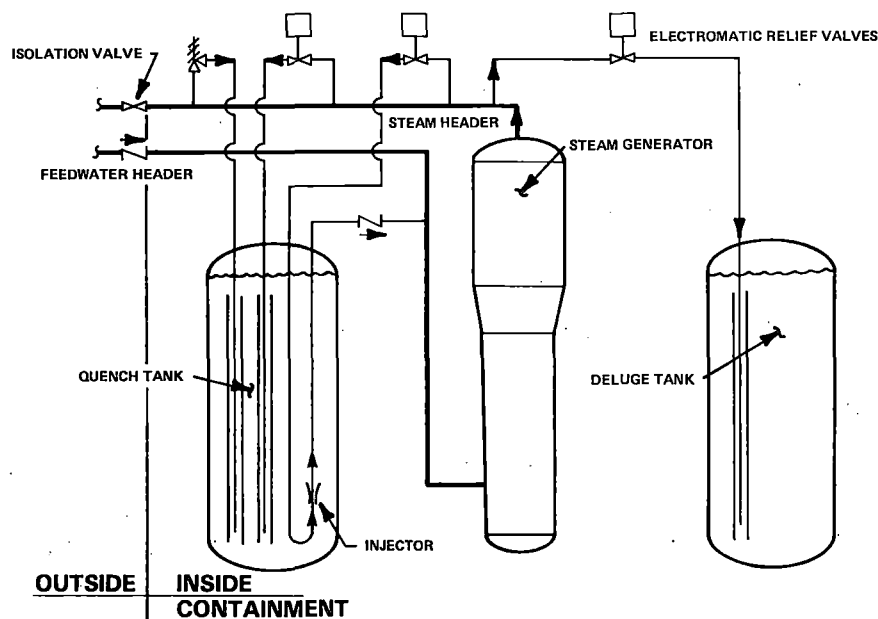


Figure 2

Alternate Decay Heat Removal System

DEPRESSURIZER SYSTEM

The system consists of two flow circuits; each circuit consists of a 1600 cu. ft. depressurizer vessel - contained within the PRC - and its associated piping, valves, instrumentation and controls actuated by the plant's redundant, safety grade DC power supplies. Each depressurizer vessel is positioned in the vicinity of the pressurizer and the bottom ends are elevated above the liquid level range of the pressurizer. Figure 3 shows the Depressurizer System and the flow circuit interconnections to the RCS and to the other plant systems.

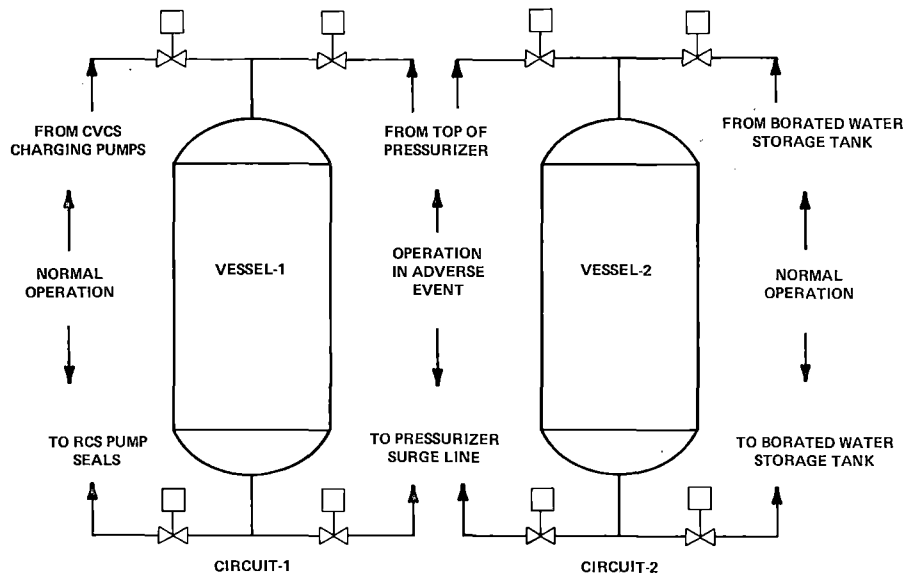


Figure 3
Depressurizer System

In Circuit-1 during reactor operation the flow of borated water from the charging pumps in the plant's Chemical and Volume Control System is routed through and out the bottom of vessel-1 to the four reactor coolant pump seals. Circuit-1 has a flow of 32 gpm, thus providing 8 gpm of cooling water at about 120F to each pump seal. Additionally, the elevated PCS deluge tanks continuously provide cooling water under natural circulation to the thermal barrier at each pump seal, as backup for limiting pump seal temperature rise.

In Circuit-2, the water in vessel-2 is maintained at four weight percent boric acid concentration. A one gpm flow is periodically recycled through vessel-2 from the plant's borated water storage tank (BWST) utilizing a positive displacement pump. The flow through Circuit-2 is isolated from the RCS during reactor operation.

In the event of an adverse plant condition; such as the loss of load, turbine trip or station blackout, the valves in Circuit-1 actuated by the DC power supply are

realigned by the same control signal that causes MSIV closure. The outlet flow from the bottom of vessel-1 switches from the pump seals to the pressurizer surge line. Also, flow into vessel-1 switches from the charging pumps to the top end of the pressurizer.

Actuation of the normally closed valves in the pressurizer connection in Circuit-1 to the open position initiates steam flow from the pressurizer displacing the water from vessel-1 into the pressurizer surge line. Steam flow into vessel-1 and the sub-cooled "makeup" help depressurize the RCS. The flow into the surge line provides 400 gpm of makeup for seal leakage, cooldown shrinkage and pipe break loss.

The valves in Circuit-2, actuated by the DC power supply, are programmed to realign about 30 minutes after initiation of the adverse plant condition. The recirculated flow through vessel-2 from the BWSI is isolated; the bottom end of vessel-2 is interconnected to the pressurizer surge line and the top end of vessel-2 is interconnected to the top end of the pressurizer to continue the 400 gpm "makeup" into the RCS through the surge line during depressurization of the RCS.

Concurrent with the actuation of the Depressurizer System on MSIV closure, the DC power supply also actuates the PORVs in two of the steam generator secondaries. The steam blowdown is discharged into the quench and deluge tanks. A sufficient amount of steam blowdown from two steam generator secondaries is provided for decay heat transfer and for RCS cooldown at the design rate of 100F/hr.

Whenever the RCS is depressurized below the pressure in the two generator secondaries, that were not used for steam blowdown, the PCS refill system flow initiates. Steam from the two generators, retained at elevated pressure and temperature, flowing through injectors entrains borated water from refill tanks and maintains the required coolant inventory in the RCS, while the other generators continue cooldown with steam blowdown to the PCS deluge and quench tanks. Also, a portion of the steam flow from these generator secondaries is directed through injectors that provide emergency feedwater from the quench tanks into the secondaries for continued steam blowdown. Sufficient heat sink capacity is provided in the Depressurizer System and the refill, deluge and quench tanks for cooldown to cold shutdown.

APPLICATION IN PWR

For this application the total RCS volume in the four-loop PWR is set at 12000 cu. ft. which includes the 1800 cu. ft. in the pressurizer. Each vessel in this Depressurizer System contains 1600 cubic feet of borated water. The liquid in each vessel is maintained slightly above 2300 psia and about 120F during reactor operation. The interconnecting piping is sized for the range of small pipe breaks such that the borated water in vessel-1 can be displaced by the steam from the pressurizer in about 30 minutes and from vessel-2 in about the next 30 minutes.

Calculations are made for the maximum pipe break size wherein the volume of liquid within the RCS can always be retained within the pressurizer normal operating range throughout RCS depressurization below 1000 psia. Pipe breaks at or above this maximum small break size depressurize the RCS rapidly enough for the refill system to be effective for the complete spectrum of LOCAs.

On a loss of all AC power for an extended period of time (station blackout), the

reactor scrams and power is lost to the RCS pump motors and to the pressurizer heaters. DC power from batteries is used to actuate the controls and instrumentation.

In the PCS these controls actuate the PORVs at the steam generator secondaries. The PORVs in two of the secondaries are sized to provide a predetermined rate of steam blowdown into the quench and deluge tanks for the transfer of decay heat, as well as for a 100F/hr cooldown of the RCS. The emergency feedwater flow rate provided by the injectors is also predetermined.

Select valves in the Depressurizer System are also programmed to open to compensate for the RCS liquid volume shrinkage resulting from the 100F/hr RCS cooldown rate. The makeup from the depressurizer vessels is routed to the pressurizer surge line.

The driving force for the makeup is the static head of water in the depressurizer vessels under the force of gravity. Steam flow from the pressurizer is routed into the depressurizer vessels to reduce the steam pressure in the pressurizer to a saturated condition corresponding to the RCS hotleg temperature. Cooldown of the RCS produced by the makeup is factored into the steam blowdown rate from the steam generator secondaries.

In the following, various malfunctions in plant operation are considered to show the benefits of the Depressurizer System in conjunction with the other PCS innovative features that provide for RCS cooldown and decay heat removal at the rate of 100F/hr.

- Case I - Station blackout with RCS cooldown via secondary system and no makeup coolant to the RCS; and,
- Case II - Station blackout with RCS cooldown via secondary system and makeup coolant to the RCS via the Depressurizer System; and,
- Case III - Station blackout in conjunction with a small break LOCA; RCS cooldown via secondary system and makeup coolant to the RCS via the Depressurizer System.

The analyses made for the above cases are in accordance with the basic laws of thermodynamics. For each case, in the event of a station blackout, the RCS is cooled down at 100F/hr by transferring heat from the RCS to the quench and deluge tanks via two selected steam generator secondaries. The energy transferred includes the decay heat from the reactor.

Case I

Assuming no makeup is available, in this Case, the shrinkage of the RCS liquid volume (resulting from RCS cooldown through two steam generator secondaries) is determined on the basis of trial and error. The specific volume of the liquid and steam at a saturated condition is used to determine the mass of liquid and steam that is contained within the 12000 cu. ft. RCS for 25F intervals of temperature as shown in Table 1, Condition A.

Although this Case assumes no coolant makeup it should be pointed out that the Depressurizer System for Case I would be effective immediately in an adverse event such as the postulated station blackout. As the pressure in the RCS approaches 1000

TABLE 1
REACTOR COOLANT SYSTEM COOLDOWN

Temperature F	Pressure psia	COOLDOWN AT:				
		A-CONSTANT MASS		Stored Energy 10 ⁶ Btu	B-CONSTANT LIQUID VOLUME	
		Volume - cu. ft. Liquid	Steam		Stored Mass lb	Stored Energy 10 ⁶ Btu
600	2250	11,280	720	303.1	484,813	303.1
575	1276	10,882	1118	284.2	501,252	293.1
550	1046	10,491	1509	268.6	519,130	286.2
544.6	1000	10,394	1606	265.3	523,838	285.2
525	848	10,106	1894	253.6	538,491	279.9
500	681	9,824	2176	238.8	554,008	271.0
475	540	9,593	2407	237.4	567,673	261.0
450	423	9,359	2641	210.4	581,201	250.5
425	326	9,272	2728	196.6	593,566	239.2
400	247	9,007	2993	183.1	605,536	226.6
375	184	8,849	3151	169.8	616,684	214.9
350	135	8,705	3295	156.8	627,230	201.9

psia (544.6F) the refill system would start to be effective in providing makeup to the RCS by utilizing the steam in the other two steam generators (not used for RCS cooldown) as the motive force for the injectors in the Refill System. It is noted that at the 1000 psia RCS pressure, when the Refill System becomes effective, the steam bubble has not expanded beyond the pressurizer.

In Table 1, Condition A, at 525F (848 psia) the steam bubble volume of 1894 cu. ft. has expanded beyond the pressurizer. At 400F (247 psia) the steam bubble (volume 2993 cu. ft.) is expanding into the RCS piping and decay heat transfer via natural circulation is starting to break down. Heat transfer reverts to a reflux condenser mode.

Case II

In this Case, makeup for RCS liquid shrinkage resulting from the RCS cooldown through the two steam generator secondaries is provided from the Depressurizer System which is maintained at about 2300 psia and 120F during reactor operation.

The makeup rate for the 100F/hr cooldown is determined by comparing the RCS mass at 500F to that at 600F in Table 1, Condition B. The mass increase is (554,008 minus 484,813) or 69,195 pounds in the first hour. The average specific volume of the makeup from the depressurizer tanks is taken at 0.1653 ft³/lb; which gives 1144 cu. ft. makeup volume in the first hour or about 143 gpm. It can be conservatively assumed that a makeup rate of 150 gpm provides sufficient liquid mass to compensate for the 100F/hr cooldown as the rate of coolant shrinkage decreases with temperature at temperatures below 500F as can be determined from Table 1, Condition B.

At the 100F/hr cooldown rate, the RCS pressure has decreased to the 1000 psia range in about 34 minutes. During this time interval a choice can be made as to the source of makeup - that is, continued makeup from the depressurizer vessels or alternatively from the Refill System.

However, it needs to be pointed out that the Depressurizer System contains over 198,000 lb. of makeup. This is more than adequate for cooldown to the 350F range. As given in Table 1, Condition B, (627,230 minus 484,813) or 142,417 lb. of makeup is required to maintain the pressurizer liquid level at the normal operating range. Decay heat transfer from the RCS to the quench and deluge tanks via the steam generator secondaries can continue for a number of hours before the restoration of AC power.

Case III

Although the nuclear industry does not postulate a station blackout in conjunction with a small break LOCA, the PCS utilizing the Depressurizer System provides cold shutdown safely even for this consideration. This derives from the fact that the PCS safety features do not require AC power for cold shutdown; rather, this is accomplished with redundant DC power supplies from storage batteries.

For Case III (as with Cases I and II) the PCS is cooled down at 100F/hr by transferring the stored energy as well as the decay heat from the RCS to the quench and deluge tanks via steam blowdown from two steam generator secondaries. The PORVs are specifically sized to accommodate this function on the loss of load, turbine trip, or station blackout.

The reduction in the PCS pressure to 1000 psia at the maximum design cooldown rate (100F/hr) is especially desirable for a small break LOCA. By providing an assured rate of cooldown, in an adverse incident, an upper limit is set on the amount of energy that needs to be rejected from the RCS before the refill system is operational. On reaching the 1000 psia range (within 34 minutes at the 100F cooldown rate) the PCS Refill System becomes operational. The two steam generator secondaries - not used for the transfer of heat during RCS cooldown - provide steam as the driving force for the jet injectors that pump makeup from the refill tanks into the RCS.

A LOCA resulting from a steam generator tube (or multiple-tube) failure results in the actuation of the Refill System at a higher steam generator pressure within a shorter time period than other types of LOCAs of the same break size. Tube failures in more than one steam generator results in Refill System actuation at a higher pressure from more than one steam generator. Sufficient heat sink capacity is provided for a steam generator tube failure concurrent with a LOCA or a main steam line break inside or outside the PRC.

Calculations have been made to approximate the maximum small break leak rate that the Depressurizer System can overcome. During RCS depressurization about 150 gpm is required to maintain the liquid level in the pressurizer that results from shrinkage. This leaves about 250 gpm for the small break leak rate. The enthalpy difference between the break flow and the makeup is 490 Btu/lb. From Table 1, Condition B, about (303.1 - 285.2) or 17.9 million Btu reduction in the stored energy depressurizes the RCS from 2250 psia/600F to 1000 psia/544.6F. On the basis of the 250 gpm makeup for leakage alone (neglecting the cooling effect of the 150 gpm makeup for shrinkage) the desired reduction in pressure takes place within 18 minutes. This enables the Refill System to actuate and maintain effective emergency core cooling and decay heat removal for the term of the adverse event.

From the preceding it can be conservatively stated that the Depressurizer System overcomes small break leak rates up to 250 gpm. Pipe break leak rates in

excess of 250 gpm result in a more rapid depressurization and actuation of the Refill System.

With the Refill System operational in the small break LOCA, the steam in the two steam generator secondaries, retained at elevated temperature and pressure, provide the motive force for continued makeup to the RCS. Steam flow through the injectors entrains borated water from the refill tanks to maintain adequate liquid inventory in the RCS. Continued steam blowdown from the other two steam generator secondaries transfer the decay heat from the RCS to the quench and deluge tanks. Emergency feed-water is provided for continued steam blowdown utilizing a portion of the steam blowdown flow through injectors that entrain water from the quench tanks for injection back into the steam generator secondaries.

The leakage from the RCS is contained within the PRC. An increase in the PRC pressure greater than 2 psia results in the venting of steam into the quench and deluge tanks. As stated previously, the heat sink capacity of the refill, deluge and quench tanks provides for at least four hours of decay heat removal without the transfer of heat outside the PRC.

SUMMARY

From the preceding it can be stated that the Depressurizer System used in conjunction with the balance of the basic PCS provides RCS cooldown to cold shutdown for the complete spectrum of LOCAs. The Depressurizer System maintains a sufficient volume of liquid within the RCS to retain the steam bubble within the pressurizer for small breaks with a 250 gpm leak rate until the Refill System is operational enabling continued rapid RCS cooldown to cold shutdown. Taking into consideration the added 150 gpm required to makeup for the liquid shrinkage during the RCS cooldown at 100F/hr, the total makeup rate from the Depressurizer System into the RCS is 400 gpm.

For breaks with leakage rates greater than 250 gpm, the energy release through the break results in the rapid cooldown of the RCS to the 1000 psia/544.6F range. The Refill System thus becomes operational to enable timely RCS cooldown to cold shutdown.

REFERENCES

1. F. W. Kleimola, N. A. Rautiola and O. B. Falls, Jr., The Passive Containment System, International Conference on World Nuclear Power, Washington, D. C. (Nov. 14-19, 1976).
2. F. W. Kleimola and O. B. Falls, Jr., The Passive Containment System in High Earthquake Motion, Proc. American Nuclear Society Topical Meeting on Thermal Reactor Safety, (1977) p. 3-766.
3. F. W. Kleimola and O. B. Falls, Jr., Passive Containment System for Boiling Water Reactors, American Nuclear Society Winter Meeting, San Francisco, California (Nov. 27 - Dec. 2, 1977).
4. O. B. Falls, Jr., Plant Surveillance with the Passive Containment System, Proc. American Power Conference, (1978), p. 121.
5. F. W. Kleimola and O. B. Falls, Jr., Recommissioning an Alternate to Decommissioning, American Nuclear Society Winter Meeting, Washington, D. C. (Nov. 12-16, 1978).
6. O. B. Falls, Jr., and F. W. Kleimola, Passive Containment System - A New Concept to Solve Safety Concerns, Proc. American Power Conference, (1979), p. 112.

UTILIZATION OF THE SAFETY FUNCTIONAL ANALYSIS TECHNIQUES
TO OPTIMIZE THE SEPARATION REQUIREMENTS IN CASE OF FIRE

Luis Martín Alvarez

Empresarios Agrupados
Magallanes, 3, Madrid - 15, Spain

ABSTRACT

The present philosophy for the fire protection of the safe shutdown capability in nuclear power plants is based on the separation of the safety-related systems in different fire areas in such a way that the redundant systems are not subject to damage from a single fire risk.

For projects of nuclear power plants in which the design of the buildings and the general arrangement were conceived before these new separation requirements, their fulfilment represents, in many cases, a considerable impact on the project. For this reason, it is advisable to perform an analysis which permits establishing the minimum redundant divisions or groups of divisions which, in truth, should be separated so as not to be affected by a single fire.

The purpose of this Paper is to show the experience gained in the application of a systematic method of analysis to minimize the number of fire barriers being compatible with the regulatory requirements and with the capability of achieving and maintaining the safe plant shutdown in the event of a fire.

As a conclusion of the analysis, the separation criteria for the divisions involved in the safe plant shutdown are obtained.

1. INTRODUCTION

The systematic method of analysis described in this Paper has been applied to the Valdecaballeros Nuclear Power Plant project to determine the necessary fire barriers to meet the separation requirements of redundant divisions according to Appendix A to Branch Technical Position ASB 9.5-1, that is, the redundant divisions should be separated by means of 3-hour rating fire barriers.

The Valdecaballeros Nuclear Power Plant is a 975 Mwe, BWR/6-type plant with Mark III Containment, located in the South-West of Spain and presently under construction. This plant is owned by Compañía Sevillana de Electricidad, S.A. and Hidroeléctrica Española, S.A.

2. THE NEED FOR A SYSTEMATIC ANALYSIS

The Valdecaballeros Nuclear Power Plant is provided with three electrical supply divisions and four instrumentation and control divisions. In general, the four instrumentation and control divisions, individually or combined in a certain manner, form the logics and generate the signals for the reactor SCRAM, NSSS isolation, initiation of the ECCS systems, etc. These four instrumentation and control divisions are supplied from electrical divisions 1 and 2.

Electrical division 3 presents certain peculiarities. This division is needed only for the operation of the High Pressure Core Spray System and its auxiliaries. In this case, the system initiation logic (belonging to instrumentation and control divisions 3 and 4) and the system operational logic (belonging to instrumentation and control division 3) are supplied from electrical division 3.

In a first attempt to obtain a suitable separation of divisions which would permit safe shutdown in case of fire, a separation of the four divisions by means of fire barriers was contemplated. The large number of barriers resulting therefrom represented a significant impact on the project (interference with pipe and cable tray runs, HVAC calculations, obstruction of envisaged through-zones, etc.).

In view of the above situation, it was considered necessary to perform a systematic analysis that would permit clearly establishing if some divisions could be grouped together in any given combination and, if so, to establish the separation criteria for the groups of divisions to guarantee the safe shutdown capability for any postulated fire. In this way, separating groups of divisions, the number of necessary fire barriers could be considerably reduced.

Although in this Paper only the separation by means of fire barriers is considered, the method of analysis is also valid if any other method of separation is applied:

- Horizontal distance of more than 20 feet with no intervening combustible or fire hazards, or
- Enclosing one redundant division in a fire barrier having a 1-hour rating.

To carry out this study, it was considered that the Safety Functional Analysis techniques could be adequate.

3. SAFETY FUNCTIONAL ANALYSIS

The Safety Functional Analysis is a systematic method of analysis at the systems level which, for a postulated event, enables verifying that the adequate protection sequences exist to perform all the required safety functions necessary to achieve and maintain the safe plant shutdown even if the worst single failure does occur.

For each analyzed event, the Safety Functional Analysis takes into account the following elements of analysis:

- Required safety functions to achieve and maintain the plant in a safe shutdown condition

- The necessary safety systems to perform the above safety functions
- Functional relationship between safety systems
- The operational sequences of the safety systems to perform the safety functions, and
- The back-up systems required for the operation of the main safety systems.

Once the relationship existing between the above-mentioned elements of analysis is established, it is possible to perform a failure analysis at the systems level to verify that all the safety functions can be accomplished assuming any single failure.

In applying this method of analysis to a fire event, it should be noted that, according to BTP ASB 9.5-1, fires need not be postulated to be concurrent with non-fire-related failures in safety systems.

4. METHOD OF ANALYSIS

The method of analysis to establish the redundant divisions separation criteria in fire areas is developed in the following phases:

4.1 Definition of Criteria

Those criteria that are considered as being necessary for the development of the analysis are taken from the applicable fire protection documents (BTP ASB 9.5-1, Appendix R to 10 CFR Part 50, etc.).

Criteria related to the following aspects should be taken into account:

- Single failure assumptions in safety systems
- Concurrence of fire and plant accidents
- Concurrence of fire and natural phenomena
- Offsite power availability, and
- Protection of equipment necessary for mitigation of consequences following design basis accidents.

4.2 Conditions to be Achieved and Maintained

Conditions to which the plant should be brought in case of fire (hot shutdown or cold shutdown) are taken from the applicable fire protection documents.

The final objective for the Valdecaballeros Nuclear Power Plant was the separation of the safety-related divisions in such a way that at least one train necessary to achieve and maintain the cold shutdown conditions remained free of fire damage for any postulated single fire event.

4.3 Necessary Safety Functions in Case of Fire

Those safety functions that must be performed in order to achieve and maintain the cold shutdown conditions are determined in this phase. For this purpose, the following safety functions have been considered:

- | | |
|--------------------------------------|-------------------------------------|
| 1. Reactivity Control | 5. Reactor Coolant Heat Removal |
| 2. Reactor Coolant Inventory Control | 6. Maintenance of Vital Auxiliaries |
| 3. Reactor Pressure Control | 7. Shutdown Variables Monitoring |
| 4. Reactor Core Heat Removal | |

4.4 Necessary Safety Systems to Perform the Safety Functions

Those safety systems that could be utilized to carry out each of the safety functions that have been identified as being necessary to achieve and maintain the cold shutdown conditions are determined in this phase.

In general, for plants of the BWR/6 type, the safety systems that could be utilized to carry out the above-mentioned safety functions are as follows:

<u>Safety Function</u>	<u>Safety System</u>
Reactivity Control	Reactor Protection System Control Rod Drive System (Hydraulic Control Units) Standby Liquid Control System Recirculation Pump Trip System
Reactor Coolant Inventory Control	High Pressure Core Spray System (HPCS) Low Pressure Core Spray System (LPCS) Low Pressure Coolant Injection System (LPCI) Reactor Core Isolation Cooling System (RCIC) Nuclear Steam Supply Shutoff System (necessary on low reactor water level)
Reactor Pressure Control	Safety/Relief Valves (including manual actuation of ADS valves)
Reactor Core Heat Removal	HPCS, LPCS, LPCI, RCIC, and Safety/Relief Valves
Reactor Coolant Heat Removal	Residual Heat Removal System (operating in the Suppression Pool Cooling Mode and in the Shutdown Cooling Mode)

Maintenance of Vital Auxiliaries	Essential Service Water System
	Essential Chilled Water System
	Essential Compressed Air System
	Essential HVAC Systems
	Emergency AC Power Supply System
	Emergency DC Power Supply System
	Emergency Lighting and Communication System
Shutdown Variables Monitoring	Reactor Vessel Level
	Reactor Vessel Pressure
	Suppression Pool Temperature, etc.

4.5 Identification of Divisions

Once the safety systems involved in the cold shutdown of the plant are obtained, the next step is to determine the division assigned to each piece of equipment and component belonging to these systems as well as the divisions assigned to the instruments and logics related to their initiation and subsequent operation. To this end, the development of tables similar to TABLE I is recommended. These tables contain the necessary information to identify the divisions involved in the operation of each piece of equipment or component.

The information contained in these tables should be as follows:

- System identification
- Equipment or component identification
- Electrical division assigned to each piece of equipment or component
- Actions required from the equipment or component (valves: open, close, control; pumps: start, stop)
- Necessary signals to initiate the actions required from the equipment or component
- Instruments involved in generating and processing the above signals
- Instrumentation and control division assigned to each instrument
- Power supply to the instruments and logics involved in the equipment initiation and operation
- Type of logic (and, or) and mode of actuation (energizing or de-energizing)

From the analysis of all this information, a conclusion can be reached regarding the involved divisions and the manner in which they intervene in the operation of each equipment item or component. Specifically, for the example considered in TABLE I, the conclusion indicated at the bottom of the table may be obtained.

TABLE I

SYSTEM	EQUIPMENT OR COMPONENT	DIV.	ACTIONS	SIGNALS	INSTRU- MENTS	I & C DIV.	POWER SUPPLY TO I & C DIV.	LOGIC
HPCS	VALVE E22-F004	3	OPEN	LOW REACTOR	<u>LEVEL</u>			
				LEVEL 2 AND/OR	B21-N073G	3	125V d.c. (Div.3)	N073G or N073R
				HIGH DRYWELL	B21-N073C	3	125V d.c. (Div.3)	and
				PRESSURE	B21-N073R	4	125V d.c. (Div.3)	N073C or N073L
					B21-N073L	4	125V d.c. (Div.3)	(ENERGIZATION)
								AND/OR
					<u>PRESSURE</u>			
					B21-N067G	3	125V d.c. (Div.3)	N067G or N067R
					B21-N067C	3	125V d.c. (Div.3)	and
					B21-N067R	4	125V d.c. (Div.3)	N067C or N067L
					B21-N067L	4	125V d.c. (Div.3)	(ENERGIZATION)
			CLOSE	HIGH REACTOR	B21-N073G	3	125V d.c. (Div.3)	N073G or N073C
				LEVEL 8	B21-N073C	3	125V d.c. (Div.3)	(ENERGIZATION)
			PERMIS- SIVE TO CLOSE	HIGH DRYWELL	B21-N067G	3	125V d.c. (Div.3)	N073G or N073R
				PRESSURE NOT	B21-N067C	3	125V d.c. (Div.3)	and
				PRESENT	B21-N067R	4	125V d.c. (Div.3)	N073C or N073L
					B21-N067L	4	125V d.c. (Div.3)	(ENERGIZATION)

CONCLUSION

DIVISION 3 IS NEEDED TO OPERATE VALVE E22-F004.

ANY FAILURE IN DIVISION 4 DOES NOT PREVENT VALVE OPERATION.

In analyzing the information contained in these tables, the worst effect is considered to occur as a consequence of the fire without taking into account its probability of occurrence. To this end, the most unfavourable of the following effects is assumed: hot shorts, shorts to ground, openings of circuits that should function on being energized, and the possibility that circuits that should function on being de-energized will become energized by other cables due to loss of isolating material.

Given the great number of equipment items and components involved in the cold shutdown of the plant, the development of this type of table for each of said equipment items or components could become extremely painstaking and this is really quite unnecessary in many cases. For example, many of the safety-related BOP systems are designed as two redundant trains, each train being assigned to a different division. Likewise, it can be said that there are some NSSS systems that are assigned to only one division (e.g. LPCS). For all these cases, the tables can be developed at a system level indicating only the division to which the system (or each of the trains) has been assigned. For the remaining systems, the tables are developed as indicated in TABLE I.

4.6 Development of Shutdown Logic Diagrams

All the information obtained from 4.2, 4.3, 4.4 and 4.5 above is grouped in the Shutdown Logic Diagrams. One diagram is developed for each of the safety functions considered to be necessary in case of fire.

Each Shutdown Logic Diagram includes all the safety systems that can be aligned in different sequences to perform the corresponding safety function. They also include all the divisions involved in the initiation and operation of each of the safety systems included in the diagram.

Figure 1 shows a simplified Shutdown Logic Diagram which corresponds to the safety functions: Reactor Core Heat Removal and Reactor Coolant Heat Removal (due to the close relationship existing between these two safety functions, they have been grouped in a single diagram).

This diagram includes all the modes of operation that permit performing the Reactor Core and Coolant Heat Removal function using only safety systems:

a. From power operating conditions to RHR operating conditions:

- Mode 1: Level control with the RCIC system and depressurization by means of manual actuation of the ADS valves
- Mode 2: Level control with the RCIC system and depressurization by means of reactor steam condensation in the RHR heat exchangers
- Mode 3: Level control with the HPCS system and depressurization by means of manual actuation of the ADS valves.
- Modes 4,5,6,7 Depressurization by means of manual actuation of the ADS valves and level control with a low pressure system (LPCS, LPCI-A, LPCI-B or LPCI-C).

The suppression pool cooling by means of RHR-A or RHR-B is necessary in all the above operating modes.

b. From RHR operating conditions to cold shutdown conditions

To reach cold shutdown conditions, the RHR may be used in the shutdown cooling mode (suction from the recirculation loop) or in the alternative shutdown mode (discharge to the suppression pool through the ADS valves and suppression pool cooling by means of the RHR system).

It has to be pointed out that this diagram only represents the primary systems necessary to perform the safety function indicated in the diagram. The analysis of the back-up systems needed for the primary systems operation is carried out in the Shutdown Logic Diagram corresponding to the Maintenance of Vital Auxiliaries safety function.

4.7 Shutdown Logic Diagram Analysis

Once the Shutdown Logic Diagrams are obtained for all the safety functions, the next step is to analyze the consequences that the loss of one or more divisions could have on the performance of each of the safety functions.

The object of this analysis is to identify those divisions or groups of divisions that must be separated so that at least one operating mode to perform the analyzed safety function remains available for any postulated fire event. A separation requirement is established for those divisions or groups of divisions that, if lost together, could disable the capability of performing the safety function by means of all the operating modes shown in its corresponding Shutdown Logic Diagram.

For the safety function analyzed in the diagram shown in Figure 1, the only unacceptable situation could arise if divisions 1 and 2 (equipment, cables, instruments, etc.) were located in the same fire areas. In this case, all the operating modes to achieve the cold shutdown could be lost. However, there are no separation requirements for divisions 3 and 4 to perform this safety function because, as may be seen in the diagram, other operating modes remain available even in the event that both divisions 3 and 4 are damaged simultaneously with division 1 or division 2. The worst case would arise if divisions 2 and 3 were located in the same fire areas and both were damaged. Nevertheless, even in this case, the safety function could be carried out by means of the operating mode indicated by a thick line in Figure 1.

The conclusion resulting from the analysis of this Shutdown Logic Diagram is that division 1 and division 2 must be separated in such a way that both divisions do not become damaged by a single fire.

5. CONCLUSIONS

All the Shutdown Logic Diagrams are analyzed in the way described above to obtain the separation criterion that requires a minimum of fire barriers and permits carrying out all the safety functions for any postulated fire event.

In applying this method of analysis to the Valdecaballeros Nuclear Power Plant, the following separation criterion was obtained:

- Divisions 1 and 4 could be located in the same fire areas

- Divisions 2 and 3 could be located in the same fire areas, and
- The group of divisions 1 and 4 must be located in fire areas different from those containing the group of divisions 2 and 3.

In this way, for a plant area containing the four divisions (e.g. a cable run area), the redundant divisions separation criteria are met by means of a single fire barrier separating the group of divisions 1 and 4 from the group of divisions 2 and 3.

It should be noted that, by using the method of analysis described in this Paper, a general criterion is obtained to meet the fire protection separation requirements; however, this criterion could be made more flexible, if required, for certain plant areas in which, because of the specific function of the equipment, cables, etc. existing therein, another different separation criterion could be acceptable. For example, divisions 1 and 3 could be located in the same fire area if they are used only for the operation of the ECCS systems, but this situation might not be acceptable if these divisions were involved in the reactor SCRAM function.

The method of analysis described in this Paper is also valid to identify all the possible exceptions to the general criterion that could be acceptable if the considered divisions were involved only in certain specific functions.

SHUTDOWN LOGIC DIAGRAM
SAFETY FUNCTION : REACTOR CORE HEAT REMOVAL AND COOLANT HEAT REMOVAL

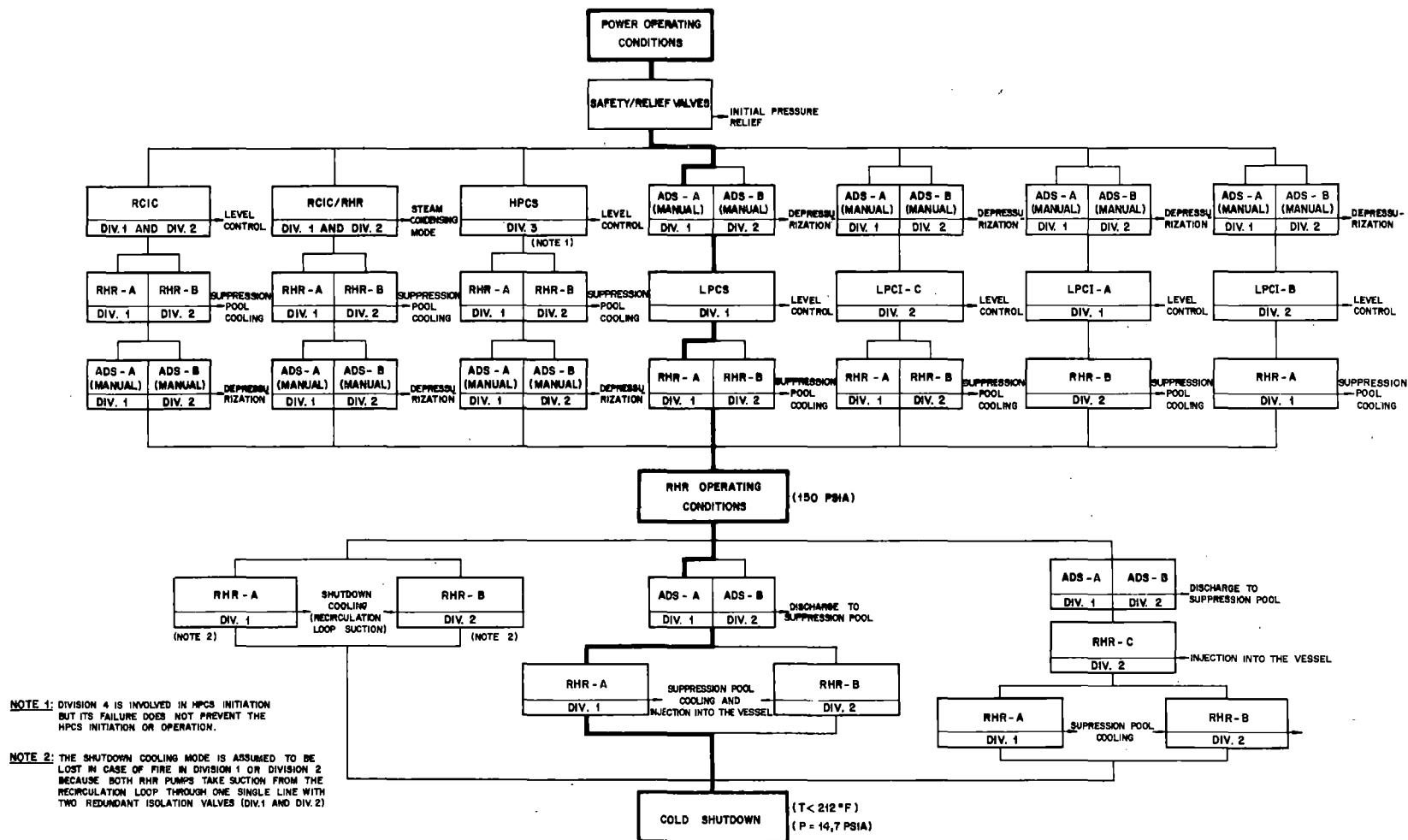


FIGURE 1

DESIGN CONSIDERATIONS FOR IMPLEMENTING A VENT-FILTER SYSTEM AT THE BARSEBACK NUCLEAR POWER PLANT

K. Johansson

Studsvik Energiteknik AB, S-611 82 Nyköping, Sweden

L. Nilsson

AB Asea-Atom, Box 53, S-721 04 Västerås, Sweden

Å. Persson

Sydskraft AB, S-217 01 Malmö, Sweden

INTRODUCTION

Equipment for filtered atmospheric venting of the reactor containments will be installed at the Barseback twin BWR Nuclear Power Plant.

A brief description of the vent-filter plant is given with an account of the design considerations guiding its implementation.

DESIGN GUIDELINES

According to a decision of Oct 15, 1981 by the Swedish government, equipment for filtered atmospheric venting of the reactor containments shall be installed at the Barseback Nuclear Power Plant and brought into operation before Sept 1, 1986.

The objectives of the vent-filter plant are to relieve excessive pressures from the containment and to reduce releases of those radioactive substances which could cause long term land contamination as a result of a containment overpressurization accident. Noble gases and methyl iodide will be vented together with the non-condensable gases through the filter plant via the stack to the atmosphere.

The equipment shall be designed so that 99.9 % of the core inventory of radioactivity, excluding inert gases, is retained in the reactor containment and filter system in the event of containment venting.

Another design guideline is to achieve passive functioning of the vent-filter plant during the first 24 hours into an accident.

SYSTEM DESCRIPTION

A joint research project named FILTRA [1, 2], sponsored by the three Swedish nuclear utilities and the Swedish Nuclear Inspectorate, has provided the information needed in support of the filter plant design. Main contractors for the FILTRA project have been Studsvik Energiteknik AB and AB Asea-Atom.

The vent-filter plant will be common to the two Boiling Water Reactors on the site. The reactors are of the ASEA-ATOM design with pressure suppression containments of the over-under type, with the reactor located centrally over the condensation pool (Mark II type).

The filter plant consists of a cylindrical vessel of 10 000 m³ volume, 20 m diameter, and 40 m height. The vessel is a cylindrical reinforced concrete structure built above ground. The vessel is filled with 1 inch size crushed quartzite rock gravel.

The gravel bed filter serves three purposes. It provides:

- a heat sink for condensation of the steam from the containment
- an expansion volume for reduction of the gas pressure in the containment
- a filtering medium for removal of the aerosols and iodine in the steam and gases from the containment.

The FILTRA plant layout includes one vent pipe from each of the two Barseback containments. The two pipes join into one common pipe, which is connected to the gravel bed at the top of the bed, see Fig. 1. All pipes are located in underground culverts. The filter vessel is placed above ground. The inflowing steam to the filter is distributed in the top layer and condenses in the gravel bed. The condensate is collected in the lower part of the gravel condenser. On the downstream side of the filter plant an off gas pipe, also located in the culvert, returns to the stack of one of the reactor units.

The vent pipes are connected to the wetwell gas volume. Outside the containment each pipe includes a rupture disc of 600 mm diameter followed by a shut-off valve. The valve is normally locked in the open position.

The vent pipes to the filter vessel have an equivalent area of 0.1 m².

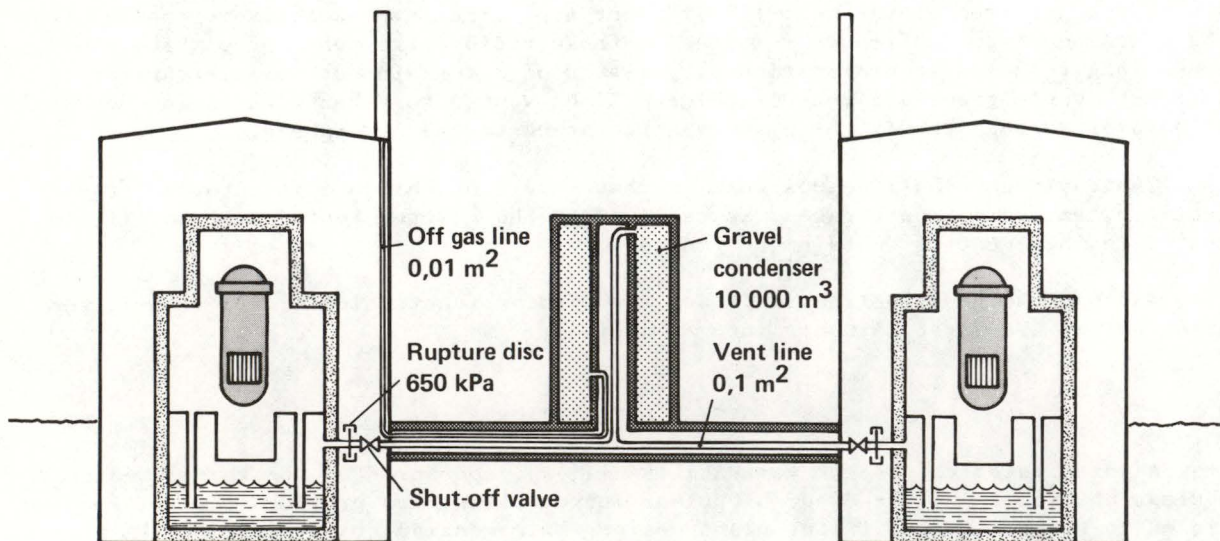


Figure 1 FILTRA Vent filter plant arrangement

In order to increase the residence time in the gravel condenser, the outlet line includes a flow restriction of approximately 0.01 m^2 area. The gas velocity through the condenser is very low, less than $2 - 3 \text{ cm/sec}$, resulting in a long residence time, 10 - 20 minutes.

The Barseback reactor containments were designed to withstand a pressure of 0.5 MPa. Later additional calculations have been made, showing the Barseback containment structures to be capable of responding to an internal pressure of 0.65 MPa in an essentially elastic manner, i.e. remaining leak-tight. Even at higher pressures, up to $0.7 - 0.8 \text{ MPa}$, only minor leakages are to be expected. The burst pressure of the rupture disc is set at 0.65 MPa.

The total amount of condensate that the gravel bed can condense and accommodate is about 500 m^3 . To facilitate the handling of contaminated condensate, the condenser layout includes pits for sumps and pumps. By using an appropriate concrete casting technique, sufficient leak tightness of the condenser vessel walls can be achieved with respect to the contaminated condensate without including a steel liner.

To prevent any hydrogen burn during the initial containment venting phase to the filter the whole filter plant, including vent pipes and gravel filter, is filled with nitrogen during normal standby conditions. After venting when the containment cooling systems are restarted, the filter plant may become partly refilled with a burnable hydrogen-air mixture, as air will be sucked back into the filter and the containment from the outlet stack. The filter plant is designed to withstand hydrogen explosions during this post accident phase.

The reactor containment is normally inerted with nitrogen to prevent any hydrogen burn prior to containment venting. Additional containment inerting capacity is available on manual initiation to prevent burnable hydrogen-air mixtures from building up in the containment following restart of the containment cooling systems after containment venting.

Hydrogen burn experiments in gravel beds have been performed, showing that the pressure caused by hydrogen explosions inside the gravel condenser will be about 0.3 MPa. In the other parts of the filter system the pressure will be about 1 MPa.

EXPERIMENTAL RESULTS

The basic requirements on the capabilities of the FILTRA system for filtered atmospheric venting of a reactor containment are:

- flow capacity for pressure relief
- heat capacity for steam condensation
- retention capacity for radioactive particles and iodine.

Large scale experiments in gravel beds have been performed in order to provide a set of experimental data for evaluating these capacities in a particular design e.g. a $10\,000 \text{ m}^3$ bed of 1 inch size crushed rock gravel.

Condensation of steam in a gravel bed

When steam and gases flow downwards into a gravel column, steam will condense on the initially cold pebble surfaces and the gases will flow downwards together with some of the condensate. The pebbles will heat up to 100°C in the upper part of the column. Below this hot zone a condensation front will move slowly downwards.

Some hundred experimental runs have been made in a fully instrumented gravel column of diameter 1 m and 30 m height in order to study the transfer of mass and heat under conditions bracketing those expected in the full scale FILTRA system.

No effects of condensate blockage were observed in the experiments, even during the initially high mass flow rates characterising a containment depressurization transient.

The results provide data in support of analytical models that permit extrapolation of the results to the full scale system. These extrapolations show that the pressure drops in the full scale gravel condenser will be small and, apart from the initial venting transient, quite negligible.

Retention of Particles and Iodine in Gravel Beds

Gravel, sand or water were held as the natural choices for filter media at the start of the FILTRA project.

Because of the potential dynamic problems with water pool scrubbers, design solutions were finally sought by applying gravel beds for the condenser and filter functions.

In a gravel bed the grain size, bed depth, gas velocity, residence time and steam fraction are the important variables that influence the retention of particles and iodine. The influence of these variables has been studied in a series of experiments. The experiments have been made with sand columns of diameter 5 cm and 1.5 m height in the laboratory scale, and with gravel columns of diameter 0.5 m and 7.5 m height in the intermediate scale.

For practical reasons concerning measurement techniques the experiments have for some tests been made at higher gas velocities and shorter residence times than would be the case in the full scale FILTRA system.

Analytical models have been developed in order to extrapolate the experimental results to a full scale system. These models are found to reproduce the experimental observations with acceptable accuracy.

Hydrogen Burns in a Gravel Bed

A flammable mixture of air and hydrogen could form in the gravel bed, if air is sucked back into the bed when the containment cooling systems are restarted at the end of an accident sequence.

Experiments have been made by exploding hydrogen air mixtures in a shock tube of diameter 0.25 m and 5 m length, partly filled with gravel.

The results show pressure pulses of 2 MPa amplitude of a short duration, less than a millisecond. The resultant impulse is not significant in impacting the concrete vessel wall of the gravel bed. The pressure pulses were followed by a quasi static pressure of 0.1 - 0.3 MPa depending on hydrogen-air mixture, gravel size etc.

ANALYTICAL RESULTS

Reference Accident Sequences

Two reference accident sequences have been chosen for detailed analysis in order to provide consistent sets of data for two core-melt accident sequences. The data can be used for assessing their possible impact on containment integrity, containment pressurization rates, vent size requirements, aerosol or fission product liberation, transport, retention and release.

These reference accident sequences are:

TB = transient (T) and loss of AC power for more than 24 hours (B).

ADB = pipe break (A), incomplete steam condensation (D) and loss of AC power for more than 24 hours (B).

The first sequence was chosen to represent a typical containment overpressurization event due to loss of heat sink. It represents a core melt sequence with modest filtering requirements.

The second sequence represents the toughest challenge to the FILTRA system in respect of both venting and filtering requirements. It has therefore been chosen as the design case for these functions.

Vent Requirements

In the TB case the pressure inside the containment will slowly rise and reach 0.65 MPa after about 13 hours. The rupture disc will open at 0.65 MPa and the containment will be vented to the filter systems.

In the ADB case the containment pressure will rise quickly because of the initial pipe break and the postulated drywell - wetwell leakage of 0.3 m² area, through which part of the steam will escape condensation in the pool at the bottom of the containment. A vent capacity equivalent to 0.1 m² area is sufficient to limit the pressure rise below 0.75 MPa in this case.

Core melt progression

The following description of the core melt progression in the reactor and in the containment is given as a result of the best estimate evaluations made. It is based on our present understanding of the art of core melt analysis.

According to the analysis made, the heat and gas evolution from a core melt accident will not cause overpressurization or excessive leakage of the containment at Barseback as long as the containment residual heat removal function remains available.

In the TB case the core will be uncovered when the automatic depressurization of the reactor pressure vessel starts automatically at low reactor water level. In the ADB case the core is uncovered as a result of the postulated pipe break. The uncovered core will heat up and a pool of melt will form in the core. After some time the pool will flow down to the lower plenum of the reactor pressure vessel. In a few minutes it will melt through the reactor vessel at one or more of the penetrations for e.g. control rods or neutron detectors.

The melt then will flow over the control rod drive mechanisms to the concrete floor of the lower drywell. The melt will be drained into the condensation pool through a 1 foot diameter drain pipe in this floor. The melt can also penetrate a steel door and drain into the pool.

The drain rates will not be very high nor very slow. Therefore the melt film flowing into the pool will break into coolable centimeter size fragments, which will be solidified by the time they reach the bottom of the 6 m deep condensation pool.

A heap of permanently coolable core fragments will form on the pool bottom.

Melt through of the containment base mat is therefore not expected.

Steam explosions if they occur in the reactor pressure vessel or in the condensation pool may damage some components or structures, but are considered not to be strong enough to cause any significant damage to the reactor or containment vessels.

Liberation, Transport and Retention of Radioactive Matter in the containment and the FILTRA plant

FILTRA will be activated in both the reference accident sequences because of loss of heat sink in reference case TB, and because of postulated incomplete steam condensation in reference case ADB.

In both cases core melt and slump will occur after about 1 hour.

In case TB bursting of the rupture disc will occur after about 13 hours. During this time most of the aerosols and iodine will settle in the containment.

In the ADB case the rupture disc will open early at the pipe break event. When the core melts, less than half of the liberated amount of aerosols and iodine will be transported by steam and hydrogen to the gravel condenser.

In the gravel aerosols will be removed by sedimentation and diffusion and by the condensing steam. Less than 10^{-4} of the mass of particles will penetrate the gravel. This can be compared to the requirement that the total atmospheric release of e.g. particulate radioactivity should be less than 10^{-3} .

Iodine will adsorb and chemisorb on the gravel surfaces and will be completely removed from the gas phase. Only that part of the iodine, which is converted to organic form - estimated at less than 1 % - will penetrate the gravel bed and be vented together with the noble gases via the stack to the atmosphere, see Fig. 2.

Leakage of radioactive condensate water at the low leakage rate expected from the gravel condenser vessel, is considered to be of little significance as a health risk.

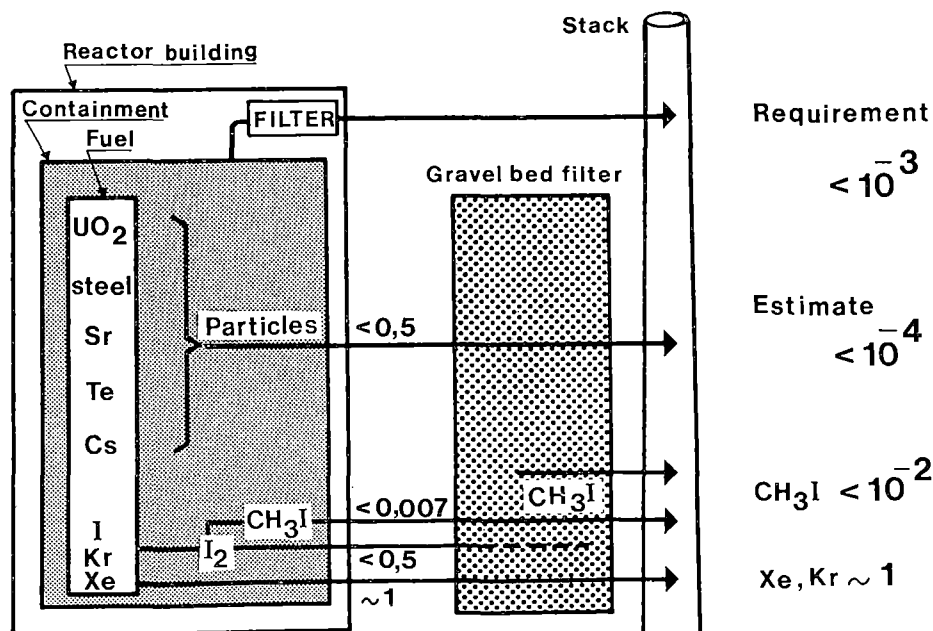


Figure 2 FILTRA Penetration Factors

SAFETY ANALYSIS

Purpose and Method

A safety analysis has been made of the influence of the FILTRA vent filter system on the safety of the Barseback plant.

The main purposes of the analysis have been to:

- study the interaction between FILTRA and the reactor safety systems and their functions during Design Basis Accidents.
- evaluate on a qualitative basis, by the use of event trees, those transients and LOCAs that will contribute dominantly to the probability of containment overpressurization or severe core damage or both.

Results

The following conclusions can be drawn from the safety analysis performed:

The FILTRA system has no significant negative impact on the intended functions of the reactor's safety systems within their current design bases.

The accident sequences can be divided into four groups with respect to their impact on the containment and the core, see Fig. 3.

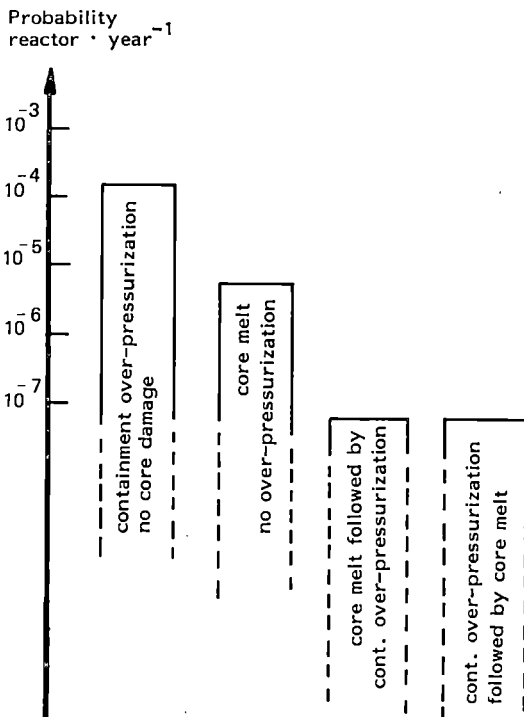


Figure 3 FILTRA Safety Analysis
Event sequences grouped according to containment and core failure modes

Containment overpressurization (group 1) would occur mainly from transients with loss of residual heat removal from the containment (TW). No core damage will occur in this case because the auxiliary feed water system will independently keep the core cooled. Containment overpressurization would occur after about 24 hours. At this point FILTRA's pressure relief function would be needed but not necessarily its filtration function.

Minor contributors to the probability of containment overpressurization would be the pipe break sequences with incomplete steam condensation (AD). Other minor contributors to the probability for containment overpressurization are the transient sequences without reactor shutdown. The latter are considered to be of low probability at Barseback because of the extra function of the electric motor driven screw mechanism that inserts the control rods.

Core melt without containment overpressurization (group 2) would occur mainly from large or medium LOCA sequences with failing emergency core cooling functions. FILTRA is not required because there is no overpressurization.

Core melt followed by containment overpressurization (group 3) would occur mainly from transients and LOCAs with simultaneous loss of both the emergency core cooling and the containment residual heat removal functions. The events in this group are characterized by a slow overpressurization, resulting in modest demands on venting and filtering, see description of the reference sequence TB above.

Containment overpressurization followed by core melt (group 4) would occur mainly from LOCAs with simultaneous impaired pressure suppression and loss of emergency core cooling functions. Events in this group provide the toughest challenge to the FILTRA system. They have been used for defining the requirements on the venting and filtering functions, see description of reference sequence ADB above.

Residual Risks

FILTRA will have little effect on some events comprising the residual risks. In this category there are accidents that could be caused mainly by external events such as earthquakes and airplane crashes and also some internal events e.g. incomplete containment isolation, reactor tank rupture, turbine missiles. At low probabilities the internal events also include some core melt events that could result from LOCAs with excessive leakage between drywell and wetwell and some of the transients without reactor shutdown.

CONCLUSIONS

The FILTRA vent-filter system as applied to the reactor containments at Barseback has no significant negative impact on the reactor safety systems' functions during Design Basis Accidents.

FILTRA protects the reactor containment from failure by overpressurization caused by loss of residual heat removal functions in transients and pipe break events. Events of this type are the dominant contributors to the probability for containment overpressurization.

FILTRA protects the reactor containment from failure by overpressurization in LOCA events combined with impaired containment pressure suppression function equivalent to a leakage of less than 0.3 m² between drywell and wetwell. Events of this type are minor contributors to the probability for containment overpressurization.

According to the best estimate description made in the safety analysis of core melt events, they will not as such cause failure of the containment by overpressurization or excessive leakage.

FILTRA protects the reactor containment from failure by overpressurization and reduces effectively releases of radioactivity in events that could cause both overpressurization and core melting. These events have very low probability ($< 10^{-6}$ per reactor year).

FILTRA will have little effect on some events comprising the residual risks. In this category there are accidents that could be caused mainly by external events such as earthquakes, but also some internal ones, e.g. lack of containment isolation, reactor tank rupture, turbine missiles. At low probabilities the internal events also include the core melt events that could result from pipe breaks with excessive leakage between drywell and wetwell and some of the transients without reactor shutdown.

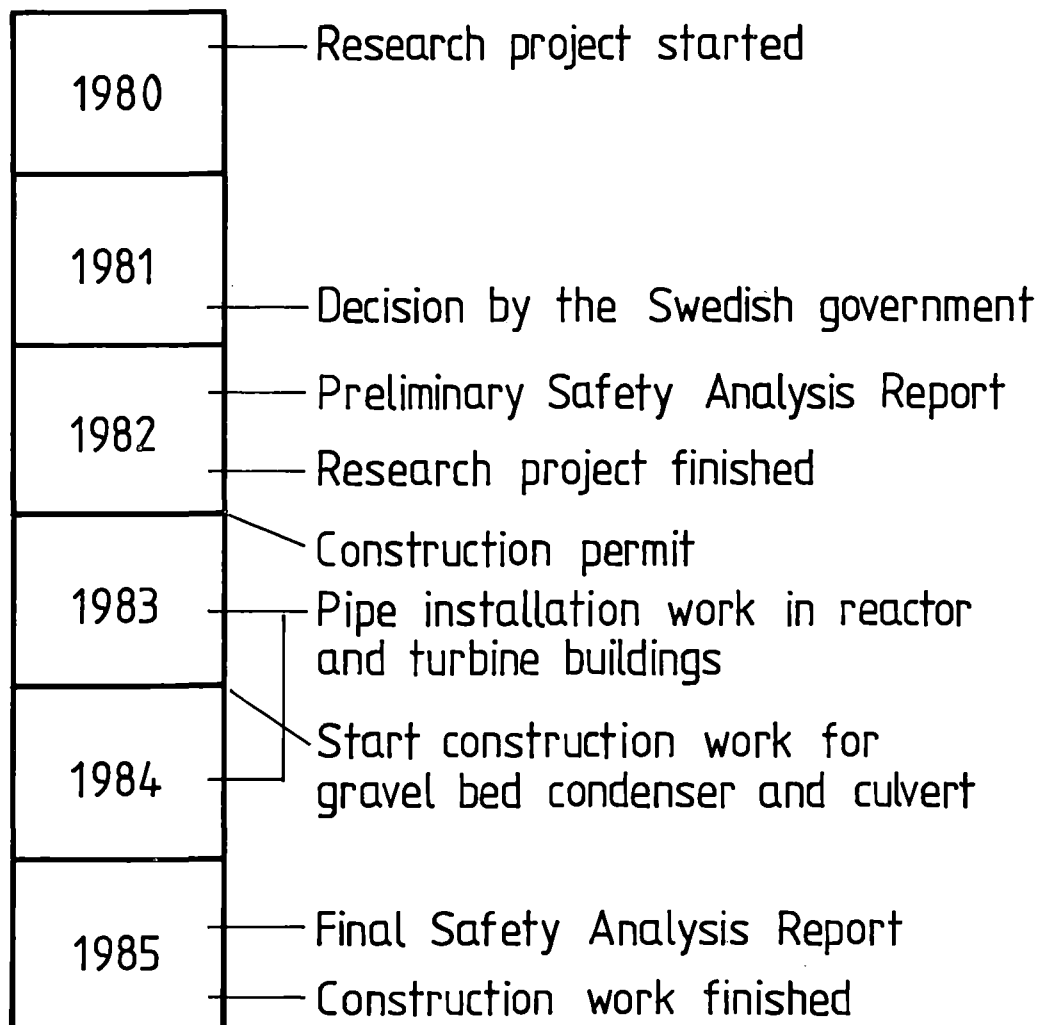


Figure 4 FILTRA Time schedules

LAYOUT, TIME SCHEDULE AND COST

On the Barseback site the rock is about 20 - 30 m below the ground level. Above the rock there is a 2 - 7 m thick layer of sand. The top layer consists of moraine. The first design approach was to site the stone condenser in the rock, but the local sandstone was not suitable for building in. A concrete vessel located partly in the rock and partly in the sand/moraine layers was therefore studied. Due to the sand layer the construction work appeared to be very difficult and expensive. Finally a concrete vessel placed above ground was found to be the most economical container for the gravel condenser. The cost is approximately 40 % lower for the above-ground location compared to the underground one. The condenser vessel will be placed beside one of the turbine buildings.

The FILTRA project work started early in 1980 and will be finished late in 1982.

Review of the Preliminary Safety Analysis Report for FILTRA at Barseback is progressing at present. A construction permit from the authorities will probably be given at the end of 1982.

The construction work for the gravel condenser and the pipe culvert will start in late 1983 and will be finished in late 1985. The pipe installation work in the reactor and turbine buildings will be carried out during the annual shut downs in 1983 and 1984, see Fig. 5.

The cost for the filter plant is estimated at approximately 20 M\$. No interest rate or index adjustment is included in this estimate.

REFERENCES

1. FILTRA final report, 1982.
2. FILTRA safety analysis, 1982.

Both are available from the Studsvik Library, S-611 82 Nyköping, Sweden, telex 64070 stubib s.

ABSTRACT

Equipment for filtered atmospheric venting of the reactor containments will be installed at the Barseback twin BWR nuclear power plant.

The objectives of the vent-filter plant are to relieve excessive pressures from the containment and to reduce releases of those radioactive substances which could cause long term land contamination as a result of a containment overpressurization accident.

Noble gases and methyl iodide will be vented together with the non-condensable gases through the filter plant via the stack to the atmosphere.

A brief description of the vent-filter plant is given with an account of the design considerations guiding its implementation.

DESCRIPTORS

SWEDEN, NUCLEAR REACTOR SAFETY ENGINEERING, CONTAINMENT, PRESSURE RELEASE, CORE MELTDOWN, LOSS OF COOLANT, BWR TYPE REACTORS, FILTERS, VENTS.

SESSION 31

DYNAMIC LOADS/STRUCTURAL ANALYSIS

Chair: T. Kuroda (*EPDC*)
L. Pease (*AECL*)

SEISMIC QUALIFICATION OF EQUIPMENT LOCATED IN CANDU NUCLEAR POWER PLANTS

A.C. Heidebrecht and W.K. Tso

Dept. of Civil Engineering and Engineering Mechanics
McMaster University
Hamilton, Ontario, L8S 4L7, CANADA

ABSTRACT

This paper provides a description of a research program on seismic qualification of equipment which was sponsored by the Atomic Energy Control Board of Canada and conducted at McMaster University. Included is a brief description of the results of several investigations which were part of this programme, including a fault tree evaluation, the development of a methodology for overall qualification of safety systems and an evaluation of qualification approaches and procedures. The primary focus of the paper concerns the development of new parameters to characterize seismic floor motions and the application of these to single and multi-frequency testing. The actual testing of an instrument cabinet, for the purpose of evaluating test procedures, is also discussed.

INTRODUCTION

The Atomic Energy Control Board of Canada has been the sponsor of a research program at McMaster University which is concerned with the seismic qualification of equipment located in CANDU nuclear power plants. The findings of this research program are summarized in reference [1].

The objectives of this program were: (i) to provide an evaluation of the current seismic qualification requirements for equipment in the CANDU reactor system, (ii) to develop a methodology for the seismic qualification of CANDU safety systems and (iii) to evaluate seismic qualification analysis and testing procedures for the purpose of providing input in the formulation of Canadian seismic qualification standards.

In order to evaluate the current seismic qualification requirements, a fault tree study was used to develop a logic diagram which identified the various paths of failure necessary to result in public release of radioactivity following an earthquake. By comparing the systems involved along each failure path under the AECL (Atomic Energy of Canada Ltd.) design requirements, it was found that the nuclear power plant as a whole would be seismically qualified if the specified AECL design requirements for each system were met.

Based on the foregoing, it is clear that the adequacy of the overall nuclear power plant depends upon the adequacy of the seismic qualification of the different systems which are designed to ensure the safety of the plant. When evaluating "safety systems", it was determined that the seismic qualification of components or individual pieces of equipment within those systems is a necessary but insufficient condition to ensure the qualification of the overall safety system. The additional requirements, over and above component qualification, were then specified in terms of two additional

types of qualification, namely location qualification and interface qualification. The methodology for these additional qualification types was illustrated by using the Shutdown System 2 (SDS2) at the Ontario Hydro Pickering B Station as an example.

In terms of component qualification, a critical evaluation of current seismic qualification procedures was included in this study. The two most common approaches are qualification by analysis and by testing, each of which has its advantages and drawbacks. The primary advantage of testing is its inherent flexibility for use in qualifying a wide variety of equipment, irrespective of shape, size or weight. If carried out properly, analysis is a viable approach for ensuring the integrity of equipment after an earthquake. On the other hand, qualification by testing has the advantage of being able to demonstrate functionality in a direct manner. Testing is limited by the shaking capacity of available testing facilities and would not be suitable for equipment of large size and/or weight. The emphasis of the evaluation in this study was on the comparison of the two different approaches and on the comparison of methods and procedures within each approach. The advantages, drawbacks, limitations and uncertainties were provided in order that engineers could choose the most suitable approach and procedure for their particular requirements.

SEISMIC FLOOR MOTION CHARACTERISTICS

In considering testing procedures, there is considerable concern about the way in which such procedures simulate anticipated seismic floor motions. While there is no evidence that current procedures have led to the installation of equipment which is underqualified, there is a real need to ensure that test procedures provide a reasonably realistic simulation of seismic floor motions which equipment is expected to withstand should an actual earthquake occur.

In order to simulate actual seismic floor motions, it is necessary to be able to properly characterize the properties of such motion. A brief description is provided of several parameters which have been proposed to be suitable for use in the characterization and classification of earthquake induced motions and structure or equipment responses. A detailed description of these parameters can be found in a report of the 1979-80 phase of this research programme [2]. The six parameters are maximum acceleration, response spectrum, cumulative damage, cumulative RMS function, duration of strong motion and root-mean-square acceleration. The first two might be considered "classical" parameters while the other four are more recent in origin; the sources of these "new" parameters are indicated in the descriptive paragraphs which follow.

The simplest parameter to obtain from a time history is the maximum acceleration. Its use as a description, however, implies that all time histories are similar in duration and frequency content and this is seldom the case. Its wide use is probably bound up in historical roots and the fact that it is used to bound the high frequency end of the response spectrum. Unfortunately, time histories having the same maximum acceleration can lead to completely different structural responses.

The second parameter is the response spectrum. A response spectrum is a plot of the maximum response versus natural frequency for different single degree of freedom systems, having the same level of damping, subjected to a particular time history. Response spectra are usually defined for the ground and for each floor of the structure. These response spectra are normally defined over the range of frequencies from 1 to 33 Hz.

The third parameter is referred to as the "cumulative damage process", which provides a technique for measuring equivalency between time histories, in terms of the equivalent number of cycles of a uniform amplitude motion required to accumulate the same damage as the random fluctuations in the time history. This process was first applied to seismic problems in nuclear power plants by Duff and Heidebrecht [3]. The

equivalent number of cycles is obtained by using the simple yet accurate cumulative damage theory proposed by Miner [4].

The particular definition of equivalent cycles used in this study is given by

$$N_{eq} = \frac{1}{2} \sum_{i=1}^n \left(\frac{R_i}{R_p} \right)^{\beta}$$

in which n is the total number of cycles

R_p is the maximum amplitude

R_i is the amplitude of cycle "i" and

β is a parameter related to material properties and test conditions.

The other three "new" parameters were applied to studies of strong ground motion characteristics by McCann and Shah [5]. The cumulative RMS function provides a time-wise indication of how the strength of a particular motion builds up and then decays. The function is defined as

$$CRF(t) = \left\{ \frac{1}{t} \int_0^t a^2(\tau) d\tau \right\}^{1/2}$$

in which $a(\tau)$ defines the acceleration time history.

The duration of strong motion can be defined qualitatively as the time taken to build up from the onset of motion to the beginning of the decay in the cumulative RMS function. Detailed expressions for duration of strong motion have been determined [2] but are not shown here.

The final parameter, root-mean-square acceleration (A_{rms}), can now be defined in terms of the cumulative RMS function and the duration of strong motion. Simply stated, the RMS acceleration is defined as the final value of the cumulative RMS function when it is evaluated from the beginning to the end of the time interval containing the strong motion. Fig. 1 illustrates CRF, for a typical earthquake ground motion record; A_{RMS} and duration can be inferred from the same diagram by using the above definition.

The use of some or all of these parameters would allow for the multiple parameter description, as opposed to the single parameter description, of seismic motion. This should provide for a more accurate description of seismic motion.

EVALUATION OF SINGLE FREQUENCY TESTING PROCEDURES

Single frequency motions of various kinds are commonly used in seismic qualification testing. The motions evaluated in this study are constant amplitude limited duration sine waves, sine beats and decaying sinusoids. In actual testing, each single frequency motion is repeated at relatively closely spaced frequency intervals (e.g. one-third octave) over the frequency range of interest, typically 1 to 33 Hz.

The characteristics of these three types of single frequency motion, using the parameters discussed in the previous section, were studied in considerable detail [2]. By selecting appropriate durations and amplitudes of motion, a certain amount of equivalence can be obtained, as can be seen in Table 1. This table shows situations in which each of the three motions has the same RMS acceleration, peak response spectrum ordinate and cumulative damage cycles N_{EQ} . However, the three motions do not equally simulate actual seismic floor motions as can be seen by examining the cumulative RMS function in Fig. 2. This figure shows that the energy build-up, as given by the CRF, is very rapid for the sine and decaying sine motion, but is much

more gradual for the sine beat. By comparing this build-up with that shown for actual seismic ground motion in Fig. 1., it can be seen that the sine beat motion provides the best simulation of the characteristics of actual seismic floor motions. Consequently, it is recommended that sine beat motion be used whenever single frequency methods are appropriate.

MULTI-FREQUENCY TIME-HISTORY TESTING

Actual seismic floor motions are multi-frequency in nature and multi-frequency time-histories are often used in seismic qualification testing. In most cases the primary requirement is that the test motion have a response spectrum which envelopes the response spectra of floor motions which are anticipated due to actual earthquakes. This section describes an experimental programme which was used to assess the implications of such an approach. The actual testing and results are described in the next section. The full programme of testing is described in a separate report [6].

Fig. 3 provides a schematic diagram of the methodology used in this phase of the study. An ensemble of twelve different actual seismic ground motion time-histories were selected (from among the large number currently available) by considering such factors as local site conditions, magnitude, maximum acceleration, duration and source distance. These twelve ground motions were then applied as inputs to a mathematical model (provided by AECL), which is a lumped mass representation of a 600 MeW CANDU nuclear power plant. The model includes four major groups of structural components (foundation base slab, containment structure, internal structure and reactor vault).

The foregoing analysis yielded an ensemble of floor motion time-histories at typical locations at which qualified equipment is located; masses 4 and 12 were used in this study. These time-histories were then normalized so that the maximum acceleration of each floor motion was 0.25 g. Individual floor response spectra were then computed for each normalized time-history; a typical spectrum is shown in Fig. 4.

The analytical phase was completed by superimposing all the twelve individual floor response spectra at each of the two locations to create an envelope response spectrum for each location. Each envelope response spectrum was then broadened, using the methodology approved by the U.S. Nuclear Regulatory Commission, in order to create a design response spectrum for the particular location. Typical envelope and design response spectra are shown in Fig. 5.

The test specimen used in the experimental phase was an instrument cabinet typical of those used in nuclear power plants. The cabinet was provided through the co-operation of AECL and Ontario Hydro. In order to bring the cabinet natural frequencies down into the range of the predominant floor motion energy, a dead weight of approximately 700 pounds was attached to the top of the cabinet.

The actual experimental phase consisted of two groups of tests. In the first group, the individual floor motion time histories were used as table motions. The cabinet responses to these motions represent an ensemble of responses which would be expected during actual seismic events. This ensemble was then used as a "base" by which to evaluate the appropriateness of a multi-frequency testing methodology using the design response spectra obtained by broadening the envelope of the individual response spectra, as described previously.

In order to conduct the second group of tests, composite floor motion time histories were created. These composite motions were composed of superimposed sine beats of different frequencies and were developed so that their response spectra enveloped the corresponding design response spectra. These composite time histories were then used as table motions in the second group of tests.

TABLE 1 EQUIVALENCE OF SINGLE FREQUENCY MOTIONS

CHARACTERISTIC	LIMITED DURATION SINE	SINE BEAT EQUIVALENT	DECAYING SINE EQUIVALENT
No. of cycles	5	7	11
Maximum acceleration	1.0 g	1.18 g	1.32 g
Strong phase RMS acceleration	.707 g	.707 g	.707 g
Peak Response Spectrum Ordinate (1 % damping)	13.5 g	13.5 g	13.5 g
Duration of Strong Motion (cycles)	5	5	3.3
N _{eq} (norm. to 1 g)	5	5	5

TABLE 2 TYPICAL INSTRUMENT CABINET TEST RESULTS
(top cabinet accelerometer in direction of table motion)

Response Parameter	Minimum	Maximum	Mean	Standard Deviation
1. Amplification* of Peak Accelerations --				
Actual	1.44	9.82	3.87	2.06
Composite	2.71	4.27	3.41	0.79
2. Amplification* of RMS Accelerations --				
Actual	1.62	16.68	6.30	3.85
Composite	4.18	4.39	4.29	0.11
3. Equivalent Damage Cycles --				
Actual	6.31	33.46	14.59	6.48
Composite	42.14	55.52	46.81	7.55
4. Duration of Strong Motion (seconds) --				
Actual	4.48	26.90	11.49	7.36
Composite	28.38	30.14	29.40	0.91

* Ratio of cabinet to table response

INSTRUMENT CABINET TEST RESULTS

The response of the cabinet was monitored by three accelerometers, two recording response in the direction of excitation at the top and mid-height and one recording transverse response at the top of the cabinet. Typical response time-histories are shown in Figs. 6 and 7. All responses were recorded and stored for analysis which included the determination of the following parameters: the duration of strong motion, the RMS acceleration, the equivalent number of damage cycles, amplification of peak acceleration (ratio of cabinet to table response), and the ratio of RMS acceleration to peak acceleration.

Four of the above parameters were analysed statistically in order to compare the responses due to "actual" and composite time histories. The mean, standard deviation, maximum and minimum values for each parameter were obtained for all responses at each cabinet accelerometer location and for each of the two building locations. These statistics were based on between 32 to 34 sample values for the "actual" time histories and 3 sample values for the composite time histories. The results are detailed in reference [6] and summarized in the following paragraphs for the four parameters which were analysed, namely peak acceleration amplification, RMS acceleration amplification, number of equivalent damage cycles and duration of string motion. Typical results are given in Table 2.

The results for the "actual" floor motions show considerable variability, due to the differing earthquake characteristics, as well as nonlinearities in cabinet response. Nonlinear cabinet response was observed because each time history was applied using different levels of excitation and the response amplification, damage cycles and durations varied with excitation level.

The results show that both the peak and RMS acceleration amplifications are substantially larger for the ensemble of "actual" time histories than for the composite time histories. This is true whether one looks at the mean or maximum values of amplification. While the reasons for this result cannot be determined directly from the experimental data, it does indicate that a simple enveloping of response spectra is insufficient to ensure that all response parameters will also be enveloped.

On the other hand, the composite time histories produce larger number of equivalent damage cycles and longer strong motion durations than are produced by the "actual" floor motions. This is likely due to the fact that the nature of the sine beat superposition in creating the composite time history is such as to ensure that the strong motion duration is very near the full 30 second duration of the time history. The longer duration of the composite time histories also contribute to a larger value of the number of equivalent damage cycles.

The general conclusion of this study is that the simple enveloping of a design response spectrum will not necessarily yield the best composite time history for testing a piece of equipment. If the amplification of motion within the piece of equipment is important, then it may be necessary to modify the composite time history (e.g. by increasing its amplitude to produce a larger response) or to use another composite time-history which produces larger amplifications. It may also be appropriate to use a small "sub-ensemble" of actual time-histories which are known to have the capability of producing large amplifications.

ACKNOWLEDGEMENT

This work was sponsored by the Atomic Energy Control Board of Canada. The assistance of Atomic Energy of Canada Limited and Ontario Hydro in providing design information, access to facilities and the instrument cabinet is also acknowledged. Computing facilities were provided by McMaster University.

REFERENCES

1. A.C. Heidebrecht and W.K. Tso, "Seismic Qualification of Equipment - A Summary of Findings", McMaster University, Hamilton, Ontario, 1982 (in preparation).
2. J.C. Wilson, A.C. Heidebrecht and W.K. Tso, "Characteristics of Seismic Floor Motions", McMaster University, Hamilton, Ontario, June 1980.
3. G.C. Duff and A.C. Heidebrecht, "Earthquake Fatigue Effects on CANDU Nuclear Power Plant Equipment", Proc. 3rd Canadian Conference on Earthquake Engineering, Vol. 1, Montreal, Canada, June 1979, pp. 325-335.
4. M.A. Miner, "Cumulative Damage in Fatigue", J. Appl. Mech., Vol. 12, no. 1, 1945, pp. 159-164.
5. N.W. McCann and H.C. Shah, "Determining Strong-Motion Duration of Earthquakes", Bull. Seism. Soc. Am., Vol. 69, no. 4, Aug. 1979, pp. 1253-1265.
6. A.C. Heidebrecht and W.K. Tso, "Qualification Testing of Instrument Cabinet", McMaster University, Hamilton, Ontario, August 1982.

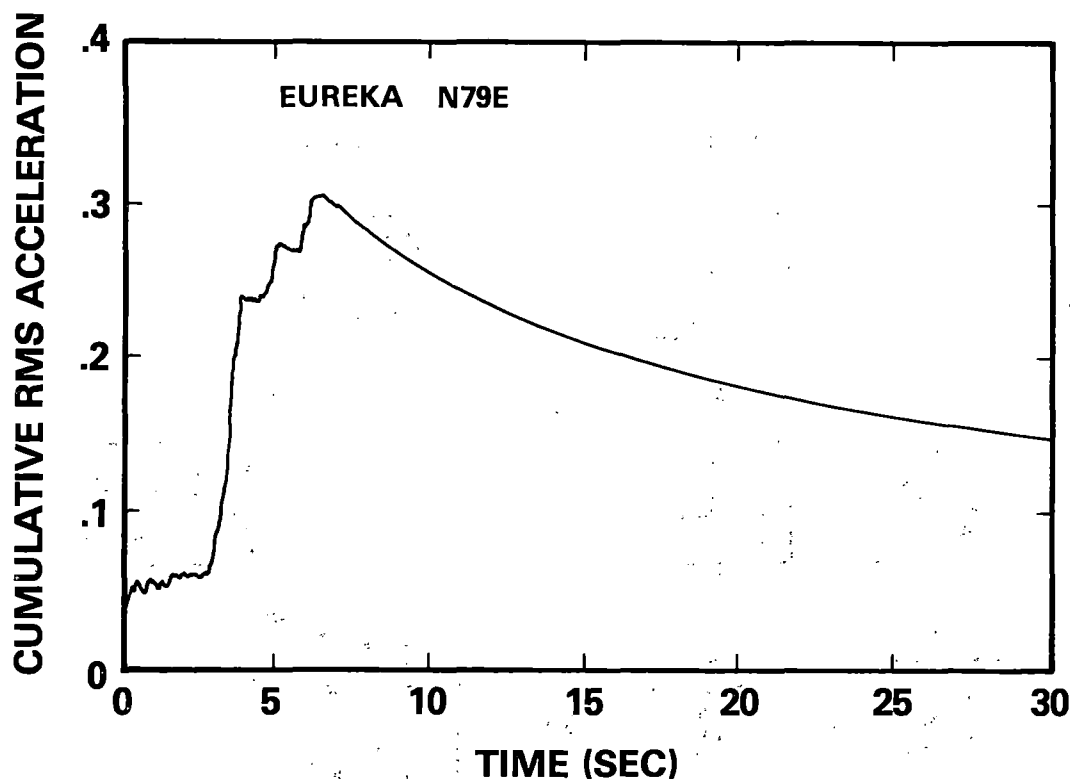


Figure 1. Typical Cumulative RMS Function, Seismic Ground Motion (Eureka N-E).

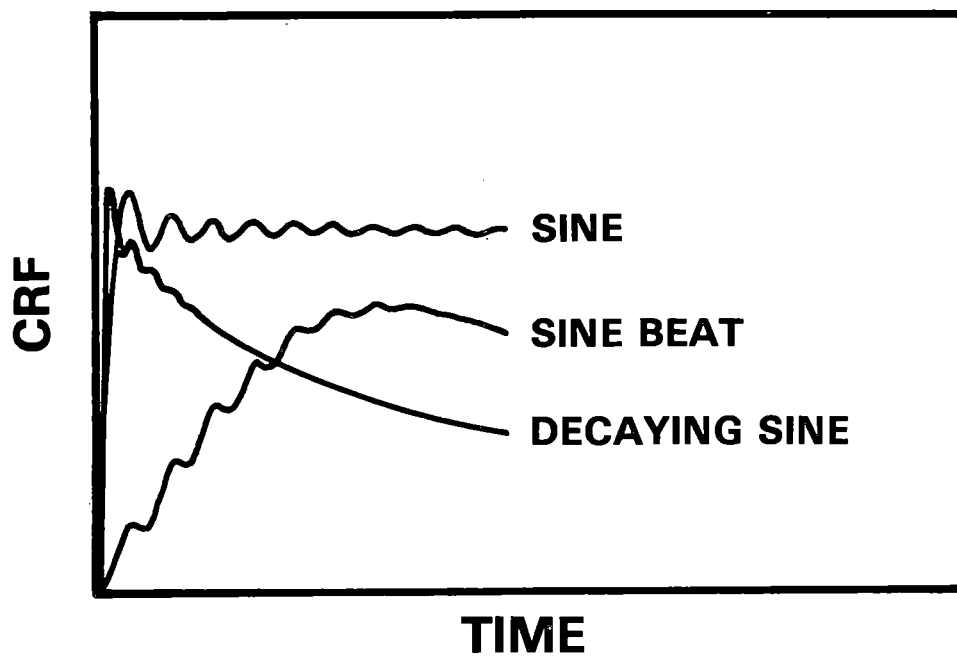


Figure 2. Cumulative RMS Functions of Single Frequency Motions.

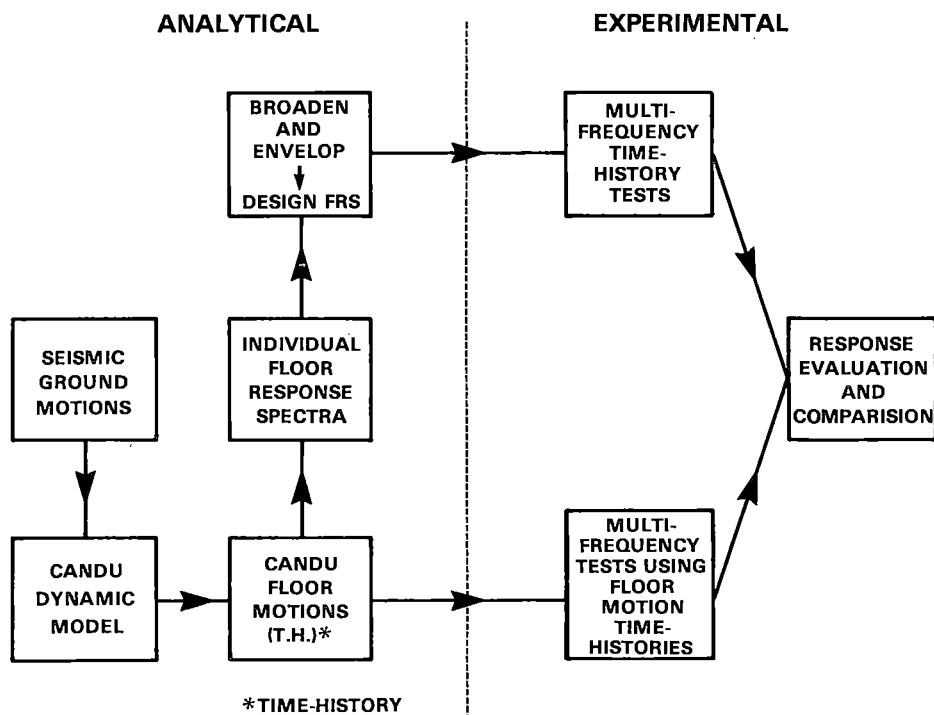


Figure 3. Schematic Outline of Test Procedure.

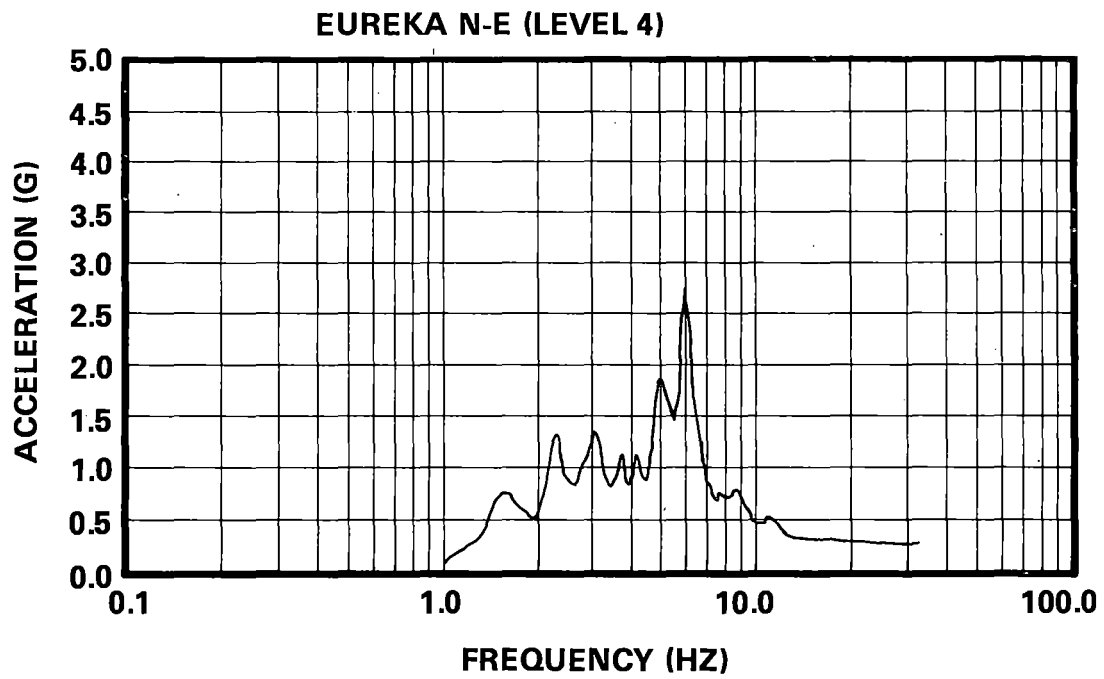


Figure 4. Sample Level 4 Response Spectrum (Eureka N-E).

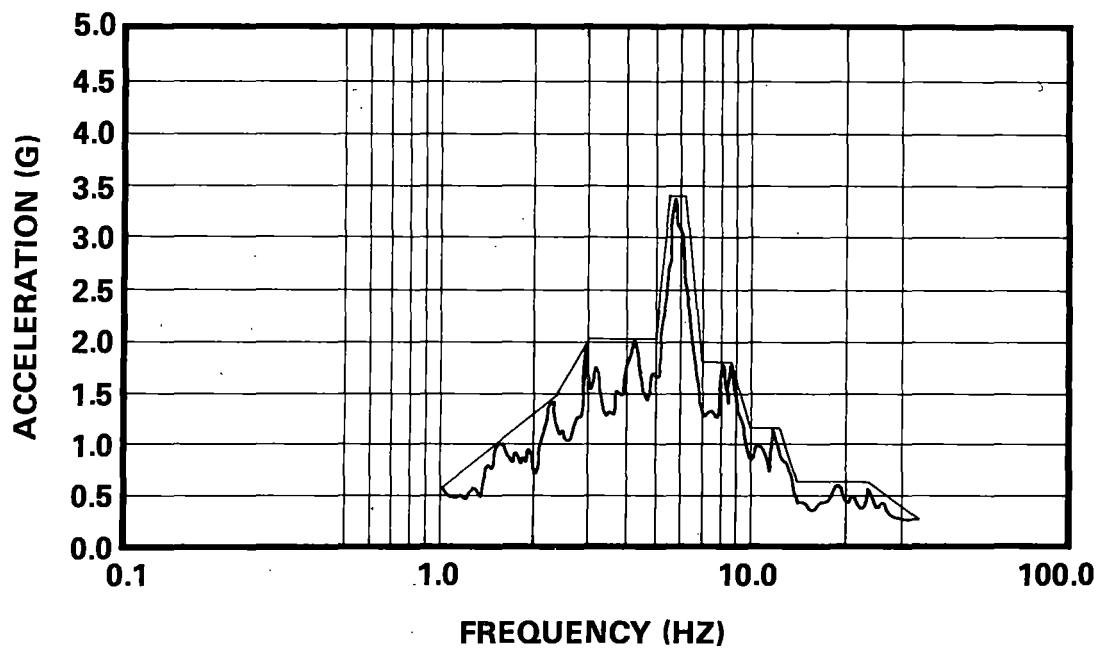


Figure 5. Level 4 Envelope and Design Response Spectra.

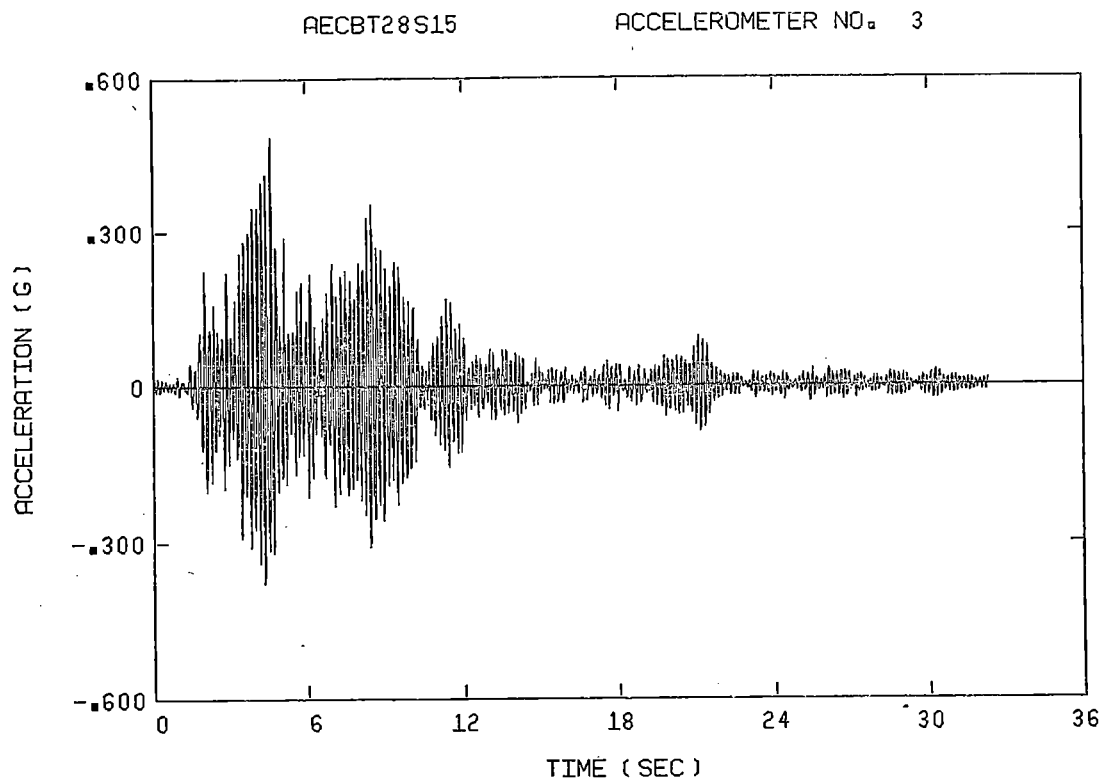


Figure 6. Longitudinal Top Acceleration of Cabinet (Eureka N-E, Level 4).

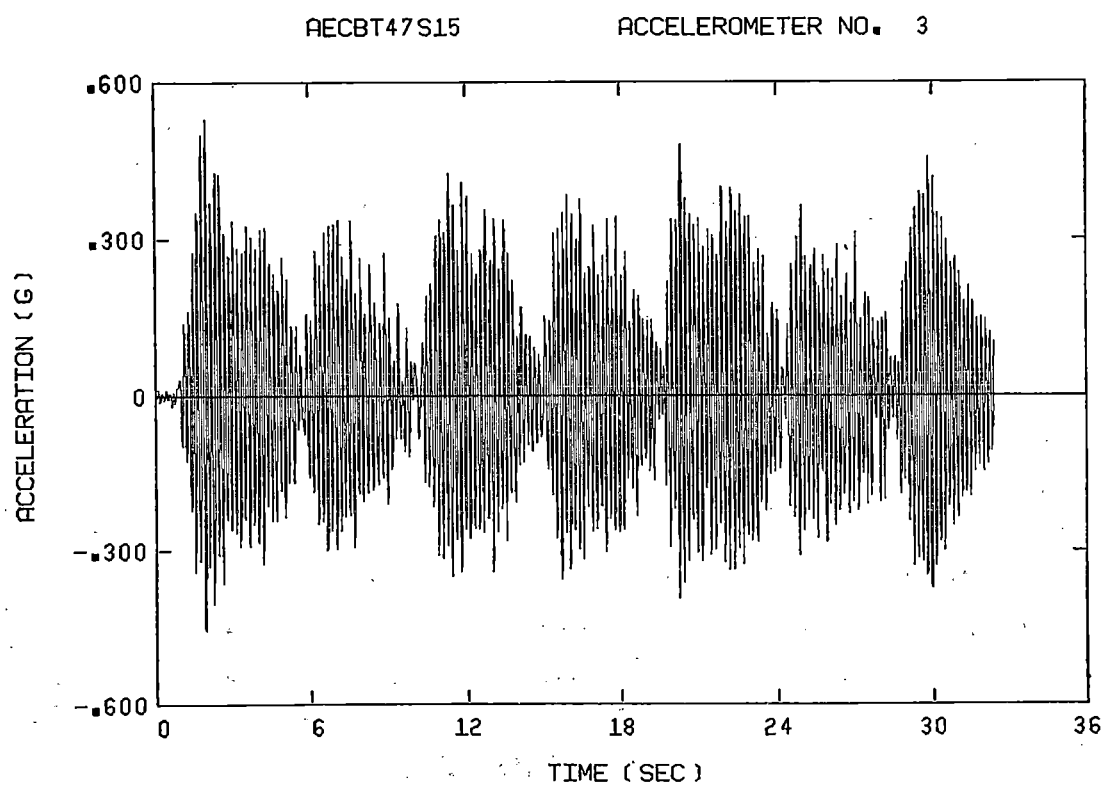


Figure 7. Longitudinal Top Acceleration of Cabinet (Composite, Level 4).

EXPERIMENTAL AND ANALYTICAL STUDIES
ON THE SEISMIC BEHAVIOUR OF
CANDU-PHW CORES

Dr. T. Kuroda
Deputy General Manager
Nuclear Power Department
Electric Power Development Co., Ltd.
8-2 Marunouchi, 1-chome, Chiyoda-ku
Tokyo, 100 JAPAN

and

C.G. Duff
Manager
Engineering Quality Assurance Department
Design and Development Division
Atomic Energy of Canada Limited
Engineering Company
Sheridan Park Research Community
Mississauga, Ontario, L5K 1B2, CANADA

ABSTRACT

The paper describes experiments conducted by EPDC in Japan on reduced and full-scale models of the CANDU-PHW pressure-tube reactor core. Correlations predicting, analytically, the behaviour of the shut-off rods and their interaction with pressure tubes during a seismic event are also discussed. Earthquake analyses carried out by AECL in Canada on the behaviour of the CANDU-PHW core, during on-power refuelling, with the fuelling machines coupled to a fuel channel, are presented. It concludes that a CANDU-PHW reactor core can survive strong earthquakes, while preserving full shutdown and on-power refuelling capability.

INTRODUCTION

The CANDU-PHW reactor is a tubed cylindrical shell-and-tube sheet structure which is housed inside a water-filled concrete vault, Fig. 1. The CANDU-PHW reactor consists primarily of a horizontal cylindrical calandria vessel containing heavy water moderator, axially oriented fuel channel assemblies, Fig. 2, and transversely oriented reactivity control mechanisms. Each of the fuel channel assemblies (hereafter referred to as CT/PT assembly) comprises a calandria tube (CT), a pressure tube (PT), fuel bundles and heavy water coolant, which is independent of the moderator.

This paper deals with a series of forced vibration tests conducted by EPDC (Electric Power Development Co.) for the models of the 600MWe CANDU-PHW core and a supportive analytical study. As illustrated in Fig. 3, the experimental portion of the study is composed of three stages; STEP I, the test using a 1/5 scale half-cut model of the core, STEP II, the test using full-scale partial models and STEP III, the safety margin test. The STEP II test is sub-divided into two parts; (1) shut-off rod (hereafter referred to as SOR) insertion capability test using a full-scale

actual unit, and (2) CT/PT assembly vibration test using full-scale partial array models (single- and nine-channel). The objective of the tests is to demonstrate the seismic qualification of the CANDU-PHW core under Japan's severe seismic excitation conditions.

The 600 MWe fuel changing system, Fig. 10, utilizes a pair of fuelling machines (hereafter designated F/M) which operate simultaneously from both ends of the reactor on any one of its 380 channels, while the reactor is running. On-power refuelling is carried out 2 to 3 times a day, so the probability of an earthquake occurring while the F/M's are in operation is quite high. Since the F/M's are coupled to end fittings (E/F's) at either end of a channel (see Fig. 2) during refuelling, it is important to know the interaction forces that are developed between the F/M's and the channel when an earthquake occurs. The paper describes the approach to seismically qualifying a coupled fuel channel and F/M.

EXPERIMENTAL STUDY

1/5 Scale Model Test [1]

The test was performed on a 1/5 scale, half-cut model of the core, Photo 1, so that the intricate seismic behaviour of the core could be visually observed through a piece of glass fitted onto the cut section.

The 380 CT/PT assemblies were modelled as cantilevers, rigidly supported at the end plate on the opposite side of the glass. The cylindrical tank, filled with ordinary light water, was located in the middle of the frame representing a concrete reactor vault. 13 guide tubes (hereafter, referred to as GT) and other reactor control guidetubes were placed together with CT/PT assemblies as they would be in the prototype.

Using a 20 ton shaking table, the model was subjected to both sinusoidal and random motions. Measurements were primarily made of acceleration of major components and drop time of SOR.

The test was instrumental in clarifying the basic and collective characteristics of tube assemblies immersed in water, as well as SOR insertion capability during an earthquake.

Shut-off Rod Insertion Capability Test [2], [3]

The test rig is indicated in Fig. 4, along with its measuring system. The rig is made up of tanks simulating the reactor vault and calandria tank, one channel of actual SOR assemblies, the longest GT and 44 channels of CT adjoining the GT. Forced vibration is induced by three, 3 ton actuators.

The model was subjected to the excitation of sinusoidal waves and random waves (floor responses) generated from dynamic analyses of the overall building model using earthquake waves, Table I. Sinusoidal waves were used for the sweep test, as well as for the GT resonance test. Both actual and synthesized earthquake motions were used as random waves, of which the synthesized waves were generated in such a manner as to satisfy the design response spectra requirements stipulated by the Japan Nuclear Safety Commission [4], [5]. Two soil conditions, soft and hard soils (50 and 100 t/cm² in Young's modulus), were considered in the building response analysis, as well as two acceleration levels representing the S₁ and S₂ design earthquakes. Measurements were mainly made of acceleration, displacement and strain of GT and CT/PT and drop time and pattern of SOR.

The SOR test results indicate that the resonant amplification factor of GT in water amounts to 3 to 6, in contrast to the very high factor of GT in air, Table II. This is primarily attributed to the higher damping factor (0.1 - 0.3) of the perforated GT in water. Of more importance for safety purposes is the drop time of the SOR. It was found that the drop time under S_1 earthquake excitation conditions ranges from 1.5 to 1.6 seconds, Fig. 5, which is well below the target time of 2.0 seconds and that the maximum time delay due to excitation is, on the average, only 0.2 second. It was also found that the drop time is not affected much by an increase in seismic intensity from S_1 to S_2 nor by an increase in trip acceleration level.

These findings, for the most part, coincide with those found in the STEP I test (1/5 scale model).

Fig. 6 shows an example of the running Fourier spectra for the response acceleration wave recorded at the center of GT during the SOR insertion test under sinusoidal excitation. It is obvious that there was a temporary decrease in the response acceleration amplitude of the GT at its first natural frequency of 4.8 Hz during the SOR insertion, and that the high frequency components caused by the collision between GT and SOR appeared in the response records after the insertion.

Fuel Channel Assembly Vibration Test [2], [3]

The single-channel model is composed of one channel of the CT/PT assembly which is enclosed in a steel cylindrical tank. The nine-channel model, Photo 2, consists of nine CT/PT assemblies and a steel, box-shaped tank.

Each CT/PT assembly of the two models is composed of an actual CT and actual and dummy PT's, in which 12 cylindrical steel bars, surrounded by ordinary water, simulate the fuel bundles and coolant in each channel.

An electro-hydraulic, 20 ton shaking table is employed for exciting the models.

The sweep test was performed at three constant acceleration levels (50, 100 and 150 gals), while floor response waves, generated by the same approach as described above, were utilized as random input motions.

Presented in Table II is a summary of major vibration characteristics of an actual CT/PT assembly identified from testing. The resonance frequency of the CT/PT assembly was obtained at 6.6 Hz in air and 5.9 Hz in water.

It was also found from the tests that a double-tubed CT/PT assembly behaves as a single element. Its damping factor when immersed in water does not increase markedly as compared with that in air (about 0.06 in water and 0.05 in air) and no discernible hydro-dynamic effect is seen between CT/PT assemblies and water. These findings are generally in good agreement with the previous findings derived from the 1/5 scale model test.

According to the nine-channel vibration test, all the channels were observed to oscillate in phase under both sinusoidal and random excitation conditions. Fig. 7 shows that the average response amplification factor of the CT/PT assembly varies with the earthquake motion applied but the difference in the amplification factors for the same earthquake motion is relatively small.

The test has indicated that the maximum response acceleration observed at the CT (600 to 1,500 gal for S_1 and 1,000 to 2,400 gal for S_2) is considerably below the allowable limit.

Safety Margin Test [3], [6]

The safety margin test is divided into two portions; (1) collision test between GT and CT/PT assembly, and (2) safety-margin checking test for SOR insertion capability.

The test rig and its measuring system for the former test is shown in Fig. 8. The rig consists of a water-filled, box-shaped tank containing three CT/PT's and six, short, cantilevered GT's, each supported by a leaf spring and fitted with an external fin and internal weight to simulate the dynamic response behaviour of the center of the actual GT in water. The model was subjected to both sinusoidal and random excitation at acceleration levels higher than those for the previous STEP II test.

It is seen from Fig. 9 (a) that collision occurs in such a manner that the GT is hit by the adjoining CT/PT assemblies by turn, which results in an increase in the deflection of the GT. Under earthquake motion excitation conditions, some collisions were found to occur when the model was subjected to synthesized near-and intermediate-field earthquakes at input levels higher than S_2 and $1.5 S_2$ respectively, Fig. 9 (b).

It was also revealed from sinusoidal 'sweeps' conducted for a model comprising one CT/PT assembly and one GT that collision was observed to occur near the CT/PT assembly's resonant frequency of 5.3 Hz when the input acceleration exceeded 250 gal.

Using the same test rig as used in STEP II, the safety-margin checking test for insertion capability was performed under both sinusoidal and random-motion excitation conditions. As shown in Fig. 5, the drop time was found to be within the target time of 2.0 sec., even for an extremely severe earthquake of $1.2 S_2$.

Analytical Study Associated With Testing [6]

Concurrent with the aforementioned tests, an analytical study was conducted in support of experimental results. A computer code was developed which is capable of simulating the interaction behaviour of the core components during a seismic event. In the code, each of the core components is idealized by a multi-degree-of-freedom lumped mass system, while the collision behaviour between the GT and CT/PT assembly is described by an impulse-momentum approach. The code was shown to provide good correlation with the test data, and then it was utilized successfully to simulate the response behaviour of an actual core involving collisions between the longest GT and 44 channels of CT/PT assemblies adjacent to it. These analyses confirmed that, with the use of the above-mentioned approach, the seismic response of the core, including the collision behaviour, could be approximated.

F/M ANALYSIS

Canadian Reactors

The earthquake response-spectrum, modal-analysis method was used, initially, in conjunction with the finite-element technique, with substructuring, for dynamic modelling purposes.

Each major component is represented by a sub-structure. The sub-structures are simulated by a finite-element model, from which the stiffness matrix is condensed to a selected number of nodes. The selected nodes for each sub-structure are then put together to form the global model which represents the overall system (see Fig. 11). Dynamic characteristics (mode shapes, frequencies, damping, etc.) of the overall system were obtained from the global model, using the Lanczos modal extraction technique in the linear computer code STARDYNE.

Dynamic responses of the F/M coupled to a fuel channel, subjected to the appropriate horizontal or vertical floor response spectra applied to the base of the global model, were then obtained using the modal superposition method. Two methods of modal combination were used: the Root Sum Square (RSS) method, with modes $< 10\%$ apart being combined by absolute sum, and the Complete Quadratic Combination (CQC) method, which resembles the RSS method but recognizes the sign of all modes, thus dealing more realistically with closely-spaced modes.

For CANDU 600 MWe reactors, particularly those situated at Pt. Lepreau, New Brunswick, Canada and Wolsung-1 in the Republic of South Korea, the earthquake analyses evaluated the combined effect of three earthquake directions: two horizontal components and one vertical. While the response-spectrum, modal-analysis method was applied initially, using 2% of critical damping for the fuelling machines, 3% damping for the calandria shell and end shields and 5% for the calandria vault and fuel channels, the final results were based on the time-history, modal-superposition method, again using STARDYNE. The results reported in Table IV for the Wolsung-1 reactor used the time-history method, because the results were more acceptable from a design point of view, as well as being more realistic.

The channel design load of 55,000 pounds, given in Table III, is the external load which, in combination with other operating and earthquake loads, including bending moments, produces stress intensity levels in the critical sections of the end fittings and pressure tube meeting the Service Level 'C' allowable limits of the ASME Code, Section III. The 55,000 pound design load is well below 80,000 pounds, which represents the minimum load at which the rolled joints between the pressure tubes and end fittings can be pulled out under operating conditions. A shakedown and fatigue analysis was also carried out under DBE earthquake conditions.

Japanese Reactor

For CANDU 600 MWe reactors and fuelling machines evaluated for earthquakes in Japan, the EPDC design criteria used are as specified in Table III. For comparison purposes, the same load combinations and ASME Service Level 'C' allowables were utilized, although somewhat lower damping factors were applied than for the Canadian reactors, viz: the F/M at 1%, the fuel channels at 2% and damping factors for calandria vault components ranging from 3% to 5%.

Several loading criteria are specified by the Japanese for the coupled F/M seismic design case which are not required in Canada. Included is Japan's concern for possible leakage of heavy water, which sets the end fitting (E/F) leakage limits. The positioning assembly, (P/A), located at one end or the other (not both) of a fuel channel (see Fig. 2), has been extensively shock and cyclically load tested and is expected to resist very much higher loads than those specified in Table III under earthquake conditions. The P/A is not specifically identified in the Canadian seismic design criteria for this reason.

For the Japanese reactor, only one horizontal earthquake component and the vertical component need be evaluated, where the horizontal component producing the more severe responses is selected for design purposes. S_1 and S_2 are for intermediate earthquakes applied to a site with relatively soft soil.

The CQC method of modal combination was utilized, together with strain-energy dependent modal damping. Studies are currently underway using time-history (T-H) analyses with the expectation that even lower seismic loads will result, based on earlier findings. This should ensure acceptable loads for the S_2 earthquake level.

These T-H studies employ the ANSYS computer code, utilizing extensive sub-structuring and super elements. The Jacobi method of eigenvalue extraction is employed, while the reduction of the mass matrix is by the Guyan procedure. ANSYS was selected to permit modelling of the various F/M non-linearities, and local as well as sub-structural damping, including Coulomb frictional damping.

The basic reason for the lower axial response loads in the Japanese study, when compared with the Canadian reactor case (36,400 pounds vs. 53,000 pounds) is modifications made to the F/M. These changes are mainly of a structural nature and do not alter the basic concept, the overall appearance or performance of the reactor or F/M. These changes include:

- heavier restraints and anchors
- motion-limiting devices
- mechanical snubbers
- stronger (stiffer) bridge and columns
- reduced clearances
- additional guides and motion locks

Further work is being undertaken in Canada to obtain the dynamic characteristics of an actual, full-sized fuelling machine and to examine its non-linear behaviour and damping characteristics. This will provide invaluable information for future F/M seismic analyses and will permit the effect of any design modifications to be evaluated directly.

CONCLUSION

The vibration characteristics and seismic response behaviour of the major core components of CANDU-PHW essential to plant safety were determined from the comprehensive test program. Furthermore, the drop time of the SOR was demonstrated to be well below the target time, even under an extremely severe seismic event. Most importantly, it was found that, despite the repeated severe loading, neither the core components nor their safety functions have been appreciably influenced by these tests.

These findings led to the conclusion that the CANDU-PHW core can maintain its safety functions, as well as its structural integrity, even when subjected to extremely strong earthquake motion excitation. A mathematical model developed in this study has also demonstrated that the seismic response of the major core components involving tube-to-tube interaction can be predicted with an acceptable degree of confidence by analytical means.

The dynamic analysis of a CANDU-PHW, 600 MWe reactor, together with a pair of fuelling machines coupled to a fuel channel during a strong earthquake, shows that the F/M's will remain operational, while the reactor and fuel channel retain their structural integrity. With the benefit of more sophisticated analytical techniques, together with available strength margins, it is possible to demonstrate that the present F/M and reactor design will be able to survive severe seismic events up to the S₂ level or even higher, with little or no modification.

ACKNOWLEDGEMENT

The authors express their sincere appreciation to Dr. K. Muto, Prof. Y. Ohsaki, Prof. H. Shibata, Prof. H. Sato and Dr. M. Watabe for their guidance and valuable comments. The STEP II test described herein was partly funded by the MITI (Ministry of International Trade and Industry) of Japan. Their support is gratefully acknowledged.

Sincere appreciation is also extended to Dr. A.S. Banwatt of AECL, Engineering Co, Canada and to the Canadian General Electric Co., Ltd., for their valuable contributions to the analytical work described in this paper.

REFERENCES

1. MUTO, K., KURODA, T., KASAI, Y., 'Forced Vibration Test of 1/5 Scale Model of CANDU Core', K12/3, 5th SMiRT, Berlin, August 1979.
2. KURODA, T., et al, 'Experimental Seismic Study on 600 MWe CANDU Core Using Full-scale Partial Model', B.4, CNS 1st Annual Conference, Montreal, June 1980.
3. KURODA, T., MURAKAMI, H., MIZUKOSHI, K., 'Experimental and Analytical Seismic Study on 600 MWe CANDU Core', CNS 2nd Annual Conference, Ottawa, June 1981.
4. JAPAN NUCLEAR SAFETY COMMISSION, 'Regulatory Guide for Aseismic Design of Nuclear Power Reactor Facilities', July 1981.
5. HISADA, T., et al, 'Design Spectra for Stiff Structures on Rock', *Proc. of the 2nd International Conference on Microzonation for Safer Construction - Research and Application*, Vol. III, San Francisco, U.S.A., November 26 - December 1, 1978.
6. KURODA, T., et al, 'Experimental and Analytical Studies on Seismic Qualification of 600 MWe CANDU Core', K9/3, 6th SMiRT, Paris, August 1981.

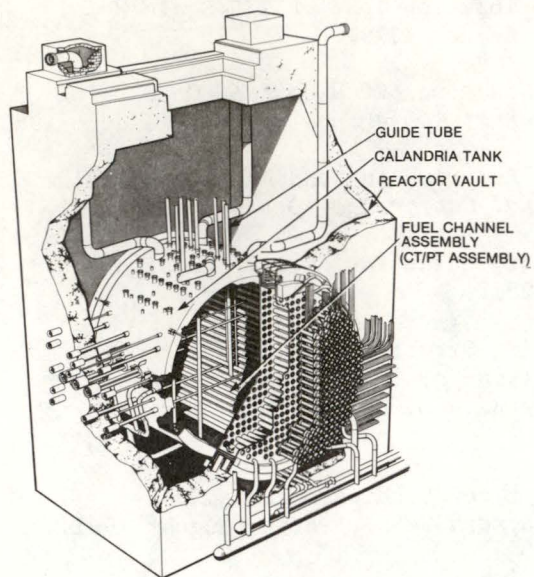


Fig. 1 CANDU 600 MWe Core

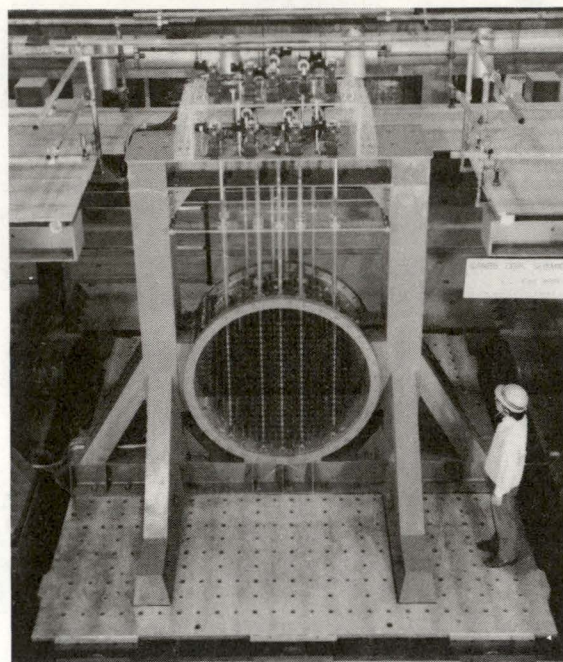


Photo 1 1/5 Scale Half-cut Model of CANDU Core

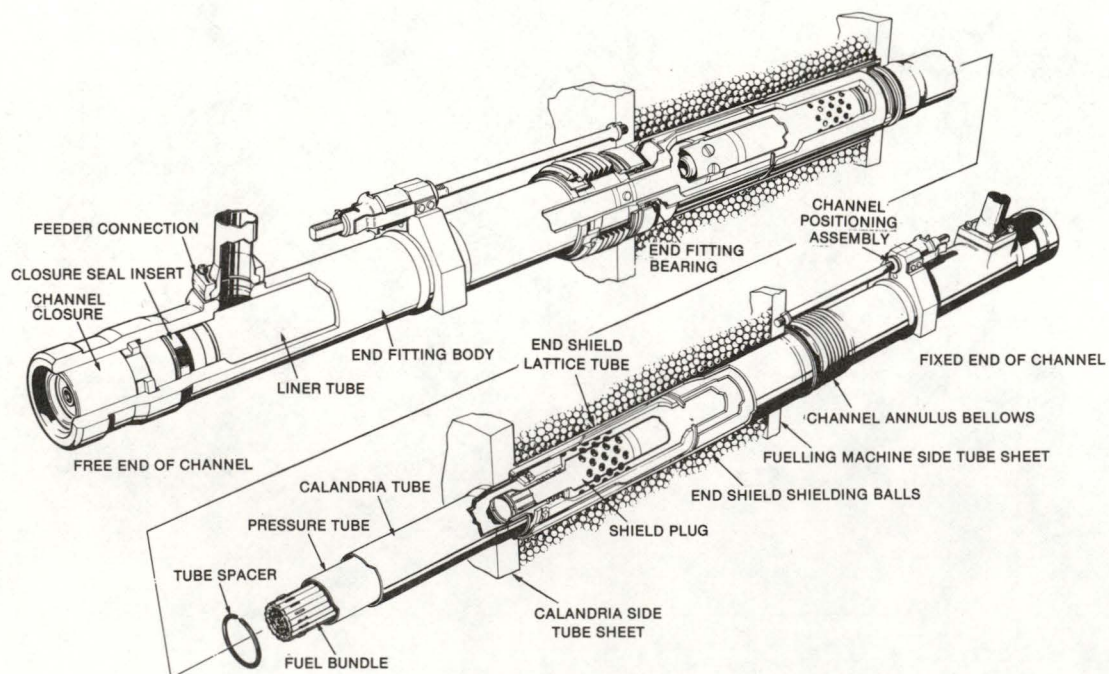


Fig. 2 600 MWe Fuel Channel Assembly

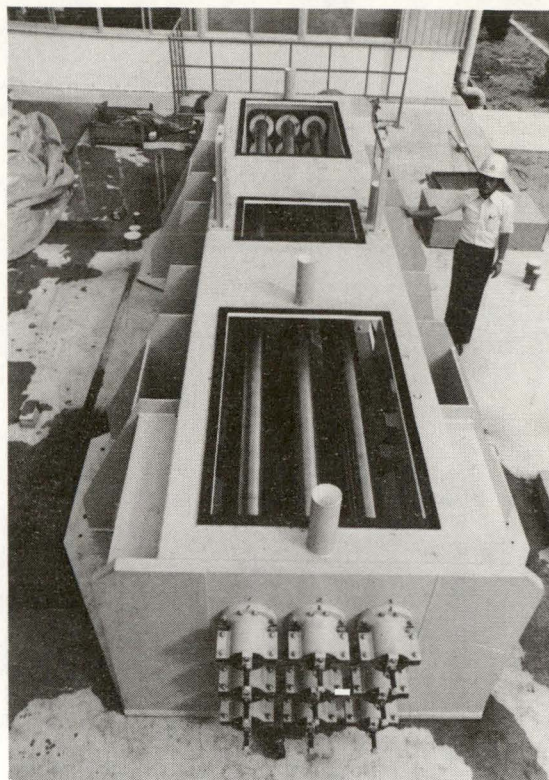
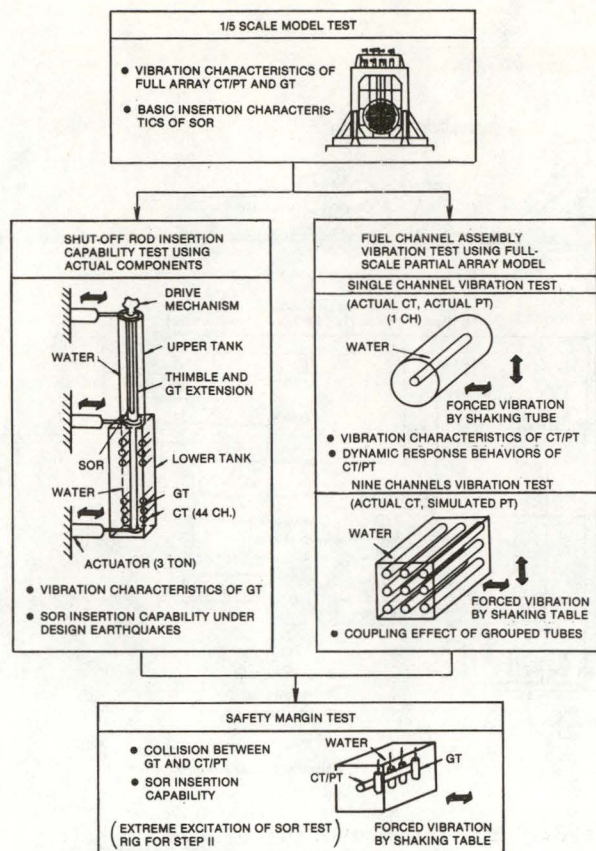


Photo 2 CT/PT Vibration Test Rig
(Nine-channel Model)

Fig. 3 CANDU Core Seismic Verification
Program

TABLE I
Input Earthquake Wave for Tests

Wave form			Max. Ground Acc. (gal)	
			S ₁	S ₂
Horizontal Direction	Recorded Earthquake	El Centro 1940 NS	300	450
		Taft 1952 EW	300	450
	Synthesized Earthquake	Far Field	270	405
		Intermediate Field	300	450
		Near Field	—	390
Vertical Direction	Recorded Earthquake	El Centro 1940 UD	180	270
		Taft 1952 UD	174	261

Note: S₁; Maximum Design Earthquake
S₂; Extreme Design Earthquake

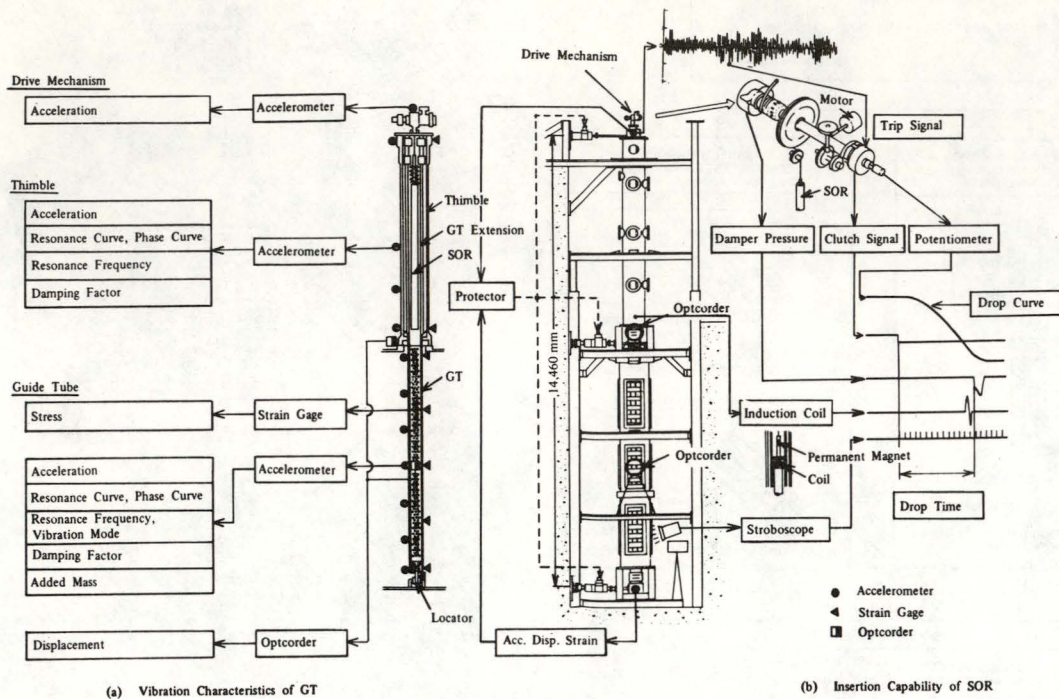


Fig. 4 SOR Insertion Capability Test Rig and its Measuring System

TABLE II
Basic Vibration Characteristics of GT and CT/PT

		GT	CT/PT
Resonant Frequency (Hz)	fa (in air)	6.6	6.6
	fw (in water)	4.8	5.9
	fw/fa	0.73	0.9
Added Mass Coefficient of Water α		0.2	1.1
Damping Factor	ha (in air)	0.005~0.01	0.05
	hw (in water)	0.1~0.3	0.06
	hw/ha	20~30	1.2
Resonance Acc. Amplification Factor (at Center)	(in air)	170	14
	(in water)	3~6	9

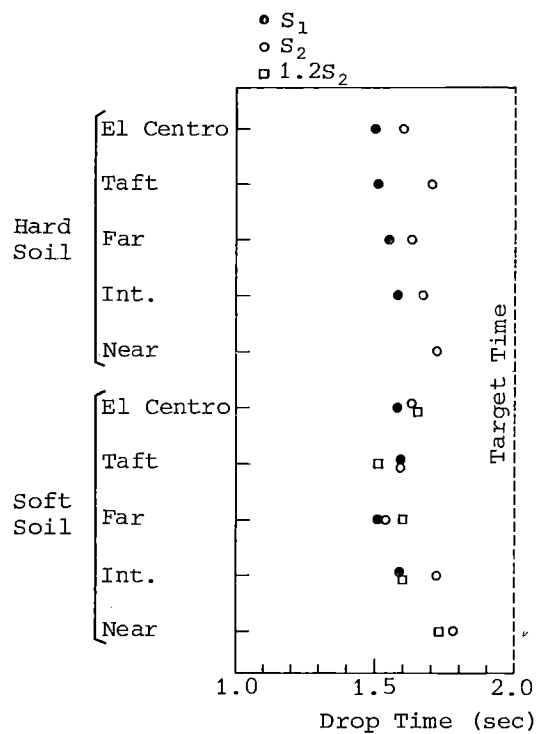


Fig. 5 Drop Time of SOR

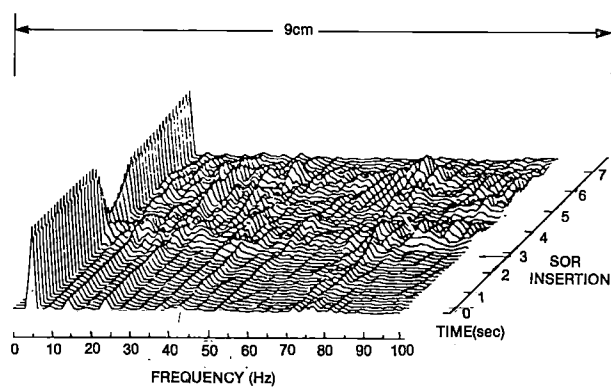


Fig. 6 Running Fourier Spectra

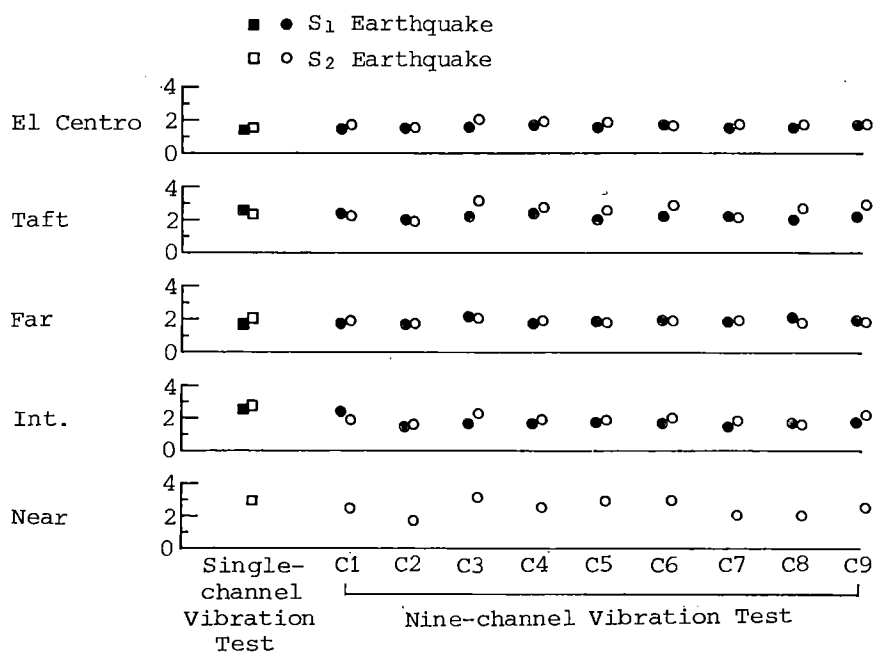


Fig. 7 Response Acc. Amplification Factor at Center of CT/PT

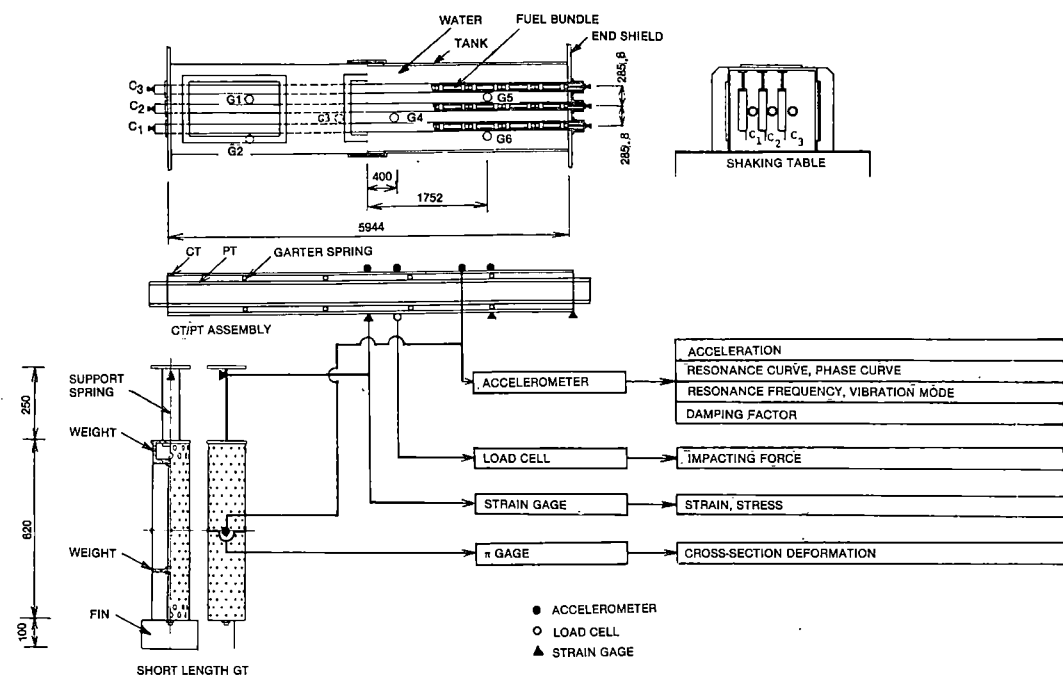
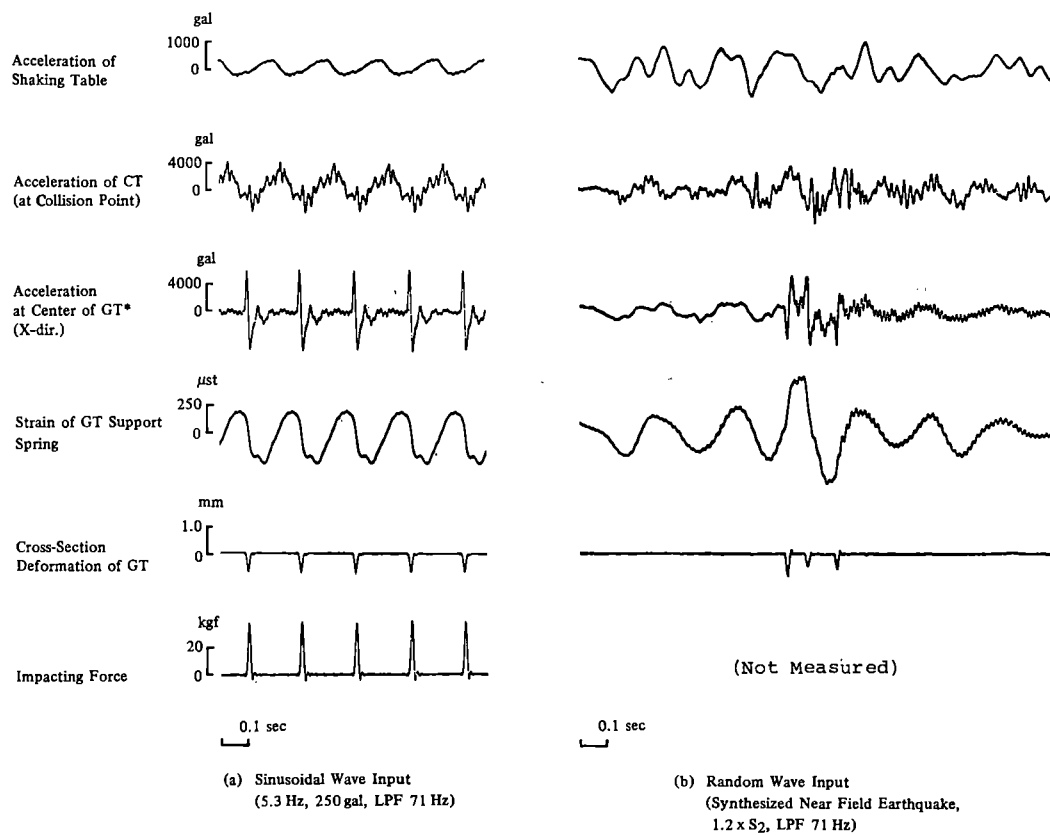


Fig. 8 Test Rig and Measuring System for Collision Test between GT and CT/PT



* Cantilever-type GT of short length simulating mid-span seismic response of actual GT

Fig. 9 Example of Collision Test Record

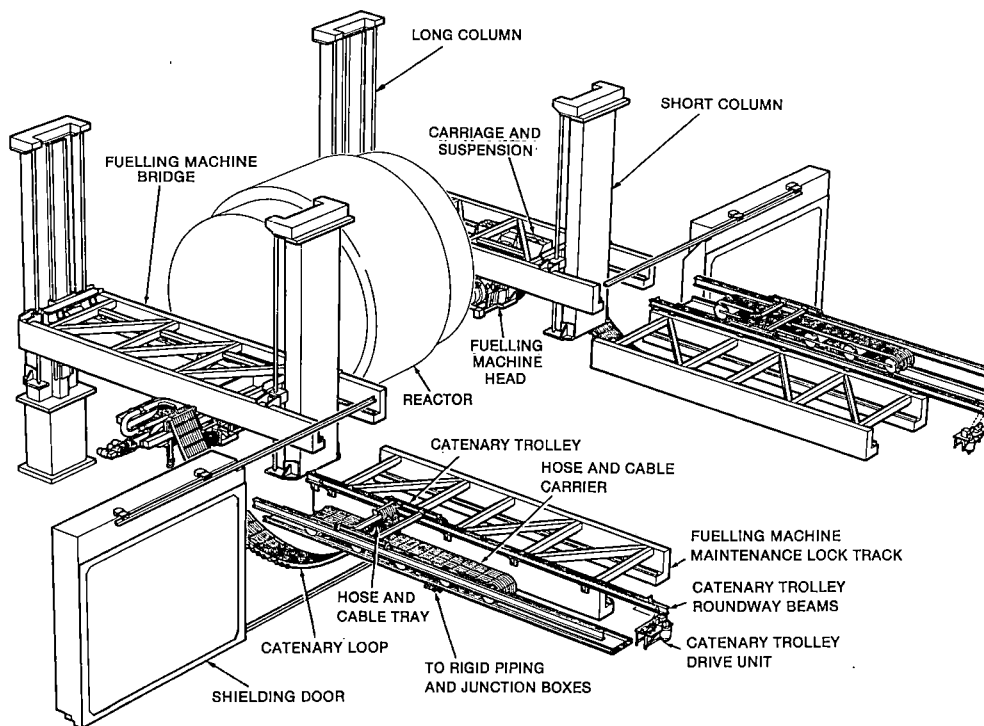


Fig. 10 Fuelling Machines

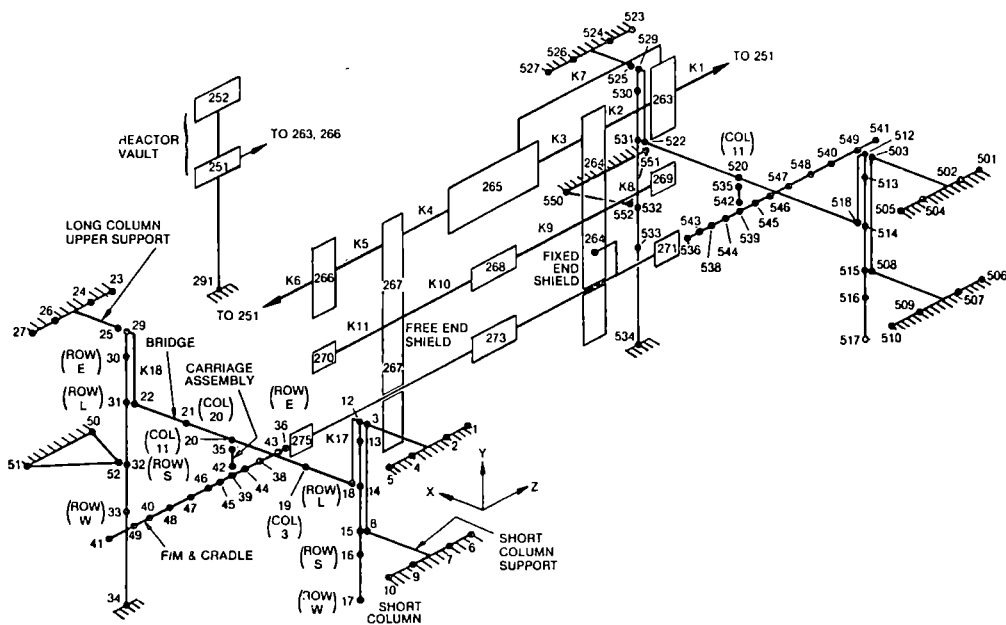


Fig. 11 F/M-Reactor Global Dynamic Model

TABLE III

F/M and Channel Seismic Design Criteria

	<u>Canada</u>	<u>Japan</u>	
Earthquake designation	DBE	S ₁	S ₂
Horizontal earthquake level	0.2g (196 gal)	300 gal	450 gal
Vertical earthquake level	0.13g (127 gal)	150 gal	225 gal
Channel axial design load	55,000	(see below)	
E/F leakage load (targets)	-----	*30,000	50,000
Rolled joint pull-out load	80,000	50,000	80,000
P/A tensile load	-----	+50,000	-----
P/A compressive load	-----	-33,700	-----

Note: All loads in pounds.

* Temporary leakage expected to commence at 46,000 pounds; permanent leakage may occur above this value.

Key: F/M, fuelling machine; E/F, end fitting; P/A, positioning assembly; DBE, design basis earthquake; S₁ and S₂, seisms 1 and 2; gal, cm/sec²; blanks -----, not applicable.

TABLE IV

F/M and Channel Seismic Analysis Results

	<u>Canada</u>	<u>Japan</u>
Earthquake	DBE (2H+V)	S ₁ (H+V)
Method	Time history	Modal (CQC)
Channel axial load	53,000 (55,000)	-----
No-leak load	-----	36,400 (30,000)*
Pull-out load	-----	10,600 (50,000)

Note: All loads are in pounds. Design targets are in brackets.

* Leakage commences at about 46,000 pounds.

Key: H = Horizontal earthquake (1 or 2 directions)
 V = Vertical earthquake
 CQC = Complete Quadratic Combination

Use of the Delphi Approach in
Seismic Qualification of Existing
Electrical and Mechanical Equipment
and Distribution Systems

J. D. Stevenson^[1]

INTRODUCTION

Seismic design verification of Category I mechanical and electrical components (vessels, pumps, valves, tanks, control panels, motor control centers, switchgear, etc.) and distribution systems (piping, duct, conduit and raceways) is both a time consuming and expensive undertaking. In current new nuclear power 1100 - 1300 MWe plant designs it is estimated that the engineering effort required to perform this seismic design verification varies between 400,000 to 700,000 manhours. For plants now in operation which were designed more than six years ago the seismic verification effort for components and distribution systems typically did not exceed 200,000 manhours.

The seismic design requirements of the Nuclear Regulatory Commission have changed and generally have increased significantly during the past ten years. There is currently underway an NRC rule making proceedings which will in all probability establish new requirements for reviewing the seismic design adequacy of operating nuclear power plants equipment and distribution systems. If this review requires a component by component, line by line reevaluation of all seismic Category I items it can be anticipated that an additional 100,000 to 300,000 engineering manhours will be required to complete the seismic reanalysis to current levels of analytical effort for each plant. This analytical effort would be further hampered by the fact that much of the original design information no longer exists and would require extensive field measurement and data gathering.

In this paper a method of seismic reevaluation is described which permits every seismic Category I component and distribution system to be evaluated and an explicit estimate of seismic capability, in terms of an acceleration level which defines limits of structural adequacy and leak-tight integrity, be defined for each item. The procedure employs the Delphi method where a team of seismic design experts independently inspect each component and distribution system in its "as installed" condition in the field and estimate the acceleration level that component or system could withstand and still meet applicable seismic design code or other criteria requirements. The accuracy and any potential bias in the estimates can be evaluated by a small control sample where selected components which were also surveyed by the Delphi team are independently evaluated in detail using current analytical techniques. This entire procedure can be accomplished for an estimated 5,000 to 10,000 manhours per plant. The procedure also directly can provide probability of failure levels at the 10, 50 and 90 percentiles which can be used to construct seismic curves for each component. These fragility curves are then available to be used in component - plant specific probability risk assessment studies.

[1] Senior Consultant, Stevenson & Associates, Cleveland, Ohio.

The Evaluation Procedure outlined in the introduction has been successfully used in the seismic evaluation of the components and distribution systems of a major nuclear facility. Typical forms used by the individual members of the Delphi team to record the condition, seismic characteristics and capabilities, recommended additional evaluation and design fixes for the components and systems are presented as shown in Figures 1a and 1b.

In Figures 1a and 1b the item being evaluated is identified and an acceleration level versus probability of failure table is prepared by each Delphi team member. Figure 1 also is used to assemble a summary of all Delphi team members observations. The team members prepare notations for each item in the following categories:

- (a) physical characteristics of the item (type of support or anchorage, dimension, weight, material used, etc.)
- (b) dominate or fundamental frequency of item
- (c) description of expected first failure mode
- (d) current condition of item (degree of corrosion, bolt tightness, weld appearance, etc.)
- (e) potential damaging effects from surrounding components
- (f) potential hazard if component fails other than system hazard
- (g) recommended analysis, tests or modifications to the item
 - (1) as a function of acceleration level
 - (2) independent of acceleration level

which will assist in qualifying the acceleration values selected and also will provide a recommendation for further evaluation or modification. The acceleration levels versus probability of survival can be based on design code criteria or actual expected failure to perform its required function and maintain leak-tight or structural integrity. In general, the failure criterion considered is compared to applicable design code allowables since this would be the criterion used if a detailed analysis were performed.

A composite of these individual forms is prepared which provides a consensus of the findings of the group as shown in Table 1.

In Table 1 in addition to summarizing the individual team member acceleration level estimates, mean values and standard deviations of the Delphi team estimates are shown. It is further assumed that the g levels to cause failure are distributed in a log normal manner. Given this assumption, it is possible using the probability of failure curve equal to 0.1 given in Figure 6, to determine lower bound probability of failure for the 90 percent probability of survival estimate equal to 0.01 probability of failure. The acceleration value established in this manner as shown in the column marked x-Ks of Table 1 is compared to the applicable response spectral curve value given in Figures 2 through 5 at the estimated dominate frequency and applicable damping values. If the x-Ks column acceleration value for 90 percent probability of survival exceeds the applicable spectral curve value then the item is said to be qualified seismically.

However, it should be noted that work sheet notation 7.2 would have to be addressed regardless of acceleration levels determined.

CONCLUSIONS

It is believed the Delphi procedure and its application as described in this paper provides a method for performing a plant and item specific seismic reevaluation of all components classified as seismic Category I in nuclear power plants in a technically adequate and cost and time effective manner.

TABLE 1
SUMMARY OF ESTIMATED LIMITING ACCELERATION, G, AT THE CENTER OF GRAVITY OF COMPONENT

SYS. I.D.	FUND. FREQ. Hz.	PROB. OF SURV	INDIVIDUAL TEAM MEMBER ESTIMATES, G'S									
			1		2		3		4		5	
			H	V	H	V	H	V	H	V	H	V
1a.	15.	10%	1.5	1.2	3.	5.	2.	1.5	3.	2.	2.00	1.75
		50%	0.8	0.8	1.5	3.5	0.85	1.0	2.	1.4	1.50	1.50
		90%	0.3	0.6	0.5	2.	0.5	0.75	1.	.7	.75	.50
1b	4.0	10%	3.0	2.0	4.0	6.0	3.0	2.0	2.0	1.5	1.50	1.00
		50%	2.0	1.5	1.0	4.0	2.0	1.0	1.0	.7	.75	.50
		90%	1.0	1.0	1.0	2.0	1.5	0.75	0.7	0.5	0.50	0.33

MEAN		X-K*s		STANDARD DEVIATION		REMARKS
H	V	H	V	S _H	S _V	
2.30	2.29	1.60	1.04	.67	1.54	4% Damping
1.33	1.64	.83	.76	.50	1.08	Fig. 2 & 3 Applicable Spectra
.61	.91	.37	.42	.27	.62	.36gH; .19gV
						..OK
2.7	2.5	1.73	1.02	.97	2.00	3% Damping
1.55	1.54	.95	.57	.62	1.43	Fig. 4 & 5 Applicable Spectra
0.94	0.92	0.57	0.40	0.38	0.66	1.4gH; .63gV
						See 7.1

*Coefficient K is determined such that x-Ks gives a 10 percent probability of being less than for the Log Normal distribution as shown in Figure 6. This results in the limiting case of 0.99 probability of survival or 0.01 prob. of failure.

x = sample mean

s = sample standard deviation.

FIGURE 1a TYPICAL COMPOSITE WORK SHEET USED FOR
JUDGEMENTAL EVALUATION OF COMPONENTS SEISMIC RESISTANCE

Data Package Number 1
Component Number a.

System Title Fire Suppression Systems
Component Title Tank - Light Water Concentrate

Horizontal resultant and vertical acceleration levels input to component that it is adjudged capable of carrying within applicable code allowables to first failure mode with probabilities noted.

Probability, Percent	g Level	
	Horizontal	Vertical
90	.61	.91
50	1.33	1.64
10	2.30	2.29

1. Comments on physical characteristics (type of supports, attachments, anchorage, dimensions, weight, material, etc.).
2. Estimate of dominant or fundamental frequencies.
3. Description of expected first failure mode.
4. Comments on the condition of the component and its support and anchorage as to the degree of corrosion, bolt tightness, etc.
5. Comments on potential damaging effects of surrounding components.
6. Comments on potential hazards other than system effects if component fails.
7. Recommended modifications, tests, analyses, etc.
 - 7.1 Comments necessary to assure design adequacy as a function of acceleration level.
 - 7.2 Comments necessary to assure design adequacy independent of acceleration level.

TYPICAL COMMENTS

1. Tank is supported by X braced cradle consisting of 4 column legs restrained by 1-5/8" expansion anchor per leg. Tank attached to cradle by two 1/2" / bar straps. No positive anchor between cradle and tank. Longitudinal restraint by friction only. Tank weight is 2500 lbs. with center of gravity located 3.0 above floor.
2. Support system in tranverse direction is rigid. Transverse frequency of tank is greater than 15 Hz. In longitudinal direction restrained only by friction of two 1/2" / bar straps; frequency less than 5 Hz. assuming straps acting.
3. Anticipated first failure mode would be by sliding of tank in cradle in longitudinal direction and anchor pull out.
4. Installed in 1973, tank surface is painted and no corrosion is apparent; some corrosion around base plates of column legs.
5. Tank is threatened by non-seismically qualified overhead piping and G-5A tank from west.
6. None identified.
- 7.1 Positive anchorage should be provided between the tank and support cradles.

FIGURE 1b TYPICAL COMPOSITE WORK SHEET USED FOR
JUDGEMENTAL EVALUATION OF COMPONENTS SEISMIC RESISTANCE

Data Package Number 1
Component Number b.

System Title Light Water Fire Suppression Systems
Component Title Piping - Light Water

Horizontal resultant and vertical acceleration levels input to component that it is adjudged capable of carrying within applicable code allowables to first failure mode with probabilities noted.

Probability, Percent	g Level	
	Horizontal	Vertical
90	.94	.92
50	1.55	1.54
10	2.7	2.5

1. Comments on physical characteristics (type of supports, attachments, anchorage, dimensions, weight, material, etc.).
2. Estimate of dominant or fundamental frequencies.
3. Description of expected first failure mode.
4. Comments on the condition of the component and its support and anchorage as to the degree of corrosion, bolt tightness, etc.
5. Comments on potential damaging effects of surrounding components.
6. Comments on potential hazards other than system effects if component fails.
7. Recommended modifications, tests, analyses, etc.
 - 7.1 Comments necessary to assure design adequacy as a function of acceleration level.
 - 7.2 Comments necessary to assure design adequacy independent of acceleration level.

TYPICAL COMMENTS

1. 3" pipe sch. 40; lateral restraint by 2" tie rods--8' long on 40' centers; vertical supports on 12' centers 1/2" - 3/8" hanger rods--friction clamped to existing supports trapeze above. These existing trapeze are 6 WF 30 supported by 2 - 1/2" rod hangers approximately 12 ft. long from ceilings. Effective horizontal restraints only in lateral direction. No restraint along axis of pipe.
2. Fundamental frequency less than 4.0 Hz.
3. Failure of vertical trapeze supports; and connection failure of branch lines (approximately 1" lines) and cast iron fittings.
4. Gaps exist in the pipe clamps used in the rod hangers; pipe joints are tight, no external corrosion noted. Bolt connections of existing lateral supports look inadequate in strength. Use of beam clamps on vertical rods is negative feature.
5. The trapeze rod hangers support additional piping and conduits which will affect the performance of the subject pipe. Piping is threatened by process piping above having no seismic restraints which are potential seismic missiles.
- 7.1 Replace vertical pipe support friction clamps with positive anchors and provide protection or evaluate hazard of pipe installed above to insure no potential for failure due to interaction with overhead piping. Improvement of lateral bracings, particularly in the longitudinal direction, based on analytical evaluations of the piping should be undertaken. Replace cast iron fittings and provide seismic support, or provide three degree restraints at each fitting (cast iron integrity would still be question).

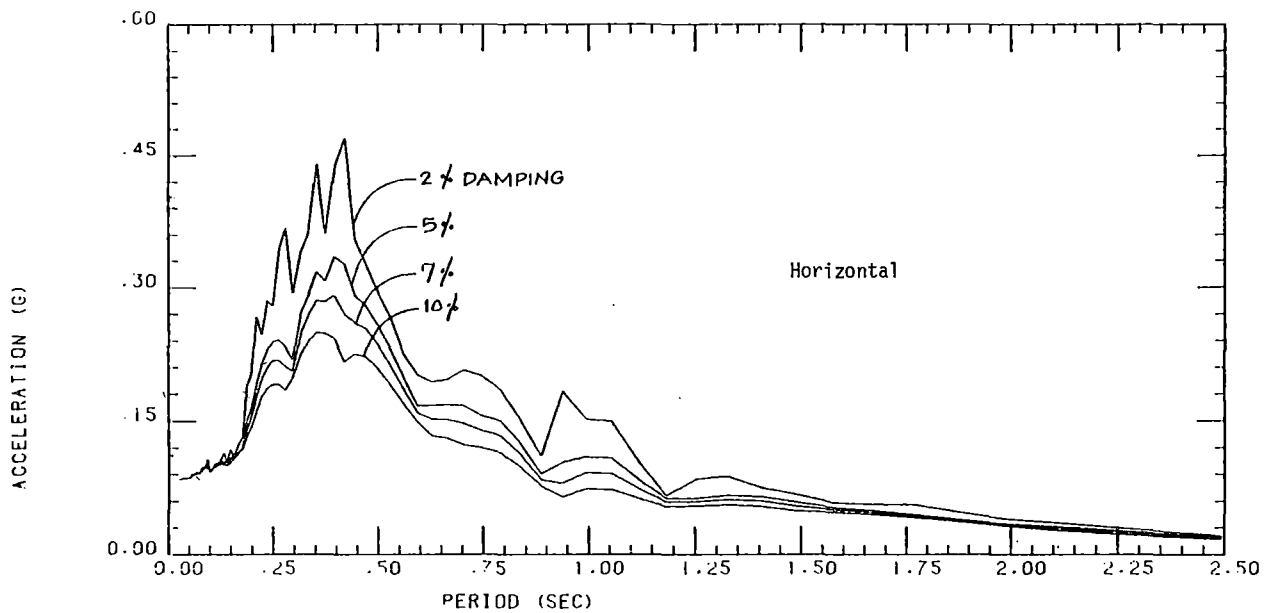


FIGURE 2 SPECTRUM VALUE AT NODAL POINT 187
0.02, 0.05, 0.07, 0.10 DAMPING RESPECTIVELY

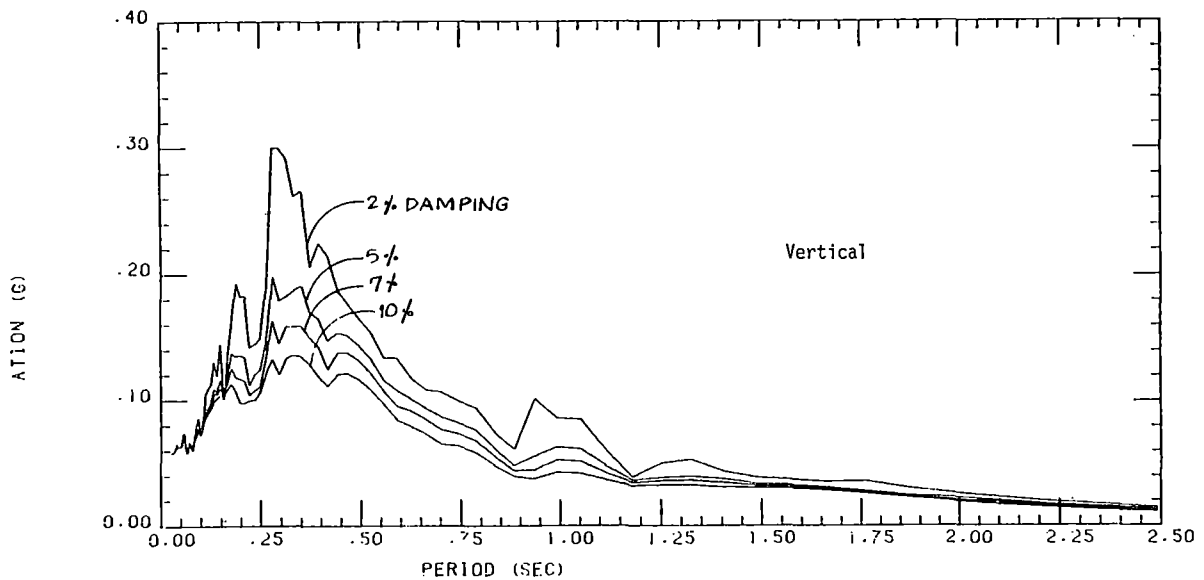


FIGURE 3 SPECTRUM VALUE AT NODAL POINT 185
0.02, 0.05, 0.07, 0.10 DAMPING RESPECTIVELY

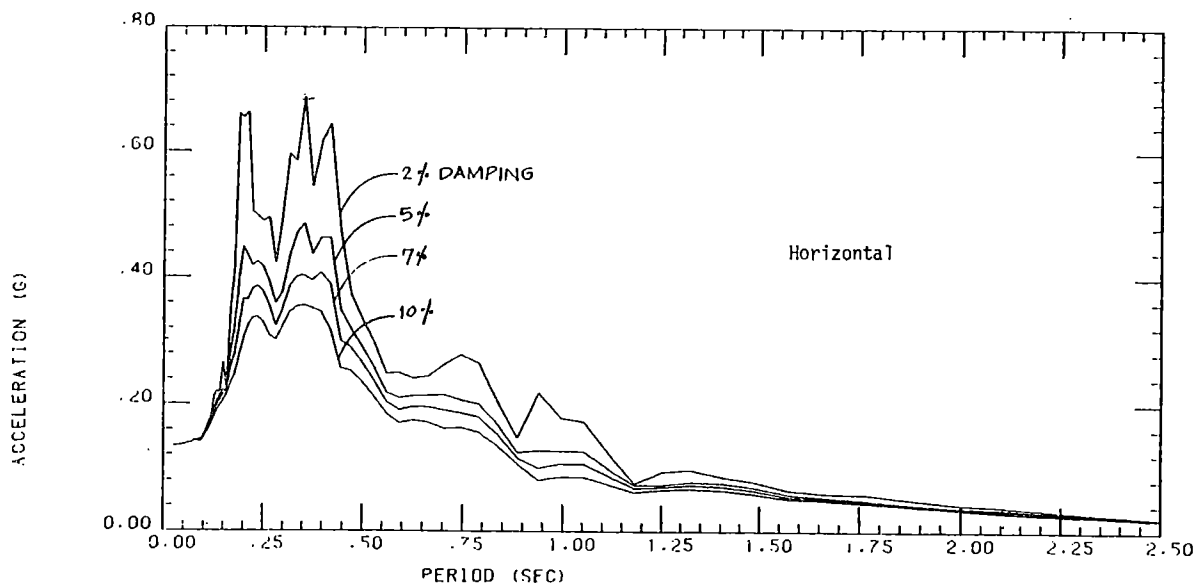


FIGURE 4 - SPECTRUM VALUE AT NODAL POINT 185
0.02, 0.05, 0.07, 0.10 DAMPING RESPECTIVELY

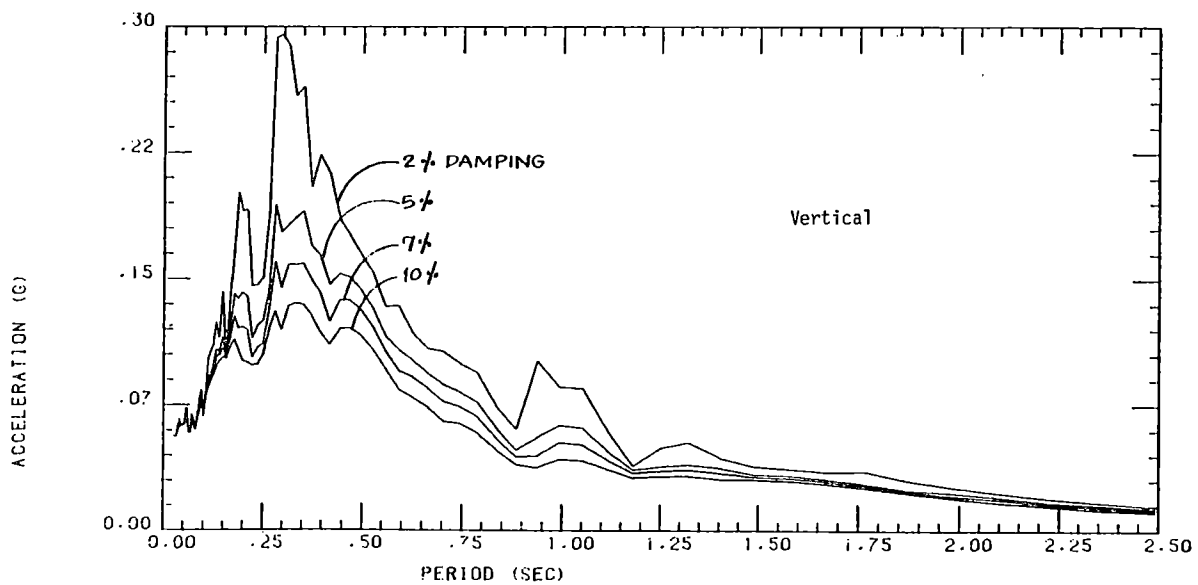


FIGURE 5 SPECTRUM VALUE AT NODAL POINT 187
0.02, 0.05, 0.07, 0.10 DAMPING RESPECTIVELY

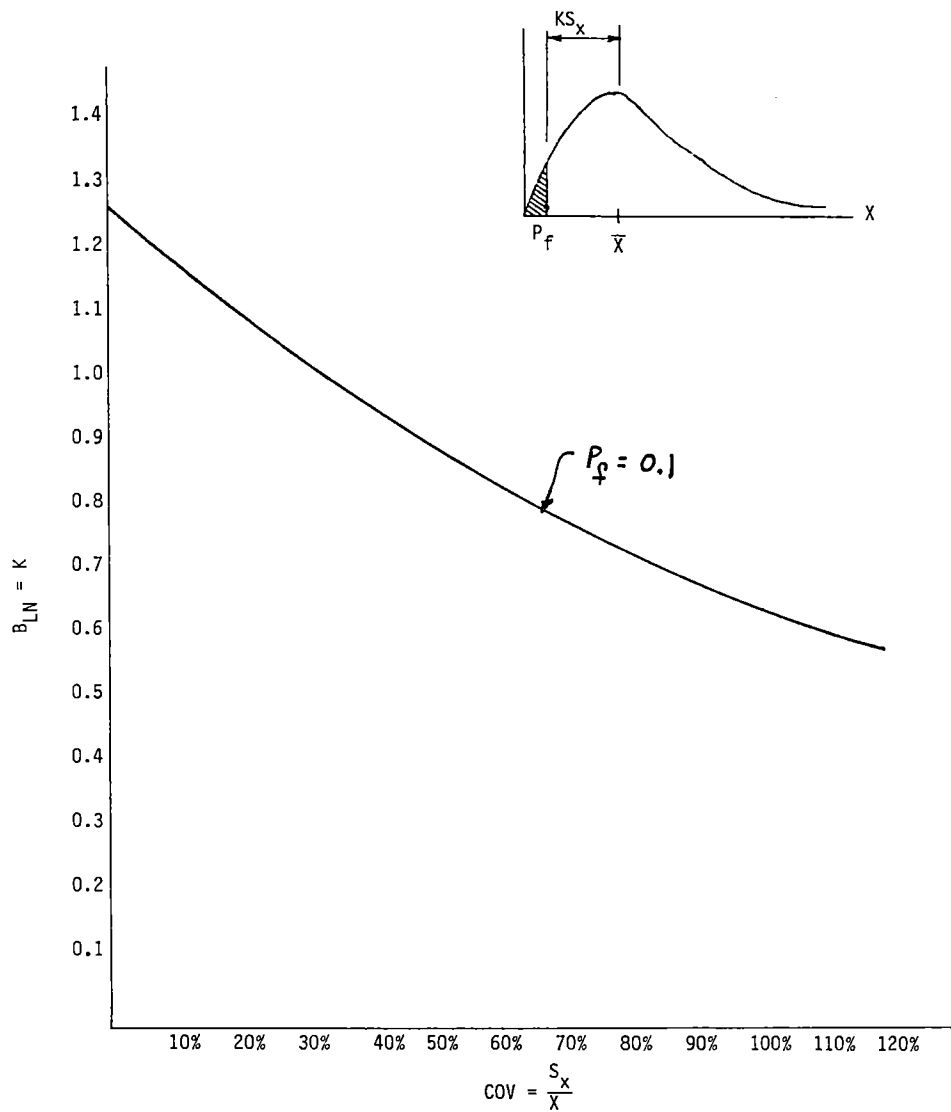


Figure 6 Number of Standard Deviations from The Mean Required to Give 10 Percent Probability of Variation of Being less Than as a Function of the Coefficient.

LARGE-SCALE, TWO-PHASE JET IMPINGEMENT EXPERIMENTS AT MARVIKEN

D.C. Slaughterbeck and D.C. Mecham
Intermountain Technologies Incorporated
Bx 1604, Idaho Falls, Idaho 83401, USA

J.E. Collén and O. Sandervåg
Studsvik Energiteknik AB
S-611 82 Nyköping, Sweden

ABSTRACT

Principal results are summarized from the Jet Impingement Test Project, the fourth in a series of large-scale, multinational, nuclear safety experiments in the Marviken power station [1]. Tests in this project involved the investigation of the behaviour of large-scale jets in the subcooled, saturated, and steam flow regimes as they exhaust beyond the choking plane. Two types of experiments were conducted. One type involved the measurement of the characteristics of freely expanding jets, and the other type concerned the measurement of loads on different targets placed in the jet stream. Comparisons of measured and theoretical loads are presented.

INTRODUCTION

The behaviour of large two-phase, critical flow jets as they exhaust beyond the choking plane is of interest in nuclear power plant design and safety analyses. In the beginning of 1980 a group of organizations from different countries agreed to jointly undertake a comprehensive program aimed at increasing their knowledge about jet behaviour. This program provided all participants with information from different small scale jet behaviour experiments and other related projects performed by the participants (in kind contributions). To quantify the actual loads from large scale jets, and to provide a basis for scaling data from laboratory experiments, the group agreed to jointly perform a complementary series of large scale tests in the Marviken testing facility. This paper summarizes the results of these tests.

The principal objective of the Jet Impingement Tests (JIT) project was to provide quasi-steady experimental data from a large scale facility on the behaviour of two phase jets as they exhaust beyond the choking plane into the containment. Free expansion tests were performed which provided information about the axial radial pressure distributions in the jet for different flow regimes, and jet impingement tests were performed which focused on the determination of the total force and the force distribution on targets in the jet stream. These data, together with data from small scale experiments, provide individual participants the information necessary to develop or verify analytical or empirical models used in estimating jet impingement loads in the safety analysis of nuclear power generating stations.

TEST FACILITY AND MEASUREMENT SYSTEM

The Marviken station was originally built to operate as a boiling heavy water direct cycle reactor with natural circulation. The station had been completed up to acceptance testing, including pre-operational light water tests when it was decided in 1969 not to complete the reactor for operation. Portions of the station were modified and the station has been used as an international test facility since 1971.

Four major components were utilized in the JIT project:

- the reactor vessel which had an internal height of 24.5 m, inside diameter of 5.2 m and a volume of about 420 m³
- a discharge pipe (about 8 m long and 750 mm dia) connected to the bottom of the vessel which contained a ball valve, rupture discs, instrumentation, and exit nozzles from 200 to 509 mm in diameter
- a jet test section which varied with the type of test. Four general configurations were used as illustrated in Figs 1 and 2
- the containment building which served as the structural housing for the experiments.

The measurement system consisted of instruments, signal conditioning units, data recording/reproducing parts and a process computer. In total, up to 169 data channels were used for individual tests. Pressure, differential pressure, temperature, density, force, and acceleration measurements were recorded using a pulse code modulation system. The transducers for pressure and differential pressure measurements were of the strain gauge type. Chromel-alumel thermocouples were used for temperature measurements. Density was measured in the discharge pipe (above the ball valve) using a three beam gamma densitometer system. Strain-gage force transducers (load cells) were used for force measurements and piezoelectric accelerometers were used for acceleration measurements.

TEST DESCRIPTIONS

Two broad categories of tests were performed in the JIT project, the free-jet tests and the tests directed toward instrumented targets. Table I summarizes the important parameter ranges from the two test groups.

Tests were conducted by first heating the vessel water to a specified temperature and pressure level. Rupture discs were then burst and the vessel contents were discharged through the nozzle to form the jet. For tests simulating water-line breaks, an initial temperature profile was established in the vessel such that a layer of high temperature (saturated) water was over the region of low temperature (subcooled) water. With the discharge pipe entrance in the region of subcooled water, the initial effluent stayed subcooled (as all flashing occurred in the saturated water zone) until the vessel pressure decreased to the saturation pressure corresponding to the low temperature water. In this way, distinct subcooled, saturated, and steam flow regimes were produced in the same test. For tests simu-

lating steam-line breaks, the discharge pipe inlet (stand-pipe) was raised through the vessel to the steam dome. Level swell was measured by a series of differential pressure probes in the vessel to determine if the mixture level reached the vicinity of the discharge pipe entrance.

TEST RESULTS AND INTERPRETATIONS

The principal result of the JIT project was the collection of the free jet and jet impingement data together with the flow related data necessary to correlate the jet behaviour with upstream conditions. The interpretations reported here represent only a very small fraction of the data and illustrate some of the more obvious trends.

Several observations have been made concerning the measured free jet pressure profiles. By combining the static pressure field measurements into a two-dimensional diagram, isobars can be drawn as shown by the example in Fig 3. In these curves, the local static pressure has been normalized by the ambient containment pressure. Dissipation of the static pressure field occurred in the close vicinity of the nozzle exit, and was dependent on the flow conditions at the nozzle entrance. Static pressure gradients in the axial direction were highest in the first nozzle diameter downstream of the exit. Likewise the highest gradients in the radial direction were observed in the first nozzle diameter away from the jet centerline.

Beyond the high static pressure region close to the nozzle exit, the jet overexpanded to pressures less than the surrounding containment pressure in both the axial and radial directions; they recovered to containment pressure at still further distances from the nozzle exit. Isobars labeled with values below 1.0 in Fig 3 indicate the region where the jet was overexpanded.

Dissipation of the total pressure field (Figs 4 and 5) occurred at somewhat farther distances from the nozzle exit than the static pressure field. In the immediate vicinity of the nozzle, the difference between the total and static axial pressure profiles was nearly constant with increasing axial distance until the elevation where the static pressure had decreased to the surrounding ambient pressure.

Four tests were performed to investigate the pressure profiles and force characteristics resulting from the jet impingement on a flat, circular plate with a diameter of 1980 mm. Three of these tests involved essentially similar blowdowns at different distances to the flat plate. In each of these tests, the nozzle inlet conditions covered a range of subcooled, saturated and steam flow conditions. The other test with impingement on a flat plate involved a steam-only blowdown. Distances to the flat impingement plate were varied from 643 to 2060 mm.

Total forces measured in the tests were compared to theoretical values by dividing the time-dependent forces by the product of the nozzle exit area and the difference between the nozzle inlet stagnation pressure and ambient pressure as shown in Figs 6 and 7. This dimensionless force is termed the thrust coefficient. Moody [2] showed that for incompressible isentropic flow, the thrust coefficient can approach 2.0. This is in good agreement with the experimentally determined maximum values near 2.0 for high subcooling as shown in Fig 6. For an ideal gas, and assuming a constant isentropic exponent of 1.3, Moody determined the thrust coefficient could approach 1.26. Again, this is in good agreement with the experimentally determined values for steam flow as shown in Fig 7.

Fig 8 shows the thrust coefficient for jet impingement into a cylindrical cavity. It is interesting that values of nearly 5.0 were computed for the early subcooled regime. The large downward force reflects a significant pressurization of the cavity relative to containment pressure, indicating that conditions in the cavity were not fully expanded. In fact, choking likely occurred near the exit of the cavity as well as in the nozzle.

Thrust coefficients were calculated for impingement on a horizontal pipe as illustrated in Fig 9. Except for the initial impact of a cold water plug, the coefficients were less than 0.1. The calculated coefficients are consistent with estimates based on the impingement plate results and assuming the pipe intercepts about 10 % of the jet.

A large number of high quality data was collected from large scale free-jet and jet-impingement tests that fulfilled the project objectives. Dissipation of the jet static pressure occurred in the close vicinity of the nozzle exit. In both types of tests, it was found that the dissipation of the jet occurred faster for two-phase flow than for single phase flow. Calculated thrust coefficients for the flat plate impingement tests were consistent with maxima predicted by incompressible isentropic flow theory.

ACKNOWLEDGEMENTS

This paper as well as the Marviken full scale jet impingement tests were sponsored by the following organizations:

Ontario Hydro, Canada

Electric Power Research Institute, USA

Studsvik Energiteknik AB, Sweden

KEMA, The Netherlands

Technical Research Centre of Finland, Finland

United States Nuclear Regulatory Commission, USA

The Company Partnership, Japan

Comitato Nazionale per L'Energia Nucleare, Italy

AMN Ansaldo Impianti, Italy

REFERENCES

1. The Marviken Full Scale Jet Impingement Tests, Summary Report, MXD-301, Studsvik Energiteknik AB, Sweden, March 1982.
2. F. J. MOODY "Prediction of Blowdown Thrust Forces", ASME 69-HT-31, August 1969.

Table 1 Summary of free-jet and jet impingement parameter ranges

FREE JET TESTS

Nozzle diameters - 200 to 509 mm

Subcooled flow regime

Nozzle inlet pressures - 2.9 to 4.8 MPa

Nozzle inlet subcooling - 0 to 41°C

Saturated flow regime

Nozzle inlet pressures - 2.6 to 4.2 MPa

Fluid qualities - 0 to 1.0

Steam flow regime

Nozzle inlet pressures - 1.1 to 4.8 MPa

Fluid qualities - ~ 1.0

JET IMPINGEMENT TESTS

Nozzle diameters - 200 to 509 mm

Distances to target - 643 to 2060 mm

Subcooled flow regime

Nozzle inlet pressure - 3.1 to 5.1 MPa

Nozzle inlet subcooling - 0 to 32°C

Saturated flow regime

Nozzle inlet pressures - 2.5 to 4.1 MPa

Fluid qualities - 0 to 1.0

Steam flow regime

Nozzle inlet pressures - 1.1 to 4.6 MPa

Fluid qualities - ~ 1.0

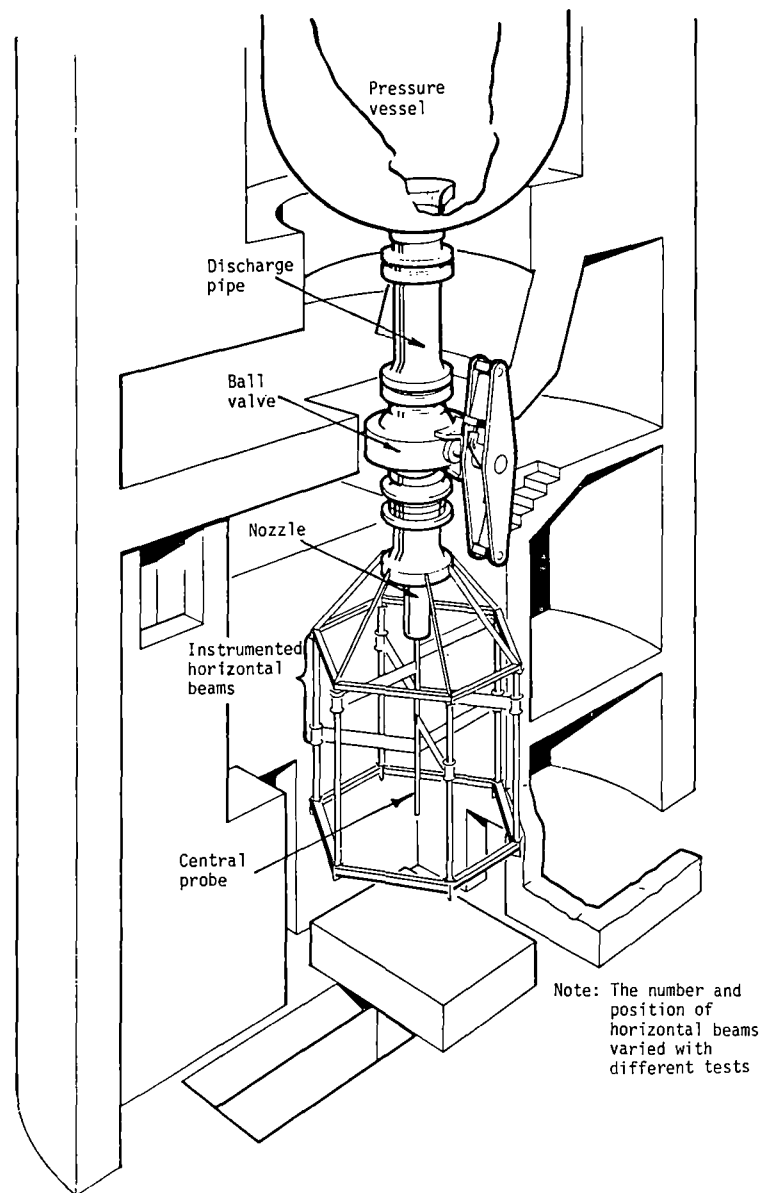


Fig. 1. Arrangement for the free jet expansion tests

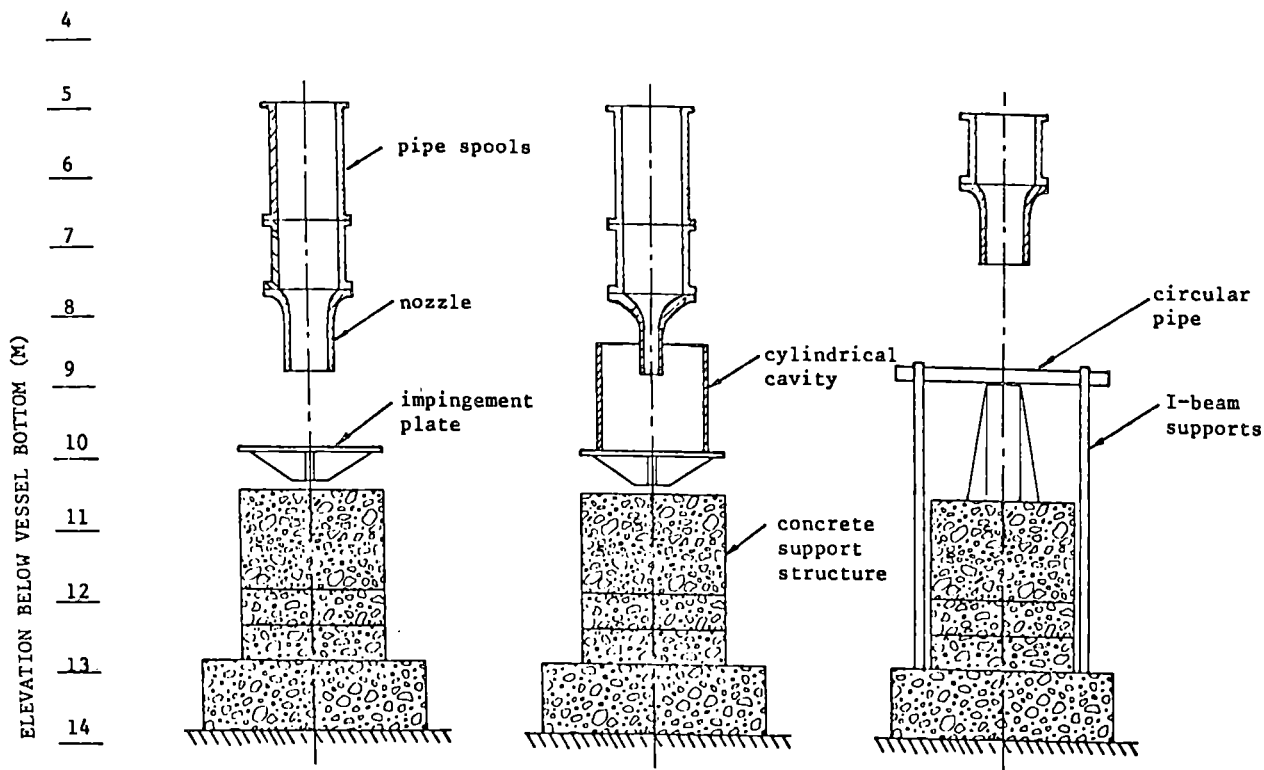


Fig. 2. Typical configurations for the jet impingement tests

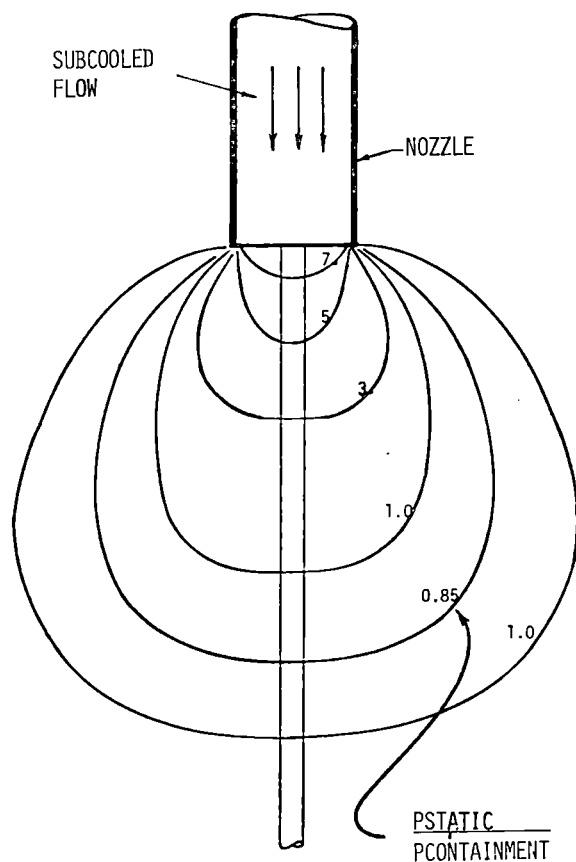


Fig. 3. Illustrative sketch showing static pressure isobars below nozzle for typical free jet test with sub-cooled flow

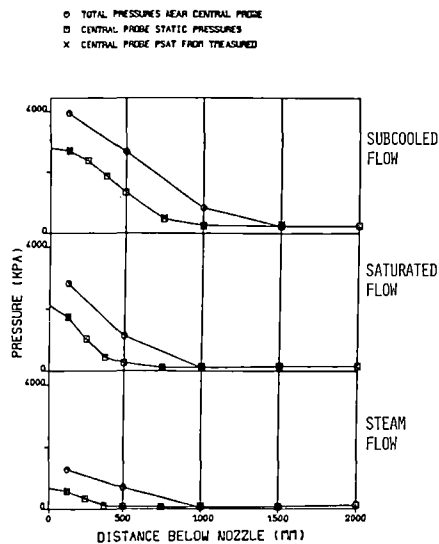


Fig. 4. Typical total and static axial pressure profiles for the sub-cooled, saturated, and steam regimes

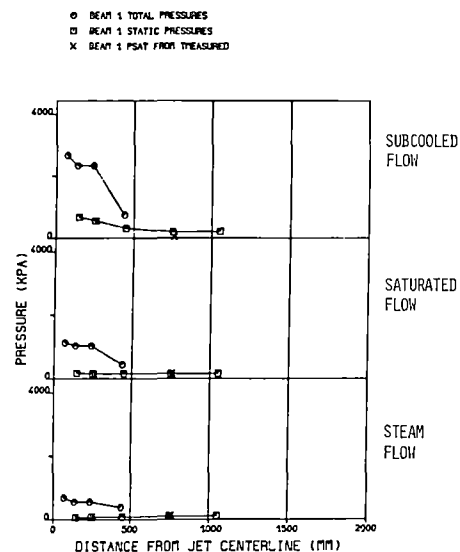


Fig. 5. Typical total and static radial pressure profiles for the sub-cooled, saturated, and steam flow regimes

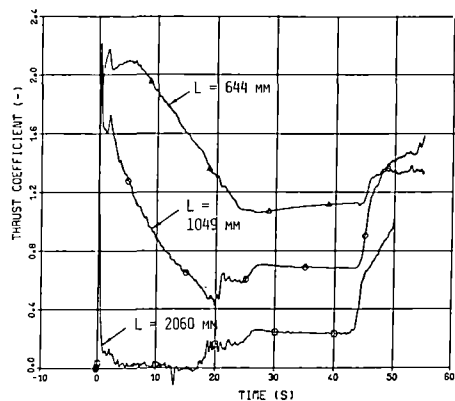


Fig. 6. Comparison of thrust coefficients as a function of the distance to the impingement plate

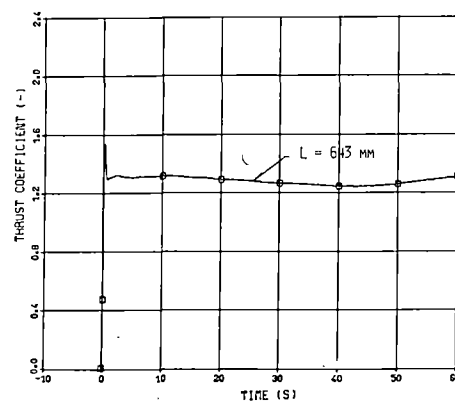


Fig. 7. Thrust coefficient for steam test only

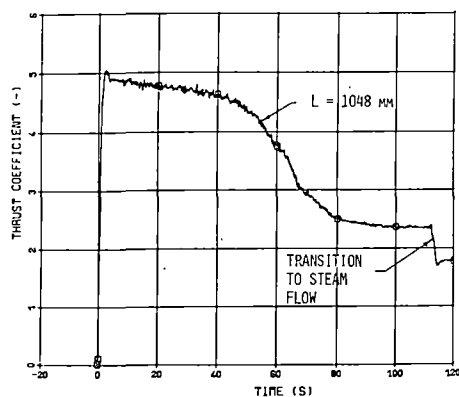


Fig. 8. Thrust coefficient for impingement into cavity

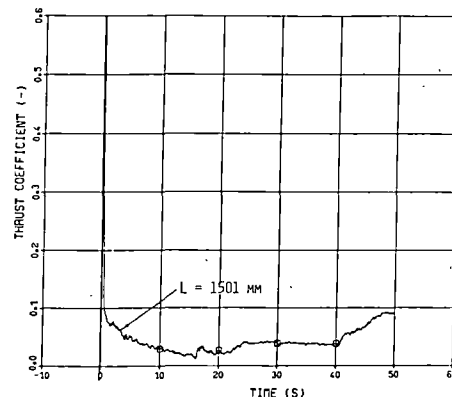


Fig. 9. Thrust coefficient for pipe impingement

CALCULATION OF STEAM-WATER JET IMPINGEMENT FORCES

Bryan A. Kashiwa and Thomas D. Butler
Theoretical Division, Group T-3
Los Alamos National Laboratory
Los Alamos, NM 87545 USA

ABSTRACT

Numerical simulations of the steam-water jet emitted from a hypothetical rupture in the primary coolant circuit have been performed. Computed jet impingement loadings are compared to both large-scale experimental data and forces computed via standard methods. Details of the constitutive relations developed for expression of the transfer of mass and momentum in a two-field, steam-water model are discussed. The existence of a super-heated, solid-liquid core in the center of the jet under subcooled discharge conditions is identified. A mechanism for the initiation of boiling, which allows such a phenomenon to occur, is proposed.

INTRODUCTION

Considerable attention has been directed toward questions of nuclear reactor safety in recent years by a large number of researchers. For the most part, the internal fluid flow events, following a hypothetical loss-of-coolant accident have been the subject of many theoretical and experimental studies. The focus of this paper is on the external effects of the steam-water jet, formed by the discharge of compressed water into the reactor containment, through a postulated rupture in the high-pressure piping of a light water reactor.

Our goal is to better the understanding of multifield flow phenomena by way of systematic scientific studies. We endeavor to explain the macroscopic nature of the steam-water jet on the basis of the microscopic interactions between and among the two phases. The approach has been to test viable interaction modes by comparing flow simulations, using modern multifield flow computational techniques, to experimental data. Such comparisons have given valuable guidance to the determination of the important interphase exchange effects in the steam-water jet.

American National Standards Institute/American Nuclear Society standard ANSI/ANS 58.2 (1980) [1] was established for the purpose of providing a design base for those structures and components that ensure public safety in the event of ruptured piping. Among the effects of postulated pipe failures considered in this standard is the impingement load experienced by an obstacle in the path of the two-phase jet emitted from a ruptured pipe.

This paper presents one of our most recent methods used in the numerical modeling of steam-water flows. Results are shown in comparison to detailed experimental data as well as results of calculations using the methods of ANSI/ANS 58.2. A full account of the work leading up to the model presented here is given in Ref. 2.

THE NUMERICAL MODEL

The two-fluid computer code K-FIX [3,4] has been used for the solution to the problems presented here. K-FIX is an Eulerian, finite-difference code which solves a complete set of field equations for each of two fluids. The field equations are coupled through the condition of pressure equilibrium between the two fluids and through exchange of mass, momentum, and energy between fields. The following is a discussion of the specific exchange functions developed for use in the K-FIX code as applied to the steam-water jet problem.

Mass Exchange

Rivard and Travis [5] have developed a nonequilibrium vapor production model in homogeneous-velocity, critical, steam-water flows. Here, their model for nonequilibrium mass exchange between liquid and vapor is extended and the coupled interaction of nonequilibrium momentum exchange (inhomogeneous-velocity) is added.

The discussion of the new mass and momentum exchange model is facilitated by the visualization of three two-phase flow regimes distinguished by the vapor volume fraction θ (volume of vapor per unit total volume of mixture). For $\theta < \theta_b$, the flow is termed bubble flow and envisioned to consist of separate vapor bubbles moving relative to a continuum of their own liquid. For $\theta_b < \theta < \theta_d$ the flow is termed churning flow, where neither a continuous liquid nor a continuous vapor can be distinguished. For $\theta > \theta_d$, the flow is termed droplet flow. Further definition of the character of these three flow regimes leads directly to the constitutive relations used for the calculations presented here.

The bubble flow regime is defined to consist of isolated bubbles moving relative to the liquid. Since the mass exchange rate is determined by the rate at which heat can be supplied from the liquid to the liquid-vapor interface, the mass exchange rate for a bubble can be derived as a function of relative velocity between the bubble and the liquid. Consider a single, spherical bubble with radius r_b and surface temperature T_s , moving in its liquid at temperature T_ℓ with relative velocity u_r , as shown in Fig. 1. An energy balance between points 1 and 2 in the liquid reveals the amount of energy per unit time E , transferred from the liquid to the bubble

$$E = (\pi r_i^2) u_r \rho_\ell c_\ell (T_\ell - T_s) ,$$

where ρ_ℓ is the liquid density, c_ℓ is the liquid specific heat at constant pressure, and r_i is the interaction radius, which relates to the thermal interaction depth d as

$$\pi r_i^2 = 2\pi r_b d .$$

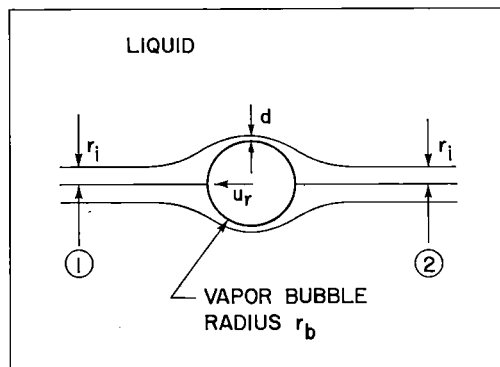


Fig. 1. Spherical vapor bubble moving relative to its liquid.

The thermal interaction depth is estimated by

$$d = \left(\frac{\alpha_l r_b}{u_r} \right)^{1/2}$$

where α_l is the thermal diffusivity of the liquid. In terms of a fraction of bubble cross-sectional area F , this is

$$F = (r_l/r_b)^2 \quad \text{or} \quad F = 2 \left(\frac{\alpha_l}{u_r r_b} \right)^{1/2}. \quad (1)$$

For a system of N bubbles per unit volume, all of radius r_b , we have

$$N = \frac{3\theta}{4\pi r_b^3}. \quad (2)$$

Hence, the mass exchange rate per unit volume J is

$$J = \frac{3}{4} F \frac{\theta}{r_b} \frac{\rho_l c_l}{\lambda} u_r (T_l - T_s). \quad (3)$$

The churning flow regime is further defined as a flow arrangement in which there is rapid mixing between liquid entities, promoted by a chaotic process of coalescence, fragmentation, and collisions between liquid parcels. The thermal transport resulting from this is so great that thermal equilibrium is maintained between the liquid and the vapor. This implies that the mass exchange rate must be large enough to maintain nearly equal liquid and vapor temperatures. To achieve this the expression

$$J = J^*(1 - \theta)(T_\ell - T_s) \quad (4)$$

is used, where J^* is a coefficient chosen such that thermal equilibrium is maintained.

In the droplet flow regime frequent collisions do not occur, so that a heat transport rate from the liquid to the liquid/vapor interface much smaller than that found in churning flow can be expected. If this heat transport rate is controlled primarily by conduction, which would be true at least until some internal droplet circulation is developed, the mass exchange rate per unit volume can be approximated by

$$J = \frac{\rho_\ell c_\ell}{\lambda} \frac{\alpha_\ell}{r_d} (T_\ell - T_s) A \quad (5)$$

in which r_b is a dimension characteristic of the liquid entities. For the area per unit volume A , we define

$$A = \frac{3\theta^*}{r^*} \quad (6)$$

where

$$\begin{aligned} \theta^* &= \theta, \quad r^* = r_b, \quad \theta < 0.5 \\ \theta^* &= (1 - \theta), \quad r^* = r_d, \quad \theta > 0.5 \end{aligned} \quad (7)$$

Hence, the mass exchange rate can be summarized

$$J = \begin{cases} \frac{F}{4} \frac{\rho_\ell c_\ell}{\lambda} u_r (T_\ell - T_s) A & \theta < \theta_b \\ J^*(1 - \theta)(T_\ell - T_s) & \theta_b < \theta < \theta_d \\ \frac{\rho_\ell c_\ell}{\lambda} \frac{\alpha_\ell}{r_d} (T_\ell - T_s) A & \theta > \theta_d \end{cases} \quad (8)$$

For the values of θ forming the boundaries between the flow regimes defined, $\theta_b = 0.6$ and $\theta_d = 0.99$ are used. These are values which give about the best fit to the large-scale data available; it is found that the results are not strongly sensitive to the values of θ_b and θ_d chosen.

Momentum Exchange

The momentum exchange function utilized is taken directly from Daly and Harlow [6], who give for the momentum exchange rate per unit volume K ,

$$K = \frac{3}{4} \theta (1 - \theta) \rho_g \frac{u_r}{r^*} \quad , \quad (9)$$

where ρ_g is the vapor density. This is accurate for dispersed, uniform spherical particles carried by a gas at large Reynolds number. For bubbles in a liquid, this is not accurate, but is used nonetheless throughout all flow regimes with good success. The reason for this is that there is little relative motion between fields in bubble flow, so that the accurate determination of K there is not required.

With this, the only remaining parameter to specify is r^* . This specification is done indirectly by use of the entity number per unit volume N . Equation (2) can be rearranged as

$$r^* = \left(\frac{3\theta}{4\pi N} \right)^{1/3} \quad . \quad (10)$$

For bubble flow, Rivard and Travis [5] use $N = 10^3 \text{ cm}^{-3}$ which is the value adopted here. For churning flow, an initially very small drag per unit volume K is expected. This is consistent with a large mass exchange rate promoted by frequent collisions and fragmentations of liquid entities. This means large liquid entities must exist for $\theta \sim \theta_b$, meaning that the entity number N_d at this point must be small. A value of $N_d = 1 \text{ cm}^{-3}$ is found to sufficiently decouple the flow fields at $\theta = \theta_b$. We here assume that in this regime, droplet coalescence and fragmentation rates exactly balance and thereby obtain an expression for N given by

$$N = N_d \left(\frac{\rho_g}{\rho_{g_1}} \right) \quad (11)$$

where ρ_{g_1} is the vapor density at $\theta = \theta_d$. These expressions for r^* and N assume that inertial effects preclude the flow reaching a Weber number equilibrium.

When the churning flow field is confined by the wall of a pipe, it is found that much larger K than that given by Eqs. (9) through (11) is needed. In this circumstance the result of Eq. (9) is simply multiplied by a factor chosen large enough to yield a homogeneous velocity field. One rationale behind this is that the additional confinement of the pipe wall restricts the vapor from escaping past the liquid with sufficient ease to allow much slip between fields to develop.

THE CALCULATIONS

Experiments have been performed at the Marviken power station in Sweden, which provide the large-scale data for comparison to these calculations [6]. In these experiments the reactor pressure vessel was allowed to discharge through a converging nozzle by way of a vertical pipe. An instrumented impingement plate was positioned with its center on the axis of the discharge pipe at a variable distance from the nozzle exit plane. As the blowdown was allowed to proceed, the vessel pressure dropped so that the initially subcooled (compressed) liquid eventually became saturated liquid, with a vapor void fraction increasing from zero to one. Data was collected for continuous change in discharge conditions ranging from subcooled to saturated liquid to steam.

One sequence of tests were carried out in which the vessel conditions were nominally identical at the start of each test, with the impingement plate spacing being the primary difference. We shall denote these by Tests A, B, and C referring to plate stand off distances of 60 cm, 105 cm, and 206 cm, respectively.

The K-FIX calculations were performed in two stages. First, a one-dimensional, variable-area calculation for the critical flow in the discharge pipe was performed. This was done by setting the high-pressure side of a one-dimensional K-FIX computational mesh equal to the measured pressure and integrating until a steady state was achieved. The second stage of the calculation involved performing a two-dimensional (axisymmetric) calculation beginning about one pipe diameter upstream of the nozzle exit plane and extending to the impingement plate. At the inflow position of the two-dimensional computational region, the flow conditions were specified using the one-dimensional results. The problem was again run until a steady state was achieved. The time required for the one- and two-dimensional calculations to reach a steady state is small compared to the time over which significant change in discharge conditions occurs in the experiments. Thus, these results represent a "snapshot" of the flow conditions at a fixed time in the blowdown.

Saturated Liquid Discharge

Because the vessel conditions in Tests A, B, and C were duplicated with precision, we were able to use a single one-dimensional critical flow calculation in combination with separate two-dimensional calculations for the analysis of saturated liquid discharge conditions. Figure 2 shows the pipe wall pressure as a function of position relative to the pipe exit for the one-dimensional calculation compared to the experimental data for Test A, during pure saturated liquid discharge. The departure in agreement near the exit plane is attributed to two-dimensional effects at that location. (In Fig. 2, P_r is a reference pressure, the value of which cannot be disclosed at this time.) Figure 3 shows the calculated vapor volume fraction contours for Test A during saturated liquid discharge; this shows the rapid manner in which the liquid is transformed to vapor upon leaving the pipe. The calculation also reveals strongly inhomogeneous velocity fields outside the pipe (not shown). Figure 4 has a plot of pressure versus radius on the surface of the impingement plate for Test A. Similar illustrations of the computed and measured results for the saturated liquid discharge period of Tests B and C are given in Figs. 5 and 6.

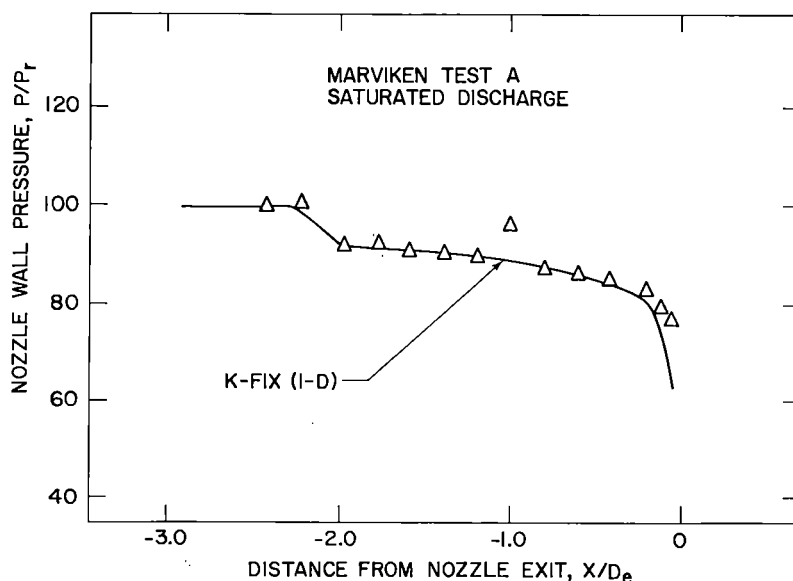


Fig. 2. Nozzle wall pressure vs axial position x for Marviken Test A, saturated liquid discharge. D_e is the nozzle diameter at the exit plane.

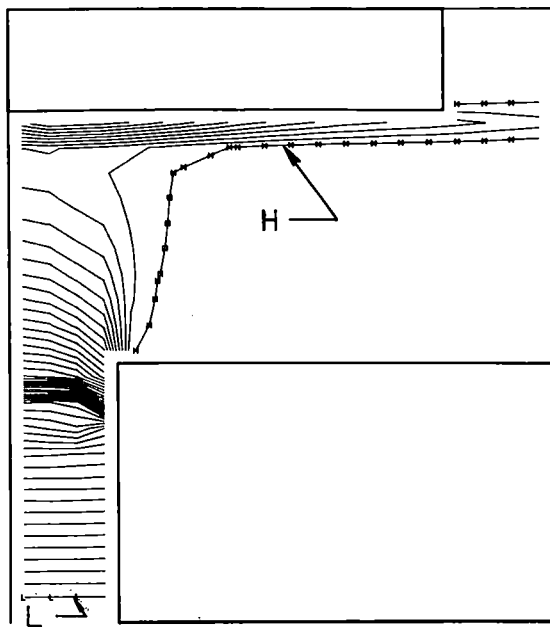


Fig. 3. K-FIX vapor void fraction contour plot for Marviken Test A, saturated liquid discharge (High = 0.98, Low = 0.18).

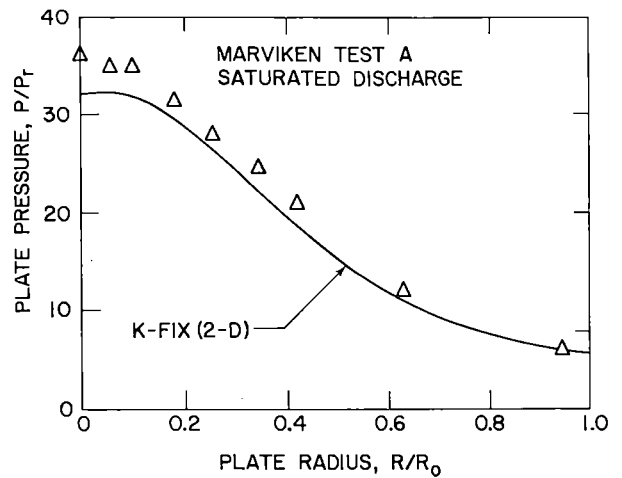


Fig. 4. Impingement plate pressure vs radial position R for Marviken Test A, saturated liquid discharge. R_0 is the outside radius for the impingement plate.

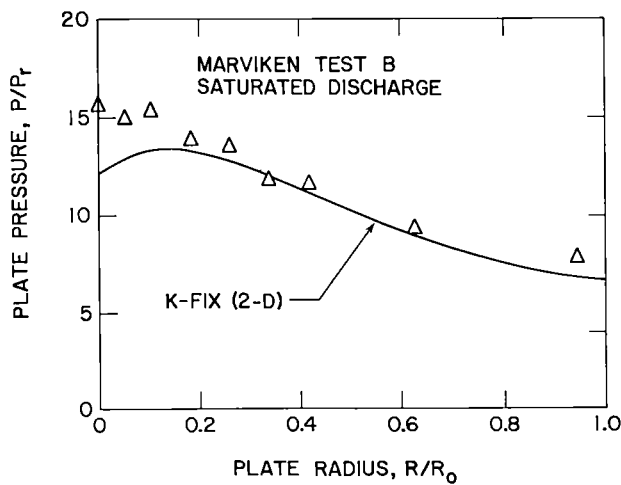


Fig. 5. Impingement plate pressure vs radial position for Marviken Test B, saturated liquid discharge.

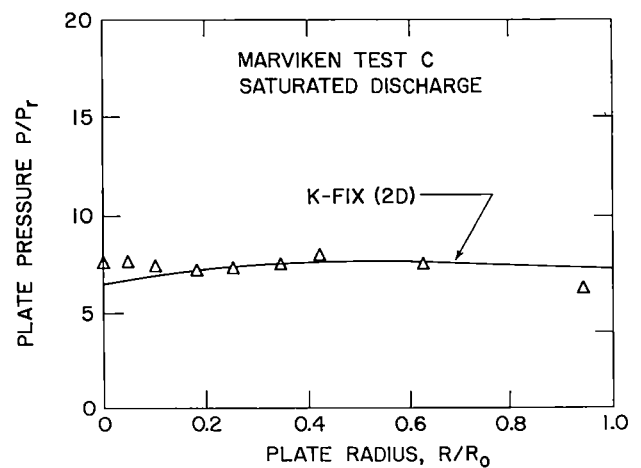


Fig. 6. Impingement plate pressure vs radial position for Marviken Test C, saturated liquid discharge.

Overall, these figures show the calculations to be in fairly good agreement with the experimental results. There are, of course, a large number of ways in which the theoretical model departs from the physical situation. Among these is the two-field assumption which neglects the existence of a spectrum in liquid entity size. The low pressure near the plate center in Figs. 4 through 6 could conceivably be owing to this simplification; one would expect the larger entities to travel in a straighter path than smaller ones, giving rise to a pressure profile more accentuated in the center than that which was computed.

Subcooled Discharge

During the initial stages of the vessel discharge in the Marviken experiments, the water approached the nozzle contraction at a pressure in excess of the saturation pressure. Thus, the water was compressed or "subcooled" at this point. For a portion of the subcooled discharge period of Test A, the central pressure on the impingement plate was significantly higher than for saturated liquid discharge. Earlier small-scale jet impingement tests have suggested the possibility of achieving full pressure recovery on a witness plate at small standoff distances [7]. This total pressure recovery or "Bernoulli" stagnation comes as somewhat of a surprise in what otherwise has been considered to be a two-phase flow event. Mjolsness [2] has given careful consideration to the possibility of full-pressure recovery in two-phase systems, and concludes that if any vapor volume is present whatsoever, complete pressure recovery is unlikely. Thus, we find it reasonable to assume that no phase change has occurred in the central part of the jet in this case. It is clear that the liquid must be strongly superheated outside of the discharge pipe and yet remain essentially unnucleated long enough to reach the impingement plate in Ref. 7.

As a first attempt at explaining this phenomenon, we hypothesize the following scenario. As the discharge liquid passes through the nozzle contraction its pressure drops to saturation by the acceleration. Boiling is not spontaneously initiated clear across the pipe, but rather is initiated only at the wall because of roughness there. Nucleation sites for boiling are then transported by turbulent diffusion from the wall toward the center of the flow channel. If the liquid passing through the nozzle contraction is sufficiently subcooled, then the critical flow speed may be high enough to enable pure liquid to reach the impingement target.

To test this scenario, we first solve the equation for transport of a passive scalar quantity s ,

$$\frac{\partial s}{\partial t} + \nabla \cdot (\vec{u}_l s) = \nabla \cdot \sigma \nabla s$$

where \vec{u}_l is the liquid velocity and σ is a turbulent diffusion coefficient estimated by

$$\sigma = 6 \times 10^{-4} R_p u$$

where R_p is the discharge pipe radius and u is the discharge flow speed. The boundary and initial conditions on s are

$$s = 0.0 \quad \text{for } \theta = 0$$

$$s = 1.0 \quad \text{for } \theta = 0.9$$

with $s = 0.5$ in the computational cells adjacent to the discharge pipe wall. We use the local value of s as a multiplier in Eq. (8) so as to represent the degree of nucleation at any point in the flow.

Results of a calculation for Marviken Test A during subcooled discharge are given in Figs. 7 and 8. The region of low void fraction in the jet is clearly evident in the vapor volume fraction contours of Fig. 7. Figure 8 shows calculated versus measured values of pressure on the impingement plate for this test.

COMPARISON OF METHODS

It is necessary to place the experimental and theoretical results presented here in perspective, with respect to their actual use in the nuclear power industry. To do this we have performed calculations for impingement loads according to the methods of ANS/ANSI-58.2 (1980) for each of the Marviken tests discussed here. The results are presented in comparison to experimental data and K-FIX calculations in Table I. This comparison shows that the methods of 58.2 are safe for steam and saturated liquid discharge for target spacings from about 60 cm to 200 cm. It is also shown that the methods of 58.2 give very high loading estimates for subcooled and saturated discharge at a separation distance of 200 cm, and a lower estimate for subcooled discharge at 60 cm separation. However, the observed total impingement load, at 60 cm separation for subcooled discharge, was less than twice the vessel pressure times the exit pipe area as predicted by single-phase, frictionless flow dynamics.

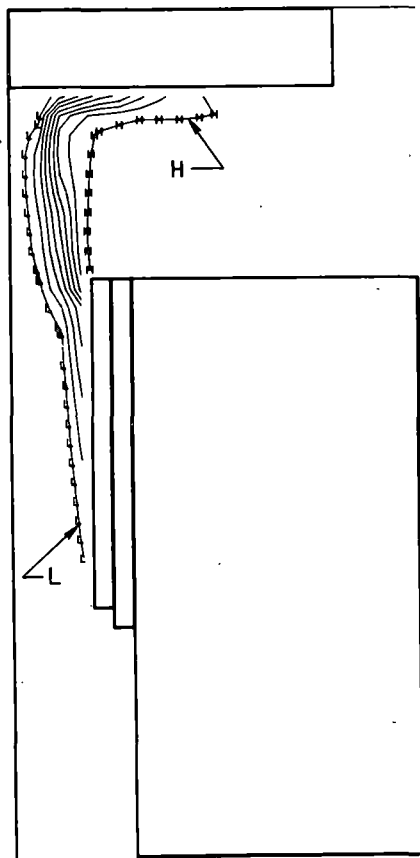


Fig. 7. K-FIX vapor volume fraction contours for Marviken Test A, subcooled liquid discharge (High = 0.90, Low = 0.10).

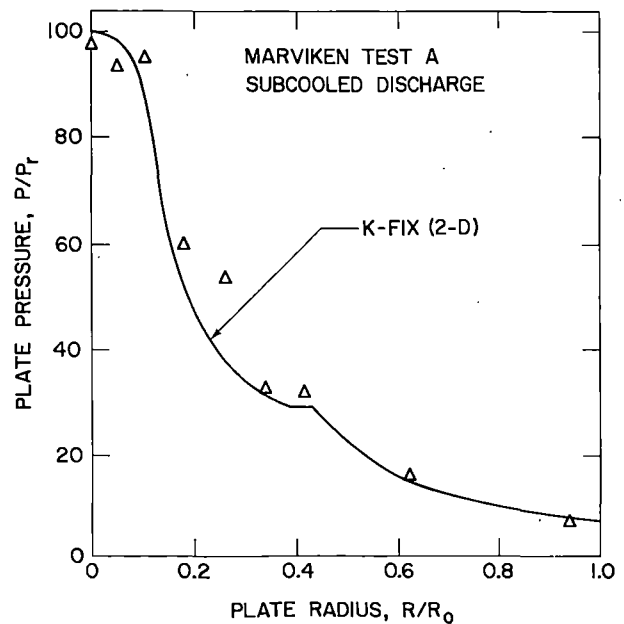


Fig. 8. Impingement plate pressure versus radial position for Marviken Test A, subcooled liquid discharge.

TABLE I

COMPARISON OF MEASURED FORCE F_{exp} TO THE FORCE COMPUTED BY ANSI/ANS 58.2 $F_{58.2}$ AND
 FORCE COMPUTED USING THE MODEL PRESENTED HERE F_{K-FIX} . L IS THE NOZZLE EXIT TO
 TARGET SPACING

Marviken Test	L (cm)	Discharge	$F_{58.2}/F_{exp}$	F_{K-FIX}/F_{exp}
C	206	Subcooled liquid	∞^1	$_{-2}$
C	206	Saturated liquid	5.8	1.1
C	206	Steam	1.2	-
B	105	Subcooled liquid	1.7	-
B	105	Saturated liquid	1.9	0.8
B	105	Steam	1.0	-
A	60	Subcooled liquid	0.7	0.8
A	60	Saturated liquid	1.2	0.9
A	60	Steam	1.1	-

¹The force measured was essentially zero.

²Calculation not yet performed.

If typical pipe-to-obstacle separation distances in nuclear power plants exceed about four pipe diameters (i.e. in the range of the Marviken experiments), then, on the basis of this study, it is reasonable to expect that the design of obstacles, such as safety baffling, is overly conservative. The source of the error appears to be the application of a jet spreading angle characteristic of single-phase jets to the two-phase jet. In the latter, the effect of boiling must be to enhance the rate of jet momentum divergence by transporting gas and liquid radially in a manner not possible with a pure steam jet.

ACKNOWLEDGMENTS

This work was performed under the Electric Power Research Institute contract RP-1324-4 in the Theoretical Division, Group T-3 of the Los Alamos National Laboratory. Many members of Group T-3 participated in the project and their contributions, especially those of Francis H. Harlow, are gratefully acknowledged.

REFERENCES

1. American National Standard - Design Basis for Protection of Nuclear Power Plants Against the Effects of Postulated Pipe Rupture, ANSI/ANS 58.2, American Nuclear Society, LaGrange Park, IL (1980).
2. B. A. Kashiwa, F. H. Harlow, R. B. Demuth, and H. M. Ruppel (R. C. Mjolsness, contributor), "Steam-Water Jet Analysis," Final report on EPRI project RP-1324-4, Electric Power Research Institute, Palo Alto, CA (1982).
3. W. C. Rivard and M. D. Torrey, "K-FIX: A Computer Program for Transient, Two-Dimensional, Two-Fluid Flow," Los Alamos Scientific Laboratory report LA-NUREG-6623 (April 1977).
4. J. R. Travis and W. C. Rivard, "PRESBC: Pressure Boundary Condition for the K-FIX Code," Los Alamos Scientific Laboratory report LA-NUREG-6623, Suppl. III (July 1980).
5. W. C. Rivard and J. R. Travis, "A Nonequilibrium Vapor Production Model for Critical Flow," Nucl. Sci. and Engr. 74, 40 (1980).
6. "The Marviken Full-Scale Jet Impingement Tests, Fourth Series," Joint Reactor Safety Experiments in the Marviken Power Station, Sweden (April-June, 1981).
7. T. F. Kanzleiter, "Experimental Investigation of the Jet Force and its Local Distribution in Case of Rupture of a Primary Circuit Pipe," Battelle-Institute, e.V., Frankfurt, Report No. BF-RS-50-62-7 (paper presented at the 1977 Reactor Conference in Mannheim, W. Germany).

BREAK FLOW AND TWO-PHASE JET LOAD MODEL

G. G. Weigand and S. L. Thompson

Sandia National Laboratories
Albuquerque, NM 87185, USA

ABSTRACT

A model has been developed for predicting two-phase, water jet loads. The model ranges in application from 60 to 170 bars pressure and 70°C subcooled liquid to 0.75 (or greater) quality -- completely covering the range of vessel conditions of interest in pressurized water or boiling water reactors. The model was developed using advanced two-dimensional computational techniques to solve the governing equations of mass, momentum, and energy. The model predicts subcooled loadings in excess of the twice (stagnation pressure) \times (exit area), one-dimensional limit, thus questioning the conservatism of current jet load models. Simple, approximate engineering models are given for estimating expansion characteristics, shock strengths, and stagnation pressures. These approximate models could be used for estimating pressures on various geometric target configurations.

INTRODUCTION

A nuclear power plant must be designed to ensure that the consequences of a pipe break (large or small) will be mitigated to prevent damage of any safety equipment or systems. A major concern in the event of a pipe break is the loading upon surrounding structures, equipment, etc., caused by the two-phase jet expanding from the break. These high energy jets have the potential to cause wide spread destruction.

In an attempt to prevent failures, due to jet loading on any of the safety equipment or control systems, a complex system of jet deflectors, snubbers, and pipe restraints has been installed in plants. The design basis for much of these structural supports can be traced to Moody's jet load model¹. Various interpretations of the actual zone of influence of the jet for this model have been made by others^{2,3}, but the one-dimensional force model from Reference 1 is nearly always applied. The error that could result from the one-dimensional approximation or the arbitrariness in deciding the zone of influence of the jet can result in costly overdesign, poor utilization of limited space inside of containment, or underdesign of restraint/barrier systems.

The use of simple one-dimensional modeling is inappropriate for two-phase jet load calculations; the jet is a complicated multidimensional flow. The high pressure and high temperature fluid that exits the break expands with supersonic velocities downstream of the break. Upon encountering a target (or obstacle) a

shock wave forms in the flow field, and it is the thermodynamic properties downstream of this shock that determine the pressure field and load on the target. A multidimensional analysis, which is capable of treating strong shocks, is required to evaluate the thermodynamic properties downstream of these shocks.

Sandia National Laboratories, with the support of the U. S. Nuclear Regulatory Commission, has completed a study using modern multidimensional computational methods to evaluate the two-phase jet load on target geometries.⁴ The governing equations of mass, momentum, and energy were solved with a high resolution Eulerian method for all calculations. The calculations form a computational data base for evaluating jet and target pressures for axisymmetric target geometries. This data base covers the range of pressures, temperatures, and distances to the target present in both pressurized water (PWR) and boiling water (BWR) reactor designs. A two-phase jet load model, which provides both pressure and load distributions, was developed using the computational data base. In addition to the load model, approximate engineering models were developed. These engineering models were developed for performing accurate interpolations within the sparse computational data base. However, they may be used for estimating the jet expansion, shock, and target load. This paper will not, because of space limitations, present in detail the two-phase jet load model. Persons interested in applying the two-phase jet load model must consult Reference 4. Reference 4 displays in a series of figures the target load and pressure distributions as a function of vessel (or break) conditions.

GENERALIZED TWO-PHASE JET BEHAVIOR

Figure 1 is a spatial illustration of the pressure field in a two-phase, impinging jet. The heavy solid lines in Figure 1 describe solid boundaries that depict the vessel, break nozzle, and target. The small plot on the right in Figure 1 describes the pressure-expansion in the vessel and piping and in the jet outside the vessel. The conditions at the dashed vertical line are the conditions at the break (pipe exit). The section of the graph to the left of the vertical dashed line corresponds to conditions outside of the pipe exit. Moving to the left corresponds to an increase in the target to pipe spacing.

In the jet flow field there are three natural divisions of the field. There is a nozzle (or break) region where the flow chokes. In this region there is a core at choked flow thermodynamic properties that projects a distance downstream of the nozzle depending upon the degree of subcooling. Downstream of this region there is the free jet region. Here the jet expands almost as a free, isentropic expansion. The flow is supersonic throughout this entire region. The free jet region terminates at a stationary shock wave near the target. This shock wave arises because of the need for the target to propagate pressure waves upstream and, thus, produce a pressure gradient that will direct the fluid around the target. Downstream of the shock is the target region where the local flow field imposes the pressure loading on the target.

The pressure P_0 is the vessel stagnation pressure, and P_1 is the choke pressure in the break nozzle. The pressure P_2 denotes a family of isentropic expansion pressures describing the jet expansion upstream of the shock wave; P_3 describes a family of pressures downstream of the shock wave that correspond to a shock wave (Hugoniot) calculation. P_4 describes the family of stagnation pressures that correspond to each of the P_3 shock wave calculations. Notice that the shock wave causes a substantial stagnation pressure loss for highly expanded jets. This stagnation pressure loss is due to the non-isentropic processes in the shock and should not be confused with the very small viscous and entrainment losses.

MODEL CALCULATIONS AND INITIAL CONDITIONS

The latter two of the above regions are evaluated using a two-dimensional, finite difference computer code, CSQ⁵; all calculations were performed using a high resolution grid. Consequently, region one, the inlet boundary zone, becomes the initial conditions for all calculations.

In the inlet zone the thermodynamic conditions are determined with the HEM critical flow model. In the inlet zone there is a conical core of fluid which remains at HEM critical flow conditions beyond the nozzle (or break). This core of fluid is traveling at supersonic velocities. Its length L_C depends upon the time it takes for a pressure wave to travel from the outer edge of the exit pipe to its center; this time is simply

$$t_c = \frac{D}{2C_s} \quad (1)$$

where C_s is the sound speed at the nozzle exit and D is the nozzle diameter. The core length, L_C , is then

$$L_C = \frac{DV_1}{2C_s} \quad (2)$$

where V_1 is the HEM critical flow velocity. The point on the centerline L_C from the pipe exit is the first point downstream of the pipe break where pressure information originating outside of the pipe would be communicated (via waves traveling at C_s) to the fluid which exited at the pipe center. For distances along the centerline less than L_C , the thermodynamic state of the fluid is the same as that inside the pipe. Figure 2 provides L_C/D as a function of the stagnation pressure P_0 and temperature T_0 . For targets located at L/D s less than L_C/D the center pressures will be equal to P_0 .

The entire jet field and the target load were evaluated with two-dimensional calculations. A matrix of calculations was developed to establish a computational data base. This data base covers the following range of vessel conditions

pressures of 60 to 170 bars

| subcooling of 0 to 70 °C |
| qualities of 0 to 0.75 |

L/D s of 0.50 to 15.0

The wall loading, P_T , is a function of these variables and the radial position on the target. Although the calculation of target pressures was the primary objective of this study, the calculations provided details of the entire jet field. Figures 3 and 4 illustrate typical results. Figure 3 shows the pressure contours for an impinging jet with stagnation conditions of $P_0 = 150$ bars and saturated liquid ($T_0 = 615.39$ K) and $L/D = 2$. Figure 4 is a three-dimensional illustration of the pressure field in Figure 3; the jet expansion followed by a shock wave near the wall is clearly shown. The last curve in the foreground in Figure 4 is the target pressure distribution.

TWO PHASE JET LOAD MODEL

The two-phase jet problem was too difficult to treat with simple engineering models, but at the same time it is impractical to run a two-dimensional, Eulerian finite difference calculation each time load calculations are made. The load model that has been developed cannot be described by a set of algebraic relations; the

phenomena involved in two-phase jets (shock waves, non-linear equation of state, 2-D expansion, etc.) are too complicated. Instead the load model is a computational data base with semi-mechanistic engineering models for interpolating within the data base. The target load and pressure distributions for the range of vessel conditions given above are displayed in 126 figures in Reference 4. There is no hope of giving that type of detail in this paper; instead some discussion of the engineering models followed by a brief example of the model will be given.

Centerline target pressure (engineering model)

The centerline target pressure model assumes the jet is an isentropic expansion and assumes the shock is normal and coincident with the target. The thermodynamic conditions are assigned an axial position using a centerline function that was developed from the spherical pressure behavior noted in the free jet in CSQ calculations. The form of this function is

$$(\rho v)_2 = (\rho v)_1 \left\{ \frac{(D/2z)^\alpha}{1 - (L_c/z)^\beta \left[1 - (D/2L_c)^\alpha \right]} \right\} \quad (3)$$

where the subscripts 1 and 2 refer to the break plane and jet field, respectively. The parameters α and β were determined by fitting equation (3) to the CSQ data base and requiring that

$$\alpha = \alpha (P_0, \Delta T_0, L/D, L_c/D) \text{ and}$$

$$\lim_{L/D \rightarrow \infty} \alpha = 2 \quad \text{and} \quad \lim_{\Delta T \rightarrow 0} \alpha = 2$$

and

$$\beta = \beta (P_0, \Delta T_0, L/D, L_c/D)$$

Figures 5 and 6 illustrate the centerline target pressure behavior for stagnation pressures of 80 and 150 bars, respectively.

Radial target pressure (engineering model)

The radial target pressure model assumes the jet is an isentropic expansion and assumes the shock is oblique and coincident with the target. The thermodynamic properties are assigned an axial position using equation (3) but redefining the length dimension as z' where

$$z' = \sqrt{R^2 + L^2} \quad .$$

R denotes a radius on the target. The shock strength is evaluated using oblique shock relations,⁶ and only the velocity component normal to the wall behind the shock wave is used to evaluate target (stagnation) pressures.

Typical Model Curves

Figures 7 through 12 are a brief set of curves which illustrate the features of the model. Figures 7 and 10 give the target load distribution as a function of target radius for stagnation conditions of $P_0 = 130$ bars with $\Delta T_0 = 35^\circ \text{C}$ and $X_0 = 0.333$ respectively. The target L/D associated with each curve is listed

in the upper right hand corner of the figure; the lowest L/D value corresponds to the uppermost curve.

Figures 8 and 11 give the target pressure distribution as a function of target radius for the same conditions noted above; in fact, Figures 7 and 10 are the integral of the pressure distributions in Figures 8 and 11. Figures 9 and 12 are composite contours of the target pressure. These figures display the extent of the exit core along with a letter indicator for pressure on a Cartesian grid of length to target (L/D) versus target radius (RADIUS/D): A = 1 bar, B = 2.5 bars, C = 5 bars, D = 10 bars, E = 15 bars, F = 20 bars, G = 25 bars, H = 30 bars, etc. When subcooling existed ($\Delta T_o > 0$ °C) and the target was located close to the break (L/D small), the loads predicted exceeded the L-D limit of $F_r/P_o A_e = 2$. This occurs because of the wide jet expansion from the break and the outer boundary shock; in subcooled cases the expansion angle can be large enough to produce velocities with components opposite to the break flow.

COMPARISON WITH EXPERIMENT

Experimental verification of the final two-phase jet load model is not straightforward because of the small amount of experimental data that exists with stagnation pressures in the 60-170 bar range. Also most data in the 60-170 bar range was recorded in small scale facilities. The data taken at the higher pressures and used here to verify the load model is reported in References 7 and 8. Reference 7 reports Kraftwerk Union (KWU) data for steady impinging jets operating at saturated conditions. Reference 8 reports a blowdown test performed by Battelle-Frankfurt for initial conditions of 140 bars and 30°C subcooled. Additional discussion of both of these data sets can be found in Reference 4.

Figures 13 to 15 show the KWU data comparisons. The stagnation conditions for these data were nominally 100 bars and saturated liquid; however, in each case the actual data showed vessel stagnation conditions between 92 and 96 bars. Because the listed experimental pressure uncertainty was about 10% and because there is some total pressure loss between the vessel and the nozzle, the exact stagnation pressure is not precisely known; however, it does range between 80 to 100 bars. Therefore, in Figures 13 to 15 target pressure distribution curves for stagnation conditions of 80 to 100 bars and saturated liquid are plotted. Figures 13 to 15 show the data comparisons for L/Ds of 1, 2, and 3, respectively; the comparison is very good. These data were not connected, in any way, with the model development -- only the CSQ data base was used.

The data comparisons for the Battelle-Frankfurt data were more difficult to perform than the KWU data comparisons; this was because the blowdown network was complicated (consisting of two interconnected vessels), and the measurements reported in Reference 8 did not completely describe the upstream stagnation conditions. Additionally, the Battle nozzle, due to geometry, does not have a clear definition of target L/D; the nozzles L/D ranges between 2.0 and 2.4 depend upon the thermodynamic conditions in the vessel. The data comparisons to be shown here are the centerline pressure on the target as a function of the blowdown time, t. Figure 16 shows the comparison with Battelle's C11 test during the subcooled portion of the blowdown, and Figure 17 shows the comparison during the saturated portion of the blowdown. Considering the large uncertainty in vessel conditions the agreement is excellent.

ACKNOWLEDGEMENTS

The authors would like to gratefully acknowledge the support of the U. S. Nuclear Regulatory Commission.

REFERENCES

1. Moody, F. J., "Fluid Reaction and Impingement Loads," Specialty Conference on Structural Design of Nuclear Plant Facilities, Vol. 1, Chicago, Illinois, December, 1973.
2. Watts Bar Nuclear Plant Final Safety Analysis Report, Section 3.6, Tennessee Valley Authority.
3. Standards Committee ANS 58.2, Design Basis for Protection of Light Water Nuclear Power Plants Against Effects of Postulated Pipe Rupture, ANSI/ANS-58.2-1980, American Nuclear Society, LaGrange Park, IL 60525, 1980.
4. Weigand, G. G., Thompson, S. L., and Tomasko, D., Two-Phase Jet Loads, NUREG/CR-2913, SAND82-1935, Sandia National Laboratories, Albuquerque, NM, 87185, 1982.
5. Thompson, S. L., CSQ-II - An Eulerian Finite Difference Program for Two-Dimensional Material Response, Part I Materials Section, SAND77-1339, Sandia National Laboratories, Albuquerque, NM, January 1979.
6. Zucrow, M. J., and Hoffman, J. D., Gas Dynamics, John Wiley & Sons, Inc., New York, 1976.
7. Eichler, R., Kastner, W., Lochner, H., and Riedle, K., Safety Project in the Area of Light Water Reactors, Studies on Critical Two-Phase Flow, NRC-477 (translation, 1978) KWU-R-512, Kraftwerk Union, FRG, 1975.
8. Vorhaben RS 50, Untersuchung der Vorgänge in einen mehrfach unterteilten Containment beim Bruch einer Kuhlmitteleitung wassergekühlter Reaktoren, Technischer Bericht BF RS 50-32-C11-1, Battelle-Frankfurt, FRG, 1976.

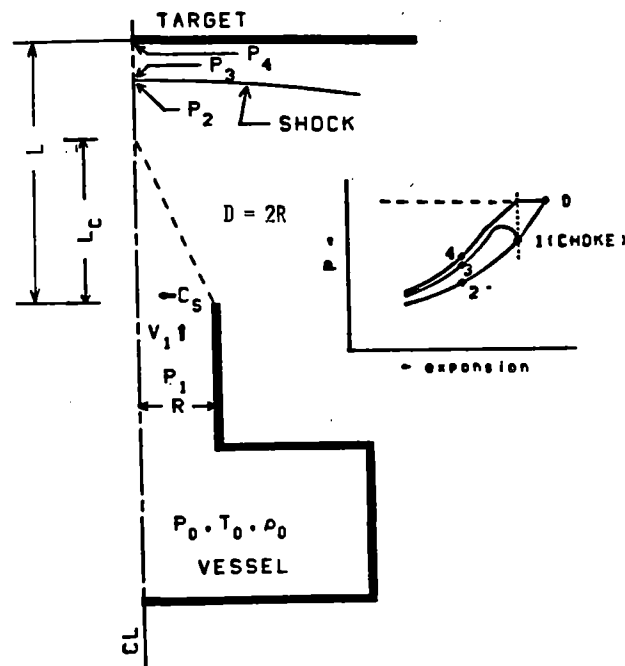


Figure 1. Expected pressure behavior along two-phase jet centerline

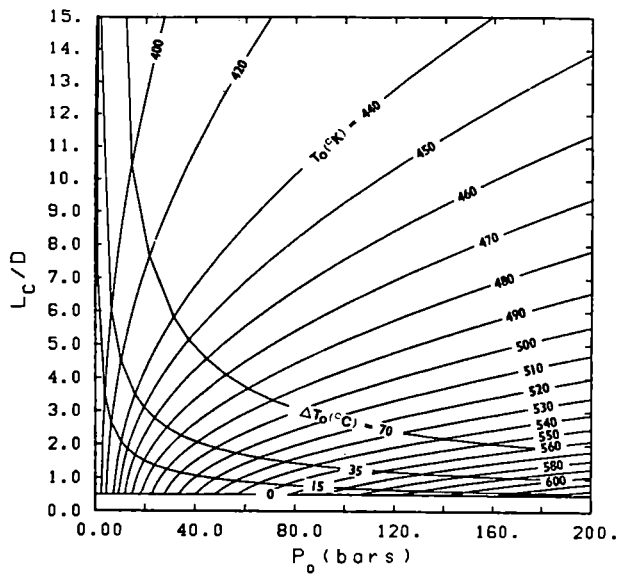


Figure 2. L_c/D as a function of upstream stagnation conditions

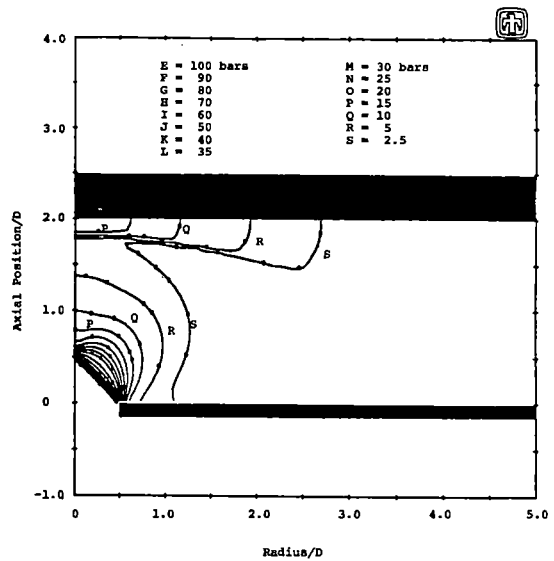


Figure 3. Pressure contours for $P_0 = 150$ bars, saturated liquid, $L/D = 2.0$

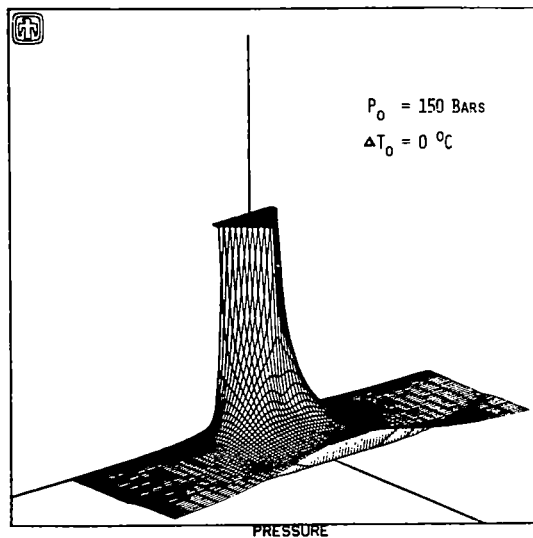


Figure 4. 3-D pressure field contour, $L/D = 2.0$

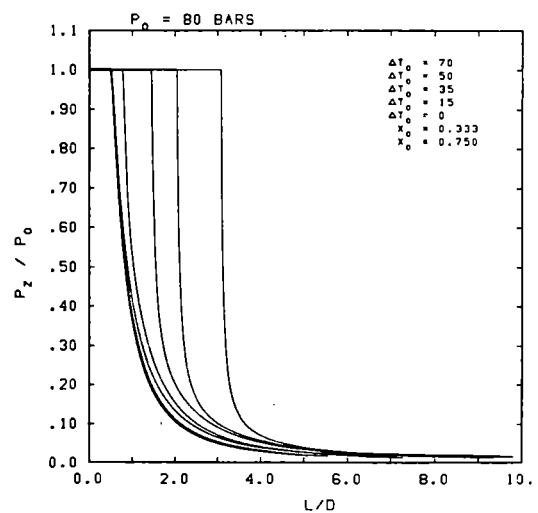


Figure 5. Centerline target pressure distributions

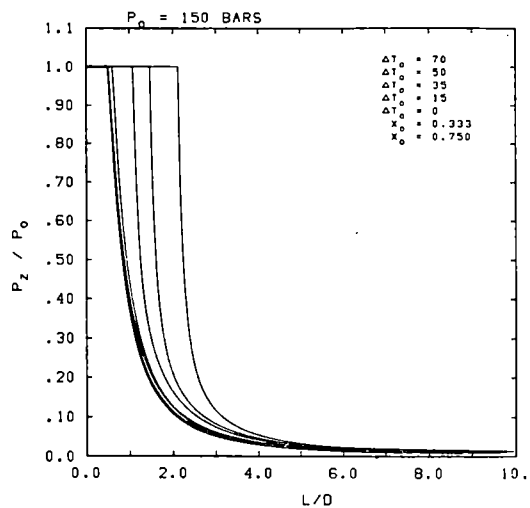


Figure 6. Centerline target pressure distributions

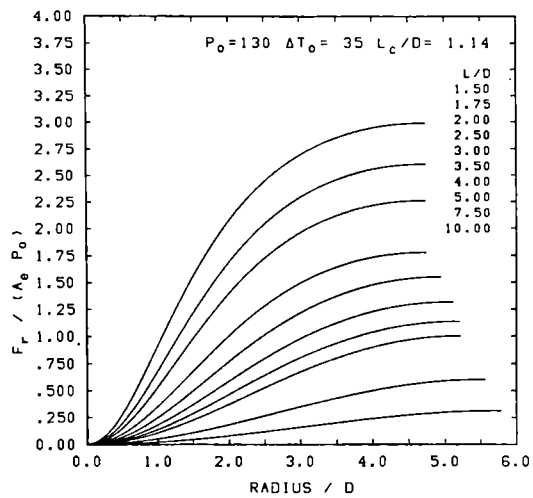


Figure 7. Target load distributions

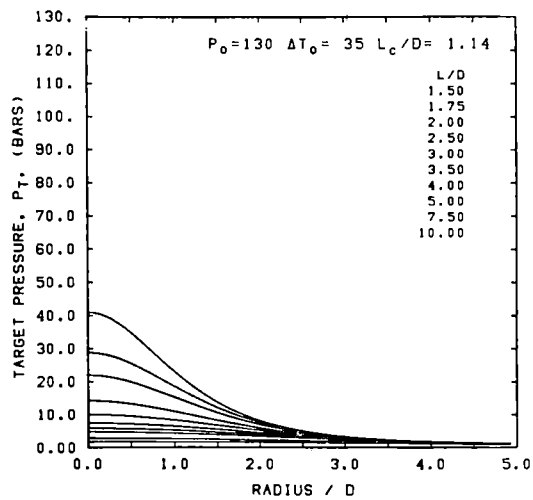


Figure 8. Target pressure distributions

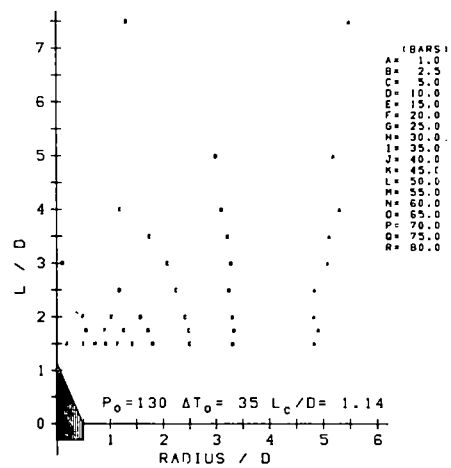


Figure 9. Composite target pressure contours

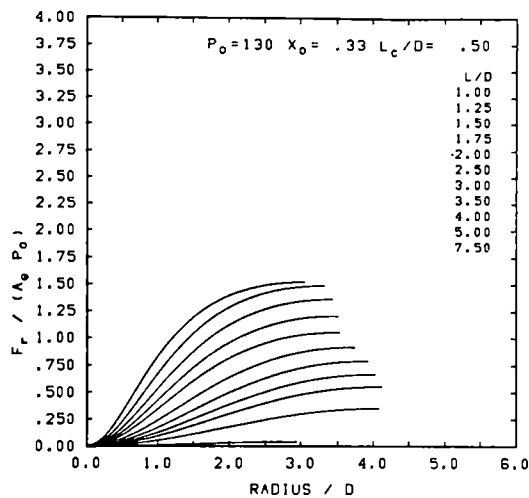


Figure 10. Target load distributions

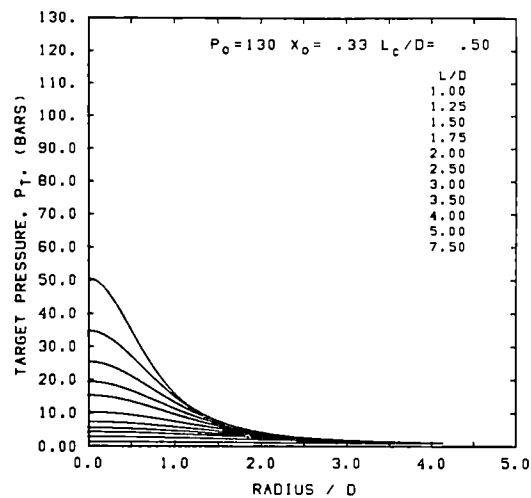


Figure 11. Target pressure distributions

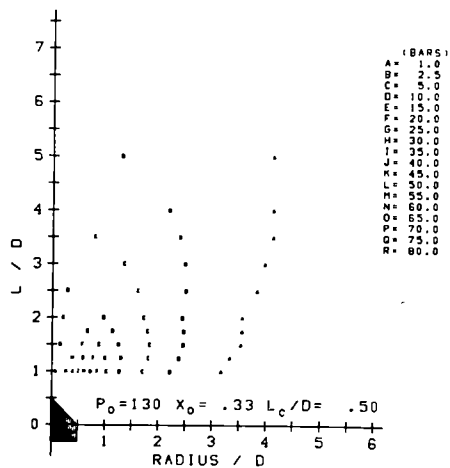


Figure 12. Composite target pressure distributions

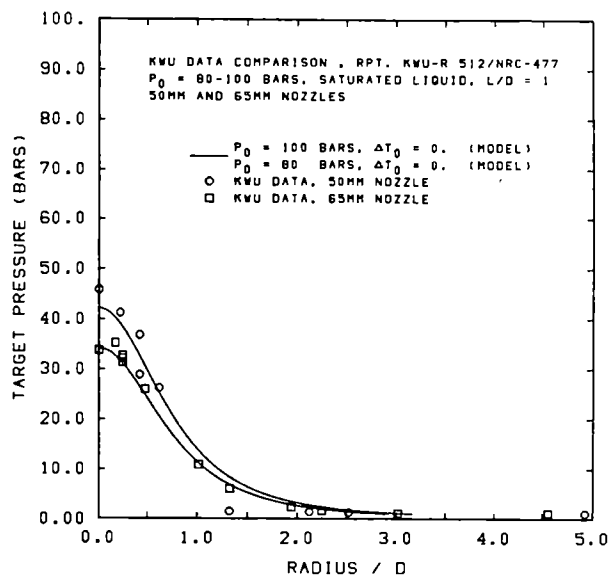


Figure 13. KWU data and load model comparisons, $L/D = 1$

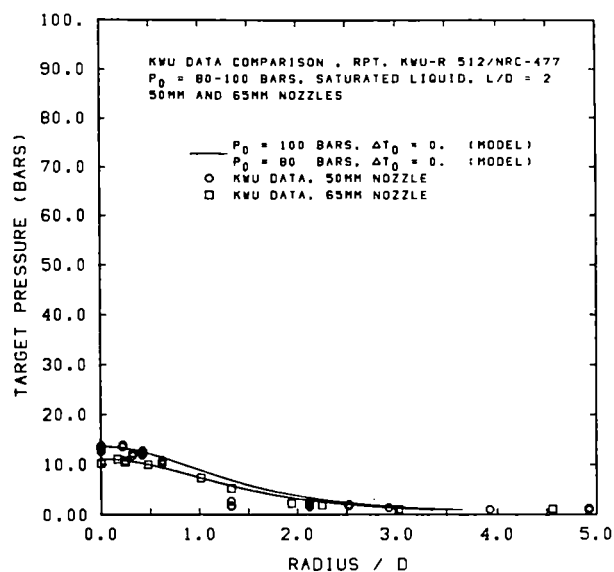


Figure 14. KWU data and load model comparisons, $L/D = 2$

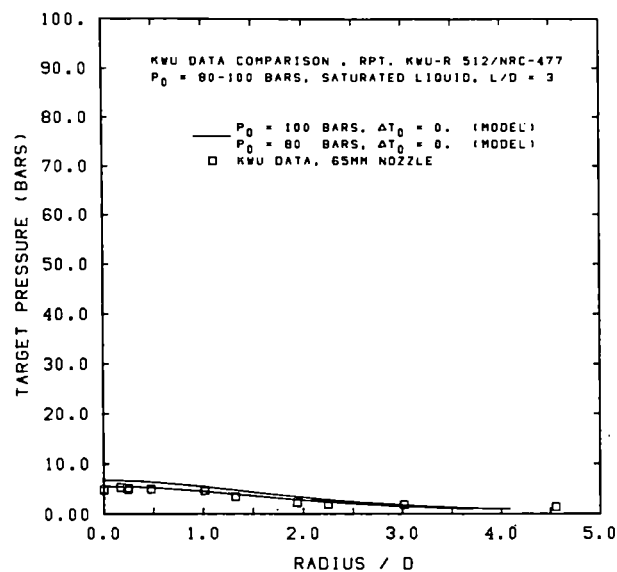


Figure 15. KWU data and load model comparisons, $L/D = 3$

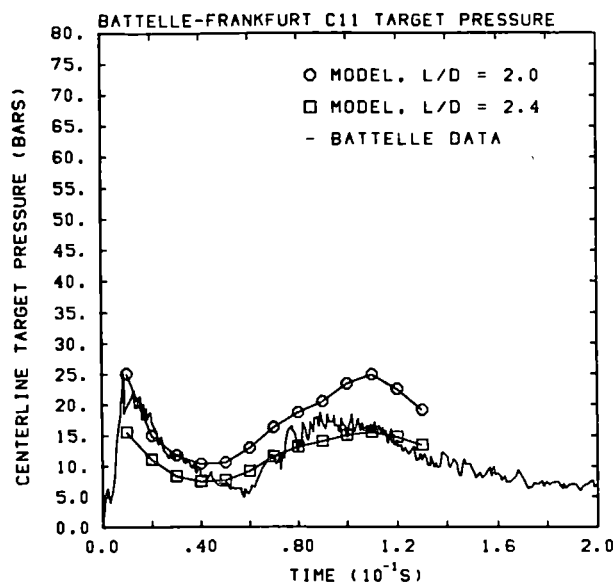


Figure 16. Battelle-Frankfurt data and load model comparison

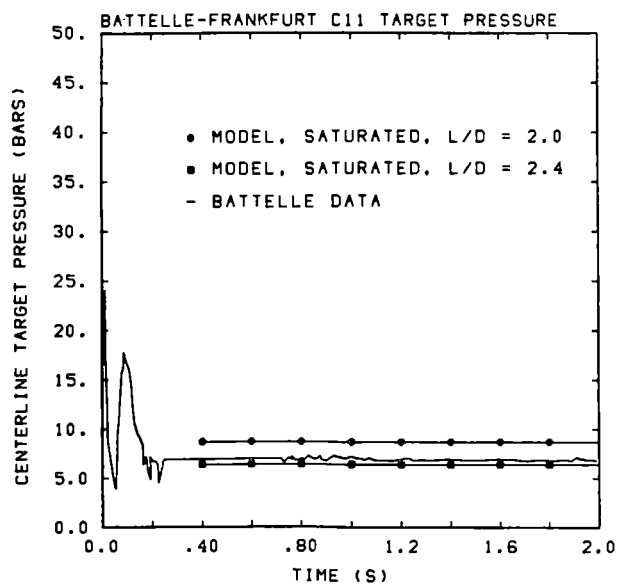


Figure 17. Battelle-Frankfurt data and load model comparison

GERMAN STANDARD PROBLEM NO. 4 AND 4a
LOADINGS AND RESPONSE OF A FEEDWATER LINE DUE TO PIPE
BREAK AND ENSUING CHECK VALVE CLOSURE

T. Grillenberger, Technische Universität München,
Forschungsgelände, D-8046 Garching, FRG

and

W. Ch. Müller, Gesellschaft für Reaktorsicherheit,
Forschungsgelände, D-8046 Garching, FRG

ABSTRACT

The German Standard Problem No. 4 investigated the closing behavior of a feedwater check valve and the fluid dynamics in its respective pipeline as a result of a simulated break in the pipeline and ensuing rapid-slow closure of the check valve. In connection with this study the German Standard Problem No. 4a investigated the structural dynamic behavior of the pipe system when subjected to the fluid forces from the problem No. 4. The test was performed at the HDR test facility. As a part of these Standard Problems several engineering firms performed "blind" calculations to predict the behavior of the fluid and the check valve and the structural response of the piping system. The main results of the experiments and the calculations will be given.

PART 1: FLUID AND VALVE DYNAMICS

1. General Aim and Participants

The fluid dynamic phenomena in the test pipe of the HDR test facility and the dynamic behavior of the feedwater check valve during the blowdown were to be pre-calculated in the German Standard Problem No. 4 (GSP 4). The participants had to solve the problem with the particular programme available in order to obtain best estimate results for the pressure, temperatures, mass flow rates and the valve lift which had been measured in the experiment. Ten institutions took part in the GSP 4. The participants (table 1) used seven different (some modified) one-dimensional codes (except for one L.P.-code). All codes use a dynamic valve model.

2. Test Facility

The test pipe line with all components is shown in figure 1. The pipe is fixed at the tee only and it has no other supports. The total length of the pipe is about 19 meters (discharge nozzle to RPV). The tested feedwater check valve is shown in figure 2. The valve cone K is connected with the damping piston D by the spindle S and can be moved into the damping cylinder Z. During the blowdown the flow of the pump loop is reversed and the valve moves with the blowdown flow to the closing position. The motion is rapid in the first milliseconds and slows down as the piston merges into the damping part of the cylinder.

Test parameters:

pressure 70 bar

damping gap 0.3mm, gap length 40 mm

temperature pipe 220 °C
 RPV bottom 220 °C
 RVP top 285 °C
 initial velocity - 4m/s

3. Comparison of Results

In table 2 the most important results are summarized for easy comparison. In the following figures only the pressure upstream of the valve (RP 2205) and the valve lift (SF 3001) are shown. For these values the results of two participants and measured data are shown in figure 3 and 4.

The pressure waves in the beginning of the blowdown are simulated well in all calculations. But the interaction of valve behavior and fluid dynamics is not always adequate. In most calculations the typical waterhammer at 0.1 sec due to the sudden decreasing mass flow does not appear or is underestimated. It is possible that a small variation of parameters would cause this effect. The high sensitivity is not only a code problem but also a problem of the experiment and was induced deliberately by the chosen parameters. The closing behavior is calculated with large discrepancies. All participants (except one) underestimate the total closing time because the flow resistance coefficient is assumed too low.

The one phase models show unrealistic high pressure oscillations. The loading of the pipe is caused mainly by the axial difference between the elbows. The pressure difference (RP 2202 - RP 2203) is proportional to the loading of the vertical pipe section. It is shown in figure 5 to 7. Since the pipe response is mainly in the low eigenfrequencies the integral values in the first 200 milliseconds in both directions are important. This integral is calculated well by participant A and poorly by participant B. In consequence the following structural dynamic calculation produces good results in the case A, and in the case B there is no chance left.

4. Conclusions from GSP No. 4

Summarizing the GSP 4 comparison it can be said that adequate results are obtained above all by participants who have great experience in the technical problem and in using the code. For the future it therefore would be advisable to pay more attention to the qualification of the engineer using the code.

PART II: PIPE DYNAMIC

1. Introduction

The Standard Problem No. 4a consists of two parts:

- 1) The "blind-blind" pretest calculations, where the fluid forces calculated in the Standard Problem No. 4 were used as input. Six institutions took part in this section (participants A - F).
- 2) The "measured-blind" pretest calculations, where measured fluid data was used as input for the structural analysis. Here eleven institutions took part (participants 1 - 11).

In the Standard Problem both displacements and stresses had to be calculated for several positions. All participants used standard piping analysis codes based on beam theory.

2. Sources of Differences in the structural analysis

A scheme of sources of disagreement and their effects is shown in figure 8. There are four types:

- a) Errors in the fluid analysis lead to discrepancies in the calculation of pressures,

which have substantial effect on the structural loads, the displacements and the stresses derived from the displacements.

- b) Errors of the structural dynamic analyst may be divided into two types:
 - Errors in transforming fluid pressures into structural loadings, which affect both displacements and stresses but not the eigenvalues.
 - Errors in modelling the structure which affects the eigenvalues and eigenmodes and by this influence displacements and stresses.
- c) Piping code errors which may consist in simple programming errors or in the fact that the codes do not adequately deal with the problem.
- d) Errors in determining the stresses from the displacements which affect the stresses only.

In the "measured-blind" calculation, errors of type a) cannot occur.

3. Interpretation of Measured and Calculated Data

When selecting and specifying the Standard Problem, great care has been taken on choosing a geometrically simple piping system without components like supports, hangers, tees or "soft" fixpoints, which might cause problems in the interpretation of the data.

In addition the position of transducers etc. was selected in a way to make sure that the positions were "undisturbed" in the sense of beam theory, i. e. at the selected positions one would expect that the pipe behaves like an elementary beam and measured and calculated data - calculated on the base of piping codes, which use beam theory - should be in reasonable agreement. The dynamic response of the piping system consists of the two lowest eigenfrequencies (5.0 Hz and 7.8 Hz) and the measured displacements are easily identified as a mixture of both eigenfrequencies.

The stresses in the test were calculated from measured strains on the base of beam theory and are difficult to interpret. The results indicate that the stresses of the piping system show deviation from those predicted by beam theory.

4. The "Blind-Blind" Pretest Calculations

For these calculations it is essential that the pressures used as input for the structural analysis are adequate. This can be easily seen from figures 9 to 10, where a relevant pressure and displacement is shown for participants A and B.

The calculation of participant A is based on a good pretest calculation of the pressure in the piping system. The structural analysis is correct and a very good agreement between measured and calculated data is reached. The result of participant A prove that existing codes are adequate for the German Standard Problem No. 4 and No. 4a and that a very good prediction of the displacements can be achieved.

5. The "Measured-Blind" Pretest Calculations

Since in this case fluid dynamics cannot cause discrepancies, it is useful to analyze the eigenvalues and eigenmodes first. The participants may be classified into three groups:

- | | |
|--|------------------|
| a) difference up to 5 % (group a) | (6 participants) |
| b) difference between 5 % and 15 % (group b) | (3 participants) |
| c) difference more than 15 % (group c) | (2 participants) |

This shows that about half of the participants modelled the structure adequately. Details can be found in table 3.

Figures 11 to 13 show the influence of the differences in the eigenvalues on the displacements. In group a) there is only a difference in the amplitudes, in group b)

the transient shows deviation in time as well, but still there is a good agreement. The results of group c) do not reproduce the characteristic features of the transient.

6. Stresses

In GSP No. 4a various stresses had to be determined. As one would expect the discrepancies of the measured and calculated stresses much higher than those for the displacements due to the fact that stresses are local parameters. But in GSP 4a the stresses calculated from measured strains do not correspond very well to the measured displacements. In figure 14 the bending stresses of participant A (displacements quite accurate) are compared to the measured data showing rather different time histories.

Even comparing calculated stresses, only shows little agreement of the participants. The reason for these discrepancies should be investigated in another GSP.

7. Conclusions from GSP 4a

The agreement between the measured data and the calculated data is lower than it had been expected, especially as far as the stresses are concerned. The reason cannot be identified due to lack of certain experimental data and due to the differences in the computational models and techniques.

It is recommended to perform another GSP on the structural dynamic behavior of the piping systems with additional measurements and detailed restriction on the computational model.

Table 1:
Participants and Codes

Institution	Abbreviation	Code
TÜV Bayern	TBY	Dapsy
TÜV Hannover	THA	Kedru
TÜV Norddeutschland	TND	Kedru
TÜV Rheinland	TRL	IFHSW
TÜV Stuttgart	TST	WHAM-6 (mod.)
IKE Stuttgart	IKE	Relap4/Mod5(mod.)
BBR	BBR	PIMOC
KWU	KWU	Eudru
GRS	GRS	Dapsy
USNRC/LASL	LAS	Sola-Loop

Table 2:
Comparison of important results

	closing time undamped/total (msec)	pressure maximum (bar)/ time (msec)	mass flow maximum (kg/sec) / time (msec)	
			valve	discharge nozzle
Experiment	90/600	115/106	≈1700/84	≈3500/≈150
BBR	73/230	110/124	1100/84	1100*/ 72
GRS	90/320	135/ 95	1550/73	1800*/132
IKE	50/600	80/ 53	1200/55	1600*/132
KWU	51/190	100/189	800/43	1250 / 44
LAS	70/290	110/ 88	1250/67	2100 / 87
TBY	60/290	135/ 72	1050/55	3500 / 7 (2450)/(77)
THA	70/250	90/ 69	1200/63	1950 /108
TND	70/270	90/ 67	1100/72	1250*/ 74
TRL	80/300	125/ 96	1450/77	1600**/66
TST	42/310	95/363	1100/70	1900 / 68

* discharge nozzle is simulated only half resp. 2/3 by TND
 **decreasing pump mass flow as boundary condition

Table 3:
First three eigenfrequencies

eigenfrequency	1	Δ	2	Δ	3
experiment	5.0	-	7.8	-	?
group a 1	5.0	0 %	7.9	1 %	9.1
2	4.7	-6 %	7.7	-1 %	9.0
3	4.8	-4 %	7.6	-2 %	8.6
4	4.8	-4 %	7.8	0 %	8.8
5	4.9	-2 %	7.6	-2 %	9.2
6	4.8	-4 %	7.6	-2 %	8.6
group b 7	4.6	-8 %	7.2	-8 %	8.4
8	4.4	-12 %	7.0	-10 %	8.1
9	5.5	10 %	8.5	9 %	9.4
group c 10	6.8	36 %	9.5	22 %	11.3
11	6.2	24 %	8.8	13 %	9.7

eigenfrequencies in Hz, Δ =(calculation - experiment)/experiment

Figure 1: Test pipe line and FWCV 350

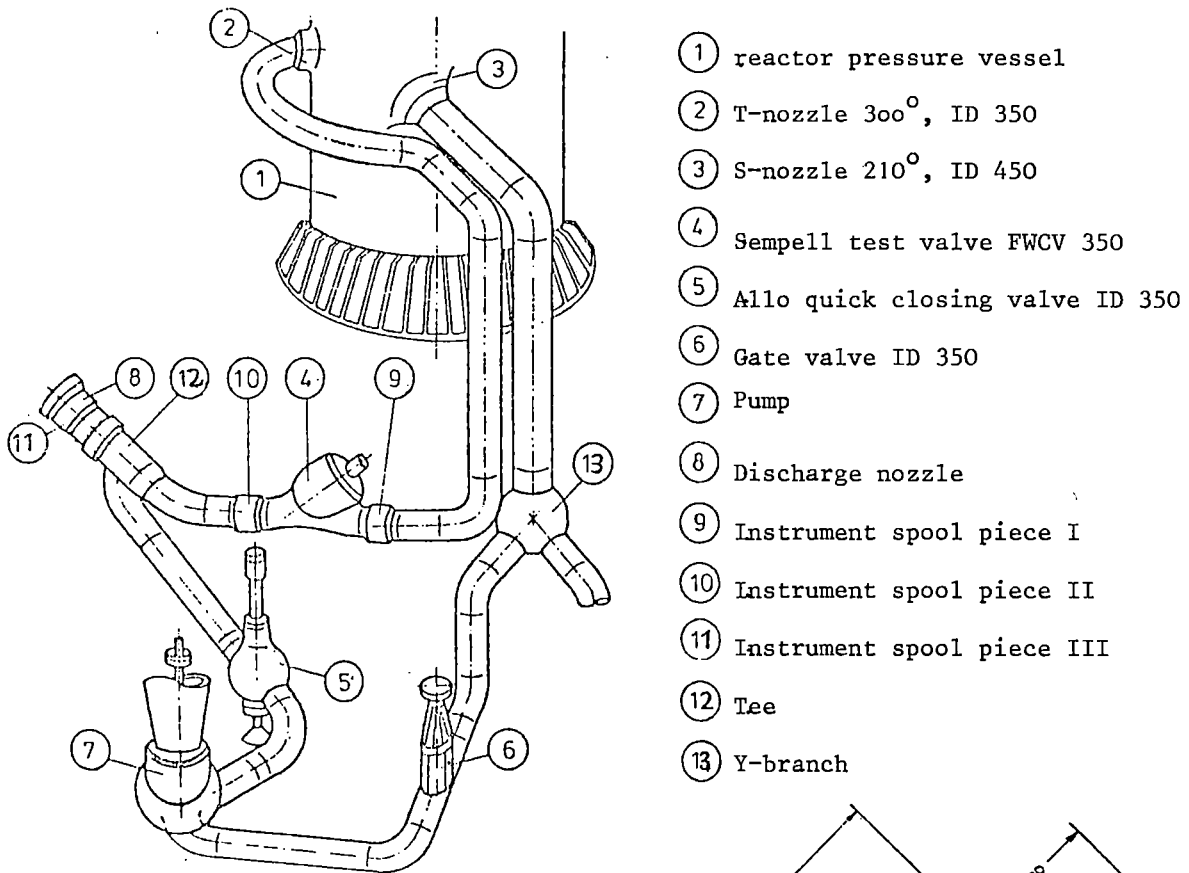
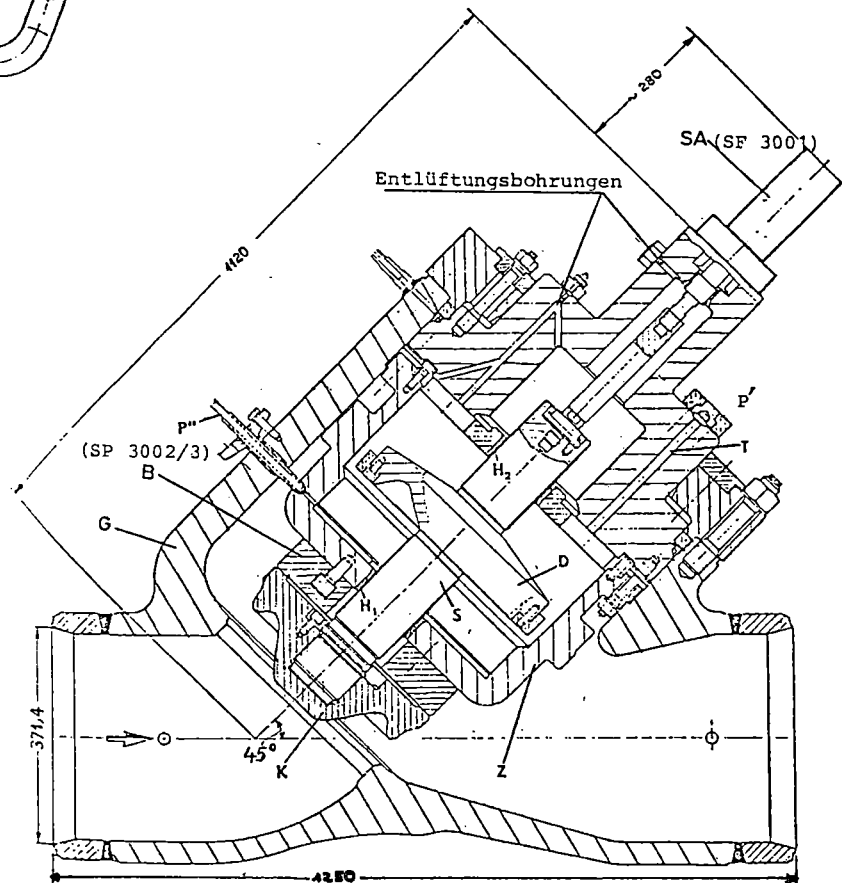


Figure 2
Scheme of FWCV 350



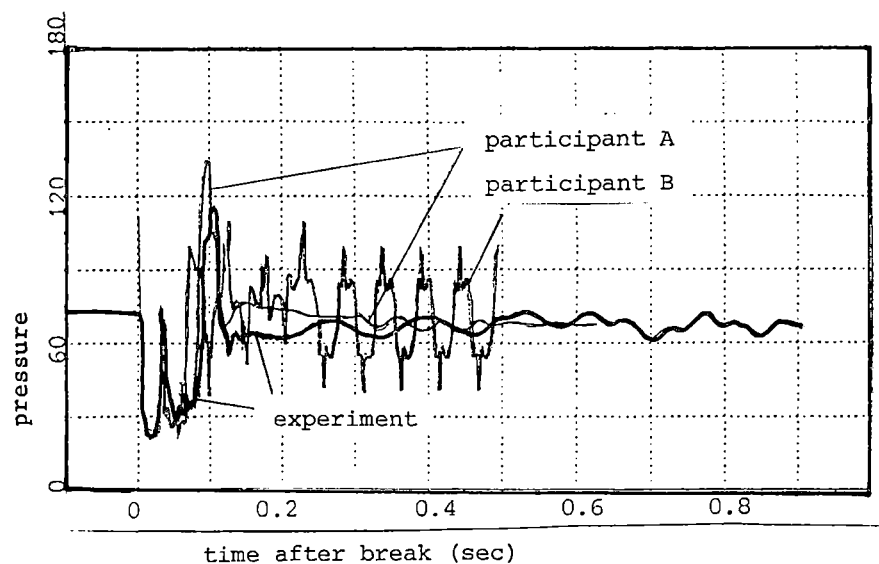


Figure 3: Pressure before valve (RP 22o5)
bar

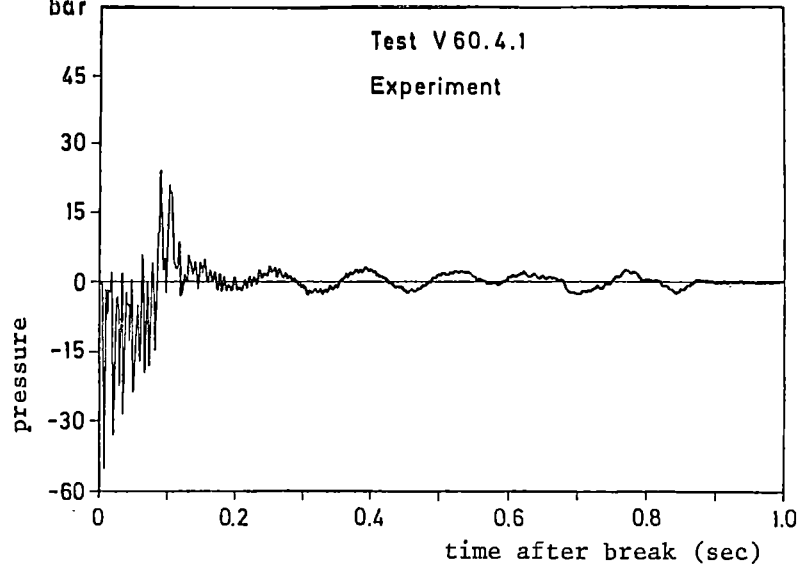


Figure 5: Experiment

Figure 5 to 7 give the pressure difference in the vertical pipe (RP 22o3 - RP 22o2)

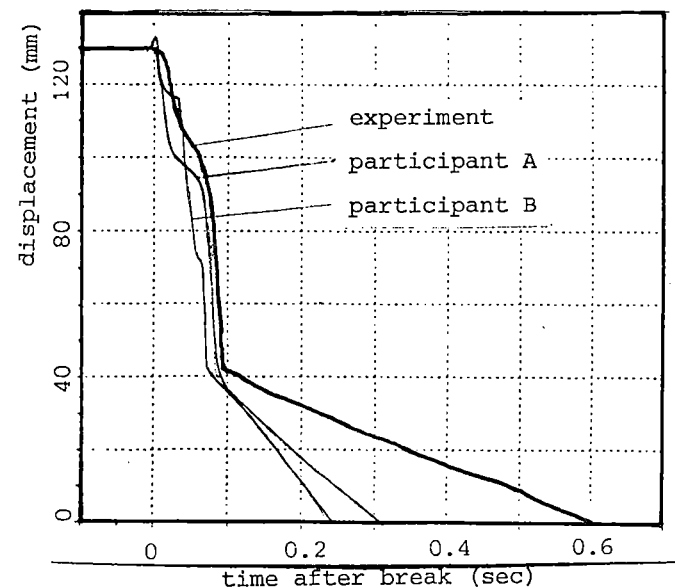


Figure 4: Valve motion (SF 3oo1)

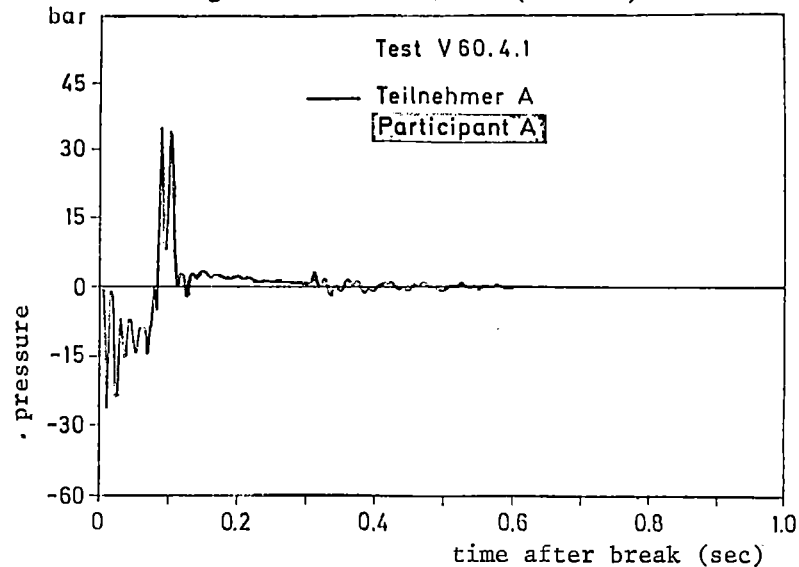


Figure 6: Participant A

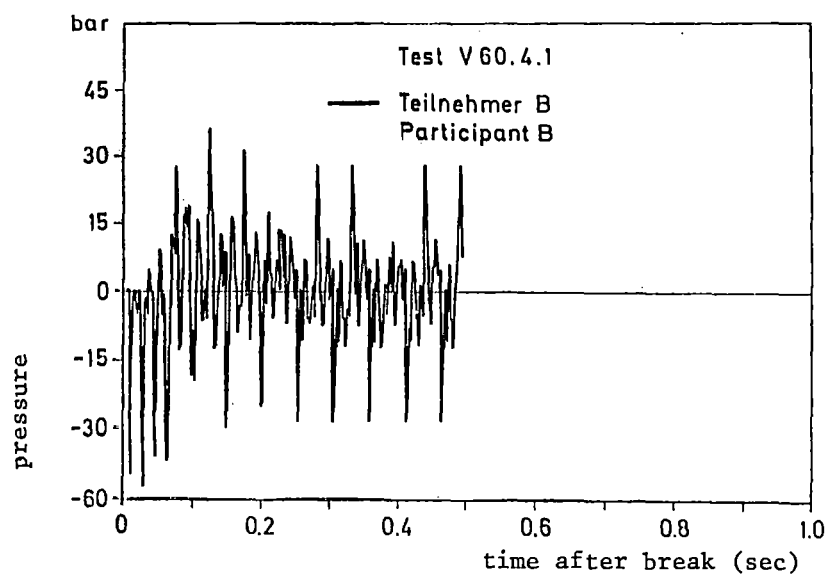


Figure 7: Participant B

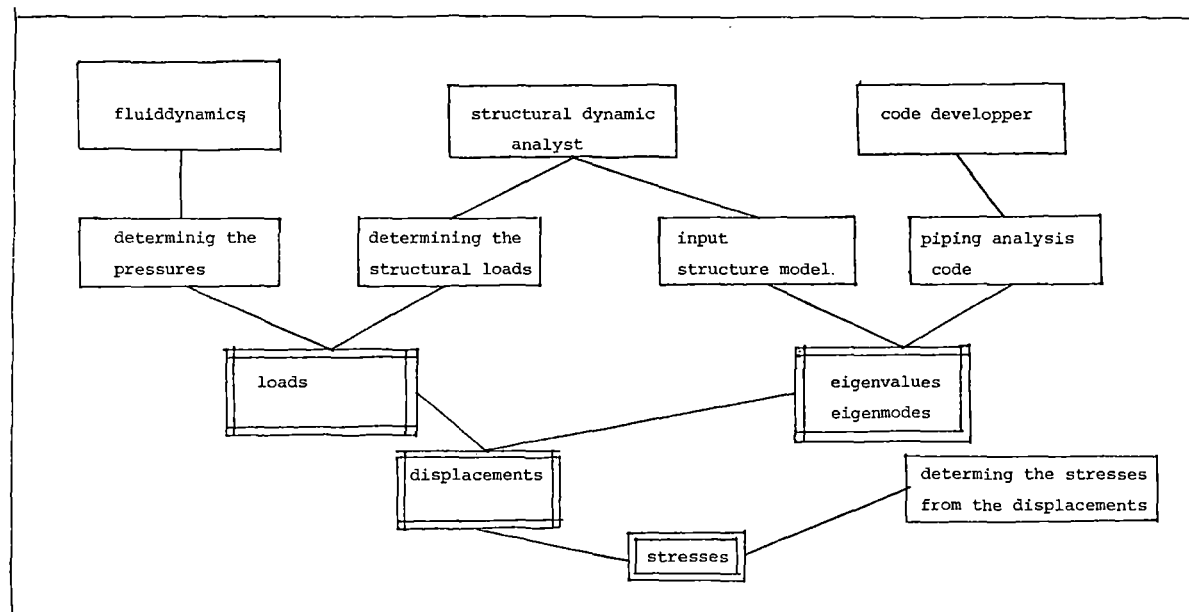


Figure 8: Sources of discrepancies

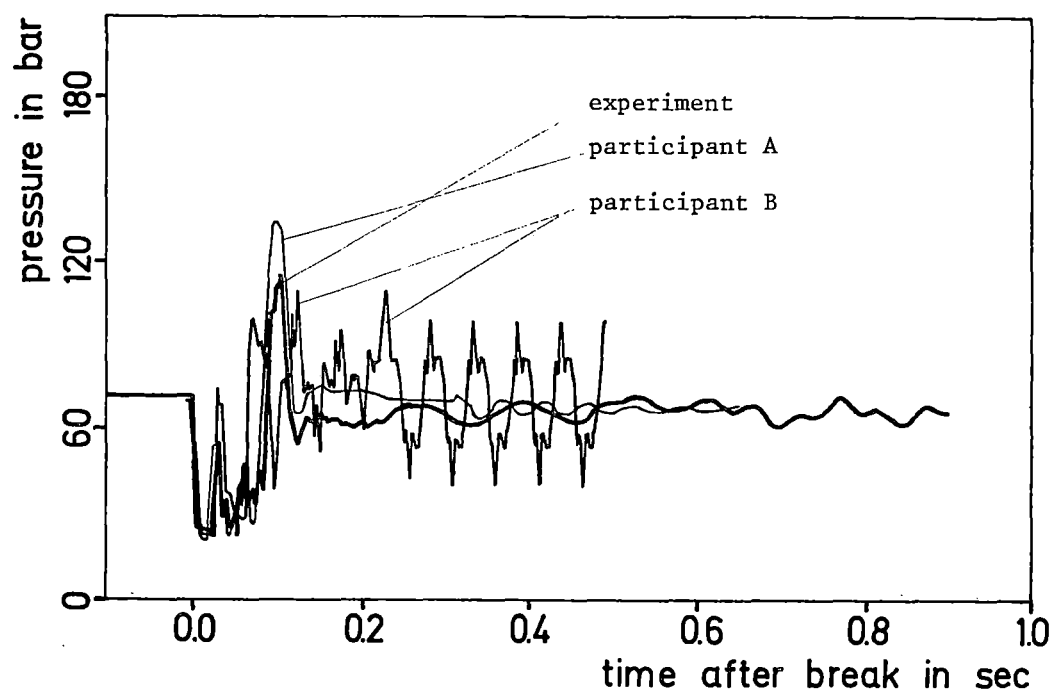


Figure 9: Pressure RP 22o5 (experiment and blind-blind calculations)

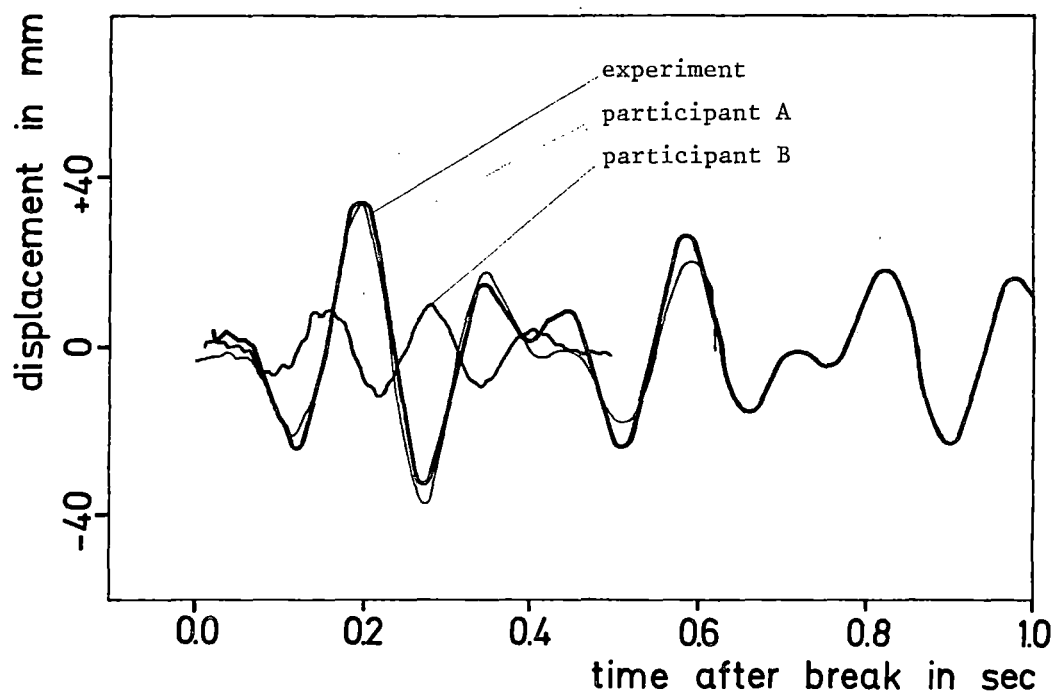


Figure 10: Displacement RS 22o1 (experiment and blind-blind calculations)

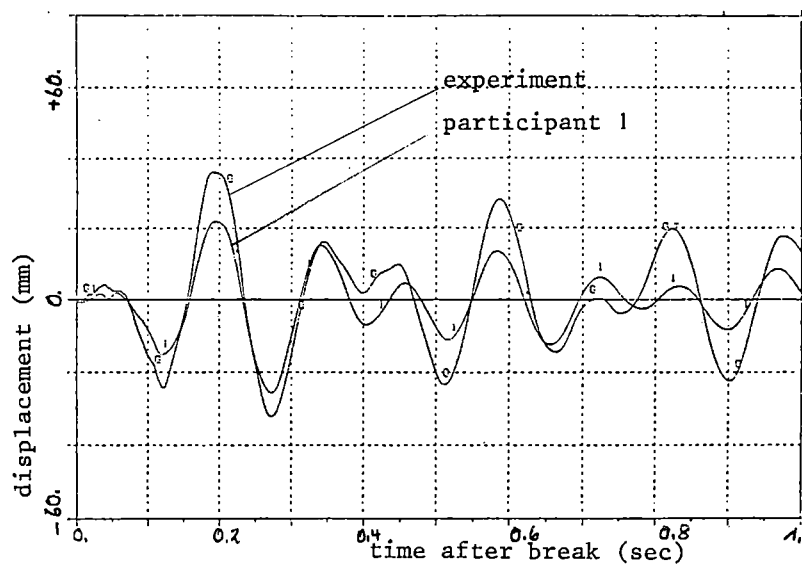


Figure 11: Displacement RS 2201

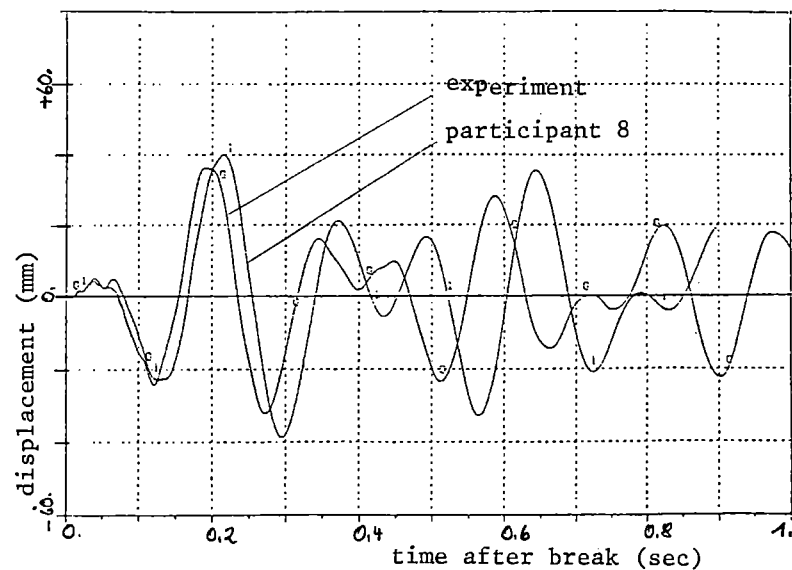


Figure 12: Displacement RS 2201

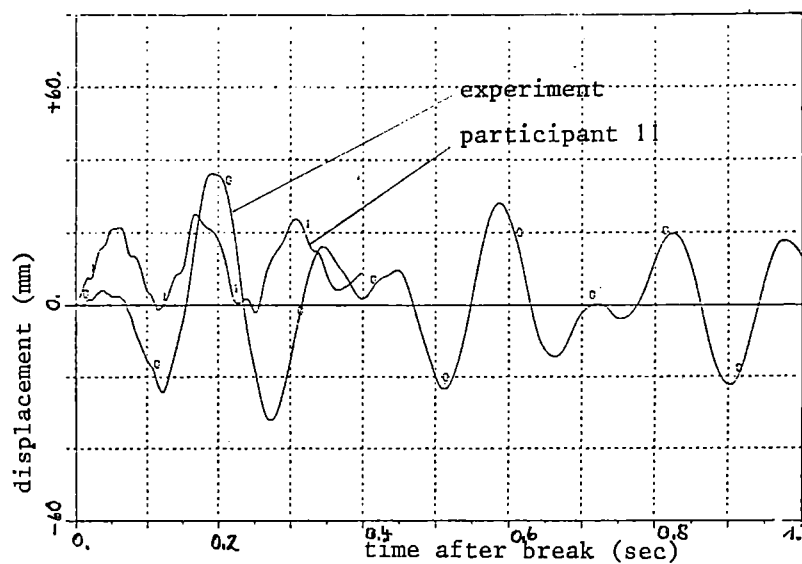


Figure 13: Displacement RS 2201

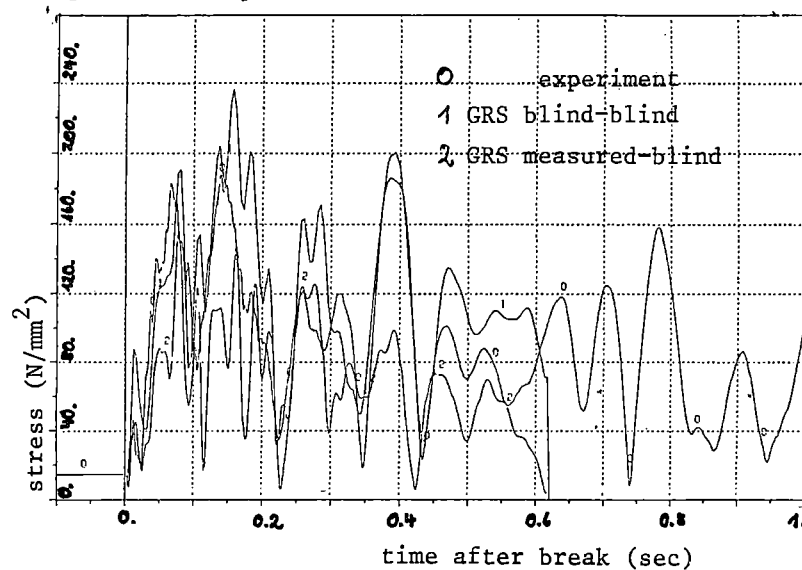


Figure 14: Bending stress RK 2014, Participant GRS

STATIC AND DYNAMIC TESTS ON REINFORCED CONCRETE SHEAR WALLS AT HIGH LOADS

E. G. Endebrock and R. C. Dove

Los Alamos National Laboratory
Los Alamos, New Mexico 87545 U.S.A.

ABSTRACT

Static and dynamic tests on small sized reinforced concrete shear walls are described and the results are presented. Monotonic and cyclic loadings were quasistatically applied to determine load-deformation characteristics of the shear walls. Classical sine sweep tests were performed to gain knowledge on the dynamic behavior of structures subjected to high loads. These tests show that reinforced concrete shear walls undergo stiffness degradation at high loads and under load reversals. The tests illustrate that classical vibration tests are not useful tools for studying the behavior of nonlinear structures.

INTRODUCTION

The information presented below is intended to increase the understanding of the behavior of Non-Containment Category I structures subjected to earthquake loads beyond the design values.

Available information on the dynamic testing of reinforced concrete shear walls, one of the principal structural elements of a Category I building, is limited; therefore the shear wall was selected for testing. Because of test facility loading capacities and the desire to fail the test structures, it was necessary to use small sized shear wall test structures. A 1 in. wall thickness was selected (actual facility wall thicknesses range from 18-48 in.). The length of the test section was 18 in. and the length to height ratio was 2.5. The shear wall test structure and reinforcement details are shown in Fig. 1.

The shear wall reinforcing consisted of a layer of 0.5 in. mesh hail screen located near each wall surface. The reinforcement ratio was 0.28% each way and each face. Anchorage was sufficient to develop the full strength of the screen wires. Threaded rods were placed near the wall ends to provide flexural reinforcement (Fig. 1). The microconcrete compressive strength ranged from 6000-7500 psi with tensile strengths of approximately 10% of the compressive strength. The modulus of elasticity was about 3.0×10^6 psi.

STATIC TESTS

Quasistatic monotonic or cyclic loads were applied to the shear walls as indicated in the schematic (Fig. 2). Direct current variable transformer (DCVT) displacement transducers were used to obtain the difference in horizontal displacements between the base and top of the shear wall. The measured data were plotted as load vs relative deformation diagrams.

Figure 3 shows a typical load-deformation relationship for a monotonically loaded shear wall and Fig. 4 shows results from a cyclic load test. A data summary of the quasistatic tests is given in Table I.

The failure mode was mostly influenced by the amount of flexural reinforcing. Test structures with the smaller amount of flexural reinforcing produced few shear cracks. A failure occurred when a large crack at the wall-base interface formed. The test structures with the larger amount of flexural reinforcing displayed numerous shear cracks and a shear failure occurred within the wall section.

The most significant observation noted from the quasistatic tests was the difference in observed and calculated initial stiffness. Observed initial stiffness values were only 30-40% of the calculated stiffness. This phenomena has also been observed by other researchers.^{1,2}

The load-deformation curves obtained from the cyclic-load tests were integrated to determine the area (measure of energy loss per cycle) inside the hysteresis loops. The results are presented in Table II. Under numerous and questionable assumptions, an equivalent viscous damping ratio can be computed. The computed damping ratios are also presented in Table II. It appears that the test structures with the smaller amount of moment reinforcement have the greater amount of energy dissipation per cycle at the higher load levels.

VIBRATION TESTS

The shear wall structures were mounted on a horizontal slip plate that is driven by a 20 000 lb force electrodynamic shaker. Added mass consisted of five steel plates with a total weight of 300 lbs. The primary data recorded were the horizontal base accelerations (input) and horizontal accelerations of the top mass (response). Sine-sweep tests were conducted with the the shaker was controlled on the response. The purpose of this was to maintain the response at a nearly constant value. An example of the input and response accelerations, as measured during a test, are shown in Fig. 5. During each sine-sweep test, the response acceleration was increased with each successive sine-sweep test until failure occurred. The usual absolute acceleration transmissibility curves for each sine-sweep test of a particular shear wall structure are shown in Fig. 6. In the dynamic tests, few shear cracks became visible. Failure occurred whenever a wall to base interface flexural crack formed at each end and then propagated until the cross-section had insufficient strength to resist the shear forces. Results of the sine-sweep tests are given in Table III.

The absolute acceleration transmissibility curves show how effective natural frequency and effective viscous damping is influenced by the response acceleration level. Effective natural frequencies decrease as the response acceleration, or load level, increases. The equivalent viscous damping increased in some cases and decreased in others as the load level increased; hence, no conclusion can be stated.

The major conclusion derived from the sine-sweep tests and subsequent tests using earthquake accelerogram loading was that classical vibration tests yield little useful information relating to prediction of earthquake response of degrading structures. Fatigue failure likely occurs because the test structures are subjected to hundred of thousands of load reversals before final failure. Classical vibration tests depend upon steady-state responses, and for degrading structures, it is doubtful that steady-state can be achieved. All subsequent dynamic tests related to this program will use earthquake accelerograms for the input signal.

FURTHER INVESTIGATIONS ON SHEAR WALL BEHAVIOR

Additional dynamic tests on one- and two-story shear wall structures have been completed but the results are not yet available. Further research will involve small box structures. In addition, the size effect will also be investigated by testing a larger structure.

ACKNOWLEDGEMENT

This work was performed under the auspices of the Mechanical/Structural Engineering Branch of the US Nuclear Regulatory Commission.

REFERENCES

1. H. Umemura, H. Aoyama, M. Ito, and Y. Hasakawa, "A Seismic Characteristics of RC Box and Cylinder Walls," Sixth World Conference on Earthquake Engineering, New Delhi, India (1976).
2. J. Gauvain, A. Hoffmann, C. Jeandidier, and M. Linolant, "Tests and Calculations of the Seismic Behavior of Concrete Structures," Proceeding, Fifth Conference On Structural Mechanics in Reactor Technology, Berlin (1979).

TABLE I
DATA SUMMARY

GROUP I, LARGE MOMENT REINFORCEMENT

Specimen No. and Load Condition	(1) Δ (in.x10 ⁻³)	(2) K_1 (lb/in.x10 ⁶)	(3) F_{ULT} (lb)	(4) U_{ULT} (in.x10 ³)	$\mu = \frac{U_{ULT}}{\Delta}$	(5) V_u (lb)
No. 2, Monotonic	4.5	0.79	6640	32	7.2	5320
No. 1, Cyclic	4.5	0.78	6470	44	9.8	4870
No. 3, Cyclic	3.2	1.0	6440	38	11.9	5630

GROUP II, SMALL MOMENT REINFORCEMENT

Specimen No. and Load Condition	Δ (in.x10 ⁻³)	K_1 (lb/in.x10 ⁶)	F_{ULT} (lb)	U_{ULT} (in.x10 ³)	$\mu = \frac{U_{ULT}}{\Delta}$	V_u (lb)
No. 4, Monotonic	3.3	1.06	6660	22	6.8	5570
No. 5, Cyclic	4.0	0.87	5880	26	6.5	5390

- Notes:
- (1) Δ = deflection at a load of 3500 lb
 - (2) K_1 = stiffness modulus in linear region
 - (3) F_{ULT} = maximum positive load, last complete cycle
 - (4) U_{ULT} = deflection at F_{ULT}
 - (5) V_u = ultimate strength computed using ACI-349

TABLE II
HYSTERETIC ENERGY LOSS

A. SPECIMEN NO. 3 - GROUP I, LARGE MOMENT REINFORCEMENT

Cycle No. (Fig. 5)	Δ (in.-lb/cycle)	F_{pk} (lb)	$K_s^{(1)}$ (lb/in. 10^6)	$\epsilon_e^{(2)}$ %
1	3	3000	1.09	5.8
11	10	4240	0.77	6.8
14	21	4920	0.65	9.0
19	23	4920	0.62	9.4
26	62	5920	0.31	8.7
28	68	5920	0.25	7.7

B. SPECIMEN NO. 5 - GROUP II, SMALL MOMENT REINFORCEMENT

Cycle No. (Fig. 5)	Δ (in.-lb/cycle)	F_{pk} (lb)	$K_s^{(1)}$ (lb/in. 10^6)	$\epsilon_e^{(2)}$ %
7	2	2740	1.18	5.0
10	7	3880	0.87	6.4
13	18	4640	0.67	8.9
15	40	4960	0.42	10.9
16	126	5600	0.34	21.7
17	173	5880	0.23	18.3

Notes: (1) K_s is the secant stiffness modulus at the corresponding peak force, that is, the slope of the straight line joining the origin and the extreme peak of the positive hysteretic loop.

(2) ϵ_e is computed as $\epsilon_e = \delta E \times K / 2\pi F^2$.

TABLE III
RESULTS OF SINE SWEEP TEST

Specimen	Test	Response Acceleration Level - \ddot{x}	Resonant Frequency- f_R	Equivalent Stiffness- K_e	Equivalent Viscous Damping- ξ_e
No.	No.	(g)	(hz)	(lb/in.) $\times 10^6$	(%)
12	1	1.19	86	0.26	3.9
	2	2.41	72	0.18	3.2
	3	3.55	56	0.11	2.6
	4	4.59	53	0.10	2.5
	5	2.33	50	0.09	2.4
13	1	1.21	75	0.20	3.4
	2	2.14	66	0.15	3.4
	3	3.37	59	0.12	3.9
	4	4.21	48	0.08	5.6
	5	5.55	42	0.06	4.3
11	1	0.97	65	0.15	6.4
	2	1.93	56	0.11	4.0
	3	3.03	50	0.09	3.5
	4	4.20	42	0.06	2.9
	5	4.33	--	--	--
10	1	0.94	132	0.61	3.8
	2	1.57	125	0.54	6.5
	3	5.44	--	--	--
	4	5.38	72	0.18	8.5
	5	9.90	--	--	--

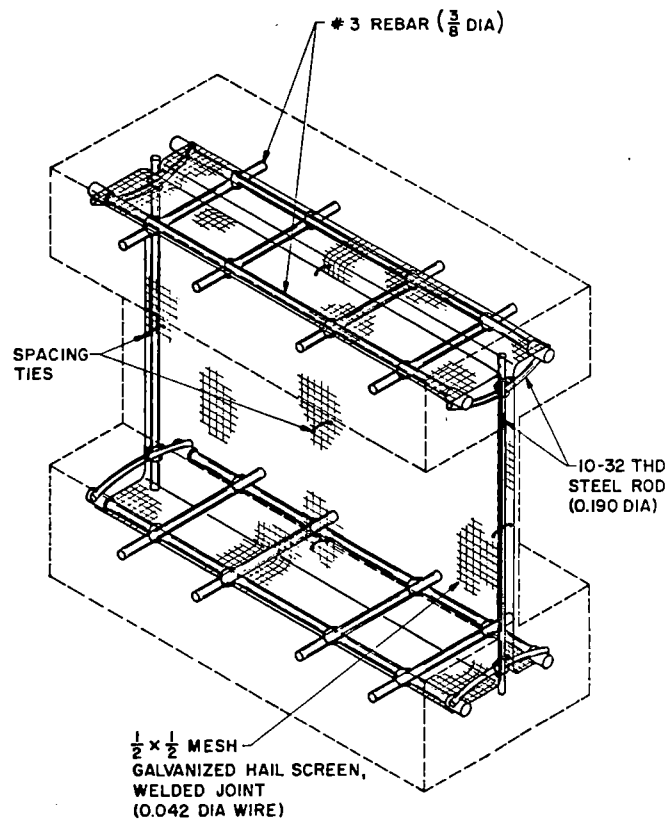


Fig. 1. Reinforcement Details of Shear Wall Structure.

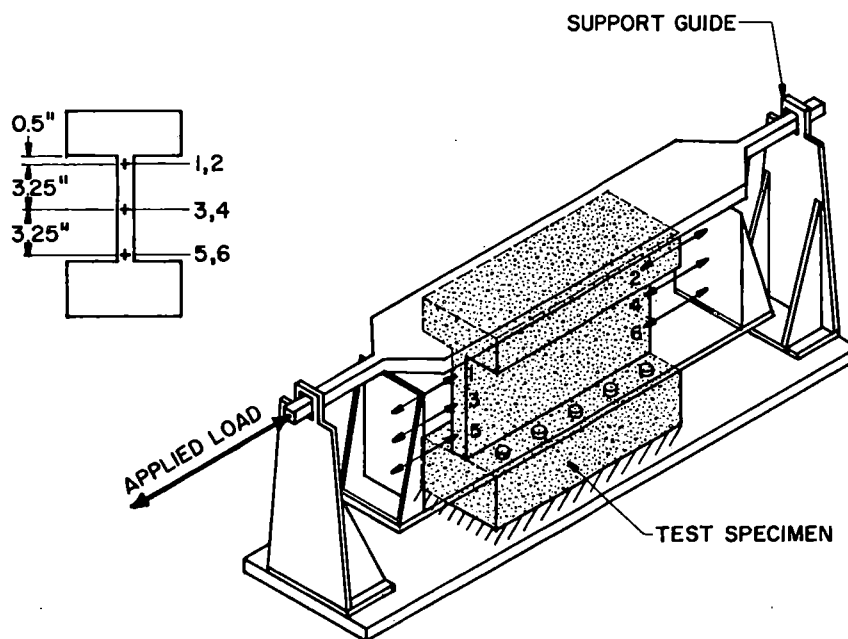


Fig. 2. Schematic of Static Test Arrangement.

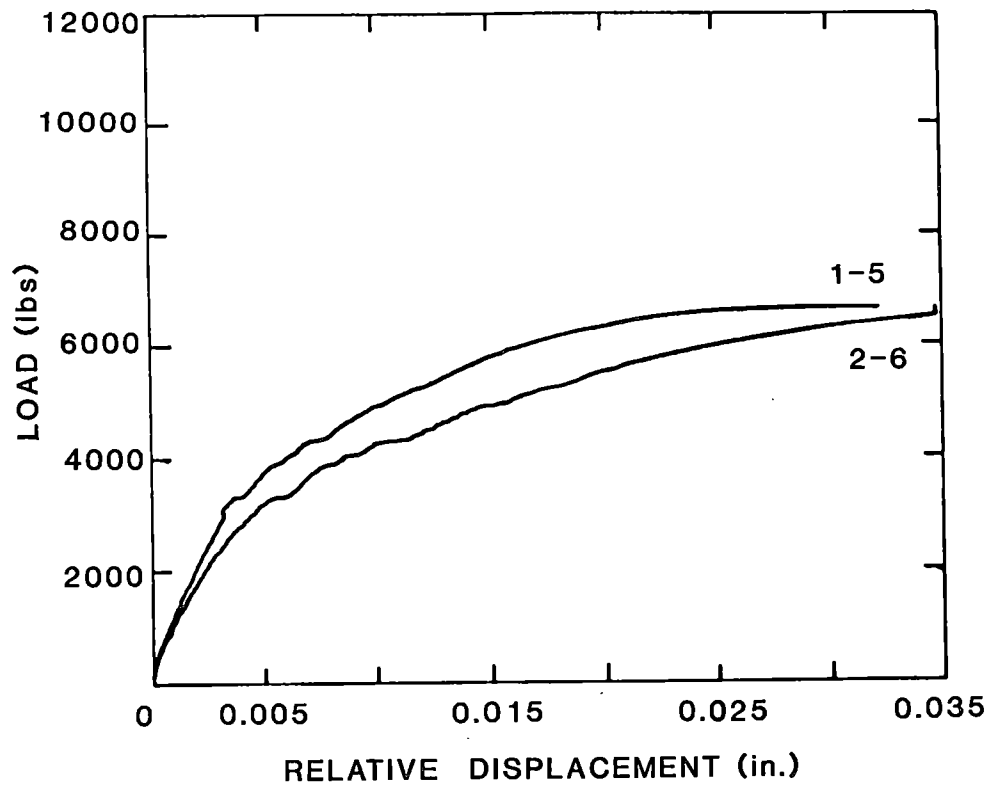


Fig. 3. Typical Static Load-Deformation Relationships

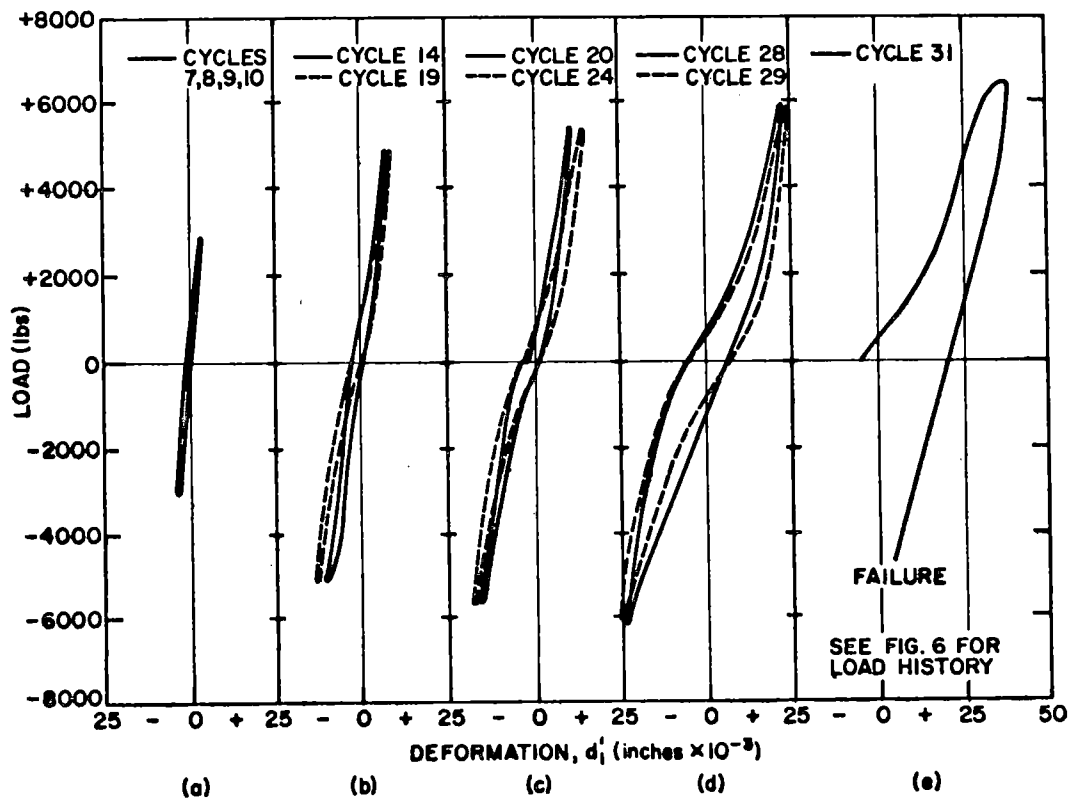


Fig. 4. Typical Quasistatic Cyclic Load Results.

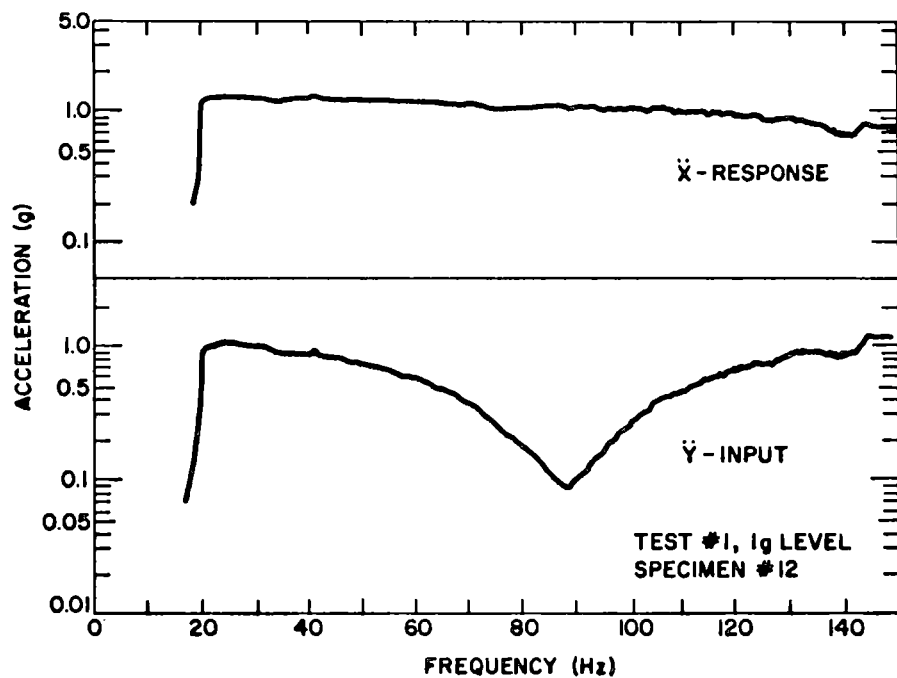


Fig. 5. Input and Response Accelerations During Sine-Sweep Tests.

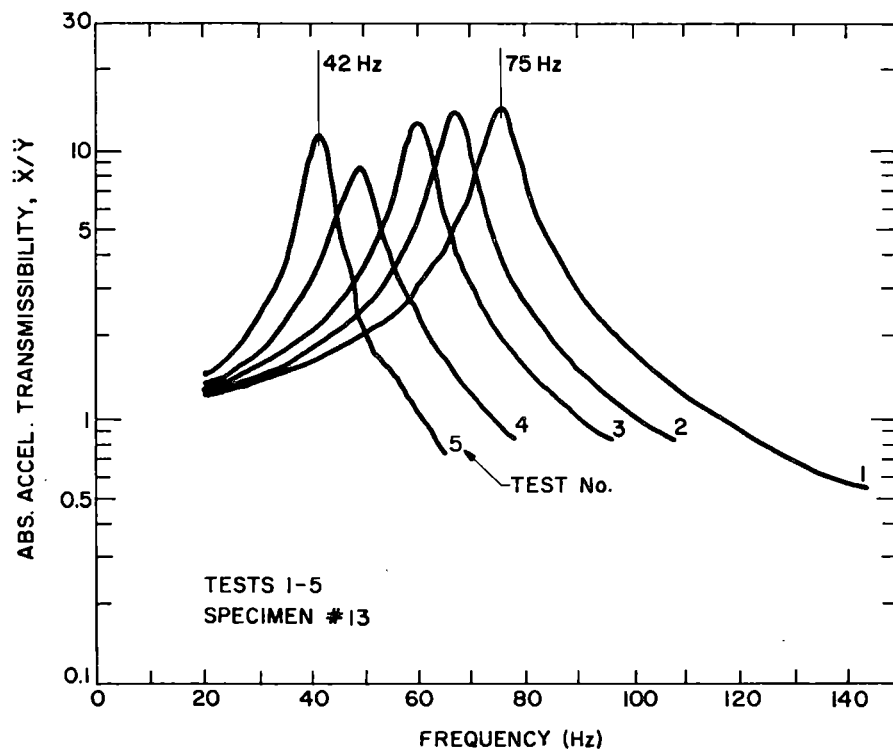


Fig. 6. Typical Absolute Acceleration Transmissibility Curves.

QUALIFICATION OF UNREINFORCED MAN-HOLES IN
THIN-WALLED PIPING OF AUXILIARY/EMERGENCY
COOLING WATER SYSTEMS

Zs. Révész

Electrowatt Engineering Services Ltd.
CH-8022 Zurich, Switzerland

ABSTRACT

Detailed stress analysis of cylindrical joints became necessary with the overstress calculated using finite-element models and stress indices according to the ASME BPV Codes for Class 2 Components. The joints in question are man-holes in thin walled, large diameter piping systems built as unreinforced tee-junctions. With more accurate calculation evaluated corresponding to alternative design procedures, numerous unreinforced man-holes have been qualified from the software side. All these are components of the emergency/auxiliary cooling water piping. The paper presents the modelling technique, derivation of the applied loads and selected results.

INTRODUCTION

In the design of nuclear power plants, safety and operational reliability require comprehensive analysis of events prior to their occurrence. In this view all safety-related equipments have to be examined before taken into operation. Safe operation of a nuclear plant requires the design of redundant heat sink systems. Although many elements of the involved piping systems have been used extensively in conventional power plants, their nuclear application is in many cases still new. Therefore, a unique and detailed stress analysis is necessary to demonstrate that the element in question will fulfill its function during the postulated events. Structural analysis of this kind lately became one of the most extensive engineering efforts required for the safety design in the nuclear industry.

This paper presents selected results from stress analysis performed for cylindrical joints in thin-walled pipes and the procedure of qualification of piping tees through detailed analysis. The investigated geometries are typical for auxiliary and emergency cooling water systems. Design and qualification of these systems for Leibstadt Nuclear Plant required several iterative steps, because piping stress analysis initially indicated overstressing at different locations under various loading conditions. The procedure described here demonstrates how one problem has been solved from the software side. The specific problem was

that the stress indices applied according to the specifications of the ASME BPV Codes for Class 2 Components [1] resulted in values above the allowable limits in case of the unreinforced man-holes of the pipings in question. To solve this problem the stress peaks of the unreinforced man-holes of the piping were analyzed, thus qualifying the components this way rather than applying subsequent reinforcements.

It has not been attempted in this work to elaborate general design rules as e.g. in [2]. The specific geometries of the applied design have been investigated and a standard method of qualification has been developed instead. This method appears feasible and economic, is fast and corresponds to the design criteria as established in Article NC-3200 (= Alternative Design Rules for Vessels) of [1].

Those efforts necessary for evaluation of the overwhelming amount of data computed with the finite element code CORTES [3] and for the engineering interpretation of the results have been minimized by using computer graphics based on the program GRFPAK [4].

DEVELOPMENT OF THE MAN-HOLE MODEL

The input data for the detailed stress analysis of man-holes has been given by piping analyses using recognized finite element technique [5]. Results of these piping structural analysis with bar elements have then been used to develop input for the shell-type FE model of the man-holes. The aim of the work has been the qualification of piping systems by separate analysis of those components which showed stresses above the allowable limits. The most critical sections are the man-holes where high stress intensification factors are to be applied if working with the corresponding codes. Detailed descriptions of the more accurate evaluations (e.g. [6]) have been prepared for the licensing authorities containing all that information which is briefly presented below.

The FE model of the piping system is illustrated in Fig. 1 by the straight lines between nodes A, B, C and D.

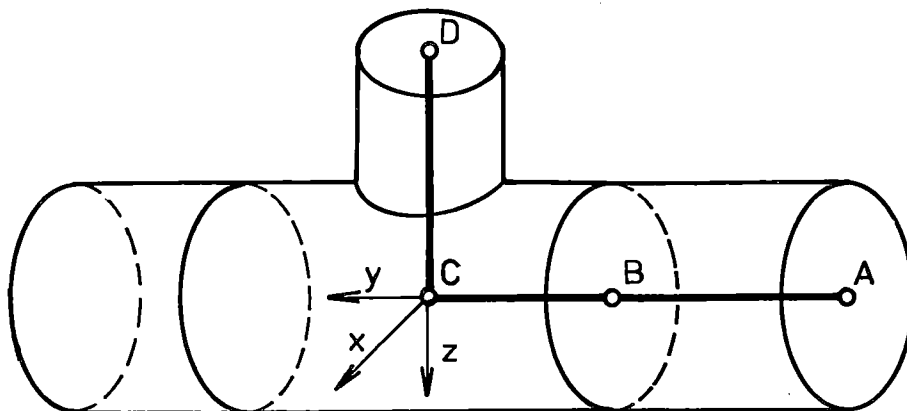


Fig. 1 Model geometry

The results provided by the piping analysis are forces and moments in these nodes where the bar-type elements have their interfacing points. The magnitude of these results is unpredictable and an interpolation between nodes is hardly possible since the data may represent combinations of different dynamic and static loads. Distances between nodes in the run pipe may be asymmetric and wall thickness may vary.

Further, the T-junction model in the applied computer code is modeled with stiff cross sections at the end of the branch and of each run section. To get realistic deformation shape in the tee, these ends must be chosen far from the end of the tee. It has been decided therefore that both halves of the tee will be modeled separately and the distances between nodes A, B, C and D will not be changed during the development of the man-hole model. So the forces and moments delivered by the piping analysis at these locations have to be transformed into those which can be introduced into the shell-type FE model.

1. 700000 N/(m*m)
2. -735 N
3. -80922 Nm
4. -43198 Nm
5. 1788 Nm
6. -5912 N
7. 2667 N
8. 0 Nm
9. 0 Nm
10. 0 Nm
11. -280 N
12. -1863 N
13. -885 N

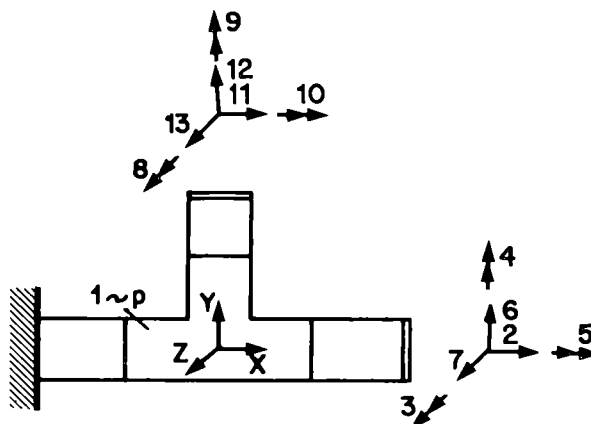


Fig. 2 The basic load cases

The 13 basic load cases are shown in Fig. 2. The input for these load cases has been derived as follows:

- LC 1 : Internal pressure uniformly distributed.
- LC 2 : Analogously to the maximum shear stress theory the difference of the forces in the nodes B and C has been input in C.
- LC 3 : The maximum of the moments in B and C will be applied in A. The moment arisen through the shift in LC 6 has been compensated with an additional moment in A so that no load will be effected by the shift in B.
- LC 4 : Analogously to LC 3.
- LC 5 : The maximum of the moments in B and C will be applied in A.
- LC 6 : Analogously to LC 2.
- LC 7 : Analogously to LC 2.

LC 8 : No loading.
 LC 9 : No loading.
 LC 10: No loading.
 LC 11: No change in the input.
 LC 12: No change in the input.
 LC 13: No change in the input.

Note that the system of coordinates in the piping (Fig. 1) and the man-hole model (Fig. 2) are not identical.

With this a standard procedure has been established using the above described transformation. This procedure is easy to follow and leads to an always conservative man-hole model with direct application of data from the piping structural analysis.

NUMERICAL RESULTS

In the computation the man-hole models have two planes of symmetry. The assumption of these symmetries allows the reduction of the model to one quarter of the original geometry. The model shown in Fig. 2 may be asymmetric i.e. the distance AB on Fig. 1 is not necessarily the same on both sides of the branch requiring that both halves of the tee were modeled separately. Each of these models describes one half of the man-hole. One quadrant of a model has been shown in Fig. 3. The unreinforced tee can be recognized by the denser grid used for its representation.

To preserve transparency, all numerical results presented here are from [6] and are related to the same half of the tee. The loads are specified in Fig. 2. The deformed mesh with the maximum stress intensities is depicted for each basic load case in Fig. 4-6.

The deformation in these figures is magnified. These plots visualize a part of the results and help the engineer to check the plausibility of them. Further the position of the critical part of the component is indicated for each component load case on these plots. It can be observed in these plots that the effect of the blockage of the ends of the structure in fact diminishes in the run and the branch of the man-hole.

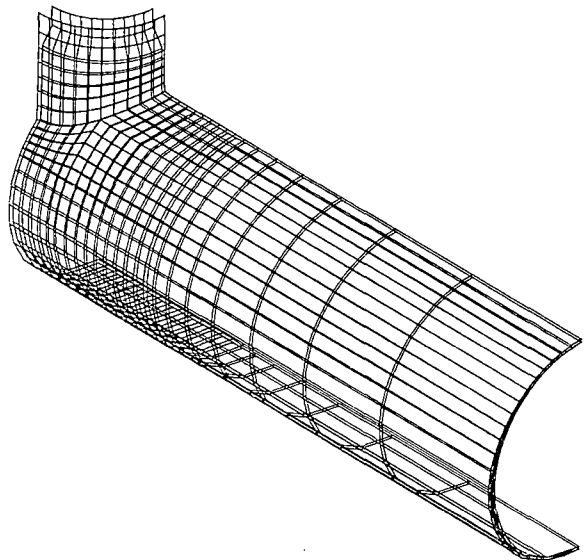


Fig. 3 FE mesh of man-hole

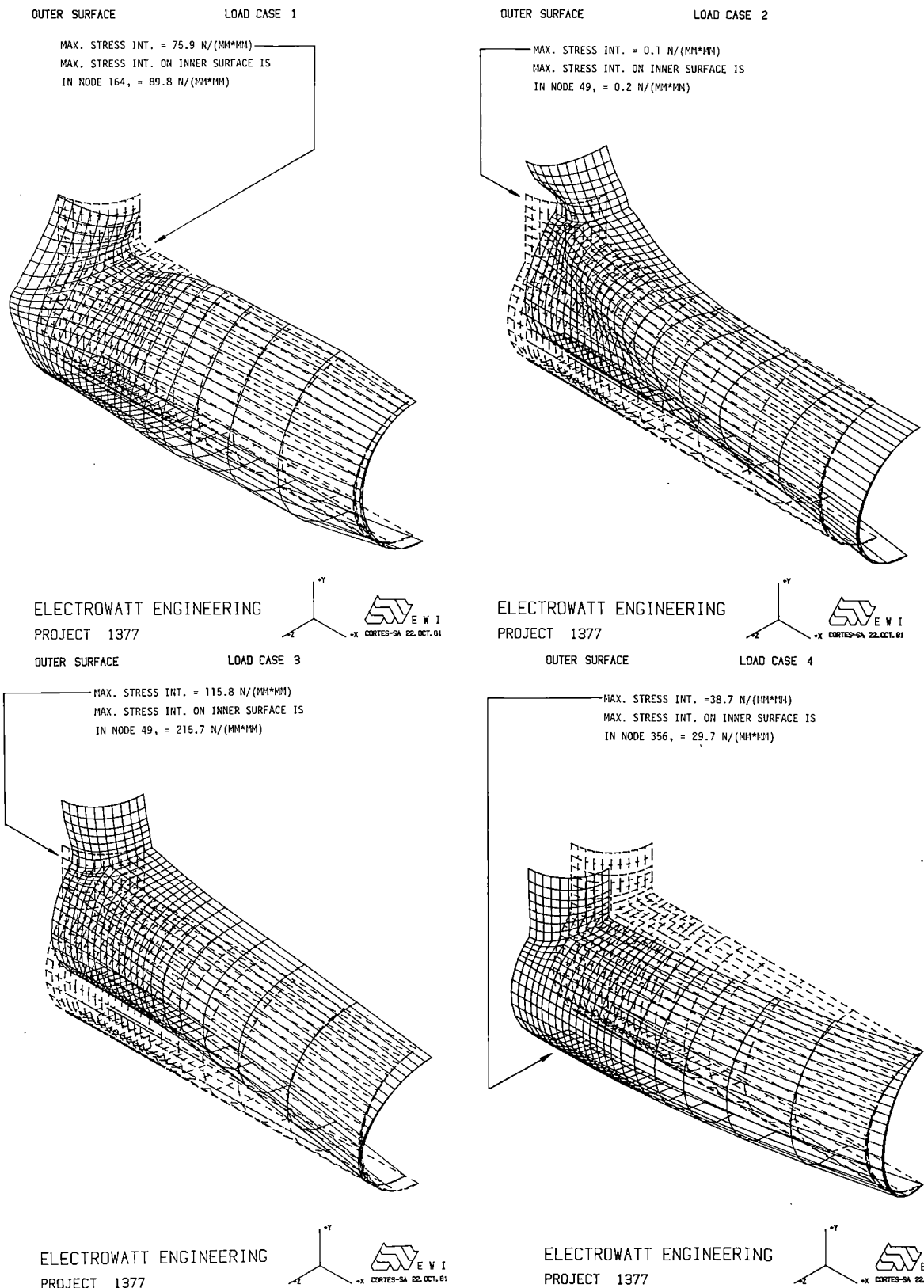
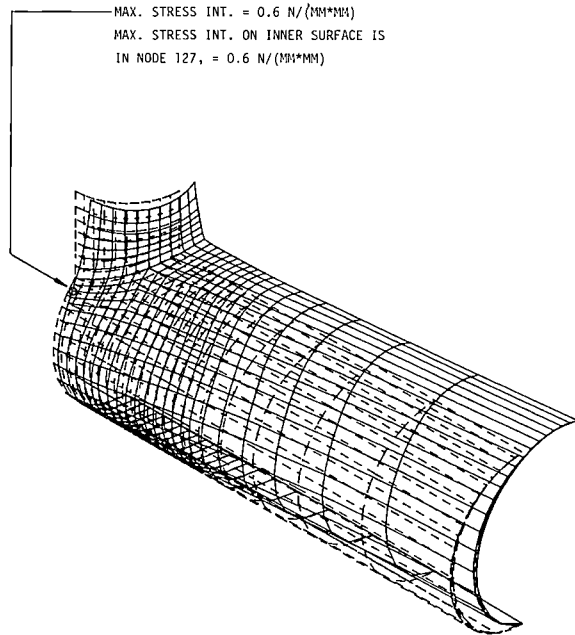


Fig. 4 Deformation shape and maximum stress intensities in the basic load cases 1, 2, 3 and 4

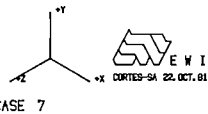
OUTER SURFACE

LOAD CASE 5

MAX. STRESS INT. = $0.6 \text{ N/(MM}^2\text{MM)}$
 MAX. STRESS INT. ON INNER SURFACE IS
 IN NODE 127, = $0.6 \text{ N/(MM}^2\text{MM)}$

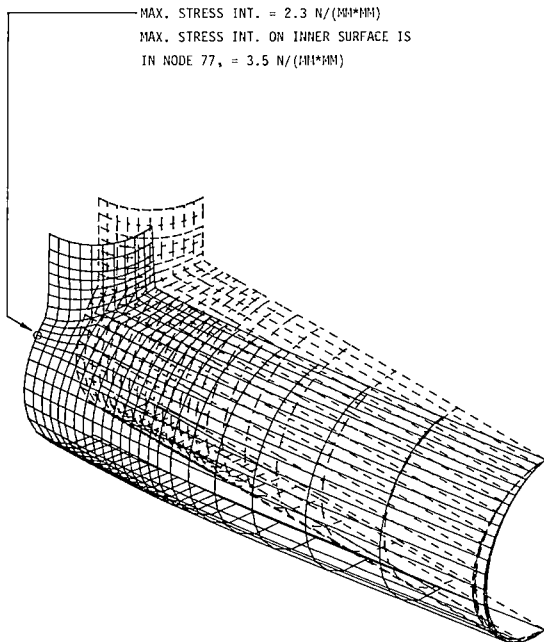


ELECTROWATT ENGINEERING
 PROJECT 1377
 OUTER SURFACE



LOAD CASE 7

MAX. STRESS INT. = $2.3 \text{ N/(MM}^2\text{MM)}$
 MAX. STRESS INT. ON INNER SURFACE IS
 IN NODE 77, = $3.5 \text{ N/(MM}^2\text{MM)}$



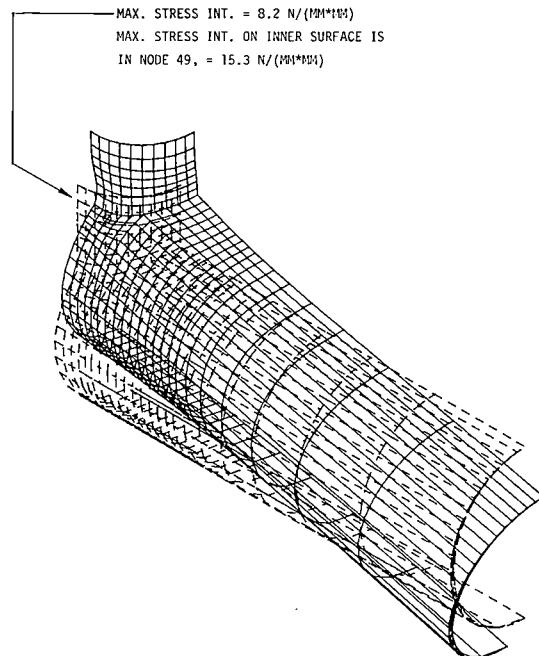
ELECTROWATT ENGINEERING
 PROJECT 1377



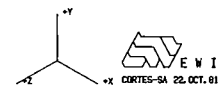
OUTER SURFACE

LOAD CASE 6

MAX. STRESS INT. = $8.2 \text{ N/(MM}^2\text{MM)}$
 MAX. STRESS INT. ON INNER SURFACE IS
 IN NODE 49, = $15.3 \text{ N/(MM}^2\text{MM)}$

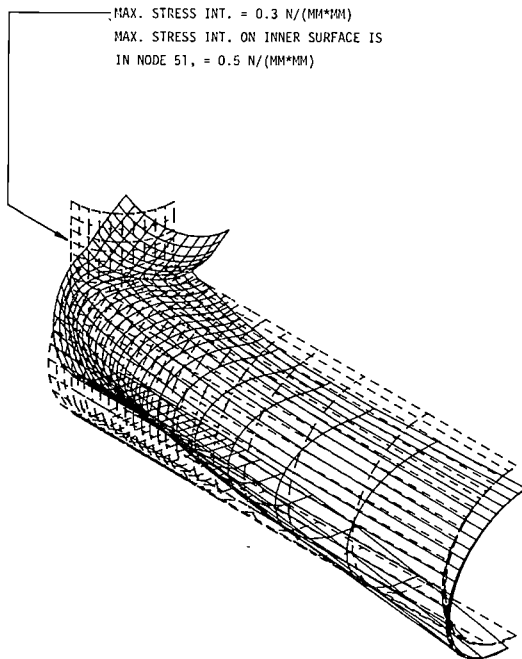


ELECTROWATT ENGINEERING
 PROJECT 1377
 OUTER SURFACE



LOAD CASE 11

MAX. STRESS INT. = $0.3 \text{ N/(MM}^2\text{MM)}$
 MAX. STRESS INT. ON INNER SURFACE IS
 IN NODE 51, = $0.5 \text{ N/(MM}^2\text{MM)}$



ELECTROWATT ENGINEERING
 PROJECT 1377



Fig. 5 Deformation shape and maximum stress intensities
 in the basic load cases 5, 6, 7 and 11

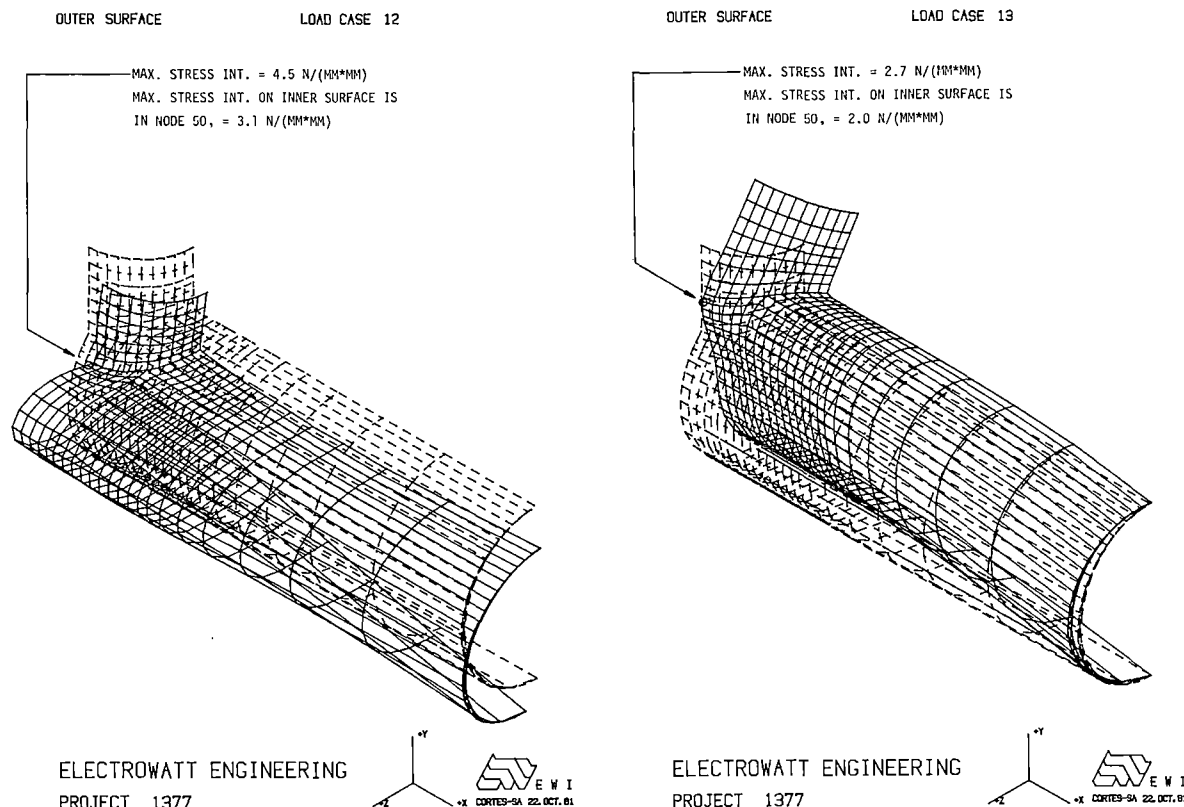
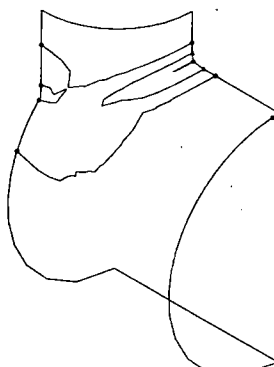
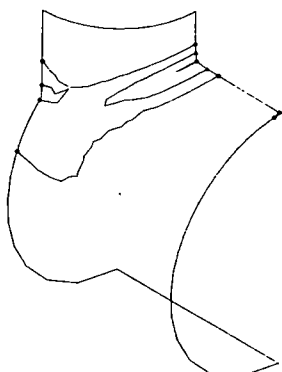
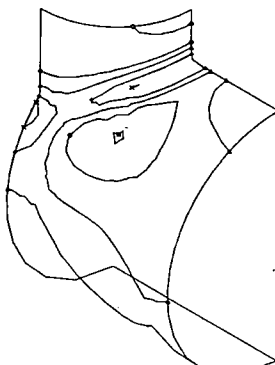
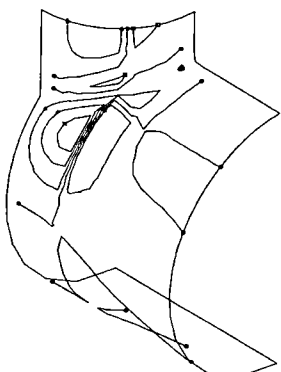
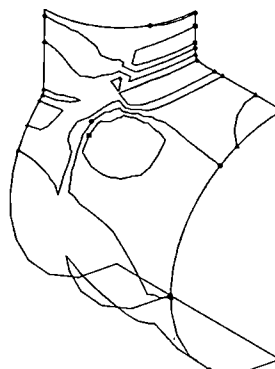
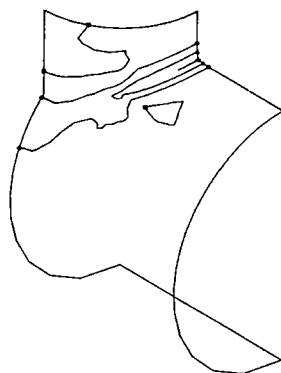


Fig. 6 Deformation shape and maximum stress intensities in the basic load cases 12 and 13

The basis for determining the limiting stress is the maximum shear stress theory saying that the quantity of strain energy stored per unit volume is responsible for material failure. The evaluation requires the computation of the differences between the algebraically largest and algebraically smallest principal stresses under combined loading and the comparison of these so called stress intensities with the mechanical properties of the material used. The evaluation of stresses in case of internal pressure is given for the outer surface in Fig. 7. It is interesting to note the good agreement in the stress intensification factors (SIF) compared to those published in [7].

For the evaluation of a certain loading condition all basic load cases have to be superimposed. The loading defined in Fig. 2 leads to a combined loading case, the result of which is summarized in Fig. 8. The figure shows the maximum stress intensities on both surfaces as well as the longitudinal and transversal stresses in the symmetry planes of the tee.

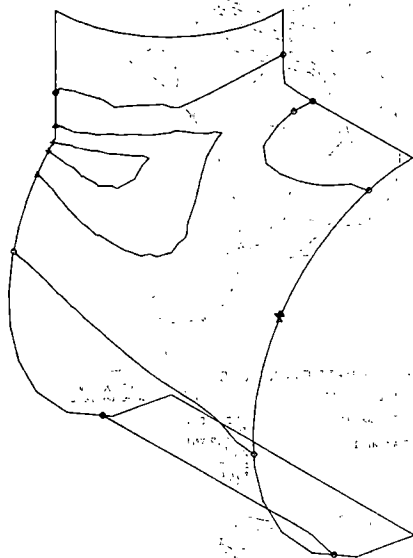
The detailed evaluation has been performed for all stress categories defined in Appendix XIII of the ASME Codes [8]. The results computed for unreinforced man-holes in thin-walled piping have generally a smaller stress maximum if computed according to the alternative design procedure rather than applying the stress intensification factors which are accepted for piping structural analysis [1]. This is the result of two different tendencies. Firstly the detailed analysis results in higher SIF-s for pressure loads, secondly moment loading leads to smaller SIF than those given in [1].



2099

OUTER SURFACE
QUADRANT 1

LOAD CASE 15
STR. INT.
CONTOUR VALUES
0 0
50.0
100.0
150.0
200.0
250.0

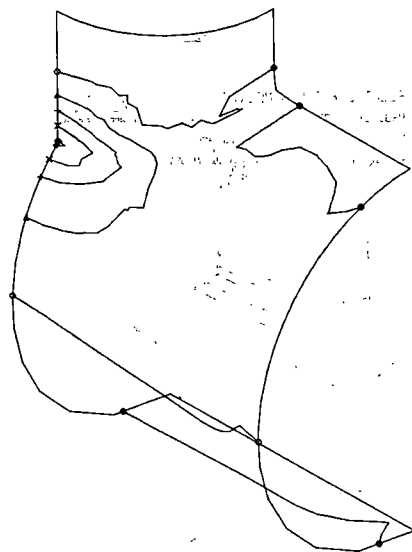


ELECTROWATT ENGINEERING
PROJECT 1377

E W I
CORTES-SA 26. OCT. 81

INNER SURFACE
QUADRANT 1

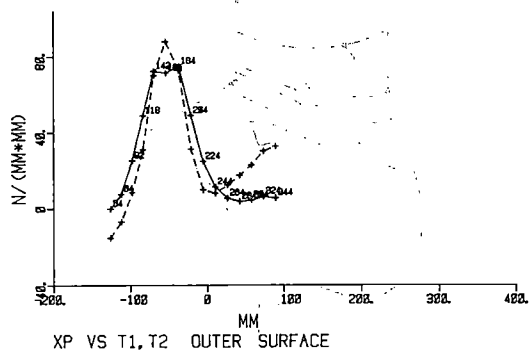
LOAD CASE 15
STR. INT.
CONTOUR VALUES
0 0
50.0
100.0
150.0
200.0
250.0



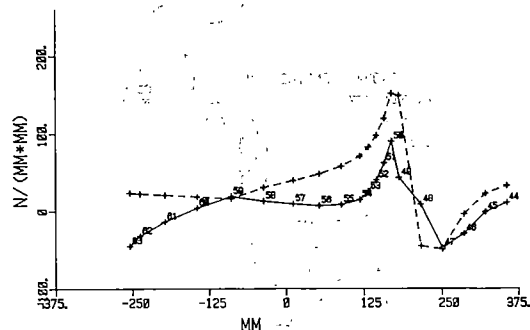
ELECTROWATT ENGINEERING
PROJECT 1377

E W I
CORTES-SA 26. OCT. 81

LOAD CASE 15
LONG. STR. - FULL, TRANSV. STR. - DOTTED



XP VS T1, T2 OUTER SURFACE

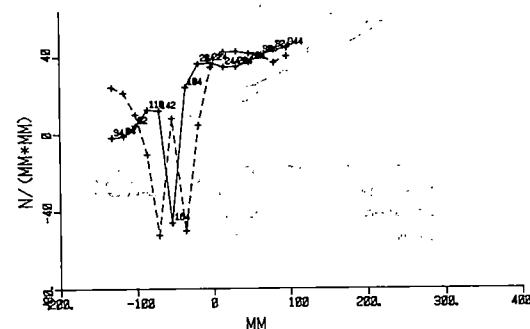


Y VS T1, T2 OUTER SURFACE

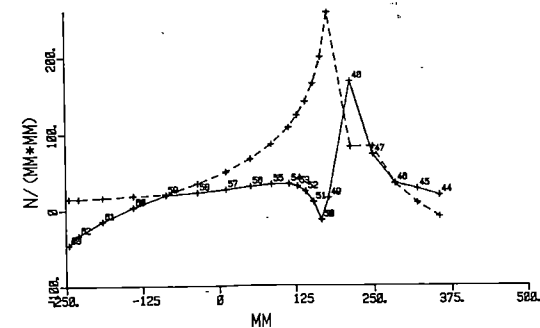
ELECTROWATT ENGINEERING PROJECT 1377
LOAD CASE 15

LONG. STR. - FULL, TRANSV. STR. - DOTTED

E W I
CORTES-SA 27. OCT. 81



XP VS T1, T2 INNER SURFACE



Y VS T1, T2 INNER SURFACE

ELECTROWATT ENGINEERING PROJECT 1377

E W I
CORTES-SA 27. OCT. 81

Fig. 8 Results of a combined load case (see Fig. 2)

The applied computer code CORTES-SA has been validated by measurements at ORNL [7]. Although the modelling technique may have a significant influence on the results there has been no need for additional validation because of geometrical similarities. The same code is being extensively used for parametric investigations for USNRC to develop recommendations for improved design rules [2].

SUMMARY

A standard procedure has been developed for detailed structural analysis of piping tees. This procedure allows the definition of the geometric and loading data straightforward from the results of piping analysis.

The procedure presented here is fast, economic and is suitable for analysis of piping tees as a routine task. Automatic generation of input data and graphic postprocessing of the results enlighten human assimilation of the overwhelming amount of computed data, thus accelerate the otherwise tedious evaluation of the results.

Using the presented analysis method numerous man-holes have been qualified from the software side making no changes in the construction necessary.

REFERENCES

1. ASME Boiler and Pressure Vessel Code Section III, Division 1, Subsection NC - Class 2 Components. New York, ASME, 1977 edition incl. Winter 1979 Addenda.
2. Bryson, J.W., W.G. Johnson and B.R. Brass: Stresses in Reinforced Nozzle-Cylinder Attachments - A Parameter Study, in Stress Indices and Stress Intensification Factors of Pressure Vessel and Piping Components edited by R.W. Schneider and E.C. Rodabough, New York, ASME (Vol. 50), 1981
3. Gantayat, A.N. and G.H. Powell: Stress Analysis of Tee Joints by the Finite Element Method, Berkeley, University of California (Ref. No. UC SESM 73-6), 1973
4. Fowler, P.G. and Bryson, J.W.: User's Manual for the CORTES Graphics Package GRFPAK, ORNL/NUREG/TM-127, Oak Ridge National Laboratory, August 1977
5. Gordis, K.: Outline of Dynamic Analysis for Piping Systems, Nuclear Engineering and Design, Vol. 52, No. 1, 1979
6. Révész, Zs.: Stress Analysis of the Man-Holes in the Emergency Cooling Water System (in German), Zurich, Electrowatt Engineering Services Ltd. (Doc. No. 1377/226.164), 1981
7. Bass, B.R., J.W. Bryson and S.E. Moore: Validation of the Finite Element Stress Analysis Computer Programme CORTES-SA for Analysing Piping Tees and Pressure Vessel Nozzles, Proceedings of ASME Petroleum and Mechanical Engineering Conference, Houston, TX, September 1977
8. ASME Boiler and Pressure Vessel Code Section III, Division 1, Appendices. New York, ASME, 1977 edition incl. Winter 1979 Addenda

SESSION 32

PANEL DISCUSSION: WHERE DO WE GO FROM HERE?

Chair: N. C. Rasmussen (*MIT*)
P. Tanguy (*CEA*)

Panelists

D. Buenemann (*GKSS*)
S. Levine (*NUS*)
D. Meneley (*OHC*)
L-S. Tong (*NRC*)

REVIEW OF MAN-MACHINE INTERFACE AND SAFETY-RELATED DESIGN CONSIDERATIONS

D. Buenemann

Gesellschaft fuer Kernenergieverwertung in Schiffbau und Schifffahrt mbH
Geesthacht, Federal Republic of Germany

The man-machine interface in nuclear power plants was discussed in three sessions, one of which was a poster session.

In Session 9, various aspects of the influence of human factors on the safety of nuclear power plants were presented. As explained in the first paper by D. L. Schurman (ASA), selection, training, job engineering, and work satisfaction are determining factors in the performance of an operator. But how can we come to a psychometric scaling? A statistical approach for a human reliability data bank, in support of probabilistic risk assessment for nuclear power plants, was described by J. S. Eckel (GPC). In any case, human reliability depends strongly on the operator aids available in the control room. As much as possible should be done in the future to improve and extend these operator aids. As an example, the paper by G. Depond (EdF) presented the powerful emergency procedure "UI" which takes into account the different educational levels of the operator and the shift technical advisor using post-accident diagnosis. This procedure should provide clear and limited information of all possible event combinations and should be sufficient for mitigating further system degradation. As R. Capel (EdF) pointed out during his presentation of the paper by M. me Griffon-Fouco (EdF) and M. Gomoliski (CEA), operator interviews and observations should be used for the development of new guidelines for periodical inspections and emergency procedures. E. M. Dougherty (TEC) tried a systematic framework for human error type classification with latent, dynamic, cognitive and recovery capabilities. The recovery capability depends strongly on logical and intensive mental processes interacting with signals during the transients. A special modelling technique is the "Event Sequence and Consequence Spectrum (ESCS)" developed by A. Amendola (JRC) and G. Reina (MESA) which includes modelling of operator intervention.

The machine side in the man-machine interface has been well described by a number of papers in Session 10 which focused on the use of computers for improvement of diagnostic tools and the quality of presenting the information as well as for reducing the tasks of the operator by increased computer control. This was well demonstrated by a paper of T. O. McNeil and N. Yanofsky (AECL) on the integrated operator/plant interface design in CANDU nuclear power plants, where, as in other thermal reactor power plants, especially diagnostic tools can be expected to undergo further developments in the future. J. M. Lanore (CEA) described the design of a future PWR simulator as a tool for safety analysis with special concern for operating actions and failures that can lead to core damage and for possible recovery actions by the operator to reach a safe status. Filtering of alarms and simplified CRT displays were the special subjects of a paper by P. J. Visuri (given by the OECD Halden-Project) on "Multivariate Alarm Handling Display." This method will certainly provide an important aid to the operator in future applications, eliminating large parts of the information overload. The STAR-concept, a new systematic approach to disturbance analysis and operator aids, was described in a paper by L. Felkel (GRS). It includes disturbance analysis and surveillance, computerized operations manual, post-trip analysis, alarm reduction and plant information processing and display. It has to be tailored to the special plant engineering design which can be quite complex, as shown in a pilot application. Future attention should be given to the question of how far the STAR system is able to handle complex multifailure accident situations in real time so as to assist the operator and the technical supervisor in the prevention of more severe damage to the plant. In any case, the trends of the physical state of the plant should be given in the displays, because accidents may follow from unforeseen error situations which the plant designer tries to counteract by means of the "defense

in depth" concept, reducing the residual risk to a very small value. It is this "defense in depth" in which the operator needs more assistance by improved computer information capabilities. It is certainly very interesting to have a Monitoring And Diagnostic System (MADS) for the fission product transport and release in the plant, as proposed by H. Kodaira, S. Kondo, and Y. Togo (UT), because it can help in identifying the event as well as in monitoring and estimating the fission product release.

In the poster session (Session 26) on man-machine interface, several interesting contributions dealt with monitoring instrumentation and surveillance systems. Accident sequence recognition in the control room display was proposed by C. D. Heising (MIT) and S. C. Dinsmore (YAP), the feasibility of an online γ -spectrometer for recognition of signatures of fission product release in the coolant and thereby determining the kind of fuel damage was brought up by D. J. Osetek et al. (EG&G). Other papers, such as that of C. H. Neuschaefer (CE) on an integrated computerized accident monitoring system and that of A. Hoeld and O. Lupas (GRS) on the computer-aided 3D core surveillance GARLIC system of a PWR, showed that considerable progress has been made in this area. In this context the regional overpower protection system for the CANDU reactor developed by C. M. Bailey et al. (AECL) may also be mentioned. Two papers from JAERI dealt with improved instrumentation such as the development of an in-vessel water level gauge and an improved multivariable noise analysis for better reactor diagnosis. Two French papers by J. Stolz et al. (EdF) were concerned with simulators of function and computer assisted training of operators.

It can be stated that great progress has been achieved in the design of better computer aids for the operator. However, it should be further evaluated to what extent automation can be applied for risk reduction, which computer-based enhancements are needed, and how they are to be integrated into a larger operational support system. This was also the main issue covered in the panel discussion following Sessions 9 and 10.

Furthermore, I wish, to give some comments on Session 30 concerning safety-related design considerations, supplementing the remarks of the session chairman. This session included a number of different topics such as a new functional design approach derived from a multilevel flow model (K. M. De et al., WEC), equipment qualification (R. F. Miller et al., S&W), value impact analyses of accident prevention and mitigation systems (A. S. Benjamin, et al., SNL), specifics of filtered/vented containment (L. Nilsson et al., ASEA/Studsvik/Sydskraft), separation requirements for fire prevention (L. Martin, EA, Spain), and a proposal for a depressurizer system for small pipe breaks (O. B. Falls, NEC). The papers suggested that generic solutions can lead to wide variations in incremental risk, depending on specific engineering details of individual plants. However, uncertainties in phenomenology (e.g., source term) and methods of analysis tend to provide large uncertainties in the realities of any "bottom line." It seems that the main steps in risk reduction have been undertaken already. A well defined methodology could probably make risk reduction investigation less speculative in the future.

REVIEW OF FUEL PERFORMANCE EVALUATION, DYNAMIC LOADS/STRUCTURAL ANALYSIS,
AND OPERATING EXPERIENCE

D. A. Meneley
Ontario Hydro
Toronto, Ont., Canada

The Chairman has asked the panel members to discuss the question of "Where do we go from here?" I wish to place my answer to this question in the context of a simple model of where we now are. My particular areas for review are fuel performance evaluation, dynamic loads/structural analysis, and operating experience.

1. Where We Are

There are three general classes of people involved in the nuclear industry, and three general types of tasks in the future. Table I identifies the elements of this matrix.

TABLE I

Major Tasks Major Actors	Maintain Return on Invested Capital	Improve the Product	Secure the Future
Station Owners	A		B
Engineering Community	B	A	
Research Community		B	A

A indicates primary interest/responsibility
B indicates supporting role

Under "Maintain Return on Invested Capital," one can include subheadings, such as (a) keep present plants running, (b) get committed plants going, and (c) convince our public (including regulatory agencies) that we are doing the right thing. These responsibilities must be assigned to plant owners because they are the prime stakeholders.

Under "Improve the Product," the main subheadings are (a) simplify systems, (b) clarify the purpose and capabilities of systems, and (c) verify the capabilities of systems. The overall purpose is to make the resulting plant financially efficient through reduced capital cost and reduced interest during construction. This is the prime role of the engineering community.

Under "Secure the Future," the purpose is to plan for the period beyond the next 20 years, and put in place the appropriate technology so that the next generation can improve on present practice. This is the prime role of the research community; plant owners and governments should provide support for this function.

2. Session Reviews

Assuming that questions are being addressed in decreasing order of priority, the first premise in our discussion of future thermal reactor safety work must be that it will not go on for many more years. Considering the large number of people working in this field, I would expect that either (a) we will soon answer all the important questions favorably, or (b) we will find one or more unacceptable answers. In both cases the work will stop.

2.1 Fuel Performance Evaluation - Session 13

The papers presented indicate that fuel is more tolerant to upsets (or in M. Gauvenet's terms, less "fragile") than has been generally assumed. In particular, a series of BWR tests found that no damage or loss of mechanical integrity occurred during transients up to 495 percent of normal rated power. Such information can be applied by the engineering community for improvement of future reload or new plant fuel designs. Plant owners may wish either to demonstrate increased margins or to increase the maximum plant rated power.

2.2 Dynamic Loads/Structural Analysis - Session 31

Both experimental and analytical results were presented. The papers showed the large gains which can be made by careful, well-verified models in place of extreme conservatism in engineering design. It appears, for example, that actual two-phase jet behavior is now well understood so that earlier conservative standards can be relaxed in many cases. Comparison of experimental and theoretical modeling of seismic behavior for critical components can provide direct assurance of design sufficiency.

A particularly valuable suggestion was made to use a judgemental rather than a strict analytical process for evaluating the seismic capability of existing plants. Highly qualified staff would make a "walk-around" inspection and provide evaluations of particular components in a DELPHI framework. Conducted on a professional basis, such an evaluation can be more valuable and much less expensive than the analytical approach. Plant owners should be particularly interested in this type of work, since it offers the best opportunity for resolution of safety design problems which arise during operation or in the late stages of construction. The engineering community should develop the methodology of the Delphi approach and identify specialists of the highest professional calibre to carry out such inspections.

2.3 Operating Experience

A large body of very important information on nuclear power plant operation is being accumulated. This was recognized by the planners of the meeting by including two sessions on the subject of operational assessment and experience. Earlier meetings in this series on thermal nuclear reactor safety in Salt Lake City (1973) and Sun Valley (1977) contained essentially no papers of this type. Knoxville (1980) did include a session on "Reactor Event Reporting Analysis." Even more papers are anticipated at future meetings in this series.

The overall impression of operating experience is that the "people factor" is more important than has been recognized by the reactor safety community. A well-designed plant may be operated in an unsafe manner, while a (theoretically) less safe plant may be operated very efficiently and safely if the operating staff understand its characteristics thoroughly.

2.3.1 NPP Operational Assessment - Session 20

The paper "Precursors to Potential Severe Core Damage Accidents 1969-1979" (Paper No. 395) by Minarick and Kukiela attracted considerable attention. The technique, using operating experience to calculate probabilities for the potential occurrence of

certain classes of events may be considered to be an important advance in reactor operational assessment. However, the project needs to have very extensive additional peer review since the work reported to date was only a status report, and considerable work remains to be done. Areas needing close scrutiny that were addressed in the paper or the question period are as follows:

- (a) The use of generic event trees, node probabilities and the long time horizons.
- (b) Since much of the data used was very plant-specific, its application in a broad sense and to other specific plants was questioned and has to be carefully evaluated,
- (c) Important events that may have been missed,
- (d) Probability overcounting.

The paper "PWR Safety-Related Operating Experience Feedback Organization of EDF" (Paper No. 383) by Capel reported on the ability to collect large quantities of operating data on components or systems manufactured by the same company. This provides very important feedback for plants using the same equipment. Sweden's experience (Paper No. 344) also supported this finding.

Several papers in the session reported on utility staff operational assessments. These types of evaluation activities are considered to be very important and are recommended to others.

2.3.2 Safety-Related Operational Experience - Session 22

This session consisted of five formal papers and a panel discussion. Three of the papers dealt with the process of detection and correction of perceived errors at operating stations; one for a single station (Oconee), one for all stations of a large integrated operating utility (EdF), and the third for a large diverse collection of utilities with widely varying equipment, policies and practices (INPO). In a very general way the conclusions were consistent. Differences in approach can be understood in terms of the history, the technical, and the socio-political context of the system being described. The steps of short-term detection and correction of "errors" (in the general sense) were visible in all papers. In short, learning is taking place. Exceptions were noted in recurring similar events, and in a difficult lack of consistency between good and poor operating experience in situations where similar equipment would lead to expectation of similar performance for different plants. The "People Factor" was hypothesized to explain the difference. A good-performance Recognition Program is in place in at least one operating utility (CECo).

The "People Factor" was further described in the fifth paper, which demonstrated that inconsistent operating procedures can lead to high operator error rates, and presented clear evidence that procedures are a powerful performance-shaping factor.

The panel consisted mainly of individuals associated with the same organizations as the presenters of the papers. They presented conceptual suggestions of how we should organize the process of learning from experience, and further the process of not forgetting what we have learned. It was pointed out that an individual's "information half-life" is very short, and formal institutional steps must be taken to efficiently retain knowledge.

A valuable concept was presented showing evidence of the use of the learning process in several diverse technologies. An estimate of the expected future event frequency can be made from sparse historical data; this estimate can be freed from the statistical burden of "lessons already learned."

It was pointed out that people (the example used was a field operator) will probably dominate initiating event frequencies in the future. The meeting was urged to consider real operators and real operations, and to place less emphasis on further hardware changes.

Consensus was reached on the need to reveal, exchange, and discuss operational experience. Both good and bad experiences should be discussed. To the extent feasible, a common set of terms, procedures, and practices should be followed to make the process more efficient.

REVIEW OF DEGRADED CORE ANALYSIS

P. Tanguy

Commissariat à l'Energie Atomique
Fontenay-aux-Roses, France

Four sessions were devoted to Degraded Core Analysis: one Poster Session, two Technical Sessions, and one Special Session which included a Panel Discussion. Such attention given to this subject is new for this type of topical meeting, which is beginning to look like a meeting on fast breeder reactors. And actually one could listen to the same concepts people have been playing with for years in fast breeder safety, such as fuel-coolant interaction, fuel dispersion, debris bed, etc. Sometimes the people were the same, making use now in LWR safety evaluation of the expertise gained in fast breeder safety studies, and taking advantage of the fact that, at least in this country, there is no longer a lot of work to do on fast breeders.

But this does not imply that laboratories are working on degraded-core issues only because they are out of work for breeders. No. The emphasis which at present is placed on the degraded core issue is directly related to the post-TMI reflections. There have been many discussions to decide whether or not TMI-2 was a Class-9 accident; certainly, as far as fuel is concerned, there is no doubt that the fuel in the TMI-2 accident has been submitted to conditions far beyond design. So it is now clear that safety analysis must consider fuel behavior beyond design limits.

Degraded core studies are aimed at three main concerns:

- Data for probabilistic risk assessments (PRA), more realistic than the ones used for WASH-1400, as well as for an evaluation of the confidence intervals deemed very important today;
- Basic data for the source term evaluation;
- Feedback on the regulatory process; a general philosophy has not been defined yet, but I can see two main issues:
 - . operating procedures, including in-vessel instrumentation,
 - . possible mitigating design features to cope with Class-9 accidents.

I shall review briefly some of the important results presented during the sessions, making use of the excellent summaries prepared by the sessions' chairmen. I shall distinguish two types of problems:

- Propagation of damage in the core;
- Accidental sequences leading to containment failure.

For what concerns the propagation of damage in the core, the emphasis was put on code development: The best known code is SCDAP, developed for NRC, but there is also a code developed by NSAC and another by the University of Stuttgart in Germany. All of these codes need to be validated. For SCDAP, I have been impressed by the NRC program, which is quite coherent, making the best use of separate effects tests, both out-of-pile and in-pile, and which includes an integral-experiment series in PBF. But when we think of validation, we have also to remember that TMI is a unique integral experiment, even if it is not entirely representative of various possible accidental sequences. We followed a very interesting and lively presentation of a German paper which did predict the core situation in TMI-2. We have been informed of DOE's plans

to examine the TMI-2 core; I am not sure that this examination program is as extensive as we could wish, for the purpose of getting a better knowledge of what really happened during the core uncovering process, and I have been very happy to learn that NRC is contemplating to extend the program of fuel sampling.

For what concerns the knowledge of phenomena involved in the degradation process, important results were presented on Zircalloy oxidation, with the reaction self-limiting due to hydrogen, and on what is called "liquefaction" of UO_2 in Zircalloy, corresponding to formation of eutectics, with also a limiting effect on temperature. My personal conclusion is that all results converge in the good direction for safety, namely lower temperatures than predicted for accidents, fission products plate out more efficiently, and less production of aerosols. I have seen no evidence of having materials become known to accidental sequences leading to the failure of containment. Also here codes are developed or improved. The MARCH code of course, is widely used; however, other codes have been developed in Germany or within the IDCOR program. But the main emphasis seems to me to be on phenomenology, and on the key issues:

- steam explosions;

- hydrogen production and burning; and
- corium-concrete interaction and debris-bed cooling. As regards steam explosions, from the chairman's summary, and from H. Fauske's contribution to the panel discussion, I get the feeling that a steam explosion energetic enough to break the containment is very unlikely indeed, if not completely impossible. It seems to me that we can probably get a consensus of all experts on that conclusion, but that it will be very difficult to go any further, and to conclude for instance that steam explosions are impossible.

On hydrogen, I have seen results, which are in part counteracting each other: On the one hand, an increase in the production of hydrogen from reaction with steel, and on the other hand, the inhibiting effect of steam on hydrogen ignition. It seems to me -- but this is a personal viewpoint -- that this is still an unresolved safety issue; one cannot exclude the possibility of containment rupture as a consequence of hydrogen deflagration coincident with a steam spike. I know that others consider it to be very unlikely. Anyway, there is going to be a workshop in October on this topic. We will get at this time a status report which could demonstrate that my present feeling is not right.

Finally what is the importance of all this work for reactor safety?

I see three steps:

(1) Core-melt probability: immaterial

(2) Conditional probability of containment failure: Very important. Today, we appear to have confirmation that the most likely failure mode

will be by slow increase of pressure, due to steam and non-condensable gases (subject to a proper demonstration of hydrogen burning).

(3) Realistic evaluation of the source term for identified sequences. Clearly, the trend is towards a reduction, at least by a decade, compared to the values used in WASH-1400.

For the regulatory process: Concerning operating procedures for the prevention of large core-melt events, and as regards appropriate instrumentation, the present research may not be quite adequate. I will come back to

this point in my conclusion. Concerning procedures aimed at reaching a safe situation, work should continue in order to get a better knowledge of possible adverse effects of restoring safety injection (mechanical effects, hydrogen production, etc.).

As regards possible safety features to be introduced in the design, we have some elements which would allow to perform a coarse cost-benefit evaluation. However, it is clear that we need a much clearer view on the source-term issue before taking a definitive standpoint.

I come now to my conclusion. All the work presented in these sessions was performed as a consequence of TMI. But we must remember that one of the fundamental lessons learned after the TMI-2 accident was that we have paid too much attention to highly improbable events, and not enough attention to frequent incidents which could degenerate into large accidents. Today, we see again that everybody seems fascinated by an improbable catastrophic fusion of the core, like in LMEBRs, and we should wonder whether enough attention is paid to the serious, but less catastrophic, accidents, where fuel temperatures can exceed the design limit of 1200°C, but stay below the 2000°C threshold, and for which a good management of the accident could well stop the accident sequence. I think that more work is needed in this area.

Along the same line, TMI has shown the importance of actions by the operators in the course of the accident sequence. This aspect is currently not very well taken into account in the studies, and more work is certainly needed on this fundamental safety question.

- RESEARCH I (1-1) - developed at INEL
- RESEARCH II (1-2) - developed at INEL
- RESEARCH III (1-3) - developed at INEL
- RESEARCH IV (1-4) - developed at INEL

All the above codes have been validated by experimental results. The basic sequence of the codes have been proven to be correct. However, some codes may need modification in specific applications, such as the use of the codes in the area of safety analysis.

The TMI experiment is reported in the following:

- (1) International Reactor Physics Experiment (IRPE) - The results of this experiment are reported in the following:

- Large scale experiment: LOFT, LOFT, LOFT
- Small scale experiment: EXEL

- (2) Separated-phase experiment: The results of this experiment are reported in the following:

- Downcomer experiment: The results of this experiment are reported in the following:

- WCCS of CANDU reactor: The results of this experiment are reported in the following:

- WCCS of CANDU reactor: The results of this experiment are reported in the following:

REVIEW OF LOCAs, TRANSIENTS, AND PRESSURIZED THERMAL SHOCK

L. S. Tong

U.S. Nuclear Regulatory Commission
Washington, D.C.

My report will cover the following two areas:

1. LOCAs and Transients
2. Pressurized Thermal Shock (PTS)

1. LOCAs and Transients

The following *computer* codes were reported on during this meeting:

- . TRAC/PF1 (3-D) - developed at LASL
- . TRAC/BD1 (3-D) - developed at INEL
- . COBRA/TRAC (3-D) - developed at PNL
- . RELAP 5 (1-D) - developed at INEL
- . RETRAN 02 (1-D) - developed at EI
- . ALMOD 3 (1-D) - developed at ENEA
- . FIREBIRD III (1-D) - developed at AECL.

All the above codes have been validated by experimental results. The basic structures of these codes have been proven to be sound. However, some physical models may need modification in specific applications, such as discharge flow correlations which are highly geometry-specific.

The *LOCA experiments* reported on may be subdivided in two categories:

- (a) Integral-system tests are aimed at understanding plant behavior during large-, medium-, and small-break LOCAs. The results presented at this meeting pertain to various experimental facilities as follows:
 - . Large and medium breaks: LOFT, LOBI, PHEBUS
 - . Small breaks: Semiscale, PKL
- (b) Separate-effect tests are aimed at understanding detailed specific phenomena such as:
 - . Downcomer-gap effect: Tests in LOBI indicated that a large downcomer gap eliminates the flow reversal in a DECL blowdown.
 - . ECCS of CANDU Reactors: Tests by Ontario Hydro and AECL to use the moderator cooling system as an alternate ECCS.
 - . Reflood oscillations on the quench front: Studies by CEA/Grenoble.

- Parallel-channel CCFL effect in BWRs: Tests by Hitachi/TEPC indicate this to be an important phenomenon.

All the above experiments show that the current ECCS is good enough to protect the core for all break sizes of LOCA alone. On the other hand, in case of a LOCA associated with multiple failures, we cannot assure the core to remain intact; we do need to know how soon the remedial actions must be started for a core recovery.

Future research effort concerning LOCAs is suggested in the following areas:

- (a) Continue to explore the effects of multiple-failures combined with LOCAs of various break sizes in order to determine the maximum delay time permissible to start the remedial actions for core recovery.
- (b) Evaluate alternate ECCS to be optimized for a spectrum of break sizes with and without simultaneous multiple failures.

2. Pressurized Thermal Shock.

Studies were conducted for both LOCA and non-LOCA conditions:

- Experiments and analyses at ORNL constitute an excellent parametric study of PTS for long flaws in the clad and in the weld which are coincidental.
- Experiments and analyses at the University of Stuttgart, FRG, are also based on long flaws.
- T-H experiments at CREARE indicate a good coolant mixing. At present CREARE is working on the temperature transient of the flow in the cold leg and downcomer.
- T-H analysis at SAI: Some computer input values seem unrealistic but there is no experimental data to check with.
- 3-D nonlinear fracture mechanics at the University of Tokyo, Japan: Calculations compared well with data.
- Residual life of reactor vessels was studied at the Joint Research Centre, Ispra, Italy by calculations.

Research on PTS is still continuing; there is no conclusion yet.

Future efforts concerning PTS are suggested as follows:

- (a) Improve the analytical capability for better evaluation of buried flaws and short flaws, which seem to occur more frequently.
- (b) Estimate the probability values and the impacts of the various assumptions in selecting the initial conditions of mechanical tests, such as the likelihood of long flaws vs. short flaws, because the pessimistic assumption of the "limiting case" of accident scenarios for scaling a severe accident may lead to unwarranted "conservatism," and may result in design requirements that inhibit the ability to cope with actual accidents. In the past, the ECCS for large-break LOCAs was very conservative, but it did not do well for the small break in TMI-2. Therefore, a PRA concept should be used to determine the realistic conditions for scaling and simulation in all severe accident studies.

LIST OF ATTENDEES

P. M. Abraham
Duke Power Company
422 S. Church Street
Charlotte NC 28242

Paul B. Abramson
Argonne National Laboratory
9700 S. Cass Ave.
Argonne IL 60439

Carmelo Addabbo
Euratom JRC
21020 Ispra (Varese) ITALY

Newal Agnihotri
Eges Inc.
505 N. Lalonde
Lombard IL 60148

Per-Eric Ahlstrom
Swedish State Power Board
S-16287 Vällingby SWEDEN

Carmine P. Aiello
S. M. Stoller Corp.
45 Oxford Rd.
Rockville Centre NY 11570

S. Akiho
Inst. of Nuclear Safety
1-8 Mita Minato-ku
Tokyo JAPAN

David C. Aldrich
Sandia National Laboratories
Division 9415
Albuquerque NM 87185

A. Alemberti
Nucleare Italiana Reattori Avanzati
Via dei Pescatori 35
16129 Genova ITALY

Joseph Alter
University of California, Los Angeles
3219 Colorado Ave.
Santa Monica CA 90404

Luis Martín Alvarez
Empresarios Agrupados
Magallanes 3
Madrid SPAIN

Paul J. Amico
Science Applications Inc.
P.O. Box 1303
McLean VA 22102

Richard P. Anderson
Argonne National Laboratory
9700 S. Cass Ave.
Argonne IL 60439

Thomas T. Anderson
Argonne National Laboratory
9700 S. Cass Ave.
Argonne IL 60439

Torbjörn Andersson
ASEA-ATOM
Box 53
S-72104 Västerås SWEDEN

R. D. Anthony
Nuclear Installations Inspectorate
Thames House North Millbank
London SW1P 4QL UNITED KINGDOM

Hideto Aoki
Toshiba
1815 Issiki Hayama
Kanagawa JAPAN

William Arcieri
NUS Corporation
910 Clopper Rd.
Gaithersburg MD 20878

K. H. Ardron
Atomic Energy of Canada Ltd.
Whiteshell Nuclear Research Estab.
Pinawa, Manitoba ROE 1L0
CANADA

Guy A. Arlotto
U.S. Nuclear Regulatory Commission
Washington DC 20555

Donn R. Armstrong
Argonne National Laboratory
9700 S. Cass Ave.
Argonne IL 60439

Ed Armstrong
Commonwealth Edison
1 First National Plaza
Chicago IL 60690

T. Asahara
Mitsubishi Research Institute
Tokyo JAPAN

Steven A. Atkinson
EG&G Idaho Inc.
WCB W-3
P.O. Box 1625
Idaho Falls ID 83415

Patrick Aujollet
Commissariat à l'Energie Atomique
231 Rue Plaine Chateau
84120 Pertuis FRANCE

Robert Avery
Argonne National Laboratory
9700 S. Cass Ave.
Argonne IL 60439

Emil A. Bachofner
OKG AB
Box 1746
S-11187 Stockholm SWEDEN

G. M. Bailey
Atomic Energy of Canada Ltd.
Sheridan Park Research Community
Mississauga, Ontario L5K 1B2
CANADA

Louis Baker, Jr.
Argonne National Laboratory
9700 S. Cass Ave.
Argonne IL 60439

M. S. Barents
Electrowatt Eng. Serv. Ltd.
Granford House 16 Carfax
Morsham, West Sussex
UNITED KINGDOM

Robert A. Bari
Brookhaven National Laboratory
Upton NY 11973

Gerd Baumgartner
Basler & Hofmann
Forchstrasse 395
8029 Zurich SWITZERLAND

Henry G. Bazydlo
Consumers Power Co.
Big Rock Point Plant
Charlevoix MI 49720

Vance L. Behr
Sandia National Laboratories
Division 9411
Albuquerque NM 87185

Barbara Jean Bell
Sandia National Laboratories
Division 7223
P.O. Box 5800
Albuquerque NM 87185

Ruben Bello
Comisión Nacional de Seguridad
Nuclear y Salvaguardias
Insurgentes sur 1806
Mexico City (20) 01730 MEXICO

Allan S. Benjamin
Sandia National Laboratories
Division 9411
Albuquerque NM 87185

Elaine D. Bergeron
Sandia National Laboratories
Division 9425
P.O. Box 5800
Albuquerque NM 87185

Kenneth D. Bergeron
Sandia National Laboratories
P.O. Box 5800
Albuquerque NM 87185

Stig O. W. Bergström
Studsvik Energiteknik AB
S-61182 Nyköping SWEDEN

Philippe Berna
Centre d'Etudes Nucleaires
13115 St. Paul-Lez-Durance
FRANCE

Adolph Birkhofer
Gesellschaft für Reaktorsicherheit
D-8046 Garching WEST GERMANY

James A. Blackburn
Illinois Department of Nuclear Safety
1035 Outer Park Drive
Springfield IL 62704

Paul E. Blackburn
Argonne National Laboratory
9700 S. Cass Ave.
Argonne IL 60439

David P. Blanchard
Consumers Power Co.
Big Rock Point Plant
Charlevoix MI 49720

Dennis C. Bley
Pickard, Lowe & Garrick
17840 Skypark Blvd.
Irvine CA 92714

William B. Bobnar
Union Electric
P.O. Box 149
St. Louis MO 63166

Kenneth R. Boldt
Sandia National Laboratories
Division 9421
P.O. Box 5800
Albuquerque NM 87185

Jim Bollinger
Argonne National Laboratory
9700 S. Cass Ave.
Argonne IL 60439

Raymond J. Borkowski
Oak Ridge National Laboratory
Bldg. 9201-3 MS-2
P.O. Box Y
Oak Ridge TN 37830

Ira Bornstein
Argonne National Laboratory
9700 S. Cass Ave.
Argonne IL 60439

Joseph D. Bowers
Commonwealth Edison
1 First National Plaza
Chicago IL 60690

Brent E. Boyack
Los Alamos National Laboratory
P.O. Box 1663
Los Alamos NM 87544

Patricia Boyle
Commonwealth Edison
P.O. Box 767
Chicago IL 60690

Robert D. Branson
Commonwealth Edison
Byron Nuclear Station
Byron IL 61010

R. J. Breen
Electric Power Research Inst., NSAC
3412 Hillview Ave.
Palo Alto CA 94303

M. J. Bridge
CEGB Berkeley Nuclear Laboratory
Berkeley Gloucester
UNITED KINGDOM

Donald R. Brindle
Commonwealth Edison
4450 N. German Church Rd.
Byron IL 61010

K. J. Brinkmann
Energie Centrum Nederland
P.O. Box 1
1755 ZG Petten THE NETHERLANDS

Wesley A. Brinsfield
Wood-Leaver & Associates Inc.
1340 Saratoga-Sunnyvale Rd.
San Jose CA 95129

Jacques Brisbois
Commissariat à l'Energie Atomique
Centre d'Etudes Nucléaires
B.P. No. 6
92260 Fontenay-aux-Roses FRANCE

G. L. Brooks
Atomic Energy of Canada Ltd.
Sheridan Park Research Community
Mississauga, Ontario L5K 1B2 CANADA

Meta Brown
Massachusetts Institute of Technology
77 Massachusetts Ave.
Cambridge MA 02139

Harry Bryant
Argonne National Laboratory
9700 S. Cass Ave.
Argonne IL 60439

Joel R. Buchanan
Oak Ridge National Laboratory
Bldg. 9711-1
P.O. Box Y
Oak Ridge TN 37830

E. Budzichowski
Commonwealth Edison
72 W. Adams St.
Chicago IL 60690

Dietrich A. L. Buenemann
GKSS Research Center
Max Planck Str.
D-2054 Geesthacht WEST GERMANY

T. R. Bump
Argonne National Laboratory
9700 S. Cass Ave.
Argonne IL 60439

M. Bustraan
Netherlands Energy Research Foundation
P.O. Box 1
NL-1755 ZG Petten THE NETHERLANDS

Thomas Butler
Los Alamos National Laboratory
Group T-3, MS B216
Los Alamos NM 87545

Per E. Bystedt
Swedish Nuclear Power Inspectorate
Box 27106
S-10252 Stockholm SWEDEN

A. Cahuzac
Electricité de France
1 Av. du General de Gaulle
92141 Clamart FRANCE

Claudio T. M. Camargo
Comissão Nacional de Energia Nuclear
Rua General Severiano 90
22290 Rio de Janeiro BRAZIL

Allen L. Camp
Sandia National Laboratories
P.O. Box 5800
Albuquerque NM 87185

David J. Campbell
JBF Associates, Inc.
1630 Downtown West Blvd.
Knoxville TN 37919

Roger Capel
Electricité de France
Service de la Production Thermique
3 Rue de Messine
75008 Paris FRANCE

Christopher Carey
University of Florida
202 Nuclear Sciences Center
Gainesville FL 32611

David D. Carlson
Sandia National Laboratories
Division 9443
Albuquerque NM 87185

Annick Carnino
Electricité de France
32 Rue de Monceau
75008 Paris FRANCE

Jose A. Carretero
Empresarios Agrupados SA
Calle Magallanes 3
Madrid SPAIN

Wade P. Carroll
Office of Breeder Reactor Technology
U.S. Department of Energy
Washington DC 20545

A. K. Chakraborty
Gesellschaft für Reaktorsicherheit
Glockengasse 2
5000 Köln 7 WEST GERMANY

Rosanna Chambers
EG&G Idaho Inc.
P.O. Box 1625
Idaho Fall ID 83415

Yao Wen Chang
Argonne National Laboratory
9700 S. Cass Ave.
Argonne IL 60439

Ira Charak
Argonne National Laboratory
9700 S. Cass Ave.
Argonne IL 60439

Ping Chee
Argonne National Laboratory
9700 S. Cass Ave.
Argonne IL 60439

Tien-Hu Chen
EG&G Idaho Inc.
P.O. Box 1625
Idaho Falls ID 83415

Steve H. Chen
Marquette University/FAI
16W070 W. 83rd Street
Burr Ridge IL 60521

R. D. Cheverton
Oak Ridge National Laboratory
Bldg. 9204-1 MS 06
P.O. Box Y
Oak Ridge TN 37830

Bindi Chexal
Electric Power Research Institute
3412 Hillview Ave.
Palo Alto CA 94303

Ronald J. Chin
Commonwealth Edison
72 W. Adams St.
Chicago IL 60690

Dae H. Cho
Argonne National Laboratory
9700 S. Cass Ave.
Argonne IL 60439

Raymond F. Choinard
Commonwealth Edison
4450 N. German Church Rd.
Byron IL 61010

C. K. Chou
Lawrence Livermore National Laboratory
P.O. Box 808
Livermore CA 94550

Hee Chung
Argonne National Laboratory
9700 S. Cass Ave.
Argonne IL 60439

K. Chung
Argonne National Laboratory
9700 S. Cass Ave.
Argonne IL 60439

Patrice Clément
Centre d'Etudes Nucléaires
85X Cedex
38041 Grenoble FRANCE

P. N. Clough
U.K. Atomic Energy Authority-SRD
Wigshaw Lane
Culcheth, Warrington WA3 4NE
UNITED KINGDOM

Enrico F. Conti
U.S. Nuclear Regulatory Commission
MS 1130-SS
Washington DC 20555

John R. Coombe
Stone & Webster Engr. Corp.
P.O. Box 2325
Boston MA 02107

Michael Corradini
The University of Wisconsin - Madison
1500 Johnson Dr.
Madison WI 53706

David C. Cox
Battelle Columbus Laboratories
505 King Ave.
Columbus OH 43201

Thomas W. Craig
General Electric Co.
175 Curtner Ave.
San Jose CA 95125

Wallis R. Cramond
Sandia National Laboratories
P.O. Box 5800
Albuquerque NM 87185

Ray M. Crawford
Science Applications Inc.
1211 W. 22nd St.
Oak Brook IL 60521

August Cronenberg
Engineering Science and Analysis
836 Claire View
Idaho Falls ID 83402

D. Cubicciotti
Electric Power Research Institute
Box 10412
Palo Alto CA 94303

James C. Cunnane
Battelle Columbus Laboratories
505 King Ave.
Columbus OH 43201

Thomas Currie
Carleton University
Colonel By Drive
Ottawa, Ontario CANADA

Peter Cybulskis
Battelle Columbus Laboratories
505 King Ave.
Columbus OH 43201

Dirk A. Dahlgren
Sandia National Laboratories
Dept. 9440
Albuquerque NM 87185

John Daily
Westinghouse WNTC-Zion
505 Shiloh Blvd.
Zion IL 60099

Francesco D'Auria
Dept. of Mech. and Nucl. Const.
Universita di Pisa
Via Diotisalvi 2
56100 Pisa ITALY

M. K. De
Westinghouse Electric Corp.
P.O. Box 355
Pittsburgh PA 15230

Bill Dean
Commonwealth Edison
101 Shiloh Blvd.
Zion IL 60099

Teun C. de Boer
Energie Centrum Nederland
P.O. Box 1
1755 ZG Petten THE NETHERLANDS

James R. Deen
Argonne National Laboratory
9700 S. Cass Ave.
Argonne IL 60439

L. Walter Deitrich
Argonne National Laboratory
9700 S. Cass Ave.
Argonne IL 60439

Roland Del Negro
Centre d'Etudes Nucléaires
13115 St. Paul-Lez-Durance
FRANCE

Madelein De La Foye
Framatome
4 Bd. Garibaldi
75015 Paris FRANCE

Paul N. Demmie
EG&G Idaho Inc.
P.O. Box 1625
Idaho Falls ID 83415

Richard S. Denning
Battelle Columbus Laboratories
505 King Ave.
Columbus OH 43201

Harold R. Denton
U.S. Nuclear Regulatory Commission
Washington DC 20555

Theodore L. Deobald
UNC Nuclear Industries
Box 490
Richland WA 99352

Gerard Depond
Electricité de France - SEPTEN
Tour EDF-GDF Cedex No. 8
92080 Paris - La Défense FRANCE

Claude Derive
Electricité de France
6 Quai Watier
78400 Chatou FRANCE

Roger W. Dettenmeier
Illinois Department of Nuclear Safety
1035 Outer Park Drive
Springfield IL 62704

C. Devillers
Centre d'Etudes Nucléaires - DSN
B.P. No. 6
92260 Fontenay-aux-Roses FRANCE

Charles E. Dickerman
Argonne National Laboratory
9700 S. Cass Ave.
Argonne IL 60439

Thomas A. Dillon
U.S. Department of Energy
1000 Independence Ave. SW
Washington DC 20585

Stephen C. Dinsmore
Yankee Atomic Electric Co.
1671 Worcester Road
Framingham MA 01701

Luigi Di Palo
ENEA
Viale Regina Margherita 125
00198 Roma ITALY

Raymond Di Salvo
Battelle Columbus Laboratories
505 King Ave.
Columbus OH 43201

Dean Dobranich
Los Alamos National Laboratory
MS K556
P.O. Box 1663
Los Alamos NM 87545

Cleon F. Dodge
Pennsylvania Power & Light Co.
2 N. 9th St.
Allentown PA 18081

Robert Doerner
Argonne National Laboratory
9700 S. Cass Ave.
Argonne IL 60439

Z. Domaratzki.
Atomic Energy Control Board
270 Albert St.
Ottawa, Ontario K1P 5S9 CANADA

Patrick M. Donnelly
Consumers Power Co.
Big Rock Point Plant
Charlevoix MI 49720

E. M. Dougherty, Jr.
Technology for Energy Corp.
One Energy Ctr./ Mississippi Pky.
Knoxville TN 37992

Joseph P. Drago
Oak Ridge National Laboratory
Bldg. 9104-1
P.O. Box Y
Oak Ridge TN 37830

C. Gordon Duff
Atomic Energy of Canada Ltd.
Sheridan Park Research Community
Mississauga, Ontario L5K 1B2
CANADA

John Stuart Duffield
Joint Research Centre
21020 Ispra (Varese) ITALY

Steve Eckel
General Physics Corporation
1010 Woodman Drive, Suite 240
Dayton OH 45432

D. T. Eggen
Dept. of Mech. and Nucl. Eng.
Northwestern University
Evanston IL 60201

Joachim Ehrhardt
Kernforschungszentrum Karlsruhe
Postfach 3640
D-7500 Karlsruhe WEST GERMANY

Jan Elliott
Los Alamos National Laboratory
MS K556
P.O. Box 1663
Los Alamos NM 87545

Richard M. Elrick
Sandia National Laboratories
Kirtland Air Force Base East
Albuquerque NM 87185

Elton G. Endebrock
Los Alamos National Laboratory
P.O. Box 1663
Los Alamos NM 87545

Ichiya Endo
Kawasaki Steel Corp.
1 Kawasaki-cho Chiba-shi
Chiba 260 JAPAN

Malcolm L. Ernst
636 Goldsborough Drive
Rockville MD 20850

Mike Estes
Westinghouse Electric Corp.
505 Shiloh Blvd.
Zion IL 60099

Rene Evenepoel
Framatome
Tour Fiat - Cedex 16
92084 - Paris 1a Défense FRANCE

O. B. Falls, Jr.
Nucledyne Engineering Corp.
728 W. Michigan Ave.
Jackson MI 49201

Hans Fauske
Fauske & Associates Inc.
16W070 W. 83rd Street
Burr Ridge IL 60521

Paul J. Fehrenbach
AECL Chalk River Nuclear Laboratories
Chalk River, Ontario K0J 1J0
CANADA

Lothar Felkel
Gesellschaft für Reaktorsicherheit
Forschungsgelände
D-8046 Garching WEST GERMANY

C. Feltin
Centre d'Etudes Nucléaires - DSN
B. P. No. 6
92260 Fontenay-aux-Roses FRANCE

Donald R. Ferguson
Argonne National Laboratory
9700 S. Cass Ave.
Argonne IL 60439

Jean Fermandjian
Centre d'Etudes Nucléaires
IPSN/DSN/SAER
B.P. No. 6
92260 Fontenay-aux-Roses FRANCE

Sidney Fiarman
Brookhaven National Laboratory
Bldg. 130
Upton NY 11973

D. E. Fields
Oak Ridge National Laboratory
Bldg. 7509
Oak Ridge TN 37830

Kenneth Finlon
University of Florida
307 SW 16th Ave.
Gainesville FL 32601

Albert K. Fischer
Argonne National Laboratory
9700 S. Cass Ave.
Argonne IL 60439

Stan Fistedis
Argonne National Laboratory
9700 S. Cass Ave.
Argonne IL 60439

Jay Fisher
C. S. Draper Laboratory
555 Technology Square
Cambridge MA 02139

George Flanagan
Oak Ridge National Laboratory
Bldg. 6025
P.O. Box X
Oak Ridge TN 37830

Paulo Victor Fleming
Universidade Federal de Rio de Janeiro
Coppe/Nuclear
Ilha do Fundão
Rio de Janeiro BRAZIL

R. I. Fluke
Ontario Hydro
700 University Ave.
Toronto, Ontario M5G 1X6 CANADA

John D. Folley, Jr.
Applied Science Associates Inc.
P.O. Box 158
Valencia PA 16059

M. H. Fontana
Technology for Energy Corp.
One Energy Ctr./Pellissippi Pky.
Knoxville TN 37922

T. R. Fortescue
Joint Research Centre
21020 Ispra (Varese) ITALY

Joseph R. Fragola
Science Applications Inc.
274 Madison Ave., Suite 1501
New York NY 10016

George Frankovich
Commonwealth Edison
72 W. Adams St.
Chicago IL 60690

Gerald Frizzell
Commonwealth Edison
72 W. Adams St.
Chicago IL 60690

Edward L. Fuller
EPRI/Technology for Energy Corp.
One Energy Ctr./Pellissippi Pky.
Knoxville TN 37922

William J. Funke
Commonwealth Edison
72 W. Adams St.
Chicago IL 60690

Jeff R. Gabor
Fauske & Associates Inc.
16W070 West 83rd St.
Burr Ridge IL 60521

R. T. Galletly
U.K. Atomic Energy Authority
Wigshaw Lane, Culcheth
Warrington, Cheshire WA3 4NE
UNITED KINGDOM

Jean-Luc Gandrille
Framatome
26 Rue Paul Olivier
92500 Rueil-Malmaison FRANCE

Jim Garrey
Commonwealth Edison
P.O. Box 767
Chicago IL 60690

André J. Gauvenet
Electricité de France
32 Rue de Monceau
75384 Paris Cedex 08 FRANCE

Steven Gehl
Argonne National Laboratory
9700 S. Cass Ave.
Argonne IL 60439

Richard G. Gido
Los Alamos National Laboratory
MS-K556
P.O. Box 1663
Los Alamos NM 87545

James A. Gieseke
Battelle Columbus Laboratories
505 King Ave.
Columbus OH 43201

G. E. Gillespie
Atomic Energy of Canada Ltd.
Whiteshell Nuclear Research Estab.
Pinawa, Manitoba ROE 1LO CANADA

Theodore Ginsberg
Brookhaven National Laboratory
Bldg. 820
Upton NY 11973

André Giraud
COGEMA
2 Rue Paul Dautier
78141 Velizy Villacoublay FRANCE

Mikio Gokan
Mitsubishi Atomic
2-4-1 Shiba-koen
Minato-ku Tokyo 105 JAPAN

Arthur J. Goldman
Argonne National Laboratory
9700 S. Cass Ave.
Argonne ILL 60439

Abel Gonzalez
Atomic Energy Commission
Av. del Libertador 8250
1429 Buenos Aires ARGENTINA

Mary Goodkind
Escor Inc.
1845 Oak St., Suite 3
Northfield IL 60093

C. W. Gordon
Ontario Hydro
700 University Ave.
Toronto, Ontario M5G 1X6 CANADA

Robert E. Grazio
Boston Edison Co.
800 Boylston St.
Boston MA 02107

Jerry D. Griffith
Office of Nuclear Energy
U.S. Department of Energy
Washington DC 20585

Larry A. Grime
Toledo Edison Co.
300 Madison Ave.
Toledo OH 43652

Everett Gruen
EG&G Idaho Inc.
210 W. Sunnyside
Idaho Falls ID 83402

Shelby L. Gubin
Commonwealth Edison
72 W. Adams St.
Chicago IL 60690

Paul H. Gudiksen
Lawrence Livermore National Laboratory
L-262
P.O. Box 808
Livermore CA 94550

Philip Gustafson
Illinois Department of Nuclear Safety
1035 Outer Park Dr.
Springfield IL 62704

Shinichi Hamaguchi
Kansai Electric Power Co. Inc.
3-3-22 Nakanoshima Kita-ku
Osaka 530 JAPAN

Kazushige Hamazaki
Japan Atomic Power Co.
1-6-1 Ohtemachi Chiyoda-ku
Tokyo 100 JAPAN

Kim E. Hammer
The University of Wisconsin-Madison
4117 Sunnyside Ave.
Madison WI 53704

William Hancox
Atomic Energy of Canada Ltd.
Whiteshell Nuclear Research Estab.
Pinawa, Manitoba ROE 1L0 CANADA

Deborah Hankins
General Electric Co.
175 Curtner Ave. MC 738
San Jose CA 95125

Bruce N. Hanna
Atomic Energy of Canada Ltd.
Whiteshell Nuclear Research Estab.
Pinawa, Manitoba ROE 1L0 CANADA

Frederick T. Harper
Sandia National Laboratories
P.O. Box 5800
Albuquerque NM 87110

Kenneth H. Harrington
JBF Associates, Inc.
1630 Downtown West Blvd.
Knoxville TN 37919

F. Eric Haskin
Sandia National Laboratories
Division 9411
Albuquerque NM 87185

Ian J. Hastings
Atomic Energy of Canada Ltd.
Chalk River Nuclear Laboratories
Chalk River, Ontario K0J 1J0
CANADA

Steven W. Hatch
Sandia National Laboratories
Division 9412
P.O. Box 5800
Albuquerque NM 87112

M. R. Hayns
U.K. Atomic Energy Authority
S & R Directorate
Wigshaw Lane
Culcheth, Warrington, Cheshire
UNITED KINGDOM

Terence Heames
Argonne National Laboratory
9700 S. Cass Ave.
Argonne IL 60439

Carol J. Hedden
Commonwealth Edison
P.O. Box 767
Chicago IL 60690

A. Heidebrecht
Dean of Engineering
McMaster University
Hamilton, Ontario L9H 1N2 CANADA

Eric Hellstrand
Studsvik Energiteknik
S-61182 Nyköping SWEDEN

Joseph H. Hendrie
Brookhaven National Laboratory
Bldg. 197
Upton NY 11973

C. D. (Dan) Henry III
ETA Engineering Inc.
415 E. Plaza Dr.
Westmont IL 60559

Robert E. Henry
Fauske & Associates Inc.
16W070 W. 83rd St.
Burr Ridge IL 60521

Joseph E. Herceg
Argonne National Laboratory
9700 S. Cass Ave.
Argonne IL 60439

E. F. Hicken
Gesellschaft für Reaktorsicherheit
Forschungsgelände
8046 Garching WEST GERMANY

Jack W. Hickman
Sandia National Laboratories
P.O. Box 5800
Albuquerque NM 87111

James Hildebrandt
W. L. Wardrop & Assoc.
77 Main St.
Winnipeg, Manitoba CANADA

D. J. Hill
U.K. Atomic Energy Authority
AEE Winfrith
Dorchester, Dorset DT2 8DH
UNITED KINGDOM

Dagmar Hippe
Gesellschaft für Reaktorsicherheit
Glockengasse 2
5000 Köln 1 WEST GERMANY

H. Hoertner
Gesellschaft für Reaktorsicherheit
Forschungsgelände
D-8046 Garching WEST GERMANY

Richard M. Hogan
Commonwealth Edison
72 W. Adams St.
Chicago IL 60690

Hermann Hohmann
Joint Research Centre
21020 Ispra (Varese) ITALY

J. E. R. Holmes
U.K. Atomic Energy Authority
AEE Winfrith
Dorchester Dorset UNITED KINGDOM

Robert A. Hommerson
University of Florida
202 NSC
Gainesville FL 32601

John H. Hopps
C. S. Draper Laboratory
555 Technology Square
Cambridge MA 02139

John J. Horwath
Commonwealth Edison
P.O. Box B
Byron IL 61010

J. Peter Hosemann
Kernforschungszentrum Karlsruhe
P.O. Box 3640
D-7500 Karlsruhe WEST GERMANY

Richard Hosteny
Argonne National Laboratory
9700 S. Cass Ave.
Argonne IL 60439

Welles Hotchkiss
Stone & Webster Engr. Corp.
245 Summer St.
Boston MA 02107

J. Q. Howieson
Atomic Energy of Canada Ltd.
2000 Argentia Rd.
Mississauga, Ontario L5K 1B2
CANADA

J. K. Hsiue
Taiwan Power Co.
242 Roosevelt Rd. Sec. 3
Taipei 107 TAIWAN

Yih-Yum Hsu
University of Maryland
College Park MD 20742

Masahide Ikerzawa
JGC Corporation
1-14-1 Besho Minami-ku
Yokohamu-shi
Kanagawa 232 JAPAN

Dan Ilberg
Israeli AEC
P.O. Box 7061
Tel Aviv ISRAEL 61070

Kouichirou Ishihara
University of Tokyo
7-3-1 Hongo Bunkyo-ku
Tokyo 113 JAPAN

Kazuhiro Isogai
Mitsui Eng. & Ship Building
1 Kaigandori Yawata
Ichihara-shi Chiba 290 JAPAN

Mathieu Israel
Electricité de France
1 Av. du Général de Gaulle
92141 Clamart Cedex FRANCE

Toshikazu Ito
Argonne National Laboratory
9700 S. Cass Ave.
Argonne IL 60439

Peter S. Jackson
Combustion Engineering Inc.
1000 Prospect Hill Rd.
Windsor CT 06095

Peter D. Jenkins
Central Electricity Generating Board
GDCD Barnwood
Gloucester GLL TRS UNITED KINGDOM

Ross Jensen
Intermountain Technologies
P.O. Box 1604
Idaho Falls ID 83401

Uffe Steiner Jensen
ELSAM
DK-7000 Fredericia DENMARK

Kjello Johansson
Studsvik
S-61182 Nyköping SWEDEN

Carl E. Johnson
Argonne National Laboratory
9700 S. Cass Ave.
Argonne IL 60439

Richard H. Johnson
Commonwealth Edison
P.O. Box 767
Chicago IL 60690

Stephen P. Johnson
Commonwealth Edison
LaSalle County Station
P.O. Box 767
Chicago IL 60690

Philip Jones
Commission of the European Communities
Joint Research Centre Ispra
21020 Varese ITALY

C. Kalverboer
PZEM
P.O. Box 48
4335 JA Middelburg THE NETHERLANDS

Manuel A. Kanter
Argonne National Laboratory
9700 S. Cass Ave.
Argonne IL 60439

David M. Kapinus
Commonwealth Edison
Braidwood Station
Braceville IL 60407

Stan Kaplan
Pickard, Lowe & Garrick
17840 Skypark Blvd.
Irvine CA 92714

Masami Kato
Nippon Atomic Industry Group
4-1 Ukishima-cho, Kawasaki-ku
Kawasaki-shi
Kanagawa-ken 210 JAPAN

Walter Y. Kato
Brookhaven National Laboratory
Upton NY 11973

Yomei Kato
Hitachi Ltd.
1168 Meviyama-cho
Hitachi-shi Ibaraki 316 JAPAN

Masayuki Kawasaki
Central Research Institute
11-1 Iwato Kita 2-chome
Komac-shi Tokyo 201 JAPAN

Valtonen Keijo
Inst. of Radiation Protection
P.O. Box 268
00101 Helsinki 10 FINLAND

Charles Kelber
U.S. Nuclear Regulatory Commission
MS 1130 SS
Washington DC 20555

Michael F. Kennedy
Argonne National Laboratory
9700 S. Cass Ave.
Argonne IL 60439

William G. Kennedy
Combustion Engineering
1000 Prospect Hill Rd.
Windsor CT 06095

Marc Kenton
Fauske & Associates Inc.
16W070 W. 83rd St.
Burr Ridge IL 60521

Hak-Sod Kim
The University of Wisconsin - Madison
1500 Johnson Dr.
Madison WI 53705

Ron Kimura
Technology Transfer Inst.
700 South Flower, Suite 918
Los Angeles CA 90017

Shigeki Kitajima
Kyushu Electric Power Co. Inc.
2-1-82 Watanabe-dori Chuo-ku
Fukuoka 810 JAPAN

Kazuo Kobayashi
Sukegawa Electric Co. Ltd.
3-19-5 Namekawa Hitachi-shi
Ibaraki-ken 317 JAPAN

Hideki Kodaira
University of Tokyo
7-3-1 Hongo Bunkyo-ku
Tokyo JAPAN

Rick J. Kohrt
Battelle Northwest Laboratories
Battelle Boulevard
Richland WA 99352

Yasuo Koizumi
EG&G Idaho Inc.
LOFT Program Division
P.O. Box 1625
Idaho Falls ID 83415

Alan M. Kolaczowski
Sandia National Laboratories
Division 9412
Albuquerque NM 87185

James S. Kolanowski
Commonwealth Edison
P.O. Box 767
Chicago IL 60690

Gregory Kolb
Sandia National Laboratories
Division 9412
Albuquerque NM 87185

H. Komoriya
Argonne National Laboratory
9700 S. Cass Ave.
Argonne IL 60439

Matti Komsa
Imatran Voima Power Company
Postilckero 138
00101 Helsinki 10 FINLAND

A. Koster
Nuclear Corp. of South Africa
4801 Massachusetts Ave., Ste. 350
Washington DC 20016

Edward J. Kozinsky
General Physics
1 Northgate Plaza, Ste. 200
Chattanooga TN 37415

Theodore E. Kraft
Argonne National Laboratory
9700 S. Cass Ave.
Argonne IL 60439

John M. Kramer
Argonne National Laboratory
9700 S. Cass Ave.
Argonne IL 60439

Tom S. Kress
Oak Ridge National Laboratory
Bldg. 9108 MS-2
P.O. Box Y
Oak Ridge TN 37830

Frank Krowzack
Commonwealth Edison
Braidwood NPS
R.R. #1, Box 84
Braceville IL 60407

R. K. Kumar
Atomic Energy of Canada Ltd.
Whiteshell Nuclear Research Estab.
Pinawa, Manitoba ROE 1L0 CANADA

David M. Kunsman
Science Applications Inc.
505 Marquette NW
Albuquerque NM 87102

Takashi Kuroda
Electric Power Development Co.
2-8-2 Marunouchi Chiyodaku
Tokyo JAPAN

Robert E. Kurth
Battelle Columbus Laboratories
505 King Ave.
Columbus OH 43201

Karl Kussmaul
MPA University of Stuttgart
32 Pfaffenwaldring
7000 Stuttgart 80 WEST GERMANY

Kari J. Laakso
AB ASEA-ATOM
Box 53
S-721 04 Västerås SWEDEN

E. T. Laats
EG&G Idaho Inc.
P.O. Box 1625
Idaho Falls ID 83415

Julio Jansen Laborne
Comissão Nacional de Energia Nuclear
Rua General Severiano 90
22290 Rio de Janeiro BRAZIL

Calvin K. Lai
Westinghouse-Bettis
P.O. Box 79
West Mifflin PA 15122

D. C. Lamken
Commonwealth Edison
P.O. Box 767
Chicago IL 60690

Raymond E. Lang
U.S. DOE-Chicago Oper. Office
9800 S. Cass Ave.
Argonne IL 60439

Jeanne Lanore
Centre d'Etudes Nucléaires - DSN
B.P. No. 6
92260 Fontenay-aux-Roses FRANCE

Cyril G. Lawson
Oak Ridge National Laboratory
P.O. Box Y
Oak Ridge TN 37830

David E. Leaver
Wood-Leaver & Associates Inc.
1340 Saratoga-Sunnyvale Rd.
San Jose CA 95129

Philippe Leboulex
Centre d'Etudes Nucléaires - DSN
B.P. No. 6
92260 Fontenay-aux-Roses FRANCE

Luis Lederman
Comissão Nacional de Energia Nuclear
Rua General Severiano 90
22290 Rio de Janeiro BRAZIL

Jack Leider
Commonwealth Edison
P.O. Box 767
Chicago IL 60690

Joseph Leon
Sentry Equipment Corp.
856 E. Armour Rd.
Oconomowoc WI 53066

Bernard A. Lerouge
Centre d'Etudes Nucléaires - DSN
B.P. No. 6
92260 Fontenay-aux-Roses FRANCE

Miles C. Leverett
15233 Via Pinto
Monte Sereno CA 95030

S. Levine
NUS Corporation
910 Clopper Rd.
Gaithersburg MD 20878

Jacques Libmann
Centre d'Etudes Nucléaires - IPSN
B.P. No. 6
92260 Fontenay-aux-Roses FRANCE

Pierre Lienart
EDF/Inst. for Nuclear Power Operations
1820 Water Place
Atlanta GA 30339

Hsuan-Chi Lin
Argonne National Laboratory
9700 S. Cass Ave.
Argonne IL 60439

Morten Lind
Risø National Laboratory
DK4000 Roskilde DENMARK

Richard Lindsay
Argonne National Laboratory
P.O. Box 2528
Idaho Falls ID 83401

W. B. Loewenstein
Electric Power Research Institute
P.O. Box 10412
Palo Alto CA 94303

J. P. Longworth
Central Electricity Generating Board
Berkeley Nuclear Laboratories
Berkeley Gloucester
UNITED KINGDOM

R. A. Lorenz
Oak Ridge National Laboratory
P.O. Box X
Oak Ridge TN 37830

Fred Lotarski
Commonwealth Edison
P.O. Box 767
Chicago IL 60690

A. L. Lotts
Oak Ridge National Laboratory
P.O. Box X
Oak Ridge TN 37830

Robert B. Lowtoll
General Electric Co.
2361 Loma Park Ct.
San Jose CA 95124

Jerry T. Lu
Houston Lighting & Power Co.
P.O. Box 1700
Houston TX 77001

A. C. Lucia
Euratom - JRC
Ispra (Varese) ITALY

P. E. MacDonald
EG&G Idaho Inc.
P.O. Box 1625
Idaho Falls ID 83415

Ray W. MacDonald
Fauske & Associates Inc.
16W070 W. 83rd St.
Burr Ridge IL 60521

Donald MacFarlane
ETA Engineering
415 E. Plaza Dr.
Westmont IL 60559

H. G. MacPherson
Inst. for Energy Analysis
P.O. Box 117
Oak Ridge TN 37830

John T. Madell
Fauske & Associates Inc.
16W070 W. 83rd St.
Burr Ridge IL 60521

Debu Majumdar
U.S. DOE-Idaho Operations Office
550 Second St.
Idaho Falls ID 83401

William J. Marble
General Electric Co.
175 Curtner Ave. M/C 165
San Jose CA 95125

John F. Marchaterre
Argonne National Laboratory
9700 S. Cass Ave.
Argonne IL 60439

A. Marchertas
Argonne National Laboratory
9700 S. Cass Ave.
Argonne IL 60439

Tim Margulies
U.S. Nuclear Regulatory Commission
Washington DC 20555

Albert C. Marshall
Sandia National Laboratories
P.O. Box 5800
Albuquerque NM 87185

John J. Mauro
Enviroshpere Co.
2 World Trade Center
New York NY 10048

Thomas A. McDonald
Argonne National Laboratory
9700 S. Cass Ave.
Argonne IL 60439

Thomas McNeil
Atomic Energy of Canada Ltd.
Sheridan Park Research Community
Mississauga, Ontario L5K 1B2 CANADA

Mark Melnikoff
Commonwealth Edison
Zion Gen. Sta.
101 Shiloh Blvd.
Zion IL 60099

Daniel A. Meneley
Ontario Hydro
700 University Ave. H16
Toronto, Ontario M5G 1X6 CANADA

Robert F. Miller
Stone & Webster Engr. Corp.
P.O. Box 2325
Boston MA 02210

Joseph Minarick
Science Applications Inc.
800 Oak Ridge Turnpike
Oak Ridge TN 37830

Robert B. Minogue
U.S. Nuclear Regulatory Commission
Washington DC 20555

Dennis E. Mitchell
Sandia National Laboratories
P.O. Box 5800
Albuquerque NM 87185

Mohammad Modarres
University of Maryland
5225 Pooks Hill Rd. 1724 N.
Bethesda MD 20814

S. M. Modro
EG&G Idaho Inc.
P.O. Box 1625
Idaho Falls ID 83415

Charles L. Mohr
Battelle Northwest Laboratories
Box 999
Richland WA 99352

Shigeru Morimoto
Sukegawa Electric Co. Ltd.
3-19-5 Namekawa Hitachi-shi
Ibaraki-ken 317 JAPAN

Edgar E. Morris
Argonne National Laboratory
9700 S. Cass Ave.
Argonne IL 60439

Fred S. Morris
Commonwealth Edison
P.O. Box 767
Chicago IL 60690

Wilbur M. Morrison
U.S. Nuclear Regulatory Commission
MS 5650 NL
Washington DC 20555

P. Mostert
KEMA
Utrechtseweg 310
Arnhem THE NETHERLANDS

Craig Mowrey
Westinghouse Nuclear Training
505 Shiloh Blvd.
Zion IL 60099

Nigel Moxley
Framatome
1 Place de la Coupole
Courbevoie 75015 FRANCE

W. Christoph Müller
Gesellschaft für Reaktorsicherheit
Forschungsgelände
D-8046 Garching WEST GERMANY

Michio Murase
Energy Research Laboratory
1168 Moriyama
Hitachi Ibaraki 316 JAPAN

Yasuo Nagai
Mitsubishi Corp.
6-3 Marunouchi 2-chome
Chiyoda-ku Tokyo 100 JAPAN

M. Nakahara
Kajima Corp.
Motoakasa 1-chome
Minato-ku Tokyo JAPAN

A. Natalizio
Atomic Energy of Canada Ltd.
Sheridan Park Research Community
Mississauga, Ontario L5K 1B2 CANADA

William F. Naughton
Commonwealth Edison
P.O. Box 767
Chicago IL 60690

Lawrence A. Neimark
Argonne National Laboratory
9700 S. Cass Ave.
Argonne IL 60439

Lloyd S. Nelson
Sandia National Laboratories
Division 9441
P.O. Box 5800
Albuquerque NM 87185

Steve L. Nicolosi
Battelle Columbus Laboratories
505 King Ave.
Columbus OH 43201

S. J. Niemczyk
Oak Ridge National Laboratory
Bldg. 4500S MS S204
P.O. Box X
Oak Ridge TN 37830

Kjell A. Nilsson
Electric Power Research Inst., NSAC
3412 Hillview Ave.
Palo Alto CA 94303

Robert Noel
Electricité de France - SEPTEN
Tour EDF/GDF - Cedex 8
92080 Paris - La Défense FRANCE

Prabhat Nunshi
Commonwealth Edison
72 W. Adams St.
Chicago IL 60690

Fridtjov Oewre
OECD Halden Reactor Project
OS Alle 13
N-1750 Halden NORWAY

David Okrent
University of California, Los Angeles
5532 Boelter Hall
Los Angeles CA 90024

Luiz F. Oliveira
Universidade Federal de Rio de Janeiro
COPPE/Nuclear
Ilha do Fundão
Rio de Janeiro BRAZIL

Erhard Ortlieb
Kraftwerk Union AG
ABT B227 PF 3220
D-8520 Erlangen WEST GERMANY

Dan J. Osetek
EG&G Idaho Inc.
P.O. Box 1625
Idaho Falls ID 83415

Kunihiro Ota
Kansai Electric Power Co.
1100 17th St. NW, Ste. 606
Washington DC 20036

Keiichi Otohara
The Tokyo Electric Power Co., Inc.
1-1-3 Uchisaiwai-cho Chiyoda-ku
Tokyo 100 JAPAN

K. O. Ott
School of Nuclear Eng.
Purdue University
West Lafayette IN 47907

John M. Otter
Rockwell Int. ESG
8900 DeSoto Ave.
Canoga Park CA 91304

Dennis F. Owen
EG&G Idaho Inc.
P.O. Box 1625
Idaho Falls ID 83415

Randall Pack
General Physics Corp.
1700 The Exchange, Ste. 120
Atlanta GA 30339

In-Kul Paik
The University of Wisconsin - Madison
1500 Johnson Dr. 142 ERB
Madison WI 53706

Bruce Palagi
Commonwealth Edison
72 W. Adams St.
Chicago IL 60690

Frank A. Palmer
Commonwealth Edison
P.O. Box 767
Chicago IL 60690

Yen-Chens Pan
Argonne National Laboratory
9700 S. Cass Ave.
Argonne IL 60439

Ioannis A. Papazoglou
Brookhaven National Laboratory
Bldg. 130
Upton NY 11973

George W. Parker
Oak Ridge National Laboratory
P.O. Box X
Oak Ridge TN 37830

Nicole Parmentier
Centre d'Etudes Nucléaires - IPSN
B.P. No. 6
92260 Fontenay-aux-Roses FRANCE

W. Paskievici
Ecole Polytechnique
4874 Cote des Neiges
Montreal H3V 1H9 CANADA

A. C. Payne, Jr.
Sandia National Laboratories
P.O. Box 5800
Albuquerque NM 87185

L. Pease
Atomic Energy of Canada Ltd
Sheridan Park Research Community
Mississauga, Ontario L5K 1B2 CANADA

Dean R. Pedersen
Argonne National Laboratory
9700 S. Cass Ave.
Argonne IL 60439

William R. Peebles
Sargent & Lundy Engineers
55 E. Monroe
Chicago IL 60603

Jean Peltier
Commissariat à l'Energie Atomique
CEN/SACLAY
Gif-sur-Yvette 91191 FRANCE

W. J. Penn
Ontario Hydro
700 University Ave.
Toronto, Ontario M5G 1X6 CANADA

Åke H. Persson
Southern Sweden Power Supply
217 01 Malmö SWEDEN

D. A. Petti
EG&G Idaho Inc.
P.O. Box 1625
Idaho Falls ID 83402

Doan Phung
Institute For Energy Analysis
P.O. Box 117
Oak Ridge TN 37830

George Pliml
Commonwealth Edison
Zion Gen. Sta.
101 Shiloh Blvd.
Zion IL 60099

Martin Plys
MIT/Fauske and Associates Inc.
16W070 W. 83rd St.
Burr Ridge IL 60521

R. Potter
U.K. Atomic Energy Authority
AEE Winfrith
NR Dorchester, Dorset DT2 8DH
UNITED KINGDOM

Wm. Trevor Pratt
Brookhaven National Laboratory
Bldg. 130
Upton NY 11973

G. Proto
Nucleare Italiana Reattori Avanzati
Via dei Pescatori 35
16129 Genova ITALY

Ralph E. Pullo
Commonwealth Edison
125 S. Clark St.
Chicago IL 60690

Blake F. Putney, Jr.
Science Applications Inc.
5 Palo Alto
Palo Alto CA 94306

W. J. Quapp
EG&G Idaho Inc.
P.O. Box 1625
Idaho Falls ID 83415

K. B. Ramsden
Commonwealth Edison
P.O. Box 767
Chicago IL 60690

Thomas Raney
Envirosphere Company
2 World Trade Center
New York NY 10048

N. Rasmussen
Massachusetts Institute of Technology
138 Albany St.
Cambridge MA 02139

A. J. Rastas
Teollisuuden Voima Oy
Kutojantie 8
02630 Espoo 63 FINLAND

Richard E. Raymond
UNC Nuclear Industries
P.O. Box 490
Richland WA 99352

G. L. Redman
Commonwealth Edison
P.O. Box 767
Chicago IL 60690

Cordell Reed
Commonwealth Edison
P.O. Box 767
Chicago IL 60690

Klaus Reinke
TÜV Baden
Dildenst. 28
D-6800 Mannheim WEST GERMANY

Forrest J. Remick
Pennsylvania State University
University Park PA 16802

J. Rest
Argonne National Laboratory
9700 S. Cass Ave.
Argonne IL 60439

Zsolt Révész
Electrowatt Engineering Services
Bellerivestrasse 36
8053 Zurich SWITZERLAND

Paul E. Rexroth
Sandia National Laboratory
Kirtland Air Force Base
Albuquerque NM 87185

Oscar Jimenez Reynaldo
Consejo Seguridad Nuclear
P. de la Castellana 135
Madrid 16 SPAIN

Howard V. Rhude
Argonne National Laboratory
9700 S. Cass Ave.
Argonne IL 60439

William J. Richardson
Westinghouse Nuclear Training
505 Shiloh Blvd.
Zion IL 60099

Marseyne Richter
Commonwealth Edison
4450 N. German Church Rd.
Byron IL 61010

William Rish
Envirosphere Co.
160 Chubb Ave.
Lyndhurst NJ 07071

R. L. Ritzman
Science Applications Inc.
5 Palo Alto Sq. Suite 200
Palo Alto CA 94304

Joseph B. Rivard
Sandia National Laboratories
P.O. Box 5800
Albuquerque NM 87185

Daniel Robeau
Centre d'Etudes Nucléaires - IPSN
B.P. No. 6
92260 Fontenay-aux-Roses FRANCE

Richard Rohrer
The University of Wisconsin - Madison
1500 Johnson Dr.
Madison WI 53705

Stig Rolandson
ASEA-ATOM
Box 53
S-72104 Västerås SWEDEN

David Rose
Argonne National Laboratory
9700 S. Cass Ave.
Argonne IL 60439

Morris Rosen
International Atomic Energy Agency
P.O. Box 100
A-1400 Vienna AUSTRIA

S. L. Rosen
Inst. for Nuclear Power Operation
1820 Water Place
Atlanta GA 30339

Gerald S. Rosenberg
Argonne National Laboratory
9700 S. Cass Ave.
Argonne IL 60439

A. David Rossin
Electric Power Research Institute
3412 Hillview Ave.
Palo Alto CA 94303

Robert S. Rudland
Westinghouse Electric Corp.
505 Shiloh Blvd.
Zion IL 60099

Roland Ruhle
University of Stuttgart - IKE
Pfaffenwaldring 31
7000 Stuttgart - 80 WEST GERMANY

K. W. Rust
Kernforschungszentrum Karlsruhe
Postfach 3640
7500 Karlsruhe WEST GERMANY

Margaret L. Ryan
McGraw Hill, "Inside NRC"
433 National Press Bldg.
Washington DC 20045

Jeffrey C. Ryman
Union Carbide Corp., Nucl. Div.
433 East Dr.
Oak Ridge TN 37830

Zeinab A. Sabri
Louisiana Power & Light Co.
Waterford 3 P.O. Box B
Killona LA 70066

Manjit S. Sahota
Los Alamos National Laboratory
P.O. Box 1663
Los Alamos NM 85745

Gary A. Sanders
Sandia National Laboratories
Division 9414
Albuquerque NM 87185

Onkichiro Sato
Genshi-Ryoku Daiko Co.
5-5-12 Ginza Chuo-ku
Tokyo 104 JAPAN

George R. Sawtelle
Energy Incorporated
P.O. Box 736
Idaho Falls ID 83402

Timothy J. Scale
Argonne National Laboratory
9700 S. Cass Ave.
Argonne IL 60439

W. O. Schikarski
Kernforschungszentrum Karlsruhe
P.O. Box 3640
7500 Karlsruhe WEST GERMANY

Fritz Schmidt
University of Stuttgart - IKE
Pfaffenwaldring 31
7000 Stuttgart - 80 WEST GERMANY

W. Schoeck
Kernforschungszentrum Karlsruhe
Postfach 3640
7500 Karlsruhe WEST GERMANY

Morris Schreim
Commonwealth Edison
1 First National Plaza
Chicago IL 60690

Erich Schroeder
GKSS Forschungszentrum
Max Planck Str.
2054 Geesthacht WEST GERMANY

Donald L. Schurman
Applied Science Associates, Inc.
Box 158
Valencia PA 16059

Terence K. Schuster
Commonwealth Edison Byron Sta.
4450 N. German Church Rd.
Byron IL 61010

Linda Scott
Commonwealth Edison
P.O. Box 767
Chicago IL 60690

G. Sdouz
Austrian Research Center
Lenaugasse 10
A-1082 Vienna AUSTRIA

Dietrich Seeliger
GKSS-Forschungszentrum-GMBH
Max Planck Str.
2054 Geesthacht WEST GERMANY

Bal Raj Sehgal
Electric Power Research Institute
3412 Hillview Ave.
Palo Alto CA 94303

Yasuhide Senda
Argonne National Laboratory
9700 S. Cass Ave.
Argonne IL 60439

Michael Senglaub
Sandia National Laboratories
Division 9424
P.O. Box 5800
Albuquerque NM 87185

Wolfgang Sengpiel
EG&G Idaho Inc.
P.O. Box 1625
Idaho Falls ID 83415

Pio Carmena Servert
Empresarios Agrupados
Magallanes 3
Madrid SPAIN

Clint Shaffer
Energy Incorporated
5345 Wyoming NE
Albuquerque NM 87109

John Shearer
Argonne National Laboratory
9700 S. Cass Ave.
Argonne IL 60439

Richard R. Sherry
U.S. Nuclear Regulatory Commission
MS 1130-SS
Washington DC 20555

N. Shirai
Nuclear Fuel Industries Ltd.
P.O. Box 1260
Lynchburg VA 24505

Louis Shotkin
U.S. Nuclear Regulatory Commission
Washington DC 20555

E. Siddall
AECL Engineering Co.
Sheridan Park Research Community
Mississauga, Ontario L5K 1B2 CANADA

John R. Siegel
Atomic Industrial Forum
7101 Wisconsin Ave.
Bethesda MD 20814

James J. Sienicki
Argonne National Laboratory
9700 S. Cass Ave.
Argonne IL 60439

F. A. Silady
General Atomic Company
P.O. Box 81608
San Diego CA 92138

John A. Silady
Commonwealth Edison
72 W. Adams St.
Chicago IL 60690

M. Silberberg
U.S. Nuclear Regulatory Commission
MS 1130-SS
Washington DC 20555

Raymond Skarda
Pacific Northwest Laboratories
P.O. Box 999
Richland WA 99352

Don Slaughterbeck
Intermountain Technologies
P.O. Box 1604
Idaho Falls ID 83401

Noval A. Smith, Jr.
Virginia Electric & Power Co.
P.O. Box 26666
Richmond VA 23261

Suzanne T. Smith
Thermal-Hydraulics GP-Q8, MS-K5
Los Alamos National Laboratory
Los Alamos NM 87545

Kunihisa Soda
Inst. of Nuclear Safety Japan
Mitakokusai Bldg. 1104
Minato-ku Tokyo 108 JAPAN

Shully I. Solomon
Department of Civil Eng.
University of Waterloo
Waterloo, Ontario N2L 3G1 CANADA

Manshik Song
Dept. of Nuclear Eng.
North Carolina State University
Raleigh NC 27650

Larry Soth
Commonwealth Edison
P.O. Box 767
Chicago IL 60690

B. W. Spencer
Argonne National Laboratory
9700 S. Cass Ave.
Argonne IL 60439

Jeremy L. Sprung
Sandia National Laboratories
P.O. Box 5800
Albuquerque NM 87185

August W. Spyksma
Commonwealth Edison
P.O. Box 767
Chicago IL 60690

K. B. Stadie
Organization for Economic Cooperation
and Development/NEA
38 Bd. Suchet
75016 Paris FRANCE

Gary Stauffer
Commonwealth Edison
4450 N. German Church Rd.
Byron IL 61010

William Stephenson
National Nuclear Corp.
Cambridge Road
Whetstone Leicester LE8 3LH
UNITED KINGDOM

John D. Stevenson
Stevenson & Associates
21099 Claythorne Rd.
Cleveland OH 44122

Jean Stolz
Electricité de France
32 Rue de Monceau
75008 Paris FRANCE

Allen H. Stretch
Atomic Energy of Canada Ltd.
Sheridan Park Research Community
Mississauga, Ontario L5K 1B2 CANADA

Bill K-H. Sun
Electric Power Research Institute
3412 Hillview Ave.
Palo Alto CA 94303

Yang-Ho Sun
Brookhaven National Laboratory
Upton NY 11873

J. A. Svensson
Sydkraft AB
21701 Malmö SWEDEN

Charles D. Swanson
Control Data Corp.
13260 Flagstaff Ave.
Apple Valley NM 55124

David Swanson
P.O. Box 2687
Palos Verdes Peninsula CA 90274

Yasumasa Tabuchi
Mitsubishi Heavy Industries
2-4-1 Shiba Koen Minato-ku
Tokyo 105 JAPAN

A. R. Taig
UKAEA/Sandia National Laboratories
Division 9415
P.O. Box 5800
Albuquerque NM 87185

Hiromi Takahashi
The Federation of Electric Power Cos.
1-9-4 Otemachi Chiyoda-ku
Tokyo 100 JAPAN

Yukio Takahashi
Argonne National Laboratory
9700 S. Cass Ave.
Argonne IL 60439

Eiji Takeuchi
Chubu Electric Power Co., Inc.
900 17th St. NW, Suite 714
Washington DC 20006

Shiu-Wing Tam
Argonne National Laboratory
9700 S. Cass Ave.
Argonne IL 60439

H. Tamm
Atomic Energy of Canada Ltd.
Whiteshell Nuclear Research Estab.
Pinawa, Manitoba ROE 1LO CANADA

Pierre Y. Tanguy
Commissariat à l'Energie Atomique
92260 Fontenay-aux-Roses FRANCE

Kanji Tasaka
Japan Atomic Energy Research Inst.
Tokai-mura
Ibaraki-ken 319-11 JAPAN

H. J. Teague
U.K. Atomic Energy Authority - SRD
Wigshaw Lane, Culcheth
Warrington Cheshire UNITED KINGDOM

Marvin Tetenbaum
Argonne National Laboratory
9700 S. Cass Ave.
Argonne IL 60439

Mohan Thadani
U.S. Nuclear Regulatory Commission
Washington DC 20555

P. J. Thomas
U.K. Atomic Energy Authority
AETB, Bldg. 329
Harwell Oxfordshire UNITED KINGDOM

David H. Thompson
Argonne National Laboratory
9700 S. Cass Ave.
Argonne IL 60439

Paul D. Thompson
Atomic Energy of Canada Ltd.
Sheridan Park Research Community
Mississauga, Ontario L5K 1B2 CANADA

Antonio G. Tiberini
Kernkraftwerk Leibstadt A.G.
4353 Leibstadt SWITZERLAND

Yasumasa Togo
Department of Nuclear Engineering
University of Tokyo
7-3-1 Hongo Bunkyo-ku
Tokyo JAPAN

Kenji Tominaga
Hitachi Ltd.
3-1-1 Saiwai-cho Hitachi City
Ibaraki-ken 317 JAPAN

L. S. Tong
U.S. Nuclear Regulatory Commission
Washington DC 20555

D. F. Torgerson
Atomic Energy of Canada Ltd.
Whiteshell Nuclear Research Estab.
Pinawa, Manitoba ROE 1LO CANADA

Alfred Torri
Pickard, Lowe & Garrick
505 Comas Santa Fe Dr., Suite 150
Solana Beach CA 72075

James G. Toscas
Commonwealth Edison
P.O. Box 767
Chicago IL 60690

Tom Tramm
Commonwealth Edison
P.O. Box 767
Chicago IL 60690

Roberto Treviño
Comisión Nacional de Seguridad
Nuclear y Salvaguardias
Insurgentes sur 1806
Mexico City (20) 01730 MEXICO

Robert W. Tsai
Commonwealth Edison
72 W. Adams St.
Chicago IL 60690

Francis Y. Tsang
EG&G Idaho Inc.
P.O. Box 1625
Idaho Falls ID 83401

Hirokuzu Tsunoda
Mitsubishi Research Institute
2-3-6 Otemachi Chiyoda-ku
Tokyo 100 JAPAN

Akira Umezu
Tokyo Electric Power Co.
1901 L St. NW, Suite 720
Washington DC 20036

Hermann Unger
University of Stuttgart - IKE
Pfaffenwaldring 31
7000 Stuttgart - 80 WEST GERMANY

Milton Vagins
U.S. Nuclear Regulatory Commission
MS 5650 NL
Washington DC 20555

J. B. van Erp
Argonne National Laboratory
9700 S. Cass Ave.
Argonne IL 60439

Timo Vanttola
Tech. Research Center of Finland
POB 169
SF-00181 Helsinki FINLAND

R. V. van Wieringen
Ministry of Social Affairs
Europasingel 14
2396 EM Koudekerk THE NETHERLANDS

Jussi K. Vaurio
Argonne National Laboratory
9700 S. Cass Ave.
Argonne IL 60439

M. Villemeur
Electricité de France
6 Quai Watier
78400 Chatou FRANCE

W. Vinck
Commission of the European Communities
200 Rue de la Loi
1049 Brussels BELGIUM

Steve Vittatoe
EG&G ORTEC
100 Midland Rd.
Oak Ridge TN 37830

Richard C. Vogel
Electric Power Research Institute
P.O. Box 10412
Palo Alto CA 94303

Antti P. Vuorinen
International Atomic Energy Agency
Nuclear Safety Division
P.O. Box 100
A-1400 Vienna AUSTRIA

Ian B. Wall
Electric Power Research Institute
P.O. Box 10412
Palo Alto CA 94303

Chester C. Wang
Atomic Energy Control Board
53 Leander St.
Bramlea, Ontario L6S 3M4 CANADA

K. R. Weaver
Atomic Energy of Canada Ltd.
Sheridan Park Research Community
Mississauga, Ontario L5K 1B2 CANADA

Walter L. Weaver
EG&G Idaho Inc.
P.O. Box 1625
Idaho Falls ID 83415

Norman Weber
Sargent & Lundy
55 E. Monroe St.
Chicago IL 60603

Ulrich Weicht
Hochtemperatur-Reaktorbau GmbH
Gottlieb Daimlerstr. 8
68 Mannheim WEST GERMANY

G. G. Weigand
Sandia National Laboratories
P.O. Box 5800
Albuquerque NM 87185

D. J. Western
Central Electricity Generating Board
Newgate St.
London UNITED KINGDOM

Michael D. White
Doub & Muntzing Chartered
1875 I St. NW, Suite 775
Washington DC 20006

G. D. Whitman
Oak Ridge National Laboratory
Bldg. 9204-1 MS 06
P.O. Box Y
Oak Ridge TN 37830

A. J. Wickett
Sandia National Laboratories
Division 9425
P.O. Box 5800
Albuquerque NM 87185

Hartmut U. Wider
Argonne National Laboratory
9700 S. Cass Ave.
Argonne IL 60439

J. Ernest Wilkins, Jr.
EG&G Idaho Inc.
P.O. Box 1625
Idaho Falls ID 83415

Michael M. Willoughby
Commonwealth Edison
Dresden Nuclear Sta.
R.R. # 1
Morris IL 60450

Randall J. Wilson
Argonne National Laboratory
9700 S. Cass Ave.
Argonne IL 60439

Kevin Winegardner
Battelle Northwest Laboratories
P.O. Box 999
Richland WA 99352

Johannes P. Wolters
Kernforschungsanlage
P.O. Box 1913
D-5170 Jülich WEST GERMANY

Douglas C. Wood
Bechtel Power Corp.
P.O. Box 1000
Ann Arbor MI 48106

P. B. Woods
Nuclear Installations Inspectorate
Thames House, North Millbank
London SW1P 4QL UNITED KINGDOM

Gary N. Wright
Illinois Department of Nuclear Safety
1035 Outer Park Drive
Springfield IL 62704

Anthony L. Wright
Oak Ridge National Laboratory
Bldg. 4500N
P.O. Box X
Oak Ridge TN 37830

A. C. D. (Dave) Wright
Atomic Energy of Canada Ltd.
Sheridan Park Research Community
Mississauga, Ontario L5K 1B2 CANADA

Yu-Chien Yuan
Argonne National Laboratory
9700 S. Cass Ave.
Argonne IL 60439

R. W. Wright
Div. of Accident Evaluation, MS-1130-SS
U.S. Nuclear Regulatory Commission
Washington DC 20555

E. L. Zebroski
Inst. for Nuclear Power Operation
1820 Water Place
Atlanta GA 30339

Wolfgang Wulff
Brookhaven National Laboratory
Bldg. 130
Upton NY 11973

Jean-Francois Zuber
Swiss Nuclear Safety Dept.
CH-5305 Würenlingen SWITZERLAND

Frank L. Wurst
Pennsylvania Power & Light
2 North 9th St.
Allentown PA 18101

Daniel A. Yakes
Commonwealth Edison
125 N. Clark St.
Chicago IL 60690

Kunio Yamana
Nissho Iwai American Corp.
1211 Ave. of the Americas
New York NY 10036

J. W. Yang
Brookhaven National Laboratory
Upton NY 11973

E. M. Yaremy
Atomic Energy of Canada Ltd.
Sheridan Park Research Community
Mississauga, Ontario L5K 1B2 CANADA

Tsunemasa Yasui
The Chubu Electric Power Co. Inc.
1 Toshin-cho Higashi-ku
Nagoya, Aichi-ken 461-91 JAPAN

L. J. Ybarrondo
EG&G Idaho Inc.
P.O. Box 1625
Idaho Falls ID 83415

Robert Youngblood
Brookhaven National Laboratory
Upton NY 11973

Vesa Yrjola
Tech. Research Ctr. of Finland
P.O. Box 169
SF-00181 Helsinki 18 FINLAND

NRC FORM 335 (11-81)		U.S. NUCLEAR REGULATORY COMMISSION BIBLIOGRAPHIC DATA SHEET		1. REPORT NUMBER (Assigned by DDC) NUREG/CP-0027 Volume 3	
4. TITLE AND SUBTITLE (Add Volume No., if appropriate) PROCEEDINGS OF THE INTERNATIONAL MEETING ON THERMAL NUCLEAR REACTOR SAFETY, Held at Chicago, Illinois, August 29—September 2, 1982				2. (Leave blank)	
7. AUTHOR(S)				3. RECIPIENT'S ACCESSION NO.	
9. PERFORMING ORGANIZATION NAME AND MAILING ADDRESS (Include Zip Code) Chicago Section of the American Nuclear Society c/o Elmer E. Lewis Dept. of Mechanical and Nuclear Engineering Northwestern University Evanston, Illinois 60201				5. DATE REPORT COMPLETED MONTH YEAR	
12. SPONSORING ORGANIZATION NAME AND MAILING ADDRESS (Include Zip Code) American Nuclear Society, European Nuclear Society, Canadian Nuclear Society, Japan Atomic Energy Society; in cooperation with U. S. Nuclear Regulatory Commission, International Atomic Energy Agency				6. (Leave blank)	
13. TYPE OF REPORT Conference Proceedings				7. (Leave blank)	
15. SUPPLEMENTARY NOTES				8. (Leave blank)	
16. ABSTRACT (200 words or less) The Proceedings of the International Meeting on Thermal Nuclear Reactor Safety, held at Chicago, Illinois, August 29—September 2, 1982, contain the entire collection of papers submitted for presentation at the meeting, as well as two special addresses, and four summarizing review articles. The papers deal with a wide spectrum of subjects pertaining to the area of thermal nuclear reactor safety, including: licensing criteria, safety goals, probabilistic risk assessment, reliability analysis, safety-related operational experience, man/machine interface, human factors, transient analysis, loss-of-coolant analysis, structural analysis, fuel performance evaluation, severe accident analysis, radiological source term evaluation, pressurized thermal shock. In addition to papers on the above technical subjects, the Proceedings contain a number of papers describing safety-related programs in a number of countries, including Argentina, Brazil, Canada, Fed. Rep. of Germany, Finland, France, Greece, Italy, Japan, Mexico, Spain, Sweden, and United Kingdom. The Meeting was jointly sponsored by the American Nuclear Society, the European Nuclear Society, the Canadian Nuclear Society, and the Japan Atomic Energy Society. It was, furthermore, organized and conducted in cooperation with the U. S. Nuclear Regulatory Commission and the International Atomic Energy Agency.					
17. KEY WORDS AND DOCUMENT ANALYSIS licensing; safety goals; probabilistic risk assessment, PRA; reliability analysis; opera- tional experience; man/machine interface; human factors; transient analysis; accident analysis; loss-of-coolant accident, LOCA; small-break LOCA analysis; large-break LOCA analysis; severe accident analysis; radiological source terms; pressurized thermal shock; degraded core cooling; structural analysis.				17a. DESCRIPTORS	
17b. IDENTIFIERS/OPEN-ENDED TERMS					
18. AVAILABILITY STATEMENT Unlimited				19. SECURITY CLASS (This report) Unclassified	
20. SECURITY CLASS (This page) Unclassified				21. NO. OF PAGES 2140 (3 volumes)	
				22. PRICE S	

UNITED STATES
NUCLEAR REGULATORY COMMISSION
WASHINGTON, D.C. 20555

FOURTH-CLASS MAIL
POSTAGE & FEES PAID
USNRC
WASH. D. C.
PERMIT No. G-67

OFFICIAL BUSINESS
PENALTY FOR PRIVATE USE, \$300

Name

Mail Stop

Due Date

Return to: 823 LIBRARY/SNL, MS 0731